

PROCEEDINGS



ASFNR ASHNR ASPNR ASSR SNIS

ASNR 52nd Annual Meeting

May 19-22, 2014

Palais de congres de Montreal

Montreal, Quebec CANADA

NOTE: Proceedings Content as of 3/28/2014...any changes made after 3/28/2014 will not be reflected in this material...for current program please check Program Planner.

All Electronic Excerptas, Education Education Exhibits, Electronic Education Exhibits, Poster and Electronic posters may be viewed using the Program Planner or ASNR Web Application.

Note: Scanned images are included in the proceedings. Some submitted images were reduced during editing thereby decreasing clarity. Also, refer to the Program Planner. Proceedings Content as of 3/28/2014.

Monday, May 19
7:25 AM – 7:30 PM
Room 517bc

Opening Remarks Gordon K. Sze, MD, FACR

Monday, May 19
7:30 AM – 8:30 AM
Room 517bc

02- Head and Neck Session (SAM)

O-01 7:30AM - 7:50AM
Frequently Missed Diagnoses in the Head and Neck

Shatzkes, D.
Lenox Hill Hospital
New York, NY

Abstract/Presentation Summary

The head and neck can be a challenging area for the radiologist, in that some findings are easily missed, and others are frequently misinterpreted. Some of the more common "misses" in H&N radiology occur because findings are subtle and will not be obvious to the examiner unless they are the subject of a specific and systematic search. A classic example is fenestral otosclerosis. This relatively common diagnosis (found in up to 10% of autopsy specimens!) will invariably be missed unless the radiologist specifically interrogates its most common site of presentation, the fissula ante fenestram, along the anterior margin of the oval window. There, only a small lucent focus may be discovered, yet this will reflect the etiology of the patient's hearing loss, while the remainder of the scan is entirely normal. The temporal bone is the site of another commonly missed diagnosis, labyrinthitis. In this scenario, the patient presents with sensorineural hearing loss, and the radiologist is able to rule out the most common listed study indication, "acoustic neuroma." Yet, labyrinthitis is a statistically more common cause of hearing loss, though the findings of abnormal signal in the membranous labyrinth may be extremely subtle. When "tunnel vision" is applied in the setting of hearing loss, and scan interrogation is limited to the internal auditory canal and cerebellopontine angle cistern, the findings of labyrinthitis will invariably be missed. Familiarity with some of the diseases specific to the H&N will help reduce the likelihood of misinterpretation of findings. An example that has recently gained attention in the literature is HPV-related squamous cell carcinoma of the oropharynx. These cancers frequently metastasize to upper jugular lymph nodes, and these nodes are frequently cystic. As such, there has been a near epidemic of cystic metastatic lymph nodes

mistakenly called second branchial cleft cysts. Beware this diagnosis in the adult patient!

O-02 7:50AM - 8:10AM
Challenging Cases in Head and Neck Radiology

Fischbein, N.
Stanford University
Stanford, CA

Abstract/Presentation Summary

The head and neck is an anatomically complex region of the body, and a strong knowledge of anatomy of this region and an understanding of the disease processes that affect this area is essential for correct interpretation of imaging studies. The anatomical complexity and variability among patients also leads to a large number of anatomical variants and pitfalls that must be recognized by interpreting radiologists. In today's presentation we will focus on areas with difficult anatomy, challenging diagnoses, and imaging of uncommon but interesting or important disease entities. One area of focus for us will be the jugular foramen. The jugular foramen is a depression on the medial and inferior surface of the petrous pyramid formed by the temporal and occipital bones. It courses anteriorly and laterally as it exits the skull base. It consists of a smaller anteromedial portion, the pars nervosa, and a larger posterolateral portion, the pars vascularis, and the two are separated by a complete or incomplete fibrous or bony septum. The pars nervosa contains CN IX (the glossopharyngeal nerve) and the inferior petrosal sinus. The pars vascularis contains CN X, CN XI, and the internal jugular vein. The classic differential of a jugular foramen mass includes paraganglioma, schwannoma, meningioma, and metastasis. An important pitfall is slow flow in the jugular bulb, which can mimic a mass lesion; conversely, a real lesion of the jugular foramen may be overlooked and mistaken for a prominent jugular bulb. Asymmetry of the larynx due to unilateral vocal cord paralysis (UVCP) is another imaging finding that can be potentially confusing for the unwary radiologist. We will review a case of a subtle lesion resulting in UVCP and will discuss the imaging features of vocal cord paralysis. We will also discuss denervation change in the laryngeal musculature as a potential pitfall in laryngeal imaging. Numerous disease processes may result in abnormalities of the retropharyngeal space, and processes such as infection in the retropharynx are of particular interest and concern as they may extend into the chest and cause severe complications for the affected patient. An uncommon but not rare disorder of this region is calcific tendinitis, and we will review an example of this process, as well as abnormalities of the retropharyngeal space secondary to trauma and foreign bodies. If time permits, we will also review the varied clinical and imaging presentations of fungal sinus disease. These include allergic fungal rhinosinusitis, mycetoma, chronic invasive fungal disease, and acute invasive fungal disease. Many of these cases, as if often true in head and neck imaging, benefit from obtaining both CT and MR scans, as each study provides different

Note: Scanned images are included in the proceedings. Some submitted images were reduced during editing thereby decreasing clarity. Also, refer to the Program Planner. Proceedings Content as of 3/28/2014.

information about the disease process and together may allow the most specific diagnosis to be made and/or offer the best chance of detecting important complications.

8:10AM - 8:30AM

Questions and Answers

Monday, May 19
8:30 AM – 10:00 AM
Room 517bc

03 - ASHNR Programming: Aerodigestive
Head and Neck Cancer

O-03 8:30AM - 9:00AM
Imaging Approach to Laryngeal and Hypopharyngeal
Cancer

Stambuk, H.
Memorial Sloan-Kettering Cancer Center
New York, NY

Abstract/Presentation Summary
CT and MRI are the two commonly used imaging modalities for imaging laryngopharyngeal tumors. CT is generally the initial study of choice because of its quicker acquisition time that makes it less susceptible to swallowing artifact compared to MRI. MRI may be reserved to answer specific questions unresolved by CT, such as questionable cartilage invasion, involvement of PES or early extralaryngeal spread. The overwhelming majority of cancers of the laryngopharynx are squamous cell carcinoma (SCC) and will be the focus of this lecture. Remember however that submucosal tumors can be of minor salivary gland origin, sarcomas can arise from the muscle and cartilage framework, thyroid cancer can invade directly, and tumors can rarely metastasize from distant sites. Tumors of the supraglottic larynx are generally asymptomatic and are not detected until later in their natural history. The supraglottic larynx is also richly supplied with lymphatics so that nodal metastases occur early. The majority of patients with supraglottic SCC therefore present with higher stage tumors. Tumors of the glottic larynx cause hoarseness and are therefore generally detected earlier compared to supraglottic tumors. The glottic larynx has sparse lymphatics so that nodal metastasis is rare, and occurs with advanced tumors. Imaging is therefore rarely useful for early glottic tumors, but radiographically demonstrable submucosal subglottic and/or supraglottic extension or cartilage invasion can upstage a clinically "early" lesion. Caudal extension into the subglottis upstages a small glottic tumor to T2 and increases risk for nodal metastases. The hypopharynx is the site with the worst prognosis among all head and neck SCC. Like patients with supraglottic tumors, these tumors are also asymptomatic until they are locally advanced and

the majority of patients present with nodal metastases. A peculiar feature of submucosal caudal spread of hypopharyngeal SCC to the cervical esophagus is that it can occur with skip areas of normal intervening tissue. A basic understanding of the mucosal anatomy as visualized through the endoscope is essential for the radiologist when communicating radiographic findings with the clinicians treating the patient. Key endoscopic features of laryngopharyngeal anatomy will therefore also be briefly reviewed during the lecture.

O-04 9:00AM - 9:30AM
Imaging Approach to Oral Cavity and Oropharyngeal
Cancer

Kirsch, C.
Ohio State Univ. Medical Center
Bexley, OH

Abstract/Presentation Summary
Presentation Summary: Imaging Approach to Oral Cavity and Oropharyngeal Cancer – Claudia Kirsch MD Associate Professor of Neuroradiology and Otolaryngology Section Chief Head and Neck Imaging Director Radiology Medical Student Teaching Wexner Medical Center The Ohio State University College of Medicine The purpose of this lecture is to outline imaging approaches to oral cavity (OC) and oropharyngeal (OP) cancers reviewing the background, incidence, and critical anatomy radiologists need to assess for treating clinicians be it otolaryngology or radiation therapy . Specifically this talk will cover five major areas including: 1- Incidence – introduce risks factors, resulting in the increased incidence of oral cavity and oropharyngeal cancers. Although risk factors from smoking and drinking have declined, the increased prevalence of the HPV virus, is associated with an increased number of both oral cavity and oropharyngeal cancers. 2- Modalities – review the currently used imaging modalities, namely CT, MRI, PET-CT, and Ultrasound, the protocols for each modality and how each modality can be utilized to help assess patients with oral cavity and oropharyngeal cancer 3- Anatomy – review the basic anatomy of the oral cavity and oropharynx that is critical in understand cancers behavior , especially the site of cancers origin and spread. Both the basic anatomy of the oral cavity and oropharynx will be reviewed, and more importantly the key subsites where these cancers can occur, and spread, with imaging examples of tumor involving the pertinent anatomical areas, with oropharyngeal carcinomas exhibiting more aggressive growth patterns. The focus is on the anatomical regions the radiologists needs to be aware of and assess, for both the primary tumor and its routes of spread. 4- Getting accurate TNM staging, and the utilization of imaging for that role, Specifically will discuss the new current AJCC (American Joint Committee on Cancer) 7th Edition. 5- Evaluation for the ENT – most importantly, evaluating the critical areas impacting patient outcomes, the ENT surgeon and radiation oncologist want to know about. Evaluation of critical areas radiographically impacts prognosis and treatment planning. This lecture provides an

Note: Scanned images are included in the proceedings. Some submitted images were reduced during editing thereby decreasing clarity. Also, refer to the Program Planner. Proceedings Content as of 3/28/2014.

approach for assessing the cancers in the oral cavity and oropharynx, to improve patient treatment and prognosis. These five goals spell out IMAGE – the intention of this talk to provide the radiologists with the information needed to allow one to be more effective when analyzing and approaching imaging studies in patients with either oral cavity or oropharyngeal cancer.

0-05 9:30AM - 10:00AM
Imaging Approach to Nasopharyngeal Cancer

Shatzkes, D.
Lenox Hill Hospital
New York, NY

Abstract/Presentation Summary

Nasopharyngeal carcinoma (NPC) differs from other carcinomas of the upper aerodigestive tract (ADT) in a number of important ways. The World Health Organization (WHO) has classified NPC into three types: I. Keratinizing squamous cell carcinoma (SCC) II. Non-keratinizing SCC III. Undifferentiated carcinoma It is only the relative uncommon Type I tumors (20% of cases in the US) that share similar histology and risk factors with others site of upper ADT SCC. In Types II and III, alcohol and tobacco use do not play a substantial etiologic role, and the primary demographic feature is origin from several southern Chinese provinces. These types are also extremely radiation sensitive and are treated primarily by radiation therapy, with surgery reserved for salvage in some recurrent cases. Other distinguishing features are the very early development of nodal metastases and the high incidence of skull base and intracranial extension. The American Joint Committee on Cancer assigns Tumor, Nodal and Metastases staging for NPC as follows: • T1: Tumor confined to nasopharynx, or tumor extends to oropharynx and/or nasal cavity without parapharyngeal extension • T2: Tumor with parapharyngeal extension • T3: Tumor involves bony structures of skull base and/or paranasal sinuses • T4: Tumor with intracranial extension and/or involvement of cranial nerves, hypopharynx, orbit, or with extension to the infratemporal fossa/masticator space • N0: No regional lymph node metastasis • N1: Unilateral cervical met(s), ≤6 cm in greatest dimension, above the supraclavicular fossa, and/or unilateral or bilateral RP met(s), ≤6 cm • N2: Bilateral cervical met(s), ≤6 cm, above the supraclavicular fossa • N3: Met(s) in lymph node(s) >6 cm and/or to supraclavicular fossa • N3a: >6 cm • N3b: Extension to the supraclavicular fossa • M0: No distant metastasis • M1: Distant metastasis Frequency of cervical nodal metastases in NPC is as follows: Nodal group Ipsilateral (%) Contralateral (%) I 7 1 II 82 36 III 31 17 IV 16 6 V 73 41 Supraclavicular 11 7 The frequency of retropharyngeal nodal metastases is approximately equivalent to that of Level II. Intensity modulated radiotherapy (IMRT) is now the modality of choice for primary treatment of NPC. Tightly conformed fields reduce side effects such as mucositis in adjacent tissues, but requires highly accurate tumor mapping. As such, the radiologist plays a crucial role in staging and treatment

planning for NPC. As skull base and intracranial invasion is frequent, particular attention should be directed to both osseous and foraminal components of the skull base, and to the cavernous sinuses.

Monday, May 19
8:30 AM – 10:00 PM
Room 517d

04 - ASFNR Programming: Pre-surgical Mapping (SAM)

0-06 8:30AM - 8:45AM
Pre-Surgical Mapping: Context, Limitations, and Potential

Ulmer, J.
Medical College of Wisconsin
Wauwatosa, WI

Abstract/Presentation Summary

Surgical excision of brain tumors is important to prolong survival, reduce steroid dependence, improve neurological function, and establish histological and genetic features that determine post-operative treatment algorithms (1,2). Presurgical brain mapping techniques, such as fMRI and DTI, can help to establish operative risks and guide operative strategies (3-5). The main goal is to better define spatial relationships between lesion borders and functional brain networks. In addition to localizing functional networks surrounding brain lesions, mapping of the actual lesions may have utility in localizing epileptogenic foci and possibly in guiding tumor biopsy site selection. Thus, presurgical mapping may characterize lesions, determine lesion resectability, influence selection of surgery to be done awake, guide surgical trajectory, and influence intraoperative testing and resection extent. The overriding goal of presurgical mapping is to help establish functional resection boundaries and thereby help to minimize operative neurological complications. Prior to the era of modern presurgical brain mapping, neurological complication rates for brain tumor resections ranged from 8-32% (6-10). BOLD fMRI has been used for presurgical mapping for two decades, but the technique has significant limitations that render it an imperfect indicator of functional risks. The most serious limitation of presurgical fMRI is the lack of functional white matter visualization (11). The addition of presurgical DTI capabilities over the last decade has enhanced the clinical impact of the BOLD technique and vice versa, by providing more complete assessments of functional networks (2). Another major limitation of BOLD fMRI is lesion-induced (or radiation-induced) neurovascular uncoupling (12). BOLD reproducibility is further affected by the indirect nature of the contrast mechanism, such that concurrence ratios of normal reactivated regions range from 55-75%. BOLD fMRI also suffers from constraints in paradigm contrast,

Note: Scanned images are included in the proceedings. Some submitted images were reduced during editing thereby decreasing clarity. Also, refer to the Program Planner. Proceedings Content as of 3/28/2014.

relatively low temporal resolution, and patient-dependent variability in task performance. DTI has limitations of its own (2), including lesion-induced decreased anisotropy and distortion of fiber tract orientation. Anatomic constraints may also limit the distinction of functional pathways coursing in the same direction, crossing with other fiber bundles, or coursing at acute angulations at the cortical interface. Because presurgical mapping data are imperfect, an integrative strategy utilizing all available localization sources is crucial. This includes functional localization based on sulcal and gyral anatomy on standard MRI. Clinical presentations including lesion-induced neurological deficits as well as seizure semiology may also provide important insights of lesion proximity to eloquent networks. This may be especially important when functional systems cannot be mapped, due to paradigm constraints or patient deficits. In such cases, Neuro-psychology testing may be risk-predictive. Presurgical localization does not obviate the need for intra-operative mapping or testing. Presurgical mapping is in fact complimentary to intraoperative mapping strategies, including intraoperative electrical stimulation and functional white matter dissection testing. Presurgical mapping can establish functional border-risk assessments that can be tested intra-operatively to establish functional resection boundaries. Case illustrations shown in this presentation demonstrate how the synergy provided by integrating localization sources, including presurgical mapping, can impact surgical decision making and produce superior postoperative neurological outcomes. A review of post-operative outcomes was recently conducted at the Medical College of Wisconsin in 76 patients with presurgical mapping and surgical navigation for resection of high risk brain tumors. At 1-month follow-up, 4 patients (5%) experienced major morbidities. Two patients experienced persistent post-operative neurologic deficits and 2 experienced regional morbidity (wound infection). Neurologic morbidity included 2 cases (<3%) of perioperative ischemic insult following Anterior Choroidal Artery and Anterior Cerebral Artery distribution strokes. In no case was there direct resection injury to eloquent networks. These outcomes compare favorably to historical controls (6-10). There is growing evidence that presurgical mapping and intraoperative utilization can improve Neurosurgical patient care.

0-07 8:45AM - 9:00AM
Clinical Applications of Resting State

Shimony, J.
Washington University School of Medicine in St. Louis
Saint Louis, MO

Abstract/Presentation Summary

Currently, a challenge in the surgical treatment of brain tumors is to preserve eloquent areas of brain function while maximizing the extent of resection. The current gold standard for localization of eloquent cortex is direct electrocortical stimulation (ECS), during an awake craniotomy where the patient is able to participate in

various cognitive tasks [1]. The requirement for patient cooperation limits its use in a significant number of patients (e.g. children and medically tenuous patients) and thus may prohibit an optimal resection for these individuals. Similarly task fMRI requires patient cooperation. Resting state functional connectivity MRI (rsfMRI) has emerged as an alternative method for localization of brain networks that requires no active patient participation and can be done under sedation [2, 3]. The purpose of this study was to explore the use of rsfMRI for localization of eloquent cortex in patients with epilepsy and brain tumors [4]. We will present results from a study in which we scanned patients with intractable epilepsy and patients with brain tumors. Epilepsy patients had electrocorticographic monitoring using an implanted grid to localize the epileptogenic zone of seizure onset and to perform functional mapping with ECS. Patients with tumors underwent intra-operative ECS mapping prior to resection of the tumor mass. Resting state fMRI data was acquired and pre-processed as per prior protocols [3, 4]. Location of the motor and language system was determined using a multi-layered perceptron (MLP) [5]. A comparison was performed between the localization of the motor and language systems using ECS and RS-fMRI via the MLP algorithm. In the epilepsy patients we were able to perform a quantitative analysis by comparing the localization of the eloquent networks using the MLP with the localization on the different grid electrodes. By adjusting the probability threshold for classifying an electrode as eloquent or not we were able to calculate receiver-operator curves (ROC) with an average area under the curve (AUC) of 0.89 for the motor network and 0.76 for the language network. The results from the tumor patients were more qualitative. Networks were preserved in the presence of a tumor, though they were often shifted with respect to their normal anatomic position. In this study [4] rsfMRI has demonstrated utility as an adjunct tool for eloquent cortex localization. We have also determined that a "no-cut" criterion of 15mm around the contour of the network determined from the MLP will limit the false negative probability to less than 2%. Minimizing the MLP false negative results are critical to reduce surgical morbidity, since resection of a false negative area could lead to a clinical deficit.

0-08 9:00AM - 9:15AM
The Value of Presurgical Functional Mapping in
Neurosurgery

Lim, M.
Johns Hopkins Hospital
Baltimore, MD

Abstract/Presentation Summary

Craniotomies for resection of various pathologies in the brain carry an inherent risk for severe morbidities in patients. The risks of causing neurologic impairment correlate with the proximity of the pathology with eloquent structures of the brain. Pioneers such as Drs. Foerster and Penfield helped define the areas of eloquence

Note: Scanned images are included in the proceedings. Some submitted images were reduced during editing thereby decreasing clarity. Also, refer to the Program Planner. Proceedings Content as of 3/28/2014.

in the 1920's that are described in traditional anatomy books. However years of intraoperative mapping have demonstrated that there areas of eloquence can be variable. The use of intraoperative mapping has decreased the morbidities associated with surgery of tumors/vascular malformations in eloquent areas. Patient's who receive intraoperative mapping do well from surgery. Initially, about 20% of patients have worsened or new speech deficits immediately after surgery but over 90% of those patients recover their function¹. fMRI now allows us to map eloquent areas of the brain before surgery to account for individual differences in anatomy and to plan for surgery. fMRI measures the amount of deoxygenated blood, which correlates to areas of activity. fMRI has been used a complement to and in some cases in lieu of intraoperative mapping. We will discuss the overall approach to fMRI, nuances associated with fMRI, and assess the appropriate situations for fMRI to replace intraoperative mapping. We will also discuss the situations where fMRI could complement intraoperative mapping.

O-09 9:15AM - 9:30AM
DTI and Pre-Surgical Mapping

Wolf, R.
University of Pennsylvania
Philadelphia, PA

Abstract/Presentation Summary

There is enough interindividual anatomic variation such that standard landmarks are not always reliable for motor or language functional cortex (1,2); and thus, there is a need for preoperative and intraoperative mapping strategies. Primary goals are to determine feasibility of resection, plan safest approach, and maximize extent of safe resection. Noninvasive and invasive cortical and subcortical electrophysiologic measurements for clinical mapping of brain function have long been available(3), but noninvasive techniques are increasingly available for routine practical neurosurgical planning. These include cortical mapping using magnetoencephalography (MEG) or functional magnetic resonance imaging (fMRI) and subcortical mapping using diffusion tensor imaging (DTI). Intraoperative electrophysiologic mapping is the reference standard, but this has inherent limitations just as for noninvasive mapping, and so these techniques can provide complementary information (4-7). The purpose of this presentation is to focus on practical aspects of DTI in neurosurgical planning. DTI methods provide microstructural information on local cellular environment and organization and macrostructural information regarding white matter tracts and connections between important cortical and subcortical functional regions in the brain. Microstructural elements including cellularity, intraaxonal organization and fiber density, myelination, and fiber diameter combine with macrostructural organization of fibers to affect diffusion anisotropy, the basis for the color fractional anisotropy (FA) and tractography maps used for planning. The color FA maps provide a 3D image data set showing direction and degree

of anisotropy on a voxel by voxel level, while fiber tractography (FT) depicts likely "connections" from voxel to voxel and thus from one region (or regions) of the brain to another. Strategies for tractography include deterministic and probabilistic approaches, deterministic methods like fiber assignment by continuous tracking (FACT) most widely used(8). These create virtual tracts and do not represent real nerve fibers, but do provide a guide for preoperative planning and intraoperative navigation, especially if updated with intraoperative MRI (8-13). DTI fiber tracking (DTI FT) and tracking with other diffusion techniques using non-tensor approaches (e.g., high-angular resolution diffusion MRI with Q ball reconstruction) are currently the only means to perform noninvasive localization of white matter tracts. There is evidence supporting the role of fMRI and fiber tracking in the presurgical setting not only for planning and navigation but also with regard to safety, postsurgical treatment and outcome.

9:30AM - 10:00AM

Questions and Answers

Monday, May 19
8:30 AM – 10:00 AM
Room 517a

05 - Young Professionals
Programming: Advances in Imaging:
How to Incorporate Them into Your
Practice

O-10 8:30AM - 8:50AM
Vessel Wall Imaging I

Wasserman, B.
Johns Hopkins University
Baltimore, MD

Abstract/Presentation Summary

High-resolution contrast-enhanced MRI has emerged as a powerful tool for characterizing atherosclerotic plaque components, ultimately enabling the identification of anatomic features that are known to predispose to rupture with the consequent clinical event. Recently, much attention has focused on the identification by MRI of the thin fibrous cap, large lipid core, the presence of intraplaque hemorrhage, and the presence of neovascularization, all of which have been shown to be important determinants of stroke risk when identified in carotid plaque. Intraplaque hemorrhage is of particular interest in that it is thought to lead to the development of the thrombogenic lipid core and contributes to plaque progression. More recent advances in high-resolution MRI imaging have enabled the evaluation of intracranial vessels also to assess stroke risk and for diagnosing

Note: Scanned images are included in the proceedings. Some submitted images were reduced during editing thereby decreasing clarity. Also, refer to the Program Planner. Proceedings Content as of 3/28/2014.

vasculopathies. In this session, an approach to evaluating these features by MRI will be presented with a focus on equipment needs, sequence considerations, and image interpretation and pitfalls.

O-11 8:50AM - 9:10AM
Vessel Wall Imaging II

DeMarco, J.
Michigan State University
East Lansing, MI

Abstract/Presentation Summary

Recent advances of carotid plaque MR imaging has made it possible to directly visualize the atherosclerotic disease in its many stages of development. The hardware and software necessary to obtain and interpret carotid plaque MR imaging will be discussed. The studies validating the in vivo MR appearance carotid plaque components utilizing dedicated research carotid coils and MR plaque sequences with histological comparison of endarterectomy specimens will be reviewed. Next, current prospective trials demonstrating the correlation of research carotid plaque MR characterization with future ipsilateral carotid cerebrovascular disease will be summarized. Recent examples to translate these research carotid MR sequences to the clinical environment by using FDA approved MR sequences and standard FDA approved carotid coils or neurovascular coils will be compared with the histologically validated research carotid MR findings. Lastly, the potential to add value to your referring clinicians by including these "clinical" carotid plaque MR sequences to routine carotid MR angiography will be reviewed.

Discussion 9:10AM - 9:15AM

O-12 9:15AM - 9:35AM
Perfusion MRI (Beyond Tumor Imaging - Additional Useful Applications)

Maldjian, J.
Wake Forest University School of Medicine
Winston-Salem, NC

Abstract/Presentation Summary

Arterial spin labeling (ASL) perfusion MRI imaging has been in development for over a decade (1-3). With the recent availability of the technique from a variety of MRI vendors, ASL is now entering more broadly into the clinical realm. Unlike conventional bolus gadolinium techniques, ASL does not require intravenous contrast, is quantitative, and is readily repeatable. There are several frequently encountered artifacts in the clinical population with ASL (4). ASL relies on a subtraction of imaging pairs to obtain the perfusion signal, making it highly susceptible to slight motion artifacts, or transient gradient hardware instability. Post-gadolinium ASL should be avoided. There are a variety of ways of implementing ASL, each of which can be

separated into a preparation phase, and an acquisition phase. Some of the more common ASL methods include pulsed ASL (PASL), continuous ASL (CASL), pseudo-continuous ASL (PCASL), and velocity-selective ASL (VS-ASL). ASL applications are evolving as clinical experience is gained with this technique. Recent studies have revealed many pathologic and physiologic processes readily identified with quantitative perfusion imaging (4-13). Normal Perfusion Patterns. ASL perfusion patterns demonstrate age-related changes in perfusion signal. Pediatric patients in the 5-15 year old range demonstrate high perfusion values (14-17). Adults demonstrate a gradual age-related decline in brain perfusion. Seizure: In the immediate post-ictal state ASL can demonstrate regional hyperperfusion (9). In the inter-ictal state, ASL can demonstrate a regional hypoperfusion pattern. Migraine: Migraine headaches imaged during the acute phase can demonstrate regional cortical hypoperfusion (8). During the headache phase, hyperperfusion can be seen in the cortex corresponding to the prior aura symptoms (8, 18-21). Posterior Reversible Encephalopathy Syndrome: PRES on ASL can have a variety of appearances. We have found that patients who are imaged acutely show hyperperfusion in the affected occipital and frontal hemispheres and patients who are imaged in the subacute phase show hypoperfusion in these regions (22). The variability and apparent discrepancies between studies investigating perfusion changes related to PRES may be secondary to the time-course of the disease. Hypercapnia: Hypercapnia is a potent cerebral vasodilatory stimulus. In the clinical population, common conditions which can result in arterial blood gas disturbances include chronic obstructive pulmonary disease, adult respiratory distress syndrome, and pulmonary edema (10).

O-13 9:35AM - 9:55AM
Perfusion MRI (Latest Update on Tumor Pre and Post Therapy)

Cha, S.
University of California San Francisco
San Francisco, CA

Perfusion MRI Discussion 9:55AM - 10:00AM

Monday, May 19
8:30 AM – 10:00 AM
Room 520

06 – Advanced Imaging Seminar:
Translational Advanced Metabolic
Imaging

Note: Scanned images are included in the proceedings. Some submitted images were reduced during editing thereby decreasing clarity. Also, refer to the Program Planner. Proceedings Content as of 3/28/2014.

O-14 8:30AM - 9:00AM
O MRI of Cerebral Oxygen Metabolism and Potential Clinical Applications

DeLaPaz, R.
Columbia University
Cave Creek, AZ

Abstract/Presentation Summary

Oxygen-17 (^{17}O) is a naturally occurring, chemically stable, non-radioactive isotope of oxygen with low natural abundance (0.037% of atmospheric oxygen). Unlike the bulk of atmospheric oxygen (^{16}O), the ^{17}O nucleus has non-integer spin (5/2), making it detectable using MR spectroscopy or proton MRI methods when metabolized to water (H_2^{17}O). Detection of the low MR sensitivity ^{17}O nucleus (gyromagnetic ratio 1/7 that of ^1H) can be improved at high magnetic fields (e.g. 7T). Proton MRI on 1.5T or 3.0T clinical systems can detect ^{17}O indirectly by utilizing its effect on high sensitivity proton relaxation in metabolized water (H_2^{17}O). Detection can be further improved by isotope enrichment using concentrated $^{17}\text{O}_2$ gas via inhalation, extracorporeal autologous blood enrichment or synthetic oxygen carriers (e.g. perfluorocarbons). In acute and chronic cerebral ischemia, measurements of cerebral blood flow (CBF) are not sensitive or specific predictors of tissue survival. Measurements of oxygen metabolism are better predictors, especially the "oxygen extraction fraction" (OEF). Elevation of OEF in both acute and chronic Stage 2 hemodynamic failure, or "misery" perfusion, indicates impending failure of oxygen metabolism and cellular necrosis, making it a sensitive and specific biomarker for the "ischemic penumbra" and tissue at risk of infarction distal to vascular stenosis. The methods now used to quantitatively image in vivo human cerebral metabolic rate of oxygen (CMRO₂) and OEF include ^{15}O -PET and MRI deoxyhemoglobin sensitive techniques (BOLD methods), which have practical and fundamental limitations for clinical use. ^{15}O -PET is limited by complex infrastructure with an on-site cyclotron for isotope production (^{15}O T_{1/2} = 2 minutes), sparse availability, radiation exposure and high cost. BOLD MRI methods are limited by dependence on complex, indirect effects of oxygen metabolism on intravascular deoxyhemoglobin concentrations which are also dependent on cerebral blood flow (CBF) and blood volume (CBV), intravascular and extravascular T₂ and T₂* relaxation effects, field strength, vessel size, perivascular water diffusion and assumptions about unmeasurable variables within the image voxel, including local hematocrit, relative arterial and venous volumes, vessel geometry, oxygen diffusion rates and oxygen concentration gradients. ^{17}O -MRI performed on conventional, clinical MRI scanners may provide a quantitative, widely available and clinically practical method for assessing CMRO₂ and OEF in human acute and chronic cerebral ischemia. Quantitative ^{17}O -MRI of oxygen metabolism may also have research and clinical utility in neurodegenerative disease, cardiology and oncology.

O-15 9:00AM - 9:30AM
Quantitative PET Biomarkers of Neuroinflammation

Mozley, P.
Nuclear Medicine
New York, NY

O-16 9:30AM - 10:00AM
Advanced Multislice Spectroscopic Imaging in Routine Clinical Practice

Shungu, D.
Weill Cornell Medical College
New York, NY

Abstract/Presentation Summary

Structural MRI with or without contrast-enhancement has developed into the preferred diagnostic imaging modality for noninvasive examinations of intracranial lesions and pathologies, producing exquisitely detailed anatomic images that have dramatically improved clinical decision-making. However, MRI often lacks the specificity to differentiate pathologic lesions from normal post-operative or post-therapy changes, such as edema and radiation-induced necrosis, and it can miss pathologic changes that do not exhibit contrast-enhancement, such as some low-grade brain neoplasms [1]. Consequently, there has been a great deal of interest in evaluating proton magnetic resonance spectroscopy (^1H MRS) – a closely related technique that permits noninvasive assessment of brain chemistry and can be performed in conjunction with MRI on virtually every clinical MR scanner, without the need to change hardware or move the patient – as a complement to MRI in the evaluation of brain lesions and diseases [2]-[5]. The clinical promise and diagnostic power of ^1H MRS is in its ability to enable the noninvasive measurement of the brain concentrations of several potential biomarkers of human disease, either from a single volume element (voxel) [3],[5], or from multiple voxels in a single or multiple brain slices simultaneously [2],[4]. The metabolic information derived by ^1H MRS can establish neuronal viability and integrity, cellular bioenergetics function or dysfunction, or the presence of rapidly proliferating cells indicative of neoplastic transformation. In this presentation, the speaker, who has had nearly two decades of experience implementing ^1H MRS imaging as a diagnostic neuroradiological tool in a clinical setting, will describe and demonstrate the promise and power of the technique as a complement to both structural and function MRI, capable of contributing highly specific information about the metabolic status of normal or diseased brain tissue that can significantly enhance decision-making in routine clinical practice.

Note: Scanned images are included in the proceedings. Some submitted images were reduced during editing thereby decreasing clarity. Also, refer to the Program Planner. Proceedings Content as of 3/28/2014.

Monday, May 19
8:30 AM – 10:00 AM
Room 524

07 – International Session: AOSNHNR
Presents the Best in 2014-Quantitative
Neuroimaging

0-17 8:30AM - 8:48AM
Recent Advances in Diffusion Weighted Imaging

Yamada, K.
Kyoto Prefectural University of Medicine
Kamigyo-ku, Kyoto

Abstract/Presentation Summary
Diffusion weighted imaging (DWI) and diffusion-tensor imaging (DTI) has now become one of the essential research/clinical tools in analyzing the brain in both normal and pathological states. Water molecules will preferentially diffuse in a direction parallel to the axon's longitudinal axis. This phenomenon can be represented mathematically by the diffusion tensor. The tensors of cerebral white matter can be reconstructed to track three-dimensional macroscopic fiber orientation. The tractography technique allows in vivo localization of neuronal fiber tracts, which was not previously possible. As a clinical tool, this technique primarily targets the intracranial space occupying lesions. This has been also utilized for other conditions, such as stroke imaging and degenerative diseases. It is important to notice that DTI is prone to partial volume averaging especially at the areas with crossing fibers. Thus, when comparing results from different institutes, it will be ideal to standardize the voxel size. The most important limitations of tractography will be that it has not yet been fully validated. Attempts to validate this technique have been made in the past, but are somewhat limited, and thus one has to interpret the results with cautions. Q-space imaging and diffusion kurtosis will be other recent advances in this field and this will be briefly touched in this talk. One last topic will be the DWI thermometry.

0-18 8:48AM - 9:06AM
Quantification of Brain Tissue - Relaxometry Studies in CNS Diseases

Lee, S.
Yonsei University College of Medicine
Seoul, CA

Abstract/Presentation Summary
In the recent decade, CNS imaging has focused on functional imaging, perfusion measurements and brain mapping studies while other many neuroscientists have tried to find quantitative brain imaging techniques in vivo.

Characterization of brain tissue by quantitative imaging is a promising field of neuroradiology because the current trends of functional and various anatomical imaging cannot provide absolute data of local tissue in cases of CNS disease. T1, T2 and T2* relaxometry studies have been applied in clinical neurology and their relevance has been proved by many studies. T2 relaxometry has been applied in quantification of signal changes in hippocampal sclerosis. However, the absolute value of T2 relaxation time of brain tissue is quite different from institution by institution. In applying the T2 relaxometry studies in epilepsy, the institute should have their own reference values for exact lateralization in cases of TLE. T2* relaxometry is more sensitive in the areas of high magnetic susceptibilities, angiogenesis and neovascularized areas. It can be applied in the assessment of iron deposition in aging process, neurodegenerative disease and even for the assessment of angiogenesis. Measurement of T1 relaxation time can be achieved by various methods. T1 relaxation time can be varied by aging process, iron deposition, neuromelanin pigmentation in cases of Parkinsonism. T1 mapping is another field of tissue characterization in CNS disease and future clinical application is expected. Although brain tissue characterization is still under progression, it is likely to be the main stream of the future brain imaging because absolute quantification of normal and diseased brain tissue is very important in imaging diagnosis of CNS disease

0-19 9:06AM - 9:24AM
Cerebral Perfusion in Angiogenesis and Stroke

Lim, C.
National Neuroscience Institute
Singapore

Abstract/Presentation Summary
Recent advances in acute stroke therapy and antiangiogenic cancer treatment have renewed interest in cerebral perfusion, and quantitative neuroimaging. For many decades, the classical Kety-Schmidt equation to determine cerebral blood flow (CBF) has been applied to positron emission tomography (PET); now, better mathematical models are being developed to study the distribution of tracer (such as contrast media) concentrations using newer MR and multi-detector CT perfusion techniques. Perfusion MR imaging may be helpful to delineate the brain territory representing the "ischemic penumbra", located downstream from vascular occlusion, and is at risk of further infarction. Combined MR angiography, diffusion-weighted (DW) MRI, and perfusion MRI parameters of mean transit time (MTT), or time to peak, may predict tissue at risk, but quantitative evidence from large scale studies have not yet been collected. Arterial spin labeling (ASL) has also become more feasible with higher field MR scanners, but perfusion CT techniques are hampered by the lack of reliable DW MRI equivalent biomarker. Intracranial neoplasm may also be studied with perfusion CT and MRI, which may be helpful for pre-surgical assessment and surveillance. Neovascularity from

Note: Scanned images are included in the proceedings. Some submitted images were reduced during editing thereby decreasing clarity. Also, refer to the Program Planner. Proceedings Content as of 3/28/2014.

tumor angiogenesis may be studied using dynamic first pass or dynamic contrast-enhanced perfusion methods, with rCBV and quantitative permeability markers being applied to research and clinical diagnostic imaging. This presentation will highlight clinical examples of perfusion CT and MRI in cerebral ischemia and brain tumors

O-20 9:24AM - 9:42AM
Quantitative Neuroimaging of End Stage Liver Disease

Lin, W.
Chang Gung Memorial Hospital - Kaohsiung Medical Center
Kaohsiung

Abstract/Presentation Summary

Although end stage liver disease is the consequence of liver function impairment and liver fibrosis, it can affect multi-systems, including the brain. Liver cirrhosis is frequently associated with a wide range of neuropsychiatric abnormalities. Personality disorders, inappropriate affective, behavioral, and sleep disturbances had been reported. Patients with acute liver failure can succumb to neurological death, with brain edema and intracranial hypertension. However, conventional neuro-images in end stage liver disease are non-specific with less clinical neurological impact. Quantitative investigation of brain in structural and functional aspects by using advanced MRI in liver cirrhosis is limited. There is still a gap between the clinical presentation and neuroanatomy in these particular subjects. Therefore, we focus on cognition function and MRI findings in these projects and try to bridge the causal-relationship between each others. In addition, liver transplantation re-normalizes the impaired liver function with subsequently cognition function improvement. We further clarified the underlining structural and functional evolution before and after transplantation by using diffusion tensor imaging and resting state functional MRI. We bridge the phenotype, neuropathology and neurophysiology in liver cirrhosis which provide a platform for further clinical assessment.

O-21 9:42AM - 10:00AM
From Flat-Detector to Quantitative DSA for Neurovascular Disorders

Guo, W.
Taipei Veterans General Hospital
Taipei, AK

Abstract/Presentation Summary

Quantitative angiography using flat detector DSA (FD-DSA or C-arm CT) is becoming a routine imaging practice in neurovascular disorders. Recently, measurement of cerebral perfusion, namely cerebral blood volume (CBV), cerebral blood flow (CBF) and circulation times, using FD-DSA is becoming feasibly available. Compared with multi-detector CT, FD-DSA provides: wider scanning coverage, better scanning efficacy, one-stop imaging that saving patient transportation, in-room real-time hemodynamics availability, and more importantly, therapeutic guidance

for various neurovascular disorders. The presentation covers the contents of quantification of cerebral hemodynamics ranging from diagnostic to intra-interventional procedures and post-therapeutic evaluation. The diseases categories included in the presentation are carotid arterial occlusive diseases (CAOD), dural arteriovenous fistula, cerebral arteriovenous malformation, post-hemorrhagic arterial spasm and moyamoya disease. The treatments employed for this patient cohort included re-vascularization and de-vascularization procedures, namely, extracranial and intracranial carotid artery stenting (CAS), intra-arterial thrombectomy/thrombolysis, EC-IC bypass, microsurgery, radiosurgery, embolization and/or their combinations. The improvement of imaging technology (high efficacy flat detector with high spatial resolution and improving contrast resolution) allows us to quantitatively study cerebral hemodynamics of patients with neurovascular disorders by using only FD-DSA. It will definitely change the scenario of our future imaging practice in neurovascular disorders.

Monday, May 19
10:30 AM – 12:00 PM
Room 517bc

08 – ASHNR Programming: Practical
Head and Neck Radiology

O-22 10:30AM - 10:55AM
Imaging of Facial Pain

Fischbein, N.
Stanford University
Stanford, CA

Abstract/Presentation Summary

Facial pain is common in the population, but must be distinguished from headache, throat pain, ear pain, and other types of pain in the head and neck region. Facial pain is typically localized to an area limited by the forehead superiorly, the masseter region laterally, and the chin inferiorly. The major mediator of facial pain is cranial nerve 5, the trigeminal nerve. Trigeminal neuralgia is a frequent indication for referral to imaging, though many patients with "classic" trigeminal neuralgia do not undergo imaging. Trigeminal neuralgia is a unilateral disorder characterized by brief electric shock-like pains, abrupt in onset and termination, limited to the distribution of one or more divisions of the trigeminal nerve. Diagnostic criteria for "classic" TN include: A. Paroxysmal attacks of pain lasting from a fraction of a second to 2 minutes, affecting one or more divisions of the trigeminal nerve and fulfilling criteria B and C B. Pain has at least one of the following characteristics: 1. intense, sharp, superficial or stabbing 2. precipitated from trigger areas or by trigger factors C.

Note: Scanned images are included in the proceedings. Some submitted images were reduced during editing thereby decreasing clarity. Also, refer to the Program Planner. Proceedings Content as of 3/28/2014.

Attacks are stereotyped in the individual patient D. There is no clinically evident neurological deficit E. Not attributed to another disorder The pain usually involves V2 or V3, with V1 affected in <5%. Many if not most patients with classic TN have compression of the trigeminal root by tortuous or aberrant vessels in the posterior fossa. In "symptomatic" TN, the pain is indistinguishable from classic TN, but it is due to a demonstrable structural lesion (neoplasm, infection, inflammation, demyelination...) other than vascular compression. In all patients with TN, the course of the trigeminal nerve should be assessed from brainstem through cisternal and foraminal segments to the end-organ points of innervation as, for the radiologist, TN is a diagnosis of exclusion. Additionally, important potential sites of disease that should be assessed in all patients with facial pain are the temporomandibular joint, paranasal sinuses, dentition/maxillary alveolus/mandible, and the salivary glands and ducts.

O-23 10:55AM - 11:20AM
Skull Base Developmental Lesions

Phillips, C.
Weill Med. College of Cornell/NY Presby'n
New York, NY

Abstract/Presentation Summary
Developmental Lesions of the Skull Base represent uncommon lesions encompassing CNS-sinonasal lesions, maldevelopmental lesions of the skull base, and potential normal variations of the skull base. It is important to recognize these lesions to avoid complications that may arise from misdiagnosis and also to properly diagnose them. Developmental lesions of the anterior skull base are largely abnormalities of the CNS that manifest via sinonasal lesions, such as encephaloceles. All nasal pathology discovered on imaging studies should prompt the radiologist to carefully scrutinize the anterior skull base. The interplay of the anterior fossa structures and the developing normal nasoethmoid region leads to a large array of potential pathology, including dermoid lesions, dermal sinuses, glial heterotopia and encephaloceles. Common encephaloceles include the frontonasal and nasoethmoidal encephaloceles. Knowledge of the normal embryology in this region is very helpful in understanding the potential imaging manifestations. In the central skull base, encephaloceles may be seen. Again, these lesions are important to diagnose to properly direct surgical management and avoid potential complications from misdiagnosis. The presence of a skull base defect must again be carefully excluded. Abnormalities of the pituitary and sella may accompany several of these central skull base abnormalities. There are a wide range of potential normal variations of the central skull base which must not be diagnosed as pathology. The posterior skull base is commonly involved in craniocervical maldevelopmental conditions. The posterior fossa structures and upper cervical spine must be carefully reviewed. Several more common variant foramina are also seen in the basiocciput. The association of posterior fossa maldevelopmental

lesions and craniocervical junction abnormalities is an important one.

O-24 11:20AM - 11:45AM
Imaging of Referred Otalgia - What You Should Look For

Gentry, L.
University of Wisconsin Hospital
Madison, WI

Abstract/Presentation Summary
Otalgia (ear pain) is most often attributable to diseases within the middle or external ear. It is not uncommon, however, for ear pain to be seen in patients with a normal ear exam and pathologies remote from the ear (referred otalgia). When patients present for workup of ear pain, it is important for the radiologist to consider the many different types of lesions that can manifest as referred otalgia. Referred ear pain is usually due to temporomandibular joint disease and dental pathology. Any lesion within the head and neck in the distribution of branches of cranial nerves 5, 7, 9, and 10, as well as the 2nd and 3rd cervical nerves can cause referred otalgia. The imaging workup should be tailored to exclude lesions along these nerves. This lecture will look at the varied pathologies that can cause referred otalgia.

11:45AM - 12:00PM

Discussion

Monday, May 19
10:30 AM – 12:00 PM
Room 517d

09 – Parallel Papers: Adult Brain:
Aneurysms

O-25 10:30AM - 10:37AM
Comparison of the Hemodynamics between Growing and Stable Cerebral Aneurysms

J Cebral¹, C Putman², D Sforza¹

¹George Mason University, Fairfax, VA, ²Texas
Neurointerventional Surgery Associates, Dallas, TX

Purpose
Increased detection of incidental cerebral aneurysms requires an objective evaluation of rupture risk for selecting the best possible patient care. However, the detailed mechanisms of cerebral aneurysm evolution are poorly understood but important for better understanding the natural history of aneurysms and improve their evaluation and treatment. Thus, the purpose of this study was to identify hemodynamic conditions that may

Note: Scanned images are included in the proceedings. Some submitted images were reduced during editing thereby decreasing clarity. Also, refer to the Program Planner. Proceedings Content as of 3/28/2014.

predispose aneurysms for growth and rupture in a series of aneurysms conservatively followed without treatment. Materials and Methods

A total of 33 untreated intracranial aneurysms longitudinally followed with 3D imaging were identified in 21 patients (19 females and 2 males) and selected for study from our database. The criteria for inclusion in the study were untreated aneurysms with at least two 3D images spaced over a period of time. Expert neuroradiologists initially identified growing aneurysms by size measurements on the images. After segmentation and geometry reconstruction, vascular models at different times were aligned and geometrical differences were measured. Aneurysms exhibiting an increase in size of more than 0.5 mm in any direction from the initial examination were classified as "growing". Aneurysms that did not enlarge more than 0.5 mm for at least nine months were classified as "stable". Patient-specific computational fluid dynamics (CFD) models were constructed and used to quantitatively characterize the hemodynamics environments of these aneurysms. Hemodynamic characteristics of growing (n=16) and stable (n=17) aneurysms then were statistically compared. Logistic regression models were constructed to test the predictability of aneurysm growth by hemodynamic features.

Results

Growing aneurysms had significantly smaller shear rate ratios ($p=0.01$), higher concentration of wall shear stress ($p=0.03$), smaller vorticity ratios ($p=0.01$), and smaller viscous dissipation ratios ($p=0.01$) than stable aneurysms. These same associations previously were found when comparing ruptured and unruptured aneurysms in cross-sectional series. Growing aneurysms also had larger areas under low wall shear stress ($p=0.06$) and larger aspect ratios ($p=0.09$); however these trends were only marginally significant. Mean wall shear stress was not significantly different between growing and stable aneurysms. Logistic regression models based on hemodynamic variables were able to discriminate between growing and stable aneurysms with a high degree of accuracy (94-100%).

Conclusions

Growing aneurysms had on average more concentrated wall shear stress distributions, more complex flow structures, lower viscous dissipation than their parent artery, and lower local deformation and rotation of fluid elements than their parent artery. The mean wall shear stress was not significantly different between growing and stable aneurysms. Statistical models based on hemodynamic features seem capable of discriminating between growing and stable aneurysms, and could be used to complement current aneurysm evaluation.

KEYWORDS: Aneurysm, Hemodynamics

0-26 10:37AM - 10:44AM

Wall Stress at Known Aneurysm Rupture Sites

J Cebra¹, D Sforza¹, C Putman²

¹George Mason University, Fairfax, VA, ²Texas Neurointerventional Surgery Associates, Dallas, TX

Purpose

The interactions between the hemodynamics, wall biomechanics and biology, and the pathways leading a cerebral aneurysm to progress to rupture are not well understood. It is thought that aneurysm evolution is driven by progressive degradation and weakening of the wall in response to abnormal hemodynamic conditions characterized by either low or high wall shear stress (WSS). Our work seeks to investigate the effects of these two different hemodynamic pathways in a series of cerebral aneurysms in which the site of rupture is known.

Materials and Methods

Nine ruptured aneurysms with associated focal intraparenchymal hemorrhages in which the rupture site could be identified in 3D images were analyzed. The wall shear stress distribution was obtained from image-based computational fluid dynamics (CFD) simulations. Wall stresses then were computed using 3D structural wall models under hemodynamic loads determined by the CFD models. Wall properties (thickness and stiffness) were modulated with the wall shear stress distribution, i.e., increased or decreased in regions of high or low WSS, in order to test possible wall degradation pathways. Regional rupture probability indices (RPI) were calculated to compare the different wall models.

Results

All possible combinations of wall thinning/thickening or stiffening/softening were compared both qualitatively and quantitatively. Qualitatively, wall models were ranked by looking at: a) the RPI within the known rupture regions, and b) the location of the maximum RPI. Quantitatively, models were compared by computing the relative rupture probability indices at the known sites of rupture. It was found that the model that best explained the rupture site (produced higher RPI) in eight of the nine aneurysms (89%) had thinner and stiffer walls in regions of abnormally high WSS. The remaining case (11%) was best explained by a model with thinner and stiffer walls in regions of abnormally low WSS. Additionally, it was observed that the regions of high RPI were in general displaced downstream towards the dome with respect to the regions of high WSS.

Conclusions

Aneurysm evolution seems to be driven by localized degradation and weakening of the wall in response to abnormal hemodynamics. Image-based computational models assuming wall thinning and stiffening in regions of abnormally high WSS were able to explain most of the observed rupture sites.

KEYWORDS: Aneurysm Rupture, Biomechanical, Hemodynamics

0-27 10:44AM - 10:51AM

Novel Applications and Quantitative Analysis of Dynamic Contrast Enhanced MRI in Neurovascular Diseases For Stroke Prediction

Note: Scanned images are included in the proceedings. Some submitted images were reduced during editing thereby decreasing clarity. Also, refer to the Program Planner. Proceedings Content as of 3/28/2014.

P Vakili¹, M Hurley¹, S Prabhakaran¹, T Carroll¹, S Ansari²

¹Northwestern University, Chicago, IL, ²Northwestern University Feinberg School, Chicago, IL

Purpose

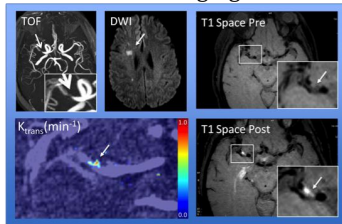
Dynamic contrast-enhanced (DCE) MR imaging (MRI) is an established method for quantifying blood-brain barrier permeability, commonly used for assessing contrast agent leakage in brain tumors (1), multiple sclerosis (2), and infectious diseases (3). However its application to neurovascular pathologies are not as thoroughly explored. In this study we demonstrate for the first time, the utility of DCE MRI in assessing the permeability of the vessel wall in patients with intracranial atherosclerotic disease (ICAD), intracranial aneurysms (IAs), Marfan's syndrome, and vasculitis.

Materials and Methods

We imaged the lumen and the vessel walls in the intracranial circulation of N=34 patients using a standard dynamic contrast-enhanced protocol based on a multiphase spoiled gradient echo pulse sequence. The imaged vessels had the following pathologies: (n=6) atherosclerotic plaques, (n=23) saccular aneurysms, (n=3) fusiform aneurysms, (n=1) Marfan's syndrome, (n=1) vasculitis. Dynamic contrast-enhanced MRI parameters kTrans, vL, and area under the curve (AUC) were derived in each case and compared against other imaging modalities (diffusion-weighted imaging, T1-SPACE dark blood imaging) and clinical findings (symptomology). Optimal imaging parameters such as slice thickness and imaging time were identified for each imaging protocol.

Results

Higher KTrans was observed in symptomatic versus asymptomatic atherosclerotic plaques versus healthy vessel walls (0.18 min⁻¹ versus 0.02 min⁻¹ versus 0.0083 min⁻¹ respectively, p<0.001). Intracranial aneurysms demonstrated larger arterial wall permeability than healthy vessel walls (IA: 0.1778 ± 0.0230 min⁻¹ versus healthy vessel: 0.0083 ± 0.0012 min⁻¹ respectively, p<0.001) but smaller contrast uptake rates than in the choroid plexus (0.4058 ± 0.0567 min⁻¹, p<0.001). Intracranial atherosclerotic disease plaques associated with acute stroke had much larger plaque KTrans than nonstroke ICAD patients (0.31 min⁻¹ versus 0.105 min⁻¹, p<0.05). Finally all ICAD and vasculitis patients with positive kTrans findings had corroborating postgadolinium enhancement on T1-SPACE Imaging.



Conclusions

Dynamic-contrast-enhanced MRI can be used to quantify the permeability of the vessel wall in a variety of neurovascular pathologies with parameters kTrans and vL. Initial results show these parameters may be used to

striate symptomatic and asymptomatic patients as well as identify those at risk for suffering stroke. Dynamic contrast-enhanced MRI studies on patients with neurovascular disease may provide useful information about disease progression especially in a longitudinal study of patients.

KEYWORDS: Aneurysm, Aneurysmal Subarachnoid Hemorrhage, Intracranial Atherosclerosis

0-28

10:51AM - 10:58AM

Local Hemodynamics at Known Aneurysm Rupture Sites

J Cebra¹, D Sforza¹, C Putman²

¹George Mason University, Fairfax, VA, ²Texas Neurointerventional Surgery Associates, Dallas, TX

Purpose

Understanding the reasons for aneurysm formation and the mechanisms leading an aneurysm to progress and ultimately rupture are important for formulating innovative medical treatments and better select factors used for future risk assessments for the many unruptured aneurysms now more frequently found on noninvasive imaging. Previous studies have identified possible pathways for aneurysm wall weakening due to both high and low wall shear stress. Thus, the purpose of this study was to investigate the local hemodynamic environment in the vicinity of the site of aneurysm rupture.

Materials and Methods

A total of nine ruptured cerebral aneurysms with associated focal intraparenchymal hemorrhages were selected from our databases of aneurysms imaged with 3D rotational angiography (3DRA). The rupture sites were identified by expert neuroradiologists by inspection of extravascular blood in volume rendered 3D angiograms and/or additional computed tomography (CT) images. Computational fluid dynamics (CFD) models were constructed using the patient-specific geometries derived from 3DRA images, and typical physiologic pulsatile flow conditions. Visualizations of the inflow jet, intrasaccular flow structures and distribution of wall shear stress were created and used to analyze the relationship between these flow features and the regions identified as the most likely point of rupture.

Results

Inspection of flow visualizations revealed that the rupture sites tended to be aligned with the inflow stream and typically were located near regions of primary or secondary flow impingement. In most of the cases (eight out of nine) the locations of aneurysm rupture did not seem to coincide with regions of sluggish flow, or with either the regions of the highest or lowest wall shear stress. All cases had at least one region of relatively high wall shear stress, and the rupture sites tended to be found downstream of the high wall shear stress region, towards the dome. In one case, the rupture point was located at the fundus of the aneurysm where the wall shear stress was the lowest.

Note: Scanned images are included in the proceedings. Some submitted images were reduced during editing thereby decreasing clarity. Also, refer to the Program Planner. Proceedings Content as of 3/28/2014.

Conclusions

In general, observed rupture sites did not coincide with regions of either low or high wall shear stress. However, they tended to be aligned with the main intrasaccular flow stream and to be located downstream of regions of high wall shear stress, towards the dome of the aneurysm. These results suggest that both the hemodynamics as well as the status of the wall are important to explain the rupture locations observed in this series.

KEYWORDS: Aneurysm, Aneurysm Rupture, Hemodynamics

0-29 10:58AM - 11:05AM
Comparison of 3D Semi-Automatic with Manual Post-Processing for Quantification of Aneurysm Pulsation

T Illies¹, A Kemmling², J Fiehler³

¹University Hospital Center Hamburg Eppendorf, Hamburg, Germany, ²University Medical Center Hamburg Eppendorf, Hamburg, Germany, ³Department of Diagnostic and Interventional Neuroradiology, Hamburg, Germany

Purpose

Due to the small volume changes encountered in the analysis of four-dimensional computed tomography angiography (4DCTA) data, precise postprocessing is critical in aneurysm pulsation analysis. We hypothesized that semi-automatic 3D segmentation offers advantages to manual 2D postprocessing.

Materials and Methods

Four-dimensional CTAs of 10 patients with a cerebral aneurysm were processed by two readers manually and semi-automatically with an in-house developed software tool. The latter creates a 3D model of the vasculature where the aneurysm/parent vessel border is defined by placing points on its surface. Then the aneurysm is segmented automatically in all time points and volumes are calculated. Absolute volumes, pulsilities (maximum volume/minimum volume) and length of postprocessing were compared between both groups.

Results

Two-dimensional and 3D postprocessing show high correlations regarding aneurysm volumes (0.92, $p=0.01$) and pulsilities (.87, $p=0.02$). Bland-Altman analysis shows similar limits of intra-observer agreement in both 2D (-1+4%) and 3D (1+5%). Total postprocessing time was 5.2+4.1min in 3D versus 12.2+6.1min in 2D.

Conclusions

Semi-automatic segmentation in 3D shows high reliability and reproducibility and considerably reduces the postprocessing time, making it a useful tool in the analysis of aneurysm pulsation.

KEYWORDS: Aneurysm

0-30 11:05AM - 11:12AM
Global Cerebral Edema in Patients with Subarachnoid Hemorrhage: Correlation with Blood Brain Barrier Permeability.

J Ivanidze¹, K Kesavabhotla¹, D Mir², A Schweitzer³, H Baradaran², A Gupta¹, P Sanelli⁴

¹New York Presbyterian Hospital, Weill Cornell Medical College, New York, NY, ²Weill Cornell Medical College, New York, NY, ³New York Presbyterian Hospital, Weill Cornell Medical Center, New York, NY, ⁴New York Presbyterian Hospital, Cornell University, New York, NY

Purpose

Global cerebral edema (GCE) in aneurysmal subarachnoid hemorrhage (SAH) is an important predictor of morbidity and mortality. Early detection of GCE remains challenging. Perfusion deficits in SAH patients who develop GCE are thought to be related to impaired autoregulation and blood-brain barrier permeability (BBBP) dysfunction. Computed tomography perfusion (CTP) with full pass technique allows measurement of BBBP in the clinical setting. We assessed whether alterations in BBBP correlate with GCE by studying PS (permeability surface area product), K-trans (flow rate constant from blood plasma to the extravascular extracellular space (EES)), Kep (flow rate constant from EES to blood plasma), and F (blood flow per unit volume of tissue).

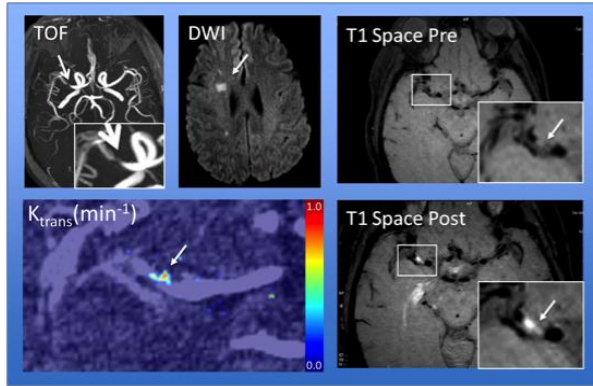
Materials and Methods

IRB approval was obtained. Thirty-three SAH patients underwent CTP on admission and at subsequent time points in the early (days 0-3) and delayed phases (days 4-16). Patients were stratified into three outcome groups as GCE, non-GCE and indeterminate based on their admission noncontrast CT using established criteria via blinded consensus reading from two board-certified neuroradiologists. Computed tomography perfusion data were postprocessed into BBBP quantitative maps of PS, K-trans, Kep and Flow using Olea Sphere software (Olea Medical, LaCiotat, France). A total of 2401 ROIs were obtained from the 31 patients included in the analysis. Unpaired t-Tests were performed. In the primary analysis comparing the GCE and non-GCE groups, the indeterminate patients were excluded. A secondary analysis was performed to include indeterminate patients with the GCE group and then the non-GCE group, separately.

Results

A total of 31 patients were included in the statistical analysis; 48.4% (15/31) were classified as GCE, 31.9% (13/31) as non-GCE and 9.7% (3/31) as indeterminate. The primary analysis revealed that PS, K-trans and F were decreased significantly in GCE compared to non-GCE both in the early and late phases. However, Kep was elevated significantly in GCE compared to non-GCE in both the early and late phases. The secondary analysis demonstrated that the results from the primary analysis are not altered when Indeterminate patients are added to the GCE or non-GCE groups (Figure 1).

Note: Scanned images are included in the proceedings. Some submitted images were reduced during editing thereby decreasing clarity. Also, refer to the Program Planner. Proceedings Content as of 3/28/2014.



Our findings support the hypothesis that altered BBBP function occurs early and remains altered in GCE after SAH. Patients with GCE have significantly decreased PS and Ktrans and significantly elevated KEP, likely due to predominance of flow in the EES to plasma direction given the high volume in the EES. These findings further contribute to our understanding of the pathophysiologic mechanisms underlying GCE.

KEYWORDS: Aneurysmal Subarachnoid Hemorrhage, Cerebral Edema, CT Perfusion

O-31 11:12AM - 11:19AM
Three-dimensional Analysis of Time-dependent Coil Changes after Embolization for Intracranial Aneurysms

D Nakagawa, H Oyama, N Saito, M Shojima, M Yoshino

The University of Tokyo, Bunkyo-ku, Tokyo, Japan

Purpose

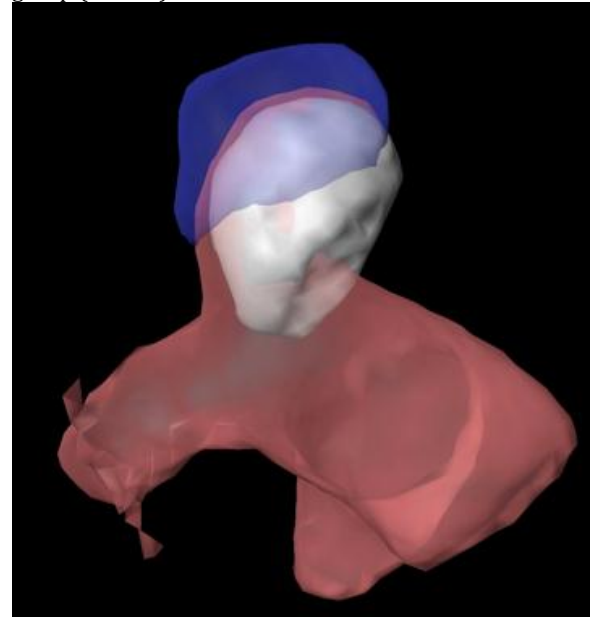
With progress in the modern technology, coil embolization is now comparable to high quality surgical clipping. But, postoperative recurrence and bleeding rates for coil embolization compared to clipping are relatively high. Three-dimensional analysis of time-dependent coil changes after embolization may be effective to predict recurrence.

Materials and Methods

A total of 13 cases of saccular unruptured intracranial aneurysm, treated with coil embolization within the period between January and December at our hospital were studied. Fusiform and dissecting aneurysms were excluded. The DICOM data of coils obtained through cerebral angiography were analyzed using Workstation, adopting the volume rendering method. On volume rendering, the threshold was set after calculating the full width at half maximum of the coil profile curve. The skull bone was regarded as a reference for the calculation of position changes, and volume changes and the lengths of shift in the center of gravity and parallel transition immediately after treatment and on follow up were analyzed and compared between those with and without recurrence. The presence of recurrence was defined as an aggravated condition, based on the classification scale established by Roy.

Results

We found that the epoch-making parameter of the recurrence following endovascular treatment was the coil occupation volume. The coil occupation volume compared to that immediately after treatment significantly increased by 23.9% in the recurrence and 3.3% in the nonrecurrence group ($P=0.05$).



Conclusions

In this study, increase in coil occupation volume, not coil compaction, was the mechanism associated with recurrence after initial coil embolization. The necessary modality is only less invasive mask images in cerebral angiography.

KEYWORDS: Aneurysm Embolization, Angiogram, Computer Modeling

O-32 11:19AM - 11:26AM
Natural history of basilar trunk artery aneurysms

G Saliou¹, R Sacho¹, S Power², A Kostynskyy¹, R Willinsky¹, M Tymianski², K TerBrugge¹, T Krings¹

¹Toronto Western Hospital, Toronto, ON, Canada,
²University Health Network/Toronto Western Hospital, Toronto, ON, Canada

Purpose

Basilar trunk artery aneurysms (BTA) are rare and challenging to manage due to difficult surgical access, frequent occurrence of broad-neck, and the incorporation of the branches of the BA within the aneurysm (1-8). We describe the epidemiology, natural history and management in 52 consecutive basilar trunk aneurysms. Materials and Methods Retrospective review approved by UHN Research Ethics Board performed on all patients with basilar trunk aneurysms followed at our institution from January 2000 to September 2013. We reviewed medical charts and

Note: Scanned images are included in the proceedings. Some submitted images were reduced during editing thereby decreasing clarity. Also, refer to the Program Planner. Proceedings Content as of 3/28/2014.

images (head CTA, MRI and cerebral angiography). Basilar trunk artery aneurysms were classified into five subtypes (9): acute dissecting aneurysms, segmental fusiform ectasia, dolichoectatic chronic dissecting aneurysms, saccular aneurysms and atherosclerotic aneurysms.

Results

From January 2000 to September 2013, 2425 patients who had at least one cerebral aneurysm (58.3% unruptured and 41.7% ruptured) were referred to our institution. Four hundred ninety-one patients had one or more brain aneurysms in the posterior circulation (53.6% unruptured and 47.3% ruptured) and 52 patients had a BTA (Table 1). Among them, 12 (23%) had multiple intracranial aneurysms. Three patients had a second aneurysm located in the basilar tip (n=2) or superior cerebellar artery (n=1) and nine patients had at least one aneurysm located outside of the basilar artery. The mean age was 55 years old (median: 55 years old; SD±19; range: 0.8-6.9). There were 29 (56%) females and 23 (44%) males. All except one of the acute dissecting aneurysms were saccular, with a total of 18 blisters-like aneurysms. All of the chronic dissecting, segmental ectasia and atherosclerotic aneurysms were fusiform, with a total of 34 fusiform aneurysms. During follow-up, nine patients (5 with segmental ectasia and 4 with chronic dissecting aneurysms) presented with an increase in the size of their aneurysm. Two of them had a SAH due to aneurysm rupture and died (1 segmental ectasia and 1 chronic dissecting aneurysm) and one patient (chronic dissecting) died from an ischemic brainstem stroke two days after surgical treatment with a bypass. Two patients had spontaneous ischemic stroke attributed to the aneurysm (2 chronic dissecting aneurysms) without any increase in aneurysm size.

Type of aneurysm	n	mean age y (#SD)	Mean clinical FU m (#SD)	male gender	SAH	TIA/Stroke	incidental aneurysms	multiple aneurysms	? 2 risk factors*	Follow up Increase	rupture	stroke
Acute dissecting	6	44 (#23)	71 (#39)	2 (33%)	5 (83%)	1 (17%)	0	0	1 (17%)	0	0	0
Segmental ectasia	11	56 (#18)	56 (#59)	6 (55%)	0 (36%)	4 (36%)	7 (64%)	2 (18%)	5 (45%)	6 (67%)*	1 (9%)	0
Chronic dissecting	19	59 (#19)	5 (#5)	11 (58%)	0 (32%)	6 (32%)	11 (58%)	3 (16%)	9 (47%)	4 (29%)**	1 (5%)	3 (16%)
Saccular	13	53 (#12)	48 (#42)	2 (15%)	5 (38%)	0	8 (62%)	7 (54%)	5 (38%)	0	0	0
Atherosclerotic	3	71 (#3)	21 (#28)	2 (67%)	0	0	3 (100%)	0	3 (100%)	0	0	0

Conclusions

There appear to be gender differences within the subtypes with saccular and acute dissecting aneurysms having a female preponderance and atherosclerotic/fusiform aneurysms being more common in males. Saccular aneurysms seem stable over time and are likely to represent an underlying predisposition to aneurysm development given that more than half of these cases are associated with multiple intracranial aneurysms. Intervention should be considered in segmental ectasia and chronic dissecting aneurysms which demonstrate an increase in size over time especially in males with significant vascular risk factors because of the increased risk of SAH.

KEYWORDS: Aneurysm Classification, Aneurysm Treatment, Basilar Artery

O-33

11:26AM - 11:33AM

Spontaneous SAH and negative initial vascular imaging-should further investigation depend upon the pattern of haemorrhage on the presenting CT?

L Yap¹, S Coley², R Dyde², T Hodgson², U Patel²

¹Royal Hallamshire Hospital Sheffield, Sheffield, UK, ²Royal Hallamshire Hospital Sheffield, South Yorkshire, UK

Purpose

Multiple repeat investigations usually are performed in patients with computed tomography (CT) or lumbar puncture proven spontaneous subarachnoid hemorrhage (SAH) who have negative initial digital subtraction angiography (DSA) or CT angiograms. Further imaging primarily is, but not exclusively, performed to identify missed intracranial aneurysms (or other significant pathologies) but there is little consensus on the most appropriate use of additional imaging studies and how this may be influenced by the findings of the initial diagnostic CT.

Materials and Methods

A retrospective analysis was performed on a prospectively collected cohort of patients referred to our neuroscience center with spontaneous SAH. Patients were included in the study if there was CT or LP confirmation (xanthochromia) of SAH and initial CTA or DSA was negative. The patients were divided into four categories based upon the distribution of blood on the initial CT (i) perimesencephalic (pSAH), (ii) diffuse (dSAH), (iii) sulcal (sSAH) and (iv) CT negative [cerebrospinal fluid (CSF) positive] (nCT-pLP). The number and the nature of the repeat imaging investigations were reviewed and the results were correlated with the findings of the presenting CT.

Results

Between January 2007 and April 2013, a total of 114 patients presented to our center with confirmed SAH and the first neurovascular investigation was negative. This cohort was classified into 41 cases of pSAH, 50 dSAHs, 6 sSAHs and 17 nCT-pLPs. The diagnostic pathway for these patients is summarized in Table 1. Repeat imaging found a total of five relevant abnormalities (3 cases of vasculitis, 1 ICA dissection and 1 spinal ependymoma). The three cases of vasculitis were diagnosed on first DSA following a negative CTA and presented with either diffuse SAH or with normal CT. The dissecting ICA aneurysm presented with diffuse SAH and only was revealed on the third neurovascular study (after normal CTA and DSA). A hemorrhagic spinal tumor presented with xanthochromia. No subsequent abnormality was found on third DSA or MRI head. No patient presenting with perimesencephalic SAH had a positive finding if the initial CTA was negative.

Note: Scanned images are included in the proceedings. Some submitted images were reduced during editing thereby decreasing clarity. Also, refer to the Program Planner. Proceedings Content as of 3/28/2014.

distribution of SAH	Table 1			
	no. of cases	pSAH	dSAH	sSAH nCT-pLP
	41	50	6	17
CTA (initial angiography)	no. of cases	39	46	5 15
DSA (initial angiography without CTA)	no. of cases	2	4	1 2
DSA following negative CTA	no. of cases	35/39	39/46	5/5 12/15
	cause of SAH identified	0	2 vasculitis (2/39)	0 1 vasculitis (1/12)
2nd DSA	no. of cases	3/37	17/43	0/6 2/14
	cause of SAH identified	0	1 ICA dissection (1/17)	0 0
3rd DSA	no. of cases	0	3	0 0
	cause of SAH identified	0	0	0 0
MRI head	no. of cases	24	27	5 7
	cause of SAH identified	0	0	0 0
MRI spine	no. of cases	6	14	1 5
	cause of SAH identified	0	0	0 1 spinal tumour (1/5)

Conclusions

Certain patterns of SAH, perimesencephalic and sulcal, are associated with a low yield of abnormalities on repeat imaging if the initial vascular study is normal and do not warrant multiple repeat examinations. Patients that present with either diffuse SAH or proven xanthochromia had a higher incidence of abnormalities on repeat imaging and therefore we advocate up to 2 DSAs and MR imaging for these patients.

KEYWORDS: Cerebral Angiography, CT Angiogram, SAH

O-34 11:33AM - 11:40AM
Delayed Angiogram in Angiography-Negative Subarachnoid Hemorrhage: A Systematic Review and Meta-Analysis

S Rawal¹, J Cruz², T Krings³, P Shah¹

¹University of Toronto, Toronto, ON, Canada, ²Hospital Clínico Pontificia Universidad Católica de Chile, Santiago, Chile, ³Toronto Western Hospital, Toronto, ON, Canada

Purpose

To systematically review and meta-analyze the evidence on the yield of performing delayed DSA on initial DSA-negative adult subarachnoid hemorrhage (SAH) patients to: (1) determine an estimate of the overall frequency of detection of occult ruptured aneurysms, and (2) determine whether this differs between perimesencephalic (PM-SAH) and nonperimesencephalic (non-PM-SAH) subgroups.

Materials and Methods

A comprehensive search was performed to detect all relevant literature. Studies had to include adult SAH patients with initial negative digital subtraction

angiography (DSA), who underwent follow-up DSA at any time interval. Outcomes had to be reported as proportion of patients with aneurysm identified on follow-up DSA among those initially DSA-negative. Risk of bias was assessed using a modified version of the Newcastle-Ottawa scale. The results of the included studies were combined using a random effects model; heterogeneity was assessed using the I-squared index. Analyses were performed for both patients with PM-SAH and non-PM-SAH.

Results

Twenty-one studies met the inclusion criteria. Overall, the studies had a low to moderate risk of bias. The overall rate of aneurysm detection on repeat DSA was 9.26% (95% CI = 6.57% to 12.36%; $I^2 = 70\%$). However, the rate in PM-SAH was 1.92% (95% CI = 0.90% to 3.32%; $I^2 = 9.4\%$), whereas that in non-PM-SAH was 14.72% (95% CI = 9.31% to 21.13%; $I^2 = 77\%$).

Conclusions

Despite limitations regarding heterogeneity, one out of seven patients with non-PM-SAH with initial negative DSA was found to have an aneurysm on repeat DSA, while the rate of detection in PM-SAH was very low. These findings have important implications for management in patients with initial DSA-negative SAH.

KEYWORDS: DSA, SAH

O-35 11:40AM - 11:47AM
Cost-effectiveness of Follow-up in Isolated Perimesencephalic Subarachnoid Hemorrhage

V Kalra, B Jeun, D Durand, C Matouk, A Malhotra

Yale University School of Medicine, New Haven, CT

Purpose

To determine the cost-effectiveness of follow-up imaging in isolated perimesencephalic subarachnoid hemorrhage as assessed on computed tomography angiography (CTA).

Materials and Methods

Two hundred thirteen CTAs containing the words "perimesencephalic hemorrhage" based on keyword search performed at a single, large academic institution in the past five years were evaluated retrospectively after obtaining IRB approval. Perimesencephalic subarachnoid hemorrhage was defined as hemorrhage centered in the anterior mesencephalon without greater than trace blood in the interhemispheric and/or proximal Sylvian fissures. Studies were excluded if there was a history of trauma or imaging findings showed extensive/diffuse subarachnoid hemorrhage. Seventeen patients met inclusion criteria. Patients ranged in age from 26 to 75 years (mean 50.4, SD 12.6) with 10 men and seven women. Number of follow-up imaging studies, including CT/CTAs, MRI/MRAs, DSAs, and transcranial dopplers, were tabulated. Literature search was performed to determine incidence of isolated perimesencephalic subarachnoid hemorrhage in the U.S. population. Costs were assessed using 2013 regional Medicare reimbursements.

Note: Scanned images are included in the proceedings. Some submitted images were reduced during editing thereby decreasing clarity. Also, refer to the Program Planner. Proceedings Content as of 3/28/2014.

Results

Of the 17 patients with isolated perimesencephalic subarachnoid hemorrhage, as confirmed with negative CTA, follow-up imaging was obtained in 15 patients. Follow-up studies of CTAs, MRI/MRAs, and DSAs were negative in all patients. There were a total of 41 follow-up CT/CTAs, 40 MRI/MRAs, and 15 DSAs, resulting in an average of 2.41 CT/CTAs, 2.35 MRI/MRAs, and 0.88 DSAs per patient. A total of 15 follow-up transcranial dopplers was performed, which showed unexplained left MCA vasospasm in three patients, with all spontaneously resolving without intervention. Using published incidence of subarachnoid hemorrhage of 8/100,000 person-years and an estimated incidence of 10% of these being isolated perimesencephalic subarachnoid hemorrhage, there are an estimated 2,560 cases per year in the U.S. Extrapolating costs from our dataset, this costs the U.S. population \$27.4 million annually using 2013 regional Medicare reimbursement values.

Conclusions

Imaging follow-up in patients who meet the strict radiographic criteria for isolated perimesencephalic subarachnoid hemorrhage with no source identified on CTA has been described as unnecessary in a previously published study from two large academic centers of 28 patients that showed completely negative DSAs and other follow-up imaging. Our study of 15 patients, all also with negative follow-up imaging, further supports that follow-up imaging is not necessary if the initial CTA is negative when strict radiographic criteria for isolated perimesencephalic subarachnoid hemorrhage are being followed. Extrapolating from our dataset, we estimate that this results in significant direct financial costs in addition to indirect and intangible costs of time lost from work and patient stress/anxiety.

KEYWORDS: Economics, Health Outcomes, Hemorrhage

O-36 11:47AM - 11:54AM

CT perfusion demonstrates changes in blood brain barrier permeability and cerebral blood flow that are associated with delayed cerebral ischemia and outcome after subarachnoid hemorrhage.

A Murphy¹, T Lee², A Manoel³, W Montanera³, R Macdonald³, A Bharatha³

¹University of Toronto, Toronto, ON, Canada, ²Robarts Research Institute, London, ON, Canada, ³St. Michael's Hospital, Toronto, ON, Canada

Purpose

Multiple factors may contribute to poor outcomes after aneurysmal subarachnoid hemorrhage (SAH) (Sanelli et al, 2013; Dankbaar et al., 2010). Computed tomography perfusion (CTP) has been used to quantify perfusion values associated with an increased risk of delayed cerebral ischemia (DCI) and poor outcome although some studies have not shown this (Cremers et al., 2013). We used a standardized management protocol for patients with SAH

that included CTP. We hypothesize that changes in CTP parameters, including decreased blood flow (CBF), increased mean transit time (MTT), and increased blood-brain barrier permeability (PS) in the early stage of SAH would be associated with worse outcomes and a greater need for rescue therapy after SAH.

Materials and Methods

In this single-center prospective investigation, there were 88 subjects with aneurysmal SAH who had CTP performed within 72 hours after admission. Computed tomography perfusion was performed at admission (day 0) and then 3-5 and 7-10 days after SAH. Admission Glasgow coma, World Federation of Neurologic Surgeons and Fisher scores were recorded, as well as systolic blood pressure, glucose and sodium levels and baseline intracranial pressure. Primary outcomes included: (1) mRS at 90 days, where poor outcome was defined as ≤ 2 and (2) infarction, quantified on MRI at discharge. Secondary outcomes were (1) DCI and (2) medical or endovascular rescue therapy. Regions of interest were drawn using standardized vascular territories; a weighted average with respect to ROI area was used to calculate the region with the lowest CBF, highest MTT, and highest PS.

Results

Of 88 patients, 25 patients have been analyzed so far. There was no difference in admission (day 0) or day 3-5 CTP parameters between subjects with and without DCI, with and without a poor outcome, or with and without infarction ($p > 0.05$). However, the percent change in PS between day 0 and day 3-5 was significantly greater in subjects that subsequently developed DCI ($47.2 \pm 13.5\%$) compared to those that did not have DCI ($-0.17 \pm 0.4\%$) ($p = 0.03$). All of the subjects that developed DCI required induced hypertension treatment. The decrease in CBF between day 0 and day 3-5 was significantly greater in subjects with a poor outcome ($p = 0.03$) and in subjects who subsequently received additional treatment with iv milrinone ($p = 0.04$).

Conclusions

The results of our standardized management algorithm in SAH demonstrate that alterations in cerebral perfusion in the early stage of SAH may help identify patients at risk of DCI and poor outcome, with an increased need for aggressive medical or endovascular therapy. Specifically, increasing blood-brain barrier permeability and decreasing CBF may be important imaging parameters to consider in the early (<72 hours) evaluation of SAH patients. We advocate for an imaging protocol that provides CTP measurements both prior to and following aneurysm securement for early identification of patients at risk of poor outcome and potentially in need of more aggressive management.

KEYWORDS: Aneurysmal Subarachnoid Hemorrhage, CT Perfusion

Note: Scanned images are included in the proceedings. Some submitted images were reduced during editing thereby decreasing clarity. Also, refer to the Program Planner. Proceedings Content as of 3/28/2014.

0-37 11:54AM - 12:01PM
CT Angiography versus Transcranial Doppler in the Assessment of Cerebral Vasospasm Following Intracranial Aneurysm Rupture

S Kennedy, A Mensinkai, R Larrazabal, D Sahlas, A Algird
McMaster University, Hamilton, ON, Canada

Purpose

Cerebral vasospasm (CV) is a complication of subarachnoid hemorrhage (SAH) from ruptured intracranial aneurysm, with a peak incidence between four and 10 days. Of those patients who survive a ruptured intracranial aneurysm, 25-30% are at risk of delayed cerebral ischemia DCI (1).

Traditionally, the gold standard for assessment of CV has been digital subtraction angiography (DSA). Both transcranial Doppler (TCD) and computed tomography angiography (CTA) are modalities with less inherent risk than DSA, which even if employed strictly as a diagnostic modality is subject to procedure-related complications.

While CTA does provide other useful nonvascular information, artifact from clips or coils might obscure the vessel, patients are exposed to radiation and require transport from the critical care setting to the diagnostic imaging department. Transcranial Doppler, however, does not utilize ionizing radiation, can evaluate vessels obscured by artifact on CT and is performed at the bedside. The purpose of this study is to evaluate the relationship between TCD and CTA in the assessment of cerebral vasospasm following SAH from ruptured aneurysm.

Materials and Methods

The study population included patients admitted to the Hamilton General Hospital between August 2011 and October 2013 for SAH from cerebral aneurysm rupture. Thirty-six patients were included in our final analysis. To meet the inclusion criteria, patients required (i) a CTA at presentation, (ii) TCD monitoring, and (iii) a subsequent CTA within 24 hours of TCD. Of the 36 patients, 44 such TCD/CTA pairs were identified. Two neuroradiologists retrospectively analyzed the CTAs, measuring the bilateral MCAs, ACAs, PCAs and the basilar artery. The agreement between TCD and CTA then was assessed.

Results

Of the 33 SAH patients, there were 23 female and 10 male. The average age at presentation was 54.8 years. Twenty aneurysms were treated with coiling, 10 were clipped. Metallic artifact from the surgical material and anatomical variants limited CTA measurement of certain vessels. The number of segments for which complete data were available for both modalities was: right MCA (40), right ACA (36), right PCA (35), left MCA (39), left ACA (38), left PCA (38) and basilar (13). Correlation was low but statistically significant for MCA segments (right MCA - 0.533, $p = 0.0004$, left MCA -0.486, $p=0.0017$). The remaining segments, though not statistically significant, had correlations ranging between -0.067 to -0.318.

Conclusions

We found a stronger correlation between CTA and TCD for the MCA measurements, which in combination afforded the best evaluation of CV. This may relate to the larger caliber

of the vessel. The dynamic nature of vasospasm could in part contribute to the variability of our findings in the other vessels, with improved correlation expected between cases conducted in shorter time intervals. The MCA will be our target for further investigation, particularly for assessment of TCD velocity and CTA percent stenosis and for stratification of vasospasm based on severity.

KEYWORDS: Aneurysm Rupture, CT Angiogram, Vasospasm

0-38 12:01PM - 12:08PM
Hippocampal damage and affective disorders after treatment of cerebral aneurysms

B Friedrich¹, M Wostrack², C Zimmer², Y Ryang²
¹University Hospital Leipzig, Leipzig, Germany, ²Klinikum rechts der Isar, München, Germany

Purpose

Despite good neurological outcome after the treatment of ruptured or incidental cerebral aneurysms, many patients complain about mood disturbances such as anxiety and depression. The present study investigated the nature of these affective disorders, their trigger factors, and corresponding structural brain changes.

Materials and Methods

We assessed 64 patients matched by history of previous subarachnoid hemorrhage (SAH) and treatment modality (clipping versus coiling) by a test battery including the Hospital Anxiety and Depression Scale (HADS) and Beck Depression Inventory-II (BDI-II). MR imaging for the evaluation of structural changes included H1-MR spectroscopy, hippocampal volumetry, and diffusion tensor imaging (DTI).

Results

The applied multimodal imaging revealed no significant differences between patients with previous SAH and patients with incidental aneurysms; there also were no substantial differences between patients with and without previous SAH with respect to depression and anxiety. However, we observed significantly higher mean HADS scores in patients treated surgically versus patients treated by coiling ($p<0.01$). BDI-II tended to be higher in surgically treated patients, but this difference appeared statistically insignificant. Surgically treated patients displayed substantial hippocampal damage in all imaging techniques: reduction in mean concentrations of N-acetylaspartate ($p = 0.04$), hippocampal volume reduction ($p = 0.012$), and diffusion disorder ($p = 0.02$). The structural alterations correlated significantly with the increased HADS scores.

Conclusions

In contrast to the endovascular treatment, aneurysm surgery seems to be associated with an increased incidence of mood disorders corresponding to the hippocampal neuronal loss, independent of the preceding SAH.

KEYWORDS: Aneurysm, MR Imaging, Stroke

Note: Scanned images are included in the proceedings. Some submitted images were reduced during editing thereby decreasing clarity. Also, refer to the Program Planner. Proceedings Content as of 3/28/2014.

Monday, May 19
10:30 AM – 12:00 PM
Room 517a

10 - Parallel Papers: Adult Brain:
Degenerative/Inflammatory/
Infectious

O-39 10:30AM - 10:37AM
MR Imaging in Clinically Isolated Syndromes and Relapsing Multiple Sclerosis after Single-Dose and Cumulative Double-Dose of Gadobutrol at 3.0T: the CUDOMS Study

A Rovira, J Corra, E Huerga, C Auger, J Sastre-Garriga, R Mitjana, X Montalban
Hospital Vall d'Hebron, Barcelona, Spain

Purpose

Several strategies have been proposed to increase the sensitivity of contrast-enhanced MR imaging (MRI) for assessing disease activity in multiple sclerosis, such as use of contrast agents achieving high T1 shortening and/or delaying scanning at least 10 minutes after gadolinium injection. The aim of this study was to prospectively compare the gadolinium-enhancing lesion detection rate with a single and a cumulative dose of one-molar gadobutrol at 3.0 T with different time intervals after contrast injection in patients with clinically isolated syndrome (CIS) and relapsing MS. The hypothesis was that the combined advantages of increasing delay and cumulative contrast dose will significantly increase the detection rate of active lesions. This would be important in terms of patient care: in CIS patients, the diagnosis of MS could be established and treatment initiated earlier, and in relapsing MS patients, MRI confirmed active disease might influence therapeutic decisions, such as initiating or changing a disease-modifying treatment.

Materials and Methods

The present study was a single site open-label Phase IV study, which was conducted according to GCP. Institutional review board and regulatory approval were granted, and written informed consent was obtained from all participating patients. A total of 115 valid patients finally were included in the study. Twenty-six (22.6%) and 89 (77.4%) were CIS and MS patients, respectively [(83 female (72%)), mean age 35 years; range 23-50 years. Forty-one patients were under treatment with immunomodulatory drugs (all but 2 with relapsing MS) at the time of the MRI examination. Patients underwent 3.0 T brain MRI consisting of transverse proton-density, T2-weighted and unenhanced T1-weighted sequences, and four sets of contrast-enhanced T1-weighted sequences performed five and 15 minutes after a single (0.1 mmol/kg) and a cumulative (0.1 + 0.1 mmol/kg) dose of gadobutrol. Each of the four sets of contrast-enhanced T1-weighted scans was evaluated for the number of gadolinium-enhancing lesions in a random fashion and using objective image interpretation criteria by three experienced neuroradiologists. They were blinded to the time point at which the enhanced sequences were obtained and used the unenhanced

sequences as references. The primary efficacy analysis was based on the number of patients presenting at least one gadolinium-enhancing lesion in the four MRI scans provided by the independent and blinded readers. Poisson regression based on generalized estimation equations were used to compare the four scans.

Results

Average number of patients showing at least one gadolinium-enhancing lesions among the three observers was 56, 54, 61 and 68 for the four scans (early and delayed single dose; and early and delayed cumulative dose), indicating that the proportion of active patients increase from 46.9- 48.7% in the single dose scans to 53.0-59.1% in the cumulative dose scans (maximum increase of 12.2%). These numbers differed significantly between the image sets with highest values for the early and delayed cumulative dose ($p=0.0008$) (Figure 1). Confidence in the diagnosis of an enhancing lesion was significantly different between the four sets, with higher values obtained with increasing delay time and dose for all readers: average proportion (%) of lesions in which the diagnosis was very confident was 15.2, 18.7, 31.7 and 34.4 for the four sets of images among the three observers ($p<0.001$).

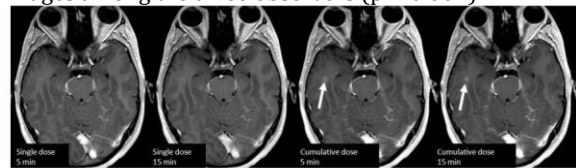


Figure: A small enhancing lesion located in the right temporal subcortical white matter seen at the 2 cumulative-dose time points (arrows), which was not identified at the two single-dose time points. Only in retrospect mild enhancement can be seen in the single-dose delay scans.

Conclusions

A cumulative gadobutrol dose associated with a longer delay time after contrast injection significantly increases the detection of gadolinium-enhancing lesions in patients with clinically isolated syndromes or relapsing multiple sclerosis, and provides higher confidence in the diagnosis of enhancing lesions. This data should be considered in clinical studies in which detection of active lesions on MRI is considered clinically relevant, as happens for the initial diagnosis of the disease, and for monitoring and predicting response to immunomodulatory treatments.

KEYWORDS: Contrast-Enhanced MR Imaging, Multiple Sclerosis

O-40 10:37AM - 10:44AM
DKI-based White Matter Modeling Identifies Decreased Myelin Integrity in Normal Controls with Hippocampal Atrophy

J Helpert¹, A Benitez¹, H Collins¹, E Fieremans², A Tabesh¹, C Chan¹, J Jensen¹

¹Medical University of South Carolina, Charleston, SC, ²New York University School of Medicine, New York, NY

Purpose

There is a critical need to develop noninvasive imaging biomarkers capable of identifying the earliest stages of Alzheimer disease (AD). While hippocampal atrophy has

Note: Scanned images are included in the proceedings. Some submitted images were reduced during editing thereby decreasing clarity. Also, refer to the Program Planner. Proceedings Content as of 3/28/2014.

been identified as one such possible biomarker, other techniques may identify concomitant changes in other regions and tissue. Thus, the purpose of this work was to investigate if diffusional kurtosis imaging (DKI)-based white matter tract integrity (WMTI) metrics could reveal alterations in white matter of normal control (NC) older adults with hippocampal atrophy.

Materials and Methods

Twenty-seven (19 female) cognitively healthy NC (age = 70.59 ± 8.26 years; range = 55-82 years) were studied, of whom 12 had hippocampal atrophy. MR imaging (MRI) experiments were conducted on a 3 T Tim Trio Siemens MR system as described previously (1) and included MPRAGE and DKI with 3 b-values (0, 1000, 2000 s/mm²) along 30 diffusion encoding directions. White matter tract integrity metrics also were estimated as previously described (1). For this analysis, we concentrated on the two WMTI metrics of axonal water fraction (AWF) and the extra-axonal radial water diffusivity (De,rad). Hippocampal atrophy was measured using NeuroQuant (i.e., hippocampal volume z-score ≤ -1.5). All parametric maps were normalized to the 1mm (isotropic) MNI-152 standard space. Voxelwise analyses were performed with Track Based Spatial Statistics (TBSS) (2) running in FSL, with analyses of covariance (controlling for age and sex) performed only in the voxels of the white matter skeleton (FA threshold = 0.4). Permutation-based statistics were computed using randomized (10,000 permutations), applying threshold-free cluster enhancement to correct for familywise error from multiple comparisons (p<0.05).

Results

Normal control subjects with (n=12) and without (n=15) hippocampal atrophy did not differ in demographic characteristics or on neuropsychological testing. However, covarying for age and sex, NC with hippocampal atrophy had increased De,rad (p=0.05) in several white matter tracts that have been implicated previously in AD (3), primarily in the left hemisphere. Axonal water fraction showed no differences between NCs with and without hippocampal atrophy when covarying for age and sex. Both (increased) De,rad and (decreased) AWF were associated with age and female gender. Conclusions

Previously, we reported that De,rad discriminated NC from amnesic mild cognitive impairment (aMCI), while AWF discriminated aMCI from AD, with high classification accuracy (1) and that WMTI metrics reflect the vulnerability of late-myelinating tracts in AD (4). We have provisionally proposed that De,rad may be a marker of myelin integrity, whereas AWF may reflect axonal density, albeit these interpretations require further validation. In extension of our prior work, in the preliminary analysis presented here we demonstrate that De,rad potentially identifies changes in the "preclinical AD" phase (5), suggesting that decreased myelin integrity may be observed very early in the AD process.

KEYWORDS: Aging, Alzheimer Disease, Diffusional Kurtosis Imaging,

O-41

10:44AM - 10:51AM

Periatrial White Matter Lesions: Potential Marker for Diagnosis of Multiple Sclerosis on MR Imaging

S Ezhapilli, S Destian, R Mehta, S Hemingway, K Craig1, A Swarnkar
SUNY Upstate Medical University, Syracuse, NY

Purpose

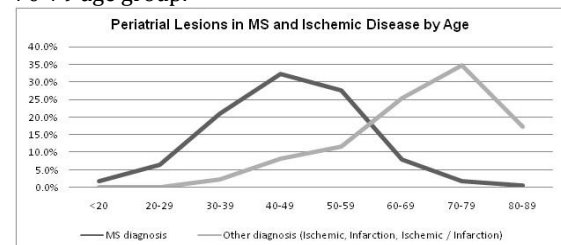
The classic multiple sclerosis (MS) plaque is an ovoid lesion within the periventricular white matter, perpendicular to the long axis of the corpus callosum. Other typical intracranial locations include the juxtacortical white matter, brainstem, brachium pontis, and cerebellum. Many MS patients present with visual findings, unaccounted for by optic neuritis. The purpose of this study was to determine whether there is a correlation between the presence of periatrial lesions, along the optic radiation, and the diagnosis of MS, and whether periatrial lesions can be used to distinguish MS from ischemic diseases.

Materials and Methods

Five hundred fifty patients with MS, ischemic disease, infarction, and combined Ischemic disease and infarction, who had an MR examination of the brain between July 1, 2010 and August 1 2011, were included initially in the study. Seventy-one examinations were excluded due to insufficient numbers in patients < 20 and > 89 years, follow-up studies of the same patient, and studies without axial T2 FLAIR images. MR examinations of patients with ischemic disease, infarction, combined ischemic disease and infarction were grouped together as "ischemic diseases". Three contiguous axial T2 FLAIR images from each examination at the level of the atrium of the lateral ventricles were evaluated by four reviewers (R1-R4), blinded to patient demographics and history. Each reviewer was asked to determine whether a lesion was present or absent in the periatrial region on any one of the images. The data were analyzed by a statistician.

Results

Of the final 479 examinations included in the study, 52.3% had a clinical diagnosis of MS while ischemic diseases accounted for the remaining 47.7%. Periatrial white matter lesions were more likely to be present in MS patients younger than 60 years than in the "ischemic diseases" group (p<.001) and as expected, MS patients tended to be younger (p < .001) than patients with ischemic diseases. Patients with "ischemic diseases" were less likely to have a periatrial lesion, compared to the MS group, except in the 70-79 age group.



Note: Scanned images are included in the proceedings. Some submitted images were reduced during editing thereby decreasing clarity. Also, refer to the Program Planner. Proceedings Content as of 3/28/2014.

Conclusions

The presence of lesions within the periaxial white matter favors a diagnosis of MS, compared to ischemic diseases, in patients younger than 60 years. Therefore, white matter lesions in the periaxial region should be considered as one of the criteria for MS, and may facilitate earlier diagnosis in patients who do not have lesions in traditionally typical locations.

KEYWORDS: MR Imaging Brain, Multiple Sclerosis

O-42 10:51AM - 10:58AM
Diffusion Tensor Tractography of the Nigropallidal-Nigrostriatal Tract Complex in Parkinson's Disease

W Tan¹, C Yeoh², N Nadkarni¹, H Rumpel², E Tan³, L Chan²

¹Duke-NUS Graduate Medical School Singapore, Singapore,

²Singapore General Hospital Singapore, Singapore,

³National Neuroscience Institute Singapore, Singapore

Purpose

Degeneration of dopaminergic nigrostriatal and nigropallidal tracts arising from the substantia nigra is a pathologic feature of Parkinson's disease (PD). Diffusion tensor imaging (DTI) is a magnetic resonance imaging (MRI) tool that can indirectly evaluate the integrity of white matter tracts by measuring the anisotropic diffusion of water. We hypothesize that DTI parameters of the nigropallidal and nigrostriatal fiber tracts, as opposed to regional parameters of the substantia nigra (SN) alone may be a more sensitive biomarker for the diagnosis and prognostication of PD. Utilizing a case control methodology, we examined DTI parameters along the striatal tracts in PD and healthy controls.

Materials and Methods

MR imaging scans were carried out in 39 subjects (21 PD patients and 18 age- and gender-matched healthy controls). Diffusion tensor imaging data were acquired using a 3 T Siemens Trio scanner (1.875x1.875x2mm resolution, b-value 800 s/mm², 30 noncollinear directions). Deterministic whole-brain tractography was performed using Diffusion Toolkit (trackvis.org, Version 0.6.2.2), and manual tract dissection and tract data analysis were performed with TrackVis (trackvis.org, Version 0.5.2). Regions of interest (ROIs) were placed in the ventral SN and ipsilateral globus pallidus (GP) to isolate the nigropallidal-nigrostriatal tract complex. Fiber count and average DTI parameters - fractional anisotropy (FA), mean diffusivity (MD), axial diffusivity (AD), radial diffusivity (RD) - along the tract were computed. Point-to-point profiles of the DTI metrics along the tract also were extracted. Results were analyzed using the average of the left and right tracts. The average fiber count and DTI metrics were compared statistically using Student's T-test, and the DTI tract profiles were compared with linear mixed effects models. The average DTI metrics also were correlated with clinical data (disease duration and Tinetti score, a validated scale for postural instability) using Pearson's correlation.

Results

Tractography was successful in 18 PD patients (age 72.2 ± 4.5, 14M:4F, Hoehn & Yahr score 2-4, disease duration 5.1 ± 2.9 years) and 17 controls (age 71.2 ± 5.2, 14M:3F). Average FA (p<0.05) and fiber count (p<0.0001) were significantly lower in the PD group compared to the control group. Radial diffusivity was significantly higher in the PD group (p<0.05), whereas MD and AD were higher in the PD group without achieving significance. Average fiber count of the right tract correlated significantly with Tinetti score (p<0.05). Average AD of both tracts, FA of the left tract, and the MD, AD, RD of the right tract correlated significantly with disease duration (p≤0.05). For the DTI profiles, preliminary modeling using DTI values at the tract midpoint suggests that AD and FA (more significantly) may be useful in predicting the odds of having PD compared to controls.

Conclusions

By isolating and quantifying the nigropallidal-nigrostriatal tract complex, we demonstrated abnormal DTI parameters of this fiber tract complex in PD patients compared to controls. Tractography of the nigropallidal-nigrostriatal tracts may be useful in the longitudinal evaluation of clinical progression in PD.

KEYWORDS: DTI Tractography, Parkinson Disease, Substantia Nigra

O-43 10:58AM - 11:05AM
Diffusion Tensor Imaging in SPG4-Related Hereditary Spastic Paraplegia

J Guzman-De-Villoria¹, F Sánchez-Navas², Y Aleman-Gomez², I Balsa², P Fernández-García¹, F Grandas¹, M Desco³

¹Hospital General Universitario Gregorio Marañón, Madrid, Spain, ²Centro de Investigación Biomédica en Red de Salud Mental, Madrid, Spain, ³University Carlos III, Madrid, Spain

Purpose

Hereditary spastic paraparesis is a clinically and genetically heterogeneous neurodegenerative disorder characterized by a progressive spasticity of lower limbs. Our aim was to identify microstructural changes in corticospinal tracts (CSTs) by diffusion tensor imaging (DTI) and their relationship to clinical impairment in a group of patients diagnosed with SPG4-related HSP.

Materials and Methods

Twenty-one patients with pure SPG4 mutation and 18 age-matched healthy controls were recruited. The patients performed the Spastic Paraparesis Rating Scale (SPRS) and Mini Mental State Examination MMSE. The evolution time of the disease is not correlative with the age of the subjects and presented from 0 to 54 years. Data were acquired with a 1.5 T MRI including a T1-weighted high-resolution image and a DTI study using a single-shot spin echo-planar imaging sequence for a b-value 50 and 800 s/mm² over 32 noncollinear directions. Diffusion-weighted studies were processed using the software package FSL 4.1. To parcel the individual FA maps into

Note: Scanned images are included in the proceedings. Some submitted images were reduced during editing thereby decreasing clarity. Also, refer to the Program Planner. Proceedings Content as of 3/28/2014.

different tracts, we used the ICBM-DTI-81 white matter atlas. We extracted the mean FA values of CSTs using a region of interest (ROI) analysis in order to generate an individualized atlas for each subject in native space. Mean FA measurements obtained were analyzed using the Univariate General Linear Model with "Group" as a fixed factor. We also explored the correlation between the FA values and SPRS in the group of the patients.

Results

Compared with healthy controls, SPG4 patients presented decreased FA in CST ($p = .015$ for the right CST, $p = .009$ for the left CST) Figure 1. Significant correlations were found between CST and SPRS (Pearson $r = -.50$ $p = .024$ for left side; $r = .58$ $p = .005$ for right side) Figure 2.

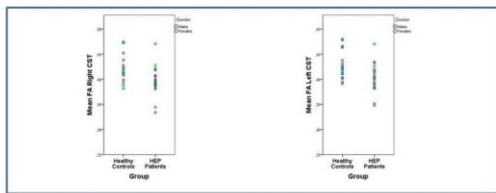


Fig. 1. Group differences in FA on the skeleton of Corticospinal Tracts.

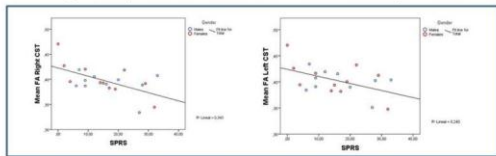


Fig. 2. Significant correlation between FA values and SPRS in patients.

Conclusions

Diffusion tensor imaging could be a sensitive technique to detect microstructural changes in SPG4 patients. The FA values in CSTs are related to disease severity.

KEYWORDS: Brain White Matter, Degenerative, DTI Tractography

0-44 11:05AM - 11:12AM
Meta-analysis of Grey Matter Atrophy and Connectivity in Progressive Supranuclear Palsy

F Yu, B Tantiwongkosi, D Barron, P Fox
University of Texas Health Science Center at San Antonio,
San Antonio, TX

Purpose

Progressive supranuclear palsy (PSP) is a neurodegenerative tauopathy which presents with gaze palsies, postural instability, bradykinesia, and dementia (1). Structural MRI (VBM) studies utilizing either voxel-based morphometry (VBM) or visual inspection have demonstrated patterns of gray matter atrophy affecting the basal ganglia and brainstem (2). However, it is unclear if these are the result of underlying anatomical pathways between affected regions, or concomitant areas of primary disease. The purpose of our study was to identify functional connectivity between areas of gray matter atrophy in PSP through the use of meta-analytic techniques.

Materials and Methods

Whole brain meta-analysis was performed, using the revised anatomical likelihood estimation method (3), on a set of 10 published voxel-based morphometry studies that met inclusion criteria (consisting of 156 PSP patients). Meta-analytic connectivity models (MACM), which have been shown to correlate with diffusion tensor imaging (DTI) and resting-state functional connectivity maps, then were generated based on the most consistent areas of gray matter structural change (4, 5).

Results

The medial dorsal nucleus of the thalamus was found to be the most significant region of gray matter atrophy in PSP based on the ALE meta-analysis. Meta-analytic connectivity models demonstrated functional co-activation of this region of interest with the bilateral insular cortices and midbrain, which also demonstrated significant convergence for gray matter atrophy in PSP (Figure 1).

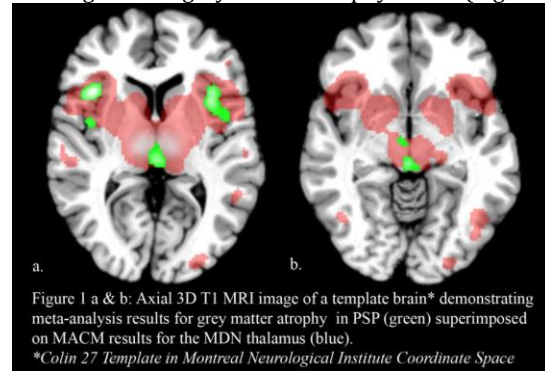


Figure 1 a & b: Axial 3D T1 MRI image of a template brain* demonstrating meta-analysis results for grey matter atrophy in PSP (green) superimposed on MACM results for the MDN thalamus (blue).

*Colin 27 Template in Montreal Neurological Institute Coordinate Space

Conclusions

Our results suggest that there are anatomical pathways between regions of gray matter atrophy in PSP, which may lead to transynaptic spread of disease. A similar process has been proposed for other neurodegenerative disorders such as human spongiform encephalopathy (6). This hypothesis will be further validated with DTI, including probabilistic tractography.

KEYWORDS: Meta Analysis, Neurodegenerative, Voxel-Based Morphometry

0-45 11:12AM - 11:19AM
MRS In The Retrosplenial Cortex May Differentiate Between aMCI, AD and Controls

D Goldsher
Isreal Institute of Technology, Haifa, Israel

Purpose

To investigate whether the spectroscopic profile of metabolites in the retrosplenial cortex (RSC) could differentiate between amnesic mild cognitive impairment (aMCI), Alzheimer disease (AD), and cognitively healthy individual.

Materials and Methods

Single voxel proton MRS in the RSC was performed for 32 individuals aged 55-80 years: 10 patients with aMCI, 12 with mild to moderate AD, and 10 cognitively healthy

Note: Scanned images are included in the proceedings. Some submitted images were reduced during editing thereby decreasing clarity. Also, refer to the Program Planner. Proceedings Content as of 3/28/2014.

individuals. Only individuals with no history of active neurological or psychiatric disorders and/or therapy that could potentially interfere with cognitive functions were included. Studies were performed with a 1.5 T system. Spectroscopy (1H MRS) was performed using the point resolved spectroscopy (PRESS) technique (TR=1500ms, TE=35ms). Spectral analysis was performed using standard software provided by the manufacturer. One voxel was located in the RSC and the second in the anterior cingulate gyrus (ACG). Nonparametric Mann-Whitney-U tests and Kruskal Wallis tests were used for statistical comparisons.

Results

A statistically significant decrease in the N-acetyl-aspartate to creatine ratio (NAA/Cr) in the RSC was found in AD patients as compared to aMCI patients and healthy individuals. The NAA to myo-Inositol (ml) ratio was found to be significantly lower in the RSC of aMCI patients than in healthy individuals.

Conclusions

N-acetyl-aspartate to creatine ratio and NAA/ml ratios in the RSC, measured by MRS, may be regarded as possible biological markers for differentiation between aMCI, AD, and cognitively HI. These markers may play an important role for clinical purposes and in clinical trial settings with potential disease-modifying drugs. Further investigation is needed to strengthen our results.

KEYWORDS: MR Imaging/Diffusion

0-46 11:19AM - 11:26AM
Neuroimaging of Pathologically Proven Cerebrovascular A-Beta Amyloid Compared to Cerebral Amyloid Angiopathy and Cerebral Amyloid Angiopathy – Related Inflammation: A Single Institution's 25 Year Experience

N Danielson¹, J Morris², C Wood², A Kotsenas²

¹Mayo School of Graduate Medical Education, Rochester, MN, ²Mayo Clinic, Rochester, MN

Purpose

Describe our institution's 25-year neuroimaging experience with pathology proven cerebrovascular amyloid, a heterogeneous group of hereditary and sporadic diseases that include cerebral amyloid angiopathy (CAA), A-beta-related angiitis (ABRA), and CAA-related inflammation (CAA-RI). Discuss the integral role of SWI and GRE imaging in guiding biopsy and elucidating the proper diagnosis.

Materials and Methods

Following approval by an Institutional Review Board, review of our pathology database identified 69 patients presenting from 1987 – 2011 with surgically and/or biopsy proven cerebrovascular amyloid. The corresponding relevant medical records and neuroimaging were reviewed to categorize the type of imaging findings, corresponding pathology results, patient presentation, and demographics. Sixty-seven unique neuroimaging time points were available for analysis from 81 amyloid cases.

Results

Three pathologic forms of amyloid were encountered: CAA (29 cases), ABRA (24 cases) and CAA-RI (14 cases). Twelve cases had CT alone, 25 cases had MRI alone, and 30 cases had a combination of the two. Twenty-nine cases had either a GRE or SWI sequence performed. Twenty-six out of 67 patients presented with lobar intraparenchymal hemorrhage, which occurred more frequently in the CAA (20/26) group than with ABRA (4/26) and CAA-RI (2/26) ($p < 0.0001$). Twenty-nine patients presented with leptomeningeal enhancement with or without underlying infiltrative T2 signal or underlying cortical infarcts. This was more common in patients with ABRA (13/29) and CAA-RI (11/29) than in patients with CAA (5/29) ($p < 0.0001$). Nine patients presented with an infiltrative white matter process mimicking a low grade astrocytoma. Although not statistically significant, this was more common in ABRA (7/9) than CAA (2/9) and not present in CAA-RI. One case of CAA-RI presented with acute multiple cortical infarcts, one case of CAA presented with focal subarachnoid hemorrhage, and one case of CAA presented as an enhancing intraparenchymal mass. Six patients (ABRA = 2, CAA-RI = 1, CAA = 3) had recurrence of their disease process at a different location. A-beta-related angiitis and CAA-RI tended to occur in younger patients.

Conclusions

A-beta-related angiitis and CAA-RI are likely part of the spectrum of one clinicopathological entity, with a distinctly different imaging presentation from CAA. The diagnosis of ABRA and CAA-RI should be suggested when the following is seen: diffuse lobar or multilobar infiltrative T2 hyperintensities, lobar hemorrhage, and/or leptomeningeal enhancement seen in association with microhemorrhages at the gray-white junction on SWI/GRE. The neuroradiologist should be aware of the findings seen with CAA, ABRA and CAA-RI, which could significantly impact patient management (immunomodulation versus biopsy). In patients where biopsies are performed, this should guide the surgeon to biopsy the gray-white junction as well as the leptomeninges rather than the underlying white matter abnormality. At our institution, we have added a susceptibility sequence to all cases that have the appearance of an infiltrative low grade glioma as well as leptomeningeal enhancement, to aid in narrowing the differential diagnosis and avoid nondiagnostic white matter biopsies in these cases.

KEYWORDS: Amyloid, GRE, Susceptibility-Weighted Imaging

Note: Scanned images are included in the proceedings. Some submitted images were reduced during editing thereby decreasing clarity. Also, refer to the Program Planner. Proceedings Content as of 3/28/2014.

O-47 11:26AM - 11:33AM
Simultaneous Pulsed Arterial Spin Labeling (PASL) MRI and 18F-FDG-PET in Neurodegenerative Dementia: a PET/MR Study

I Riederer, C Preibisch, P Alexopoulos¹, T Grimmer, I Yakushev, C Zimmer, S Förster
Klinikum Rechts der Isar, Technical University of Munich, Munich, Germany

Purpose

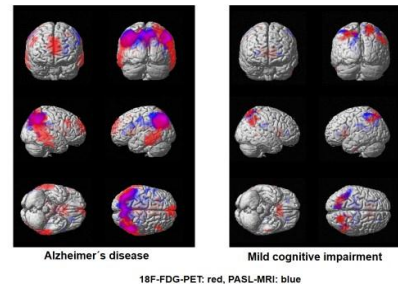
Previous studies in Alzheimer disease (AD) and mild cognitive impairment (MCI) reported disease-typical abnormality patterns and also high pattern similarity in brain perfusion arterial spin labeling (ASL) magnetic resonance imaging (MRI) and brain metabolism (18-fluorodeoxyglucose positron emission tomography, 18F-FDG-PET) relative to healthy controls. Though these studies either applied only one modality or were performed on separate MRI and PET scanners at different time points. We now compare these two methods, for the first time, using a simultaneous acquisition protocol on an integrated PET/MR system in different dementia groups and healthy controls.

Materials and Methods

So far 19 patients with AD, 14 patients with MCI and 11 matched healthy control subjects (HC) have been examined on a Siemens mMR Biograph using a simultaneous acquisition protocol including pulsed arterial spin labeling (PASL: 11 slices aligned with the hippocampus and including the parietal cortex), T1-weighted MPRAGE MRI and 18F-FDG-PET. Matlab and SPM8-based preprocessing of cerebral blood flow (CBF) and FDG-PET images comprised motion correction, coregistration, segmentation, partial-volume correction, spatial normalization and smoothing. Voxelwise statistical comparisons between patient groups and controls were performed using t-tests (threshold $p > 0.001$; $kE = 20$). Additionally regional perfusion and metabolism values were extracted using a region of interest (ROI) analysis.

Results

Large regional overlap between the patterns of hypoperfusion and hypometabolism was detected in patients with AD (left figure) as well as MCI (right figure) relative to HCs, while abnormalities were restricted to the bilateral parietal cortex in patients with MCI, more widespread abnormalities including temporal and frontal cortex were detected in patients with AD. Peak overlap areas between hypometabolism and hypoperfusion were detected in the bilateral posterior cingulate gyrus and bilateral superior parietal cortex for AD and the left posterior cingulate gyrus as well as left superior parietal cortex for MCI. Patients with MCI and AD had significantly lower perfusion and metabolism values in the posterior cingulate gyrus and the parietal cortex compared to HC.



Conclusions

In patients with MCI and AD there was a good congruence between the patterns of hypoperfusion and hypometabolism, especially with overlap in the posterior cingulate gyrus and parietal cortex. Our preliminary data suggests that PASL MRI is comparable to 18F-FDG-PET in the evaluation of patients with varying cognitive impairment due to neurodegenerative AD. Pulsed arterial spin labeling MRI, having the advantage of being absolutely noninvasive, needs further validation but may come up as an alternative to the well established 18F-FDG-PET in the diagnosis of AD in the near future.

KEYWORDS: Alzheimer Disease, MR Imaging/PET, PASL

O-48 11:33AM - 11:40AM
Regional Brain Volume and Cognition: A Population-based MRI Study

R Srinivasa¹, R Peshock¹, H Rossetti¹, M Weiner¹, R McColl¹, R Lucarelli², K King¹

¹University of Texas Southwestern Medical Center, Dallas, TX, ²Massachusetts General Hospital, Boston, MA

Purpose

The Montreal Cognitive Assessment (MoCA) is a clinically useful tool for detecting mild cognitive impairment and early Alzheimer disease (AD). Previous studies have shown that low volume of the posterior cingulate cortex (PCC), precuneus and hippocampus may serve as preclinical biomarkers for vulnerability to AD. Our goal was to determine if low volume in these regions measured by volumetric brain MR imaging (MRI) was associated with lower clinical measures of cognitive performance, and if the best predictor varied among the older versus younger members of our cohort.

Materials and Methods

We examined volumetric brain MRI data from a subset of the population-based Dallas Heart Study, mean age 49.9 ± 10.6 years, without a diagnosis of dementia or stroke who underwent cognitive testing using the MoCA ($n = 1675$). Cortical and subcortical segmental volumes were generated automatically using FreeSurfer. Regions of interest in this study included the PCC, precuneus and hippocampi. Total brain volume also was evaluated. Multiple linear regression analysis was performed with a threshold for significance of $p < 0.05$ predicting MoCA performance using PCC, precuneus, hippocampal and total brain volumes as regressors. Data were adjusted for age,

Note: Scanned images are included in the proceedings. Some submitted images were reduced during editing thereby decreasing clarity. Also, refer to the Program Planner. Proceedings Content as of 3/28/2014.

gender, ethnicity and education. Secondary analysis was performed stratified for age above and below 50 years.

Results

In the multiple regression model, PCC volume correlated with performance on MoCA ($p < 0.001$), with no other volume independently significant. Total brain ($p = 0.004$) and hippocampal ($p = 0.04$), but not precuneus volumes ($p = 0.07$), correlated with MoCA scores when considered individually. In secondary analysis, PCC volume also had the strongest association with MoCA scores among those below age 50 ($n = 834$, $p = 0.001$) but after age 50 ($n = 841$) hippocampus ($p = 0.05$) and precuneus ($p = 0.02$) were the best independent predictors of MoCA scores.

Conclusions

The MoCA is a clinical tool with validated utility for detecting mild cognitive impairment and early AD. In our population, lower performance on the MoCA was associated with decreased PCC volume. As shown in previous studies, low PCC volume may be an early finding in both sporadic and early-onset AD. In secondary analysis, PCC was the best predictor below age 50, but after age 50 the hippocampal and precuneus volumes were better predictors. Our findings suggest that low PCC volume may be a biomarker for vulnerability to cognitive insult in a younger community population but hippocampus and precuneus volumes may be better predictors in late adulthood.

KEYWORDS: Atrophy, Cognitive Deficit, Volumetric Measurements

0-49

11:40AM - 11:47AM

The brain damage in patients with early type 2 diabetes: a preliminary cognitive functional imaging study using fMRI, DTI and MR spectroscopy

W Tian, X Liu

University of Rochester Medical Center, Rochester, NY

Purpose

Diabetes mellitus (DM) is a common metabolic disease and is associated with impaired cognitive function and an increased risk of dementia. Cognitive impairments are more pronounced in type 2 than in type 1 diabetes patients. There are few studies about the brain dysfunction in early type 2 diabetes using advanced functional MR techniques. We try to evaluate the cognitive dysfunction in early type 2 diabetic patients with psychological tests and BOLD functional MR imaging (fMRI); To detect the microstructure change and metabolite abnormality with diffusion tensor imaging (DTI) and MR spectroscopy.

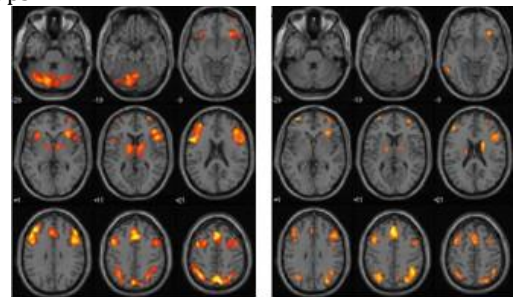
Materials and Methods

Twenty patients with early type 2 diabetes mellitus and 15 demographically similar, healthy subjects were enrolled. All subjects with microalbuminuria, hypoglycemia and ketonic acidosis, visible cerebral lesions on MR were ruled out. Psychology tests-Wechsler memory scale-revised (WMS-R), trail making test A and the personality and affective states were assessed in both groups. Then nback task fMRI and single-voxel MRS with TE 30 on bilateral

Prefrontal cortex (PFC) and DTI were performed. Regions of interest (ROIs) were located on prefrontal white matter area (PF WM), corpus callosum, internal capsule, anterior cingulate. The statistic differences of neuropsychological tests and MRS result and DTI parameters (FA, MD) between the two groups were evaluated. The fMRI data were analyzed by SPM2.

Results

(1) psychological tests showed that the scores of cognitive tests in diabetes group were significantly lower than those in control group. Diabetic patients were more depressive and anxious than controls. (2) Functional MRI examinations revealed that the activation pattern in diabetes group was similar with the control group, but less activation in prefrontal, parietal lobe and cerebellar was demonstrated on figure. There was additional activation in right temporal lobe (including inferior temporal gyrus and parahippocampus gyrus) and anterior cingulate cortex in diabetes group. (3) MR spectroscopy data showed that comparing with control group, the mean value of Glx/Cr, Glx/Cho, Glx/(Cho+Cr) were significantly elevated in right PFC ($p < 0.05$), while the value of Cho/Cr was significantly reduced ($p < 0.01$). The value of NAA/Cr was reduced in right side, but did not reach statistical significance. Transit memory was negatively correlated with Glx/Cho ($F = -0.546$, P value = 0.013) and Glx/(Cr+Cho) ($F = -0.471$, P value = 0.036). The number of errors in trail making test A was positively related to NAA/Cr (4). Diffusion tensor imaging data showed that the mean FA value in prefrontal white matter area in diabetes group was significant lower (0.32 ± 0.008) than in control group (0.38 ± 0.01), there was no significant difference in other areas between two groups.



Left image: nback task brain activation area in control group. Right image shows brain activation in patient group: decreased activation especially on PFC.

Conclusions

Early type 2 diabetic patients have cognitive dysfunction, especially decreased memory at verbal working memory. Functional MRI using nback test shows the hypofunction in PFC, DTI showed reduced FA in prefrontal white matter. The hypofunction in PFC plays an important role in cognitive dysfunction and the emotional abnormality. The MRS results reveal that increase of Glx and the degeneration of choline neuron system may contribute to the pathophysiological basis of PFC hypofunction in early type 2 diabetes.

KEYWORDS: Brain Abnormalities, Diffusion Tensor Image, MR Spectroscopy

Note: Scanned images are included in the proceedings. Some submitted images were reduced during editing thereby decreasing clarity. Also, refer to the Program Planner. Proceedings Content as of 3/28/2014.

0-50 11:47AM - 11:54AM
The Role Of T2*-Weighted Perfusion MRI In Therapeutic Response Assessment Of Brain Tuberculomas

A Gudipati¹, R Bharath¹, C Sasi¹, A Gupta²

¹National Institute of Mental Health & Neurosciences, Bangalore, Karnataka, ²National Institute of Mental Health & Neurosciences, Bangalore, India

Purpose

The purpose of this study was 1) To evaluate the rCBV values in patients with brain tuberculomas before the start of standard treatment with antituberculous therapy (ATT) and after completion of treatment. 2) To compare the rCBV values in responders and nonresponders to treatment and thereby assess the response to treatment.

Materials and Methods

Nineteen patients in the age range of 4-50 years were serially evaluated using T2* Perfusion on 3 T MR imaging system. rCBV ratio was calculated. All patients were proven to have brain tuberculomas based on the response to the ATT (n = 13), detection of pulmonary tuberculosis and associated tubercular meningitis (n = 3), and histopathology (n = 3). All patients subsequently were treated with standard antituberculous treatment for 12-22 months. Patients were classified into two groups based on clinical and imaging findings after treatment. Responders (n = 13) included those patients who showed clinical and imaging improvement. Nonresponders (n = 6) included patients who did not show response to treatment. Out of the six in three patients the lesions were excised.

Results

The rCBV values measured from central area of the lesions in responders group ranged from 0.25 to 1.85 (mean ± SD: 0.98 ± 0.44). The rCBV of the peripheral wall of lesions in responders group varied from 0.87 to 3.5 (mean ± SD: 1.57 ± 0.66). The rCBV values measured from central area of the lesions in nonresponders ranged from 0.10 to 0.74 (mean ± SD: 0.29 ± 0.26). The rCBV of peripheral wall of the lesions in nonresponders varied from 0.15 to 1.44 (mean ± SD: 0.66 ± 0.51). Nonresponders showed very low rCBV values on initial scan. Follow-up scan of three patients showed same low rCBV values. The lesions in the responders had significantly higher rCBV ratios in the center and periphery of lesions than those in the nonresponders (p < 0.05).

Conclusions

Treatment responders showed statistically significant higher values of rCBV as compared to both nonresponders and surgically excised lesions. We conclude that presence of very low rCBV values on initial scan in a tuberculoma may be the reason for nonresponse to antituberculous therapy.

KEYWORDS: Tuberculosis

0-51 11:54AM - 12:01PM
Changing Face of Intracranial Cryptococcal Infection

J Lammering¹, M Booker¹, J Grimm², R Larsen¹, E Law¹, P Kim¹, M Shiroishi³, J Go¹

¹University of Southern California, Los Angeles, CA, ²Childrens Hospital Los Angeles, Los Angeles, CA, ³University of Southern California Keck School of Medicine, Los Angeles, CA

Purpose

To characterize the changing imaging characteristics of intracranial Cryptococcal infection with correlation to CD4 count and prior treatment with protease inhibitor and highly active antiretroviral therapy (HAART).

Materials and Methods

Fifty-seven patients with culture-proven Cryptococcal infection and with brain MRIs performed between 11/2005-11/2013 at the LAC+USC Medical Center were assessed retrospectively for the presence of pseudocysts, perivascular space abnormality, hydrocephalus, cryptococcoma and stroke. Abnormal enhancement of leptomeninges, choroid plexus and ependyma also was assessed. Imaging findings were reviewed by two neuroradiologists and correlated with CD4 counts and prior treatment with protease inhibitor and HAART. Chi-square odds ratios with Pearson significance values were calculated using JMP 10.

Results

Of the 57 patients identified, 32 had CD4 counts <50, 20 were actively on HAART therapy, and 11 were receiving treatment with at least one protease inhibitor. Those patients with a CD4 count <50 were significantly more likely to have perivascular space enhancement and cerebritis, with ORs of 5.23 and 3.53, respectively. Those patients who had been treated with protease inhibitors were significantly more likely to have pseudocysts with enhancement, although there was only one recorded case. Patients on protease inhibitors also were more likely to have leptomeningeal enhancement with an OR of 3.47, although this did not reach the level of statistical significance (p-value 0.08). In contrast, none of the imaging characteristics of HAART versus non-HAART patients were statistically significant. Overall, the most common imaging findings were leptomeningeal enhancement, cerebritis, perivascular enhancement, perivascular space edema, hydrocephalus, and stroke with total incidence rates of 49%, 35%, 21%, 17%, and 15%, respectively (Table 1).

Note: Scanned images are included in the proceedings. Some submitted images were reduced during editing thereby decreasing clarity. Also, refer to the Program Planner. Proceedings Content as of 3/28/2014.

	Total Incidence	CD4 < 50 Incidence	OR	P-Value	Protease Inhibitor Incidence	OR	P-Value	HAART Incidence
Total	57	32						
Pseudocyst	4 (7.0%)	4 (12%)	Inf.	0.07	1 (9.0%)	1.43	0.76	1 (5.0%)
Pseudocyst w/ edema	2 (3.5%)	2 (6.2%)	Inf.	0.20	1 (9.0%)	4.50	0.26	1 (5.0%)
Pseudocyst w/ enhancement	1 (1.7%)	1 (3.1%)	Inf.	0.37	1 (9.0%)	Inf.	*0.04	1 (5.0%)
Widened	7 (12%)	5 (15%)	2.13	0.38	1 (9.0%)	0.67	0.72	2 (1.0%)
Perivascular spaces								
Perivascular space edema	11 (19%)	7 (21%)	1.47	0.58	4 (36%)	3.18	0.11	5 (25%)
Perivascular space enhancement	12 (21%)	10 (31%)	5.23	*0.03	3 (27%)	1.54	0.57	5 (25%)
Lepto-Meningeal Enhancement	28 (49%)	17 (53%)	1.44	0.49	8 (72%)	3.47	0.08	11 (55%)
Choroid Plexus Enhancement	1 (1.7%)	1 (3.1%)	Inf.	0.37	0 (0%)	0.00	0.62	0 (0%)
Ependymal Enhancement	1 (1.7%)	1 (3.1%)	Inf.	0.37	0 (0%)	0.00	0.62	0 (0%)
Hydrocephalus	10 (17%)	4 (12%)	0.45	0.26	1 (9.0%)	0.41	0.41	2 (1.0%)
Cerebritis	20 (35%)	15 (46%)	3.53	*0.03	6 (54%)	2.74	0.13	9 (45%)
Enhancing Mass/ cryptococcoma	8 (14%)	5 (15%)	1.36	0.70	1 (9.0%)	0.56	0.60	2 (1.0%)
Stroke	9 (15%)	4 (12%)	0.57	0.44	1 (9.0%)	0.48	0.50	1 (5.0%)

Conclusions

The imaging characteristics of intracranial Cryptococcal infection has changed over the past few decades, with findings previously thought to be atypical becoming more common. Awareness of imaging trends in relation to clinical lab values as well as treatment will assist in accurate diagnosis and management.

KEYWORDS: Cryptococcal Meningitis

Monday, May 19
10:30 AM – 12:08 PM
Room 520

11 - Parallel Papers: Adult Brain:
Neoplasms and New Techniques

O-52 10:30AM - 10:37AM
SWI micro-hemorrhages do not represent metastases in patients with primary breast cancer or melanoma.

A Franceschi¹, S Moschos², J Ramalho², C Kernodle Anders², M Castillo², Y Lee²

¹SUNY Stony Brook, Stony Brook, NY, ²University of North Carolina Chapel Hill, Chapel Hill, NC

Purpose

Susceptibility-weighted imaging (SWI) has substantially increased detection of hemorrhage in intracranial lesions and it has been suggested that microhemorrhages may serve as markers of small metastases even in absence of contrast enhancement (1). We sought to examine SWI findings in commonly hemorrhagic brain metastases to better understand if its presence is related to lesion size.

Materials and Methods

Patients with either melanoma or primary breast cancer underwent SWI imaging and high resolution T1 images (immediate postcontrast T1 MPRage, Multihance 0.1

ml/kg) at either 1.5 T or 3.0 T. Lesion volume was estimated by measuring three orthogonal dimensions and calculating it for an ellipsoid ($V = 4/3 \pi abc$). All enhancing lesions were presumed to be metastases based on clinical history of primary tumors. Susceptibility-weighted imaging findings on the corresponding image slices were categorized as either positive or negative based on presence/absence of signal dropout in the same locations. The percentage of SWI positivity then was estimated as a function of lesion size using 0.1 cm³ as a cutoff for micrometastases. A two-tailed Fisher exact test was performed to examine differences in the contingency tables.

Results

We studied 73 patients with 1173 enhancing metastases for which 952 had SWI. Thirty-eight patients had breast cancer (467 analyzed lesions) and 35 had melanoma (485 analyzed lesions). Only 10 of 342 micrometastases had SWI abnormalities while 410 of 610 larger ones were SWI positive (67.2%, p-value of < 0.0001). When examined by primary tumor type, 76.9% (melanoma) versus 55.6% (breast cancer) were SWI positive (p-value < 0.0001). No melanoma lesions larger than 1.5 cm³ were SWI negative while 14 of 15 of similar breast cancer lesions were SWI negative.

Conclusions

Using SWI and contrast-enhanced high resolution imaging we found that presence of hemorrhage is uncommon in micrometastases but common in larger metastases regardless of primary source. Thus, microhemorrhages even in presence of a primary breast cancer and melanoma cannot be used as sole markers of underlying metastases. Large metastases commonly harbor hemorrhage which occurs more often in presence of melanoma than in primary breast cancer.

KEYWORDS: Adult Brain, Advanced MR Imaging, Brain Metastases

O-53 10:37AM - 10:44AM
Brain radiation-related black dots on Susceptibility-Weighted Imaging

D Varon¹, F Chiang¹, G Tedeschi¹, M Simons¹, T Panyaping², M Castillo¹, G Pacheco³

¹University of North Carolina Chapel Hill, Chapel Hill, NC, ²University of North Carolina Hospital/University of North Carolina, Chapel Hill, NC, ³Hospital Rebagliati, Lima, Peru

Purpose

Brain irradiation may result in changes months to years after treatment of intracranial tumors and small-vessel injury is a prominent feature of delayed injury.

Susceptibility-weighted imaging (SWI) is a technique that exploits the magnetic properties of tissues, such as blood and iron content. The purpose of this study is to describe the SWI findings following cranial irradiation.

Note: Scanned images are included in the proceedings. Some submitted images were reduced during editing thereby decreasing clarity. Also, refer to the Program Planner. Proceedings Content as of 3/28/2014.

Materials and Methods

We evaluated 13 patients with MR imaging (MRI) follow up who underwent cranial irradiation for primary or metastatic tumors. From the clinical records, the latency interval, type of radiation, and total dose were established. The number and the distribution of "black dots" were analyzed. We also compared the findings on SWI with the those on conventional MRI.

Results

In all patients, black dots were clearly identified on SWI, while on conventional MRI (T2 and FLAIR) none were visible. In 10 patients (83%) diffuse black dots were observed and in two patients (17%) these were located near the surgical beds. All black dots were seen after whole brain radiation. When it could be established, the latent period for development of black dots was four months and doses varied from 45-54 Gy. None of these dots showed enhancement making them unlikely to represent hemorrhagic metastases. Black dots occurred in the cerebrum, cerebellum, and even choroid plexuses. Follow-up (3-6 months) in four instances showed that the numbers of these black dots increased.

Conclusions

Radiation-related black dots are not an uncommon effect of cranial irradiation. Susceptibility-weighted imaging is an accurate technique for evaluation of black dots presumably induced by radiation. The etiology of these black dots is uncertain and they could be related to microbleeds, capillary telangiectasias, and/or small cavernomas but they are unlikely to be metastases as none enhanced.

KEYWORDS: Radiation, Susceptibility-Weighted Imaging

O-54 10:44AM - 10:51AM
Dynamic contrast enhancement MR perfusion of pituitary adenomas

V Cuvinciuc, M Viallon, I Barnaure-Nachbar, M Vargas, S Haller, K Lovblad
University Hospitals of Geneva, Geneva, Switzerland

Purpose

To evaluate and describe pituitary adenomas with dynamic contrast enhancement MR perfusion.

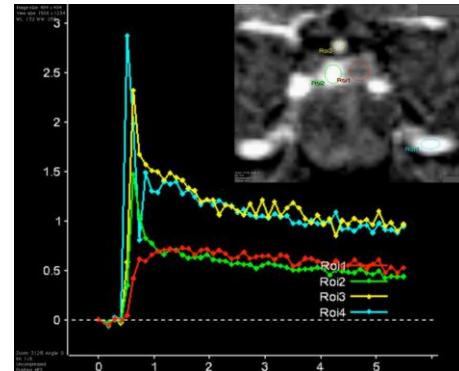
Materials and Methods

Fourteen patients with pituitary adenomas were explored with on optimized digital contrast enhancement (DCE) MR perfusion sequence between June 2013 and December 2013. Three patients presented with microadenomas, and the rest with macroadenomas. The dynamic acquisition was performed in a coronal plane with 1.2 mm thickness slices and a temporal resolution of 5 seconds acquired with time-resolved angiography with stochastic trajectories (TWIST) sequence on a 3 T machine. The dynamic acquisition was preceded by two T1 volumetric interpolated breath-hold examination (VIBE) sequences with 2 and 15 degrees flip angle, in order to compute the T1 map. Model-independent semiquantitative maps and quantitative maps based on multiple pharmacokinetic models [Tofts extended, adiabatic approximation of tissue

homogeneity (AATH) and AATH with delay] were generated with commercially available software. Analysis of quantitative parameters based on the pharmacokinetic models for both normal pituitary gland and pituitary adenomas was performed using Spearman's coefficient of correlation and Mann-Whitney test.

Results

Visual analysis of the enhancement curves showed in two out of the three cases of microadenomas that the difference between normal pituitary tissue and tumor tissue was most striking during the first minute after gadolinium injection, with a vascular peak of enhancement of the normal tissue and a slow washin of the adenoma; after one minute, the differences become minimal (Figure). Quantitative analysis showed that normal pituitary tissue and tumor tissue could be differentiated with most parameters used (Ktrans, ve, vp, washin, and washout) and with all the pharmacokinetic models ($p < 0.01$). Tofts extended model had the worst correlation with the other models (Spearman's rho between 0.552 and 0.670) for Ktrans measurements of adenomas; the Spearman's rho between the other models was more than 0.8 (excellent correlation). Area under the curve (AUC) could not differentiate normal tissue and tumor tissue on any of the models used.



Conclusions

Based on this preliminary experience, microadenomas are best depicted during the first minute after gadolinium injection. Most quantitative parameters derived from multiple pharmacokinetic models differentiate tumor from normal pituitary tissue.

KEYWORDS: Dynamic Contrast Enhancement, Pituitary Adenoma

O-55 10:51AM - 10:58AM
Apparent Diffusion Coefficient (ADC) and Pituitary Macroadenomas: Preoperative Assessment of Tumor Atypia

B Tamrazi, M Pekmezci, T Tihan, C Glastonbury
University of California San Francisco, San Francisco, CA

Purpose

Pituitary macroadenomas are predominantly benign intracranial neoplasms that can be locally aggressive with invasion of adjacent structures. This often renders gross

Note: Scanned images are included in the proceedings. Some submitted images were reduced during editing thereby decreasing clarity. Also, refer to the Program Planner. Proceedings Content as of 3/28/2014.

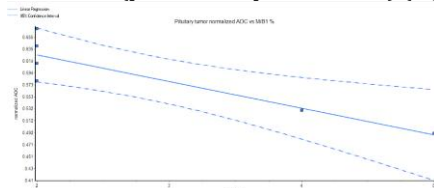
total resection challenging, resulting in higher recurrence rates and potentially adjuvant radiation for disease control. Although these tumors can be invasive, they are seldom histologically atypical and biomarkers of aggressive behavior have been identified previously in the pathology literature, including the proliferative marker MIB-1. In the radiology literature, diffusion-weighted imaging with low apparent diffusion coefficient (ADC) values have been reported as imaging markers of aggressive behavior in tumors of the brain and head and neck. The purpose of this study was to determine whether there was any correlation between ADC values, cellular atypia and MIB-1 in pituitary macroadenomas.

Materials and Methods

A retrospective review of imaging and immunohistochemical characteristics of pituitary macroadenomas was performed. A total of 25 patients were identified over a five-year period with MR imaging (MRI) including ADC maps at time of diagnosis. Patients with adenomas <2cm in size, with predominantly hemorrhagic or cystic components were excluded. The MR imaging features of the adenomas were evaluated for local invasion and restricted diffusion. The ADC values were normalized to ADC value of white matter to account for scaling factors during imaging acquisition (normalized ADC ratio). Tumor proliferation indices were reported as a percentage of tumor nuclei labeling with Ki-67 (clone MIB-1) monoclonal antibody in resected tissue. Linear regression analysis was performed to compare the normalized ADC ratio and MIB-1.

Results

Of the 25 patients, 21 demonstrated local invasion on imaging, which was confirmed intraoperatively. The mean ADC ratio was 0.91 in these patients. A subset of six patients was identified within this group in which the ADC values were significantly lower, with a mean ratio of 0.59. In these six patients, MIB-1 (Ki-67 index) was reported, ranging from 2-5%. Linear regression analysis of normalized ADC values versus MIB-1 demonstrates a negative correlation, with a linear slope significantly different from zero ($p = 0.02$, r squared = 0.80) (Figure 1).



Conclusions

Prior studies involving both ADC and MIB-1 have independently demonstrated the potential of these indices in the assessment of tumor behavior. To our knowledge, this is the first study to evaluate the relationship between ADC and MIB-1 in pituitary macroadenomas. We determine a strong correlation of low ADC values and MIB-1, demonstrating the potential of diffusion imaging as a possible biomarker for cellular, proliferative tumor, which may ultimately affect the surgical approach and postoperative management.

KEYWORDS: Pituitary Adenoma

0-56

10:58AM - 11:05AM

Accuracy and Reproducibility of ADC maps and CT for Diagnosis of Solid Pineal Masses

M Al-Sabbagh¹, D Dodig¹, T Amrhein¹, M Vittoria-Spampinato¹, Z Patay², C Welsh¹, Z Rumboldt¹

¹Medical University of South Carolina, Charleston, SC, ²St. Jude's Research Children's Hospital, Memphis, TN

Purpose

Pineal region tumors usually are of either germ cell or pineal cell origin [including pineal parenchymal tumor of intermediate differentiation (PPTID)]. These two groups have different prognoses and treatments. Apparent diffusion coefficient (ADC) values on MR imaging (MRI) and pineal calcification characteristics on computed tomography (CT) have been proposed for their differentiation. However, other lesions also arise in this location, which may exhibit overlapping imaging characteristics. The purpose of this study was to establish the accuracy and reproducibility of pineal mass differentiation using ADC maps and calcification patterns.

Materials and Methods

Four radiologists retrospectively reviewed imaging studies of 55 patients with histologically confirmed solid pineal masses at two institutions from 2003 to 2012. Reader experience spanned resident to neuroradiologist with 13 years of practice. Each blinded reader independently compared lesion signal intensity on ADC maps to normal brain (similar, darker, or brighter), and, in a separate session, the morphology of the pineal calcification on CT (preserved or "exploded"). Low ADC signal and exploded pineal calcification were the criteria for pineal cell tumors and atypical teratoid rhabdoid tumor (ATRT), while isointense to high ADC signal and intact calcification were considered consistent with germ cell tumors. Readers selected one of four options: definitive pineal cell tumor/ATRT, favor pineal cell tumor /ATRT, favor germ cell tumors, or definitive germ cell tumor. Interobserver agreement was assessed using kappa statistics. Final imaging diagnosis was established by the most senior neuroradiologist via evaluation of all available images.

Results

Both CT and MRI were available in seven patients, with ADC maps showing higher accuracy and interobserver agreement. Apparent diffusion coefficient maps had 100% sensitivity for germ cell tumors, with only 50% specificity. Computed tomography had a sensitivity of 88.9% for pineal cell tumors/ATRT and 100% for pineoblastoma, with lower specificity. Two cases of PPTID showed either low ADC values with preserved calcifications or "exploded" calcifications with higher ADC values. Overall sensitivity of 94.1% was found for germ cell tumors on ADC maps, with specificity under 50%. Apparent diffusion coefficient maps demonstrated a high specificity for pineal cell tumors/ATRT (89.5%), with a poor sensitivity (65.4%). Computed tomography showed a very high sensitivity for pineal cell tumors/ATRT (88.9%) and even higher for pineoblastoma (100%), with lower specificity (72.7%).

Note: Scanned images are included in the proceedings. Some submitted images were reduced during editing thereby decreasing clarity. Also, refer to the Program Planner. Proceedings Content as of 3/28/2014.

Gliomas of various grades and metastases simulated germ cell tumors based on calcification pattern and ADC signal. The agreement between pairs of raters was substantial in four and moderate in two cases for the ADC maps, substantial in two and moderate in four for the CT scans. Readers' experience did not appear to have an impact on kappa statistics.

Conclusions

Apparent diffusion coefficient signal intensity appears more reproducible than CT calcification pattern for pineal masses. Apparent diffusion coefficient maps are very sensitive but not specific for germ cell tumors, while CT is very sensitive and ADC maps are very specific for pineoblastoma and ATRT. "CT/MRI mismatch" ("exploded" calcification with isointense ADC signal or intact calcification with low diffusion values) appears suggestive of PPTID. Some of the pineoblastomas before the 2007 WHO classification actually might have been PPTIDs.

KEYWORDS: MR Imaging/Diffusion, Pineal Calcification, Pineal Cell Tumor

O-57 11:05AM - 11:12AM
Magnetic Resonance Fingerprinting of Brain Tumors:
Initial Clinical Experience

C Badve¹, D Ma², Y Jiang², A Yu³, A Sloan¹, V Gulani¹, M Griswold², J Sunshine¹

¹University Hospitals Case Medical Center, Cleveland, OH, ²Case Western Reserve University, Cleveland, OH, ³Case School of Medicine, Cleveland, OH

Purpose

Magnetic resonance fingerprinting (MRF) is a novel framework for simultaneous accurate quantitation of multiple MR tissue properties (1). The purpose of this study is to apply MRF for evaluating intra-axial brain tumors.

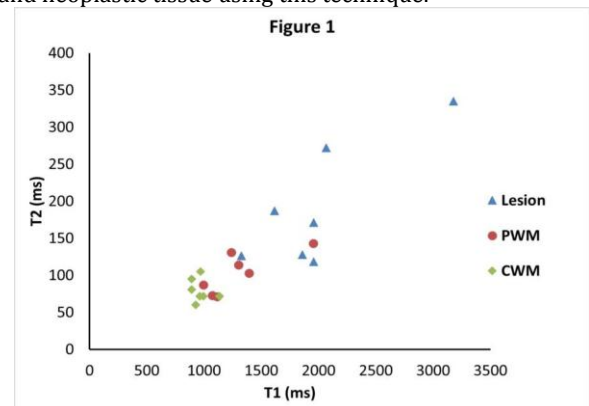
Materials and Methods

Seven patients (4 females 3 males, age 56-82) with intra-axial brain tumors, three high grade gliomas (HGG), two low grade gliomas (LGG) and two metastases (esophageal and lung adenocarcinoma) were scanned using a previously described MRF protocol (1). Clinical MRI images were used for region of interest (ROI) planning. T1 and T2 quantification of solid tumor, perilesional white matter (PWM), and contralateral white matter (CWM) was performed. In HGG, abnormal signal beyond the enhancement but within the expansile portion of lesion also was analyzed separately. Student's t-test for paired data was performed to compare T1, T2 values between different locations across subjects.

Results

Mean T1 and T2 values of solid parenchyma in gliomas (n = 5) were 1890 ± 170 ms and 219 ± 60 ms, respectively. Mean T1 and T2 of abnormal signal beyond the enhancement but within the expansile portion of lesion in HGG (n = 3) were 1789 ± 223 ms and 128 ± 24 ms. Intralesional T1, T2 of cystic metastasis from esophageal adenocarcinoma were 3177 and 335 ms and of lung

adenocarcinoma metastasis were 1324 and 126 ms. Mean T1 and T2 of perilesional white matter (n = 7) were 1272 ± 311 ms and 104 ± 25 ms. Mean T1 and T2 for (n = 7) contralateral normal white matter were 982 ± 77 ms and 77 ± 13 ms. Tumor relaxometry values are in good agreement with the limited published literature (2, 3). T1 and T2 values of tumor were significantly different than those of CWM (n=7, p<0.002, p<0.003 and PWM (n=7, p<0.02, p<0.02). There was significant difference between T1 and T2 of PWM and CWM (n=7, p<0.02, p<0.03). Figure 1 shows distribution of T1/T2 for all tumors. As seen, tissue characteristics for each region are distinct from each other, suggesting quantitative distinction between normal and neoplastic tissue using this technique.



Conclusions

These preliminary results suggest that MR Fingerprinting can quantitatively distinguish tumors, PWM changes and CWM from each other. Preliminary measurements also support using MRF to identify regions of infiltrative nonenhancing tumor in high grade gliomas. These results suggest application of this technique in tumor differentiation, delineation of tumor margins beyond enhancing borders, and therapeutic response evaluation.

KEYWORDS: Brain Neoplasms, MR Imaging, Relaxivity

O-58 11:12AM - 11:19AM
Is Remote Site Diffusion Restriction an Early Marker of Tumor Progression in Patients with Known Glioblastoma Multiforme?

J Newsome, S Lu, G Landinez, A Rizvi, S Tahvilian
Monmouth Medical Center, Long Branch, NJ

Purpose

The most commonly accepted method of assessing tumor progression in treated glioblastoma multiforme (GBM) is the presence of a new enhancing lesion. However, at sites that are remote from the original tumor, we propose that diffusion restriction precedes enhancement, as an early marker of tumor progression.

Materials and Methods

A retrospective review of standard protocol MR imaging (MRI) examinations of the brain, including diffusion-weighting imaging and their associated apparent diffusion coefficient (ADC) maps, was performed in patients with a

Note: Scanned images are included in the proceedings. Some submitted images were reduced during editing thereby decreasing clarity. Also, refer to the Program Planner. Proceedings Content as of 3/28/2014.

known history of GBM. The inclusion criteria included all GBM patients that had been followed longitudinally at Monmouth Medical Center over a 5.5 year period, from January 1, 2008 to August 6, 2013. Ninety patients were identified, and a board-certified neuroradiologist (S.L.) reviewed all of the images for these patients, in order to identify those patients with remote-site diffusion restriction. The patients were followed radiographically and/or surgically (i.e., re-resection) to determine the etiology of the remote-site diffusion restriction. Patients who subsequently developed an enhancing mass at the remote site were considered to have tumor progression. Patients with eventual resolution of the remote-site diffusion restriction or with subsequent development of encephalomalacia at the remote site were presumed to have had a focal infarct.

Results

In 18 of the 90 patients with GBM (20%), remote-site diffusion restriction without enhancement was seen following diagnosis and treatment. Upon longitudinal follow up, 10 (56%) of these 18 patients developed enhancing tumor at the remote site of diffusion restriction. Six (33%) of these patients were determined to have developed infarct. Two (11%) of these patients expired prior to an established etiology.

Conclusions

Remote-site diffusion restriction can be an early marker for the progression of tumor in patients with known glioblastoma multiforme. However, a significant portion of these patients with remote-site diffusion restriction suffer from focal infarction, rather than progression.

KEYWORDS: GBM, Glioblastoma, Glioma

0-59 11:19AM - 11:26AM

Predicting the spread of glial tumors: Lessons from the Insular Connections to the Frontal Lobe

V Kumar¹, L Chavali¹, J Hamilton¹, F Lang¹, J Hunter², M Thiebaut de schotten³, D O'Donoghue⁴, G Fuller¹, T Naidich⁵, A Kumar¹, L Hayman⁶

¹University of Texas MD Anderson Cancer Center, Houston, TX, ²Texas Children's Hospital, Houston, TX, ³King's College London, Houston, TX, ⁴University of Oklahoma Health Science Center, Oklahoma City, OK, ⁵Mount Sinai Hospital, New York, NY, ⁶Anatom-e Information Systems, Ltd, Houston, TX

Purpose

To demonstrate the 4 U-fiber tracts which are responsible for the spread of glioma between the insula (Brodmann area 13) and the frontal lobe (Brodmann areas 6, 43, 44 and 45/47).

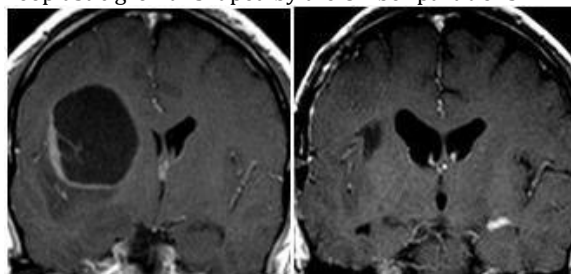
Materials and Methods

One thousand histologically proven gliomas in adults were analyzed retrospectively by MR imaging prior to surgical resection of tumor. One hundred and seven cases of insular tumor were subdivided into: a) 42 cases confined to the

insula, b) 24 of the remaining 65 cases demonstrated glioma spread between the insula and frontal lobe.

Results

In the 24 cases of insular tumor with spread to the frontal lobe, 12 occurred via the U fibers to the pars opercularis (Brodmann area 44), 9 occurred via U fibers to the pars orbitalis/pars triangularis (Brodmann area 45/47). Two cases spread via the U fibers between the insula and the subcentral gyrus (Brodmann area 43). Only one case used the U fibers between the opercular part of Brodmann area 6. Tumor infiltration between the concentric fibers which make up the U-fiber tracts occurred in 4 locations relative to the Sylvian fissure. Tumors which expanded the entire U fiber tract formed superficial rounded masses on both sides of the Sylvian fissure. This shape contrasted with the tumors which arose from either the insular or opercular limbs of the U fibers. Their growth displaced the Sylvian away from the expanded gyrus. The last location of tumor growth was in the junctional U fibers. These deep white matter tumors could reach considerable size. Tumors in any of the 4 locations can have a crescentic-shaped internal architecture which represents successive layers of neoplastic growth shaped by the U fiber partitions.



Conclusions

Insular gliomas can arise and dissect in 4 U-fiber tracts. They form unique shapes that can be described by using Brodmann area nomenclature. In our tertiary referral hospital 24/65 (37%) of insular tumors have spread to the frontal lobe at the time of diagnosis. Better understanding of these pathways of tumor spread is useful in planning neurosurgery and radiotherapy treatment. Figure legend. Coronal postcontrast MR images of a large astrocytoma trapped in the junctional part of the U fibers between the insula and Brodmann 44. Comparison of the preoperative (A) and postoperative (B) images confirms the site of tumor origin.

KEYWORDS: Insula

0-60 11:26AM - 11:33AM

Comparison of Qualitative Assessment Versus Semi-automated, Computer-assisted Quantitative Neuroimaging Feature Analysis of Glioblastomas in The Cancer Genome Atlas

J Soun, D Chow, F Hao, X Guo, B Zhao, C Filippi
Columbia University Medical Center, New York, NY

Purpose

Careful evaluation of the MR features of glioblastomas (GBM) is important for treatment planning and prognosis.

Note: Scanned images are included in the proceedings. Some submitted images were reduced during editing thereby decreasing clarity. Also, refer to the Program Planner. Proceedings Content as of 3/28/2014.

VASARI, a standardized vocabulary set that describes the 30 most common imaging features of GBMs, has been created to guide GBM evaluation. Our institution has developed a semi-automated, computer-assisted volumetric (CAV) algorithm that can potentially evaluate a subset of the VASARI features in a reproducible and objective way. Previous studies have shown the feasibility of semi-automated CAV algorithms for the assessment of GBM tumor core. In addition, researchers have demonstrated concordance between qualitative technique and semi-automated CAV assessment of GBMs. The purpose of this study is to assess concordance of traditional qualitative assessment versus a semi-automated CAV technique and to assess the inter-reader variability of these two techniques in evaluating GBMs from The Cancer Genome Atlas (TCGA) database.

Materials and Methods

This was a retrospective review using pathology results and images from the TCGA database and Cancer Imaging Archive, respectively. The Cancer Imaging Archive maintains images corresponding to TCGA patients. Only patients with presurgical MR imaging (MRI) with T1 precontrast, T1 postcontrast, and FLAIR imaging were included. Each tumor was assessed by two neuroradiologists independently using qualitative and semi-automated, quantitative CAV techniques. For the qualitative assessment, four key features based on VASARI scoring criteria were evaluated for each tumor: proportions of enhancement, noncontrast enhancement, necrosis, and surrounding edema. For semi-automated CAV assessment, the same criteria were evaluated by drawing a region of interest on one image of the tumor and using a CAV algorithm to automatically propagate that region of interest to the rest of the images. The semi-automated algorithm used combines a region-based active contours and level set approach. Intraclass correlation coefficient (ICC) analysis was performed to assess concordance between the qualitative technique and the semi-automated CAV technique to grade the four GBM features. Additional ICC analysis was examined for each technique. All analyses were performed with SPSS.

Results

Preoperative imaging with pathology was available for 59 GBMs obtained from the TCGA database. The ICC to assess concordance between the qualitative technique and semi-automated CAV technique were 0.85 (95% CI 0.75-0.91), 0.85 (95% CI 0.74-0.91), 0.96 (95% CI 0.93-0.98), and 0.90 (95% CI 0.83-0.94) for proportions of enhancement, noncontrast enhancement, necrosis, and surrounding edema, respectively. The ICC to assess inter-reader agreement for the qualitative technique were 0.75 (95% CI 0.57-0.85), 0.73 (95% CI 0.55-0.84), 0.68 (95% CI 0.46-0.81), and 0.72 (95% CI 0.57-0.83) for the same features. The ICC to assess inter-reader agreement for the semi-automated CAV technique were 0.87 (95% CI 0.79-0.93), 0.98 (95% CI 0.96-0.99), 0.90 (95% CI 0.82-0.95), and 0.89 (0.81-0.94) for the same features. Figure 1 shows a comparison of the inter-reader agreement for qualitative and semi-automated CAV techniques.

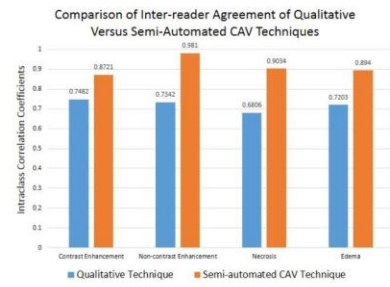


Figure 1. Intraclass correlation coefficients to assess inter-reader agreement of qualitative versus semi-automated CAV technique.

Conclusions

Our study shows high concordance between the qualitative technique and semi-automated CAV technique for evaluating GBM features. The ICC was higher using the semi-automated CAV technique. This study shows that semi-automated CAV technique is a viable quantitative tool for the evaluation of GBM characteristics in the clinical setting because of its reliability and reproducibility.

KEYWORDS: Glioblastoma, Volumetric Analysis

O-61

11:33AM - 11:40AM

Characteristic Computed Tomography and Magnetic Resonance Imaging Findings of Myeloid Sarcoma: A Retrospective Study

A Chaudhry¹, M Gul², A Chaudhry³, J Dunkin⁴

¹Stony Brook University Medical Center, Westbury, NY, ²Winthrop University Hospital, Mineola, NY, ³St Johns University, Westbury, NY, ⁴Stony Brook University Medical Center, Stony Brook, NY

Purpose

Myeloid sarcoma is a rare cause of extramedullary leukemia presenting as soft tissue mass and can occur anywhere in the body. It can be the initial presentation of aleukemic leukemia that either resulted from myelodysplastic syndrome conversion into leukemia, de novo aleukemic leukemia or leukemia relapse. It can present weeks to months before the peripheral presence of leukemia. The purpose of this study is to retrospectively evaluate imaging characteristics of myeloid sarcoma on computed tomography (CT) and MR imaging (MRI). Additionally, we aim to identify if there is a possible age, sex, organ system predilection and if specific subtypes of leukemia are more likely to result in development of myeloid sarcoma.

Materials and Methods

A retrospective study of 100 patients with pathologically proven myeloid sarcoma included 29 patients (18 men, 11 women; mean age, 55 years; range, 9-80 years) who underwent pretreatment CT and/or MRI at our institution from January 1993 to December 2012. A total of 60

Note: Scanned images are included in the proceedings. Some submitted images were reduced during editing thereby decreasing clarity. Also, refer to the Program Planner. Proceedings Content as of 3/28/2014.

examinations (25 MRI and 35 CT) were evaluated by two radiologists in consensus.

Results

There were 82 total sites of involvement of myeloid sarcoma were noted, most commonly CNS (30/82, 36.6%), head and neck (16/82, 19.5%), abdominopelvic viscera (13/82, 15.9%), thorax (11/82, 13.4%), musculoskeletal (7/82, 8.5%), lymphatics (6/82, 7.3%), gonads (3/82, 3.7%) and breast (2/82, 2.4%). Most of these sarcomas were AML subtype of which majority were M3 and M5. Of all of the patients, only 40% had evidence of leukemia on peripheral smear. The mean size of measurable lesions was 2.8 cm (range, 1-8 cm). On CT, 30 of the 35 lesions were solid and measurable. These lesions were isodense to spleen, liver and muscle measuring 40-70 HU on unenhanced CT. Twenty-five sites were noted on MR images obtained for evaluation of a new sign or symptom, most commonly CNS (20 sites), MSK (4 sites) and abdomen (1 sites). Compared with gray matter and muscle, the lesions were isointense (78.4%) or hypointense (21.6%) on T1-weighted images and hyperintense (96%) on T2 and FLAIR images and had homogeneous enhancement (88%). On diffusion-weighted imaging (DWI), 96% images showed restricted diffusion. Only 16% of images showed susceptibility artifact on gradient and none of these lesions demonstrated observable calcium on CT.

Conclusions

Myeloid sarcoma is a rare form of extramedullary leukemia which can be initial presentation of leukemia (de Novo, concurrent or recurrence) and commonly is seen without evidence of leukemia in peripheral blood. In patients with history of leukemia or other lymphoproliferative disorder, identification of a soft tissue mass can be indicative of myeloid sarcoma. Our study shows that the nervous system and head & neck are the two most common systems in which myeloid sarcoma arises. Imaging characteristics of myeloid sarcoma include homogenous mass isodense to muscle on CT, T1 isointense, T2/FLAIR hyperintense with restricted diffusion and homogenous postcontrast enhancement without significant susceptibility artifact.

KEYWORDS: MR Imaging, MR Imaging Brain, MR Imaging/Diffusion

0-62 11:40AM - 11:47AM

Usefulness of Diffusion Tensor Imaging based Intratumoral fiber tracking magnetic resonance imaging for the differentiation of schwannoma and classic meningioma in the cerebellopontine angle.

A Gudipati
Krishna Institute of Medical Sciences, Hyderabad, Andhra Pradesh, India

Purpose

The differentiation between schwannoma and meningiomas may have implications in pre-operative planning but may not be possible on the basis of conventional MR imaging (MRI). Diffusion tensor imaging (DTI) provides information about magnitude and

directionality of water diffusion and thus fiber tracking may be able to measure the differences in intratumoral diffusion anisotropy as a result of histologic differences between schwannoma and classic meningiomas.

Materials and Methods

Pre-operative DTI was performed in eight schwannoma and six classic meningiomas. In addition to MR imaging with all basic sequences, Medium DTI was acquired using a 3 T MR imaging scanner (Philips, Achieva) and postprocessed with fibretrak package to obtain intratumoral fiber tracking.

Results

Classic meningiomas showed whorly pattern of fibers inside the tumors. Intratumoral fiber tracking in all schwannoma is due to displaced facial nerve which was confirmed with surgical findings.

Conclusions

Diffusion tensor imaging-based intratumoral fiber tracking showed that the degree of contribution of intracellular environment is responsible for fiber tracking findings. This feature may allow for noninvasive differentiation between schwannoma and classic meningiomas.

KEYWORDS: Diffusion Tensor Image

0-63 11:47AM - 11:54AM

Primary CNS Lymphoma : Is Absence of Intratumoral Hemorrhage a Characteristic Finding on MRI?

A Sakata, T Okada, A Yamamoto, M Kanagaki, Y Fushimi, T Dodo1, K Togashi
Kyoto University Graduate School of Medicine, Kyoto, Japan

Purpose

Previous studies have shown that intratumoral hemorrhage is a common finding in glioblastoma multiforme (GBM), but rarely is observed in primary central nervous system lymphoma (PCNSL). Our aim was to re-evaluate whether intratumoral hemorrhage observed on T2-weighted imaging (T2WI) as gross intratumoral hemorrhage (GITH) and on susceptibility-weighted imaging (SWI) as an intratumoral susceptibility signal (ITSS) can differentiate PCNSL from GBM.

Materials and Methods

A retrospective cohort of brain tumors from August 2008 to March 2013 was searched, and 58 patients (19 PCNSL, 39 GBM) satisfied the inclusion criteria. Absence of GITH was examined on T2WI, and ITSS was graded using a 3-point scale on SWI. Results were compared between PCNSL and GBM, and values of $P < .05$ were considered significant.

Results

Gross intratumoral hemorrhage on T2WI was absent in 15 patients (79%) with PCNSL and 23 patients (59%) with GBM. Absence of GITH could not differentiate between the two disorders ($P = 0.20$). However, ITSS grade 1 or 2 was diagnostic of PCNSL with 79.0% sensitivity and 67.5% specificity ($P < 0.0001$), irrespective of GITH.

Note: Scanned images are included in the proceedings. Some submitted images were reduced during editing thereby decreasing clarity. Also, refer to the Program Planner. Proceedings Content as of 3/28/2014.

Conclusions

Gross intratumoral hemorrhage on T2WI had no differential capability, whereas ITSS score on SWI could differentiate PCNSL from GBM. However, specificity was not as high as previously reported. Primary central nervous system lymphoma cannot be excluded based solely on the presence of positive ITSS.

KEYWORDS: Lymphoma, Primary CNS Neoplasms, Susceptibility-Weighted Imaging

O-64 11:54AM - 12:01PM
Follow-Up MR in Inflammatory Cerebral Amyloid Angiopathy

F Cattin, K Gete, E Pomero, C Billon-Grand, A Biondi
Besancon University Hospital, Besancon, France

Purpose

Inflammatory form of cerebral amyloid angiopathy (CAA) is rare. The aim of this study is to report MR imaging (MRI) follow-up findings in patients presenting with inflammatory CAA disease and in those presenting with primary CAA complicated with an inflammatory evolution. Materials and Methods

We report a series of four patients (3 females and 1 male, ranging in age from 78 to 83 years). Two patients with an already known common form of CAA (i.e., microbleeds, macrobleeds, intracranial hemorrhages, hemosiderosis and T2 hypersignal in periventricular white matter) presented with acute neurological deficit (hemianopia 1 case, brachiofacial deficit 1 case). Two other patients were admitted with confusion (1 case) and hemianopia (1 case). MR protocol included diffusion imaging, axial T1, T2 FLAIR, T2 *-W images. 3D TOF MRA was performed in all of the four cases. Magnetic susceptibility images (SWAN) were obtained in three cases. Axial T1-weighted images and/or 3D T1 acquisition after gadolinium injection were performed in all cases. MR follow up ranged from four to nine months.

Results

In all patients, multiple large areas of high intensity signal on T2-weighted images were observed in the white matter associated with bilateral and asymmetrical U fibers and cortex involvement. The lesions were hypointense on T1-weighted images. There was no diffusion restriction. The data were in favor of vasogenic edema. The sulci adjacent to the parenchymal abnormalities were collapsed. Faint focal leptomeningeal cortical enhancement was observed in two cases. In the patients with previously diagnosed CAA, MR images showed an acute parenchymal hemorrhage in contact with the T2 parenchymal hyperintensities in addition to typical CAA findings. On the follow-up MR studies, a quite complete regression of the edematous lesions was observed. Nevertheless the number of microbleeds lesions increased.

Conclusions

In our series, inflammatory CAA occurred in patients with previously diagnosed common form of CAA or with the primary manifestation of CAA. Clinical presentation of

inflammatory form of CAA is not specific. MR imaging, including T2* and SWAN images, and MR follow up are crucial to confirm the diagnosis and avoid invasive diagnostic procedure as cerebral biopsy.

KEYWORDS: Amyloid, Inflammatory, MR Imaging Brain

Monday, May 19
10:30 AM – 12:00 PM
Room 524

12 - Parallel Papers: Pediatrics: Vascular

O-65 10:30AM - 10:37AM
Developmental Trajectories of Cerebrovascular Reactivity in Healthy Children

J Leung, A Kassner
The Hospital for Sick Children, Toronto, Ontario, Canada

Purpose

Noninvasive imaging strategies can assess vessel distensibility by quantifying the relative changes in cerebral blood flow (CBF) in response to a vasoactive stimulus. The resulting measure is expressed as cerebrovascular reactivity (CVR) and is a useful tool in the clinical assessment of cerebrovascular disease (1, 2). Although we know that baseline CBF undergoes significant developmental changes during childhood (3, 4), very little data are currently available on how this affects CVR in children. Understanding the healthy developmental trajectories of CVR in relation to CBF could aid in the interpretation of future studies in children with cerebrovascular disease. The purpose of this study was to measure CVR at various ages and compare them to corresponding changes in CBF throughout childhood.

Materials and Methods

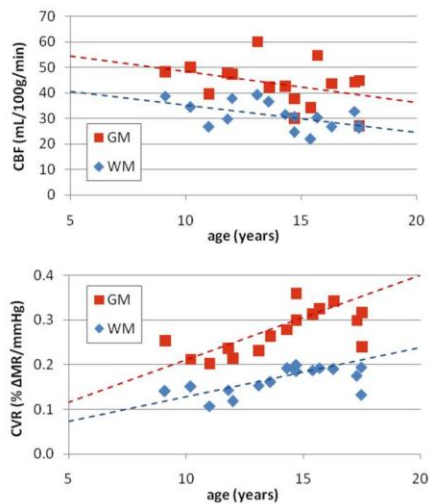
Sixteen healthy volunteers (7 males, 9 females) between nine and 18 years old were imaged on a clinical 3 T MRI scanner (MAGNETOM Tim Trio; Siemens Medical Solutions, Erlangen, Germany) using a 32-channel head coil. Blood-oxygen level-dependent (BOLD) imaging was used to assess changes in CBF during the administration of a CO2 stimulus via a computer-controlled gas sequencer (RespirAct; Thornhill Research Inc., Toronto, Canada). The BOLD sequence parameters were as follows: TR/TE=2000/40ms, FOV=220mm, matrix size=64x64, slices=25, thickness=4.5mm, volumes=240, time=8min. Cerebrovascular reactivity maps were computed offline using FSL v4.1 (<http://www.fmrib.ox.ac.uk/fsl/>) by correlating the voxel-wise BOLD signal change to the measured end-tidal CO2 waveform. Baseline CBF was measured using a PICORE Q2TIPS pulsed arterial spin labeling sequence (TR/TE=2500/13ms, T1=700ms, T12=1800ms, FA=90°, FOV=220mm, matrix=64x64, slices=13, thickness=4.5mm) and quantified using the vendor processing pipeline (5). Cerebrovascular reactivity and CBF maps were averaged over gray matter (GM) and

Note: Scanned images are included in the proceedings. Some submitted images were reduced during editing thereby decreasing clarity. Also, refer to the Program Planner. Proceedings Content as of 3/28/2014.

white matter (WM) regions and Pearson correlation analysis was performed on the resulting data.

Results

Cerebral blood flow and CVR values in each subject are plotted as a function of age. A linear decline in CBF was observed for both GM and WM with respective correlation coefficients $r^2 = -0.375$ and $r^2 = -0.531$. The change in mean GM and WM CVR exhibited an opposite pattern as CVR linearly increases with age up to age 17. The relation does not hold afterwards as CVR values showed a dramatic decline. The correlation for a linear fit was $r^2 = 0.660$ and $r^2 = 0.600$ for GM and WM, respectively, for data points up to age 17.



Conclusions

Our study shows a linear upward trend in the evolution of CVR with age in healthy subjects, corresponding to the normal change in CBF. The eventual peak and decline in CVR, however, indicate that other factors beside CBF may be influencing CVR in the late teen years. Additional data will further substantiate this finding and provide a more comprehensive understanding of CVR changes with age.

KEYWORDS: BOLD FMRI, Cerebral Hemodynamics, Cerebrovascular Reserve

0-66 10:37AM - 10:44AM
Reproducibility of MR Based Measures of Cerebrovascular Reactivity in Children Using a Computer Controlled Vasoactive Stimulus

J Leung, A Kassner
The Hospital for Sick Children, Toronto, Ontario, Canada

Purpose

Cerebrovascular reactivity (CVR) is a measure that assesses vessel distensibility in the brain, which is important for maintaining normal blood flow and pressure. Noninvasive CVR imaging strategies that quantify cerebral blood flow (CBF) changes in response to a vasoactive stimulus has become a useful tool in the clinical assessment of cerebrovascular disease (1, 2). A successful

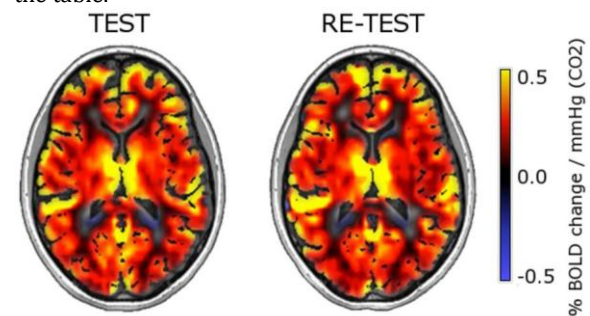
approach for mapping regional CVR is by measuring MRI blood-oxygen level dependent (BOLD) signal changes during the administration of a computer-controlled CO₂ stimulus. This method has been shown to be reproducible in adults (3), but not yet in children. The purpose of this study was to demonstrate BOLD-CVR reproducibility using precise targeting of end-tidal partial pressures of CO₂ (PetCO₂) in pediatric subjects.

Materials and Methods

Three healthy volunteers (1 male, 2 females) between 15 and 16 years old were imaged on a clinical 3 T MRI scanner (MAGNETOM Tim Trio; Siemens Medical Solutions, Erlangen, Germany) using a 32-channel head coil. We assessed long-term reproducibility by collecting test-retest BOLD-CVR measurements performed on two separate days, approximately two weeks apart. BOLD-CVR data was acquired during an eight minute long CO₂ breathing challenge consisting of four block cycles of normocapnia (PetCO₂ = 40 mmHg) and hypercapnia (PetCO₂ = 45 mmHg), which was administered via a computer-controlled gas sequencer (RespirAct™; Thornhill Research Inc., Toronto, Canada). Cerebrovascular reactivity maps were computed offline using FSL v4.1 (<http://www.fmrib.ox.ac.uk/fsl/>) by correlating the voxel-wise BOLD signal change to the measured end-tidal CO₂ waveform, followed by normalization into units of % BOLD change/mmHg (CO₂). High resolution T1-weighted anatomical images also were acquired for the purposes of coregistration of the CVR maps as well as brain tissue segmentation into gray matter (GM) and white matter (WM) regions. Mean CVR values over GM and WM were calculated for each subject. Reproducibility was assessed using the between-day coefficient of variation (CV).

Results

Representative test-retest BOLD-CVR maps overlaid on T1 images are provided in the figure. Mean (\pm SEM) BOLD-CVR measures exhibited good between-day reproducibility for both the GM and WM regions (CV < 14%) as shown in the table.



Test-retest BOLD-CVR mean \pm SEM (% BOLD change / mmHg) and CV mean \pm SEM (%).

Region	Trial 1 Mean	Trial 2 Mean	CV (%)
GM	0.257 \pm 0.032	0.280 \pm 0.036	9.7 \pm 6.9
WM	0.158 \pm 0.016	0.163 \pm 0.024	13.6 \pm 6.4

Conclusions

Note: Scanned images are included in the proceedings. Some submitted images were reduced during editing thereby decreasing clarity. Also, refer to the Program Planner. Proceedings Content as of 3/28/2014.

In this study, we have demonstrated the reproducibility of BOLD-CVR data in children using a precisely controlled vasoactive stimulus. While additional data needs to be acquired to expand on these initial results, they provide support for the feasibility of pediatric CVR imaging studies.

KEYWORDS: Cerebrovascular Reserve, Pediatric Brain, Reproducibility

O-67 10:44AM - 10:51AM
Assessing the Effect of Red Cell Transfusion on MR Based Cerebrovascular Reactivity in Children with Sickle Cell Disease

P Kosinski, J Leung, S Williams, A Kassner
The Hospital for Sick Children, Toronto, Ontario, Canada

Purpose

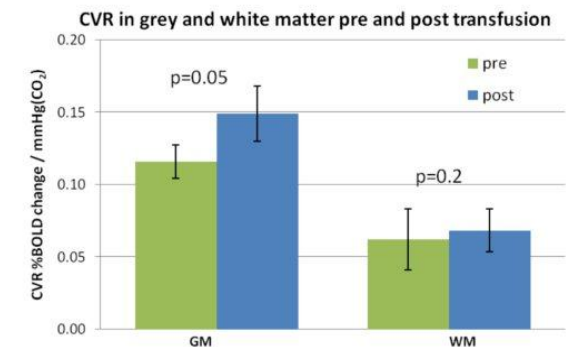
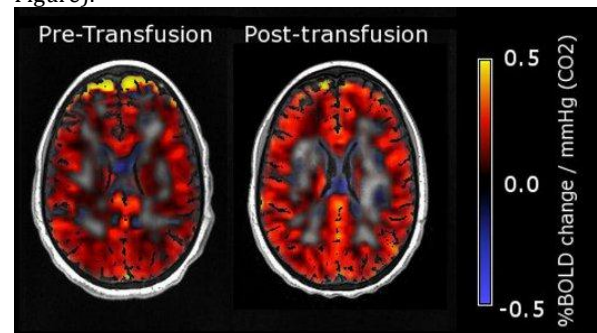
Sickle cell disease (SCD) is a genetic disorder and the most common cause of ischemic stroke in the pediatric population. More than 10% of SCD patients will experience an overt stroke by the age of 20 (1). Patients presenting with abnormal cerebral arterial blood flow velocities (> 200cm/s), as measured by transcranial Doppler, are treated with prophylactic monthly blood transfusions to reduce the rate of either primary or recurrent stroke (2). The attenuation of stroke risk following transfusion may be due potentially to the restoration of cerebrovascular reactivity, which is known to be compromised in SCD (3, 4). Cerebrovascular reactivity (CVR) is a marker that reflects the cerebral vasculature's capacity for vasodilation in the presence of a vasoactive stimulus (3) and can be assessed using blood-oxygen-level-dependent (BOLD) MRI. The purpose of this study was to assess the effect of transfusion on cerebrovascular reactivity using MR-based measures of CVR in children with SCD.

Materials and Methods

Three SCD patients (11-12 years old) without a history of overt stroke, requiring transfusion therapy were imaged on a 3 T MRI (Siemens). Imaging data were acquired at two time points, just prior to transfusion and a few days afterwards. Cerebrovascular reactivity data were obtained using a standard BOLD MRI sequence in combination with a CO₂ breathing challenge. The BOLD parameters were: TR/TE=2000/40ms, FOV=220mm, matrix size=64×64, slices=25, thickness=4.5mm, volumes=240, time=8min. CO₂ was administered using a re-breathing mask in cycles of targeted normocapnia for one minute followed by a 5mmHg step increase in CO₂ tension for 45 seconds. Correlations of voxel-based BOLD changes to end-tidal CO₂ waveforms were performed on FSL v4.1 to generate CVR maps that then were coregistered on T1-weighted anatomical scans. A Student's T-test was used to compare significant changes (p<0.05) in mean CVR pre- and post-transfusion. The equation by Levin, et al. was used to account for the effect of hematocrit (Hct) on the BOLD signal (6).

Results

Representative CVR maps are provided in the figure. Following transfusion, mean CVR increased in the gray matter from 0.131 ± 0.011 to 0.167 ± 0.019 (p<0.05) and in the white matter from 0.077 ± 0.021 to 0.086 ± 0.014 (p=0.11). After correcting for Hct, mean CVR following transfusion increased in the gray matter from 0.116 ± 0.012 to 0.149 ± 0.02 (p=0.052) and in the white matter from 0.062 ± 0.023 to 0.068 ± 0.015 (p=0.2) (refer to Figure).



Conclusions

In this study, we have demonstrated that CVR increases following transfusion in patients with SCD. The increase in CVR probably is due to an increased capacity for cerebral vasculature to dilate, which plays an important role in preventing cerebral ischemia. Further studies are needed to validate this.

KEYWORDS: Cerebrovascular Reserve, MR Imaging Brain, Sickle Cell Disease

O-68 10:51AM - 10:58AM
Effect of Obstructive Sleep Apnea on Cerebrovascular Health in Children with Sickle Cell Disease

J Kim, J Leung, I Narang, S Williams, A Kassner
The Hospital for Sick Children, Toronto, Ontario, Canada

Purpose

Sickle cell disease (SCD) is a genetic disorder that causes hemolytic anemia and occlusive vasculopathy (1). Previous work has demonstrated that cerebrovascular reactivity (CVR), a measure for vascular health, was globally reduced compared to healthy controls in the pediatric SCD population (2). Cerebrovascular reactivity reflects the capacity of blood vessels to regulate blood flow in the

Note: Scanned images are included in the proceedings. Some submitted images were reduced during editing thereby decreasing clarity. Also, refer to the Program Planner. Proceedings Content as of 3/28/2014.

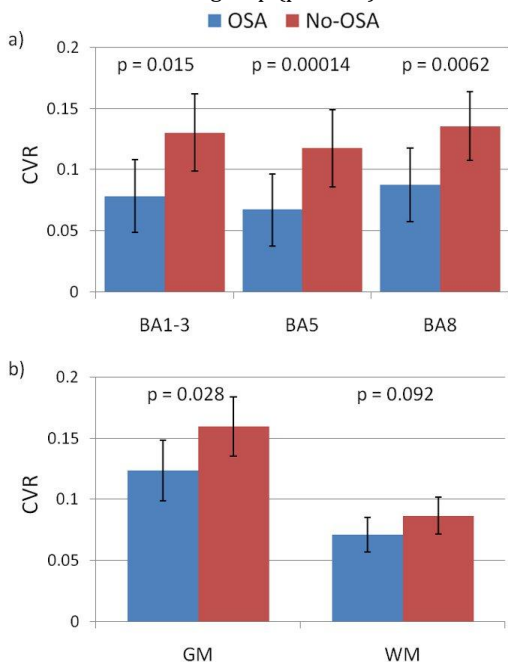
presence of a vasoactive stimulus. In addition, a high percentage of individuals with SCD suffer from obstructive sleep apnea (OSA) (3). This can lead to repeated episodes of nocturnal hypoxia, hypercapnia and sleep disruption. It is currently unknown if the presence of OSA in the pediatric SCD population will further impair cerebrovascular health. Therefore, by comparing the MRI derived CVR values in the OSA versus the non-OSA cases in the pediatric SCD population, we will gain valuable insight into their combined effect on cerebrovascular health.

Materials and Methods

Seventeen SCD patients, seven with OSA (8-18 years) and 10 without OSA were imaged on a 3 T MRI scanner using a 32-channel head coil. Cerebrovascular reactivity data were acquired using a blood-oxygen level dependent (BOLD) sequence during a computer-controlled administration of a vasoactive stimulus delivered in programmed cycles of low and increased levels of CO₂ through a rebreathing mask. The BOLD images were acquired with TR/TE = 2000/40ms, FOV = 220mm, matrix size = 64×64, slices = 25, slice thickness = 4.5mm, volumes = 240, time = 8 min. High resolution CVR maps were computed using FSL v4.1 and then converted into surface maps through the CIVET pipeline (4). Next, the surface maps were coregistered into the MNI pediatric MRI Atlas, which was segmented manually into the corresponding Brodmann regions. The MATLAB based program SurfStat was used to perform Student's t-tests on CVR between the groups (5).

Results

From the CVR group comparison analysis, we observed that global CVR levels in gray matter was significantly lower in SCD patients with OSA compared to the non-OSA group. The regions of interest analysis revealed several Brodmann areas that showed significantly reduced CVR levels in the OSA SCD group ($p < 0.05$).



Conclusions

In this study, we have demonstrated significantly reduced CVR values in SCD patients with OSA compared to SCD patients without OSA in different parts of the brain. Reduced CVR may expose individuals who suffer from SCD and OSA to a higher risk for serious vasculopathies such as stroke and they should, therefore, be considered for treatments such as adenotonsillectomy or CPAP therapy to reduce stroke risk.

KEYWORDS: Cerebrovascular Reserve, Obstructive Sleep Apnea, Sickle Cell Disease

O-69

10:58AM - 11:05AM

Pediatric syndromic CNS vascular disorders: imaging clues to a diagnosis

P Muthusami, H Branson, M Seed, T Bradley, S Bowdin, S Blaser

The Hospital for Sick Children, Toronto, Ontario, Canada

Purpose

Syndromic central nervous system (CNS) vascular disorders are being increasingly recognized. Imaging is performed for screening in family members of affected individuals or may be obtained only after a catastrophic complication in a child not diagnosed previously. Imaging patterns may be specific or could be useful in suggesting a diagnosis. The purpose of this study was to describe the CNS and non-CNS vascular and nonvascular imaging manifestations of these disorders.

Materials and Methods

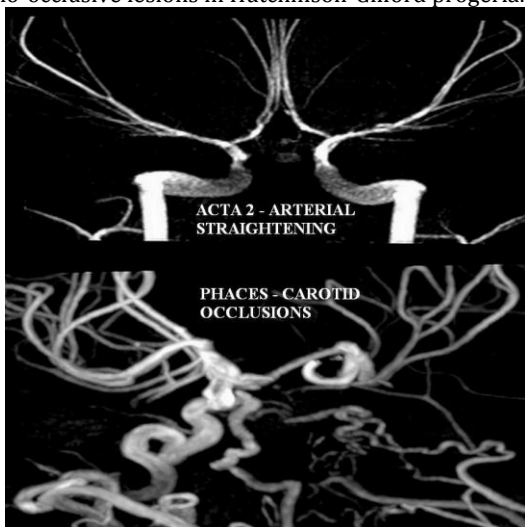
Two hundred fifty patients with syndromic CNS vascular disorders were identified via an IRB/REB approved retrospective radiology text search. Arterial MIP reconstructions were evaluated for specific patterns. Additional clues to the diagnosis were sought on extra CNS imaging studies.

Results

Our findings could be grouped into conditions with predominantly CNS involvement (Neurofibromatosis 1-NF1, moyamoya disease and PHACES association were the most common), predominantly extra-CNS with frequent CNS manifestations [ACTA2 mutation, Takayasu arteritis, Loeys-Dietz syndrome (LDS)], and predominantly extra-CNS with infrequent CNS involvement (Blue rubber bleb nevus syndrome, velocardiofacial syndrome and hereditary hemorrhagic telangiectasia-HHT). Characteristic CNS vascular patterns were found that could define certain conditions, like arterial straightening in ACTA-2, tortuosity in LDS and progressive stenosis in moyamoya disease. Complementary nonvascular CNS findings aided diagnosis in several cases, like posterior fossa abnormalities with persistent primitive arteries and steno-occlusions in PHACES, characteristically distributed white matter abnormalities (FASI) with steno-occlusions in NF1 and colobomas associated with congenital vascular occlusions in Morning Glory syndrome. Some less specific

Note: Scanned images are included in the proceedings. Some submitted images were reduced during editing thereby decreasing clarity. Also, refer to the Program Planner. Proceedings Content as of 3/28/2014.

CNS imaging findings were complemented by extra-CNS findings. Examples are aneurysms in polycystic kidney disease and microcephalic-osteodysplastic-primordial-dwarfism type-II, cerebral and pulmonary arteriovenous malformations in HHT, aortic ectasia in LDS and ATS, aortic and branch steno-occlusions in Takayasu arteritis, medially deviated pharyngeal carotid arteries in 22q11 deletion and steno-occlusive lesions in Hutchinson-Gilford progeria.



Conclusions

Central nervous system vascular abnormalities may be specific like the arterial straightening in ACTA-2 mutation. Less specific vascular patterns such as tortuosity or moyamoya appearance may be seen. Additional CNS and non-CNS imaging clues may aid in suggesting and planning an appropriate diagnostic approach.

KEYWORDS: Loeys-Dietz Syndrome, Moyamoya, MR Angiography

O-70 11:05AM - 11:12AM
Vascular Causes of Pediatric Intracranial Hypertension

O Pasternak-Wise¹, A Honarmand², M Hurley¹, T Alden³, R Bowman³, Y Curran¹, A DiPatri³, S Ansari¹, A Shaiban^{1,2}
¹Northwestern University Feinberg School of Medicine, Chicago, IL, ²Northwestern University, Chicago, IL, ³Ann & Robert H. Lurie Children's Hospital of Chicago, Chicago, IL

Purpose

After space-occupying lesions and mechanical disruptions of CSF drainage have been excluded, intracranial venous hypertension (ICVH) often is the central mechanism leading to intracranial hypertension and its causes can be categorized into primary venous outflow compromise (PVOC), arteriovenous shunting (AVS) and idiopathic intracranial hypertension syndrome (IIH). We identified pediatric cases of intracranial venous hypertension (ICVH) to investigate the precipitant vascular causes and the role of endovascular intervention.

Materials and Methods

Following IRB approval, a retrospective pediatric neurointerventional database review identified patients

with known ICVH. Cross-sectional imaging and catheter studies were reviewed for direct intravascular pressure measurements and angiographic evidence of disturbed cerebral venous drainage including venous dilation, stenosis, occlusion and abnormal collateral drainage. Demographic data, clinical presentation, type and grade of the underlying vascular lesion, treatment strategy, follow-up imaging and clinical course were obtained accordingly. Results

Eleven patients (3F/8M) with mean age of 4.6 years (range: 20 days - 13 years) at the time of presentation were identified. The presenting signs and symptoms included increased head circumference (IHC) (n=6), failure to thrive (n=3), visual disturbance/papilledema (n=3), seizure (n=2), prominent scalp and/or facial veins (n=2), head tilt (n=1), and cardiovascular/respiratory complications (1). Preprocedural imaging findings included: hydrocephalus (n=5), ventriculomegaly (n=4), anatomical sinus variant (n=4), venous sinus thrombosis (n=2), and bilateral subdural hematoma (n=1). ICVH was verified by transcatheter venous pressure measurement in four cases. The underlying vascular lesions leading to ICVH were subclassified into three groups: PVOC, AVS and IIH. Three cases were classified as PVOC including 2 cases of focal web-like stenosis of the dominant sigmoid sinus and 1 case of venous sinus thrombosis. Six cases of AVS included vein of Galen aneurysmal malformation (n=2), high-flow pial/dural AVF (n=2) and congenital high-flow torcular arteriovenous fistula (n=2) with one of the latter complicated by a secondary venous outflow obstruction. Two cases were consistent with IIH. The AVS group comprised younger patients (mean age: 2.6 months) and the most common clinical findings were IHC and hydrocephalus compared with headache, decreased visual acuity and papilledema in IIH. PVOC had a more heterogenous presentation with an overlap of presenting symptoms and signs with the AVS group (IHC and hydrocephalus) and IIH group (headache, papilledema). The endovascular treatment included multiple sessions of endovascular embolization, stent placement, and intra-arterial thrombectomy/thrombolysis depending on lesion type and was technically successful without perioperative complications in all cases. Follow-up imaging and clinical outcome revealed significant improvement in intracranial venous drainage and remarkable clinical and developmental improvement except for one case. Conclusions

Intracranial venous hypertension may be caused by primary outflow obstruction, arteriovenous shunting or idiopathic intracranial hypertension, with significant overlap of clinical presentations as well as hybrid lesions mandating a thorough endovascular work up. Whereas most lesions are amenable to endovascular therapy, the management of idiopathic intracranial hypertension remains controversial.

KEYWORDS: Intracranial Hypertension, Pediatric Brain, Venous Malformations

Note: Scanned images are included in the proceedings. Some submitted images were reduced during editing thereby decreasing clarity. Also, refer to the Program Planner. Proceedings Content as of 3/28/2014.

0-71 11:12AM - 11:19AM
Degree of Collateralization Predicts Symptomatic Cerebral Vasospasm Among Pediatric Patients: Correlation Between Angiography, TCD, and Clinical Findings.

P Moftakhar, M Amans, D Cooke, N Ko, S Hetts
University of California San Francisco, San Francisco, CA

Purpose

Cerebral vasospasm is a significant cause of morbidity and mortality following subarachnoid hemorrhage (SAH). Although vasospasm has been investigated extensively in the adult population, minimal data exists about this phenomenon in the pediatric population primarily because vasospasm is rarely diagnosed clinically in children. We hypothesize that even though children have highly vasoreactive arteries, they rarely develop clinically evident symptoms of cerebral vasospasm due to robust cerebral collateral blood flow.

Materials and Methods

Retrospective review of our tertiary care hospital's neurointerventional radiology database and medical records was performed under an IRB-approved protocol. Thirty-seven children (21 boys) who presented with SAH (32 aneurysmal: Hunt Hess 1-5, Fisher 1-4 and 5 traumatic) under the age of 18 years (average age 11.8 years) were identified. Digital subtraction angiograms (DSA) were analyzed for degree of vasospasm based on luminal narrowing (none, mild (<30%), moderate (30-50%), or severe (>50%). To assess degree of collateralization in our vasospasm patients, we adapted a scoring system which has been established in ischemic stroke (Table 1) (1). Transcranial Doppler (TCD) ultrasound was correlated with DSA. Vasospasm on TCD was defined using established adult criteria (MCA ≥ 120 cm/s and Lindegaard ratio [(LR)>3, basilar artery ≥ 90 cm/s). Clinical outcome was assessed by the pediatric modified Rankin Scale (mRS) (2).

Results

Seventeen (46%) children demonstrated angiographic vasospasm (21% mild, 50% moderate, 29% severe). Only three children demonstrated symptomatic vasospasm and all three demonstrated poor collaterals (collateral score of 5). Ten (71%) of the asymptomatic children demonstrated some degree of collateralization (collateral score 1-4). All 5 five children with traumatic SAH demonstrated angiographic vasospasm. Sixteen children had TCDs that could be correlated with catheter angiography. Thirteen (81%) of these children demonstrated vasospasm by TCD criteria. Only one of these children demonstrated symptomatic vasospasm, however. In 12 instances that vasospasm was identified in a particular vascular territory by TCD criteria, there was no evidence of vasospasm in that vessel by DSA. Time to onset of vasospasm by TCD was 5+/-3 days (range 2-10). Twenty-five (68%) of children had good outcomes (mRS of 0-2) (average follow-up time 19.7 months).

Table 1. DSA-Based Scale for Collateral Blood Flow in Pediatric Cerebral Vasospasm

Score

- 1 Collaterals reconstitute the distal portion of the narrowed segment
- 2 Collaterals reconstitute proximal portion of segment adjacent to narrowed segment
- 3 Collaterals reconstitute distal portion of segment adjacent to narrowed segment
- 4 Collaterals reconstituted two segments distal to narrowed segment
- 5 Little or no significant reconstitution of the territory served by the narrowed vessel segment.

Conclusions

Based on DSA, children appear to have a relatively high incidence of vasospasm, which often is moderate to severe in nature possibly due to their increased vasoreactivity as compared to adults. However, children rarely develop symptomatic vasospasm and have good long term outcomes, perhaps due in part to their robust cerebral collateral blood flow. Transcranial Doppler using adult criteria tends to overestimate the incidence of cerebral vasospasm in the pediatric population. Future studies with larger populations are needed to help define TCD vasospasm criteria for children.

KEYWORDS: Aneurysmal Subarachnoid Hemorrhage, Pediatric Cerebrovascular Disease, Vasospasm

0-72 11:19AM - 11:26AM
Semi-automated Computer Segmentation of Core Infarct Volume and Percentage of Infarcted Brain Parenchyma in Pediatric Acute Stroke: Developing Quantitative Metrics for Outcome Prediction

C Filippi¹, A El-ali², V Miloushev³, D Chow¹, J Choi⁴, X Guo¹, B Zhao¹

¹Columbia University Medical Center, New York, NY, ²Columbia University College of Physicians and Surgeons, New York, NY, ³Columbia University, New York, NY, ⁴University of Chicago School of Medicine, Chicago, IL

Purpose

The purpose of this study was to quantify core infarct volume and percentage of infarcted brain parenchyma on diffusion-weighted imaging in the setting of acute infarct in pediatric patients and to compare these quantitative metrics with clinical outcome.

Materials and Methods

Twelve male and 11 female patients, (age range 0-17.6 years, mean age 4.6 years) presenting with acute stroke were included. Exclusion criteria (4 patients) included inadequate follow up, inadequate imaging, prior infarction, and/or hemorrhagic transformation. Clinical follow up ranged from 0.8 to 19.3 months (mean 5.1 months). Clinical outcome was scored using the Pediatric Stroke Outcome Measure (PSOM). PSOM typically are scored as good (normal or mild deficit) and poor (moderate or severe). Validity of PSOM is not significantly affected when performed retrospectively (1-2). Using semi-automated

Note: Scanned images are included in the proceedings. Some submitted images were reduced during editing thereby decreasing clarity. Also, refer to the Program Planner. Proceedings Content as of 3/28/2014.

computer-assisted segmentation, core infarct volumes and total brain parenchymal volume were quantified by a medical student, radiology resident, and neuroradiologist with CAQ. Core infarct volumes and percentage of infarcted parenchymal volumes were compared among patients with good and poor outcomes using Wilcoxon rank sum test. Linear regression analysis was performed comparing PSOM to core infarct volume and percent volume of brain infarction. Inter-rater reliability was assessed using intraclass correlation coefficient (ICC).

Results

The ACA was affected in 30.0% (n=7), the MCA in 91.3% (n=21) of patients, and PCA and vertebrobasilar system in 52.1% (n=12) of patients. Eighteen patients had poor outcomes, including five deaths, and five had good outcomes. Mean core infarct volume for the good outcome group was 7.4 cc, 95% CI (0-24.2cc) and 75.7cc, 95% CI (35.5cc-177cc) for the poor outcome group, which was statistically significant ($p < .007$). Mean percentage of infarcted brain parenchyma was 0.6% for the good outcome group (95% CI of 0-2.1%) and was 10.4% for the poor outcome group (95% CI 1.8-31%), which was statistically significant ($p < 0.006$). There was a significant relationship between PSOM and infarct volume ($p < .01$) and percentage of brain parenchymal infarction ($p < .04$). Core infarct volumes greater than 32cc and percentage of infarcted brain parenchyma greater than 3% had poor outcomes in all cases. There was significant agreement between all the raters with an intraclass correlation coefficient (ICC) of 0.915 (range 0.831-0.961), $p < 0.001$.

Conclusions

Both core infarct volumes and percentage of infarcted brain parenchyma correlated with severity of outcome in pediatric acute infarct. Cut-off values above 32 cc for core infarct volume and 3% for percentage of infarcted brain parenchymal volume always were associated with a bad outcome.

KEYWORDS: Pediatric Brain, Stroke

0-73 11:26AM - 11:33AM

Brain Maturation is Delayed in Fetuses with Congenital Heart disease

A Vossough¹, C Limperopoulos², D Licht³

¹University of Pennsylvania/Children's Hospital of Philadelphia, Philadelphia, PA, ²Children's National Medical Center, Washington, DC, ³Children's Hospital of Philadelphia, Philadelphia, PA

Purpose

Congenital heart disease (CHD) is the most common birth defect. Brain injury and long term neuropsychological sequelae are common in children with complex congenital heart disease. Often these injuries are similar to the injuries seen in the immature brains of preterm neonates despite being born at term. Previously, it has been shown that infants with CHD have delayed brain maturation compared to normal newborns and brain immaturity is an important independent risk factor for brain injury in these

patients. The purpose of this study was to assess prenatal brain maturation in fetuses with complex CHD in the second half of pregnancy.

Materials and Methods

Fetal brain maturation was assessed by MR imaging (MRI) in 46 fetuses with CHD and compared to 48 normal controls. No fetus with a brain malformation or focal detectable abnormality was included in the study. A previously validated semiquantitative fetal total maturation score (fTMS) based on fetal brain MRI was utilized. The fTMS assesses fetal cortical sulcation in the frontal and occipital regions, insula, and temporal lobes, the degree of fetal brain myelination, and evolution of the germinal matrix, providing a single combined numerical value as a marker of brain maturity. Intraclass correlation coefficient was calculated to assess inter-rater reliability of the two independent and blinded readers. Linear regression analysis of fTMS versus gestational age was performed in the two groups and compared by an F test. Subgroup analysis also was performed for fetuses with the diagnosis of transposition of the great arteries and hypoplastic left heart syndrome as these two groups have a relatively high incidence of postnatal brain injury.

Results

The fetuses ranged from 25.1 to 36.7 weeks gestational age (median 29.0 weeks). The intraclass correlation coefficient for the readers was 0.89. Regression plots were constructed for normals (adjusted $R^2=0.94$, $p < 0.001$) and fetuses with CHD (adjusted $R^2=0.91$, $p < 0.001$). Statistical comparison of the regression analyses revealed that fetuses with CHD had a slower rate of brain maturation compared to healthy control fetuses ($p < 0.001$). The digression of the brain maturation trajectories started in the beginning of the third trimester. There was no difference in fetuses with transposition of the great arteries and hypoplastic left heart ($p=0.31$).

Conclusions

Brain maturation is delayed in fetuses with congenital heart disease compared to healthy controls, even in those without overt brain abnormalities, starting as early as the beginning of the third trimester. Future therapeutic trials aimed at prevention of brain injury in CHD should probably start during the fetal period.

KEYWORDS: Fetal Brain Development, Fetal Brain Injury, Fetal MR Imaging

0-74 11:33AM - 11:40AM

Susceptibility-weighted imaging in predicting neurodevelopmental outcome of early childhood in neonatal hypoxic ischemic injury after hypothermia therapy

T Bosemani¹, G Gerner², V Burton², M Leppert², E Cristofalo¹, M Allen¹, F Northington¹, M Johnston², T Huisman¹, A Poretti¹

¹The Johns Hopkins University School of Medicine, Baltimore, MD, ²Kennedy Krieger Institute, Baltimore, MD

Note: Scanned images are included in the proceedings. Some submitted images were reduced during editing thereby decreasing clarity. Also, refer to the Program Planner. Proceedings Content as of 3/28/2014.

Purpose

Susceptibility-weighted imaging (SWI) is a high-spatial-resolution, 3D, fully velocity compensated, gradient-echo magnetic resonance imaging (MRI) technique which accentuates the magnetic properties of blood, blood products, non-heme iron and calcification. The blood oxygen level dependent (BOLD) venography principle in SWI determines the signal intensity and prominence of the veins: veins draining critically perfused brain regions are more prominent/ hypointense due to increased oxygen extraction fraction and increased deoxyhemoglobin in the sulcal, subependymal and intramedullary veins. Hypoxic-ischemic injury (HII) occurs in 1-6/1000 live full-term newborns and carries a high-risk for subsequent neurodevelopmental disabilities. In neonatal HII, biomarkers for long-term neurodevelopmental prognosis are needed. In this preliminary study, we aim to study the role of SWI as a potential biomarker for HII. We hypothesize a correlation between hypointensity and prominence of veins on neonatal SWI and neurodevelopmental outcome at two years of age.

Materials and Methods

Inclusion criteria for this retrospective study were: neonates with HII and hypothermia therapy, SWI dataset in postcooling MRI and measurement of neurodevelopmental outcome at two years of age. Intubation and ventilation during MRI was an exclusion criterion. Susceptibility-weighted imaging acquisition parameters were: TR 49 ms, TE 40 ms, flip angle 15°, bandwidth 80 kHz, slice thickness 1.2 mm, FOV 201x230, matrix size 320x221, iPAT factor of two and axial minIP thickness accounts for 9.6 mm (8 slices). The prominence of intramedullary, sulcal and subependymal veins were graded for severity as: grade 0 = normal (healthy term neonate), grade 1 = mildly prominent and grade 2 = markedly prominent. Neurodevelopmental assessment using the Mullen Scales of Early Learning was conducted with all surviving children between 20 and 32 months. Statistical analysis with Spearman Rho was performed to correlate SWI grading with individual Mullen score criteria.

Results

Seven boys and seven girls with mean gestational age of 39 weeks (range: 37-41 weeks) and MRI performed at a mean postnatal life of 8.3 days (range: 4-14 days) were included. A significant correlation between higher hypointensity/prominence of subependymal veins and a lower standard Mullen score ($p=0.014$) as well as lower Mullen scores for visual reception ($p=0.026$) and expressive language ($p=0.009$) was identified. A positive correlation between severity of grading of sulcal veins and Mullen score for gross motor outcome also was noted.

Conclusions

Our preliminary data suggests that neonatal SWI (particularly hypointensity/prominence of subependymal veins) may play a role as a biomarker for neurodevelopmental outcome in neonates with HII and hypothermia therapy. Subependymal veins drain basal ganglia and thalami that have been shown to play a role in visual reception and expressive language in other neurological disorders. The positive correlation between

prominence of sulcal veins and gross motor score remains unexplained. Further studies including a higher number of patients are needed to corroborate our results.

KEYWORDS: Hypoxia, Outcome, Susceptibility-Weighted Imaging

O-75

11:40AM - 11:47AM

Pallidal Index: A Potential Predictor of Motor Outcome in Hypoxic Ischemic Encephalopathy

A Radmanesh¹, A Mathur, MD², P Srinivasakumar³, J Zempel², J Shimony⁴

¹Mallinckrodt Institute of Radiology, Saint Louis, MO, ²Washington University, Saint Louis, MO, ³Akron's Children Hospital, Youngstown, OH, ⁴Washington University School of Medicine, Saint Louis, MO

Purpose

To determine the value of Pallidal Index (PI) in predicting motor outcome in newborns with hypoxic ischemic encephalopathy (HIE).

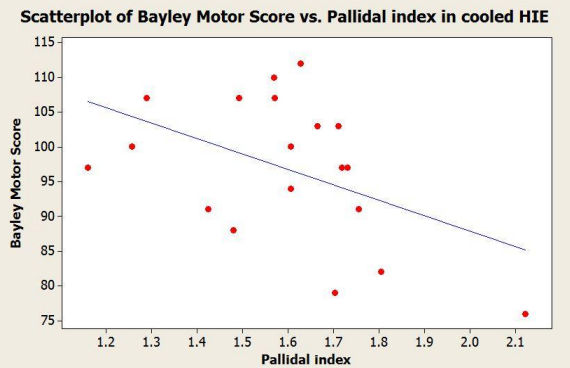
Materials and Methods

Infants with clinical diagnosis of HIE who were born at or referred to a tertiary Children's Hospital in 2010 and 2011 were selected for this retrospective study. Bayley scores documented by a pediatrician were retrieved from the patients' charts. Those who expired early, or had no Bayley scores available were excluded. Brain MR imaging (MRI) of the remaining 27 newborns were reviewed. Pallidal index was measured for each scan using axial T1-weighted images. Pallidal index was defined as the ratio of the signal intensity in the medial aspect of the right globus pallidus over the signal intensity of the right frontal subcortical white matter. Measurements of the signal intensity were performed using institutional image viewer, by drawing small regions of interest. Regression analysis was performed to assess correlation between the PI and sum composite scores for motor, language, or cognitive development in cooled and not cooled groups separately. The relationship between the PI and history of anticonvulsant therapy in the newborns also was evaluated.

Results

Twenty-seven MRI scans were reviewed (20 status postcooling; average gestational age:38.5 weeks; average age at the time of MRI: 6.6 days). The mean PI was 1.63 (SD=0.24). Lower PI was associated with higher Bayley motor score in the cooled group (P value = 0.04). There was no such significant correlation in newborns without cooling. There is no significant correlation between the PI and cognitive or language Bayley scores. The preliminary analysis of our data demonstrates lower PI in babies treated with anticonvulsant therapy.

Note: Scanned images are included in the proceedings. Some submitted images were reduced during editing thereby decreasing clarity. Also, refer to the Program Planner. Proceedings Content as of 3/28/2014.



Conclusions

Pallidal index, although originally introduced to be used in metabolic encephalopathies, correlates with Bayley composite motor score as an index of motor outcome in newborns with HIE. Therefore, PI should be considered as a potential predictor of motor outcome in HIE. In our preliminary analysis, newborns with prior anticonvulsant therapy had lower PI, which is an interesting observation worthy of further investigation in larger number of cases.

KEYWORDS: Encephalopathy, Globus Pallidus, Hypoxia

O-76 11:47AM - 11:54AM
 Pediatric Intracranial Aneurysms: A Spectrum of Underlying Pathological Conditions and Presentations in 15 Patients

M Pearl¹, E Wyse²

¹Johns Hopkins University School of Medicine, Baltimore, MD, ²Johns Hopkins Hospital, Baltimore, MD

Purpose

Intracranial aneurysms (IA) are rare in the general pediatric population and account for less than 2% of all cerebral aneurysms. Of the over 700 reported cases of pediatric aneurysms, the most common presentation is subarachnoid hemorrhage (80%) and the most common location is the internal carotid artery terminus. The purpose of this study was to describe the spectrum of underlying pathological conditions and clinical presentations in pediatric patients with intracranial aneurysms.

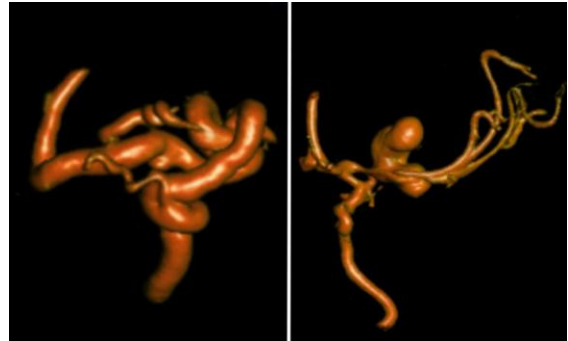
Materials and Methods

A retrospective review of the author's prospectively collected pediatric cerebral angiography database from July 2010 to October 2013 was performed. All pediatric patients with cerebral aneurysms (fusiform, saccular, and pseudoaneurysms) were included. Medical records were reviewed for age, gender, past medical history, clinical presentation, and treatment plan.

Results

From July 2010 to October 2013, 117 children underwent diagnostic or therapeutic cerebral angiograms. Of these, 15 children (7 boys and 8 girls), from 15 days to 19 years, had a total of 32 intracranial aneurysms. Clinical presentation was varied: subarachnoid hemorrhage (n = 3), stroke (n = 1), headache (n = 2), post-traumatic (n = 2), feeding artery

aneurysm for AVM (n = 1), incidental finding (n = 6). Underlying pathologies: sickle cell disease (n = 6), transcarbamylase deficiency (n = 1), AVM (n = 1), no significant past medical history (n = 7). Two patients underwent coil embolization. Two patients underwent surgical aneurysm clipping. The other eleven patients were managed conservatively with stability of their aneurysms documented by regularly scheduled MRI/MRAs and/or DSA.



Conclusions

Pediatric intracranial aneurysms are rare. Unlike the majority of cases reported in the literature, an increasing number of aneurysms are being detected as incidental findings in a number of underlying disease pathologies.

KEYWORDS: Aneurysm

O-77 11:54AM - 12:01PM
 Osseous Intramedullary Signal Alteration and Enhancement in Sturge-Weber Syndrome: An Early Diagnostic Clue

M Whitehead¹, G Vezina²

¹Children's National Medical Center, Arlington, VA, ²Children's National Medical Center, Washington, DC

Purpose

Sturge-Weber syndrome (SWS) is a sporadic phakomatosis with variable intracranial involvement. The full disease spectrum is typified by a facial nevus flammeus, ipsilateral choroidal angioma, and ipsilateral leptomeningeal angiomatosis of varying severity. Over time, imaging manifestations often evolve toward cerebral hemiatrophy and compensatory hemicalvarial enlargement known as the Dyke-Davidoff-Mason syndrome. However, recognizable imaging correlates may be lacking early in the disease process and in milder phenotypes. We have observed bone marrow signal changes to be quite prevalent across all SWS disease durations and phenotypes. The purpose of this study is to evaluate the presence and extent of bone marrow signal abnormalities and enhancement in patients with Sturge-Weber syndrome.

Materials and Methods

The Montage brain MR imaging database at a single academic children's hospital was queried for the term "Sturge-Weber" to build a cohort for retrospective analysis. The electronic medical record for each patient was

Note: Scanned images are included in the proceedings. Some submitted images were reduced during editing thereby decreasing clarity. Also, refer to the Program Planner. Proceedings Content as of 3/28/2014.

reviewed for the presence of a Sturge-Weber syndrome diagnosis. All relevant clinical information was collected. Images from each SWS patient's brain MR were reviewed by a board certified neuroradiologist. Bone marrow volume, signal, and enhancement patterns were specifically evaluated.

Results

A total of 20 brain MR exams from different SWS patients, with a mean age of 4.8 +/- 5.8 years (range 6 months - 16 years) met inclusion criteria. In all patients exhibiting a port wine stain (18/20), leptomeningeal enhancement, bone marrow T2 prolongation, and/or marrow enhancement was present ipsilaterally. Leptomeningeal enhancement was only present in 50% of all patients. However, 80% (16/20 patients), had unilateral bone marrow abnormalities (T2 prolongation and/or enhancement). In 35% (7/20 patients), unilateral bone marrow abnormalities occurred without accompanying leptomeningeal angiomas. The age of these patients were all < five years (6/7 < 2 years).



Conclusions

Bone marrow signal abnormality and enhancement is common ipsilateral to the nevus flammeus in Sturge-Weber syndrome. As this may be the sole brain MR abnormality in some patients, it may reflect mild SWS phenotypes or early disease manifestations prior to visible leptomeningeal angiomas. Adjunctive fat saturation techniques should be considered for bone marrow evaluation on brain MR work up in these patients.

KEYWORDS: Angioma, Bone Marrow, Phakomatoses

Monday, May 19
1:00 PM – 2:30 PM
517bc

13 - ASPNR PROGRAMMING:
PEDIATRICS TRAUMA (SAM)

O-78
Mild Accidental Brain Injury

1:00PM - 1:20PM

Girard, N.
Hopital Nord
Marseille

Abstract/Presentation Summary

TBI in children is one of the leading causes of childhood morbidity and mortality. Injuries can be divided by severity into mild, moderate, and severe cases. Mild TBI accounts for approximately 80% to 90% of all TBIs. Although long-term neurocognitive deficits are rare following mild TBI, children with mild TBI are more likely to display post concussive symptoms (PCS) than children with other types of injuries (1). Mild TBI was defined as head injury producing a Glasgow Coma Scale (GCS) of 13-15. Children are awake, may be confused but can communicate. However, studies showed that up to 40% of patients with an initial GCS of 13 had abnormal CT scans and 10% required neurosurgical treatment with outcome similar to moderate TBI. The accepted definition includes patients who have a GCS of 14-15 at initial presentation. In preverbal children a modified scale is used (2, 3). CT is recommended in children younger than 2 years who present altered mental status, palpable skull fracture, scalp hematoma, loss of consciousness (LOC), severe mechanism of injury, or not acting normally. Repeated vomiting, posttraumatic fit, and bulging tense fontanel are also clinically important to CT (4-7). In patients older than 2 years CT is recommended in patients with altered mental status or signs of basilar skull fracture. CT is also often performed in patients with history of LOC, vomiting, severe mechanism of injury, or severe headaches. CT scanning is the investigation of choice for patients with mild TBI at presentation to detect underlying pathology and the presence of surgically defined lesions that require neurosurgical treatment or hospitalization in the neurosurgical centre. MRI is not performed in all cases of mild TBI, but in selected cases because of neurologic symptoms after 2 days of follow up. Symptoms include subtle and nonspecific clinical signs as dizziness, worsening headaches and seizures. Because these symptoms may be delayed (15 days to 1 month), clinical follow up after discharge from the hospital is done at 3 weeks (or early). In the presence of such symptoms MRI is recommended to look for diffuse axonal injury (DAI). MRI protocol includes susceptibility weighting imaging, diffusion weighting imaging and tensor diffusion imaging (8-10). Spectroscopy is also reported. A group of older patients with frequent concussion injuries (football, ice hockey and soccer players) for several years has emerged in the past years. Structural changes are seen on brain imaging. MRI with advanced techniques is mostly performed in research setting (11).

Note: Scanned images are included in the proceedings. Some submitted images were reduced during editing thereby decreasing clarity. Also, refer to the Program Planner. Proceedings Content as of 3/28/2014.

0-79

1:20PM - 1:40PM

Abusive Head Trauma

Silvera, V.
Boston Children's Hospital
Boston, MA

Abstract/Presentation Summary

In young children, traumatic CNS injury is a leading cause of morbidity and mortality. In the United States, the incidence of abusive head trauma in children less than 2 years of age is estimated to be 17/100,000 person-years.¹ Classically, infants with abusive head trauma will present with retinal hemorrhages, subdural hematomas and encephalopathy. External signs of trauma are absent in as many as 50% of cases.² The history provided by the caretaker is often not reliable and will typically change over time or may be developmentally incompatible with the child's age. Radiographs, CT and MRI play an important role in the assessment of children with abusive head trauma. Skull radiographs and CT are most sensitive for detecting skull fractures and intracranial hemorrhage,³ while MRI is sensitive in the detection of hypoxic ischemic injury and white matter contusional tears.⁴ Hypoxic ischemic injury is often multifocal and in a non-arterial vascular distribution. Subdural hematomas, considered hallmark findings in infants with abusive head trauma, are most commonly located within the interhemispheric fissure and over the cerebral hemispheres.⁵ The appearance of subdural hematomas in these children is highly variable and may be challenging to interpret in regard to the timing of the subdural hemorrhage.⁶ In regard to outcome, 7-30% of children with abusive head injury die, 30-50% suffer significant cognitive or neurological deficits, and 30% have a chance for full recovery.⁷ In fatal cases of abusive head trauma, the cause of death is most commonly increased intracranial pressure related to severe brain edema. In this presentation attention will be focused on head imaging patterns that are most suggestive of abusive head trauma, the temporal evolution of imaging findings, and challenges related to dating of subdural hematomas.

0-80

1:40PM - 2:00PM

Clinical Management Directions in Mild TBI

Meehan, W.
Boston Children's Hospital
Boston, MA

Abstract/Presentation Summary

Recent studies have shown a 4 fold increase in the incidence of diagnosed concussions sustained by high school athletes,¹ and a 2-3 fold increase in the number of emergency department patients diagnosed with concussion.^{2,3} Approximately 23-30% of all pediatric patients diagnosed with a concussion in the emergency department sustained their injury during sports participation.³⁻⁵ The CDC estimates that as many as 3.8 million sport-related traumatic brain injuries occur each

year, the vast majority of which are concussions.⁶ Concussion is caused by a rapid spinning or rotational acceleration of the brain. Biomechanical forces that result in a rotational acceleration of the brain and impart a shear strain on the underlying parenchyma, induce the signs and symptoms of concussion.^{7,8} The leading hypothesis regarding the pathophysiology of concussion suggests that this shear strain results in deformation of the axonal membrane, leading to a massive influx of sodium and calcium, and a corresponding efflux of potassium. An unorganized depolarization of neurons ensues, causing a spreading depression-like phenomenon, with the release of excitatory amino acids such as glutamate.⁹⁻¹² The sodium-potassium pump works to return sodium to outside of the axonal membrane, a process which requires adenosine triphosphate (ATP). Given the large disruption of ionic gradients, large amounts of ATP are required.¹³ ATP is derived from glucose, delivered by blood flow to the neurons. For a period of days to weeks after concussion, however, there is decreased blood flow to the brain.^{11,14} Thus, there is an inadequate supply to meet the increased demand for ATP, and this supply-demand mismatch is thought to result in the prolongation of concussion symptoms. Concussions are assessed by using symptom inventories, standardized balance assessments, and neurocognitive evaluations, either computerized or in person with a neuropsychologist. Once it has been established that an athlete has sustained a concussion, and other potential concomitant injuries have been addressed or ruled out, treatment may begin. The foundations of treatment begin with physical and cognitive rest. Most athletes recover quickly from concussions, in a matter of days to weeks. Studies show that well over 90% of collegiate and high school athletes that sustain a sport-related concussion have full resolution of their symptoms and are deemed recovered by medical personnel within a month.¹⁵⁻¹⁸ Thus, physical and cognitive rest is often the only treatment required for the vast majority of athletes suffering sport-related concussions. If symptoms persist beyond a month, referral to a clinician specializing in the management of concussions should be considered. Such clinicians can offer a thorough assessment for other potential contributing etiologies and therapies for prolonged headaches, sleep disturbance, vestibular dysfunction, mood disorders, and cognitive difficulties.¹⁹⁻²² Once recovered, athletes are gradually returned to their sports, starting with light aerobic activity, and progressing in a stepwise fashion through the return-to-play stages outlined by the international consensus on concussion in sport, so long as they remain symptom free.²³

2:00PM - 2:30PM

Questions and Answers

Note: Scanned images are included in the proceedings. Some submitted images were reduced during editing thereby decreasing clarity. Also, refer to the Program Planner. Proceedings Content as of 3/28/2014.

Monday, May 19
1:00 PM – 2:30 PM
517d

14 - ASHNR PROGRAMMING:
THYROID/ORBIT/PET

O-81 1:00PM - 1:30PM
Imaging of Visual Loss

Juliano, A.
Massachusetts Eye & Ear Infirmary
Boston, MA

Abstract/Presentation Summary

The visual pathway begins in the globe, where light makes its initial encounter, and includes sequentially the cornea, aqueous humor, lens, vitreous humor, and retina. It continues with the optic nerve, optic chiasm, optic tract, lateral geniculate nucleus of the thalamus, finally reaching the occipital lobe via the optic radiation. Abnormalities of the globe are frequently diagnosed clinically by ophthalmologists, with imaging playing a secondary though sometimes important and confirmatory role especially in the setting of trauma or a congenital anomaly. Optic nerve abnormality is usually suspected based on the classic clinical findings of visual field defect, dyschromatopsia, and afferent pupillary defect, but requires imaging evaluation for more precise delineation and characterization of the pathology, as well as for search of a potential underlying cause. As an example, MR imaging can confirm the presence of optic neuritis, but in addition may demonstrate white matter lesions in the brain suggesting to the clinician the diagnosis of a demyelinating disease. MR imaging can also distinguish between the more common causes of visual loss related to the optic nerve seen in adults, namely optic neuritis, optic nerve atrophy, and compressive optic neuropathy from a perioptic meningioma. Disturbance of the optic chiasm produces the infamous bitemporal hemianopsia. Here, imaging again plays an important role in assessment for any pituitary or suprasellar lesion. Symptoms pointing to lesions affecting the optic radiation or occipital lobe require imaging evaluation for a parenchymal lesion in the brain. In this presentation, the role of radiology in the evaluation of more common pathologies involving the globe, optic nerve, and optic chiasm is explored, including discussion of important associated findings that should be included in the radiologist's checklist and noted in our reports.

O-82 1:30PM - 2:00PM
Imaging of Congenital Hearing Loss

Moonis, G.
Beth Israel Deaconess Medical Center
Boston, MA

O-83 2:00PM - 2:30PM
Imaging of Salivary Gland Lesions

Kassel, E.
Princess Margaret Hospital
Toronto, ON

Abstract/Presentation Summary

This presentation will have greater discussion directed to the parotid glands as the most frequently directed salivary imaging request and will emphasize mass lesions and their variable imaging presentations, with limitations as to their benign vs. malignant character. Comments will include solitary/ multiple/ diffuse and cystic lesions and include non-neoplastic entities (congenital) with limited discussion of obstructive salivary disease, with proportionate emphasis on the more common parotid masses or those lesions with characteristics allowing identification such as recurrent pleomorphic adenoma and carcinoma ex pleomorphic adenoma. Implications re character of the parotid capsule and its late encapsulation will be mentioned. Perineural tumor spread emphasizes the need to fully assess a proper field of study and not just the primary space of the involved salivary gland. Only 20% of parotid masses are malignant yet diligence to detect the malignant nature/ extent or to suggest tissue sampling or further follow up studies, or consider a role apparent diffusion coefficient (ADC) mapping of salivary gland tumors may play. Submandibular gland discussion includes mass lesions, benign and malignant, clues to the nature of the mass/ whether the mass arises within or external to the gland. Abutting nodal adenopathy, especially lymphoma or nodal SCCa metastasis, need to be differentiated from a primary SMG neoplasm. Primary SMG malignancy occurs in 45-50% of SMG neoplastic masses (usually Adenoid Cystic Ca (ACCa), mucoepidermoid ca (MEC) or adenoca (AdCa). Masses centered within the SMG invading adjacent tissues suggest malignancy. Main differential from malignant SMG mass includes pleomorphic adenoma (BMT), sialadenitis, SMG mucocele. Sublingual gland lesions, as with SMG masses, require attention because of likelihood for malignancy, recent data having SLG tumors approaching 80% malignancy rate. As with SMG masses, adjacent adenopathy favors mucoepidermoid carcinoma while perineural spread favors adenoid cystic ca. Hematogenous spread (usually lungs) favors ACCa. Main differentials include carcinoma of the FOM (usually clinical diagnosis), venolymphatic malformation and ranula. Dehiscence of the mylohyoid muscle, extension of the SLG into the submandibular space is discussed. Minor salivary gland tumors include lesions arising within the oral cavity/oropharynx, nasopharynx and sinonasal cavity. This presentation will be practical,

Note: Scanned images are included in the proceedings. Some submitted images were reduced during editing thereby decreasing clarity. Also, refer to the Program Planner. Proceedings Content as of 3/28/2014.

includes common salivary gland pathologies but also pitfalls in diagnosis by misinterpretation of anatomic landmarks or limitations by the imaging modality chosen.

Monday, May 19
1:00 PM – 2:30 PM
Room 517a

**15 - GENERAL PROGRAMMING: PAIN AS
 A BRAIN DISEASE: NATURE VERSUS
 NURTURE**

O-84 1:00PM - 1:30PM
 Pain and Brain Structure and Function

Prabhakaran, V.
 University of Wisconsin-Madison
 Madison, WI

Abstract/Presentation Summary

In the United States, the prevalence of chronic pain has been estimated to be approximately 30% and about 116 million Americans are living with chronic pain (Debono et al., Institute of Medicine). Neuroimaging using fMRI can help elucidate the mechanisms underlying pain (Tracey and Bushnell, 2009) and several studies have shown altered cerebral processing due to either experimentally induced or disease-related pain in different patient groups (fibromyalgia, irritable bowel syndrome, chronic back pain etc.). Functional MRI (fMRI) has helped to identify brain regions underlying the experience of pain and dissected these into anatomically distinct activities of different functional systems (e.g. somatosensory, limbic systems)(Tracey, 2005). This has clinical significance because it identifies distinct targets for therapeutic modulation. fMRI can capture the variability of responses even on a single subject level; for example, inter-individual differences in pain responses can be found in the primary somatosensory, anterior cingulate and prefrontal cortices (Coghill et al., 2003). In this review, I will focus on the brain regions associated with pain processing, modulation of activity in these regions due to manipulations that reduce pain perception, and alterations in functional connectivity due to chronic pain.

O-85 1:30PM - 2:00PM
 fMRI Biomarkers of Pain

Wager, T.
 University of Colorado at Boulder
 Boulder, CO

O-86 2:00PM - 2:30PM
 Structural Abnormalities in Migraines

Filippi, M.
 San Raffaele Scientific Institute, Vita-Salute San Raffaele
 University
 Milan

Abstract/Presentation Summary

In the past few years, the application of magnetic resonance imaging (MRI) techniques to study patients with migraine has changed our view of migraine from primarily a vascular disorder to a neurovascular disease and currently to a central nervous system (CNS) disorder. Abnormal function of key brain areas and networks, mainly involved in pain processing, has been shown to occur in the brain of migraineurs. Numerous conventional MRI studies have described an increased risk of harbouring white matter hyperintense lesions in migraineurs, that might be influenced by headache frequency, disease duration and the presence of aura. The application of modern MRI techniques has also revealed diffuse structural abnormalities of the brain gray and white matter. Specifically, the involvement of key brain areas and networks, mainly involved in pain, visual and sensorymotor processing, has been shown to occur in the brain of migraineurs. In addition, the application of morphometric techniques is contributing to identify the structural correlates of some of the clinical deficits that are typically detected in migraineurs in clinical practice. All of this is critical not only to improve the understanding of migraine pathophysiology, but also to characterize better its heterogeneous clinical manifestations, and to develop imaging biomarkers to be applied in treatment trials of new experimental drugs.

Monday, May 19
1:00 PM – 2:30 PM
Room 520

**16 - YOUNG PROFESSIONALS
 PROGRAMMING: HEALTH CARE
 REFORM EDUCATION AND UPDATE**

O-88 1:00PM - 1:40PM
 Political Advocacy for the Neuroradiologist

Turski, P. · Tu, R.
 University of Wisconsin · Progressive Radiology
 Madison, WI · Washington, DC

Abstract/Presentation Summary

The presentations will provide an overview of the opportunities for neuroradiologists to advocate for their specialty through the American Society of Neuroradiology (ASNR), the American College of Radiology (ACR) the

Note: Scanned images are included in the proceedings. Some submitted images were reduced during editing thereby decreasing clarity. Also, refer to the Program Planner. Proceedings Content as of 3/28/2014.

American Medical Association as well as local and national organizations. Dr. Turski is past Chair of the ASNR Health Policy Steering Committee which oversees the Quality, Safety and Value Committee, the Economics Committee and the Standards and Guidelines Committee. Dr. Turski will review the activities and personnel associated with each committee. A case example will be presented demonstrating how Dr. Turski became a political advocate for neuroradiology when magnetic resonance angiography was introduced into clinical practice 25 years ago. He will further use this example to explain the relationship of AMA CPT Codes, AMA Relative Value Units, ACR standards and Guidelines, ACR Appropriateness criteria and the coordination between the ASNR Health Policy Committee and the ACR Neuroradiology Commission. Dr. Tu is a radiologist in Washington, DC. He is Clinical Associate Professor of Radiology at The George Washington University in Washington DC, Chairman of Radiology at United Medical Center and Partner of Progressive Radiology, the largest physician owned imaging company in the State of Maryland. Dr. Tu is a native Washingtonian and will share his story how his involvement in local life in the District of Columbia brought insight and access to health policy from the local to national scene. As the sole radiologist to have served on the DC Board of Medicine during his tenure, ACR Chapter President, hospital Chairman, Chair of the ACR Medicaid Network and ASNR Advisor to CPT his dedication to public service Dr. Tu will show how he did it.

O-89 1:40PM - 2:20PM
Healthcare Reform Impact on Neuroradiology

Bello, J.
Montefiore Medical Center
Bronx, NY

Abstract/Presentation Summary

This presentation will attempt to decipher the "alphabet soup" that comprises the undercurrent within the stormy sea of Healthcare Reform. The underpinnings of Healthcare Reform will be addressed from a recent historical perspective. Contributing components of the reimbursement cycle will be defined, including the Current Procedural Terminology (CPT) and Relative Value Update Committee (RUC) processes. Their relative importance and relationship to CMS will be described. Radiology's position in today's challenging and changing climate of healthcare reform will be analyzed; potential future roles for Radiology in alternative delivery models will be explored. Neuroradiology's current status in organized medicine will be discussed, including ASNR's involvement in both the AMA and ACR. A summary of recent legislative challenges will be presented and ongoing advocacy efforts will be reviewed. Strategies for protecting our profession will be suggested, including the need to integrate radiology and stewardship into the undergraduate medical curriculum at an early stage, and to include healthcare policy and economics within our graduate medical education

curriculum. Emphasis will be placed on the importance of being or becoming involved.

2:20PM - 2:30PM

Discussion

Monday, May 19
1:00 PM – 2:30 PM
Room 524

17 - PARALLEL PAPERS: ADULT BRAIN: STRUCTURAL AND FUNCTIONAL IMAGING

O-90 1:00PM - 1:07PM
Music and the Brain: fMRI Activation Patterns of Classical and Rap Music

Y Safriel
Radiology Associates of Clearwater/University of South Florida, Belleair Beach, Florida

Purpose

Music therapy has been used successfully in rehabilitation by health care professionals. Athletes and performers also use music to prepare for events. While the effects of music and music therapy have been published, the activation pattern, connectivity and mechanism of action is not completely understood. As part of a pilot study evaluating the effect of different types of music on patients and performance athletes, we compared the activation pattern of two markedly different types of music.

Materials and Methods

Review Board approval was obtained. Volunteers between the age of 25 and 49 were recruited. Eight subjects were scanned, two females and six males. BOLD acquisition was obtained with the subjects listening to two separate paradigms each comprising 5 cycles of 30 seconds of active/rest (green/red on attached figure respectively). The first paradigm was classical music (Violin Concerto #5 in A, WA Mozart, Berlin Philharmonic, Deutsch Gramophone) and the second paradigm was rap music (Low, Flo Rida, Mail on Sunday, Atlantic and Poe Boy). The rest state was 30 seconds of silence. Prior to BOLD scanning, 3D volumetric acquisition and GRE field map of the head was obtained. BOLD functional MRI (fMRI) was performed on a Siemens 3 T Trio using standard parameters that also are used for presurgical evaluation. Images were analyzed using the in-line workstation (Leonardo, Siemens, Germany) with a visually supervised measurement routine.

Results

There were striking differences in activation for both 'music' (active) and 'silence' (rest) between the classical and rap paradigms. Rap music showed strong activation in the auditory cortex symmetrically bilaterally. Classical music showed activation in similar areas but of markedly

Note: Scanned images are included in the proceedings. Some submitted images were reduced during editing thereby decreasing clarity. Also, refer to the Program Planner. Proceedings Content as of 3/28/2014.

lesser magnitude. The silent state was similar for both paradigms and significantly less than the active state.



Conclusions

Functional MRI shows striking differences between classical and rap music. This information may have impact on music therapy and the type of music played to patients during MRI, amongst other implications. Future study directions include defining the connectivity related to various types of music and evaluation of variations of measurements between different pieces in the same music type.

KEYWORDS: FMRI, Functional Connectivity MR, Functional Networks

0-91 1:07PM - 1:14PM
Identification of the hand motor cortex: comparison of structural imaging with functional MR imaging and corticospinal tractography

N Sahin¹, S Mohan², P Maralani², S Duddukuri³, E Melhem⁴, R Wolf²

¹Sifa University School of Medicine, Izmir, Turkey, ²University of Pennsylvania, Philadelphia, PA, ³K.V.G Medical College and Hospital, Hyderabad, India, ⁴University of Maryland Medical Center, Baltimore, MD

Purpose

Identification of the central sulcus for localizing primary motor cortex is crucial in presurgical planning for brain lesions in proximity; however, localization of this region based on morphologic features is not always straightforward. Normal anatomical variations, mass effect from space-occupying lesions, and congenital malformations such as cortical dysplasias can create uncertainty. In addition, reorganization can occur with chronic injuries and slowly progressing pathology. The purpose of this study was to compare the accuracies of different methods for identification of primary motor cortex based on structural MRI as compared to functional MR imaging (fMRI) and diffusion tensor imaging (DTI) fiber tracking of the corticospinal tract (CST) in the involved and contralateral hemisphere of patients with brain lesions.

Materials and Methods

Fifty-five patients (22 men and 33 women; mean age: 54.5 years) with brain lesions and prior MRI with motor fMRI were identified for this HIPAA-compliant retrospective

study. At least one motor task for each fMRI was available in 109 hemispheres. Diffusion tensor imaging fiber tracking of the CST was available in 86 hemispheres. Three different methods were used to define the central sulcus on 3D MPRAGE T1-weighted sequences for structural analysis: (1) following the typical course of the superior frontal and precentral sulci (the axial method), (2) identification of the typical shape of the motor hand area (the precentral knob), and (3) difference of cortical thickness in precentral gyrus. One radiologist with 10 years of experience applied each method in all hemispheres and a confidence rating was assigned to each method, using a 5-point scale. Concordance between structural analysis and fMRI and DTI fiber tracking was assessed by two neuroradiologists with 13 and seven years of experience after training.

Results

All three structural anatomical localization methods could be applied to all hemispheres, except for two failures using the axial method secondary to anatomical variation. On fMRI studies, task-related activation localized central sulcus with high confidence in all but six hemispheres. Tracking of CST identified the central sulcus in all 86 hemispheres, concordant with fMRI. Central sulcus identification based on cortical thickness was the most accurate method, with the highest confidence rating (mean score: 4.99) in 100% of the patients. Precentral knob morphology also permitted the recognition of the central sulcus in all of the patients, but confidence rating (mean score: 4.7) was lower. The axial method was least accurate (mean score: 4.35).

Conclusions

The difference in cortical thickness across the central sulcus is a reliable anatomical landmark for identification of the precentral gyrus as compared to localization with fMRI and DTI fiber tracking; however, cases of decreased confidence or failure also occur with fMRI and DTI fiber tracking and thus structural assessment remains complimentary to these techniques. In addition, localization of specific motor functions is not sufficiently accurate based on anatomical landmarks and requires fMRI, especially when anatomical landmarks are distorted or reorganization may have occurred. Functional MRI and DTI fiber tracking improves the confidence and efficiency of presurgical planning in patients with brain lesions.

KEYWORDS: Diffusion Tensor Image, FMRI, Glioma

0-92 1:14PM - 1:21PM
The Effect of Hyperbaric Oxygen Treatment on Resting State Networks

M Allen¹, J Davidson², J Davidson², M Benzaquen², B Ances¹, T Benzinger³, J Rutlin¹, M Brier⁴, E Leuthardt¹, J Shimony¹
¹Washington University, Saint Louis, MO, ²St Luke's Hospital, Chesterfield, MO, ³Mallinckrodt Institute of Radiology/Washington University, Saint Louis, MO, ⁴Washington University in St. Louis School of Medicine, Saint Louis, MO

Note: Scanned images are included in the proceedings. Some submitted images were reduced during editing thereby decreasing clarity. Also, refer to the Program Planner. Proceedings Content as of 3/28/2014.

Purpose

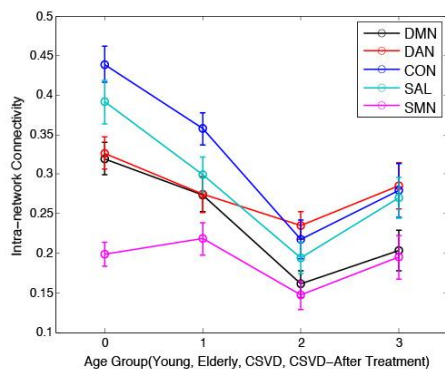
Hyperbaric oxygen (HBO) treatment is an established method to improve wound healing in the extremities by stimulating angiogenesis. A similar effect in the brain has not been well established. Resting-state functional magnetic resonance imaging (rsfMRI) has been used to reliably identify and study resting state networks (RSN) in the brain. The purpose of this project was to evaluate if HBO treatment can help patients with chronic cerebral small vessel disease (CSVD) by measuring changes in connectivity of RSN.

Materials and Methods

Twenty patients >50 years of age with chronic cerebrovascular disease were recruited from the community. Patients were scanned using rsfMRI before and approximately four weeks after they were treated with hyperbaric oxygen therapy. Subjects were treated in Sechrist Monoplace Hyperbaric Chambers at a pressure of two atmospheres absolute for 45 minutes using 100% oxygen. Subjects were given 10 treatments over a span of two weeks (5 treatments per week). Twenty age-matched controls and 17 young adult healthy controls were selected from other ongoing studies at our institute. Resting-state fMRI preprocessing was performed using standard methods. Thirty-six regions of interest associated with the following RSN were selected for analysis: Default Mode (DMN), Dorsal Attention (DAN), Control (CON), Salience (SAL), and Somatomotor (SMN). The correlation matrix between all regions was calculated and transformed using the Fisher z-transform to obtain normal distributions. The internetwork and intranetwork connectivity for these five RSN was measured and compared across groups.

Results

The figure demonstrates the changes in the different intranetwork connectivity across the groups. The intranetwork connectivity of all five RSN in the young control group was highest of all and decreased in the elderly normal controls in all networks, except for the SMN network, which increased slightly. In every network, the connectivity decreased in the elderly patients with CSVD. The connectivity in this group of patients shows improvement after HBO therapy in each of the five networks.



Conclusions

Resting-state networks can be used to monitor treatment of disease in the brain, and the current study provides

preliminary evidence that HBO treatment can be used to improve RSN connectivity in patients with CSVD.

KEYWORDS: Cerebrovascular Disease, Functional Connectivity, Resting-State fMRI

O-93

1:21PM - 1:28PM

RESTING STATE NETWORKS (rs-fcMRI) in HIV ASSOCIATED NEUROCOGNITIVE DISORDER (HAND) AND CORRELATION WITH BLOOD BRAIN BARRIER DISRUPTION AND MR SPECTROSCOPY

J Chaganti¹, B Brew²

¹St. Vincents Hospital, Sydney, Australia, ²University of New South Wales, New South Wales

Purpose

Resting-state functional connectivity could be a sensitive marker for neurocognitive impairment in HIV-associated neurocognitive disorder in the era of highly active antiretroviral therapy and may provide an understanding to the association of the accelerated aging in HIV.

Materials and Methods

We used resting state fMRI study to measure the intermodal and intranodal connectivity among five functional brain networks in 30 HIV-infected participants who are on highly active antiretroviral therapy and seven age- and sex-matched healthy volunteers. We compared the results with the blood-brain barrier integrity and neuronal integrity measures by MRS and plasma and CSF viral load.

Results
The HIV-infected patients demonstrated decreased rs-fcMRI intra network correlations in the salience networks (SN), default mode networks (DMN), control networks (CN) and dorsal attention networks (DAN) while sensorimotor network (SMN) showed no significant change. Internodal correlation demonstrated reduced correlation between DMN-DAN as well as DMN-SAL while there appears to be a trend in increase between the CN-SAL and CN-SMN. Correlative studies with plasma and CSF viral load as well as CD-4 count did not show any correlation with rs-fcMRI results. There is a trend towards positive correlation with disrupted blood-brain barrier and neuronal loss on spectroscopy.

Conclusions

HIV-associated neurocognitive disorder could be a causative factor in decrease in the rs-fcMRI and appear identical to the age-associated cognitive decline. Reduced neuronal integrity and blood-brain barrier disruption could be contributory/comorbid factors for affection of the resting state networks.

KEYWORDS: Highly Active Antiretroviral, HIV, Neurocognition

Note: Scanned images are included in the proceedings. Some submitted images were reduced during editing thereby decreasing clarity. Also, refer to the Program Planner. Proceedings Content as of 3/28/2014.

0-94 1:28PM - 1:35PM
Diffusion Tensor Imaging Detects Early Microstructural Hypothalamic Changes Associated with Cognitive Dysfunction in Obese Subjects

J Puig¹, G Blasco¹, J Daunis-i-Estadella², X Molina³, R Rodriguez⁴, M Serrano⁴, G Xifra⁴, W Ricart⁴, F Fernandez-Aranda⁵, S Pedraza¹, J Fernandez-Real⁴

¹Girona Biomedical Research Institute (IDIBGI), Hospital Dr Josep Trueta, Girona, Spain, ²University of Girona, Girona, Spain, ³Biomedical Research Institute (IDIBGI), (IDI), Hospital Universitari de Girona, Girona, Spain, ⁴IDIBGI, Hospital University Dr Josep Trueta, CIBERobn, Girona, Spain, ⁵Hospital Universitari de Bellvitge, CIBERobn Hospitalet de Llobregat, Barcelona, Spain

Purpose

Despite progress in understanding the neurobiology of energy homeostasis, little is known regarding how brain systems that promote weight stability are altered in obesity. Growing evidence implicates hypothalamic inflammation in the pathogenesis of diet-induced obesity and cognitive dysfunction in rodent models. Few studies have addressed the association between obesity and hypothalamic damage in humans and its relevance. We sought to evaluate obesity-associated hypothalamic damage by diffusion tensor imaging (DTI) together with its impact on cognitive function.

Materials and Methods

We prospectively studied 24 consecutive middle-aged obese subjects (13 women; 49.8±8.1 years; BMI 43.9 ± 0.92 Kg/m²) and 20 healthy volunteers (10 women; 48.8±9.5 years; BMI 24.3 ± 0.79 Kg/m²). All patients underwent 1.5 T MRI (Intera, Philips Healthcare, Best, the Netherlands) including axial FLAIR and DTI sequences. Diffusion-sensitized gradients were applied along 15 noncollinear directions with a b-value of 1000 s/mm². Diffusion tensor images were coregistered, and a neuroradiologist blinded to all clinical information placed free-hand regions of interest in the right and left sides of the hypothalamus using dedicated software (Olea Sphere V.2.0, Olea Medical, La Ciotat, France). Primary (λ_1), secondary (λ_2), and tertiary (λ_3) eigenvalues, FA, and mean diffusivity (MD) were calculated. Cognitive function was evaluated with neuropsychological tests. Receiver operator characteristic curves were used to calculate the DTI-metrics cutoffs to predict obesity-associated hypothalamic damage.

Results

Mean λ_1 values for the hypothalamus were significantly lower in obese subjects ($P<0.001$). The mean hypothalamic λ_1 cutoff point that best discriminated obese and control subjects was 1.072, yielding 75% sensitivity, 87.5% specificity, 83.3% PPV, and 80.7% NPV for hypothalamic damage (AUC, 0.854; 95% CI, 0.742-0.96) (Figure). No significant differences were found for λ_2 , λ_3 , FA, or MD (Table). Patients with hypothalamic $\lambda_1<1.072$ had significantly increased BMI and blood inflammatory markers. Loss of hypothalamus gray matter defined as $\lambda_1<1.072$ significantly correlated with cognitive impairment. Combined

BMI and alanine aminotransferase was the strongest predictor of obesity-associated hypothalamic damage (AUC=0.89).

	Obese (n=24)	Control (n=20)	p-value
Sex (male/female)	13-Nov	10-Oct	0.783
Age (years)	49.875(8.158)	48.85(9.511)	0.706
BMI (kg/m ²)	43.987(4.548)	24.305(3.548)	<0.001
Waist circumference (cm)	115.896(37.612)	84.35(10.261)	0.001
Systolic blood pressure (mmHg)	142.625(20.334)	120.9(11.947)	<0.001
Total cholesterol (mg/dl)	190.75(46.731)	202.9(30.953)	0.309
HDL-cholesterol (mg/dl)	46.875(11.078)	63.35(15.618)	<0.001
Triglyceride (mg/dl) log transformation	4.61(0.532)	4.203(0.454)	0.009
HOMA-IR (mean ± SD)	4.838(3.149)	0.97(0.906)	<0.001
Ultrasensitive CRP (mg/dl)	0.877 (0.843)	0.137(0.152)	<0.001
Primary eigenvalue	1.014(0.984 - 1.040)	1.112(1.046 - 1.162)	<0.001
Secondary eigenvalue	0.673(0.611 - 0.728)	0.767(0.665 - 0.812)	0.105
Tertiary eigenvalue	0.395(0.334 - 0.433)	0.440(0.351 - 0.535)	0.096
Fractional anisotropy	0.393(0.369 - 0.444)	0.410(0.380 - 0.440)	0.427
Mean diffusivity	0.755(0.724 - 0.817)	0.802(0.727 - 0.843)	0.337

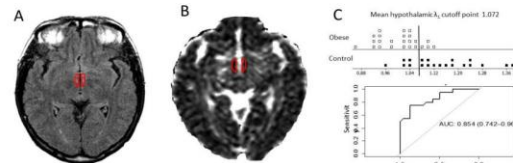


Figure. FLAIR images (a) and diffusion tensor images (b) were coregistered and a free-hand region of interest was placed on the hypothalamus. c, Primary eigenvalues (λ_1) for the hypothalamus were lower in obese subjects ($P<0.001$). We calculated the λ_1 cutoff to predict hypothalamic damage with receiver operator characteristic curves.

Conclusions

Our preliminary data indicate that λ_1 could be a useful DTI-metric for assessing hypothalamic damage in obese individuals. Further studies are needed to validate the quantification of DTI-metrics as a noninvasive tool for detecting obesity-induced damage in the hypothalamus.

KEYWORDS: Cognitive Deficit, Diffusion Tensor Image, Hypothalamus

0-95 1:35PM - 1:42PM
Diffusion Tensor Tractography of Pyramidal Tract in Brainstem: A Study on Optimal Reduction Factor in Parallel Imaging

Y Bae, Park, J Kim, B Choi, E Kim, C Jung
Seoul National University Bundang Hospital, Seongnam-si, Gyeonggi-do, Korea

Purpose

Single-shot echo planar imaging (EPI) has inherent drawbacks including low signal-to-noise ratio (SNR) and susceptibility artifact. Susceptibility artifact in EPI is remarkable particularly at the pons-sphenoid interface causing severe image distortion of the pons. This makes the use of diffusion tensor tractography (DTT) based on EPI limited at the pons level. However, parallel imaging applied to EPI can mitigate aforementioned drawbacks owing to the reduction of phase encoding steps. In parallel imaging, reduction (R) factor indicates a ratio of original phase encoding steps to reduced phase encoding steps. Therefore, parallel imaging for DTT through the pons needs an optimal R to achieve both higher SNR and less image distortion. The purpose of this study is to find optimal R factor for DTT through the pons.

Materials and Methods

We measured SNR, image distortion and the number of the corticospinal tract fiber at different values of R. This study was conducted with ten healthy volunteers (9 male, 1 female; median age, 30 years, range 27 - 43 years).

Note: Scanned images are included in the proceedings. Some submitted images were reduced during editing thereby decreasing clarity. Also, refer to the Program Planner. Proceedings Content as of 3/28/2014.

Diffusion tensor imaging was performed at 3 T based on single-shot EPI with following parameters: diffusion gradient direction = 15, b value = 1000 s/mm², voxel size = 2 x 2 x 2 mm³ and was repeated with R = 1, 2, 3, 4, 5. First, SNR was calculated using signal intensity measured on b = 0 image and noise value measured on noise map. Second, image distortion was evaluated by measuring anteroposterior diameter of the pons on b = 0 image. Lastly, the number of the corticospinal tract fiber was calculated. Diffusion tensor tractography was conducted for right and left pyramidal tracts passing through the pons in 10 subjects (total 20 tracts). Signal to noise ratio, image distortion and the fiber number of the tract were compared between different R using Friedman test. P value less than 0.05 was considered to be statistically significant.

Results

Each of SNR, image distortion and fiber number of the tracts was significantly different between different R. Maximal SNR was achieved at R factor 2 in nine out of 10 subjects and at R factor 3 in only one subject ($p < 0.01$). Image distortion was decreased continuously with the increase in R factor. The least image distortion was achieved at R factor 5 in nine out of 10 subjects ($p < 0.01$). The fiber number of the corticospinal tracts through pons was maximal at R factor 3 in 11 out of 20 tracts, followed by R factor 4 (6 tracts) and R factor 2 (2 tracts) ($p < 0.01$). Conclusions

For DTT of corticospinal fiber tracking at brainstem, R factor 3 is considered optimal, balancing between SNR and image distortion. Our results reflect that DTT is influenced by a combination of SNR and image distortion which vary differently depending on R factors. Further technical improvement in parallel imaging such as better coil design and less reconstruction artifact may allow higher R factor useful in DTT in the future.

KEYWORDS: Corticospinal Tract, Diffusion Tensor Image, Parallel Imaging

0-96 1:42PM - 1:49PM
Relationship between white matter integrity and serum cortisol levels in drug-naïve major depressive disorder patients: a diffusion tensor imaging study using tract-based spatial statistics

X Liu¹, K Watanabe², S Kakeda², R Yoshimura², O Abe³, S Ide², K Hayashi², A Katsuki², W Umene-Nakano⁴, R Watanabe², I Ueda², J Nakamura², Y Korogi²

¹University of Occupational and Environmental Health & First Affiliated Hospital of Jinan University, Guangzhou, Guangdong, China, ²University of Occupational and Environmental Health, School of Medicine, Kitakyushu-shi, Fukuoka-ken, Japan, ³Nihon University School of Medicine, Tokyo, Japan, ⁴University of Occupational and Environmental Health, School of Medicine, Kitakyushu-shi, Fukuoka-ken, Japan

Purpose

In major depressive disorder (MDD) patients, the frontal-subcortical circuits and frontal-limbic circuits are proposed as important pathogenic elements. A higher daytime cortisol level due to a hyperactive hypothalamic-pituitary-adrenal axis also have been reported in MDD. Our aim was to evaluate the relationship between the white matter (WM) integrity and serum cortisol levels during the first depressive episode in drug-naïve MDD patients using a tract-based spatial statistics (TBSS) method.

Materials and Methods

Twenty-nine drug-naïve MDD patients with first depressive episode and 47 age- and gender-matched healthy subjects (HS) underwent diffusion tensor imaging (DTI) scans, and the analysis was conducted using TBSS. Morning blood samples were extracted from all MDD patients and HS for cortisol measurement.

Results

The serum cortisol levels were significantly higher in the MDD patients than in the HS. Compared with the HS, the MDD patients had significantly reduced FA values ($p < 0.05$, FWE-corrected) in the inferior fronto-occipital fasciculus (IFOF), uncinate fasciculus (UF), and anterior thalamic radiation (ATR) (Table). The FA values of the IFOF, ATR, and UF had significantly negative correlations with the serum cortisol levels in the MDD patients ($p < 0.05$; FWE-corrected). There were no regions that showed a positive correlation between FA and cortisol levels.

Table. Results of image analyses

Anatomical regions	Cluster size	p-value (FWE-corrected)	MNI coordinates (mm)		
FA values					
Between-groups comparison(HS>MDD)					
R.corticospinal tract	53	0.049	69	105	114
R.SCR					
L.IFOF	283	0.039	114	147	72
L.UF					
L.external capsule					
L.corticospinal tract	1221	0.036	111	104	116
L.ATR					
Negative correlation to cortisol levels in MDD patients					
R.IFOF	96	0.047	56	113	73
R.external capsule					
L.ATR	706	0.045	111	169	88
L.UF					
L.IFOF					
L.cingulum	1036	0.031	107	144	100
L.ACR					
R.ATR	3921	0.031	65	161	78

R= right, L= left, MNI= Montreal Neurologic Institute, SCR= superior corona radiation, IFOF = inferior fronto-occipital fasciculus, UF = uncinate fasciculus, ATR = anterior thalamic radiation, ACR = anterior corona radiation

Conclusions

In early stage of the MDD patients, the FA values of the IFOF, UF and ATR were decreased significantly compared with HS, and also showed significant inverse correlations with the cortisol levels. Since the IFOF, UF and ATR are essential elements for the frontal-subcortical circuits and frontal-limbic circuits, high levels of cortisol in MDD might injure the microstructures in these specific WM circuits.

KEYWORDS: Diffusion Tensor Image, White Matter Tracts

Note: Scanned images are included in the proceedings. Some submitted images were reduced during editing thereby decreasing clarity. Also, refer to the Program Planner. Proceedings Content as of 3/28/2014.

0-97 1:49PM - 1:56PM
White and Gray Matter Segmentation of the Human Brain Stem Using Diffusion Tensor Imaging

L Curley¹, R Desikan¹, V Rao², H Bartsch¹, N White³, C Hess⁴, T Jernigan¹, A Dale¹

¹University of California San Diego, La Jolla, CA,

²Massachusetts Institute of Technology, Cambridge, MA,

³University of California San Diego, San Diego, CA,

⁴University of California San Francisco, San Francisco, CA

Purpose

In this study, we tested the reproducibility of manually subdividing the brainstem based on diffusion tensor MRI (DTI) into gray and white matter based neuroanatomical regions.

Materials and Methods

Using DTI and T1- and T2-weighted MRI scans from 20 participants (age range = 3 to 20) we manually delineated 20 gray and white matter regions of interest (ROIs) per hemisphere. For T1 images, we used an SPGR sequence on a GE scanner. For DTI images, we used a b value of 1000 with 30 directions, slice thickness of 2.5mm and field view was 24. Regions of interest included inferior, middle and superior cerebellar peduncles, medial lemniscus, corticospinal tract, crus cerebri, decussation of the middle and superior cerebellar peduncles, pontocerebellar fibers, cranial nerves V and VII/VIII, red nucleus, substantia nigra, inferior olive, mammillary bodies, superior and inferior colliculi, central tegmental tract, rubrothalamic and dentatorubral tracts (see Figure 1). Three neuroanatomically trained operators manually labeled all ROIs. Using intraclass correlation coefficients (ICCs), we evaluated intra- and inter-rater reliability.

Results

Across all ROIs, the average ICCs for intra- and inter-rater reliability ranged from approximately 0.75 (dentatorubral and rubrothalamic tracts) to 0.95 (decussation of the pontocerebellar fibers). Larger ROIs demonstrated higher ICC values than smaller ROIs.

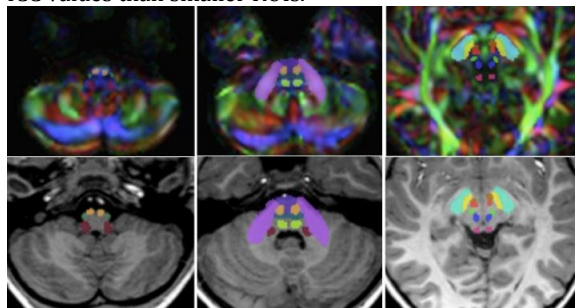


Figure 1
Axial view of ROIs in the brainstem, progressing from superior to inferior (left to right). Top row shows diffusion encoded color images of DTI scans and bottom row shows T1 weighted scans. ROIs: inferior (red), middle (purple) and superior (pink) cerebellar peduncles, medial lemniscus (green), corticospinal tract (burnt orange), crus cerebri (light blue), decussation of the middle and superior cerebellar peduncles (dark purple), pontocerebellar fibers (teal), cranial nerve V (dark blue), red nucleus (red), substantia nigra (yellow), inferior olive (green), and inferior colliculus (brown).

Conclusions

Our findings suggest that gray and matter areas can be manually parcellated with high reproducibility using DTI and high-resolution T1-weighted images. Future work will focus on utilizing this information to develop an automated

atlas-based method for quantitative analysis of brainstem structures.

KEYWORDS: Anatomy, Brainstem, White Matter Tracts

0-98 1:56PM - 2:03PM
Transient hypothyroidism: An arterial spin labeling magnetic resonance study

Y Kaichi¹, M Kenjo¹, T Higaki¹, Y Akiyama², W Fukumoto¹, K Kajiwara¹, C Tani¹, D Komoto¹, Y Nagata¹, K Awai¹

¹Hiroshima University, Hiroshima, Japan, ²Hiroshima University Hospital, Hiroshima, Japan

Purpose

Thyroid dysfunction is a contributor to the depression. We used arterial spin labeling (ASL) to investigate changes in the regional cerebral blood flow (rCBF) distribution in patients with transient post-thyroidectomy hypothyroidism.

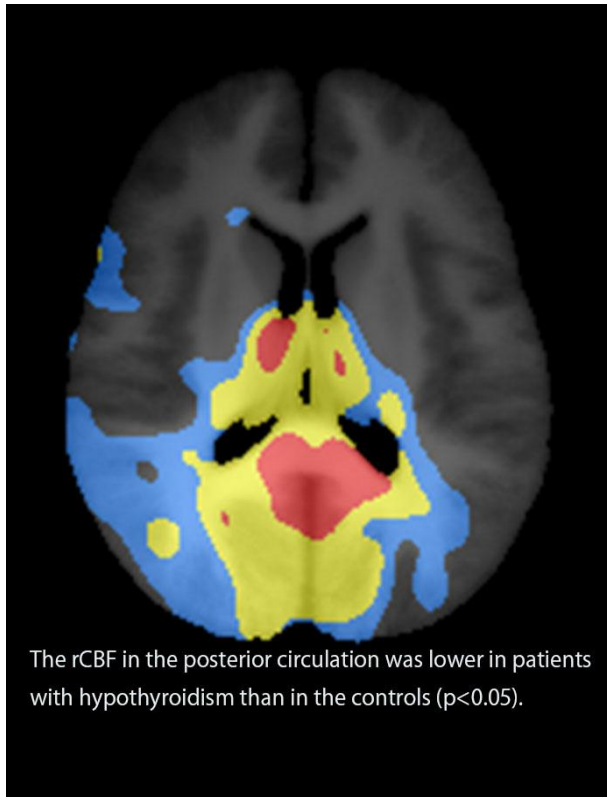
Materials and Methods

Our study included 24 patients with transient hypothyroidism and 40 healthy control subjects. We acquired scans with ASL on a 3 T MR system. On the day of the MR studies we quantified the severity of depression using the 21-question Beck Depression Index (BDI) and the 17-item Hamilton Depression Scale (HAM-D). We used voxel-based analysis to compare the absolute rCBF value of the patients and control subjects. We also performed region-of-interest (ROI) analysis of the whole brain, white and gray matter, cerebellum, bilateral caudate nuclei, amygdala, hippocampus, lentiform nucleus, and thalamus to examine the correlation between the rCBF and depression severity (BDI score, HAM-D score). After thyroid hormone replacement therapy (HRT) we again obtained ASL images and the BDI and HAM-D scores. Based on these scores the patients were categorized as unchanged and improved. To confirm the reversal of rCBF diminution after thyroid HRT we used group comparisons between control subjects and patients showing improvement and between the controls and patients with no change. We also performed ROI analysis to investigate the correlation between the rCBF and the severity of depression after thyroid HRT.

Results

The rCBF in the posterior circulation was lower in patients with hypothyroidism than in the controls ($p < 0.05$). After thyroid HRT the rCBF was enhanced in patients showing improvement. In patients with no change the area with significantly low rCBF remained unchanged. There was a significant correlation between the BDI score and the rCBF in the whole brain, white and gray matter, the left amygdala, bilateral hippocampi, and right thalamus (correlation coefficient: -0.57 to -0.51 , $p = 0.01$ to 0.04). In patients manifesting no change the rCBF of the whole brain, white and gray matter, and the left amygdala showed a significant decrease as the HAM-D score increased (correlation coefficient: -0.47 to -0.44 , $p = 0.02$ to 0.04).

Note: Scanned images are included in the proceedings. Some submitted images were reduced during editing thereby decreasing clarity. Also, refer to the Program Planner. Proceedings Content as of 3/28/2014.



Conclusions

On ASL images there was a significant rCBF decrease in the posterior circulation of patients with transient hypothyroidism after thyroidectomy, a phenomenon that may help to explain their depression. In some but not all patients we observed recovery of the rCBF after thyroid HRT. Our findings suggest that a lack in the improvement of depression after thyroid hormone replacement may reflect a persistent decrease in the rCBF.

KEYWORDS: ASL, Cerebral Blood Flow, Thyroid

0-99 2:03PM - 2:10PM
Regional cerebral blood flow in depressive disorders:
Arterial spin labeling magnetic resonance study

Y Matsubara¹, Y Akiyama², K Awai¹, S Date¹, T Higaki¹, Y Kaichi¹, Y Nakamura¹, Y Okamoto¹, T Yamagami¹, S Yamawaki¹

¹Hiroshima University, Hiroshima, Japan, ²Hiroshima University Hospital, Hiroshima, Japan

Purpose

Findings in the limited number of studies that addressed changes in cerebral blood flow (CBF) in depressed individuals are inconsistent. They suggest a complex neuropathophysiology in patients with depressive disorder that may be related to differences in disease development and treatment responses. We used arterial spin labeling (ASL) magnetic resonance imaging (MRI) to investigate

CBF changes in patients with refractory and nonrefractory depressive disorders (RDD, NDD) and healthy subjects.

Materials and Methods

Our study included 68 participants, 40 were the healthy controls and 28 suffered from depression. They underwent imaging on a 3 T MRI system between February 2012 and September 2013. ASL- and echo-planar images were subtracted and averaged to yield perfusion-weighted images. On the day of the MR studies we quantified the severity of depression using the 21-question Beck Depression Index (BDI) and the 17-item Hamilton Depression Scale (HAM-D). After treatment with antidepressants we again acquired ASL images and recorded the BDI and HAM-D scores. Based on these scores the patients were categorized into an RDD group (n=16) and an NDD group (n=12). Then we performed voxel-based comparison of the regional CBF (rCBF) among the patients and controls. To reduce possible interindividual variability in rCBF we normalized all CBF voxel data by dividing each participant's voxel data by his/her global mean CBF value for the cerebellum. We also performed region-of-interest (ROI) analysis of the gray and white matter and of the bilateral caudate nucleus, amygdala, hippocampus, lentiform nucleus, and thalamus. To reduce the possible interindividual variability in rCBF we normalized all CBF ROI data by dividing each participant's ROI data by his/her global mean CBF value for the cerebellum. We defined this as the normalized CBF (nCBF). Lastly we investigated the correlation between the nCBF in patients with RDD and NDD and the severity of depression (BDI- and HAM-D score) before and after antidepressant treatment.

Results

In patients with NDD, perfusion in the left frontal and parietal lobe and the caudate nucleus was lower than in the control subjects. In patients with RDD, perfusion in the bilateral temporal lobes was significantly lower than in the controls (p<0.05). Before antidepressant treatment, there was a significant inverse correlation between the BDI score and the nCBF value of the bilateral amygdalae and lentiform nuclei in patients with RDD (correlation coefficient: -0.61 to -0.49, p=0.01 to 0.04). After treatment, there was a significant correlation between the HAM-D score and the nCBF value of the right lentiform nucleus in patients with NDD (correlation coefficient: 0.58, p= 0.04). In the control subjects, there was no significant correlation between the BDI score and the rCBF in all ROI examined.

Conclusions

Our study revealed that the rCBF distribution is different in patients with RDD and NDD. An understanding of differences in the neurophysiologic blood flow patterns in RDD and NDD may help to select appropriate treatments for particular patient subgroups.

KEYWORDS: ASL, MR Imaging Perfusion, Psychiatry

Note: Scanned images are included in the proceedings. Some submitted images were reduced during editing thereby decreasing clarity. Also, refer to the Program Planner. Proceedings Content as of 3/28/2014.

O-100 2:10PM - 2:17PM
Symmetric T1 hyperintensity in globus pallidi in a patient with posterior reversible encephalopathy syndrome

S Pungavkar¹, R Saraogi², M Lawande¹, D Patkar¹, S Narkar¹
¹Dr. Balabhai Nanavati Hospital, Mumbai, Maharashtra, India, ²Dr. R.N.Cooper Hospital, Mumbai, Maharashtra, India

Purpose

We present a case, where an MR imaging (MRI) scan of brain performed on an eclamptic patient for evaluation of seizures, within 24 hours of treatment with magnesium sulphate revealed a symmetric hyperintense signal in the basal ganglia on T1-weighted images in addition to features of posterior reversible encephalopathy syndrome (PRES). Other conditions which could have a similar appearance of the basal ganglia were ruled out with appropriate tests. We also report MR spectroscopy (MRS) findings in the basal ganglia of the same patient. We have followed up this patient at one-month interval and have documented gradual decrease in the T1 signal in the basal ganglia, with disappearance of the signal on a scan performed at six months. MR imaging scans also were performed on two other patients who also were administered magnesium sulphate. These scans showed similar signal intensity changes. We postulate it to be secondary to deposition of magnesium in the brain parenchyma. It has to be determined whether deposition of magnesium in the brain parenchyma could have implications in the use of magnesium sulphate in pregnant patients.

Materials and Methods

Our index patient was a 28-year-old female, primigravida with 29 weeks gestation and with no significant prior history presenting to our hospital with two episodes of generalized tonic clonic convulsions. The blood pressure was elevated (180/120 mm Hg). Other findings were unremarkable. The patient was treated with anticonvulsants and injections as per Pritchard's regimen. Magnesium sulfate was administered for 24 hours as 4 grams intravenous and 10 grams loading dose followed by 5 grams intramuscularly 4 hourly [total dose: 14+ (5x6) = 44gms]. The seizures responded to treatment and the blood pressure normalized. However, patient persisted to be drowsy. Neurological examination did not reveal any focal deficit. On the second day postictus, the patient underwent an MRI scan of brain using T1 fluid attenuation inversion recovery (FLAIR), fast spin echo (FSE) T1 and T2. For T1 FLAIR, a repetition time (TR) of 1500 ms, echo time (TE) of 7.5 ms, inversion time (IR) of 750 ms, matrix of 256 x 192 were used with two number of excitations (NEX). For SE T1 sequence, TE of 400 ms, TR of 21 ms and a matrix of 320 x 192 were used with 2 NEX. T2-weighted images were obtained using TE of 4200 ms, TR of 80 ms and matrix of 320 x 224 with 3 NEX. Slice thickness of 3 to 5 mm and field of view of 24 cm were used. Single voxel spectroscopy was performed using 2 x 2 x 2 cm sized voxel and a short TE (30 ms). Liver and renal function tests and serum levels of copper, manganese and magnesium were

assessed. Follow-up MR scans using axial T1 FLAIR and T2-weighted images were performed at week one on index patient with further follow up at one month and six monthly intervals. Two other pregnant patients who also had convulsions and were administered magnesium sulphate as part of the treatment protocol were scanned within 24 hours of the first episode, with follow-up scans at one and six monthly intervals.

Results

The scan in the index patient revealed more or less symmetric, hyperintensities on T2-weighted sequences in bilateral posterior parietal cortex and subcortical white matter consistent with a diagnosis of PRES. There was no venous sinus thrombosis. Also seen was a symmetric hyperintense signal in the globus pallidi on T1-weighted imaging. The globus pallidi appeared normal on T2-weighted images. On single voxel MR spectroscopy study, there was reduction in the height of ml peak and ml/Cr ratio. No abnormal peak could be detected. Liver and renal function tests were normal. Serum levels of copper and manganese too were within the normal range. Serum magnesium levels were found to be elevated. Follow-up MR scans conducted after a week on the index patient, revealed resolution of the lesions in bilateral parietal parenchyma which were considered to represent PRES. However, the signal changes seen on T1-weighted imaging in the globus pallidi were persistent. It was, thus, hypothesized that the T1 hyperintensity seen in the globus pallidi could be secondary to magnesium deposition following intramuscular magnesium sulfate injections for control of blood pressure. Further follow-up MRI in the index patient at one month interval revealed reduction in the T1 signal intensity by about 50 % with normal appearance at six months. The serum magnesium levels at six months were within normal range. The two subsequent patients were scanned within 24 hours of injection. T1 hyperintense signal was seen in both these patients, which decreased on follow-up MRI performed at one and six months. Serum magnesium levels were elevated at the time of the first MR scan and within normal range at six months in both patients. Neurological examination of these patients also was normal.

Conclusions

Although, magnesium has been used for almost a century in several clinical conditions, this is the first report raising possibility of deposition of magnesium in the brain, when administered in pharmacological dosages. It appears as a symmetric high signal on T1-weighted MR scan. The intensity is likely to be dependent on the dosage of administered drug and time to scan since the injection. Hence, magnesium deposition must be considered in the differential diagnosis of bilateral symmetric T1 hyperintensity in the globus pallidi in the given clinical setting.

KEYWORDS: Globus Pallidus

Note: Scanned images are included in the proceedings. Some submitted images were reduced during editing thereby decreasing clarity. Also, refer to the Program Planner. Proceedings Content as of 3/28/2014.

O-101 2:17PM - 2:24PM
Relationship Between Lactate Dehydrogenase and the Development of PRES in Cancer Patients Receiving Systemic Chemotherapy

S Wright, R Fitzgerald, R Samant, M Kumar, R Ramakrishnaiah, R Van Hemert, E Angtuaco
University of Arkansas for Medical Sciences, Little Rock, AR

Purpose

Posterior reversible encephalopathy syndrome (PRES) is a neurotoxic process that occurs in the setting of hypertension, infection, transplantation, pregnancy, autoimmune disease, and cancer. Although the pathophysiology of PRES remains unclear, an underlying state of immune dysregulation and endothelial dysfunction has been proposed. The purpose of this investigation was to examine alterations of serum lactate dehydrogenase (LDH), a marker of endothelial dysfunction, relative to the development PRES.

Materials and Methods

A retrospective database of 88 PRES patients was compiled via an IRB-approved electronic medical record search for those treated for PRES at our institution from 2007-2012. Clinical diagnosis of PRES was confirmed by review of brain MR exams by two subspecialty certified neuroradiologists. Clinical features at presentation and initial blood pressure were recorded. Blood pressure was classified according to American Heart Association criteria. Serum LDH values were collected at three time points: prior to, at the time of, and following PRES diagnosis. Student's T-test was used to analyze the normal distribution of serum LDH measurement at the three measured time points.

Results

Twenty patients (23%) developed PRES while undergoing chemotherapeutic treatment for malignancy. Within this subset, serum LDH values were available during the course of treatment in 12 patients (9 female; mean age 57.8 years (range 33-75 years). Among the subset of 20 chemotherapy-related PRES patients, five (25%) were normotensive, seven (35%) hypertensive, and eight (40%) exhibited extreme hypertension. Normal blood pressure at presentation was less commonly encountered in the nonchemotherapy group (9%). Fourteen (70%) of chemotherapy-related PRES patients presented with seizure. Additional or alternative presentations included: altered mental status (6), headache (4), and vision changes (7). Lactate dehydrogenase levels at the time of PRES diagnosis were higher than those before and after ($p=0.0263$), with a mean difference of 114.8 IU/L. Mean time intervals between LDH measurement prior to and following PRES diagnosis were 44.8 days and 51.4 days respectively. Mean elapsed time between last chemotherapy administration (mean 3.5 chemotherapeutic agents/patient) and PRES onset was 11.1 days.

Conclusions

Serum LDH, a marker of endothelial dysfunction, shows statistically significant elevation at the onset of PRES toxicity in cancer patients receiving chemotherapy. Our

findings support a systemic process characterized by endothelial injury/dysfunction as a factor, if not the prime event, in the pathophysiology of PRES.

KEYWORDS: Chemotherapy, Hypertension, Posterior Reversible Encephalopathy

O-102 2:24PM - 2:31PM
Initial assessment of MRI/PET in patients with neurofibromatosis type 1

J Ramalho, Y Lee, M Castillo
University of North Carolina Chapel Hill, Chapel Hill, NC

Purpose

In NF1 patients, plexiform neurofibromas (PNFs) and optic pathway gliomas (OPGs) are commonly imaged to assess their progression/degeneration and progression respectively. Clinical examination, imaging, and even biopsies often are inconclusive in these assessments. PET/CT has limited soft tissue contrast and exposes patients to high radiation which is important in children and young adults who require multiple studies. Whole body FDG PET/MRI is a novel metabolic-anatomical imaging technique that overcomes these limitations but is limited by time and field of view constraints and its utility in this setting has not been described. Our purpose is to assess PET/MRI sensitivity for detection of PNFs and OPGs, its sensitivity for FDG avid lesions localization and compare its results with those of conventional MRI studies.

Materials and Methods

Using whole body PET/MRI we evaluated 11 NF1 patients with (n=4) or without (n=7) focal pain. Whole body MR sequences included coronal STIR, T1 VIBE pre and postcontrast with 4-6 stations covered depending on patient size (n=11). Coronal STIR and axial T2 thin sections through the optic pathways were acquired additionally in patients with OPGs (n=3). Patients received a standard IV dose of FDG one hour prior to the examination. Total imaging time was approximately 35 minutes (range: 25-45 min). Fused MR/PET images were analyzed and maximum standardized uptake value (SUV_{max}) was recorded for all lesions. We also correlated all MR images with conventional MR images obtained previously.

Results

We studied a total of 11 patients (2 males, 9 females; mean age: 23.3±18.1, median age: 17 years), of which four had recently developed local pain. Of the asymptomatic ones, whole body MR images showed all lesions when compared to dedicated MR images obtained previously and were enough to assess location and extension but not intrinsic mass characteristics. The PET portion of the study showed no uptake of FDG in any lesions. In symptomatic patients, the whole body MR images also identified all lesions when compared to previous MRI studies. PET study showed one tumor with FDG uptake (maxSUV>4) and also areas of uptake not in the tumors (n=3) but rather in muscles adjacent to them suggesting that the pain did not originate from progressive and/or degenerating tumors.

Note: Scanned images are included in the proceedings. Some submitted images were reduced during editing thereby decreasing clarity. Also, refer to the Program Planner. Proceedings Content as of 3/28/2014.

Conclusions

Whole body MR images obtained as part of MR PET studies were sufficient to identify all mass lesions when compared to conventional dedicated MR studies. Masses in asymptomatic patients did not show FDG uptake but in three of the four symptomatic patients MR PET showed areas of high uptake not in the masses but in muscles adjacent to them suggesting that the cause of pain in them was not the tumors.

KEYWORDS: MR Imaging/PET, Neurofibromatosis, PET

Monday, May 19
3:00 PM – 4:30 PM
Room 517bc

18 - PARALLEL PAPERS: New
Techniques and Orbits

O-103 3:00PM - 3:07PM
Permeability Measures of Normal Structures of Head and Neck: A Proof-of-Principle Study Utilizing DCE Imaging with Radial-VIBE and GRASP Technique.

L Bangiyev¹, X Wu¹, K Block¹, R Grimm², C Rossi Espagnet¹, M Hagiwara¹, M Bruno¹, J Babb¹, G Fatterpekar¹
¹New York University Langone Medical Center, New York, NY, ²Pattern Recognition Lab, FAU Erlangen-Nuremberg, Nuremberg, Germany

Purpose

In the head and neck, cross-sectional imaging provides only one index of biological activity, i.e., morphologic evaluation, which is nonspecific. Most current advances in MR imaging (MRI) allow exploring physiologic alterations that can be used as imaging biomarkers. Radial-VIBE with GRASP assesses for structural dynamic contrast-enhanced (DCE) permeability. Our hypothesis is that the permeability patterns of every normal anatomical structure in the neck should be distinct. The purpose of this study therefore is to evaluate the role of Radial-VIBE with GRASP to establish the unique permeability characteristics of the different normal anatomical structures of the neck. Materials and Methods

This retrospective HIPPA-compliant study evaluated 10 patients who underwent clinically indicated MRI of the neck at 1.5 T. Along with standard MRI sequences, dynamic Radial-VIBE sequence with GRASP was performed during administration of 0.01 mmol/kg of gadolinium-based contrast at 3 mL/second. The following acquisition parameters were used: spatial resolution=1.0x1.0x2.0 mm; 800 spokes; flip angle=12°; TR=4.57 ms; TE=2.06 ms; matrix=256x256; bandwidth=400 Hz/px; field of view=256 mm²; acquisition time=4'43". Signal-time curves (Figure 1) were generated along with the following parameters: Ktrans (transfer constant, aka permeability), VE (volume of extravascular-extracellular space), VP

(blood plasma volume), KEP (rate constant), wash-in, wash-out, AUC (area under the curve), peak maximum enhancement (MPeak) and time to maximum enhancement (MTime). Normal structures of the neck such as the jugular vein, sternocleidomastoid muscle (SCM), lymph node (LN), thyroid gland, and vocalis muscle (vocalis) were evaluated. Results

Mixed model analysis of variance (ANOVA) was used to compare normal structures of the neck in terms of each imaging measure. All statistical tests were conducted at the two-sided 5% significance level using SAS 9.3 (SAS Institute, Cary, N.C.). As outlined in Table 1, VP and wash-in demonstrated statistically significant ($p < 0.05$) differences in all measured structures of the neck. Most of the remaining permeability parameters also demonstrated significant differences among the different anatomical structures of the neck.

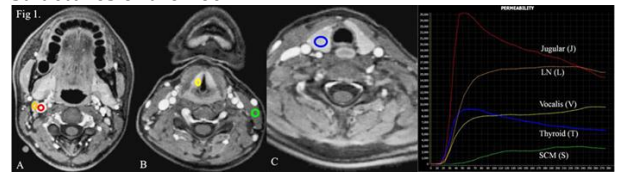


Table 1: p-Values from the ANOVA analysis, comparing regions in terms of each DCE measure.

Regions	AUC	KEP	Ktrans	MPeak	MTime	VE	VP	Wash-in	Wash-out
Compared									
Jugular LN	<0.001	<0.001	<0.001	<0.001	<0.001	<0.001	<0.001	<0.001	<0.001
Jugular SCM	<0.001	0.895	0.108	<0.001	<0.001	0.987	<0.001	<0.001	<0.001
Jugular Thyroid	<0.001	0.463	0.224	<0.001	0.173	0.235	<0.001	0.010	<0.001
Jugular Vocalis	<0.001	0.085	0.094	<0.001	<0.001	<0.001	<0.001	<0.001	<0.001
LN SCM	<0.001	<0.001	<0.001	<0.001	0.726	<0.001	<0.001	<0.001	<0.001
LN Thyroid	0.011	0.002	<0.001	0.021	<0.001	<0.001	0.041	0.040	0.234
LN Vocalis	<0.001	0.019	0.009	0.002	<0.001	0.818	<0.001	0.001	<0.001
SCM Thyroid	<0.001	0.257	0.698	<0.001	<0.001	0.010	<0.001	<0.001	<0.001
SCM Vocalis	<0.001	0.010	<0.001	<0.001	0.001	<0.001	<0.001	<0.001	<0.001
Thyroid Vocalis	0.157	0.316	<0.001	0.371	<0.001	<0.001	<0.001	<0.001	<0.001

Conclusions

The results from this proof-of-principle study are consistent with the hypothesis that each normal structure of the neck has a unique permeability pattern. The GRASP technique is a new viable method for assessing permeability patterns in the head and neck.

KEYWORDS: Head And Neck, Permeability MR Imaging

O-104 3:07PM - 3:14PM
Molecular MR Imaging of Myeloperoxidase Activity is a Potential Imaging Biomarker for Head and Neck Cancer

J Li¹, R Forghani², L Bure², G Wojtkiewicz³, Y Iwamoto³, A Muhammad³, A Li³, C Wang³, H Curtin⁴, J Chen³
¹Tongji University, Shanghai, China, ²Jewish General Hospital & McGill University, Montreal, Quebec, Canada, ³Massachusetts General Hospital, Boston, MA, ⁴Massachusetts Eye and Ear Infirmary, Boston, MA

Purpose

Head and neck squamous cell carcinomas (HNSCC) can be associated with an intense inflammatory response. Myeloperoxidase (MPO) is a highly oxidative inflammatory enzyme abundantly secreted by macrophages and neutrophils. In this study we evaluated whether MPO-Gd, an activatable MR molecular imaging agent highly specific and sensitive to MPO activity, would be superior in detecting tumor extent compared to a conventional

Note: Scanned images are included in the proceedings. Some submitted images were reduced during editing thereby decreasing clarity. Also, refer to the Program Planner. Proceedings Content as of 3/28/2014.

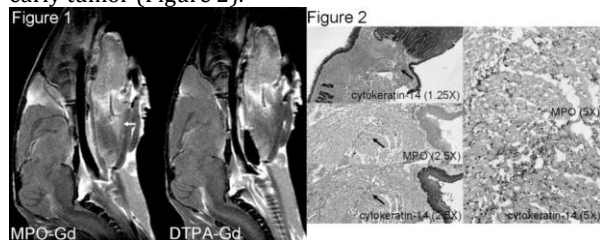
gadolinium contrast agent (DTPA-Gd) in a murine model of HNSCC.

Materials and Methods

Head and neck squamous cell carcinoma was induced in ten 8-week C57Bl/6 mice with 4-niroquinoline-N-oxide (100 ug/ml) dissolved in drinking water for four months. Five age-matched C57Bl/6 mice on normal water were used as control. After another eight to 10 weeks, the mice were screened for tumor using bioluminescence imaging (BLI) of MPO activity (with luminol). When BLI imaging was positive, MR imaging (MRI) was performed with DTPA-Gd and MPO-Gd. The mice then were sacrificed for histopathological analysis of the tongue samples, with anti-MPO antibody and anti-cytokeratin 14 antibody to validate the imaging findings.

Results

Nine out of 10 mice developed tumor, three mice died before imaging was performed, and six mice were imaged. The luminol BLI signal (total flux) in the head and neck region of the tumor group was higher than that in the control group (tumor: $40,011 \pm 5,179$ p/s; control: $16,326 \pm 2,179$ p/s; $p=0.0018$), confirming the development of inflammation. On MRI, lesions were detected within the tongue. The enhancing volume detected by MPO-Gd was higher than that by DTPA-Gd (MPO-Gd: 0.0232 cm³; DTPA: 0.0097 cm³; $p=0.013$). Furthermore, MPO-Gd imaging detected areas that were absent with DTPA-Gd imaging (Figure 1), confirmed histopathologically to represent early tumor (Figure 2).



Conclusions

Molecular MR imaging targeting MPO activity is superior at detecting early HNSCC and identifying tumor extent than Gd-DTPA.

KEYWORDS: Head And Neck, MR Imaging, Squamous Cell Carcinoma

O-105

3:14PM - 3:21PM

Impact of Model-Based Iterative Reconstruction on image quality of contrast enhanced Neck CT

S Gaddikeri¹, J Andre¹, J Benjert², D Hippe¹, Y Anzai¹

¹University of Washington, Seattle, WA, ²University of Washington/VA Puget Sound, Seattle, WA

Purpose

To compare adaptive statistical iterative reconstruction (ASiR30) and model-based iterative reconstruction (MBIR) algorithms for the assessment of image quality of contrast-enhanced neck CT.

Materials and Methods

The imaging data of 64 consecutive patients undergoing contrast-enhanced neck CT with a noise index of 23.4 were reconstructed retrospectively by ASiR30 as well as MBIR. Objective image quality was assessed by comparing signal to noise ratio (SNR), contrast to noise ratio (CNR) and background noise (BN) at two different levels; at the levels of mandible (level I) and superior mediastinum (level II). Two experienced blinded reviewers subjectively graded the image quality and overall image quality on a scale of 1 to 5 grading system, (Grade 5 = excellent image quality without artifacts and grade 1 = nondiagnostic image quality with significant artifacts). The subjective image quality assessment was performed at four different levels, including the level of nasopharynx, oropharynx, true vocal cords (VC) and sterno-calvicular (SC) junction. Interobserver agreement was assessed with Cohen's kappa analysis. Thyroid shield was placed over the lower neck for all patients as a part of radiation safety exercise in our institution.

Results

Compared with ASiR30, MBIR significantly improved SNR [(mean \pm SD) 12 ± 4.3 versus 16 ± 7.2 , $p<0.001$], CNR (6.8 ± 2.4 versus 7.6 ± 2.6 , $p<0.001$) at the level I and (3.9 ± 3.4 versus 6.9 ± 8.1 , $p<0.001$), (3.7 ± 1.6 versus 4.9 ± 2.0 , $p<0.001$) at the level II, respectively. Model-based iterative reconstruction also significantly decrease BN at the level I (7.8 ± 9.2 versus 6.3 ± 9.2 , $p<0.016$), although there was no significant difference at the level II (34 ± 31 versus 32 ± 33 , $p=0.61$). Model-based iterative reconstruction scored significantly higher over ASiR30 by both reviewers, at the level of nasopharynx (4.8 ± 0.3 versus 4.2 ± 0.3 , $p<0.001$), oropharynx (3.7 ± 0.6 versus 3.1 ± 0.6 , $p<0.001$) and overall image quality (3.9 ± 0.3 versus 3.7 ± 0.3 , $p<0.001$). Model-based iterative reconstruction scored significantly lower at the level of VC (3.7 ± 0.5 versus 4.0 ± 0.4 , $p<0.001$) and SC junction (3.4 ± 0.5 versus 3.8 ± 0.2 , $p<0.001$), due to artifacts related to thyroid shield specific for MBIR. Interobserver agreement was relatively low at all levels ($k = 0.04, 0.31, 0.17, 0.05$, and 0.02 for MBIR and $0.02, 0.30, 0.02, 0.00$, and 0.06 for ASiR30 at the level of nasopharynx, oropharynx, VC, SC, and overall image quality respectively) reflecting the bias in ratings between the two reviewers.

Conclusions

Model-based iterative reconstruction offers improved subjective and objective image quality as evident by higher SNR and CNR and lower BN within the same data set for contrast-enhanced neck CT. This raises a great potential of MBIR to reduce radiation dose while maintaining the image quality. Only minor downside was prominent artifact related to thyroid shield on MBIR. Further studies are necessary to assess how much radiation dose saving can be achieved with application of newer model-based iterative reconstruction algorithm.

KEYWORDS: Head And Neck, Image Quality, Iterative Reconstruction

Note: Scanned images are included in the proceedings. Some submitted images were reduced during editing thereby decreasing clarity. Also, refer to the Program Planner. Proceedings Content as of 3/28/2014.

O-106 3:21PM - 3:28PM
Radiologic Findings in Patients with Persistent Hemifacial Spasm After Microvascular Surgical Decompression

C Taylor¹, M Hughes¹, A Frederickson², B Branstetter¹, R Sekula¹

¹University of Pittsburgh Medical Center, Pittsburgh, PA,

²University of Pittsburgh, Pittsburgh, PA

Purpose

To identify common anatomical locations of persistent unaddressed vascular compression of the facial nerve in patients with a history of a failed microvascular decompression.

Materials and Methods

Fifteen patients with persistent hemifacial spasm following a previous microvascular decompression were included in this retrospective study. The patients were evaluated clinically by a neurosurgeon specializing in cranial nerve disorders and had findings consistent with persistent hemifacial spasm. All patients underwent thin section steady-state free precession MR images. Blinded to the surgical results, a single neuroradiologist reviewed the imaging to identify: presence of a vessel contacting the facial nerve, whether the contacting vessel was an artery, vein or both, which artery was responsible, which segment of the nerve was involved, and whether this point of contact was medial or lateral to the existing pledget. If the patient underwent a repeat microvascular surgical decompression, the imaging findings were compared to the operative findings.

Results

In 11 of the 15 patients persistent arterial compression was identified; one of these patients also had venous contact with the facial nerve. Eleven patients underwent repeat microvascular decompression. Of these 11 patients 10 had imaging evidence of persistent vascular compression of the facial nerve. The PICA was the sole culprit vessel in three patients, the AICA was the sole culprit vessel in six patients, and both the AICA and PICA contacted to the facial nerve in one patient. Compression of the adherent segment (along the undersurface of the pons) was identified in six patients (60%), the root detachment point in one patient (10%), and the transition zone in three patients (30%). The point of contact was medial to the pledget in eight patients (80%) and was lateral to the pledget in two patients (20%). These findings were confirmed at surgery. One patient without imaging evidence of arterial compression underwent repeat surgical decompression, and small arterioles were noted intra-operatively compressing the facial nerve. Long term outcome data are being acquired. Four patients were not offered repeat decompression. Three of these patients had no evidence of persistent vascular compression and one patient had arterial contact of the cisternal segment of the facial nerve, lateral to the existing pledget.

Conclusions

In patients with persistent hemifacial spasm despite microvascular decompression, the unaddressed vascular compression when present is typically medial to the

previously placed pledget. In the majority of patients in this small series, the compression occurred at the adherent segment that extends along the undersurface of the pons. Special attention should be paid to the proximal portions of the seventh nerve, particularly the portions medial to the existing pledget, in patients with persistent hemifacial spasm to identify residual compression.

KEYWORDS: Cranial Nerves, Facial Nerve

O-107 3:28PM - 3:35PM
Ultrasound Diagnosis of Intra-Thyroid Parathyroid Adenoma: The Importance of Identification of the Dominant Polar Vessel

M Kwon¹, M Debnam¹, T Vu¹, D DiVito², E Grubbs¹, N Perrier¹, W Wei¹, B Fornage¹, B Edeiken-Monroe¹
¹University of Texas MD Anderson Cancer Center, Houston, TX, ²St. Joseph Hospital, Chicago, IL

Purpose

Intrathyroid parathyroid adenomas (ITPA) are uncommon but do occur. When clinical and laboratory findings of hyperparathyroid function are present, imaging localization of the parathyroid adenoma (PA) may remain elusive particularly if the adenoma is intrathyroid. The purpose of this study is to evaluate the impact of a dominant polar vessel (DPV) in the ultrasound (US) localization of an ITPA. While the DVP has been recognized previously as a characteristic of a parathyroid adenoma, the significance of this sign in localizing a parathyroid adenoma has not been established.

Materials and Methods

The appearance of ITPAs localized on US were reviewed retrospectively and where possible were compared to the CT and sestamibi findings. Inclusion criteria were the preoperative US suspicion of ITPA and FNA/cytologic/pathologic documentation of a parathyroid adenoma. The following US features were recorded: size, margins, echotexture, echogenicity, comet tail artifact, calcification and vascular flow were assessed. Power Doppler was performed to identify a dominant polar vessel (DPV) that partially encircled the nodule and/or extended into the nodule. FNA was performed based on the US suspicion of an ITPA.

Results

Intrathyroid parathyroid adenomas were diagnosed by US in 25 patients, four men and 21 women based on the presence of a DPV and absence of localization of an alternate site of parathyroid adenoma by US, CT, and sestamibi scans. The characteristics of the ITPAs diagnosed by US were nonspecific in size, echotexture, and echogenicity. Each ITPA had a well defined margin. Calcification and comet tail artifact due to crystalline colloid were absent in all of the ITPAs. A DPV on power Doppler US was present in 22 of 25 (88%) suspected ITPAs. Correlation between the presence of a DPV and ITPA was statistically significant (p-value < 0.0001 by Fisher's exact test). Accuracy of the test was 0.89 (58/65; 95% exact CI: 0.79, 0.96). Sensitivity of the test was 0.88

Note: Scanned images are included in the proceedings. Some submitted images were reduced during editing thereby decreasing clarity. Also, refer to the Program Planner. Proceedings Content as of 3/28/2014.

(22/25 with DVP; 95% exact CI: 0.69, 0.97). Specificity was 0.90 (36/40 without DVP; 95% exact CI: 0.76, 0.97). Thus, the demonstration of DPV is a valid indicator for the presence of an ITPA and the absence of a DLV is highly specific for absence of an ITPA. Of 25 ITPAs localized by US, eight of 21 (38%) were detected by 4D CT scan and four of 24 (17%) were detected by sestamibi scan. FNA and/or surgical resection/surgical pathology documented that lesion localized by US was a parathyroid adenoma. Surgical resection/surgical pathology suggested that 17 of 24 (71%) were true ITPAs, and seven of 24 (29%) were closely adjacent to the margin of the thyroid gland and possibly extrathyroid.

Conclusions

In a patient undergoing pre-operative evaluation for primary hyperparathyroidism and absence of imaging localization of a parathyroid adenoma, the DPV is a distinguishing US characteristic that can raise the suspicion for, and facilitate the diagnosis, of an ITPA.

KEYWORDS: Parathyroid, Thyroid, Ultrasonography

O-108 3:35PM - 3:42PM
DCE-MRI Evaluation of Pathologic Cervical Lymphadenopathy Using Radial-VIBE acquisition with Dynamic GRASP Reconstruction.

X Wu¹, L Bangiyev¹, M Hagiwara¹, A Davis¹, K Block¹, C Rossi Espagnet², J Babb¹, G Fatterpekar¹
¹New York University Langone Medical Center, New York, NY, ²New York University Medical Center, New York, NY

Purpose

Cross-sectional imaging is limited in evaluation of pathologic lymphadenopathy. Positron emission tomography-computed tomography (PET-CT) has proven to be helpful. However, there are certain limitations. Neck dissection therefore remains the gold standard. Radial-VIBE in combination with the new GRASP technique can be used for dynamic contrast-enhanced (DCE) structural assessment. Our hypothesis is that normal lymph nodes will demonstrate difference DCE parameters when compared with pathologic lymphadenopathy. The purpose of this study is therefore to evaluate the role of Radial-VIBE with GRASP to distinguish metastatic lymphadenopathy from normal lymph nodes in primary head and neck cancers.

Materials and Methods

In this HIPAA-approved retrospective study, 27 lymph nodes from 10 patients were evaluated. Of the 27 lymph nodes, there were nine pathologically proven metastatic and 18 normal lymph nodes. All patients were imaged on 1.5 T system utilizing standard MRI protocols and DCE-MRI with Radial-VIBE and GRASP. The Radial-VIBE sequence was acquired during administration of 0.01 mmol/kg of gadolinium-based contrast at 3 mL/second using: spatial resolution=1.0 x1.0 x 2.0 mm; 800 spokes; flip angle=12°; TR=4.57 ms; TE=2.06 ms; matrix=256 x 256; bandwidth=400 Hz/px; field of view=256 mm²; acquisition time=4'43". Signal-time curves were generated from ROIs along with K-trans (transfer constant,

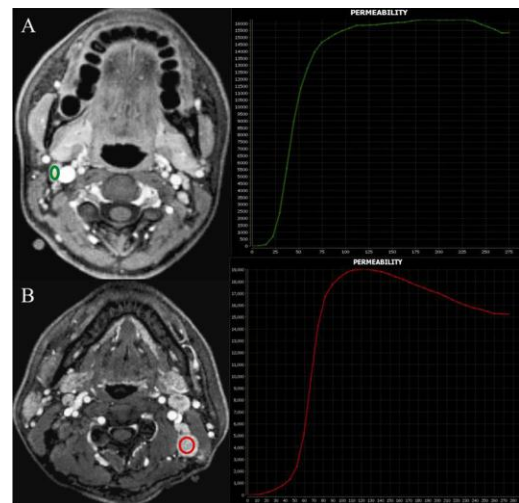
permeability coefficient), VE (volume of extravascular-extracellular space), VP (blood plasma volume), KEP (rate constant), wash-in, wash-out, AUC (area under the curve), peak maximum enhancement, and time to maximum enhancement.

Results

Statistical analysis was performed using mixed model analysis of variance (ANOVA) for each imaging measure. The lack of statistical independence among observations from the same patient was accounted for by assuming data to be correlated only when acquired from the same subject. All statistical tests were conducted at the two-sided 5% significance level using SAS 9.3 (SAS Institute, Cary, N.C.). The mean, standard deviation, and median values are listed in Table 1, and p-values are listed in Table 2. Most of the measured parameters demonstrated significant ($p < 0.05$) difference with exception of VE and Ktrans. VE demonstrated a statistical trend with $p=0.075$.

Table 1. The mean, standard deviation (SD), median, and P value of each measure among abnormal and normal

Measure	Abnormal (n=9)		Normal (n=18)		P Value		
	Mean	SD	Mean	SD			
AUC	3465246.92	507897.63	3577033.93	2458779.66	846361.57	2507250.08	0.019
KEP	1.76	0.46	1.82	0.92	0.34	0.83	0.008
KTRANS	0.43	0.15	0.49	0.28	0.10	0.28	0.240
PEAK	17522.77	2349.25	17842.10	12028.88	3748.72	12717.20	0.008
TIME	118.2	8.95	119.23	139.64	25.80	138.70	0.011
VE	0.21	0.06	0.20	0.29	0.09	0.29	0.075
VP	0.19	0.05	0.19	0.15	0.08	0.13	<0.001
WASHIN	202.75	26.72	206.04	106.91	46.94	107.99	<0.001
WASHOUT	27.45	3.69	28.58	14.21	6.10	14.44	<0.001



Conclusions

Our pilot study demonstrates significant difference in permeability parameters of pathologic lymphadenopathy when compared with normal lymph nodes using Radial VIBE with GRASP technique.

KEYWORDS: Lymph Node Metastasis, Permeability MR Imaging

O-109 3:42PM - 3:49PM
High-resolution Flat-panel CT in the Post-operative Evaluation of Cochlear Implants

M Pearl, A Roy, C Limb
Johns Hopkins University School of Medicine, Baltimore, MD

Note: Scanned images are included in the proceedings. Some submitted images were reduced during editing thereby decreasing clarity. Also, refer to the Program Planner. Proceedings Content as of 3/28/2014.

Purpose

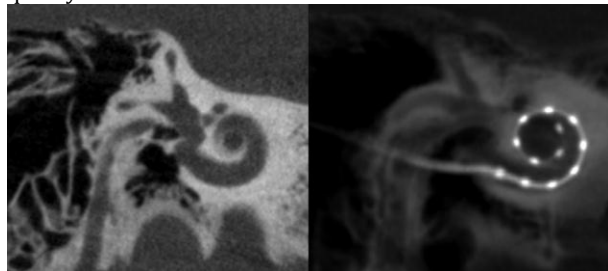
Clinical outcomes following cochlear implantation vary considerably in the degree and quality of hearing recovery. Cochlear implant (CI) location, insertion depth, scalar localization, and relationship to the facial nerve are important factors for CI outcomes. This study investigates the utility of flat-panel computed tomography (FPCT) in the postoperative evaluation of patients with CI.

Materials and Methods

All patients gave written informed consent to participate in this IRB approved study. Fifteen patients with 19 previously placed CIs (18 Med-El standard 31.5-mm arrays, 1 Med-El medium 24-mm array) underwent postoperative FPCT (DynaCT, Siemens, Erlangen, Germany) evaluation on a flat-panel angiography system (Axiom Artis Zee, Siemens) using commercially available software (Syngo DynaCT, Siemens). A collimated 20-second FPCT of the head was performed: 109 kV, small focus, 200-degree rotation angle, and 0.4-degree/frame angulation step. Postprocessing was performed on a commercially available workstation (Leonardo; Siemens). Secondary reconstructions were created using the following parameters: manually generated VOI to include only the electrode array, voxel size 0.07 mm - 0.08 mm, 512 x 512 matrix, Hounsfield units (HU) and edge enhancement (EE) kernel types, and very smooth, normal, auto, and sharp image characteristics. Images were analyzed for the ability to identify distinct electrode contacts, CI insertion point, relationship to the facial nerve, and scalar localization. The four different types of image characteristics and two different kernel types used in the creation of secondary reconstructions were compared to identify the optimal reconstruction parameters for CI visualization.

Results

Flat-panel CT could depict the insertion site, CI course, relationship to the facial nerve, and all 228 individual electrode contacts. Scalar localization could be inferred based on the relationship to the cochlear walls, yet discrete visualization of the CI and adjacent osseous spiral lamina throughout CI course was not possible. The HU kernel type and sharp image characteristic provided the highest quality combination for CI visualization.



Conclusions

Flat-panel CT is a promising imaging tool for the evaluation of patients with CIs and produces high-resolution images that identify the CI insertion point, all individual electrode contacts, and the relationship to the facial nerve.

KEYWORDS: Facial Nerve, Flat-Detector Cone-Beam CT, Hearing Loss

O-110

3:49PM - 3:56PM

C-Arm CT Imaging of the Temporal Bone: Image Quality and 3D Radiation Dose Distribution

T Kennedy¹, T Szczykutowicz², K Royalty³, S Schafer³, S Nace¹, B Gartrell¹, S Gubbels¹

¹University of Wisconsin Hospital and Clinics, Madison, WI,

²University of Wisconsin Madison, Madison, WI, ³Siemens Medical Solutions, USA, Hoffman Estates, IL

Purpose

In recent years there have been substantial developments in the field of C-Arm-based CT acquisitions (CACT), especially when focusing on small volume, high contrast targets. The relatively small area and osseous anatomy of the temporal bone make this structure an ideal candidate for CACT imaging. The purpose of this study was to compare the image quality and the relative radiation dose to the ocular lens between multidetector CT (MDCT) and CACT using a cadaveric model and an anthropomorphic head phantom.

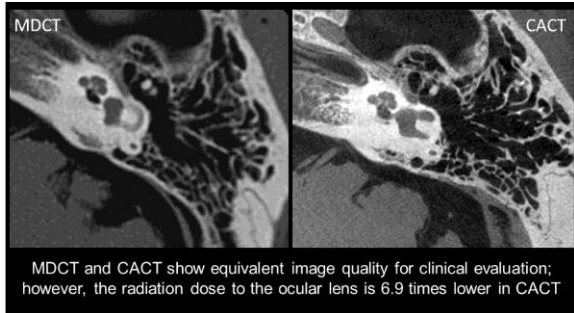
Materials and Methods

Five cadaveric heads were scanned on a C-Arm biplane system with CACT capability, and on a clinical 64-slice MDCT. A small field of view high resolution scan mode was used for CACT using a micro focal spot, 6.5 cm by 11 cm coverage and 0.154 mm detector pitch. The center of the field of view was the right temporal bone in all acquisitions. For MDCT scans, a standard clinical temporal bone protocol was used with a 0.531 pitch, noise index 6.7, acquisition slice thickness 2.5 mm, and axial bone reconstructions of 0.625 mm. Image quality was qualitatively evaluated by a panel of experienced neuroradiologists. Dose measurements were performed using thermoluminescent dosimeters (TLDs). The dose to the lens was estimated by placing TLD chips under the eyelids of intact whole cadaver heads. Volumetric dose measurements were taken using an anthropomorphic head phantom to compare the different dose distributions of each modality qualitatively. All TLD measurements were repeated three times and averaged. A total of 35 measurement locations were used to create the volumetric dose maps for the phantom study.

Results

Image quality between the MDCT and CACT were judged to be equivalent for clinical evaluation (Figure). The radiation dose to the lens was 6.9 times lower in CACT. The volumetric dose distribution for MDCT showed a relatively uniform dose distribution compared to an asymmetric dose distribution for CACT. In the region of the orbits, the dose was higher for MDCT than for CACT, which is consistent with the cadaveric result. For CACT, the dose was highest over the right temporal bone with a large gradient that decreased markedly away from the temporal bone.

Note: Scanned images are included in the proceedings. Some submitted images were reduced during editing thereby decreasing clarity. Also, refer to the Program Planner. Proceedings Content as of 3/28/2014.



Conclusions

Due to the geometry of the scan range and collimation of the CACT system, a substantial dose reduction was observed for CACT over MDCT for the ocular lens. Future applications of this imaging technique include the potential usability of flat-panel-based C-Arm systems for cochlear implant staging, delivery under fluoroscopic guidance, as well as postdelivery assessment of surgical position.

KEYWORDS: Flat-Panel Angiographic CT, Radiation Dosage, Temporal Bone

0-111 3:56PM - 4:03PM
Optic nerve elevation in children: causes, imaging appearance and clinical significance.

A Shifrin¹, D Gold², E Pitkin³, A Bhatia², A Pollock², A Vossough³, T Feygin²

¹Mount Auburn Hospital, Cambridge, MA, ²Children's Hospital of Philadelphia, Philadelphia, PA, ³University of Pennsylvania, Philadelphia, PA

Purpose

To define the spectrum of disorders manifested clinically as optic disk elevation; to define reliable MR imaging features of true papilledema; and to evaluate the prognostic value of restricted diffusion within the optic disks.

Materials and Methods

MR imaging (MRI) of the brain and orbits in 127 patients referred for papilledema were reviewed by two neuroradiologists blinded to the clinical history. In addition to routine MR brain imaging with and without gadolinium, thin section T2 and post-gadolinium T1 images in axial and coronal planes with fat suppression and diffusion imaging were obtained. The subjects' ages ranged from six months to 15 years. Comparison was performed with orbital MRIs of 46 patients imaged for reasons other than suspected papilledema. All imaging was performed on 1.5 or 3 T MRI scanners.

Results

Evaluation of MRI examinations reveals that 68% of patients referred for papilledema had positive imaging findings of true papilledema; 8% of patients had an imaging diagnosis of pseudopapilledema; and 24% had a normal imaging exam. The spectrum of imaging findings of true papilledema in the orbits includes: protrusion (inversion), restricted diffusion, and enhancement of the optic nerve heads, and enlargement of the optic nerve

sheath greater than 8 mm. The spectrum of underlying pathologies includes, in decreasing order of prevalence: hydrocephalus, predominantly due to brain tumors; pseudotumor cerebri; venous sinus thrombosis, intracranial hemorrhage, vascular anomalies; and miscellaneous causes including local orbital pathology such as optic neuritis, trauma, and inflammatory disorders. Patients with papilledema were categorized into three groups depending on their visual outcome (normal, subnormal and abnormal). A comparison between these groups was made using a chi-square test for association, and pairwise comparisons were conducted with a two-sample t-test. Our findings indicate that restricted diffusion of the optic nerve heads was seen in 73.7% of patients with clinical papilledema. Visual outcomes were subnormal or normal in 86.8% of our patients with papilledema. However, there was no statistically significant association between visual outcome and prevalence of diffusion restriction.

Conclusions

A significant number of pediatric patients referred for papilledema had positive MRI findings. The largest subset of patients with positive imaging findings was due to hydrocephalus, predominantly as a result of tumors or other causes of increased intracranial pressure. However, there was no statistically significant association between visual outcome and prevalence of restricted diffusion within the optic disks.

KEYWORDS: Optic Nerve, Orbits, Pseudotumor Cerebrii

0-112 4:03PM - 4:10PM
Superior Oblique Muscle Size Variations in Congenital Superior Oblique Muscle Palsy

I Davagnanam¹, A Dahlmann-Noor², J Sowden³, T Yousry¹
¹UCL Institute of Neurology, London, UK, ²UCL Institute of Ophthalmology, London, UK, ³UCL Institute of Child Health, London, UK

Purpose

Congenital superior oblique palsy (CSOP) is the most common congenital cranial nerve palsy and cause of strabismus. Recent animal and human studies have provided strong candidate genes involved in the development of the superior oblique muscle (SO) and/or its cranial nerve, indicating that this condition may be due to primary muscle hypoplasia or primary misdevelopment of the nerve/nucleus. We aimed to demonstrate structural MR imaging (MRI) of the SO, 4th cranial nerve (CN4) and its nucleus, and to correlate the imaging phenotype with candidate genes responsible for the structural development of each component. Data from the initial analysis of SO muscle is presented and will be supplemented with subsequent data from cranial nerve and nucleus imaging as well as correlations with genetic tests.

Materials and Methods

Clinically confirmed patients with unilateral CSOP were recruited from a tertiary referral Ophthalmological

Note: Scanned images are included in the proceedings. Some submitted images were reduced during editing thereby decreasing clarity. Also, refer to the Program Planner. Proceedings Content as of 3/28/2014.

institution underwent 3 T MRI of the brain and orbits using a standardized imaging protocol. Maximal cross-sectional areas of the SO (MaxA) were outlined and calculated on ITKSNAP (PICSL, Pennsylvania) by an experienced neuroradiologist blinded to the diagnosis. The data were tabulated and the following parameters calculated: mean MaxA for controls and the nonaffected side of patients, mean MaxA affected side of patients, mean difference in MaxA in patients (affect versus nonaffected) and controls. Results

Twenty-two subjects were recruited consisting of 11 patients and 11 aged-matched controls. In all 11 patients, there was a measurable difference in MaxA between the affected and asymptomatic side. Mean MaxA of controls and the nonaffected side of patients: 24.98 ± 3.88 (19.94-33.37)mm², mean MaxA of affected side of patients: 19.38 ± 5.51 (5.29-25.23)mm², mean difference in MaxA in patients (affect versus nonaffected): 8.03 ± 7.66 (2.85-24.41)mm², and controls: 0.54 ± 0.33 (0-0.81)mm².

Conclusions

A wide variation in maximal cross-sectional area of the affected SO is demonstrated in patients with CSOP which overlaps with normal control SO areas. There is a measurable difference in cross-sectional area of the SO between the affected and nonaffected SO in CSOP patients and between the affected side in CSOP SO areas and control SO areas. Correlations with the presence of CN4 and its nucleus as well as with genotypic will provide insight into the pathophysiological mechanism of CSOP.

KEYWORDS: Congenital

O-113 4:10PM - 4:17PM
Distinguishing Recurrent Thyroid Cancer from Normal Thyroid Tissue Using Multiphasic Multidetector CT-Enhancing Characteristics

J Debnam, N Guha-Thakurta, W Wei, D Schellingerhout
University of Texas MD Anderson Cancer Center, Houston, TX

Purpose

Normal thyroid tissue frequently persists in the thyroid bed following total thyroidectomy and distinguishing this tissue from recurrent disease on follow-up CT images is a diagnostic challenge. We performed multiphase multidetector dynamic CT studies (4D-MDCT) to assess the contrast patterns of recurrent disease and normal thyroid tissue and determine a way to differentiate between these two.

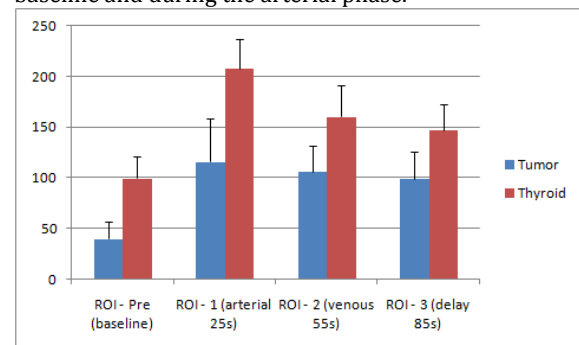
Materials and Methods

Twenty-four patients with 29 nodules of pathologically proven recurrent thyroid carcinoma underwent 4D-MDCT imaging of the neck prior to surgical resection or biopsy. We selected 17 random patients undergoing 4D-MDCT for parathyroid disease without evidence of thyroid cancer to serve as case controls for thyroid enhancing characteristics. Our 4D-MDCT protocol included 4 phases: baseline noncontrast, 25 seconds (arterial phase), 55 seconds (venous phase) and 85 seconds (delayed phase)

after injection. Regions of interest (ROIs) were placed over lesions by identifying the lesion on the most conspicuous phase, defining the lesion with a freehand ROI, and copying this ROI over to the other phases without size variation. Statistical analysis is by Student's T-test.

Results

Thyroid cancer recurrences had baseline Hounsfield densities of 40 ± 16 versus normal thyroid tissue with 100 ± 21 (mean \pm standard deviation). Arterial phase was 115 ± 43 versus 208 ± 29 , venous phase was 106 ± 26 versus 163 ± 30 and delayed phase was 99 ± 27 versus 147 ± 25 . Simple T-test comparisons showed all these differences to be highly statistically significant ($p < 0.01$). It is clear that normal thyroid tissue has a higher density than recurrent disease at baseline and all phases of enhancement, and that these differences are greatest at baseline and during the arterial phase.



Conclusions

Normal thyroid tissue can be differentiated from recurrent thyroid cancer by means of a distinctly different enhancement pattern. These data serve as justification for future prospective human studies.

KEYWORDS: CT, Neoplasm, Thyroid

O-114 4:17PM - 4:24PM
Multimodal Imaging of Pediatric Ocular Syndromes with CNS Involvement

V Batmanabane, M Shroff, P Muthusami, E Heon
Hospital for Sick Children, Toronto, Ontario, Canada

Purpose

Children with ocular syndromes involving the brain need investigation with a variety of imaging modalities to arrive at a specific clinical diagnosis and aid genetic testing and ultimate management of the patient. This pictorial essay illustrates the importance of multimodal imaging and the distinct contribution each makes toward arriving at a comprehensive diagnosis. The classical ocular and intracranial manifestations of these syndromes using ocular imaging like optical coherence tomography (OCT), fundus autofluorescence (FA), and orbital imaging by ultrasonography which complement cranial imaging with computed tomography (CT) and MR imaging (MRI) are described.

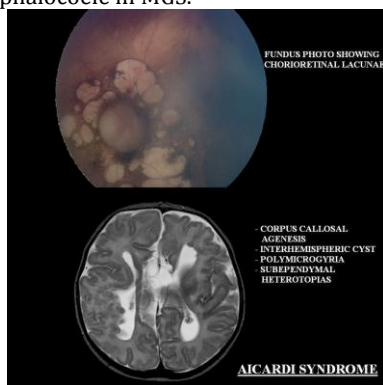
Note: Scanned images are included in the proceedings. Some submitted images were reduced during editing thereby decreasing clarity. Also, refer to the Program Planner. Proceedings Content as of 3/28/2014.

Materials and Methods

Patients with congenital ocular syndromes were identified via a retrospective text search program using relevant keywords. Additional clues to the diagnosis were sought on clinical examination, ocular and fundus photographs, ocular and orbital USG, and brain imaging studies. Pertinent images of each modality were analyzed for diagnostic clues characteristic of a particular syndrome. The confirmation of the genetic diagnosis was accessed from the genetics database.

Results

Optical coherence tomography in Bardet-Biedl and Joubert syndromes reveal characteristic findings of absent or rarefied cone outer segment tips line, and vitreoretinal interface abnormalities. Defects or absence of all retinal layers are seen in morning glory syndrome (MGS), CHARGE (chorioretinal colobomata), and Aicardi syndrome (chorioretinal lacunae). Enlarged optic cups with nerve fiber layer thinning are characteristic of Sturge Weber syndrome (SWS). Retinal capillary hemangioblastomas in von Hippel Lindau (VHL) disease, diffuse choroidal hemangioma in SWS, and retinal hamartomas in tuberous sclerosis are noted on OCT, USG and CT/MRI. Characteristic CT and MRI findings are noted in trilateral retinoblastoma and optic pathway gliomas in neurofibromatosis 1, in addition to the molar-tooth sign in Joubert syndrome, hemangioblastomas in VHL, leptomeningeal angiomatosis in SWS, and trans-sphenoidal basal encephalocele in MGS.



Conclusions

Ocular imaging by OCT and FA can help determine retinal morphological alterations such as thickening, atrophy or excavations which can help explain defective vision in these patients. Abnormal findings will prompt further testing by complementary investigative tools like USG, CT and MRI which provide an extended view into the orbit and cranium, which offer diagnostic clues about nonocular lesions in these syndromes. Such comprehensive imaging not only aids in planning the best approach to diagnosis and management but also serves to prognosticate these disorders.

KEYWORDS: Childhood, CNS, MR Imaging

O-115

4:24PM - 4:31PM

Venous sampling for Cushing's Disease: Comparison of Internal Jugular Vein (IJV) and Inferior Petrosal Sinus (IPS) Sampling

D Sorte, P Gailloud, R Salvatori, M Radvany
The Johns Hopkins University School of Medicine,
Baltimore, MD

Purpose

To compare the accuracy of venous sampling from the internal jugular vein (IJV) with sampling from the inferior petrosal sinus in the setting of Cushing's disease (CD).

Materials and Methods

Twenty consecutive patients who were referred for venous sampling for suspected Cushing's disease underwent a modified venous sampling technique using a coaxial catheter system. Simultaneous baseline venous sampling was performed at five sites: the inferior petrosal sinuses, internal jugular veins and right femoral vein. Venous sampling was repeated after the administration of either corticotrophin releasing hormone (CRH) or desmopressin (DDAVP). The blood samples were analyzed for adrenocorticotropic hormone (ACTH) levels.

Results

Review of the venograms demonstrated appropriate catheter position in 17 of 20 cases. There were no complications associated with the procedures. When measured in the IPS, 17 of 17 cases had ratios diagnostic of CD. When the ratio was measured in the IJV, 9 of 17 (53%) cases had ratios diagnostic of CD. In 14 of 17 cases the IPS ratio lateralized. Of the 13 patients who have undergone surgery, nine had pathology consistent with an adenoma. One additional patient had a clinical cure despite normal tissue in the pathological specimen for a 77% cure rate. In only four cases was there lateralization when IJ ACTH levels were evaluated. In one case this was associated with aberrant drainage of the IPSS. There were not enough cases in the DDAVP group to compare outcomes between the stimulating agents.

Conclusions

Sampling of the IJV is not useful for the evaluation of Cushing's disease, with the exception of rare instances of aberrant IPS drainage.

KEYWORDS: Pituitary Adenoma

O-116

4:31PM - 4:38PM

Retrospective Analysis of Correlation between Computed Tomography (CT) Density and Functional Status of the Thyroid Gland

Y Zhou, V Pandey
Saint Louis University School of Medicine, Saint Louis, MO

Purpose

It has long been known that there is a significant correlation between thyroid CT density and the iodine concentration of the tissue (1), and has been suggested that CT density may have the potential to reflect thyroid

Note: Scanned images are included in the proceedings. Some submitted images were reduced during editing thereby decreasing clarity. Also, refer to the Program Planner. Proceedings Content as of 3/28/2014.

functional status (1, 2). However, the relationship of CT density and thyroid function has not been studied fully. The purpose of this study is to determine the correlation between the CT density (Hounsfield units, HU) of the thyroid gland and its functional status measured by serum thyroid-stimulating hormone (TSH) levels.

Materials and Methods

In this retrospective study, the medical records of patients who had a cervical spine CT examination for a reason not related to thyroid pathologies between June 2012 and August 2013 were reviewed to identify subjects who also had a thyroid functional test (TSH) within three months of the CT scan. A total of 157 patients met the inclusion criteria and were included. The TSH levels were retrieved from the medical record system and the thyroid CT densities (Hounsfield units) were determined on axial images of the noncontrast CT scan using a soft tissue window. For each patient, the CT densities of two regions of interest (ROIs) of at least 20 mm² were measured for each lobe of the thyroid gland and the average of the four measurements was used as the CT density of the corresponding thyroid. The sternocleidomastoid muscles were used as internal controls. The CT densities of both right and left sternocleidomastoid muscles were determined and the mean muscle densities were calculated in the same manner. In this study, 0.4-4.0 μ IU/mL was considered as the normal range for serum TSH levels. The subjects were divided into three groups based on the TSH levels (Low TSH < 0.4 μ IU/mL, Normal TSH 0.4 - 4.0 μ IU/mL and High TSH > 4.0 μ IU/mL) for statistical analyses. In correlation analysis, the patients were divided into two groups, those with TSH < 3.0 μ IU/mL and those \geq 3.0 μ IU/mL.

Results

There were 77 female and 80 male patients, with ages ranging from 20 to 112 years and an average age of 60.7 years. The mean thyroid CT densities for the Low, Normal and High TSH groups were 83.1 ± 16.5 HU (n = 51), 97.4 ± 16.7 HU (n = 78) and 83.0 ± 21.5 HU (n = 28), respectively. Both Low and High TSH groups demonstrated significantly decreased thyroid CT densities when compared to the normal group (P < 0.0001, for both groups). In contrast, the mean densities of the sternocleidomastoid muscles for the same groups were 54.1 ± 9.0 HU (n = 51), 55.5 ± 10.8 HU (n = 78) and 52.6 ± 8.1 HU (n = 28), respectively, with P values of 0.47 and 0.20 for the Low and High TSH groups, respectively, when compared with the Normal TSH group. This result suggested that there was no significant difference in the CT densities of the muscles between the normal and abnormal TSH groups. In addition, correlation analysis demonstrated a weak positive correlation between the thyroid CT densities and TSH levels (r = 0.42; P < 0.00001, n = 125) for subjects with a TSH level < 3.0 μ IU/mL and a moderate negative correlation (r = -0.64; P < 0.0001, n = 30) for those with a TSH level \geq 3.0 μ IU/mL.

Conclusions

The CT density of the thyroid gland is correlated to its functional status as measured by the serum TSH levels. Patients with both abnormally increased and decreased TSH levels demonstrated significantly decreased CT

densities, a relationship not observed in the muscle tissue. There is a weak positive correlation between the thyroid CT density and the TSH levels for subjects with TSH levels < 3.0 μ IU/mL and a moderate negative correlation for patients with TSH levels \geq 3.0 μ IU/mL. Therefore, the CT density of thyroid may be an indicator of the thyroid function status, and when CT density of the thyroid gland is below 80 HU on a routine noncontrast cervical spine CT, it may be warranted to recommend a thyroid function test.

KEYWORDS: CT, Density, Thyroid

Monday, May 19
3:00 PM – 4:30 PM
Room 517d

19 - PARALLEL PAPERS: Brain:
Neoplasms II

O-117 3:00PM - 3:07PM
Added Value of Dynamic-susceptibility contrast (DSC) MRI and Susceptibility Weighted Imaging in Differential Diagnosis of Solitary Brain Masses

S Sood, R Gupta, J Sharma, J Modi
Medanta-The Medicity, Gurgaon, India

Purpose

Susceptibility-weighted imaging (SWI) and dynamic susceptibility contrast (DSC) perfusion images are used routinely for characterization of brain lesions. The purpose of this study was to determine the added value of these for differentiating solitary intra-axial brain lesions (tumoral versus nontumoral; differentiating tumor types) by combined assessment of intralesional susceptibility artifacts (ILSA) and the relative cerebral blood volume rCBV.

Materials and Methods

Thirty-five patients with solitary intra-axial brain lesions, without previous surgery, were reviewed retrospectively. Independent reviews were performed by two neuroradiologists blinded to the histopathology results using conventional MR images alone and with adjunctive SWI and DSC perfusion MR imaging (MRI). The solitary lesions were assessed with presence of intralesional susceptibility artifacts (ILSA) (0,1+,2+,3+) and rCBV (hypoperfusion/moderate perfusion/high perfusion) and the imaging diagnosis were compared with specific histopathologic types of lesions. Clinical diagnosis/response to treatment on follow up was considered in case histopathology was not available as in infective lesions.

Results

Two observers diagnosed lesional pathology accurately in 18 (51.4%) of 35 lesions after reviewing the conventional images alone and 26 (74.2%) of 35 lesions after reviewing

Note: Scanned images are included in the proceedings. Some submitted images were reduced during editing thereby decreasing clarity. Also, refer to the Program Planner. Proceedings Content as of 3/28/2014.

the adjunctive SWI and DSC perfusion MRI. Intralesional susceptibility signal were seen in 10 (100%) of 10 glioblastoma multiformes (GBMs) usually 3+, in one (25%) of five anaplastic astrocytomas, in two (40%) of five metastatic tumors, two (40%) of five anaplastic oligodendrogliomas and 1(25%) of five tuberculoma. No susceptibility signal was seen in three of the lymphomas, one toxoplasmosis and low grade gliomas. There was a significant difference in ILSA being more prominent in GBM (3+) than other lesions. On DSC perfusion MRI high rCBV was in all of the GBMs (solid portions) and metastasis (100%), moderately high perfusion in lymphomas (100%) and low perfusion in anaplastic astrocytomas (grade II-III), anaplastic oligodendrogliomas, low grade glioma and tuberculomas. A combination of high (3+) intralesional susceptibility artifacts (ILSA) and high perfusion significantly adds to the correct diagnosis of glioblastomas over metastasis. No ILSA seen was in moderately perfused lymphomas. Solitary enhancing circumscribed lesions showing low perfusion with no/low ILSA favor tuberculoma over infiltrative/low grade gliomas (infiltrative, nonenhancing with low perfusion and no ILSA). Diagnosis of tumefactive demyelination versus low to indeterminate grade glioma can be challenging even with perfusion MRI and SWI.

Conclusions

The use of DSC MRI and SWI together significantly improves the diagnostic accuracy for the differential diagnosis of solitary brain lesions compared with the use of conventional MR imaging alone.

KEYWORDS: MR Imaging Perfusion, Neoplasm, Susceptibility-Weighted Imaging

O-119 3:14PM - 3:21PM
Assessment of Recurrent Glioblastoma Multiforme Response to Treatment with Bevacizumab: A Diffusional Kurtosis Imaging Study

C Lee, A Kalra, M Vittoria-Spampinato, A Tabesh, J Jensen, J Helpert, M Falangola, M Van Horn, P Giglio
Medical University of South Carolina, Charleston, SC

Purpose

Bevacizumab has been used increasingly in treating recurrent glioblastoma multiforme (GBM). However, only a fraction of patients respond to the treatment, and effective assessment of treatment response remains difficult. Standard postcontrast T1 and FLAIR images can either exhibit 'pseudoresponse' or 'pseudoprogression' (1, 2). Recently, diffusion-weighted imaging (DWI) was shown to predict or correlate with tumor response to Bevacizumab treatment (3-6). In this study, we investigate whether diffusional kurtosis imaging (DKI) (7) can effectively evaluate recurrent GBM response to Bevacizumab treatment. We hypothesized that volumetric analysis of DKI-derived diffusion parameters may help stratify patients into "responders" and "nonresponders".

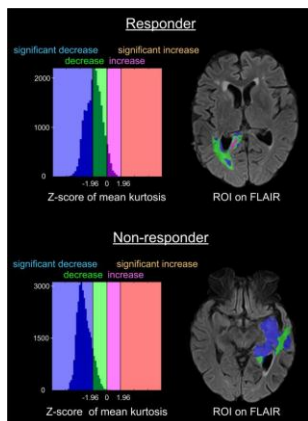
Materials and Methods

Patients: Ten patients (56.7 ± 9.2 years, 6 females) diagnosed with recurrent GBM were included in this study. All patients previously underwent postoperative therapy, including radiation combined with chemotherapy (Temozolomide) or radiation alone. Bevacizumab was given every two weeks. One patient was later excluded from the study due to Bevacizumab induced thrombocytopenia. The remaining nine patients were classified into two groups based on a threshold of 90 days progression free survival (PFS): responders (n = 5) with PFS mean of 234 days (range: 90-255 days) and nonresponders (n = 4) with PFS mean of 35 days (range: 28-56 days). **MR imaging (MRI):** Baseline (1-3 days before treatment) and posttreatment (28 days after treatment) MRI scans were obtained from each patient. MR imaging scans were performed on a Siemens 3 T scanner and included standard postcontrast T1, FLAIR, and DKI with b = 0, 1000, and 2000 s/mm² along 30 encoding directions. Diffusional kurtosis images were used to estimate diffusion and diffusional kurtosis tensors (8), from which parametric maps of mean diffusivity (MD), fractional anisotropy (FA), and mean kurtosis (MK) were generated. **Image Analysis:** Diffusion maps and FLAIR images were first coregistered to T1-weighted images to ensure the same anatomical space for all images. Regions-of-interest (ROIs) were defined by FLAIR hyperintensity excluding necrosis. Z-scores of each image voxel in the ROI were computed to quantify the changes in MD, FA, and MK with respect to normal appearing white matter (NAWM) (6). Region of interest image voxels then were classified into "significant increase", "increase", "significant decrease", and "decrease" based on a 95% confidence interval of z-scores (Figure 1). These statistically quantified changes were compared between the responder and nonresponder groups using the two-samples t-test (one-tailed, unequal variances assumed) with a significance level p = 0.05.

Results

In post-treatment MK maps (28 days after treatment), responders showed a significantly smaller ratio of significantly decreased MK volume to decreased MK volume than nonresponders (ratio: 1.4 ± 0.8 versus 5.8 ± 3.8, p = 0.048). This indicates that responders had a smaller portion of significantly decreased MK volume than nonresponders (Figure 1). MD, FA, and volume of abnormal FLAIR signal showed no significant changes.

Note: Scanned images are included in the proceedings. Some submitted images were reduced during editing thereby decreasing clarity. Also, refer to the Program Planner. Proceedings Content as of 3/28/2014.



Conclusions

Our preliminary results demonstrated that post-treatment (28 days after treatment) volumetric changes in MK may help stratify patients into responders and nonresponders (mean PFS: 234 versus 35 days). This suggests that DKI may be useful for early assessment of recurrent GBM response to Bevacizumab treatment.

KEYWORDS: Diffusion Kurtosis Imaging, Glioblastoma, MR Imaging

O-120 3:21PM - 3:28PM
T1-Rho Imaging of Brain Tumors: A Novel Method to Predict Histology of Intracranial Masses

S Hipko¹, V Kalia¹, R Watts¹, T Andrews², J Gonyea¹, K Ducis¹, C Lin¹, C Filippi³, J Nickerson¹

¹University of Vermont College of Medicine, Burlington, VT,
²Philips Healthcare Cleveland Ohio, Burlington, VT,
³Columbia University Medical Center, New York, NY

Purpose

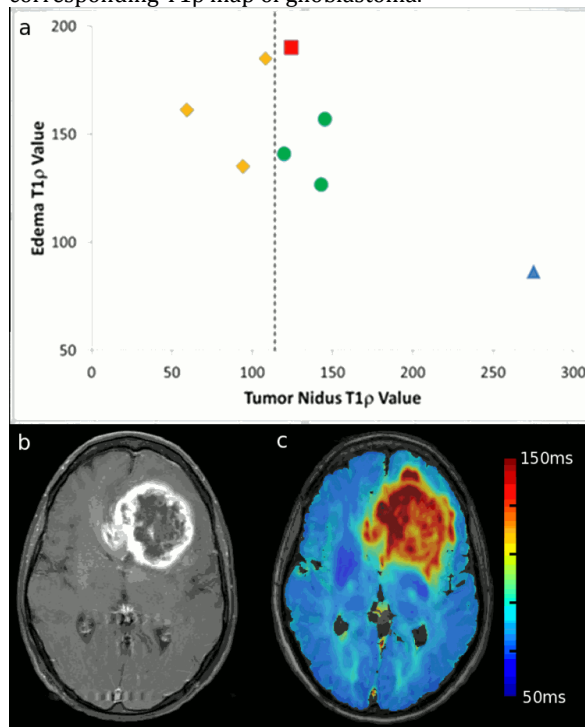
T1-Rho ($T1\rho$) is an inherent tissue contrast in MR imaging (MRI) that has shown sensitivity to macromolecules (proteins). Our aim in this study is to investigate whether the $T1\rho$ sequence may provide a useful biomarker for differentiation of intracranial masses.

Materials and Methods

Eight subjects (1 male and 7 females, aged 27-72 years) with newly diagnosed intracranial masses (3 glioblastoma, 2 metastatic melanoma, 1 metastatic rectal cancer, 1 hemangiopericytoma, and 1 hemangioblastoma) were imaged at 3.0 T utilizing a novel a 3D whole brain fluid suppressed turbo spin echo $T1\rho$ -weighted sequence along with standard intracranial mass MRI sequences such as T1, T1 postcontrast, and FLAIR sequences. All subjects were scanned with spin-lock (SL) times of 0, 20, 40, 60, 80, and 100 msec at 500 Hz. After image acquisition, two regions of interest were defined by a neuroradiologist for each patient: one in the tumor nidus and one in the surrounding peritumoral T2 hyperintensity, and also in ipsilateral and contralateral normal-appearing white matter. Quantitative $T1\rho$ and T2 values were obtained for each of these regions of interest.

Results

Figure 1A shows a scatterplot comparing $T1\rho$ values (A) of tumor nidus versus tumor edema in eight patients with intracranial masses (Yellow diamonds = metastatic lesions, Green circles = glioblastoma, Red square = anaplastic hemangiopericytoma, Blue triangle = hemangioblastoma). Metastatic lesions demonstrate lower $T1\rho$ values compared to both low and high-grade primary intracranial masses (Figure 1). Within the peritumoral T2 hyperintensity, the high grade primary tumors (glioblastoma) are of lower $T1\rho$ value than the low grade neoplasm. Figure 1B shows a T1 postcontrast MRI image of glioblastoma in left frontal lobe and Figure 1C shows the corresponding $T1\rho$ map of glioblastoma.



Conclusions

Though these data were collected in a small group of patients, they suggest that further research into $T1\rho$ characteristics of various intracranial masses holds potential and value in aiding diagnosis, treatment planning, and prognostication before final pathology results may be available.

KEYWORDS: Contrast, Grading Scale, Neoplasm

O-121 3:28PM - 3:35PM
Diagnostic Performance Of Magnetic Resonance Imaging In The Diagnosis Of Intracranial Tumors - Comparison With Pathology Results

M Diogo, I Fragata, J Ramalho, J Jacinto, J Pamplona, C Conceição, C Martins, N Caçador, M Mafra, J Reis
Centro Hospitalar Lisboa Central, Lisbon, Portugal

Note: Scanned images are included in the proceedings. Some submitted images were reduced during editing thereby decreasing clarity. Also, refer to the Program Planner. Proceedings Content as of 3/28/2014.

Purpose

A correct diagnosis of intracranial tumors on magnetic resonance imaging (MRI) implies an accurate distinction of tumor characteristics, specifically its location (intra versus extra-axial), its nature (benign versus malignant), and its origin (primary versus secondary). We analyzed the diagnostic performance of MR imaging (MRI) in our center in pathology proven intracranial tumors.

Materials and Methods

Patients with brain tumors were searched in MRI and pathology databases between January 1, 2010 and April 1, 2010. One hundred sixty-four consecutive patients constituted our study population (81 males, 83 females, minimum age 3 years old, maximum age 87 years old). The MRI reports were performed by board-certified neuroradiologists and retrospectively analyzed regarding the diagnostic impression and compared with the pathology reports. Agreement on intra/extra-axial location, benign/malignant, primary/secondary, and diagnostic impression of tumor histology were analyzed. Performance diagnostic tests, including sensitivity, specificity, positive predictive value, and accuracy were calculated.

Results

Sensitivity and specificity were calculated as follow: 90.5% and 94% for the diagnosis of intra/extra-axial location; 80.5% and 92.6% for benign/malignant tumor; and 73.5% and 76.5% for primary/secondary tumor. The accuracy of the diagnostic impression compared with tumor histology was 57%. There was a total of 10% false negatives for tumor diagnosis. Overall diagnostic accuracy was highest for the diagnosis of extra-axial versus intra-axial lesions (96%). Positive predictive value was highest for intra/extra-axial location (95%) and for benign/malignant tumor (94%), and significantly lower in distinguishing primary from secondary tumors (74%).

Conclusions

MR imaging is reliable in the diagnosis and characterization of intracranial tumors. Higher sensitivity, specificity and positive predictive values were found for the differentiation of intra-axial versus extra-axial lesions, and of benign versus malignant lesions.

KEYWORDS: MR Imaging Brain, Neoplasm, Quality Control

O-121 3:35PM - 3:42PM
Imaging Genomic Mapping of Tumor Volume MRI phenotypes in Glioblastoma Multiforme and Correlation with the Survival and Treatment Response

Z Mahmood, J Wang, G Thomas, M ElBanan, P Zinn, R Colen
MD Anderson Cancer Center, Houston, TX

Purpose

The search for the effective therapy for glioblastoma (GBM) continues despite the recent discoveries of new molecular targets and pathways. MR imaging (MRI) is a noninvasive diagnostic modality previously validated to be able to perform robust radiogenomic (imaging genomic) screens for uncovering potential novel molecular targets/determinants (1, 2). Thus, we seek to provide

comprehensive image genomic analysis in GBM using quantitative MRI enhancing volume and large scale gene and microRNA expression profiles and correlating with survival.

Materials and Methods

Based on The Cancer Genome Atlas (TCGA), discovery and validation sets with gene, microRNA and quantitative MR imaging data were created. Top concordant genes and microRNAs correlated with high CE volumes obtained from the contrast-enhanced MRI (downloaded from the Cancer Imaging Archive); both sets were further characterized by Kaplan Meier survival statistics, microRNA-gene-imaging correlation analysis, and GBM molecular subtype-specific distribution.

Note: Scanned images are included in the proceedings. Some submitted images were reduced during editing thereby decreasing clarity. Also, refer to the Program Planner. Proceedings Content as of 3/28/2014.

Results

The top upregulated and downregulated gene in both the discovery and validation sets was identified in those patients with high CE volume. Patients with high CE volume demonstrated gene and microRNA signatures associated with angiogenesis. These patients also had poor survival.

Conclusions

Here, we present our imaging screening method for molecular cancer subtypes and genomic correlates of contrast enhancing tumor volume. Our findings also have potential therapeutic significance since successful molecular targeting of those genes, microRNA and pathways involved in the growth of high contrast enhancing tumor volumes will improve therapy and patient survival in GBM.

KEYWORDS: Contrast Enhancement, Glioblastoma, Imaging Genomics

O-122 3:42PM - 3:49PM
Imaging Genomic Biomarker Signature for 1p/19q Deletion Identification in Glioblastoma

A Amer, M ElBanan, Z Mahmood, G Thomas, J Wang, P Zinn, R Colen
MD Anderson Cancer Center, Houston, TX

Purpose

To create an imaging genomic biomarker signature in order to identify those glioblastoma patients (GBM) with 1p/19q deletion. Recent prospective randomized clinical trials have validated associations between 1p/19q codeletion and increased overall survival of patients treated with radiation therapy with or without chemotherapy.

Materials and Methods

Using The Cancer Genome Atlas (TCGA), we identified 99 treatment naive GBM patients for whom both gene and miRNA expression profiles including the 1p/19q deletion status, and pretreatment MR neuroimaging from The Cancer Imaging Archive (TCIA) were available. The VASARI feature set and 3D Slicer software 3.6

(<http://www.slicer.org>) were used for image analysis and image review was done in consensus by two neuroradiologists. Fluid attenuated inversion recovery (FLAIR) was used for segmentation of the edema and postcontrast T1-weighted imaging (T1WI) for segmentation of enhancement (defined as tumor) and necrosis. Imaging parameters then were correlated with 1p/19q deletion status and gene expression profiles. Complex biomarker signatures based on profiling and survival were created.

Results

A specific imaging biomarker signature using multiple imaging parameters predicted the presence of 1p/19q codeletion in patients with GBM. These also were associated with overall and progressive-free survival.

Conclusions

Imaging genomic signatures can be expected to promote a more robust personalized approach to patient care and accelerate drug development and clinical trials. An imaging biomarker signature was created using both qualitative and quantitative imaging parameters that predicted 1p/19 deletion status and expression.

KEYWORDS: Glioblastoma, Imaging Biomarker, Imaging Genomics

O-124 3:56PM - 4:03PM
Pitfalls of Inoperative Magnetic Resonance Imaging (IoMRI) of Pediatric Brain Tumors: Results of a Four-Years' Experience

C Saint-Martin, J Atkinson, J Farmer, J Montes
McGill University Health Center, Montreal, Quebec, Canada

Purpose

To review causes of false positive, false negative, misread inoperative MR images (IoMRI) obtained during surgery of pediatric brain tumors.

Materials and Methods

We retrospectively reviewed the inoperative MR images obtained during the surgery of pediatric brain tumors performed between October 2009 and 2013 at the Montreal Children's Hospital. All of the patients underwent inoperative MRI during and/or at the surgery. Inoperative MRI was obtained on 3 T magnet with an 8-channel inoperative head coil. Images were analyzed at the time of acquisition by a senior pediatric neuroradiologist and the operating neurosurgeon in consensus. Correlation with first postoperative MRI follow-up findings was performed in terms of evaluation of degree of resection, immediate complications and limitations.

Results

Among all of the pediatric neurosurgical procedures done at the Montreal Children's Hospital between 2009 and 2013, 176 benefit from IoMRI, 126 (108 patients) were indicated for intracranial tumor and 50 (45 patients) for epilepsy surgery. Eighteen patients were excluded due to nonavailable follow-up examination. Mean age was 8.9 years. Among the 90 patients included (53 male, 37 female), a total of 108 surgeries was performed for supratentorial (70), infratentorial (35) and extra-axial (3) mass lesion. Based on IoMRI results, gross total resection (GT) was achieved in 57/108 surgeries, subtotal resection (ST) in 33/108 cases, including cases with further resection and no residual (ST-GT) or residual (ST-EXT) tumor at end of surgery. Eighteen surgeries initially were planned partial or biopsies (PP). On the follow-up MRI obtained with a mean postoperative interval of 104 days, 52/57 GT were confirmed with no residual or recurrence seen; 4/33 ST did not have residual corresponding to false positive cases. Overall, accuracy of the IoMRI findings was 90%. Out of the 57 cases with GT resection assessed on IoMRI, five showed tumoral tissue on the first postoperative follow-up MRI. In all of these cases, the resected tumor was of high grade malignancy

Note: Scanned images are included in the proceedings. Some submitted images were reduced during editing thereby decreasing clarity. Also, refer to the Program Planner. Proceedings Content as of 3/28/2014.

(glioblastoma multiformis, supratentorial anaplastic ependymoma, metastasis of rhabdomyosarcoma, undifferentiated medulloblastoma). Rapid local recurrence of these malignant lesions could explain the discrepancy between inoperative and follow-up MRIs. In the four false-positive cases with misread IoMRI, several causes were identified, including venous enhancement, surgical bed enhancement as well as blood by product deposits in the surgical cavity. In addition to assessing degree of tumor resection, IoMRI revealed unexpected complications of potential clinical significance on patient's outcome including acute ischemic arterial infarct, active bleed in the surgical bed as well as vascular injury.



Conclusions

Inoperative MRI is a valuable tool to help neurosurgeons achieve gross total resection of pediatric brain tumors. Reading IoMRI is still a challenge to radiologists. We illustrate and explicit causes of potential errors and difficulties of MR interpretation including unexpected complications.

KEYWORDS: MR Imaging, Neuronavigation, Pediatric Brain Tumors

0-125 4:03PM - 4:10PM
CT In The Diagnosis Of Intracranial Tumors: Is The Diagnostic Performance Of The Attending Neuroradiologists Better Than The Resident's?

M Diogo, I Fragata, J Ramalho, J Jacinto, J Pamplona, C Conceição, C Martins, N Caçador, M Mafra¹, J Reis
Centro Hospitalar Lisboa Central, Lisbon, Portugal

Purpose

Computed tomography (CT) is usually the first exam performed for the diagnosis of intracranial tumors, many times in the emergency setting, and frequently by the resident on call. Accurate distinction between intra- and extra-axial, benign or malignant and primary versus secondary lesions is important to reach a correct diagnostic impression and follow-up approach. We hypothesized that experienced certified board

neuroradiologists would be able to better analyze CT images and obtain correct diagnosis of intracranial tumors when compared to neuroradiology residents.

Materials and Methods

Patients with brain tumors were searched in CT and pathology databases between January 2010 and April 2010. Reports of 86 CT in 86 patients (36 male and 50 female, minimum age 3 years, maximum age 85 years) with pathology proven intracranial tumors were analyzed retrospectively, and diagnostic impressions were compared to the final pathology reports. The diagnostic performance of the neuroradiology residents and attending neuroradiologists in the diagnosis of intracranial tumors were compared. Agreement on intra-/extra-axial location, benign/malignant, primary/secondary tumor, and diagnostic impression of tumor histology were analyzed separately for reports performed by residents and attending neuroradiologists. Sensitivity, specificity, positive predictive value, and accuracy were calculated for these parameters.

Results

Sensitivity, specificity and positive predictive value for neuroradiology residents on CT were respectively 75%, 100% and 100% for intra-/extra-axial location of tumor, 60%, 67% and 78% for benign/malignant tumor and 50%, 82% and 33% for primary/secondary tumor. For attending neuroradiologists the sensitivity, specificity and positive predictive value were significantly higher and calculated in 80%, 100% and 100% for intra-/extra-axial location of tumor, 71%, 100% and 100% for benign/malignant tumor and 66%, 97% and 66% for primary/secondary tumor, respectively ($p < 0.05$). There also were significant differences between residents and attending neuroradiologists concerning the accuracy of the diagnostic impression for tumor histology, with 37% and 66%, respectively ($p < 0.05$).

Conclusions

There were significant differences between residents and attending neuroradiologists in the interpretation of CT scans of intracranial tumors. Attending neuroradiologists had consistently higher scores in every parameter analyzed. Our study highlights the importance of routine supervision and validation of the resident reports, especially in the emergency setting.

KEYWORDS: Neoplasm, Report Content, Resident Training

0-127 4:17PM - 4:24PM
Comparison of cerebral blood volume and plasma volume in untreated intracranial lesions.

S Bazyar¹, J Ramalho², A Franceschi³, Y Lee²

¹University of North Carolina, Raleigh, NC, ²University of North Carolina Chapel Hill, Chapel Hill, NC, ³SUNY Stony Brook, Stony Brook, NY

Purpose

Cerebral blood volume (CBV) and plasma volume (Vp) permit the noninvasive assessment of the microvasculature of brain tumors. Cerebral blood volume

Note: Scanned images are included in the proceedings. Some submitted images were reduced during editing thereby decreasing clarity. Also, refer to the Program Planner. Proceedings Content as of 3/28/2014.

and Vp should represent related vascular spaces, differentiated by hematocrit, and thus theoretically should be directly related. However, the acquisition of the two parameters utilizes not only significantly different MR imaging (MRI) approaches, but significantly different modeling assumptions. Our purpose was to examine the equivalence of CBV and Vp, and the potential for using these parameters to distinguish different types of intracranial lesions.

Materials and Methods

In this retrospective study patients were scanned with a standard clinical protocol that included both dynamic contrast enhancement (DCE) and dynamic susceptibility contrast (DSC) imaging after the gadolinium contrast agent injection (gadobenate dimeglumine, 0.1 mmol/kg). Our study population included 27 histologically proven untreated newly diagnosed brain tumor patients: Glioblastoma multiformis (GBM) WHO grade IV (n=6), Meningiomas (n=7), and Metastasis (n=14: four from breast cancer, three from gastrointestinal cancer, three from urogenital cancer, three from nonsmall cell lung cancer and one from melanoma). Regions of interest (ROIs) were delineated manually avoiding hemorrhage and necrosis. The lesion shape guided the shape of the ROI to minimize confounding factors. The ROIs size varied between 0.2-0.3cm² and multiple ROIs were drawn in same lesion, based on the lesion size. A total of 86 ROIs [GBM (n=34), meningiomas (n=33), and metastasis (n=19)] were drawn. The ROIs were propagated to DSC-MR images to calculate the CBV in same region. Rational regional CBV (rrCBV) were calculated based on the contralateral white-matter CBV. The hematocrit (HCT) effect was eliminated in our calculations. In metastatic lesions we assessed the rrCBV and Vp correlation in all metastatic lesions and also in lesions with same type of primary tumors separately. Statistical analyses were performed with Pearson and Spearman correlations.

Results

rrCBV and Vp correlation was improved in meningioma (Pearson correlation=0.859, Spearman correlation coefficient=0.641, P <0.01), followed by GBM (Pearson correlation=0.546, Spearman correlation coefficient=0.649, P <0.01). This relation was not significant in metastatic lesions even in patients with the same type of primary tumor. The pattern remained the same even after eliminating the HCT effect.

Conclusions

rrCBV and Vp correlate well in meningioma and moderately well in GBM. Metastatic lesions did not show adequate correlation. This difference in correlation suggests that Vp and rrCBV represent more significantly different vascular processes than their definitions would initially suggest. Furthermore, in cases of an unknown diagnosis, examining the relationship between rrCBV and Vp may help differentiate between metastases and GBMs, while rrCBV and Vp range have a huge overlap in these two pathologies.

KEYWORDS: Brain Neoplasms, Cerebral Blood Volume, Permeability MR Imaging

0-128

4:24PM - 4:31PM

Comprehensive Motion-Corrected Neuroimaging Protocol

S Amukotuwa¹, M Aksoy¹, J Maclaren¹, R Bammer²

¹Stanford University, Stanford, CA, ²Stanford University Hospital, Stanford, CA

Purpose

Motion artifacts degrade roughly one third of MR imaging (MRI) studies and render approximately one study per day nondiagnostic, therefore patient motion persists to be a considerable problem in MRI studies of the brain. In the U.S., the estimated economic impact has been estimated recently to amount to \$150-200k/year/MR scanner. Despite attempts to correct for motion with specific MRI acquisition methods that allow for retrospective corrections (e.g., PROPELLER/BLADE) or adaptive approaches (e.g., PACE, PROMO), one major limitation is the lack of a comprehensive solution that applies to all MR pulse sequences. Here, we present an approach that allows one to perform motion correction for a complete suite of brain MR sequences, without an accompanying scan time penalty.

Materials and Methods

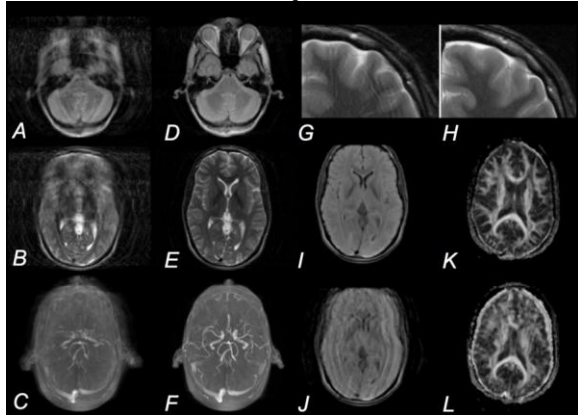
A comprehensive neuroimaging protocol was augmented by the ability to adapt to patient head position changes in real time for each pulse sequence. Specifically, the protocol implemented on a GE 3 T (750w) comprised: 3D T1w BRAVO, PDw/T2w FSE, T1 FLAIR, T2 FLAIR, 3D TOF COW, 3D PCASL, 3D SWAN, high-resolution T2w FSE and DWI. The pulse sequences were updated with patient head position information at a rate of 60 times per second using a MR-compatible, in-bore optical tracking system (HobbitView, Atherton, CA) that was independent of the MR acquisition process. All experiments were IRB approved and informed consent was obtained. Eight volunteers performed prespecified motion maneuvers mimicking patterns commonly encountered on routine brain scans: (i) sustained motion for the entire exam; (ii) rapid abrupt motion; (iii) coughing; (iv) "falling asleep"/nodding; (v) no motion.

Results

In all subjects, motion caused substantial artifacts that rendered all sequences diagnostically inadequate. Some sequences (e.g., FSE) were more prone to motion than others (e.g., BRAVO, EPI). Our adaptive motion correction technique was able to fix motion artifacts in all subjects and all sequences. Most importantly, all studies could be rendered diagnostically adequate by application of this technique. A few residual artifacts remained on certain sequences that are more prone to motion than others, but this did not impact the radiologists' ability to make a diagnosis. High-resolution T2-weighted FSE often suffers from ringing/ghosting artifacts even in cooperative subjects who try to hold still. Thus, there is a diminishing return from going to higher resolution. However, pristine image quality could be achieved when motion correction was turned on indicating that these artifacts are due to motion and emphasizing that even in cooperative subjects motion correction is beneficial. Since the pose tracking

Note: Scanned images are included in the proceedings. Some submitted images were reduced during editing thereby decreasing clarity. Also, refer to the Program Planner. Proceedings Content as of 3/28/2014.

focuses on one landmark, all scans are perfectly registered to each other. An added benefit of this registration step is that it even allows the patient to leave the scanner in between exams as long as the tracking marker on the forebrain is not removed or its position altered; this is potentially of value in many settings, such as delayed postcontrast studies and scenarios where the patient has to be recalled for further sequences.



Conclusions

Currently available motion correction methods, which are pulse sequence specific, may result in inadequate correction of diagnostically important "money shot" sequences, and consequently missed diagnoses. Optical motion correction allows tracking motion independent of the MR acquisition process, and can be applied to virtually any pulse sequence. Therefore, our method provides a comprehensive solution for every pulse sequence. The speed and precision of the presented optical method allows one to adaptively correct for motion. In this study, this led to a change from 100% technically inadequate studies to 100% diagnostic studies.

KEYWORDS: Motion Correction, MR Imaging

O-129 4:31PM - 4:38PM
Postcontrast T1 FLAIR versus T1 Fast Spin Echo: Which is the better choice for intracranial lesion evaluation?

N Nouri¹, N Nagornaya¹, P Pattany², k shah², R Quencer³, E Sklar⁴

¹Jackson Memorial Hospital, Miami, FL, ²University of Miami School of Medicine, Miami, FL, ³University of Miami Miller School of Medicine/Jackson Memorial Hospital, Miami, FL, ⁴Jackson Memorial Hospital/University of Miami, Miami, FL

Purpose

Loss of cerebrospinal fluid (CSF) and tissue contrast on 3 T MR imaging (MRI) scanners is a widely known limitation of 3 T MRI. Inversion recovery is used to adjust for this loss but its efficacy postcontrast has not been investigated extensively. Previous studies have evaluated differences in conspicuity of spinal cord lesions on 3 T versus 1.5 T MR imaging in gadolinium-enhanced T1-weighted fast spin echo (FSE) and T1-weighted FLAIR, finding that use of FLAIR may yield increased conspicuity of lesions. The

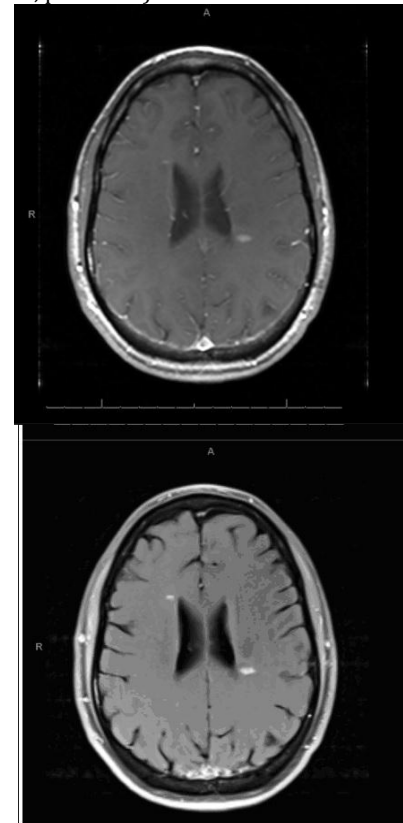
purpose of this study is to determine whether a similar conclusion can be made in the evaluation of intracranial lesions.

Materials and Methods

After the iv administration of gadolinium, T1 FSE and T1 FLAIR sequences were obtained in 30 consecutive patients. Three experienced radiologists were asked to evaluate and compare the conspicuity of abnormal enhancing intracranial lesions between the two sequences. Of the 30 patients, 19 had abnormal enhancing lesions and thus were evaluated. A 5-point number scale was used to score the overall conspicuity of lesions found in each MRI study, with lower numbers representing increased conspicuity of lesions on FLAIR and higher numbers representing increased conspicuity of lesions on FSE.

Results

An increase in conspicuity was consistently seen on T1-weighted FLAIR in comparison to T1-weighted FSE. Utilizing chi-square analysis, the difference in conspicuity between the studies was found to be statistically significant (mean: 2.02, $p < 0.0001$).



Conclusions

In postgadolinium T1 3T MR imaging, T1-weighted FLAIR increases the visualization enhancing brain lesions when compared to T-1 weighted fast spin echo and is therefore recommended as the preferred sequence in routine MR imaging.

KEYWORDS: Fast Spin-Echo, FLAIR, Fluid-Attenuated Inversion Recovery

Note: Scanned images are included in the proceedings. Some submitted images were reduced during editing thereby decreasing clarity. Also, refer to the Program Planner. Proceedings Content as of 3/28/2014.

Monday, May 19
3:00 PM – 4:30 PM
Room 517a

20 - Scenario Planning and the ASNR

O-130 3:00PM - 3:30PM
Scenario Planning: Principles, Theory and Practice

Lexa, F.
Wharton School, Univ. of Pennsylvania, Global Consulting
Practicum
Philadelphia, PA

O-131 3:30PM - 4:00PM
Scenario Planning: The SCARD Experience

Norbash, A.
Boston Medical Center
Boston, MA

O-132 4:00PM - 4:20PM
Relevance to ASNR

Dillon, W.
Univ of California, San Francisco Med Ctr
San Francisco, CA

4:20PM - 4:30PM
Discussion

Monday, May 19
3:00 PM – 4:38 PM
Room 520

21 - Parallel Papers: Trauma

O-906 4:31PM - 4:38PM
Spinal injury, ischemic-anoxic brain injury and its
correlation between abusive head trauma versus
accidental trauma

A Choudhary
Nemours A I DuPont Children's Hospital, Wilmington, DE

Purpose
The purpose of this study is 1. to compare the relative
incidence of spinal ligamentous and soft tissue
abnormalities on spinal magnetic resonance imaging (MRI)
among three groups of children aged < 48 months: 1) those
with abusive head trauma (AHT), 2) those with accidental

trauma, and 3) those with nontraumatic conditions. 2. to
correlate the incidence of ischemic-anoxic brain injury
with ligamentous injury amongst these cohorts.

Materials and Methods

This comparative study included 183 children who
underwent spine MRI: 67 with AHT, 46 with accidental
trauma and a clinical suspicion of spinal injury, and 70 with
nontraumatic conditions. Clinical and radiographic findings
were collected in all cases and were analyzed
retrospectively to identify MRI evidence of traumatic
spinal injuries. The incidence of spinal injuries among the
three groups was compared. The incidence of spinal
ligamentous injuries were calculated for those with and
without radiographic evidence of hypoxic-ischemic
encephalopathy. All comparisons were performed using
Fisher's exact test with $p < 0.05$ considered statistically
significant.

Results

Injuries to the cervical spine ligamentous injuries
(predominantly the nuchal, atlanto-occipital and atlanto-
axial ligaments) were present in 78% of the AHT group,
46% of the accidental trauma group, and 1% of the
nontrauma group; all of these differences were statistically
significant. Among the AHT group, ligamentous injuries
were correlated statistically with evidence of brain
ischemia.

Conclusions

Injury to the cervical spinal posterior ligamentous complex
is common in AHT and even more prevalent than in
clinically symptomatic traumatic cases. The high
correlation between the radiographic findings of
occipitocervical ligamentous injuries and ischemic-anoxic
brain injury is consistent with an interpretation that
transient upper occipitocervical spinal cord injury in AHT
leads to disordered breathing and results in hypoxic-
ischemic encephalopathy. We recommend imaging the
entire spine in AHT to properly identify and classify these
injuries.

KEYWORDS: Abusive Head Trauma, Atlantoaxial, Spinal
Trauma

O-133 3:00PM - 3:07PM
Brain CT and the Detection of Subdural Hematomas in
Trauma: Do coronal and sagittal reformations improve
sensitivity?

W Mostertz, G Maass, K Sharma, M Matheus, W Bartynski1,
Z Rumboldt, T Amrhein
Medical University of South Carolina, Charleston, SC

Purpose

Current standard of care employs emergent noncontrast
brain computed tomography (CT) in the axial plane only as
the initial imaging evaluation for acute head trauma. At our
institution, orthogonal images (coronal and sagittal) have
been included routinely. Our goal was to determine if the
addition of orthogonal imaging planes (coronal and
sagittal) improves the sensitivity for detection of subdural
hematoma (SDH) compared with standard axial brain CT.

Note: Scanned images are included in the proceedings. Some submitted images were reduced during editing thereby decreasing clarity. Also, refer to the Program Planner. Proceedings Content as of 3/28/2014.

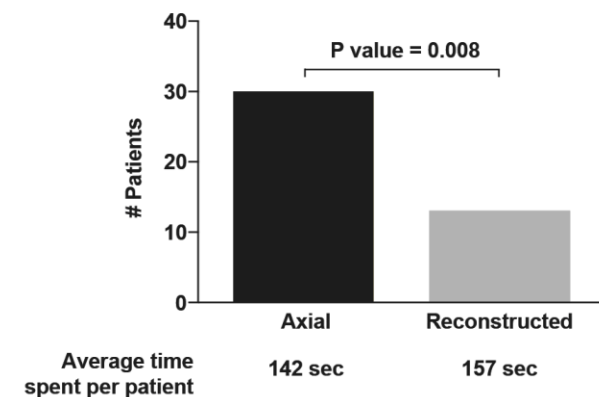
We assumed a null hypothesis of no difference in sensitivity. We also hypothesized that the reading times for the multiplanar CT would not be significantly longer.

Materials and Methods

In this retrospective single institution study, 200 consecutive patients receiving noncontrast brain CT for an indication of trauma met inclusion criteria. By design, equal numbers of patients were assigned to each group: 100 SDHs and 100 controls (negative exams). All patients were anonymized and randomly divided into five sets of 40 (each with 20 SDH, 20 control). Each patient's scan was presented twice, once with axial images only and once with axial, coronal, and sagittal images. Four readers (two CAQ-certified neuroradiologists, a neuroradiology fellow, and one radiology resident) were blinded to the purpose of the study and asked to provide their diagnostic impressions. There were 10 sessions per reader (5 axial, 5 reconstructed). The scan order was randomized for each session, so that no two sessions were identical. Final impressions and average reading times were recorded. Detection rates of SDHs (using the final report as the standard of reference) were compared between axial and reconstructed reading sessions.

Results

Gender distribution was equal between the SDH and control groups (both: 58 male; 42 female). The SDH cohort was significantly older (average 50.6 versus 39.6, $p = 0.0002$). To date, a total of 16 reading sessions have been completed: eight reconstructed and eight axial only. On average, reading time spent per scan was not significantly different between groups (142s axial; 157s reconstructed, $p=0.54$). For axial images only (320 readings), 18.8% of SDHs were not identified (30 of 160) compared to 8.1% (13 of 160) with reconstructed images ($p = 0.008$) (Figure 1).



Conclusions

There was a significantly increased detection rate of SDH with the addition of orthogonal reconstructions, without a significant increase in reading times. Further work will include an assessment of the clinical significance of "missed" SDHs through patient chart review. Increased SDH detection rates in the setting of trauma may reduce patient morbidity and mortality.

KEYWORDS: CT, Subdural Hemorrhage, Traumatic Brain Injury

O-134

3:07PM - 3:14PM

Repeated Head CT in the Neurosurgical ICU: Feasibility of SAFIRE based Ultra - low dose CT for Surveillance

I Corcuera-Solano, A Doshi, A Noor, L Tanenbaum
Mount Sinai Hospital, New York, NY

Purpose

Patients in the neurosurgical intensive care unit (NICU) undergo multiple head CT scans, resulting in high cumulative radiation exposures. Our aim was to assess the acceptability of a dedicated, special purpose SAFIRE iterative reconstruction-based ultra-low dose CT (ULDCT) protocol for NICU surveillance head CT exams, by quantitatively and qualitatively comparing image quality to routine studies on the same patients performed with our standard of care SAFIRE LDCT and legacy FBP SDCT protocols.

Materials and Methods

A retrospective analysis was performed of 54 head CT exams - ULDCT (n=22), LDCT (n=12) and SDCT (n=20) in 22 NICU patients. SDCT were reconstructed using FBP on a Somatom Sensation 64 (Siemens, Erlangen, Germany). LDCT and ULDCT exams were obtained on a Siemens AS+128 scanner with commercially available SAFIRE. Qualitative and quantitative parameters including image quality and dose were evaluated.

Results

SAFIRE ULDCT represented a 68% lower CT DIvol compared to FBP SDCT techniques in the same patients while maintaining similar quality and SNR levels. SAFIRE LDCT offered higher image quality than FBP SDCT ($p < 0.05$) with no differences in SNR at 24 % lower CT DIvol. Compared to LDCT, ULDCT had significantly lower SNR ($p=0.001$) but demonstrated clinically satisfactory measures of image quality.

Table 1. Radiation exposure for the ULDCT, LDCT and SDCT.

	ULDCT (n=22)	LDCT (n=12)	SDCT (n= 20)	SDDCT- ULDCT	(%) [*]	SDCT- LDCT	(%) [*]	LDCT- ULDCT	(%) [*]
CT dose index volume - CTDI _{vol} (mGy)									
Max	20.46	54.71	60.69	40.23	(56)	5.99	(10)	34.24	(62)
Min	11.77	26.79	33.80	22.03	(65)	7.01	(20)	15.03	(56)
Mean	15.55	36.47	48.38	32.83	(68)	11.92	(24)	20.91	(57)
Dose length product -DLP (mGy-cm)									
Max	375.00	958.00	1128.20	753.20	(67)	170.20	(15)	583.00	(61)
Min	188.00	471.00	574.65	386.65	(67)	103.65	(18)	283.00	(61)
Mean	273.39	668.58	843.30	569.91	(67)	174.82	(21)	395.09	(59)
Effective Dose- ED (mSv)									
Max	0.86	2.20	2.59	1.73	(67)	0.39	(15)	1.34	(61)
Min	0.43	1.08	1.32	0.89	(67)	0.24	(17)	0.65	(60)
Mean	0.62	1.53	1.93	1.31	(68)	0.4	(21)	0.91	(59)

Conclusions

In this cohort of NICU patients, dedicated ULDCT for surveillance head CT imaging leads to a significant dose reduction while maintaining adequate image quality.

KEYWORDS: CT, Dose Reduction, Iterative Reconstruction

Note: Scanned images are included in the proceedings. Some submitted images were reduced during editing thereby decreasing clarity. Also, refer to the Program Planner. Proceedings Content as of 3/28/2014.

O-135 3:14PM - 3:21PM
Utility of CT Perfusion in the setting of a false-negative CTA for brain death due to a decompressive craniectomy or major skull fracture

A Pauranik¹, R Aviv², S Symons¹

¹University of Toronto and Sunnybrook Health Sciences Centre, Toronto, ON, ²Sunnybrook and Women's College HSC, Toronto, ON

Purpose

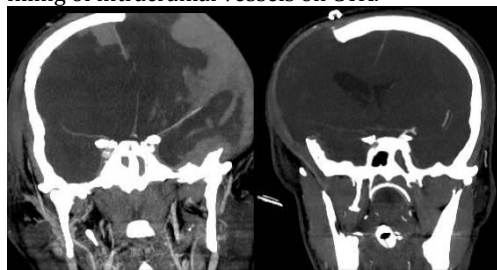
CT angiogram (CTA) is the most commonly used ancillary test in the determination of brain death. However it can be falsely positive (that is negative for brain death) in patients with a decompressive craniectomy or major skull fractures. This is due to the reduction in intracerebral pressure allowing sufficient filling of the intracranial vessels. False negative CTAs can lead to unnecessary delay in diagnosis with implications on organ transplantation as well as use of limited resources on brain dead patients. We explore the utility of CT perfusion (CTP) in these situations.

Materials and Methods

Between January 2013 and August 2013, CTP was performed in five patients with decompressive craniectomy or major skull fracture with clinically and radiologically suspected brain death but negative CTA results. All these patients had adequate opacification of cortical segments of the middle cerebral arteries and internal cerebral veins and thus scored four on the four-point CTA scale. Regions of interest (ROIs) were drawn in bilateral cerebral parenchyma and in deep gray nuclei to assess cerebral blood volume (CBV) and cerebral blood flow (CBF). Mean CBV and CBF were calculated. Values for CBF x CBV were used to assess level of perfusion, with levels below a threshold of 19.72 being regarded as tissue infarction, and thus brain death.

Results

All the patients showed CBV x CBF values less than 19.72 indicating tissue infarction despite presence of adequate filling of intracranial vessels on CTA.



Subject	NCCT findings	CTA SCORE	MEAN CBF	MEAN CBV	MEAN MTT	CBV/CBF
1	diffuse hypodensity, loss of gray white differentiation, large tentorial hematoma, right frontotemporal craniectomy	4	3.56	0.263	10.65	7
2	diffuse hypodensity, loss of gray white differentiation, right frontotemporal craniectomy	4	13.33	1.07	12.49	14.23
3	loss of gray white differentiation, subdural hemorrhage	4	13.1	1.08	12.45	14.31
4	diffuse hypodensity, loss of gray white differentiation, large displaced fracture left skull base	4	13.86	1.09	12.15	15.1
5	loss of gray white differentiation, left hemispheric craniectomy	4	13.54	1.08	12.3	14.6

Conclusions

Computed tomography angiography may be inadequate and falsely negative for the diagnosis of brain death in patients with decompressive craniectomy or major skull fracture. Computed tomography perfusion should be considered in the guidelines as a valid ancillary test in

order to reach conclusive diagnosis early in the management of these patients.

KEYWORDS: Brain Death, Craniectomy, CT Perfusion

O-136 3:21PM - 3:28PM
Aging effect in the alterations of frontoparietal network after mild traumatic brain injury

D Chen, C Chen W Wang, F Yen

Taipei Medical University - Shuang Ho Hospital, Taipei, Taiwan, Province of China

Purpose

Poor attention and memory impairment are symptoms frequently complained after mild traumatic brain injury (mTBI). However, behavioral performance usually was normal in these patients. Frontoparietal network (FPN) is an intrinsic brain network involved in tasks of numerous executive cognitive processes such as attention, motor inhibition and working memory and is constantly observed in the resting-state functional MR imaging (rs-fMRI) studies. Alterations of the FPN after mTBI have been reported in several studies. This study aims to evaluate the influence of age on frontoparietal network connectivity after mTBI.

Materials and Methods

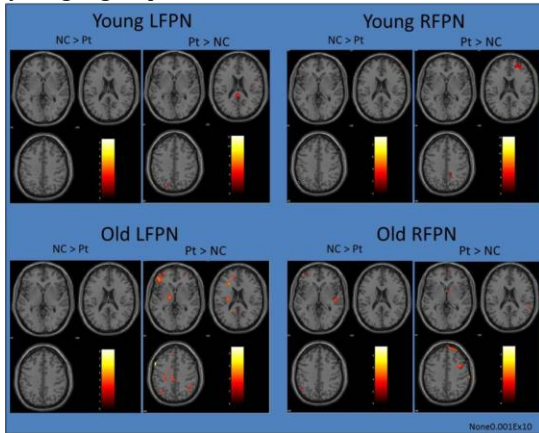
Research ethics committee approval and patient written informed consent were obtained. We collected two groups of mTBI patients (age > 50 years and age < 30 years). The older group contains 13 patients (51~68 years; average 57.7 years) and the younger group contains 13 patients (21~29 years; average 24.7 years). Thirteen age- and gender-matched normal controls (NC) for the older group (51~68 years; average 60.1 years) and 13 age- and gender-matched normal controls for the younger group (21~29 years; average 26.1 years) were recruited. All patients received resting-state fMRIs within two weeks after mTBI on a GE Discovery MR750 3 T MRI scanner. Data preprocessing using SPM8 (www.fil.ion.ucl.ac.uk/spm) included slice timing correction, head motion correction, spatial normalization to the MNI template, and spatial smoothing. Group independent component analysis (ICA) was performed using GIFT (<http://icatb.sourceforge.net>). For each group, the preprocessed images from all subjects were concatenated and reduced by two-step principal component analysis, followed by independent component estimation with the Infomax algorithm. The group ICA analysis on each group was run 20 times using the ICASSO function to ensure stability and reliability of the 20 estimated components. A set of average group components were created and back-reconstructed into single-subject space. The individual subjects' components were scaled to spatial z-score maps by subtracting the global mean from each voxel and dividing by the global standard deviation and then entered into a one-sample t test ($p < 0.01$, corrected for multiple comparisons with false discovery rate criterion; cluster threshold = 10 voxels). Two-sample t test were performed to assess group differences between

Note: Scanned images are included in the proceedings. Some submitted images were reduced during editing thereby decreasing clarity. Also, refer to the Program Planner. Proceedings Content as of 3/28/2014.

carriers and noncarriers results ($p < 0.001$ uncorrected; cluster threshold = 10 voxels).

Results

One-sample t test results showed bilateral FPN connectivity in the younger and older groups. The lateralized FPN component included the brain regions in the ipsilateral intraparietal sulcus, inferior parietal lobe, and dorsal premotor cortex, as well as some minor brain regions in the contralateral dorsal premotor and inferior parietal cortex, which were consistent with previous reports. Figure 1 shows two-sample t test results of bilateral FPN connectivity compared between the mTBI patients and the normal controls. In the younger group, increased FPN connectivity was found both in the RFPN and LFPN relative to the normal control. In the older group, there also was increase in bilateral FPN connectivity relative to the normal control. However, the older group showed greater extent of increase in FPN connectivity than the younger group.



Conclusions

This study found that bilateral FPN connectivity was increased in both the younger and older adults after mTBI. However, greater extent of increase in FPN connectivity was found in the older group than the younger group.

KEYWORDS: Aging, Functional Connectivity, Mild TBI

O-137

3:28PM - 3:35PM

Diffusion Tensor Imaging for Outcome Prediction in Complicated and Uncomplicated Mild Traumatic Brain Injury

E Yuh¹, S Cooper¹, P Mukherjee¹, J Yue¹, H Lingsma², W Gordon³, A Valadka⁴, D Okonkwo⁵, D Schnyer⁶, M Vassar¹, A Maas⁷, S Casey¹, M Cheong¹, K Dams-O'Connor³, A Hricik⁵, T Inoue¹, D Menon⁸, J Pacheco⁶, A Puccio⁵, G Manley¹

¹University of California San Francisco, San Francisco, CA, ²Erasmus Medical Center, Rotterdam, Netherlands, ³Mount Sinai School of Medicine, New York, NY, ⁴Seton Brain and Spine Institute, Austin, TX, ⁵University of Pittsburgh, Pittsburgh, PA, ⁶University of Texas Austin, Austin, TX, ⁷Antwerp University Hospital, Edegem, Belgium, ⁸University of Cambridge, Cambridge, UK

Purpose

There is growing recognition that current classification schemes for mild traumatic brain injury (MTBI) based solely on Glasgow Coma Scale and duration of post-traumatic amnesia and loss of consciousness are very limited, with small mean effect sizes in long-term impairment obscuring differences among diverse subgroups of MTBI patients with very different prognoses. Diffusion tensor imaging (DTI) is a promising technique for identification of microstructural white matter damage after traumatic brain injury. Although group differences in DTI parameters between MTBI patients and controls have been demonstrated, we sought to explore the practical use of acute or subacute DTI data for outcome prediction in the individual patient after controlling for demographic, clinical, and CT and conventional MRI predictors.

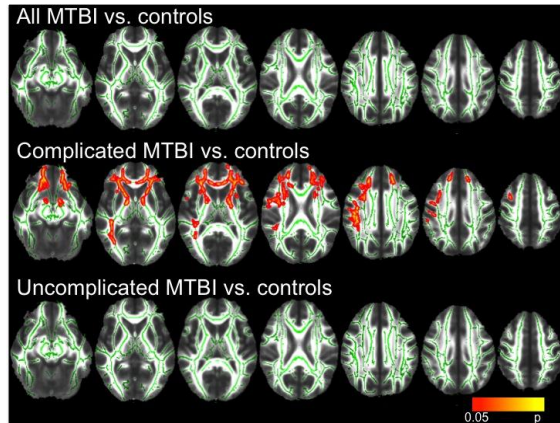
Materials and Methods

We evaluated DTI at 3 T for evidence of white matter injury in 37 adult MTBI patients at the semi-acute stage (10.9±3.6 days) after injury, employing both whole-brain voxelwise analysis and a complementary region-of-interest (ROI) approach. Because whole-brain voxelwise approaches may have limited sensitivity due to the heterogeneity of spatial distribution of white matter injury in MTBI, while the ROI approach may be limited by failure to interrogate less common areas of white matter injury, we employed both of these methods as complementary approaches in the current study.

Results

Complicated MTBI, defined as presence of any acute traumatic intracranial lesion and/or depressed skull fracture on day-of-admission CT or semi-acute 3 T MRI, was associated with significantly reduced fractional anisotropy (FA) in the internal and external capsules, uncinate fasciculi, genu of corpus callosum, and corona radiata compared to 50 control subjects. In contrast, we found no significant group differences in FA between uncomplicated MTBI and control subjects, using either whole-brain voxelwise or ROI methods. To determine the clinical relevance of DTI findings to outcome, we assessed for correlations between 3- and 6-month outcome measures and DTI, CT and MRI findings and demographic, socioeconomic and clinical predictors. MR imaging features, including DTI parameters, surpassed other variables for prediction of 3- and 6-month outcome. The best predictors of 3-month Extended Glasgow Outcome Scale (GOS-E) were DTI evidence of one or more ROIs with severely reduced FA (univariate odds ratio 8.0 per unit decrease in 3-month GOS-E, $p=0.008$) and MRI evidence for contusion (univariate odds ratio 12.6, $p=0.02$). The only statistically significant predictor of 6-month GOS-E was combined conventional MRI and DTI evidence of any traumatic intracranial lesion (odds ratio 4.8, $p=0.03$).

Note: Scanned images are included in the proceedings. Some submitted images were reduced during editing thereby decreasing clarity. Also, refer to the Program Planner. Proceedings Content as of 3/28/2014.



Conclusions

We employed both whole-brain voxelwise and ROI analyses as complementary approaches to show that microstructural white matter injury severity does vary, on a group level, according to the presence of more familiar macroscopic pathoanatomical lesions on CT and conventional MRI. In addition, this is the first study to compare DTI features in individual MTBI patients to conventional MRI, CT, clinical, demographic and socioeconomic features for the prediction of 3- and 6-month outcome in individual patients. We show that conventional MRI and DTI are useful, complementary imaging biomarkers for prediction of 3- and 6-month outcome in MTBI.

KEYWORDS: Diffusion Tensor Image, Traumatic Brain Injury

O-138 3:35PM - 3:42PM
Resting State Networks of Traumatic Brain Injury

L Lin¹, M Brier¹, S Chleboun², A Snyder¹, C MacDonald¹, J Shimony³
¹Washington University/St. Louis School of Medicine, Saint Louis, MO, ²Southern Illinois University in Edwardsville, Edwardsville, IL, ³Washington University, Saint Louis, MO

Purpose

Patients with traumatic brain injury (TBI) often have difficulty with cognition, sensory processing, communication, and mood. It is thought that the axonal injury and consequent disruption of functional networks contributes to the cognitive dysfunction. Previous studies of functional connectivity in TBI patients has been mainly in the acute phase of injury, and focused on the default mode network (DMN). The purpose of this study was to look at changes in several resting state networks (RSN) in patients with chronic (1-7 years from injury) TBI using resting state functional MRI (rsfMRI).

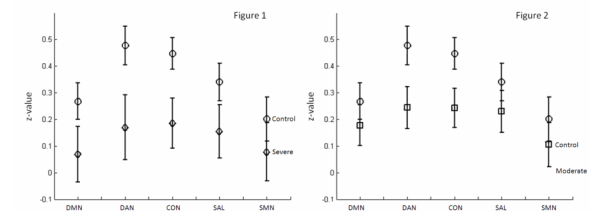
Materials and Methods

Eighteen chronic TBI patients (13 moderate and 5 severe by GOSE criteria) ranging from 1-7 years since initial injury and 16 age-matched controls were enrolled. Subjects were scanned in a 3 T Allegra MRI scanner (Siemens, Erlagen, Germany) while awake with eyes open and not performing

any tasks. Following previously described protocols, we acquired rsfMRI [TE = 25 ms, 90° flip, (4 mm) 3 voxels, 438 frames], high resolution MPRAGE and T2-weighted fast spin echo scans. Preprocessing included compensation for asynchronous slice timing, retrospective correction for head motion and atlas transformation ((3 mm) three voxels). Thirty-six regions of interest (ROIs) representing five resting state networks were used to extract the time course of the blood oxygen level dependent (BOLD) signal from the rsfMRI. A Pearson correlation coefficient (r) was computed between the time course of each ROI with all other ROIs and normalized with the Fisher's z-transformation. The resulting z-values were averaged within each of the five resting state networks.

Results

As seen in the figure, the within network correlations decreased in both TBI groups, with the decrease more noticeable in the severe TBI group. The differences between control and severe groups are significant in every network except for the sensory-motor network (SMN) (Figure 1), while the differences between control and moderate groups are significant in the dorsal attention (DAN) and control networks (CON) (Figure 2). Differences seen in the DMN and salience network (SAL) are significant between control and severe groups, but are not significant between the control and moderate groups.



Conclusions

Intranetwork correlations, on average, are decreased in moderate and severe TBI patients as compared to controls. Although each TBI is different the current results suggest that moderate and severe injury cause more global dysfunction in neural networks.

KEYWORDS: Resting-State fMRI, TBI, Traumatic Brain Injury

O-139 3:42PM - 3:49PM
FDG-PET Precuneus hypometabolism in Veterans with history of Traumatic Brain Injury (TBI)

S Soman¹, M Adamson², J Ashford², S Chao³, J Cheng⁴, A Furst², J Kong³
¹Stanford University/Palo Alto WRIISC, Menlo Park, CA, ²Stanford University, Palo Alto, CA, ³VA Palo Alto Health Care System, Palo Alto, CA, ⁴Palo Alto Veterans Affairs Hospital, Palo Alto, CA

Purpose

To investigate whether traumatic brain injury (TBI) severity is associated with Alzheimer disease (AD)-like metabolic decline independent of age in a cohort of mid-life veterans. There is increasing evidence suggesting that a

Note: Scanned images are included in the proceedings. Some submitted images were reduced during editing thereby decreasing clarity. Also, refer to the Program Planner. Proceedings Content as of 3/28/2014.

history of TBI is increasing the risk for dementia and may hasten its onset. However, it is unclear to what extent there is a specific link between TBI and AD.

Materials and Methods

A convenience sample of mid-life veterans was selected from our study center. Diagnosis of TBI severity and post-traumatic stress disorder (PTSD) was established using alteration of consciousness (AOC), loss of consciousness (LOC), post-traumatic amnesia (PTA) and clinician-administered PTSD scale (CAPS). All patients underwent FDG imaging within one week of the examination.

Fluorodeoxyglucose scans were spatially normalized to the MNI FDG template in SPM8 and smoothed with a 6mm kernel. Scans then were entered into a multiple regression analysis with TBI severity as variable of interest and age as nuisance variable. T maps exploring negative correlations between TBI severity and metabolic decline were initially thresholded at $p < .001$ (uncorrected) followed by a volume-of-interest (VOI) analysis (30 mm sphere).

Results

The sample consisted of 57 veterans (7 females), mean age of 46.8 years (median: 45.1), 31 mild TBI, 5 moderate TBI and 43 with PTSD. Glucose metabolism decreased significantly with increasing TBI severity in the right precuneus and left angular gyrus. Volume-of-interest analyses with FWE multiple comparison correction at $p < .05$ confirmed the robustness of the effect.

Conclusions

Traumatic brain injury severity is associated with AD-like metabolic decline within the precuneus and angular gyrus, independent of age.

KEYWORDS: PET/CT, TBI, Traumatic Brain Injury

O-140 3:49PM - 3:56PM

Longitudinal Assessment of Executive Working Memory with fMRI in Athletes Participating in Contact Sports, Baseline and Post-Concussion Evaluation

K Peters, A Mancuso, J Clugston, R Sitaram, A Old Crow, J Bennett
University of Florida, Gainesville, FL

Purpose

To develop a rapidly performable objective functional MR imaging (fMRI) paradigm to assess executive decision making and memory in the evaluation of concussion following sports-related injury. There are an estimated 1.6-3.8 million sports-related concussions each year in the United States. Postconcussive symptoms include lowered cognitive function and resolution of this is used as a clinical indicator of recovery. Cognitive function usually is assessed by standardized neuropsychometric tests compared with baseline results or against established population-specific normative data. Limitations of these tests include subjective components related to the player's responses, especially at time of baseline testing and a potentially high false positive rate (40%) as suggested by other investigators. There has been increased assessment of functional abnormalities in symptomatic athletes

utilizing fMRI, however most of these studies compare fMRI findings to the results of normative group data. To further refine this testing, a cohort of players engaged in competitive contact sports underwent baseline and postconcussion imaging.

Materials and Methods

Prior to the beginning of the scheduled season baseline MR and fMRI imaging was obtained on players participating in contact sports as part of an IRB-approved research protocol. MR imaging was performed on a 3 T Toshiba Titan scanner and included high resolution volumetric T1, a blood sensitive sequence, FLAIR, and diffusion tensor imaging (DTI). Functional MRI testing consisted of a six minute BOLD contrast scan using an n-Back test paradigm with alternating 0-Back and 2-Back tests of working memory function. Total scan time was 25 minutes.

Following a sports related concussion diagnosed by team physicians, the players underwent repeat imaging using the same protocol 1-3 days postinjury. Analysis of fMRI BOLD data was performed with FSL fMRI Expert Analysis Tool (FEAT) and group maps created to compare baseline and postconcussion regions of activation.

Results

Sixty-six players enrolled in the study and underwent baseline imaging per protocol. During the season there were four practice- or play-related concussions, all of which had follow-up imaging. Baseline memory test results for the group of players that subsequently had a concussion demonstrated a correct performance rate on the baseline 0-Back and 2-Back tests of 100% and 100% respectively. Correct group performance rate on the postconcussion 0-Back and 2-Back tests was 98% and 93% respectively. Functional MRI group analysis maps demonstrated a decrease in activation in the dorsal lateral prefrontal cortex (DLPC) following concussion which was most significant on the right.

Conclusions

An fMRI task of executive working memory can be performed in addition to routine sequences following mTBI to provide activation information. Although there was not a significant change in performance on n-Back testing, there were definite changes in the pattern of cortical activation. Following mTBI there was decreased activation in the DLPC, especially on the right in our cohort. This correlates well with the work of other investigators that have used control populations as their comparison group. These findings further confirm that there are different physiological responses to memory following injury and suggests this testing paradigm may be of utility in the diagnosis of mTBI.

KEYWORDS: FMRI, Memory, Traumatic Brain Injury

Note: Scanned images are included in the proceedings. Some submitted images were reduced during editing thereby decreasing clarity. Also, refer to the Program Planner. Proceedings Content as of 3/28/2014.

O-142 3:56PM - 4:03PM
White Matter Integrity Changes and Head Impact Exposure in a Season of High School Varsity Football

E Davenport¹, C Whitlow¹, J Urban¹, M Espeland¹, Y Jung¹, D Rosenbaum¹, G Gioia², A Powers¹, J Stitzel¹, J Maldjian¹
¹Wake Forest University School of Medicine, Winston-Salem, NC, ²Children's National Medical Center, Rockville, MD

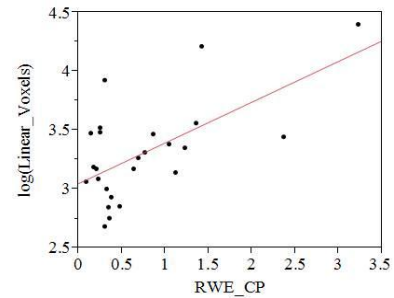
Purpose

The purpose of this study is to determine if the cumulative effects of head impacts from a season of high school football produce magnetic resonance imaging (MRI) measurable changes in the brain in the absence of clinically diagnosed concussion.

Materials and Methods

Twenty-seven players from a local high school football team (mean age=17.2; age range=16-18) were instrumented with the head impact telemetry system (HITS) during all practices and games. All players received pre and postseason MR imaging (MRI). Diffusion tensor imaging (DTI) images were acquired using a 2D single-shot EPI sequence (TR=10500 msec; TE=99 msec; FA=90 degrees; spatial resolution= 2.2x2.2 mm; slice thickness = 3 mm; 54 slices; 10 b = 0 volumes; 15 diffusion directions with b = 1000/2000 each). Immediate postconcussion assessment and cognitive testing (ImPACT) also was conducted. The biomechanical metric computed from the HITS data for this study was the risk weighted cumulative exposure (RWE). This metric represents the collected risk of concussion over the course of the season. Total impacts and risk weighted cumulative exposure (RWE), including linear (RWELinear), rotational (RWERotational), and combined components (RWECP) were computed for each subject. Fractional, linear, planar and spherical anisotropies (FA, CL, CP, CS, respectively), as well as mean diffusivity (MD), were used to determine total number of abnormal white matter voxels (defined as 2 standard deviations above or below the group mean). Delta (post minus preseason) ImPACT scores for each individual were computed and compared to the DTI measures using the Spearman's rank correlation coefficient. None of the players analyzed experienced clinical concussion (N = 25). Results

Regression analysis revealed a statistically significant linear relationship between RWECP and FA. Secondary analyses demonstrated additional statistically significant linear associations between RWE (RWECP and RWELinear) and all DTI measures. There also was a strong correlation between DTI measures and change in verbal memory subscore of the ImPACT.



Conclusions

We demonstrate that a single season of football can produce brain MRI changes in the absence of clinical concussion. Similar brain MRI changes have been previously associated with mild traumatic brain injury.

KEYWORDS: Concussion, Diffusion Tensor Image, DTI

O-143 4:03PM - 4:10PM
Interhemispheric Connectivity Changes Associated with a Season of High School Football

F Mokhtari¹, E Davenport², J Urban², N Bahrami², C Whitlow², A Powers², J Stitzel², J Maldjian²
¹Wake Forest University, Winston Salem, NC, ²Wake Forest University School of Medicine, Winston Salem, NC

Purpose

The goal of this study is to determine if cumulative head impacts over a season of high school football has an effect on brain network connectivity.

Materials and Methods

Thirty high school football players without history of prior concussion (age: 14-18, gender: male) participated in the study. None of the players included in the study experienced clinical concussion during the season. For each subject, biomechanical data were acquired using the head impact telemetry (HIT) system during practices and games using helmet-embedded sensors. Six minutes of resting-state fMRI pre and postseason were obtained using a Siemens Trio 3 T scanner in each subject. The biomechanical metric utilized to capture each player's head impact exposure was the risk weighted cumulative exposure (RWECP) (1). This metric is defined as the combined risk of concussion calculated from the peak resultant linear and rotational acceleration for each impact. fMRI data preprocessing was performed using SPM8. For each subject, fMRI data were motion corrected, normalized to MNI space and band-pass filtered at 0.01 - 0.1 Hz. The 6 rigid-body motion parameters, as well as parameters for the white matter signal, global mean signal, and cerebrospinal fluid signal were regressed from the time series. Interhemispheric connectivity was calculated between regions of the AAL atlas including 54 regions in each hemisphere using a correlation metric. For each subject, connectivity differences between post and preseason for each ROI were computed. In order to investigate the relationship between RWECP versus prepost difference in functional connectivity a multiple linear regression analysis was performed. Body mass index

Note: Scanned images are included in the proceedings. Some submitted images were reduced during editing thereby decreasing clarity. Also, refer to the Program Planner. Proceedings Content as of 3/28/2014.

(BMI), time between scans, and participant age were included in the model as confounders. Significance was determined using a bootstrap analysis with 1000 resamplings.

Results

Eight interhemispheric connectivities out of 54 connectivities were identified as significant ($p < 0.05$). The likelihood of identifying eight significant connectivities at an alpha of 0.05 among 54 tests is less than 1%. Table 1 shows the results obtained using univariate and multivariate linear regression analysis and the bootstrapping multiple linear regression analysis for RWECP versus prepost season difference of interhemispheric connectivity.

Table 1. Statistical results of univariate and multivariate linear regression analysis for RWECP vs. pre-post season difference in whole-brain network interhemispheric connectivity.

Interhemispheric connectivities	T-stat and P-value without bootstrapping				P-value with bootstrapping
	Univariate Model	P-value	Multivariate Model	P-value	
Precentral	-2.10	0.0449	-2.36	0.0262	0.0230
Frontal midline	-1.88	0.0712	-2.28	0.0315	0.0330
Frontal inferior triangular	-2.02	0.0528	-2.68	0.0129	0.0140
Lingual	-4.25	0.0002	-3.92	0.0006	0.0000
Thalamus	-1.98	0.0576	-2.10	0.0461	0.0480
Cerebellum3	2.20	0.0359	2.55	0.0171	0.0150
Cerebellum7b	-2.31	0.0282	-2.13	0.0435	0.0430
Cerebellum8	-4.37	0.0002	-3.81	0.0171	0.0000

Conclusions

These results indicate changes (predominantly decreases) in the interhemispheric connectivity between frontal lobe, thalamic and cerebellar structures in nonconcussed subjects during a single season of football. This is in accordance with several studies which have shown significant changes in frontal lobe and cerebellum interhemispheric connectivities associated with mTBI (2, 3).

KEYWORDS: Concussion, FMRI, Functional Connectivity

O-144 4:10PM - 4:17PM
Mild Neck Compression Alters Intracranial Venous Sinus Volume: Implications for a Novel Neuroprotective Effect in Concussion

J Leach, G Myer, D Smith
Cincinnati Children's Hospital Medical Center, Cincinnati, OH

Purpose

Recent animal models indicate that internal jugular vein compression may mitigate traumatic axonal injury by potentially reducing intracranial SLOSH effect by increasing intracranial blood volume and altering intracranial compliance (1). Additional recent population studies have documented a decrease in reported concussions in athletes at higher altitudes, potentially related to altitude-related changes in cerebral volume (2). Understanding how jugular venous compression may alter venous volume in humans is necessary to see if this approach can be applied as a potential neuroprotective mechanism. The purpose of the current study was to investigate the effect of mild neck compression on the volume of the intracranial dural sinuses in normal subjects.

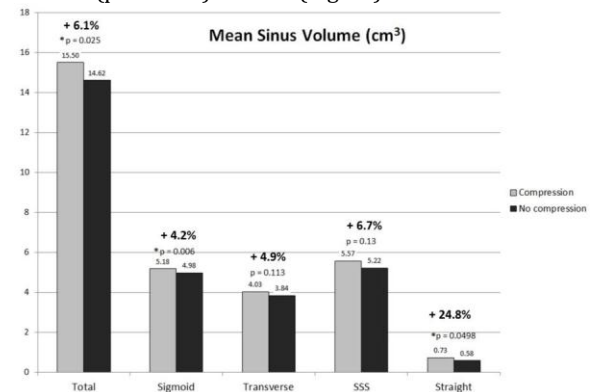
Materials and Methods

Four normal subjects (ages: 28-38, M:2, F:2) participated in the study cohort. A pneumatically operated band

compression device was used to provide transient mild neck compression during the procedure. Previous internal safety studies of the maneuver have documented safety and adequacy of venous compression by US evaluation. Intracranial 2D TOF MRV (coronal plane, 1.6 mm ST, inferior sat pulse) was performed at baseline (NC) and with jugular compression (C) in each subject. Semi-automated segmentation of flow signal within the transverse (TS), sigmoid (SS), straight sinus (StS), and superior sagittal sinus (SSS) was performed using BrainLab iPlan 3.0. Volumes of the venous segments were analyzed in each subject with and without jugular venous compression.

Results

Jugular compression was tolerated well in all subjects with no reported discomfort or symptoms. Volumes of the SS and StS, as well as total dural sinus (TDS) volume increased in all subjects (mean change: + 4.2%, + 25.65%, + 6.3% respectively) with neck compression; SSS volume increased in two and TS volume increased in four. As a group, mean dural sinus volume increased in all segments with a significant increase in TDS ($p=0.25$), SS ($p=0.006$), and StS ($p=0.0498$) volume (Figure).



Conclusions

Jugular venous compression results in increased total dural sinus volume in normal subjects in the MR environment. Significant segmental increases were noted in the sigmoid and straight sinuses. Future research is warranted to determine if mild jugular compression alters intracranial compliance in humans and if reductions in brain damage in response to concussion might be achieved with this maneuver as previously noted in animal studies.

KEYWORDS: TBI, Venous Anatomy, Venous Drainage

O-145 4:17PM - 4:24PM
Role of MR Neurography in the Management of Entrapment Neuropathies

K Sharma, A Varma, A Buchholz, Z Rumboldt, M Vittoria-Spampinato
Medical University of South Carolina, Charleston, SC

Purpose

Magnetic resonance neurography (MRN) is a noninvasive high-resolution magnetic resonance imaging technique

Note: Scanned images are included in the proceedings. Some submitted images were reduced during editing thereby decreasing clarity. Also, refer to the Program Planner. Proceedings Content as of 3/28/2014.

increasingly used in the evaluation of the peripheral nerves. The ability of MRN to alter the management of patients with peripheral neuropathy requires further investigation. Our goal was to assess the impact of MRN on the treatment plan in patients with suspected upper and lower extremity entrapment neuropathy.

Materials and Methods

We retrospectively identified 17 patients with suspected upper and lower extremity entrapment neuropathy (10 ulnar; 7 peroneal) that had undergone MRN on 3 T MR scanner with a dedicated extremity coil. Anonymized clinical exam and electrophysiological data were presented to a neurosurgeon who had not been involved in the care of these patients. The neurosurgeon completed a questionnaire on each patient twice, before and after receiving access to the MRN imaging data. The information collected included the following: degree of confidence of a peripheral nerve abnormality (1: low, 2: moderate, 3: high), specific nerve involved, degree of confidence of need for surgery (1: low, 2: moderate, 3: high), timing of surgery (1: immediate, 2: not sure and follow up in 3 months, 3: surgery not needed), approach to surgery (site and length of incision), confidence in approach to surgery (1: low, 2: moderate, 3: high) and estimated length of surgery (1: < 2 hours, 2: 2-4 hours, 3: 4-6 hours, 4: 6-8 hours, 5: >8 hours). Change in evaluation of these parameters before and after access to MRN data was calculated using Wilcoxon signed-rank test. Results were considered significant when $p < 0.05$.

Results

Before obtaining access to the MRN data the neurosurgeon made the diagnosis of neuropathy in 15 out of 17 peripheral neuropathy subjects. After review of the MRN data there was no significant change in the level of confidence of the neuropathy diagnosis ($p = 0.18$). The surgeon became significantly more confident about the need for surgery in seven (41.2%) patients ($p = 0.003$). Furthermore in 11 (64.7%) patients there was a change in timing of surgery recommendation [no surgery to immediate surgery (5.9%), follow up to immediate surgery (29.4%), follow up to no surgery (11.8%), and immediate surgery to follow up (11.8%)]. In eight (47.1%) patients there was a statistically significant increase in confidence level of the surgical approach ($p = 0.04$). The length of incision was increased in five (29.4%) patients and in one patient the proposed site of incision changed from the lumbar spine to the lateral knee following MRN, as the initial diagnosis of radiculopathy was changed to peroneal nerve entrapment syndrome.

Conclusions

MR neurography is an excellent technique with established technical effectiveness and high diagnostic accuracy. MR neurography has great potential in helping with patient management decisions, such as surgical versus nonsurgical treatment of neuropathies and surgical planning, which may positively affect patient outcome.

KEYWORDS: MR Neurography, Neurography

O-146 4:24PM - 4:31PM
BOLD Functional Connectivity Differences between Contact and Non-contact Sports Collegiate Athletes

M Pollock, D Hwang, M Shiroishi, M Law, C Liu
University of Southern California, Los Angeles, CA

Purpose

There is increasing awareness of the long-term effects of cognitive impairment following mild traumatic brain injury (mTBI) in athletics, particularly those who participate in contact sports. We used resting-state functional MR imaging (fMRI) to assess for imaging correlates to the effects of mTBI.

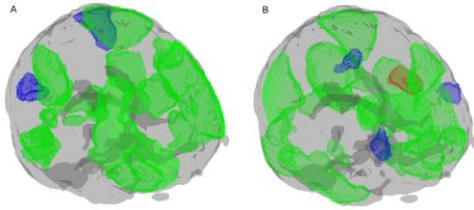
Materials and Methods

College students, eight of whom participate in contact sports and 14 of whom participate in noncontact sports, were imaged on a 3 T scanner with a whole-brain 2D multislice single-shot gradient echo blood oxygenation level-dependent (BOLD) sequence (TE 30 ms, TR 3000 s, 44 axial acquisitions per TR). One hundred sixty brain volumes were acquired. Motion-corrected data were analyzed for statistical significance using SPM 8 and CONN. Eighteen seed regions of interest (ROIs) for computing resting-state networks were chosen based on a literature review of BOLD functional connectivity following head trauma as well as from morphologic analysis of cortical differences in mTBI subjects. Second-level analyses of between-subjects contrasts using the ROIs were performed to generate group functional connectivity maps. The resultant maps were thresholded by cluster area size and then corrected for multiple comparisons at a false discovery rate of $p < 0.05$.

Results

Using the bilateral dorsolateral prefrontal cortices (DLPC, BA 46) as seeds, connectivity map corresponding to the dorsal attention network (green) was noted in the two groups, with decreased connectivity (blue) predominantly seen in the angular gyri bilaterally in the contact sports group relative to the noncontact sports group (Figure 1a). The left inferior parietal lobule seed generated connectivity map corresponding to a combination of the dorsal attention network as well as the default mode network, with increased connectivity (red) predominantly seen in the left middle temporal gyrus and decreased connectivity seen in the DLPC bilaterally as well as the right premotor cortex in the contact sports group relative to the noncontact sports group (Figure 1b). The bilateral secondary visual cortices seed (BA 18) generated connectivity map corresponding predominantly to the visual system, with decreased connectivity predominantly in the right supramarginal gyrus noted in the contact sports group relative to the noncontact sports group.

Note: Scanned images are included in the proceedings. Some submitted images were reduced during editing thereby decreasing clarity. Also, refer to the Program Planner. Proceedings Content as of 3/28/2014.



Conclusions

Statistically significant changes in functional connectivity are demonstrable between contact and noncontact sport athletes, with the changes primarily affecting working memory and attentional processes. The findings correspond to clinical anecdotes of cognitive impairment in those suffering from mTBI and may help target future therapies.

KEYWORDS: Resting-State fMRI, Traumatic Brain Injury

Monday, May 19
3:00 PM – 4:30 PM
Room 524

22 - Parallel Papers: Pediatrics:
Demyelinating and Inflammatory,
Trauma. Radiation

O-147 3:00PM - 3:07PM
Rate of Agreement for Manual and Automated Techniques for Determination of New T2 Lesions in Children with Multiple Sclerosis and Acute Demyelination

L Verhey¹, C Elliott², H Branson³, C Philpott³, M Shroff³, T Arbel², B Banwell⁴, D Arnold²

¹The Hospital for Sick Children Research Institute, Toronto, Ontario, Canada, ²McGill University, Montreal, Quebec, Canada, ³The Hospital for Sick Children, University of Toronto, Toronto, Ontario, Canada, ⁴The Children's Hospital of Philadelphia, Philadelphia, PA

Purpose

Determination of new lesions on serial magnetic resonance imaging (MRI) is important in multiple sclerosis (MS) diagnosis, and new T2 lesions serve as a surrogate outcome for relapses in clinical trials. Absence of new lesions confirms a monophasic illness in children with an acute demyelinating syndrome (ADS). The objective of this study was to evaluate inter-rater variability in new T2 lesion determination based on a manual lesion identification method (1) and an automated probabilistic segmentation technique (2, 3).

Materials and Methods

Scans were acquired according to a standard protocol at onset, 3, 6, and 12 months and annually as part of a national prospective study of children with ADS. New T2 lesions were identified manually independently by three experts (2 pediatric neuroradiologists, 1 imaging scientist) using an optimized standard scoring tool (1). T1-weighted pre and postcontrast, PD-weighted, T2-weighted, and

FLAIR sequences were used. Readers were blinded to clinical information. Automated new T2 lesion segmentation was performed on the same cohort using an optimized, computer-assisted method in which a voxelwise Bayesian and lesion-level random forest classification (2, 3) is performed on T1-weighted pre and postcontrast, T2-weighted, PD-weighted, and FLAIR sequences of reference, follow up and difference images. Active scans were defined as having ≥ 1 new T2 lesion. New T2 lesion counts were categorized into 0, 1, 2 and ≥ 3 lesions. Rate of agreement was assessed for scan activity and new T2 lesion count.

Results

From 19 children included (10 MS, 9 monophasic ADS), 130 scans were analyzed; 12 scans not meeting predetermined quality specifications were excluded. A mean of 101 new lesions was identified on all scans [expert readers (delineated as R1, R2 and R3): R1=87, R2=90, R3=106]; automated method (delineated as A1): A1=122]. Mean rate of agreement on scan activity between the automated method and expert readers was 87% (R1-A1=91%, R2-A1=83%, R3-A1=88%), compared to 91% between readers. Mean agreement on lesion count of the automated method with expert readers was 82% (R1-A1=85%, R2-A1=77%, R3-A1=84%) compared to 85% between readers; when zero counts were removed, the mean was 53% (R1-A1=61%, R2-A1=39%, R3-A1=59%), compared to 61% between readers.

Conclusions

Agreement is high between manual and automated methods for new T2 lesion determination. Overall, the automated method is more sensitive than the manual readers and identifies a higher number of lesions. The automated method can feasibly aid in the determination of new T2 lesions for diagnosis and monitoring as well as in pediatric MS clinical trials. Discrepancies on agreement between manual and automated methods currently are being arbitrated independently by an expert reader who was not involved in previous aspects of the work; a comparison of sensitivity and specificity of the manual and automated methods will be presented.

KEYWORDS: Demyelination, Multiple Sclerosis, Pediatric Brain

O-148 3:07PM - 3:14PM
Standardized MRI Protocol and Structured Reporting for Pediatric CNS Inflammatory Demyelination and Multiple Sclerosis: Consensus Recommendations from the Canadian Pediatric Demyelinating Disease Program

L Verhey¹, H Branson², S Laughlin², B Banwell³, M Shroff²

¹The Hospital for Sick Children Research Institute, Toronto, Ontario, Canada, ²The Hospital for Sick Children, University of Toronto, Toronto, Ontario, Canada, ³The Children's Hospital of Philadelphia, Philadelphia, PA

Purpose

In children with acute demyelination of the central nervous system (CNS), magnetic resonance imaging (MRI) plays an important role in excluding alternative diagnoses (1),

Note: Scanned images are included in the proceedings. Some submitted images were reduced during editing thereby decreasing clarity. Also, refer to the Program Planner. Proceedings Content as of 3/28/2014.

determining risk for multiple sclerosis (MS) (2), confirming an MS diagnosis prior to second attack (3, 4) and monitoring recovery in children with a monophasic illness and disease progression and treatment response in those with MS. The value of MRI in informing the clinical management of children with inflammatory demyelination is largely predicated on the use of a standardized protocol and lexicon. We recently developed a standardized MRI scoring tool for pediatric CNS demyelination (5). We expand on this work and propose an evidence-based MRI acquisition protocol and lexicon for structured reporting in children with acute demyelination and MS.

Materials and Methods

The proposed MRI protocol and structured reporting method is based on findings from the Canadian Pediatric Demyelinating Disease Program, a national prospective cohort study of children less than 16 years of age with an incident attack of CNS demyelination in which standardized clinical and MRI data are acquired at onset, 3, 6, and 12 months after onset and annually for eight years. The MRI acquisition protocol entails a set of scans that have been optimized by a group of MS imaging experts for use at the 23 sites in the prospective study. The lexicon is derived from a standardized semiquantitative scoring tool that was developed to score scans acquired in the prospective study. Parameters included in the tool were identified based on a literature review and expert input. A panel of neurologists and radiologists with expertise in demyelination and MS met to refine the definition of each parameter, and those parameters with good inter-rater agreement ($\kappa \geq 0.6$), deemed important in predicting MS diagnosis, and visualized on routine clinical imaging were retained in the final lexicon. The structured reporting template is proposed based on the network's experience with the standardized acquisition protocol and lexicon used in the prospective study.

Results

The recommended minimum brain MRI protocol includes: precontrast 3D T1-weighted SPGR, postcontrast axial T1-weighted SPGR, axial T2-weighted FSE or TSE, sagittal and axial FLAIR, and axial diffusion-weighted imaging (DWI). Focused imaging of the optic nerves and spinal cord should be performed as clinically indicated for optic neuritis or transverse myelitis. With the assistance of MRI-compatible movie goggles and headphones, children tolerate lying still for the duration of the protocol. Unique aspects to imaging children (e.g., artifact from dental hardware) are considered. The lexicon consists of 16 parameters: 15 are binary (yes/no) variables, and one is a count (i.e., number of T2 lesions; counts greater than 15 are grouped as ">15"). Parameters include descriptions of lesion location (e.g., periventricular, brainstem, corpus callosum) and features (e.g., T1-hypointense, diffusion restricted, contrast enhancing). A textual and pictographic atlas for each parameter has been defined. A template for structured reporting is proposed that includes a description of lesions on a single scan (i.e., the lexicon), description of lesion changes on serial scans (e.g., new T2 or contrast-enhancing lesions, lesion resolution or stability, changes in brain

volume), and statements on whether the scan meets published predictive and diagnostic criteria for MS.

Conclusions

An evidence-based algorithm for standardized MRI acquisition and reporting in pediatric central nervous system (CNS) demyelination is proposed, providing a framework that will permit revisions and refinements to enhance its applicability and implementation across centers. A standard acquisition protocol and lexicon provides necessary groundwork for implementation of structured reporting in diagnostic radiology, and will facilitate aggregation of data to achieve adequate sample sizes in clinical trials of pediatric MS involving surrogate MRI endpoints.

KEYWORDS: Demyelination, Multiple Sclerosis, Structured Report

O-149

3:14PM - 3:21PM

Magnetic Resonance Spectroscopic Imaging in Pediatric CNS Inflammatory Demyelination: Assessing the Risk of Relapse

D Lin¹, E Kossoff², T Crawford², A Fatemi², P Barker¹
¹Johns Hopkins University School of Medicine, Baltimore, MD, ²Johns Hopkins University, Baltimore, MD

Purpose

The long-term prognosis of children presenting with acute inflammatory demyelination is highly variable, and difficult to predict. In this study, it was investigated whether brain metabolite levels, as measured by proton magnetic resonance spectroscopic imaging (MRSI), show differences between subjects with monophasic disease and good recovery, versus those with recurrent illness.

Materials and Methods

Fifteen consecutive children presenting with acute central nervous system (CNS) inflammatory demyelination prospectively underwent MRSI (TR/TE: 2300/280ms, 3-4 axial slices, thickness: 15 mm, gap: 2.5 mm, matrix 32x32, nominal voxel size: 0.8 cm³) and clinical MR imaging (MRI) at 1.5 T between 1995 and 2006. Clinical follow-up data were used to classify the subjects as either monophasic or polyphasic, according to current consensus criteria. The metabolic ratios Choline(Cho)/Creatine (Cr), NAA/Cr and NAA/Cho were compared between groups from voxels in the white matter lesions and contralateral normal appearing white matter (NAWM). Pair-wise ANOVA corrected for multiple comparisons was applied to assess statistical significance.

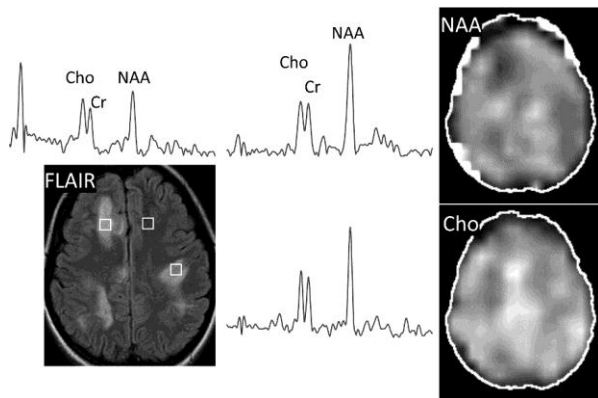
Results

Eight children (3 male, mean age 8.9 ± 4.5, range 3-17 years) were classified in the polyphasic group and seven children (3 male, mean age 8.7 ± 4.7, range 2-16 years) in the monophasic group. Only in the polyphasic group, both NAA/Cr and NAA/Cho ratios were significantly lower in the demyelinating lesions compared to the NAWM (see Table 1). In the polyphasic group, Cho/Cr showed a trend of elevation compared to the NAWM (P=0.06), unlike in the monophasic group, in which Cho/Cr was similar to the

Note: Scanned images are included in the proceedings. Some submitted images were reduced during editing thereby decreasing clarity. Also, refer to the Program Planner. Proceedings Content as of 3/28/2014.

NAWM. MRSI in a case of monophasic ADEM in a 16-year-old girl with multifocal FLAIR hyperintense lesions is shown in Figure 1. The lesions are primarily characterized by moderately diminished NAA levels, with Cho and Cr levels similar to those in NAWM.

	WM lesion	NAWM	P	
polyphasic	Cho/Cr	1.88 ± 0.48	1.39 ± 0.12	0.06
	NAA/Cr	1.43 ± 0.52	2.23 ± 0.32	0.01*
	NAA/Cho	0.83 ± 0.36	1.64 ± 0.23	0.00**
monophasic	Cho/Cr	1.39 ± 0.39	1.39 ± 0.34	2.94
	NAA/Cr	1.60 ± 0.30	2.06 ± 0.30	0.06
	NAA/Cho	1.23 ± 0.33	1.58 ± 0.46	0.42



Conclusions

Central nervous system inflammatory demyelinating lesions in children with subsequent relapse show greater abnormalities on MRSI compared to children with monophasic disease. MR spectroscopic imaging may be useful, either alone or in combination with other clinical and imaging data, in predicting the risk of relapse and long term prognosis.

KEYWORDS: Acute Disseminated Encephalomyelitis, ADEM, MR Spectroscopy

0-150 3:21PM - 3:28PM
Pediatric Autoimmune Encephalitis: Antibody Markers and MRI Abnormalities

C Pluto, J Rusin, L Ruess
Nationwide Children's Hospital, Columbus, OH

Purpose

Autoimmune encephalitis (AE) can pose a diagnostic dilemma to both clinician and radiologist. Common clinical features have been described in children with probable AE whether positive or negative for antibody markers. Although variable MR imaging (MRI) findings have been described in the adult population, pediatric MRI descriptions have been sparse. Our purpose was to analyze the clinical and MRI findings of AE in a pediatric population

in order to improve the diagnostic algorithm for AE at our institution as well as to further describe MRI findings of AE in the pediatric age group.

Materials and Methods

An IRB approved this retrospective review of clinical and radiology records to identify suspected and confirmed cases of AE at a large pediatric hospital over the past four years based on clinical, laboratory, and treatment response criteria. Clinical information was recorded. Neuroimaging studies were reviewed and the findings in these patients were characterized and compared.

Results

Of 553 patients with a diagnosis of encephalopathy, 17 patients with MR images met the clinical inclusion criteria for AE (encephalopathy with neuropsychiatric symptoms, seizures, movement disorders and/or cognitive dysfunction; and either laboratory evidence of central nervous system (CNS) inflammation, a history of other autoimmune disorder and/or a positive response to immunotherapy). There were 10 (59%) females and seven males. Median age was 10 (range 4-17). Nine (53%) patients had positive antibody markers (in CSF or serum): four NMDA, two GAD-65, two TPO, one GAD-65 and TPO. Marker positive patients had MRI abnormalities primarily within limbic structures including anterior medial temporal lobes (7, 78%); hippocampus, amygdala and uncini (6, 67%); and gyrus rectus (2, 22%). Insular cortex involvement (7/17, 41%) included marker positive (4/9, 44%) and negative (3/8, 38%) patients. Marker negative patients also had temporal lobe lesions (4/8, 50%) however none involved the anterior medial temporal cortex. Only marker negative patients had nontemporal lobe cerebral cortex lesions (parietal 4; occipital 5). Increased T2 signal in sulci also was seen only in marker negative patients (3/8, 38%). Enhancement was seen in 7/17 (41%): 3/9 (33%) marker positive and 4/8 (50%) marker negative patients. Atrophy affected 8/17 (47%): 4/9 (44%) marker positive and 4/8 (50%) marker negative patients. Nine patients had either normal CTA or MRA, and three of these had confirmatory negative catheter cerebral angiograms.

Conclusions

Pediatric patients with suspected and confirmed AE have a narrow spectrum of MRI abnormalities. Limbic structures including the anterior medial temporal lobes are involved more typically in patients with positive antibody markers. However, MRI still may be helpful to suggest the diagnosis of AE, even when antibody markers are negative.

KEYWORDS: Autoimmune, Encephalitis, Encephalopathy

Note: Scanned images are included in the proceedings. Some submitted images were reduced during editing thereby decreasing clarity. Also, refer to the Program Planner. Proceedings Content as of 3/28/2014.

O-151 3:28PM - 3:35PM
Rapid MRI Protocol for Pediatric Patients with Traumatic Head Injury

J Acharya¹, L LeCompte², K Clark², H Mehta²

¹Westchester Medical Center PMB 578, Valhalla, NY,

²Westchester Medical Center, Valhalla, NY

Purpose

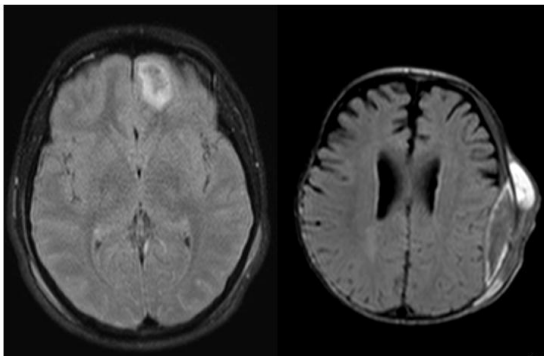
Traumatic brain injury results in over 500,000 pediatric ER visits yearly. After initial evaluation with noncontrast head CT, we utilized a rapid sequence MR imaging (MRI) protocol to monitor evolution of traumatic injury without use of ionizing radiation. We offer a report of our protocol.

Materials and Methods

Rapid MR imaging of the brain was established initially at our institution for monitoring of hydrocephalus in children with ventricular diversion catheters in order to reduce lifetime ionizing radiation exposure. After proven success with high quality diagnostic imaging without the need for sedation, we quickly realized the potential for other applications. As a major regional Level 1 trauma center, the monitoring of traumatic brain injury was an ideal application of our rapid MRI protocol and may become a possible substitution for initial trauma screening in certain patients. Our rapid MR imaging sequences include echo planar imaging (EPI), single shot, and ultra fast half fourier imaging techniques, with additional optional sequences as tolerated.

Results

Rapid MR imaging of the brain was established initially at our institution for monitoring of hydrocephalus in children with ventricular diversion catheters in order to reduce lifetime ionizing radiation exposure. After proven success with high quality diagnostic imaging without the need for sedation, we quickly realized the potential for other applications. As a major regional Level 1 trauma center, the monitoring of traumatic brain injury was an ideal application of our rapid MRI protocol and may become a possible substitution for initial trauma screening in certain patients. Our rapid MR imaging sequences include echo planar imaging (EPI), single shot, and ultra fast half fourier imaging techniques, with additional optional sequences as tolerated.



Conclusions

Our rapid sequence MRI protocol has been optimized to not only follow patients with chronic hydrocephalus, but

also to be used to monitor traumatic brain injury without the use of ionizing radiation and sedation.

KEYWORDS: Pediatric Brain, Radiation Dose Reduction, Traumatic Brain Injury

O-152 3:35PM - 3:42PM
Pediatric Sports-Related Concussion Produces Alterations in Frontal Lobe Activation: a Functional MRI Study.

L Hayes¹, S Palasis¹, T King², R Jones¹, B Sun¹, A Arenivas¹, D Kloehs¹, T Burns¹

¹Children's Healthcare of Atlanta, Atlanta, GA, ²Georgia State University, Atlanta, GA

Purpose

The pathophysiology of pediatric sports-related concussion (SRC) is not well understood. Therefore, functional MRI was employed in an effort to identify alterations in brain activity in concussed children by comparing the fMRI BOLD responses between acute SRC patients and matched controls. Historically, fMRI studies have shown disrupted frontal activation patterns during working memory (WM) tasks with mixed results demonstrating either increased or decreased activation during WM tasks in patients versus controls. Our study evaluated neural activation in high school boys with sports-related concussion versus controls using a multi-level (0,1,2,3,control) n-back fMRI paradigm on a 3 T MRI scanner in an attempt to further elucidate the neural alterations that occur with pediatric concussions.

Materials and Methods

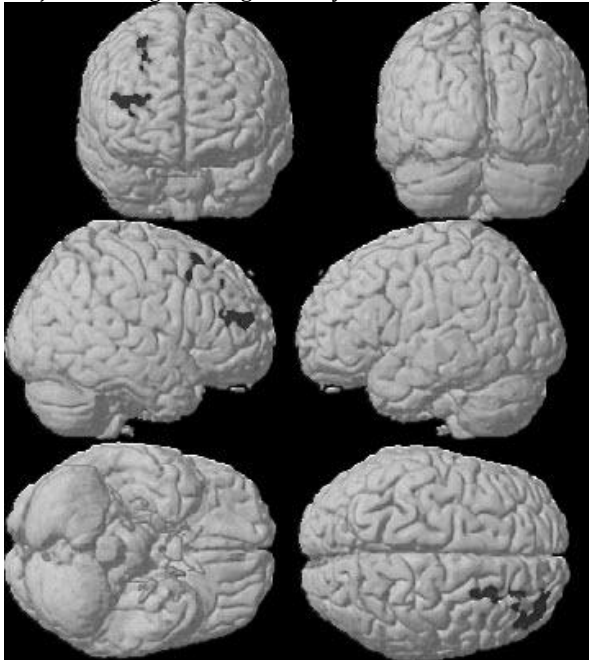
Twenty-four participants, all right-handed boys aged 15-18 years, were enrolled in our study. Of these participants, 13 had SRC within past seven days at the time of the study and 11 were normal controls (reaffirmed with retrospective inspection of the anatomical MRI). The respective age for the control and SRC groups is 16.16 ± 1.05 and 15.89 ± 1.07 . All subjects took a WASI IQ exam and had a MRI session. The MRI session lasts about an hour and includes anatomical MRI, DTI, ASL, and working memory fMRI. The scanning parameters for the fMRI are: TE=30ms; TR=2.13s; FA=90 degree; FOV=204mm and Slice Thickness=3mm. The working memory fMRI is conducted with a letter n back paradigm. The fMRI session includes three separate trials (runs), each with different randomization of task ordering. Each run lasts approximately four minutes, with the entire fMRI session lasting about 15 minutes. Accuracy and reaction times are recorded. The lower n tasks (i.e., target and 1 back) primarily test vigilance while higher n tasks (2 and 3 back) target the working memory networks. The fMRI analysis was conducted using the FSL software package (fMRIB's Software Library, www.fmrib.ox.ac.uk/fsl). Because each participant had fMRI scan with three separate runs, a three level GLM was used. The fMRI data from each trial for each participant was processed individually using the first level GLM based on the paradigm setup, following typical fMRI preprocessing including motion correction, denoising, etc. The three first level results for each subject subsequently

Note: Scanned images are included in the proceedings. Some submitted images were reduced during editing thereby decreasing clarity. Also, refer to the Program Planner. Proceedings Content as of 3/28/2014.

were averaged using a second level GLM. The second level results then were grouped based on subject condition and compared statistically using a third level regression. A Z value greater than 1.9 and cluster corrected $p < 0.05$ were used. The results of the mean activation for the controls, SRC, and controls-SRC for working memory minus vigilance were targeted.

Results

Groups did not differ in accuracy or reaction time across n-back conditions, however the SRC group demonstrated a statistically significant decrease in activation in the right frontal lobe relative to controls during working memory tasks. No other areas of statistically significant differences in activation were detected between the control and SRC subjects during working memory tasks.



Conclusions

Alterations in neural activation were present on fMRI scans of the brain in children who sustained a single concussion within 2-7 days after the injury compared to controls. Despite similar IQs, differences in neural activation are demonstrated, with significantly reduced activation in the right frontal lobe compared to controls. This is hypothesized to be related to deficits in attention in these recently concussed children. These findings correlate with the working memory literature that implicates frontal lobe dysfunction in patients with recent concussion. Decreased activation could be related to decreased cerebral blood flow in these children as recently described in the pediatric SRC literature. Moving forward, we are now comparing fMRI findings and ASL-based cerebral blood flow (CBF) measures in an effort to help decipher the complex, likely multifactorial, pathophysiological states responsible for SRC in children.

KEYWORDS: Functional Brain Mapping, Pediatric Brain, Traumatic Brain Injury

0-153

3:42PM - 3:49PM

Parenchymal Brain Lacerations in Abusive Head Trauma

L Palifka¹, L Frasier², R Metzger³, G Hedlund³

¹Dartmouth-Hitchcock Medical Center, Lebanon, NH, ²Penn State Hershey Children's Hospital, Hershey, PA, ³Primary Children's Medical Center, Salt Lake City, UT

Purpose

Abusive head trauma (AHT) is a significant cause of neurologic morbidity and mortality in infants and young children. Signs and symptoms of inflicted injury may range from nonspecific to severe. Additionally, historical information on the cause of injury may be difficult to obtain. Up to 30% of AHT is missed in initial evaluation by physicians due to confounding history and vague presenting symptoms. Typical pathology in AHT includes subarachnoid hemorrhage, subdural hemorrhage, and primary and secondary brain injuries. Parenchymal brain lacerations (PBLs) have been identified on imaging of some AHT patients, but no study to date has compared the incidence of PBLs in AHT versus accidental brain injury. The purpose of this observational study is to determine if the presence of parenchymal brain lacerations are a pattern of primary brain injury unique to AHT in children three years and younger. The recognition of PBLs in infants may provide an additional imaging criterion to discriminate between AHT and accidental head injury.

Materials and Methods

We retrospectively reviewed the medical charts, autopsy reports in fatal cases when available, and cross-sectional brain imaging (CT and MRI) in two age-matched patient cohorts (AHT and accidental head injury) of infants and children up to three years of age between January 2005 and November 2013. Abusive head trauma was determined by confession and/or confirmed evaluation by the institutional child abuse medical evaluation team. The second cohort comprised of patients who were coded as moderate to severe accidental head trauma as defined by a Glasgow Coma Scale < 13 . MR imaging was utilized as the gold standard for the detection of parenchymal brain lacerations; therefore, cases were excluded when supporting MRI was not available. A parenchymal brain laceration is typically subcortical and defined by a linear or oval morphology with length ≥ 5 mm. It may contain a fluid-fluid level or demonstrate variable signal alteration depending on the chronicity of injury.

Results

In the AHT cohort, PBLs were observed in 18 of 137 patients, while no PBLs were observed in the 28 accidental head injury patients. MR imaging is performed much less frequently in accidental head injury than in victims of possible AHT and is primarily reserved for those with the most severe clinically evident injuries. These results indicate an association between head injury mechanisms and parenchymal brain laceration ($p = 0.045$), with sensitivity, specificity, PPV and NPV of 13.1%, 100%, 100% and 19.0%, respectively, for AHT.

Note: Scanned images are included in the proceedings. Some submitted images were reduced during editing thereby decreasing clarity. Also, refer to the Program Planner. Proceedings Content as of 3/28/2014.

Conclusions

Our retrospective observational review of age-matched pediatric head trauma groups, one with AHT and the other with accidental injury, demonstrates that PBLs are reflective of the complex motion mechanisms observed frequently in AHT. Parenchymal brain lacerations serve as a reliable predictive indicator of AHT in infants and children up to three years of age as they are not seen in cases of accidental trauma, even with profound impact injuries resulting in death.

KEYWORDS: Abusive Head Trauma, MR Imaging Brain

O-154 3:49PM - 3:56PM
Value of Multiplanar 3-Dimensional Reconstruction of Head Computed Tomography in the Diagnosis of Pediatric Skull Fractures

G Orman, T Bosemani, D Seeburg, C Zamora, A Oshmyansky, L Hines, A Tekes, A Poretti, T Huisman
The Johns Hopkins University School of Medicine, Baltimore, MD

Purpose

Head trauma is a leading cause of mortality and high morbidity in children. Skull fractures occur in 2.1% to 26.6% of children with head trauma. Skull fractures commonly are associated with intracranial brain injury and their presence should lead to careful search for associated lesions. A high sensitivity in the diagnosis of a skull fracture is important. We aim to compare axial 2-dimensional (D) with axial 2D and 3D multiplanar reconstruction of head computed tomography (CT) data in the diagnosis of skull fractures. We hypothesize that 2D CT images with 3D reconstruction has a higher sensitivity and specificity in detecting skull fractures compared to axial 2D CT images alone.

Materials and Methods

Head CT studies of 250 consecutive children with a history of minor or major head trauma were included in this retrospective study. All head CT studies were evaluated independently by a third year radiology resident (DS), a neuroradiology fellow (CZ) and a junior pediatric neuroradiology attending (TB). All readers evaluated first only axial 2D images and subsequently axial 2D images with 3D multiplanar reconstruction. The individual evaluations by the three readers were compared with a reference evaluation in consensus by two pediatric neuroradiologists with 18 (TAGMH) and six (AT) years of experience, respectively.

Results

The children of our study included 167 males and 83 females. At the CT study, the mean age of the patients was 7.82 ± 5.63 years (range 0.01 to 17.4 years). Eighty-two skull fractures in 76 children were diagnosed. The sensitivity to depict skull fractures was significantly higher for axial 2D CT images with 3D multiplanar reconstruction (81.3%) compared to axial 2D images alone (74.5%, $p=0.015$). The specificity was similar for both evaluations:

89.1% for axial 2D images alone and 90.5% for axial 2D CT images with 3D multiplanar reconstruction ($p>0.05$).

Conclusions

Our study shows that 3D multiplanar reconstruction increased the sensitivity of head CT studies significantly in the diagnosis of pediatric skull fractures. Three-dimensional multiplanar reconstruction is particularly helpful to detect skull fractures located in the plane of the axial 2D CT slices. Three-dimensional multiplanar reconstruction, however, does not reduce the misinterpretation of cranial sutures as skull fractures. Three-dimensional multiplanar reconstruction is cost-effective, does not require additional radiation, adds clinically valuable information and should be performed routinely for head CT studies in children with head trauma.

KEYWORDS: CT, Fracture, Skull

O-155 3:56PM - 4:03PM
Acute Imaging in Pediatric Encephalitis: What Do We See and What Don't We Know

J Bykowski¹, P Kruk², J Gold³, J Crawford³
¹University of California San Diego Health System, La Jolla, CA, ²San Diego Imaging/Rady Children's Hospital San Diego, San Diego, CA, ³Rady Children's Hospital San Diego, San Diego, CA

Purpose

The diagnosis of acute infectious pediatric encephalitis can be difficult and confounded by noninfectious mimics such as vasculitis, collagen vascular disorders, paraneoplastic syndromes, autoimmune conditions, or white matter disease. Our aim was to review acute brain imaging findings of the full spectrum of clinically suspected cases of pediatric encephalitis to identify any imaging factors that may correlate with clinical course.

Materials and Methods

Data were collected prospectively, as part of the IRB-approved California Encephalitis Project (CEP). A five year retrospective review of the clinical and imaging database of a participating regional children's medical center was performed to identify pediatric patients who met clinical suspicion for encephalitis and who had CT and/or MR imaging of the brain prospectively within the acute phase of presentation. Imaging studies were reviewed and graded by a pediatric radiologist and neuroradiology fellow independently, blinded to the initial imaging interpretation, clinical symptoms and outcome. Extent of findings including white matter disease, meningeal and/or parenchymal enhancement, diffusion restriction, hemorrhage, infarct, and hydrocephalus were scored and compared to patient age, gender, length of stay, confirmed pathogens, and outcome. Serial imaging studies were included in the analysis when available.

Results

One hundred forty-one children ages 2 days–19 years (avg 8 years) met inclusion criteria. Abnormal findings were seen in 22/94 children on head CT and 67/134 children on MR. Of the 52 with normal noncontrast head CT and MR

Note: Scanned images are included in the proceedings. Some submitted images were reduced during editing thereby decreasing clarity. Also, refer to the Program Planner. Proceedings Content as of 3/28/2014.

imaging within 2 days, abnormal findings were identified on the MR in 20 (38%). T2-hyperintense lesions were seen in the following prevalence: subcortical white matter (52%), periventricular/deep white matter (21%), brainstem (21%), cortex (20%), basal ganglia (20%), cerebellum (15%), thalami (13%), corpus callosum (8%), internal capsule (7%), hippocampus (3%), optic chiasm (2%). Lesions involved 2 or more of the above areas in 46% of those children; lesions were confluent in 30%. Additional findings included: parenchymal enhancement(18%); meningeal enhancement(45%), restricted diffusion(39%), necrotizing lesions(3%), intracranial hemorrhage(10%), hydrocephalus(8%), and subfalcine herniation in 1 child. Pathogens were identified in 52%, the most common being *M. Pneumoniae*(30), and included one or more viral agents (38), bacterial (24), both viral and bacterial(6), *M. tuberculosis*(3), rickettsia(1) and amoebae(1). MR imaging was abnormal in 40% of children where no pathogen was identified on CSF or serological screening and 49% of children where a pathogen was identified. Acute MR imaging was negative in 3 children who developed MR abnormalities within 2, 5 and 7 days respectively. Of the 51 children with serial MR based on clinical symptoms, 33% showed progression of MR findings. Five children died shortly after presentation. Clinical follow-up was available for 63/73 patients where a pathogen was identified, with 48% returning to clinical baseline. Length of stay did not correlate with age or pathogen status. While 62% of children with normal acute MR were discharged within 7 days, compared to 24% of children with abnormal acute MR, the severity of white matter and additional imaging findings did not independently correlate with length of stay.

Conclusions

Abnormal MR findings are common in pediatric encephalitis patients, and imaging may lag clinical symptom onset and recovery. In the acute evaluation of pediatric encephalitis, noncontrast head CT can serve as a primary screen for complications such as hemorrhage, mass effect or herniation in the absence of MRI availability; however, should not be considered a definitive evaluation.

KEYWORDS: Encephalitis

0-156 4:03PM - 4:10PM
Pseudo-Leptomeningeal Contrast Enhancement at 3.0T in Pediatric Patients Sedated by Propofol

R Gawande¹, B Knoll², C Truwit², A McKinney³

¹University of Minnesota and Hennepin County Medical Centers, Minneapolis, MN, ²Hennepin County Medical Center, Minneapolis, MN, ³University of Minnesota and Hennepin County Medical Centers, Roseville, MN

Purpose

Preliminary studies have shown that propofol can modulate cerebral blood flow by decreasing the metabolic rate of oxygen, and also can dilate vascular smooth muscle (1-2). As pediatric patients undergoing MR imaging (MRI) often receive intravenous sedation, the purpose of our

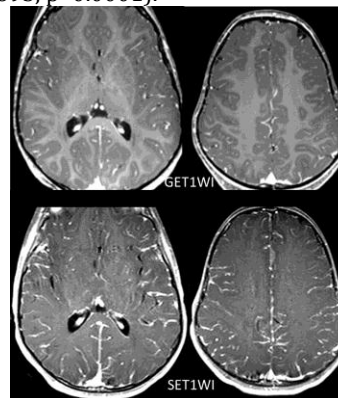
study was to evaluate the degree of leptomeningeal contrast enhancement (LMCE) on postcontrast brain MRIs at 3.0 T, in order to determine if differences exist between spin echo (SET1-weighted imaging) and gradient echo FFE (GET1-weighted imaging) T1-weighted images.

Materials and Methods

From 154 pediatric patients sedated with propofol between ages one to six years who underwent a brain MRI on a 3 T magnet between 11/2010-11/2013, 99 were excluded due to an absence of postcontrast imaging (n=96) or being on a 1.5 T magnet (n=3), moderate-severe brain abnormalities (n=10), or limited evaluation (n=2). The standard weight-based dosage of contrast was 0.1 mmol/kg of intravenous gadobutrol. A total of 43 were included who had received postcontrast GET1-weighted imaging (n=23) and SET1-weighted imaging (n=20). Three neuroradiologist reviewers separately graded the presence of LCME as follows: Grade 0: no vascular structures visualized within the sulci, Grade 1: small vascular structures barely visible within sulci, Grade 2: LCME/vascular structures that extend throughout the depths of the sulci, Grade 3: irregular and slightly thickened LCME, Grade 4: nodular or moderate-severe LCME or involvement of adjacent parenchyma. Interobserver variability between LMCE grades were compared using Cohen's kappa, and the grades were correlated with the TTI (time to imaging postcontrast administration).

Results

The mean patient age was 3.1 years. The range of LMCE grades for the three reviewers on GET1-weighted imaging was 1.2-1.4, and on SET1-weighted imaging was 1.9-2.1. There was a significant difference in mean TTI between GET1-weighted imaging (range 7-18 minutes, mean 12.63) and SET1-weighted imaging (range 7-18 minutes, mean 11.00 minutes); Mann-Whitney $p < 0.0001$. The TTI did not have a significant correlation with the LMCE grade on GET1-weighted imaging ($r = 0.015-0.19$, $p = 0.371-0.940$) or SET1-weighted imaging ($r = -0.358$ to -0.475 , $p = 0.036-0.122$), although the SET1-weighted imaging correlation was weak-moderate. Notably, in six patients who underwent both sequences, the LMCE grades were higher on SET1-weighted imaging. The range of interobserver kappa's were strong on both GET1-weighted imaging ($k = 0.567-0.698$, $p < 0.0001$) and SET1-weighted imaging ($k = 0.609-0.693$, $p < 0.0001$).



Note: Scanned images are included in the proceedings. Some submitted images were reduced during editing thereby decreasing clarity. Also, refer to the Program Planner. Proceedings Content as of 3/28/2014.

Conclusions

The appearance of LMCE or pseudo-LMCE is common on postcontrast MRI of pediatric patients sedated by propofol, and should not be mistaken for disease. This occurs more commonly, and to a greater degree, on SET1-weighted imaging as compared to GET1-weighted imaging. Such findings could relate to propofol-induced vascular smooth muscle dilation, while such vascular structures may be more visible on SET1-weighted imaging at 3.0 T possibly due to its higher contrast to noise ratio, as described previously (3-4). Ongoing or future research could also evaluate if this phenomenon relates to dosage of intravenous propofol or oxygen saturation.

KEYWORDS: Leptomenigeal Disease, Pediatric Brain, Sedation

O-157 4:10PM - 4:17PM
Cerebral Necrosis in Pediatric Brain Tumor Patients Treated with Proton Radiotherapy

W Finke¹, C Ho², C Shih², S Kralik²

¹Indiana University, Indianapolis, IN, ²Indiana University School of Medicine, Indianapolis, IN

Purpose

The purpose of this research is to evaluate post-treatment imaging for cerebral necrosis among pediatric brain tumor patients treated with proton radiotherapy.

Materials and Methods

Following institutional review board approval, a retrospective review of clinical and radiological data was performed of a total of 61 pediatric patients with primary brain tumors who had undergone cranial proton radiotherapy from 1/11/2010 to 10/25/2012 at our institution. Patients were scanned at three-month intervals or sooner, if suspicious findings were found on imaging. Patients without 12 months of imaging follow up from the completion of proton radiotherapy were excluded unless cerebral necrosis or death occurred prior to 12 months. Clinical variables included age at diagnosis, tumor pathology, chemotherapy, radiation dose, and date of radiotherapy completion. Two fellowship trained board certified neuroradiologists with certificates of added qualification (CAQ) in neuroradiology evaluated all available preoperative, immediate postoperative and subsequent follow-up brain MR imaging (MRIs) of included patients. Data recorded included preoperative tumor location and size, presence of leptomenigeal disease, extent of tumor resection, immediate postoperative complications, and postradiotherapy imaging were evaluated for tumor progression as well as for any post-treatment effects including volume loss, microhemorrhages, parenchymal T2/FLAIR hyperintensities indicative of gliosis, and cerebral necrosis. A diagnosis of cerebral necrosis was reached following consensus agreement between the two neuroradiologists and was defined as new areas of parenchymal contrast enhancement which resolve without intervention within six months. Statistical analysis of cerebral necrosis and

clinical variables was performed using Fisher exact test. Incidence and timing to development of cerebral necrosis was compared with historical information from conventional radiotherapy.

Results

Patient Characteristics: Ten patients were excluded due to lack of the required 12 months of follow-up imaging, for a total 51 patients evaluated. Average patient age was 6.8 years (range 0.9-18 years) with 9/51 (18%) of children less than two years of age. There was a male:female ratio of 2.4:1. **Tumor Characteristics:** Tumor pathology is listed in Table 1. Supratentorial tumors composed 17/51 (33%) patients involving the Cerebral Hemisphere (15.7%), Pineal (7.8%), and Sella (9.8%). Infratentorial tumors composed 34/51 (66%) patients involving the Brainstem (7.8%), and Cerebellar Hemisphere (58.8%). Surgical treatment included: Gross Total Resection (56.8%), Subtotal Resection (29.4%), Biopsy (7.8%), or None (5.9%). **Imaging Outcome:** Average follow up from completion of proton radiotherapy was 19.2 months (range 3-34 months). A total of five patients died prior to 12 month follow up. A total of 16/51 (31%) of patients developed cerebral necrosis as defined above. This compares to a typical expected incidence of radiation necrosis with conventional radiotherapy in the adult population 5-10%, and a range of 5-37% reported in pediatric patients (1-3). Average time to development of cerebral necrosis was 5.8 months (median 5 months, range 2-11 months). This compares to a typical median of 1-2 years to development of radiation necrosis with conventional radiotherapy in adults, and a reported range of 1-12 months in pediatric patients (1-3). Age less than two was found to demonstrate statistically significant association with cerebral necrosis (Fisher's exact test p=0.034). Gross total surgical resection, tumor pathology, and tumor location did not demonstrate statistical correlation with presence of cerebral necrosis (Fisher's exact test p=0.35; Fisher's exact test p= 0.19; Fisher's exact test p=1.0 respectively).

Tumor	Total
Medulloblastoma	17
Ependymoma	12
Brainstem Glioma	4
ATRT	3
Craniopharyngioma	3
Germinoma	2
PNET	2
Mature Teratoma	2
Pilocytic Astrocytoma, Grade I	2
High grade neuroepithelial tumor with glial differentiation	1
Pilomyxoid Astrocytoma, WHO Grade II	1
Pineal Parenchyma tumor, WHO Grade II	1
Choroid meningioma, grade II	1

Conclusions

Pediatric brain tumor patients treated with proton radiotherapy demonstrate a high incidence of cerebral necrosis and a short time frame to development of necrosis compared to historical data from conventional radiotherapy in adults, and at the upper end of reported necrosis in pediatric patients. Radiologists should be aware of the relative high rate of necrosis and the timing to

Note: Scanned images are included in the proceedings. Some submitted images were reduced during editing thereby decreasing clarity. Also, refer to the Program Planner. Proceedings Content as of 3/28/2014.

development of necrosis when evaluating these patients for tumor recurrence or progression. Ultimately, the clinical outcome in these patients should be compared to a similar patient population treated with conventional radiotherapy to assess the risk and efficacy of proton radiotherapy in the pediatric brain tumor population.

KEYWORDS: Pediatric Brain, Pediatric Brain Tumors, Radiation Necrosis

0-158 4:17PM - 4:24PM
Brain MR Imaging Abnormalities in Children after Treatment with High-Dose Sequential Chemotherapy and Hyperfractionated Accelerated Radiotherapy.

S Thust, E Blanco, A Michalski, K Mankad, W Chong
Great Ormond Street Hospital for Children, London, UK

Purpose

To characterize brain MR signal abnormalities encountered in children following treatment for medulloblastoma and primitive neuroectodermal tumor (CNS-PNET). Treatment-related changes including pseudoprogression are increasingly recognized in adults, but few reports are found on the subject in the pediatric literature. The distinction of therapy-related changes from tumor continues to be a challenge, even for specialists, highlighting the need for further investigation.

Materials and Methods

Institutional approval was obtained for a retrospective review of patients with medulloblastoma or CNS-PNET treated at Great Ormond Street Children's Hospital using high-dose sequential chemotherapy, hyperfractionated accelerated radiotherapy (HART) with or without thiotepa according to the recently introduced 'Milan' protocol. Patient demographic data, chemotherapy and radiotherapy treatment details and outcomes were recorded. Serial MR imaging (MRI) from presentation until the latest follow up or death was re-analyzed by two independent reviewers blinded to the original report and each other's analysis. Brain abnormalities were documented in a descriptive manner through serial imaging over several years and retrospectively categorized as tumor, treatment-related focal abnormalities and generalized parenchymal changes. Postsurgical parenchymal changes were recorded, but discounted from the analysis.

Results

In the study period, 14 children (aged 2-13 years, mean 7.5 years) received 153 serial MR examinations before and after treatment. Nine of 14 patients demonstrated a total of 11 episodes of new focal enhancing lesions (FEL). Over serial scans, 3/11 FEL episodes proved to represent definite recurrence, two at the resection site and one distant. However, 6/11 FEL episodes were treatment-related changes, which resolved or regressed spontaneously. Treatment-FEL occurred in the cerebellum and brainstem in the medulloblastoma group and within the cerebral hemispheres in the CNS-PNET group. In one episode of new multifocal enhancement, this was felt to represent a combination of tumor progression and

treatment change. One episode of FEL could not be characterized with certainty, the disease burden being too gross to make a distinction. All primary tumors and tumor-FEL demonstrated marked restricted diffusion even in small lesions, whereas none of the treatment-FEL restricted on DWI/ADC. This was felt to represent an important feature, which could aid diagnosis in future and warrants quantitative evaluation. In most of the treatment-FEL, there was evidence of regression of pre-existing residual tumor on the same scan, which could possibly aid interpretation in patients with residual disease. On the contrary, for the tumor-FEL pre-existing neoplasia was progressive or static at the onset of new FEL. In all but one child, a degree of generalized neuroparenchymal volume loss and diffuse white matter signal abnormality were noted, which were moderate or severe in 6/14 children and more pronounced in the medulloblastoma group. Generalized white matter atrophy has not been described previously in children on the 'Milan' treatment and appears frequent from our data with possible implications for long-term neurocognitive outcome.

Conclusions

In this retrospective analysis, two patterns of treatment-related brain parenchymal signal abnormality emerged: Transient focal enhancing lesions and a leukodystrophy-like pattern, both of which appear frequently. Recognition of treatment-FEL is extremely important to avoid misdiagnosis as tumor with potential devastating consequences for patient management. Lack of diffusion restriction in FEL (with restriction in the primary tumor) may prove to be a useful diagnostic feature.

KEYWORDS: Chemotherapy, Pediatric Neoplasms, Radiation Toxicity

0-159 4:24PM - 4:31PM
Brain Imaging of Methotrexate-Related Leucoencephalopathy in Patients Treated for Osteosarcoma

P Brugieres¹, A Longuad², N Gaspar², A Maraval¹, J Lincot¹, L Brugieres²

¹Henri Mondor, Creteil, France, ²Institut Gustave Roussy, Villejuif, France

Purpose

To evaluate the incidence of methotrexate-related leucoencephalopathy (MRLE) in patients treated with high-dose methotrexate (HDMTX) for an osteosarcoma and to describe the morphological, metabolic and diffusion patterns of the disease.

Materials and Methods

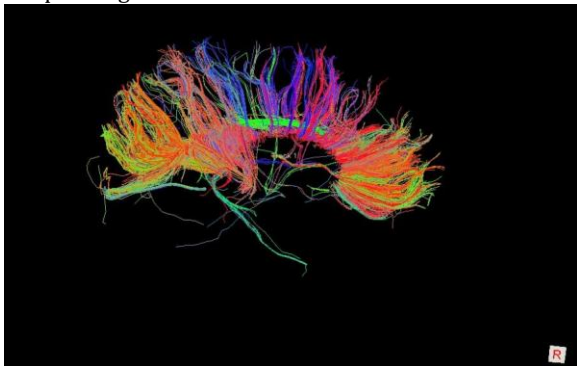
Thirty-eight patients included in the French on-going OS2006 trial who received at least three courses of HDMTX (12g/m²) had brain MR imaging (MRI) FLAIR sequences, diffusion tensor imaging (DTI) and 1H-MR spectroscopy in the week following the last course on a 1.5 T Siemens Avanto system. We used the Wilson's Grading scale for the quantification of MRLE. We calculate the ratio of apparent diffusion coefficient (ADC) in the MRLE relatively to the

Note: Scanned images are included in the proceedings. Some submitted images were reduced during editing thereby decreasing clarity. Also, refer to the Program Planner. Proceedings Content as of 3/28/2014.

ADC value of the normal-appearing white matter (NAWM). 1H-MRS metabolites (NAA, Cho, Cr, ml) were quantified by reference to brain water. Lactate were semi-quantitatively quantified (absent, small peak, well-defined peak). We used Diffusion-Toolkit[®] and TrackVis[®] softwares for fibers reconstruction. Interhemispheric fibers were reconstructed from a midsagittal region-of-interest (ROI) delineating the corpus callosum. Apparent diffusion coefficient and FA values from total brain fibers (ADCTB, FATB) and from interhemispheric fibers (ADCcc, FAcc) were registered.

Results

Thirty-one patients presented a MRLE (grade 1 =13, grade 2 = 12, grade 3 = 6). Twenty patients were asymptomatic at the time of MR study, 10 had headaches, eight had transient neurological symptoms. Patients with a severe MRLE (grade 2&3) had significant lower NAA/H2O (0.22 versus 0.27 p=0.001) and Cho/H2O (0.144 versus 0.169, p=0.009) ratios, a higher ADC (MRLE/NAWM) ratio (1.35 versus 1.12, p=0.0005), presented more often (6/18 versus 2/21) a lactate peak, and had higher ADCTB (90.01E-5 mm²/s versus 85.11E-5 m²/s, p=0.0007) and ADCcc (85.2E-5 mm²/s versus 92.03E-5 mm²/s, p=0.007) values. Patients with neurological symptoms and/or headaches had significant lower FATB (0.406 versus 0.439, p= 0.002) and FAcc (0.558 versus 0.608, p= 0.0005), higher ADCTB (88.97E-5 mm²/s versus 86.05E-5 mm²/s p= 0.04), lower NAA/H2O (0.227 versus 0.264, p= 0.02) and higher Cho/H2O (0.167 versus 0.147, p= 0.04) and 8/18 presented a lactate peak. Most (6/8) of the patients with neurological symptoms showed a clear rarefaction of interhemispheric fibers mainly in frontal and parieto-occipital regions.



Conclusions

Leuco-encephalopathy linked to high dose methotrexate is a frequent complication of the treatment of osteosarcoma. High choline peak indicative of a high membrane turn-over is encountered in patients with neurological symptoms and frequently is associated with the presence of lactates and with a disorganization of the white matter tracts demonstrated by the decreased FATB and FAcc. A prospective evaluation of neurocognitive tests during and after treatment is warranted in order to evaluate the clinical consequences of this treatment.

KEYWORDS: Brain White Matter, Leukoencephalopathy, MR Spectroscopy

O-160

4:31PM - 4:38PM

Correlation of Imaging Location of Pediatric Posterior Fossa Ependymoma with Extent of Surgical Resection, Pattern of Tumor Recurrence, Patient Survival and Survival Time

N Sabin, Y Yuan, A Coan, P Klimo, D Ellison, T Merchant
St. Jude Children's Research Hospital, Memphis, TN

Purpose

Previous reports have suggested that posterior fossa ependymoma may be divided into two groups based on tumor location: lateral cerebellopontine angle (CPA) centered tumors and those centered in the IVth ventricle. Lateral tumors have been associated with incomplete resection and poor prognosis. We examined the association between the imaging location of posterior fossa ependymoma, extent of surgical resection, pattern of tumor recurrence, and patient survival status and survival time.

Materials and Methods

After institutional review board approval, pre-operative MR imaging (MRI) examinations for 107 children and adolescents diagnosed with posterior fossa ependymoma were reviewed systematically. The subjects were participants in a larger institutional trial of conformal radiotherapy following definitive surgery. Tumors centered in the IVth ventricle were categorized as central and those not centered in the IVth ventricle were categorized as lateral tumors. The extent of resection was recorded based on postoperative MRI studies. Recurrent tumor, when it was present on follow-up MRI examinations, was classified as local when present in the region of the original tumor or distant when present at a site discontinuous from the original lesion. Fisher's exact test was used to assess the association between the location of the primary tumors, extent of resection, and outcome including patient survival status and pattern of tumor recurrence. The log-rank (L-R) test was used to test for survival time differences between patients with central tumors and those with lateral tumors. A two-sided significance level of p<0.05 was used for all statistical tests.

Results

No statistically significant association was detected between the location of posterior fossa ependymoma and extent of resection, pattern of tumor recurrence or overall survival. Analysis of all subjects, regardless of survival status, showed no significant difference in survival time between individuals with central tumors and those with lateral ependymomas (L-R, p=0.0879). Among patients who died of their tumors, however, there was a statistically significant difference in survival time comparing those with central ependymomas and subjects with lateral tumors (L-R, p=0.0377).

Conclusions

After the detailed evaluation of more than 100 subjects with posterior fossa ependymoma, no association was found between tumor location, extent of surgical resection, pattern of tumor recurrence or patient survival time. These results do not substantiate those of previous studies that have found lateral tumors to be associated with incomplete

Note: Scanned images are included in the proceedings. Some submitted images were reduced during editing thereby decreasing clarity. Also, refer to the Program Planner. Proceedings Content as of 3/28/2014.

resections and worse outcomes. We did find that among subjects who died of ependymoma, those with central tumors survived longer. The reason for this is unclear but could be related to comorbidities and other difficulties associated with resection of the lateral lesions. Our analysis of pediatric posterior fossa ependymomas is ongoing and will evaluate histopathological and genetic differences among the tumors as well as associations with additional clinical and demographic data.

KEYWORDS: Ependymoma, Outcomes, Pediatric Brain Tumors

Monday, May 19
 4:45 PM – 6:15 PM
 Room 517bc

23 - General Programming: The Foundation of the ASNR Special Session on Traumatic Brain Injury: Is DTI Ready for Prime Time?

FASNR Introduction 4:45PM - 4:50PM

Russell, E.
 Northwestern University
 Chicago, IL

O-161 4:45PM - 5:15PM
 State of the Art

Mukherjee, P.
 University of California San Francisco
 San Francisco, CA

O-162 5:15PM - 5:25PM
 MEG in TBI

Lee, R.
 UCSD/VA Medical Center
 San Diego, CA

O-164 5:25PM - 6:00PM
 Pro: Academic

Lipton, M.
 Albert Einstein College of Medicine
 Bronx, NY

O-165 5:25PM - 6:00PM
 Pro: Clinical

Bigler, E.
 Brigham Young University
 Provo, UT

O-163 5:25PM - 6:00PM
 Pro: Private Practice

Walker, A.
 Florida Imaging Consultants, PA
 Stuart, FL

O-166 6:00PM - 6:15PM
 Con: Academic

Zimmerman, R. · Niogi, S.
 New York Presbyterian Hospital
 New York, NY

O-168 6:00PM - 6:15PM
 Con: Clinical

Wortzel, H.
 VISN 10 MIRECC & University of Colorado
 Denver, CO

Monday, May 19
 4:45 PM – 6:15 PM
 Room 517d

24 - General Programming: Toxic and Occupational Diseases

O-169 4:45PM - 5:15PM
 Toxic Encephalopathies

Mandell, D.
 University Health Network and the University of Toronto
 Toronto, Ontario

Abstract/Presentation Summary
 Toxic encephalopathies were described in Roman writings more than two thousand years ago, and patients with toxic exposures not uncommonly present to emergency departments and outpatient clinics today. Clinical toxicity can be reversible if diagnosis and treatment is prompt, but few physicians have expertise in the full spectrum of toxic disease. I will begin the session by discussing the unique susceptibility of the central nervous system to toxic injury. I will then briefly cover the cellular pathophysiology of toxic injury, particularly emphasizing the relationship between pathophysiological terminology (eg. glutamate excitotoxicity) and imaging findings. I will discuss the environmental exposure clinical history, the role of laboratory testing, and the role of imaging for diagnosis of toxic encephalopathy. Finally, I will focus on the imaging patterns of two particular categories of toxic encephalopathy: heavy metal toxicity and pharmaceutical toxicity.

Note: Scanned images are included in the proceedings. Some submitted images were reduced during editing thereby decreasing clarity. Also, refer to the Program Planner. Proceedings Content as of 3/28/2014.

O-170 5:15PM - 5:35PM
Toxic Encephalopathies II

Gallagher, T.
Northwestern University Feinberg School of Medicine
Chicago, IL

O-171 5:35PM - 5:55PM
Cased Based Differential Diagnosis

Huang, B.
University of North Carolina
Chapel Hill, NC

Abstract/Presentation Summary

In this case based review, the audience will be presented with patient vignettes in which the clinical and imaging differentials may include toxic disorders as part of a broader list of diagnostic considerations. In these cases, differentials for entities which typically affect the subcortical white matter and entities which involve the deep gray matter nuclei symmetrically will be discussed. In addition to selected toxic disorders, topics reviewed will include ADEM, PRES, CNS infections, hypoxic brain injury, and hemolytic-uremic syndrome. Specific distinguishing clinical and imaging features of these each of these disorders will be highlighted.

Questions and Discussion 5:55PM - 6:15PM

Monday, May 19
4:45 PM – 6:15 PM
Room 517a

25 - Young Professionals Programming:
Career Choices and Development

O-172 4:45PM - 5:00PM
Benefits of Academic Medicine

Meltzer, C.
Emory University School Of Medicine
Atlanta, GA

O-173 5:00PM - 5:15PM
Benefits of Private Practice

Pramanik, B.
Medical Center Radiology Group
Orlando, FL

Abstract/Presentation Summary

Private practice radiology offers a number of considerable advantages over academic radiology. One key advantage is

personal freedom. There is much more autonomy to make decisions as there is less bureaucracy. The workload is predominantly clinical and there is no research or very little teaching responsibilities. Private practice enables radiologists to capitalize on a broader range of their training. Most private practice radiologists practice general radiology and see a broad range of patients encompassing every radiologic subspecialty and modality. By seeing a breadth of cases, there is more flexibility to adapt. Finally, the major advantage is compensation. Private practice salaries are higher than academic radiology. Moreover, the benefits packages including vacation are frequently more generous.

O-174 5:15PM - 5:30PM
Negotiating a Position of Academic Medicine

Mukherji, S.
Michigan State University
Ann Arbor, MI

Abstract/Presentation Summary

The intent of this presentation will be to review important aspects about negotiating an academic radiology position. The attendees will be familiar with important information that will permit them to properly assess different academic opportunities.

O-175 5:30PM - 5:45PM
Negotiating a Contract in Private Practice

Barr, R.
Mecklenburg Radiology Associates, P.A.
Charlotte, NC

Abstract/Presentation Summary

This will be a practical, "how to" session for attendees preparing to enter the private practice radiology workforce. The basics of the employment contract will be discussed from the perspective of the group practice. The speaker hopes to make up for a lack of legal expertise with a plethora of common-sense advice. The typical steps from recruitment to contracting will be reviewed. The talk will highlight the most important elements of the contract, including the elements that tend to raise the most questions, such as noncompete clauses and tail coverage responsibility. We'll discuss what's typically missing from the contract, and the most common mistakes job seekers make when contracting.

O-176 5:45PM - 6:00PM
Why I Did What I Did and Did I Make the Right Decision

Seidenwurm, D.
Radiological Associates
Sacramento, CA

Note: Scanned images are included in the proceedings. Some submitted images were reduced during editing thereby decreasing clarity. Also, refer to the Program Planner. Proceedings Content as of 3/28/2014.

Abstract/Presentation Summary

Choose a career that reflects a realistic assessment of your interests and capabilities, and one that will make you happy based on your priorities in life.

6:00PM - 6:15PM

Discussion

Monday, May 19

4:45 PM – 6:15 PM

Room 520

26 - Comparative Effectiveness Research: What's Being Done, Who's Paying for it, What it Takes to Get Funded

O-177 4:45PM - 5:00PM
PCORI, Pragmatic Trials and CER: What is it and Who Funds It?

Jarvik, J.
Univ of Washington
Seattle, WA

Abstract/Presentation Summary

In this presentation, I will discuss comparative effectiveness research and present an example of a pragmatic randomized trial. Low back pain, an Institute of Medicine priority condition for comparative effectiveness research, is of major public health importance. It is one of the most common reasons for physician visits and an important cause of functional limitation and disability. Imaging is frequently performed as part of the diagnostic evaluation and is an important contributor to the cost of back pain care, which totaled more than \$86 billion in 2005. It is well known that, even without back pain, magnetic resonance (MR) imaging of the lumbar spine frequently reveals findings such as disc desiccation or bulging. Patients and their providers may attribute greater importance to these findings, which are often age-related, than they should, because they do not have an appropriate frame of reference in which to interpret the findings. These "incidental" findings may initiate a cascade of events leading possibly even to surgery, without improving patient outcomes. The Lumbar Imaging with Reporting of Epidemiology (LIRE) Trial is a pragmatic, randomized trial to determine the effectiveness of inserting epidemiological benchmarks into imaging reports at reducing subsequent tests and treatments.¹ Our intervention is simple, inexpensive and easy to deploy. We are passively collecting primary outcome measures of healthcare utilization both pre- and post-intervention, using robust electronic health records at our participating sites. LIRE is an example of a trial that falls at the pragmatic end of the explanatory-pragmatic spectrum described by Thorpe et al. ² LIRE was

funded by the NIH Health Care Systems Collaboratory, but other entities such as PCORI and AHRQ, are playing a leading role in promoting and funding CER.

O-178 5:00PM - 5:15PM
Costs Studies and Cost Effective Analysis

Medina, L.
Miami Children's Hosp
Miami, FL

Abstract/Presentation Summary

There are multiple types of cost studies in medical imaging. Lecture will focus on (1) cost studies such as time motion analysis and (2) cost-effectiveness analysis (CEA).

O-179 5:15PM - 5:30PM
Involving Trainees in Comparative Effective Research

Anzai, Y.
Univ. Washington Medical Center
Seattle, WA

O-180 5:30PM - 6:15PM
Panel Discussion on Promoting CER with Academic Research Enterprise and Breaking Down Barriers

Sanelli, P. · Fink, J. · Hoang, J. · Gupta, A.
Weill Cornell Medical College · Univ Of Washington · Duke University Medical Center · NY Presbyterian Hosp./Cornell Univ.
New York, NY · Seattle, WA · Durham, NC

Monday, May 19

4:45 PM – 6:15 PM

Room 524

27 - CSI: Montreal Programming: Making a Scientific Presentation

O-185a 4:45PM - 5:30PM
Tips on Preparing and Giving an Oral Presentation

Wiggins, R.
University of Utah
Salt Lake City, UT

Abstract/Presentation Summary

There is an art to teaching and lecturing, which is not taught in medical school. While the lecture or oral presentation is the most commonly used method of passing along knowledge in medical education, it is not the best method of educating. Our problem is that students only capture about 30% of the main points in a lecture in their notes, and 3-4 weeks later, most students remember <10% of lecture facts. So as a teacher in medical education, how

Note: Scanned images are included in the proceedings. Some submitted images were reduced during editing thereby decreasing clarity. Also, refer to the Program Planner. Proceedings Content as of 3/28/2014.

can we change this? In thinking about these problems, we have 2 main goals with our oral presentations. The first is: (1) what can I do as a teacher to ensure that my students understand and recognize the main teaching points of my oral presentation, and (2) how can I create and deliver an oral presentation that will allow my students to remember these important points longer than a few days after the talk?

O-185b 5:15PM - 5:45PM
How to Create an Award Winning Scientific Exhibit

Reede, D.
The Long Island College Hospital
Brooklyn, NY

Abstract/Presentation Summary

Electronic exhibits are the major format used for scientific posters at most national meetings. There are many advantages in using this format such as the ability to vary the presentation style (quiz based vs lecture format, animated vs non-animated etc.). However, many steps need to be completed before an exhibit is uploaded. This presentation will focus on choosing a topic, writing an abstract, concept development, gathering materials (cases and illustrations) and organizing the team to produce an award winning exhibit.

O-185c 5:45PM - 6:15PM
How to Create an Award Winning Scientific Exhibit - II

Ledermann, E.
The long Island College Hospital
Brooklyn, NY

Abstract/Presentation Summary

PowerPoint is the standard medium for lectures and scientific exhibits at most national and subspecialty radiology meetings. Understanding its applications, limitations and design capabilities will enable you to enhance the presentation of research data and educational materials. Basic and advanced techniques that can improve the overall style and design of a PowerPoint presentation will be shown. Strategies will be demonstrated to increase effectiveness and streamline the exhibit making process.

Tuesday, May 20
7:30 AM – 8:30 AM
Room 517bc

28 - Pediatrics Session (SAM)

O-186 7:30AM - 7:50AM
Pediatric Brain-Part I: Congenital Abnormalities

Dietrich, R.
UCSD Medical Center
San Diego, CA

Abstract/Presentation Summary

This session comprises a case-based review presentation of common and uncommon congenital disorders involving the pediatric brain with a focus on the approach to the differential diagnosis. Congenital central nervous system anomalies occur due to abnormal or arrested development of the brain and/or spine during the intrauterine period. As the brain and spine form within a limited period of time, insults leading to the development of congenital anomalies often affect multiple brain structures. Both prenatal and postnatal multiplanar imaging techniques are extremely useful in demonstrating the spectrum of abnormalities seen in each entity and help diagnose and give prognostic information to treating physicians and parents. This information together with increasing understanding of the genetic origins of many of these entities is giving additional insight into many of the congenital brain anomalies discussed in this session. Covered topics include: Disorders of dorsal induction including cephaloceles and Chiari malformations. Disorders of ventral induction including holoprosencephalies and septooptic dysplasia. Posterior fossa hypoplastic and dysplastic anomalies including Dandy-Walker malformation, vermian and hemispheric hypoplasia, Joubert syndrome, rhombencephalosynapsis and Llermitte-Dulcos syndrome. Migrational anomalies including lissencephaly (agyria/pachygyria), polymicrogyria, heterotopias, cortical dysplasias, schizencephaly and hemimegalencephaly. Corpus callosum anomalies including dysgenesis and hypoplasia of the corpus callosum and associated anomalies such as lipomas and interhemispheric arachnoid cysts. Neurophakomatoses including neurofibromatosis type 2, tuberous sclerosis complex and von Hippel-Lindau disease.

O-187 7:50AM - 8:10AM
Pediatric Brain-Part II: Acquired Disorders

Poussaint, T.
Children's Hospital
Boston, MA

Abstract/Presentation Summary

Pediatric Neuroradiology, a radiologic discipline in which neuroimaging techniques are used to assess central

Note: Scanned images are included in the proceedings. Some submitted images were reduced during editing thereby decreasing clarity. Also, refer to the Program Planner. Proceedings Content as of 3/28/2014.

nervous system (CNS) disease in the infant, child, and teenager, relies on 1) an understanding of normal brain development and maturation from gestation through adolescence; 2) a technical mastery of the neuroimaging techniques that are used in evaluating brain diseases of childhood; 3) an overall grasp of the imaging features of acquired numerous brain pathologies; and 4) the ability to select the most appropriate modality or modalities in evaluating a suspected or diagnosed case of acquired pediatric CNS disease. This presentation will provide a case-based overview of a subset of various CNS acquired diseases of childhood as well as the basic imaging features that inhere in each. The acquired disorders that will be covered in this session include metabolic white matter diseases of childhood, pediatric brain tumors, congenital infections, and vascular diseases of childhood described in the paragraphs below. Regarding white matter diseases of childhood, these disorders that primarily involve the white matter are known as leukoencephalopathies and include the peroxisomal disorders (e.g., adrenoleukodystrophies), the lysosomal leukodystrophies (e.g., metachromatic globoid cell) and other white matter diseases (e.g., Pelizaeus-Merzbacher, Canavan, Alexander, Cockayne). Brain tumors are the most common solid pediatric tumors and the leading cause of death in children with solid tumors. The classification of CNS tumors is primarily based on histopathological criteria, molecular genetics and imaging features. Anatomic predilection and corresponding clinical signs provide other measures for classifying intracranial tumors in childhood including cerebral hemispheric tumors, tumors about the third ventricle, and posterior fossa tumors which will be reviewed. Deep or hemispheric cerebral tumors of childhood include astrocytoma (e.g., pilocytic), choroid plexus papilloma, ganglioglioma, other glial tumors, and embryonic tumors (e.g., PNET). Tumors that develop around the third ventricle (i.e., the suprasellar or pineal regions) are frequently encountered in childhood. These lesions include optic glioma, craniopharyngioma, and germ cell tumors (i.e., germinoma, teratoma). Common posterior fossa tumors of childhood include medulloblastoma, cerebellar astrocytoma, brainstem glioma, and ependymoma. Congenital infections of the CNS, which usually infect via the transplacental route, can affect the developing nervous system. Depending on the fetal age at the time of insult, manifestations of infection may vary. Congenital infections include, but are not limited to toxoplasmosis and others- syphilis, rubella, cytomegalovirus, herpes 2 and HIV (mnemonically termed, TORCH). Infections contracted during the first two trimesters may result in congenital malformations, while those occurring in the third trimester typically manifest as destructive lesions. On neuroimaging, the chronic sequelae of congenital infections include disorders of cortical development, calcifications, hydrocephalus, atrophy, demyelination, and porencephaly. There are numerous vascular diseases in childhood. Occlusive neurovascular disease in the child may be arterial or venous in origin and typically results in focal or multifocal lesions distributed within the occluded vessel or vessels. Arterial occlusive

disease may occur as a prenatal or perinatal event (emboli of placental origin or from involuting fetal vessels), as a complication of infection (e.g., meningitis), with congenital heart disease, or from a hypercoagulopathy. Other causes include trauma (e.g., dissection), moyamoya disease, and metabolic disorders (e.g., mitochondrial cytopathies). Vascular conditions such as vein of Galen malformations and the associations of hemangioma with PHACE syndrome will be included.

8:10AM - 8:30AM

Questions and Answers

Tuesday, May 20
8:30 AM – 10:00 AM
Room 517bc

29 - ASFNR Programming: Emerging
Techniques

O-188
7T-Potential Clinical

8:30AM - 9:00AM

Hess, C.
University of California, San Francisco
San Francisco, CA

O-189
Simultaneous Multi-slice (Multiband, Multiplexed) Sub-second fMRI and Ultrafast Imaging

9:00AM - 9:30AM

Feinberg, D.
University California, Berkeley
Berkeley, CA

Abstract/Presentation Summary

Echo planar imaging (EPI) is most commonly used for fMRI due to its high BOLD contrast sensitivity, greatly reduced physiological noise compared to segmented or multi-shot imaging techniques and its high SNR/time rate during acquisition. Each EPI brain image is created from a single excitation pulse and the subsequent echo train readout in under a 100 ms, hence the image signal is recorded within a similar cardiac phase which minimizes physiological artifacts arising from pulsatile blood and CSF movement. Multi-slice EPI acquisition independently excites slices within a TR period to achieve very high efficiency in terms of image SNR per acquisition time. To date, gradient echo (GE) EPI is the workhorse of fMRI studies. Discussed here is a rapidly developing MRI technology, recently impacting EPI based fMRI and diffusion imaging, as used in the NIH Human Connectome Project, and is a technology that will likely impact other neuroimaging sequences more widely used for clinical brain and spine imaging. Simultaneous Multi-Slice (SMS) EPI, also referred to as Multiplexed and Multiband (MB) EPI, (1-6) is a powerful new MRI development that is providing unprecedented speed in

Note: Scanned images are included in the proceedings. Some submitted images were reduced during editing thereby decreasing clarity. Also, refer to the Program Planner. Proceedings Content as of 3/28/2014.

brain imaging for fMRI. SMS EPI has recently undergone improvements in its ability to separate the simultaneously recorded images, to reduce g-factor, reduce artifacts and substantially increase SNR. Improved separation of slices through dealiasing using a generalizable approach of blipped controlled aliasing in parallel imaging (blipped-CAIPI) (4) now allows much higher slice acceleration (5,6), up to 12 slices recorded simultaneously, however the spatial inhomogeneity of g-factor becomes limiting in studies (4-6). A major advantage of SMS EPI over in-plane parallel imaging (Grappa, SENSE) is that SMS EPI does not accelerate by an undersampling factor R to shorten the echo train, consequently it does not incur the $\frac{1}{R}$ reduction in SNR as does parallel imaging. SMS EPI records slices simultaneously and can be used to increase brain coverage (2) or reduce TR for higher sampling rates (3). At 7T thinner slices reduce signal loss from intravoxel Bo inhomogeneity while SMS EPI allows whole brain fMRI without prohibitively long TR (2). In functional connectivity studies at 3T, SMS EPI reduced the TR required for whole brain coverage from typical TR 2s-3s down to sub-second TR 0.3-0.8s, which improved statistical definition of networks and provided additional important information on resting state connectivity (3). Recent use of SMS EPI for ASL perfusion imaging and for CSF phase velocity imaging has been evaluated.

O-190 9:30AM - 10:00AM
ASL Perfusion – Is It Reliable in Advanced Steno-Occlusive Disease?

Zaharchuk, G.
Lucille Packard Children's Hosp. at Stanford
Stanford, CA

Tuesday, May 20
8:30 AM – 10:00 AM
Room 517d

30 - Mini Symposium – Tumor – Part I

O-191 8:30AM - 8:45AM
Blood Brain Barrier Imaging: Key Concepts When Evaluating Primary Brain Tumors

Cha, S.
University of California San Francisco
San Francisco, CA

O-192 8:45AM - 8:51AM
Comparison of DCE- and DSC-MRI at 3T in the Grading of Gliomas

T Nguyen¹, G Cron¹, K Bezzina², P Kirstin¹, I Cameron¹, S Chakraborty¹, M Hogan¹, G Jansen¹, J Sinclair¹, R Thornhill¹, C Torres¹, J Wolfe¹

¹The Ottawa Hospital, Ottawa, Ontario, Canada, ²University of Ottawa, Ottawa, Ontario, Canada

Purpose

Tumor plasma volume (Vp) and the volume transfer constant (Ktrans) estimated by dynamic contrast enhanced MR imaging (DCE-MRI) can be biased by poor measurement of the vascular input function (VIF) (1). We have compared a novel DCE-MRI technique using a phase-derived VIF and "bookend" T1 measurements with dynamic susceptibility contrast (DSC) MRI, in terms of diagnostic accuracy for pre-operative grading of gliomas.

Materials and Methods

This prospective study included 44 patients with new pathologically confirmed diagnosis of glioma (grade II, n=8; grade III, n=10; grade IV, n=26). Each patient underwent a preoperative MRI at 3 T which included two injections of 5ccs Gadobutrol 1.0 for DCE- and DSC-MRI. During DCE-MRI, both magnitude and phase images were acquired to estimate Vp_Φ and Ktrans_Φ (calculated using a phase-derived VIF and bookend T1 measurements) as well as for Vp_SI and Ktrans_SI (calculated from a magnitude-derived VIF without T1 measurements). From DSC-MRI, both the corrected cerebral blood volume normalized to the contralateral white matter (rCBV) and leakage factor (K2) maps were computed. For each patient, four regions-of-interest (ROIs) were placed over the solid part of the tumor and the highest value among the ROIs was recorded (hot spot). A neuropathologist diagnosed and graded the tumor according to the 2007 WHO criteria. A Mann-Whitney U test was used to test for difference between grades. Diagnostic accuracy was assessed using ROC analysis.

Results

Vp_Φ, Ktrans_Φ and rCBV values were statistically different between grade 2 and grade 3 as well as between grade 3 and grade 4 (P<0.05). Such a difference was not found for Vp_SI, Ktrans_SI and K2 (P>0.05). In differentiating low grade from high grade gliomas, there was no statistically significant difference between AUCs of Vp_Φ, Ktrans_Φ, and rCBV which were 0.96 (0.90-1), 0.91 (0.74-1) and 0.87 (0.68-1) respectively. AUCs for Ktrans_SI, Vp_SI, and K2 were 0.84 (0.71-0.97), 0.82 (0.61-1) and 0.71 (0.48-0.95). A statistical difference in AUCs was found between Vp_Φ and Ktrans_SI, and also between Vp_Φ and K2.

Conclusions

In the pre-operative grading of gliomas, diagnostic accuracy of DCE-MRI parameters obtained from phase-derived VIF and bookend T1 mapping is similar to DSC-MRI-derived rCBV.

Note: Scanned images are included in the proceedings. Some submitted images were reduced during editing thereby decreasing clarity. Also, refer to the Program Planner. Proceedings Content as of 3/28/2014.

O-194 9:00AM - 9:15AM
ASL in the Evaluation of Primary CNS Tumors: Are We There Yet?

Maldjian, J.
Wake Forest University School of Medicine
Winston-Salem, NC

Abstract/Presentation Summary

Arterial spin labeling (ASL) perfusion MRI imaging has been in development for over a decade (1-3). During this time, it has remained predominantly a research tool. With the recent availability of the technique from a variety of MRI vendors, ASL is now entering more broadly into the clinical realm. Unlike conventional bolus gadolinium techniques, ASL does not require intravenous contrast, is quantitative, and is readily repeatable. Perfusion studies can provide useful information in the evaluation of patients with CNS tumors. Tumor grade frequently correlates with a variety of perfusion parameters, based predominantly on bolus gadolinium techniques (4-7). Tumor studies using ASL are now emerging. Hypoperfused tumors on ASL are frequently of lower histologic grade (4), and for malignant neoplasms, the higher the perfusion of the mass, the higher the histologic grade (4-7). High ASL perfusion can be seen frequently in non-malignant tumors such as meningiomas and hemangioblastomas. Metastatic lesions demonstrate a variety of perfusion patterns, with solid tumors tending to be hyperperfused.

O-198 9:30AM - 9:45AM
Update on MRS in Brain Tumor Evaluation

Castillo, M.
UNC Chapel Hill
Chapel Hill, NC

Abstract/Presentation Summary

This lecture explores the following issues: Do we understand what MRS means? Is it reliable and reproducible? Is it helpful in initial tumor evaluation and biopsy planning and treatment planning? Is it useful after treatment? We know that NAA is a neuron-marker only but that its function is unknown although it serves as marker of neuron density and viability. Choline reflects cellularity but not its origin which can be due to proliferation or accumulation. Creatine is a marker of energy and may be elevated in low grade gliomas. Lactate indirectly measures aerobic metabolism and although it generally implies ischemia (high grade) it may be elevated in pilocytic astrocytomas. Finally, lipids are markers of necrosis but many times are contaminants from outside of voxel sampling. The reproducibility of MRS has improved but it remains limited in the evaluation of small changes in metabolites due to its inherent low signal-to-noise and the fact that major biological alterations must be present before being reflected by MRS. MRS is perhaps not helpful in initial tumor evaluation and low grade gliomas may have falsely low choline levels while some glioblastomas may show a normal spectral pattern. MRS may be helpful in

distinguishing between 1ry gliomas and metastasis and tumefactive demyelinating lesions but perfusion is equally helpful in these situations and easier to perform and interpret. MRS may be helpful in guiding biopsy towards areas containing high choline levels especially in heterogeneous tumors such as gliomatosis. Finally, finding elevated myoinositol and glutamine in a hemisphere contralateral to a glioma may indicate diffuse tumor spread and in some gliomas the presence of certain metabolites may correlate with genetic alterations such as mutation of the IDH1 gene. MRS may add certainty to the diagnosis of treatment-induced necrosis but is limited in cases of pseudoprogression. Unfortunately, MRS is not covered by most insurances due to the fact that most articles are levels of evidence 3 or 4 and its impact in diagnosis and tumor treatment have not been proven.

O-192 8:45AM - 8:51AM
Comparison of DCE- and DSC-MRI at 3T in the Grading of Gliomas

T Nguyen¹, G Cron¹, K Bezzina², P Kirstin¹, I Cameron¹, S Chakraborty¹, M Hogan¹, G Jansen¹, J Sinclair¹, R Thornhill¹, C Torres¹, J Woulfe¹

¹The Ottawa Hospital, Ottawa, Ontario, Canada, ²University of Ottawa, Ottawa, Ontario, Canada

Purpose

Tumor plasma volume (Vp) and the volume transfer constant (Ktrans) estimated by dynamic contrast enhanced MR imaging (DCE-MRI) can be biased by poor measurement of the vascular input function (VIF) (1). We have compared a novel DCE-MRI technique using a phase-derived VIF and "bookend" T1 measurements with dynamic susceptibility contrast (DSC) MRI, in terms of diagnostic accuracy for pre-operative grading of gliomas.

Materials and Methods

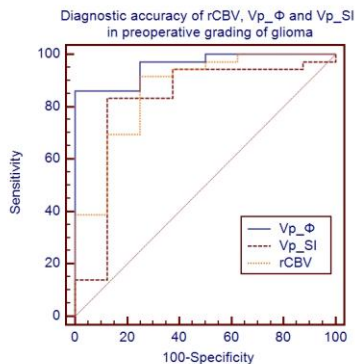
This prospective study included 44 patients with new pathologically confirmed diagnosis of glioma (grade II, n=8; grade III, n=10; grade IV, n=26). Each patient underwent a preoperative MRI at 3 T which included two injections of 5ccs Gadobutrol 1.0 for DCE- and DSC-MRI. During DCE-MRI, both magnitude and phase images were acquired to estimate Vp_Φ and Ktrans_Φ (calculated using a phase-derived VIF and bookend T1 measurements) as well as for Vp_SI and Ktrans_SI (calculated from a magnitude-derived VIF without T1 measurements). From DSC-MRI, both the corrected cerebral blood volume normalized to the contralateral white matter (rCBV) and leakage factor (K2) maps were computed. For each patient, four regions-of-interest (ROIs) were placed over the solid part of the tumor and the highest value among the ROIs was recorded (hot spot). A neuropathologist diagnosed and graded the tumor according to the 2007 WHO criteria. A Mann-Whitney U test was used to test for difference between grades. Diagnostic accuracy was assessed using ROC analysis.

Results

Vp_Φ, Ktrans_Φ and rCBV values were statistically different between grade 2 and grade 3 as well as between

Note: Scanned images are included in the proceedings. Some submitted images were reduced during editing thereby decreasing clarity. Also, refer to the Program Planner. Proceedings Content as of 3/28/2014.

grade 3 and grade 4 ($P < 0.05$). Such a difference was not found for Vp_SI, Ktrans_SI and K2 ($P > 0.05$). In differentiating low grade from high grade gliomas, there was no statistically significant difference between AUCs of Vp_Φ, Ktrans_Φ, and rCBV which were 0.96 (0.90-1), 0.91 (0.74-1) and 0.87 (0.68-1) respectively. AUCs for Ktrans_SI, Vp_SI, and K2 were 0.84 (0.71-0.97), 0.82 (0.61-1) and 0.71 (0.48-0.95). A statistical difference in AUCs was found between Vp_Φ and Ktrans_SI, and also between Vp_Φ and K2.



Median values of the maximal perfusion parameters for different grades of gliomas

	Grade					
	2		3		4	
	Median	95% CI	Median	95% CI	Median	95% CI
Ktrans_Φ	0.000425	0.0000973 - 0.0141	0.0191	0.00398 - 0.0447	0.0584	0.0403 - 0.0860
Ktrans_SI	0.0116	0.00126 - 0.0696	0.0615	0.00927 - 0.217	0.112	0.0728 - 0.162
Vp_Φ	0.228	0.000 - 1.062	1.668	0.913 - 3.545	3.636	2.739 - 4.700
Vp_SI	1.200	0.805 - 6.210	7.268	2.474 - 20.817	9.559	6.991 - 11.970
rCBV	2.326	1.380 - 9.214	6.343	4.018 - 15.697	12.302	9.181 - 16.381
K2	1.150	-0.0375 - 5.225	2.052	0.448 - 3.320	3.557	2.191 - 6.029

Conclusions

In the pre-operative grading of gliomas, diagnostic accuracy of DCE-MRI parameters obtained from phase-derived VIF and bookend T1 mapping is similar to DSC-MRI-derived rCBV.

KEYWORDS: Dynamic Contrast-Enhanced MR, Neoplasm, Permeability MR Imaging

0-193 8:51AM - 8:57AM
A New Mosaic Pattern in Glioma Vascularization:
Endothelial Progenitor Cells may Become a Therapeutic
and Imaging Probe to Overcome Antiangiogenic Resistance

X Chen, J Fang, W Zhang
Institute of Surgery Research, Daping Hospital, Third
Military Medical University, Chongqing, China

Purpose

Emerging evidence suggests that glioma stem-like cells (GSCs) transdifferentiating into vascular endothelial cells (ECs) possibly contributes to tumor resistance to antiangiogenic therapy. Endothelial progenitor cells

(EPCs), showing active migration and incorporation into neovasculature of glioma, may be a good vehicle for delivering genes to target GSCs transdifferentiation. Thus we aimed to investigate whether exogenous EPCs integrated into the vessels containing the tumor-derived ECs in C6 glioma rat model. Furthermore, to show the feasibility of using MR imaging (MRI) to track and quantify these cells.

Materials and Methods

Forty-eight C6 glioma rat models *in situ* were established. Spleen-derived EPCs from healthy Sprague-Dawley rats were obtained, maintained and identified, then labeled with USPIO and fluorescein. Rats in the EPC group were transplanted with double labeled EPCs via tail vein on 10 days after glioma established. MR imaging was performed at a 3.0 T MR system using specific small animal head coil before EPCs transplantation and on 1, 3, 5, 7 day post-transplantation of EPCs. The MRI sequences included T2-weighted imaging and susceptibility-weighted imaging (SWI) were used to track the migration of these double labeled EPCs, additionally, T2-map was used to detect the T2 value and corresponding $\Delta R2$ value. The distribution of double labeled EPCs was detected by Prussian blue staining and immunofluorescent staining. The corporation of these homing EPCs into tumor vessels was performed by immunofluorescent staining and TEM.

Results

We found a new mosaic pattern that exogenous EPCs integrated into the vessels containing the tumor-derived ECs in C6 glioma rat model. Further, the transdifferentiation frequency of C6 glioma cells and the expressions of key factors on GSCs transdifferentiation, i.e., HIF-1 α , Notch1, and Flk1 in gliomas with or without EPCs transplantation showed no significant difference between these two groups. Similar results were observed in a series of *in vitro* experiments, including flow cytometry, tube formation and western blot analysis of transdifferentiation-induced C6 glioma cells treated with or without EPCs conditioned medium. Additionally, magnetic resonance imaging could track the migration and incorporation of EPCs into glioma *in vivo*, which was confirmed by Prussian blue staining. The number of magnetically labeled EPCs estimated from T2 maps correlated well with direct measurements of labeled cell counts by flow cytometry.

Conclusions

Our findings may provide a rational base for the future application of EPCs as a therapeutic and imaging probe targeting GSCs transdifferentiation to overcome antiangiogenic resistance for glioma and monitor the efficacy of this treatment.

KEYWORDS: Glioma, MR Imaging, Stem Cell

Note: Scanned images are included in the proceedings. Some submitted images were reduced during editing thereby decreasing clarity. Also, refer to the Program Planner. Proceedings Content as of 3/28/2014.

O-195 9:15AM - 9:21AM
Blood Pool Contrast Agent High-resolution MR
Angiography in Glioblastoma: Tumor Vasculature as a
Biomarker for Survival

J Puig¹, G Blasco¹, J Daunis-i-Estadella², S Remollo³, D Hernandez⁴, M Essig⁵, R Jain⁶, J Sanchez-Gonzalez⁷, S Pedraza¹

¹Girona Biomedical Research Institute (IDIBGI), Hospital Dr Josep Trueta, Girona, Spain, ²University of Girona, Girona, Spain, ³Hospital Dr Josep Trueta, Girona, Spain, ⁴Hospital Vall Hebron, Barcelona, Spain, ⁵University of Manitoba, Winnipeg, Manitoba, Canada, ⁶New York University Langone Medical Center, New York, NY, ⁷Philips Healthcare Ibérica, Madrid, Spain

Purpose

Vascularity, defined histologically or with molecular techniques, correlates with poor survival in patients with glioblastoma. Regionally heterogeneous vascularization limits histologic markers, which are measured only in some tissue sections. More accurate assessment of valid vascular biomarkers such as digital subtraction angiography or dynamic susceptibility contrast (DSC) perfusion MRI represents a challenge; thus far, MR angiography has been unable to characterize glioblastoma vascularity. Gadofosveset is an albumin-binding contrast agent approved for imaging blood vessels. It remains largely intravascular because it forms reversible noncovalent bonds with albumin, resulting in a 4- to 5-fold increase in blood relaxivity at 1.5 T compared to extracellular contrast agents. We aimed to (a) assess the vascularity of newly diagnosed glioblastomas using gadofosveset high-resolution MR angiography, (b) correlate the findings with dynamic DSC and diffusion MR imaging (MRI) parameters for contrast-enhancing lesion (CEL) and surrounding non-CEL, and (c) determine whether high resolution MR angiography of tumor is useful in predicting survival.

Materials and Methods

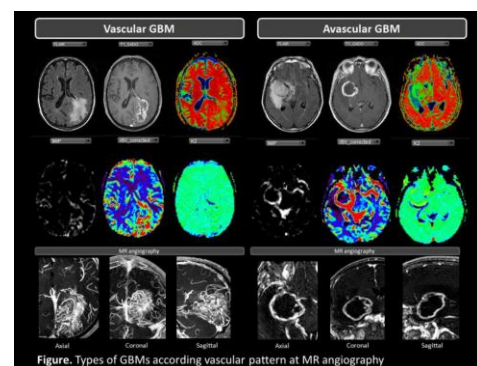
Before treatment, 33 patients (23 men; mean age, 63 years) with histologically proven glioblastoma underwent MRI including anatomical sequences, first-pass DSC images and postcontrast T1-weighted SE images after gadobutrol (Gadovist; Bayer Schering Pharma, Berlin, Germany) at 0.1 mmol/kg and, 48 hours later, high-resolution MR angiography acquired after gadofosveset (Ablavar, Lantheus Medical Imaging, North Billerica, USA) at 0.03 mmol/kg with a 0.6 mm isometric voxel. Two independent observers evaluated presence of vessels on high resolution MR angiography. Volumes of interest for CEL, NCEL, and contralateral tissue were obtained for cerebral blood volume ratio (rCBV), cerebral blood flow ratio (rCBF), permeability constant (k₂), mean temporal maximal intensity projection (tMIP), and apparent diffusion coefficient (ADC) using Olea Sphere V.2.0 software (Olea Medical, La Ciotat, France). Statistical analyses included Pearson correlation, linear regression analysis, and interclass correlation coefficients. Prognostic factors were

evaluated by Kaplan-Meier survival and Cox proportional hazards analysis.

Results

Eighteen (52.94%) glioblastomas were vascular and 16 (40.5%) avascular on high resolution MR angiography (Figure); interobserver reliability was good (K=0.745). In vascular glioblastomas, mean tMIP values were higher (p=0.024) and there was a trend to lower mean ADC values (p=0.068) (Table). Median survival for avascular and vascular glioblastomas treated with surgery and with radiotherapy plus chemotherapy was 15 months (95% CI, 4.5-30.2) and 8.5 months (95% CI, 2.9-14.1), respectively. When treatment was incomplete, median survival for avascular and vascular glioblastomas was 6.5 months (95% CI, 3.1-9.8) and 3.5 months (95% CI, 2.1-4.9), respectively. Vascular pattern was the best survival predictor for glioblastoma at 5.25 months (AUC 0.794, 81.2% sensitivity, 77.8% specificity, 76.5% positive predictive value, 82.4% negative predictive value). Vascular pattern yielded the highest hazard ratio (14.012; 95% CI: 2.436,80.579; P=0.003).

	Contralateral gray matter			Non contrast-enhancing lesion			Contrast-enhancing lesion		
	Avascular	Vascular	p-value	Avascular	Vascular	p-value	Avascular	Vascular	p-value
rCBF	18.3 (5.66)	16.58 (6.48)	0.429	20.81 (8.67)	18.34 (10.29)	0.432	44.65 (21.79)	55.53 (23.78)	0.193
rCBV	1.68 (0.63)	1.46 (0.7)	0.343	1.93 (0.71)	1.61 (0.99)	0.305	3.92 (1.82)	4.54 (2.25)	0.408
rCBVc	1.25 (0.49)	1.03 (0.52)	0.219	1.41 (0.5)	1.17 (0.8)	0.324	3.15 (1.92)	3.51 (1.55)	0.512
MTT	5.74 (1.31)	5.29 (1.07)	0.385	5.73 (1.59)	5.24 (2.02)	0.451	5.1 (1.19)	4.91 (1.3)	0.685
Tmax	3.06 (0.61)	3.11 (0.59)	0.81	5.32 (2.61)	6.91 (3.86)	0.184	5.59 (3.76)	5.21 (3.66)	0.775
TTP	38.12 (18.47)	42.47 (17.71)	0.495	38.09 (18.05)	41.85 (16.64)	0.539	39.81 (18.29)	41.8 (17.48)	0.756
k ₂	-46.75 (33.34)	-41.31 (18.08)	0.555	-48.32 (60.66)	-27.48 (38.07)	0.23	-62.96 (117.32)	-69.31 (87.32)	0.862
Cmax	0.12 (0.04)	0.12 (0.03)	0.676	0.13 (0.06)	0.13 (0.04)	0.948	0.29 (0.11)	0.41 (0.16)	0.024
ADC	79.6 (4.17)	82.05 (3.89)	0.091	130.18 (16.77)	134.59 (14.1)	0.417	120.86 (20)	109.73 (13.16)	0.068



Conclusions

High resolution MR angiography using gadofosveset can detect vascularity in glioblastoma. Vascularity is a useful imaging biomarker that correlates with worse survival in newly diagnosed glioblastoma.

KEYWORDS: Glioblastoma, MR Imaging/MR Angiography, Outcome

Note: Scanned images are included in the proceedings. Some submitted images were reduced during editing thereby decreasing clarity. Also, refer to the Program Planner. Proceedings Content as of 3/28/2014.

O-196 9:21AM - 9:27AM
Non-invasive Assessment of Intratumoral Vasculature Using Arterial Spin Labeling: a Comparison to Susceptibility-weighted Imaging for the Differentiation of Primary Cerebral Lymphoma and Glioblastoma

J Furtner, V Schoepf, M Preusser, U Asenbaum, R Woitek, A Woehrer, J Hainfellner, S Wolfsberger, D Prayer
Medical University of Vienna, Vienna, Austria

Purpose

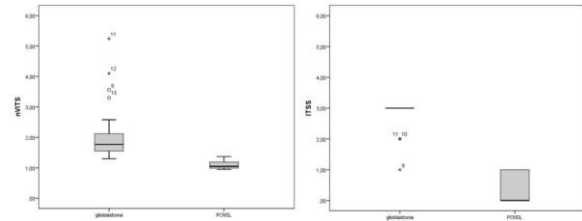
Using conventional MR imaging (MRI) methods, the differentiation of primary cerebral lymphomas (PCNSL) and other primary brain tumors, such as glioblastomas, is difficult due to overlapping imaging characteristics. The purpose of this study was to determine the utility of normalized vascular intratumoral signal intensity values (nVITS) obtained from pulsed arterial spin labeling (PASL) to differentiate between PCNSL and glioblastomas in a routine clinical setting, and to compare the diagnostic accuracy of this new method with the accuracy of intratumoral susceptibility signals (ITSS) values obtained from susceptibility-weighted imaging (SWI). This could ultimately result in a totally noninvasive method to differentiate lymphoma and glioblastoma.

Materials and Methods

Using conventional MRI methods, the differentiation of PCNSL and other primary brain tumors, such as glioblastomas, is difficult due to overlapping imaging characteristics. This study was designed to discriminate tumor entities using nVITS obtained from PASL, combined with ITSS from SWI. Thirty consecutive patients with glioblastoma (n=22) and PCNSL (n=8), histologically classified according to the WHO brain tumor classification, were included. MR images were acquired on a 3 T scanner, and included PASL and SWI sequences. nVITS was defined by the signal intensity ratio between the tumor and the contralateral normal brain tissue, as obtained by PASL images. Intratumoral susceptibility signal was determined as intratumoral low signal intensity structures detected on SWI sequences and were divided into four different grades. Potential differences in the nVITS and ITSS between glioblastomas and PCNSLs were revealed using statistical testing. To determine sensitivity, specificity, and diagnostic accuracy, as well as an optimum cut-off value for the differentiation of PCNSL and glioblastoma, a receiver operating characteristic analysis was used.

Results

We found that nVITS (p=0.011) and ITSS (p=0.001) values were significantly higher in glioblastoma than in PCNSL. The mean of the ITSS value was 0.43 for lymphoma and 2.77 for glioblastoma. For nVITS values, the mean was 1.10 for lymphoma and 2.16 for glioblastoma. For illustration, also see the box-and-whisker plots in Figure 1. The optimal cut-off value for nVITS was 1.41 and 1.5 for ITSS, with a sensitivity of 100%, a specificity of 95.5%, and an accuracy of 95.5%. Intratumoral susceptibility signals were detected in all glioblastomas (100%) and in three of seven lymphomas (0.43%). One T-cell PCNSL was excluded due to extensive intralesional macrohemorrhage.



Conclusions

nVITS and ITSS values, obtained from PASL and SWI sequences, provide truly noninvasive approaches to the differentiation of glioblastomas and lymphomas on the basis of tumor vascularization. The cut-off values determined in this study could serve as an objective support for decision-making in the routine clinical diagnostic protocol to distinguish these two tumor entities. These methods offer beneficial, fast, and easily applicable tools for integration into routine MRI diagnostics, which would result in a potentially high clinical impact for the treatment and management of patients with these tumors.

KEYWORDS: Arterial Spin-Labeling, Primary CNS Neoplasms, Susceptibility-Weighted Imaging

O-197 9:27AM - 9:33AM
Evaluation of a Novel Pulsed Arterial Spin Labeling Protocol in Pediatric Brain Tumors: a Feasibility Study in Comparison with Dynamic Susceptibility Contrast Perfusion

C Ho¹, S Kralik¹, J Smith², J Boaz², L Ackerman², D Fulkerson², Y Wang¹

¹Indiana University School of Medicine, Indianapolis, IN,
²Goodman Campbell Brain and Spine, Indianapolis, IN

Purpose

To compare a novel pulsed arterial spin labeling (PASL) method to dynamic susceptibility contrast (DSC) perfusion in the clinical setting of pediatric central nervous system (CNS) tumors. The experimental PASL protocol uses multiple inversion times (TI) to minimize bias in rCBF estimates due to regional differences in arterial arrival time, in addition to improving the signal to noise ratio by combining two consecutive PASL scans in ascending and descending slice order for the same TI.

Materials and Methods

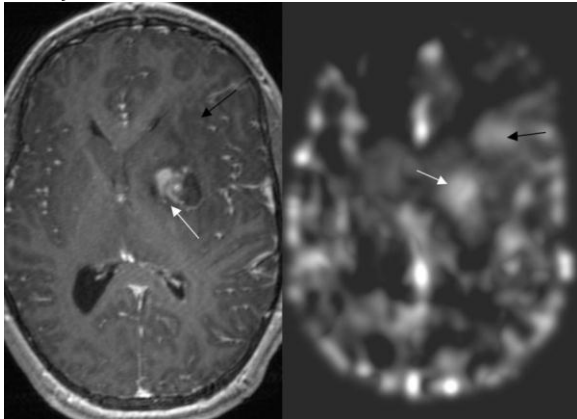
IRB approval was obtained for this study. Nine children with primary CNS tumors were imaged with our PASL technique followed by DSC perfusion. Tumor diagnosis and tumor grade were recorded by available pathologic data or consensus from expertise and follow-up imaging. For each case, CBF maps were generated from the PASL scan, as well as CBF and CBV maps from DSC. Regions of interest (ROIs) were placed in the tumor areas with highest perfusion on the CBF maps and compared to normal contralateral gray matter (GM) with both types of perfusion techniques. For DSC, the highest ROI values in the tumor also were compared to normal contralateral white matter (WM) for both CBV and CBF maps. Spearman's rho was calculated for the resulting ratios compared to the tumor grade. Multiple

Note: Scanned images are included in the proceedings. Some submitted images were reduced during editing thereby decreasing clarity. Also, refer to the Program Planner. Proceedings Content as of 3/28/2014.

regression analysis was performed for all ratios and tumor grade.

Results

To date, six low grade tumors and three high grade neoplasms were studied. All cases were pathologically confirmed, except two presumed low grade tumors from multidisciplinary consensus, lack of symptomatic change, imaging characteristics, and stability. The PASL protocol averaged 11 minutes for acquisition. Positive Spearman's rho was found for all ratios compared to tumor grade. Significant positive correlation was noted between rCBV-DSC and tumor grade (0.67, p=0.04), rCBF-DSC and tumor grade (0.74, p=0.02) and rrCBF-PASL and tumor grade (0.72, p=0.05). Multiple regression analysis demonstrates positive correlation between all ratios and tumor grade with the strongest correlation between rCBV(WM) and rCBF(WM) for DSC (0.89, 0.55-0.98), rCBF(WM) and rCBF(GM) for DSC (0.88, 0.52-0.97), and rCBF-DSC(GM) and rrCBF-PASL(GM) (0.86, 0.46-0.97). Figures: Sixteen-year-old male with pathology proven primitive neuroectodermal tumor. Axial postcontrast 3D T1-weighted image shows an enhancing mass in the left lentiform nucleus with corresponding increased perfusion on rCBF-PASL map (white arrows). An area which does not show enhancement in the anterior insular cortex also shows increased rCBF indicating tumor involvement (black arrows).



Conclusions

A novel PASL protocol with multiple-TI was introduced at clinically acceptable scan durations and demonstrates good correlation with DSC and tumor grade in pediatric brain tumors. This allows perfusion data with less bias from differences in arterial arrival time to be obtained without the use of gadolinium-based contrast in children.

KEYWORDS: ASL, Dynamic Susceptibility Contrast-Enhanced, Pediatric Brain Tumors

O-199

9:45AM - 9:51AM

PH-Weighted Molecular MRI in Human Glioblastoma using Chemical Exchange Saturation Transfer (CEST) Imaging of Glutamine at 3T

B Ellingson¹, R Harris¹, Q Liu², D Li², W Pope¹, T Cloughesy¹

¹University of California Los Angeles, Los Angeles, CA,

²Cedars-Sinai Medical Center, Los Angeles, CA

Purpose

A decrease in pH within the tumor microenvironment has been shown to result in malignant transformation, resistance to radiation therapy, resistance to specific chemotherapies, increased probability of metastasis, immunosuppression, increased tumor invasion, increased rate of mutations, increased chromosomal rearrangements, altered gene expression, and angiogenesis. Thus, a noninvasive imaging method for evaluating tumor tissue pH would be valuable for early detection of treatment response, tumor progression, and/or treatment failure in malignant gliomas. In the current study we used chemical exchange saturation transfer (CEST) imaging, a new MR imaging (MRI) technique, to identify tumor tissue with low pH (acidic tissue) by targeting MR excitation of amine protons on glutamine, one of the major sources of fuel for tumor cells.

Materials and Methods

All experiments were performed on a 3 T Siemens Trio (Siemens Healthcare, Erlangen, Germany). We performed extensive experiments involving glutamine in solution at various concentrations and pH in order to establish the relationship between extracellular glutamine and pH. We performed serial CEST imaging at 3 T in 10 patients with glioblastoma before, during, and after radiation therapy and concurrent temozolomide. Additionally, we performed CEST imaging in select patients with suspected tumor recurrence and patients treated with bevacizumab, an anti-angiogenic agent. Chemical exchange saturation transfer imaging was performed by selecting 51 offset frequencies ranging from -5 ppm to 5 ppm with respect to water resonance, using a saturation power of $B_1 = 2 \mu\text{T}$ and a series of 100 ms Gaussian pulses at 50% duty cycle. B0 homogeneity correction was performed. Chemical exchange saturation transfer asymmetry was calculated at 2.8 ppm, corresponding to glutamine proton resonance, by $[\text{Asym} = (+2.8\text{ppm} - -2.8\text{ppm})] + 2.8 \text{ ppm} \times 100\%$.

Results

Results suggest that a positive asymmetry exists for acidic pH environments when targeting glutamine. This asymmetry increased with increasing concentration of glutamine. Serial pH-weighted imaging during radiation therapy showed increasing volume of tissue with low pH in areas of the tumor not responding to therapy as indicated by growing tumor on subsequent follow-up scans. Patients with new regions of contrast enhancement after radiotherapy and no corresponding change in pH-weighted imaging were shown to have characteristics of pseudoprogression. Areas of necrosis also showed low pH, consistent with known biology. At tumor recurrence, the volume of tissue with low pH corresponded to areas of

Note: Scanned images are included in the proceedings. Some submitted images were reduced during editing thereby decreasing clarity. Also, refer to the Program Planner. Proceedings Content as of 3/28/2014.

contrast enhancement along with areas surrounding the tumor. Patients with prolonged bevacizumab therapy showed areas of low pH within atypical necrotic regions, consistent with previous reports.

Conclusions

Chemical exchange saturation transfer imaging targeting glutamine proton exchange is a novel approach to visualizing and quantifying tumor tissue with low pH. This information may be valuable for early identification of treatment failure and differentiating tumor recurrence from pseudoprogression.

KEYWORDS: Glioblastoma, Magnetization Transfer Imaging, Molecular Imaging

O-200 9:51AM - 9:57AM
Variable density interleaved spiral MRI for amide proton transfer imaging on U87 glioblastoma xenograft model at clinical 3T scanner

J Kim¹, P Sun²

¹University of Iowa, Iowa City, IA, ²Massachusetts General Hospital/Harvard Medical School, Boston, MA

Purpose

Amide proton transfer (APT) imaging has demonstrated promising potentials in brain tumor activity measure which may be useful as a biomarker for evaluating therapeutic response to glioblastoma (GBM). Preclinical imaging on GBM xenograft models is crucial to test validity and reliability of this new technique. However lack of easy access to small animal MRI facility have been hampering clinical translation of APT imaging. Variable density (VD) spiral sequence has many desirable properties that come from its concentric circular geometry allowing oversampling near the origin of k-space and reduced hardware demand on gradient switching. In this work, we developed a new APT imaging sequence with VD interleaved spiral readout and applied this method on orthotopic GBM xenograft models in immune-deficient rats to test feasibility of preclinical APT imaging at clinical 3 T scanner.

Materials and Methods

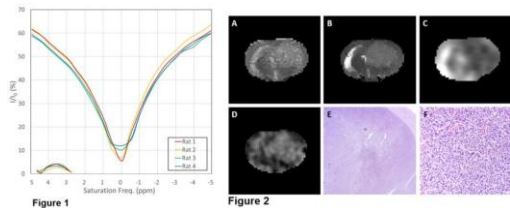
Four male athymic nude rats 7-8 weeks of age were implanted with U87 MG cells in the right frontal caudate region stereotaxically, and imaged at 20-25 days after tumor implantation on a 3 T clinical MR imaging (MRI) scanner equipped with a quadrature transmit/receive RF coil. Local shimming was followed by acquisition of multi-shot VD spiral-out APT-weighted images with 31 pulsed saturation RF irradiation ($B_1=1.5 \mu\text{T}$) and 21 frequency-labeling offsets from -5 ppm to 5 ppm with respect to water (TR/TE=1600/1.7 msec, spiral interleaves=20, slice thickness=3 mm, FoV=40 mm, matrix=96x96, average=2, acquisition time=14:25 min). B_0 inhomogeneity was corrected with Z-spectrum fitting on double-echo gradient field maps. The APT effect was calculated based on the MT-ratio asymmetry. Additionally T1 mapping with variable flip angle FLASH, T2 mapping with multi-echo turbo SE, and ADC mapping on RESOLVE DWI with a three-point

multi-exponential fitting ($b=0, 1000$ and 2800 s/mm^2) were performed.

Results

All U87 GBM xenograft demonstrated enhanced APT effect compared to the normal brain. Figure 1 shows the Z-spectra and APTR plots from each GBM xenograft model. Amide proton transfer ratio measured from the tumors were ranged from 3.40 to 5.28% (4.2 ± 0.83 ; mean \pm S.D.) higher than those from the normal side of the brain (Table 1). Figure 2 shows example images of T1 map (A), T2 map (B), ADC map (C), APTR map (D), and histopathologic correlation of a U87 GBM xenograft (E,F).

GBM bearing rats	APTR (%)	T1 (ms)	T2 (ms)	ADC ($\times 10^3 \text{ mm}^2/\text{s}$)
1	5.28	1479.1	157.41	0.60
2	3.71	1545.2	172.89	0.46
3	4.38	1407.4	151.06	0.54
4	3.40	1262.9	196.12	0.51



Conclusions

Efficient use of gradient hardware in VD spiral sequence allowed small field-of-view acquisition while maintaining reasonable signal-to-noise ratio for small animal brain scan at clinical 3 T scanner. This method also can significantly reduce scanning time and still maintain spatial resolution which are desirable attributes for practical translation of APT-weighted imaging. In this small study, we observed a trend of APT effect measures positively correlate with degree of pseudopalisading necrosis within the GBM on microscopy, which needs to be further investigated in a larger scale study.

KEYWORDS: Animal Model, Glioblastoma

Tuesday, May 20
8:30 AM – 10:00 AM
Room 517a

31 - ASPNR Programming: Vascular Anomalies

O-201 8:30AM - 9:00AM
Vascular Malformations in Neonates
Rossi, A.
G. Gaslini Children's Hospital
Genova

Note: Scanned images are included in the proceedings. Some submitted images were reduced during editing thereby decreasing clarity. Also, refer to the Program Planner. Proceedings Content as of 3/28/2014.

Abstract/Presentation Summary

Vascular malformations in neonates comprise arteriovenous malformations (AVM), mainly represented by the vein of Galen aneurysmal malformation (VGAM), and dural sinus malformations (DSM). Other vascular malformations that are proper of older age groups, such as pial AVMs and cavernomas/developmental venous anomalies (AVMs) are more seldom encountered in the neonate. Frequently, the diagnosis of these disorders is already made prenatally thanks to a combined use of ultrasound and MRI. A challenge of fetal MRI is represented by the absence of reliable MR angiography techniques; thus, appraisal of the vascular nature of the lesion must be made by a combination of "conventional" T1 and T2-weighted sequences, complemented by Doppler ultrasound. VGAM accounts for 30% of vascular malformations in the pediatric age group, and is the most common in neonates. It results from abnormal connections established between choroidal arteries and the median prosencephalic vein at 6-11 weeks gestation, which prevent the physiologic regression of this vein. MRI allows for classification between choroidal (>4 afferents) and mural (<4 afferents) types, and is crucial for assessing parenchymal trophism and presence of negative prognostic factors such as encephalomalacia, calcifications, and hydrocephalus. DSM is a giant venous lake, usually but not necessarily involving the torcular. It may be fed by AV fistulas, and intraluminal thrombosis is part of its natural history. Although it accounts for fewer than 2% of vascular malformations in the pediatric age group, it is the second most common in neonates. Outcome is satisfactory in the majority of cases, but the role of endovascular treatment remains controversial. Lateral DSM (ie, involving only one transverse-sigmoid sinus) has a better prognosis than median DSM (involving the torcular). "Anterior" DSM (involving the inferior sagittal sinus) is an uncommon entity which we have seen in association with large DVAs.

O-202 9:00AM - 9:30AM
Pediatric Aneurysms

Vossough, A.
University of Pennsylvania
Philadelphia, PA

Abstract/Presentation Summary

Pediatric intracranial arterial aneurysms are uncommon compared to adults and despite many similarities, there are distinct differences between pediatric and adult aneurysms. The epidemiology of pediatric intracranial aneurysms will be first presented and how it can differ from adult aneurysm statistics. The features of pediatric intracranial aneurysms and classifications into traumatic, dissecting, saccular, vasculopathic, and infectious types of aneurysms will be discussed. The pathophysiologic mechanisms of aneurysms will be briefly reviewed in the context of the various types. A number of underlying disorders have an increased incidence of cerebral aneurysms in the child. The associated comorbidities and the various congenital cerebral aneurysmal vasculopathies

will be briefly examined in the context of pediatric cerebral aneurysms. The incidence of subarachnoid hemorrhage and subsequent intracranial vasospasm is also different in children and will be discussed. Basic treatment strategies will be briefly reviewed. Finally, prognosis and outcome of treatment of pediatric aneurysms will also be discussed.

O-203 9:30AM - 10:00AM
Endovascular Treatment

Rodesch, G.
Hopital Foch
Suresnes

Abstract/Presentation Summary

AVMs in neonates (from birth to 1 month of age) represent challenging lesions far beyond pure technique, and their treatment cannot be indeed summarized to a miniaturized endovascular therapy. Two main types of lesions share this age group: Vein of Galen Arterio-venous Malformations (VGAMs) and Dural Sinus Malformations (DSMs). They can both be considered as "true" congenital embryologic malformations. High Flow arterio-venous fistulas (AVFs) and malformations (AVMs) are rarely seen in neonates, pointing to the fact that this type of shunts is created later in life, most often after infancy. Symptoms of VGAMs and DSMs in neonates differ from the usual ones associated to "adult type" malformations. VGAMs often present in neonates with systemic disorders that can even have begun in utero. Application of specific clinical scores allows to recognize which patients will benefit from embolization and at what moment this treatment should be applied (delayed until 5-6 months of age under close radio-clinical follow up, or in emergency). Endovascular occlusion with acrylic glue has proven to be the most efficient therapy in these diseases. DSMs may also present at that age with hemodynamic symptoms. The challenge in these latter malformations is however different because of the associated immaturity of the venous system and the risk of spontaneous thrombosis. Midline locations have usually poor prognosis as compared to lateral ones. Cavernous sinus capture and maturation of the sigmoido-jugular junction will dictate clinical outcomes. Precise recognition of the type of the disease, of its patho-physiology and consequences on the brain (melting brain or focal atrophies...) or other body organs, as proper evaluation of the optimal therapeutic window to treat the patients represent the most important steps to follow to obtain satisfactory results. The main primary goals to reach in this age group are obviously not obligatorily the cure of the malformation, but are represented by the relief of the symptoms presented by the baby and the maturation of the brain, allowing normal neurologic and neurocognitive development.

Note: Scanned images are included in the proceedings. Some submitted images were reduced during editing thereby decreasing clarity. Also, refer to the Program Planner. Proceedings Content as of 3/28/2014.

Tuesday, May 20
8:30 AM – 10:00 AM
Room 520

32 - International Session: ESNR:
European Teaching Carousel

O-204 8:30AM - 8:50AM
Neuroradiological Assessment of Traumatic Brain Injury: A
Pattern-Based Approach

Parizel, P.
Antwerp University Hospital/University of Antwerp

Abstract/Presentation Summary
CT and MRI examinations constitute an essential part of the diagnostic work-up of patients admitted with (acute) traumatic brain injury. Imaging studies often direct patient management and greatly influence the clinical course, especially the acute setting. CT remains the preferred technique to determine the presence and extent of injuries (such as fractures, intra- and extra-axial hemorrhage, mass effect, etc.). CT findings are crucial in planning and guiding neurosurgical intervention. Multi-detector CT scanning allows simultaneous assessment of head and cervical spine, thereby obviating the need for plain X-rays. MRI of the brain plays an increasingly important role in the assessment of craniocerebral trauma, especially in those individuals in whom there is a discrepancy between the patient's clinical status and the CT findings. In these cases, MRI may reveal evidence of parenchymal damage (e.g. diffuse axonal injury) or hemorrhage, not seen on CT. During this presentation, we shall propose a pattern-based approach, in order to obtain a quick and complete inventory of the traumatic brain lesions. It is important to distinguish primary and secondary lesions. Primary injuries occur as a direct result of the impact with damage to brain tissue. Examples include fractures, different types of traumatic haemorrhage (epidural, subdural, intracerebral, subarachnoid), cerebral contusion, diffuse axonal injury (DAI). CT- and/or MR-angiography are useful techniques to document traumatic blood vessel injury. Secondary injuries are caused by systemic factors such as increased intracranial pressure, edema, brain herniation, decreased cerebral blood flow, excitotoxic damage. Increasingly, there is an important role for MRI of the brain in patients admitted with traumatic brain injury. In the head-injured patient, a multiparametric MRI examination should include diffusion, perfusion, and susceptibility-weighted imaging. Diffusion tensor imaging with fractional anisotropy mapping may show microstructural abnormalities in patients with mild TBI, even when traditional MRI sequences appear normal. Neuroimaging also plays a role in the chronic stage, identifying sequelae, determining prognosis, and guiding rehabilitation. In

conclusion, recent technological advances in CT and MRI have greatly improved our understanding of the pathophysiology of craniocerebral trauma and allow us to detect abnormalities, even in patients with mild head trauma, when routine imaging studies appear normal.

O-205 8:50AM - 9:10AM
Infections

Tali, E.
Gazi University School of Medicine
Besevler, Ankara

Abstract/Presentation Summary
Infections of the CNS frequently present diagnostic and therapeutic challenges. Central nervous system infections are not frequent, accounting for 1% of primary hospital admissions and 2% of nosocomially acquired infections, 2-7% of osteomyelitis. When encountered, prompt diagnosis and initiation of specific treatment often are necessary to allow the best chance of recovery without sequelae. The prognosis depends on rapid identification of the site of the inflammation and pathogen. Most CNS infections can be treated successfully as long as they are detected early. Delayed diagnosis remains a major cause of disability. It is particularly unfortunate if a rapidly progressive but treatable disease remains undetected until irreversible damage is caused. Even at present, many cases reaching a neurosurgical centre could have been detected and referred early if the imaging had been correctly interpreted in the clinical setting. Radiological evaluation plays an important role in the diagnosis, subsequent treatment and treatment monitoring. Improvements in diagnostic imaging, in particular computed tomography (CT) and magnetic resonance imaging (MRI) have greatly facilitated the diagnosis and treatment planning, treatment and treatment monitoring of intracranial and spinal infections.

O-206 9:10AM - 9:30AM
Demyelination

Thurnher, M.
Medical University Of Vienna
Vienna

Abstract/Presentation Summary
Evaluation of MR imaging in a patient with an intramedullary lesion should focus on key-features: a) the location of the lesion on the cross sectional area of the cord, best evaluated on axial images, b) the length of the lesion evaluated on sagittal images, c) the presence of cavitation and cysts, d) signal intensity on T2-WI, e) the presence of enhancement and enhancement type, and f) associated leptomeningeal enhancement. The knowledge of the presence or absence of the brain lesions is important information for narrowing the differential diagnosis. Finally, clinical information, demographics, and immune status should be incorporated. In this lecture imaging characteristics and typical patterns of intramedullary lesions will be presented. A diagnostic

Note: Scanned images are included in the proceedings. Some submitted images were reduced during editing thereby decreasing clarity. Also, refer to the Program Planner. Proceedings Content as of 3/28/2014.

algorithm, which includes imaging, clinics and CSF analysis, will be discussed.

O-207 9:30AM - 9:50AM
Tumors

Rossi, A.
G. Gaslini Children's Hospital
Genova

Abstract/Presentation Summary

Brain tumors are the most common solid pediatric tumors and are the leading cause of death in children from solid tumors. The estimated incidence of all childhood primary brain and central nervous system tumors is 4.8 cases per 100,000 person-years. In neonates and infants up to the age of 3 years, supratentorial tumors are more common, whereas infratentorial tumors predominate until adolescence. The wide availability of CT for diagnosing patients presenting acutely, particularly in the emergency room setting, has produced several advantages including its ability to detect a sizable mass lesion, identify mass effect, and check for ventricular enlargement, lesional hemorrhage, calcification, and osseous involvement. Owing to its superior soft tissue resolution, multi-planar capability, and lack of ionizing radiation, MRI with contrast is the modality of choice for determining lesion size, location and characterization. Conventional sequences for MR evaluation include T1, T2, FLAIR and post gadolinium (multiplanar T1) images. While contrast enhancement typically reflects disruption of the blood-brain barrier; the degree of contrast enhancement does not always correlate with tumor grade. For example, benign tumors (e.g., choroid plexus papillomas and pilocytic astrocytomas) can enhance avidly, whereas anaplastic astrocytomas or primitive neuroectodermal tumors may not enhance at all. MRI is also used to assess tumor response and progression and monitor treatment effects. Craniospinal MR with gadolinium is useful in evaluating the degree to which tumor may have disseminated in the CSF pathways. Advanced MR imaging modalities, such as diffusion-weighted imaging (DWI), diffusion tensor imaging (DTI), perfusion-weighted imaging (PWI), magnetic resonance spectroscopy (MRS), and functional MRI have significantly improved our understanding of the physiopathology of brain tumours and have provided invaluable additional information for treatment planning and monitoring of treatment results.

9:50AM - 10:00AM
Questions

Tuesday, May 20
8:30 AM – 10:00 AM
Room 524

**33 - Socioeconomic Programming:
Current Payment Policy**

O-208 8:30AM - 8:50AM
CPT Update

Tu, R.
Progressive Radiology
Washington, DC

Abstract/Presentation Summary

CPT has identified procedures which occur together with request for bundling. ASNR was the lead society in the code change proposal for myelography as the injection procedure and imaging guidance codes for myelography were identified as codes reported together 75% or more of the time. The Relativity Assessment Workgroup requested that a bundled coding solution be perused for this family of codes. ASNR as lead with ACR, ARRS, and RSNA submitted 4 code change proposals bundling injection and image guidance for myelography procedures. The current injection and radiologic supervision and interpretation codes for myelography were retained as myelography is occasionally performed by 2 physicians, one performing the contrast media injection and the second providing radiology radiological supervision and interpretation. The code change was accepted by CPT and reviewed by National Correct Coding Initiative. SIR was the lead presenter for Percutaneous Vertebroplasty and Augmentation and ASNR with ACR, ARRS, RSNA, AANS, AAOS, ASNR, and SNS as cosponsors for code change proposal describing vertebral augmentation including imaging which was approved.

O-209 8:50AM - 9:10AM
RUC Update

Nicola, G.
Hackensack University Medical Center
Hackensack, NJ

Abstract/Presentation Summary

Update talk will focus on the fundamental role the "Relative Value Scale Update Committee" (RUC) plays in the current fee for service physician Medicare payment system, and, how does the American Society of Neuroradiology (ASNR) participate in the process. Key topics will include detailing the composition of the RUC, meeting schedule, and its influences on Medicare payment policy. The concept of "relative value units" (RVU) for professional and technical component payments will be

Note: Scanned images are included in the proceedings. Some submitted images were reduced during editing thereby decreasing clarity. Also, refer to the Program Planner. Proceedings Content as of 3/28/2014.

introduced. An expanded look will be made into the RUC survey process, data collection, data analysis, and data presentation used to determine relative value units. Recent results of the ASNR/RUC interaction will be critiqued. Trends in health care economics and statutory requirements changing the way the RUC operates, and potential impacts on radiology will be reviewed. Examples of how the general membership may take part in supporting the ASNR in its dealing with RUC are explored.

O-300 9:10AM - 9:30AM
CMS Update

Silva, E.
South Texas Radiology Group
San Antonio, TX

Abstract/Presentation Summary

This presentation will build upon the earlier discussions of actions taking place at the CPT Editorial Panel and the RVS Update Committee, the RUC. The CMS update will highlight the broader regulatory climate at the Centers for Medicare and Medicaid Services (CMS). Focus will be paid upon policies which impact radiology including changes to the Medicare Physician Fee Schedule, the Hospital Outpatient Prospective Payment System and the Inpatient Prospective Payment System. A discussion of the various pay for performance initiatives impacting radiology payment will occur with focus paid upon two major changes to the PQRS program this year: (1) the emergence of a radiology specific quality measures group, Optimizing Patient Exposure to Ionizing Radiation (OPEIR) and (2) the emergence of Qualified Clinical Data Registries as a means to report. Comments will be made regarding challenges faced by CMS in implementing the Patient Protection and Affordable Care Act, including the impact of the health insurance exchanges on local insurance networks.

O-301 9:10AM - 9:50AM
Guidelines Update

Bello, J.
Montefiore Medical Center
Bronx, NY

Abstract/Presentation Summary

This presentation will outline the ACR Collaborative Guidelines Process, including the Neuroradiology Guidelines Committee structure and function. The current status of the Guidelines Committee activity, including recently reviewed guidelines, those currently in the pipeline, and those up for review in the upcoming cycle will be summarized. In addition, the debate over harmonizing guideline prescriptive elements with ACR Accreditation requirements will be presented. Ongoing discussions of an accelerated course for guideline approval, as well as conforming pertinent guidelines to meet the IOM Guideline criteria will be addressed. Distinct features of the Technical Standards, Guidelines and Appropriateness Criteria will be

emphasized. Finally, the ASNR's role in extramural guideline endorsement will be reviewed.

9:50AM - 10:00AM

Discussion

Tuesday, May 20
10:30 AM – 12:00 PM
Room 517bc

34 - Parallel Papers: Interventional:
Aneurysms I

O-302 10:30AM - 10:37AM

The natural history and clinical outcome of unruptured fusiform intracranial aneurysms

R Sacho¹, A Kostynskyy¹, G Saliou¹, M Tymianski², T Krings¹, R Willinsky¹

¹Toronto Western Hospital, Toronto, Ontario, Canada,
²Toronto Western Hospital/University Health Network,
Toronto, Ontario, Canada

Purpose

The management of unruptured fusiform intracranial aneurysms is controversial, largely due to the paucity of data related to their natural history. Although more uncommon and etiologically different than their saccular counterparts, it is unclear whether approaches to management decisions should differ. Both surgical and endovascular therapy to repair or exclude fusiform aneurysms often are challenging and accompanied by a definite risk which must outweigh the natural history of the disease in order to be of benefit. We undertook a retrospective study of the natural history in this population to help guide management decisions in these patients.

Materials and Methods

We performed a retrospective analysis on all patients with unruptured fusiform intracranial aneurysms seen in our multidisciplinary neurovascular clinic between January 2000 and October 2013. Exclusion criteria were aneurysms that were giant (>2.5cm), entirely extradural or associated with intracranial atherosclerosis (presence of thick eccentric wall plaques in the presence of systemic risk factors). Natural history was assessed using change in MR spectroscopy (MRS) scale at last follow up and aneurysm growth measurements on serial imaging follow-up studies. Patients who underwent treatment of their aneurysm were analyzed separately for outcomes of treatment.

Results

We identified 108 aneurysms in 96 patients. Thirty-nine aneurysms (36%) were located in the posterior circulation. Aneurysm dimensions were mean diameter 7.49mm (2.4mm – 23mm) and mean length 12.80mm (2mm – 39.4mm). Fifteen patients (16%) were symptomatic at

Note: Scanned images are included in the proceedings. Some submitted images were reduced during editing thereby decreasing clarity. Also, refer to the Program Planner. Proceedings Content as of 3/28/2014.

presentation [8 stroke/TIAs, 5 with mass effect (two ophthalmoplegia) and two occipitocervical headache secondary to dissection]. Natural history follow-up data were available in 87 patients (91%) and imaging follow up in 82 patients/94 aneurysms (85%/87%). There were 193 person years clinical follow up (mean 27 months), and 477 aneurysm years of imaging follow up (mean 61 months). There was one aneurysm-related death from SAH during follow up (rupture rate 0.51% per year) but no other significant aneurysm-related change in the MRS scale for the remaining cohort. Eight patients (9%) showed evidence of aneurysm growth, with an overall risk of aneurysm progression of 1.6 % per year. Risk factors for growth were larger aneurysm diameter (13.5mm versus 6.9mm) ($p<0.01$) and symptomatic clinical presentation (63% versus 9%, $p<0.01$). Receiver operating characteristic (ROC) curve analysis (AUC 0.89, 95% CI: 0.79-0.99) showed aneurysms >6.7 mm were more likely to enlarge. Twenty-three patients (24%) underwent aneurysm treatment (15 surgical and 8 endovascular). Ten (43%) of these patients were symptomatic. Clinical follow up in treated patients was death in three patients (12.5%, two as a treatment complication and one from SAH) and moderate disability (MRS 3) in a further three patients (12.5%, all due to treatment-related events) at last follow up.

Conclusions

For patients harboring nonatherosclerotic fusiform intracranial aneurysms the overall risk of rupture is 0.51%/year. Aneurysms that are symptomatic on presentation or that are larger than 7mm in maximum diameter are more likely to enlarge and may warrant closer follow up or consideration of treatment. The high risks of treatment associated with these aneurysms should be taken into consideration when evaluating their natural history.

KEYWORDS: Aneurysm Rupture, Aneurysm Sizes, Aneurysm Treatment

O-303 10:37AM - 10:44AM
Unruptured intracranial aneurysms in children with sickle cell disease: analysis of 23 lesions in six patients

M Pearl¹, S Saini², B Speller-Brown², E Wyse³, E Meier², R Fasano²

¹The Johns Hopkins University School of Medicine, Baltimore, MD, ²Children's National Medical Center, Washington, DC, ³Johns Hopkins Hospital, Baltimore, MD

Purpose

Intracranial aneurysms (IA) are rare in the general pediatric population and account for less than 2% of all cerebral aneurysms. Children with sickle hemoglobinopathy and IA are even more rare as only nine patients (< 22 years) with sickle cell disease (SCD) and documented aneurysms have been reported to date. The purpose of this study was to determine the prevalence of unruptured IAs in children with SCD and to describe the

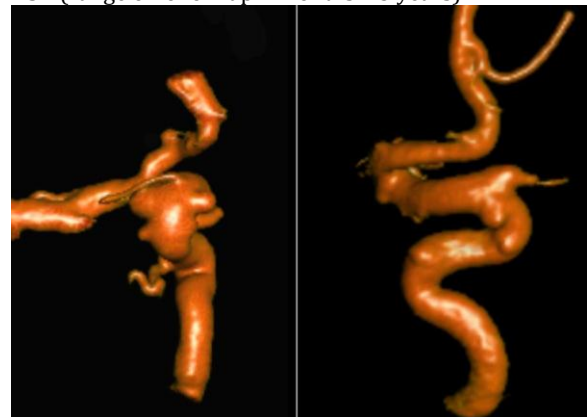
morphological characteristics, management, and long-term outcomes of this patient population.

Materials and Methods

This study was approved by our Institutional Review Board. A retrospective review of the electronic radiology database for all children with SCD (HbSS, HbSC, HbS β +, and HbS β 0) who underwent MR imaging (MRI)/MR angiography (MRA) of the brain from January 2002 to August 2013 was performed. Medical records were reviewed for age, gender, sickle cell genotype, neurologic symptoms, baseline hematological indices, transcranial Doppler findings, treatment approach, and long term neurological outcome.

Results

From January 2002 to August 2013, 192 children with SCD underwent MRI/MRA of the brain. Six patients (3 boys and 3 girls) were diagnosed with IA (3.1%), all confirmed by digital subtraction angiography (DSA). One patient presented with the acute onset of a third nerve palsy, whereas all other patients were asymptomatic. No instance of subarachnoid hemorrhage was noted. The mean age was 15 years (range 7-19 years) at the time of diagnosis. Five patients (83.3%) had homozygous HbSS disease, while one patient had HbSC disease. A total of 23 aneurysms were detected, of which 22 (95.6%) were in the anterior circulation. The average aneurysm size was 3 mm (range 1-5.6 mm). Five patients (83.3%) had multiple aneurysms, with bilateral distribution in four instances (67%). The maximum number of aneurysms detected in a single patient was eight. Two patients underwent uneventful surgical aneurysm clipping. The other four patients were managed conservatively with stability of their aneurysms documented by regularly scheduled MRI/MRAs and/or DSA (range of follow up 2 months – 3 years).



Conclusions

Children with SCD are at risk for developing multiple intracranial aneurysms and a high index of suspicion must be maintained when interpreting MRI/MRAs of the brain in this population. Unlike IA in the general pediatric population, we found no gender predilection, and the majority of lesions were small and involved in the anterior circulation.

KEYWORDS: Aneurysm, Sickle Cell Disease

Note: Scanned images are included in the proceedings. Some submitted images were reduced during editing thereby decreasing clarity. Also, refer to the Program Planner. Proceedings Content as of 3/28/2014.

O-304 10:44AM - 10:51AM
Influence of Iterative Reconstruction Algorithm (AIDR) on the Quantification of Cerebral Aneurysms

T Illies¹, A Kemmling², J Fiehler³

¹University Hospital Center Hamburg Eppendorf, Hamburg, Germany, ²University Medical Center Hamburg Eppendorf, Hamburg, Germany, ³Department of Interventional Radiology, Hamburg, Germany

Purpose

Four-dimensional computed tomography angiography (4DCTA) is currently the only technique allowing the investigation of aneurysm pulsation to achieve new pathophysiological insights and possibly enable more accurate prediction of aneurysm rupture risk. Its widespread use is limited by its radiation exposure, which might be improved by use of iterative reconstruction methods. We hypothesized that filtered backprojection (FBP) and AIDR reconstruction are equal regarding pulsatility analysis.

Materials and Methods

Four-dimensional computed tomography angiography of 10 patients with a cerebral aneurysm were reconstructed using FBP and Toshiba AIDR algorithm. Volume changes throughout the cardiac cycle were computed with an in-house developed software. Absolute volumes and pulsilities (maximum volume/ minimum volume) were compared between both groups.

Results

Absolute aneurysm volumes and pulsilities show very high correlations (0/93 and 0.95).

Conclusions

Absolute aneurysm volumes and pulsilities correlate highly when obtained from data reconstructed with IR and FBP. This work shows that FBP has the potential to reduce radiation dose substantially in 4DTCA, possibly facilitating the application of this technique for further investigation of aneurysm dynamics.

KEYWORDS: Aneurysm, Cerebellar

O-305 10:51AM - 10:58AM
High-Quality Low-dose C-arm CT imaging of flow diverting devices in the angiography suite

A Ahmed¹, Z Clark¹, B Patel¹, B Aagaard-Kienitz¹, D Niemann¹, K Royalty², S Schafer², C Strother¹

¹University of Wisconsin, Madison, WI, ²Siemens Medical Solutions, USA, Hoffman Estates, IL

Purpose

Flow diverting devices can be complex to deploy and difficult to see clearly with standard projection x-ray imaging. Careful assessment after deployment is required to ensure the device is well positioned and opposed to the vascular anatomy. Current state-of-the-art high-quality C-arm computed tomography (CT) acquisitions in the angiography suite can approach the dose of a CT scan, and provide high resolution details of the device. We

investigated a collimated volumetric acquisition approach aimed at significantly reducing radiation dose by limiting radiation exposure to a small field of view, while still supplying desired device visibility.

Materials and Methods

Thirty patients were imaged with a volume of interest (VOI) scan following aneurysm treatment via flow diverter placement or stent assisted coiling. The exposed area of the scan was collimated to 12% of the full acquisition field. For each scan, the radiation dose-area-product (DAP) was recorded. Retrospectively, thirty full field acquisitions were identified and the respective DAP was recorded. Blinded readers were presented with VOI 3D images and assessed device apposition, proximal and distal end visualization, relationship of device to coils, as well as possible twisting and stretching. Thermoluminescence dosimetry (TLD) was performed for full field and VOI acquisition using an anthropomorphic head phantom with 35 TLDs evenly distributed.

Results

Visualization of the device and wall apposition and device visualization were judged of good diagnostic quality for VOI imaging, as well as visualization of fine details such as device porosity and for assessment of device twisting and stretching (Figure 1a, b). Flow diverter and coil relationship assessment in VOI imaging varied with packing density due to metal artifacts, with higher density packing severely impacting image quality. Dose-area-product measurements showed a reduction of 85% compared to full field acquisitions. Thermoluminescence dosimetry evaluations showed dose reduction throughout the volume (Figure 1c, d).

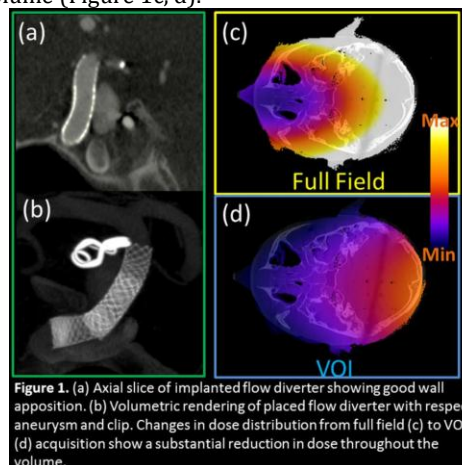


Figure 1. (a) Axial slice of implanted flow diverter showing good wall apposition. (b) Volumetric rendering of placed flow diverter with respect to aneurysm and clip. Changes in dose distribution from full field (c) to VOI (d) acquisition show a substantial reduction in dose throughout the volume.

Conclusions

Volume of interest imaging offers a significant reduction in radiation to the patient, while still providing diagnostic quality 3D device imaging. The significant reduction of radiation dose may allow for multiple image acquisitions of focused anatomical regions during critical stages of device deployment.

KEYWORDS: Flat-Detector Cone-Beam CT, Flow Diverter, High-Resolution Imaging

Note: Scanned images are included in the proceedings. Some submitted images were reduced during editing thereby decreasing clarity. Also, refer to the Program Planner. Proceedings Content as of 3/28/2014.

O-306 10:58AM - 11:05AM
Comparison of Measurements from Automatic Intracranial Aneurysm Analysis Software and an Experienced Rater

M Jagani¹, G Chintalapani¹, P Chinnadurai¹, H Shaltoni², H Morsi², M Mawad³

¹Siemens Medical Solutions USA, Inc., Hoffman Estates, IL, ²St. Luke's Hospital, Houston, TX, ³Baylor College of Medicine, Houston, TX

Purpose

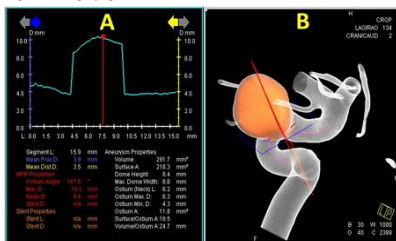
Endovascular treatment of intracranial aneurysms with stent-assisted coiling or flow diverter devices requires precise measurements of the aneurysm and the parent artery. Typically, aneurysm measurements are performed manually on two-dimensional (2D) or three-dimensional (3D) images. However, these can be prone to significant errors based on the viewing angle. Several computer-assisted approaches have been proposed recently to assess the aneurysm geometry from 3D images. The primary goal of this study is to evaluate the efficacy and accuracy of a 3D digital subtraction angiography (DSA)-based automatic vessel analysis tool and compare the results with the measurements of an experienced radiologist.

Materials and Methods

Intracranial aneurysms from thirty patients that underwent endovascular treatment were evaluated in this study. Commercially available software, Intracranial Aneurysm Analysis version VC21 (Siemens AG, Forchheim, Germany), was applied to the 3D DSA images from each patient and the measurements of the aneurysm [dome height (H), neck length (L), maximum neck diameter (D)] were recorded. The software requires the operator to manually place a point in the aneurysm dome and in the proximal and distal parent vessel. These measurements were compared to the manual measurements taken by an experienced radiologist using correlation analysis.

Results

Software successfully segmented 27 out of the 30 aneurysm datasets. Seventeen of these datasets were segmented successfully on the first try, and 10 datasets required minor postprocessing modifications such as cropping vessels originating from the aneurysm. The software could not segment three datasets due to touching vessels and ill-defined neck. The average software to experienced rater errors with standard deviations were H = 0.87 ± 0.74 mm, L = 0.67 ± 0.52 mm, and D = 1.13 ± 0.87 mm. The maximum errors were H = 2.77 mm, L = 1.72 mm, and D = 3.3 mm. Correlation between the software and rater was calculated using Pearson's r, for which H = 0.96, L = 0.90, and D = 0.90.



Conclusions

The software was able to segment the aneurysm in a large majority of cases either on the first try or after minor manual corrections. Results indicate that the measurements from aneurysm analysis software are comparable ($r \geq 0.9$) to an experienced radiologist for each aneurysm characteristic. Hence, the software can provide a reliable means of extracting aneurysm measurements. Further studies using phantoms based on patient geometry are currently underway.

KEYWORDS: Aneurysm, Aneurysm Sizes, Aneurysm Treatment

O-307 11:05AM - 11:12AM
Role of vascular smooth muscle cells in the pathogenesis of cerebral aneurysm: inflammatory mediators and angiogenesis-related factors production in proinflammatory cytokine stimulation

S Suh, J Kim, T Kwon, H Seol
Korea University Guro Hospital, Seoul, Korea

Purpose

The inflammation and angiogenesis have been suggested as the critical process in the pathogenesis of cerebral aneurysms. The purpose of this study is to evaluate the pattern of production of matrix metalloproteinase (MMP) and angiogenesis-related cytokines by cultured human arterial smooth muscle cells (SMC) in the tumor necrosis factor- α (TNF- α) stimulation.

Materials and Methods

Smooth muscle cells were isolated from human superficial temporal artery wall tissues during brain surgery, and confirmed as vascular SMCs by immunohistochemical staining, and cultured according to the protocol. Cultured arterial SMCs were stimulated by different concentration (1, 10, 100 ng/ml) of TNF- α for 48 hours and also treated for various periods of time (24, 48, 72 hours) by 10 ng/ml of TNF- α . The productions of inflammatory mediator (MMPs) and angiogenesis-related factors (IL-6, IL-8, IL-17, VEGF, IFN- γ) in the stimulated SMCs were assayed by enzyme-linked immunosorbent assay (ELISA).

Results

All cultured cells expressed α smooth muscle actin, suggesting the SMC-type origin. Tumor necrosis factor- α stimulated SMCs produced the MMP-3, IL-6, IL-8, and VEGF with dose- and time-dependent pattern and showed statistically significant amount comparing with nonstimulated one. The MMP-1 production was demonstrated at nonstimulated SMCs, but not significantly increased in response to variable concentration of TNF- α . The SMCs did not produce the detectable amount of the MMP-9, IL-17, and IFN- γ .

Conclusions

The cultured arterial SMCs produced inflammatory mediator and angiogenesis-related factors in response to proinflammatory cytokines stimulation with a concentration- and time-dependent manner. The arterial SMCs may play an important role in the pathogenesis of cerebral aneurysm.

Note: Scanned images are included in the proceedings. Some submitted images were reduced during editing thereby decreasing clarity. Also, refer to the Program Planner. Proceedings Content as of 3/28/2014.

KEYWORDS: Aneurysm Formation, Experimental Aneurysms

0-308 11:12AM - 11:19AM
Developing a better Understanding of the Importance of Ostium Hemodynamics for Aneurysm Rupture: Velocities at the Aneurysm Ostium correlate with the Pressure Loss Coefficient

C Karmonik¹, O Diaz², R Klucznik³, R Grossman¹, Y Zhang⁴, G Britz¹, N Lv⁵, Q Huang⁵
¹Houston Methodist Hospital, Houston, TX, ²The Methodist Hospital, Bellaire, TX, ³The Methodist Hospital, Houston, TX, ⁴Weill Medical College of Cornell University; Houston Methodist Hospital, Houston, TX, ⁵Affiliated Changhai Hospital of Second Military Medical University, Shanghai, China

Purpose

To quantify the relationship between the pressure loss coefficient (PLC), a potential surrogate marker for aneurysm rupture (1), with the inflow and outflow characteristics at the aneurysm ostium. Ostium hemodynamics are of interest as they are altered by flow diverter (FD) treatment.

Materials and Methods

From computational fluid dynamics simulations (Star-CCM+, cd-adapco) of eight cerebral aneurysms, inflow and outflow mean velocities were determined at the aneurysm ostium. Statistical significance of correlations with blood velocities and pressures in the parent artery, in the aneurysm dome and with the PLC were investigated.

Results

Statistically significant correlations ($p < 0.05$) between PLC and mean inflow (correlation coefficient $CC = 0.96$) and outflow ($CC = -0.88$) at the ostium were found. In addition, statistically significant correlation of the PLC with the mean blood velocity inside the aneurysm was established ($CC = 0.89$). None of the hemodynamic parameters correlated with the area of the inflow or outflow region at the ostium.

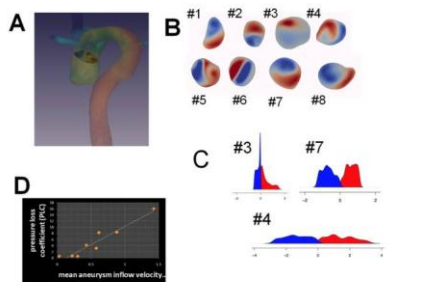


Figure 1: A: Illustration of segmented aneurysm ostium in one computational aneurysm model (case #4; color coding shows total pressure - blue: low, red: high). B: Aneurysm ostia for all eight cases (red: area of inflow into the aneurysm, blue: area of outflow from the aneurysm). C: Blood velocity distributions for three representative cases (#3, #4 and #7) visualizing variety in between cases. D: High correlation of pressure loss coefficient and blood inflow velocity into the aneurysm at the ostium ($R = 0.96$).

Conclusions

Inflow and outflow velocities into cerebral aneurysms at the ostium were found to strongly correlate with the pressure loss coefficient, a potential surrogate marker for aneurysm rupture. This finding is of interest towards a better understanding of hemodynamic alterations at the ostium caused by FD treatment which aims at reducing aneurysm rupture risk.

KEYWORDS: Computational Fluid Dynamics, Intracranial Aneurysms

0-309 11:19AM - 11:26AM
Half-Year Follow-Up after Coil-Embolization of Cerebral Aneurysms. Is DSA Mandatory?

C Gramsch, S Zülw, J Schelhorn, F Nensa, I Wanke, S Goericke, M Forsting, M Schlamann
University Hospital Essen, Essen, Germany

Purpose

Whereas long term follow ups normally are performed using MR imaging (MRI) techniques the combination of catheter angiography (DSA) and MR angiography (MRA) is concerned as gold standard for half-year follow ups in endovascularly treated patients. In case of congruent results in both techniques, further control examinations with digital subtraction angiography (DSA) may be omitted. The purpose of our study was to determine whether the initial follow-up DSA half a year after the embolization is already dispensable, because MRI with at least 1.5 T provides similar results.

Materials and Methods

Five hundred and ninety-seven half-year follow-up examinations consisting of DSA, contrast-enhanced MRA (CE-MRA) and time-of-flight MRA (TOF-MRA) of 468 consecutive patients, treated endovascularly between 2003 and 2012 were reviewed retrospectively. Visualization of residual aneurysm patency with each of the MRA techniques was compared with DSA as the reference standard by two experienced readers ($>10y$).

Results

Recurrences could be detected in 245 aneurysms half a year after embolization. In five cases recurrence was only detectable in DSA examinations but neither in CE-MRA nor in TOF-MRA. These recurrences, however, were small ($<2mm$) and therapy concept was not changed. All recurrences that required treatment were detectable with at least one of the MRI techniques. In seven cases aneurysm recurrence was only visible in the DSA and TOF-MRA but not in the CE-MRA and in four cases it was not visible in the TOF-MRA but in both of the other imaging procedures.

Conclusions

Catheter angiography is dispensable in the half-year follow up. MR imaging is as effective as DSA in detection of residually patent aneurysms if CE-MRA and TOF angiography are performed.

KEYWORDS: Aneurysm, Angiography, Coil Embolization

Note: Scanned images are included in the proceedings. Some submitted images were reduced during editing thereby decreasing clarity. Also, refer to the Program Planner. Proceedings Content as of 3/28/2014.

O-310 11:26AM - 11:33AM
BUENOS AIRES EXPERIENCE WITH SURPASS (SNEG)

P Lylyk¹, C Ingino¹, R Romero¹, R Ceratto¹, A Ferrario¹, C Bleise¹, J Chudyk²

¹Eneri - Sagrada Familia, Buenos Aires, Argentina, ²Eneri, Buenos Aires, Argentina

Purpose

Surpass device (SNEG) is indicated for the treatment of saccular, wide neck or fusiform intracranial aneurysms (IA) arising from a parent vessel with a diameter between 2mm and 6mm. We present our initial experience in the treatment of IA with SP device and early follow-up results.

Materials and Methods

Patients with IA considered having a high probability of failure or recurrence with conventional endovascular techniques were selected for treatment with SNEG. All patients were pretreated with dual antiplatelet medication. Angiographic and clinical follow up was performed at three, six and 12 months.

Results

Fifty-seven patients with 66 IA, 48 female, were treated with the SNEG device; 44 had saccular IA; 20, fusiform IA; and two, blister like IA. A total of 64 SNEG were used. Eighty percent were treated with a single SNEG. Complete angiographic occlusion was achieved at three months in 40 of 52 aneurysms (77%); at six months, in 29 of 33 (88%); and at 12 months, in 22 of 24 (92%). 75.4% IA were symptomatic, (14 had an acute stroke; 12, mass effect; and 17 with previous SAH; 14 were incidental). Two patients had thrombotic complications: one patient who suffered a brainstem stroke finally died due to a pseudomonas pneumonia during follow up, and it was the only major complication within this series. Four patients with TISS were observed in the follow up without clinical consequences. Morbimortality rate was 5.2%.

Conclusions Our initial experience in the endovascular treatment of selected IA with the Surpass device shows that it can be safely achieved with a low rate of complications. A longer follow up is needed.

KEYWORDS: Aneurysm Treatment, Flow Diverter

O-311 11:33AM - 11:40AM
COVERED STENT VS FLOW DIVERTER IN THE
TREATMENT OF COMPLEX ANEURYSMS OF THE
INTERNAL CAROTID ARTERY

W Escobar, A Pedroza
Imbanaco Medical Center, Cali Valle, Colombia, SA

Purpose

To demonstrate that covered stents are an excellent option for treating complex aneurysms that originate proximal to the anterior choroidal artery. **Background:** The recanalization rate in wide-necked, large or giant aneurysms treated with detachable coils is very high. Additionally, such aneurysms also represent serious difficulties for surgeons because of bony obstacles and

difficulty in proximal control. Recently these aneurysms have been treated with flow diverters that have been associated with late occlusion, thrombosis, hemorrhage and embolism without resolving the problem.

Materials and Methods

From November 2003 to November 2013, 19 patients with big and wide-necked aneurysms located under the anterior carotid artery have been treated with covered stents. Under general anesthesia with a triaxial system, premedicated with antiagregants (Clopidogrel and Aspirin) three days before the procedure. Five thousand units of heparin in bolus were used at the beginning of the procedure followed by 1500 units per hour. After the procedure, patients stayed on Aspirin and Clopidogrel during six months followed by Aspirin for life. Jostent Graftmasters Coronary stent grafts were utilized along with Tracker Excel 14 microcatheters, Transed EX micro guides, PT Choice extra support 300 cms and Envoy guide catheter 6F.

Results

Twelve aneurysms were excluded immediately from circulation after stent deployment without contrast material filling into the aneurysm cavity. Eight were thrombosed as shown by late control in angiography, computed tomography (CT) or MRI imaging (MRI) evaluations. The patients treated had complex aneurysms and the internal carotid artery was favorable for navigation. There was no mortality and morbidity because embolism was present in one patient who did not take the antiagregant medication after the procedure. At three-month follow up this patient had recovered completely. All patients had three to 36 month follow ups with angiography, showing exclusion of the aneurysm from the circulation and permeability of the internal carotid artery.

Conclusions

Covered stents would be a very effective alternative treatment for complex carotid aneurysms located under the origin of the anterior choroidal artery whenever anatomy is favorable for navigation. Covered stents occlude aneurysms faster and in a higher percentage than flow diverters. Although the initial results are promising, longer follow up and larger clinical trials are required.

KEYWORDS: Aneurysm Treatment, Carotid Artery, Stents

O-312 11:40AM - 11:47AM
Initial experience with p64, a retrievable and controlled detachable intraluminal flow modulation implant, in the treatment of neurovascular dissections and aneurysms

M Aguilar-Pérez, W Kurre, E Henkes, C Serna-Candel, H Bätzner, H Henke
Neurozentrum, Klinikum Stuttgart, Stuttgart, Baden-Württemberg, Germany

Purpose

Endovascular flow diversion and modulation recently became an accepted method for the treatment of neurovascular dissections, fusiform and side-wall aneurysms. p64 is a braided, self-expanding Nitinol

Note: Scanned images are included in the proceedings. Some submitted images were reduced during editing thereby decreasing clarity. Also, refer to the Program Planner. Proceedings Content as of 3/28/2014.

implant, which is connected to an insertion wire and is accepted by an 0.027". In comparison with most other devices with a similar function, p64 has a radial force in the same range, offers denser vessel wall coverage and can be withdrawn after complete deployment. The initial clinical experience with this device will be presented. We sought to evaluate both safety and efficacy effects of p64.

Materials and Methods

One hundred thirty-six patients (59 male) with 139 target lesions underwent 159 treatment sessions in a single neurovascular center. The target lesions (per procedure) included 81 saccular aneurysms, 56 fusiform aneurysms, 13 neurovascular dissections and seven CCFs. Apart from 88 unruptured lesions without any previous treatment, 33 target lesions were treated previously with a flow diverter or a stent, 19 were remnants after coiling and six were treated after partial clipping or failed surgery. The majority of target lesions (123) were located in the anterior circulation, with 34 lesions in the posterior circulation. The fundus of the saccular aneurysms had a median diameter of 4 mm. In 118/157 procedures a single p64 was deployed.

Results

Complete coverage of the target lesion was achieved in 94%. No device malposition was encountered. Predilatation was performed in 17 cases, postdilatation in nine. During the first angiographic follow up after 91 days (median), complete occlusion was confirmed in 52/110 lesions, minor remnants were found in 25/110 and significant remnants were present in 33/110. For 38 lesions a second DSA follow up was available after 8.6 months (median). Complete occlusion and a minor remnant was observed in 24 and five lesions, respectively. A significant remnant was present in nine lesions. Neither a SAH from a target lesion nor an ICH in the dependent brain or in a remote location occurred. Neurological deficits due to ischemic events were transient in 11 and permanent in three patients. Two patients died (1 from pneumonia, 1 from access related ICA dissection). Seven out of 10 side branch occlusions remained asymptomatic. All 11 patients with minor to moderate intimal hyperplasia developed no related symptoms.

Conclusions

p64 allows safe and efficacious reconstruction of extra and intracranial vessel dissections. In saccular aneurysms a single device is mostly sufficient to induce vessel remodeling, resulting in aneurysm obliteration. Fusiform aneurysms may need more complex procedures with the use of several devices.

KEYWORDS: Aneurysm, Flow Diverter

0-313 11:47AM - 11:54AM
LONG TERM FOLLOW-UP FOR ENDOVASCULAR TREATED RUPTURE INTERNAL CAROTID ARTERY PSEUDOANEURYSM AFTER RADIOTHERAPY FOR NASOPHARYNGEAL CARCINOMA

S Lo, W Poon, Y Cheung, C Chan, K Shek, K Tang, D Wong1 K Fok
Queen Elizabeth Hospital, Hong Kong, China

Purpose

Internal carotid artery pseudoaneurysm developed after postradiotherapy in nasopharyngeal carcinoma is a rare but life-threatening condition. The methods and safety of endovascular treatment in this life-threatening disease is still equivocal. Our aim of this study is to evaluate the efficacy, complications, and clinical outcome of different methods of endovascular treatment of ruptured internal carotid artery pseudoaneurysm developed after postradiotherapy in nasopharyngeal carcinoma patients.

Materials and Methods

From a prospective data repository, we retrieved records of 24 consecutive patients with ruptured radiation-induced internal carotid artery (ICA) pseudoaneurysm that were treated endovascularly between October 1999 and October 2013, in Queen Elizabeth Hospital. Hospital records, angiographic findings, intraprocedural and 30 days clinical morbidity and mortality, long-term clinical outcome were retrieved and analyzed after treatment, with subsequent clinical and imaging follow up. Descriptive statistical analysis was carried out by using Statistical Package for the Social Sciences for Windows, version 19.0 (SPSS, IBM).

Results

During the 14 years study period, 24 patients (21 male; age range 33-78 years) with history of nasopharyngeal carcinoma treated with radiotherapy, developed ICA pseudoaneurysms, and were treated by endovascular means in our hospital. The average time interval for pseudoaneurysm development after completion of radiotherapy was 11 years (range 2-19 years). Presenting symptoms were epistaxis in 13 patients (54%), otorrhagia (bleeding from ear) in eight patients (21%), and two (8%) with both epistaxis and otorrhagia. Most pseudoaneurysms were arising from petrous segment of ICA (46%), followed by cervical segment (33%) and lacerum segment (17%). Therapeutic complete occlusion of the affected internal carotid artery was performed in five patients, and stenting of the affected artery (with or without coils obliteration of pseudoaneurysm) was performed in 19 patients. Immediate hemostasis was achieved in all patients. Nineteen (80%) patients were discharged successfully from hospital, 17 patients (71%) without any major neurological defects (mRS <2), and two patients have cerebral infarcts with mRS >2. There were total seven complications encountered within 30 days after the procedure. Two patients rebleed during hospitalization and five patients encountered cerebral infarctions. Three (16%) complications (2 rebleed and 1 cerebral infarct) occurred in patient with stenting performed; whereas, four (80%) cerebral infarctions occurred in parent artery

Note: Scanned images are included in the proceedings. Some submitted images were reduced during editing thereby decreasing clarity. Also, refer to the Program Planner. Proceedings Content as of 3/28/2014.

occlusion. Five mortalities (20%) happened within 30 days postop, three (60%) occurred in parent artery occlusion and two (11%) in parent artery stenting. The result of this study showed statistical significant differences in complication rates ($p=0.01$) and mortality ($p=0.04$) between parent artery occlusion versus parent artery stenting procedures in ruptured postradiotherapy related ICA pseudoaneurysm.

Conclusions

Ruptured internal carotid artery pseudoaneurysms following radiotherapy is a rare complication but life-threatening condition. Endovascular treatment by endoluminal vascular reconstruction of internal carotid artery with stents, provide immediate hemostasis and obliteration of the pseudoaneurysms. Long term results from this study showed lower complication and mortality rates for endoluminal vascular stent reconstruction than parent artery occlusion in treating postradiotherapy related ICA pseudoaneurysm.

KEYWORDS: Aneurysm, Aneurysm Embolization, Aneurysm Treatment

O-314 11:54AM - 12:01PM
LARGE AND GIANT INTRACRANIAL ANEURYSMS
TREATED WITH FLOW DIVERTER EMBOLIZATION DEVICE
(PED) : BUENOS AIRES COHORT.

P Lylyk¹, J Lundquist¹, E Scrivano¹, R Ceratto¹, A Ferrario¹, C Bleise¹, J Chudyk²

¹Eneri - Sagrada Familia, Buenos Aires, Argentina, ²Eneri, Buenos Aires, Argentina

Purpose

We present our results with Pipeline embolization device (PED) in the treatment of large and giant intracranial aneurysm (IA), focused on clinical and angiographic results and long term follow up.

Materials and Methods

Patients with giant and large IAs were treated with PED. Clinical presentation was: mass effect in 147 IAs; 57 IAs were incidental; 69 IAs had previous subarachnoid hemorrhage; others seven IAs; 58 had previous treatment. Anterior/posterior circulation IAs were 229 and 51, respectively.

Results

Between March 2006 and October 2013, 280 patients with 99 giant and 181 large IAs were treated with PED; 209 patients were female; average age was 62.1 years (7-85). One hundred and forty-two IAs were treated with 1 PED, 61 with 2 PED, and 32 IAs required three or more PED (mean, 1.38 PED/IA). Follow-up angiograms were performed between 1 and 84 months. The follow-up occlusion rate at 12 months was 85.4 %. All patients with an initial mRS of 0-1 were unchanged at 3-6 month of follow-up. The global morbimortality was 6.3%. Six patients died (2.14%) and 11 patients (3.9%) experienced transient neurologic deficit or exacerbations of pre-existing cranial neuropathies or headache after PED treatment, but these symptoms were resolved within the first month.

Conclusions

Our results have shown that large/giant IAs can be safely treated with PEDs. This clinical result is highly encouraging, and our technique may significantly improve the endovascular treatment of this kind of intracranial aneurysms.

KEYWORDS: Aneurysm Treatment, Flow Diverter

O-315 12:01PM - 12:08PM
Experimental Testing of New Generation of Flow Diverter
"FRED" in Sidewall Aneurysms in Rabbits

Y Ding¹, T Tieu², D Kallme^{s1}

¹Mayo Clinic, Rochester, MN, ²MicroVention Company Inc., Tustin, CA

Purpose

The Flow Re-Direction Endoluminal Device (FRED™) system (MicroVention, Inc., Tustin, CA) is a dual layer, aneurysm hemodynamic disturbing device. The purpose of this study was to evaluate the effectiveness and tissue reaction of FRED device in sidewall aneurysm model in rabbits.

Materials and Methods

The FRED devices were implanted in 22 sidewall aneurysms and 22 abdominal aortas in the New Zealand white rabbits and followed for one (n = 5), three (n = 5), six (n = 4) and 12 months (n = 8). Rabbits at each time-point were classified as Group 1, 2, 3, 4 accordingly. Extent of intra-aneurysmal flow disruption was graded on a 3-point scale based on digital subtraction angiography (DSA) immediately following device implantation and before sacrifice, including Grade 1 (complete flow cessation); Grade 2 (near complete flow cessation); Grade 3 (incomplete flow cessation). Comparison of aneurysm occlusion situation at follow up was based on angiographic images immediately after treatment and before sacrifice. Toluidine blue and basic fuchsin (TB-BF) staining was used for histologic specimen process. Scanning electronic microscopy (SEM) examination of abdominal aorta with device attached was performed. Histological healing at aneurysm lumen and neck were evaluated. Aneurysm sizes between different groups were compared by using the Student's t-test.

Results

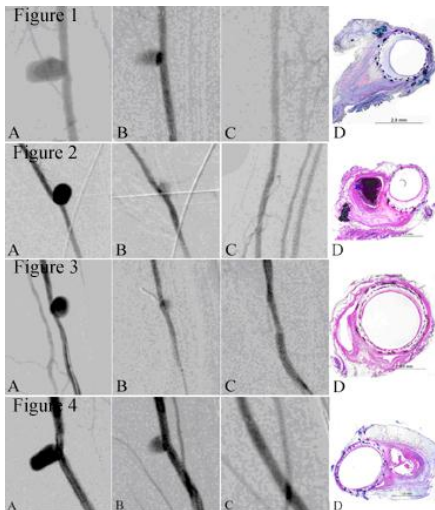
Mean aneurysm sizes (including aneurysm neck, width, and height) of the 22 aneurysms in four groups were shown in Table 1. There was no significant difference of aneurysm neck, width, and height among different groups ($p > .05$). Incomplete aneurysm occlusion was shown in 19 (86%) cases immediately after device deployment. The other three (14%) aneurysms were occluded nearly completely. At one month follow up, complete occlusion was noted in four (80%) of five cases, near complete in one (20%) case (Figure 1 A-C). At three-month follow up, complete occlusion was noted in four (80%) of five cases, near complete in one (20%) case (Figure 2 A-C). At six-month follow up, all (100%) of the aneurysms were completely occluded (Figure 3 A-C). At 12-month follow up,

Note: Scanned images are included in the proceedings. Some submitted images were reduced during editing thereby decreasing clarity. Also, refer to the Program Planner. Proceedings Content as of 3/28/2014.

complete occlusion was noted in seven (88%) of eight cases, near complete in one (12%) cases (Figure 4 A-C). Histological images indicated partially unorganized or organized thrombus within aneurysm and neointima coverage at aneurysm neck (Figures 1 D, 2 D, 3 D, 4 D). Scanning electronic microscopy indicated vessel branches along the device remained patent in all the cases.

Table 1. Mean Aneurysm Sizes in Four Groups

	Neck (mm)	Width (mm)	Height (mm)
Group 1	4.1+/-1.1	6.5+/-2.1	7.0+/-1.7
Group 2	3.5+/-1.0	5.5+/-1.6	5.5+/-1.2
Group 3	3.7+/-1.1	6.3+/-1.7	5.9+/-1.4
Group 4	3.6+/-1.0	5.5+/-1.5	6.0+/-1.4



Conclusions
The FRED device in experimental aneurysms demonstrated high rates of progress and complete aneurysm occlusion.

KEYWORDS: Endovascular Flow Diverter, Experimental Aneurysms

Tuesday, May 20
10:30 AM – 12:00 PM
Room 517d

35 - Mini Symposium: Tumor – Part II

O-316 10:30AM - 10:50AM
Diffusion - Weighted Imaging and Primary CNS Tumors: Application and caveats

Ellingson, B.
University of California Los Angeles
Los Angeles, CA

O-320 11:00AM - 11:15AM
Pre-Surgical Brain Mapping of Intracranial CNS Tumors

Ulmer, J.
Medical College of Wisconsin
Wauwatosa, WI

O-323 11:30AM - 11:45AM
HIFU: Principles, Current Applications and Future Possibilities

Colen, R.
MD Anderson Cancer Center
Houston, TX

O-317 10:45AM - 10:51AM
Correlation of FA values and Mean Diffusivity (MD) with the Ki-67 Proliferation Index in Gliomas

S Sood, J Modi
Medanta-The Medicity, Gurgaon, India

Purpose
Assessment of glioma grade is important in predicting the response to treatment and survival. The purpose of this study was to correlate fractional anisotropy (FA) and mean diffusivity (MD) values in newly diagnosed gliomas with Ki-67 proliferation index. **Materials and Methods**
Ten patients with newly diagnosed gliomas who underwent diffusion tensor imaging (DTI) for presurgical evaluation followed by biopsy/surgery were retrospectively reviewed. MR imaging (MRI) was done on 3 T scanner in all patients using multishot EPI sequence. Fractional anisotropy and mean diffusivity values were calculated at the point of infiltration in white matter tracts and within the estimated tumor margins. The values were correlated with Ki-67 proliferation index.

Results
Higher FA and lower MD values correlated with a high Ki-67 labeling index representing higher tumor cell density. **Conclusions**
Fractional anisotropy and MD values tend to represent the histology of gliomas and the tumor cell density correlating well with Ki-67 labeling index. Higher FA and lower MD values represent higher tumor cell density and malignant potential.

KEYWORDS: Diffusion Tensor Image, Mean Diffusivity, Neoplasm

Note: Scanned images are included in the proceedings. Some submitted images were reduced during editing thereby decreasing clarity. Also, refer to the Program Planner. Proceedings Content as of 3/28/2014.

O-318 10:51AM - 10:57AM
Combined ADC Diffusion and CBV Perfusion Maps predict Survival in Patients with Newly Diagnosed Glioblastoma

A Radbruch¹, M Bendszus¹, K Deike¹, R Floca², M Graf², S Heiland¹, W Wick¹, B Wiestler¹

¹University of Heidelberg, Heidelberg, Germany, ²German Cancer Research Center (DKFZ), Heidelberg, Germany

Purpose

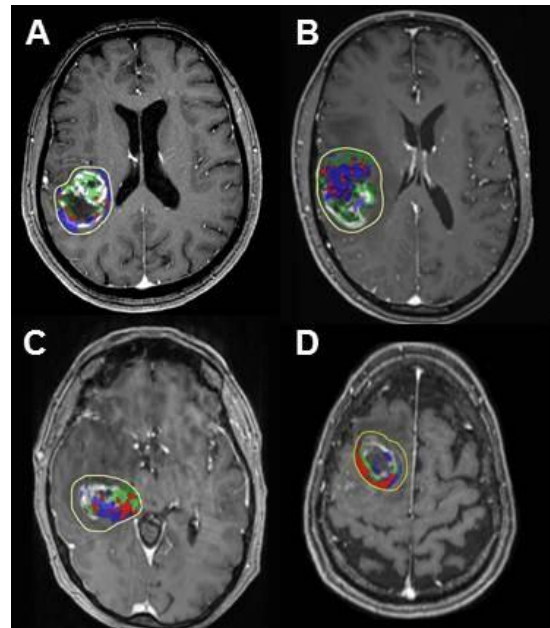
Minimum apparent diffusion coefficient (MinADC) values on diffusion MR imaging (MRI) maps are supposed to be correlated with high cellularity and hence malignancy in patients with glioblastoma. In contrast maximum cerebral blood volume (MaxCBV) values on dynamic susceptibility contrast (DSC)-weighted perfusion maps should be correlated with increased vascularity and hence malignancy. In this study we investigated if a specific distribution of MaxCBV values and MinADC values either in the enhancing area or the surrounding area of the tumor can identify subtypes of glioblastoma with different prognosis.

Materials and Methods

Diffusion-weighted imaging (DWI), DSC and contrast-enhanced T1-weighted (ce-T1) imaging using DOTAREM (Gadoterate meglumine) was performed in 67 patients with newly diagnosed and histologically proven glioblastoma before surgery on a 3 T MR system. Apparent diffusion coefficient and CBV maps were calculated and coregistered on ce-T1 images. A region of interest (ROI) was delineated manually on ce-T1 images encompassing the enhancing lesion with a 1 cm margin. Within this ROI, pixels with ADC < the 30th percentile (MinADC), pixels with CBV > the 70th percentile (MaxCBV) and the corresponding overlap were calculated automatically and visualized (MinADC blue, MaxCBV green, intersection red; Figure 1) on ce-T1 images. The acquired maps were assessed by two neuroradiologists and qualified as "infiltrative subtype" if MinADC values were located mainly in the surrounding area and MaxCBV values mainly within the enhancement (Figure 1 A) and as "vascular subtype" for the opposite distribution (Figure 1 B). If the intersection of MinADC and MaxCBV was larger than 25% of the visualized area (MinADC and MaxCBV) patients were subgrouped as "big intersection subtype" (Figure 1 D). In case of an intersection below 25% and no specific distribution of MinADC and MaxCBV values, patients were subgrouped as "nonspecific subtype".

Results

Thirty patients were classified as "invasive subtype", five as "vascular subtype", 17 as "big intersection subtype" and 15 as "nonspecific subtype". Patients of the "invasive subtype" showed a significantly shorter overall survival (8.2 ± 8.4 months, logrank-test $p < 0.00028$) than those of the "vascular subtype" (21.0 ± 11.2 months), "nonspecific subtype" (13.5 ± 9.1 months) and "big intersection subtype" (18.8 ± 8.5 months).



Conclusions

A possible explanation for the bad prognosis of the "invasive subtype" may be that this subtype is characterized by an early and extensive invasion of tumor cells in the surrounding tissue, resulting in the specific localization of MinADC within the surrounding tumor area. The pathophysiological mechanism underlying this distribution might be that migrating tumor cells in the invasion front, represented by areas of MinADC, produce and secrete neoangiogenic factors, leading to a "trailing behind" of the vascular-rich tumor border, represented by MaxCBV. In subtypes with a big intersection of MinADC and MaxCBV the above-mentioned "trailing behind mechanism" might be less pronounced, resulting in a decreased invasiveness of the tumor and a prolonged survival of the patients.

KEYWORDS: Glioblastoma

O-319 10:57AM - 11:03AM
Comparison of Compressed-Sensing Accelerated Diffusion Spectrum Imaging vs. Diffusion Tensor Imaging in Patients with Brain Tumors

R Young¹, E Tan², K Peck¹, J Tisnado¹, X Liu², M Jenab¹, A Holodny³, L Marinelli²

¹Memorial Sloan-Kettering Cancer Center, New York, NY, ²GE Global Research, Niskayuna, NY, ³Memorial Sloan-Kettering Cancer Center, Weill Medical College of Cornell University, New York, NY

Purpose

To compare tractography results from compressed-sensing diffusion spectrum imaging (CS-DSI) and diffusion tensor imaging (DTI) in patients with brain tumors.

Note: Scanned images are included in the proceedings. Some submitted images were reduced during editing thereby decreasing clarity. Also, refer to the Program Planner. Proceedings Content as of 3/28/2014.

Materials and Methods

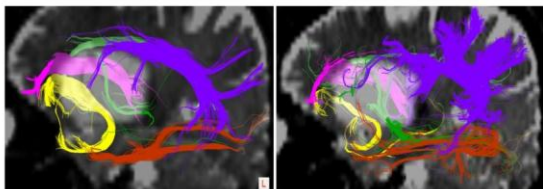
Using 3 T MR imaging (MRI) (Discovery MR750, GE Healthcare, Milwaukee, WI), DTI and CS-DSI were performed in 11 patients with brain tumors (6 high-grade gliomas, 3 low-grade gliomas, 1 meningioma, 1 metastasis). The median age was 49 years (range, 35-86) with seven males and four females. Diffusion tensor imaging was acquired at 25 directions (n=11) with ASSET R=2, b=1,000 sec/mm², matrix=128×128, thickness=3mm, TR/TE=11,000/64msec, time=4.5min. Diffusion spectrum imaging was acquired at 127 directions (n=7; R=4; slices=34; time=14 min) and 102 directions (n=4; slices=50; time=10 min) with 11-cube q-space, b=6,000-10,000sec/mm², thickness=3mm, TR/TE=5,000/116msec). Compressed-sensing-DSI was processed on parallelized code written in Matlab (Mathworks, Natick, MA). Diffusion tensor imaging and CS-DSI tract quantification were performed using Trackvis (Wang, Boston, MA). Based on prior experience, angle thresholds were set to 38°. Total 2-5 tracts/patient were selected by an experienced neuroradiologist as potentially affected by the tumor and/or peritumoral abnormality. Semi-automatic segmentation with manual editing was performed to seed the selected tracts. Diffusion tensor imaging and CS-DSI tract counts (TCs) were compared using Wilcoxon signed rank tests with p<.05. For both DTI and CS-DSI, the tumor and normal contralateral tracts were compared within patients, and designated as consistent with pathology if TCratio<0.9 (decreased TC on side of tumor) and inconsistent if TCratio>1.2.

Results

Compressed-sensing DSI provided greater TCs than DTI overall, with median difference=255 (p<.00001) and qualitatively fewer extraneous tracts. Specifically, CS-DSI yielded greater TCs in four tracts (anterior thalamic radiations, cingulum, inferior fronto-occipital fasciculus, superior longitudinal fasciculus) with median difference =66-392 (p<.0007). Similar TCs were found in the other two tracts (inferior longitudinal fasciculus, uncinate fasciculus) with median TC difference =8-66 (p>.377). For DTI, total of 21 tracts were predicted to be consistent with pathology and nine to be inconsistent. For CS-DSI, total of 26 tracts were consistent with pathology and 0 were inconsistent.

Figure. In a patient with a low grade oligodendroglioma in the left temporal lobe, CS-DSI (LEFT) shows greater tract counts (yellow, brown) than DTI (RIGHT), and fewer extraneous tracts (purple).

Key: yellow=uncinate fasciculus; brown=inferior longitudinal fasciculus; purple=superior longitudinal fasciculus; pink=anterior thalamic radiations; green=inferior fronto-occipital fasciculus; light green=cingulum



Conclusions

Compressed-sensing DSI provided greater TCs in tumor affected white matter tracts than DTI. Compressed-sensing DSI also revealed greater differences in TC ratios between tumor and nontumoral sides, suggesting greater consistency in predicting tracts affected by tumor and/or

peritumoral abnormality. These results suggest that CS-DSI outperforms DTI in tracking in brain tumor patients through areas of low anisotropy and in following small and/or crossing fibers. Further work is necessary to investigate the role of CS-DSI for preoperative planning and potential correlations with white matter infiltration.

KEYWORDS: Diffusion Tensor Image, MR Imaging Brain, MR Imaging/Diffusion

O-321 11:15AM - 11:21AM
Comprehensive Survival Analysis of Preoperative Imaging Features in Patients with Glioblastoma

P Wangaryattawanich, J Wang, A Kumar, P Zinn, R Colen
MD Anderson Cancer Center, Houston, TX

Purpose

Glioblastoma (GBM) is the most common and most aggressive primary brain tumor in adults which carries poor prognosis, with median survival of approximately 14.6 months. Neuroimaging plays a pivotal role in diagnosis and monitoring therapeutic response. The prognostic role of pretreatment imaging characteristics of GBM has been studied but remains controversial. The purpose of this study was to assess the significance of over 35 quantitative and qualitative preoperative imaging variables with regards to overall and progression free survival of these patients.

Materials and Methods

We retrospectively analyzed magnetic resonance imaging (MRI) characteristics of 111 patients with previously untreated GBM using the collection of the original material and data provided by The Cancer Imaging Archive (TCIA) corresponding to the patients of The Cancer Genome Atlas (TCGA) project. The imaging data set based upon Visually Accessible Rembrandt Images (VASARI) feature set for human glioma consists of 26 imaging features, with standardized terminologies. Volumetric analysis using Slicer 3.6 (slicer.org) and volumes were obtained from the area of contrast enhancement, necrosis, and edema/invasion, as previously described by our lab. Ratios, groupings and subgrouping were performed of the quantitative volumetric parameters. The Kaplan Meier curve was used to measure patient survival. The statistical significance of relationship between each imaging variable and survival was identified by performing multivariate Cox regression analysis. The statistical analyses also were performed after adjustment for the potential explanatory clinical variables including age, Karnofsky Performance Status (KPS) scale, gender, and regimens of therapy.

Results

A total of 15 quantitative and qualitative imaging parameters were statistically significant robust predictors of survival.

Conclusions

Specific pre-operative MR parameters have a significant role in the prognosis of patients with GBM. Given the statistical significance of specific pre-operative MRI brain tumors features with regards to survival, these imaging

Note: Scanned images are included in the proceedings. Some submitted images were reduced during editing thereby decreasing clarity. Also, refer to the Program Planner. Proceedings Content as of 3/28/2014.

prognostic parameters can now be used for imaging biomarker and imaging genomic biomarker development and validation. Imaging signatures derived from these can be used as stratification and endpoint imaging biomarkers in clinical trials.

KEYWORDS: Glioblastoma, Image Processing, Imaging Biomarker

O-322 11:21AM - 11:27AM
Using Diffusion Tensor Tractography to Predict Routes of Progression and Design Theoretical Radiation Therapy Plans in Patients with High Grade Gliomas

M Hirano¹, M Lattanzi², K Beal², P Litkowski², N Martinez³, Z Zhang², K Peck², A Holodny⁴, V Liu², R Young²
¹Memorial Sloan Kettering Cancer Center, North Chicago, IL, ²Memorial Sloan Kettering Cancer Center, New York, NY, ³North Shore University Health System, Evanston, IL, ⁴Memorial Sloan Kettering Cancer Center, Weill Medical College of Cornell University, New York, NY

Purpose

To examine the utility of tractography to predict recurrent tumor growth patterns in patients with high grade gliomas (HGGs). We hypothesize that tractography-driven anisotropic radiation therapy (RT) plans will provide superior coverage of the recurrent tumor while decreasing total patient radiation dose.

Materials and Methods

The prospective study cohort consisted of 39 patients (mean age 54 years, range 29-76) with pathologically proven glioblastoma (n=30) or anaplastic astrocytoma (n=9). Diffusion tensor imaging (DTI) was acquired as part of the treatment planning MRI and streamline tractography was performed using Nordic BrainEx (NordicNeuroLabs, Milwaukee, WI). The major (largest) and maximal length (longest) fiber tracts originating from the tumor region were identified. Standard RT (RTStand) and theoretical tractography-driven RT (RTTract) plans were developed and compared in terms of dose, volume and coverage. Based on Response Assessment in Neuro-Oncology (RANO) criteria, tumor recurrence was determined on follow-up scans and categorized as central, regional or remote.

Progression-free survival (PFS) was measured.

Results

For the 39 patients, RTTract resulted in smaller planning target volume (PTV) than RTStand (mean decrease=26.1%, 95%CI 15.4-36.8%) with p<.0001 (Wilcoxon signed-rank test) and provided equivalent or slightly superior coverage of the recurrent tumor in 24/31 (77.4%) patients. Of the 31 recurrent tumors, RTTract yielded a smaller PTV than the conventional RT plan in 25/31 (80.6%) patients and a larger PTV in 6/31 (19.4%) patients. RTTract resulted in a smaller PTV and equivalent or superior coverage in 18/31 (58.1%) patients and a smaller PTV but inferior coverage in seven patients (22.6%). For 6/31 (19.4%) patients, RTTract provided equivalent or superior coverage but with a larger PTV. A total of 31/39 (79.5%) patients developed recurrence during the follow-up period, with mean PFS of

7.9 months (range, 0.5-19.7). The most common recurrence pattern was central (n=20), then regional (n=5), remote (n=4), and central/remote and central/regional/remote (n=1 each). The majority of recurrences (27/31, 87.1%) occurred along a generated fiber tract: maximal length (n=9, 29.0%), maximal/major (n=8, 25.8%), major (n=7, 22.6%), unlabeled (n=3, 9.7%). Recurrence was local rather than along any tract in two (6.5%) patients, and tractography failed for technical reasons in the remaining two (6.5%) patients.

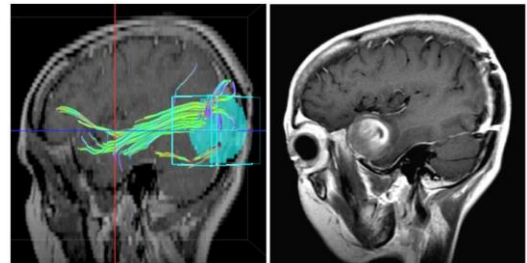


Figure. (Left) Pre-RT tractography overlaid on contrast sagittal T1-weighted image shows major/maximal length tracts (green) emerging along the inferior fronto-occipital fasciculus from the anterior superior medial margin of the seed region-of-interest (blue sphere) placed at the surgical cavity in the occipital lobe. (Right) 13 months post-RT, contrast sagittal T1-weighted image reveals recurrent tumor in the anterior temporal lobe. Expanded to specifically include the inferior fronto-occipital fasciculus, the theoretical RT_{max} still achieved a 7.7% decrease in PTV (not shown).

Conclusions

We found that theoretical tractography-driven RT plans may be helpful in predicting the site of recurrent tumor. Tractography results may be helpful in designing anisotropic RT plans to achieve superior or equivalent coverage of the tumor site with smaller treatment volumes.

KEYWORDS: Diffusion Tensor Image, Glioma, Radiation Therapy

O-324 11:45AM - 11:51AM
Towards Improved Characterization of Brain Tumors by Sodium (Na)-MR Neuroimaging

A Biller¹, A Nagel², A Hertenstein¹, J Neumann¹, F Sahn¹, J Kleesiek¹

¹University of Heidelberg, Heidelberg, Germany, ²German Cancer Research Center, Heidelberg, Germany

Purpose

Sodium (Na)-MRI can provide three different image contrasts, which reflect the average tissue Na concentration (NaT contrast) and Na ions with short relaxation times (NaR and NaS contrast). The NaR signal is obtained by an inversion-recovery pulse, whereas the NaS contrast is based on weighted subtraction of images at different echo times (1). Previous work demonstrated a strong association between the Ki-67 proliferation index of brain tumor cells and both, the NaR and NaS signal (1). This finding emphasizes the added benefit of Na-MRI to canonical neuro-oncological imaging as used in clinical routine. In this study, we examined a larger patient population suffering from brain tumors to evaluate the robustness of the Ki-67/NaR association. Furthermore, Na-MRI is compared to conventional T1-weighted gadolinium enhanced (T1W GAD+), T2-weighted (T2W) and FLAIR imaging.

Note: Scanned images are included in the proceedings. Some submitted images were reduced during editing thereby decreasing clarity. Also, refer to the Program Planner. Proceedings Content as of 3/28/2014.

Materials and Methods

Na-MRI was conducted on a 7 Te MR system (Magnetom, Siemens Healthcare, Erlangen, Germany) using a double-resonant (H/Na) quadrature birdcage coil (Rapid Biomed, Rimpar, Germany). Na-MR sequences were based on a 3D density-adapted projection reconstruction technique (2). To detect the tissue Na signal (NaT) relaxation weighting was minimized using a short echo time (TE = 0.35 ms) and a long repetition time (TR = 160 ms). A nominal spatial resolution of $3 \times 3 \times 3 \text{ mm}^3$ was achieved in an acquisition time of TAQ = 10 min 40 s. A second echo (TE = 12 ms) was used to calculate a weighted subtraction image (NaS) as described previously (1). To suppress signal from extracellular fluids such as cerebrospinal fluid, an inversion recovery sequence (NaR) was applied with the following parameters: TE = 0.75 ms; TR = 185 ms; TRO = 16.7 ms; inversion time: TI = 41 ms; TAQ = 9 min 52 s; nominal spatial resolution: $4.4 \times 4.4 \times 4.4 \text{ mm}^3$. Canonical T1w GAD+, T2w and FLAIR imaging was performed on a 3 T MR system (Tim Trio, Siemens Healthcare, Erlangen, Germany). N = 20 patients suffering from naïve brain tumors WHO grade 1 to 4 were measured including 2 Pilocytic Astrocytomas, 2 Astrocytomas, 1 Oligodendroglioma, 4 Anaplastic Astrocytomas, 2 Anaplastic Oligodendrogliomas, 1 Anaplastic Ependymoma, 1 Gliomatosis Cerebri, 7 Glioblastomas. For all patients, histopathologic evaluation of tumor specimens was performed including Ki-67 monoclonal antibody staining. Ki-67 is a cellular marker for proliferation (3) and is known to correlate with tumor growth (4, 5). Na and proton images were coregistered to the individual standard space by FLIRT (part of FSL) (6).

Results

Correlation analyses revealed strong correlations between the NaR signal of the tumor and its Ki-67 index ($r = 0.85$, $p < 0.001$; Fig. 1a) and between the NaS signal and the Ki-67 index ($r = 0.87$, $p < 0.001$). There was no correlation between histopathologic tissue parameters and NaT, conventional T1w GAD+, T2w and FLAIR imaging.

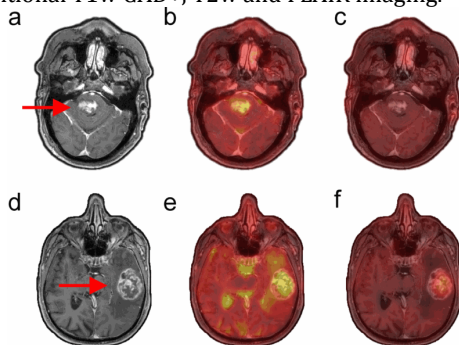


Figure: Exemplary T1w GAD+ (a, d), NaT (b, e) and NaR (c, f) data of a Pilocytic Astrocytoma (PA, WHO 1, a-e) and a Glioblastoma (GBM, WHO 4, d-f) demonstrate the benefit of relaxation-weighted Na-MRI: T1w GAD+ imaging exhibits high signals in both the PA (a) and the GBM (d). A distinction between both tumors is impossible. However, the NaR contrast reveals a low signal of the PA (c) and a high signal of the GBM (f) which enables the correct diagnosis. The improved accuracy of relaxation-weighted Na neuroimaging compared to conventional T1w GAD+ (and T2w and FLAIR imaging; data not shown) is owed to the strong association with the Ki-67 proliferation index of the tumor cells [1].

Conclusions

In this study, we are able to reproduce previous findings (1) on the association between the relaxation-weighted Na

signals (NaR and NaS) and the Ki-67 proliferation index of brain tumors, despite the differing tumor subtypes between both studies. A local cellular energetic breakdown mainly of the Na^+/K^+ ATPase, changes in Na^+/H^+ exchange kinetics (7) and a sustained cell depolarization initiating cell division might represent the pathophysiological correlates of this association (8). All mechanisms result in an elevated intracellular Na^+ concentration, which is reflected by the NaR and NaS contrast. NaT and clinical routine MR sequences including T2, T1 GAD+ and FLAIR imaging failed to detect these specific changes of tumor tissue (cf. Figure). This underlines the limited specificity (9) in tumor characterization of these sequences but also emphasizes the added value of NaR and NaS imaging to conventional neuro-oncological MRI. In future, Na-MRI might help to limit the use of contrast media and stereotactic biopsies for brain tumor diagnosis.

KEYWORDS: Brain Neoplasms, Glioma, MR Imaging

O-325

11:51AM - 11:57AM

Multifrequency Magnetic Resonance Elastography: high resolution assessment of viscoelastic properties in intracranial tumors

M Reiss-Zimmermann¹, K Streitberger², I Sack², F Arlt¹, K Hoffmann¹

¹University Hospital Leipzig, Leipzig, Germany, ²Charité Universitätsmedizin Berlin, Berlin, Germany

Purpose

While magnetic resonance elastography (MRE) is already a clinically available imaging technique for liver examinations, the intracranial utilization lags behind, due to the more difficult accessibility of the skull-surrounded brain tissue. Recent studies proved, that MRE is capable of measuring global changes of the viscoelastic properties of cerebral tissue in aging, as well as in diseases like Alzheimer, Parkinson and Multiple Sclerosis (1-4). The purpose of our study was to implement latest developments of high-resolution multifrequent three-dimensional cerebral MRE for evaluation of focal viscoelastic properties in intracranial tumors.

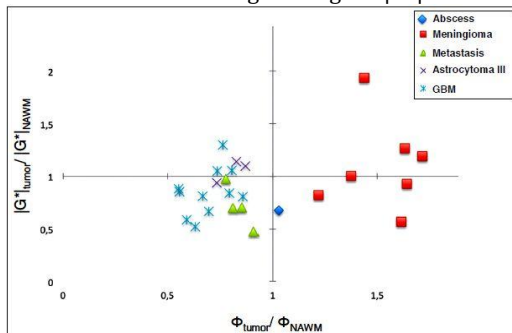
Materials and Methods

Twenty-six patients (63 ± 13 years, 18 female) were included in our study and examined on a clinical 3 T scanner before neurosurgical resection or biopsy. A spin-echo EPI sequence with flow-compensated motion encoding gradient (15 slices, TR/TE 3000/71 ms; FoV $250 \times 187 \text{ mm}$, iPAT=2, spatial resolution $2 \times 2 \times 2 \text{ mm}$ temporal resolution 8 dynamics per wave cycle, scan time 75 sec) was used. Seven harmonic vibration frequencies (30 to 60 Hz, 5 Hz increment) were induced by an acoustic driver, connected to a head cradle. Data postprocessing included the proposed multifrequency dual elasto-visco (MDEV) inversion (5) to generate high-resolution maps of the magnitude $|G^*|$ and the phase angle Φ of the complex shear modulus of the human brain.

Note: Scanned images are included in the proceedings. Some submitted images were reduced during editing thereby decreasing clarity. Also, refer to the Program Planner. Proceedings Content as of 3/28/2014.

Results

The tumor entities included in this study were all located supratentorial and consisted of: glioblastoma multiforme WHO °IV (n=11), anaplastic astrocytoma WHO °III (n=3), meningioma (n=7), cerebral metastasis (n=4), and intracerebral abscess formation (n=1). Compared to the normal appearing contralateral white matter (NAWM) as well as to all other entities, meningiomas appeared to be more viscous giving rise to a higher ratio of $\Phi_{\text{tumor}}/\Phi_{\text{NAWM}}$ as can be seen in Figure 1. Primary brain tumors and cerebral metastases were not distinguishable in terms of $|G^*|$ and Φ . In our group, a trend was delineable that WHO grade II and III tumors are stiffer compared to grade IV glioblastoma. The group of glioblastoma multiforme exhibited the largest range of $|G^*|$ values.



Conclusions

In this pilot study, using 3D multifrequent MRE and MDEV inversion, it is possible to characterize intracranial tumors by their mechanical properties with improved spatial resolution compared to previous work in MRE on tumors (6, 7). We were able to clearly delineate meningiomas from intra-axial tumors, while for the latter group an overlap remains in viscoelastic terms.

KEYWORDS: Brain Neoplasms, Metastases, MR Elastography

Tuesday, May 20
10:30 AM – 12:10 PM
Room 517a

36 - Parallel Papers: New Techniques II

0-905 12:01PM - 12:08PM
BMD Values Derived from Routine Lumbar Spine MDCT
Predict Osteoporotic Vertebral Fractures and Screw
Loosening

B Schwaiger, A Gersing, T Baum, P Noel, C Zimmer, J Bauer
Klinikum rechts der Isar der TU Muenchen, Munich,
Germany

Purpose

Established methods available for measuring bone mineral density (BMD) such as quantitative computed tomography

(qCT) or dual energy x-ray absorptiometry are associated with radiation exposure of the patient. Validating a method to assess BMD in routine lumbar MDCT data could avoid additional radiation exposure and examination time for patients. First aim of this study was to correlate BMD values derived from routine lumbar spine MDCT scans (BMDMDCT) to BMD values obtained from qCT (BMDqCT). Second, we analyzed the use of baseline BMDMDCT values to differentiate between patients with and without baseline fractures and whether these values predict incidental fractures and screw loosening in patients with spondylolysis.

Materials and Methods

In 38 patients (mean age \pm SD 74 \pm 6.5; 25 female), BMD was assessed in qCT as a standard of reference, as well as in sagittal reformations derived from standard MDCT studies without iv contrast. For this purpose, standard built-in PACS measurement tools were used. MDCT-to-qCT conversion equations were calculated and then applied to baseline MDCT scans of further 62 patients (mean age \pm SD 71 \pm 5.8; 29 female), using a linear regression model. After a mean follow-up time of 15 \pm 6 months, patients were re-assessed for incidental fractures (n=62) and screw loosening after spondylolysis (n=49). Correlation analysis was performed using general models adjusting for age, gender, follow-up time and application of intrathecal contrast medium.

Results

The conversion equations

BMDMDCT=0.78xHUMDCTmg/ml (correlation with BMDqCT R²=0.92, p<0.001) for 120 kVp tube voltage and BMDMDCT=0.86xHUMDCTmg/ml (R²=0.81, p<0.001) for 140 kVp were observed, respectively. Seven patients (11.3%) had existing osteoporotic vertebral fractures at baseline while eight patients (12.9%) showed incidental osteoporotic vertebral fractures. Screw loosening was detected in 28 patients (57.1% of patients with spondylolysis). Patients with existing vertebral fractures showed significantly lower BMDMDCT than patients without fractures (p<0.01). At follow up, significantly lower baseline BMDMDCT values were found in patients with incidental fractures and screw loosening after spondylolysis, respectively (p<0.001 each).

Conclusions

This study presented an easy and fast method to obtain converted BMD values from standard lumbar spine MDCT scans. This method may be easily integrated into routine clinical practice using already available standard PACS tools. Converted BMD values are able to differentiate not only between patients with and without baseline fractures, they also are able to show increased risk for incidental fractures and screw loosening in patients with spondylolysis. Thus, such a quantification adds significant information to a standard preoperative MDCT exam of the lumbar spine.

KEYWORDS: CT, Osteoporosis

Note: Scanned images are included in the proceedings. Some submitted images were reduced during editing thereby decreasing clarity. Also, refer to the Program Planner. Proceedings Content as of 3/28/2014.

0-326 10:30AM - 10:37AM
 Permeability imaging of the pituitary gland: a novel application of RADIAL VIBE with GRASP technique

C Rossi Espagnet, L Bangiyev, K Block, J Babb, T Shepherd, G Fatterpekar
 New York University Langone Medical Center, New York, NY

Purpose

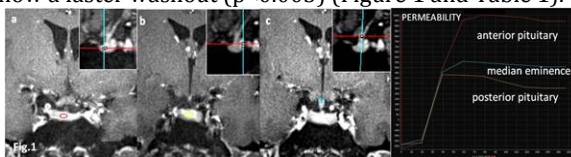
The pituitary gland is located outside of the blood-brain barrier. Dynamic T1-weighted contrast-enhanced sequence is considered to be the gold standard to evaluate this region. However, it does not allow assessment of permeability characteristics of the gland. The purpose of this study was to demonstrate the utility of recently developed Radial-VIBE with GRASP to evaluate permeability characteristics of individual components (anterior, posterior gland and median eminence) of pituitary gland in routine patients.

Materials and Methods

A retrospective study was performed in 79 patients with normal appearing pituitary gland (M:F=20:59). Imaging was performed at 1.5 T and at 3 T. Regions of interest (ROI) were placed in the anterior gland, median eminence, and posterior pituitary gland to generate signal-time curves. A statistical analysis was performed using a paired-sample Wilcoxon signed rank test to evaluate the mean peak values, mean time of maximum enhancement (TME), mean area under the curves (AUC), and mean wash-in and wash-out in the ROIs.

Results

Curves from the posterior pituitary gland and median eminence demonstrate a faster wash-in and TME with a lower peak of enhancement compared to anterior pituitary gland, which shows a slower wash-in, delayed TME and higher peak of enhancement. Compared to the posterior pituitary gland, anterior pituitary and median eminence show a faster washout (p<0.005) (Figure 1 and Table 1).



Measure	Anterior		Posterior		Median Eminence	
	Mean	SD	Mean	SD	Mean	SD
AUC	69980.65	20169.32	37500.10	17701.73	40246.39	16686.70
PEAK	754.94	242.04	439.61	205.67	446.62	192.66
TME	86.55	19.23	58.96	16.23	62.60	18.70
WASHIN	10.92	3.89	9.14	4.20	8.54	3.71
WASHOUT	1.52	1.34	1.90	1.48	1.56	1.27

Conclusions

This validation study, by demonstrating unique signal-time curves distinct for each component of the pituitary gland, confirms the ability of GRASP technique to evaluate the hitherto unexplored permeability characteristics of the pituitary gland.

KEYWORDS: Permeability MR Imaging, Pituitary Gland

0-327 10:37AM - 10:44AM
 Novel Permeability Criteria to Assess Function of Morphologically Normal Pituitary Gland in Patients with Central Endocrinologic Disturbances

C Rossi Espagnet, L Bangiyev, A Davis, K Block, A George, J Babb, G Fatterpekar
 New York University Langone Medical Center, New York, NY

Purpose

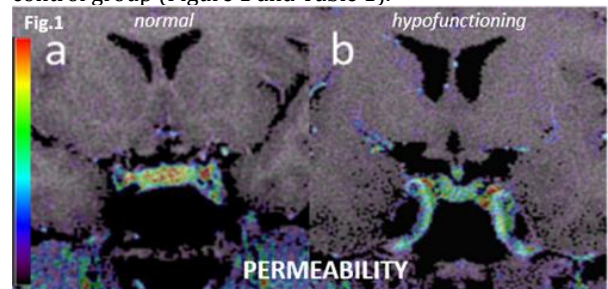
Conventional dynamic pituitary MR imaging (MRI) is routinely employed to evaluate for pituitary lesions in patients with endocrinologic disturbances. However, often times a normal sized pituitary gland with no focal areas of differential enhancement is seen in patients with endocrine disturbances suspected to be of central origin. We hypothesize clinical hypopituitarism without any structural abnormality could be associated with abnormal permeability characteristics of the pituitary gland. The purpose of our study therefore is to evaluate the permeability parameters using radial-VIBE with GRASP in patients with "central" endocrine disturbances and a normal appearing pituitary gland.

Materials and Methods

A retrospective study was performed in 43 patients (M:F =14:29). The control group (group 1) consisted of 33 patients with normal appearing anterior and posterior pituitary glands. Group 2 consisted of 10 patients with clinical and laboratory evaluation consistent with hormonal deficiency of suspected central "pituitary" origin, and no morphological abnormalities on routine dynamic MR imaging. All 43 patients were evaluated on 3 T utilizing radial-VIBE with GRASP. Regions of interest (ROI)-based method was used to obtain signal-time curves (STCs) from the anterior and posterior pituitary gland. Statistical analysis was performed to compare the mean area under the curves (AUC), mean peak, mean time of maximum enhancement (TME), mean washin and washout parameters for the anterior and posterior pituitary glands between the two patient groups.

Results

Signal-time curves from anterior and posterior pituitary gland demonstrated a statistically significant difference (p < 0.05) in the AUC, peak, washin and washout parameters between the patient population when compared to the control group (Figure 1 and Table 1).



Note: Scanned images are included in the proceedings. Some submitted images were reduced during editing thereby decreasing clarity. Also, refer to the Program Planner. Proceedings Content as of 3/28/2014.

TABLE 1	Anterior		Posterior		Median Eminence	
	Mean	SD	Mean	SD	Mean	SD
AUC	69980.65	20169.32	37500.10	17701.73	40246.39	16686.70
PEAK	754.04	242.04	439.61	205.67	446.62	192.66
TME	86.55	19.23	58.96	16.23	62.60	18.70
WASHIN	10.92	3.89	9.14	4.20	8.54	3.71
WASHOUT	1.52	1.34	1.90	1.48	1.56	1.27

Conclusions

This pilot study utilizing radial-VIBE with GRASP demonstrates relative hypoperfusion within the "normal appearing pituitary gland" in patients with "central" endocrinologic disturbances.

KEYWORDS: Permeability MR Imaging, Pituitary Gland

O-328 10:44AM - 10:51AM
Optimizing MR acquisition time for dynamic pituitary gland evaluation utilizing Radial-VIBE with GRASP Reconstruction

C Rossi Espagnet, L Bangiyev, R Jain, K Block, J Babb, G Fatterpekar
New York University Langone Medical Center, New York, NY

Purpose

Dynamic postcontrast T1-weighted sequence remains the gold standard to evaluate the pituitary gland. This sequence is especially utilized to evaluate a microadenoma, the most common indication. The acquisition time for this sequence varies among different institutions ranging from 150 seconds to 180 seconds. Radial-VIBE with GRASP technique allows adequate evaluation for structural permeability providing excellent temporal information with high spatial resolution. The purpose of our study is to evaluate the signal-time curves (STCs) obtained utilizing Radial-VIBE with GRASP technique to optimize the acquisition time for dynamic pituitary gland evaluation.

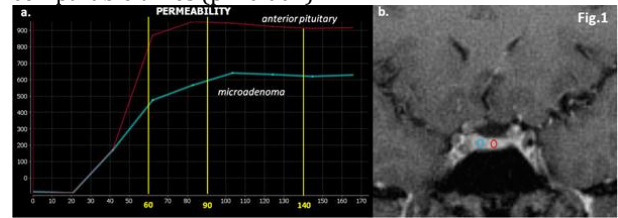
Materials and Methods

A retrospective study was performed in 20 patients with known microadenomas. All patients were evaluated on a 3T MR imaging (MRI). Using GRASP images, ROI-based STCs were generated from normal appearing anterior pituitary gland and the microadenoma to evaluate peak enhancement (PE) values every 10 seconds beginning at 60 seconds (T1) following contrast administration, for a total time period of 140 seconds (T9) (Figure 1). For each time T>1, the mean, standard deviation (SD), median, maximum and the lower and upper limits of a 95% confidence interval of the mean for the percentage change in the peak enhancement was estimated from time T-1 to time T.

Results

The mean PE for the anterior pituitary gland was reached at T = 80 seconds (± 19 seconds) without significant change in the values after time T4 (90 seconds) (Table 1). The PE values for the microadenoma measured from time T1 (60 seconds) to time T4 (90 seconds) showed a statistically significant difference when compared to peak

enhancement values of the anterior pituitary gland at comparable times ($p < 0.001$).



Time T	Mean	SD	Median	Maximum	Lower	Upper
2	9.82	9.97	5.25	30.99	5.16	14.49
3	6.11	6.65	4.52	21.69	3.00	9.23
4	2.00	2.52	1.05	8.53	0.82	3.18
5	2.17	2.55	1.18	8.98	0.97	3.36
6	1.41	0.87	1.06	2.76	1.01	1.82
7	1.38	0.87	0.71	3.28	0.53	1.35
8	0.94	0.87	0.71	3.28	0.53	1.35
9	0.57	0.33	0.62	1.30	0.42	0.73

Conclusions

We successfully demonstrate that an acquisition time of 90 seconds following contrast administration is sufficient to provide adequate dynamic evaluation of the pituitary gland and microadenoma. This significantly shortens acquisition time of dynamic T1-weighted sequences from 150 – 180 seconds as reported in current imaging literature, allowing optimum utilization of magnet scanning time. According to our literature search, this is the first pilot study to evaluate STCs to optimize acquisition time of the dynamic contrast enhanced sequence for pituitary gland evaluation.

KEYWORDS: Permeability MR Imaging, Pituitary Gland

O-329 10:51AM - 10:58AM
Development of an Automated Quantification Method for Cerebrospinal Fluid Dynamics in the Cerebral Ventricles using an MR Spin Labeling Real Time Imaging Technique

T Shiodera¹, S Nitta¹, T Takeguchi¹, M Yui², T Yamaoto², S Yamada³

¹Toshiba Corporation, Kawasaki, Japan, ²Toshiba Medical Systems Corporation, Tochigi, Japan, ³Toshiba Rinkan Hospital, Kanagawa, Japan

Purpose

The Time-Spatial Labeling Inversion Pulse (Time-SLIP) technique, which is based on selective inversion recovery technique, can provide visual information for blood flows and for cerebrospinal fluid (CSF) flows without using contrast medium. Previous studies have evaluated visual assessments of CSF dynamics using the Time-SLIP technique. Our previous work has shown an automated quantification method for CSF dynamics using a half-Fourier fast spin-echo sequence as pseudo cine imaging. The objective of this study is automated quantification of CSF dynamics in the cerebral ventricles using the Time-SLIP real time imaging technique.

Materials and Methods

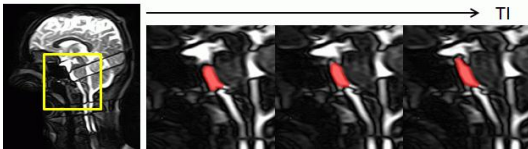
A series of 2D images with incremental inversion recovery times were acquired by 1.5 T MR imaging (MRI) scanner

Note: Scanned images are included in the proceedings. Some submitted images were reduced during editing thereby decreasing clarity. Also, refer to the Program Planner. Proceedings Content as of 3/28/2014.

using Time-SLIP sequence with balanced steady-state free precession (bSSFP) real time imaging. The bSSFP scanning conditions were FOV = 24.0 x 26.3 cm, matrix = 64 x 192, slice thickness = 7 mm, TR/TE = 4.2/2.1, FA = 90, initial inversion time (TI) = 0.6 s and TI step = 0.101 s. Region of interest was outlined automatically based on signal intensity analysis and shape of region for a given point. Subsequently, labeled CSF regions were detected using the image binarization method. Cerebrospinal fluid average speed and total variation was calculated using TI values and the corresponding traveling CSF positions. Correlations between the proposed method and manual annotations of the quantified values were evaluated in the prepontine cisterns.

Results

Thirty-two datasets from four healthy volunteers were studied. The proposed method detected the labeled CSF region as examples shown in Figure 1. The correlation factors between the proposed method and manual annotations were $R^2 = 0.91$ ($p < 0.001$) for the CSF velocity and $R^2 = 0.85$ ($p < 0.001$) for the CSF total variation. The processing time was less than 3 seconds per data.



Conclusions

This paper presented a new automated quantification method of CSF dynamics using the Time-SLIP real time imaging technique.

KEYWORDS: Cerebrospinal Fluid, Image Processing, MR Imaging

O-330 10:58AM - 11:05AM
IVIM Perfusion in Acute Stroke

C Federau¹, S Sumer², F Becce¹, K O'Brien³, R Meuli¹, M Wintermark²

¹CHUV, Lausanne, Switzerland, ²University of Virginia, Charlottesville, VA, ³CIBM, Lausanne, Switzerland

Purpose

Local brain perfusion measurement, either with MR imaging (MRI) dynamic susceptibility contrast (DSC) or CT perfusion (CTP), currently is used clinically in the context of acute stroke to assess altered perfusion, while restriction in diffusion-weighted imaging is used to assess the ischemic core, and their mismatch the salvageable tissue, also called penumbra. Because both DSC and CTP depend on the arterial input function (AIF), both may fail to properly take into account leptomeningeal collateral blood flow supply, which is essential for clinical prognosis (1). Measuring perfusion with intravoxel incoherent motion (IVIM) MRI (2) might theoretically solve this issue, as it is independent on the AIF, and thought to be mainly dependent on the local microvascular perfusion. It also would allow a gain of time, as no iv contrast medium is needed, and therefore, no vein puncture before imaging is

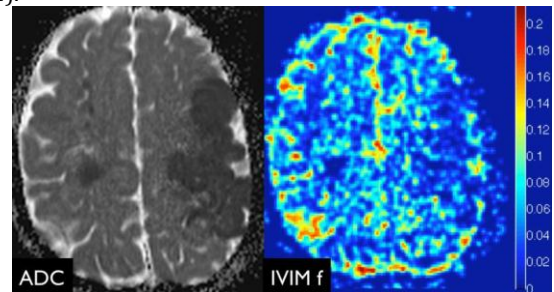
necessary. To our knowledge, only one study of IVIM perfusion fraction measurement in acute ischemic stroke in human patients has been reported (3), without maps, and with somewhat counterintuitive quantitative results, the majority of f values being reported as negative in the infarcted area. In the context of a regain of interest in IVIM as a method to measure brain perfusion (4-6), we re-evaluated IVIM perfusion measurement in the context of acute stroke.

Materials and Methods

Images were collected in patients who presented with symptoms of acute ischemic stroke. Exclusion criteria were onset of symptoms to imaging > 5 days, hemorrhagic transformation, infratentorial lesions, and small lesions < 0.5 cm in minimal diameter. We collected 17 cases (Table 1). Intravoxel incoherent motion images were performed at 3 T, using a spin-echo sequence with embedded Stejskal-Tanner pulsed gradients, with parameters as previously described (4), using 16 b-values from 0 to 900 s/mm² in three orthogonal directions. Quantitative analysis was performed by placing a region of interest (ROI) around the largest stroke area on an axial slice, as defined by reduced apparent diffusion coefficient (ADC), and in the collateral region, avoiding cerebrospinal fluid. The trace of the signal was first averaged for each b value, before fitting the bi-exponential IVIM model (2).

Results

Parametric IVIM perfusion maps showed an area of decreased perfusion fraction f in 14/17 patients (Figure 1). Two patients showed a mismatch, while two other patients showed a not fully overlapping ischemic core and hypoperfusion area, without quantitative mismatch. Quantitative analysis showed high statistically significant decrease in both IVIM perfusion fraction f (0.026 ± 0.019 versus 0.056 ± 0.025 ; $p = 1.1 \cdot 10^{-6}$) and diffusion coefficient D in comparison to the contralateral side ($3.9 \pm 0.79 \cdot 10^{-4}$ versus $7.5 \pm 0.86 \cdot 10^{-4}$ mm²/s; $p = 6.5 \cdot 10^{-21}$).



Patient demographics: age (years), sex, NIHSS clinical severity score, onset of symptoms to IVIM imaging (hours), and number of patients treated with i.v. tPA before imaging. Avg \pm std dev, when appropriate.

Age	56.2 \pm 23.4
Sex	12 males, 5 females
NIHSS at entry	7.7 \pm 5.4
Onset to imaging	45.5 \pm 40.3
Treated with tPA i.v.	6

Conclusions

Intravoxel incoherent motion perfusion measurement is feasible in the context of acute stroke. Because this permits acquisition of both perfusion and diffusion information in a single 3 min MRI sequence, without iv contrast injection, a

Note: Scanned images are included in the proceedings. Some submitted images were reduced during editing thereby decreasing clarity. Also, refer to the Program Planner. Proceedings Content as of 3/28/2014.

significant gain in imaging time could be achieved in the context where minimal time to treatment is seen as the most critical predictor of positive outcome. Further studies should evaluate the potential for IVIM in predicting clinical outcome and treatment response.

KEYWORDS: Ischemia, Penumbra, Stroke

O-331 11:05AM - 11:12AM
Whole Brain Perfusion Imaging at 70 kVp with Adaptive Temporal Sampling: Reduced Dose, Superior Quality and Improved Consistency.

A McLellan, I Corcuera-Solano, R De Leacy, A Doshi, P Pawha, L Tanenbaum
Icahn School of Medicine at Mount Sinai, New York, NY

Purpose

Despite the widespread application of perfusion CT for neurologic steno-occlusive disease, radiation dose concerns remain. In the effort to minimize dose via lower tube current (mA), image quality and signal to noise ratio can suffer. Restricting the sampling period length can lead to inconsistency as variability in cardiac output can mean that scanning ends before venous return to baseline, challenging rendering based on deconvolution principles. Perfusion studies typically employ fixed sampling intervals (every 1-3 seconds) and a limited scanning period (40-50 seconds) with sampling time directly proportional to dose. Inevitably, in a modest percentage of cases, sampling stops before baseline signal is restored, making longer scanning periods desirable. As certain segments of the contrast passage have a lesser need for high sampling frequency, such as the pre-enhancement baseline and the downward slope toward the return to baseline, scanning at variable intervals is appealing: slow (every 3 seconds) during the pre-arrival baseline, fast (every 1.5 seconds) targeting the rise and fall of enhancement and slower (every 7.5 seconds) to extend the temporal sampling window. The recent availability of lower kVp for perfusion scanning also is attractive as a dose reduction method. As 70 kV more closely approximates the k-edge of iodine, lower tube current values and net CTDI values may be acceptable. The purpose of this retrospective study was to evaluate the impact on quality, consistency and radiation dose of these two clinical innovations: the use of lower kV values – 70 rather than the traditional 80 kVp, and the use of longer sampling periods with variable rather than fixed sampling intervals -- by comparing to studies performed with traditional 80 kV and regular sampling within the same institution.

Materials and Methods

Forty consecutive stroke patients who underwent CT perfusion between 1/2013 and 12/2013 were enrolled in this retrospective study. Nineteen low dose 70 kV adaptive CTA perfusion examinations performed on a Siemens AS+ 128 scanner, and 21 80 kV CT performed on a GE Lightspeed VCT scanner were evaluated. All perfusion studies were processed with CT Perfusion 4D on a GE Advantage Workstation 4.6 by a neuroradiologist. Three

experienced neuroradiologists independently subjectively rated overall quality and cortex-white matter differentiation of the CBF, CBF and transit time maps on a three-point scale (Table 1). The first-pass perfusion temporal enhancement curves were analyzed objectively to assess the rate at which each protocol captured the desired portions of the enhancement cycle as intended: fast sampling during the contrast transit through the brain and successful capture of the venous return to baseline. Radiation doses were recorded and compared for all studies.

Results

Qualitative Analysis. The inter-rater reliability in the assessment of image quality parameters was high. Overall image quality was significantly better at 70 kV for all three parameters: transit time ($p=0.01$), CBF ($p=0.02$) and CBV ($p=0.04$). Gray white differentiation with CBV was significantly higher at 70 kV ($p=0.03$) but not statistically different on CBF and transit time maps.

Quantitative Analysis. Dose: The low kV, adaptively sampled protocol was 15% lower in overall dose than the fixed sampling protocol at 80 kV (1538 versus 1831 DLP). The CTDI at 70 kV was 106 and at 80 kV was 193, 55% lower per whole brain pass for the 70 kV protocol. **Temporal enhancement curves:** Analysis of the temporal enhancement curves revealed that with the fixed interval, limited length protocol (38-43 seconds) did not go long enough to capture the venous return to baseline in 53% of cases, provoking a change in protocol for these scanners at our institution at the cost of some increase in dose. The adaptively sampled longer protocol (52 seconds) captured the venous return to baseline in 95% of cases. **Rapid sampling during the critical arterial arrival and washout period** was captured in 100% for both protocols.

Conclusions

Whole brain adaptive perfusion imaging at 70 kVp produces statistically significant improvement in image quality compared to traditional 80 kV acquisitions with greater consistency of capture of the critical phases of contrast passage at lower radiation doses. As low kV and variable sampling capability become more widely available these techniques should be integrated into clinical practice.

KEYWORDS: CT And Stroke, CT Brain Perfusion, CT Perfusion

O-332 11:12AM - 11:19AM
Brain Dynamic Susceptibility Contrast (DSC) Perfusion Using a Reduced Contrast-dose at 3.0T: Comparison of Bayesian Method and Circulant Singular Value Deconvolution (cSVD)

K Nael¹, B Mossadeghi¹, R Khan¹, A Meshksar¹, W Kubal¹, E Krupinski¹, B Ellingson²

¹University of Arizona, Tucson, AZ, ²University of California Los Angeles, Los Angeles, CA

Purpose

Increased use of brain dynamic susceptibility contrast (DSC) perfusion in combination with other enhanced applications such as contrast-enhanced MR angiography (MRA) for evaluation of patients with acute stroke (1) or with DCE perfusion in evaluation of brain tumors (2), has

Note: Scanned images are included in the proceedings. Some submitted images were reduced during editing thereby decreasing clarity. Also, refer to the Program Planner. Proceedings Content as of 3/28/2014.

necessitated a demand for contrast dose reduction. The lower signal to noise ratio (SNR) associated with reduced contrast dose remains a limiting factor (3). Bayesian probabilistic method, which is inherently less sensitive to noise (4) has the potential for more accurate calculation of cerebral perfusion in low-dose protocols. The purpose of this study was to establish the feasibility of a reduced contrast dose (0.05 mmol/kg) brain DSC perfusion using Bayesian method and compare the result with block-circulant singular value deconvolution (cSVD) that is used routinely in clinical practice.

Materials and Methods

In this prospective study, 20 patients (12 male, 34-70 years old) who were referred for contrast-enhanced brain MRI underwent two consecutive DSC-perfusion (gradient-EPI, TR/TE: 1450/22 msec, FA 90°) at 3 T using two different doses of gadolinium (Gd). A total of 0.1 and 0.05 mmol/kg of Gd was used for full-dose (FD) and half-dose (HD) scans which were performed eight minutes apart. Using a FDA approved software (Olea Medical, La Ciotat, France), all DSC scans were processed with cSVD and Bayesian probabilistic method. Coregistered parametric maps of cerebral blood flow (CBF), cerebral blood volume (CBV) and mean transit time (MTT) from both FD and HD scans were analyzed for quantitative measurement along the middle cerebral artery distribution using a ROI-based analysis. The quantitative perfusion values between the cSVD and Bayesian methods in FD and HD groups were compared with regression analysis and unpaired t-test.

Results

The mean of SNR values was significantly ($p < 0.0001$) lower in the HD group (12.9) compared to FD group (20.1). Using Bayesian method, the mean of CBF (ml/100 g/min), CBV (ml/g) and MTT (sec) values in FD/HD group were 48.6/38.9 ($p=0.16$), 1.8/1.5 ($p=0.1$) and 3.6/3.4 ($p=0.9$) respectively. Using cSVD method, the mean of CBF (ml/100 g/min), CBV (ml/g) and MTT (sec) values in FD/HD group were 44/25 ($p < 0.0001$), 1.9/1.3 ($p=0.004$) and 4/5.2 ($p=0.01$) respectively. In FD scans, there was no statistically significant difference between Bayesian and cSVD for calculation of CBF ($P=0.52$), CBV ($p=0.61$) and MTT ($p=0.17$). In HD scans, there was statistically significant difference between Bayesian and cSVD for calculation of CBF ($P=0.009$), and MTT ($p=0.001$) but not for the CBV values ($p=0.14$).

Conclusions

Bayesian probabilistic method is inherently less sensitive to low SNR (4) and outperforms cSVD in HD group where the SNR is lower by approximately 36%. Reduced contrast dose (0.05-mmol/kg) DSC perfusion of the brain is feasible at 3.0 T using Bayesian probabilistic method with comparable quantitative results to 0.1 mmol/kg.

KEYWORDS: Deconvolution, Dose Reduction, Dynamic Susceptibility Contrast-Enhanced

O-333 11:19AM - 11:26AM
Patient Motion: Small Annoyance or Call To Action?

J Andre¹, M Hoff¹, M Mossa-Basha², B Bresnahan¹, W Cohen¹

¹University of Washington, Seattle, WA, ²University of Washington, Kirkland, WA

Purpose

Patient motion frequently degrades MR examinations, often resulting in suboptimal image quality that negatively impacts radiological interpretation. While many motion-correction techniques have been proposed (1-4), often the most promising methods are available in the research domain only. Additionally, the prevalence of patient motion that results in significantly degraded MR examinations is documented poorly in the literature. We sought to assess the prevalence of significant patient motion in MR examinations of the neuroaxis at an academic level 1 trauma center. Within our population there are a wide range of patients and illnesses and a focus on neurological diseases (especially vascular, traumatic, and infectious), and a large spine population (both traumatic and degenerative).

Materials and Methods

HIPAA and informed consent were waived. The patient population presenting for MR imaging at our institution is comprised of ~50% inpatient (IP) and emergency department (ED) patients and ~50% outpatients (OP). This study included manual review of one full calendar week of MR examinations sent to the picture archiving and communication system (PACS). All exams were performed at a single institution on three different MR scanners: a 1.5 T OP only scanner, and 1.5 T and 3 T in-hospital scanners capable of accommodating IP and OP examinations. All patient images were reviewed manually at a PACS station for the detection of significant patient motion; subtle movement within the globes, pulsation artifact, and mild interleaved motion artifacts were generally disregarded.

Results

Seventy percent of the MR examinations performed at our institution are of the neuroaxis (brain, head & neck, and spine). The remaining 30% primarily involve imaging of the musculoskeletal system (~25%), with some general body MR imaging (MRI) performed (~5%). In this study, 175 total MRI examinations were completed in one calendar week (53.1% were OP examinations; 46.9% were IP and/or ED examinations). Of these, 55 (31.4%) were sent to PACS with at least some motion degradation (47.6% of IP/ED exams; 17.2% of OP exams). Within the 55 motion degraded exams, 29 contained additional "repeat" sequences sent to PACS (16.6% prevalence among total cases), for which 27 of these (49.1% of all motion degraded exams) were examinations of the brain, head and/or neck (including MR angiograms), representing 15.4% of total completed examinations. Thus, a total of 84 sequences were motion degraded, and 47 of these were dedicated to imaging the human brain (56%). These numbers likely represent an underestimation of the exact prevalence of motion degradation affecting MR examinations, since

Note: Scanned images are included in the proceedings. Some submitted images were reduced during editing thereby decreasing clarity. Also, refer to the Program Planner. Proceedings Content as of 3/28/2014.

partially completed sequences and failed examinations not sent to PACS were not included in our evaluation.

Furthermore, examinations requiring sedation for motion control were not differentiated. While an exact dollar amount is difficult to calculate given complex and nontransparent hospital costs, the current reimbursement scale, the variability in sedation requirements, and in-hospital referral and practice patterns, we estimate the cost to the hospital in correcting patient motion may be as much as \$813/hour* (\$13/min), which can be lost due to patient motion (lower than the associated outpatient reimbursement rate for MR examinations). This would represent a cost, using conservative estimates, of \$5,694 per week at our institution, assuming 5-minutes lost per repeat sequence.

Conclusions

Patient motion represents a frequent cause of MR image degradation affecting up to 31% of neuroaxis MR examinations in this patient population, similar to a prior report that significant motion may be seen in 10-42% of images (based on computed percent of missing data) (5). Motion degradation and repeat sequences represent an additional, unclear cost not reimbursed in the current system. Since the indication for patient sedation is multifactorial (and may include the anticipation of motion), this may increase motion-related imaging costs, which we conservatively estimate to approach \$296,092.00/year. The retrospective nature of this study, small sample size, and short duration may appear to weaken the results; however we think these costs are underestimated given that not all attempted/failed examinations may have been captured by this study design. Patient motion represents a formidable challenge, potentially affecting the global MR community, and may result in significant inefficient use of hospital resources and suboptimal radiological interpretations. Elimination of wasted effort and unnecessary work is increasingly important as payors focus on controlling reimbursement for medical services as part of the general trend toward decreasing the cost of U.S. medical care. The results of this study suggest that this represents an opportunity to improve efficiencies in health costs and that more attention should be directed toward providing practical solutions to this dilemma.

KEYWORDS: Economics, Motion Correction

O-334

11:26AM - 11:33AM

Acute Ischemic Stroke in Non-Human Primates: A Validation Study Using Near Infrared Spectroscopic Tomography for Cerebral Monitoring of Stroke and Intracranial Hemorrhage

S Mangla, F Barone, T Gevorgyan, H Graber, D Pfeil, Y Xu, J Libien, J Charchafli, J Kral, R Barbour, D Lee
SUNY Downstate Health Science Center, Brooklyn, NY

Purpose

Near-infrared spectroscopic (NIRS) tomography is an evolving and exciting portable technology for continuous cerebral monitoring in critical care and operative

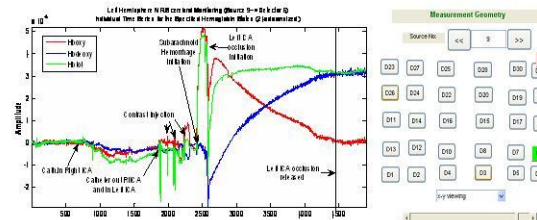
procedures. We developed and validated an endovascular acute ischemic stroke nonhuman primate (NHP) model with NIRS monitoring of acute cerebral ischemic and hemorrhagic events in real-time.

Materials and Methods

During stroke induced by unilateral microcatheter occlusion of the middle cerebral artery, we used a NIRS imager with a 270 source-detector (5 X 6 measurement geometry; see Figure: Individual Channel Monitoring) channel array for cerebral monitoring of anesthetized Bonnet Macaques. We performed experiments in five Macaques using three hours of reversible unilateral occlusion of the middle cerebral artery (MCA) to induce ischemia/stroke, with continuous recordings of total hemoglobin (Hbtot) levels and hemoglobin saturation (HbsO2) from each channel comparing pre/post events and bilateral hemisphere measurements. Near-infrared spectroscopic data also were used to construct three-dimensional tomographic functional images of the scalp and brain. Comparative analyses were performed for pre- and post-stroke events within and between cerebral hemispheres. We also performed immediate post-stroke CT perfusion, MR imaging (MRI), and postmortem brain histopathology to confirm ischemic and hemorrhagic stroke injury.

Results

Ischemia was achieved in five of five animals as confirmed by CT perfusion and/or MRI diffusion imaging and pathology at autopsy. After refinements in the NIRS monitoring protocol during the first three experiments, successful recordings were obtained in the last two subjects. Inadvertent vessel perforation in one case allowed us to study subarachnoid hemorrhage. Near-infrared spectroscopic tomography findings correlated with histopathology, CT, and MRI during acute cerebral ischemia and subarachnoid hemorrhage in these two subjects. Significant localized decreases in Hbtot resulting from contrast boluses mimicking transient ischemia were noted [19 injections: statistically significant left-right differences in 15 (79%) cases ($p < 0.0001$); inter-hemispheric differences had expected directionality in 18 of 19 (94.7%) cases]. Regional verapamil injections increased Hbtot levels on the ipsilateral side ($p = 2 \times 10^{-8}$), whereas diffuse subarachnoid hemorrhage produced bilaterally increased Hbtot compared to baseline levels ($p = 0.0001$). Following microcatheter-induced cerebral ischemia, Hbtot levels fell in the region corresponding to the occluded artery, compared to the same region in the contralateral cerebral hemisphere ($p < 0.0001$).



Conclusions

Endovascular microcatheter occlusion of the MCA successfully created acute strokes in anesthetized adult

Note: Scanned images are included in the proceedings. Some submitted images were reduced during editing thereby decreasing clarity. Also, refer to the Program Planner. Proceedings Content as of 3/28/2014.

male nonhuman primates. Near-infrared spectroscopic tomography accurately captured both cerebral ischemia and hemorrhage in real time. These findings demonstrate the potential of NIRS tomography for noninvasive cerebral monitoring in a critical care setting.

KEYWORDS: Acute Stroke, Animal Model, Functional Brain Mapping

O-335 11:33AM - 11:40AM
ASL Reveals Subtle Perfusion Changes in DWI-Negative TIA: Comparison with DSC

B Yoo¹, J Lee², J Qiao¹, D Wang¹, D Liebeskind¹, N Salamon¹
¹David Geffen School of Medicine at University of California Los Angeles, Los Angeles, CA, ²University of California, Los Angeles, Cerritos, CA

Purpose

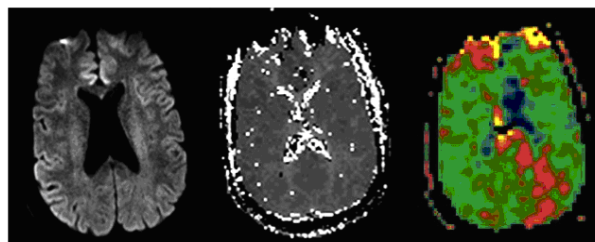
Determining a vascular etiology for transient ischemic attack (TIA) symptoms and negative diffusion-weighted imaging (DWI) is a clinical challenge. The purpose of this study is to compare arterial spin labeling (ASL) and dynamic susceptibility contrast-perfusion (DSC) in the detection of perfusion deficits in DWI-negative TIA.

Materials and Methods

Pseudocontinuous ASL with 3D background-suppressed gradient and spin-echo with four second post-label delay and DSC-perfusion were acquired in 145 patients presenting with stroke-like symptoms. All patients had DWI-negative scans and MR angiographies (MRAs) without significant intracranial stenosis. Arterial spin labeling arterial-transit-time (ATT) and DSC-time-to-peak (TTP) maps were generated and scored from 1-3 based on the presence and conspicuity of perfusion deficits by two independent observers blinded to patient history. Disagreements between the observers were resolved by consensus. The laterality of the perfusion disturbance was recorded in patients with hemispheric TIA for comparison with neurologic symptoms at onset.

Results

Arterial spin labeling detected 23 perfusion defects in DWI-negative TIA (16%), while DSC detected five perfusion deficits (3%). Of the 23 perfusion defects detected by ASL, 14 patients had symptoms referable to a specific hemisphere; nine of these lesions were lateralized to the symptomatic hemisphere. Of the five perfusion defects detected by DSC, one of these lesions was lateralized to the symptomatic hemisphere. The average conspicuity ratings on ASL ATT maps was 1.2 ± 0.49 versus 1.05 ± 0.27 on DSC TTP maps ($p=0.00164$).



DWI

DSC

ASL

Conclusions

Arterial spin labeling-perfusion may be more sensitive than DSC-perfusion in the detection of subtle perfusion deficits in patients presenting with TIA symptoms and DWI-negative MRI.

KEYWORDS: Arterial Spin-Labeling, Dynamic Susceptibility Contrast-Enhanced, TIA

O-336 11:40AM - 11:47AM
MEG Delta wave changes related to Impact location in High School Football

J Urban¹, L Miller², E Davenport¹, J Maldjian¹, C Whitlow¹, A Powers¹, J Stitzel¹

¹Wake Forest University School of Medicine, Winston-Salem, NC, ²Wake Forest University, Winston-Salem, NC

Purpose

Injured brain tissue can produce low-frequency signals in the delta band (0-4 Hz) that are measurable with magnetoencephalography (MEG) (1). The purpose of this study is to determine if the location on the helmet with the greatest exposure to head impacts during a season of high school football is associated with detectable changes in MEG delta band power.

Materials and Methods

Head impact exposure was measured by instrumenting the helmets of 31 high school football players (ages 14-18) with helmet-mounted accelerometer arrays to measure linear and rotational acceleration using the head impact telemetry (HIT) system. Helmet impact locations were computed as azimuth (AZ) and elevation (EL) relative to the center of gravity of the head. Impact locations were divided into equally spaced increments of AZ and EL. Peak linear acceleration within each increment was summed to compute the cumulative linear acceleration experienced by the athlete to each impact increment. The AZ/EL increments were converted to Cartesian coordinates and mapped to MNI space. The impact location with the greatest exposure was correlated visually with the location of greatest change in delta wave power. Eight minutes of eyes-open, resting-state MEG data were acquired for each subject using a 275 channel CTF whole-head system pre and postseason, and structural MR imaging (MRI) was acquired using a 3 T Siemens Skyra scanner for coregistration. Using the SPM12b software, the MEG data were down-sampled to 100Hz, baseline corrected, band-stop filtered at 60Hz, band-pass filtered to 1-4Hz (delta spectrum), and divided into 10000ms epochs.

Note: Scanned images are included in the proceedings. Some submitted images were reduced during editing thereby decreasing clarity. Also, refer to the Program Planner. Proceedings Content as of 3/28/2014.

Magnetoencephalographic data then were projected into standard (MNI) source space using the Bayesian group inversion and greedy search constraint within SPM. These data for each subject were exported to a 4D file where each voxel represented the power for the delta range for each 10000ms epoch. Two athletes sustained clinically diagnosed concussions and were excluded from this analysis. Impact locations with the greatest exposure were compared visually with areas of greatest increase in delta band power from pre to postseason.

Results

Table 1 demonstrates the HITS maximum impact locations and brain areas of increased MEG delta power. For most of the head impact locations, coup and contra-coup relationships were apparent in the MEG spatial locations. Players with frontal impacts tended to have increased MEG delta wave changes in the occipital lobes, particularly near the falx.

Table 1: Impact Locations and increased delta waves

Impact	Occipital	Frontal	Parietal
Front: 18	12	1	5
Top: 4	3	0	1
Top/Front: 4	0	4	0
Back: 2	2	0	0

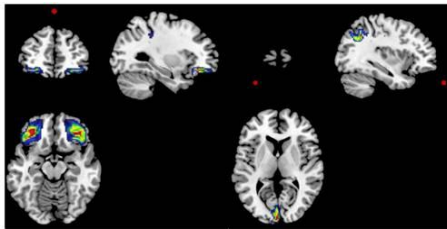


Figure 1: Maximum Impact location (red dot) and MEG delta wave power maps for 2 subjects.

Conclusions

The impact location with the greatest exposure in high school football players may demonstrate relationships to areas of increased brain MEG delta wave activity. This adds to a growing body of literature that a season of high school football can result in brain changes that have been associated with mTBI, even in the absence of clinically diagnosed concussion.

KEYWORDS: Biomechanical, Concussion, MEG

O-337 11:47AM - 11:54AM

The accuracy of Flat Detector CT Cerebral Blood Volume Mapping Source Images in Diagnosing Intracranial Arterial Stenosis

S Hung, W Guo, C Lin
Taipei Veterans General Hospital, Taipei, Taipei

Purpose

Flat detector cerebral blood volume mapping (FDCT-CBV) can provide intracranial hemodynamic information in the angiographic suite without patient transfer. CTA-like datasets can be reconstructed from the fill-run of

FDCT-CBV. The aim of our study was to evaluate the reliability of FDCTCBV source images for detection of intracranial stenosis and occlusion with digital subtraction angiography (DSA) as the reference.

Materials and Methods

Eleven DSA exams were included in this retrospective analysis. FDCTCBV and DSA were performed simultaneously for all the patients with suspected acute infarction or post-SAH vasospasm. Axial, coronal and sagittal maximum intensity projections were reconstructed from the source images of FDCT-CBV. The imaging quality and degrees of stenosis were read by two independent neuroradiologists, who were both blind to the results of DSA.

Results

The imaging quality of the reconstructed FDCT-CBV source images was all sufficient for diagnosis. The intraclass correlation between two raters was excellent (ICC = 0.876). The FDCT-CBV source images had an averaged sensitivity of 86.6% and a specificity of 62% for detecting intracranial stenosis ($\geq 50\%$) compared with DSA.

Conclusions

Flat detector cerebral blood volume mapping can provide valuable intracranial hemodynamic information by using the angiographic C- arm FDCT without patient's transfer. The reconstructed source images of FDCT-CBV can be a feasible and time-saving tool for evaluating intracranial vasculature.

KEYWORDS: Flat-Detector Cone-Beam CT, Flat-Panel Angiographic CT, Vasospasm

O-338 11:54AM - 12:01PM

CT Metal Artifact Reduction in the Spine: Can an Iterative 3D Reconstruction Technique Really Improve Visualization?

A Kotsenas¹, G Michalak¹, D DeLone¹, F Diehn¹, K Grant², C McCollough¹, J Fletcher¹

¹Mayo Clinic, Rochester, MN, ²Siemens Healthcare, Rochester, MN

Purpose

Metal-related artifacts from spine instrumentation can obscure relevant anatomy and disease in neuroimaging. We evaluated the utility of a new prototype three-dimensional iterative metal artifact reduction (3D-IMAR) technique for spine CT.

Materials and Methods

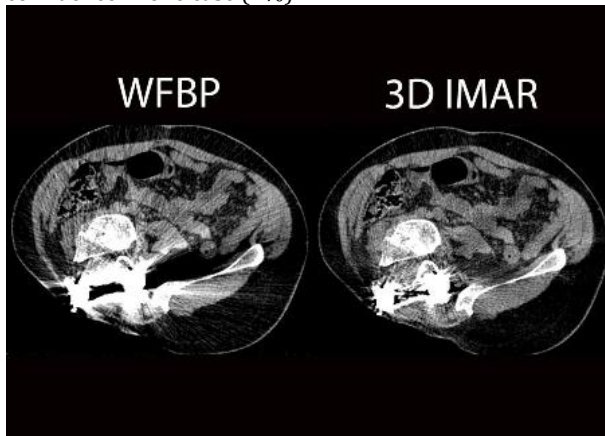
After IRB approval, we performed a retrospective analysis of imaging data collected between July 2012 and August 2013. Inclusion criteria were prior instrumented fusion and CT imaging of the spine (Definition FLASH; Siemens Healthcare). Computed tomography (CT) images were reconstructed using weighted filtered back projection (WFBP) and a prototype 3D-IMAR using spine hardware setting, 0.6mm slice thickness and B35s kernel. Two neuroradiologists (ALK, DRD) reviewed both WFBP and 3D-IMAR exams in soft tissue (ST) and bone windows in consensus. On ST window settings, the paravertebral

Note: Scanned images are included in the proceedings. Some submitted images were reduced during editing thereby decreasing clarity. Also, refer to the Program Planner. Proceedings Content as of 3/28/2014.

anatomy was given an overall visualization score in the region of the spinal hardware (0= totally obscured to 5 = seen with high confidence), with a separate artifact score (analogous 0-5 scale, 0 worst) given in the region of the worst visualized anatomical structure. Using bone windows, the angle (degrees) of vertebral cortex obscured by artifact and length of "flame" artifact (lower-attenuation linear projection from ends of hardware, mm) also were measured. Radiologists estimated impact on diagnostic confidence (unclear, probable or definite increase or decrease). Statistical analysis was performed using two-tailed paired t-tests.

Results

Sixty-eight patients met inclusion criteria with one failure of 3D-IMAR (additional metallic dental work). In the ST images, the mean visualization scores for overall anatomical appearance were 1.38 and 2.79 for WFBP and 3D-IMAR image respectively ($p < 0.0001$). The mean artifact scores were 0.85 and 2.44, respectively ($p < 0.0001$). There was overall improvement in visualization and artifact scores > 1 point in 55 and 60 cases, respectively. Mean angular obscuration of the vertebral body cortex for WFBP and 3D-IMAR images were 36 and 16° respectively ($p = 0.002$). Mean "flame" artifact lengths were 29 mm and 11mm, respectively ($p < 0.0001$). Iterative metal artifact reduction resulted in probable or definite improvement in diagnostic confidence in 24 (36%) and 22 (33%) cases, respectively, and decreased confidence in one case (1%).



Conclusions

The prototype 3D-IMAR improves anatomical visualization and reduces metal artifacts by subjective and objective measurement, resulting in improved diagnostic confidence in the large majority of patients.

KEYWORDS: CT Artifacts, Spinal Instrumentation

Tuesday, May 20
10:30 AM – 12:00 PM
Room 520

37 - Parallel Papers: Pediatrics:
Neonatal and Developmental/
Metabolic

O-345

11:12AM - 11:19AM

Study of Cerebro-Cerebellar Connectivity Development in Preterm Neonates Using MR Imaging Tractography

M Thompson¹, D Ferriero², T Flynn², O Tymofiyeva², A Barkovich³, D Xu²

¹University of California Berkeley-San Francisco, Berkeley, CA, ²University of California San Francisco, San Francisco, CA, ³University of California San Francisco Medical Center, San Francisco, CA

Purpose

The cerebellum has been associated with a wide variety of normal motor and nonmotor functions and behaviors. It serves a vital role in normal development, and developmental impairment in the cerebellum has been correlated with motor, behavior, attention, socialization, and cognition deficits (1). Early diagnosis of abnormalities in the white matter microstructure connecting this crucial region with the cerebral cortex will allow for earlier identification of children who require clinical intervention. This will enable targeted therapy to be provided as early as possible and potentially result in improved clinical outcomes. With this aim in mind, this study characterized typical development of cerebro-cerebellar connectivity as indicated by MR imaging (MRI) tractography streamlines in preterm neonates with good outcome on neuromotor scores at six months of age.

Materials and Methods

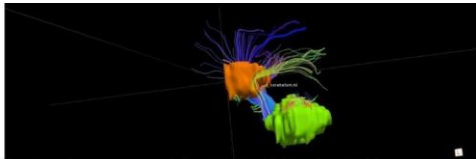
As part of an ongoing study at the University of California, San Francisco, 23 diffusion tensor imaging (DTI) scans were taken of 19 neonates born prematurely [gestational age of 25-32 weeks, postmenstrual age (PMA) of 30-40 weeks at time of scan]. A 3 T GE MR scanner was used and the images were collected using half-Fourier SE EPI, with a FOV of 25.6 cm, 128x128, 2 mm slice thickness, min TE, 30 directions, b-value 600 s/mm². The cerebellum and thalamus regions of interest (ROIs) composed of the entire cerebellum and thalamus were manually selected using the TrackVis (2) tool for analyzing diffusion tractography. These regions were connected by streamlines, mathematical representations of white matter tracts based on the varying diffusivity of water through the neural tracts of the brain. The spatial extent of the streamlines connecting the regions (corrected for the total number of voxels present in the brain) as well as the average fractional anisotropy (FA) over these voxels were calculated for each subject. Of the 23 neonatal scans that

Note: Scanned images are included in the proceedings. Some submitted images were reduced during editing thereby decreasing clarity. Also, refer to the Program Planner. Proceedings Content as of 3/28/2014.

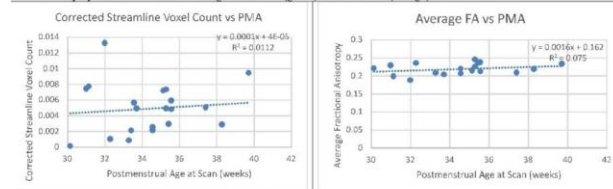
were analyzed, three were excluded because no streamlines connected the ROIs, indicating a tractography error. A further two scans were excluded from FA analysis for values more than two standard deviations outside of the mean, leaving 20 scans of postmenstrual ages of 30.4-39.71 weeks for streamline spatial extent analysis and 18 scans for FA analysis.

Results

Both the spatial extent of streamlines connecting the regions and the average FA showed an increasing trend with PMA of the neonate at the time of the scan (See Figure). A linear regression model of the relation between the corrected spatial extent of the streamlines and the PMA resulted in $r^2=0.0112$ and $p=0.6572$. A linear regression model of the relation between the FA and the PMA resulted in $r^2=0.0750$ and $p=0.2716$. The FA values ranged between 0.1876 and 0.2449.



TrackVis display of streamlines connecting cerebellum (green) and thalamus (orange) ROIs.



Scatter plots of the individual data of the association between the spatial extent of streamlines (corrected for the total number of voxels in the brain) and PMA at MRI scan.

Conclusions

Both streamline voxel count and FA values increased slightly with PMA in the final stages of development preceding term-equivalent age. The range of the FA values and this increase with PMA is consistent with previously reported FA values during this developmental period in other white matter regions (3). This mild trend to increase both FA and streamline count indicates cerebro-cerebellar connectivity may develop faster in the final stages of development preceding term-equivalent age. It should be noted that both streamline spatial extent and FA as measures of connectivity must be interpreted with care, as streamline voxel count is not a direct indicator of axonal fiber volume and FA is not a direct measure of white matter integrity (4). However, the short, direct streamlines connecting the cerebellum and the thalamus were selected as a measure of cerebro-cerebellar connectivity to avoid errors due to fiber crossings, curvature, length and branching. By investigating the connectivity in neonates who have shown good neuromotor scores at six months age, we have developed a basis of comparison for further study of atypically developing neonates. Future directions include investigating this measure in premature neonates with poor neurological outcome.

KEYWORDS: Cerebellum, Fractional Anisotropy, Neonatal

0-339

10:30AM - 10:37AM

Brain Development and Myelination is Influenced by Route of Nutrition in a Preterm Pig Model

A Choudhri¹, K Buddington², H Cohen¹, R Buddington²

¹University of Tennessee Health Science Center, Memphis, TN, ²University of Memphis, Memphis, TN

Purpose

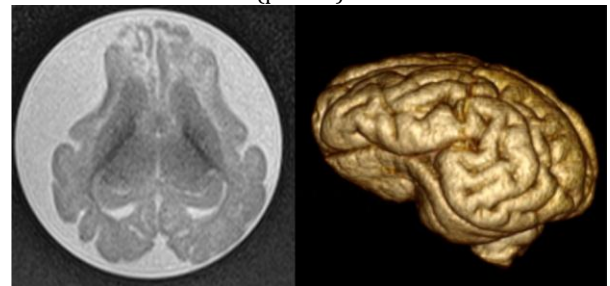
Perinatal brain development is sensitive to nutrition. Preterm infants are at greater risk of behavioral, cognitive, and motor developmental impairment. Intensive care unit (ICU) support of preterm infants is often reliant upon long-term parenteral nutrition (PN), however the impact of this on brain development as opposed to enteral nutrition (EN) is unknown. We used a preterm pig model of neonatal ICU support to evaluate the differences of EN and PN on brain growth and myelin maturation.

Materials and Methods

Eight preterm pigs harvested by caesarian section at 92% of term gestation were randomized to EN (n=4) and PN (n=4). After 12 days of support in a preterm-pig neonatal intensive care unit, animals were euthanized and the brains were explanted. Brains were weighed, formalin fixed, and evaluated using high spatial resolution T1-, T2-weighted MR imaging (MRI) and diffusion tensor imaging on a 3 T scanner. MR images were reviewed in a blinded manner by a neuroradiologist and the extent of myelination in the corticospinal tract, corticobulbar tract, and optic radiations were assessed on a four-point Likert Scale.

Results

All pigs survived the 12 day observation period without need for ventilator support. Brains of pigs receiving EN weighed 32.9 ± 1.8 g, compared to 27.9 ± 2.0 g for pigs dependent upon PN ($p=0.009$). The PN group had higher somatic growth with a $73 \pm 11\%$ gain from birth weight, compared to $30 \pm 2\%$ increase in the EN pigs ($p<0.001$). Myelination in the pyramidal tracts and optic radiations was more mature, and involved a larger volume of white matter in the EN brains ($p<0.05$).



Conclusions

Brain volume and myelination are impacted by route of nutrition in preterm pigs harvested at a stage of development analogous to late preterm humans. In this model of 12 days of NICU care, PN fostered higher somatic growth, whereas EN elicited greater growth in brain mass and accelerated myelin maturation in visual and motor pathways. These findings are novel and correspond with the developmental impairment often reported for preterm

Note: Scanned images are included in the proceedings. Some submitted images were reduced during editing thereby decreasing clarity. Also, refer to the Program Planner. Proceedings Content as of 3/28/2014.

infants. Parenteral nutrition often is administered to preterm infants to reduce complications such as necrotizing enterocolitis, however PN may compromise brain development compared to EN, independent of somatic growth.

KEYWORDS: Brain Development, Myelination

O-340 10:37AM - 10:44AM
Fetal MR Quantitative Ontogenetic Study: Progressive Normal Relative Diminution of the Mesencephalon Through Fetal Development

V Kalra¹, C Filippi², S Saulja³, L Kier¹
¹Yale University School of Medicine, New Haven, CT, ²Columbia University, New York, NY, ³Berkeley Medical Center, Martinsburg, WV

Purpose

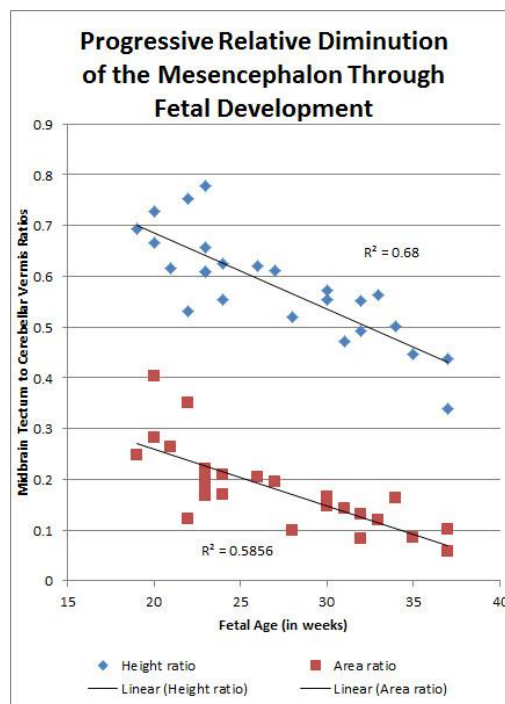
To address the appearance of the disproportionately large size of the quadrigeminal plate in the second trimester, sometimes mistaken for causing aqueductal stenosis in fetuses with isolated bilateral and third ventricular enlargement. We perform a quantitative ontogenetic study using midsagittal T2-weighted fetal MR images to measure the size ratios of the mesencephalon, specifically the quadrigeminal plate, compared to the cerebellar vermis through fetal development.

Materials and Methods

Two hundred fetal MR images (MRIs) performed at a single, large academic institution were evaluated retrospectively after obtaining IRB approval. Studies were excluded if imaging findings demonstrated a fetal neurologic abnormality, if no diagnostic midsagittal T2-weighted fetal MR images were acquired, or if estimated fetal age by either ultrasound or last menstrual period was not available. Twenty-five studies met inclusion criteria. Estimated fetal age ranged from 19 to 37 weeks (mean 27 weeks, SD 5.5 weeks). Height and freehand region of interest (ROI) areas of the quadrigeminal plate (midbrain tectum) were used for the mesencephalon. Height and freehand ROI areas of the cerebellar vermis were used for baseline measurement. Linear regression analyses of mesencephalon to cerebellar vermis height and area ratios were performed to determine R squared values. Spearman's rank correlation coefficients were calculated to determine statistical dependence of height and area ratios to fetal age. Spearman's rank-order calculations were performed to determine p values.

Results

The relative sizes of the midbrain tectum to the cerebellar vermis decreased with greater fetal age. Both mesencephalon to cerebellar vermis height and area ratios demonstrate an inverse relationship to fetal age. Height ratios demonstrated an R squared value of 0.68, a Spearman rho of statistical dependence of -0.82, and a p value of < 0.00001. Area ratios demonstrated an R squared value of 0.59, a Spearman rho of statistical dependence of -0.83, and a p value of < 0.00001.



Conclusions

The disproportionately large relative size of the quadrigeminal plate to the cerebellar vermis, especially in the second trimester, is a normal phase of fetal development and should not be mistaken for causing aqueductal stenosis. Fetal MR quantitatively demonstrates a strong inverse linear size relationship between the mesencephalon and the cerebellar vermis on both height and area ratios. These findings are consistent with ontogenetic, phylogenetic, qualitative, and anatomical fetal studies previously published. Recent advances in fetal MR imaging with rapid, high spatial resolution sequences allow for quantitative ontogenetic studies to be performed.

KEYWORDS: Embryology, Neonatal, Neonatal MR Imaging

O-341 10:44AM - 10:51AM
Fetal brain injury in survivors of twin pregnancies complicated by demise of one twin as assessed by in utero MR imaging

F Williams¹, P Griffiths²
¹Royal Hallamshire Hospital, Sheffield, UK, ²University of Sheffield, Sheffield, UK

Purpose

Twin pregnancies are the commonest type of multiple pregnancy, occurring in 2% of pregnancies and twin pregnancies are considered high risk. In a particular subtype both types share the placenta, i.e., are monozygotic. The shared placenta that defines monozygotic pregnancies often contains blood vessels that may carry blood to either fetus and can be the source of potentially serious problems. If one fetus in a monozygotic pregnancy dies there is opportunity for either hemodynamic changes to affect the other fetus or for

Note: Scanned images are included in the proceedings. Some submitted images were reduced during editing thereby decreasing clarity. Also, refer to the Program Planner. Proceedings Content as of 3/28/2014.

harmful blood-borne materials (e.g., embolus, substances affecting clotting) to pass from the dead twin to the healthy one. In this situation there is a high risk of injury to the brain of the surviving twin. One complication of monochorionic twin pregnancies that produces very high risks is twin-twin transfusion syndrome (TTTS) where one fetus 'donates' blood supply to the other. In these cases prognosis is poor with death of one or both twins occurring in 60% to 100% of cases. We report our experience of performing in utero magnetic resonance (iuMR) imaging of the fetal brain in survivors of monochorionic pregnancies complicated by fetal demise of the co-twin.

Materials and Methods

This was a retrospective, observational study of monochorionic twin pregnancies complicated by demise of one twin. Two groups were created, one where there was a history of TTTS and some type of ante-natal intervention (treated TTTS group) and the other where the pregnancy was not complicated by TTTS (spontaneous demise group). The pregnant women were referred from nine fetomaternal centers in Britain but all had their iuMR examination at the Academic Unit of Radiology, University of Sheffield. The women had ante-natal ultrasonography performed by an experienced fetomaternal consultant prior to the iuMR examination. In cases of treated TTTS the type of intervention and gestational age at which it performed was recorded as well as the time at which the twin demise was first recorded and the demise-to-scan time. For cases of spontaneous demise of a twin only the estimated demise-to-scan time was recorded. All iuMR procedures were carried out on 1.5 T whole body systems, from 2004 to 2007 - Infinion (Philips Medical Systems, Best, Netherlands) and from 2008 to 2013 - HDx (GE Healthcare, Milwaukee, USA). The reports of the ante-natal ultrasound and the co-temporaneous iuMR examinations were compared in order to make assessments of the overall rate of acquired brain pathology in the surviving twin and to make an assessment of the differences in diagnosis between the ultrasound and iuMR examinations.

Results

A search of our institutional MR database located 73 appropriate cases from 2004 to 2013, 32 with treated TTTS and 41 with spontaneous demise of one twin. Of the 34 cases with treated TTTS 29 had laser ablation of placental blood vessels and five had selective reduction of the pregnancy (RF ablation or cord occlusion). The ultrasound and iuMR examinations both were reported as showing no evidence of acquired brain injury in 64/73 (88%) overall, including 28/32 (88%) of the treated TTTS group and 36/41 (88%) of the spontaneous demise group. The rate of brain pathology was approximately the same in both groups (12%). In the abnormal group (n=9) three of nine cases ultrasound and iuMR findings agreed (all cases of ventriculomegaly as the only finding). In two of nine cases the ultrasound examinations were reported as showing ventriculomegaly only but iuMR showed VM and some other brain abnormality (extensive encephalomalacia in one case and extensive encephalomalacia and reparative polymicrogyria in the

other). In one further case the ultrasound examination showed ventriculomegaly and raised the possibility of brain infarction. In utero MR imaging showed extensive unilateral brain injury with a focal infarction and reparative polymicrogyria. In three of nine cases the ultrasound examination was reported as normal but iuMR in all three cases showed extensive or focal areas of encephalomalacia and reparative polymicrogyria. Thus ultrasound failed to demonstrate or underestimated the brain injury in 66%. Outcome details of the pregnancy were available in 59/73 cases (81%). Fifty-eight percent of the fetuses resulted in a preterm delivery (49% moderate/late, 10% very preterm and 5% extreme preterm) in comparison with 7.1% in the general population. Six of the fetuses with brain abnormalities were delivered preterm including four that were very preterm.

Conclusions

In utero MR imaging is superior to ultrasound in the detection and characterization of the neurologic sequelae of cotwin demise in monochorionic twin pregnancies. The rate of such sequelae in the surviving twins in cases of TTTS is not increased in our subgroups, which is at odds with several previously published studies. Nonetheless, our study adds valuable experience to the in utero imaging of a high risk pregnancy group.

KEYWORDS: Fetal, Fetal Brain Injury, Fetal MR Imaging

O-342 10:51AM - 10:58AM
Charting the Prenatal Development of Regional Functional Connectivity: an in Utero Functional MRI Study

A Jakob¹, E Schwartz¹, G Kasprian¹, G Gruber², D Prayer¹, V Schoepf¹, G Langs¹

¹Medical University of Vienna, Vienna, Austria, ²University of Vienna, Vienna, Austria

Purpose

The characterization of prenatal neural functional development has been so far limited to indirect observations on fetal behavior, electrophysiological measurements, invasive measurements and translation of knowledge from animal models. Advances of fast in utero magnetic resonance imaging (MRI) enable the application of functional MRI (fMRI) approaches to critical periods of human brain development, to the time of extensive synaptogenesis during the mid- and late gestation. We aimed to portray the prenatal emergence of functioning neuronal ensembles by noninvasive neuroimaging, providing normative data of how regional, macroscopic scale functional interactions become detectable.

Materials and Methods

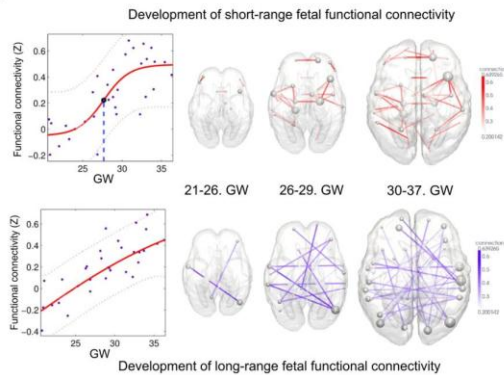
Our study relied on the functional examinations of 32 fetuses with no detectable morphological abnormalities. By adapting the functional magnetic resonance acquisition, motion correction and nuisance signal reduction procedures of the commonly modeled resting-state functional brain networks to fetal data we extracted BOLD activation information for major cortical and subcortical

Note: Scanned images are included in the proceedings. Some submitted images were reduced during editing thereby decreasing clarity. Also, refer to the Program Planner. Proceedings Content as of 3/28/2014.

structures. Resting fMRI networks were observed for increasing regional functional connectivity during the 21-38 gestational weeks (GW) with a network-based statistical inference approach.

Results

The overall functional connectivity network, short range and interhemispheric connections showed sigmoid expansion curve peaking at the 26-29 GW. In contrast, long-range connections exhibited linear increase with no periods of peaking development. Region-specific increase of functional signal synchrony followed a sequence of occipital (peak: 24.8 GW), temporal (peak: 26 GW), frontal (peak: 26.4 GW) and parietal expansion (peak: 27.5 GW).



Conclusions

We successfully adapted functional neuroimaging and postprocessing approaches to correlate macroscopic scale activations in the fetal brain with gestational age. Our in vivo data confirm that the mid-fetal period hosts events that cause the architecture brain circuitry to mature. This is supported by the developing complexity and increasing strengths of intra and interhemispheric functional connectivity. We characterized a diverging developmental trajectory of short- and long-range connectivity presumably marking different mechanisms that contribute to the increasing functional connectivity. The use of functional connectivity approach on a region of interest basis will allow future investigations on disease development and their correlation to healthy characteristics of connectivity strength development curves as shown in this work.

KEYWORDS: Fetal, Fetal fMRI, Fetal MR Imaging

O-343 10:58AM - 11:05AM
Diagnosis of Polymicrogyria on Fetal MRI.

M Tenenbaum¹, J Soul¹, J Estroff¹, P Grant², E Yang¹
¹Boston Children's Hospital, Boston, MA, ²Children's Hospital Boston, Enders 961, Boston, MA

Purpose

Fetal MR imaging (MRI) can detect and characterize brain malformations that may be difficult or impossible to diagnose on ultrasound examination. As a result, fetal MRI now is recommended for the confirmation of fetal brain anomalies suspected by ultrasound and to search for

additional brain anomalies when abnormalities such as ventriculomegaly or callosal agenesis are observed. Polymicrogyria (PMG) is one of the most common cortical anomalies diagnosed on fetal MRI. While difficult to detect on ultrasound, the diagnosis of polymicrogyria remains challenging even on fetal MRI, and there is limited data on the accuracy of fetal MRI for this malformation. The purpose of this study was to assess accuracy of fetal polymicrogyria diagnosis through a retrospective analysis of cases interpreted as polymicrogyria and correlate clinical interpretations with pathology or postnatal imaging. In addition we set out to determine the impact of gestational age on accuracy, imaging findings commonly associated with polymicrogyria, and underlying etiologies where ascertainable.

Materials and Methods

The radiology database was queried for instances of polymicrogyria diagnosed on fetal MRI from January 2003 through August 2013. Reasons for referral, fetal sex, gestational age, and associated abnormalities were recorded. Where available, follow-up imaging, clinical information, and underlying etiology was obtained for these cases. One scan was performed on a Siemens Skyra 3 T system, with the remainder performed on a GE Signa HDxt 1.5 T system. Fetal and postnatal images were reviewed by three pediatric neuroradiologists, two of whom are senior members of the American Society of Neuroradiology and board certified neuroradiologists with a focus on pediatric neuroimaging.

Results

Database query yielded 27 cases where PMG was diagnosed or questioned, 14 females and 13 males. The reason for referral of these cases was enlargement of the ventricles in 44%, other brain abnormalities in 16%, spine or body anomalies in 26%, cleft lip in 7%, and for follow up of previously abnormal fetal brain MRI from an outside institution in one case. Average age of gestation at time of fetal diagnosis of definite or possible PMG was 30 weeks 2 days. MR imaging manifestations of fetal PMG were similar to postnatal imaging findings including cortical thickening/irregularity and presence of excessive number of gyral folds in locations departing from standard gyral anatomy for age. Two thirds of the cases were bilateral with 26% of total cases representing bilateral perisylvian involvement and 22% diffusely involving the cerebral cortex. Associated findings included ventriculomegaly in 48%, abnormalities of the corpus callosum in 22%, heterotopic gray matter in 15%, and cystic changes/encephalomalacia in 15%. Ultrasound reports were available for 26 of the 27 patients where PMG was suspected, in which the possibility of PMG was mentioned in two cases. Postnatal or fetopsy follow up was obtained for 16 fetuses, confirming the diagnosis in 10 instances. Retrospective analysis of the false positive cases of PMG suggested that abnormalities of sylvian fissure configuration without discrete cortical nodularity and technical factors may contribute to spurious diagnosis of PMG in utero. False positive cases also were associated with less diagnostic certainty than true positive cases and invariably had significant other abnormalities. There was

Note: Scanned images are included in the proceedings. Some submitted images were reduced during editing thereby decreasing clarity. Also, refer to the Program Planner. Proceedings Content as of 3/28/2014.

no statistically significant difference in gestational age for confirmed versus nonconfirmed PMG ($p=0.4961$). Of the cases with followup, confirmed etiologies included CMV infection, 11p15.4 deletion, Aicardi Syndrome, and Megaencephaly-Capillary malformation – polymicrogyria syndrome. In the majority a cause was not confirmed.

Conclusions

Polymicrogyria is a challenging diagnosis with significant implications for neurologic outcome. As such, close attention for this abnormality should be paid on fetal MRI studies in which brain anomalies are suspected. Characteristic imaging findings include areas of cortical nodularity and abnormal frequency of gyral folding in a pattern departing from normal sulcal anatomy. Associated abnormalities that may suggest a specific etiology include microcephaly with parenchymal destruction/cysts (i.e., CMV); periventricular nodular heterotopia, agenesis of the corpus callosum, and interhemispheric cysts (i.e., Aicardi syndrome); and megalencephaly with distal extremity anomalies (i.e., megalencephaly polymicrogyria polydactyly hydrocephaly, MPPH, syndrome). Potential pitfalls include acquisition factors (e.g., angulation, image artifacts, and field strength) and difficulties in resolving abnormal gyral folds in the early third trimester, a time period when secondary sulci have formed but the overall brain size remains quite small. With improvements in fetal MRI technique, these technical pitfalls are anticipated to be less frequent in the future.

KEYWORDS: Fetal, Fetal MR Imaging, Polymicrogyria

O-344 11:05AM - 11:12AM
Ultrasound and MRI in the Neonate: A Head to Head Comparison.

S Ortiz-Romero, B Kline-Fath, S O'Hara
Cincinnati Children's Hospital Medical Center, Cincinnati, OH

Purpose

Ultrasonography has been a standard in imaging the premature and critically ill neonate as most neonates are too unstable to leave the confines of the neonatal intensive care unit. The recent installation of a 1.5 T MR imaging (MRI) scanner in our neonatal intensive care unit has been advantageous in directing the care of these delicate patients. Because some may question the advantages of brain MRI over bedside head US, a study was performed to directly compare neonatal brain imaging findings and the sensitivity of the two techniques.

Materials and Methods

The study was IRB approved and parental consent was obtained. A total of 42 neonates which had both MRI of the brain and head ultrasound within a 72-hour window were enrolled. The MR exams were interpreted by a pediatric neuroradiologist and ultrasound exams by a pediatric radiologist specialized in sonography. Blinded to clinical history, the imaging was graded utilizing a brain pathology scale. Statistical comparison of the two techniques was obtained utilizing the Kappa test.

Results

Of the 42 patients with corrected gestational age ranging from 32 – 47 weeks (mean 40.1) concordance between ultrasound and MRI findings varied widely. As expected, ventriculomegaly and enlarged extra-axial fluid spaces showed good agreement. MR imaging and US showed the worst agreement when identifying cerebellar hemorrhage (0-US, 6-MRI), anomalies of the corpus callosum (1-US, 6-MRI), and extra-axial hemorrhage (1-US, 9-MRI). White matter injury and parenchymal hemorrhage also had significant discordance with US overcalling normal white matter in 9/29 cases but undercalling grade 3 injury in 8/11 cases. In cases of parenchymal hemorrhage, US overcalled in 5/31 cases and undercalled 7/11 cases. Moderate agreement was noted when comparing migrational abnormalities and germinal matrix hemorrhage. The lack of agreement in the germinal matrix injury was unexpected but was due to subacute injuries being more difficult to detect via US when compared to MRI susceptibility sequences.

Conclusions

Both US and MRI are valuable techniques in directing medical care for the neonate. Ultrasound is extremely helpful in assessing the CSF spaces. MR imaging is sensitive at detecting parenchymal abnormalities, many of which are important with regard to long term outcome. Data from our study should help guide clinicians in choosing between US and MRI in the evaluation of these youngest, critically ill neonates.

KEYWORDS: Neonatal, Neonatal MR Imaging, Ultrasonography

O-346 11:19AM - 11:26AM
Auditory Neuropathy Spectrum Disorder due to Infantile Thiamine Deficiency: MR Findings.

A Aizer Dannon¹, P Caruso², G Bachar³, E Raveh⁴, J Attias⁵
¹Schneider Children's Medical Center of Israel, Petah Tikva, Israel, ²Massachusetts General Hospital, Boston, MA, ³Rabin Medical Center, Petah Tikva, Israel, ⁴Institute of Audiology and Clinical Neurophysiology, Petah Tikva, Israel, ⁵Sackler Faculty of Medicine, Petah Tikva, Israel

Purpose

To report the MRI findings of seven children who were fed with thiamine deficient formula in infancy and developed hearing impairment attributed to the auditory neuropathy spectrum disorder.

Materials and Methods

A pediatric radiologist and a neuroradiologist retrospectively reviewed the pretreatment brain MR imaging (MRI) examinations of the seven infants with auditory neuropathy spectrum disorder due to thiamine deficiency. Four patients had post-treatment MRIs following the initiation of thiamine supplementation. All MRIs included T2, FLAIR images, either IRT1 or T1-weighted images. Postgadolinium T1-weighted were available in six out of seven patients and diffusion-weighted images (DWI) were available in five patients. The

Note: Scanned images are included in the proceedings. Some submitted images were reduced during editing thereby decreasing clarity. Also, refer to the Program Planner. Proceedings Content as of 3/28/2014.

MRIs were evaluated for abnormal signal and enhancement with attention to the central auditory pathway including the cochlear nuclei, the auditory fiber tracts, the inferior colliculi and the medial geniculate bodies.

Results

The time of imaging of the MRIs ranged from two to 16 months of age. Along the auditory pathway, abnormal elevated signal on the T2-weighted images was seen in the cochlear nuclei in six patients and the inferior colliculi in five patients. Abnormal elevated signal was seen on the T2-weighted images also in the posterior thalami in four patients, and in the cortex and subcortical white matter in three patients, and in other cranial nerve nuclei such as the hypoglossal and vagal nuclei. Abnormal diminished diffusion was seen in the tectum, brainstem, posterior thalami, and the basal ganglia. After the administration of thiamine, follow-up MRI exams were performed in four of the patients. Improvement in the signal abnormality was found in the brain stem in all four patients, in the posterior thalami in three patients and in all three patients with tectal involvement.

Conclusions

Our report describes for the first time the MR findings along the central auditory pathway and in the supratentorium and brain stem of infants with auditory neuropathy spectrum disorder due to thiamine deficiency.

KEYWORDS: Hearing Loss, MR Imaging Brain, Wernicke Encephalopathy

O-347 11:26AM - 11:33AM
Physiologic Pineal Region and Choroid Plexus Calcifications in the First Decade of Life

M Whitehead¹, C Oh², A Raju², A Choudhri²
¹Children's National Medical Center, Arlington, VA,
²UTHSC/LeBonheur Children's Hospital, Memphis, TN

Purpose

Benign intracranial calcifications commonly are encountered on head CT exams. Physiologic calcifications of the pineal gland, habenula, choroid plexus, and dura may be present in both children and adults. In the modern CT era with thinner image sections and multiplanar reformats, intracranial calcifications have become increasingly visible. We sought to discover the prevalence of pineal region and choroid plexus calcifications on head CTs in the first decade of life.

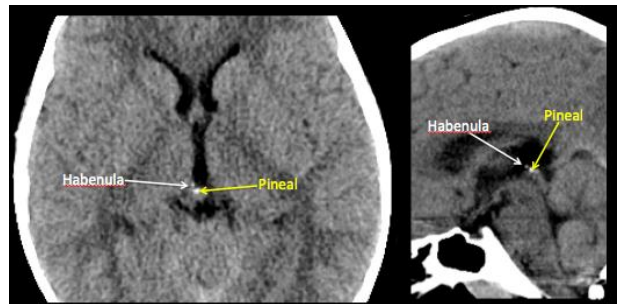
Materials and Methods

Head CT exams from 507 consecutive new patients at a single academic children's hospital were identified by a RIS search. Five exams were excluded due to excessive artifact or hemorrhage. A total of 502 exams were analyzed. Axial, coronal, and sagittal 5mm section bone and soft tissue algorithm images were evaluated for calcifications associated with the pineal gland, habenula, choroid plexus, and dura. Images were reviewed independently by two CAQ holding board certified neuroradiologists. A consensus reading was reached in all cases.

Type of Calcification	Number Of Patients	Age Range (Years)
Pineal	25/502 (5%)	4.2-9.9 (median 7)
Habenular	50/502 (10%)	3.2-9.9 (median 7)
Choroid Plexus	58/502 (12%)	1.1-9.9 (median 7)
Dural	7/502 (1%)	3.9-9.8 (median 4)

Results

Pineal region (pineal and/or habenular) calcifications were present in 13% (65/502) of patients. Pineal calcifications were visible in 5% (25/502; range 4.2 to 9.9 years, median 7 years) and habenular calcifications were identified in 10% (50/502; range 3.2 to 9.9 years, median 7 years). Twelve percent of patients had choroid plexus calcifications (58/502; range 1.1 to 9.9 years, median 7 years). Dural calcifications were present in 1% (7/502; range 3.9 to 9.8 years, median 4 years). The vast majority (96%; 483/502) of intracranial calcifications were found in patients over five. There was no significant difference in the sex or race of patients with and without pineal region and choroid calcifications.



Conclusions

Physiologic pineal region and choroid plexus calcifications may be present on head CT in patients in the first decade of life, principally in children older than five. The majority of pineal region calcifications are habenular in location. Pineal and habenular calcifications were never present in children less than four and three years, respectively.

KEYWORDS: Choroid Plexus, Pediatric Brain, Pineal Calcification

O-348 11:33AM - 11:40AM
Hypomyelination with atrophy of basal ganglia and cerebellum (HABC) due to TUBB4A mutations: expansion of the neuroimaging phenotype

A Poretti¹, C Ferreira¹, J Cohen², A Hamosh¹, S Naidu²
¹Johns Hopkins University School of Medicine, Baltimore, MD, ²Kennedy Krieger Institute, Baltimore, MD

Purpose

Hypomyelination with atrophy of basal ganglia and cerebellum (HABC) is a rare and sporadic leukodystrophy that is characterized by childhood onset, developmental delay, a variety of extrapyramidal movement disorders, ataxia, progressive spasticity and seizures. The diagnosis of

Note: Scanned images are included in the proceedings. Some submitted images were reduced during editing thereby decreasing clarity. Also, refer to the Program Planner. Proceedings Content as of 3/28/2014.

HABC is based on the characteristic neuroimaging findings including hypomyelination and selective atrophy of the neostriatum and cerebellum. Recently, a single de novo mutation in TUBB4A has been associated with HABC. The aim of this study is to report on three new patients with HABC, describe two novel mutations in the TUBB4A gene and expand the neuroimaging phenotype of HABC.

Materials and Methods

Clinical and neuroimaging data of three patients with HABC were collected by the senior author. All neuroimaging data (including at least sagittal T1- and axial T2-weighted images) were evaluated retrospectively for qualitative assessment of size and signal intensity of infra and supratentorial gray and white matter structures. Whole-exome sequencing (WES) was performed in all patients.

Results

At last follow-up, the patients were 24, 14 and 12 years old, respectively. At this age, all patients had spasticity, dystonia, microcephaly and abnormal language. Choreoathetotic movements, speech difficulties (dysarthria or anarthria), impairment of visual acuity and eye movement disorders (exotropia or nystagmus) were present in two patients, tremor in one. Ataxia was present in one patient and not testable in the other two patients. Cognitive functions were normal in one patient, while the other two patients had severe intellectual disability. For all patients, two neuroimaging studies were available. Age at first MR imaging (MRI) was between 11 months and 2.7 years, age at follow-up MRI between 8.2 and 9.8 years. In patient one and two, hypomyelination was diffuse, while in patient three it was less severe: genu and splenium of the corpus callosum as well as the posterior limbs of the internal capsule appeared to be partially myelinated at two years of age, but no progression in myelination occurred up to the next neuroimaging follow up at 8.7 years of age. In all patients, progressive cerebellar atrophy was seen over time and thalami as well as globi pallid had a normal size on all MR studies. In patient one and two, progressive atrophy of putamina and head of caudate nuclei was seen at follow up, while in patient three the size and signal of the putamina and caudate nuclei remained normal over the course of seven years. Whole-exome sequencing revealed heterozygous missense mutations in TUBB4A in all patients. Mutation in patient three appears to result in similar clinical severity, but more benign neuroimaging findings compared to mutations in patients one and two.

Conclusions

We confirm the association between mutations in TUBB4A and HABC. We expand the neuroimaging phenotype of HABC including a less severe degree of hypomyelination and lack of atrophy of putamina and caudate in one patient. Mutations in TUBB4A should be suspected in all cases of diffuse hypomyelination even in the absence of putaminal or caudate atrophy.

KEYWORDS: Cerebellar, Hypomyelination, Neurogenetics

0-349

11:40AM - 11:47AM

Autism and Sensory Processing Disorders: Shared White Matter Disruption in Sensory Pathways but Divergent Connectivity in Social-Emotional Pathways

Y Chang, J Owen, S Desai, S Hill, A Arnett, J Harris, E Marco, P Mukherjee

University of California San Francisco, San Francisco, CA

Purpose

Over 90% of children with Autism Spectrum Disorders (ASD) demonstrate atypical sensory behaviors. In fact, hyper- or hyporeactivity to sensory input or unusual interest in sensory aspects of the environment is included in the DSM-5 diagnostic criteria for ASD. There is, however, a group of children with isolated sensory processing disorders (SPD) who do not show primary language or social deficits, but do show atypical sensory reactivity and/or sensory interests to the same, or greater, extent as children who meet an ASD diagnosis. The comparison of children with SPD and ASD will help to define the neural underpinnings of each of these conditions. It has been demonstrated previously that these children with Sensory Processing Disorders (SPD) have impaired white matter microstructure, primarily in posterior cerebral tracts involved in unimodal sensory processing as well as multisensory integration (MSI). It was further found that this white matter microstructural pathology correlates with atypical sensory behavior. In this study, we use a diffusion tensor imaging (DTI) fiber tractography approach to compare the structural connectivity of specific white matter tracts in children with ASD and SPD.

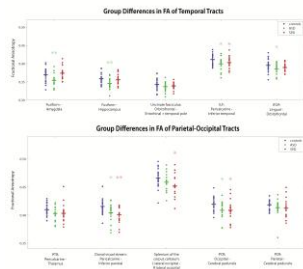
Materials and Methods

Diffusion tensor imaging (DTI) was acquired in 16 boys with SPD, 15 boys with ASD, and 23 neurotypical boys, all ages 8-11 years. Probabilistic diffusion fiber tractography was used to define white matter tracts, and strength of tract connectivity was assessed using mean fractional anisotropy. Group differences in connectivity were assessed with two-tailed nonparametric permutation tests, using a two-sample t-statistic, at a significance level of $p < 0.05$.

Results

Both the SPD and ASD cohorts demonstrate decreased connectivity relative to controls in parieto- and temporo-occipital tracts involved in sensory perception and multisensory integration. However, the ASD group alone shows impaired connectivity in the lingual-orbitofrontal tracts and the fusiform-amygdala and fusiform-hippocampus tracts, which are associated with social emotional processing.

Note: Scanned images are included in the proceedings. Some submitted images were reduced during editing thereby decreasing clarity. Also, refer to the Program Planner. Proceedings Content as of 3/28/2014.



Conclusions

Our results demonstrate both overlapping and divergent white matter pathology affecting SPD and ASD, with temporal tracts traditionally associated with ASD being relatively unaffected in SPD, and with SPD subjects demonstrating more extensive white matter pathology in parieto-occipital sensory processing tracts. These observations help elucidate the roles of specific neural circuits in neurodevelopmental disorders.

KEYWORDS: Autism Spectrum Disorder, Connectivity, Diffusion MR Imaging

O-350 11:47AM - 11:54AM
Thiamine transporter-2 deficiency due to SLC19A3 mutations in the differential diagnosis of Leigh syndrome in the pediatric age

M Rebollo Polo, J Ortigoza Escobar, B Perez Dueñas, M Serrano Gimare, J Muchart
Hospital Sant Joan de Deu, Barcelona, Spain

Purpose

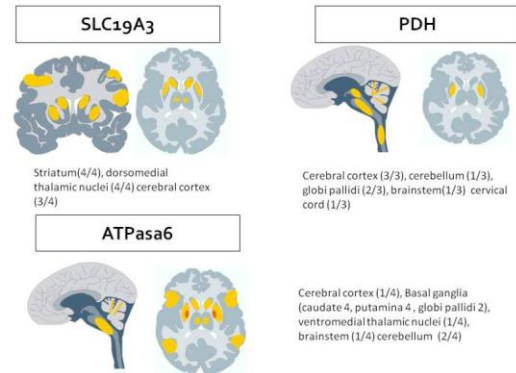
SLC19A3 deficiency causes acute/recurrent encephalopathy with symmetric lesions on MR imaging (MRI) and lactic acid accumulation, being initially indistinguishable from mitochondrial encephalopathy, especially Leigh syndrome (LS). We aimed to compare radiological features between patients with SLC19A3 defects and LS, and to establish neuroimaging clues for early diagnosis.

Materials and Methods

Neuroimaging features were compared between four children with SLC19A3 defects and eight children with LS [ATPase 6 (N=4), PDH-E1 α (N=3)], unknown genetic defect (N=1).

Results

As compared to LS, SLC19A3 patients had lesions in the striatum (4/4), dorsal-medial thalamic nuclei (4/4) and cerebral cortex (3/4). Thiamine dramatically reversed the phenotype (clinical and radiological) only in SLC19A3 children. The following radiological criteria were established: a) Symmetric lesions affecting the striatum and medial thalami, b) Symmetric lesions in areas of higher metabolic demands of the cerebral cortex (i.e., perirolandic cortex in the neonate), c) Infratentorial involvement: tegmental part of the midbrain, pons, cerebellar white matter or dentate nuclei, d) Resolution of the lesions after thiamine supplementation.



Leigh syndrome with known mutation, lesions pattern distribution (unpublished preliminary data from our Center)

Conclusions

Thiamine transporter-2 deficiency due to SLC19A3 mutations is in the differential diagnosis of Leigh syndrome in children, being clinically indistinguishable at onset. In children with acute encephalopathy, an excellent response to thiamine is highly suggestive of SLC19A3 deficiency. Specific brain lesions affecting the striatum, dorsal-medial thalami and cerebral cortex also are helpful in the differential diagnosis with mitochondrial encephalopathies.

KEYWORDS: Mitochondrial Disease

O-351 11:54AM - 12:01PM
Cavitary Leukoencephalopathy in infants with Complex I Deficiency

P Krishnan¹, K Siriwardena¹, A Feigenbaum¹, S Laughlin¹, J Raiman¹, A Schulze¹, B Meaney², M Van der Knaap³, S Blaser¹

¹The Hospital for Children Sick, Toronto, Ontario, Canada,

²McMaster Children Hospital, Hamilton, Ontario, Canada,

³VU University Medical Centre, Amsterdam, Holland

Purpose

To illustrate the pattern of cavitary leukoencephalopathy in infants with nuclear encoded Complex I deficiency. The mitochondrial oxidative phosphorylation system (OXPHOS) uses the electron transport chain complexes I through IV and ATP synthetase (complex V) to generate cellular energy in the form of ATP. Defects of the OXPHOS system are present in ~1 in 3-5,000 live births and affect high energy demand organs, including the brain. Complex I is the largest respiratory chain complex and is the deficiency most frequently involved in human OXPHOS disorders. There are at least 45 core subunits of Complex I; 38 are nuclear gene-encoded (NADH dehydrogenase ubiquinone or 'NDU'). The prefixes 'NDU' is followed by the subunit number, itself a description of the subunit's function or location. For example, FS denotes iron-sulfur protein region, while FV denotes the flavoprotein region. The resultant 'NDU' subunits include NDUFS1, NDUFS4, NDUFS8 and NDUFV1, amongst others. Complex I deficiency may cause a myriad of central nervous system (CNS) imaging manifestations. These include: normal

Note: Scanned images are included in the proceedings. Some submitted images were reduced during editing thereby decreasing clarity. Also, refer to the Program Planner. Proceedings Content as of 3/28/2014.

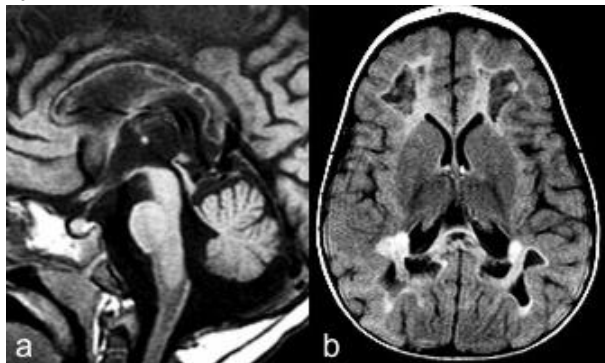
imaging (+/- lactate on MR spectroscopy (MRS); isolated subependymal cysts; atrophy; Leigh or Leigh-like deep gray nuclei and brainstem involvement; and leukoencephalopathy progressing to cavitation. Genotype-phenotype correlation is not exact.

Materials and Methods

Research ethics board approved retrospective review of imaging in leukodystrophies sought infants with Complex 1 mutations and leukoencephalopathies via a word search of radiology texts (ISYS tm). MRI, DWI/DTI, MRS and change over time were assessed.

Results

We identified 13 patients with Complex I deficiency and leukoencephalopathy. Nuclear gene-encoded deficiencies included: NDUFV1 (n = 4), NDUFS4 (n = 1), NDUFS8 (n = 2), NDUFS1 (n = 1). Results of Complex I sequencing were pending or unavailable in four, although three had respiratory chain analysis on muscle tissue/fibroblast culture confirming Complex I deficiency. An additional patient with mutations in BOLA3, which plays a role in biogenesis of the iron-sulfur clusters needed for respiratory chain function had similar imaging appearance. Imaging findings: White matter swelling was present in all. Cavitory white matter changes were present in 10 patients on the initial study with progression in all six patients who had follow-up imaging. Diffuse white matter swelling on presentation with cystic changes on follow-up study was seen in two patients. Corpus callosum, brainstem, and corticospinal tract involvement was universal. Diffusion restriction (93%) and WM lactate (93.7%) were other associated significant findings. Patchy enhancement was present in 61%. Signal change in cerebellar white matter, peduncles and spinal cord were present in approximately half.



Conclusions

The presence of progressive cavitory leukoencephalopathy is a useful imaging feature suggestive of mutations in nuclear encoded Complex I.

KEYWORDS: Leukoencephalopathy, Mitochondrial Disease, MR Imaging Brain

Tuesday, May 20
10:30 AM – 12:00 PM
Room 524

38 - Parallel Papers: Epilepsy

0-352 10:30AM - 10:37AM
 Machine Learning Classification of Neuroimaging Measures in Epilepsy Patients with and without Mesial Temporal Sclerosis

J Rudie, J Colby, S Dua, N Salamon
 David Geffen School of Medicine at University of California
 Los Angeles, Los Angeles, CA

Purpose

A major goal of neuroimaging research is to develop individualized measures that aid in the diagnosis and treatment of neuropsychiatric disorders. Although converging evidence suggests that temporal lobe epilepsy with mesial temporal sclerosis (MTS) is associated with alterations in cortical morphology and white matter integrity, differences at the individual level is not well established. Machine learning approaches are promising methods that may help overcome this challenge. We sought to 1) characterize alterations in cortical morphology and white matter integrity in a large cohort of epilepsy patients with and without MTS and 2) develop a robust method for automatically classifying patients based on neuroimaging measures.

Materials and Methods

Our sample consisted of high resolution T1 structural scans of 182 adults with epilepsy collected across five different 1.5 T and four different 3 T scanners at UCLA over the past 10 years. Of the 182 patients, 81 had a diagnosis of epilepsy with left or right MTS and 101 were diagnosed with epilepsy without evidence of MTS or other structural abnormalities. In 165 of these patients (70 with MTS), diffusion tensor imaging (DTI) data also were collected. Groups were matched for age, scanner strength and data resolution. Raw T1-weighted anatomical MRI scans were processed with Freesurfer's recon-all processing pipeline for whole brain segmentation and parcellation. This pipeline generated segmentations of 68 cortical and 45 noncortical regions. Nine metrics per cortical region and three metrics per subcortical region, including volume, thickness and curvature, were used as features for machine learning classification. FSL was used to generate average fractional anisotropy values for 48 white matter tracts as additional features. A multiple support vector machine recursive feature elimination algorithm (mSVM-RFE) was used to obtain classification accuracy and a ranked list of features. This process was wrapped in an external layer of 10-fold cross validation. Estimates of generalization error were obtained by averaging the performance of a tuned

Note: Scanned images are included in the proceedings. Some submitted images were reduced during editing thereby decreasing clarity. Also, refer to the Program Planner. Proceedings Content as of 3/28/2014.

and trained radial basis function SVM classifier on the respective hold-out samples across these 10 folds.

Results

Despite high variability across different scanners and imaging acquisition parameters, we were able to obtain an overall classification accuracy of 70% ($p = 1.6 \times 10^{-5}$) for epilepsy patients with left or right MTS compared to epilepsy patients without significant structural abnormalities. Accuracy reached 82% ($p = 5.4 \times 10^{-15}$) when comparing the ipsilateral MTS hemisphere versus epilepsy patients without significant structural abnormalities. Consistent with the clinical diagnosis of MTS, the most reliable feature was decreased hippocampal volume. Peak classification accuracy was obtained with an average of ~ 10 features, suggesting that only a few other features contributed to accuracy. Additional features useful for classification included putamen volume, entorhinal cortical thickness, and surface area of the inferior temporal lobe, temporal pole, pars orbitalis, pars triangularis, pars opercularis and frontal pole. Measures of fractional anisotropy did not significantly contribute to classification accuracy.

Conclusions

An automated classification algorithm was able to distinguish epilepsy patients with and without MTS with 82% accuracy. In addition to reductions in hippocampal volume, we found that reduced cortical volume and thickness in inferior frontal and anterior and inferior temporal regions contributed to classification accuracy. These findings provide a novel marker of MTS by implicating extrahippocampal involvement of MTS and thus may allow clinicians to detect more subtle cases of epilepsy with MTS. Larger and more homogenous sample sizes with improved data quality would improve classification accuracy and thus aid in the eventual development of automated neuroimaging-based classification algorithms that should assist in the global neurocognitive evaluation of epilepsy patients and may help predict clinical outcomes.

KEYWORDS: Cortical Thickness, Hippocampus, Temporal Lobe Epilepsy

0-353

10:37AM - 10:44AM

Hippocampal sub-field volumes in patients with temporal lobe epilepsy: a 7T MRI study

P Barker¹, H Trinh², T Ratnanather², D Lin¹, G Bergey¹

¹Johns Hopkins University School of Medicine, Baltimore, MD, ²Johns Hopkins University Center for Imaging Science, Baltimore, MD

Purpose

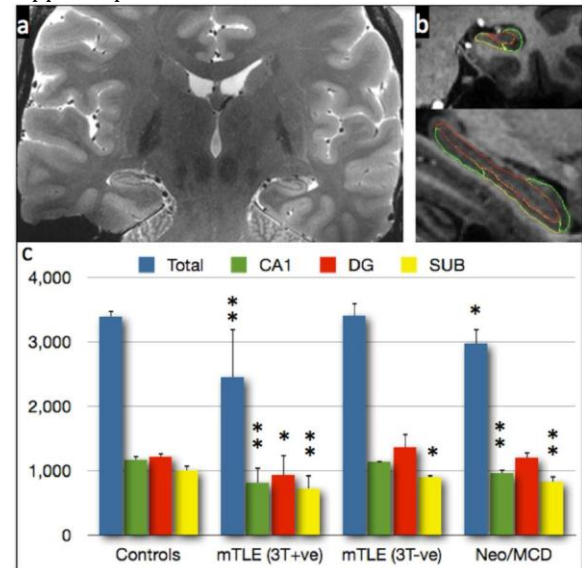
To investigate the use of high resolution MR imaging (MRI) at 7 T combined with automated analysis of hippocampal subfield volumes, for the detection of structural abnormalities in patients with suspected mesial temporal lobe epilepsy (mTLE).

Materials and Methods

Seventeen patients with medically intractable epilepsy (10 male, 32 ± 12 years) and seven normal control subjects (4 male, 36 ± 10 years) underwent 7 T MRI using a 32-channel head coil (Philips, Best, The Netherlands). The protocol included T1-weighted 3D MP-RAGE (0.6 mm isotropic resolution) and a coronal 2D FSE T2-weighted sequence (0.5x0.5x1 mm). Volumetric images were segmented into hippocampal substructures using an automated LDDMM-SBM pipeline, which was validated by comparison to manual segmentation in the control subjects. Final diagnosis was based on invasive EEG, clinical evaluation and (when available) pathology.

Results

Of the 17 patients, 11 had a final diagnosis of mTLE (3 with normal conventional 3 T MRI scans) and six either neocortical or cortical malformation (MCD). Segmentation Dice coefficients were on the order of ~ 0.8 . Figure 1 shows (a) an example of a coronal 7 T T2-weighted image, (b) the results of the automated subfield segmentation in a normal volunteer, and (c) average hippocampal, CA1, dentate gyrus plus CA2/3 (DG), and subiculum (SUB) volumes ($(L+R)/2$, $\text{cm}^3 \times 10^3$, $**P < 0.001$, $*P < 0.05$ vs. controls). In 3 T+ve cases, volume loss is apparent in all subfields, while in 3T-ve cases, only selective subiculum volume loss was found. In the neocortical/MCD cases, both CA1 and subiculum were reduced significantly, as well as total hippocampal volume.



Conclusions

The high spatial resolution available at 7 T allows accurate automated determination of hippocampal subfield volumes. Subfield volumes are significantly reduced in mTLE, even in cases where conventional 3 T MRI is considered normal.

KEYWORDS: High Field, MR Imaging Brain, Temporal Lobe Epilepsy

Note: Scanned images are included in the proceedings. Some submitted images were reduced during editing thereby decreasing clarity. Also, refer to the Program Planner. Proceedings Content as of 3/28/2014.

O-354 10:44AM - 10:51AM
« Pliers sign », a new typical MR pattern of focal cortical dysplasia in the central region

C Mellerio¹, F Chassoux¹, J Meder¹, P Roca¹, M Tisserand¹, C Oppenheim²

¹CH Sainte Anne, Paris, France, ²CH Sainte-Anne, Université Paris Descartes, INSERM U894, Paris, France

Purpose

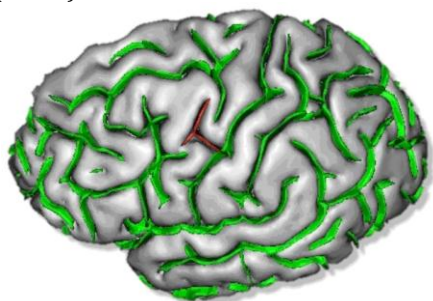
Type 2 focal cortical dysplasia (FCD2) is one of the main causes of refractory partial epilepsy, but often remains overlooked by MR imaging (MRI), even with optimized protocol. This study aimed to analyze and characterize sulcal abnormalities near lesions located in the central region and especially to evaluate the contribution of a new sulcal pattern ("pliers sign") in FCD2 detection.

Materials and Methods

Four readers reviewed the 3DT1 MR images of 37 patients (among which 13 had negative MRI) with histologically proven FCD2 of the central region and 19 controls using a three-dimensional, mesh-based reconstruction of cortical folds (BrainVisa-Anatomist). Pliers sign referred to the interposition of a precentral segment inside "pliers" materialized respectively by a small unusual branch ascending anteriorly from central sulcus and the central sulcus itself (cf. figure). Inter- and intra-observer reliability, specificity, sensitivity were calculated. Other central sulcus variations such as interruptions, side branches and connections also were reviewed.

Results

Pliers sign was found in 62% of the patients (70% when MRI was positive and 49% if not) near the lesion, but was never found in controls (Specificity = 100%, Sensitivity = 62%). FCD2 was located precisely in the depth of the abnormal branch in 60% of the patients with pliers. In other cases, FCD2 was located in its immediate vicinity. Inter- and intra-observer rate were excellent (0.87 and 0.92 respectively). Other sulcal variations were more frequent in patients than in controls, such as the number of side branches ($p=0.008$) and connections with central sulcus ($p=0.01$).



Conclusions

Sulcal abnormalities and especially "Pliers sign" can provide additional criteria for FCD2 detection and localization, even in patients with negative MRI.

KEYWORDS: Focal Cortical Dysplasia, MR Imaging Brain, Sulcation

O-355 10:51AM - 10:58AM
Voxel-based Morphometric MRI Post-processing in "Nonlesional" Pharmacoresistant Focal Epilepsies

S Jones, I Wang, B Krishnan, R Burgess, J Mosher, I Najm, A Alexopoulos

Cleveland Clinic, Cleveland, OH

Purpose

MR imaging (MRI)-negative ("nonlesional") pharmacoresistant focal epilepsy (PFE) patients are most challenging for surgical management. Discovering a previously undetected lesion can drastically change the evaluation, treatment plan, and surgical outcome. We present results from applying a voxel-based MRI postprocessing technique, implemented in a morphometric analysis program (MAP), to significantly enhance detection of subtle focal cortical dysplasia (FCD) in a consecutive cohort of MRI-negative surgical candidates.

Materials and Methods

We retrospectively reviewed the consecutive surgical series of the Cleveland Clinic Epilepsy Center from 1999 to 2012. Patients were included if they: (1) had a preoperative 1.5 T or 3 T MRI; (2) were considered MRI-negative prior to surgery; and (3) had > 12 months of postsurgical follow up. Morphometric analysis program was performed on T1-weighted Magnetization Prepared Rapid Acquisition with Gradient Echo (MPRAGE) sequence in Matlab SPM5, consistent with methodology published by Huppertz et al. The gray-white junction z-score map was calculated by comparing the patient with a scanner-specific normal database. Regions with z-score > four were considered indicative of significant gray-white blurring. These areas were presented to a neuroradiologist (SEJ), who was the final judge of whether they present true lesions. The neuroradiologist was blinded to patients' clinical information. The concordance among MAP+ region and surgical resection was determined on a sublobar level. All patients were analyzed as an overall group and further divided for subgroup analysis, based on a review of the clinical notes from the patient management conference, during which focused re-review of the MRI was performed based on noninvasive evaluation data (EEG, PET, SPECT, magnetoencephalography). Two subgroups were studied: (1) a group in which subtle/questionable abnormalities were noted; (2) another group in which the MRI was still considered negative. Surgical outcome at 12 months was dichotomized into two groups: seizure-free and not seizure-free. Statistical significance was assessed using Fisher's Exact test and Cochran-Armitage test (for trend). Significance was defined as $p \leq 0.05$.

Results

A total of 150 MRI-negative patients were identified (mean age = 28.5 years, 45% females, 63% seizure-free). Morphometric analysis program showed an overall 43% positive rate. The overall sensitivity of MAP was 0.9 and specificity was 0.67. With complete resection of the MAP+ region, 90% of patients were seizure-free; 67% of those with partial resection/no resection of the MAP+ region had recurring seizures. In the MAP negative group, 52% were

Note: Scanned images are included in the proceedings. Some submitted images were reduced during editing thereby decreasing clarity. Also, refer to the Program Planner. Proceedings Content as of 3/28/2014.

seizure-free. Overall, patients whose MAP+ region was resected completely had the best seizure outcomes, followed by the MAP negative patients, and patients who had partial resection/no resection of the MAP+ region had the worst outcome ($p < 0.001$). The outcome trend was consistent in both subgroups. Additionally, our subgroup analysis revealed that, although complete resection of the visually noted abnormalities indeed correlated with seizure-free outcomes ($p = 0.014$), the significance was concentrated in the patients who were also MAP+ ($p = 0.01$) and not in the MAP- subgroup ($p = 0.36$). False-positive rate in a group of 54 age- and gender-matched normal control was 2%. Surgical pathology of the resected MAP+ abnormalities contained mainly none-balloon-cell FCD. Multiple MAP+ abnormalities were present in 7% of patients.

Conclusions

We present the largest-to-date cohort of MRI-negative epilepsy patients evaluated with MRI postprocessing. Our study reveals the usefulness of MAP in identifying subtle epileptogenic lesions, and in particular cortical dysplasia. A MAP+ region, when concordant with the patient's electro-clinical presentation, can be targeted surgically, and thus has the potential to improve surgical outcome of "nonlesional" epilepsies.

KEYWORDS: Epilepsy, Focal Cortical Dysplasia, Voxel-Based Morphometry

O-356 10:58AM - 11:05AM
Diffusional Kurtosis Imaging Evaluation of Recent-Onset Medial Temporal Lobe Epilepsy

A Tabesh, T Nesland, J Jensen, M Vittoria-Spampinato, J Edwards, J Helpert, L Bonilha
Medical University of South Carolina, Charleston, SC

Purpose

Medial temporal lobe epilepsy (MTLE) is a common neurological disorder, affecting about one million people in the U.S. alone. Despite its prevalence, however, there is a lack of reliable biomarkers for clinical management of MTLE. Diffusion MRI (dMRI) is a unique and sensitive modality for quantitative assessment of brain microstructure and axonal connectivity, and as such it may serve as a complementary tool for evaluation of network abnormalities in MTLE. Prior dMRI studies have shown microstructure and connectivity alterations in patients with chronic MTLE (1, 2). This study aims to complement previous work by investigating diffusion changes in recent onset MTLE. We hypothesize that microstructure and connectivity abnormalities are present early in the course of the disease.

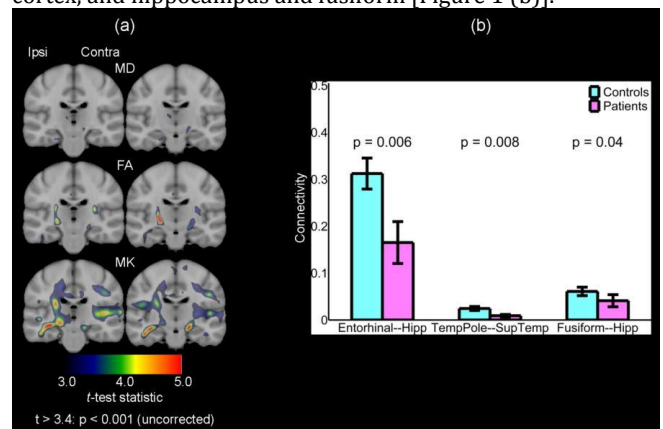
Materials and Methods

Twelve patients with recent onset MTLE (duration of disease < 2.2 years) and 24 age- and sex-matched healthy control subjects underwent diffusional kurtosis imaging (DKI) scans. Image acquisition was performed on a Siemens 3 T scanner using a twice-refocused echo planar sequence with three diffusion weightings ($b = 0, 1000$, and

2000 s/mm^2) along 30 diffusion encoding directions. Diffusivity and kurtosis parametric maps as well as the kurtosis orientation distribution function (ODF) (3) then were obtained using in-house software (4, 5). Voxel-wise analyses in standard space were employed to compare the parametric maps between patients and controls. Streamline tractography based on the kurtosis ODF was used to quantify the axonal connectivity of the temporal lobe ipsilateral to the side of seizures. The degree of connectivity between each pair of gray matter regions was calculated as the density of streamlines terminating in the two regions.

Results

Figure 1 (a) shows voxel-wise comparisons of mean diffusivity (MD), fractional anisotropy (FA), and mean kurtosis (MK) between patients with recent onset MTLE and controls. Compared to controls, patients showed increased axial, radial, and mean diffusivity in the cingulum ipsilateral to the side of seizures as well as increased axial diffusivity in the ipsilateral thalamus. Patients also showed reduced FA in the ipsilateral uncinate fasciculus, posterior limb of internal capsule, and splenium of corpus callosum. Reduced axial kurtosis was observed in the genu and body of corpus callosum, and in the retrolenticular part of internal capsule. In contrast, MK and, particularly, radial kurtosis were reduced in extensive brain regions. These included the superior corona radiata, fimbria and crus of fornix, and posterior thalamic radiation. Impaired ipsilateral temporal connectivity in patients was observed in the connections between the hippocampus and entorhinal cortex, temporal pole and superior temporal cortex, and hippocampus and fusiform [Figure 1 (b)].



Conclusions

Our results indicate that alterations in tissue microstructure and connectivity are present in patients with recent onset MTLE. This observation is consistent with the hypothesis that certain temporal network alterations may precede the abnormalities induced by chronic seizures. Moreover, kurtosis metrics appeared to capture more extensive microstructural abnormalities than diffusivity measures. Ongoing research will determine whether the observed diffusion abnormalities can predict the clinical course of the disease, such as response to anti-epileptic medications, in recent onset patients.

Note: Scanned images are included in the proceedings. Some submitted images were reduced during editing thereby decreasing clarity. Also, refer to the Program Planner. Proceedings Content as of 3/28/2014.

KEYWORDS: Diffusional Kurtosis Imaging, Fiber Tracking, Temporal Lobe Epilepsy

O-357 11:05AM - 11:12AM
3D CT and MR Registration, Fusion and Data Merge with 3D Post Processing for EEG Lead Placement Verification for Pre-Operative Surgical Guidance in Intractable Epilepsy

S Todorova¹, H Shin², E Hadar³, M Elkay³, V Jewells³
¹University of North Carolina Hospitals, Chapel Hill, NC, ²University of North Carolina, Chapel Hill, NC, ³David Geffen School of Medicine at University of California Los Angeles, Los Angeles, CA

Purpose

Epilepsy surgery is the standard of care for refractory partial onset epilepsy. Prior to surgery, patients undergo extensive evaluation to verify seizure type, focus and etiology as well as prediction of resection risk, and prognosis. Three-dimensional computed tomography (CT) has been vital for the localization of the epileptogenic zone compared to subdural electrodes during invasive EEG monitoring. Despite ubiquitous use of CT localization, it is still difficult to ensure electrode to sulcal/gyral orientation and localization. In addition, CT has limited resolution compared to MR imaging (MRI). Therefore, we propose to use MRI and CT merge and reconstruction for localization of electrodes to the underlying anatomy.

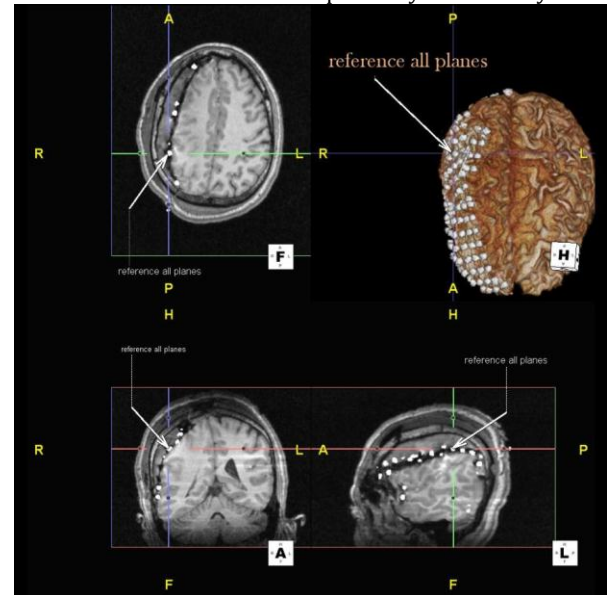
Materials and Methods

High resolution brain MRI and spiral 0.75 mm CT were performed status postplacement of electrodes in 14 patients for presurgical planning. Subsequently, CT and MR images were merged and 3D reconstructions performed for concurrent visualization of electrodes and underlying brain on high resolution MR for surgical planning. Merging allows for 3D localization with cross-hair function. This was performed using TeraRecon an FDA approved software for fully automated registration.

Results

This new postimaging process requires approximately ½ hour of radiological technologist time in an imaging lab opposed to multiple hours of processing time by a post doc. This technique results in improved neurosurgical guidance due to clarity of anatomical structures on MRI compared to CT as well as prior authors methods using Insite ITK tool kit and Amira software (1, 2, 3), which are not FDA approved. This technique allows the formation of interactive images for localization of electrodes and the underlying brain. Of the 14 patients whose seizure foci were localized with this technique, 13 are postsurgery to the extent that Engle Outcome can be assessed. Our outcome for those 13 patients is Engle I for nine (seizure free), Engle of II for nine (>90% reduction), and an Engle of 4 (less than 50% reduction) for one patient. These are good outcomes based upon the literature since our single Engle IV patient is a extratemporal epilepsy case (4, 5, 6). We are continuing to add patients to this data base. Our imaging method is depicted in Figure 1 in a postoperative patient who exhibits a postop SDH. Despite the SDH, there is good localization of electrodes to the underlying brain

for surgical guidance. These images can be rotated for interactive evaluation and cross-hair function for localization in three reference planes synchronously.



Conclusions

Multimodality, 3D CT and MR preoperative imaging with merging and reconstruction provides interactive virtual 3D models for better delineation, correlation of electrode placement to morphologic/anatomical brain foci, and surgical guidance for resection of the epileptogenic zone with less reconstruction time. Additionally, this technique can be performed by a radiological technologist under physician supervision. Epilepsy is the second most common neurological disorder. Despite over 20 anti-epileptic drugs, refractory epilepsy is common. For presurgical planning, accurate localization of electrodes compared to electrode-identified seizure foci with brain anatomical localization is necessary for optimal resection and epilepsy free results, and our technique improves localization compared to previously reported methods.

KEYWORDS: Brain, Epilepsy, Postprocessing

O-358 11:12AM - 11:19AM
A Comparison of MRI MPRAGE T1 sequences with Double Inversion Recovery Sequences in Identifying Focal Cortical Dysplasia in Patients with Epilepsy

K Kelly¹, J Britton¹, L Wong-Kisiel¹, R Watson¹, A Kotsenas¹, K Krecke¹, A Patton¹, C Shin¹, J Thomas¹, D Rettmann², R Witte¹

¹Mayo Clinic Rochester, Rochester, MN, ²General Electric, Rochester, MN

Purpose

Seizures remain refractory to medical treatment in 30-40% of the 50 million people worldwide with epilepsy. Surgery provides a definitive option for a subset of patients with intractable seizures. Surgical outcomes generally are higher in patients with a radiologic evident resectable

Note: Scanned images are included in the proceedings. Some submitted images were reduced during editing thereby decreasing clarity. Also, refer to the Program Planner. Proceedings Content as of 3/28/2014.

abnormality. Focal cortical dysplasias (FCDs) are a surgically remediable cause of epilepsy. These lesions can be very difficult to detect on MR imaging (MRI), often leading to a "nonlesional" report. IR-prepped heavily T1-weighted gradient echo sequences such as MPRAGE traditionally have been helpful to detect malformations of cortical development. Double inversion recovery (DIR) pulse sequences provide unique tissue contrast in brain MRI by suppressing cerebrospinal fluid (CSF) and white matter. Recent MR technical advances have enabled faster acquisition of high resolution DIR sequences in clinically acceptable times. Few reports have demonstrated the usefulness of DIR in multiple sclerosis, tuberous sclerosis, and neocortical epilepsy. None has evaluated DIR in FCD. The aim of our study was to compare DIR versus MPRAGE sequences in the identification of FCD.

Materials and Methods

We performed a case-control study in patients with radiologically and surgically identified FCD. The cases included 16 patients with FCD (7 pathology confirmed). The control groups were 13 patients with periventricular nodular heterotopias (PVNH) and 20 healthy subjects without neurologic disease. A senior neuroradiologist (RJW) re-reviewed all images and classified subjects as cases (FCD) or controls (PVNH or normal). Focal cortical dysplasia was defined as areas of gray-white blurring, subcortical signal, usually tapering to the ventricle (transmantle sign). As part of the institution's MR protocol for seizure patients, a 3D fast GRE T1-weighted MPRAGE with typical imaging parameters: TR/TE=7.5/3.1 ms, 256x256x200 matrix, FOV 24.0x24.0cm, section thickness 1.0mm, BW=±31.25kHz, 1.0 NEX, TD=2300ms was acquired. Additionally a 3D FSE DIR sequence with typical imaging parameters: TR/TE=5000/12.7 ms, 256x256x180 matrix, FOV 25.0x22.5cm, section thickness 1.0mm, BW=±62.5kHz, ETL=72, 0.5 NEX, TI/TI2=2437/456 ms, 2x2 parallel imaging was acquired. All DIR scans were obtained under an IRB-approved protocol and scanned on 3.0 T and 1.5 T MR scanners. A custom software was created to display and review DIR and MPRAGE sequences in sagittal, axial, and coronal planes. Two neuroradiologists blinded to diagnosis and imaging sequence determined whether images were FCD, PVNH or normal. Sensitivity, specificity and likelihood ratios for detecting FCD using MPRAGE and DIR were calculated for each reviewer. Correct FCD identification between MPRAGE and DIR was analyzed using McNemar's test on paired proportions.

Results

Reviewer A correctly identified 81% of FCD cases using DIR versus 19% of FCD cases with MPRAGE ($p=0.0016$). Reviewer B correctly identified 81% of FCD cases using DIR versus 31% of FCD cases with MPRAGE ($p=0.0047$). Table 1 summarizes percent of correctly identified diagnosis for each reviewer by MR sequence. The sensitivity for the DIR sequence in the FCD cases was 0.88 for reviewer A and 0.88 for reviewer B. Sensitivity for DIR studies in agreement between reviewer A and reviewer B in FCD cases was 0.81. Sensitivity for the MPRAGE sequence in FCD cases was 0.38 for reviewer A, 0.25 for

reviewer B, and 0.18 for the cases in agreement between both reviewers (Table 2).

Conclusions

This blinded study showed greater sensitivity for DIR sequences compared to MPRAGE in the detection of FCD. DIR sequences should be considered in patients with intractable focal epilepsy of unknown etiology. These results have implications for the selection of sequences to be used in imaging protocols for intractable epilepsy.

KEYWORDS: Congenital Brain Malformations, Cortical Dysplasia, Epilepsy

O-359

11:19AM - 11:26AM

Differences in the White Matter of Patients with Mesial Temporal Sclerosis Presenting Discordant and Concordant Data: a Magnetization Transfer MRI study

L Minami, V Passarelli, C Jorge, R Valerio, L Castro, M Otaduy
Medical School, University of São Paulo, São Paulo, Brazil

Purpose

New evidences suggest that patients with mesial temporal sclerosis (MTS) present diffuse brain alterations not restricted to the temporal lobe. In unilateral MTS we can distinguish two type of MTS patients, regarding the concordance of the laterality of the epilepsy seizure detected by EEG and the laterality of the MTS observed in the MR imaging (MRI). When the observed activity in the EEG is restricted to the hemisphere of the MTS observed in MRI, we consider the patient to be concordant. A discordant patient also will present EEG activity in the contralateral hemisphere. Magnetization transfer ratio (MTR) is a quantitative magnetic resonance imaging technique sensitive to myelin and white matter integrity. The aim of this study was to evaluate by MTR whether the white matter is affected in patients with MTS, and whether there is a difference between concordant and discordant patients.

Materials and Methods

A total of 35 patients with unilateral MTS (mean age: 34.8+/-10.0) and a sex- and age-matched group of 22 healthy controls (mean age: 32.8+/-10.6) were examined by MRI using a 3 T Intera Achieva (Philips, Best, The Netherlands) magnet and an eight-channel head coil. MR imaging exam included acquisition of three-dimensional high resolution T1-weighted images (3D-T1-TFE) and axial images with and without the application of a MT preparation pulse with 1mm³ isotropic resolution. Magnetization transfer ratio maps were constructed subtracting the axial images acquired with the MT prepulse preparation from the corresponding axial images without using this preparation. Furthermore the result of the subtraction was divided by the images without MT prepulse, and the result was multiplied by 100, in order to obtain values of MTR for each pixel (a MTR map) expressed as a percentage. FSL software was used to segment the white matter from anatomical T1-weighted 3D images and subsequently to coregister the white matter mask to the

Note: Scanned images are included in the proceedings. Some submitted images were reduced during editing thereby decreasing clarity. Also, refer to the Program Planner. Proceedings Content as of 3/28/2014.

MTR map. The MTR histogram of the white matter mask was calculated for each subject, and mean +/- SD values, and the 25th, 50th and 75th percentiles were calculated for each subject. Patients were divided in two groups: concordant and discordant, regarding the concordancy of the laterality observed in the MRI and the laterality observed in the EEG. Multiple comparisons were performed for the different MTR histogram parameters between the groups: patients versus controls; and discordant patients versus concordant patients and versus controls. Statistical analysis was performed using SPSS software.

Results

All MR images were examined by two experienced radiologists and 17 patients were classified as right MTS. By comparing the MRI to the EEG results, nine patients presented discordant data. Table 1 summarizes the obtained white matter MTR histogram parameters for three groups: controls, concordant and discordant patients. An ANOVA analysis found significant differences for the mean MTR and 25th percentile of the MTR histogram ($p=0.051$ and 0.025 , respectively), but no differences for the other higher percentiles. For the mean MTR and the 25th percentile the discordant group presented lower values than the other two groups. Concordant patients showed also slightly lower MTR values than controls, but this decrease was not statistically significant. There was no significant differences in age among the three groups.

Group	Age	Mean MTR	25 th percentile	50 th percentile	75 th percentile
Controls	33±13	53.4 ± 2.6	51.2 ± 2.7	56.0 ± 1.4	59.0 ± 0.7
Concordants	35±10	52.5 ± 3.1	50.1 ± 3.5	53.7 ± 1.6	59.1 ± 0.7
Discordants	34±11	50.5 ± 2.9	47.7 ± 3.4	54.7 ± 1.9	58.9 ± 1.1
ANOVA	0.72	0.051	0.025	0.11	0.50

Table 1: Mean and SD values of the average and percentiles of the MTR histograms obtained from white matter in controls, concordant and discordant patients.

Conclusions

With MTR it was possible to detect a diffuse alteration of the white matter in patients with epilepsy and MTS, more specifically in patients presenting discordant data regarding laterality between MRI and EEG exams. Discordant patients presented a significantly lower MTR, suggesting an impairment of white matter integrity.

KEYWORDS: Epilepsy, Magnetization Transfer Imaging, MR Imaging Brain

0-360 11:26AM - 11:33AM
Early MRI Characteristics After MRI-guided Laser Assisted Cingulotomy For Intractable Pain Control.

P Belani¹, S Sundararajan¹, S Danish¹, I Keller²
¹Rutgers - Robert Wood Johnson University Hospital, New Brunswick, NJ, ²University Radiology Group, P.C., East Brunswick, NJ

Purpose

Anterior cingulotomy is a well accepted stereotactic procedure in the treatment of both refractory OCD and debilitating pain syndromes. The procedure to this date has been done using a radiofrequency probe with or without MRI stereotaxis. At our institution, we recently have introduced the use of a 980-nm diode laser to

perform this procedure: MR imaging (MRI)-guided Laser assisted cingulotomy (MRgLAC). The MRI characteristics after ablation of the cingulum with this technology have not been described. The purpose of this study is to report the early MRI changes associated with cingulotomy using a 980-nm diode laser.

Materials and Methods

Five bilateral procedures were performed in four patients with intractable pain secondary to metastatic disease under an approved IRB protocol. The patients were imaged at multiple time points within 60 hours of the procedure. We retrospectively analyzed the changes in MRI signal characteristics during that time frame. One patient had a four-month follow-up MRI. Imaging was performed on 1.5 T GE and Phillips MRIs.

Results

At 0-60 hours, a characteristic pattern of zonal architecture consisting of four concentric rings in an "owl eye" shape was noted in the cingulum on T1-weighted and T2-weighted imaging. We observed four areas of injury with distinct signal intensity characteristics created by the ablation. These have been labeled zones 1-4. The central zone (zone 1) represents a laser probe void filled with fluid, with appropriate signal intensity characteristics. Initially, zones 2 and 3 have signal characteristics that represent hemorrhage, which matures differentially into two distinct zones (zone 2 and 3) over our measured time interval. Zone 4 has a peripheral ring of infarction with restricted diffusion-weighted imaging (DWI), and enhances postgadolinium administration. The lesions enlarged over the 60-hour time frame. The patient with the 4-month follow-up MRI demonstrated persistent concentric rings but resolution of the surrounding edema. We believe these areas represent a continuum of injury created by the laser probe and have an almost linear relationship to the transmitted "energy".

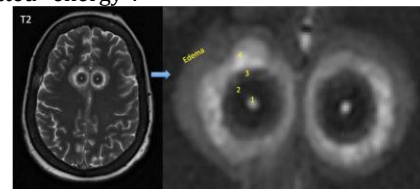


FIGURE: The above "owl eyes" appearing lesions are recorded 20-24 hours post laser ablation of the cingulate gyri. Four discrete zones are noted, arbitrarily labeled 1 through 4 from central to peripheral.

Zone 1 represents the CSF-filled cavity created post-thermal ablation. Zones 2 and 3 demonstrate varying T1-T2 signal with associated GRE, suggesting blood products of varying age (T1 not included above). Zone 4 demonstrates restricted diffusion and enhancement, relating to peripheral infarction with associated blood-brain barrier break down (T1 post and DWI not included above). Surrounding edema is better seen on T2 imaging.

Conclusions

MRgLAC is a newly introduced technique to perform bilateral anterior cingulotomies. The perioperative imaging changes seem similar to that described for laser ablation of tumor infiltrated tissue with a 1064-nm laser. This is the first study to characterize early MRI changes after MRgLAC using a 980-nm laser. As minimally invasive laser ablation cingulotomy re-emerges to treat intractable pain in these patients, it becomes important for the neuroradiologist to understand the expected imaging findings.

KEYWORDS: Laser, Pain

Note: Scanned images are included in the proceedings. Some submitted images were reduced during editing thereby decreasing clarity. Also, refer to the Program Planner. Proceedings Content as of 3/28/2014.

O-361 11:33AM - 11:40AM
Identification of Heschl's gyrus on phase difference enhanced imaging

S Ide¹, S Kakeda¹, T Yoneda², Y Korogi¹, K Futatsuya¹, Y Hiai³, J Moriya¹, K Watanabe¹

¹University of Occupational and Environmental Health, School of Medicine, Kitakyushu-shi, Fukuoka-ken, Japan, ²Kumamoto University, Kumamoto-shi, Kumamoto-ken, Japan, ³Kumamoto University, Kitakyushu-shi, Fukuoka-ken, Japan

Purpose

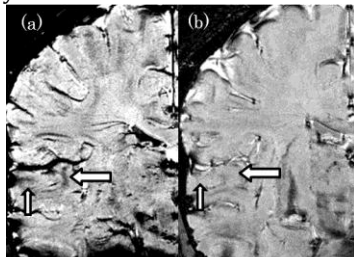
Human primary auditory cortex locates on the superior surface of the temporal lobe in the region known as Heschl's gyrus (HG). A previous study at 7 T evaluated the T2* signal intensity of the HG cortex (1). However, no studies have analyzed the signal intensity of the white matter (WM) in the HG. The phase difference enhanced (PADRE) imaging was developed to enhance the contrast between the target tissue and surrounding tissue by choosing the appropriate phase difference. On PADRE images, the signal-intensity (SI) of a certain WM may reflect its myelin content. Our purpose is to evaluate relative SI of the WM in the HG on PADRE images in comparison with the susceptibility-weighted imaging (SWI)-like images.

Materials and Methods

The subjects comprised four healthy volunteers (8 sides, 2 women, 2 men: mean age 29.0 years: range 28-30 years). Coronal high spatial resolution PADRE images were acquired covering the entire HG and superior temporal gyrus (STG) using a 3 T MR system. By consensus of two observers, the HG and STG were identified based on previously established anatomical methods (2, 3). The SI of WM in the HG on the PADRE images and SWI-like images were divided into three grades in comparison with that of the STG; grade I: isointense, grade II: slightly hypointense, and grade III: markedly hypointense.

Results

For the SI of WM, the grade II and grade III appearances were found in three (38%) and five (62%) of eight HG (4 subjects) on PADRE images, respectively (Figure). On the other hand, all eight HG were rated as grade I on SWI-like images, suggesting that there was no difference of susceptibility between the HG and STG.



PADRE (a) and SWI-like (b) images of a 28-year-old male. On PADRE image (a), the white matter of the right Heschl's gyrus (large arrow) is definitely hypointense (grade III) to the ipsilateral superior temporal gyrus (small arrow). On SWI-like image (b), however, the white matter of the Heschl's gyrus (large arrow) is isointense to the superior temporal gyrus (small arrow).

Conclusions

The WM in the HG shows hypointense on PADRE, which probably reflects the higher myelin content. PADRE may be useful for identification of the HG by assessing the SI of the WM.

KEYWORDS: Phase Contrast Imaging

O-362 11:40AM - 11:47AM
Microarchitecture Of Hippocampus: How Much Can Be Resolved On Clinical 3T MRI?

V Gupta, P Vibhute
Mayo Clinic, Jacksonville, FL

Purpose

Alterations of hippocampal volume and signal are the standard MR criteria in localization of temporal lobe epilepsy. In absence of the above, the internal architecture of hippocampus may become critical in seizure lateralization. Although the hippocampal microanatomy is well understood, there is no literature investigating what extent of the microarchitecture detail is reproducible on clinical high resolution MR imaging (MRI). Hence, there are no consistent and objective criteria for evaluating hippocampal architecture on clinical MRI. This study attempts to assess the extent to which the microanatomy of hippocampus can be resolved on high resolution techniques at 3 T and thereby, establish clinical MR criteria of hippocampal architecture.

Materials and Methods

Ninety-five consecutive technically optimal 3 T MRI (Skyra, Siemens) scans of patients with seizures were viewed independently by two neuroradiologists experienced in epilepsy imaging. Hippocampal architecture was evaluated on high resolution coronal 3D SPACE True Inversion Recovery T1- and T2-weighted sequences. A total of 154 hippocampi remote or contralateral to seizure onset, and appearing normal in volume and signal were included in the study. These hippocampi were scrutinized for morphological details previously published in cadaveric ultra high field MR and histologic studies of hippocampal architecture.

Results

The following features of hippocampal microarchitecture were agreed upon by both observers in greater than 95% hippocampi: 1. Cornu ammonis (CA1-CA3): a. A dark outer stripe representing the strata oriens and pyramidale, tapering from CA1 to CA3, b. An inner bright stripe comprising of strata radiatum and lacunosum-moleculare, becoming thicker from CA1 to CA3. 2. End-folium (CA4 and dentate gyrus): a. Dentate gyrus: an outer bright molecular layer, and inner dark band comprising of granular and polymorphic layers, b. CA4: seen as an intermediate signal zone enveloped by the dentate gyrus. In the hippocampal head digitations, the bright stripes of inner cornu ammonis and outer dentate merge into a single band; while in the body, these are separated by the hippocampal fissure.

Conclusions

Clinical high resolution 3T MRI can reliably replicate the above details of hippocampal microarchitecture previously

Note: Scanned images are included in the proceedings. Some submitted images were reduced during editing thereby decreasing clarity. Also, refer to the Program Planner. Proceedings Content as of 3/28/2014.

described on cadaveric MR and histological studies. These can be used as objective criteria to evaluate and describe hippocampal architecture both in practice and clinical research.

KEYWORDS: Epilepsy, Hippocampus, MR Imaging Brain

O-363 11:47AM - 11:54AM
Pre-operative Imaging and Clinical Predictors of Post-operative Seizure, Development, and Motor Outcomes in Hemispherectomy Patients.

G Shiferman¹, A Yogi¹, Y Hirata¹, R Sankar¹, G Mathern¹, N Salamon²

¹University of California Los Angeles, Los Angeles, CA,

²David Geffen School of Medicine at University of California Los Angeles, Los Angeles, CA

Purpose

Hemispherectomy and modified hemispherotomy are surgical procedures that are indicated for intractable seizures of various congenital and acquired etiologies. These procedures can be highly effective methods of long term seizure control and allow consequent discontinuation of antiepileptic drugs in selected candidates. The use of hemispherectomy and comparable epilepsy surgery is becoming more widespread and patient outcomes continue to improve. For this reason, further evaluation of this patient population is warranted. The purpose of this study is to correlate pre-operative imaging and clinical findings in hemispherectomy patients with postoperative seizure, development, and cognitive outcomes.

Materials and Methods

After obtaining IRB approval, a retrospective review of the University of California Los Angeles Neuroradiology PACS system was performed to identify 44 patients that underwent hemispherectomy from 2006-2013. After reviewing the available images and medical records of these patients, pre-operative imaging and clinical findings were documented. These included the regions of brain involved, presence of signal and morphologic abnormalities in the affected and contralateral hemispheres, age at seizure onset, age at time of surgery, gender, seizure type, congenital versus acquired etiology, pre-operative development quotient, and severity of any pre-operative motor or language deficits. Postoperative seizure, motor, language, and development quotient outcomes also were documented. Spearman's correlation coefficients with P values were calculated for every possible pairing of pre-operative and postoperative variables.

Results

Preliminary results show a positive correlation between the following variables: temporal lobectomy and seizure outcome, age at seizure onset and postoperative language outcome, pre-operative language development and postoperative language development, pre-operative cognitive development and postoperative cognitive development. Preliminary results also show a negative correlation between the following variables: number of

lobes involved and postoperative seizure outcome, left hemispherectomy and postoperative language development, contralateral anomalies and postoperative seizure outcomes, hemimegalencephaly patients and postoperative seizure, development, and cognitive outcomes, age at time of surgery and postoperative seizure and motor outcomes.

Conclusions

Hemispherectomy and modified hemispherotomy are highly effective methods of long term seizure control. Better postoperative outcomes are seen in patients with younger age at seizure onset, younger age at time of surgery, temporal lobectomy, higher pre-operative language and cognitive development, fewer lobes involved, fewer contralateral brain anomalies, and acquired seizure etiology versus hemimegalencephaly.

KEYWORDS: Epilepsy, Hemimegalencephaly

O-364 11:54AM - 12:01PM
MR Imaging in Pediatric Non-convulsive Status Epilepticus

K Fath, H Greiner, J Leach, P Horn, F Mangano
1Cincinnati Children's Hospital Medical Center, Cincinnati, OH

Purpose

Nonconvulsive status epilepticus (NCSE) is defined as prolonged seizure activity identified by electroencephalogram (EEG) with no obvious clinical symptoms other than encephalopathy (1). A high prevalence of NCSE has been reported in encephalopathic children in the ICU (1, 3, 5). Diagnosis of NCSE is made with continuous EEG (cEEG) monitoring which changes the management of these patients and affects prognosis. Acute imaging findings in convulsive status epilepticus have been well described (2), however recent studies have suggested that MR imaging (MRI) may be abnormal in NCSE patients as well (4). We hypothesized that certain MR imaging features are prevalent in children with NCSE concordant to hemispheric lateralization of seizure onset that may suggest the diagnosis, leading to more rapid identification of this patient subset.

Materials and Methods

Study patients were identified retrospectively from search of the electronic medical record. Criteria for inclusion were an EEG demonstrating NCSE and a brain MRI performed within 14 days of the EEG (peri-ictal MRI). Information was obtained on pertinent clinical, EEG, and MRI variables via retrospective chart review. All peri-ictal MRI exams (including all previous and follow-up MRIs) were blindly assessed for several variables, including acute T2/FLAIR signal [increased signal with associated swelling or lack of volume loss, new from prior exams (when available)], diffusion restriction, and hippocampal volume loss (on the initial or follow-up exams). Hemispheric lateralization and lobar localization of findings was recorded.

Electroencephalogram reports were blindly assessed by an experienced epileptologist. When reported findings were

Note: Scanned images are included in the proceedings. Some submitted images were reduced during editing thereby decreasing clarity. Also, refer to the Program Planner. Proceedings Content as of 3/28/2014.

unclear regarding lateralization or localization, tracings were assessed and scored independently.

Results

Thirty-three children formed the study group (age range: 3 mos – 20 years). Seventeen children had a past history of epilepsy. Thirteen of thirty-three (39.3%) had a structural etiology identified on imaging, 20/33 (60.6%) had a metabolic, toxic, or infectious etiology. Thirty of thirty-three (90.9%) had abnormal peri-ictal MRI exams. Twenty of thirty-three (60.6%) exhibited diffusion restriction, 22/33 (66.7%) had acute t2/FLAIR signal, 8/33 (24.2%) had hippocampal signal abnormalities, and 10/33 (30.3%) had hippocampal volume loss on follow-up exams. Those with no history of epilepsy were more likely to have acute T2/FLAIR abnormalities on MRI ($p = 0.035$) and hippocampal volume loss on follow-up MRI ($p = 0.05$). Younger patients were more likely to show hippocampal volume loss on follow-up MRI ($p = 0.039$). Significant hemispheric concordance of MRI and EEG abnormalities was noted ($p = 0.016$).

Conclusions

MR imaging abnormalities are common in children with NCSE and may represent an important clue in the evaluation of encephalopathic children. Younger children with NCSE and those with no history of epilepsy were more likely to develop hippocampal atrophy on follow-up exams. MR imaging and EEG abnormality locations were correlated by hemisphere, a relationship that should be further evaluated by future studies.

KEYWORDS: Status Epilepticus

O-365 12:01PM - 12:08PM
Brain FDG PET versus brain MRI in epilepsy patients: Diagnostic accuracy and correlation to post-surgical outcome.

N Mallak¹, A Capizzano¹, T Moritani¹, P Kirbuy², Y Menda²

¹University of Iowa Hospitals and Clinics, Iowa City, IA,

²University of Iowa, Iowa City, IA

Purpose

A significant number of epilepsy patients do not respond fully to medical treatment, and become eligible for surgical treatment. In this group of patients, lesion localization is critical for pre-operative planning. The purpose of this study is to assess the MR imaging (MRI) and fluorodeoxyglucose positron emission tomography (FDG PET) findings in patients with epilepsy, in order to compare the sensitivity and specificity of each modality for lesion detection as well as the impact on the postsurgical outcome.

Materials and Methods

This is a descriptive retrospective analysis of cases diagnosed with epilepsy who underwent MRI and FDG PET of the brain no more than six months apart in the past five years at our institution, including a total of 106 patients. After the IRB approval, data concerning the epidemiologic distribution of the patients, the imaging findings on both modalities, the EEG results, and the surgical outcome were

reviewed. The patients were divided into three subgroups: Patients having mesial temporal sclerosis (MTS) (pathologically proven or on MRI if surgery was not performed), lesional epilepsy, defined as parenchymal lesion other than MTS responsible for the epilepsy (pathologically proven or on MRI if surgery was not performed), and patients with negative MRI (this subgroup includes patients who had a negative MRI with no pathology available). Data were analyzed to compare both imaging modalities in terms of localization and impact on the surgical outcome. The EEG was considered the gold standard for seizure localization.

Results

Of 106 patients included, mean age \pm SD was 33.97 years \pm 16.71, and gender distribution was 54 females and 52 males. Thirty-nine patients underwent epilepsy surgery, of which 29 (74.4%) were seizure free or had a worthwhile improvement. Thirty-seven patients were diagnosed with MTS: PET and MRI were both positive and concordant in 91.9% of cases (34 patients), PET was positive with a negative MRI in 5.4 % of cases (2 patients), and PET was negative with a positive MRI in 2.7 % of cases (1 patient). Sensitivity was 94.6% for MRI and 97.3% for PET. Twenty-seven patients were diagnosed with lesional epilepsy, these patients were classified into two subgroups. The first included patients with MCD (16 patients), in this subgroup PET and MRI were both positive and concordant in 50% of cases (8 patients), PET was positive with a negative MRI in 31.2% of cases (5 patients), and PET was negative or nonconcordant with the EEG with a positive MRI in 18.8% of cases (3 patients). These data show that MRI has a sensitivity of 68.8%, and the PET has a sensitivity of 81.2%. The second subgroup included patients with lesional epilepsy other than MCD (11 patients), with the following diagnoses: encephalomalacia (5 patients), tumors (3 patients), tuberous sclerosis (2 patients) and cavernoma (1 patient). In this subgroup PET and MRI were both positive and concordant in 81.8% of cases (9 patients), and MRI showed the pathology with a negative PET in 18.2% of cases (2 patients). Thus, the sensitivity of MRI in this subgroup is 100% and 81.8% for PET. Finally, the negative MRI subgroup included forty-two patients. Positron emission tomography was positive in 66.7% (28 patients) and correlated with EEG in 85.7% of cases (24 patients) while it did not correlate with EEG in 14.3% (4 patients). Positron emission tomography was negative in the remainder 33.3% of cases (14 patients).

Conclusions

In patients with MTS, both FDG PET and MRI have very high and comparable sensitivity. In patients with MCD, PET is superior to MRI with a sensitivity of 81.8%, probably because the included MCDs were located mostly in the mesial temporal lobes corresponding to types I and IIA in the 2011 ILAE classification, which have lower MRI detectability compared to IIB (with balloon cells). Regarding lesional epilepsy not related to MCD, we would like to point out the selection bias of our sample, since most of the patients diagnosed with an epileptogenic abnormality on MRI such as tumor or vascular malformation do not undergo FDG PET. Notwithstanding,

Note: Scanned images are included in the proceedings. Some submitted images were reduced during editing thereby decreasing clarity. Also, refer to the Program Planner. Proceedings Content as of 3/28/2014.

our study still showed the expected higher sensitivity of MRI, approaching 100%. FDG PET shows high sensitivity in the negative MRI subgroup, and it correlated with the EEG in 85.7% of cases. However, only one patient in this subgroup underwent surgery with a good outcome, therefore, PET results did not have a high impact on the patients' care since no surgeries were done in the vast majority of MRI negative patients.

KEYWORDS: Epilepsy, MR Imaging Brain, PET

Tuesday, May 20
1:00 PM – 2:30 PM
Room 517bc

39 - ASHNR Programming: Head and Neck Staging and Treatment Assessment (SAM)

0-366 1:00PM - 1:20PM
Imaging of Lymph Node Metastasis - Practical Approach

Aiken, A.
Emory University School of Medicine
Atlanta, GA

Abstract/Presentation Summary

Imaging of cervical lymph nodes is one of the greatest challenges for the head and neck radiologist. There is no perfect test, but an understanding of the anatomy and the clinical context is key to providing useful information to clinicians. The three most common clinical scenarios for nodal assessment include: 1) Nodal staging with a known head and neck squamous cell carcinoma (HNSCC) primary 2) SCCA nodes with an occult primary 3) palpable nodes without a pathologic diagnosis. HNSCC comprises the majority of head and neck malignancies. The presence of a single metastatic node decreases the five -year survival by 50%, bilateral lymphadenopathy reduces prognosis by another 50% and the presence of extracapsular spread by another 50%. Therefore, lymph node status one of the most important predictors of the prognosis in HNSCC.(1,2) The first step in assessing the neck for metastatic nodes is knowledge of the anatomic nodal classification defined by the American Joint Committee on Cancer Staging (AJCC) as level I through VII. (See Table below) Level I refers to submental and submandibular nodes, levels II-IV refers to jugular chain nodes, level V refers to posterior cervical space nodes, level VI refers to visceral nodes and finally level VII refers to superior mediastinal nodes. Additional important named nodal groups include parotid nodes, lateral retropharyngeal nodes of rouvier, supraclavicular nodes (Virchow). Table 1: Imaging-based nodal classification (3) Level I Submental and submandibular nodes, located above the hyoid bone, below the mylohyoid muscle, and anterior to the back of the SMGs IA Submental nodes lie between the medial margins of the anterior

bellies of the digastric muscles. IB Submandibular nodes lie lateral to the anterior bellies of the digastric and anterior to the back of the SMGs. II Upper internal jugular nodes, lying from the skull base to the bottom of the body of the hyoid bone, posterior to the back of the SMG, and anterior to the back of the SCM IIA Anterior, medial, lateral, and immediately posterior/ touching the IJV IIB Posterior to the IJV & separated by a fat plane III Mid-jugular nodes, located from the bottom of the body of the hyoid bone to the level of the bottom of the cricoid arch and anterior to the back of the SCM. IV Low jugular nodes, located from the bottom of the cricoid arch to the level of the clavicle and lie anterior to the back of the SCM. V Posterior triangle nodes, located posterior to the back of the SCM from the skull base to the level of the clavicles. VA Upper level V nodes from skull base to the bottom of the cricoid arch posterior to the SCM. VB Lower level V nodes from the bottom of the cricoid arch to the level of the clavicles as seen on axial images. VI Visceral nodes, located between the carotid arteries from the level of the bottom of the body of the hyoid bone to the top of the manubrium. VII Superior mediastinal nodes, located between the carotid arteries below the level of the manubrium and above the level of the innominate vein. SPN Supraclavicular nodes are located caudal to the level of the clavicle on axial images and lateral to the carotid arteries on each side of the neck. RPN Retropharyngeal nodes are located within 2 cm of the skull base and medial to the internal carotid arteries. Most studies that have compared the accuracy of CT and MRI for assessment of lymph nodes in known HNSCC have found no difference. Several recent studies have demonstrated high sensitivity and specificity for PET-CT (4-6) in the evaluation of nodal metastasis, but reactive or inflammatory nodes may cause false positives and false negatives may occur with largely necrotic nodes. At Emory, we recommend performing a fully diagnostic CECT for attenuation correction for PET and in general most HNSCC patients should undergo PET-CT for staging. Although size criteria for lymph nodes have been established, they are somewhat arbitrary and controversial. A commonly used size criterion is a maximal longitudinal diameter of 15mm for level I and II and 10mm for all other levels except retropharyngeal nodes which should have a maximum diameter of 8mm. (7,8) If minimal diameter is used, then the threshold of 11mm for level II nodes and 10 mm for all other levels have been used. The imaging assessment of cervical lymphadenopathy is complex and includes not only determination of size, but also evaluation of morphology, borders, density and number. Regardless of the size, central low density is indicative of central necrosis and a metastatic node. Other highly suspicious features include rounded morphology with loss of the fatty hilum, clustered nodes (>3 nodes measuring >8mm) and ill-defined margins suggesting extracapsular spread. (9) The most important question to keep in mind when staging the neck is, "how will the presence/ absence of a metastatic node change treatment, surgery or prognosis?" For example, many head and neck surgeons will perform an ipsilateral prophylactic neck dissection for the N0 neck in patients with oral cavity carcinoma because of the high risk

Note: Scanned images are included in the proceedings. Some submitted images were reduced during editing thereby decreasing clarity. Also, refer to the Program Planner. Proceedings Content as of 3/28/2014.

of occult cervical metastasis (up to 35%), regardless of the radiographic N stage. So what is the role of imaging in this scenario? The major role would be to detect unexpected nodal metastases in the contralateral neck or in an unusual nodal chain. On the contrary, when treatment is nonsurgical as in many oropharyngeal cancers, radiographic N stage will affect radiation planning. Also, upfront surgical management with TORS (transoral robotic surgery) has gained momentum for select oropharyngeal cancers to avoid the toxic effects of radiation and chemotherapy. However, features such as extracapsular spread (which often means that chemotherapy is added to treatment) may sway the surgeon away from upfront surgery. Unfortunately, recent data has shown that although CT can be specific (97%) for detecting ECS (47%), it is not sensitive. Knowledge of the clinicians' practice at a particular institution will dictate when careful discrimination of nodes is most critical to plan treatment and when it is not. Ultrasound guided FNA of a suspicious node may be helpful for the clinically N0 neck, if this would affect surgical management. For the remaining two clinical scenarios- SCC node with an occult primary and palpable nodes without a pathologic diagnosis- knowledge of typical imaging patterns and nodal drainage is key. For level II nodes, the diagnosis of exclusion is HNSCC in one of the following sites: oropharynx (90%), lingual and palatine tonsils), nasopharynx or hypopharynx. For an infrahyoid node without any upper neck nodes, systemic metastases (lung, breast and GI) should be considered, particularly with a "Virchow" node. The radiologist should suspect nasopharyngeal carcinoma, lymphoma, thyroid cancer or hypopharyngeal cancer in an adult with an abnormal retropharyngeal node. In a child, reactive retropharyngeal nodes can be seen or suppurative retropharyngeal adenitis. Skin cancers often present with parotid lymphadenopathy. Bilateral non-necrotic bulky lymph nodes involving unusual chains should suggest lymphoma. Papillary thyroid cancer should be suspected with lower jugular chain and paratracheal nodes, especially with cystic change or calcification.

O-367 1:20PM - 1:40PM
Imaging of Post-Operative Neck - What Radiologists Should Know

Mukherji, S.
Michigan State University
Ann Arbor, MI

Abstract/Presentation Summary

This presentation will review the various options for treating lymph node metastases in the neck. The presentation will begin with reviewing the normal anatomy of the cervical lymph nodes. We will then review the standard neck dissection and their indications. The section of the talk will end by review the post-operative imaging appearance of each form of lymph node dissection. The next portion of the talk will review the expected and abnormal appearance of the neck following non-surgical organ preservation therapy. The content will focus on how

to distinguish between expected changes versus recurrent tumor.

O-368 1:40PM - 2:00PM
Inoperable Head and Neck Cancer - What to Look For

Anzai, Y.
Univ. Washington Medical Center
Seattle, WA

Abstract/Presentation Summary

Imaging plays a major role in the initial staging of head and neck aerodigestive tract cancers. In particular, the imaging assessment of the extent of a primary tumor is essential for determining the treatment choice. Despite the wide application of chemoradiotherapy for advanced head and neck cancer, toxicity associated with chemoradiotherapy is difficult for some patients to tolerate. Primary surgery remains a preferred treatment choice for patients with certain head and neck cancers. Head and neck surgeons rely heavily on imaging findings to determine if a neoplasm is operable (resectable). The American Joint Commission on Cancer (AJCC) revised the T staging classifications of head and neck cancers in 2002. One of the major changes of the T staging classification is to divide T4 lesions to T4a (resectable) and T4b (unresectable). In this review, we will discuss pertinent radiological findings that make head and neck cancer unresectable. These findings should be clearly communicated to head and neck surgeons in order to make an impact on patient care and treatment decision. There are three imaging findings that clearly define the lesion unresectable at all anatomical sub sites of the head and neck: 1) Vascular encasement and invasion 2) Prevertebral fascia invasion 3) Mediastinal invasion 1) Vascular encasement - Imaging findings to indicate vascular invasion include a) compression and deformation of the carotid artery, b) partial fat or fascia defect between tumor and artery, and c) involvement of 270° or more of the circumference of the carotid artery. Yousem et al found that single criterion using involvement of 270° or more of the circumference of the carotid artery was accurate in predicting inoperability to strip tumor off from the carotid artery. 2) Prevertebral fascia invasion - Clinically, prevertebral fascia invasion is suspected by fixation of the tumor to the prevertebral musculature. Surgical resection of tumor from the longus colli /capitis muscle complex has been shown to be challenging and does not improve patient's prognosis. Patients with prevertebral fascia invasion are often associated with retropharyngeal nodal metastasis, indicating a dismal prognosis. Loevner et al demonstrated that preservation of a retropharyngeal fat stripe on T1 weighted non-contrast images served as an excellent imaging indicator for absence of tumor invasion. The findings suggestive of the presence of prevertebral invasion include abnormal muscle concavity or T2 signal changes and contrast enhancement in the longus capitis or colli muscle. 3) Mediastinal invasion - It is commonly seen in patients with advanced laryngeal, hypopharyngeal, or thyroid cancer. When the lesion extends below the sternal notch, it requires participation of thoracic surgeons.

Note: Scanned images are included in the proceedings. Some submitted images were reduced during editing thereby decreasing clarity. Also, refer to the Program Planner. Proceedings Content as of 3/28/2014.

Imaging findings include obliteration of mediastinal fat and encasement of supra-aortic vessels. The combination of abnormal signal intensity of tracheal cartilage, intraluminal mass and circumferential tracheal encasement more than 180 degree is suggestive of tracheal invasion. Additionally, the followings are generally considered unresectable findings. These include skull base invasion, dural/brain invasion, and perineural spread of tumor. 4) Skull base invasion – skull base invasion is most commonly seen in nasopharyngeal cancer, sinonasal cancer or salivary gland tumors. When skull base bone is grossly involved, the lesion is clearly inoperable. MR is far more sensitive to detect the skull base invasion than CT. Replacement of fatty marrow by tumor infiltration on non-contrast T1 weighted images, associated with contrast enhancement is highly suggestive of tumor invasion. A study based on 943 patients by Chen L, et al, with NPC demonstrates difference in prognosis based on the location of skull base invasion. Patients with invasion to the pterygoid process, base of sphenoid, petrous apex, clivus, and foramen lacerum had better prognosis than those with invasion in the pterygoid canal, great wing of sphenoid bone, pterygopalantine fossa, foramen rotundum, foramen ovale, jugular foramen, and hypoglossal canal. 5) Dural/brain invasion – Intracranial extension, often seen in the sinonasal cancer, is another critical finding to determine surgical resectability. Dural invasion is the first step toward intracranial extension of squamous cell carcinoma. Although linear dural thickening seen on post contrast MR imaging is suggestive of tumor infiltration, often thin dural enhancement can be reactive or inflammatory, as seen in "dural tail" sign for meningioma. Linear dural thickening greater than 5 mm and nodular dural thickening are highly suggestive of actual tumor infiltration. Once pial arachnoid enhancement or actual brain invasion with vasogenic edema is seen, the lesion is considered unresectable. Exception for this rule is esthesioneuroblastoma, where surgical resection is a reasonable option and provides good outcomes even with presence of brain invasion. 6) Perineural spread (PNS) – HNC often spread along the neural sheath, a phenomenon well known as perineural tumor spread. Imaging manifestation of PNS has been beautifully described by Ginsberg et al. It is critically important for radiologists to pay attention to subtle findings of PNS as this clearly impacts therapeutic decision. Adenoid cystic cancer is commonly present with PNS, though virtually any HNC may be associated with PNS. Salivary gland tumor, oral cavity cancer, sinonasal cancer are often present with PNS. Enlargement and enhancement of neural foramen with loss of perineural foraminal fat, as well as asymmetric enhancement of cranial nerve is highly suggestive of PNS. Although there are certain structures that are not technically unresectable, these require tremendous functional or cosmetic loss leading to substantial morbidity, thus considered not suitable for surgical treatment. These are considered "functional unresectability". These include orbital apex invasion and brachial plexus invasion. Currently, these cases will be treated with chemoradiation and surgery remains a salvage option. 7) Orbital invasion – Sinonasal cancer is

often associated with orbital invasion. Invasion to orbital wall itself does not necessary require orbital exenteration, allowing orbital sparing without compromising overall survival. Periorbital soft tissue invasion (extra-ocular muscles, optic nerve, etc), which often requires orbital exenteration, is not technically inoperable, if a patient accepts the degree of morbidity. Orbital apex invasion as a result of PNS along pterygopalantine fossa and inferior orbital fissure is thus considered inoperable. Orbital fat infiltration and enhancement of extraocular muscles and/or intraconal fat are key findings to make the determination. 8) Brachial plexus invasion – although brachial plexus invasion is not listed under T4b description of AJCC staging classification, once tumor involves the brachial plexus, similar to PNS to cranial nerves, it is generally inoperable. This is often seen in large nodal metastases with extracapsular spread or advanced thyroid cancer. The useful imaging feature is loss of fat surrounding the anterior scalene muscle as well as enhancement of anterior scalene muscle. STIR or heavily T2 weighted images are particularly useful to delineate brachial plexus and tumor margin.

2:00PM - 2:30PM

Questions and Answers

Tuesday, May 20
1:00 PM – 2:30 PM
Room 517d

40 - Mini Symposium – Tumor – Part III

O-369

1:00PM - 1:15PM

Integrative Informatics for Brain tumor Gene Expression: Correlation with Imaging

Gevaert, O.
Stanford
Stanford, CA

Abstract/Presentation Summary

Vast amounts of molecular data characterizing the genome, epi-genome and transcriptome are becoming available for a wide range of cancers. In addition, new computational tools for quantitatively analyzing medical and pathological images are creating new types of phenotypic data. Now we have the opportunity to integrate the data at molecular, cellular and tissue scale to create a more comprehensive view of key biological processes underlying cancer. Our goal is to develop computational methods to realize multi-scale biomedical data fusion. To accomplish this we develop computational methods to derive quantitative image features from MR images that characterize the radiographic phenotype of glioblastoma lesions. Based on these quantitative image features we create radiogenomic maps by associating the radiographic phenotype with

Note: Scanned images are included in the proceedings. Some submitted images were reduced during editing thereby decreasing clarity. Also, refer to the Program Planner. Proceedings Content as of 3/28/2014.

various molecular data. These models can have profound contributions towards predicting diagnosis and treatment. Preliminary results show that radiogenomic approaches in glioblastoma have the potential to predict clinical and molecular characteristics of tumors non-invasively.

O-373 1:30PM - 1:45PM
Understanding the Molecular Signature of the Glioblastoma: Why This Represents the Future in Neuro-Oncology

Pope, W.
University of California Los Angeles
Los Angeles, CA

O-376 2:00PM - 2:15PM
Biomarkers in Brain Tumor Imaging: Definition and Beyond

Shiroishi, M.
USC Keck School of Medicine, Univ of So CA
Los Angeles, CA

Abstract/Presentation Summary
With recent emphasis on individualized cancer care, biomarkers have taken on a prominent role in cancer medicine. Biomarkers have been defined as "a characteristic that is objectively measured and evaluated as an indicator of normal biological processes, pathogenic processes, or pharmacologic responses to a therapeutic intervention." There are 2 general categories of biomarkers: 1. Bio-specimen biomarkers (genetic/molecular/biochemical/histological, etc) and 2. Imaging biomarkers. Imaging biomarkers have been specifically defined as "anatomic, physiologic, biochemical or molecular parameters detectable with imaging methods used to establish the presence or severity of disease." In order to obtain bio-specimen biomarkers, biological material, such as tissue or fluid, is taken from a patient. On the other hand, imaging biomarkers have the advantage of being essentially non-invasive. Other appealing characteristics of imaging biomarkers are that they can be repeated and are also spatially resolved. The potential for a particular imaging biomarker to overcome limitations of traditional reference standards such as histological analysis from invasive biopsy are particularly desirable because biopsy is inherently risky, may be inconclusive and are subject to sampling error. Like other biomarkers, imaging biomarker development is a difficult process that proceeds in sequential steps similar to the process for a new drug (i.e. discovery, verification in multiple laboratories, validation and qualification) before it can be put into routine clinical use. Accuracy, reproducibility/repeatability, standardization and quality control are central to these efforts. In brain tumor imaging, advanced MRI methods such as spectroscopy, perfusion and diffusion techniques as well and PET imaging have played a central role to provide quantitative imaging biomarkers for a number of applications including: tumor diagnosis, tumor grading/prognosis, treatment planning,

prediction/markers of treatment response and functioning as surrogate endpoints. Techniques such as molecular MRI and radiogenomics methods are emerging techniques which may provide novel biomarkers for brain tumor imaging in the future. However, despite their "added value", the evidence for these biomarkers is largely from small case series performed in single centers and, as such, their role as a complement to conventional anatomic imaging in clinical research and clinical care remains limited. While a prospective, multi-center imaging trial is complex and expensive, evaluation of a validated imaging biomarker in this context is critical to establish it as a part of "standard of care" and directly impact patient management and outcome.

O-370 1:15PM - 1:21PM
Imaging Genomic Features are predictive of EGFR mutation status in Glioblastoma

R Colen, J Wang, G Thomas, Z Mahmood, M ElBanan, P Zinn
MD Anderson Cancer Center, Houston, TX

Purpose

To develop a imaging biomarker signature that predicts the epidermal growth factor receptor (EGFR) mutation status in glioblastoma (GBM). Epidermal growth factor receptor mutations (mostly commonly these are extracellular) occur in GBM and are more sensitive to type 2 EGFR kinase inhibitors; in patients with this mutation, clinical responses to EGFR kinase inhibitor therapy is demonstrated. Thus, a noninvasive imaging surrogate that predicts EGFR mutation status will help stratify patients into therapy and clinical trials.

Materials and Methods

Using The Cancer Genome Atlas (TCGA), we identified 99 treatment naive GBM patients for whom both gene-and miRNA expression profiles including the EGFR mutation status, and pretreatment MR neuroimaging from The Cancer Imaging Archive (TCIA) were available. The 3D Slicer software 3.6 (<http://www.slicer.org>) was used for image analysis and image review was done in consensus by two neuroradiologists. Fluid attenuated inversion recovery (FLAIR) was used for segmentation of the edema and postcontrast T1-weighted imaging (T1WI) for segmentation of enhancement (defined as tumor) and necrosis. Imaging parameters then were correlated with EGFR mutation status and gene expression profiles. Complex biomarker signatures based on profiling and survival were created.

Results

We created a imaging signature that predicted EGFR mutation status and correlated with patient overall and progression-free survival.

Conclusions

The development of an imaging biomarker signature that predicts EGFR mutation status is of significant clinical significance as it remains a therapeutic target. The ability to noninvasively identify the presence of the EGFR mutation can help stratify patients into clinical trials and can serve as an imaging endpoint.

Note: Scanned images are included in the proceedings. Some submitted images were reduced during editing thereby decreasing clarity. Also, refer to the Program Planner. Proceedings Content as of 3/28/2014.

KEYWORDS: Image Processing, Imaging Biomarker, Imaging Genomics

O-371 1:21PM - 1:27PM

Integrated Imageomic Analysis Identifies Clinically Relevant Imaging Subtypes of Glioblastoma

R Colen, A Chaddad, P Zinn
University of Texas MD Anderson Cancer Center, Houston, TX

Purpose

To develop a classification of glioblastoma based solely on imaging that are clinically relevant and meaningful. Verhaak et al (Cancer Cell 2010) published the molecular classification of glioblastoma based on its genomic characterization. We seek to do the same with imaging, which we term imaging-omics (radiomics).

Materials and Methods

We retrospectively identified 80 patients with pretreatment, pre-operative MR imaging (MRI) from the Cancer Genome Atlas (TCGA). Each image (T1 axial image both before and after gadolinium contrast administration, and axial T2/FLAIR image), we performed volumetric analysis using the 3-D Slicer platform to quantitatively measure actual volumes of each individual region. The flair-volume, contrast-enhancing region, and necrotic core were independently segmented and verified by a trained neuroradiologist experienced in tumor volumetry, as previously done in our lab. Feature extraction (contrast, correlation, homogeneity and entropy) of each of the three segmented regions were performed using GLCM.

Results

A total of 628 imaging features were extracted for each of the segmented regions. The top 10 imaging features of each of the segmented regions were calculated and demonstrated to be robust and clinically predictive and relevant.

Conclusions

A novel robust classification based solely on imaging features was developed.

KEYWORDS: Imaging Biomarker, Imaging Genomics

O-372 1:27PM - 1:33PM

Association between genomic analysis of mammalian target of rapamycin (mTOR) and quantitative dynamic susceptibility contrast (DSC)-MR perfusion imaging evaluation and their implication in prediction of survival time in patients with glioblastoma

X Liu, S Ekholm, R Mangla, W Tian
University of Rochester Medical Center, Rochester, NY

Purpose

Glioblastoma is the most common malignant primary brain tumor in adults. Phosphatidylinositol-3 kinases (PI3Ks) constitute a family of intracellular lipid kinases that frequently are hyperactivated in glioblastoma, mammalian target of rapamycin (mTOR), a key mediator of PI3K signaling, which has emerged as a compelling molecular target in glioblastoma patients. The purpose of this study is to evaluate association between the activation status of mTOR and relative blood volume (rCBV) value derived from dynamic susceptibility contrast (DSC) MR perfusion imaging in patients with glioblastoma, and their clinical implication in predicting survival outcome.

Materials and Methods

Thirty-one cases (mean age is 62.06 ± 11.5) with new pathology confirmed glioblastomas were enrolled in this study. Mean and maximal rCBV ratio of the enhancing tumor (rCBVmean and rCBVmax), maximal rCBV ratio of peri-enhancing tumor area (rCBVperitumor) were measured as well as Ki-67, IDH, and mTOR. The correlations between rCBVmean, rCBVmax and rCBVperitumor and mTOR were assessed, the Cox regression was used to evaluate their implication on overall survival time (OS). The difference of age, rCBVmean, rCBVmax, rCBVperitumor and mTOR between the patients who survived less than 14 months and more than 14 months was compared.

Results

The rCBVmean, and rCBVperitumor had significant correlation with mTOR, (p value was 0.04 and 0.037 separately). The rCBVperitumor also showed significant correlation with OS (p < 0.001). The Cox regression analysis showed that age and rCBVmax were the two strongest predictors of OS. There were 17 patients who survived less than 14 months after initial diagnosis, and 14 patients survived more than 14 months. There was significant difference of rCBVperitumor between these two groups (p value was 0.003), but combination of rCBVperitumor and mTOR had better predication of survival time (>14 months) than other parameters.

Conclusions

The quantitative rCBV measurement is useful in predicting survival time of patients with glioblastoma. The rCBVmean, and rCBVperitumor correlated with mTOR status in glioblastoma, which suggested that mTOR pathway may moderate increase of neoplastic vasculature within the tumor and vasculature infiltration in the peri-enhancing tumor area. The rCBVmax is an independent imaging biomarker to predict patient overall survival. The combination of rCBVperitumor and mTOR could provide additional predictive information regarding to survival time of 14 months.

KEYWORDS: Genomic Analysis, Glioblastoma, MR Perfusion-Weighted Imaging

Note: Scanned images are included in the proceedings. Some submitted images were reduced during editing thereby decreasing clarity. Also, refer to the Program Planner. Proceedings Content as of 3/28/2014.

O-374 1:45PM - 1:51PM
MR imaging Based Analysis of Glioblastoma multiforme: Estimation of IDH1 Mutation Status

K Yamashita, A Hiwatashi, H Honda, K Kikuchi, O Togao, K Yoshimoto¹, T Yoshiura¹
Kyushu University, Fukuoka, Japan

Purpose

Glioblastoma multiforme (GBM) is the most common and highly aggressive primary malignant brain tumor.

Recently, glioma patients with isocitrate dehydrogenase (IDH) 1 mutations were found to have better clinical outcomes than those without. Therefore, the detection of IDH1 mutation is of great importance for GBM patients.

Our purpose was to predict the IDH1 mutation status in GBM using MR imaging.

Materials and Methods

Eighty patients including 65 with IDH1 wild type and 15 with IDH1 mutant in GBM were studied retrospectively. Absolute tumor blood flow (aTBF) and a relative tumor blood flow (rTBF) within the enhancing portion of each tumor were measured using arterial spin labeling (ASL) data. In addition, the percentage of cross-sectional necrosis area inside the enhancing lesions (%necrosis) and the minimum apparent diffusion coefficient (ADC_{min}) were obtained from contrast-enhanced T1-weighted images and diffusion-weighted imaging (DWI) data, respectively. Each of the four parameters was compared between tumors with IDH1 mutation and those without using Kruskal-Wallis test. The performance in discriminating between the two groups was evaluated using the receiver operating characteristics analysis. Area under the curve (AUC) values were compared among the four parameters using a nonparametric method.

Results

The aTBF, rTBF and %necrosis were significantly higher in IDH1 wild type (mean aTBF±SD = 86.5±56.0 mL/100g/min, mean rTBF±SD = 2.43±1.34, mean %necrosis±SD = 34.9±21.1 %) than in IDH1 mutant (mean aTBF±SD = 50.3±25.0 mL/100g/min, mean rTBF±SD = 1.49±0.64, mean %necrosis±SD = 15.7±17.8 %) (p<0.05, respectively). In contrast, no significant difference was found in the ADC_{min} value. The AUC for %necrosis, aTBF and rTBF were 0.764, 0.741, and 0.759, respectively. Combined rTBF and %necrosis resulted in higher AUC value (0.818) than that for each parameter alone, although their difference was not statistically significant.

Conclusions

MR imaging is useful to predict IDH1 mutation status.

KEYWORDS: Glioblastoma, MR Imaging Brain

O-375 1:51PM - 1:57PM
Imaging Genomic Biomarker Signature predicts IDH-1 mutation in Glioblastoma Patients

M ElBanan, J Wang, Z Mahmood, G Thomas, P Zinn, R Colen
MD Anderson Cancer Center, Houston, TX

Purpose

The IDH-1 (R132H) mutation is one of the strongest prognostic predictors and a diagnostic hallmark of gliomas that is independent of other known prognostic factors, including age, grade, and O6-methylguanine-DNA methyltransferase (MGMT) methylation status and thus has a major clinical relevance. Given the latter, it will likely be integrated into the new WHO classification for GBM. Currently used methods to determine the IDH-1 mutation status of GBM include immunohistochemical analysis and genotyping of the DNA extracted from the brain tumor specimens. Thus, we seek to identify an imaging signature associated with IDH-1 mutated tumors that can be considered as a noninvasive predictor of the IDH1 status in glioblastoma patients.

Materials and Methods

We identified 99 GBM patients from The Cancer Genome Atlas (TCGA) who had both genetic expression profiles of IDH-1 and mutation status and neuroimaging available at The Cancer Imaging Archive (TCIA). All morphological image analyses and segmentation were done using Slicer 3.6 (slicer.org) and reviewed in consensus by two neuroradiologists. Fluid attenuated inversion recovery (FLAIR) was used for segmentation of the edema and postcontrast T1-weighted imaging (T1WI) for segmentation of enhancement (defined as tumor) and necrosis. The nonenhancing perilesional FLAIR hyperintensity reflected a mixture of edema/tumor infiltration. Multiple quantitative imaging features were identified and combined to create the imaging biomarker signature predictive of IDH-1 mutation status.

Results

We created a complex imaging biomarker signature using quantitative MR imaging features to predict those GBM patients with IDH-1 mutation and furthermore that was predictive of patient survival.

Conclusions

Glioblastoma multiforme tumors with IDH-1 mutation hold a specific imaging biomarker signature that can be used as a predictive and prognostic biomarker and noninvasive surrogate for IDH-1 status detection.

KEYWORDS: Glioblastoma, Imaging Biomarker, Imaging Genomics

Note: Scanned images are included in the proceedings. Some submitted images were reduced during editing thereby decreasing clarity. Also, refer to the Program Planner. Proceedings Content as of 3/28/2014.

0-377 2:15PM - 2:21PM
Feasibility of Perfusion Fraction from Intravoxel Incoherent Motion as a Biomarker in Contrast-Enhanced Tumor: A Pilot Study in Glioblastoma Patients

J Puig¹, J Sanchez-Gonzalez², G Blasco¹, J Daunis-i-Estadella³, M Essig⁴, R Jain⁵, S Pedraza¹

¹Girona Biomedical Research Institute (IDIBGI), Hospital Dr Josep Trueta, Girona, Spain, ²Philips Healthcare Ibérica, Madrid, Spain, ³University of Girona, Girona, Spain, ⁴University of Manitoba, Winnipeg, Manitoba, Canada, ⁵New York University Langone Medical Center, New York, NY

Purpose

Effective monitoring of antiangiogenic drugs in patients with glioblastoma requires accurate assessment of vascularization. Dynamic susceptibility contrast (DSC) echo-planar MR imaging (MRI) enables noninvasive assessment of tumor angiogenesis by estimating regional cerebral blood flow (CBF) and cerebral blood volume (CBV). Other perfusion techniques based on endogenous tracers, such as intravoxel incoherent motion (IVIM) MRI, are potentially useful in clinical protocols. Considering the vascular floor as a random network of vessels where blood freely flows, IVIM uses a single diffusion-weighted imaging (DWI) acquisition to distinguish pure molecular diffusion from water molecules moving in the capillary network. We compare perfusion fraction (f) measured by IVIM with CBV and CBF on DSC to determine whether f is useful in predicting survival in newly diagnosed glioblastoma.

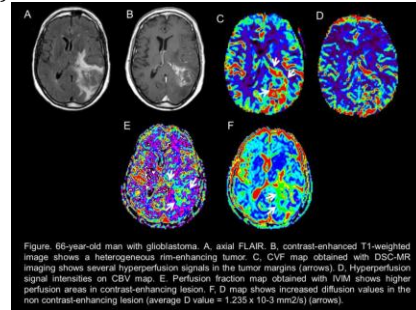
Materials and Methods

Seventeen patients (14 men; mean age, 64 years) with histologically proven glioblastoma underwent MRI including echo-planar imaging with IVIM-encoding gradients using 13 b-values (0-1000 s/mm²). Diffusion-weighted imaging (DWI) were fitted to an IVIM biexponential model to elaborate diffusion-coefficient (D), pseudodiffusion-coefficient (D*), and perfusion-fraction (f) maps for contrast-enhancing region (CER) and nonenhancing region (NCER). Anatomical images were reviewed using Olea Sphere V.2.0 software (Olea Medical, La Ciotat, France). The measured tissue concentration-versus-time curve was deconvoluted with an arterial input function to generate CBV and CBF maps. Intravoxel incoherent motion imaging was analyzed with a program developed within the research group using Interactive Data Language 6.3 (Research Systems Inc., Boulder, CO, USA). Statistical analysis included Pearson correlation, linear regression analysis, and intraclass correlation coefficients. Prognostic factors were evaluated by Kaplan-Meier survival and Cox proportional hazards analyses.

Results

We found significant linear correlations between fCER and both CBF_{CER} and CBV_{CER} (R=0.878 and R₂=0.77 (P<0.001) and R=0.599, R₂=0.36; (P=0.011), respectively) (Figure). The best cutoffs for 7-month survival were fCER > 15.37% and CBF_{CER} > 223.01 ml/min/100g (44% sensitivity, 100% specificity, 100% PPV, and 61.5% NPV;

AUC 0.722 and 0.694, respectively). fCER yielded the highest hazard ratio (1.579; 95% CI: 1.028, 2.424; P=0.036).



Conclusions

fCER correlated with CBF_{CER} and CBV_{CER} indexes in newly diagnosed glioblastoma and promises to be useful in predicting survival; IVIM using endogenous tracers can potentially obviate the need for contrast media in clinical imaging. Patients with high fCER may benefit from more aggressive and experimental treatments for newly diagnosed glioblastoma.

KEYWORDS: Diffusion MR Imaging, Glioblastoma, MR Perfusion-Weighted Imaging

0-378 2:21PM - 2:27PM
Fractional Anisotropy as a Quantitative Imaging Biomarker for Prediction of Tumor Grade in Glioma: A Meta-analysis Research Study.

V Miloshev¹, D Chow², A Lignelli¹, C Filippi²

¹Columbia University, New York, NY, ²Columbia University Medical Center, New York, NY

Purpose

Diffusion tensor metrics have been investigated as a potential in vivo quantitative neuroimaging biomarker for the characterization of brain tumor subtype and degree of invasion into the surrounding brain tissue. Fractional anisotropy is an indirect, quantitative measure of tissue microstructure. Multiple publications have evaluated the ability of fractional anisotropy (FA) to distinguish low grade from high grade glioma in the identifiable tumor core and the peripheral edematous/infiltrated region. This meta-analysis analyzes the statistical consensus of quantitative values in the published literature.

Materials and Methods

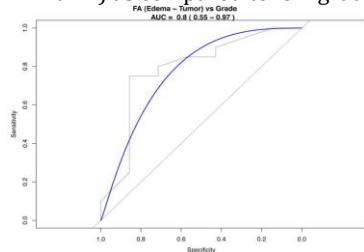
A meta-analysis of all published fractional anisotropy data for World Health Organization (WHO) low grade (I, II) and high grade (III, IV) gliomas was performed. Meta-regression, standardized mean difference, approximate back calculation of axial and radial diffusivity, and receiver operator characteristic curve (ROC) analysis was performed.

Results

The fractional anisotropy of the solid tumor component is larger in high grade gliomas than low grade gliomas (60 studies, 772 patients, p-value = 0.009). The difference in fractional anisotropy, or a combination of axial and radial

Note: Scanned images are included in the proceedings. Some submitted images were reduced during editing thereby decreasing clarity. Also, refer to the Program Planner. Proceedings Content as of 3/28/2014.

diffusivity, in the peripheral region of signal abnormality (the region of T2-prolongation) is not statistically significant in the cohort of studies with respect to tumor grade. However, the fractional anisotropy difference between the tumor core and peritumoral region of signal abnormality is significantly smaller in high grade gliomas (27 studies, 335 patients, p-value = 0.001, optimal threshold $\Delta FA = 0.21$) as compared to low grade gliomas.



Conclusions

High grade gliomas have larger fractional anisotropy values compared to low grade gliomas in the tumor core and have a smaller fractional anisotropy difference between the tumor core and peripheral region of signal abnormality. However, fractional anisotropy in the peripheral region of signal abnormality is not statistically significant with respect to tumor grade in the current literature. Considerable heterogeneity in the published literature may be addressed by use of standardization in image acquisition, processing, and analysis techniques as well as genomic histopathological differentiation of tumor subtypes in future studies.

KEYWORDS: DTI, Fractional Anisotropy, Glioma

Tuesday, May 20
1:00 PM – 2:30 PM
Room 517a

41 - ASPNR Programming: Pediatric Spine

O-379 1:00PM - 1:30PM
Advanced Techniques in Spine Imaging

Thurnher, M.
Medical University of Vienna
Vienna

Abstract/Presentation Summary
Challenging advanced MR imaging techniques have been successfully applied to the brain, and now could be applied on even more challenging part of the central nervous system, namely the spinal cord. Despite all difficulties several diffusion-weighted MR imaging (DWI) methods have been introduced and used for the evaluation of the spinal cord. DWI became a method of choice in detection of spinal cord ischemia. Diffusion tensor imaging (DTI) metrics and fiber tracking (FT) allowing more accurate

characterization of intrinsic integrity of tissues including cellular density and architecture have been increasingly used in evaluation of spinal cord neoplasms. Perfusion MR imaging may be helpful in preoperative and postoperative evaluation of the spinal cord in patients with severe degenerative disease and cervical compression myelopathy. Methodological challenges for MR spectroscopy (MRS) of the spinal cord such as anatomical tissue heterogeneity, small diameter of the spinal cord, pulsatile flow of the CSF and patients motion have been partly effectively solved. In this lecture the clinical impact of advanced MR imaging techniques in evaluation of the spine will be discussed.

O-380
Developmental Spine

1:30PM - 2:00PM

Huisman, T.
The Johns Hopkins University School of Medicine
Baltimore, MD

Abstract/Presentation Summary

The most common spinal dysraphias and malformations that may be encountered at birth or in the neonatal time period will be discussed and correlated with our current understanding of the normal and abnormal development/embryology of the spinal cord and canal. Pathologies to be covered include skin and non-skin covered myelomeningoceles, dorsal dermal sinus malformation, diastematomyelia, caudal regression syndrome, sacrococcygeal teratoma and various frequent pathologies that may involve the filum terminale.

O-381 2:00PM - 2:30PM
Acquired Pediatric Spine Abnormalities

Shroff, M.
The Hospital for Sick Children
Toronto, Ontario

Abstract/Presentation Summary

Imaging is critical in the diagnosis of acquired spinal diseases in children. Conventional radiographs are often used as an initial screening study with more definitive evaluation with MRI and/or CT scan and sometimes with nuclear medicine studies. In this presentation, we will review imaging features of the following acquired conditions and will discuss features specific to the pediatric age group: 1) Infective and inflammatory conditions, 2) Tumors, 3) Trauma, 4) Discogenic disease, 5) Idiopathic & unusual conditions. The discussion will include spinal and intraspinal abnormalities. Cases that will be discussed for the spine will be inflammatory conditions of the craniovertebral region, CRMO of the spine, eosinophilic granulomas, osteoid osteoma / osteoblastoma, aneurysmal bone cyst, chordomas, trauma specific to children such as atlanto-axial dissociation and non-accidental injury, disc disease associated with posterior lumbar apophyseal ring fracture and unusual discogenic conditions like idiopathic intervertebral disc calcification. Intraspinal inflammatory (MS, transverse

Note: Scanned images are included in the proceedings. Some submitted images were reduced during editing thereby decreasing clarity. Also, refer to the Program Planner. Proceedings Content as of 3/28/2014.

myelitis, GBM) and neoplastic conditions will also be briefly discussed. The presentation will be based on personal experience and review of literature. It will follow a case based format and where appropriate relevant differential diagnoses will be discussed.

Tuesday, May 20
1:00 PM – 2:30 PM
Room 520

42 - Socioeconomic Programming: New Payment and Practice Models

O-382 1:00PM - 1:25PM
 Obamacare's Impact on Radiology Payment

Silva, E.
 South Texas Radiology Group
 San Antonio, TX

Abstract/Presentation Summary
 This presentation will discuss in depth the emergence, implementation and impact of the Patient Protection and Affordable Care Act, aka Obamacare. A perfect political storm allowed this legislation to pass and the long term implications of that political storm will be highlighted. Comments will be made regarding the internal debates which occurred during the crafting of this legislation and how that impacts policy today. Focus will be paid upon the impacts of Obamacare on the Medicare Physician Fee Schedule, including the most common means of physician payment: fee for service. A detailed discussion of the Health Insurance Marketplace roll out will take place with comments provided regarding the future status of insurance networks and Medicaid across the country. Reference to the Massachusetts experience will be included. New payment models will be discussed including the demonstration projects taking place as well as the status of ACOs around the country.

O-383 1:25PM - 1:50PM
 National Entrepreneurial Radiology Initiatives - Evolution of Corporate Radiology

Muroff, L.
 Imaging Consultant, Inc
 Tampa, FL

Abstract/Presentation Summary
 This presentation will discuss the emergence and evolution of national entrepreneurial radiology companies. The topic will cover what these companies offer to hospitals, what they deliver, why they may be appealing to hospital administrators, and how radiologists might respond to this non-traditional competitive challenge. Radiologists must understand that this is not "business as usual". Strategies

for radiology groups to succeed in a changed environment will be covered. QUESTIONS: 1) Which of the following statements about national entrepreneurial radiology companies is true: A) Joining them is always voluntary for a radiology practice and its members. B) A common goal of these companies is to "go public" or be acquired by a publicly traded company. C) Radiologists who join these entities usually have a major say in how the company is run. D) The emergence of these companies is a new phenomenon seen only in the past five years.

O-384 1:50PM - 2:15PM
 Future of Neuroradiology

Mukherji, S.
 Michigan State University
 Ann Arbor, MI

Discussion 2:15PM - 2:30PM

Tuesday, May 20
1:00 PM – 2:30 PM
Room 524

43 - CSI Montreal Programming: Social Media and the Neuroradiologist

O-385 1:00PM - 1:30PM
 Social Media and the Neuroradiologist

Chen, J.
 San Diego VA / UCSD Med. Center
 La Jolla, CA

Abstract/Presentation Summary
 Is your practice ready? The Affordable Care Act is expected to increase the number of patients with health insurance. Many of them will need diagnostic imaging studies. All of them will have access to the internet. Are you ready to differentiate your practice to patients who all have access to the internet? Whether or not you are familiar with social media, social media can help with practice building and marketing. The concept of social media, social media mistakes, and selected content ideas will be introduced. The different metrics for effectiveness and return-on-investment compared to traditional marketing will be introduced.

Note: Scanned images are included in the proceedings. Some submitted images were reduced during editing thereby decreasing clarity. Also, refer to the Program Planner. Proceedings Content as of 3/28/2014.

O-386 1:30PM - 2:00PM
Using Social Media: Separating Your Personal Life from Your Professional Life

Patel, J.
Baltimore VA Medical Center
Baltimore, MD

Abstract/Presentation Summary

Social media has established itself as a powerful medium to connect people. Companies like Facebook, LinkedIn, Google, and Twitter have developed widely used communication tools and websites which facilitate networking, messaging, and sharing. "One to one" and "one to many" communication has never been easier. These tools have found applications across all disciplines including medicine. Social media can play a role in both the personal and professional lives of physicians. The session targets physicians who engage in or plan to engage in social media. The discussion will outline specific ethical, legal, and financial conflicts at the intersection of personal and professional social media. These conflicts will be described through representative case examples and analyzed from multiple perspectives. The session will conclude with strategies to minimize these conflicts and effectively integrate one's personal and professional online presence.

O-387 2:00PM - 2:30PM
Disruption Innovation: What Is It and What It Means for You

Chokshi, F.
Emory University School of Medicine
Marietta, GA

Abstract/Presentation Summary

Disruptive Innovation (DI) is all around us and many of us don't even know it. From your smartphone and tablet, to the PACS station you work on, to the diffusion weighted imaging that has revolutionized MR imaging, DI a phenomenon that upsets the status quo and breaks through the dogmatic thinking and processes afflicting any industries and professions. Find out about the way DI affects both your personal and professional life, especially how it has revolutionized radiology (especially Neuroradiology). Moreover, find out why it's so important to you. Background: Introduced by Clayton Christensen, Ph.D. (Harvard Business School) in 1997, Disruptive Innovation (DI) refers to a new technology or innovation that is rapidly adopted in an industry or profession, essentially replacing the "older", established status quo. Radiology is a field full of examples of DI, which may go unnoticed or under-appreciated by radiologists, possibly related a lack of exposure to the history behind DI and its implications to our field. From the advent of CT to the amazing power of MRI, and the workflow changing effect of PACS, DI has changed the face of radiology over the last half century.

Tuesday, May 20
3:00 PM – 4:30 PM
Room 517bc

44 - Parallel Papers: Head and Neck:
Neoplasia

O-388 3:00PM - 3:07PM
Osteoradionecrosis after Radiation Therapy for Head and Neck Cancer: Differentiation from Recurrent Disease with CT and PET-CT Imaging

S Fakhran A Reynolds L Alhilali
University of Pittsburgh Medical Center, Pittsburgh, PA

Purpose

To compare the CT and PET-CT imaging features of osteoradionecrosis (ORN) with those of recurrent disease after treatment of head and neck malignancy.

Materials and Methods

We retrospectively reviewed maxillofacial and neck CT scans performed for suspected ORN or tumor recurrence for the presence of 1) discrete solid mass, 2) cystic mass, 3) interruption of the bony cortex, 4) bony fragmentation, 5) bony trabecular loss, 6) intraosseous gas and 7) bony sclerosis. Trabecular bone loss was further categorized as permeative (<75% loss of trabecula) or lucent (>75% loss). Positron emission tomography (PET)-CT studies performed for suspected ORN or tumor recurrence were evaluated for SUVmean and SUVmax.

Results

Ten maxillofacial CT, 53 neck CT, and 23 PET/CT studies were performed in a total of 63 patients. Osteoradionecrosis was diagnosed by pathology or imaging stability in 46 patients, and tumor recurrence in 17 patients. Bony sclerosis was seen and found to be significantly more prevalent in ORN, and never seen with tumor recurrence (p=0.013). Patients with tumor recurrence were more likely to have a solid (p<0.001) or cystic mass (p=0.025), which was rare in ORN. While patients with tumor recurrence had significantly higher SUVmean and SUVmax, there was significant overlap in SUVmean and SUVmax between the two groups.

Conclusions

There is significant overlap of SUV values in patients with ORN and tumor recurrence. CT imaging findings provide more reliable diagnostic tools, with a solid or cystic mass strongly associated with tumor recurrence and bony sclerosis seen only with ORN.

KEYWORDS: Mandible

Note: Scanned images are included in the proceedings. Some submitted images were reduced during editing thereby decreasing clarity. Also, refer to the Program Planner. Proceedings Content as of 3/28/2014.

0-389 3:07PM - 3:14PM
Discordant Parathyroid 4DCT and Sestamibi Scintigraphy Results for Localization of Parathyroid Adenomas and Hyperplasia: What Factors Contribute to Missed Parathyroid Lesions?

L Galvin, J Oldan, J Sosa, J Hoang
Duke University Medical Center, Durham, NC

Purpose

To determine the prevalence of discordant results for parathyroid four-dimensional (4D) computed tomography (CT) and sestamibi scintigraphy and describe factors leading to missed adenomas for both modalities.

Materials and Methods

This was a retrospective review of 40 patients with primary hyperparathyroidism with pathologically proven parathyroid lesions that underwent both sestamibi scintigraphy with SPECT and 4DCT prior to parathyroidectomy between July 2009 and October 2013. Ultrasound was performed in 14 patients. The original radiology reports were reviewed with knowledge of the surgical results. The parathyroid lesions were categorized into four groups based on the radiology reports: a) both modalities correctly identified the lesion; b) neither modality correctly identified the lesion; c) 4DCT was correct and scintigraphy was incorrect; and d) 4DCT was incorrect and scintigraphy was correct. Interpretation of imaging studies could have been biased by availability of the other study, but this does not significantly favor one modality over the other since 16 patients had both modalities performed on the same day and two patients had 4DCT before scintigraphy. Imaging studies of missed lesions were reviewed by three radiologists (fellowship-trained in neuroradiology and nuclear medicine) for whether the lesion was seen in retrospect and potential factors limiting the original interpretation.

Results

There were 51 lesions in 40 patients with six cases of multiglandular disease. The sensitivities of 4DCT and scintigraphy were 85% (29/34) and 50% (17/34), respectively, for single adenomas; and 53% (9/17) and 24% (4/17), respectively, for multiglandular disease. Overall sensitivities for detection of all lesions by 4DCT and scintigraphy were 71% (36/51) and 41% (21/51), respectively. The sensitivity of ultrasound was 21%. The four categories of results and factors contributing to missed lesions are summarized in Table 1. In 20 patients with discordant imaging results, 4DCT was correct in 90% and scintigraphy was correct in 10%. Both modalities missed at least one lesion in 18% of all patients (7/40). Of 13 lesions missed on 4DCT, 10 were not evident on retrospective review. Of 30 missed lesions on scintigraphy, 21 were not evident on retrospective review.

Table 1. Radiology report result and factors contributing to missed parathyroid lesions

Radiology report results		Number of lesions as % of total lesions (n=51 lesions, 40 patients)	Predominant reason for missed lesions (n)	
4DCT	Scintigraphy		4DCT	Scintigraphy
Correct	Correct	19% (n=10, 20 patients)	---	---
Incorrect	Incorrect	22% (n=11, 7 patients)	Multiglandular disease (7) Heterogeneous thyroid (2) Low dose protocol (1) Large body habitus (1)	Multiglandular disease (7) Heterogeneous thyroid (2) Small lesion adjacent to the thyroid (2)
Correct	Incorrect	35% (n=18, 16 patients)	---	Small lesion adjacent to thyroid (6) Heterogeneous thyroid (3) Atrophylaryngeal location (2) High atrophylaryngeal space location (1) Multiglandular disease (2) Poor iodopic uptake (1)
Incorrect	Correct	4% (n=2, 2 patients)	Heterogeneous thyroid (1) Large body habitus (1)	---

*Low dose protocol with subcurrent modulation and maximum tube current of 500mA. Current protocol has a maximum tube current of 700 mA for the original phase.

Conclusions

Detection rates of 4DCT and sestamibi scintigraphy are discordant in 39% of lesions, with 4DCT correctly identifying the lesion in the majority of these cases. If the institution has experience in both modalities, 4DCT has higher sensitivity than scintigraphy and could have a role as the first line imaging modality. However, additional imaging with scintigraphy may be helpful in patients with heterogeneous/nodular thyroid glands or large body habitus. Multiglandular disease is a challenge for both modalities but 4DCT is more likely than scintigraphy to detect multiple lesions.

KEYWORDS: CT, Parathyroid

0-390 3:14PM - 3:21PM
Cystic lymph nodes as a predictor of prognosis in HPV-positive oropharyngeal squamous cell carcinoma.

S Narayanan, T Rath, M Hughes, R Ferris, B Branstetter
University of Pittsburgh Medical Center, Pittsburgh, PA

Purpose

Human papillomavirus (HPV) now is recognized to play an important role in oropharyngeal squamous cell carcinoma (OPSCC) pathogenesis. HPV-positive OPSCC is considered a distinct entity with better prognosis than HPV-negative cases. However, some patients with HPV-positive OPSCC have aggressive disease with higher recurrence and metastatic rates. The purpose of this study is to determine whether the presence of cystic lymph nodes on staging CT can act as an imaging bio-marker to predict prognosis in HPV-positive OPSCC.

Materials and Methods

This is an IRB approved HIPAA compliant retrospective study. Two hundred eighty-eight patients with HPV-positive OPSCC were identified from our tumor registry. Subjects were divided into two groups; those with and without recurrent disease. Staging CT was evaluated for patterns of nodal metastases. The presence of solid or cystic lymph nodes, size and cystic change of index LN and

Note: Scanned images are included in the proceedings. Some submitted images were reduced during editing thereby decreasing clarity. Also, refer to the Program Planner. Proceedings Content as of 3/28/2014.

overall percent of cystic lymph nodes were calculated. Patients were categorized based on the overall fraction of cystic versus solid lymphadenopathy into one of the three categories: predominantly solid (<20% cystic change), mixed (20-80% cystic change) and predominantly cystic (>80% cystic change). Recurrence rates were tabulated for each group, and Kaplan-Meier curves were plotted for disease-free survival.

Results

Recurrence was identified in 28 of the 288 patients (10%). Patients with predominantly cystic lymph nodes at staging had a recurrence rate of 4% (1/26), while patients with mixed cystic and solid nodes had a rate of 8% (11/141), and patients with solid nodes recurred at a rate of 13% (16/121). Kaplan-Meier curves also reflected these differences in disease-free survival.

Conclusions

In patients with HPV-positive OPSCC, greater cystic change in lymph node metastases on staging CT predicts better prognosis. This imaging biomarker may help to identify patients who would be more appropriate candidates for treatment de-escalation.

KEYWORDS: Head And Neck, Oropharynx

O-391 3:21PM - 3:28PM
How Do Radiologists Report Incidental Thyroid Nodules on CT and MRI? High Variability Across Subspecialties

A Grady, T Tanpitukpongse, K Choudhury, J Sosa¹, R Gupta, J Hoang
Duke University Medical Center, Durham, NC

Purpose

There are currently no widely accepted guidelines for reporting incidental thyroid nodules (ITNs) seen on computed tomography (CT) and MR imaging (MRI), and lack of guidelines may lead to variable practices. The purpose of this study is to describe the reporting practices of radiologists for ITNs seen on CT and MRI and to determine the factors that influence reporting.

Materials and Methods

This is a retrospective review of 401 patients with ITNs reported on CT and MRI examinations between January and December 2011. Patients were identified by searching CT and MRI reports for the phrase "thyroid nodule".

Patients were excluded if they had prior thyroid workup or a history of thyroid cancer. Data obtained from the reports included characteristics of patients, nodules, and reading radiologists. Radiology report outcomes of interest were whether the ITN was reported in the impression section of the report and whether further workup was recommended. Analyses were performed to identify factors associated with these outcomes.

Results

Three hundred seventy-five patients met the inclusion criteria (Table 1). The reporting styles were as follows: impression with ultrasound recommendation (n=67, 18%), impression with no recommendation (n=71, 19%), body of report only with ultrasound recommendation (n=2, 0.5%),

and body only with no recommendation (n=235, 63%). Three hundred fifty-three (94%) patients had ITNs reported on CT, and chest CT accounted for 62% (n=231) of all studies. Mean ITN size was 14.5 mm (range 3-56 mm) in those with reported sizes, but 185 (49%) reports did not provide nodule size. The factors that determined if an ITN was reported in the impression of the report were radiology division and nodule size on multivariate analysis (p<0.03, Table 1). Body division radiologists were least likely to report a nodule in the impression. Large ITNs were more likely to be reported in the impression (73% of nodules ≥20 mm). However, there was variability in reporting ITNs measuring 10-14 mm and 15-19 mm, which were reported in the impression in 61% and 50% of patients, respectively. The factors that determined if an ITN was recommended for ultrasound were radiology division and study indication on multivariate analysis (p<0.05, Table 1). Body division radiologists were least likely to recommend workup. Patients having imaging for another malignancy were least likely to have recommendation for workup.

Table 1. Characteristics of incidental thyroid nodules reported on CT and MRI by reporting styles

	All nodules	Reported in impression		Ultrasound recommended	
		Nodules Univariate p-value	Multivariate p-value	Nodules Univariate p-value	Multivariate p-value
n (%)	375	138 (37)		69 (18)	
Female, n (%)	250 (67)	93 (67)	0.82	46 (67)	1
Mean age, years (SD)	64 (14)	64 (15)	0.62	62 (13)	0.21
Study indication, n (%)					
Malignancy	196 (52)	44 (32)	<0.0001	13 (19)	<0.0001
Vascular	63 (17)	30 (22)	0.45	16 (23)	0.003
Trauma	43 (11)	21 (15)		8 (12)	
Inflammation/infection	24 (6)	15 (11)		11 (16)	
Other	49 (13)	28 (20)		21 (30)	
Radiologist experience, n (%)					
0-4 years	144 (38)	50 (36)	0.12	24 (35)	0.028
5-9 years	78 (21)	23 (17)		8 (12)	
7-10 years	153 (41)	65 (47)		37 (54)	
Radiology division, n (%)					
Chest imaging	92 (25)	40 (29)	<0.0001	29 (42)	<0.0001
Neuroradiology	103 (27)	52 (38)	0.028	25 (36)	0.049
Body imaging	172 (46)	40 (29)		10 (14)	

Conclusions

Reporting styles and recommendations for ITNs seen on CT and MRI are variable. The predominant factor that influences how a nodule is reported is the subspecialty of the radiologist, and not nodule and patient characteristics. Ideally, size should be used to categorize nodules for workup, as is the case for ultrasound guidelines. Development of CT/MRI practice guidelines for reporting ITNs has the potential to standardize ITN reporting by radiologists and thereby improve quality of care.

KEYWORDS: Incidental Findings, Report Style, Thyroid

O-392 3:28PM - 3:35PM
PET/CT in Head and Neck Squamous Cell Carcinoma: Should We Include the Head and the Abdomen?

U Yankevich¹, M Hughes¹, T Rath¹, S Fakhran¹, L Alhilali¹, J Grandis¹, S Kim², B Branstetter¹

¹University of Pittsburgh Medical Center, Pittsburgh, PA,
²University of Pittsburgh School of Medicine, Pittsburgh, PA

Purpose

Note: Scanned images are included in the proceedings. Some submitted images were reduced during editing thereby decreasing clarity. Also, refer to the Program Planner. Proceedings Content as of 3/28/2014.

Optimizing the utilization of positron emission tomography (PET)/computed tomography (CT) in patients with head and neck squamous cell carcinoma (HNSCC) is an important area of ongoing research. Although metastases from HNSCC to the head and to the abdomen are rare, these regions are often included in PET/CT protocols. These additional images create a financial burden on the health care system and require more time of the interpreting radiologist. The purpose of our study was to determine the diagnostic and therapeutic yield of the head and abdomen portions of PET/CT scans performed in patients with HNSCC to determine if these areas should be included routinely with PET/CT of the neck and chest.

Materials and Methods

We evaluated patients with pathologically proven HNSCC who had PET/CT scans for staging, restaging or surveillance of HNSCC from January 2007 to December 2012. Medical records were extracted from a dedicated Head and Neck Oncologic Data Repository. Patients with intracranial and intra-abdominal metastases were identified. All metastatic lesions were confirmed via biopsy or clinical follow up. The fraction of patients with evidence of HNSCC to the head and abdomen was tallied. Medical records then were reviewed to determine whether the abdominal and head findings changed the management of the patients, above and beyond the findings in the neck and chest.

Results

Seven hundred and four patients (1881 PET/CT scans) were included in the study. Eight patients (1.1%) had cranial involvement by cancer: in six patients (0.85%), this was a result of local tumor extension; two patients (0.3%) had distant calvarial metastases. None of the calvarial metastases changed patient management. Fourteen patients (2.0%) had intra-abdominal metastases. In nine patients (1.3%) the intra-abdominal findings changed the patient's management (surgical intervention in two patients, external radiation in one patient, and chemotherapy modification in six patients). In both patients with distant calvarial metastases and in 10 out of 14 patients with intra-abdominal metastases, the cranial and abdominal lesions coexisted with chest metastases and were part of multifocal disease progression. In four patients (0.6%) the intra-abdominal metastases were the only evidence of distant metastases.

Conclusions

Routine extension of PET/CT scans to include the head and abdomen in patients with HNSCC is not indicated. If other signs of metastatic disease are present (radiologic evidence of chest metastases or clinical evidence of spinal or abdominal metastases), then extension to these regions may be warranted. In patients without evidence of systemic metastases, routine PET/CT examinations should include the neck and chest only.

KEYWORDS: Cancer, Head And Neck, PET/CT

0-393 3:35PM - 3:42PM
Localization of Parathyroid Adenomas by Tc99m Sestamibi SPECT-CT, Contrast-enhanced Multi-phase CT (4D-CT) and Combination of SPECT-CT and 4D-CT

T Vu¹, F Wong¹, C Kappadth¹, S Wong², N Perrier¹, N Guha-Thakurta¹, H Chuang¹, E Rohren¹, D Schellingerhout¹
¹The University of Texas M.D. Anderson Cancer Center, Houston, TX, ²Methodist Hospital Research Institution in Houston, Houston, TX

Purpose

This study is designed to compare the abilities of Tc99m Sestamibi (MIBI) SPECT-CT, dynamic contrast-enhanced CT (4DCT) and combination of both modalities to identify parathyroid adenomas.

Materials and Methods

A retrospective study was conducted under an IRB-approved chart review for patients undergoing parathyroid adenoma resection in January 2010-June 2010. Parathyroid SPECT-CT was conducted after the patient received 20 mCi of Tc99m MIBI, 4DCT was conducted within two days from MIBI. All images were display in planar digital displays. Three teams of nuclear physicians and radiologist were assigned to interpret anonymized imaging studies without clinical or pathologic information. The surgical pathology is used as the gold standard. An A-F type location scheme was applied to identify the location of the lesions.

Results

A total of 41 evaluable patients were collected. Histopathology reported 46 lesions with 21 in the left and 25 in the right size. SPECT-CT correctly lateralized 36 lesion and identify 21 correct surgical types; 4DCT also lateralized 36 lesions but correctly identify 18 lesion types while combination of both correctly lateral 37 lesions and identified 24 lesion types.

Conclusions

The combination of 4DCT and MIBI SPECT CT may have additional diagnostic values for identification of parathyroid adenomas.

KEYWORDS: Parathyroid

0-394 3:42PM - 3:49PM
Diffuse metastases to the Thyroid Gland.

N Guha-Thakurta, (Debnam
The University of Texas M.D. Anderson Cancer Center, Houston, TX

Purpose

Metastases to the thyroid gland are rare and account for 2-3% of all malignant tumors of the thyroid. The most common primary malignancy is renal cell carcinoma, but thyroid metastases also have been reported from primary cancers in the gastrointestinal tract, lung, breast, and sarcoma. Metastases can be discovered incidentally or present with clinical complaints such as a new thyroid nodule, enlarged thyroid gland, neck swelling, dysphonia,

Note: Scanned images are included in the proceedings. Some submitted images were reduced during editing thereby decreasing clarity. Also, refer to the Program Planner. Proceedings Content as of 3/28/2014.

dysphagia or cough. Rarely they can present in a dramatic fashion with respiratory compromise requiring emergent tracheostomy. While previous reports have stated that thyroid metastases can occur as single or multiple masses, diffuse infiltration of the thyroid gland by metastases has not been described and characterized.

Materials and Methods

The patient demographics, clinical history, and multidetector computed tomography (MDCT) imaging findings of patients who demonstrated diffuse metastases to the thyroid gland from nonthyroid primary cancers were reviewed retrospectively.

Results

Diffuse thyroid metastases were identified in 15 patients (10 men and 5 women), age range 33-71 years (median 58 years). The primary malignancies included prostate (n=1), renal (n=1), melanoma (n=1), breast (n=3), lung (n=4), and head and neck cancer (n=5). The median time of detection of metastatic disease within the thyroid was two years after the initial diagnosis of the primary nonthyroid cancer. The imaging patterns include, diffuse hypodensity, or multiple coalescent nodules. Metastases to the thyroid either remained confined to the gland, or extended beyond the thyroid capsule to encase the adjacent vessels and structures.

Conclusions

Metastases to the thyroid gland should be considered following development of a new, diffuse enlargement of the thyroid gland in the context of a known primary elsewhere in the body irrespective of the remoteness of the history of prior malignancy. Diffuse infiltration of the gland by metastases can mimic primary thyroid cancer, lymphoma or thyroiditis. The diagnosis of metastases to the thyroid gland can be a challenge and a high index of suspicion is warranted especially in cases with an atypical infiltrative appearance.

KEYWORDS: Metastases, Thyroid

0-395 3:49PM - 3:56PM
Needle in a haystack: Diagnosing metastatic papillary thyroid carcinoma in patients with concurrent cervical nodal involvement by lymphoma.

S Ahmed¹, H Elamir², M Williams¹, B Edeiken-Monroe¹, M Debnam¹

¹The University of Texas M.D. Anderson Cancer Center, Houston, TX, ²The University of Texas Health Science Center at Houston, Houston, TX

Purpose

Ultrasound (US)-guided fine needle aspiration (FNA) biopsy is performed to document the presence or absence of lateral compartment metastasis to determine the need for neck dissection at the time of thyroidectomy. Pre-operative evaluation, including nodal selection for FNA, in the lateral compartments of the neck for metastatic papillary thyroid carcinoma (PTC) is challenging in patients with concurrent active lymphoma. The purpose of

this study was to evaluate the nodal imaging characteristics of concurrent lymphoma and PTC, and to describe differentiating features of adenopathy from each disease.

Materials and Methods

Hospital databases were queried for FNA diagnoses of PTC and lymphoma since 2004, yielding 53 patients with both diagnoses. Selection criteria included biopsy proven cervical lymphomatous involvement and co-existing PTC. Demographic and pathology data were obtained through retrospective chart review. Computed tomography (CT) and US examinations were evaluated retrospectively. Lymph nodes, status-post FNA, were identified on CT and US examinations, and nodal characteristics including morphology, echogenicity, calcification, and cystic change were recorded.

Results

Eleven patients, seven male and four female ranging in age from 38 to 75 years (median = 60 years) were included in the study. Total of 18 lymph nodes were evaluated preoperatively by US-guided FNA biopsy. Fourteen of 18 nodes demonstrated lymphoma and four demonstrated metastatic PTC. The 14 nodes demonstrating lymphoma showed the following characteristics: solid (n=14), cystic change (n=0), hypoechoic to muscle (n=12), isoechoic to muscle (n=2), calcification (n=0). The four nodes demonstrating PTC showed the following characteristics: solid (n=2), partially cystic (n=1), completely cystic (n=1). One of the solid nodes was hypoechoic with calcification, and the other was hyperechoic. The entirely cystic node biopsy initially yielded a nondiagnostic sample, and thyroglobulin washout assay was performed on the cystic fluid contents to confirm metastasis.

Conclusions

Calcification and cystic change of lateral compartment nodes suggest involvement by metastatic PTC in patients with active lymphoma (p=0.0049). These features can be used for nodal FNA selection to ensure that the correct diagnosis is made and the appropriate therapy is instituted. Thyroglobulin washout assay of the aspirate can be used to establish a diagnosis of PTC when the sample is acellular. Nodes with lymphomatous involvement are more likely to be solid and hypoechoic, whereas hyperechogenicity raises the concern for metastatic PTC.

KEYWORDS: Biopsies, Lymphoma, Thyroid

0-396 3:56PM - 4:03PM
Intra-tympanic contrast enhanced MRI evaluation of Meniere's Disease

J Bykowski¹, M Miller², J Du³, G Bydder³, J Harris³, M Mafee³
¹University of California San Diego Health System, La Jolla, CA, ²University of California San Francisco, San Francisco, CA, ³University of California San Diego Health System, San Diego, CA

Purpose

Dilute gadolinium-based MR contrast has been used in an off-label manner for the delineation of membranous

Note: Scanned images are included in the proceedings. Some submitted images were reduced during editing thereby decreasing clarity. Also, refer to the Program Planner. Proceedings Content as of 3/28/2014.

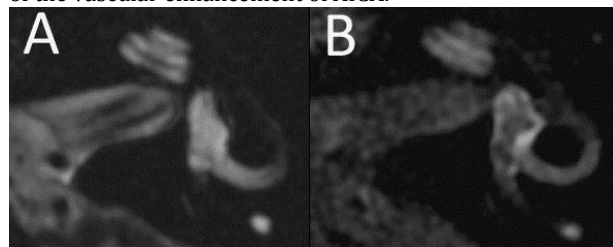
labyrinthine structures, and studies propose that the extent of endolymphatic hydrops in patients with Meniere's disease can be assessed with this technique. Our aim was to optimize a protocol for 3T MR imaging (MRI) after intratympanic contrast injection for the clinical setting, improving resolution and reducing the time for sequence acquisition.

Materials and Methods

FDA IND #115,342 was obtained for intratympanic injection of 1:7 v/v diluted Gd-DTPA (Magnevist) contrast. With IRB approval, five consenting adults with Meniere's symptoms refractory to medical therapy underwent 3T MR imaging 20-28 hours after intratympanic injection of dilute contrast into their more severely affected ear. Series were acquired with a standard head coil and a three-inch surface coil with sequences including high resolution heavily T2-weighted (FIESTA), T2 FLAIR, and T1 spin echo imaging pre- and postintravenous contrast administration. The area of the endolymphatic space (FLAIR signal void) and the perilymphatic space (contrast enhancement) were segmented manually for comparison. Mean signal intensity of an ROI placed in the basal turn of the cochlea of the injected ear was compared to that in the cochlear basal turn of the noninjected ear, and to that of a vertical segment of AICA for determination of relative signal intensity (rSI) ratios.

Results

In-plane resolution of 0.23 x 0.23 mm was achieved on FIESTA imaging, without resolution of Reissner's membrane. On FIESTA, the signal intensity of the perilymphatic space could not be distinguished from that of the endolymphatic space (Figure A). On FLAIR imaging, contrast was evident in the perilymphatic space of the vestibule, semicircular canals and cochlea of the injected ear in all patients after 20-28 hour delay (Figure B). Signal void corresponding to the endolymphatic space represented 34-50% of the vestibule in three participants and >50% in two participants, corresponding to mild and significant hydrops respectively per the proposed grading scale of Nakashima et al (1). By using the surface coil, in-plane resolution of 0.375 x 0.375 mm was achieved on FLAIR with a scan time of 4 min 12 sec. Contrast was detectable in the labyrinth on T1 images, however less visually conspicuous than on FLAIR sequences. Comparing the mean signal intensity of the cochlear basal turn in the injected versus noninjected ear yielded rSI ratios of 1.2 – 5.1 (average 2.8+/-1.6). T1 signal intensity in the injected cochlear basal turn was 0.5 – 0.8 (average 0.6 +/-0.1) that of the vascular enhancement of AICA.



Conclusions

Evaluation of the endolymphatic volume in patients with Meniere's symptoms can be accomplished using high

resolution FLAIR with minimal additional time added on to a standard internal auditory canal MR protocol. Contrast within the labyrinth on T1 sequences was not sufficiently intense that it should obscure an enhancing intralabyrinthine mass such as schwannoma, if present; however correlation for any filling defect on a heavily T2-weighted sequence is recommended. Performing the MR exam 20-28 hours after intratympanic diluted contrast injection allows for optimal contrast penetration of the perilymphatic spaces and facilitates patient scheduling.

KEYWORDS: Meniere, MR Contrast Agents

O-397

4:03PM - 4:10PM

CT Findings of the EAC in Patients After Middle Ear Surgery

V Mingkwansook¹, H Kelly², H Curtin³

¹Thammasat University, Prathumthani, Thailand,

²Massachusetts Eye and Ear Infirmary and Massachusetts General Hospital, Boston, MA, ³Massachusetts Eye and Ear Infirmary, Boston, MA

Purpose

Middle ear surgery performed through the external auditory canal (EAC) often involves drilling of a portion of the bony canal wall. On computed tomography (CT), such postoperative changes can mimic bony changes typically associated with neoplasms or aggressive infections of the EAC. The objective of this study was to evaluate and describe the CT appearance of the EAC after transcanal surgery so that erroneous diagnoses can be avoided.

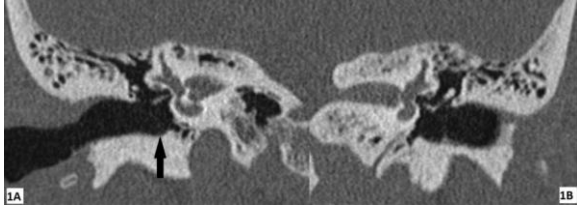
Materials and Methods

We retrospectively reviewed the CT examinations of 15 patients with a history of transcanal surgery who underwent postoperative multidetector CT (MDCT) or cone beam CT (CBCT) between July 2008 and January 2013. Two experienced neuroradiologists, reviewed the images for findings in the EAC including bony change, wall defects and soft tissue thickening. Demographic and operative data were subsequently collected.

Results

Time since operative intervention ranged from 10 months to 30 years. All 15 patients had osseous changes along the inferior wall (floor) of the EAC. The bony changes observed included thinning and flattening of the EAC floor resulting in loss of the normal tympanic sulcus (Figure 1). Similar osseous changes were seen in the anterior and superior walls of the EAC in seven out of 15 patients. The inferior wall was the most common site for bony defects (5 out of 15 patients), with the defects ranging in size from 2.0 – 8.1 mm. Soft tissue thickening also was seen most commonly along the floor of the EAC. The posterior wall was the least often involved, with osseous changes in four of 15 patients and a bony defect in a single patient. No patient was found to have a superimposed pathologic process of the EAC. Figure 1, coronal reformatted CT images demonstrate the typical convexity of the EAC floor in a normal right temporal bone (1A), with a well formed tympanic sulcus (arrow); compared to flattening of the EAC floor in the postoperative left ear (1B).

Note: Scanned images are included in the proceedings. Some submitted images were reduced during editing thereby decreasing clarity. Also, refer to the Program Planner. Proceedings Content as of 3/28/2014.



Conclusions

Computed tomography findings in the EAC after transcanal surgery include thinning, irregularity and/or flattening of the bone, soft tissue thickening and bony wall defects. The most common findings include involvement of the inferior wall with loss of the normal tympanic sulcus and flattening of the anterior wall of the EAC, as seen on axial images. Bony defects and soft tissue thickening also can be seen and should not prompt concern for a pathologic process. Knowledge of this normal postoperative appearance is useful to avoid misdiagnosis of external canal disease.

KEYWORDS: CT, Head And Neck, Temporal Bone

O-398 4:10PM - 4:17PM
Combined Contrast Enhanced CT of the Neck with PET/CT in the Baseline Assessment of Oral Cavity Cancer Post Treatment.

M Foley¹, A Aiken², K Baugnon³, A Kendi¹, J Wadsworth³
¹Emory University, Atlanta, GA, ²Emory University Hospital, Atlanta, GA, ³Emory University School of Medicine, Atlanta, GA

Purpose

The National Cancer Comprehensive Network (NCCN) guidelines for surveillance imaging in oral cavity cancer recommend imaging of the head and neck within six months of completion of therapy (surgery with or without radiation/chemotherapy). At our institution, there has been a transition towards a combined positron emission tomography (PET) and contrast-enhanced neck computed tomography (CECT) to serve as this baseline assessment. The purpose of this study was to assess the performance of both components alone and together in the assessment of local, regional and metastatic disease. We hypothesize that PET alone may lead to a higher number of false positives for local recurrence due to recognized pitfalls in the post-treatment oral cavity.

Materials and Methods

A database inquiry of all patients who received a PET/CECT between 2009 and 2012 and an ICD 9 code for oral cavity cancer was performed. This identified 348 studies involving 287 patients. Of this group, 37 patients met the following inclusion criteria: 1. Primary squamous cell carcinoma (SCCA) of the oral cavity, 2. First staging study post-treatment was a PET/CECT, 3. At least three months imaging and clinical follow up. The PET/CT portion of the study (without the diagnostic CECT Neck) was reviewed independently and retrospectively by a nuclear medicine physician. The CECT of the neck was reviewed retrospectively by a consensus of two neuroradiologists specializing in head and neck imaging. Finally, the initial

reports generated by a consensus read between nuclear medicine and head and neck radiology were reviewed. Both modalities were assessed for local, regional and distant metastasis. Findings were categorized as positive, negative and indeterminate for recurrent or metastatic disease. Clinical and imaging follow up, with biopsy results where available served as the gold standard for imaging performance.

Results

Of the 37 patients, four patients had local recurrence and five patients had regional recurrence on the initial post-treatment scan, one of which with both local and regional disease. Both CECT and PET/CT correctly identified local recurrence in three cases (Sens 75%). PET/CT had a higher number of false positives (3, PPV 50%) for local recurrence than CECT (0, PPV 100%). CECT had a higher number of indeterminate classifications (6) than PET/CT (2). Of the CECT indeterminate findings, PET/CT helped to correctly downgrade to a negative read in five of the six cases, but incorrectly upgrade to a positive read in one case (false positive). However, in four of those cases (66%), the area of imaging concern localized to the mucosal surface, which could be assessed clinically. The remaining two cases had imaging concerns in the deep tissues of the surgical site. For regional disease, CECT correctly identified four of five cases of regional recurrence, while the fifth recurrence had been assigned an indeterminate value. PET/CT correctly identified five of five cases of regional recurrence. For distant metastasis, PET/CT identified four of four patients and CECT neck identified three of four patients (as disease was localized to upper mediastinum) The fourth case of distant disease manifested as pulmonary nodules, included only on the CT portion of the PET/CT.

Conclusions

This initial study suggests that combined PET/ CECT may not be cost-effective as a routine screening tool in the baseline post-treatment assessment for all oral cavity cancers. While PET imaging was helpful in downgrading the indeterminate findings on CECT for local disease recurrence, in four of six of those cases, the abnormality was on the mucosal surface and could be assessed clinically. This was countered by a significantly higher false positive rate on PET/CT, with such pitfalls as muscle fasciculations, mucositis, and physiological asymmetry contributing to this finding. CECT of the neck may suffice as a baseline study in the post-treatment setting of oral cavity cancer, with PET/ CECT reserved for cases where there is a concern for deep recurrence or patients at high risk for regional and distant metastasis. A larger study of cost-effectiveness and patient outcomes would be needed to determine which oral cavity cancers should undergo upfront surveillance with PET/CECT.

KEYWORDS: Contrast-Enhanced CT, Oral Cavity, PET/CT

Note: Scanned images are included in the proceedings. Some submitted images were reduced during editing thereby decreasing clarity. Also, refer to the Program Planner. Proceedings Content as of 3/28/2014.

0-399 4:17PM - 4:24PM
Errors in Radiology Reports for Head and Neck Cancer: Types and Frequencies for Cases Stratified by History, Primary Site, Cancer Stage, and Imaging Center

J Lysack, M Hudon, J Dort
University of Calgary, Calgary, Alberta, Canada

Purpose

Patients with head and neck cancer often present to academic tertiary referral centers with imaging studies that have been performed and interpreted elsewhere (1). Prior studies show that formal review of these outside imaging studies by an academic neuroradiologist with expertise in head and neck imaging frequently leads to clinically meaningful changes in the cancer stage and treatment plan (2-4). We hypothesize that subspecialty radiologist second opinions may be of greater value in particular subsets of these cases. The purpose of this study was to determine the radiology error rates for groups of cases stratified by history, primary site, cancer stage, and imaging center.

Materials and Methods

Our institutional review board approved the retrospective review of electronic medical records, including original and second opinion radiology reports, for 100 consecutive cases of biopsy proven or clinically suspected head and neck cancer referred to our academic tertiary cancer center. The presence or absence of "misses" and "misinterpretations", with regard to the primary tumor and lymph node metastases, was determined for each original radiology report. A "miss" was defined as the absence of a reported finding in the original report that would correspond to clinically significant pathology when it was identified correctly in the second opinion report. A "misinterpretation" was defined as a finding that was interpreted incorrectly as benign versus malignant or was described insufficiently to allow for local tumor staging in the original radiology report when it was interpreted correctly and sufficiently described in the second opinion report. Correct identifications and interpretations were defined as those corresponding to the recorded TNM cancer staging as had been determined by the multidisciplinary cancer care team as part of routine clinical practice. The 100 cases were stratified by: (1) history (initial staging for known cancer versus imaging investigation for nonspecific symptoms – e.g., "lump in neck"), (2) primary site (oral cavity, oropharynx, larynx, other), (3) cancer stage (high stage versus low stage), and (4) imaging center (urban versus rural). The error rates for the entire cohort and for the stratified groups were calculated, and Fisher's exact test using a threshold for statistical significance of $P < .05$ was used to reject the null hypothesis that the error rate for each group was the same.

Results

At least one clinically significant error was present in 66.0% of the original radiology reports (95% CI: 56.3-74.6%). There was at least one "miss" in 33.0% of reports (95% CI: 24.5-42.7%) and at least one "misinterpretation" in 41.0% of reports (95% CI: 31.9-50.8%). The primary tumor was missed in 20.0% of cases (95% CI: 13.3-

29.0%) and was misinterpreted in another 35.0% of cases (95% CI: 26.4-44.8%). Metastatic lymphadenopathy was missed 19.0% of the time (95% CI: 12.4-27.9%) and was misinterpreted 11.0% of the time (95% CI: 6.1-18.8%). There was a trend toward fewer primary tumors being missed when the scan was done for a known history of cancer than when the scan was done for nonspecific symptoms, but this was not statistically significant (15.9% versus 38.9%; $P=0.128$). Even when the specific primary site was known, the primary tumor was missed 17.0% of the time (95% CI: 9.0-29.5%). Oral cavity primaries were missed more often than other primaries (40.0% versus 13.3%; $P=0.033$). There was no significant difference in error rates for high stage (69.1%) versus low stage (52.6%) cancers or for rural (67.5%) versus urban (65.0%) imaging centers.

Conclusions

Clinically significant errors occur in the majority of outside radiology reports for patients presenting to an academic tertiary referral center with a known or suspected head and neck cancer. Risk stratification based on history, primary site, cancer stage, and imaging center location did not reveal a low risk group. Outside imaging for all patients with head and neck cancer should be reviewed by a neuroradiologist with expertise in head and neck imaging as part of a multidisciplinary team.

KEYWORDS: Head And Neck, Quality Improvement, Report Content

0-400 4:24PM - 4:31PM
Pediatric Parotid Neoplasms: A 10-Year Retrospective Review of These Rare Tumors

M Mamlouk, K Rosbe, C Glastonbury
University of California San Francisco, San Francisco, CA

Purpose

Most adult primary parotid gland neoplasms are benign and are pleomorphic adenomas. We aimed to identify the types and distribution of pediatric parotid gland neoplastic masses, and to determine imaging or presenting clinical features that might suggest malignancy.

Materials and Methods

Institutional review board approval was obtained. Hospital electronic medical records were reviewed for all patients younger than 18 years with pathology proven parotid neoplasms presenting to our tertiary referral center over the 10-year period from 2003 to 2013. Infantile hemangiomas and neurofibromas secondarily involving the parotid gland in patients with known neurofibromatosis type 1 were excluded from evaluation. Imaging features of all lesions were analyzed, and the presenting clinical features were reviewed.

Results

Eighteen patients (10 boys, 8 girls; age range: 2-17 years) were identified with neoplastic parotid masses; 11 were malignant and seven were benign. The malignant tumors consisted of three acinic cell carcinomas, two mucoepidermoid carcinomas, one alveolar rhabdomyosarcoma, one poorly differentiated carcinoma, one low-grade adenocarcinoma, and three nodal metastases (2 melanoma, 1 orbital medulloepithelioma). The seven benign tumors consisted of

Note: Scanned images are included in the proceedings. Some submitted images were reduced during editing thereby decreasing clarity. Also, refer to the Program Planner. Proceedings Content as of 3/28/2014.

six pleomorphic adenomas and one schwannoma. Radiologic imaging was available in 14/18 patients; 13 MR imaging (MRI) and three computed tomography (CT). Imaging features that were highly suggestive of malignancy included: low T2 signal, reduced diffusion, and ill-defined borders. Pleomorphic adenomas had similar characteristics to those in adults in two of four of the patients with available imaging appearing well circumscribed with homogeneously hyperintense T2 signal and heterogeneous enhancement. Two patients, one with acinic cell carcinoma and the other with alveolar rhabdomyosarcoma, had imaging features indistinguishable from this despite their malignant histology. The two patients with confirmed pleomorphic adenoma and nontypical imaging findings had low T2 signal and focal internal hemorrhage in one and multifocal nodular recurrent disease presenting as a mass in the other. A painless enlarging mass was the most common symptom in 10 patients (5 benign, 5 malignant), followed by asymptomatic in four patients (all malignant), and painful enlarging mass in one patient with a pleomorphic adenoma.

Conclusions

While pediatric primary parotid neoplasms are rare, even at a tertiary referral hospital, there is a greater likelihood that a new parotid mass is malignant. This is in distinction to adult parotid tumors, which are statistically likely to be benign. MR imaging features that should raise concern for malignancy include: ill-defined borders, low T2 signal, and reduced diffusion; however, some malignant tumors in our patient group had imaging appearances identical to classic pleomorphic adenomas. Clinical presenting symptoms did not differ between the benign and malignant tumors. It is thus important when evaluating pediatric parotid masses to have a high degree of suspicion of malignancy, and recommend FNA in order to enable timely correct clinical management.

KEYWORDS: Masses, Parotid Gland, Pediatric Head And Neck

Tuesday, May 20
3:00 PM – 4:30 PM
Room 517d

45 - Mini Symposium: Tumor – Part IV

O-401 3:00PM - 3:15PM
DSC-MRI and the Identification of Tumor Recurrence in the Setting of Pseudoprogression and Pseudoresponse

Boxerman, J.
Rhode Island Hospital
Providence, RI

Abstract/Presentation Summary

Increased enhancement on post-treatment MRI of high-grade gliomas can represent treatment-related effects, including early-delayed pseudoprogression (PsP) and late-delayed radionecrosis, or true progressive disease (PD). Whereas conventional MRI has proved unreliable for

prospectively distinguishing PsP and radionecrosis from PD, DSC-MRI with measures of relative cerebral blood volume (rCBV) has shown promise. Although rCBV is generally higher in PD compared with radionecrosis, its ability to distinguish PsP from PD is more controversial, with some studies concluding that specific thresholds are helpful, and others asserting the opposite. Overlapping rCBV measurements in PsP and PD are common, and fractional tumor burden maps of enhancing lesions reveal rCBV patterns consistent with mixtures of PsP and PD, emphasizing the limitations of single-mean rCBV values for discrimination. PsP appears to lie somewhere between radionecrosis and active tumor in a histopathological spectrum, and coexistent viable irradiated tumor and necrosis present wide-ranging vascular morphologies that likely explain overlapping mean rCBV between PsP and PD at initial progressive enhancement. Measures of spatial (histogram analysis, parametric perfusion maps) and temporal (longitudinal trends) rCBV variation are therefore likely to be more useful than mean rCBV for predicting lesion destiny because over time, tumor-to-PsP ratios increase when PD dominates, with correspondingly increased rCBV, and the converse should be true for PsP domination. Pseudoresponse (improved contrast enhancement not necessarily reflecting true anti-tumor effect) is commonly seen with anti-angiogenic drugs interfering with VEGF signaling and reducing blood-brain barrier permeability. Whereas progressive enhancement of recurrent GBM treated with anti-angiogenic therapy correlates significantly with poor overall survival (OS), decreased enhancement does not (responsive and non-responsive/non-responsive enhancement have similar OS). Although progression of non-enhancing disease (FLAIR) may occur following anti-angiogenic therapy, evidence that FLAIR progression correlates with OS is controversial. However, recent data suggest that decreased rCBV shortly after treatment predicts longer PFS and OS in bevacizumab-treated tumors, and that rCBV can prognosticate patients with non-progressive enhancement and select patients with greater likelihood of response to bevacizumab treatment. DSC-MRI parameters, including pulse sequence (GE versus SE, TE, flip angle, field strength), contrast agent (relaxivity, pre-load dose and incubation time, bolus dose and injection rate), and post-processing (leakage correction, integration methodology) can substantially impact quantitative rCBV estimates, as can inter-reader variability in segmentation of tumor and reference brain. Intra- and inter-subject comparisons of rCBV therefore require consistent methodology. Because contrast agent leakage confounds Gd-based rCBV measures, ferumoxytol-based rCBV measures have been proposed as a better alternative for assessing treatment response. Vessel size index and percent signal recovery are additional computed DSC-MRI parameters that may provide complimentary information about treatment response.

Note: Scanned images are included in the proceedings. Some submitted images were reduced during editing thereby decreasing clarity. Also, refer to the Program Planner. Proceedings Content as of 3/28/2014.

O-404 3:30PM - 3:45PM
DCE-MR: Evaluating Tumor Recurrence from Treatment-Induced Change

Jain, R.
NYU Langone Medical Center
New York, NY

Abstract/Presentation Summary

Various imaging techniques have been employed to evaluate blood-brain-barrier leakiness in brain tumors as higher tumor vascular leakiness is known to be associated with higher grade and malignant potential of the tumor, and hence can help provide additional diagnostic and prognostic information. These imaging techniques range from routine post-contrast T1-weighted images that highlight degree of contrast enhancement to absolute measurement of quantitative metrics of vascular leakiness employing pharmacokinetic modeling methods (1-3). Brain tumor patients undergo various combination therapies, which can lead to complex and confusing imaging appearance on follow-up MRI. Therefore, the differentiation of recurrent or progressive tumor from treatment-induced necrosis (4) or effects has always been a challenge in neuro-oncologic imaging. The purpose of this presentation is to discuss the clinical utility of dynamic contrast-enhanced T1-weighted MR imaging (DCE-MRI) to differentiate tumor recurrence from treatment-induced changes.

O-407 4:00PM - 4:15PM
RANO Criteria: How it Evolved and Where it Currently Stands

Fatterpekar, G.
NYU Langone Medical Center
New York, NY

Abstract/Presentation Summary

Discussion will include: 1. Evolution in the "standard of care" treatment strategies in patients with high-grade gliomas. 2. Understanding the terms tumor progression, pseudoprogression, and pseudoresponse, and the underlying pathophysiology. 3. Evolution of imaging based-response assessment from MacDonald to RECIST to PERCIST to currently accepted RANO criteria to keep up with the change in treatment strategies. 4. Comparison of these various response assessment criteria in high-grade gliomas. 5. Are the currently accepted RANO criteria sufficient? 6. Role played by advanced imaging and the different contrast agents in assessing treatment response. 7. Future directions for monitoring treatment response in high-grade gliomas.

O-402 3:15PM - 3:21PM
Prediction of response to concurrent chemoradiotherapy with temozolomide in glioblastoma: application of immediate post-operative dynamic susceptibility contrast and diffusion-weighted imaging

S Choi
Seoul National University Hospital, Seoul, Korea

Purpose

Even though the immediate postoperative MR imaging (MRI) can be used to evaluate the presence of residual tumor or operation-related complications in glioblastoma patients, there have been no reports regarding its application for the prediction of response to concurrent chemoradiotherapy (CCRT) with temozolomide using dynamic susceptibility contrast (DSC) and diffusion-weighted imaging (DWI). The purpose of this study was to determine whether histogram analysis of apparent diffusion coefficient (ADC) and normalized cerebral blood volume (nCBV) maps of enhancing lesions detected by immediate postoperative MR images could predict the response to CCRT with temozolomide, and to correlate parameters from histogram analysis of ADC and nCBV maps with the progression-free survival (PFS).

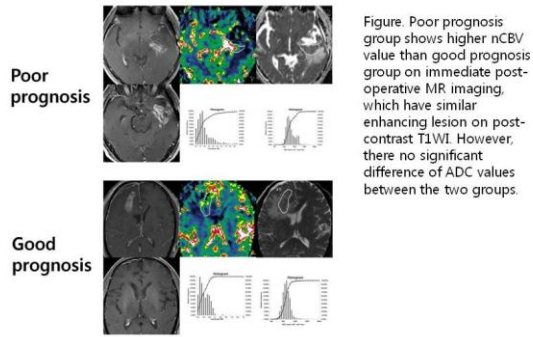
Materials and Methods

We enrolled 24 patients with glioblastoma, who showed measurable contrast enhancement on immediate postoperative MRI. In all patients, DSC perfusion imaging and DWI ($b = 0, 1000 \text{ sec/mm}^2$) were obtained. The corresponding nCBV and ADC maps were calculated for the measurable enhancing lesions. Among them, 11 patients showed progression after 2–6 cycles of adjuvant TMZ (progression group), while complete response or stable status was observed in 13 patients (nonprogression group). The histogram parameters from nCBV and ADC maps between the two groups were compared using an unpaired Student's T-test. Receiver operating characteristics (ROC) analysis was used to find the best cutoff value of each parameter for the prediction of progression after CCRT. One year progression-free survival was determined by using the Kaplan-Meier method with log-rank test.

Results

The 99th percentile of the cumulative nCBV histogram (nCBV C99) on immediate postoperative MR imaging was a significant predictor for true progression after CCRT ($P = 0.033$). However, we could not find significant differences of mean nCBV, mean ADC, and other histogram values from nCBV and ADC maps between two groups. Receiver operating characteristics analysis showed that the best cutoff value was 5.537 for the prediction of progression after CCRT, and sensitivity and specificity was 72.7% (8 of 11 patients) and 76.9% (10 of 13), respectively.

Note: Scanned images are included in the proceedings. Some submitted images were reduced during editing thereby decreasing clarity. Also, refer to the Program Planner. Proceedings Content as of 3/28/2014.



Conclusions

The nCBV C99 of the cumulative histogram analysis of nCBV from immediate postoperative MRI can be a useful method for the prediction of progression and PFS after CCRT in glioblastoma.

KEYWORDS: DSC MR Imaging, Glioblastoma, Radiation Therapy

O-403 3:21PM - 3:27PM
Functional Imaging for Follow-up of Brain Gliomas: Comparison between Dynamic Susceptibility Contrast Perfusion MR and Methionine Metabolism

M Beltran Marin¹, C Mathey¹, S Goldman², F Lefranc¹, N Sadeghi²

¹ULB-Erasme Hospital, Brussels, Belgium, ²Erasme Hospital, Brussels, Belgium

Purpose

Dynamic susceptibility contrast (DSC) MR and positron emission tomography (PET) using carbon-11 methionine (MET) are both used in the follow up of patients with brain gliomas for the early detection of tumor recurrence as well as for the distinction between tumor recurrence and post-treatment effects (1-3). The access to MET is restricted in many sites because of the short half-life of carbon-11 methionine, whereas DSC MR imaging and CBV measurements now are performed routinely in most centers with no additional cost during the follow-up imaging of brain tumors. The purpose of this study is to compare quantitatively the information provided by cerebral blood volume (CBV) based on DSC-MR and by maximum carbon-11 methionine uptake based on PET performed during the follow-up imaging work up of brain gliomas.

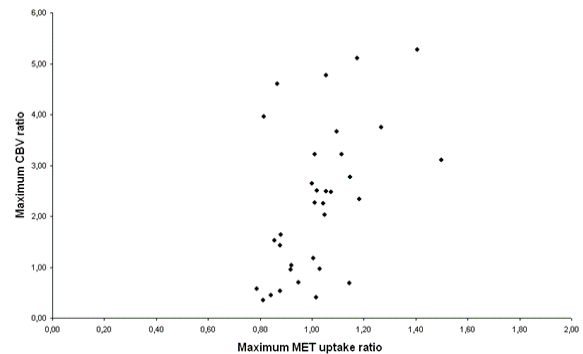
Materials and Methods

Thirty-three patients with histologically proven primary brain gliomas were included in the study. In addition to conventional MR sequences, dynamic contrast-enhanced MR and PET study using MET, were acquired on the same day during their follow up. Fifteen patients had low grade gliomas and eighteen patients had high grade gliomas. Patients with low grade gliomas had been treated by surgery only, whereas those with high grade tumors had been treated by surgery and radiation and/or chemotherapy. Maximum CBV as well as maximum MET uptake values were recorded and normalized to normal

brain values. The sites of CBV measurements were based on FLAIR/T2 abnormality and/or enhancement on T1-weighted with contrast. Cerebral blood volume values also were measured at the site of maximum PET-MET uptake measurements for a local comparison. Cerebral blood volume ratios and MET-uptake ratios were compared using Spearman rank order correlation test.

Results

Maximum CBV ratios ranged from 0.35 to 5.27 (n= 33, Mean= 2.27, SD=1.46) and maximum MET uptake ratios ranged between 0.79 and 1.50 (n= 33, Mean= 1.02, SD= 0.16). Cerebral blood volume ratios measured at the same region as maximum MET uptake ranged between 0.28 and 6.15 (Mean= 2.11, SD= 1.51). A positive significant correlation was found between maximum MET uptake ratios and maximum CBV ratios (Spearman rank order correlation: $r = 0.53$, $p < 0.01$) (Figure 1). The correlation was stronger when MET values were correlated to CBV values measured at the site of PET measurement (Spearman rank order correlation: $r = 0.58$, $p < 0.001$).



Conclusions

During the follow up of treated brain gliomas, we found a relation between metabolic information provided by PET-MET studies and vascularity information provided by DSC MR studies.

KEYWORDS: Cerebral Blood Volume, Glioma, PET

O-405 3:45PM - 3:51PM
Complimentary Role of Brain Dynamic Contrast-Enhanced MR Perfusion for Posttreatment Evaluation of Brain Tumors: Use of 'Stack-of-Stars' Scheme and k-Space Weighted Image Contrast

K Nael, R Khan, W Erly, M Lemole, S Sckolnik, B Stea, A Bilgin
University of Arizona, Tucson, AZ

Purpose

In comparison to dynamic susceptibility contrast (DSC), dynamic contrast-enhanced (DCE) is technically a more demanding technique but provides a different prospective of blood-brain barrier and tumor angiogenesis and may be of additional value, where DSC could be affected by susceptibility artifacts. Introduction of imaging tools such as radial k-space sampling 1 and echo-sharing techniques such as k-space weighted image contrast (KWIC) 2 have

Note: Scanned images are included in the proceedings. Some submitted images were reduced during editing thereby decreasing clarity. Also, refer to the Program Planner. Proceedings Content as of 3/28/2014.

improved the efficiency of dynamic contrast imaging in terms of coverage, spatial and temporal resolutions. The purpose of this study was to prospectively assess the added value of an improved DCE perfusion technique in evaluation of post-treated brain tumors and compare the result to DSC perfusion and surgical pathology in a subset of patients.

Materials and Methods

In this prospective study, 20 consecutive patients (12 males, age range: 36-72 years old) who were being treated for brain tumors underwent MR imaging (MRI) on a 3.0 T MR scanner (Siemens Skyra) including DCE and DSC perfusion. The DCE perfusion was acquired by a 3D radial VIBE (volumetric interpolated examination) sequence (TR/TE: 3.6/1.7 ms, voxel size 1.4 x 1.4 x 3mm). A total of 328 radial views were acquired in eight rotations (42 views/rotation) with 'stack-of-stars' scheme. Three measurements were obtained each divided to eight subframes by applying KWIC, resulting in whole brain coverage with three minutes acquisition time and a four sec temporal resolution. Subsequently DSC perfusion was performed using a gradient-EPI sequence (TR/TE: 1450/22 ms, voxel size 1.7 x 1.7 x 4 mm³). A total of 0.2 mmol/kg of gadolinium was used to accomplish both DCE and DSC. The DCE image quality was evaluated independently by two neuroradiologists using a 1-4 grading scale in respect to motion and pulsation artifact, brain edge sharpness and vascular conspicuity. Perfusion datasets were processed using a commercially available FDA approved software (Olea Medical, La Ciotat, France). The arterial input function was selected automatically and multiparametric perfusion maps were calculated using an extended toft model for DCE and block-circulant singular value decomposition technique for DSC. The perfusion maps, FLAIR and T1 postcontrast images for each patient were coregistered using the Olea software. K-trans (minutes⁻¹) and rCBV values were calculated from the region of interests for each patient.

Results

All DCE studies were rated with diagnostic image quality (median: 3, range: 3-4) by both observers and with excellent interobserver agreement (k=0.82). In 11 patients the k-trans values and perfusion permeability curve pattern were suggestive of tumor recurrence and concordant with rCBV values >1.5 3-4. In six patients the k-trans values and perfusion permeability curve pattern were suggestive of radiation necrosis and concordant with rCBV < 1. In three patients (15%), DSC maps were nondiagnostic due to blood-product susceptibility artifact within the surgical bed, in whom DCE was able to predict tumor recurrence. In seven patients (35%) the perfusion findings were confirmed subsequently by surgical pathology.

Conclusions

The described DCE perfusion technique is feasible with acceptable result in comparison to DSC perfusion and can provide additional diagnostic value in a subset of patients with brain tumor in whom DSC may be limited by susceptibility artifact related to post-treatment surgical bed. Radial k-space sampling provides several advantages including lower motion sensitivity, benign undersampling

behavior and lack of aliasing artifact, while KWIC helps to maintain the temporal resolution.

KEYWORDS: Brain Neoplasms, DCE MR Imaging, Radiation Necrosis

O-406

3:51PM - 3:57PM

Differentiation of True Progression and Pseudoprogression by Use of Quantitative Dynamic Contrast-Enhanced MR Imaging in Glioblastoma Treated with Radiation Therapy and Concomitant Temozolomide

S Choi

Seoul National University Hospital, Seoul, Korea

Purpose

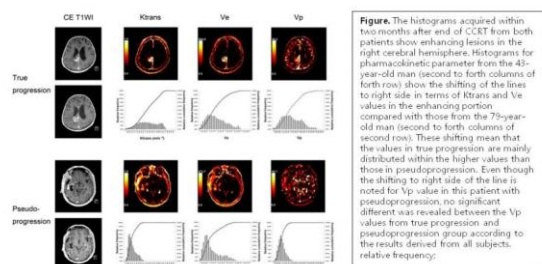
To assess the ability of dynamic contrast-enhanced (DCE) MR imaging (MRI) to discriminate true progression from pseudoprogression in glioblastoma treated with concurrent chemoradiotherapy.

Materials and Methods

We conducted a prospective study in 33 patients with histopathologically proven glioblastoma, who had undergone concurrent chemoradiotherapy. Dynamic contrast-enhanced-derived pharmacokinetic parameters including Ktrans, Ve, and Vp were calculated from the newly developed or enlarged enhancing lesions. The pharmacokinetic parameters between true progression (n=17) and pseudoprogression groups (n=16) were compared using unpaired t-tests, which also were compared using multivariable analysis.

Results

The mean Ktrans value was higher in the true progression group than that in the pseudoprogression group (0.44 ± 0.25 and 0.23 ± 0.10 min⁻¹, retrospectively, $p = .004$). In terms of the cumulative Ktrans histograms, 5th, 10th, and 50th percentile points also were significantly higher in the true progression group than those in the pseudoprogression group ($p \leq .020$). We also observed the higher mean Ve value in the true progression group than in the pseudoprogression group (1.26 ± 0.78 and 0.75 ± 0.49 , retrospectively, $p = .034$). With regards to the cumulative Ve histograms, we found the higher 5th and 10th percentile points in the true progression group than those in the pseudoprogression group ($p \leq .015$). Multivariable analysis showed that mean Ktrans value was the only independently differentiating variable ($p = .004$).



Note: Scanned images are included in the proceedings. Some submitted images were reduced during editing thereby decreasing clarity. Also, refer to the Program Planner. Proceedings Content as of 3/28/2014.

Conclusions

The mean Ktrans parameter is the most promising parameter in the differentiation of true progression from pseudoprogession among the useful Ktrans and Ve values of the DCE MR imaging.

KEYWORDS: DCE MR Imaging, Glioblastoma, Radiation Therapy

O-408 3:51PM - 3:57PM
Differentiation of Pseudoprogession and Real Progression in Glioblastoma Using Apparent Diffusion Coefficient Parametric Response Maps

A Radbruch¹, M Bendszus¹, C Reimer¹, W Wick¹, B Wiestler¹, H Schlemmer², R Floca²

¹University of Heidelberg, Heidelberg, Germany, ²German Cancer Research Center (DKFZ), Heidelberg, Germany

Purpose

Pseudoprogession describes the radiologic phenomenon that patients with high grade glioma undergoing their first or second radiation MR imaging (MRI) show increased contrast enhancement that eventually subsides without any change in treatment. Currently it is not possible to differentiate real progression and pseudoprogession using conventional T1- and T2-weighted images. Here we tested if a voxelwise analysis of apparent diffusion coefficient (ADC) values can differentiate between true progression and pseudoprogession using the parametric response map, a new postprocessing procedure.

Materials and Methods

Twenty-nine patients with proven progression and seven patients with pseudoprogession were identified in a retrospective case study. For all patients ADC baseline and follow-up maps were available. The ADC baseline map and the ADC follow-up map were coregistered on the contrast-enhanced T1-weighted follow-up images. Subsequently the enhancement in the follow-up contrast-enhanced [Dotarem (Gadoterate meglumine)] T1-weighted image was delineated manually and a reference region of interest (ROI) was drawn in the contralateral white matter. Both ROIs were transferred to the ADC images. Relative ADC (rADC) (baseline)/reference ROI (baseline) values and ADC (follow up)/reference ROI (follow up) values were calculated for each voxel within the ROI. The corresponding voxels of rADC (follow up) and rADC (baseline) were subtracted and the percentage of all voxels within the ROI that exceeded the threshold of 0.25 was quantified.

Results

Relative ADC voxels showed an increase of 21.9+-26.3% above 0.25 in patients with real progression and in 55.7 +/- 28.3% in patients with pseudoprogession. Receiver operating characteristic (ROC) analysis revealed a very good diagnostic performance (AUC = 0.82).

Conclusions

The introduced parametric response map for rADC maps provides a potential tool for the differentiation between pseudoprogession and real progression. Generally an ADC

increase is supposed to be correlated with a decrease of cellularity and hence with therapy response. Therefore our findings of an increased number of voxels with increased ADC values in patients with pseudoprogession are in line with these basic pathophysiologic considerations.

KEYWORDS: Glioblastoma, Pseudoprogession

Tuesday, May 20
3:00 PM – 4:30 PM
Room 517a

46 - Parallel Papers: Brain: Functional Imaging II

O-411 3:00PM - 3:07PM
MEG Graph Theoretic Connectivity Analysis

J Maldjian, E Davenport, C Whitlow
Wake Forest University School of Medicine, Winston-Salem, NC

Purpose

Interhemispheric connectivity with resting state magnetoencephalographic (MEG) has been elusive, and demonstration of the default mode network (DMN) yet more challenging. Recent seed-based MEG analyses have shown interhemispheric connectivity using power envelope correlations. The purpose of this study is to compare graph theoretic maps of brain connectivity generated using MEG with and without signal leakage correction to evaluate for the presence of interhemispheric connectivity.

Materials and Methods

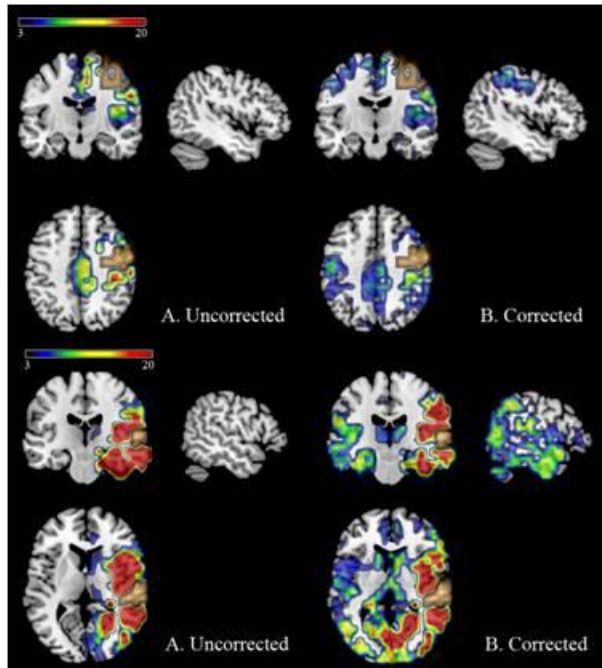
Eight minutes of resting state eyes-open MEG data were obtained in 22 normal male subjects enrolled in a larger IRB-approved study (ages 16-18 years). Data were processed using an in-house automated MEG processing pipeline including synthetic third-order gradient balancing, DC filtering (60 Hz), automated artifact rejection, baseline correction, high and low-pass filtering at 0.5 and 100 Hz for environmental noise, frequency filtering at 13-30Hz (β band) and projection into standard (MNI) source space at 5 mm resolution using a scalar beamformer. Mean beta band amplitude was sampled at 2.5 second epochs from the 4D source space time series. Leakage correction was performed in the time domain of the source space beamformed signal prior to amplitude transformation as a 0-phase lag regressor. Graph theoretic voxel-wise source space correlation connectivity analysis was performed (~20K gray matter nodes) for corrected and uncorrected data. Degree maps were thresholded across subjects for the top 20% of connected nodes to identify hubs. Log-log plots of the complementary cumulative degree distribution were generated to determine scale-free behavior. Additional degree maps for visual, motor, and temporal

Note: Scanned images are included in the proceedings. Some submitted images were reduced during editing thereby decreasing clarity. Also, refer to the Program Planner. Proceedings Content as of 3/28/2014.

regions were generated to identify interhemispheric connectivity using laterality indices.

Results

Hubs for the uncorrected MEG networks were predominantly symmetric and midline, bearing some resemblance to functional MRI (fMRI) networks. These included the cingulate cortex, bilateral inferior frontal lobes, bilateral hippocampal formations and bilateral cerebellar hemispheres. These uncorrected networks however, demonstrated little to no interhemispheric connectivity using the region of interest (ROI)-based degree maps. Leakage-corrected MEG data identified the DMN, with hubs in the posterior cingulate and biparietal areas. These corrected networks demonstrated symmetric interhemispheric connectivity for the ROI-based degree maps. Degree distributions for corrected and noncorrected MEG networks followed a truncated exponential power law.



Conclusions

Graph theoretic analysis of MEG resting state data without signal leakage correction can demonstrate symmetric networks with some resemblance to fMRI networks. These networks however, are an artifact of high local correlation from signal leakage and lack interhemispheric connectivity. Following signal leakage correction, MEG hubs emerge in the DMN, with strong interhemispheric connectivity.

KEYWORDS: Graph Theory, Magnetoencephalography, MEG

O-412

3:07PM - 3:14PM

Subject Based Registration: Patient-Centered Analysis Of Diffusion Tensor MRI (dtMRI)

A Suri¹, R Fleyshe¹, M Lipton²

¹Albert Einstein College of Medicine, Bronx, NY, ²Albert Einstein College of Medicine, Montefiore Medical Center, Bronx, NY

Purpose

Detection of patient specific pathological changes in diffusion MRI requires comparison of individual patients to a control group (1 versus many analysis). The typical approach to this problem entails coregistration of the imaging of the patient and a set of controls to a canonical brain atlas in order to facilitate comparisons. Although appropriately registered brains more closely resemble the template brain, morphological variations still can be readily verified by visual inspection. Thus, a voxelwise comparison of a set of coregistered brains for the purpose of identifying salient differences will incorporate a systematic limitation of the registration process as a confounding factor. In addition to this systematic error, an additional error is introduced due to differences between the template, the target of the registration process, and the patient's brain, the target of the analysis. In this study, we propose a novel approach where the patient of interest is the target of the registration process as well as the analysis. Using this approach, systematic registration errors of the control brains, although present, will be distributed across the subject rather than an alternate target, such as a brain atlas. The result is elimination of registration error for the patient of interest.

Materials and Methods

3 T diffusion tensor MR imaging (MRI) (2mm³, 32 directions, b=800) was performed on 20 acute TBI patients and 48 normal individuals using a Philips Achieva scanner and 32 channel head coil. Fractional anisotropy (FA) images were derived and registration and segmentation procedures applied as described previously (1). A voxelwise ANCOVA then was performed comparing the white matter of the patient to the controls to identify clusters of abnormally low FA defined as at least 100 contiguous voxels with p<0.01. Three distinct analyses were performed: (1) all subjects and controls were transformed to the Johns Hopkins University (JHU) T1-weighted atlas, (2) all subjects and controls were transformed to the Montreal Neurological Institute (MNI) T1-weighted atlas, (3) all controls were transformed to the patient's T1-weighted volume, which we term the patient-centered approach.

Results

We found a significant reduction in the total volume of abnormally low FA values in analyses carried out in the patient's anatomical space compared to either atlas-based analysis. More than 50% of the patients (11/20) demonstrated no abnormally low FA clusters in the patient space analysis. This is in contrast to registrations to a brain atlas which demonstrated near ubiquitous presence of

Note: Scanned images are included in the proceedings. Some submitted images were reduced during editing thereby decreasing clarity. Also, refer to the Program Planner. Proceedings Content as of 3/28/2014.

abnormally low FA clusters, seen in 95% to 100% of patients. The nine patients that did demonstrate low FA clusters using the subject-based registration method showed average increases of approximately 400% in total number of abnormally low FA voxels detected when using the atlas-based analyses. Furthermore, atlas-based analysis demonstrated an average range of 9.8% to 13.3% overlap of gray matter/CSF voxels of the coregistered patient volume and the white matter of the atlas template, which may contribute to the excess number of low FA voxels detected in atlas-based analyses. Without careful evaluation, such misregistrations could be misinterpreted as pathology. Since subject-based registrations does not involve any manipulation of patient data, these misregistrations cannot occur.

Conclusions

Brain templates facilitate comparison across subjects and can be used as a basis for delineating regions of abnormal diffusion in individual patients. However, systematic limitations of the registration process as well as morphological differences between template and subject brains can introduce error in identification of diffusion abnormalities. Through a simple change in the registration process, we eliminate inaccuracies due to differences between a brain template and the patient's anatomy. Although registration errors still persist, these errors are distributed across the subject rather than a brain atlas and therefore are less problematic. Although expert assessment can identify misregistration in atlas-based analyses, the patient-centered analysis can provide more accurate identification of diffusion abnormalities. An additional benefit of our patient-centered approach is that diffusion abnormalities now can be visualized directly in the patient's anatomical space, rather than interpolating results from a brain atlas registration, thereby enhancing clinical correlation across image series within an exam and facilitating MR tractography using regions of diffusion abnormality as seed regions of interest (ROI).

KEYWORDS: DTI, Fractional Anisotropy, Postprocessing

O-413 3:14PM - 3:21PM
Regional Brain T1 and T2 Relaxometry in Healthy Adults using Magnetic Resonance Fingerprinting

C Badve¹, A Yu², D Ma³, V Gulani¹, M Griswold³, J Sunshine¹
¹University Hospitals Case Medical Center, Cleveland, OH,
²Case School of Medicine, Cleveland, OH, ³Case Western Reserve University, Cleveland, OH

Purpose

To quantify T1 and T2 relaxation times of different brain regions in normal adults by using the novel magnetic resonance fingerprinting (MRF) technique and to analyze differences in relaxometry measurements based on gender and age.

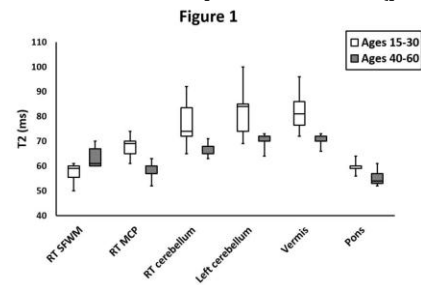
Materials and Methods

We scanned 12 healthy volunteers (M:F 1:1; 7 between age 18 to 30 years, 5 between age 40-60 years) on a 3 T MR imaging (MRI) scanner using the already described MR

fingerprinting protocol (1). Imaging was acquired through the representative areas of brain and quantitative T1 and T2 maps were generated. Multiple regions of interest (ROIs) were manually outlined at predetermined locations and T1 and T2 relaxation values at these sites were extracted. Each slice acquisition was less than 15 seconds in duration. The ROIs included representative white matter regions in all lobes, centrum semiovale, corpus callosum, internal capsule and cerebral peduncles, deep nuclei, thalami, cerebellar structures and pons. A total of 38 ROIs were drawn in each subject. Independent sample t-tests were used to determine differences between males and females, and age groups 18-30 and 40-60 years.

Results

Normal T1 and T2 values of selected brain ROIs were established. The T2 relaxometry values in right superior frontal white matter (SFWM) were higher ($p < 0.03$) in the older age group (Figure 1). Similar trend also was seen in T1 values of right centrum semiovale ($p < 0.06$). The T2 values of several posterior fossa structures were significantly lower in the older age group (all $p < 0.05$) (Figure 1). Similar trend also was seen with T1 of left dentate nucleus ($p < 0.06$). The T2 values of different regions and age-related changes were comparable to the published data in literature (2). There was a trend for higher T1 values in rostrum and right cerebellar hemisphere in males as compared to females ($p < 0.07$).



Conclusions

Magnetic resonance fingerprinting allows simultaneous, rapid, in vivo quantification of relaxation parameters of brain. Normal T1 and T2 relaxometry values in different brain regions provide baseline measurements for comparison with different disease-related states. Age-based analysis shows significant differences in relaxation parameters of certain brain regions in concurrence with published literature.

KEYWORDS: Brain Aging, Brain Mapping, Relaxivity

O-414 3:21PM - 3:28PM
Correlation of Size of Primary Motor Hand Region or "Hand knob" to Individual Handedness

J Chang, P Shen, A Nidecker, G Runner
University of California Davis, Sacramento, CA

Purpose

MR imaging (MRI) evaluation of individual handedness may be a noninvasive way to identify the dominant cerebral hemisphere, especially in seizure patients. By

Note: Scanned images are included in the proceedings. Some submitted images were reduced during editing thereby decreasing clarity. Also, refer to the Program Planner. Proceedings Content as of 3/28/2014.

measuring the dimensions of the primary motor hand region, or "hand knob," we hope to establish asymmetry between the two cerebral hemispheres, and thus improve predictive value of handedness.

Materials and Methods

Twenty-one subjects (16 right handed, 3 left handed, and 2 ambidextrous) were identified retrospectively after a search for individuals who had both MRI with 3D isotropic imaging and a clinical note from neurology assessing handedness. Only subjects ranging in age from 10-50 were included. Subjects were excluded from analysis if there was no documentation of handedness, or a confounding disability was identified, including congenital abnormalities, hemiplegia, quadriplegia, cerebral palsy, traumatic brain injury, brain tumor, and infection. From axial T1 3D spoiled gradient echo sequences, types of "hand knob" morphology were identified as omega, epsilon, null, or medially or laterally asymmetric epsilon. Length and height of the "hand knob" were measured in the axial plane (see Figure A). Length and height dimensions of the "hand knob" then were added together as a sum for both dominant and nondominant hemispheres. Paired two-tail method T test was used to compare the dominant versus nondominant hemisphere summed height and length measurement total in the axial plane for both right, left and ambidextrous patients.

Results

The left hand knob taken as the sum of the length plus height measured in the axial plane, was larger than the right in 16 right handed subjects ($p < 0.001$) (Graph B). Statistical significance in the size of the hand knobs in the three left-handed subjects ($p = 0.19$) and the two ambidextrous subjects ($p = 0.5$) could not be established given the small sample size. Combining both right and left handed patients, the dominant versus nondominant primary motor hand cortex summed measurements of the length and height were taken and compared and also yielded statistic significant, $p < 0.01$.

Figure A: Left hemisphere primary motor hand region or "hand knob" is omega in shape and highlighted in blue. Right hemisphere "hand knob" is epsilon in shape and highlighted in yellow. The length and height measurements are shown as white lines.

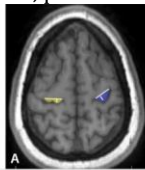
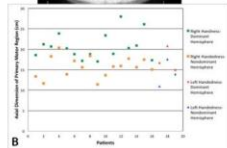


Figure B: Scatter plot of dominant and non-dominant "hand knob" axial dimensions of both right and left handed patients. The dominant hemisphere dimensions are overall larger than the non-dominant hemisphere for both groups.



Conclusions

This pilot study suggests that there is a direct correlation between dominant hemisphere primary motor cortex size and handedness. The study is limited by the small number of subjects, particularly in the left handed and ambidextrous groups. Ongoing data collection will increase sample size, and along with future volumetric analysis of the primary motor hand regions (which will be made with Free Surfer software application, developed at the Martinos center for Biomedical Imaging) of the primary motor hand region, may support the conclusion of a

statistically significant difference in size of dominant versus nondominant "hand knob" region.

KEYWORDS: Motor Cortex

O-416

3:35PM - 3:42PM

In Vivo Assessment of White Matter Damage in Neuromyelitis Optica Patients: a Diffusion Tensor and Diffusion Kurtosis MR Imaging Study

M Kimura, T Doring, F Rueda, G Tukamoto, E Gasparetto
CDPI-Clinica de Diagnostico por Imagem, Rio de Janeiro, Brazil

Purpose

In patients with neuromyelitis optica (NMO), damage to extensive regions of normal-appearing white matter (WM) has been observed. To investigate the possibility that microstructural alterations are present in these WM tracts, diffusion tensor imaging (DTI) and diffusion kurtosis imaging (DKI) techniques were applied and compared.

Materials and Methods

Thirteen patients with NMO and 13 demographically and gender-matched controls underwent MR imaging (MRI) using a 3 T MR scanner, with both DTI and DKI sequences acquired. Parametric fractional anisotropy maps were derived from diffusion tensor (FADTI) values using b values of 0 s/mm² and 1000 s/mm². Parametric fractional anisotropy maps derived from diffusion kurtosis tensor (FADKI) values also were acquired using b-values of 0, 1000, and 2000 s/mm². Mean FADTI and FADKI values also were calculated. A region of interest (ROI) analysis of the genu and splenium of the corpus callosum (CC), cerebral peduncle (CP), and optic radiation (OR) also were performed. Student's T-test and corrections for multiple comparisons were used to evaluate the data obtained.

Results

In the present study, a ROI-driven DTI and DKI analysis of WM tracts previously found to have altered FA values in NMO patients were performed. Both the splenium of the CC and the left OR of NMO patients were found to have significantly reduced FADTI values compared to controls ($p < 0.05$). The FADKI ROI values of NMO patients also were slightly lower than those of the controls for the same WM tracts, demonstrating only a positive trend ($0.1 > p > 0.05$). The other WM tracts analyzed in this study did not display significant decrease in the FA values obtained for NMO patients versus controls for both the DTI and DKI techniques. Diffusion tensor imaging employs a water diffusion displacement probability function that obeys Gaussian distribution. However, while Gaussian diffusion of water is observed in homogeneous solutions, diffusion of water in biological tissues, such as the brain, often do not show Gaussian behavior. This is consistent with the presence of cell membranes and organelles in the brain, which create differing extents of water diffusion, thereby resulting in a non-Gaussian probability of distribution. Therefore, theoretically, DKI is better able to characterize the microstructure of brain tissue. However, differently of DTI technique, the DKI technique could not assess the

Note: Scanned images are included in the proceedings. Some submitted images were reduced during editing thereby decreasing clarity. Also, refer to the Program Planner. Proceedings Content as of 3/28/2014.

microstructure alterations of the brain in patients with NMO.

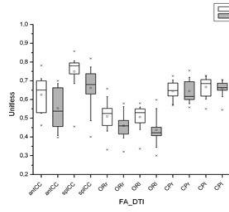


Figure 2. Box-and-whisker plots show the distribution of diffusion tensor imaging fractional anisotropy (FADTI) for the genu of the CC (antCC), splenium of the CC (spCC), right OR (OR), left OR (OR), right cerebral peduncle (CP), and left cerebral peduncle (CP) for healthy controls (white boxes) and NMO patients (gray boxes).

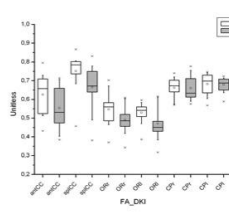


Figure 3. Box-and-whisker plots show the distribution of diffusion kurtosis imaging fractional anisotropy (FADKI) for the genu of the CC (antCC), splenium of the CC (spCC), right OR (OR), left OR (OR), right cerebral peduncle (CP), and left cerebral peduncle (CP) for healthy controls (white boxes) and NMO patients (gray boxes).

	FADTI Patients	FADTI Controls	FADKI Patients	FADKI Controls
Splenium of corpus callosum	0.66 +/- 0.11	0.75 +/- 0.09	0.66 +/- 0.12	0.75 +/- 0.09
Left optic radiation	0.43 +/- 0.08	0.50 +/- 0.06	0.47 +/- 0.08	0.53 +/- 0.05

Conclusions

To our knowledge, this is the first study to analyze WM tracts of NMO patients using DTI and DKI. These data indicate that DKI could not be used to evaluate WM integrity in NMO patients. Furthermore, the results obtained with FADTI are consistent with the hypothesis that diffuse brain involvement characterizes NMO.

KEYWORDS: Diffusion Kurtosis Imaging, Diffusion Tensor Image, Neuromyelitis Optica

O-417 3:42PM - 3:49PM
Cortical Atrophy and Relative Increase of Interhemispheric Connections in Relapsing Remitting Multiple Sclerosis With Low Scores of Disability

C Rimkus¹, M Otaduy¹, D Callegaro², C Leite¹
¹Laboratory of Medical Investigation (LIM-44), University of São Paulo, São Paulo, Brazil, ²University of São Paulo, São Paulo, Brazil

Purpose

The chronic inflammation in multiple sclerosis (MS) leads to axon and myelin damage, which can induce functional and anatomical reorganization of brain connections. Studies have reported increases in cortical activity in the initial stages of MS (1, 2), as a possible compensatory response to the beginning process of tissue degeneration. We propose to study the white matter (WM) connections in areas of cortical atrophy in relapsing remitting MS (RRMS) patients with low Expanded Disability Status Scale (EDSS) scores by diffusion tensor imaging (DTI), in an attempt to observe adaptive changes in the WM pathways associated to the early cortical degeneration.

Materials and Methods

Fifteen RRMS patients (12 female, mean age 30.3 years ± 8.3, mean EDSS 1.3 ± 0.9) and 15 healthy controls (HC) (13 female, mean age 32.5 years ± 5.4) underwent brain exams with a 3 T MR scanner. The MRI exam included acquisition of 3DT1-weighted images (time of echo (TE)/time of repetition (TR)= 2.7/6.2 ms; time of inversion (TI)= 700 ms; 1mm³ isotropic voxel) and DTI (b-values= 0 and 1000 s/mm²; 32 encoding directions; 2mm³ isometric voxel). Cortical segmentation was obtained with FreeSurfer v5.1.0. Group analysis based on General Linear Modeling was

performed searching for areas of significant cortical atrophy (p< 0.05) and using age as a cofactor. The resulting labels of cortical atrophy were coregistered to each individual DTI space. From the labeled areas of cortical atrophy we extracted the regional fiber tracts (Figure 1), fractional anisotropy (FA), mean diffusivity (MD), the total number of cortical fibers and the number of connections to the corpus callosum (CC).

Results

The main results are shown in Table 1, showing a greater ratio of cortical fibers connecting to the CC in RRMS patients, associated to an increase in MD. The increase of interhemispheric fibers was derived predominantly from the right hemisphere, which also showed a greater extension of cortical atrophy (Figure 1).

Table 1. DTI and tractography characteristics of the fiber tracts derived from clusters of cortical atrophy in RRMS patients

	MD (10 ⁻³ mm ² /s)		Total cortical fibers (CF)		Connections to the CC (CCF) (%)					
	Right	Left	Right	Left	Right	Left				
RRMS	0.38 ± 0.03	0.37 ± 0.03	0.83 ± 0.04	0.82 ± 0.03	7287 ± 999	4122 ± 402	29.7 ± 31.3	28.1 ± 40.0	1.0% ± 1%	0.8% ± 0.9%
HC	0.38 ± 0.02	0.37 ± 0.02	0.8 ± 0.02	0.81 ± 0.03	7138 ± 911	4052 ± 422	10.1 ± 12.2	10.1 ± 18.1	0.3% ± 0.5%	0.3% ± 0.5%
p value	0.8	0.8	0.03*	0.09**	0.86	0.9	0.02*	0.12	0.06**	0.14

The cells show the mean results ± standard deviation of each measurement for the right and left hemispheres in the RRMS and HC groups. The bottom row contains the p-value of the test showing the differences between the groups, being significant p< 0.05 (*) and the p-values between 0.05 and 0.1 were considered trends (**).

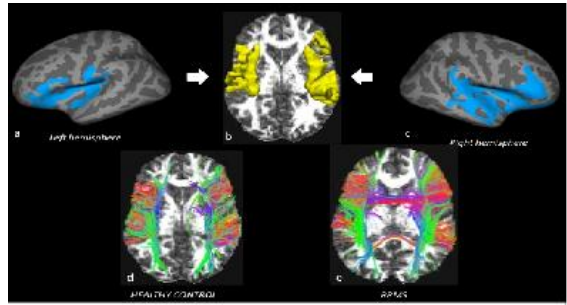


Figure 1. Clusters of cortical atrophy in RRMS patients and the derived DTI fiber tracts in RRMS patients and healthy controls. The clusters of cortical atrophy in the left (a) and right (b) hemispheres were coregistered in the individual FA maps (a), used as seeds to the tractography. The bottom images represent the derived fiber tracts in a healthy control (c) and a RRMS patient (d), with more fibers crossing the corpus callosum in the RRMS patient.

Conclusions

Cortical degeneration has been reported previously from the earlier stages of MS. Some patients may compensate the initial neurological dysfunction by adaptive changes in cortical activity and connectivity (1, 2). The DTI results of our study show that the cortical degeneration also may be followed by microstructural reorganization of WM tracts, resulting in an increase of interhemispheric connections.

KEYWORDS: Degenerative, Diffusion Tensor Image, Multiple Sclerosis

O-418 3:49PM - 3:56PM
Quantitative MR and Histopathologic Features of CNS Remyelination Correlate with Functional Recovery in Felines: The Role of Vitamin B12 As An Independent Promoter of Myelination.

J Brucker¹, A Field²
¹University of Wisconsin, Madison, WI, ²University of Wisconsin Hospital, Madison, WI

Purpose

In this study we investigate the outcome of various quantitative MR parameters – obtained from quantitative

Note: Scanned images are included in the proceedings. Some submitted images were reduced during editing thereby decreasing clarity. Also, refer to the Program Planner. Proceedings Content as of 3/28/2014.

magnetization transfer (MT), diffusion tensor (DTI), q-space, and myelin water fraction imaging - during sequential stages of central nervous system (CNS) demyelination and remyelination in felines, as corroborated by functional assessments and histopathologic correlation.

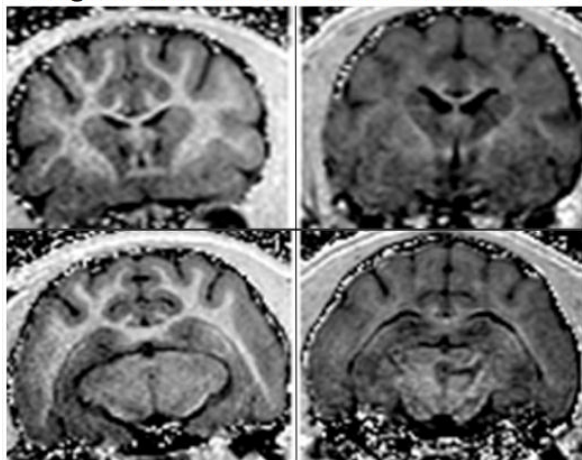
Materials and Methods

This is a case-control study that enrolled a total of 13 cats, 11 of which were placed on a diet of irradiated food, which induces global CNS demyelination. A subset of the diseased group was supplemented with vitamin B12 while others were either maintained on the irradiated diet or switched to nonirradiated food. Quantitative MR imaging (MRI) of the whole brain, spinal cord, and optic nerves were obtained at baseline, during partial disease onset, at peak disease, and during recovery; MRI data were obtained on a 3 T clinical scanner with a standard knee coil. Subjects from each representative group were euthanized at different stages for the purpose of histologic analysis and comparison.

Results

The diseased group demonstrated decreased MT ratio and MT saturation values, in comparison to the non-diseased subjects. However, MT parameters were seen to rebound during the recovery phase, which correlated with functional outcomes and histologic confirmation of remyelination. A similar relationship was observed with diffusion parameters, with a decrease in fractional anisotropy, axial diffusivity, and mean diffusivity - and accordingly an increase in radial diffusivity - when comparing the diseased state to the baseline and recovery phases. Myelin water fraction values correlate with the degree of myelination at various disease stages.

Magnetization Transfer Ratio – Whole Brain



Normal

Peak Disease

Conclusions

The unique phenomenon of nonimmune mediated CNS demyelination in felines that are fed irradiated food offers a powerful large animal model with which to study "pure" demyelination and subsequent recovery, without the confounding factors of inflammatory changes and axonal degeneration that are encountered in other animal models. Recovery from the peak disease state is observed in both

cats that are switched to a nonirradiated diet, or cats supplemented with vitamin B12 regardless of diet. The latter effect is observed irrespective of serum levels or other markers of vitamin B12 status, which suggests that vitamin B12 supplementation may independently promote remyelination. We confirm this with functional outcomes, histologic analysis, and multiparametric quantitative MRI. Quantitative MRI values are shown to correlate with various degrees of myelination in this model, which confirms that these sequences potentially offer a noninvasive, clinically feasible means for assessing this facet of white matter disease. Furthermore, the feline model may translate to subacute combined degeneration (SCD), observed in vitamin B12-deficient humans, or can be treated as a reductionist model of multiple sclerosis in which demyelination and remyelination can be studied in isolation from confounding effects.

KEYWORDS: Animal Model, Demyelination, FMRI

O-419

3:56PM - 4:03PM

Evaluation of the Brain Gray Matter Structures in Adults Perinatally-infected with HIV Using DKI

M Post¹, A Cuadra², E Willen², S Sheriff², K Arheart², V Govind²

¹Jackson Memorial Hospital/University of Miami, Miami, FL, ²University of Miami, Miami, FL

Purpose

To evaluate the long term impact of persistent reservoirs of HIV in the central nervous system (CNS) and the potential effects of long term use of some of its antiretroviral therapeutics on the tissue structural integrity of the brain subcortical and deep gray matter (GM) regions in people living with HIV infection. In this study, a whole-brain diffusion kurtosis imaging (DKI) method is used to obtain mean diffusivity (MD) and mean kurtosis (MK) metric maps in adults perinatally infected with HIV and a matched community control group for comparisons.

Materials and Methods

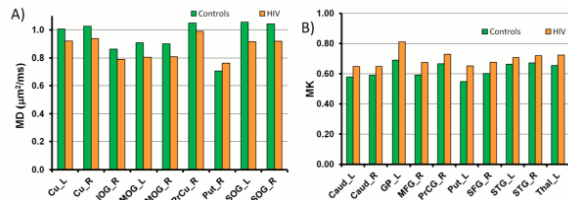
MR imaging (MRI) data were acquired from 24 adults perinatally infected with HIV (mean±SD: 20±1.9 years) and nine control subjects (mean±SD: 22±1.4 years) using a 3 T scanner. The MR protocol included diffusion-weighted imaging (DWI) (b: 0, 1000, 2000 s/mm²; number of diffusion gradient directions: 30; TR: 6100 ms; TE: 101 ms; slices: 45; resolution: 2.7 mm isotropic; 2 ave) and T2 (for distortion correction) sequences. Data were processed using DKE1 and DtiStudio (www.mristudio.org). The DKE-processed maps of MD and MK were transformed spatially to a template in MNI space at 1 mm resolution. To obtain data from GM regions in these maps, we used a brain atlas² with 130 regions of interest (ROI). Furthermore, to avoid inclusion of voxels with predominantly CSF or white matter (WM) in the ROIs, a GM mask was created for each subject by setting appropriate thresholds in their MD and FA images, respectively. Finally, data were selected only from 60 predominantly GM ROIs for analysis. Between

Note: Scanned images are included in the proceedings. Some submitted images were reduced during editing thereby decreasing clarity. Also, refer to the Program Planner. Proceedings Content as of 3/28/2014.

group analysis of MD and MK metrics of the ROIs was carried out using ANCOVA with age and sex as covariates. A p value of <0.05 was considered significant.

Results

In Figure 1A are shown the mean MD values of nine GM ROIs that showed significant changes in the HIV group. The nine ROIs comprised of cuneus - left (Cu_L) and right (Cu_R), inferior occipital gyrus right (IOG_R), middle occipital gyrus - left (MOG_L) and right (MOG_R), pre-cuneus right (PrCu_R), putamen right (Put_R), and superior occipital gyrus - left (SOG_L) and right (SOG_R). In Figure 1B are shown ten GM ROIs with significant mean MK changes in the HIV group. The ten ROIs included caudate nucleus - left (Caud_L) and right (Caud_R), globus pallidus left (GP_L), middle frontal gyrus right (MFG_L), precentral gyrus right (PrCG_R), putamen left (Put_L), superior frontal gyrus right (SFG_R), superior temporal gyrus - left (STG_L) and right (STG_R), and thalamus left (Thal_L). In the HIV group compared to controls, the MD values were lower across the ROIs, except in Put_R, and the MK values were consistently higher in all the ROIs.



Conclusions

The significant changes observed in the MD and MK metrics of the subcortical and deep GM brain regions in individuals with HIV infection indicate that these regions also are affected in addition to previously known WM regions. There was no overlap of the ROIs found with significant MD and MK changes; this result indicates that the tissue water in these ROIs experiences different degrees of Gaussian and non-Gaussian diffusion effects. The significantly reduced MD values and increased MK values in the GM ROIs indicate that tissue structural and cellular compositional changes occur in the intra- and extra-cellular environments of the brain of individuals with HIV infection. In conclusion, microstructural changes occur in the subcortical and deep GM brain regions of adults infected with HIV. These changes indicate underlying cellular pathologies that may be responsible for HIV-associated neurocognitive disorders (HAND) prevalent in people living with HIV infection. The neuroimaging methodology described here will be useful in developing biomarkers for evaluating the impact of HIV infection and its therapeutics on the brain. Acknowledgements: This work is supported by a pilot grant from the Center for AIDS Research, University of Miami.

KEYWORDS: Brain Abnormalities, Diffusional Kurtosis Imaging, HIV

O-420

4:03PM - 4:10PM

White Matter Microstructure Abnormalities in Pediatric Migraine Patients: In-Vivo Measures of Brain Hyperexcitability?

R Messina, M Rocca, B Colombo, E Pagani, G Comi, A Falini, M Filippi
San Raffaele Scientific Institute, Vita-Salute San Raffaele University, Milan, Italy

Purpose

By exploiting diffusion characteristics of water molecules in the central nervous system, diffusion tensor (DT) magnetic resonance imaging (MRI) provides several quantities with the potential to disclose white matter (WM) microstructure abnormalities. Among these, fractional anisotropy (FA) reflects axonal integrity and fiber organization, mean diffusivity (MD) measures the overall magnitude of diffusion, axial diffusivity ($\lambda_{||}$) is associated with fiber density and axon intrinsic characteristics, whereas radial diffusivity (λ_{\perp}) reflects the degree of myelination (1). In this study, we explored abnormalities of WM microstructure in pediatric patients with migraine using DT MRI and two different methods of analysis.

Materials and Methods

Using a 3.0 T scanner, dual-echo and DT scans were acquired from 15 pediatric migraine patients (8 girls, mean age = 14.1 years, mean disease duration = 3 years, mean attack frequency = 21 attacks per year, 8 with visual aura and 7 without aura) and 15 age-matched controls. Tract-based spatial statistics (TBSS) analysis (2) was performed using FMRIB's Diffusion Toolbox. In order to confirm TBSS results, we also performed a DT probabilistic tractography of the major brain WM tracts (3).

Results

Both TBSS and DT tractography analysis showed that compared to controls, pediatric migraine patients had significant lower MD, $\lambda_{||}$ and λ_{\perp} in the brainstem, thalamus, fronto-temporo-occipital lobes, including the right cingulum, corpus callosum, optic radiation, fronto-occipital fasciculus and corticospinal tract, bilaterally. They also experienced increased FA of the left optic radiation. No correlation was found between WM abnormalities and disease duration and frequency of attacks.

Conclusions

Pediatric migraine patients present diffuse WM microstructural abnormalities. Higher FA and lower MD, $\lambda_{||}$ and λ_{\perp} might be explained by repeated neuronal activation, that is likely to lead to cells swelling and might stimulate the activity-dependent myelo-modulation, or by the presence of higher neuronal and synaptic densities in migraine patients compared to controls (4, 5). Both these mechanisms would reflect an hyperexcitability of the brain in migraine patients.

KEYWORDS: Migraine, MR Imaging/Diffusion, White Matter Disease

Note: Scanned images are included in the proceedings. Some submitted images were reduced during editing thereby decreasing clarity. Also, refer to the Program Planner. Proceedings Content as of 3/28/2014.

O-421 4:10PM - 4:17PM
Using Quantitative Imaging to Evaluate Correlation Between Diffusion MRI and DCE MRI in Intracranial Human Gliomas, Meningiomas, Metastases, and Cerebral Lymphomas

H Huhdanpaa¹, D Hwang¹, S Cen¹, M Booker², N Muradyan³, C Liu¹, A Lerner¹, D Commins¹, A Rajamohan¹, P Kim¹, O Boyko¹, J Go⁴, M Law⁵, M Shiroishi¹
¹University of Southern California, Los Angeles, CA, ²Keck School of Medicine, Los Angeles, CA, ³iCAD, Nashua, NH, ⁴LAC/University of Southern California Medical Center, Los Angeles, CA, ⁵Keck Medical Center of University of Southern California, Los Angeles, CA

Purpose

Quantitative imaging biomarkers are needed to better characterize tumor cell number, cell size, and cell packing (1). Determination of the relationship between diffusivity metrics derived from diffusion MRI and dynamic contrast-enhanced (DCE) MR imaging (MRI) metrics such as extravascular-extracellular space (EES) volume fraction (ve) may help develop new imaging biomarkers of brain tumor cellularity. Monitoring of cellular proliferation and cell death is needed in neuro-oncology practice to monitor tumor response to novel therapeutics. Apparent diffusion coefficient (ADC) determined from diffusion weighted imaging (DWI) MRI and the equivalent concept of mean diffusivity (MD) determined from diffusion tensor imaging (DTI) can both give an impression of the EES and have been shown to be inversely correlated with tumor cell density. Upon successful treatment, the tumor cellularity, with its associated barriers, would be expected to decrease, therefore increasing diffusivity. Likewise, EES would be expected to increase upon successful treatment due to tumor necrosis. As such, one would expect diffusivity and ve to be positively correlated. The purpose of this study was to determine the correlation between DCE metrics such as ve, blood-brain barrier transfer constant (Ktrans), Kep (Ktrans/ve), and fractional plasma volume (vp), and diffusivity, as characterized by ADC in the case of DWI MRI, and axial diffusivity (DA) and MD in the case of DTI MRI, focusing on gliomas, lymphomas, metastases, and meningiomas.

Materials and Methods

Fifty intracranial tumors (21 gliomas (grade I-IV), 13 metastases, 7 lymphomas and 9 meningiomas) were evaluated retrospectively. Diffusion tensor imaging/DWI and DCE images were acquired during the same MRI exam on a GE 3T HDxT scanner. Dynamic contrast-enhanced MRI images were postprocessed in CADvue. Metrics extracted from DCE MRI were: ve, vp, Ktrans, and Kep. Metrics for diffusivity were calculated using custom Matlab software. Dynamic contrast-enhanced and diffusion images were coregistered and 3-dimensional (3D) regions of interest were drawn on parametric maps using the area of enhancement on postcontrast imaging. Mean and median values were extracted using Pearson correlation.

Results

When all the tumors were considered together, no statistically significant correlation was observed between DCE parameters and diffusion parameters either with DTI or DWI, although for cases imaged with DWI the negative correlation observed between mean ADC and mean Kep ($r=-0.51$, $p = 0.05$) as well as the negative correlation observed between mean ADC and median Kep ($r=-0.51$, $p = 0.05$) did both approach statistical significance (see Table). These negative correlations are suggestive of positive correlation between ADC and ve as $Kep = Ktrans/ve$. However, when analyzing by specific tumor type (see Table), a strong positive correlation was observed for gliomas between mean MD and mean ve ($r=0.60$, $p = 0.01$) as well as between mean AD and mean ve ($r=0.66$, $p < 0.01$). No statistically significant correlation was observed between measures of diffusivity and mean ve for the other tumor types in the study.

Table: Correlation coefficients between Diffusion MRI parameters and DCE MRI parameters - both for all tumors combined as well as for specific tumor types
Pearson Correlation Coefficients and (p-values), all tumors combined, DTI vs. DCE, N = 35

	Mean v_e	Mean K_{ep}	Median K_{ep}	Median K^{trans}
Mean MD	0.2599 (0.132)	-0.2046 (0.240)	-0.1203 (0.491)	-0.0284 (0.871)
Mean AD	0.3134 (0.067)	0.2435 (0.159)	-0.1162 (0.506)	-0.0006 (0.997)

Pearson Correlation Coefficients and (p-values), all tumors combined, DWI vs. DCE, N = 15

	Mean v_e	Mean K_{ep}	Median K_{ep}	Median K^{trans}
Mean ADC	0.1668 (0.552)	-0.5141 (0.050)	-0.5102 (0.052)	-0.4050 (0.134)
Median ADC	0.0374 (0.895)	-0.3632 (0.183)	-0.3961 (0.144)	-0.4659 (0.080)

Pearson Correlation Coefficients and (p-values), by tumor type, DTI vs. DCE

	Glioma N = 17		Lymphoma N = 5		Meningioma N = 5		Metastases N = 8	
	Mean AD	Mean MD	Mean AD	Mean MD	Mean AD	Mean MD	Mean AD	Mean MD
Mean v_e	0.6587 (0.0040)	0.6024 (0.0105)	0.3180 (0.6020)	0.2671 (0.6640)	-0.2764 (0.6526)	-0.2134 (0.7303)	-0.3739 (0.3615)	-0.2143 (0.6104)

Conclusions

Our results showed a strong positive correlation between DTI measures of diffusivity, MD and AD, and ve for gliomas, while no statistically significant correlation was observed for the other tumor types. A prior study performed in breast cancer (2) found a negative correlation while another study in breast cancer (3) as well as one in glioblastoma (1) found no correlation between measures of diffusivity and DCE parameters. Multiple factors contribute to measures of diffusivity other than extravascular extracellular space volume. For example, different geometries of the available extravascular extracellular space may impact diffusivity, while the overall volume remains unchanged (2). Likewise, diffusivity is affected by the spatial configuration of the EES, intracellular diffusion coefficients, and membrane permeability (1). Yankeelov et al. (2) also suggested interstitial fluid pressure may decrease in tumors following treatment, which in turn aids elimination of cellular debris and increases diffusivity, while the overall volume of extravascular extracellular space may decrease as a result of this decreased interstitial fluid pressure. To conclude, our results suggest that the way these multiple factors impact diffusivity, and its relationship to DCE parameters such as ve, is tumor type specific, and that meaningful

Note: Scanned images are included in the proceedings. Some submitted images were reduced during editing thereby decreasing clarity. Also, refer to the Program Planner. Proceedings Content as of 3/28/2014.

combination of these different MRI sequences to build predictive models should be tumor type specific.

KEYWORDS: DCE MR Imaging, Diffusion MR Imaging, Postprocessing

O-422

4:17PM - 4:24PM

Glioblastoma: Evaluation of the nonenhancing peritumoral region using resting state BOLD MRI

D Chow¹, C Horenstein², M Kozberg¹, A Lignelli³, C Filippi¹, J Grinband¹

¹Columbia University Medical Center, New York, NY, ²North Shore Long Island Jewish Medical Center, Manhasset, NY, ³Columbia University, New York, NY

Purpose

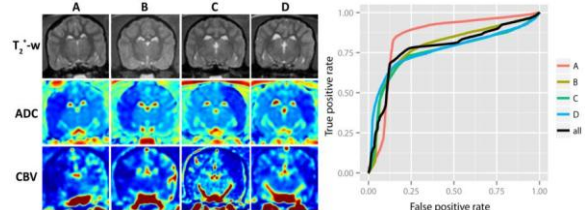
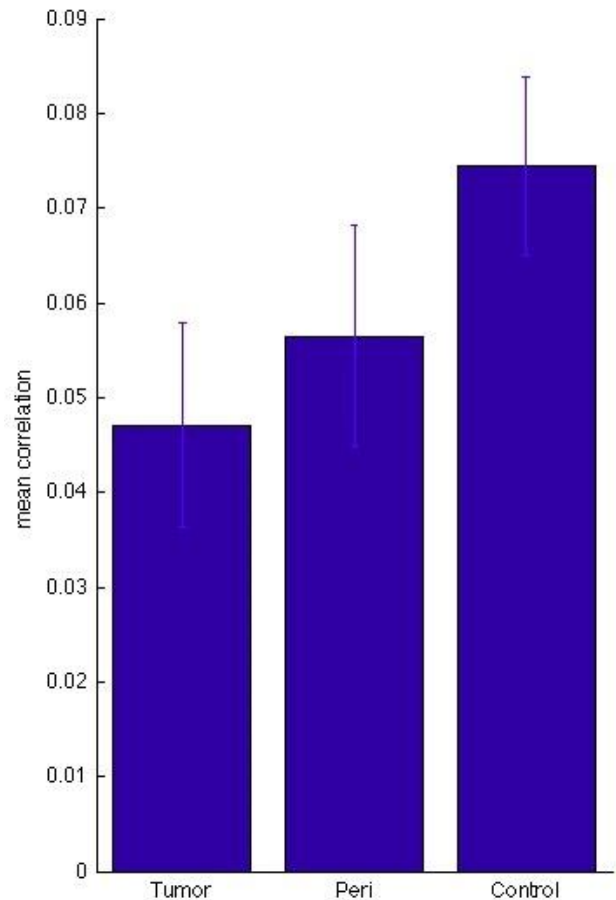
Glioblastoma (GBM) is an invasive primary brain malignancy, which may infiltrate the peritumoral edema with malignant cells. Identification of this nonenhancing disease remains a radiographic challenge. Given that GBMs may disrupt cerebral blood flow modulation through a variety of mechanisms (i.e., vascular compression, invasion, shunting), imaging focused at identifying regions of vascular deregulation may represent a possible biomarker for nonenhancing disease. One possible means of objectively quantifying disruptions in blood flow modulation is resting state BOLD MR imaging (MRI). In this study, we aim to objectively measure the BOLD blood flow correlations as a potential marker for tumor-impaired neural tissue. We hypothesize that regions of dysfunction in the vascular regulation will display lower correlative values.

Materials and Methods

This was a retrospective review of 15 patients with pathology proven GBMs that had resting state BOLD functional MR imaging (fMRI) at 3 T prior to tumor resection. Motion correction and slice timing correction was performed on the raw datasets. Global functional connectivity (FC) maps were generated to obtain an objective measure for correlative blood flow. Each voxel time series was correlated to the time series of a set of Talarach-identified regions of interest (ROIs) to derive a measure of global functional connectivity. Patterns of functional connectivity within the tumor and peritumoral edema (defined by the peritumoral FLAIR abnormality) were characterized qualitatively and quantitatively.

Results

The contrast-enhancing tumor had significantly lower correlative blood flow measures compared to the contralateral normal white matter ($p < 0.05$). The nonenhancing peritumoral edema region also displayed significantly lower correlative blood flow measures compared to the contralateral normal white matter ($p < 0.05$).



Conclusions

These findings suggest that objective assessment of the correlative blood flow using resting state BOLD MRI may provide a potential biomarker for tumor invasion in the nonenhancing peritumoral edema. Further study is required to determine whether different signatures on these BOLD connectivity maps relate to tumor subtype and/or prognosis.

KEYWORDS: Biomarkers, Functional Connectivity MR, Glioblastoma

Note: Scanned images are included in the proceedings. Some submitted images were reduced during editing thereby decreasing clarity. Also, refer to the Program Planner. Proceedings Content as of 3/28/2014.

0-423 4:24PM - 4:31PM
Automatic lesion detection on C-arm CT CBV-maps in a canine model of ischemic stroke

K van der Marel¹, I van der Bom², J Chueh¹, A Wakhloo¹, M Gounis¹

¹University of Massachusetts Medical School, Worcester, MA, ²Philips Healthcare, Andover, MA

Purpose

Perfusion imaging may identify viable brain tissue in ischemic stroke that critically guides patient and treatment selection for endovascular therapy. Tissue viability may change rapidly after stroke onset, suggesting the need for accurate perfusion imaging immediately prior to intra-arterial treatment. In pursuit of bringing cerebral blood flow (CBF) and volume (CBV) measurements to the angiography suite, recent studies have focused on perfusion imaging using C-arm cone-beam CT (CBCT) systems (1, 2). The purpose of this study was to explore the potential of a machine learning algorithm to automatically identify voxels belonging to the ischemic lesion on CBCT-based CBV maps.

Materials and Methods

Adult beagle dogs (n=4) received stroke by injection of an autologous blood clot unilaterally in the internal carotid artery (ICA) inducing an M1-occlusion which was confirmed by digital subtraction angiography (DSA). Subsequently, animals were imaged on an x-ray angiographic C-arm system and a 3 T whole-body MR imaging MRI scanner (Philips Healthcare) as described before (1). Four and on half hours after stroke onset, CBV maps were calculated from CBCT images obtained during a 20-second 220°-sweep, before and after intravenous contrast agent injection (1). Diffusion weighted imaging (DWI) for calculation of apparent diffusion coefficient (ADC) maps and anatomical MRI was performed within 10 minutes after CBV assessment. True infarct volumes were measured on post mortem TTC-stained coronal brain sections (1). After coregistration, voxel-wise analysis was performed. The ischemic lesion was determined on the ADC map by thresholding (1) and a mirrored control region was obtained in the contralateral hemisphere. A nonlinear support vector machine (SVM) classifier (3) then was trained ($C = 1$, $\sigma = 40$, 15000 samples) to discriminate between lesion and control voxels in the combined control and lesion area, based on CBV values that were normalized with respect to the average control CBV. Classification performance was assessed with leave-one-out cross-validation.

Results

The left panel of the figure shows the anatomical MRI (top row), ADC map (second row; values between 0 and $3.0 \cdot 10^{-3} \text{ mm}^2/\text{s}$), and CBV map (bottom row; a.u.) for each of the four animals (A-D). The ischemic lesion is clearly identified on the ADC map at a threshold of $5.3 \cdot 10^{-4} \text{ mm}^2/\text{s}$, which yields lesion volume estimates that are in agreement with TTC-based lesion volumes (1). Support vector machines were trained in a leave-one-out cross-validation on a limited set of voxels that

encompassed the lesion and contralateral control areas. The performances of the SVMs are depicted in the right panel of the figure. The receiver operating characteristic (ROC) curve indicates reasonable performance of the classifier in each case, with the area under the ROC curve (AUC) between 0.75-0.85 (see Table). The AUC of the combined predictions was 0.78.

A	9.6	13.8	15.2	0.85
B	5.6	6.2	6.0	0.79
C	13.4	12.2	8.1	0.75
D	3.6	3.4	2.8	0.77

Conclusions

The current approach shows that nonlinear machine learning algorithms are capable of detecting ischemic lesion voxels with reasonable sensitivity and specificity. As the current training and evaluation was confined to a restricted area of the brain that encompassed ischemic and unaffected contralesional tissue, its performance on whole-brain CBV maps remains to be evaluated.

KEYWORDS: Acute Ischemic Stroke, C-Arm CT CBV, Image Processing

Tuesday, May 20
3:00 PM – 4:30 PM
Room 520

47 - Parallel Papers: Adult Brain:
Degenerative Disease

0-424 3:00PM - 3:07PM
Hypertrophic Olivary Degeneration Resulting from Posterior Fossa Masses and Their Treatments

M Hirano¹, V Hatzoglou², S Karimi², T Kaley², R Young²
¹Memorial Sloan Kettering Cancer Center, North Chicago, IL, ²Memorial Sloan Kettering Cancer Center, New York, NY

Purpose

The purpose of this study was to characterize hypertrophic olivary degeneration (HOD) that develops from posterior fossa masses and their treatments.

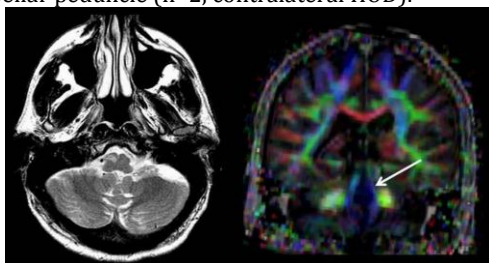
Materials and Methods

We retrospectively queried a departmental database from January 1997 to June 2013 to find patients with posterior fossa masses and HOD. Total 10 patients had MR imaging and other clinical data available for review. HOD was defined as abnormal T2 hyperintensity and/or enlargement of the inferior olive by MR imaging (MRI) with an inciting lesion in an afferent limb of the Guillain-Mollaret triangle. Four patients also had diffusion tensor imaging (DTI) available for analysis and streamline tractography.

Note: Scanned images are included in the proceedings. Some submitted images were reduced during editing thereby decreasing clarity. Also, refer to the Program Planner. Proceedings Content as of 3/28/2014.

Results

Patients had unilateral cerebellar lesions (n=4, developed contralateral HOD), midline cerebellar lesions (n=4, bilateral HOD) or unilateral pontine lesions (n=2, ipsilateral HOD). These consisted of tumors (n=8), demyelination (n=1) and nonspecific necrosis (n=1). Eight patients had dysphagia and/or nystagmus, including four patients a median 87 days before HOD. MR imaging showed T2 hyperintense signal in the inferior olive median 86 days (range, 0-363) after the diagnosis of a posterior fossa lesion. Hypertrophic olivary degeneration presented prior to surgery (n=2), after surgery (n=3), after surgery and radiation therapy (n=4), or without any treatment (n=1). Diffusion tensor imaging in four patients revealed decreased anisotropy and fiber tracts in the central tegmental tract (n=2, ipsilateral HOD) or the superior cerebellar peduncle (n=2, contralateral HOD).



Conclusions

Hypertrophic olivary degeneration may develop from posterior fossa masses and surgical and/or radiation therapy treatments. Proper recognition of the characteristic features of HOD is necessary to avoid misdiagnosis of a recurrent tumor in cancer patients.

KEYWORDS: Anatomy, Brain Neoplasms, Hypertrophic Olivary Degeneration

O-425 3:07PM - 3:14PM
Estrogen and Brain Structure in a Community Cohort of Elderly Women

C Raji¹, J Becker², C Boyle³, H Gach², W Longstreth⁴, O Lopez², P Thompson³

¹University of California Los Angeles Medical Center, Los Angeles, CA, ²University of Pittsburgh Medical Center, Pittsburgh, PA, ³University of Southern California, Los Angeles, CA, ⁴University of Washington, Seattle, WA

Purpose

Alzheimer disease (AD) is the most common cause of dementia, and women are at higher risk than men (1). Prior studies suggest that estrogen may reduce the risk of Alzheimer dementia (2). Such risk modifying influence may occur by estrogen strengthening brain structural integrity with neurotrophic effects. Here we aimed to understand how estrogen use influences brain structure in a cohort of elderly women.

Materials and Methods

Female participants were recruited from the multisite Cardiovascular Health Study (n = 560). Of this cohort, 100 subjects were actively taking estrogen at the time of

assessment with 3D volumetric spoiled gradient echo T1-weighted MR imaging (MRI). The average age of this group was 78.1 years (range: 69-93); 137 subjects had either AD or mild cognitive impairment (MCI). Women using estrogen were more likely to be better educated [(557) = 2.71, p = .007] and younger [(557) = -2.64, p = .008] compared to the nonestrogen group. There were no statistically significant differences in BMI, physical activity, type II diabetes, alcohol use, smoking, MRI infarcts, white matter lesions, or cognitive impairment (p < .05). The relationship between estrogen use and brain structure was quantified with tensor-based morphometry. Multivariable regression modeled this relationship and controlled for multiple comparisons, age, site, education, physical activity, BMI, cognitive impairment, and white matter lesions.

Results

Women taking estrogen had greater gray and white matter volumes in the frontal, temporal, and parietal lobes, compared to the nonestrogen group (Figure 1). A darker shade of blue on the color scale denotes a stronger effect size in the frontal lobes. The positive influences of estrogen use on brain structure remained statistically significant after adjusting for potential confounders.



Conclusions

History of estrogen use in older women of the CHS was related to greater gray and white matter volumes in the frontal, temporal, and parietal lobes. Stronger main effects were observed in the frontal cortex; these results persisted even when controlling for multiple potential confounding variables. These results may reflect the underlying neurotrophic influence of estrogen known from prior work (3, 4).

KEYWORDS: Aging, Brain Mapping

O-426 3:14PM - 3:21PM
Cerebral Microbleeds and White Matter Hyperintensity in Alzheimers Disease, Significance and Incidence in Australian Population and its effect on Cognition

S Bhuta¹, M Bilska¹, C Hsu¹, R Jones², G Kwan¹

¹Gold Coast University Hospital, Gold Coast, Australia, ²James Cook University, Townsville, Australia

Note: Scanned images are included in the proceedings. Some submitted images were reduced during editing thereby decreasing clarity. Also, refer to the Program Planner. Proceedings Content as of 3/28/2014.

Purpose

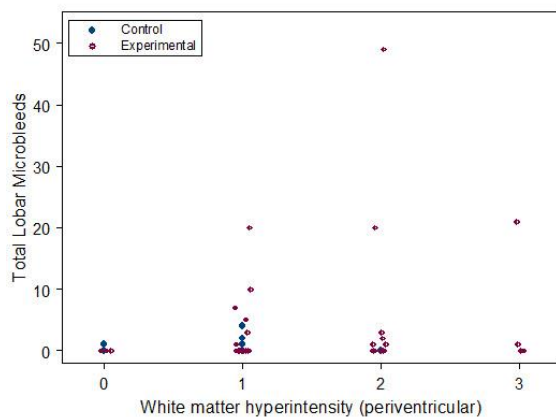
The aim of the study was to determine the incidence and distribution of lobar microbleeds in probable Alzheimer disease (AD) and mild cognitive impairment (MCI) patients and to assess its association with white matter hyperintensities (WMH) and its effect on cognition and higher executive function.

Materials and Methods

Patients with presumed clinical diagnosis of AD and MCI (n=38) referred from Specialist Dementia Clinic were included in the study and healthy age-matched controls (n=26) also were used. Retrospective review of MR imaging (MRI) was performed by two independent readers (CC-TH and SB). Susceptibility-weighted imaging (SWI) and phase sequences and T2/FLAIR were included in dementia imaging protocol. Location and number of microbleeds as lobar or basal ganglia was discerned with SWI and phase sequences. White matter hyperintensity was rated on T2-weighted images using a modified Age-Related White Matter Changes Rating Scale (ARWMC). Mini mental score examination (MMSE) was used as an index to assess patients cognitive status. To evaluate the association and effect of proposed variables, the data were modelled as negative binomial regression. SPlus 8.2 (Tibco Software) or R 3.0.1 (R Foundation for Statistical Computing) was used for statistical analysis.

Results

The average number of microbleeds was 4.7 times higher in the AD and MCI group versus the control group ($p = 0.043$). Microbleeds increased progressively with age in the 70+ age group ($p = 0.010$) at a rate of 11% per year. There was occipital predominance of lobar microbleeds in AD and MCI compared to control group ($p = 0.007$). Basal ganglia microbleeds were less frequent and demonstrated no significant difference between groups. Increase in modified ARWMC scores was associated with higher number of lobar microbleeds from score 0 to 2 but not between score 2 to 3. There was no consistent relationship between number of lobar microbleeds and MMSE in the AD and MCI group, similarly no consistent relationship was seen with Superficial Siderosis (SS) and AD although sample size of SS was small.



Conclusions

Alzheimer disease and MCI patients have higher incidence and number of microbleeds with an occipital predominance compared to normal aging subjects, this may implies vasculopathy in AD and possible vascular basis for neuronal damage and neurodegeneration. Microbleeds number increases with higher modified ARWMC score 0-2 but not so from 2-3. Numerical value of lobar microbleeds is not a reliable marker of cognition (MMSE). A larger patient cohort may be required to elucidate the complexity of microbleeds in AD and MCI patients.

KEYWORDS: Microbleeds

O-427 3:21PM - 3:28PM
Effect of Age and Gender on Cerebral Microbleeds of Alzheimer's Disease on 3T Susceptibility-Weighted Images - A University Hospital-Based Dementia Study

H Uetani, Y Ando, M Azuma, M Hashimoto, M Ikeda, M Kitajima, T Hirai, Y Yamashita
Kumamoto University, Kumamoto, Japan

Purpose

The aim of this study was to investigate the effect of age and gender on cerebral microbleeds (MBs) on 3 T susceptibility-weighted images (SWI) in Alzheimer disease (AD) patients seen at our memory clinic.

Materials and Methods

We studied 299 consecutive AD patients (89 men, 210 women, mean age 76 ± 8.5 years) who attended our memory clinic and were diagnosed on the basis of the criteria for probable AD of the National Institute of Neurologic Disorders and Stroke/Alzheimer Disease and Related Disorders Association by two neuropsychiatrists. All underwent dementia screening, neurologic and comprehensive neuropsychiatric assessments, and 3 T MR imaging (MRI) including susceptibility-weighted imaging (SWI) studies of the brain. For each patient, two neuroradiologists independently evaluated MBs defined as small (<10 mm diameter) round foci of low signal intensity on SWI. Statistical analyses were performed to evaluate the difference between male and female on the prevalence of MBs.

Results

Of the 299 patients, at least one MBs was exhibited in 163 (55%) on whole brain and 128 (43%) on the cortex or subcortical white matter (C/S). There were no MBs on the whole brain and the C/S in female AD patients in their fifties. The prevalence of MBs on the whole brain increased with age in both male and female groups; it was higher for male than female at any age group. Male patients in their sixties had a significantly higher prevalence of MBs on the C/S than female (58% versus 24%; odds ratio adjusted by hypertension, 4.53; $P = 0.041$). In the prevalence of MBs on the C/S, no significant difference between the male and female groups was found in their seventies (42% versus 51%, adjusted odds ratio was 0.69, $P = 0.395$) and in their

Note: Scanned images are included in the proceedings. Some submitted images were reduced during editing thereby decreasing clarity. Also, refer to the Program Planner. Proceedings Content as of 3/28/2014.

eighties (51% versus 43%, adjusted odds ratio was 1.47, P = 0.345).

Conclusions

On 3 T SWI in AD patients, the prevalence of cerebral MBs increased with age in both male and female groups. The appearance of MBs was later for female than male.

KEYWORDS: Alzheimer Disease, Microbleeds, Susceptibility-Weighted Imaging

0-428 3:28PM - 3:35PM
Quantitative MRI discrimination of Alzheimer's dementia, mild cognitive impairment, and other memory disorders using volumetric MRI

S Jones¹, Z Berman², S Mahmoud¹, A Rae-Grant¹

¹Cleveland Clinic, Cleveland, OH, ²Case Medical School, Cleveland, OH

Purpose

Alzheimer disease (AD) is a debilitating neurodegenerative process, and a core part of the clinical investigation is qualitative brain MR imaging (MRI). Recently quantitative MRI is being applied, with FDA-approved commercialized software yielding detailed brain volumes. Due to considerable overlap of these volumes compared with normal brains, the most useful clinical parameter is a statistical comparison of a given patient compared with a normal control distribution. We extend this concept except to compare a given patient against a distribution of patients with known AD, in addition to a set of patients with mild cognitive impairment (MCI), and those with age-related memory loss. Lastly to measure the clinical impact of these volumetric MRI reports, we measure the impact of a report during a weekly interdisciplinary degenerative disease conference using a survey method, with clinical decisions recorded both before and after the introduction of a quantitative report.

Materials and Methods

The clinical records were reviewed of 663 consecutive patients at the Lou Ruvo Center for Brain Health who underwent quantitative MRI using commercially available NeuroQuant (Cortech Inc., La Jolla, CA), which computes the brain volumes of 48 parenchymal and extraparenchymal regions. These numbers were compared with the presence and type of dementia, whose gold standard was the clinical diagnosis. This cohort was randomized to a group of 496 patients for a "training set" and 167 patients for a "test set." The training set volumetric data and clinical diagnosis were used to form a library and three models to evaluate the ability to correctly place the test set's patient into their correct clinical diagnosis. The model yielded three probabilities, for any new patient, that their volumetric numbers could belong to each of the library sets of AD, MCI, or age-related memory loss. The second portion of this project evaluated the effect of these probabilities on clinical decision-making during a weekly conference, during which clinical diagnoses and treatment plans were recorded both before and after introduction of the three probabilities.

Results

Of the 663 patients scanned with volumetric MRI: 322 were with Alzheimer dementia, 262 with mild cognitive impairment, and 79 with age-related nonneurodegenerative memory loss (AR-ML). After randomization, three probability models using multinomial logistic regression were derived from the training group. A statistical, a clinical, and a hybrid model were created. The accuracy of correctly placing the test set was 0.691, 0.740, and 0.744, respectively. The hybrid model achieved 0.753, 0.625, and 0.444 positive predictive values for correctly assigning patients to AD, MCI, or AR-ML, respectively. To date, 12 patients have been discussed during weekly conferences, with inclusion of probabilities that a given patient could belong to each of the three disease groups. Two of the 12 patients have had their clinical decisions affected by the volumetric report. This activity is ongoing and we will present further data during conference.

Conclusions

A center specific library of quantitative brain measures may be useful in generating probabilistic models to categorize patients with cognitive disorders. Preliminary data suggest that inclusion of these volumetric results affect a given patient's clinical decision-making during a weekly conference about 10% of the time.

KEYWORDS: Alzheimer Disease, Degenerative, MR Imaging Brain

0-429 3:35PM - 3:42PM
Functional Neuroimaging: Trends in Utilization of PET in Alzheimer's Disease as Analyzed from a NonDenial Approach to Radiology Benefit Management

O Boyko¹, L Boyko¹, M Tankersley², M Law¹

¹University of Southern California, Los Angeles, CA,

²HealthHelp Inc, Houston, TX

Purpose

Analyze utilization trends over a 36-month period for functional neuroimaging of PET scan for clinical indication of Alzheimer disease assessment in a nondenial approach to radiology benefit management.

Materials and Methods

Request for neuroimaging positron emission tomography (PET) pre-authorization by an Radiology Benefit Management (RBM) using a nondenial system, retrospectively reviewed over a 36-months trend for CPT codes 78608 and 78609 for commercial provider (Humana) as to three categories. 1. Total studies ordered by provider two. 2. Total number withdrawn by provider three. 3. Total number changed by consensus/nonconsensus.

Results

Over a 36-month analysis the total number of studies ordered were 1196 with total approved of 922 (77%), withdrawn by the provider 257 (21.5%) and procedure changed 17 (1.7%). The trend broken down per year were: Year 1 Year 2 Year 3 Total 3 Years Withdrawn PET 57 83 117 257 Approved PET 260 305 357 922

Note: Scanned images are included in the proceedings. Some submitted images were reduced during editing thereby decreasing clarity. Also, refer to the Program Planner. Proceedings Content as of 3/28/2014.

Conclusions

In an RBM environment with increasing utilization demand for functional neuroimaging using PET a nondental RBM system with providers working in a collaborative environment (in which result of disagreement = defer to treating clinician) was not associated with a greater utilization with the upward trend of utilization being offset by upward trend of provider withdrawal allowing for appropriateness criteria and collaborative environment to "bend the cost curve" without a confrontational atmosphere with a patient safety achievement of decreasing radiation exposure (equivalent of 179,900 CXRs for 257 withdrawn PET studies).

KEYWORDS: Alzheimer Disease, PET

O-430 3:42PM - 3:49PM
Comparison of Automated Brain Segmentation to Subjective Assessment in Discriminating Shunt-Responsive Normal Pressure Hydrocephalus, Alzheimer Disease and Normal Elderly

Y Serulle, H Rusinek, J McMenamy, A Baxter, R Jain, J Golomb, O Gonen, A George
New York University Langone Medical Center, New York, NY

Purpose

Normal pressure hydrocephalus (NPH) is increasingly recognized as a treatable disorder characterized by motor deficits, urinary incontinence and cognitive impairment. Differentiating NPH from cerebral atrophy associated with neurodegenerative diseases such as Alzheimer disease (AD) is often a challenge due to their overlapping clinical features and similar age groups they affect. Using clinically validated ground truth cases we assessed the subjective diagnostic performance of three experienced radiologists in discriminating shunt-responsive NPH from AD and age-matched healthy controls. We compared the subjective radiologic assessments with a multivariate predictive model based on brain tissue volumetry.

Materials and Methods

The study involved high resolution 3D T1-weighted MRI examinations of 15 NPH patients who showed subsequent positive response to shunt, 21 AD patients and 18 healthy controls. The groups were matched on age and gender. Subjective assessment: Three radiologists (with 3-18 years of experience in the interpretation of brain MR images) independently and in a blinded fashion rated each case as NPH, AD or healthy elderly. Automated model: Images were segmented into gray and white matter and intra and extraventricular CSF using automated software. A multivariate prediction model was generated based on tissue volumes and gender. The model was compared to the radiologists' subjective assessments in regards of diagnostic accuracy.

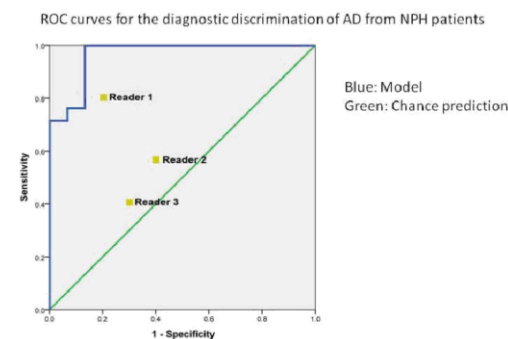
Results

Subjective assessments: The diagnostic accuracy for the three readers was 75.9%, 70.4% and 64.8% (Table 1). There was a 'fair agreement' across the readers with an

intraclass correlation coefficient of 0.49 (95% confidence interval 0.33 - 0.64). There were 12 (22%) discordant diagnoses between readers one and two, and 16 (29%) between readers one and three and readers two and three. Automated model: A binary logistic regression model that includes gender (to account for larger head size in male subjects), gray matter volume and ventricular volume, had accuracy of 96.3%, significantly ($P < 0.005$) higher than each reader (Table 1). Receiver operating characteristic (ROC) analysis demonstrated higher sensitivity and specificity for the regression model compared to the readers (area under the curve 0.965) (Figure 1).

Diagnostic accuracy (%) for the three readers and the model based on brain segmentation

	Overall	Normal elderly	NPH	AD
Reader 1	75.9	72.2	73.3	81
Reader 2	70.4	94.4	60.0	57.1
Reader 3	64.8	94.4	60.0	42.9
Model	96.3	100	86.7	100



Conclusions

Automated brain segmentation differentiates shunt-responsive NPH from Alzheimer disease and healthy elderly with higher accuracy than subjective assessment.

KEYWORDS: Alzheimer Disease, Neurodegenerative, Normal Pressure Hydrocephalus

O-431 3:49PM - 3:56PM
Using Structural Connectivity Graph Analysis to Predict Cognitive Decline in Patients After Carotid Endarterectomy

S Soman¹, G Prasad², E Hitchner³, M Moseley⁴, A Rosen⁴, W Zhou³

¹Stanford University/Palo Alto WRIISC, Menlo Park, CA, ²University of Southern California - LONI/Stanford University, Menlo Park, CA, ³Stanford Vascular Surgery, Menlo Park, CA, ⁴Stanford University, Menlo Park, CA

Purpose

While carotid endarterectomy or stenting has been noted to reduce the risk of future stroke in patients with high grade carotid stenosis, many patients still experience postoperative neurocognitive decline. We sought to apply structural connectivity metrics to identify patients at increased risk for postoperative decline.

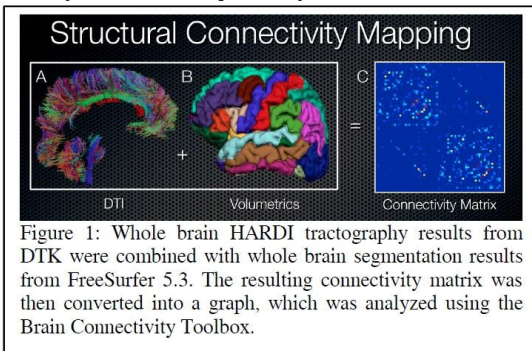
Materials and Methods

Note: Scanned images are included in the proceedings. Some submitted images were reduced during editing thereby decreasing clarity. Also, refer to the Program Planner. Proceedings Content as of 3/28/2014.

Twenty-eight patients underwent presurgical evaluation under an IRB approved protocol that included T1 structural and 30 direction diffusion tensor imaging (DTI) MRI and a battery of neuropsychological tests both before and one month after surgery. Patients were classified as decliners based on decreased performance on the Rey-AVLT on one month follow up. The T1 images were processed using FreeSurfer, with resulting segmentations being reviewed and edited as needed under the supervision of a neuroradiologist. Whole brain tractography was performed using Diffusion Toolkit and visually inspected. Connectivity matrices then were generated from the FreeSurfer segmentation and DTK fiber tracking using Matlab, and graph metrics were computed using the Brain Connectivity Toolbox.

Results

Controlling for age, classifiers using the graph analysis metrics "weighted optimal community structure" and "binary component sizes" were able to identify patients that would experience cognitive decline with 81% sensitivity 83% and specificity ($p > .05$, false discovery rate .05). These two measures were computed at 10 proportion edge thresholds from .1 to 1 at intervals of .1 in weighted and binary networks respectively.



Conclusions

Applying structural connectivity analysis may be capable of identifying patients at increased risk for postoperative cognitive decline, and may help guide therapy and provide patients' families guidance regarding prognosis.

KEYWORDS: Carotid Artery, Carotid Artery Stenting, Connectivity

O-432 3:56PM - 4:03PM
DTI Evidence of Asymmetric Progression in Parkinson's Disease

L Chan¹, K Ng², C Yeoh¹, H Rumpel¹, E Tan³
¹Singapore General Hospital, Singapore, ²Duke-NUS Graduate Medical School, Singapore, ³National Neuroscience Institute, Singapore

Purpose

Parkinson's disease (PD), a common neurodegenerative disease, may be differentially affected between sides (left & right). There is limited data on side differences in PD and to our knowledge no studies that have examined the rate of change of diffusion tensor imaging (DTI) parameters on

MRI between the right and left side over time. Utilizing a longitudinal follow-up methodology, we investigated the rate of change in DTI-metrics between the right and left side in PD patients.

Materials and Methods

Subjects diagnosed with PD using standardized clinical criteria were prospectively recruited. All subjects underwent DTI MR brain imaging at baseline and about 5 years later using identical MR protocol. We measured the FA and ADC values in the right and left caudate, putamen, thalamus and substantia nigra. We evaluated the FA, ADC and their rate of change in the right and left sides of the ROIs in all subjects. Statistical significance is defined at $p < 0.5$.

Results

Forty-six PD patients (average age 70 years, 22 men) were included. There was a significant difference in the FA value between the right and left SN at baseline (0.45 vs 0.43, $p = 0.001$) and the second time point (0.48 vs 0.47, $p = 0.047$). The FA was not significantly different between right and left putamen at baseline (0.28 vs 0.28, $p = 0.49$), but this became significant at the second time point (0.36 vs 0.32, $p = 0.001$). Similar findings were found in the thalamus at baseline (0.37 vs 0.37, $p = 0.59$) and the second time point (0.39 vs 0.42, $p = 0.003$). The rate of change of change in some brain regions appears to be different between the right and left at baseline and the second time point.

Conclusions

We demonstrated significant right - left differences in FA values in the SN, putamen and thalamus in PD. These side differences became more significant for some brain regions 5 years later, suggesting asymmetric progression of neurodegeneration. These observations would be pertinent to consider in the long-term evaluation of clinical progression in PD patients using DTI.

KEYWORDS: Degenerative, Diffusion Tensor Image, Parkinson Disease

O-433 4:03PM - 4:10PM
Comparison of subcortical tissue distortion in MR images at 3T and 1.5T for deep brain stimulation patients

S Sarkar¹, R Rojas², E Papavassiliou², R Alterman², L Shih², D Teich¹, D Hackney²
¹Beth Israel Deaconess Medical Center/Harvard Medical School, Boston, MA, ²Beth Israel Deaconess Medical Center, Boston, MA

Purpose

MR-based presurgical stereotactic planning for deep-brain stimulation (DBS) surgery for placing electrodes within subcortical targets is a widely used and reliable method. However, potential MR distortion has been much debated (1) as a confounding factor toward estimating presurgical target coordinates leading to errors in electrode placement particularly for small targets like subthalamic nucleus (STN) or globus pallidus interna (GPi). Duchin et al. (2) compared several anatomical landmarks from MR images at 7 T and 1.5 T to show that 7 T images of the central brain

Note: Scanned images are included in the proceedings. Some submitted images were reduced during editing thereby decreasing clarity. Also, refer to the Program Planner. Proceedings Content as of 3/28/2014.

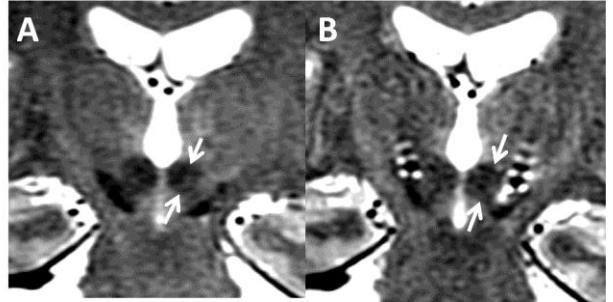
regions have comparable while the distal brain regions have higher distortions than images obtained at 1.5 T, and hence concluded that targeting of central structures such as the STN are reliable at 7 T. In this work we analyzed the difference in various distance and size measurements for common subcortical tissues for six patients scanned first at 3 T for identifying and estimating presurgical target coordinates followed by imaging at 1.5 T after DBS implantation in order to assess lead placement accuracy. Our assumption, along with those of many practitioners, is that 1.5 T being the lower field strength would produce less geometric distortion and should be considered the preferred tool. However, often the MR-based surgical planning for various subcortical nuclei has been unsatisfactory due to the variability in anatomical position and size of these structures at lower field strengths (3) although inadequate surgical atlas and mechanical variation involving brain shifts also have played significant roles in DBS targeting errors (4, 5).

Materials and Methods

Six patients (age 59-76, 3 males) with medically refractory Parkinson's disease were scanned using an axial T1-weighted MPRAGE and a coronal T2-weighted sequence in a 3 T GE MR scanner with Leksell frame and fiducials for presurgical stereotactic planning for DBS surgery for placing quadripolar electrodes (Medtronic Inc., Minneapolis, MN) in the subthalamic nuclei. After DBS placement the patients were re-imaged in a GE 1.5 T MR system with identical software and MR sequences appropriately modified to maintain SAR and other hardware conditional guidelines of FDA and DBS manufacturer. Qualitative and quantitative assessments of global and regional distortion were evaluated by a physicist and a neurosurgeon based on the dimensions and distances of the following: the AC-PC length, the diagonal distance between the outer fiducials of the Leksell frame, the length of the caudate head (CN) and the hippocampus body (Hb) as well as the diameter of bilateral red nuclei (RN) along the frequency encode direction in which the geometric distortion is maximum.

Results

Mean variation in the measured dimensions for various tissues between the two field strengths were less than one percent for AC-PC and fiducial distances as well as for dimensions of CN and Hb. However, the dimension of RN varied by 3-7% in our patient group when compared between 3 T and 1.5 T (Figure 1 below shows coronal T2-weighted images for a typical DBS candidate). Note in this case the RN dimension is 7.3 mm at 3 T prior to surgery (A, arrows) and 7.7 mm at 1.5 T 24 hours after surgery (B). Subthalamic nucleus and GPi boundaries were not equally identifiable at both fields and were not analyzed for distortion at this time.



Conclusions

The larger variation observed only for the dimension for RN indicates a greater geometric distortion perhaps due to the higher susceptibility at the iron-rich RN. Similar effects are expected for other iron-rich nuclei including STN and GPi and currently are being studied. This may be an important contributor to the lead placement errors in addition to ones caused by the brain shift (4, 5) in MR-based stereotactic DBS surgery.

KEYWORDS: Deep Brain Stimulator, High Field, Subthalamic Nucleus

O-434

4:10PM - 4:17PM

Patterns of Chronic Venous Insufficiency in the Dural Sinuses and Extracranial Draining Veins and Their Relationship with White Matter Hyperintensities for Patients with Parkinson's Disease

E Haacke¹, M Liu¹, D Utriainen²

¹Wayne State University, Detroit, MI, ²Magnetic Resonance Innovations, Inc., Detroit, MI

Purpose

Idiopathic Parkinson's disease (IPD) remains one of those neurodegenerative diseases where the cause remains unknown. Many clinically diagnosed cases of IPD are associated with cerebrovascular disease and white matter hyperintensities (WMH) (1). The purpose of this study was to investigate the presence of transverse sinus and extracranial venous abnormalities in IPD patients and their relationship with brain WMH.

Materials and Methods

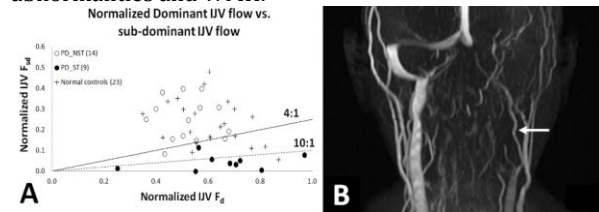
Twenty-three IPD patients and 23 age-matched normal controls were recruited from the same site in this study. They had conventional neurological MR structural and angiographic scans. In addition, blood flow in the extracranial vessels were quantified with 2D phase contrast (PC) including the internal jugular veins (IJVs), vertebral veins, common carotid arteries, vertebral arteries. The IJV flow was normalized by the total arterial flow. Venous structures were evaluated with 2D-time-of-flight (TOF); and WMH volume was quantified with T2-weighted fluid attenuated inversion recovery (FLAIR). The ratio of the flow in the dominant IJV (which carries the most flow) and the subdominant IJV (Fd/Fsd) was calculated for each case (Figure 1A). The IPD and normal subjects were classified using both the MR TOF and PC images into four categories: 1) complete missing

Note: Scanned images are included in the proceedings. Some submitted images were reduced during editing thereby decreasing clarity. Also, refer to the Program Planner. Proceedings Content as of 3/28/2014.

transverse sinus and partially missing IJVs on the TOF images with high Fd/Fsd (Figure 1B); 2) missing transverse sinus and stenotic IJVs with high Fd/Fsd; 3) reduced flow in the subdominant IJV with high Fd/Fsd; and 4) normal flow and no stenosis.

Results

When broken into the above four categories with categories one through three combined, a significant difference in the distribution of the IPD patients and normal controls ($\chi^2=7.7$, $p<0.01$) was observed. Venous abnormalities (categories 1, 2 and 3) were seen in 57% of IPD subjects and only in 30% of controls. Patients with venous abnormalities tended to show higher volume WMH. In IPD subjects, category type correlated with both flow abnormalities and WMH.



Conclusions

A major fraction of IPD patients appear to have abnormal venous anatomy and flow on the left side of the brain and neck and the flow abnormalities in particular appear to correlate with WMH volume.

KEYWORDS: Parkinson Disease, Venous Drainage, Venous Stenosis

0-435 4:17PM - 4:24PM
Hypertrophic Olivary Degeneration and Cerebellar Atrophy

A Mironov
Creighton University Medical Center, Omaha, NE

Purpose

It is well acknowledged that the primary (ischemia, hemorrhage, mass, trauma) or secondary (surgical treatment) injury of the dentato-rubro-olivary pathway may generate a unique pathological and imaging condition representing the phenomenon of hypertrophic olivary degeneration (HOD). The hallmarks include, depending on the level of injury, ipsilateral or bilateral increased T2 signal intensity and hypertrophy of the olive, and may be associated variably with dentatorubral tremor or palatal, cervical or ocular myoclonus. The purpose is to present two cases with classical acquired features of HOD associated with progressive cerebellar atrophy in the very late period. The progressive global cerebellar atrophy has not been considered previously in the definition of the HOD.

Materials and Methods

The first patient (50-year-old male) suffered symptomatic pontine hemorrhage due to cavernoma. He was followed up for up to 10 years after surgery. The second patient (32-year-old female) had history of systemic lupus erythematosus (SLE) and developed vasculitis with lacunar insults of the brain stem. The patient was followed up to

five year after the first onset. The patients were evaluated by imaging studies (CT, MRI, MRA, catheter angiography).
Results

The first case was found to have - 10 months after surgery for pontine cavernoma with symptomatic hemorrhage - an abnormal T2 symmetrical signal in the olives of medulla oblongata bilateral, which persisted over the following three years. Two years after the surgery the patient developed progressive diplopia, numbness, poor coordination, dysarthria and intractable tremor. The patient was considered to be treated by deep brain stimulators. Repeated imaging in the following 10 years after surgery showed progressive general cerebellar atrophy. The second case suffered SLE and developed lacunar ischemic lesions of pons and thalamus. Three weeks later repeated MRI revealed abnormal T2 hyperintensity of olives involving the entire medulla oblongata. Repeated MRIs in the following four years showed persistent abnormal T2 signal of olives, shrinking of the superior medulla, and impressive progressive atrophy of pons and cerebellum. The chronological development of HOD in both cases showed initial T2 abnormality 10 months/3 weeks after ictus, with persistent increased T2 signal and mild olivary hypertrophy for three years/four years followed by continued signal decrease and olivary shrinking and impressive cerebellar atrophy.

Conclusions

The pathological changes within the olivary nucleus had been considered neuronal cell enlargement, cytoplasmic vacuolation, fibrillary gliosis, demyelination, and astrocytic proliferation. The progressive involvement of the cerebellum in our cases may suggest similarities with the primary autosomal-inherited cerebello-olivary degeneration of Holmes, in which the olivary changes has been suggested to be secondary to transynaptic degeneration from the primary cortical degeneration. Some neuronal loss may be encountered in the dentate nucleus, but usually the afferent and efferent connections are uninvolved as are the motor and sensory tracts of the spinal canal. The evolution of the acquired HOD may suggest that the primary injury of dentato-rubro-olivary pathway may have the same impact on the cerebellum.

KEYWORDS: Hypertrophic Olivary Degeneration

0-436 4:24PM - 4:31PM
Schizophrenia, Exercise and Hippocampal and Frontal Cortex Plasticity Assessed By High-Field Structural Imaging in MR

O McDonnell¹, A Rauscher², D Warburton², A Thornton³, G Smith², W Su², B Humphries², A Vertinsky¹, D Lang²
¹Vancouver General Hospital, Vancouver, BC, Canada,
²University of British Columbia, Vancouver, BC, Canada,
³Simon Fraser University, Vancouver, BC, Canada

Purpose

Previous imaging studies have suggested that reduced hippocampal volumes and frontal cortical thickness in

Note: Scanned images are included in the proceedings. Some submitted images were reduced during editing thereby decreasing clarity. Also, refer to the Program Planner. Proceedings Content as of 3/28/2014.

schizophrenia are part of the underlying mechanism that gives rise to components of both psychiatric and cognitive impairment. Antipsychotic medications provide some alleviation of psychiatric deficits, but offer little to no amelioration of cortical or hippocampal deficits.

Additionally, antipsychotic medications have deleterious metabolic and cardiovascular sequelae. In contrast, regular exercise is associated with improved cardiovascular health, enhanced mood state, weight loss, and increased hippocampal volumes in the normal population. We examined the effects of exercise on cortical thickness and hippocampal volume in a cohort of chronic hospitalized schizophrenia patients to determine if exercise could increase hippocampal volumes or frontal cortical thickness in chronically medicated patients.

Materials and Methods

a). Study Design: Measures of clinical symptoms and imaging were conducted at baseline, and at six weeks and 12 weeks following an exercise intervention. b). Subjects: 26 chronic refractory DSM-IV schizophrenia in-patients (10 female, 16 male) were recruited from the BC Psychosis Ward, UBC Hospital, and enrolled in a progressive 12-week supervised exercise program. Fourteen of 26 had completed all imaging research protocols at the time of this submission. c). Imaging: Standard whole brain 3D IR-weighted SPGR were collected at 3 T (Philips Achieva). Volumetric segmentation of hippocampal volumes and gray matter thicknesses were ascertained with FSL versus 4.1 and FreeSurfer 5.1 tools. d) Analysis: All repeated measures comparisons were based on baseline and 12 week follow-up scores. Preliminary repeated measures t-tests were used to investigate left-right differences. ANCOVAs with gender and total brain volume entered as covariates were used to test baseline versus follow-up differences in hippocampal volume or frontal gray matter thickness. Relationships between hippocampal volume and frontal thickness were explored with Pearson's linear correlations.

Results

All subjects were receiving antipsychotic treatment during the course of the study. Subjects were a mean age of 30.2 years and had been ill an average of 9.7 years at study entry. No significant left-right differences in any volumes were observed (all p-values >.10). Subsequent analyses used total left + right volumes. Total hippocampal volumes increased significantly after 12 weeks exercise ($F(1,11)=9.4$, $p=.01$, particularly on the left ($1,27)=6.2$, $p=.03$, but not the right ($F(1,27)=.12$, $p>.50$). Mean frontal lobe gray matter thickness did not increase after exercise ($F(1,27)=.60$, $p.>.40$), nor were hippocampal volumes and mean frontal lobe gray matter thicknesses correlated at baseline or follow up (all p-values >.10).

Conclusions

Twelve weeks of regular exercise was associated with increased hippocampal volume in chronically medicated schizophrenia patients, particularly on the left side. Exercise was not associated with overall frontal cortex thickness increases; however, a more focused assessment of the frontal subregions may be more fruitful in determining potential benefits. These observations

indicate that regular exercise is a potentially effective method of addressing the brain volume deficits associated with chronic schizophrenia and may result in improved cognitive functionality.

KEYWORDS: Cognitive Deficit, Cortical Thickness, Hippocampus

Tuesday, May 20
3:00 PM – 4:30 PM
Room 524

48 - Parallel Papers: Congenital Malformations and Seizures

O-437 3:00PM - 3:07PM
Prenatal MR morphology of occipital encephaloceles

G Kasprian¹, M Paldino², A Mehollin-Ray³, A Shetty³, J Williams³, W Lee³, C Cassady²

¹Medical University of Vienna, Vienna, Austria, ²Texas Children's Hospital, Houston, TX, ³Baylor College of Medicine, Houston, TX

Purpose

Meningoencephaloceles are congenital malformations of the central nervous system, characterized by the protrusion of meninges and cerebral tissue through a bony defect of the skull. When encephaloceles are detected prenatally, there is a need for detailed diagnostic assessment and characterization of a possible underlying syndrome. However, systematic studies on the prenatal MR appearance of encephaloceles are limited. This retrospective fetal MR study aims to systematically characterize cerebral MR morphology in cases with occipital and parietal meningoencephaloceles.

Materials and Methods

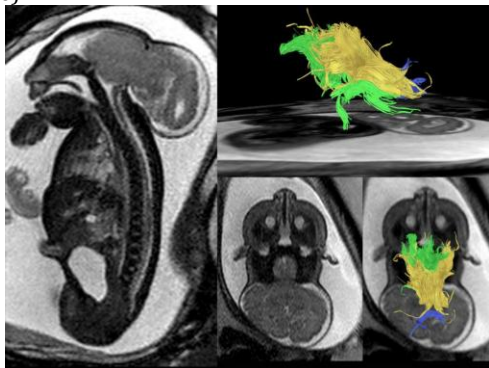
The 1.5-Tesla MR examinations (T2w, T1w, EPI, DWI) of 14 fetuses (mean gestational age: 26+3 gestational weeks {GW}) with occipital/parietal meningoencephaloceles were retrospectively analyzed for classification of anatomic characteristics. In five cases, a diffusion tensor sequence (16 gradient encoding directions, TR/TE = 2189/60 ms. FOV 230 x 230 x 72, resolution: 2mm x 2mm x 4mm, b = 0, 700 s/mm², scan time = 1 min 12 sec.) was performed.

Results

Displaced structures involved the occipital poles (3/14), occipital lobes (bilaterally 2/14, unilaterally 1/14), parietal and occipital lobes (bilaterally 1/14, unilaterally 2/14), and the parietal lobe only (1/14). In 2/14 cases, parts of the brainstem, the cerebellum, temporal and occipital lobes bilaterally were exteriorized. The typical features of Chiari III malformation¹ were seen in 6/14 cases, no skull deformity with or without external CSF spaces in 3/14 cases. The encephalocele appeared grossly disorganized in 6/14 with hemorrhage in 3/14 and polymicrogyria in

Note: Scanned images are included in the proceedings. Some submitted images were reduced during editing thereby decreasing clarity. Also, refer to the Program Planner. Proceedings Content as of 3/28/2014.

2/14. In 3/14 the brainstem displayed abnormal kinking/rotation, a Z shape (1/14), and/or a molar tooth like configuration of the midbrain (3/14). Tractography revealed the presence and position of sensorimotor tracts in 5/5 and parts of the corpus callosum in 3/4. The displaced brain tissue showed diffusion restriction in 8/9 with massive frontooccipitally oriented tracts on DTI (3/5, Figure).



Conclusions

Fetal MRI allows prenatal characterization of the macro- and micro- structural heterogeneity of occipital encephaloceles and may provide important information in the genetic workup and counseling of affected pregnancies.

KEYWORDS: Fetal Brain Development, Fetal Brain Injury

O-438 3:07PM - 3:14PM
Corpus callosum anomalies in Joubert syndrome: low prevalence and weak phenotype-genotype correlation

A Poretti¹, F Mancini², M Romani², A Micalizzi², J Koch³, J Fluss⁴, E Del Giudice⁵, A Simonati⁶, M Cirillo Silengo⁷, M Mirabelli⁸, R Biancheri⁸, T Huisman⁹, E Valente², E Boltshauser¹⁰

¹Johns Hopkins University School of Medicine, Baltimore, MD, ²Mendel Laboratory, IRCCS Casa Sollievo della Sofferenza Institute, Roma, Italy, ³University Hospital, Salzburg, Austria, ⁴University Children's Hospital, Genève, Switzerland, ⁵University "Federico II", Napoli, Italy, ⁶University of Verona, Verona, Italy, ⁷University of Torino, Torino, Italy, ⁸G. Gaslini Institute, Genova, Italy, ⁹The Johns Hopkins University School of Medicine, Baltimore, MD, ¹⁰University Children's Hospital, Zürich, Switzerland

Purpose
The molar tooth sign (MTS) is the neuroimaging hallmark of Joubert syndrome (JS) and results from a midbrain-hindbrain malformation characterized by vermian hypoplasia, thickened, elongated and horizontally orientated superior cerebellar peduncles and an abnormally deep interpeduncular fossa. Recently, we reported supratentorial neuroimaging findings including hippocampal malrotation, callosal dysgenesis, migration abnormalities, cephaloceles and ventriculomegaly in about 30% of JS patients. Mutations in KIF7, one of the 23 genes associated so far with JS, have been reported recently in patients with acrocallosal syndrome (ACS), a disease characterized by callosal agenesis and polydactyly.

Additionally, the MTS have been reported in few children with a phenotype reminiscent of ACS. This suggests that there may be some overlap between JS and ACS. We aimed to 1) estimate the prevalence of anomalies of the corpus callosum in JS and 2) evaluate whether KIF7 is a major gene causative of this specific phenotype.

Materials and Methods

The inclusion criterion was neuroimaging findings consistent with JS (unequivocal presence of MTS). The evaluation included qualitative assessment of the corpus callosum. Genetic analysis performed in a subset of patients included sequencing of 21 JS genes (including KIF7).

Results

Neuroimaging studies of 533 patients with confirmed diagnosis of JS were included in this study. Complete agenesis of the corpus callosum was found in five patients. Other morphological abnormalities of the corpus callosum were found in eight additional patients and included partial agenesis (absence of the splenium and hypoplasia in three patients, respectively), and dysplasia (abnormal shape) in two. Screening for mutations in 21 genes associated with JS (including KIF7) was performed in 280 of 533 JS patients including four patients with complete callosal agenesis and three patients with other callosal abnormalities. Genetic analysis revealed causative mutations in KIF7 in one patient with complete callosal agenesis and another patient with a dysplastic corpus callosum. Mutations in KIF7 were excluded in 273 JS patients without callosal abnormalities.

Conclusions

Abnormalities of the corpus callosum are rare in JS and were found in 2.4% of JS patients. In our series, KIF7 mutations were rare and always associated with corpus callosum abnormalities. In the literature, however, mutations in KIF7 have been reported in JS patients with a normal corpus callosum, weakening the genotype-phenotype correlation between KIF7 mutations and the occurrence of callosal anomalies. Neuroimaging findings are mandatory for the diagnosis of JS, but remain of limited value in classifying patients into specific subtypes.

KEYWORDS: Cerebellum, Corpus Callosum, Joubert Syndrome

O-439 3:14PM - 3:21PM
Anatomical Connectome Reveals Abnormal Connectivity in Complete Corpus Callosum Agenesis

A Meoded, T Bosemani, T Huisman, A Poretti
The Johns Hopkins University School of Medicine, Baltimore, MD

Purpose

The corpus callosum (CC) is the major commissure in the human brain. In complete CC agenesis, the fibers of the CC are not missing, but heterotopic and form abnormal white matter tracts. Investigating the anatomical brain connectivity is crucial for understanding the structural reorganization of white matter circuits in children with CC

Note: Scanned images are included in the proceedings. Some submitted images were reduced during editing thereby decreasing clarity. Also, refer to the Program Planner. Proceedings Content as of 3/28/2014.

agenesis. The structural connectome is an innovative technique suitable for the study of large-scale white matter connectivity of the human brain and the cerebral organization. Here, we apply a multiscale structural connectomics analysis to investigate white matter connectivity in children with complete CC agenesis. In more detail, we aim to 1) investigate connected/disconnected subnetworks, 2) characterize the topological network measures and 3) search for aberrant circuits in children with CC agenesis.

Materials and Methods

Patients were selected from our pediatric neuroradiology database based on 1) complete CC agenesis by conventional MR imaging (MRI) and 2) availability of diffusion tensor imaging (DTI) data without artifacts enabling high quality postprocessing. Age- and gender-matched controls also were selected. Diffusion tensor imaging data were acquired using a 1.5 T scanner. Postprocessing was performed using TORTOISE software. After nonlinear registration to MNI space, the cerebral and cerebellar cortex were parcellated into 108 regions using the AAL template. Probabilistic tractography was used to define connections between any pair of gray matter regions and an association matrix of structural connectivity was created for every subject. Structural connectomes for controls were created after excluding the CC (virtual callosotomy). Further analysis included 1) network-based statistics (NBS) to detect interconnected subnetwork as a whole and 2) topological network measures analysis to perform quantitative analysis of network metrics across different densities.

Results

Eleven patients (6 males, mean age 11.7 years) and 11 healthy controls were included in this study. One patient with two aberrant interhemispheric tracts was excluded from network analysis. Network-based statistics revealed three highly connected subnetworks (two intrahemispheric, one interhemispheric) in patients compared to controls. Topological network measure analysis showed higher clustering coefficient, smaller characteristic path length, higher global efficiency, slightly higher local efficiency (at higher density level), smaller assortativity and higher transitivity values across the range of densities in patients compared to controls. Network hubs were found in both insular and the left and right insula, and precuneus gyri and right lingual gyrus in patients and in the right postcentral gyrus and cerebellar 8th lobule and bilateral precuneus gyri in controls.

Conclusions

In patients with CC agenesis, the structural network is more segregated and less integrated compared to controls. This represents more local (between neighboring anatomical regions) rather than global interactions. In patients, the absence of hubs in the cerebellum may reflect compensatory mechanisms to maintain local efficiency at the cost of global connectivity. Highly interconnected subnetworks in patients also suggest effective local connectivity and may reflect compensatory rewiring mechanism in CC agenesis. Connectome analysis provides new information about abnormal connectivity and potential reorganization of white matter tracts in CC agenesis.

KEYWORDS: Connectivity, Corpus Callosum, Diffusion Tensor Image

O-440

3:21PM - 3:28PM

Correlation of Prenatal and Postnatal MRI Findings in Schizencephaly

S Nabavizadeh¹, D Zarnow¹, L Bilaniuk¹, E Schwartz¹, R Zimmerman¹, A Vossough²

¹Children's Hospital of Philadelphia, Philadelphia, PA,

²University of Pennsylvania/Children's Hospital of Philadelphia, Philadelphia, PA

Purpose

Schizencephaly is a rare malformation of the central nervous system characterized by a gray matter lined defect extending from the pial surface to the lateral ventricles. Previously it has been reported that the prenatal and postnatal appearances of schizencephaly are identical. The purpose of this study was to correlate imaging findings of schizencephaly and associated anomalies on fetal and postnatal MR imaging (MRI) and assess possible changes which may occur from the prenatal to postnatal state.

Materials and Methods

A retrospective review of 32 fetal subjects diagnosed with schizencephaly on prenatal MRI at our institution was performed. Those without postnatal MRI follow up at our institution were excluded. Subject age, cleft type, number, location, status of cortex lining the defect, presence or absence of a covering membrane (thin linear membrane along the surface or depth of the cleft), presence of signs of hemorrhage, and presence of other anomalies were assessed. Normalized dimensions of the defect at three levels and normalized width of the ipsilateral ventricle were measured on pre and postnatal imaging. These features and measurements were compared statistically and correlated to changes in the clefts between pre and postnatal imaging in order to assess whether these factors play a role in the observed changes in the schizencephalic clefts.

Results

Ten subjects with 18 clefts (8 bilateral) were included. The majority of defects (83%) were open on prenatal MRI, but 47% of those were found to subsequently have closed on postnatal imaging. Evidence of prior hemorrhage was seen in 83%. Prenatal MRI detected all cases of absent septum pellucidum, but detected a fraction of gross polymicrogyria and missed all cases of optic nerve hypoplasia. A covering membrane was detected in 10 defects prenatally, but only persisted in two defects postnatally. The normalized ipsilateral ventricular and inner and middle width dimensions of the defects were significantly decreased at postnatal imaging ($P < 0.05$). The widths of the defects, ventricular width, presence of a cleft membrane, and presence of hemorrhage were not predictors of closure of prenatally diagnosed open defects ($P > 0.05$).

Conclusions

In our series, nearly half of prenatally diagnosed open schizencephaly defects had closed on postnatal imaging. Prenatal MRI was only able to demonstrate some of the

Note: Scanned images are included in the proceedings. Some submitted images were reduced during editing thereby decreasing clarity. Also, refer to the Program Planner. Proceedings Content as of 3/28/2014.

associated anomalies. Our analysis could not predict which prenatally diagnosed open schizencephalic clefts will close.

KEYWORDS: Fetal, Fetal Brain Development, Schizencephaly

O-441 3:28PM - 3:35PM
What is different in the acallosal fetal brain?

G Kasprian, E Schwartz, P Brugger, G Langs, D Prayer
Medical University of Vienna, Vienna, Austria

Purpose

Complete agenesis of the corpus callosum (CCA) is a rather common developmental brain defect, with a reported incidence of 0.05-1% (1, 2) in the general population and 2-3% in patients with mental retardation (2). In cases of CCA, accompanied by associated brain or body malformations, severe psychomotor deficits and intractable epileptic seizures frequently are encountered (3). In contrast, the isolated finding of CCA leads more frequently (>80%) to a close to normal postnatal intellectual development (4). This study aims to detect and describe abnormalities and differences in cortical folding patterns of fetuses with CCA.

Materials and Methods

Three orthogonal T2-w sequences (1.5 T, slice thickness 4.4 mm, FOV 230 mm, TE=140 ms) of 15 fetuses with isolated and 15 cases with associated forms of CCA were compared to 15 age-matched normal fetuses. For 3D modeling axial, coronal and sagittal sequences were combined into isotropic volumes (resolution 0.78-1.02 mm) using intraslice motion correction and super-resolution reconstruction. The program ITK snap was used for manual segmentation of the surface of the fetal brain and the ventricles. In these, the shape of the manually delineated cortical contour was described using a 3D Gaussian model.

Results

Three-dimensional modeling could readily visualize the dynamic cortical folding patterns in CCA fetuses. Super-resolution datasets allowed the identification of subtle differences between normal fetuses and cases with isolated forms of CCA, whereas differences (ventricular size, brain size, cortical surface) were more pronounced in cases with associated anomalies.

Conclusions

In this preliminary work we used the technique of super-resolution 3D modeling to detect subtle differences of atypical cortical folding patterns of fetuses with CCA. In future, these tools may be further suitable to differentiate cases of isolated CCA with adverse neurodevelopmental outcome from those with close to normal development.

KEYWORDS: Callosal Dysgenesis, Fetal, Fetal MR Imaging

O-442 3:35PM - 3:42PM
CNS Imaging Findings Associated with Parry-Romberg Syndrome/En Coup de Sabre and Correlation to Cutaneous and Neurological Abnormalities.

D Doolittle, V Lehman, J Lehman, K Schwartz, M Tollefson, L Wong-Kisiel
Mayo Clinic-Rochester, Rochester, MN

Purpose

Parry-Romberg syndrome (PRS) and en coup de sabre (ECS) are both variants of morphea along a spectrum. Although numerous central nervous system (CNS) imaging findings of PRS/ECS have been reported, the prevalence of CNS imaging findings and relationship to cutaneous and neurological abnormalities has not been well characterized.

Materials and Methods

We performed a retrospective review of all patients less than 50 years of age at our institution over a 16-year interval with a confirmed clinical diagnosis of PRS/ECS by a skin/facial subspecialist. Two neuroradiologists evaluated the available imaging and characterized CNS imaging findings. These were correlated to the cutaneous and neurological abnormalities.

Results

Eighty-eight patients with PRS/ECS were identified [62 females (70.4%); average age: 28.8 years]. Nineteen of 43 (44%) patients with CNS imaging exams had abnormal imaging findings, although the only abnormal imaging finding in one patient was lateral ventricle asymmetry. Of the remaining 18 patients, findings were bilateral in 11 (61%), strictly ipsilateral to the side of facial involvement in six (33%), and strictly contralateral in 0 (6%). The two most common CNS imaging findings were white matter T2 hyperintensity in 14 of 43 (33%) patients and atrophy/encephalomalacia in five of 43 (12%) patients. Sixteen patients had serial imaging examinations over an average interval of 632 days (range 118-3438 days), of whom 13 (81%) had stable imaging findings. Three of 16 (19%) patients with serial imaging had change over time. One patient had decreased white matter T2 hyperintensity, progression of right atrophy, and development of right cortical T2 hyperintensity. Another had decrease in white matter T2 hyperintensity, development of encephalomalacia in left basal ganglia, and enlargement of a porencephalic cyst. The third patient had development of new areas of white matter T2 hyperintensity with subtle enhancement. Of 23 patients with a clinical neurologic abnormality and imaging, 12 (52%) had abnormal imaging findings. These included six of 18 (33%) with headaches and 7 of 7 (100%) with seizures. Six patients with PRS/ECS were evaluated by neurology and found to have no neurologic abnormality. Of those six, 4 (67%) had imaging and two (33%) had abnormal imaging findings, including 1 patient with bilateral cerebral aneurysms and 1 with a left cerebellar hemorrhage, prominent deep and subcortical WM T2 hyperintensities, and an area of T2 hyperintensity in the thalamus. Five of 6 (83%) patients with progressive cutaneous findings over the interval of serial examinations

Note: Scanned images are included in the proceedings. Some submitted images were reduced during editing thereby decreasing clarity. Also, refer to the Program Planner. Proceedings Content as of 3/28/2014.

had stable imaging findings, with the other displaying increasing white matter T2 hyperintensities.

Conclusions

This study represents the largest study on neuroimaging studies in patients with PRS/ECS to date and is unique in that imaging findings were correlated with cutaneous and neurologic findings, all followed over time. Unlike prior reports, this study found that imaging findings are frequently bilateral. Imaging findings are inconsistently associated with clinical neurologic abnormality, are frequently present in the setting of seizures, are usually stable over time, and often do not correlate with cutaneous disease activity.

KEYWORDS: Atrophy, Headaches, Seizure

O-443 3:42PM - 3:49PM
Volumetric changes in hippocampal subregions and their relation to memory in pediatric non-lesional localization-related epilepsy

E Widjaja, C Raybaud, M Smith, O Snead, M Zamyadi
Hospital for Sick Children, Toronto, Ontario, Canada

Purpose

Developmental differences in structure and function have been reported along the hippocampal subregions. The aims of this study were to determine if there were volumetric differences in hippocampal head (HH), body (HB), tail (HT) and total hippocampus (TotH) in children with nonlesional localization-related epilepsy relative to controls, and the relation between hippocampal subregions with episodic memory and clinical parameters.

Materials and Methods

Forty-eight children with nonlesional localization-related epilepsy, consisting of 29 left- and 19 right-sided epilepsy, and 27 healthy controls were recruited. All patients and controls underwent volumetric T1-weighted imaging, verbal and nonverbal memory testing. The volume of hippocampal subregions was compared between patients and controls. The associations between left hippocampal subregions with verbal memory, right hippocampal subregions with nonverbal memory, and hippocampal subregions with age at seizure onset and seizure frequency were assessed.

Results

Patients with left-sided epilepsy had smaller left HH ($p=0.003$) and HB ($p=0.012$), right HB ($p=0.021$) and HT ($p=0.015$), and right TotH ($p=0.020$) volumes. Those with right-sided epilepsy had smaller right HT ($p=0.018$) volume. There were no significant differences between verbal and nonverbal memory in left- and right-sided epilepsy relative to controls (all $p>0.025$). In left-sided epilepsy, there was a significant association between left HH volume with verbal memory ($\beta=0.492$, $p=0.001$). There was no significant association between left and right hippocampal subregions with verbal and nonverbal memory respectively in right-sided epilepsy and controls (all $p>0.002$). In left- and right-sided epilepsy, there was no significant association between hippocampal subregions

with age at seizure onset and seizure frequency (all $p>0.002$).

Conclusions

We have found hippocampal volume reduction, but did not identify a gradient in the severity of volume reduction along the hippocampal axis in children with localization-related epilepsy. We also have found a significant association between reduced left HH volume with reduced verbal memory in left lateralized epilepsy, suggesting that the left HH may play a greater role in verbal episodic memory than the remaining hippocampus. Longitudinal study is needed to clarify whether there is a differential rate of volume reduction along the axis of the hippocampus in children with continuing seizures.

KEYWORDS: Hippocampus, Pediatric Epilepsy

O-444 3:49PM - 3:56PM
Subtraction imaging and MR co-registration to increase diagnostic yield of ictal and interictal SPECT in localization of epileptogenic foci in patients with intractable seizures.

Z Abramson¹, H Magill², J Wheless², A Choudhri³
¹University of Tennessee Health Science Center, Memphis, TN, ²LeBonheur Children's Hospital, Memphis, TN, ³UTHSC/LeBonheur Children's Hospital, Memphis, TN

Purpose

Patients with intractable epilepsy are candidates for surgical resection if an epileptogenic focus can be identified. Current multidisciplinary evaluation, including neuro-clinical data, electroencephalogram (EEG), MR imaging (MRI), magnetoencephalographic (MEG) and nuclear medicine imaging has allowed for the ability to localize epileptogenic foci. SPECT perfusion imaging, in particular, is an important tool in identifying epileptogenic foci in patients with intractable seizures, however analysis typically has been performed subjectively. Improved quantitative processing of ictal and interictal SPECT perfusion data with MR coregistration may increase the ability to identify and localize seizure foci. In this study, we sought to determine the diagnostic yield of ictal-interictal subtraction imaging and MRI coregistration at a single institution.

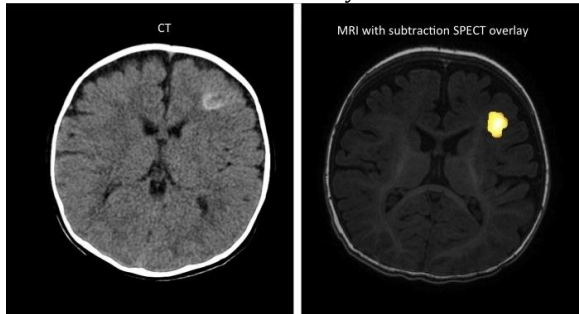
Materials and Methods

All patients who underwent HMPAO-SPECT perfusion imaging for the evaluation of intractable seizures at a single tertiary care pediatric neuroscience institute over a two and one half year period were reviewed retrospectively. For patients with ictal SPECT (IS) and interictal SPECT (IIS), subtraction imaging was performed. All images were coregistered to volumetric T1-weighted MR images using a FDA approved software package (MIM-Vista, MIM Software, Cleveland, OH). Abnormal SPECT results were defined as visual hypoperfusion on interictal SPECT and/or statistically significant hyperperfusion on ictal SPECT with postprocessing subtraction. The presence of abnormality on pre-SPECT MRI was recorded for comparison.

Results

Note: Scanned images are included in the proceedings. Some submitted images were reduced during editing thereby decreasing clarity. Also, refer to the Program Planner. Proceedings Content as of 3/28/2014.

One hundred and sixteen patients with intractable epilepsy underwent SPECT imaging as part of their evaluation, including 60 (52%) with IS-IIS subtraction imaging, and 56 (48%) with IIS only. Ninety-six of 116 (83%) had an abnormality identified on SPECT. Of the 96 patients with abnormal SPECT studies, 50 had abnormal ictal scans, 77 had abnormalities on interictal SPECT, and 30 had abnormalities on both ictal and interictal SPECT. Twenty patients showed no abnormality on SPECT imaging. In total, 94 patients had an abnormality noted on MRI. The most common MRI abnormality noted was volume loss, followed by nonspecific white matter signal abnormality. Of the 116 patients, seven patients demonstrated normal findings on both MRI and SPECT. Fifteen patients demonstrated a normal MRI but an abnormal SPECT study. Thirteen patients had abnormalities on MRI without SPECT abnormalities. The remaining 81 patients had abnormalities on both MRI and SPECT. Only 56 of these 81 MRI findings were considered "corresponding abnormalities" to the SPECT study.



Conclusions

In patients with intractable epilepsy, SPECT perfusion imaging employing IS-IIS subtraction with MRI coregistration identifies likely seizure foci in a majority of patients, with a diagnostic yield higher than historical reports of qualitative analysis.

KEYWORDS: Epilepsy, Pediatric Epilepsy, Seizure

0-445 3:56PM - 4:03PM
MR Guided LASER ablation of non-lesional epileptic foci in pediatric patients utilizing Magnetoencephalography (MEG) scan and EEG.

A Ghassemi, M Chez, S Ciricillo, A Krishnan
Sutter Medical Center Sacramento, Sacramento, CA

Purpose

Medically refractory epilepsy affects approximately 300,000 patients in the United States. Early surgery reduces long term impact, comorbidities and improves quality of life. Patient fear of an open craniotomy and the use of intracranial electrode monitoring, combined with more extratemporal foci in pediatric cases delays surgical decisions. Often electroencephalogram (EEG) tracing localization may not correlate with any obvious MR imaging (MRI) abnormality. Multimodality studies [EEG, magnetoencephalography (MEG) scan, positron emission tomography (PET) scan and functional MRI (fMRI)] can be

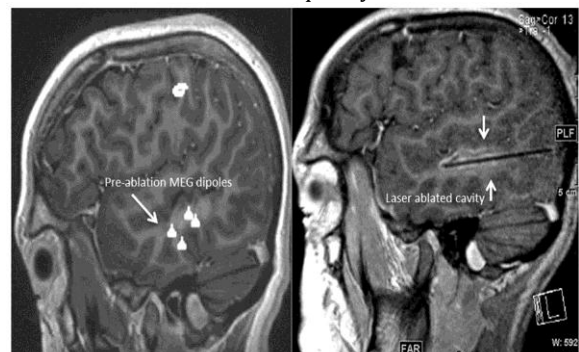
used to identify nonlesional epileptic foci and plan stereotactic laser ablation (SLA), a minimally invasive technique offering less morbidity and quicker recovery. To our knowledge, we present the largest cohort of pediatric patients in the literature who were treated using MR-guided SLA of nonlesional epileptic foci.

Materials and Methods

All patients with medically refractory epilepsy were studied with video-EEG, then correlated the seizure onset of scalp EEG with MEG scan dipoles. All the patients had a normal MRI showing no signs of cortical dysplasia. Language and motor centers were localized by fMRI. A total of 19 pediatric patients aged between 4-20 years (mean age of 13.7, Table 1) underwent SLA. We combined EEG, MEG scan, fMRI, PET scan and utilized frameless BrainLab localization to perform minimally invasive MRI-guided SLA (Visualase Thermal Therapy System; Visualase, Inc., Houston, TX) was employed in this work. Critical safety points were placed near location of critical structures to limit temperatures below 50 C. A baseline pre-ablation EEG was performed in the OR with MR compatible plastic electrodes. Stereotactic laser ablation was performed while simultaneously observing the evolution of the estimated ablated cavity calculated from real time thermal images. A postablation EEG was repeated with the patient still in the MR suite demonstrating complete resolution of the abnormal spikes seen on the pre-ablation EEG. This defined successful ablation. Improved clinical outcome was characterized by seizure freedom or seizure reduction by more than 50%.

Results

The laser ablations were performed in frontal lobe (5/19), temporal lobe (3/19), occipital (1/19) and multilobar (10/19). All patients showed reduction of pattern of abnormal spikes on postablation EEG. Duration of follow up ranged anywhere from two to 24 months from SLA. Sixty-three and one half percent (12/19) of them are seizure free, 31.5% (6/19) have 50-96% reduction in seizures, 5% (1/19) patient only had 10% reduction in seizure. Two patients were treated twice, one became seizure free after the second SLA and the other had over 90% reduction in seizure frequency.



Note: Scanned images are included in the proceedings. Some submitted images were reduced during editing thereby decreasing clarity. Also, refer to the Program Planner. Proceedings Content as of 3/28/2014.

Patients Demographics and Outcome							
Age	Sex	Laser ablation location	Follow-up (months)	Seizure Free	50-96% seizure reduction	<50% seizure reduction	
1	11	M	L Frontal	24	X		
2	20	F	R Temporal	19		X	
3	10	M	R Frontal	19	X		
4	13	F	R Frontal	19	X		
5	12	M	R Occipital temporal	15		X	
6	7	F	L Occipital Temporal	15	X		
7	11	F	L parietal Cingulate	13	X		
8	20	F	L Temporal	13	X		
9	4	F	R Occipital	10		X	
10	13	F	R Parietal Temporal	10		X	
11	20	F	R Frontal Temporal	10	X		
12	14	F	L Frontal Temporal	7			X
13	19	F	R Temporal	7		X	
14	20	F	R frontal Cingulate	6	X		
15	17	M	R Temporal Occipital	5	X		
16	13	F	L Frontal	5	X		
17	18	F	L Temporal Frontal	3	X		
18	7	M	R Frontal Temporal	2	X		
19	13	F	R Frontal Temporal	2		X	

Conclusions

MR-guided SLA of epileptic foci in this large cohort of pediatric patients showed that 95% of patients became seizure free or had significant reduction in seizure frequency. Our outcomes are better than standard resective surgery and similar to success rate for standard mesial temporal resection. Stereotactic laser ablation could be a superior alternative to routine cortical resection given the significant decrease in morbidity, safety/precision of the technology and the quick recovery associated with this procedure. The utilization of MEG scan combined with EEG surface recording and fMRI allows multimodal localization of epileptic foci in patients with normal MRIs and no clear evidence of cortical dysplasia. Given the minimally invasive nature of SLA, patients can safely have a repeat laser ablation if the seizures do not resolve or significantly decrease in frequency.

KEYWORDS: Epilepsy, Laser, MEG

O-446

4:03PM - 4:10PM

Clinical, EEG, MRI and surgical outcomes of pediatric epilepsy with Astrocytic Inclusions versus Focal Cortical Dysplasia

L Alshafai¹, O Snead², E Widjaja³, A Ochi, C Go, B McCoy, H Otsubo, J Rutka

¹University of Toronto, Toronto, Ontario, ²Hospital for Sick Children, Toronto, Ontario, ³The Hospital for Sick Children, Toronto, Ontario

Purpose

To compare the clinical, electroencephalography (EEG), magnetoencephalography (MEG), MR imaging (MRI), and surgical outcomes of children with astrocytic inclusions (AI) relative to focal cortical dysplasia (FCD).

Materials and Methods

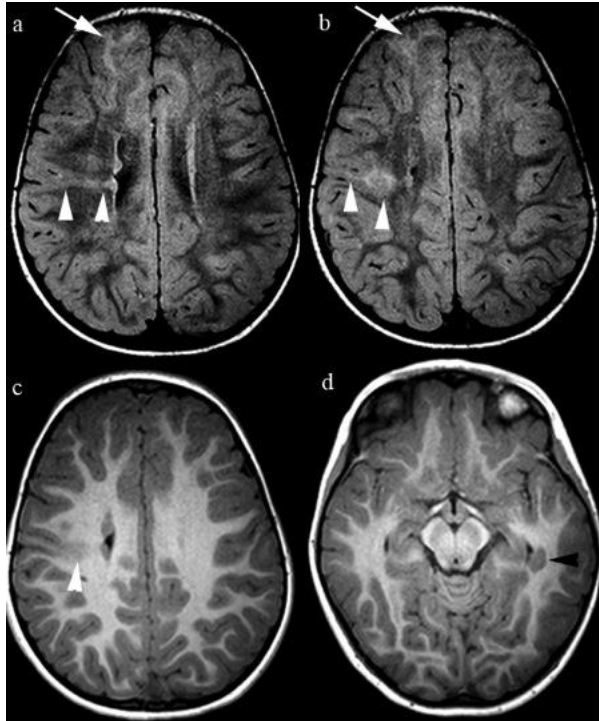
The clinical manifestations (including age at seizure onset, duration of epilepsy), video EEG (including seizure semiology and characteristics of interictal and ictal discharges), MEG, MRI features (including abnormal signal in cortex and subcortical white matter, increased cortical thickness, blurring of gray-white matter junction, abnormal sulcation and gyration pattern, reduced white matter volume and gray matter heterotopia) and surgical outcomes of children with histologically proven AI were compared to those with FCD.

Results

Six children had AI and 27 had FCD. Children with AI had early age at seizure onset, periodic spasms, and have unusual interictal epileptiform discharges consisting of mixture of generalized or diffuse hemispheric slow waves, sharp waves, spikes and polyspikes. Patients with AI were less likely to have clusters on MEG ($p=0.057$) or high T2/FLAIR in the subcortical white matter on MRI ($p=0.015$), more likely to demonstrate abnormal sulcation and gyration pattern ($p=0.001$) and have gray matter heterotopia ($p=0.002$) than FCD. Children with AI (25%) have a lower proportion of seizure-free outcome after surgery compared to FCD (55.5%), even though this was not statistically significant.

MRI features of astrocytic inclusions and focal cortical dysplasia	Astrocytic Inclusions (n=6)	Focal Cortical Dysplasia (n=27)	p-value
High T1 signal in cortex	1 (17%)	10 (37%)	0.338
High T2/FLAIR signal in cortex	0 (0%)	10 (37%)	0.074
High T2/FLAIR signal in subcortical white matter	1 (17%)	19 (70%)	0.015
Increased cortical thickness	0 (0%)	6 (22%)	0.202
Blurring of gray-white matter junction	1 (17%)	9 (33%)	0.422
Abnormal sulcation and gyration pattern	4 (67%)	2 (7%)	0.001
Reduced white matter volume	0 (0%)	1 (4%)	0.632
Abnormal signal in the white matter extending towards ventricle	1 (17%)	1 (4%)	0.229
Gray matter heterotopia	2 (33%)	0 (0%)	0.002

Note: Scanned images are included in the proceedings. Some submitted images were reduced during editing thereby decreasing clarity. Also, refer to the Program Planner. Proceedings Content as of 3/28/2014.



Conclusions

The clinical, EEG and MRI findings could help distinguish AI from FCD, and AI may have poorer prognosis following surgical resection. There have been several reports of eosinophilic astrocytic inclusions from histological brain specimens of patients with early onset epilepsy, with or without developmental delay and structural brain malformations (Hazrati et al., 2008; Hedley-Whyte et al., 2009; Horoupian et al., 2003; Kato et al., 1992; Minagawa et al., 1992; Van den Veyver et al., 2004; Visanji et al., 2012). These inclusions have been shown to be positive for filamin A in patients with intractable epilepsy (Hazrati et al., 2008; Hedley-Whyte et al., 2009) and Aicardi syndrome (Van den Veyver et al., 2004). Filamin A is an actin binding protein involved in neuronal migration. Other proteins such as cytoglobin and glutamate transporter I, also have been shown to be present. These inclusions also demonstrated increased expression of catalase and carbonic anhydrase I (Visanji et al., 2012). Animal model of status epilepticus has shown increase catalase levels in the hippocampus, striatum and frontal cortex (Freitas et al., 2004), suggesting that the increase catalase may be a reaction to oxidative stress and cell injury during epileptic seizures. Increased carbonic anhydrase II and XII also have been shown in animal model of status epilepticus (Halmi et al., 2006), suggesting a link between carbonic anhydrase and seizures. Although the proteomic content of the AI is increasingly recognized, less is known about the clinical, electrophysiological and neuroimaging manifestations of this condition. The reported cases of AI from resected brain tissue to date have been from patients with early onset epilepsy (Hazrati et al., 2008; Hedley-Whyte et al., 2009; Visanji et al., 2012). However, the surgical outcomes of patients with AI have not been well documented. Also, it is

unknown if there are distinct clinical and diagnostic tests that could differentiate these epileptogenic lesions.

KEYWORDS: Epilepsy, Focal Cortical Dysplasia

O-447 4:10PM - 4:17PM
Presurgical Language Evaluation with fMRI in Intractable Pediatric Epilepsy: Validation with Extraoperative Electrocortical Stimulation Mapping Under Different Clinical Scenarios

C Hansen, H Greiner, D Kadis, F Mangano, J Leach
Cincinnati Children's Hospital Medical Center, Cincinnati, OH

Purpose

Surgical therapy is employed increasingly for treating intractable epilepsy in children. Correct assessment of language lateralization is critical for operative planning as language centers must be spared, and children with intractable epilepsy more commonly have atypical language distribution. Extraoperative electrocortical stimulation mapping (ESM) is a clinical gold standard for language lateralization and localization prior to surgery, however is limited by surgical exposure and is invasive. Validation of functional MR imaging (fMRI) in children with epilepsy is limited but is critical to inform use of this technique. This study aims to assess agreement between clinical fMRI language laterality measures and objective assessments of language laterality in pediatric epilepsy surgery patients using different interpretation scenarios. Materials and Methods

Thirty pediatric epilepsy surgery patients with subdural grid placement and ESM covering typical language areas (29), Wada testing (1), or both (3) and language fMRI were identified. All fMRI examinations included verb generation (VG) and story processing (SP). Functional MRI was processed in a clinical system (BrainLAB iPlan 3.0) without knowledge of side of surgery or ESM results. Functional MRI examinations were evaluated by: 1. Visual inspection (VI), at the workstation with continuous thresholding, specifically evaluating the inferior frontal (FL) and temporal lobes (TL), and 2. Using standardized region of interest (ROI) calculations in the FL and TL. Lateralization indices (LI) comparing volumes of activation, left versus right, were calculated at: median statistical significance (mtROI, mid-way between peak significance and excessive artifact determined by VI), and lowest threshold (ltROI, before appearance of artifact): 0.2 used as the LI cutoff. Clinical objective language laterality (COL) was determined by ESM [Left: left stimulation sites (+) or right stimulation sites (-). Right: right stimulation sites (+) or left stimulation sites (-).] and Wada. Functional MRI scenarios included: left versus not left (LvNL); bilateral/right lateralization were "not left"; left versus right (LvR); bilateral were excluded; left + bilateral versus right (LBvR) bilateral/left lateralizing were left. LPV (probability of true left COL), RPV (probability of true right COL), and Concordance (overall agreement) were calculated.

Note: Scanned images are included in the proceedings. Some submitted images were reduced during editing thereby decreasing clarity. Also, refer to the Program Planner. Proceedings Content as of 3/28/2014.

Results

Average age was 13.7 years and 70% were right-handed. All had diagnostic VG and 22 /30 had diagnostic SP paradigms. Nine patients (30%) had atypical (right, bilateral, or mixed) language lateralization by fMRI. See Figure for overall results. VI of VG fMRI in the FL demonstrated excellent agreement with ESM/Wada (LPV:0.96,RPV:0.8,Concordance:0.93), identical to ROI-based analysis, using the LBvR scenario. VI of VG fMRI in the TL performed similar or better than ROI in all three comparison scenarios. While exhibiting a perfect LPV in all scenarios, SP fMRI had worse RPV and concordance using VI than VG, and in most other scenarios. SP demonstrated perfect LPV and RPV at ltROI, but a diagnostic exam could be completed in only 22/30 (73%) subjects. ltROI showed better performance than mtROI analyses in most scenarios. Best performance measures occurred using the LBvR scenario with worst performance using TL assessment and LvNL scenarios. An improvement in performance was noted using ROI analysis compared with VI with SP at ltROI.

Scenario	VI - VG Frontal			ROI - VG Frontal, MID t			ROI - VG Frontal, LOW t		
	LPV	RPV	concordance	LPV	RPV	concordance	LPV	RPV	concordance
LvNL	0.96	0.67	0.9	0.96	0.57	0.87	0.96	0.67	0.9
LvR	0.96	0.8	0.9	0.96	0.6	0.89	0.96	0.8	0.93
LBvR	0.96	0.8	0.93	0.96	0.6	0.9	0.96	0.8	0.93

Scenario	VI - VG Temporal			ROI - VG Temporal, MID t			ROI - VG Temporal, LOW t		
	LPV	RPV	concordance	LPV	RPV	concordance	LPV	RPV	concordance
LvNL	0.95	0.5	0.83	0.95	0.36	0.73	0.94	0.33	0.7
LvR	0.95	0.8	0.83	0.95	0.5	0.81	0.94	0.67	0.88
LBvR	0.96	0.8	0.93	0.95	0.5	0.83	0.96	0.67	0.9

Scenario	VI - SP Temporal			ROI - SP Temporal, MID t			ROI - SP Temporal, LOW t		
	LPV	RPV	concordance	LPV	RPV	concordance	LPV	RPV	concordance
LvNL	1	0.5	0.7	1	0.4	0.87	1	0.25	0.73
LvR	1	0.67	0.7	1	0.5	0.91	1	1	1
LBvR	1	0.67	0.73	1	0.5	0.91	1	1	1

Conclusions

Functional MRI demonstrated excellent agreement with objective measures of language lateralization in pediatric epilepsy patients. VG paradigms, evaluating the frontal lobe, performed the best and visual inspection of fMRI data was as good as ROI-based laterality in most tested scenarios. SP paradigms, while exhibiting excellent performance, especially using ltROI analysis, was more variable and was nondiagnostic in 8/30 patients suggesting the need for improved evaluation techniques for temporal language areas. Combination of VI and ROI analysis likely maximizes performance, especially using SP paradigms.

KEYWORDS: Language, Preoperative Language Lateralization

0-448 4:17PM - 4:24PM

Usefulness of DTI analysis of brain tissue surrounding the cortical tuber for predicting epileptogenicity in tuberous sclerosis patients

A Yogi, Y Hiarata, E Karavaeva, J Wu, S Yudovin, B Ellingson, N Salamon
David Geffen School of Medicine at University of California Los Angeles, Los Angeles, CA

Purpose

Up to 90% of patients with tuberous sclerosis complex (TSC) have seizures, and 25-30% will develop intractable

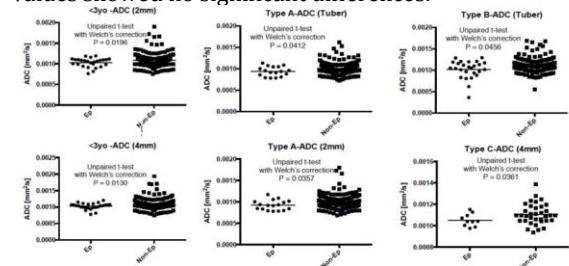
epilepsy. For these patients, neurosurgery is essential treatment of choice for seizure control. Based on electrophysiological data, epileptogenic tissue is found in the tissue around tubers. The purpose of this study is to evaluate if diffusion tensor imaging (DTI) can detect the epileptogenic tissue in TSC.

Materials and Methods

From the UCLA epilepsy program TSC cohort, twenty-three patients underwent surgery between 2004 and 2011. Total of 699 tubers were included in the study. All patients had preoperative DTI. Tubers were divided in three groups according to T2 changes. The DTI analysis was performed using AFNI (Analysis of Functional NeuroImages). One neuroradiologist and one neurosurgeon manually outlined all tubers on T2-weighted images or FLAIR images in consensus, and created region of interests of tubers (ROI tuber). Region of interest tuber then was inflated by 2mm and 4mm and the original ROI tuber was subtracted to create an ROI of brain tissue which surrounds the tuber (ROI 2mm, ROI 4mm). Regions of interest which include tuber and surrounding tissue by 2mm and 4mm were generated as ROI tuber+2mm and ROI tuber+4mm respectively. Calcification, flow void, cerebrospinal fluid, bone, and air were carefully eliminated from those ROIs. All created ROIs were overlaid on apparent diffusion coefficient (ADC) maps and FA maps, and median and maximum values of ADC and FA were calculated in all ROIs. Epileptogenicity was defined by pre-operative EEG, MSI and intra-operative electrocorticography. This is confirmed by postoperative seizure control. We compare the DTI parameters between epileptogenic tubers and nonepileptogenic tubers, and each patient groups divided by age and tuber type, using Mann-Whitney U test and unpaired t test.

Results

Six hundred ninety-nine cortical tubers were identified by preoperative MRI, and 73 epileptogenic cortical tubers and 626 nonepileptogenic cortical tubers were identified. Five hundred fifty-three cortical tubers were available for ADC analysis (54 epileptogenic, 499 nonepileptogenic), and 411 were available for FA analysis (43 epileptogenic, 358 nonepileptogenic). The median ADC values of cortical tuber ($p < .0018$), surrounding tissue by 2mm ($p < .006$) and 4mm ($p < .008$), and cortical tuber with surrounding tissue by 2mm ($p < .0045$) and 4mm ($p < .0014$) in epileptogenic group were significantly lower than those in nonepileptogenic group. Maximum ADC values and all FA values showed no significant differences.



Note: Scanned images are included in the proceedings. Some submitted images were reduced during editing thereby decreasing clarity. Also, refer to the Program Planner. Proceedings Content as of 3/28/2014.

Conclusions

This is the first study demonstrating the ADC values of brain tissue surrounding epileptogenic tuber is significantly lower than nonepileptogenic group. Diffusion tensor imaging can be a promising tool to predict the epileptogenic tissue in tuberous sclerosis.

KEYWORDS: Diffusion Tensor Image, Epilepsy, Tuberous Sclerosis

0-449 4:24PM - 4:31PM
Independent Contribution of Individual White Matter Pathways to Language Function in a Cohort of Pediatric Epilepsy Patients

M Paldino, J Monsalves, W Zhang
Texas Children's Hospital, Houston, TX

Purpose

Patients with epilepsy and malformations of cortical development (MCD) are at high risk for language and other cognitive impairment. Specific impairments, however, are not well correlated with the extent and locale of dysplastic cortex (1). Such findings highlight the relevance of aberrant cortico-cortical interactions, or connectivity, to the clinical phenotype. Abnormalities within several white matter pathways have been reported in association with language dysfunction. However, in patient populations whose cerebral connectivity and brain function are both extensively abnormal, an association between a proposed biomarker and a particular cognitive function may be indirect (i.e., epiphenomenon). The goal of this study was to determine the independent contribution of well described white matter pathways to language function in a cohort of pediatric patients with epilepsy.

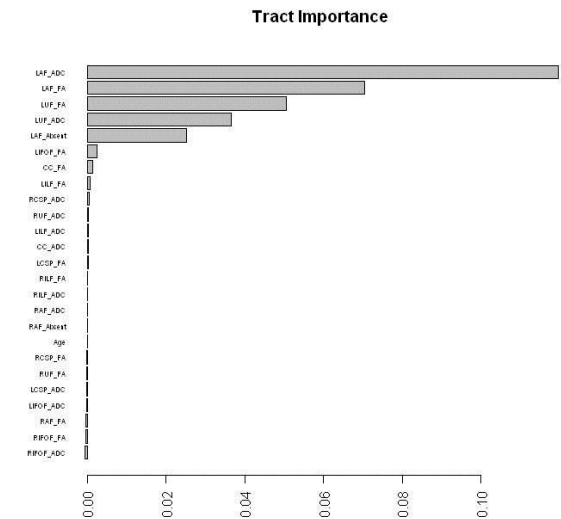
Materials and Methods

Patients were identified retrospectively from an existing database of pediatric epilepsy patients with the following inclusion criteria: 1. Diagnosis of MCD. 2. Diffusion tensor imaging performed at 3 T. 3. Language characterized by a pediatric neurologist. Diffusion Toolkit and Trackvis (www.trackvis.org) were used for segmentation and analysis of the following tracts: corpus callosum, corticospinal tracts, inferior longitudinal fasciculi (ILF), inferior fronto-occipital fasciculi (IFOF), uncinate fasciculi (UF), and arcuate fasciculi (AF). Mean diffusivity (MD) and fractional anisotropy (FA) were calculated for each tract. Wilcoxon rank sum test (corrected for multiple comparisons) was used to assess potential differences in tract parameters between language-impaired and language-intact patients. In a separate analysis, a machine learning algorithm (random forest approach) was applied to measure the independent contribution of the measured diffusion parameters for each tract to the clinical phenotype (language impairment). In other words, the importance of each tract parameter was measured after adjusting for the contribution of all other tracts.

Results

Thirty-three MCD patients were included (age range: 3-18 years). Twenty-one patients had intact language, 12 were

impaired. All tracts were identified bilaterally in all patients except for the AF, which was not identified on the right in 10 subjects and not identified on the left in 11 subjects. Mean diffusivity and/or FA within the left AF, UF, ILF, and IFOF differed between language-intact and language-impaired groups. However, only parameters related to the left uncinate and arcuate fasciculi were independently associated with the clinical phenotype (Figure 1).



Conclusions

Quantitative metrics derived from the left uncinate and arcuate fasciculi were associated independently with language function. These results support the importance of these pathways in human language function.

KEYWORDS: Diffusion MR Imaging, Epilepsy, Language

Tuesday, May 20
4:45 PM – 6:15 PM
Room 517bc

49 - ASPNR Programming: 2014 ASPNR
Interesting Case-based Session

0-450 4:45PM - 6:15PM
Interesting Cases Panelists

Vossough, A. · Panigrahy, A. · Chong, W. · Hoffmann, C. · Soares, B.
University of Pennsylvania · Children's Hospital of Pittsburgh of UPMC · Great Ormond Street Hospital for Children · Sheba Medical Center · Emory University Philadelphia, PA · Pittsburgh, PA · London · Ramat-Gan · Atlanta, GA

Note: Scanned images are included in the proceedings. Some submitted images were reduced during editing thereby decreasing clarity. Also, refer to the Program Planner. Proceedings Content as of 3/28/2014.

Tuesday, May 20
4:45 PM – 6:15 PM
Room 517d

50 - Mini-Symposium – Tumor – Part V

0-453 4:45PM - 5:00PM

Advanced Imaging in Pediatric Gliomas: Diagnostic and Therapeutic Implications

Panigrahy, A.
Children's Hospital of Pittsburgh of UPMC
Pittsburgh, PA

0-454
Advanced Diffusion-Weighted MR Imaging Analysis for
Brain Tumor Tissue Characterization in Pediatric Patients

J Deng, D Burrowes, S Goldman, E Boylan
Ann & Robert H. Lurie Children's Hospital of Chicago,
Chicago, IL

Purpose:

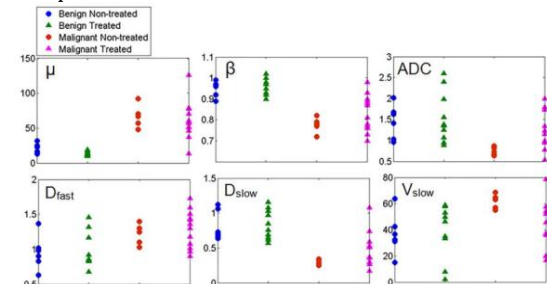
The purpose of this study was to exploit the high b-value diffusion-weighted magnetic resonance imaging (DW-MRI) with advanced diffusion analysis using the anomalous diffusion model and the bi-exponential two-compartment model, for differentiation of malignant and benign brain tumor tissues in pediatric patients.

Materials and Methods:

All MRI exams were performed on 1.5 T and 3.0 T scanners (Magnetom Aera/Skyra, Siemens Medical Solution). Diffusion-weighted MRI covering the entire tumor area was acquired with single shot echo planar sequence using 16 extended b-values (0-3500 s/mm²) applied in three orthogonal directions. A region of interest (ROI) was placed on each solid tumor region and the averaged signal intensity (S) at all b-values was measured within each tumor ROI. Conventional apparent diffusion coefficient (ADC) was calculated using a mono-exponential model fitting signal decay ($b=0-1000$ s/mm²). Extended diffusion parameters were derived from two advanced diffusion models: anomalous diffusion model and bi-exponential two-compartment model, by the Levenberg-Marquardt nonlinear fitting (Matlab program). 1) In the anomalous diffusion model, the signal intensity at all 16 b-values (0-3500 s/mm²) were fitted based on the equation $S(b)/S_0 = \exp[-D \cdot \mu^{\beta-1} \cdot (\gamma G \delta)^{2\beta} \cdot (\Delta - (2\beta - 1) \cdot \delta / (2\beta + 1))]$, where Gd is diffusion gradient amplitude, δ and Δ are diffusion gradient pulse width and interval, respectively. Two anomalous diffusion parameters -space constant μ (unit: μm) and complex parameter β ($0 < \beta < 1$) were derived. 2) In the two-compartment model, signal intensity at 11 higher b-values 150-3500 s/mm² (to avoid perfusion effect) were fitted based on the equation

$S(b)/S_0 = V_{\text{fast}} \cdot \exp(-D_{\text{fast}} \cdot b) + V_{\text{slow}} \cdot \exp(-D_{\text{slow}} \cdot b)$. Extracellular diffusion coefficient (D_{fast}) and volume (V_{fast}), and intracellular diffusion coefficient (D_{slow}) and volume (V_{slow}) were derived. Each of the diffusion parameters (ADC, μ , β , D_{slow} , V_{slow} and D_{fast}) was compared between malignant and benign tumor types using a nonpaired t-test with unequal variance ($\alpha = 0.05$). Results:

A total of 33 patients (1-25 years old) with biopsy-proven brain tumors were enrolled and divided into malignant (n=17: 5 nontreated and 12 treated tumors) and benign groups (n=16: 6 nontreated and 10 treated tumors) All diffusion measurements including μ , β , ADC, D_{fast} , D_{slow} and V_{slow} for all nontreated and treated benign and malignant tumors were plotted in the Figure. By comparing all benign and malignant tumors regardless of the treatment status, μ , β , D_{fast} and D_{slow} all demonstrated strongly significant differences between malignant and benign tumors with $p < 0.005$, whereas ADC showed weaker significance ($p = 0.01$). In addition, to avoid the treatment efficacy variation, only nontreated tumors were compared, where μ , β , D_{slow} , V_{slow} and ADC all demonstrated significant differences between malignant and benign tumors ($p < 0.005$ for all except p of $V_{\text{slow}} = 0.01$ and p of $\text{ADC} = 0.007$). Specifically, two treated malignant tumors that demonstrated closer measurements as the benign tumors showed clinically proven improved disease and complete remission after treatment.



Conclusions:

Malignant tumors are characterized with more compact tissue density, higher intracellular volume and increased tortuosity and heterogeneity, which are reflected by lower ADC, lower β (i.e., increased complexity), higher space constant μ , lower intracellular diffusion (D_{slow}) and higher intracellular volume (V_{slow}), compared to benign tumors. This study provided in-depth explanations of tissue water diffusion behavior reflective of complex microstructural tumor tissue properties. These advanced diffusion analyses may prove to be useful in improving the accuracy and confidence in the diagnosis of various brain tumors, facilitating treatment planning, targeting treated tumor areas and in therapeutic response assessment.

0-457 5:15PM - 5:30PM
Radiosurgery of Brain Metastasis - Radiologic and
Histologic Consequences

Minja, F.
Yale University
New Haven, CT

Note: Scanned images are included in the proceedings. Some submitted images were reduced during editing thereby decreasing clarity. Also, refer to the Program Planner. Proceedings Content as of 3/28/2014.

Abstract/Presentation Summary

Patients with intracranial metastatic lesions are increasingly being treated with single fraction high dose stereotactic radiosurgery (SRS), as first line therapy. For most patients SRS is an effective means of intracranial metastatic lesion control. However, following SRS, a significant number of patients develop enlarging enhancing lesions, often with extensive surrounding T2 signal abnormality on magnetic resonance (MR) imaging at the original tumor site. We have previously reported that although most metastatic lesions are stable or smaller in size during the first 36 months post-SRS, a transient increase in volume is seen in approximately one-third of lesions [Patel TR et al, 2011]. These enlarging enhancing lesions raise the challenging clinical dilemma between tumor recurrence (TR) versus a radiation induced inflammatory process, often referred to as radiation necrosis (RN). The differentiation between TR and RN is challenging on routine MR imaging, as both entities can present with enlarging enhancing lesions with surrounding abnormal T2 signal. We will review the enhancement pattern of metastatic lesions following SRS, together with histopathology correlation. We will also briefly explore the role of advanced imaging modalities (MR perfusion, MR spectroscopy and FDG-PET) for differentiating TR from RN.

0-454

5:00PM - 5:06PM

Advanced Diffusion-Weighted MRI Analysis for Brain Tumor Tissue Characterization in Pediatric Patients

J Deng, D Burrowes, S Goldman, E Boylan
Ann & Robert H. Lurie Children's Hospital of Chicago,
Chicago, IL

Purpose

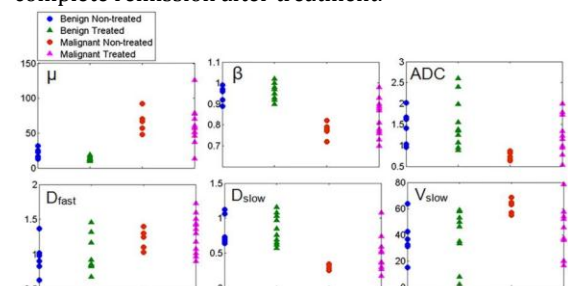
The purpose of this study was to exploit the high b-value diffusion-weighted magnetic resonance imaging (DW-MRI) with advanced diffusion analysis using the anomalous diffusion model and the bi-exponential two-compartment model, for differentiation of malignant and benign brain tumor tissues in pediatric patients.

Materials and Methods

All MRI exams were performed on 1.5 T and 3.0 T scanners (Magnetom Aera/Skyra, Siemens Medical Solution). Diffusion-weighted MRI covering the entire tumor area was acquired with single shot echo planar sequence using 16 extended b-values (0-3500 s/mm²) applied in three orthogonal directions. A region of interest (ROI) was placed on each solid tumor region and the averaged signal intensity (S) at all b-values was measured within each tumor ROI. Conventional apparent diffusion coefficient (ADC) was calculated using a mono-exponential model fitting signal decay ($b=0-1000$ s/mm²). Extended diffusion parameters were derived from two advanced diffusion models: anomalous diffusion model and bi-exponential two-compartment model, by the Levenberg-Marquardt nonlinear fitting (Matlab program). 1) In the anomalous diffusion model, the signal intensity at all 16 b-values (0-3500 s/mm²) were fitted based on the equation $S(b)/S_0 = \exp[-D \cdot \mu^2 (\beta - 1) \cdot (\gamma G d \delta)^2 \beta \cdot (\Delta - (2\beta -$

$1) \cdot \delta / (2\beta + 1)]]$, where Gd is diffusion gradient amplitude, δ and Δ are diffusion gradient pulse width and interval, respectively. Two anomalous diffusion parameters - space constant μ (unit: μm) and complex parameter β ($0 < \beta < 1$) were derived. 2) In the two-compartment model, signal intensity at 11 higher b-values 150-3500 s/mm² (to avoid perfusion effect) were fitted based on the equation $S(b)/S_0 = V_{\text{fast}} \cdot \exp(-D_{\text{fast}} \cdot b) + V_{\text{slow}} \cdot \exp(-D_{\text{slow}} \cdot b)$. Extracellular diffusion coefficient (D_{fast}) and volume (V_{fast}), and intracellular diffusion coefficient (D_{slow}) and volume (V_{slow}) were derived. Each of the diffusion parameters (ADC, μ , β , D_{slow} , V_{slow} and D_{fast}) was compared between malignant and benign tumor types using a nonpaired t-test with unequal variance ($\alpha = 0.05$). Results

A total of 33 patients (1-25 years old) with biopsy-proven brain tumors were enrolled and divided into malignant (n=17: 5 nontreated and 12 treated tumors) and benign groups (n=16: 6 nontreated and 10 treated tumors). All diffusion measurements including μ , β , ADC, D_{fast} , D_{slow} and V_{slow} for all nontreated and treated benign and malignant tumors were plotted in the Figure. By comparing all benign and malignant tumors regardless of the treatment status, μ , β , D_{fast} and D_{slow} all demonstrated strongly significant differences between malignant and benign tumors with $p < 0.005$, whereas ADC showed weaker significance ($p = 0.01$). In addition, to avoid the treatment efficacy variation, only nontreated tumors were compared, where μ , β , D_{slow} , V_{slow} and ADC all demonstrated significant differences between malignant and benign tumors ($p < 0.005$ for all except p of $V_{\text{slow}} = 0.01$ and p of $\text{ADC} = 0.007$). Specifically, two treated malignant tumors that demonstrated closer measurements as the benign tumors showed clinically proven improved disease and complete remission after treatment.



Conclusions

Malignant tumors are characterized with more compact tissue density, higher intracellular volume and increased tortuosity and heterogeneity, which are reflected by lower ADC, lower β (i.e., increased complexity), higher space constant μ , lower intracellular diffusion (D_{slow}) and higher intracellular volume (V_{slow}), compared to benign tumors. This study provided in-depth explanations of tissue water diffusion behavior reflective of complex microstructural tumor tissue properties. These advanced diffusion analyses may prove to be useful in improving the accuracy and confidence in the diagnosis of various brain tumors, facilitating treatment planning, targeting treated tumor areas and in therapeutic response assessment.

Note: Scanned images are included in the proceedings. Some submitted images were reduced during editing thereby decreasing clarity. Also, refer to the Program Planner. Proceedings Content as of 3/28/2014.

KEYWORDS: Diffusion MR Imaging, Neoplasm Recurrence, Diagnosis

0-455 5:06PM - 5:12PM
Pediatric cerebellar tumors: Apparent diffusion coefficient of the solid contrast enhancing component appears to predict tumor grade best.

G Orman¹, T Bosemani¹, L Higgins¹, K Carson², T Huisman¹, A Poretti¹

¹The Johns Hopkins University School of Medicine, Baltimore, MD, ²The Johns Hopkins Bloomberg School of Public Health, Baltimore, MD

Purpose

The role of apparent diffusion coefficient (ADC) in differentiating high and low grade pediatric cerebellar tumors has been shown previously and was attributed to differences in cellularity between tumors. In previous studies, ADC values have been measured only in the solid, enhancing component of the tumor. Accordingly, a large tumor component has been excluded from the evaluation and the measured ADC value may not be representative for the entire tumor. Our purpose is to compare the role of ADC measurement in 1) the solid, enhancing component and 2) the entire tumor in predicting the tumor grade of pediatric cerebellar tumors.

Materials and Methods

A retrospective study was performed including patients with histologically proven cerebellar tumors evaluated presurgically. For each patient, three regions of interest (ROI) were positioned manually a) within the solid enhancing component and b) covering the entire tumor. Median ADC values were calculated. Control ADC values were obtained within macroscopically normal appearing cerebellum and thalami. Evaluation was performed by two observers. Ratios between 1) both ADC measurements of the tumors and 2) control ADC values of the normal cerebellum and thalami were calculated. The absolute ADC values and the ratios were correlated with the tumor grade. Statistical analysis included intraclass correlation, a two-sample Wilcoxon test, logistic regression and receiver operating characteristic (ROC) curves (only for absolute ADC values).

Results

Thirty-two patients (15 boys and 17 girls) were included in the study. The median age at presurgical MRI was 7.66 years (range 0.08-17.38 years). Fifteen patients had a high grade tumor, 17 a low grade tumor. Intra class correlation coefficients ranged between 0.98 and 1.0 for both measurements. For the solid enhancing tumor component, absolute ADC values (median 1.49×10^{-3} mm/s² vs. 0.61×10^{-3} mm/s²), cerebellar ADC ratio (2.11 versus 0.88), and thalamic ratio (1.88 versus 0.75) were higher in low grade versus high grade tumors ($p < 0.0001$). For the "entire tumor", absolute ADC values (1.79×10^{-3} mm/s² versus 1.05×10^{-3} mm/s², $p = 0.003$), cerebellar ADC ratio (2.25 versus 1.38, $p = 0.006$), and thalamic ratio (2.16 versus 1.24, $p = 0.003$) were higher in low grade compared to high grade tumors. The area under the ROC curve was 0.961 and 0.812

for ADC measurements in the solid enhancing component and "entire tumor", respectively. Cutoff ADC values to differentiate between high and low grade tumors were calculated: 0.9×10^{-3} mm/s² (sensitivity 93%, specificity 94%) and 1.5×10^{-3} mm/s² (sensitivity 87%, specificity 71%) for ADC measurements in the solid enhancing component and "entire tumor", respectively.

Conclusions

Our study confirms the value of ADC measurement in predicting tumor grade in pediatric cerebellar tumors. Although both ADC measurements are able to predict histology, ADC measurements covering only the solid, contrast-enhancing tumor component has a higher sensitivity and specificity. Careful positioning of the ROIs within the enhancing, non-necrotic, nonedematous, contrast-enhancing tumor component appears to be essential for highly predictive ADC measurement.

KEYWORDS: Apparent Diffusion Coefficient, Cerebellar, Childhood

0-456 5:12PM - 5:18PM
Perfusion MR Imaging for Grading Pediatric Brain Tumors

J Cardinal¹, S Kralik², A Kamer², C Ho²

¹Indiana University School of Medicine, Zionsville, IN, ²Indiana University School of Medicine, Indianapolis, IN

Purpose

Relative cerebral blood volume (rCBV) has been demonstrated to correlate with glial tumor grade and improve sensitivity and positive predictive value (PPV) of glial tumor grade assessment. Vascular permeability and contrast leakage also has been hypothesized to have diagnostic value. We evaluate the use of rCBV and time-signal intensity curves (TIC) in the assessment of pediatric brain tumor grade.

Materials and Methods

After IRB approval, 63 cases of pediatric brain tumors with perfusion imaging were collected retrospectively at our institution. Inclusion criteria included pathology proven diagnosis with WHO grade and preoperative dynamic susceptibility contrast perfusion MR imaging (DSC). Dynamic susceptibility contrast images were obtained using an echo-planar imaging sequence during the first pass of a bolus of gadopentetate dimeglumine (MultiHance, Bracco Diagnostics Inc., Princeton, NJ) on 1.5 and 3 T MRI scanners (Siemens Avanto and Verio, Erlangen, Germany). Two fellowship-trained neuroradiologists independently obtained 3-5 mm² ROIs for maximum rCBV values of each tumor while blinded to pathologic diagnosis. Relative CBV measurements and qualitative analysis of TIC was performed using a commercially available workstation (DynaSuite Neuro, InVivo, Pewaukee, WI). The maximum rCBV value obtained by each neuroradiologist was averaged for each tumor and correlated to WHO grade using Spearman's rho. Receiver operating characteristic (ROC) analyses were performed to determine the optimum rCBV threshold for tumor grading. TIC from the ROI with the maximum CBV value were evaluated by each

Note: Scanned images are included in the proceedings. Some submitted images were reduced during editing thereby decreasing clarity. Also, refer to the Program Planner. Proceedings Content as of 3/28/2014.

neuroradiologist independently and categorized as demonstrating no contrast leakage effects (signal returns to baseline after first pass bolus), contrast leakage with T1-dominant effects (signal returns to baseline and continues to increase beyond the baseline), or contrast leakage with T2* dominant effects (signal never returns to baseline). Interobserver agreement was assessed using Cohen's kappa statistic. Consensus opinion was obtained in cases with discrepant impressions of contrast leakage and compared with tumor grade.

Results

Patient ages ranged from 1.0 to 16.8 years with a mean of 6.3 years. The series included 25 high and 38 low grade tumors. Thirty-nine of the tumors were in the posterior fossa, and 24 tumors were supratentorial. A positive correlation exists between tumor maximum rCBV and tumor grade ($r=0.30$, $p=0.0155$). Receiver operating characteristic analysis of rCBV to predict tumor grade demonstrated an area under the curve of 0.65 (0.52-0.77, $p=0.029$). An rCBV cut off value of 1.38 was selected by maximizing Youden's index, which resulted in a sensitivity of 92% (74-99) and specificity of 39.5% (24.0-56.6). Independent assessment of contrast leakage effects by two neuroradiologists had a Cohen's kappa of 0.69 (0.54 – 0.84). 25/25 tumors with T1-dominant leakage were low grade (1.00 PPV, 0.83-1.0, $p<.0001$). By comparison, tumors with a T2* (10/15, 0.67 PPV, 0.39-0.87) and no (15/23, 0.65 PPV, 0.43-0.82) leakage patterns were predominantly high grade. Figure: Cerebral blood volume map of a 4-year-old male with pilocytic astrocytoma of the left brachium pontis. Region of interest of the maximum rCBV value shows a TIC with T1 dominant leakage.

Conclusions

Maximum rCBV values of pediatric brain tumors obtained from DSC techniques have positive correlation with increasing brain tumor WHO grade. The recognition of a T1 predominant leakage curve on the time-signal intensity profile is 100% predictive for a low grade tumor.

KEYWORDS: Dynamic Susceptibility Contrast-Enhanced, Pediatric Brain Tumors

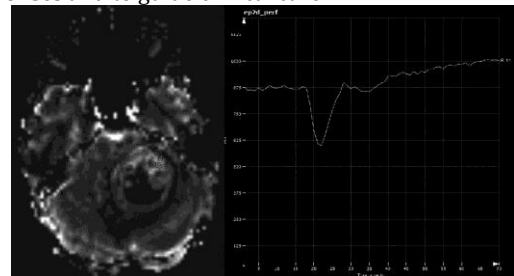
0-460 5:45PM - 6:00PM
Clinical Trials in Neuro-oncology: What the
Neuroradiologist Needs to Know

Barboriak, D.
Duke University Medical Center
Durham, NC

Abstract/Presentation Summary

In this presentation, the importance of neuroimaging in multicenter trials for patients with brain tumors will be discussed. Whenever a new use of neuroimaging is proposed, whether that imaging is routine and standard of care or advanced and experimental, a multicenter clinical trial remains the most effective means available to provide the strong evidence needed to bring about a change in clinical practice, and to support reimbursement for the procedure. Unfortunately, clinical trials have important

drawbacks; they may not definitively answer the question being studied, and because of the expense and the length of time needed to accrue sufficient numbers of patients to the trials, it is impractical to study every important imaging question with a trial. The status of clinical trials in neuro-oncology, for both primary brain tumors and metastatic disease, will be reviewed with an emphasis on trials that have important implications for the imaging assessment of these conditions. Imaging continues to play important role for determining the progression free survival endpoint that has been used, generally successfully, in the evaluation of new therapies for primary brain tumors. The Response Assessment in Neuro-oncology (RANO) criteria is currently the most commonly used paradigm used to evaluate primary brain tumors in clinical trials, but these measurements may also be requested as part of clinical practice. The justification for the RANO criteria and the challenges faced in implementing it will therefore be discussed. The role of ACRIN and ECOG-ACRIN will be outlined in the context of the new National Clinical Trials Network program for cancer. Increasingly, the limitations of standard of care structural MR imaging (as currently being practiced) for the evaluation of brain tumors are being recognized. Efforts to evaluate advanced imaging such as spectroscopy, diffusion-weighted imaging and dynamic susceptibility weighted imaging in multicenter trials will be reviewed, as well as initiatives to improve the ability of structural imaging to evaluate therapeutic responses and to guide clinical care.



Case Summary

Total Cases = 63
Max age (years) = 16.8
Min age (years) = 1.0
Avg age (years) = 6.3
Posterior fossa = 39
Supratentorial = 24
WHO I = 25
WHO II = 13
WHO III = 9
WHO IV = 16
Pilocytic astrocytoma = 17
Medulloblastoma = 9
Ependymoma WHO III = 7
Piloxyoid astrocytoma = 6
Ependymoma WHO II = 3
ATRT = 3
GBM = 3
Choroid plexus papilloma = 2
Fibrillary astrocytoma = 1
Craniopharyngioma = 1
Desmoplastic infantile ganglioglioma = 1
Ganglioglioma = 1

Note: Scanned images are included in the proceedings. Some submitted images were reduced during editing thereby decreasing clarity. Also, refer to the Program Planner. Proceedings Content as of 3/28/2014.

Ganglion cell tumor 1=
 High grade diffuse glioma = 1
 Low grade glioma = 1
 Low grade glioneuronal tumor = 1
 Low grade oligoastrocytoma = 1
 Oligodendroglioma = 1
 Pineal parenchymal tumor of intermediate differentiation = 1
 PNET = 1
 Anaplastic astrocytoma = 1

O-458 5:30PM - 5:36PM
 Pseudoprogression and lesion response in metastatic disease of the brain treated by radiosurgery.

J Knitter¹, W Erly², B Stea¹, M Lemole¹, K Nael¹
¹University of Arizona, Tucson, AZ, ²University of Arizona Medical Center, Tucson, AZ

Purpose

In this HIPPA-compliant, IRB-approved retrospective study, 104 patients were identified who had metastatic disease to the brain that was treated by SRS. Patients were excluded who had less than two scans or medical records that were inadequate and/or incomplete. A total of 41 SRS-treated lesions in 22 patients were identified. One hundred sixty-eight scans were reviewed by a CAQ-certified neuroradiologist and bidimensional measurements were obtained of the targeted metastases. Scans were assessed for percent change of the product of the bidimensional measurements as a function of time. Lesions were stratified into those which, on the last included examination, had increased in size, those which had decreased in size, and those which did not change in size.

Materials and Methods

In this HIPPA-compliant, IRB-approved retrospective study, 104 patients were identified who had metastatic disease to the brain that was treated by SRS. Patients were excluded who had less than two scans or medical records that were inadequate and/or incomplete. A total of 41 SRS-treated lesions in 22 patients were identified. One hundred sixty-eight scans were reviewed by a CAQ-certified neuroradiologist and bidimensional measurements were obtained of the targeted metastases. Scans were assessed for percent change of the product of the bidimensional measurements as a function of time. Lesions were stratified into those which, on the last included examination, had increased in size, those which had decreased in size, and those which did not change in size.

Results

Of the 41 SRS-treated lesions, 22 regressed by the final examination. Of these, two lesions demonstrated an early increase in size with subsequent spontaneous regression (pseudoprogression). The increase in the bidimensional cross product of the lesions showing pseudoprogression ranged from 30% to 64% above baseline measurements. These lesions first demonstrated pseudoprogression 0.5 to 4.3 months after treatment and regressed 1.9 to 6.2 months after treatment. Of the remaining lesions that regressed, 89% had regressed at four months and all had regressed by six months following treatment. The mean time between treatment and the first scan showing

regression was 2.4 months. Of the lesions that ultimately increased in size, 38% showed an initial decrease. The mean time between the decrease in size and the ultimate increase in size over baseline measurements was 7.0 months.

Conclusions

Among all lesions treated in this series, 5% demonstrated an initial increase in size prior to spontaneously regressing below baseline measurements. Successfully treated tumors responded quickly to treatment, with 93% decreasing in size by two months and regression occurring in a mean of 2.4 months after treatment (range, 0.8-7.6 months).

KEYWORDS: Metastases, Pseudoprogression, Radiation

O-459 5:36PM - 5:42PM
 Screening for Brain Metastases: A Post Contrast 3D T1 High Resolution Sequence is Sufficient

J Butman¹, E Baker¹, N Patronas¹, D Pham², E Magrath², A Stewart¹, R Sherry¹

¹National Institutes of Health, Bethesda, MD, ²Center for Neuroscience and Regenerative Medicine, Bethesda, MD

Purpose

To demonstrate that the postcontrast 3D T1-FFE sequence is sufficient to screen for brain metastases for oncologic clinical trials in neurologically asymptomatic individuals.

Materials and Methods

Review of the intramural NCI database identified patients with Stage IV melanoma enrolled into clinical immunotherapy trials for which MR imaging (MRI) to exclude brain metastases is a requirement. For retrospective MRI review, 98 cases (38 with brain metastases) met the following inclusion criteria: (1) stage IV melanoma with no history of brain metastases (2) absence of neurological symptoms and (3) maximal metastasis diameter of 1 cm. Clinical MRI included precontrast 5mm sagittal and axial SE T1, axial FSE T2, and postcontrast 5mm axial SE T1, T2 FLAIR and ~ 1 mm isotropic sagittal 3D T1-FFE (Philips 1.5 T or 3.0 T Achieva) or FLASH (Siemens 3.0 T Verio). The 3D T1 sequence was anonymized and sent to the PACS (Carestream) as a coded study for interpretation by three neuroradiologists. Readers were asked to count metastases using a presentation state including native slices, MPR and slab MIP reconstructions. In addition, one reader performed an interpretation of the complete MRI (all sequences). The clinical diagnosis (a combination of the initial MRI interpretation and subsequent clinical course) and consensus review of discordant cases was used as gold standard. The study was powered to detect a 10% difference in sensitivity and a 5% difference in specificity from the gold standard (100% for both).

Results

Using the 3D T1 sequence alone, each reader had a sensitivity of 92%, and specificities from 95% to 98%. For reinterpretation of the complete MRI, the sensitivity and specificity was 95% and 97%. None were significantly different than the gold standard.

Note: Scanned images are included in the proceedings. Some submitted images were reduced during editing thereby decreasing clarity. Also, refer to the Program Planner. Proceedings Content as of 3/28/2014.

Conclusions

High resolution postcontrast 3D T1 sequences commonly are reserved for planning of stereotactic radiosurgery or biopsy and not performed routinely. However, this sequence has been shown to be more sensitive than the routine spin echo T1 sequences for metastasis detection (1). For this and other reasons (e.g., image registration), we perform the 3D T1 routinely. In practice, we focus on this as the most important component of the exam for metastasis detection. Anecdotally, the review of the additional sequences presents "information overload" that actually distract from the primary purpose of the exam (detecting brain metastases). In this study, the postcontrast 3D T1 performs no differently than a complete diagnostic MRI for detection of metastasis in the stage IV melanoma patients with a high prevalence of brain metastases. The applicability of these results to other patient populations requiring screening for brain metastases may be influenced by differences in MRI signal characteristics of different tumor types. To summarize, in neurologically asymptomatic patients with stage IV melanoma, a single postcontrast 3D T1 sequence is sufficient to screen for metastases to meet entry criteria for clinical trial enrollment.

KEYWORDS: Metastases

0-461 6:00PM - 6:06PM
Blood Brain Barrier Disruption and Intra-arterial
Chemotherapy in Malignant Brain Tumors: An Institutional
Review

E Bourekas, W Slone, M Luttrull, W Marashdeh, S Bell, J
McGregor
The Ohio State University, Columbus, OH

Purpose

To review risks and outcomes associated with treatment of patients with malignant brain tumors with intra-arterial chemotherapy after blood-brain barrier disruption at a single institution.

Materials and Methods

During the period from 1995-2010, patients with primary malignant brain tumors including glioblastoma multiforme, anaplastic astrocytomas, anaplastic oligodendrogliomas, oligodendrogliomas, primary central nervous system (CNS) lymphomas and germinomas were treated with repeated courses of osmotic blood-brain barrier disruption with mannitol followed by intra-arterial methotrexate or carboplatin. Following treatment, follow up was conducted for a number of years and included complete physical examinations, CT and MRI imaging of the brain, and standard laboratory tests. Complications arising during or after treatment and outcomes were documented.

Results

Forty-nine patients were treated. A total of 606 procedures were performed with seizures being the most common procedure-related complication (2.1% of procedures) and one permanent neurological deficit noted (0.2% of procedures). For primary CNS lymphoma, the overall

response rate was 94% (59% complete, 35% partial) with a median overall survival of 3.6 years. For germinomas the response rate was 100%. Response rates and median overall survival were less with gliomas.

Response	Tumor Type						Overall N = 49
	GBM N=27	AA N=3	AO N=3	Oligo N=2	PCNSL N=17	Germ N=2	
CR	1	0	0	0	10	2	13
PR	0	0	0	0	6±	0	6
SD	15±	3±	3	2*	0	0	23
PD	6	0	0	0	1	0	7
Alive	0	0	0	0	5**	2	7
Median Follow up (days)					2384	3249.5	
TTP	198.95	136	224	71	775.9	1318**	
Range (days)	(8-749)	(65-256)	(216-465)	(70-72)	(40-2098)		
Expired	22	3	3	2	11	0	41
Mean OS	347	449	795	589	1433**	NA	
Range (days)	(33-772)	(185-868)	(260-1544)	(120-1058)	(121-3444)		
Median OS (days)	382	295	582	589	1303	NA	

+ 2 = PT stopped TX; 2 = PT switched to IA or RT; 1 = stopped due to AE

1 = patient switched to RT

* 1 = stopped due to AE

± 1 = PT stopped TX; 1 = PT switched to IA

**1 = missing data

***1 = progression

Conclusions

Intra-arterial chemotherapy after blood-brain barrier disruption with mannitol is safe and well tolerated with a low incidence of catheter-related complications and with very good response rates for primary CNS lymphoma and germinomas and excellent median overall survival for primary CNS lymphoma. Whether this treatment can offer superior response rates and overall survival as compared to conventional therapies needs to be investigated with multicenter randomized trials.

KEYWORDS: Blood-Brain Barrier, Brain Neoplasms,
Intraarterial Chemotherapy

AA: anaplastic astrocytoma; AE: adverse event; AO: anaplastic oligodendroglioma; BBBB: blood brain barrier disruption; CR: complete response; IA: Intra-arterial; GBM: glioblastoma multiforme; GERM: germinoma; NA: :not applicable; OLIGO: oligodendroglioma; OS: Overall survival; PCNSL: primary central nervous system lymphoma; PD: progressive disease; PR: partial response; PT: Patient; RT: radiation therapy; SD: stable disease; TTP: time to progression; TX: Treatment

0-462 6:06PM - 6:12PM
Paradoxical Perfusion Characteristics in Response to an
IGF-1R Antisense (AS) Treatment Protocol for Human
Glioblastoma (GBM) (ID#NCT01550523)

K Talekar, A Flanders, R Gorniak, I Hayden, D Andrews
Thomas Jefferson University Hospital, Philadelphia, PA

Purpose

Antisense (AS) agents have potential as immunotherapeutic agents and are being assessed as a means to stimulate a patients immune system to combat certain forms of cancer. The purpose of this preliminary investigation is to determine whether MR perfusion techniques can serve as a response biomarker for endstage human glioblastoma (GBM) treated with an AS

Note: Scanned images are included in the proceedings. Some submitted images were reduced during editing thereby decreasing clarity. Also, refer to the Program Planner. Proceedings Content as of 3/28/2014.

oligodeoxynucleotide directed against the insulin-like growth factor type 1 receptor.

Materials and Methods

Twelve GBM patients were enrolled in this safety trial using an antisense DNA regimen. Criteria include end stage disease with failure to respond to a conventional therapeutic regimen. A "vaccine" was created using recently harvested GBM tissue and antisense DNA. Ten semipermeable biodiffusion chambers were filled with sterilized and irradiated autologous tumor cells with 2.5 µg of exogenous free antisense and implanted into the patient's rectus sheath for 24 hours and removed. Baseline and serial MR imaging was performed at regular time intervals using dynamic susceptibility contrast (DSC) perfusion and 15 direction diffusion tensor imaging. Serial clinical assessment included Karnofsky performance scale and peripheral white blood cell (WBC) counts as well as multiplex cytokine assays to assess immune response. Hemispheric regions of interest (ROIs), tumor "hot-spot" ROIs and ROIs of contralateral hemisphere were used to generate relative cerebral blood volume (rCBV) values. Twelve anatomical features were assessed to identify serial changes in enhancement characteristics, invasiveness of the normal white matter, as well as changes in noncontrast-enhancing tumor and peritumoral edema. Temporal changes in anatomical MR, rCBV were compared to conventional response criteria, tumor progression/response and clinical status in five patients. Results

Of all 12 patients treated, seven died of disease progression, one of hemorrhage, and one of sepsis. Two patients remained clinically stable for over a year before succumbing to disease progression and one patient continues to survive with a Karnofsky score of 80 at six months after treatment. All patients were categorized clinically into either a short survival cohort (N=9) or a longer survival cohort (N=3); eight patients were characterized as having no immune response while four patients had a quantifiable immune response reflected as an increase in WBC counts, T cells, B cells and a decrease in M2 macrophages (immunosuppressive CD163+ monocytes). Of the longer term survivors, enhancement characteristics progressed while the rCBV initially increased and then normalized in the affected hemisphere within two months after treatment compared to two nonresponders in which the rCBV values remained elevated. An example of a long term survivor is shown in the Figure.

Conclusions

Elevations in rCBV may occur with use of immunotherapies in the treatment of GBM. This paradoxical effect may not be indicative of interval tumor growth but may be a reflection instead of an inflammatory response after induction vaccination. Perfusion MRI may demonstrate a paradoxical response when novel therapies are employed to treat GBM. MR biomarkers should be reconsidered with immunotherapies and GBM.

KEYWORDS: Glioblastoma, Immune

Tuesday, May 20
4:45 PM – 6:15 PM
Room 517a

51 - General Programming: Challenges of Clinical Practice

0-463 4:45PM - 5:05PM
Imaging Technology: When Is Enough - Enough

Seidenwurm, D.
Radiological Associates
Sacramento, CA

Abstract/Presentation Summary

There is emerging consensus, except perhaps among radiologists, that recent imaging growth has been excessive. There are several reasons why imaging rates are higher in the US than other OECD countries. Systemic causes like fee for service payment, rapid commercialization and dissemination of new technologies and research based techniques, competition at the level of the provider and referral source rather than at the consumer or payer level, and medical legal concerns contribute to the problem. Another contributor is our increasing Mannerism, a response to declining rates of innovation through demonstration of superfluous technological virtuosity. A similar phenomenon occurred among artists post renaissance. Solutions to the problems of excessive imaging rates may include economic and regulatory forces. However, the optimal approach is through professionalism and scientific reasoning among radiologists and other physicians. We need to think harder before we scan "better", and rigorously analyze the incremental benefits of thinner slices, more sequences, contrast agents and techniques applied to clinical patients outside of controlled research studies. An organizing principle might be "number needed to scan", which would allow the application of Bayesian inference to everyday clinical circumstances. This will permit application of advanced imaging to targeted populations most likely to benefit, preserving resources for optimal allocation within and outside of imaging.

0-464 5:05PM - 5:20PM
The Role of Imaging in Pre-Operative Planning and Guidance in Modern Skull Base Surgery

Bhatia, R.
Jackson Memorial Hospital/ University of Miami
Miami, FL

Note: Scanned images are included in the proceedings. Some submitted images were reduced during editing thereby decreasing clarity. Also, refer to the Program Planner. Proceedings Content as of 3/28/2014.

O-465 5:20PM - 5:40PM
3D Computerized Evaluation of Aneurysms

Truweit, C.
Hennepin County Medical Center
Minneapolis, MN

Abstract/Presentation Summary

Until recently, DSA has been considered the gold standard in the search for intracranial aneurysms (1). Most studies find a false negative rate on the order of 5%, largely related to vessel overlap and failure to find the optimal view (2). This has been mitigated to considerable extent by the advent of 3DRA which, like CTA and MRA, offers views not as easily or reliably obtained in the angiography suite. Likewise, studies of the sensitivity of CTA and MRA show a false negative rate on the order of 5-10%. In this case, the rate limiting factors are different, typically related to failure to focus on one vessel at a time, incomplete assessment beneath the anterior clinoid processes, incomplete assessment of the post-circle of Willis cerebral vasculature, and failure to perform a systematic search through the cerebral vasculature, allowing for missed mirror and multiple aneurysms. That said, as recently noted by the UCLA group (1), adoption of systematic review processes can offer improved sensitivity of CTA over DSA, especially for very small aneurysms measure 4mm or less. Thus, in the search for, and evaluation of, intracranial aneurysms, the role of advanced visualization cannot be understated. Whereas earlier efforts were somewhat limited by the speed of advanced visualization workstations, this is no longer the case, as almost all such systems allow for near real-time processing. In addition, whereas previous efforts were generally limited to MIP, surface rendered, and MPR, current systems also display endoluminal views which allow for proper characterization of the aneurysm neck and potential branch vessels arising from the aneurysm wall (away from the neck). As noted above, during catheter angiographic studies, one vessel is assessed at a time. This rule is not universally followed when performing advanced visualization of CTA and MRA, unfortunately, affording the reviewer the opportunity for distraction and incomplete assessment. In addition, neuroradiologists often state that careful attention to the individual axial slices is imperative to the proper interrogation of a CTA dataset. While this is undoubtedly true, as noted by the UCLA group, this is not enough: by this method alone, as many as 10% of aneurysms are missed (3). On the other hand, review of 3D images alone, in the absence of careful review of the axial slices and MPR slices, also exposes the reviewer to a 10% miss rate (3). During this presentation, the concept of a systematic approach to the evaluation of CTA (and MRA) on advanced visualization workstations will be discussed. This includes identifying and reviewing those areas of known fall negatives, such as intra- and infracaloid aneurysms, as well as small, second aneurysms that can be overlooked. In addition, such a methodological approach can generally be performed just a few minutes in most cases, allowing it to be a routine rather than an exceptional, part of the evaluation of CTA and MRA of the cerebral vasculature.

O-466 5:40PM - 6:00PM
Do We Need to Follow All Aneurysms?

Villablanca, J.
David Geffen School of Medicine at UCLA
Malibu, CA

Abstract/Presentation Summary

This presentation will review the incidence and pathophysiology of cerebral aneurysms. We will explore the role of imaging in the detection, characterization and triage of brain aneurysms including a brief review of the literature. Using clinical examples, the role of imaging in treatment selection will be discussed. Comparative advantages and limitations of CTA, BS-CTA, TOF-MRA and CE-MRA will be outlined. Recent evidence on the management of asymptomatic incidental cerebral aneurysms will be presented. Finally, we will identify common sources of interpretational error, review recent studies on cost effectiveness strategies, and summarize major points.

O-467 6:00PM - 6:15PM
Confessions of a Dictaphone

Chapman, P.
Radiology Of Huntsville
Huntsville, AL

Tuesday, May 20
4:45 PM – 6:15 PM
Room 520

52 - Advanced Imaging Seminar:
Translational Advanced Imaging for
Tissue Characterization

O-468 4:45PM - 5:15PM
The Role of SWI in Neurodegenerative Disease: From the Fetus to Dementia

Haacke, E.
Wayne State University
Detroit, MI

Abstract/Presentation Summary

In this presentation, we shall introduce the basic elements of susceptibility weighted imaging (SWI) and how one can use phase information to enhance image contrast. SWI is a 3D phase enhanced gradient echo imaging method that shows increased sensitivity in the detection of venous blood and blood products such as clot or hemorrhages. In this presentation, we will review the main process of producing an SWI data set from the phase information and discuss issues related to signal-to-noise and resolution. We will introduce the concept of a fully flow compensated double echo sequence and how it will be useful when there is high iron content present in tissue. The ME approach also makes it possible to collect T2* maps and to compare these results with quantitative susceptibility mapping. At 3T, we have been using a resolution of between 0.5mm3 and 1mm3 while at 7T we have been using 0.2 x 0.2 x

Note: Scanned images are included in the proceedings. Some submitted images were reduced during editing thereby decreasing clarity. Also, refer to the Program Planner. Proceedings Content as of 3/28/2014.

1mm3. More specifically, among other diseases, we consider the application of SWI to traumatic brain injury (TBI), stroke, tumors, Sturge-Webber disease (SWD) and multiple sclerosis (MS). 1) trauma: High resolution SWI has been shown to be superior to conventional gradient echo imaging in detecting hemorrhages caused by TBI. Small lesions are more visible on SWI compared to conventional GRE. 2) stroke: Both computed tomography (CT) and MRI have been used for initial radiologic evaluation of acute stroke and patient selection for thrombolytic therapy. MRI is more sensitive than CT for identifying acute infarcts. 3) SWD: We have studied many cases of SWD and found that SWI shows abnormalities in the white matter consistent with abnormal transmedullary veins. Many patients also have prominent cortical SWI abnormalities as well. 4) MS: SWI reveals lesions with increased iron content as well as increased iron content in the basal ganglia. 5) fetal imaging: SWI has been used to map the development of the venous system from 20 to 37 weeks and to look at oxygen saturation levels in the superior sagittal sinus. 6) dementia: SWI has been used to study cerebral amyloid angiopathy (CAA) and monitor changes in microbleeds over time. 7) developmental venous anomalies: SWI is perhaps the best method for evaluating telangiectasias and other DVAs. Recent advances in inverting phase into a source image called quantitative susceptibility mapping (QSM) can be applied to any case where SWI is being used since the phase is available. SWI is exquisitely sensitive to even small microbleeds and has excellent diagnostic capabilities while QSM provides a quantitative map of the iron content independent of local geometry. In summary, SWI and SWIM provide a powerful means to study neurological diseases.

0-469 5:15PM - 5:45PM
Latest in Clinical Applications of Quantitative Susceptibility Mapping (QSM)

Wang, Y.
Weill Medical College of Cornell University
New York, NY

Abstract/Presentation Summary
Quantitative susceptibility mapping (QSM) has become sufficiently accurate for measuring strong susceptibilities of biomaterials including iron distribution (ferritin) in the deep brain nuclei and basal ganglia, deoxyhemoglobin (dHb) in the veins, blood degradation products (hemosiderin in late stage), concentrated calcifications and exogenous species such as gadolinium. Clinical applications of QSM are being developed to use these imaging biomarkers to probe iron distribution in neurodegenerative and inflammatory diseases, hemorrhage, metabolic consumption of oxygen, and calcium deposition, and to guide and monitor therapy. QSM can also remove blooming artifacts in traditional T2* weighted imaging, providing an accurate definition of the geometries of magnetic biomaterials in MRI. This presentation will illustrate QSM applications in the following areas: • Diamagnetic biomaterial based

applications to differentiate diamagnetic calcifications from paramagnetic materials such as hemosiderin • Paramagnetic heme iron (deoxyhemoglobin, methemoglobin, hemosiderin) based applications to measure metabolic rate of oxygen consumption and to define microbleeds and hemorrhage • Paramagnetic nonheme iron (ferritin) based applications to measure iron overload in neurodegenerative disease and to define targets for deep brain stimulation • Paramagnetic contrast agent biodistribution quantification based application in contrast enhanced MRI and molecular MRI, and • Mixed diamagnetic and paramagnetic applications to measure demyelination and iron content in multiple sclerosis.

0-470 5:45PM - 6:15PM
Susceptibility Tensor Imaging and Fiber Tracking

Liu, C.
Duke University, School of Medicine
Durham, NC

Abstract/Presentation Summary
Susceptibility tensor imaging (STI) is a recently developed MRI technique for imaging and quantifying tissue magnetic susceptibility (Liu, 2010). STI utilizes images acquired with the 3D gradient echo sequence. From the phase maps of gradient echo images, STI is able to compute a susceptibility tensor for each voxel by solving a system of linear equations. A susceptibility tensor can be either isotropic such as in the cerebral spinal fluid or anisotropic such as in the brain white matter; susceptibility tensor may also be paramagnetic or diamagnetic. Susceptibility tensor can be decomposed in two three eigenvectors and corresponding principal susceptibility values. These eigenvalues and eigenvectors are rotationally invariant and are independent of the coordinate system, thus providing a quantitative measure of tissue property. In the white matter, the largest principal susceptibility is shown to be in the direction parallel to the axonal fibers (Li et al., 2012a; Liu, 2010). This relationship can be utilized to reconstruct fiber tracts of the brain in a fashion similar to diffusion tensor imaging tractography (Liu et al., 2012). Further constraints on the tensor may be applied to simplify the acquisition of STI (Li et al., 2012b; Wisnieff et al., 2013). In the brain white matter, anisotropic susceptibility tensor originates from the anisotropic molecular susceptibility of lipids in the myelin sheaths and the ordered microstructures of axons (Lee et al., 2012; Li et al., 2012a; Liu, 2010; Wharton and Bowtell, 2013). Neonatal brains and demyelination in multiple sclerosis have thus reduced diamagnetic susceptibility and susceptibility anisotropy (Liu et al., 2011). Magnetic susceptibility anisotropy also exists outside brain, for example, in the kidney and heart. Consequently, STI provides a new technique that may have broad applications in imaging and characterizing tissue microstructure.

Note: Scanned images are included in the proceedings. Some submitted images were reduced during editing thereby decreasing clarity. Also, refer to the Program Planner. Proceedings Content as of 3/28/2014.

Tuesday, May 20
4:45 PM – 6:15 PM
Room 524

53 - GENERAL PROGRAMMING - ASNR
INTRODUCES THE STUDY GROUPS

O-471 4:45PM - 4:50PM
Introduction

Wintermark, M.
University of Virginia
Charlottesville, VA

O-472 4:50PM - 5:10PM
CSF Flow

Bradley, W.
USD Medical Center
San Diego, CA

Abstract/Presentation Summary
The International Hydrocephalus Imaging Working Group (IHIWG) is an informal group of neuroradiologists, neurosurgeons, neurologists, bioengineers and basic scientists which meets twice a year at the ASNR and at the ISHCSF (International Society for Hydrocephalus and CSF Disorders). We discuss basic concepts like where CSF is formed and taken up and the possible role of AQ4 receptors. We discuss issues related to the diagnosis and treatment of various forms of hydrocephalus and related diseases, eg, pseudotumor. We discuss various MRI-based techniques for demonstrating CSF flow, eg, Phase-Contrast and TimeSLIP, as they help in the management of diseases such as NPH and Chiari I. In the context of NPH we discuss possible causes of the idiopathic form, eg, benign external hydrocephalus. We compare various methods to predict response to shunting, eg, phase contrast measurements of the aqueductal CSF Stroke Volume, the DESH (Disproportionately Enlarged Subarchnoid space Hydrocephalus) pattern on a coronal MRI, the high volume tap test, saline infusion, and external lumbar drainage. We discuss new findings using DTI and MR elastography for evaluation of NPH. In the context of Chiari I, we discuss computational flow dynamics based on PC MRI using the Navier-Stokes equation to predict CSF pressures over the cardiac cycle and the impact on syrinx formation. By coupling PC MRI measurements of CSF, arterial blood, and venous blood flow over the cardiac cycle, we discuss the ability to noninvasively estimate intracranial pressure. We discuss new techniques like TimeSLIP (basically arterial spin labeling of CSF) and the many applications in the evaluation of intracranial diseases.

O-474 5:10PM - 5:30PM
Tumor Genomics

Colen, R. · Pope, W.
MD Anderson Cancer Center · University of California Los Angeles
Houston, TX · Los Angeles, CA

O-475 5:30PM - 5:50PM
Translational Imaging

Druzgal, T. · Whitlow, C.
University of Virginia · Wake Forest School of Medicine
Charlottesville, VA · Winston-Salem, NC

O-477 5:50PM - 6:00PM
Vessel Wall Imaging

Wasserman, B. · Mikulis, D.
Johns Hopkins University · Toronto Western Hospital
Baltimore, MD · Toronto, ON

Abstract/Presentation Summary
An overview of the activities of the recently formed vessel wall imaging study group will be presented. The group has conducted four webinars since the study group formed a year ago where interesting intracranial and extracranial cases have been shown and discussed. Committees have been formed to promote networking, protocol standardization, research, and education. Some of the successful milestones achieved by the group in this first year include: • Development of a 3-D T1 weighted black blood sequence that should work effectively on Siemens 3T platform. This has been achieved with the help and hard work of MR physicist David Saloner. The sequence is close to being in a distributable form. Meetings are being planned with other vendors to enable similar sequences for other platforms. • White papers are being led by Luca Saba and Danny Mandell on cervical carotid wall imaging and intracranial arterial wall imaging, respectively. • The first collaborative research paper is being developed with a target publication for the end of 2014. • A web site is being developed with the assistance of the ASNR and should become available within the next few months. We are encouraging ASNR members to join the study group, contribute cases to the webinars, participate in the working committees, and participate in research activities.

Questions 6:00PM - 6:15PM

Wednesday, May 21
7:30 AM – 8:30 AM
Room 517bc

54 - Brain Imaging Session (SAM)

Note: Scanned images are included in the proceedings. Some submitted images were reduced during editing thereby decreasing clarity. Also, refer to the Program Planner. Proceedings Content as of 3/28/2014.

O-479 7:30AM - 7:45AM
Vasculitis and Demyelinating Diseases

Johnson, C.
New York-Presbyterian Hospital
New York, NY

Abstract/Presentation Summary

Cerebral vasculopathies include atheromatous and nonatheromatous diseases. Cerebral atherosclerosis is the most frequent etiology of intracranial vascular stenosis and the third most common cause for thromboembolic stroke following cardiac and carotid sources. Nonatheromatous vasculopathies are a heterogeneous group of disorders that include true vasculitis and noninflammatory vasculopathies such as amyloid angiopathy, CADASIL syndrome and vasomotor disorders. Vasculitis is characterized pathologically by inflammation and variable necrosis of the vessel wall and can be grouped according to involvement of large, medium or small vessels. Large vessel vasculidities include giant cell arteritis such as temporal arteritis and polyarteritis nodosa. Other systemic vasculidities involve small vessels. Primary angiitis of the central nervous system affects medium and small sized vessels. In addition to primary systemic vasculidities causes of secondary CNS vasculitis include multiple infectious agents, connective tissue diseases, various drugs, oncologic disease such as lymphoma, Behcet's disease and sarcoidosis. Clinical presentations related to cerebral vasculopathies are varied but include headache, focal neurologic deficits, ataxia, nonspecific encephalopathy, seizure and visual disturbance. In vasculitis cerebrospinal fluid analysis shows evidence of inflammation including elevated protein and lymphocytic pleocytosis. Neuroimaging is important in diagnosing cerebral vasculopathy. MRI/MRA is the mainstay in the initial imaging evaluation. CT angiography is utilized in selected cases. MR imaging findings are varied but include multifocal T2 hyperintensities in white and gray matter, hemorrhage and areas of parenchymal or leptomeningeal enhancement. Vessel wall imaging can aid in the diagnosis. Diffusion weighted imaging may show areas of recent ischemia while susceptibility weighted imaging is useful to show recent or chronic hemorrhage. MR or CT angiography may be normal or show multisegmental vascular stenoses. Conventional angiography may be considered the "gold standard" but is infrequently performed unless there is a high clinical suspicion in the absence of findings at MR or CT angiography. Demyelinating diseases have clinical and imaging findings in common with those found in cerebral vasculopathies. Demyelinating diseases can be classified into several categories among which are inflammatory demyelination and viral demyelination. The most common form of inflammatory demyelination is multiple sclerosis. MR is the primary imaging modality. The diagnosis can be suggested based on classic characteristic appearance of white matter lesions and use of the McDonald criteria. Demyelinating diseases which have unique imaging findings include Balo's concentric sclerosis, a subtype of MS, and neuromyelitis optica. Acute disseminated

encephalomyelitis (ADEM) is characteristically a monophasic disease though recurrent ADEM can occur. ADEM is immune mediated, more common in children and typically occurs within 2 weeks following an infection or vaccination. Imaging findings may be similar to those in multiple sclerosis but the white matter lesions are more often asymmetric and spare the callosal-septal interface. Tumefactive demyelination may be difficult to differentiate from tumor though some imaging findings including those at spectroscopy may suggest this diagnosis. The primary viral demyelinating disease is progressive multifocal leukoencephalopathy (PML) caused by the JC virus in an immunocompromised host. PML has been associated with the use of natalizumab (Tysabri), a monoclonal antibody, for treatment of multiple sclerosis. MR imaging screening of patient's receiving Tysabri is routinely obtained. Findings related to immune reconstitution in patient's with JC virus infection need to be differentiated from those from those related to progressive demyelinating disease. Imaging plays an important role in the diagnosis and subsequent followup of cerebral vasculopathies and demyelinating diseases. Characteristic imaging findings often suggest the appropriate diagnosis and aid in monitoring of treatment response.

O-480 7:45AM - 8:00AM
Primary Brain Tumors in Adulthood

Tampieri, D.
Montreal Neurological Hospital and Institute
Montreal, Quebec

Abstract/Presentation Summary

The latest WHO classification of CNS Brain tumors was published in 2007. The tumors are classified depending of their cellular origin and few new tumors types were added including angiocentric glioma, papillary glioneuronal tumour, rosette-forming glioneuronal tumour of the fourth ventricle and others. The classification from Grade I to IV reflects the degree of malignancy. Grade I are usually considered benign tumors without malignant transformation. Grade IV are the most aggressive with local invasive feature and may lead to metastasis mainly via the CSF. Grade II and III are aggressive tumors that tend to evolve to grade IV in time. The diagnosis is histological based on the presence of atypical cells, neovascularity, necrosis and mitotic index. The imaging findings of brain tumors may vary according to the tumors grade, and advanced imaging techniques such as spectroscopy, diffusion and perfusion sequences may help in the differential diagnosis of certain tumors type. The molecular markers in high grade gliomas are important, they have both a diagnostic and prognostic value and they help to predict the response to treatment. In Primary GBM, usually the most aggressive type of tumor with shortest survival rate, the presence of MGMT (O-Methylguanine-DNA Methyltransferase) has a favorable prognostic value. This is a DNA repair gene, if is methylated the response to Temozolamide is better because the DNA of the tumor cell can not be repaired. Therefore GBMs with MGMT methylated have longer survival rate. In consideration of the advanced neurosurgical techniques available when anatomically possible, gross total resection is the goal of the intervention. Subsequently patients are usually enrolled in specific

Note: Scanned images are included in the proceedings. Some submitted images were reduced during editing thereby decreasing clarity. Also, refer to the Program Planner. Proceedings Content as of 3/28/2014.

protocols based on the histological type of the tumors. For high grade gliomas the combination of Temozolimide and radiotherapy has become the standard of practice. However this combination may lead to confusing imaging findings in the follow up MRI exams and the differential diagnosis of recurrent tumor versus pseudo-progression still remain difficult. The assessment of the MRI characteristics of these lesions using also advanced imaging techniques is paramount to the patient's clinical evolution and treatment.

0-481 8:00AM - 8:15AM
Emergency Imaging in Neuroinfections

Del Carpio-O'Donovan, R.
McGill University Health Center, Montreal General Hospital
Montreal, QC

Abstract/Presentation Summary
Infectious diseases involving the brain require prompt and accurate diagnosis. Imaging in the Emergency Department (ED) consists initially of CT scanning. With this first approach, certain key decisions can be taken: medical vs surgical management, proceed to CSF testing, complement study with iv. contrast medium or MRI. Adequate clinical information is possibly more relevant than with other categories of disease. The geographical origin of the patient, personal contacts, work, lifestyle, immune status, extreme ages constitute key information. Emergent infectious diseases are a considerable challenge. MRI is proving indispensable in the ED and for infectious acute pathology besides obvious advantages for children and pregnant women. It is useful in differentiating abscess from glioblastoma, more sensitive for meningeal processes and for complications such as subdural or epidural empyema. Appropriate localization of the lesion is of paramount importance. Potential for rapid progression and permanent neurological deficits gives great urgency to the diagnosis and appropriate treatment.

8:15AM - 8:30AM
Questions and Answers

Wednesday, May 21
8:30 AM – 10:00 AM
Room 517bc

55 - General Programming – Evidence Based Medicine: Imaging in Alzheimer's Disease – What Is the Evidence?

0-483 8:30AM - 8:40AM
Clinical Practice Guidelines and Appropriateness Criteria

Anzai, Y.
Univ. Washington Medical Center
Seattle, WA

0-484 8:40AM - 9:00AM
Brain Imaging for Alzheimer's Disease

Larvie, M.
Massachusetts General Hospital
Boston, MA

Abstract/Presentation Summary
The diagnostic criteria for neurodegenerative diseases generally, and Alzheimer's disease (AD) specifically, have evolved in concert with advances in brain imaging. Although until very recently the diagnosis of AD was based solely on clinical examination, it is now recognized that brain imaging can strongly add to the sensitive and specific diagnosis. The major imaging modalities for AD are CT, MRI, FDG PET and amyloid PET, and the selection of appropriate imaging is dependent upon the clinical circumstance. We will consider three different scenarios: 1) Evaluation of acutely recognized diminished mental status in a patient whose cognitive baseline is not well-established; 2) Evaluation of subtle cognitive deficits (such as mild cognitive impairment) of insidious onset; 3) Identification of early AD pathology in a patient with no clinical symptoms (that is, pre-clinical AD). The optimal approach to these scenarios will make use of imaging examinations with different receiver operating curves, ranging from less sensitive and less specific to more sensitive and more specific. In support of evidence-based practice, the utility of different imaging modalities will be presented in the context of specific clinical applications.

0-485 9:00AM - 9:20AM
Advanced Imaging of Alzheimer's Disease - The Role of DTI and ASL

Petrella, J.
Duke University Medical Center
Durham, NC

0-486 9:20AM - 9:40AM
Amyloid Imaging for Alzheimer's Disease

Nasrallah, I.
University of Pennsylvania
Philadelphia, PA

Abstract/Presentation Summary
Alzheimer disease is neuropathologically characterized by aggregation of amyloid beta plaques and tau-containing neurofibrillary tangles. Over the past decade, a number of Positron Emission Tomography (PET) tracers have been developed to evaluate one of these pathophysiological hallmarks: cerebral amyloid aggregates. These agents have

Note: Scanned images are included in the proceedings. Some submitted images were reduced during editing thereby decreasing clarity. Also, refer to the Program Planner. Proceedings Content as of 3/28/2014.

had significant impact on Alzheimer disease research over this period and have potential to benefit clinical trial design and clinical evaluation of patients with cognitive decline. This presentation will: • Discuss the various PET agents currently available for cerebral amyloid imaging. • Review approaches to standard clinical interpretation of amyloid PET and methods for quantification of radiotracer uptake. • Explore the utility of amyloid imaging radiotracers in reference to other biomarkers of Alzheimer disease, including diagnostic and prognostic value of amyloid PET. • Outline suggested appropriate use criteria proposed by the Amyloid Imaging Task Force of the Society of Nuclear Medicine and Molecular Imaging and Alzheimer's Association.

9:40AM - 10:00AM

Panel Discussion

Wednesday, May 21
8:30 AM – 10:00 AM
Room 517d

56 - ASSR Programming: Advanced
Imaging of the Spine

O-487 8:30AM - 8:50AM
Demyelinating Diseases of the Cord

Thurnher, M.
Medical University Of Vienna
Vienna

Abstract/Presentation Summary
Evaluation of MR imaging in a patient with an intramedullary lesion should focus on key-features: a) the location of the lesion on the cross sectional area of the cord, best evaluated on axial images, b) the length of the lesion evaluated on sagittal images, c) the presence of cavitation and cysts, d) signal intensity on T2-WI, e) the presence of enhancement and enhancement type, and f) associated leptomeningeal enhancement. The knowledge of the presence or absence of the brain lesions is important information for narrowing the differential diagnosis. Finally, clinical information, demographics, and immune status should be incorporated. In this lecture imaging characteristics and typical patterns of intramedullary lesions will be presented. A diagnostic algorithm, which includes imaging, clinics and CSF analysis, will be discussed.

O-488 8:50AM - 9:10AM
New Concepts of CSF Flow Studies or Higher Field Spine Imaging

Bradley, W.
USD Medical Center
San Diego, CA

Abstract/Presentation Summary
This talk will discuss new applications for CSF flow in the spine and other new applications in the pipeline over the next decade generally at higher field. The CSF flow applications are based on Vic Haughton's group's work using computational flow dynamics to model flow and pressure gradients in the upper cervical spine, particularly in the context of Chiari I (Hentschel S, Haughton V, et al, AJNR 2010; 31:997-1002). By using the Navier-Stokes equation pressures can be calculated in the spinal subarachnoid space over the cardiac cycle and the tendency for CSF to enter the central canal via the perivascular spaces can be demonstrated computationally (Drosdal IN, Mardal K-A, Stoverud K, Haughton V, The Neuroradiology Journal 26: 585-590, 2013).

O-489 9:10AM - 9:30AM
DWI and MRS of the Spine

Tanenbaum, L.
Mount Sinai Medical Center
New York, NY

Abstract/Presentation Summary
The role of diffusion weighted imaging has expanded beyond the brain to whole body applications. This presentation will explore the contribution of DWI in the routine evaluation of spinal conditions focusing on its role in the detection, characterization and surveillance of neoplastic, degenerative and infectious diseases. MR spectroscopy has the power to delineate the chemical signature of tissues in health and disease. Research suggests detection of key MRS biomarkers may have a role analogous to provocative discography in identification of the painful disc. This presentation will cover the key findings in the painful disc and review the research work done to date.

O-490 9:30AM - 9:50AM
New Concepts About CSF Flow and What I Learned in a Recent CSF Symposium with Bill Bradley

Law, M.
USC Keck School of Medicine & Medical Center of USC
Los Angeles, CA

9:50AM - 10:00AM

Questions

Note: Scanned images are included in the proceedings. Some submitted images were reduced during editing thereby decreasing clarity. Also, refer to the Program Planner. Proceedings Content as of 3/28/2014.

Wednesday, May 21
8:30 AM – 10:00 AM
Room 517a

57 - ASPNR Programming – CVR

0-500 8:30AM - 9:00AM
Quantitative CVR Mapping

Mikulis, D.
Toronto Western Hospital
Toronto, ON
Abstract/Presentation Summary
Quantitative imaging methods have primarily been applied for research investigation of normal and pathophysiological conditions. However, there are numerous examples where quantitative imaging research has translated into the clinical environment. For example, measurement of blood flow metrics (CBF, CBV, MTT, TMAX), and vascular permeability has found clinical application in the assessment of cerebral ischemia and CNS neoplasia. Measurement of CVR has also been available for many years and has likewise been used primarily for research. The major contribution that the body of CVR research has made is establishment of the relationship between steal physiology in patients with cerebrovascular steno-occlusive disease and the risk of disabling ischemic stroke. More recent work has shown that there is a relationship between steal physiology and subacute brain injury in patients who are not experiencing ischemic events. In view of the clinical potential of CVR for assessing vascular risk both in terms of stroke risk and for distinguishing embolic from hemodynamic transient ischemic events, as well as the ability of MR to make this assessment without the need for injectable tracers, interest in clinical MRI CVR mapping is increasing. Further impetus is derived from the notion that the normal brain operates under the framework of demand vasodilatation. That is, activation of neurons is accompanied by a considerable increase in blood flow to support increased metabolic demand as the brain is poor in storing high-energy metabolites. The brain depends on this flow support. It is therefore not surprising that resting blood measurements are ineffective in assessing the impact of steno-occlusive disease under resting blood flow conditions as autoregulatory compensation can maintain normal blood flow albeit with increased transit time. Transit time could be considered an important metric in this regard but there is no consensus on a threshold for significance. In fact CVR can be normal with carotid occlusion and increased transit time secondary to excellent collaterals. This presentation will therefore focus on the application of CVR as a metric for assessing the significance of cerebrovascular steno-occlusive disease. The key CVR finding is the detection of decreased blood flow in response to a global vasodilatory stimulus (CO₂), i.e. steal physiology (lack of demand

vasodilatation). The detection of decreased blood flow to a global vasodilatory stimulus can be identified with either qualitative or quantitative CVR approaches. Both methods including advantages and disadvantages will be discussed. "Chronic Neurovascular Uncoupling Syndrome" In 1954, C. Miller Fisher first described the relationship between carotid occlusive disease and rapidly progressive dementia in patients who were not experiencing ischemic events. More recently it has been shown that activation of neural networks is accompanied by a significant increase in local cerebral blood flow (on the order of 50%) that is spatially congruent with those networks. Interestingly, the increase in blood flow secondary to neural activation is greater than the consumption of additional oxygen provided by this flow increase. This interaction has been termed neurovascular coupling (or uncoupling by some in the sense that the additional oxygen delivered is not fully consumed - we have preferred the term neurovascular coupling since we feel it is a normal physiological response). There are numerous theories as to why such high increases in flow occur including removal of waste products and maximization of microvascular surface area for optimal tissue transfer of oxygen. An important consideration is that the brain is poor at storing high-energy metabolites. An increase in energy demand during activation of neural networks must therefore be accompanied by rapid synthesis of high-energy metabolites. An important issue arises in the setting of high-grade steno-occlusive disease of the major cervical and cerebral arteries. Under these conditions vasodilatation of the vasculature distal to the steno-occlusive process occurs in order to compensate for a potential blood flow deficit, but this consumes vascular reserve and the ability to further vasodilate in response to neural activation is diminished. When compensatory collaterals are poor, vascular reserve can become exhausted leaving no further vasodilatory response. The key question is, if blood flow cannot increase to support the metabolic demand of the tissue during neural activation, does this result in injury to the brain as this, by definition, is ischemia? Initial evidence indicates that this in fact is true. Under these conditions, neurovascular coupling becomes uncoupled. Evidence for the effects of neurovascular uncoupling will therefore be discussed in this presentation.

0-501 9:00AM - 9:30AM
Clinical Relevance of CVR Mapping

Derdeyn, C.
Mallinckrodt Inst. Radiology
St. Louis, MO

Abstract/Presentation Summary
The brain and brain vasculature can compensate for reductions in oxygen delivery through autoregulatory vasodilation to maintain cerebral blood flow and through increased oxygen extraction [1]. Oxygen delivery can be reduced in a variety of situations, including reduced cerebral blood flow (arterial stenosis, hypotension) and

Note: Scanned images are included in the proceedings. Some submitted images were reduced during editing thereby decreasing clarity. Also, refer to the Program Planner. Proceedings Content as of 3/28/2014.

anemia. A number of imaging tools have been developed to assess for the presence of these compensatory mechanisms. Some of the most commonly used methods evaluate cerebrovascular reserve (CVR). CVR describes the degree to which the brain vasculature can respond to a vasodilatory stimulus, such as acetazolamide or hypercapnia. A normal response is a robust increase in flow or flow velocity. When the response is absent, muted, or paradoxically worsened (steal physiology) after the stimulus, the presence of pre-existing autoregulatory vasodilation is inferred. The strongest evidence for clinical utility for CVR is for predicting the risk of future stroke in patients with atherosclerotic carotid occlusive disease [2, 3]. Tests of CVR have great potential for clinical use in other situations as well. These include subarachnoid hemorrhage-induced vasospasm [4], non-atherosclerotic vasculopathies (moyamoya) [5], sickle cell disease [6] and prediction of hyperperfusion syndrome. These tests may have value in predicting stroke risk and identifying patients that may benefit from revascularization procedures. This talk will review the physiology of hemodynamic impairment, a brief overview of the available tools for assessment, and then a discussion of clinical applications and the evidence to support them.

O-502 9:30AM - 10:00AM
Breathhold CVR

Pillai, J.
The Johns Hopkins Hospital
Baltimore, MD

Abstract/Presentation Summary
Breath-hold Blood Oxygen Level Dependent (BOLD) cerebrovascular reactivity (CVR) mapping will be introduced in this lecture. The importance of this technique in clinical presurgical mapping will be stressed, both as an important quality control tool for assessing reliability of clinical BOLD fMRI and as a method for detection of neurovascular decoupling or uncoupling (NVU) potential. The phenomenon of NVU and how it may affect the BOLD signal will be discussed from both pathophysiologic and practical standpoints. Some important differences between the breath hold CVR technique and conventional exogenous CO₂ delivery approaches will be discussed including advantages and disadvantages of each approach. Brief mention will be made of research applications of this method related to NVU involving brain tumors of different grades. The great clinical utility of BOLD breath hold CVR mapping will be demonstrated using case examples from Johns Hopkins Hospital. These examples will show how this technique can make a difference in neurosurgical planning and why this technique will likely rapidly evolve into a standard of care for clinical fMRI.

Wednesday, May 21
8:30 AM – 10:00 AM
Room 520

58 - ASNR Annual Business Meeting
(members only)

Wednesday, May 21
8:30 AM – 10:15 AM
Room 524

59 - Parallel Papers: Interventional
Aneurysms II

O-123 10:08AM - 10:14AM
MRI Features Distinguish Subtypes of Infratentorial
Ganglioglioma with High Specificity.

J Harrell, K Gupta, W Orisme, J Dalton, R Tatevossian, I
Qaddoumi, Y Yuan, D Ellison
St. Jude Children's Research Hospital, Memphis, TN

Purpose
Abnormalities involving BRAF, a regulator in the mitogen-activated protein (MAP) kinase signaling pathway crucial to cell growth and differentiation, have been found in many cancers including ganglioglioma, a low-grade glioneuronal tumor that is rare below the tentorium. Recently, we identified two histopathologically and genetically distinct subtypes of infratentorial ganglioglioma: classic tumors with a high frequency of BRAF:p.V600E mutation (Group I), and pilocytic astrocytomas with gangliocytic differentiation with a high frequency of KIAA1549-BRAF fusion (Group II). The purpose of this study was to determine whether MR imaging (MRI) phenotype could differentiate between subtypes of infratentorial gangliogliomas.

Materials and Methods

After pathologic and genetic analysis of 27 infratentorial gangliogliomas involving the cerebellum, brainstem and spinal cord, a neuroradiologist blinded to pathologic/genetic analysis evaluated MR imaging available in 25/27 subjects (14 Group I, 11 Group II) for tumor cysts/necrosis, hemorrhage, enhancement, restricted diffusion, circumscription, edema and location. Radiologic features then were compared between histopathologic/genetic subtypes, and sensitivity and specificity for distinction of tumor subtypes calculated.

Results

Group I gangliogliomas were most frequently poorly circumscribed (79%) and rarely cystic/necrotic (14%).

Note: Scanned images are included in the proceedings. Some submitted images were reduced during editing thereby decreasing clarity. Also, refer to the Program Planner. Proceedings Content as of 3/28/2014.

Three of eight (38%) with diffusion-weighted imaging (DWI) were diffusion-restricted; none were midline or hemorrhagic. Group II gangliogliomas were more frequently cystic/necrotic (91%), midline (55%), hemorrhagic (45%) and well circumscribed (64%); five of six (83%) with DWI were diffusion-restricted. The presence of cysts/necrosis was 91% sensitive and 86% specific for differentiating Group II from Group I gangliogliomas. The presence of hemorrhage and/or midline location increased specificity to 100%.

Conclusions

Radiologic phenotype differentiates subtypes of infratentorial ganglioglioma with high sensitivity and specificity.

KEYWORDS: Genetics, MR Imaging, Pediatric Brain Tumors

O-504 8:30AM - 8:37AM
A Randomized Trial Comparing Platinum and Hydrogel Coiling in Patients Prone to Recurrence After Endovascular Treatment - The PRET Trial: Immediate Procedural results

J Raymond, F Guilbert, A Weill, D Roy
Centre Hospitalier de l'Université de Montréal - Notre Dame Hospital, Montreal, Quebec, Canada

Purpose

Some patients are at high risk of aneurysm recurrence following endovascular treatment. The PRET trial, sponsored by the Centre Hospitalier de l'Université de Montréal and funded by MicroVention Inc., aimed to compare hydrogel to bare platinum coiling in patients with aneurysms prone to recurrence, i.e., in patients with large aneurysms (≥ 10 mm; PRET-1) or in patients with a major recurrence after previous coiling (PRET-2). We report periprocedural safety and operator-assessed immediate angiographic results.

Materials and Methods

Patients were randomized to the hydrogel coil or control arms (concealed allocation) by using minimization criteria. Recently ruptured and unruptured aneurysms (UAs) were included. Any type of bare platinum coils were allowed in the control arm. The present abstract includes aggregated results. Safety was evaluated according to the number of days in hospital, the modified Rankin score (mRs) at discharge and the discharge location (home or not). Angiographic results were graded according to the Montreal scale.

Results

Thirty-four centers recruited 443 patients in six countries. Mean age was 58 +/- 11; mean aneurysm sizes were 14 +/- 4 mm for 247 PRET-1 and 11 +/- 7mm for 196 PRET-2 patients; 18% were ruptured aneurysms (29% in PRET-1; 4% in PRET-2); 42% of aneurysms were in the posterior circulation. Coiling was successful in 95% of patients. Forty-three (9.7%) periprocedural complications were reported. Patients were hospitalized for less than five days in 81.5% (93.5% of unruptured cases) and discharged home in 91% of cases (97% of UA cases). Two patients with ruptured aneurysms died (unrelated to treatment). At

discharge and one month, 28 (6.6%) and 15 patients (4%) had a mRS >2. At discharge, 0 and five (1.4%) of 357 treated UA patients were dead or dependent (mRS>2). Operators assessed immediate angiographic results as complete obliteration or residual neck in 78% of cases. Analyses per allocated groups will be available at the time of the meeting.

Conclusions

Although immediate angiographic results may be suboptimal, bare platinum and hydrogel coiling can be performed very safely, even in large and recurrent aneurysms.

KEYWORDS: Aneurysm Embolization, Hydrocoil

O-505 8:37AM - 8:44AM
WEB device for intracranial aneurysm embolisation: A case series

M Igra¹, A Lawson², T Patankar¹, T Goddard¹
¹Leeds Teaching Hospitals, Leeds, UK, ²Leeds General Infirmary, Leeds, United Kingdom

Purpose

The WEB device is a novel device for the endovascular treatment of both ruptured and unruptured intracranial aneurysms. We present our experience in a series of patients treated at our institution.

Materials and Methods

This prospective study included 16 patients who were treated with the WEB device over a nine-month period. Aneurysm size, location and whether the aneurysm was ruptured or not was recorded, along with type and size of WEB device. Complications in the postoperative period also were documented.

Results

In all 16 cases a WEB device was deployed successfully. One case involved an acutely ruptured aneurysm. Complications were recorded in five cases, including thromboembolic events, aneurysm rupture and the necessity of a second stent. A right facial palsy and left sensory deficit was the result of a thromboembolic event. All 16 patients have survived at the time of submission.

Conclusions

This initial series of 16 patients shows that aneurysm embolization is feasible with WEB device. Long term follow up of these patients, along with larger cohort studies are needed to further evaluate this new technique.

KEYWORDS: Aneurysm Embolization, Aneurysm Treatment, Endovascular Embolization

O-506 8:44AM - 8:51AM
Low-Profile Visible Intraluminal Support Device (LVIS) Jr: Initial Multicenter Experience

D Iancu¹, A Quateen¹, J Raymond², A Weill², D Roy², H Lesiuk¹, M dos Santos¹, C Lum¹

Note: Scanned images are included in the proceedings. Some submitted images were reduced during editing thereby decreasing clarity. Also, refer to the Program Planner. Proceedings Content as of 3/28/2014.

¹University of Ottawa, Ottawa, Ontario, Canada, ²Centre Hospitalier de l'Université de Montréal - Notre Dame Hospital, Montreal, Quebec, Canada

Purpose

Wide-neck aneurysms incorporating a portion of the parent artery can be challenging to treat and may require combined balloon-remodeling and stent-assisted techniques. Low profile visible intraluminal support device (LVIS) Jr can be delivered through a remodeling balloon and is a new hybrid stent design that incorporates a lower porosity, is more navigable than current generation stents and also possesses some flow diversion characteristics. Study reports the initial multicenter experience using the LVIS Jr stent.

Materials and Methods

We reviewed the cases in which LVIS Jr was used in conjunction with coil embolization. Aneurysm characteristics, technical details, and periprocedural events were recorded. All patients were premedicated and maintained on dual antiplatelet therapy.

Results

We had 20 patients (13 females, 7 males) with 20 aneurysms (12 AComA, 3 MCA bifurcations, 4 BA termination and 1 LICA) treated using LVIS Jr devices. Two patients have been treated during acute phase of SAH. All but one stent were deployed successfully. The stent was placed before aneurysm coiling in 12 cases and as a bail out situation in seven cases, via a remodeling balloon in five cases. A "Y" stent construction was planned in five cases however, was only required in three cases, since only a single stent placement resulted in satisfactory coverage of the neck in two cases. Fourteen aneurysms were completely occluded initially and remained so at follow up, one patient progressed to complete occlusion on follow up. There were no permanent neurological procedural complications.

Conclusions

The LVIS Jr stent is a promising device for stent-assisted coiling. It has high navigability, can be delivered through a remodeling balloon and has flow-diversion characteristics which potentially expand the options currently available for management of wide-neck aneurysms.

KEYWORDS: Aneurysm, Aneurysm Treatment, Stents

0-507 8:51AM - 8:58AM
OVERALL BUENOS AIRES FLOW DIVERTERS EXPERIENCE AT SEVEN YEARS FOLLOW-UP

E Scrivano¹, R Nella Castro¹, P Lylyk¹, R Ceratto¹, A Ferrario¹, J Chudyk², J Chudyk¹, C Bleise¹

¹Eneri - Sagrada Familia, Buenos Aires, Argentina, ²Eneri, Buenos Aires, Argentina

Purpose

The aim of the study was to show the results of the use of flow diversion devices (FDD) in the treatment of wide neck, recanalized, dissecting, fusiform, giant and/or complex intracranial aneurysms (IA).

Materials and Methods

Between March 2006 and October 2013, 673 patients with 804 IA were treated. Female, 65.4%, median age was 58 years (Range 6-82 years). Pipeline (PED) was used in 497 patients with 599 IA; 57 patients with 66 IA with Surpass; 61 patients with 67 IA with CMFM; Silk was implanted in four patients (4 aneurysms); Sequent was used in 24 patients, (26 IA); and P64 in 29 patients (41 IA). Nine hundred fifty-nine devices were implanted.

Results

Intracranial aneurysms were 85.3% in anterior circulation; 22% were incidental and 78% were symptomatic IA; 51% were large and giant IA; 19% had been treated previously. All patients were under double antiplatelet drugs for 6-12 months post-treatment. Therefore our global morbimortality rate was 4.6% and 1.9% related to the procedure. The range of clinical and angiographic follow up was between three months and seven years.

Conclusions

Flow diversion device implantation showed low complications and high occlusion rate. In our seven-year experience with FDD we concluded that vessel repair is feasible, durable and achieves a definite endovascular reconstruction of parent vessel.

KEYWORDS: Aneurysm, Aneurysm Treatment, Flow Diverter

0-508 8:58AM - 9:05AM
SILK flow diverter for complex intracranial aneurysms- A Canadian registry

J Shankar¹, R Agid², J Ghostine³, D Iancu⁴, B Shettar⁵, A Weill⁶, J Wong⁷, D Tampieri⁸, M Cortes⁹, T Krings²
¹QE II Hospital, Halifax, Nova Scotia, ²Toronto Western Hospital, Toronto, Ontario, Canada, ³University of Montreal, Montreal, Quebec, Canada, ⁴The Ottawa Hospital, Ottawa, Ontario, Canada, ⁵Dalhousie University, Halifax, Nova Scotia, ⁶Centre Hospitalier de l'Université de Montréal - Notre Dame Hospital, Montreal, Quebec, Canada, ⁷University of Calgary, Calgary, Alberta, Canada, ⁸Montreal Neurological Institute and Hospital, Montreal, Quebec, Canada, ⁹Montreal Neurological Institute, Montreal, Quebec, Canada

Purpose

Flow diverter is a relatively new technology for treatment of complex intracranial aneurysms. There have been small case series in the literature with very few studies with larger number of patients. We are presenting the results of registry of patients treated with SILK flow diverter (SFD) in Canada.

Materials and Methods

Seven centers across Canada were contacted to fill out case report forms for patients treated with SFD in their center. The case report forms were sent to Dr. Jai Shankar in Halifax, where the final analysis was performed. Individual centers were responsible for approval from their ethics committee. The information then was collected and analyzed. The image analysis was performed by individual

Note: Scanned images are included in the proceedings. Some submitted images were reduced during editing thereby decreasing clarity. Also, refer to the Program Planner. Proceedings Content as of 3/28/2014.

operators. All patients were followed at least until aneurysms were completely obliterated.

Results

Total of 88 patients were treated with SFD in six centers in Canada since 2009. The number of patients varied from three to 25 across centers. The aneurysms were located on posterior circulation in 11 patients (Basilar-4; vertebral-7) and in anterior circulation in 69 patients (Cavernous ICA-20; Intracranial ICA-45; ACA-2; MCA-2). Most of the aneurysms were saccular in shape except 13 fusiform and three blister aneurysms. The size of aneurysms varied from 2 mm to 60 mm with the neck varying from 2- 48. Twelve and one half percent (Thromboembolic-7, Hemorrhagic-4) patients had peri-operative complications but only 8% had clinical manifestation. Two (2.3%) patients died. Thirty-four (39%) of patients had complete obliteration of the aneurysm; 19 (22%) had partial obliteration and another 35 (40%) had no information on this.

Conclusions

Overall SFD appears to be a safe and effective tool to treat complex intracranial aneurysms.

KEYWORDS: Aneurysm, Flow Diverter

O-509 9:05AM - 9:12AM
BLISTER-LIKE ANEURYSMS: ENDOVASCULAR
TREATMENT WITH FLOW-DIVERTING STRATEGY

E Scrivano, J Chudyk, D Prieto, P Lylyk, R Ceratto, J Lundquist, A Ferrario
Eneri- Sagrada Familia, Buenos Aires, Argentina

Purpose

The current literature describing neurosurgical and endovascular treatment of fragile blister-like aneurysms (BLA) offers no clear consensus on the optimal treatment modality. We present our experience in treating BLA with endovascular techniques.

Materials and Methods

We report 20 patients with 30 BLA, mean age 51 years, (range 30-70) that were treated using reconstructive endovascular technique with FD. Treatment, angiographic and clinical outcomes were evaluated retrospectively.

Results

Between October 2008 and October 2013, 23 patients with 33 BLA were seen. In this special cohort, 23 patients presented with subarachnoid hemorrhage (blood BLA), seven headache and three were incidental; 7 patients had multiple aneurysms. Dual antiplatelet therapy was indicated for the entire group. All patients were treated initially with 36 FD embolization devices. Three patients with subarachnoid hemorrhage required coiling before stenting. No rebleeding or thrombotic complication occurred periprocedurally. Long term control angiography was available in all patients. The occlusion rate at three, six and 12 months, was 90%, 100% and 100% respectively. Clinical outcome (mRS) was 0-2 in 16 patients and three in three patients. One patient died due to clinical complication.

Conclusions

Endovascular treatment of BA/Like-BA using a FD device may represent a valid alternative and a promising strategy that can be performed with acceptable clinical and radiological results.

KEYWORDS: Blister Aneurysm, Flow Diverter

O-510 9:12AM - 9:19AM
Flow Diverter Stenting in recanalized Intracranial
Aneurysms previously treated with a regular stent

A Biondi, E Pomeroy, F Descourvieres, E Farah, A Flores1
Besancon University Hospital, Besancon, France

Purpose

To evaluate clinical and angiographic results and long term follow up in a series of patients with a recanalized intracranial aneurysm previously treated using a regular stent.

Materials and Methods

Nine patients with a recanalized intracranial aneurysms treated by a regular stent and coils (1 neuroform stent in three patients, 1 enterprise stent in three patients, 2 enterprise stents in two patients and 1 Leo stent in one patient) were included in the study. Flow diverter stents were Pipeline stent (ev3 company) in six cases and Surpass stents in three. DynaCt or XperCT was used in all cases in order to evaluate correct deployment of the stent.

Results

Flow diverter stent deployment failed in one case and was very challenging in two. No clinical complications were observed immediately after the procedure and at follow up. All patients underwent long term angiographic and MR follow-up studies. Complete occlusion was observed in six of eight patients in whom the procedure was successful.

Conclusions

Flow diverter stenting in aneurysms previously treated with a regular stent remains a challenging procedure and should be reserved for selective cases. The evaluation of the full deployment of the previous stent could be difficult, however this information is crucial in order to plan a correct indication for flow diverter stenting.

KEYWORDS: Aneurysm Embolization, Flow Diverter, Interventional

O-511 9:19AM - 9:26AM
INTRASACCULAR FLOW DIVERSION FOR BIFURCATION
AND TERMINAL ANEURYSMS: BUENOS AIRES
EXPERIENCE

P Lylyk, C Bleise, R Ceratto, J Lundquist, E Scrivano, J Chudyk
Eneri - Sagrada Familia, Buenos Aires, Argentina

Purpose

WEB dual layer or WEB II, is the second generation of an intrasaccular flow diversion device planned for the treatment of bifurcation and terminal intracranial

Note: Scanned images are included in the proceedings. Some submitted images were reduced during editing thereby decreasing clarity. Also, refer to the Program Planner. Proceedings Content as of 3/28/2014.

aneurysms (IA). We report our initial experience in a series of patients treated with this device, regarding the feasibility, safety and mid-term follow up.

Materials and Methods

Between April 2012 and October 2013, the WEB II was implanted in 18 patients with 20 IA. Eighteen IA were in anterior circulation (1 ruptured). Middle cerebral artery (MCA) was the most common location (14 IA). Clinical or angiographic controls were performed at three and 12 months.

Results

The WEB II was deployed successfully in all patients; in three cases it was necessary to reposition the device. No hemorrhagic complications were observed; two patients presented thromboembolic complications, successfully treated with IA fibrinolytic. At three months the occlusion rate was 77.7%. Six aneurysms were controlled at 12 months: four showed complete occlusion, and two required retreatment with stent and coils. No hemorrhagic or ischemic complications in the follow up period. mRS 0 in all patients.

Conclusions

WEB II showed to be a safe alternative for the treatment of bifurcation and terminal aneurysms, with low rate of complications and retreatment. Longer follow up is necessary.

KEYWORDS: Aneurysm Treatment, Flow Diverter

0-512 9:26AM - 9:33AM
Utility of C-arm CT in Flow-Diverter Stent Imaging and Re-Expansion During Treatment of Intracranial Aneurysms.

B Mitchell¹, J Hartranft², G Chintalapani², P Chinnadurai², H Morsi³, H Shaltoni³, M Mawad¹

¹Baylor College of Medicine, Houston, TX, ²Siemens Medical Solutions USA Inc., Hoffman Estates, IL, ³St. Luke's Hospital, Houston, TX

Purpose

Treatment for intracranial aneurysms using flow-diverting stents has become more predominant over the past five years. Given the higher rate of flow-diverter stent usage and the often tortuous vessel anatomy and dense skull-base bone structure, stent disfiguration and flow disruption can occur, but this may be difficult to analyze with standard angiographic views. However, the use of intraprocedural C-arm computed tomography (CT) can greatly enhance an operator's ability to evaluate stent stenosis, aiding in stent apposition to vessel walls and correcting stenotic regions.

Materials and Methods

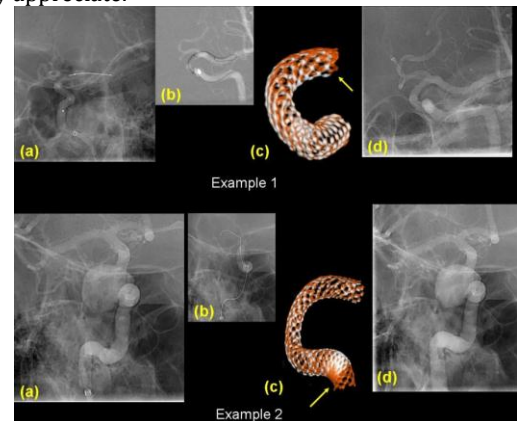
Intraprocedural C-arm computed tomography was used in a series of five patients undergoing endovascular treatment to determine areas of maximal stent stenosis during flow-diversion treatment of intracranial cerebral aneurysms. Following balloon angioplasty expansion of stenotic regions, C-arm CT was again used to re-evaluate stent conformation and apposition.

Results

Incomplete stent expansion and apposition to vessel walls was seen in five cases, using C-arm CT, after which balloon angioplasty was used in stenotic regions. C-arm CT was useful in predicting successful stent expansion in all five cases. Stent shortening could also be seen on postangioplasty C-arm CT, which may be a necessary component to successfully expanding the highly dense configuration of flow-diverting stents.

Conclusions

Use of C-arm CT in conjunction with standard angiography successfully allows for accurate visualization and optimal re-expansion of stenotic or distorted flow-diverter stents, especially in areas of dense or tortuous skull-base vascular anatomy that may otherwise be difficult or impossible to fully appreciate.



Examples of Pipeline Embolic Devices (PED) being deployed near the skull base, with poor visualization under fluoroscopic guidance alone (A, both examples). (B) Balloon angioplasty of the stenotic regions of the PED. (C) C-Arm CT reconstruction of the pre-angioplasty stent shape (red) and the post-angioplasty (white), showing expansion of previously stenotic regions as well as some stent shortening as a result of the stent expansion. (D) Post-Angioplasty fluoroscopy views.

KEYWORDS: C-Arm CT, Stenosis, Stents

0-513 9:33AM - 9:40AM
Prospective Study of Early MRI Appearances Following Flow Diverting Stent Placement for Intracranial Aneurysms.

S Memon¹, A Hope², B McGuinness²

¹Vancouver General Hospital, University of British Columbia, Vancouver, British Columbia, ²Auckland Hospital, Auckland, New Zealand

Purpose

Following pipeline embolization device (PED) and other flow diverting stent placement to treat intracranial arterial aneurysms, complications of delayed aneurysmal and parenchymal hemorrhage, with or without preceding symptomatology have been described (1-4). Speculation remains regarding the etiology of both forms of hemorrhage, with hemorrhage risk of 0-6% in reported series (4, 5). MR imaging (MRI) case reports (1, 2) have identified perianeurysmal edema, aneurysm expansion and

Note: Scanned images are included in the proceedings. Some submitted images were reduced during editing thereby decreasing clarity. Also, refer to the Program Planner. Proceedings Content as of 3/28/2014.

aneurysm wall enhancement in symptomatic patients prior to delayed aneurysm rupture. We sought to document whether such MR findings were common in asymptomatic patients following flow diverting stent insertion. There is limited literature on routine MR findings following flow diverting stents (6).

Materials and Methods

Patients requiring flow diverting stent placement for treatment or retreatment of cerebral aneurysms were included prospectively in the study over a 20-month period. Early postprocedure MRI studies were obtained between two and 10 days poststent placement and compared with pre-operative imaging. Aneurysm size, shape, surrounding edema, wall enhancement and the occurrence of parenchymal diffusion-weighted imaging (DWI) positive lesions were noted. Clinical data were gathered as to neurological symptomatology and clinical complications.

Results

Twenty-eight aneurysms in 27 patients were included in the study. Early postprocedure MRI studies were obtained in 24 patients. There were exclusions for claustrophobia (one) and booking errors (two). Two patients had delayed MRI beyond the target time, both at day 16. Two aneurysms were in the vertebrobasilar territory with the remainder anterior circulation. Median age was 53 years and median aneurysm pretreatment diameter was 13mm. Aneurysm mural enhancement was present in 64% of cases measuring 1-3mm thick. Mild (3mm or less) new perianeurysmal edema was present in 25% without clear association with headache. Aneurysm size was stable, or within 1mm of pretreatment dimension in all cases except one where the aneurysm asymptotically increased by 4mm (26mm from 22mm). Any DWI lesion was present in 54% cases. Thirty-three percent had more than five DWI lesions or any lesion greater than 5mm; two (2/27 or 8% overall) of these cases experienced clinical ischemic complications. New foci of susceptibility effect ipsilateral to the stent and almost always not associated with diffusion restriction were found in 43% (9/21) of cases that had susceptibility-weighted sequences performed. A further 29% of these studies (6/21) had susceptibility foci ipsilateral to the stent which were possibly new but did not have an earlier comparison SWI sequence. There were no cases of intracranial hemorrhage and no deaths.

Conclusions

Asymptomatic aneurysm mural enhancement and perianeurysmal edema frequently are seen following flow diverting stent placement. Such findings early after flow diversion should not necessarily be interpreted as a sign of impending aneurysm rupture. Diffusion-weighted imaging data suggest a comparable embolic risk to that reported with aneurysm coiling (7). New susceptibility foci following stent placement has not been reported previously but is common in our series. The etiology of this signal change is uncertain but may warrant further investigation with regard to its potential relevance to ipsilateral parenchymal hemorrhage following flow diversion.

KEYWORDS: Aneurysm Thrombosis, Flow Diverter, MR Imaging/MR Angiography

O-514

9:40AM - 9:47AM

3D-DSA reconstruction from Sparse Projections with C-arm CT

S Oishi¹, Y Chang², X Han³, X Pan³, T Satow⁴, M Silver², M Yamada⁴, H Yokoyama⁴

¹Toshiba Medical Systems Corp., Otawara, Tochigi, Japan,

²Toshiba Medical Research Institute USA, Vernon Hills, IL,

³The University of Chicago, Chicago, IL, ⁴National Cerebral and Cardiovascular Center, Suita, Osaka, Japan

Purpose

Three-dimensional digital subtraction angiography (3D-DSA) is the 3D imaging tool to provide detailed vessel structures, and is becoming indispensable in making decisions of treatment plans, especially for aneurysm cases. However, a certain amount of dose and contrast media are required in order to get feasible information for those purposes. We show the possibility that dose and contrast can be reduced without compromising image quality with total variation (TV), a form of iterative reconstruction.

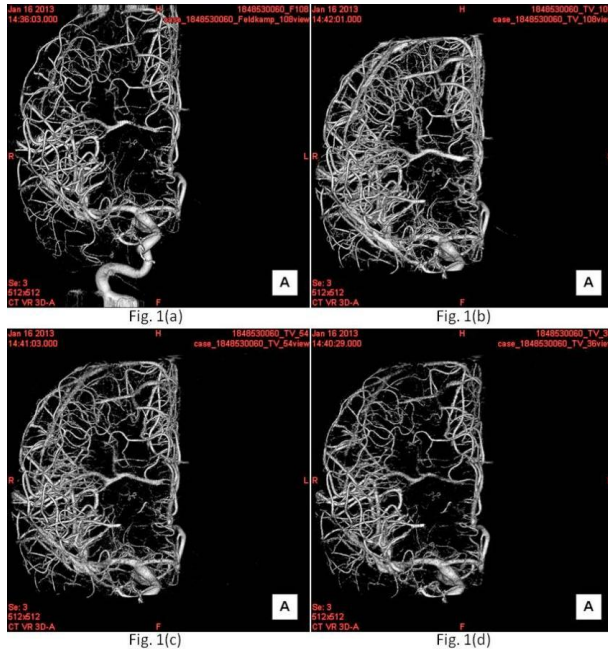
Materials and Methods

Ten sets of 3D-DSA projection data were used for this study, and each 3D-DSA projection data had 108 projections. Standard 3D-DSA images used in practice were reconstructed from 108 projections with the Feldkamp method. New 3D-DSA images, TV1s, TV2s and TV3s, were reconstructed with the TV method from 108, 54 and 36 projections, respectively. Projection data sets of 54 and 36 projections were retrieved by sampling every two and three projections, respectively. The TV1s, TV2s and TV3s were compared individually with the standard images by two experienced neuroradiologists/neurosurgeons, and a semi-quantitative five-point grading scale (1=poor, 4=comparative with the standard images 5= even better) were used for visibility of fine vessels and aneurysms.

Results

The standard image, TV1, TV2 and TV3 were shown on Figure 1(a), 1(b), 1(c) and 1(d), respectively. We could see comparable fine vessels on the standard image and TV2, and TV1 showed even finer vessels. Averaged five-point grading scales were 5, 3.9 and 3.3 for TV1s, TV2s and TV3s, respectively. TV3s would be inappropriate for diagnostic purposes, but would have significant information for guide-wire or catheter navigational purposes.

Note: Scanned images are included in the proceedings. Some submitted images were reduced during editing thereby decreasing clarity. Also, refer to the Program Planner. Proceedings Content as of 3/28/2014.



Conclusions

TV method showed image quality improvement compared with Feldkamp method to enhance clinical usefulness, and also showed that potential reduction of either x-ray dose or amount of contrast media.

KEYWORDS: Angiography

0-515 9:47AM - 9:54AM
Magnetically Assisted Remote Controlled Endovascular Catheter for Interventional MRI: In Vitro Navigation at 1.5T versus X-ray Fluoroscopy

S Hetts, R Arenson, D Cooke, P Lillaney, A Losey, A Martin, P Moftakhar, M Saeed, B Thorne, M Wilson, J Yang
University of California San Francisco, San Francisco, CA

Purpose

To compare in vitro navigation in a vascular phantom of a magnetically assisted remote controlled (MARC) catheter under real-time MR imaging (MRI with manual navigation under MRI and x-ray guidance in endovascular catheterization procedures.

Materials and Methods

A custom 2.9 French clinical grade microcatheter prototype with a solenoid coil at the distal tip was deflected with a foot pedal actuator used to deliver ± 300 mA. Investigators navigated the catheter into branch vessels in a custom cryogel abdominal aortic phantom. This was repeated under MRI guidance without magnetic assistance and under conventional x-ray fluoroscopy. MR imaging experiments were performed at 1.5 T using a b-SSFP sequence. The mean procedure times and percent success were determined and analyzed with a linear mixed effects regression analysis.

Results

The catheter was clearly visible under real-time MRI. One hundred and ninety-two (80%) of 240 turns were completed successfully with magnetically assisted guidance versus 144 (60%) of 240 turns with nonassisted guidance ($P < .001$) and 119 (74%) of 160 turns with x-ray guidance ($P = .028$). Overall mean procedure time was shorter with magnetically assisted than with nonassisted guidance under MRI (37 ± 6 s versus 55 ± 3 s, $P < .001$), and between magnetically assisted and standard guidance under x-ray (37 ± 6 s versus 44 ± 3 s, $P = .045$). When stratified by angle of branch vessel, magnetic assistance was faster than nonassisted MR guidance at turns of 45° , 60° , and 75° .

Conclusions

We have developed and tested a MARC catheter for endovascular navigation under real-time MRI guidance. For catheterization of branch vessels arising at large angles relative to the parent vessel, magnetic-assisted catheterization was faster than manual catheterization under MRI guidance and comparable to x-ray guidance. This work forms the foundation for improved endovascular catheter navigation under MRI, enabling further exploration of simulated interventions for the treatment of stroke, vascular malformations, and tumors - all of which may benefit from the physiologic information available through real-time MRI but not x-ray fluoroscopic guidance.

KEYWORDS: Devices, Image-Guided Procedures

0-516 9:54AM - 10:01AM
Does Configuration And Location Of Intracranial Aneurysm Influence Pipeline Stent Deployment? Single Center Analysis

K Malhotra, R Ramanathan, A Ku
Allegheny General Hospital, Pittsburgh, PA

Purpose

Pipeline embolization device (PED) is an FDA approved flow diverting stent indicated for endovascular treatment of large or giant wide-necked intracranial aneurysms (IAs) located in anterior circulation. Pipeline embolization devices have shown encouraging results in PITA and PUFs studies, but limited data exists on their use in posterior fossa IAs and the number of stents used in different types of aneurysms. We hypothesize that fusiform aneurysms require more PEDs to achieve complete occlusion.

Materials and Methods

We reviewed 15 patients who underwent pipeline stenting for various IAs between June 2011 and July 2013. Inclusion criteria included patients who were unsuitable for coiling/clipping, had nonruptured aneurysms and without any prior interventions. Several patients had pre-existing neurological deficits with cranial nerve or brain stem compression. All patients were continued on dual antiplatelet therapy and platelet assays were obtained before and after the surgery. Follow-up conventional angiograms were performed at six and 12 months with

Note: Scanned images are included in the proceedings. Some submitted images were reduced during editing thereby decreasing clarity. Also, refer to the Program Planner. Proceedings Content as of 3/28/2014.

CTA at 24 months, while morbidity was evaluated using Barthel Index before and three months after the procedure. Presence of a residual aneurysm was assessed on catheter angiograms using Raymond criteria.

Results

Mean size and volume of aneurysms recorded were 17.3 mm and 2940.5 mm³ respectively. There were eight fusiform (n=8) and eight saccular (n=7) aneurysms in our cohort. A total of 59 PEDs were placed with 15 stents in saccular and 44 stents in fusiform type of IAs. There were no long term clinical complications, in-stent stenosis, aneurysmal ruptures or lobar hemorrhages; while five patients developed restricted diffusion on MR imaging (MRI) scans during peri-operative period (<30 days). Complete resolution of aneurysmal sac was noted in 11 (73.3%) patients on follow-up angiograms, while two of four failure cases were basilar fusiform IAs which did not show complete resolution.

Conclusions

We conclude that fusiform IAs require more PEDs to achieve successful occlusion. Interestingly, deliberate lower mesh density used in treatment of basilar aneurysms due to risk to perforators result in higher rates of incomplete occlusion.

KEYWORDS: Aneurysm Sizes, Pipeline Embolization Device

0-517 10:01AM - 10:08AM
The Penumbra Coil 400 System Beyond Intracranial Aneurysms - Initial Experience with 19 Unusual Lesions

E Wyse¹, M Pearl², M Radvany², P Gailloud¹

¹The Johns Hopkins Hospital, Baltimore, MD, ²The Johns Hopkins University School of Medicine, Baltimore, MD

Purpose

The Penumbra Coil 400 is a new large size detachable coil system (coil diameter 0.020, coil length up to 60cm). This increased coil size requires the use of a larger delivery microcatheter (Penumbra PX Slim). While the system has proved to be efficient for the embolization of intracranial saccular aneurysms, its potential role in the treatment of more unusual lesions remains unclear. This report describes a series of patients treated with the Penumbra Coil 400 system for indications other than intracranial saccular aneurysms.

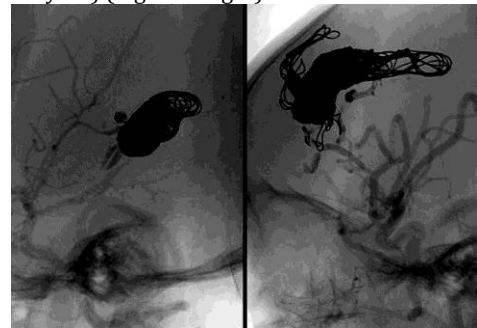
Materials and Methods

We report 19 consecutive procedures performed over a one-year period in 13 adult and six pediatric patients (age range 1 week to 75 years), including embolizations for transverse sinus dural arteriovenous fistulas (DAVF) (5 cases), other cranial, cervical, or spinal arteriovenous fistulas (AVF) (6 cases), vein of Galen arteriovenous malformations (VGAM) (2 cases), as well as four cases of internal carotid artery sacrifice, and two cases of splenic or renal aneurysms embolizations. The endovascular access was either transarterial (8 cases) or transvenous (9 cases). In pediatric cases, a 4-French diagnostic catheter was used as the guiding catheter. In two instances (diploic AVF and

DAVF), the lesion was accessed by direct puncture using the outer dilator of a micropuncture set.

Results

All the procedures were technically successful, without periprocedural or immediate postprocedural complications. Each of the targeted lesions could be accessed with the Penumbra PX catheter, in spite of its larger caliber, including navigating tortuous spinal venous networks or access via a micropuncture dilator in cases performed by direct puncture. Complete occlusion of the lesions was achieved in all but one case. The latter patient was a one-week old baby with a VGAM, who remained in cardiorespiratory failure in spite of three transarterial embolizations; transvenous occlusion of the venous aneurysm was performed, with persistent minimal flow through the coil pack at the end of the procedure, while still fully heparinized. The large size of the coils was found to be particularly advantageous in pediatric cases, where the reduced number of needed coils directly translated into shorter procedural times, limiting radiation exposure. As illustrative examples, the embolization of a VGAM in a two-year-old boy was achieved with a total of 18 coils (radiation dose: 124.3 mGy, 834.13 uGym²) (Figure 1 left), the treatment of a complex intracranial AVF in a six-month-old girl with 30 coils (radiation dose: 139.5 mGy, 346.68 uGym²) (Figure 1 right).



Conclusions

The Penumbra Coil 400 system was, in our experience, successful in treating a range of unusual lesions both in adults and children. Besides potential financial and logistic advantages, the decreased procedural times made possible by the reduced number of coils needed to achieve complete embolization was felt to be particularly advantageous in children, where radiation dose limitation is critically important.

KEYWORDS: Devices, Endovascular Therapy

Wednesday, May 21
10:30 AM – 12:00 PM
Room 517bc

60 - Special Session

Note: Scanned images are included in the proceedings. Some submitted images were reduced during editing thereby decreasing clarity. Also, refer to the Program Planner. Proceedings Content as of 3/28/2014.

0-518 10:30AM - 11:00AM
Keynote Speaker: A Unifying Role for Prions in
Neurodegenerative Diseases

Prusiner, S.
University of California, San Francisco
San Francisco, CA

Abstract/Presentation Summary

Mounting evidence argues that prions feature in the pathogenesis of many, if not all, neurodegenerative diseases. Such disorders include Alzheimer's, Parkinson's, Lou Gehrig's and Creutzfeldt-Jakob diseases as well as the frontotemporal dementias. In each of these illnesses, aberrant forms of a particular protein accumulate as pathological deposits referred to as amyloid plaques, neurofibrillary tangles, Lewy bodies, as well as glial cytoplasmic and/or nuclear inclusions. The heritable forms of the neurodegenerative diseases are often caused by mutations in the genes encoding the mutant, prion proteins that accumulate in the CNS of patients with these fatal disorders. The late onset of the inherited neurodegenerative diseases seems likely to be explained by the protein quality control systems being less efficient in older neurons and thus, more permissive for prion accumulation. To date, there is not a single drug that halts or even slows one neurodegenerative disease.

0-519 11:00AM - 11:15AM
Neurodegeneration and Brain Connections: The Role of
Neuroimaging

Petrella, J.
Duke University Medical Center
Durham, NC

0-520 11:15AM - 11:30AM
CLARITY & Beyond: Towards Integrative Understanding of
the Brain in Health and Disease

Chung, K.
Massachusetts Institute of Technology
Cambridge, MA

Abstract/Presentation Summary

Obtaining detailed structural and molecular information from complex biological systems while simultaneously maintaining the global perspective has long been a fundamental challenge in neuroscience and throughout biology. Current pioneering methods, while proven adequate to study small-scale fine structures, fall short of providing integrated system-wide information. To address this challenge, we have developed a novel technology (which we term CLARITY) that rapidly transforms intact tissue into a hydrogel hybrid that is optically-transparent and macromolecule-permeable while retaining structural and molecular information. This unique framework enables effective and complete access of intact tissue using both light microscopy and molecular phenotyping techniques (immunohistochemistry and in situ hybridization). Exogenous macromolecules can rapidly penetrate deep into transmuted tissue for labeling and can be completely removed after imaging, enabling multiple

rounds of molecular interrogation in 3D volumes of tissue. The application of CLARITY to the adult mouse brain has enabled imaging of long-range circuits, local circuits, subcellular morphological details, and molecular architectures. Finally, we find that this technique allows fine structural analysis of postmortem human brain, opening the door to the possibility of mapping the human brain at single cellular resolution with integrated molecular information. Taken together, this technology promises to provide high-content system-wide structural and molecular information that may enable integrative understanding of large-scale intact biological systems.

0-521 11:30AM - 12:00PM
The Human Connectome Project

Van Essen, D.
Washington University School of Medicine
St. Louis, MO

Abstract/Presentation Summary

Recent advances in noninvasive neuroimaging enable the systematic exploration of human brain circuits in health and disease. The Human Connectome Project (HCP) is systematically characterizing brain circuitry, its variability, and its relation to behavior in a population of 1,200 healthy adults (twins and their non-twin siblings). This talk will review progress by the HCP consortium in acquiring, analyzing, and freely sharing these massive and highly informative datasets. The HCP obtains information about structural and functional connectivity using diffusion MRI and resting-state fMRI, respectively. Additional modalities include task-evoked fMRI and MEG, plus extensive behavioral testing and genotyping. Each of these methods is powerful, yet faces significant technical limitations that are important to characterize and be mindful of when interpreting neuroimaging data. Comparisons with anatomical data obtained in nonhuman primates aid in evaluating different imaging methods and also yield insights regarding the evolution of human cerebral cortex. Advanced visualization and analysis methods developed by the HCP enable characterization of brain circuits in individuals and group averages at high spatial resolution and at the level of functionally distinct brain parcels. Comparisons across subjects are beginning to reveal aspects of brain circuitry that are related to particular behavioral capacities and which are heritable or related to specific genetic variants. Data from the HCP is being made freely available to the neuroscience community via a user-friendly informatics platform. Altogether, the HCP is providing invaluable information about the healthy human brain and its variability. It will set the stage for characterizing brain circuits during healthy development and in abnormal brain connectivity in many brain disorders and diseases.

Note: Scanned images are included in the proceedings. Some submitted images were reduced during editing thereby decreasing clarity. Also, refer to the Program Planner. Proceedings Content as of 3/28/2014.

Wednesday, May 21

1:00 PM – 2:30 PM

Room 517bc

61 - ASSR Programming: Controversies
in Spine Trauma (SAM)

O-522 1:00PM - 1:15PM
MRI in Spinal Injury

Van Goethem, J.
University Hospital Antwerp
Antwerp

Abstract/Presentation Summary

MRI has gained importance in imaging of spinal trauma with its increased availability for the emergency room physician. It is apparent that the depiction of the spinal cord is of primary importance, and with the adoption of MR, the utility of myelography and post-myelography CT has diminished to the point of vanishing (in the absence of contraindications to MR). MR is capable of depicting the vertebra and supporting structures, intervertebral disks, the spinal cord and nerve roots, and trauma-associated injuries such as hemorrhage, traumatic disk herniations, and primary cord injury such as hematomas, edema, and even cord transection. Any patient with presumed spinal cord injury should undergo an emergent MR study. MR is superior at depicting the previously mentioned lesions which guide surgical management in these patients. Careful clinical examination with a determined level of injury is an excellent means of directing the level to be studied. Many trauma protocols may also mandate evaluation of the other spinal segments to exclude additional injury which may be masked by a higher level spinal cord injury. The sensitivity of MR for injuries of the soft tissue associated with trauma is well known, but MR may also demonstrate changes within the bone marrow of traumatized vertebrae which are inapparent on plain film studies, and even on CT, such as bone contusions. MR has also been shown to be both sensitive and specific for ligamentous injury in the trauma setting. We have used MR to provide a "ligament screen" exam for major trauma patients for several years now, with consistent results. The typical exam protocol for this purpose includes sagittal T1, sagittal T2, and sagittal STIR images, as well as axial imaging. Edema in the interspinous or supraspinous ligaments is particularly conspicuous on STIR images. Some observers may prefer fat-suppressed T2 images, which provide similar conspicuity of the changes of ligamentous injury. In whiplash patients special attention to the ligaments of the craniocervical junction is important. In these patients a dedicated 3D proton density sequence with thin reconstructed slices is able to show lesions to the transverse, alar and atlanto-occipital ligaments as well as the tectorial membrane.

O-523 1:15PM - 1:30PM
Dynamic or Static Imaging? Flexion/Extension Imaging of
the Spine

Go, J.
LAC/USC Medical Center
Los Angeles, CA

Abstract/Presentation Summary

Flexion/extension imaging of the cervical spine has been used to examine spinal alignment, ligamentous integrity, and instability. Different methodologies have been used including the use of static and dynamic imaging with or without weight bearing as well as different modalities including plain radiography, fluoroscopy, CT and MRI. The use of flexion/extension imaging still remains controversial and currently there is no level I data in spine literature which verifies its use in imaging. This lecture will examine the controversial role of flexion/extension imaging in the assessment of ligamentous integrity and laxity, instability, and presence or absence of pseudoarthrosis or non-union. The information gained from flexion/extension imaging will be reviewed as well as normative values used in the different imaging modalities. Though controversial, the information used from flexion/extension imaging is still used to determine medical and surgical management.

O-524 1:30PM - 1:45PM
Is There a Role for MRI in Ligamentous Injury of the Spine?

Parizel, P.
Antwerp University Hospital/University of Antwerp

Abstract/Presentation Summary

Traumatic injuries of the spine and spinal cord are common, devastating and potentially lethal lesions. Imaging studies are essential to ascertain the exact location of the injury, to discern between stable and instable lesions, to evaluate the impact of the traumatic event on the spinal cord and nerve roots, and on the diameters of the spinal canal and neural foramina. Increasingly, MRI has become a useful and even mandatory adjunct to 'clearing' the spine. In obtunded patients with cervical spine injury, while multi-detector row CT is reported to have negative predictive values as high as 98.9% for ligament injury and 100% for unstable cervical spine injury, still MRI remains the method of choice for showing spinal cord contusion, ligamentous injury, intervertebral disk edema and bone marrow edema. MRI provides direct evaluation of the spinal soft tissue structures, including ligaments, neural structures (spinal cord and nerve roots), intervertebral disks, and vasculature. An abnormal MRI after normal plain X-ray films and CT cervical spine examinations can result in a change of management. Moreover, it has been shown that an initial MRI evaluation after spinal cord injury provides supplemental prognostic information on the recovery of motor function in the upper and lower extremities. Correct identification of soft tissue injuries has a direct influence on patient management, helps to make a decision about acute surgery, and impacts prognosis. Literature data indicate that reliance on CT imaging alone to "clear the cervical spine" after blunt trauma can lead to missed injuries. There is increasing evidence to support the

Note: Scanned images are included in the proceedings. Some submitted images were reduced during editing thereby decreasing clarity. Also, refer to the Program Planner. Proceedings Content as of 3/28/2014.

addition of MRI in evaluating spine trauma patients who are obtunded, or unexaminable, despite a negative CT scan. While multidetector CT is still the modality of choice for most patients admitted with spine trauma, the role of MRI is rapidly growing, because of its ability to directly evaluate the soft tissues of the spine. Early and accurate identification of injury to the neural structures (spinal cord and nerve roots), soft tissues (intervertebral disks, ligaments, muscles) and vascular structures has a great impact on patient management and outcome. Moreover, the identification of ligamentous injury of the spine may have important medicolegal consequences.

0-525 1:45PM - 2:00PM
Medicolegal Aspects of Imaging Spine Trauma

Kim, P.
University of Southern California
Los Angeles, CA

Abstract/Presentation Summary
One of the major pitfalls faced by physicians is a lack of understanding of the basic legal aspects of medical malpractice. There are several salient points to consider . Vigilance and minimizing errors is always most desirable, but error-free neuroradiology is unattainable. Best medical judgment, although not error free, is at least defensible as noted in the case law discussed here. Errors of protocol, on the other hand, are extremely difficult to defend, particular failure to communicate significant results. Understanding this alone will reduce risk immeasurably. Errors resulting from bias, particularly alliterative errors, are most insidious and require significant self-vigilance. Many of these errors, as well as perceptual errors, are the result of rushing, distraction, or fatigue resulting from high-volume workloads. Other pitfalls are not under the radiologist's control. One unfortunately cannot easily choose the clinical colleagues associated with his or her practice but vigilance for their errors can certainly reduce the risk of being sued. Finally, because cervical spine trauma are is commonly associated with malpractice litigation, heightened caution and vigilance for potential missed diagnoses is emphasized.

2:00PM - 2:30PM

Discussion and Questions

Wednesday, May 21
1:00 PM – 2:30 PM
Room 517d

62 - SNIS Programming: Acute Stroke
Imaging and the Real World

0-526 1:00PM - 1:30PM
Acute Stroke Imaging: Use of CT Modalities for
Endovascular Management Triage Decisions - Denver
Experience

Frei, D.
Radiology Imaging Assoc.
Lakewood, CO

0-527 1:30PM - 2:00PM
Acute Stroke Imaging: Use of Combined CT and MRI
Modalities for Endovascular Management Triage Decisions
- Cleveland Clinic Experience

Hussain, M.
Cleveland Clinic
Cleveland, OH

Abstract/Presentation Summary
Stroke secondary to large vessel occlusion remains a devastating disorder. Intra-arterial stroke therapy shows promise as a treatment for this condition. However, despite improved recanalization rates, patient outcomes have not shown improvement in clinical trials of intra-arterial stroke therapy. This likely is due to issues of patient selection. In order to improve patient selection, a "Hyperacute MRI" protocol was initiated at the Cleveland Clinic in 2010. Since implementation, the volume of procedures for IAT was cut in half, with substantial improvement in outcomes and reduced mortality. The talk will focus on the development and implementation of the Hyperacute MRI protocol, with a discussion of the changes in outcomes and future directions.

0-528 2:00PM - 2:30PM
Care Paths and Advanced Stroke Imaging Triage:
Implications for Cost Repositioning and Longitudinal Care
Strategies

Modic, M.
Cleveland Clinic Foundation
Cleveland, OH

Abstract/Presentation Summary
CarePaths are organized around a medical condition in order to reduce unnecessary variations in patient care over time, venue and provider. Validated health status measures/outcomes, process, cost and patient experience are tied together and embedded within the electronic medical record. This construct provides the infrastructure necessary for continuous improvement, cost repositioning and longitudinal care strategies. The stroke carePath model will be used to illustrate the interplay between care coordination, innovation, care transformation and cost using examples at the individual patient and population levels. The importance of the interplay of workflow, regional implementation and care management will be illustrated.

Note: Scanned images are included in the proceedings. Some submitted images were reduced during editing thereby decreasing clarity. Also, refer to the Program Planner. Proceedings Content as of 3/28/2014.

Wednesday, May 21
1:00 PM – 2:30 PM
Room 517a

63 - International Session: ASNR
Introduces Its First Bilingual Session:
Society of French Neuroradiology

O-529 1:00PM - 1:10PM
Brain Perfusion Imaging Techniques in Neonates

Proisy, M.
CHU Rennes Hospital SUD
Rennes

O-530 1:10PM - 1:20PM
Quantitative DTI for Prognostic Evaluation in Acute Brain Injury

Galanaud, D.
UPMC Paris Universit s
Paris

O-531 1:20PM - 1:30PM
Cerebrovascular Reserve in Clinical Practice

Krainik, A.
University Hospital of Grenoble
Grenoble

O-532 1:30PM - 1:40PM
MRI Red Flags Against the Diagnosis of Multiple Sclerosis

Dousset, V.
Universite Bordeaux Segalen
Bordeaux, Bordeaux

O-533 1:40PM - 1:50PM
Exome Sequencing of Familial Form of Intracranial Aneurysm

Bourcier, R. · Desal, H.
University Hospital of Nantes
Nantes

Abstract/Presentation Summary
Introduction : Familial form of intracranial aneurysm (ICA) is defined by the presence of two or more first-degree relatives with ICA. It is considered that about 10% of all ICA occurs in a familial context but this may be an underestimation. Nowadays genetic analysis has not allowed identifying any gene involved in familial forms of ICA. In the present study, we aim to discover rare genetic variants causally related to ICA in large French families. Material and methods : Among families followed in our center (Departement of Neuroradiology of CHU Nantes, France), we have selected two large families with more

than 5 siblings affected by ICA. Disease segregation in these families is consistent with autosomal-dominant inheritance model. Syndromic forms of ICA were ruled out in the index case by medical genetic consultations. First- and second-degree relatives aged over 20 years were screened with encephalic MRI for the presence of ICA. Blood sample was taken from each patient. Whole-exome sequencing was performed for two relatives in each family with IAC. Sequence data analysis was carried out with Samtools and GATK algorithms. Series of filters were applied to exclude variants which are unlikely to contribute to ICA, such as those with a minor allele frequency above 1% in the general population. The remaining variants were prioritized using the following criteria. Genes were given higher priority if (1) they were related to selected categories and genes of interest in the Gene Ontology (GO) database; (2) more affected individuals within the family carried the variant; (3) any controls sent from the family of interest did not carry a variant within the gene; (4) the variants within the gene were predicted to be deleterious by protein prediction programs (SIFT, Polyphen2); (5) they were within a highly conserved region as defined by GERP. Results : After whole-exome sequencing, a mean coverage of 124X was achieved for the coding portion of the genome. On average, 89% of the targeted bases were covered by at least 20 sequencing reads. Among the 29 rare non synonymous variants shared by two affected relatives from the first family, we have identified one non sense variant within a gene involved in angiogenesis. We are currently sequencing this gene in additional ICA cases. Functional investigations are also ongoing. Conclusion : Our study has already led to the identification of a rare variant in a gene potentially involved in the aneurysm formation in a large ICA family. This could help us to identify pathways and mechanisms causing the formation and rupture of ICA. We could then, based on this information, better select which patient to screen, to follow and to treat among people with IAC.

O-534 1:50PM - 2:00PM
State of the Art and New Algorithms of Endovascular Treatment for Intracranial Aneurysm

Spelle, L.
Beaujon Hospital
Paris, Paris

O-535 2:00PM - 2:10PM
Advanced Hemodynamic Profiling of Intracranial Aneurysms Prior to Flow Diversion

Eker, O.
CHU Montpellier
Montpellier, --

O-536 2:10PM - 2:20PM
Randomized Trial in Acute Stroke Therapy: THRACE Intermediate Results

Bracard, S.

Note: Scanned images are included in the proceedings. Some submitted images were reduced during editing thereby decreasing clarity. Also, refer to the Program Planner. Proceedings Content as of 3/28/2014.

CHU Nancy
Nancy, Nancy

Abstract/Presentation Summary

Methods All patients aged between 18 and 80 years with an acute ischemic stroke occurred within 4 hours are eligible for the study. Inclusion criteria are an occlusion of the intracranial carotid artery, the M1 portion of the middle cerebral artery or the upper third of the basilar and with a NIHSS score between 10 and 25. All the patients are treated with the reference IV treatment (0,9 mg/kg of rTpa). In the thrombectomy arm, thrombectomy is performed at the end of IV perfusion, with one of the thrombectomy device available. The modified Rankin Score at 3 month after treatment is the primary outcome. Secondary outcomes are the Barthel score at 3 month and the Quality of Life with Euroqol EQ-5D generic questionnaire at 3 and 12 months after treatment. The sample size was estimated at 480 patients. 325 were already included at the end of 2013. After the intermediate analysis of the first 220 patients, the Safety Committee recommendation was to continue the study.

O-537 2:20PM - 2:30PM
Diversion: French Prospective Observational Registry in Flow Diversion for Intracranial Aneurysms

Turjman, F.
University of Lyon
Lyon

Abstract/Presentation Summary

F.Turjman (1), L. Spelle (2), J. Berge (3), L. Pierot (4), L. Huot (6), F. Chapuis (6), A. Bonafe(5), Department of Neuroradiology from Lyon (1), Paris Beaujon (2), Bordeaux (3), Reims (4) and Montpellier (5) and Pôle Information Médicale Evaluation et Recherche (IMER) Hospices Civils de Lyon (6). INTRODUCTION: The goal of this study was to assess the impact of flow diverter (FD) devices in the treatment of intracranial aneurysms on aneurysmal occlusion rates, morbidity, mortality, and complication rates in an unselected cohort subjected to real life clinical practice. The current study was designed by the French Society of Neuroradiology in collaboration with the French Agency for drugs and devices safety (ANSM) in order to monitor all flow diverters (FD) used in France in the treatment of intracranial aneurysms from October 8th, 2012 to February, 7th 2014. We report here an interim analysis concerning the immediate (intra and peri-procedural) results of endovascular treatment of intracranial aneurysms with FD. of patients enrolled during the first year of the study. METHODS: The inclusion criteria were the use of a FD in the treatment of an intracranial aneurysm in patient older than 18 year who agreed to participate to the study. The primary endpoint was the rate of morbi-mortality at 1-year. This prospective study involved all active French centers. SAEs were assessed by an independent DSMB and the imaging data were reviewed by 2 interventional neuroradiologists independent to the study. Exhaustivity of the data will be assessed by crossing

the reported data in a given center with the sales reported by the companies. The study was funded by the neuroendovascular companies and sponsored by the French Society of Neuroradiology. Data of patients enrolled during the first year of the study in the centers having included 10 patients or more are considered here. 10% of all files and all SAE were monitored by an independent CRO. Descriptive analysis of aneurysms characteristics and clinical results of the procedures was performed. RESULTS: From October 8th 2012 to October 7th 2013, 308 patients were enrolled in the study in 17 centers in France and treated with the flow-diverter devices (FD). Among these patients, data from 223 (72.4%) with 266 cerebral aneurysms treated, representing 228 procedures, were available for the analysis. Aneurysm size was >15 mm for 31 (11.7 %), 5-15 mm for 129 (48.5%), and <5 mm for 106 (39.9%). Aneurysm locations were extradural in 38 cases and intradural in 224. For intradural aneurysms, the location was supraclinoid internal carotid artery (ICA) in 117 cases (52.2%), middle cerebral artery in 30 (13.4 %), posterior communicating artery (PCoA) in 9 (4.0%), and anterior communicating artery (ACoA) in 14 (6.3%). The vertebrobasilar system accounted for 12 cases (5.4%) and paraclinoid for 27 (12.1%). Three aneurysms were not treated. At least 274 FD were used: 165 (60.2%) were PIPELINE Embolisation Devices (Covidien); 76 (27.7%) Silk (Balt); 20 (7.3%) FRED (Microvention); 11 (4.0%) SURPASS Neuroendograft System (Stryker); and 2 devices were not identified. In 38 (14.5 %) case aneurysms, devices were used with coils. Success rate was 94.9%. Complete stasis was obtained in 38 (14.7%) aneurysms, significant flow reduction in 69 (26.7%), Adverse events occurred during 39 patients procedures (17.1%). During hospitalization, 27 SAEs occurred, including 7 hemorrhages, 12 ischemic events, and 1 visual impairment. Three patients died from cerebral hemorrhage. At discharge, overall morbidity rate were was 20.6%. CONCLUSION: Our prospective study confirms that morbidity and mortality rates in treatment with FD rates in an unselected cohort subjected to real life clinical practice do not differ from those reported in the largest series.

Wednesday, May 21

1:00 PM – 2:30 PM

Room 520

64 - Advanced Imaging Seminar:
Translational Advanced Non-Gaussian
Diffusion Imaging

O-538 1:00PM - 1:30PM
Gaussian vs. Non-Gaussian Diffusion - Who Cares and Why You Should!

Jensen, J.
Medical University of South Carolina
Charleston, SC

Note: Scanned images are included in the proceedings. Some submitted images were reduced during editing thereby decreasing clarity. Also, refer to the Program Planner. Proceedings Content as of 3/28/2014.

Abstract/Presentation Summary

Diffusion MRI (dMRI) encompasses a variety of specific methods that exploit the ability to sensitize the MRI signal to water diffusion by applying strong magnetic field gradients during the pulse sequence. These "diffusion gradients" cause spin dephasing that is enhanced by molecular motion. Thus tissues with stronger diffusion will have a reduced dMRI signal. The various dMRI methods differ in the choice of the diffusion gradients (e.g., their strengths, directions, and durations) and in the algorithms used for post-processing of the data. These distinctions determine what aspects of water diffusion can be quantified. For clinical dMRI, the most widely used technique is diffusion tensor imaging (DTI) [1]. However, DTI is based on an approximation that water diffusion is Gaussian. This means that the distribution of water molecule displacements for a given time interval is idealized as obeying a Gaussian (i.e., normal) probability distribution. For water in a homogeneous solution, this would typically be an excellent assumption. In contrast, water diffusion in brain departs significantly from a Gaussian form and is therefore referred to as "non-Gaussian diffusion." This diffusional non-Gaussianity is a consequence of restrictions, such as cell membranes, and compartmentalization, such as for the inter- and extra-cellular water pools [2]. For this reason, diffusional non-Gaussianity is a natural indicator of microstructural complexity in brain tissue. Nonetheless, there are no measures provided by DTI that quantify this property, and DTI imaging protocols are, in fact, designed to minimize non-Gaussian diffusion effects, in order to be consistent with the assumptions underlying this technique. To access the information associated with non-Gaussian diffusion, several "advanced" dMRI methods have been proposed, including high angular resolution diffusion imaging (HARDI) [3-5], diffusion spectrum imaging (DSI) [6], and diffusional kurtosis imaging (DKI) [7]. All these approaches share the feature that dMRI data is acquired with somewhat larger diffusion weightings than typical for DTI, which increases the sensitivity to non-Gaussianity. HARDI, which refers to several related techniques, focusses on trying to improve the angular resolution to which the water diffusion can be characterized. This is particularly useful for white matter fiber tractography and provides a resolution to the so-called "fiber crossing problem" of DTI-based fiber tractography [8]. DSI is a method of quantifying the distribution of diffusion displacements without making any assumptions about its form. DKI is designed to be a minimal extension of DTI that includes metrics of non-Gaussianity and aims to maintain the practical advantages of DTI to the extent possible.

0-539 1:30PM - 2:00PM
Selected Application: Stroke

Sun, P.
A. Martinos Center for Biomedical Imaging, Radiology,
MGH and Harvard Medical School
Charlestown, MA

0-540 2:00PM - 2:30PM
Selected Applications: Brain Tumor & Huntington's Disease

Van Caeter, S.
University Hospitals Leuven
Belgium

Abstract/Presentation Summary

Although different methods have been proposed to measure non-Gaussian diffusion, most clinical studies investigating the non-monoexponential diffusion related signal decay, apply the DKI model. The intuitive concept of DKI as an extension of the widely used DTI technique and the implementation of b-values, readily implementable in routine clinical and experimental scanners, have proven this technique attractive in the non-invasive investigation of several neuropathologies. In this lecture, we will focus on the role of DKI in characterizing the microstructural complexity in gliomatous brain tumours. Kurtosis related parameters have proven to be more accurate than conventional diffusion metrics in determining glioma grade. Furthermore, we will discuss a potential role of DKI in differentiating therapy related changes from tumor relapse in glioblastoma patients. The second part of the lecture will focus on the added value of DKI in the identification of biomarkers in Huntington's disease. Although this devastating disease is most often diagnosed in mid-life, it is known that the key to its clinical expression may be found during brain maturation. Recent experimental studies have shown the DKI-related parameters are promising to assess changes in tissue microstructure and detect alterations during neurodevelopment.

Wednesday, May 21
1:00 PM – 2:30 PM
Room 524

65 - General Programming –
Subspecialty and Regional Society and
Regional Society Award Papers, Dyke
Award, Foundation of the ASNR Papers

0-547 1:00PM - 1:20PM
Gold Medal Award Winner Presents

Naidich, T.
Mount Sinai Hospital
New York, NY

0-542 1:20PM - 1:30PM

Note: Scanned images are included in the proceedings. Some submitted images were reduced during editing thereby decreasing clarity. Also, refer to the Program Planner. Proceedings Content as of 3/28/2014.

Louis A. Gilula, MD Mentor Award - American Society of Spine Radiology (ASSR) - Simulation-Based Educational Curriculum for Lumbar Puncture to Improve Operator Confidence and Efficiency

McLaren, T.
Medical University of South Carolina
Johnson City, TN

Abstract/Presentation Summary

A Bourgeois¹, T McLaren², K Hudson, MD¹, A Pasciak¹, A Faulkner¹, E Heidel¹, Y Bradley¹ ¹ University of Tennessee Department of Radiology and Graduate School of Medicine. Knoxville, TN. ² East Tennessee State University Quillen School of Medicine. Johnson City, TN. Introduction: The use of anthropomorphic detail phantoms in simulation-based medical education has rapidly increased in the past few decades, aimed at improving operator confidence and patient outcomes. However, further adaptation of simulation-based procedural instruction is often cost-prohibitive and provides uncertain clinical benefit. We describe the integration of a novel, low-cost, durable lumbar spine phantom and formal educational curriculum for performing lumbar punctures (LP) with the aim to increase operator efficiency and confidence. Methods: Following IRB approval, 6 PGY-2 residents were enrolled in an educational curriculum including 2 formal didactic lectures, an instructional video, and 20 simulated fluoroscopically-guided lumbar punctures performed on a novel phantom created for the purposes of this study. Data from 114 lumbar punctures performed by the six enrolled residents were compared with retrospective data from 514 LP's performed by 17 residents who underwent no formal training. A 10-question survey analyzing the operators' confidence, understanding of anatomic landmarks and knowledge of procedural risks was administered to the test group before and after their first 15-25 LP's. Results: The LP curriculum test group had significantly decreased procedural fluoroscopy time (0.87 min) compared to the control group (1.09 min) for all lumbar punctures, including both diagnostic LP and LP for myelogram on an aggregate basis ($p = 0.002$). This relationship is preserved when independently accounting for diagnostic LP alone ($p = 0.002$) and LP for myelogram alone ($p = 0.001$). No statistically significant relationship in failed LP's between the two groups or variability in outcomes among different clinical indications for LP were observed. Survey-based subjective measures of operator confidence showed improvement following completion of the curriculum. Conclusion: The didactic and simulation-based curriculum for fluoroscopically guided lumbar puncture produces tangible improvement in operator confidence, procedural efficiency, and likely reduces patient radiation exposure.

O-543 1:30PM - 1:40PM
The Norman E. Leeds Award - Eastern Neuroradiological Society (ENRS) - Management of Delayed Cerebral Ischemia in Subarachnoid Hemorrhage: Is Imaging for Vasospasm Necessary?

Rawal, S.
University of Toronto
Toronto, Ontario

Abstract/Presentation Summary

Background and Purpose: Delayed cerebral ischemia (DCI) is a serious complication that may occur following aneurysmal subarachnoid hemorrhage. If DCI is suspected, imaging methods designed to detect vasospasm or regional hypoperfusion are often employed prior to instituting therapy. Uncertainty in the strength of the relationship between angiographic vasospasm and DCI-related outcomes raises the question of whether imaging to select patients for therapy is effective in improving outcome in patients suspected to have DCI. Methods: A decision analysis was performed using a Markov model. In the context of suspected DCI, strategies were to either treat all patients immediately, or to first undergo diagnostic testing by digital subtraction angiography (DSA), CT angiography, or CT perfusion to assess vasospasm. According to current practice guidelines, treatment consisted of induced hypertension. Outcomes were survival in terms of life-years and quality-adjusted life-years (QALYs). Results: When treatment was assumed to be ineffective in non-vasospasm patients, Treat All and DSA were equivalent strategies; when a moderate treatment effect was assumed also in non-vasospasm patients, Treat All became the superior strategy. One-way sensitivity analyses demonstrated that the model was robust; two and three-way sensitivity analyses with variation of disease and treatment parameters reinforced dominance of the Treat All strategy. Conclusions: Testing for the presence of vasospasm in patients suspected of DCI before initiating hypertensive treatment did not lead to improved outcomes. In patients suspected of having DCI, imaging studies to rule in or rule out vasospasm are not beneficial, and should not be performed before initiating medical therapy.

O-544 1:40PM - 1:50PM
The Gabriel H. Wilson Award - Western Neuroradiological Society (WNRS) - Atypical Age-Related Cortical Thinning in Episodic Migraine

Chong, C.
Mayo Clinic Arizona
Scottsdale, AZ

Abstract/Presentation Summary

Purpose: Migraine is a debilitating neurological disorder affecting over 36 million people in the U.S. Although the clinical manifestations of the disease are well described, the pathophysiology of migraine remains poorly understood. It has been proposed that migraine is a progressive disorder with cumulative effects on brain structure and function. In this study, we assessed age-related cortical thinning patterns in migraine patients compared to healthy controls to test the hypothesis that migraine is associated with greater age-related thinning in areas subserving pain processing. Methods: 32 healthy controls (mean age=35.3 years; SD=11.6) and 27 age and gender matched episodic

Note: Scanned images are included in the proceedings. Some submitted images were reduced during editing thereby decreasing clarity. Also, refer to the Program Planner. Proceedings Content as of 3/28/2014.

migraine patients (mean age=33.6 years; SD=12.3) underwent highresolution 3T structural scanning. Scans were post-processed using a surface based semi-automatic analysis technique and cortical thickness was estimated with a General Linear Model vertex-by-vertex approach. Results were modeled for each hemisphere using a group-by-age, main effect analysis to estimate the effect of age on cortical thickness for each group separately, and an age-by-diagnosis analysis to estimate differences in age-related cortical thinning between migraine patients and normal controls. Results: Although migraineurs and normal controls both have expected age-related thinning in many regions along the cortical mantle, migraineurs have age-related thinning of regions that do not thin in healthy controls, including: somatosensory cortex, precuneus, fusiform and anterior insular cortex. Cortical thinning of these regions is more prominent with advancing age. There were no regions where normal controls had greater age-related cortical decline relative to migraineurs. Conclusion: Results suggest that migraine is associated with atypical cortical thinning of pain processing regions. Recurring migraines could have a cumulative effect on cortical structure that becomes more prominent with advancing age in regions associated with sensory-discriminatory and affective pain processing.

O-545 1:50PM - 2:00PM
Southeastern Neuroradiology Society (SENRS) -
Pseudoprogession in Glioblastoma: Clinical Features &
Imaging Assessment

Holder, C.
Emory Univ. School Of Med.
Atlanta, GA

Abstract/Presentation Summary
Pseudoprogession (PsP) is a relatively recently recognized phenomenon that presents a difficult challenge in the imaging assessment of patients undergoing standard treatment (resection followed by temozolomide and radiation therapy) for glioblastoma. This lecture will review the phenomenon of PsP and the current Response Assessment in Neuro-Oncology (RANO) guidelines and recommendations with regard to this entity. PsP can be indistinguishable from early true progression (TP) by MR imaging. As a result, a patient with PsP may be incorrectly assumed to have early TP, in which case treatment may be altered, such as addition of an anti-angiogenic agent, or enrollment in a clinical trial for 'recurrent or progressive' glioblastoma. If enrolled in a clinical trial, a patient with PsP may then go on to improve (in the normal course of evolution of PsP), and the clinical trial agent may be incorrectly given credit for the improvement. Some factors to consider with regard to PsP include: Timing – most cases of PsP occur within 90 days after completion of radiation therapy, with almost all cases occurring within 180 days. MGMT promoter methylation status – Methylation of the MGMT gene promoter turns off the DNA repair mechanism of the tumor cells, and therefore confers a more favorable prognosis. Although PsP can occur in

MGMT-unmethylated tumors, MGMT-methylated tumors are more likely to have PsP. Also, PsP is a favorable phenomenon in terms of prognosis (UN-methylated is UN-favorable). Clinical status of the patient – patients with TP are generally worsening clinically, whereas patients with PsP are usually clinically stable or even improving. Communication between neuroradiologists and our colleagues in neuro-oncology, radiation oncology and neurosurgery is invaluable. Without change in treatment, patients may go on to have marked regression of enhancing tumor, which is diagnostic of PsP; therefore, no final clinical decisions should be made on the basis of the first post XRT-chemo MRI scan.

O-546 2:00PM - 2:10PM
AJNR Editorial Fellow: Article Citations: Title Features That
Lead to Higher Citations

F Chokshi¹, J Kang², M Castillo³
¹Emory University School of Medicine, Marietta, GA,
²Emory University, Atlanta, GA, ³UNC Chapel Hill, Chapel
Hill, NC

Purpose
When the effect of title characteristics on number of citations (NOC) was evaluated in 2010 for the Lancet, British Medical Journal (BMJ), and Journal of Clinical Pathology (JCP) it was found that 3 title characteristics were statistically associated with higher NOC: 1) total number of words (NOW), 2) presence of a colon symbol (POC) & 3) presence of acronym (POA). We aimed to demonstrate if similar associations are found in radiology journals.

Materials and Methods
We queried Web of Science for all original research and review articles published in AJNR, Radiology and AJR from Jan 1, 2006 to Dec 31, 2012. Article titles characteristics listed above were tabulated for all 3 journals. First, we fit a Poisson regression model to investigate the association between the NOC and the 3 title characteristics named above for each journal. We also adjusted for the potential confounders year. Second, regression coefficients estimates and standard errors were computed; coefficient of significance was assessed using the Wald test. Third, we used the Wald test to detect the pairwise difference in the effect of title characteristics and year of publication on the NOC between journals (AJNR vs. Radiology, AJNR vs. AJR, Radiology vs. AJR). Standardized differences in effects (Z-value) and p-values for different title characteristics were computed.

Results
Between 2006-2012 published manuscript counts were: AJNR 2581, AJR 3998, and Radiology 2662. **TITLE CHARACTERISTICS AND NOC PER JOURNAL** If 1 word increased in title, then NOC increased 1.6% in AJNR and 2.6% in AJR. NOC decreased by 0.8% in Radiology (all p<0.001). POC led to 16%, 15%, and 7.4% increases of NOC in AJNR, Radiology, and AJR, respectively (all p<0.001). POA resulted in 10%, 14%, and 13.3% increases of NOC for

Note: Scanned images are included in the proceedings. Some submitted images were reduced during editing thereby decreasing clarity. Also, refer to the Program Planner. Proceedings Content as of 3/28/2014.

AJNR, Radiology, and AJR, respectively (all $p < 0.001$).
COMPARISON OF EFFECT OF TITLE CHARACTERISTICS AND NOC BETWEEN JOURNALS (Table 1) NOW: AJR had the strongest association with NOC compared to AJNR and Radiology. All differences are significant. POC: Radiology and AJNR have stronger associations with NOC compared to AJR, however there was no significant difference between AJNR and Radiology. POA: AJR has a stronger association with NOC than AJNR; no significant differences between AJNR and Radiology or between AJR and Radiology were found. Effect of Year of Publication: Radiology has the strongest effect on NOC compared to AJNR and AJR.

Table 1

	<i>AJNR vs. Radiology</i>		<i>Radiology vs. AJR</i>		<i>AJR vs. AJNR</i>	
	Z	P-value	Z	P-value	Z	P-value
NOW	15.079	<0.001	-23.896	<0.001	6.436	<0.001
POC	0.465	0.321	4.744	<0.001	-5.412	<0.001
POA	-0.959	0.169	0.146	0.442	1.91	0.028
Effect-Year	-1.353	0.088	5.752	<0.001	-3.229	<0.001

Conclusions

Manuscript title characteristics (NOW, POC, and POA) are highly associated with higher NOC within 2 robust specialty journals (AJR & Radiology) and a subspecialty journal (AJNR). Attention to these factors during title selection/modification can have significant impact on NOC.

KEYWORDS: Outcome, Outcomes

0-541 2:10PM - 2:20PM
 ASNR Cornelius G. Dyke Memorial Award - Anatomical Connectome Reveals Abnormal Connectivity in Complete Corpus Callosum Agenesis

Meoded, A.
 The Johns Hopkins University School of Medicine
 Baltimore, MD

Abstract/Presentation Summary

Purpose: The corpus callosum (CC) is the major commissure in the human brain. In complete CC agenesis, the fibers of the CC are not missing, but heterotopic and form abnormal white matter tracts. Investigating the anatomical brain connectivity is crucial for understanding the structural reorganization of white matter circuits in children with CC agenesis. The structural connectome is an innovative technique suitable for the study of large-scale white matter connectivity of the human brain and the cerebral organization. Here, we apply a multiscale structural connectomics analysis to investigate white matter connectivity in children with complete CC agenesis. In more detail, we aim to 1) investigate connected/disconnected subnetworks, 2) characterize the topological network measures and 3) search for aberrant circuits in children with CC agenesis. **Materials and Methods:** Patients were selected from our pediatric neuroradiology database based on 1) complete CC agenesis by conventional MR imaging (MRI) and 2) availability of

diffusion tensor imaging (DTI) data without artifacts enabling high quality postprocessing. Age- and gender-matched controls also were selected. Diffusion tensor imaging data were acquired using a 1.5 T scanner. Postprocessing was performed using TORTOISE software. After nonlinear registration to MNI space, the cerebral and cerebellar cortex were parcellated into 108 regions using the AAL template. Probabilistic tractography was used to define connections between any pair of gray matter regions and an association matrix of structural connectivity was created for every subject. Structural connectomes for controls were created after excluding the CC (virtual callosotomy). Further analysis included 1) network-based statistics (NBS) to detect interconnected subnetwork as a whole and 2) topological network measures analysis to perform quantitative analysis of network metrics across different densities. **Results:** Eleven patients (6 males, mean age 11.7 years) and 11 healthy controls were included in this study. One patient with two aberrant interhemispheric tracks was excluded from network analysis. Network-based statistics revealed three highly connected subnetworks (two intrahemispheric, one interhemispheric) in patients compared to controls. Topological network measure analysis showed higher clustering coefficient, smaller characteristic path length, higher global efficiency, slightly higher local efficiency (at higher density level), smaller assortativity and higher transitivity values across the range of densities in patients compared to controls. Network hubs were found in both insular and the left and right insula, and precuneus gyri and right lingual gyrus in patients and in the right postcentral gyrus and cerebellar 8th lobule and bilateral precuneus gyri in controls. **Conclusions:** In patients with CC agenesis, the structural network is more segregated and less integrated compared to controls. This represents more local (between neighboring anatomical regions) rather than global interactions. In patients, the absence of hubs in the cerebellum may reflect compensatory mechanisms to maintain local efficiency at the cost of global connectivity. Highly interconnected subnetworks in patients also suggest effective local connectivity and may reflect compensatory rewiring mechanism in CC agenesis. Connectome analysis provides new information about abnormal connectivity and potential reorganization of white matter tracts in CC agenesis.

2:20PM - 2:30PM

Questions

Wednesday, May 21
 3:00 PM – 4:30 PM
 Room 517bc

66 - General Programming – Psychiatric Disorders and the Emotional Brain: Normal and Deranged

Note: Scanned images are included in the proceedings. Some submitted images were reduced during editing thereby decreasing clarity. Also, refer to the Program Planner. Proceedings Content as of 3/28/2014.

O-550 3:00PM - 3:30PM
Anatomic Foundation and Relevant Networks

Naidich, T.
The Icahn School of Medicine at Mt. Sinai
New York, NY

Abstract/Presentation Summary

Part I of this presentation (TP Naidich) will discuss the I. Anatomic Foundation, including the Insula and cingulate-insular connections, Nucleus accumbens: Core and shell; Amygdala, Periamygdaloid cortex and extended amygdaloid complex; Septum-Hypothalamus and Olfactory cortex; Substantia nigra and dopamine system; Periaqueductal gray matter (PAG) and Ventral tegmental area (VTA), and Cerebellum II. Relevant Networks, including the Default mode network vs. Task-directed network; Reward system, and Stress system: pituitary-hypothalamic axis, amygdaloid corticotrophic releasing hormone (CRH), and extracranial CRH III. Affective States, including Empathy, Negative affective states, and Homeostasis vs. Allostasis

O-551 3:30PM - 4:15PM
Circuitry of Affective States and Disorders of Emotion

Schmahmann, J.
Massachusetts General Hospital
Boston, MA

Abstract/Presentation Summary

Part II of this presentation (JD Schmahmann) will discuss the IV. Disorders of Emotion, including Major Depressive Disorder (MDD), Obsessive Compulsive Disorder (OCD), Addictive States; Schizophrenia, Links to Alzheimer disease V. Anatomic-Biochemical-Circuitry of Emotional Disorders, including Disrupted insular-cingulate-amygdaloid interactions; and Deranged interactions of amygdala and Extended amygdaloid complex with the Stress system (adrenal, amygdala and hypothalamic-pituitary axis); Allostasis VI. Neuromodulation by Deep brain stimulation (DBS); Serotonin reuptake inhibitors (SRIs); Ketamine; and Interactive-adversive training; VII. Pulling it Together: Present Consensus and Understanding

Wednesday, May 21
3:00 PM – 4:30 PM
Room 517d

67 - Parallel Papers: Adult Stroke

O-817 4:31PM - 4:38PM
BOLD-based MRI reveals relative oxygen extraction fraction changes in patients with stroke or severe arterial stenosis

A Gersing, M Ankenbrank, V Toth, B Schwaiger, N Hirsch, S Wunderlich, C Zimmer, C Preibisch

Technical University of Munich, Klinikum rechts der Isar, Munich, Germany

Purpose

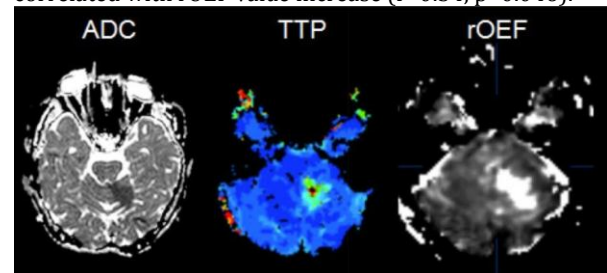
Hypoxia plays an important role for the outcome in cerebral ischemia. Recently, a new method based on the quantitative blood-oxygenation-level dependent (BOLD) effect and independent measurement of T2, T2* and cerebral blood volume (CBV) was proposed for qualitative mapping of the relative oxygen extraction fraction (rOEF). In this study, we applied this BOLD-based method for assessment of rOEF in patients with stroke or severe arterial stenosis. Purpose of this study was to evaluate whether rOEF maps are an improved predictor for penumbra estimation, compared to the established method of the apparent diffusion coefficient (ADC) and time to peak (TTP) mismatch.

Materials and Methods

Thirty-six patients (63 ± 16 years old; 14 males) with suspected ischemia or severe carotid artery stenosis were examined with a 3 T scanner. Quantitative measurements of T2 multi-echo GRASE and T2* multi-GE were performed with a measurement time of 3.5 minutes. Cerebral blood volume was derived from the routine DSC PWI. For assessment of hypoxic areas, $rOEF = R2' / (c \cdot rCBV)$ was calculated with $R2' = (1/T2^*) - (1/T2)$, relative rCBV and $c = 4/3 \cdot \pi \cdot \gamma \cdot \Delta\chi \cdot B_0 = 317\text{Hz}$ at 3 T. Relative OEF maps were compared with FLAIR, ADC, TTP and CBV maps and correlated with the clinical outcome in order to evaluate its prognostic value for patient selection regarding therapy.

Results

Twenty-three patients (15 with acute, 3 with subacute ischemia and 5 with severe arterial stenosis) showed areas of prolonged TTP (> 4s) and/or diffusion restriction. On the lesion side in areas with prolonged TTP without diffusion restriction, rOEF presented a signal intensity increase from 0.59 ± 0.19 to 1.44 ± 0.85 ($p=0.077$). In regions with diffusion restriction this effect was less pronounced (1.03 ± 0.62 , $p=0.082$). Relative OEF lesion was associated with TTP lesion in size and location (Figure). Prolonged TTP values correlated with rOEF value increase ($r=0.50$, $p<0.05$). Regional CBV reduction correlated with rOEF value increase ($r=0.54$, $p=0.046$).



Conclusions

In stroke patients, rOEF measurements were able to detect ischemic areas as well as differences between ischemic core and surrounding tissue. Relative OEF values correlate with perfusion prolongation. These results underline the assumption that areas with increased rOEF outside the ischemic core represent tissue with potentially reversible metabolic and functional impairment. Further work is

Note: Scanned images are included in the proceedings. Some submitted images were reduced during editing thereby decreasing clarity. Also, refer to the Program Planner. Proceedings Content as of 3/28/2014.

needed to delineate the utility of rOEF for the penumbra concept.

KEYWORDS: MR Imaging Brain, Penumbra, Stroke

O-552 3:00PM - 3:07PM
Imatinib Reduces Infarction and Blood-Brain Barrier Permeability in a Transient Occlusion-Reperfusion Rodent Model: a MRI Study

Z Merali¹, J Leung¹, D Mikulis², F Silver², A Kassner¹
¹The Hospital for Sick Children, Toronto, Ontario, Canada,
²Toronto Western Hospital, Toronto, Ontario, Canada

Purpose

Permeability imaging using dynamic contrast-enhanced (DCE) MR imaging (MRI) can assess early blood-brain barrier (BBB) breakdown in acute ischemic stroke (AIS). Previous studies have shown a correlation between BBB permeability (KPS) and subsequent hemorrhagic transformation (HT) in patients with AIS (1). Agents that can stabilize the BBB such as Imatinib could play an important role in reducing the risk of HT in AIS. One study using a permanent occlusion rodent model found that mice given Imatinib had lower BBB leakage and were less likely to proceed to HT after thrombolytic therapy (2). However, this type of model neglects reperfusion injury, which is a significant factor in the development of HT and did not include imaging. The purpose of our study was to use a transient occlusion AIS model combined with MRI to quantify the BBB stabilizing effect of Imatinib in a rodent, to measure infarct size and validate the results with histology.

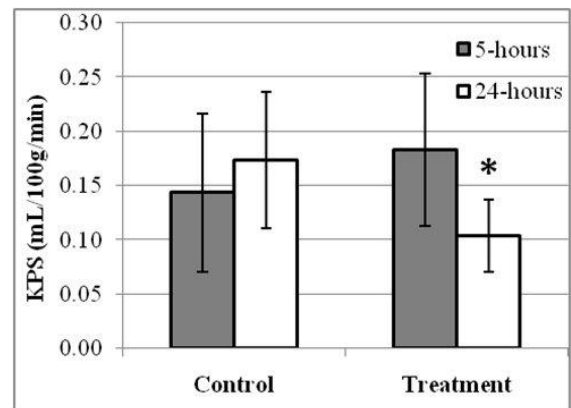
Materials and Methods

Male Sprague-Dawley rats (n=18, 250-300g) underwent a 60 minute occlusion of the middle cerebral artery as described by Longa et al (3). Either Imatinib (100mg/kg) or saline was administered at 1-hour and 20-hours after reperfusion. DCE-MRI performed on a 3 T clinical magnet (Philips Acheiva 3.0 T TX) using an eight-channel wrist coil was conducted at five hours and 24 hours after reperfusion. A 60uL bolus of contrast (Gadovist, 2mmol/mL) was injected via tail vein catheter over 12 seconds shortly after the start of the DCE scan (TR/TE=6.3/2.2 ms, FOV=100×85 mm², matrix=168×142, slice=1 mm, volumes=36, time=4:20 min). T2-weighted images were acquired to quantify lesion volume. Imaging data were coregistered and analyzed using an in-house tool (MR Analyst v2.1; University of Toronto, Canada). Infarct regions of interest (ROIs) were manually defined on the T2-weighted images then applied to the DCE-MRI data to calculate mean KPS using a two-compartment pharmacokinetic model (4). A Student's T-test was performed between control and treatment groups to detect significant differences (p<0.05) in KPS as well as lesion volume. In addition, Evans blue extravasation and Western blot protein analysis was performed in three animals (5).

Results

KPS and infarct size quantified from data at the five-hour time point were not significantly different between groups.

At 24 hours after occlusion, the group treated with Imatinib had reduced infarct sizes (226mm³±38.6 treatment versus 288mm³±38.6 control, p<0.05) and KPS (0.104mL/100g/min±0.034 treatment versus 0.173mL/100g/min±0.063 control, p<0.05). Also, the treatment group had reduced extravasation of Evans blue into the central nervous system (CNS) tissue at 24 hours (0.49ng/mg±0.03 treatment versus 0.57ng/mg±0.08 control, p<0.05). In addition, Western blot analysis revealed that the tight junction protein ZO-1 was expressed at significantly higher (p<0.05) levels in the infarcted hemispheres of the Imatinib-treated rats compared to controls.



Conclusions

Using transient occlusion model, we observed that Imatinib has BBB stabilization properties after 24 hours, as assessed by structural and DCE-MRI as well as histology. Further studies will investigate if Imatinib can reduce the risk of HT after administration of a thrombolytic agent.

KEYWORDS: Acute Stroke, Animal Model, Permeability MR Imaging

O-553 3:07PM - 3:14PM

MR Imaging Findings in Middle Cerebral Artery Stroke Patients Implanted with Mesenchymal Stem Cells: Initial Findings

C Wanamaker, L Alhilali, S Fakhran
University of Pittsburgh Medical Center, Pittsburgh, PA

Purpose

The primary purpose of this study was to describe MR findings seen after mesenchymal stem cell (MSC) implantation in patients with chronic stable infarcts in the middle cerebral artery (MCA) territories and to compare changes in brain volume in stem cell transplanted patients to age-matched normal controls and age-matched control patients with chronic MCA infarcts.

Materials and Methods

MR examinations in five patients with stable chronic MCA territory infarcts who underwent MSC implantation into the peri-infarct region via stereotactic surgery were reviewed retrospectively. Patients were imaged

Note: Scanned images are included in the proceedings. Some submitted images were reduced during editing thereby decreasing clarity. Also, refer to the Program Planner. Proceedings Content as of 3/28/2014.

immediately after MSC implantation and at one year. Imaging findings after implantation and at one year were recorded. Images immediately postimplantation and at one year underwent quantitative volumetric comparison using automated brain extraction and registration software (SIENA, FSL software library) to determine the percent brain volume change (PBVC). Images for controls at initial imaging and at one year also were analyzed for PBVC. Comparison of PBVC for MSC implantation patients and controls was determined using a two-tailed unpaired t-test.

Results

MR findings immediately post-implantation included susceptibility signal loss and enhancement at the site of implantation, with enhancement persisting up to one year in some patients. Immediate postprocedural complications included a small subdural hemorrhage in one patient. No acute infarct was seen as result of the implantation. No findings suggestive of a teratoma, tumor, or heterotopia were seen at either imaging time point. Volumetric analysis showed slight increase in brain volume in the MSC patients (0.736, range -0.726 to 5.05), which was higher than that of control patients with encephalomalacia without MSC implantation (-0.271, range -2.31 to -0.535) but less than age-matched normal controls (2.90, range 0.881 to 4.491), although due to the small sample size, this did not reach statistical significance ($p=0.24$ and 0.52 , respectively).

Conclusions

Enhancement and susceptibility signal loss after MSC implantation can be seen up to one year after the procedure. Complications after the procedure were limited to typical postsurgical complications and no complications unique to the MSC implantation such as teratoma, tumor, or heterotopia were seen. Initial findings suggest a possible trend in increased brain volume in patients receiving MSC implantation compared to infarcted patients who did not receive stem cells; however, this was limited by the small number of patients who undergo this procedure and further investigation is warranted.

KEYWORDS: Stem Cell, Stroke

0-554 3:14PM - 3:21PM
Black Holes on Time to Peak Map: Is it the core of the core

R Meagher¹, J Shankar²

¹Diagnostic Imaging, Dalhousie University, Halifax, Nova Scotia, YNeuroradiology, QE II Hospital, Halifax, Nova Scotia

Purpose

CT perfusion (CTP) is widely used and established in multimodality imaging of acute stroke. In CTP, time to peak (TTP) image maps represent the time from the beginning of contrast material injection to the maximum concentration of contrast material within a region of interest. A black hole is a frequently observed, yet not yet formally defined, phenomenon seen on TTP image maps where black, or no color, is assigned to an area of brain parenchyma. As of now it is unclear the meaning or significance of this finding. The purpose of this study was

to describe the black hole phenomenon seen on TTP image maps for acute stroke perfusion imaging, and to propose a framework for future characterization and analysis while promoting awareness and discussion into the significance of TTP black holes.

Materials and Methods

Perfusion analysis was performed for all patients with a single vendor-supplied software package, by using a semiautomatic deconvolution algorithm. Images were analyzed first on whether an acute stroke was present. A black hole is defined as an area color coded black on the TTP image map which is not assigned a TTP value and does not correspond with cerebral spinal fluid containing spaces, vessels or bone on the unenhanced CT exam of the brain. Furthermore a black hole must have a surrounding area of increased TTP unless present within brain parenchyma supplied by perforating arteries. Regions of interest (ROIs) were randomly drawn on an area of the black hole and on an immediately adjacent area of brain parenchyma which was not color coded black (any other color was accepted). Within the respected ROI, values for cerebral blood volume (CBV), cerebral blood flow (CBF) and TTP were recorded. Follow-up CT or MRI exams of the brain performed at least one day post CTP acquisition were interpreted and parenchyma corresponding to black holes was assessed for the signs of infarction.

Results

In the five month interval 84 CTP exams were performed 42 of which had follow-up imaging available for review. Of these 23 patients were diagnosed with acute stroke on CTP. Twenty-three of 23 patients (100%) demonstrated black holes. Twelve patients had follow-up CT and 11 follow-up MRI. All black holes corresponded with areas of infarcted brain on follow-up studies (specificity of 100%). Of the 23 black holes 16 received iv TPA, one of which also underwent mechanical thrombectomy, and seven received no intervention. Cerebral blood flow values of black holes (mean 6.10 ml/100ml/min) and adjacent brain (mean 35.85 ml/100ml/min) parenchyma were significantly different ($P < .000001$). Cerebral blood volume values in black holes (mean 0.84 mL/100ml) and adjacent brain (mean 2.55 mL/100ml) parenchyma also were significantly different ($P < .000001$).

Conclusions

In conclusion, our result shows that black holes on TTP image maps represent areas of infarct at the time of acquisition. All CTP exams positive for acute stroke demonstrated corresponding black holes. Time to peak image maps can be challenging to interpret and appear to contain more information than initially appreciated.

KEYWORDS: CT, CT Perfusion

0-555 3:21PM - 3:28PM
Characterization of carotid artery plaque using CT multi-spectral imaging: comparison between 2 different systems

L Saba¹, G Argiolas², P Lucatelli³, M Piga⁴, F Zaccagna⁵, E Genovese⁴

Note: Scanned images are included in the proceedings. Some submitted images were reduced during editing thereby decreasing clarity. Also, refer to the Program Planner. Proceedings Content as of 3/28/2014.

¹University of Cagliari, Monserrato, Italy, ²AOB, Cagliari, Italy, ³University la Sapienza, Roma, Italy, ⁴University of Cagliari, Cagliari, Italy, ⁵University of Rome - Sapienza, Rome, Italy

Purpose

Previous studies have demonstrated that the carotid artery plaque's attenuation values significantly change according to the selected keV. The purpose of this study was to compare the two different computed tomography (CT) scanners in the multispectral analysis of carotid artery plaque.

Materials and Methods

Sixty consecutive (males 47; median age 69 years) patients were analyzed prospectively. Carotid arteries were studied with two different multi-energy CT scanners (Discovery HD 750, GE Healthcare and Somatom Definition, Siemens) that use two different modality to produce the multi-energy values (dual tube versus fast switching technologies). All patients received a 15 mL timing bolus of contrast medium to synchronize the data acquisition followed by an injection of a volume of 60 mL of contrast medium at 5 mL/sec flow rate. Plaque analysis in 120 carotid arteries was performed (4 excluded because absence of detectable). Plaque and datasets were reconstructed by using a dedicated workstation. For each plaque HU value was quantified with a square region of interest (ROI) at mono-energy values of 66, 70, 77 and 86 keV (equivalent to 80, 100, 120 and 140 kV). Wilcoxon test was used to test the differences between the HU values in the plaques at different keV.

Results

Eleven plaques were excluded because no plaque was present. In the remaining 109 Wilcoxon analysis showed a statistically significant difference in HU values among the mono-energy values of 66, 70, 77 and 86 keV ($P = 0.0001$) both for GE and Siemens systems. A statistically significant reduction of HU values was found by increasing the monochromatic keV values.

Conclusions

Results of this study suggest that using multi-energy CT scanners, independently from the model and technology implemented, the plaque's HU values significantly change according to the selected keV.

KEYWORDS: Carotid Artery, Carotid Plaque, Dual Energy Spectral

O-556 3:28PM - 3:35PM
Imaging of Cerebral Air Embolism

G McNeill, J Kerrie, J Chew
Vancouver General Hospital, Vancouver, BC

Purpose

Cerebral air embolism (CAE) is the result of the inadvertent entry of air into the venous or arterial systems. The iatrogenic sources of CAE are multiple, the most common origins that have been reported in the literature

include central venous catheters, lung biopsy and at angiography. A right hemispheric predominance in CAE neurological syndromes has been described due to a preferential pathway to the right common carotid artery from the heart. Reported cases of CAE imaging findings are consistent with expected findings from an 'embolic shower', with multiple areas of peripheral infarction or ischemia in different arterial territories. The detection of intracranial locules of air has been described; however noncontrast-enhanced computed tomography (NECT) has a relatively low sensitivity for the detection of intracranial gas. Sensitivity depends upon the volume of gas present and, more crucially, the time interval between CAE and NECT. The goal of this study is to establish the expected imaging findings in patients with confirmed iatrogenic CAE.

Materials and Methods

A comprehensive medical chart review of all patients admitted for hyperbaric oxygen therapy (HBOT) for iatrogenic cerebral embolism at a tertiary referral center between May 2002 and January 2013 was performed. Imaging on these patients was read by two fellowship-trained neuroradiologists, blinded to clinical examination findings.

Results

Sixty-six patients were admitted for HBOT, of which 49 patients (74%) underwent neuroimaging. Of these, 10 patients (20%) had a reduced level of consciousness, 21 (42.8%) suffered seizures, 14 (28.5%) had localizing signs (50% right hemispheric) and two (4%) had witnessed air embolism during surgery and were transferred directly for HBOT. Time interval between documented event and initial neuroimaging was broad (15 minutes - more than 48 hours), 17 (25.8%) patients had imaging performed less than 240 minutes postevent (15-232 minutes, median 98 minutes). Air was demonstrated in 2/49 (4%) of initial studies and 0/49 (0%) of follow-up studies. Sixteen of 49 (32.6%) patients demonstrated early infarct changes on initial imaging, of which 8/16 (50%) involved several different arterial territories, when unilateral, equal involvement (4/16 25%) of left and right hemispheres was present. Follow-up imaging was performed on 24 patients, with a time interval of (7-74 hours, median 29 hours) between initial and follow-up imaging. All patients with early infarct changes on initial imaging demonstrated expected evolution. Eight of 24 (33.33%) patients demonstrated new infarct changes on follow-up imaging with 2/8 (25%) involving multiple arterial territories, 4/8 (50%) left hemisphere and 2/8 (25%) right hemisphere.

Conclusions

The detection of intracranial air following documented CAE is an unusual finding. The majority of initial studies are normal, thus the clinical scenario and examination findings are vital in patient management decisions. In our study, 50% of those with early infarct changes on initial imaging had multiple arterial territories involved. In this study, there was no predilection for right hemispheric syndromes.

KEYWORDS: Emboli, Stroke

Note: Scanned images are included in the proceedings. Some submitted images were reduced during editing thereby decreasing clarity. Also, refer to the Program Planner. Proceedings Content as of 3/28/2014.

O-557 3:35PM - 3:42PM
Analysis of hyperdense sign on non-contrast CT for diagnosing cerebral venous thrombosis

S Zaheer, R Glikstein, S Patro¹, N Seppala, N Steffenhagen, D Iancu
University of Ottawa, Ottawa, Ontario, Canada

Purpose

Timely diagnosis of cerebral venous thrombosis (CVT) is essential. Noncontrast CT (NCCT) is the initial investigation of choice, where the occluded sinus appears hyperdense. The purpose of this study was to assess the value of hyperdense sign and attenuation ratios in diagnosing CVT on NCCT.

Materials and Methods

Using a case control retrospective study we evaluated 19 patients with acute CVT and 20 control patients without CVT who presented to ER with similar symptoms. Final diagnosis of CVT was confirmed or ruled out with CT/MR venogram for all the patients. Three blinded readers (junior resident, fellow and staff neuroradiologist) evaluated the initial NCCT for hyperdense sign first using only axial slices, then axial, coronal and sagittal reformats, and finally using region of interest (ROI) attenuation measurements. In addition to absolute values, attenuation ratios were measured to better differentiate thrombosed from nonthrombosed sinuses. These ratios were measured as follows: target sinus/lowest attenuation sinus (ratio 1), target sinus/basilar artery (ratio 2), target sinus/internal carotid artery (ICA) (ratio 3), target sinus/nonhemorrhagic temporal lobe (ratio 4) and target sinus/nonhemorrhagic frontal lobe (ratio 5).

Results

Overall, the hyperdense sign was found to be: 61.4% sensitive (95% CI 51.8%-70.2%), 96.8% specific (95% CI 95.7%-97.6%), and 94.1% accurate (95% CI 92.9%-95.2%) on axial slices only; 64.9% sensitive (95% CI 55.3%-73.4%), 98.8% specific (95% CI 98.0%-99.2%), and 96.2% accurate (95% CI 95.2%-97.1%) with the addition of coronal and sagittal reformats, and 62.3% sensitive (95% CI 52.7%-71.1%), 98.7% specific (95% CI 97.9%-99.2%), and 96.0% accurate (95% CI 94.9%-96.9%) with absolute attenuation measurement. The expertise of the reader, addition of sagittal and coronal reformats to axial slices, and objective measurement of ROI did not have any significant effect on sensitivity, specificity or accuracy of hyperdense sign. There was statistically significant difference in average attenuation between acutely thrombosed sinuses (68.6HU, 95% CI 65.3-71.9) and nonthrombosed sinuses (52.1HU, 95% CI 50.7-53.5). Sixty-one HU was the optimal cut-off for diagnosis of CVT with 84.4% sensitivity and 89.6% specificity. The proposed attenuation ratios showed varying results: Ratio 1: thrombosed 1.43 (95% CI 1.36-1.51) versus nonthrombosed 1.06 (95% CI 1.05-1.08). Optimal cut-off of 1.29 lead to sensitivity of 87.5% and specificity of 96.0%. Ratio 2: thrombosed 1.95 (95% CI 1.80-2.09) versus nonthrombosed 1.45 (95% CI 1.40-1.49). Optimal cut-off of

1.68 gave 81.3% sensitivity and 81.6% specificity. Ratio 3: thrombosed 1.81 (95% CI 1.68-1.93) versus nonthrombosed 1.37 (95% CI 1.33-1.42). Optimal cut-off of 1.54 resulted in sensitivity of 78.2% and specificity of 79.2%. Ratio 4: thrombosed 1.89 (95% CI 1.77-2.00) versus nonthrombosed 1.42 (95% CI 1.38-1.46). Optimal cut-off of 1.63 lead to sensitivity of 84.4% and specificity of 83.2%. Ratio 5: thrombosed 1.95 (95% CI 1.84-2.07) versus nonthrombosed 1.47 (95% CI 1.43-1.51). Optimal cut-off of 1.80 gave 78.1% sensitivity and 94.4% specificity. Conclusions

Although subjective assessment of hyperdense sign on NCCT to diagnose CVT has rather low sensitivity, an objective threshold for hyperattenuation (> 61HU) and attenuation ratio of the suspected sinus/normal appearing sinus (> 1.29) may improve sensitivity. These findings need to be validated in further prospective studies.

KEYWORDS: Cerebral Venous Thrombosis, CT

O-558 3:42PM - 3:49PM
Temporal Resolution of Microvascular Dysfunction in Aneurysmal Subarachnoid Hemorrhage

A Schweitzer¹, D Mir², K Kesavabhotla³, J Ivanidze³, A Gupta³, P Sanelli²

¹New York-Presbyterian Hospital, Weill Cornell Medical Center, New York, NY, ²Weill Cornell Medical College, New York, NY, ³New York-Presbyterian Hospital, Weill Cornell Medical College, New York, NY

Purpose

After aneurysmal subarachnoid hemorrhage (SAH), delayed cerebral ischemia (DCI) contributes significantly to functional and cognitive disability (1). It has long been thought that DCI is primarily related to reduced cerebral blood flow (CBF) from proximal vasospasm (2), but recent evidence suggests that microvascular and neuronal dysfunction may be involved (3). Due to the inability to predict which patients will develop DCI, therapeutic interventions often are delayed and target proximal vasospasm only, thus infarction still occurs frequently. We sought to characterize the changes in microvascular dysfunction by evaluating cerebral blood flow (CBF) and permeability surface (PS) in DCI after SAH.

Materials and Methods

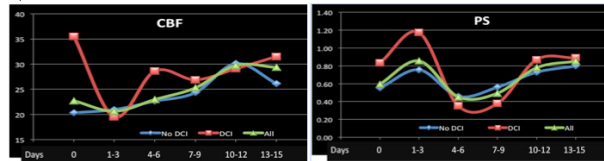
IRB approval was obtained. Thirty-three SAH patients underwent multiple CTA and CTP exams on admission and at subsequent time points in the early (days 0-3) and delayed phases (days 4-16). Patients were stratified into DCI and nonDCI groups based on outcome measures of cerebral infarction and permanent neurologic deficits. All CTP data were postprocessed into CBF and PS quantitative maps using CT Perfusion software program 4D version (General Electric Healthcare, Milwaukee, WI). Region of interest (ROI) placement was performed using standardize protocol sampling the cortex of the anterior, middle and posterior cerebral artery vascular territories. If a perfusion deficit was present, then the ROIs sampling the perfusion

Note: Scanned images are included in the proceedings. Some submitted images were reduced during editing thereby decreasing clarity. Also, refer to the Program Planner. Proceedings Content as of 3/28/2014.

deficit were included in the statistical analysis. If no perfusion deficit was present, then all ROIs were used. Cerebral blood flow and PS quantitative data were plotted in time-series curves to describe the temporal resolution of these parameters after SAH in patients with and without DCI.

Results

Figure 1a shows the CBF pattern after SAH with reduced CBF in the early phase (days 1-3) followed by a gradual increase of CBF into the delayed phase. In the early phase, there is a 45% decline in CBF in DCI compared to no significant change in patients without DCI. Significant angiographic vasospasm on CTA, defined as >50% narrowing, occurred on mean day 8. At this time point, there was a 24% decline in CBF in DCI patients compared to a 20% increase in patients without DCI. Figure 1b reveals a biphasic pattern of PS after SAH with peaks in the early and delayed phases (days 1-3 and 10-12). This temporal pattern is maintained in patients with and without DCI; however, the mean PS is statistically significantly higher in the DCI group ($p < 0.05$) at these time points.



Conclusions

Cerebral blood flow and PS have characteristic temporal patterns after SAH. In the early phase (days 1 – 3), PS, a surrogate marker for blood-brain barrier permeability, is significantly higher in patients who eventually develop DCI compared to those who do not. Further study is necessary to determine whether the relationship between CBF and PS could be used to prospectively distinguish between patients with and without DCI so that early treatments can be targeted towards prevention of DCI.

KEYWORDS: Aneurysmal Subarachnoid Hemorrhage, Blood-Brain Barrier, CT Brain Perfusion

O-559 3:49PM - 3:56PM
Reliability and Performance of a User-Independent Platform for CT-Perfusion Analysis: Threshold-Derived Automated Systems Outperform Examiner-Driven Approaches to Prognosis and Outcome Prediction in Acute Ischemic Stroke

S Dehkharghani¹, L Albin², O Kass-Hout³, M Winningham¹, A Saindane⁴, D Qiu⁴, M Straka⁵, S Christensen⁶, R Bammer⁶, G Albers⁶, M Lansberg⁶, F Nahab¹

¹Emory University Hospital, Atlanta, GA, ²Emory University School of Medicine, Atlanta, GA, ³University of Buffalo, Buffalo, NY, ⁴Emory University, Atlanta, GA, ⁵Kantonsspital Winterthur, Zurich, Switzerland, ⁶Stanford University Hospital, Stanford, CA

Purpose

Revascularization strategies aim to curtail ischemic progression in acute ischemic stroke (AIS). Emerging paradigms propose subselection of a target treatment population, and include the profile of imaging biomarkers such as those defined within the ischemic penumbra formalism. The characteristic features of this population remain controversial, and advanced techniques such as CT perfusion or angiography (CTP, CTA) have met with skepticism compared with faster approaches to triage such as the Alberta Stroke Program Early CT Scale (ASPECTS). Computed tomography perfusion may suffer interpretability bias engendered by the qualitative nature of most approaches. We propose the retrospective evaluation of the performance of a high-speed computational tool, providing automated parametric thresholding and segmentation, hypothesizing enhancements compared with traditional approaches to NCCT, CTA, and CTP analysis in widespread use. We report performance and correlation with favorable clinical outcomes in a cohort of AIS patients.

Materials and Methods

Forty-four patients (36 female, age 70 ± 17 years) with AIS (<12 hours) and MCA or intracranial ICA occlusion, were seen at a single institution. Imaging included NCCT, followed by CTA and subsequently two CTP acquisition volumes providing 8 cm supratentorial coverage on a 64 detector-row system (GE Healthcare, Milwaukee, WI, USA). Analysis was performed independently by a neuroradiologist or stroke neurologist blinded to clinical and outcomes data. Perfusion analysis was performed on a fully operator-independent platform (RAPID 2.0, iSchemaView Inc., Stanford, USA). Parametric maps of CBF, CBV, and time-to-maximum of the tissue residue function (Tmax) were computed and followed by automated normalization and segmentation for display purposes (~5 minutes). Estimated ischemic core (rCBV or rCBF) and hypoperfused volumes were established at voxel-wise thresholds, and for Tmax varied at 2s increments between 4-10s. Qualitative analysis included application of ASPECTS methodology to NCCT and CTP (CTP-ASPECTS), and were scored on a descending scale from 10 (normal) to 0 (severe); CTA-collateral score (CS), defined by vascular density overlying the diseased hemisphere, was scored from 3 (normal) to 0 (absent); CTA-clot burden score (CBS), describing clot extent, ranged from 10 (absent) to 0 (complete multisegment occlusion). Variables were analyzed for performance as predictors of favorable outcome (90-day modified Rankin scale (mRS) ≤ 2) by receiver-operating characteristic (ROC) analysis, after adjustment for baseline differences.

Results

Median admission NIHSS=19 (IQR=12-22); median final infarct volume=37cc. All variables of interest exhibited correlation with dichotomized favorable outcome. Receiver-operating characteristic analysis highlighted disparities in performance. RAPID-derived core estimates (rCBV, rCBF) were found to outperform all qualitative approaches including CTP-ASPECTS (AUC rCBV=0.89 $p < 0.0001$; AUC rCBF=0.81, vs. AUC ASPECTS=0.72 $p = 0.012$). Strongest overall performance was observed

Note: Scanned images are included in the proceedings. Some submitted images were reduced during editing thereby decreasing clarity. Also, refer to the Program Planner. Proceedings Content as of 3/28/2014.

with final infarct volume (AUC=0.96 P<0.0001). RAPID hypoperfusion estimates across all Tmax thresholds outperformed all qualitative approaches, with the exception of Tmax>10s (AUC=0.737 p=0.008) versus CBV-ASPECTS (AUC=0.756 p=0.005), which demonstrated the strongest performance among qualitative approaches. Conclusions

Computed tomography perfusion-ASPECTS, previously shown to outperform NCCT-ASPECTS as outcome predictors, are themselves limited by their inherently qualitative nature. Voxel-wise semiquantitation enhances immunity to such limitations, but generally prove impractical as integrations to clinical workflow. Our findings establish the benefits of high-speed automated analysis in AIS, outperforming conventional methodologies, while avoiding delays in management.

KEYWORDS: Stroke, Thrombolysis

0-560 3:56PM - 4:03PM
Hyperintense basilar artery on fluid attenuated inversion recovery magnetic resonance imaging: Diagnostic accuracy and clinical impact in patients with acute brain stem stroke

M Gawlitza, U Quäschling, J Otto, P Voigt, C Hobohm, K Hoffmann, D Lobsien
University Hospital Leipzig, Leipzig, Germany

Purpose

To evaluate the hyperintense configuration of the basilar artery (FLAIR-hyperintense basilar artery - FHBA) as a marker of basilar artery occlusion (BAO) and as a predictor of patient survival.

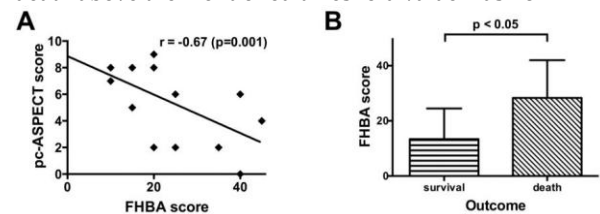
Materials and Methods

We retrospectively identified 20 patients with BAO who initially received MR imaging (MRI) with subsequent DSA. The diagnostic performance of FHBA was tested by defining a control group: one control patient without BAO that had undergone an MRI for suspected stroke - matched for age, sex and MR tomograph with which the examination was performed - was randomly selected for each patient with proven BAO from the PACS. Only the FLAIR images of the aforementioned 40 patients (20 with and 20 without BAO) were read independently by four readers in one session: two board certified, subspecialized neuroradiologists with 13 and eight years, and two radiologists in training with three and four years of experience. Visual hyperintensity of the basilar artery was graded in a 5-point Likert scale (1 = no; 2 = little; 3 = equivocal; 4 = distinct; 5 = sure). Scores of 4 and 5 were defined as positive FHBA-sign. To grade the extent of FHBA sign in patients with BAO, a score (called FHBA score in the further course of the manuscript) was generated by counting the number of slices from the basilar tip down to the foramen magnum - including the dominant vertebral artery - in which a hyperintense signal in the vessel lumen was present multiplied by the slice thickness (for example three slices with FHBA at a slice thickness of 5 mm would result in a score of 15). These measurements were performed in consensus by two readers who also

calculated the posterior circulation-ASPECTS (pc-ASPECTS) scores on DWI sequences.

Results

Assigning visual hyperintensity ratings of 4 and 5 to "positive FHBA sign" and 1, 2 and 3 to "negative FHBA sign" the following sensitivity, specificity and accuracy values for BAO were achieved: 70%, 100% and 85% for reader 1; 65%, 95% and 80% for reader 2; 85%, 95% and 90% for reader 3; 90%, 95% and 93% for reader 4. Substantial to excellent inter-reader agreement measures (using Cohen's κ 0.64 - 0.85) were observed. The FHBA sign was unequivocally present in 17 patients (85%). Mean FHBA score was 18.5 ± 13.3 (median 15.0, range 0-45). Eighteen patients (90%) had DWI lesions on the initial MRI scan with a mean pc-ASPECTS score of 6.2 ± 2.9 (median 7.5, range 0-10). FHBA and pc-ASPECTS scores showed a highly significant negative correlation ($r = -0.67$; $p = 0.01$, Figure 1A). There was a tendency towards a moderate correlation between FHBA and mRS scores at discharge ($r = 0.41$; $p = 0.09$) and patient survival was associated with significantly lower FHBA values (13.4 ± 11.1 versus 28.3 ± 13.7 ; $p < 0.05$; Figure 1B). Whereas ROC analysis for patient outcome prediction (mRS) revealed no statistically significant result (AUC 0.71, $p = 0.15$), an AUC of 0.81 ($p < 0.05$) for the prediction of patient death was calculated. An optimal discrimination threshold for the FHBA score of 17.5 or higher was determined which yielded a sensitivity of 83% and a specificity of 77%. The odds ratio for patient death above the mentioned threshold value was 16.7.



Conclusions

The FHBA sign proved to be a reliable, moderately sensitive but specific and robust sign of basilar artery occlusion that may have significant implications for the correct diagnosis of BAO. It might be of particular importance if MR angiography is degraded by artifacts or if MR angiography is primarily not scheduled, for example in patients with atypical neurological symptoms not suggestive of acute stroke. Beside its diagnostic capabilities, the FHBA sign might also have prognostic relevance since high FHBA scores were associated with more extensive ischemic lesion patterns - analogous to hemispheric stroke, the extent of the FHBA sign might be a marker of impaired hemodynamics in BAO with pronounced FHBA meaning larger brain areas being hypoperfused. Furthermore, the FHBA sign may be helpful in the prediction of patient survival.

KEYWORDS: Basilar Artery Occlusion, Diagnostic Accuracy, Fluid-Attenuated Inversion Recovery

0-561 4:03PM - 4:10PM
CSF flow quantification in acute subarachnoid hemorrhage: a predictor of hydrocephalus?

Note: Scanned images are included in the proceedings. Some submitted images were reduced during editing thereby decreasing clarity. Also, refer to the Program Planner. Proceedings Content as of 3/28/2014.

I Fragata¹, J Fialho¹, P Canhao², S Afonso¹, R Moreno¹, J Reis¹

¹Centro Hospitalar Lisboa Central, Lisbon, Portugal,

²Faculdade Medicina Lisboa, Lisbon, Portugal

Purpose

Hydrocephalus is a frequent complication of acute subarachnoid hemorrhage (SAH), occurring in about 20% of patients. Clinical grade of SAH and intraventricular blood are known predictors of hydrocephalus in SAH. Cerebrospinal fluid (CSF) flow dynamics can be quantified with phase-contrast MR imaging (MRI). We hypothesized that in the first 72h after SAH, CSF stroke volume and flow velocity could be predictors of acute hydrocephalus.

Materials and Methods

We prospectively included 30 patients with acute SAH, and performed MR on the first 72 hours after symptoms onset. Informed consent and IRB approval were obtained. We obtained CSF dynamic flow studies, and quantified average flow, average velocity, and stroke volume at the level of the aqueduct. We recorded demographic data, Hunt & Hess scale (HH) at admission, Fisher score and acute hydrocephalus on admission CT, and the need of external CSF drainage during hospital stay. Statistical analysis was performed using Student-T test and Wilcoxon Signed Ranks test, as appropriate, to assess the association between CSF parameters and the development of hydrocephalus.

Results

Of these 30 patients 17 were female, and the mean age was 58 years old. Median HH was 2, and mean Fisher was 3.4. Six patients were diagnosed acute hydrocephalus, and four needed CSF shunt. Of the six patients with hydrocephalus, all had Fisher 4 on CT at admission. However, 11 patients with Fisher 4 had no hydrocephalus. A mean $19.9 \pm 8.3 \mu\text{l}$ stroke volume was found in this SAH population. Mean peak velocity was $2.4 \pm 2.3 \text{ cm/sec}$, mean average velocity was $0.09 \pm 0.13 \text{ cm/sec}$, and mean average flow was $1.92 \pm 1.9 \text{ ml/min}$. A lower CSF stroke volume, average velocity and average flow were associated with Fisher grades 3 and 4 ($p < 0.05$). Patients with acute hydrocephalus presented lower CSF stroke volume than those without hydrocephalus ($12.5 \pm 4 \mu\text{l}$ versus $23.1 \pm 9 \mu\text{l}$, $p = 0.025$), as well as higher average flow of CSF ($2.8 \pm 1.9 \text{ ml/min}$ versus $1.7 \pm 2.0 \text{ cm/sec}$, $p = 0.03$). Average velocity, although lower in hydrocephalus patients ($0.083 \pm 0.5 \text{ cm/sec}$ versus $0.116 \pm 0.8 \text{ cm/sec}$, $p = 0.106$), did not reach a statistically significant difference between patients with and without hydrocephalus. There were no significant differences in CSF flow parameters in patients that needed acute CSF shunting.

Conclusions

Quantitative analysis with phase-contrast MR imaging in acute SAH patients showed lower CSF stroke volume and average velocity and increased average flow in patients with acute hydrocephalus. Lower CSF stroke volume and velocity probably reflect increased resistance to CSF flow in the aqueduct due to the presence of blood mixed with CSF. We speculate that increased average flow might

reflect higher intraventricular pressure in acute hydrocephalus. Cerebrospinal fluid flow parameters were not predictors of the need for acute CSF shunting, although the number of shunted patients was probably too small to reach statistical significance.

KEYWORDS: Aneurysmal Subarachnoid Hemorrhage, Cerebrospinal Fluid, Hydrocephalus

O-562

4:10PM - 4:17PM

What is the significance of wall thickening in intracranial vertebral arteries?

A Halimi-Cohen¹, P Roux¹, F Charbonneau¹, A Gueguen¹, V Macaigne², K Malkani³, S Khung-Savatovsky⁴, J Savatovsky⁵

¹Fondation Rothschild, Paris, France, ²Chu de Rouen, Rouen, Haute Normandie, France, ³Faculty of Medicine, University of Angers, Saint Sylvain d'Anjou, Pays de la Loire, France, ⁴Hopital Robert Debré, Paris, France, ⁵Fondation Ophtalmologique Adolphe de Rothschild, Paris, France

Purpose

The techniques currently used for intracranial vascular imaging, i.e., computed tomography (CT) angiography, MR angiography and digital subtraction angiography, rely mainly on the imaging of the arterial lumen. However, the direct evaluation of the arterial wall is expected to provide more information than the mere appreciation of the arterial lumen. Here we make a retrospective assessment of the prevalence of wall thickening in the intracranial vertebral and basilar arteries in patients free from known vascular disease.

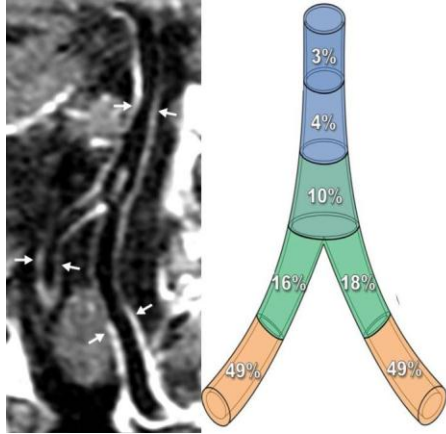
Materials and Methods

We collected the records of 300 consecutive eligible patients, free from arterial disease, having undergone contrast-enhanced brain MR imaging (MRI) examinations from April to June 2013 as part of routine care (multiple sclerosis, internal auditory canal workup, visual pathway workup, headaches). All MRI examinations included contrast-enhanced 3D turbo spin-echo T1-weighted black-blood sequences. Interobserver agreement, prevalence of wall thickening in the vertebral and basilar arteries and its relationships with the patients' age and sex were studied.

Results

The interobserver reproducibility of the results was good ($\text{Kappa} = 0.746$). Wall thickening in the proximal intracranial vertebral artery was found in 49% of the patients and had occurred in 16% of patients under 40 years of age. In contrast, wall thickening in the distal vertebral and basilar arteries had been noted in only 10% of the patients. None of the patients under 40 years of age had suffered any basilar arterial wall thickening. Multivariate analysis revealed that intracranial arterial wall thickening was more prominent in male than in female patients, with a statistically significant risk of wall thickening increasing with age.

Note: Scanned images are included in the proceedings. Some submitted images were reduced during editing thereby decreasing clarity. Also, refer to the Program Planner. Proceedings Content as of 3/28/2014.



Conclusions

The higher incidence of wall thickening observed in the proximal vertebral arteries than in the distal vertebral and basilar arteries in patients free from any known vascular disease was possibly favored by normal anatomical features. Thus, the finding of proximal intracranial vertebral arterial wall thickening should not automatically lead to the diagnosis of arteritis or any similar pathology. However, distal vertebral and basilar arterial wall thickening may reflect certain pathologic conditions, such as intracranial atherosclerosis, but should be interpreted with caution since it occurs in elderly patients in the absence of any vascular symptoms.

KEYWORDS: Basilar Artery, Vertebral Artery, Vessel Wall

0-563

4:17PM - 4:24PM

Detection of Ischemic Cerebral Lesions following Left Heart Radiofrequency Ablation: Prospective Analysis including Diffusion-Tensor Trace Imaging.

R Watson, T Kaufmann, M Madhavan, S Asirvatham
Mayo Clinic, Rochester, MN

Purpose

Catheter-based ablation techniques are a well accepted and increasingly common means of controlling cardiac arrhythmias. An accepted risk of the procedure is producing embolic cerebral infarcts (1-3). In an effort to explore the frequency of these infarcts, a prospective study was conducted to evaluate infarct production using MR imaging (MRI), including diffusion techniques (4). The study included comparison of the frequency with which diffusion abnormalities were detected with routine diffusion-weighted imaging (DWI) and diffusion tensor trace imaging (DTI).

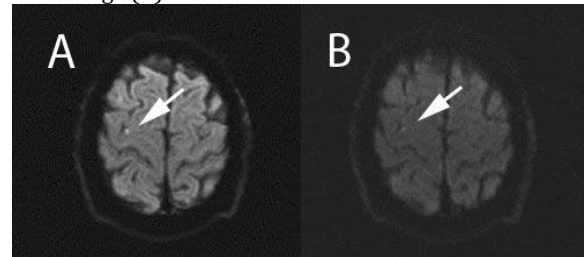
Materials and Methods

Head MRIs, including diffusion-weighted and diffusion tensor-trace imaging were acquired 1 - 2 days prior to and following radiofrequency ablation for atrial fibrillation (n=25) and left ventricular tachycardia (n=3) (age 58 (±8) years, 46% males). Scanning was performed on 1.5 T GE magnets running 16.0 software using an 8 channel head coil. Conventional DWI as well as DTI images were acquired at 4mm and 5mm (respectively), 128 x 128

matrix, and B value of 1000. DWI and DTI included 3 and 25 direction acquisition, respectively. Acquisition time was 0:50 for DWI, 3:50 for DTI. Exams also included sagittal T1, axial T2 FLAIR, axial T2 FSE, axial EPI GRE, and 3D SWAN sequences. Two CAQ certified neuroradiologists independently evaluated the scans, scoring DWI or DTI series and their corresponding ADC maps for presence, location, size, and contrast to noise (CNR) and conspicuity of sites of restricted diffusion. A 5-point incremental scoring system qualitatively evaluating the lesion's DWI versus DTI contrast to noise ratio was employed: +2, +1, =, -1, -2.

Results

New DWI or DTI ischemic lesions (N=12) were detected in 7(25%) patients, with positive cases demonstrating 1-3 lesions, ranging in size from 2-5 mm. None had clinically overt stroke or TIA. Independent neuroradiologist reads of the 12 lesions were in agreement; CNR was judged to be markedly superior in the the DTI versus DWI (score "2+") in six (including some lesions undetectable with conventional DWI); superior in five (score "1+"); and equivalent in one (score "="). The figure demonstrates increased CNR and conspicuity of a small infarct at the right frontal lobe (arrows) in the DTI image (A) versus the DWI image (B).



Conclusions

This prospective study has demonstrated that, to this point, ischemic cerebral lesions occurred in 25% of patients undergoing catheter-based ablation procedures for treatment of cardiac arrhythmias. Our experience has been that these lesions are typically small, ranging from 2-5 mm. Detectability of these small lesions is enhanced by 25-direction diffusion tensor trace imaging compared with conventional DWI. Improved detection of ischemic lesions with DTI should serve as a basis upon which to improve catheter-based ablation techniques and minimize associated ischemic events. As such, this approach should be generalizable to analyses of cerebrovascular consequences of other invasive procedures.

KEYWORDS: Diffusion MR Imaging, Diffusion Tensor Image, Infarct

0-564

4:24PM - 4:31PM

Whole brain mean-ADC predicts death in patients after cardiac arrest.

J Mettenburg¹, L Calderon¹, J Carlson², J Rittenberger¹, V Agarwal¹

¹University of Pittsburgh Medical Center, Pittsburgh, PA,

²Saint Vincent Emergency Services, Erie, PA

Note: Scanned images are included in the proceedings. Some submitted images were reduced during editing thereby decreasing clarity. Also, refer to the Program Planner. Proceedings Content as of 3/28/2014.

Purpose

The purpose of this study is to characterize the relationship of whole brain apparent diffusion coefficient (wb-ADC) measurements with regard to rhythm at presentation and follow up scores of outcome, including cerebral performance category (CPC), in patients presenting with cardiac arrest. Our hypothesis is that higher mean wb-ADC values correlate with better outcome (CPC <3) and that specific ADC values can inform clinical prognosis with regard to survival and good outcome.

Materials and Methods

The study was IRB approved. One hundred fifty-two patients presented from 2006-2011 with cardiac arrest (asystole, PEA, VF/VT, unknown rhythm) and were stabilized in the intensive care unit. Routine clinical brain MR imagings (MRIs) including 3-direction diffusion-weighted imaging (DWI) and calculated apparent diffusion coefficient (ADC) maps, were obtained at 1.5 T an average of 4.5 days (+/- 5.4 days, range (1-22 days) postarrest. Cerebral performance category scores were calculated during follow-up visits after discharge. One hundred twenty-five of the 152 MRIs included diffusion-weighted imaging (DWI) and ADC maps free from artifacts. The DWI was skull stripped using the brain extraction tool (FSL, Oxford, UK) and the resulting mask was applied to the ADC map, visually inspected and mean wb-ADC values were determined using FSL, excluding CSF containing spaces with ADC > 1000 mm²/sec. Mean wb-ADC values then were compared based upon the patient demographics, presentation and clinical outcomes. A p-value of <0.05 was considered significant.

Results

Sixty-three men and 61 women ranging in age from 17 to 84 (56 +/- 15.1 years) had usable DWI. Mean wb-ADC was significantly lower for patients that died (761.2 +/- 83.4 mm²/sec) when compared to survivors (812.3 +/- 33 mm²/sec, p<0.00001), and only one patient with mean wb-ADC < 750 mm²/sec survived (n=19), with a clinically bad outcome. There was no significant difference in mean wb-ADC values between those that survived with good (814.5 +/- 21.6 mm²/sec) versus bad (809.1 +/- 45.0 mm²/sec) outcome (p=0.5) based on CPC scores. Mean wb-ADC was not significantly correlated with age or sex. Patients presenting with asystole trended to a lower mean wb-ADC compared to other rhythms (asystole: 768.9 +/- 85.7, PEA: 796.2 +/- 64.8, VF/VT: 794.4 +/- 53.7, unknown: 804.2 +/- 55.9 mm²/sec), without reaching significance.

Conclusions

Mean wb-ADC shortly after presentation is significantly different for postcardiac arrest patients that die following stabilization and admission to the ICU. A mean wb-ADC value of <750 mm²/sec is highly specific for identifying patients who ultimately die. Age and sex of the patient had no influence on the mean wb-ADC after presentation. Mean wb-ADC did not significantly vary depending on the rhythm of presentation, although there was a trend to lower mean wb-ADC with asystole. Importantly, the mean wb-ADC did not vary between survivors with good or bad outcomes, suggesting region specific injury not characterized by this whole brain calculation. Future

studies will investigate region- and vascular territory-specific differences in ADC between these groups.

KEYWORDS: Apparent Diffusion Coefficient, Hypoxia, Ischemia

Wednesday, May 21

3:00 PM – 4:30 PM

Room 517a

68 - Parallel Papers: Adult Brain:
Noninvasive Evaluation of Vascular
Pathology

0-565

3:00PM - 3:07PM

Intravascular Papillary Endothelial Hyperplasia Following Stereotactic Radiosurgery Ablation of Arteriovenous Malformations: Clinical and Imaging Characteristics and Theories of Pathogenesis

P Thurlow¹, S Nabavizadeh², M Martinez-Lage², F Cloran², R Hurst², L Bagley², M Goldberg¹

¹Allegheny General Hospital, Pittsburgh, PA, ²Hospital of the University of Pennsylvania, Philadelphia, PA

Purpose

Intravascular papillary endothelial hyperplasia (IPEH), also known as Masson's tumor, is a benign proliferation of endothelial cells that is thought to result from an excessive reaction to normal thrombus reorganization. Although relatively common in the extremities, intracranial IPEH is exceedingly rare. While various theories of pathogenesis have been proposed, an exact mechanism remains elusive. Isolated reports in the literature describe an association between IPEH and arteriovenous malformations (AVM) treated with stereotactic radiosurgery (SRS). We have encountered aggressive lesions arising at the site of prior SRS-treated AVMs that have been diagnosed pathologically as IPEH. We sought to better define the clinical and imaging features of this rare intra-axial entity in an effort to work towards a theory of pathogenesis and elucidate any implications for the treatment of vascular malformations.

Materials and Methods

Four cases of presumed intracranial IPEH arising at the site of a previously SRS-ablated AVM were found at two institutions. Clinical characteristics of the cases, including patient demographics, site of the original AVM, treatment history, type of radiosurgery, radiation dose, latency period for IPEH, and histopathology were reviewed. Available CT and MR imaging data were reviewed in this cohort.

Results

Two cases of IPEH were histologically proven. The third case was diagnosed as AVM with necrosis on histopathology, but exhibited clinical and imaging features consistent with IPEH. A fourth case exhibited clinical and

Note: Scanned images are included in the proceedings. Some submitted images were reduced during editing thereby decreasing clarity. Also, refer to the Program Planner. Proceedings Content as of 3/28/2014.

imaging features consistent with IPEH but has not been resected, and is being observed without adverse consequences. There was no gender predisposition. Age at time of SRS ranged from 52 to 71 years (mean 61 years). Three of four patients underwent endovascular embolization of the AVM nidus between one month and three years prior to radiosurgery. Three patients underwent linear accelerator radiosurgery and one patient underwent gamma knife radiosurgery. Radiation doses were similar, with a 90% isodose ranging from 1800-2000 cGy. Latency period between radiosurgery and IPEH presentation ranged from 5 to 13 years (mean 9 years). All lesions arose in the intra-axial compartment, occurred within the irradiated field, and demonstrated similar characteristic imaging features including: hyperdensity on CT; lobulated, circumscribed mass with a T2 hypointense rim, avid enhancement, and extensive vasogenic edema on MRI; and aggressive growth over short term imaging surveillance. Two of four lesions extended across either the tentorium or the falx cerebri, unusual behavior for an intra-axial, non-neoplastic process.

Conclusions

We present the clinical and imaging features of intraaxial IPEH following SRS for AVM, the only reported case series of SRS-associated IPEH. This aggressive entity can be a diagnostic dilemma, given that its imaging features may overlap with radiation necrosis, neoplasia, and cavernoma. The mechanism of radiosurgical ablation of AVMs is thought to relate to endothelial proliferation, hyalinization, and thrombosis leading to vessel occlusion. Interestingly, the histopathology of IPEH seems to reflect an unrestrained form of radiation-related effects. As such, IPEH may represent a complication of SRS and should be considered when an aggressive intra-axial mass is encountered at the site of prior SRS.

KEYWORDS: Arteriovenous Malformation, Radiation, Radiation Effects

0-566 3:07PM - 3:14PM
The Supreme Intercostal Artery Includes the Last Cervical Intersegmental Artery (C7) - Angiographic Validation of Dorcas Padget's Intersegmental Nomenclature

P Gailloud
The Johns Hopkins Hospital, Baltimore, MD

Purpose

In 1954, Dorcas Padget settled the debate over the labeling of the intersegmental arteries (ISAs) and the level of origin of the subclavian artery (SubA). Her proposed nomenclature introduced the name of proatlantal artery and confirmed that the SubA was associated with the sixth ISA rather than the seventh. However, a generally unnoticed consequence of this now widely accepted terminology lays in its incompatibility with the traditional view of the costocervical trunk, regarding in particular the anatomy of the supreme intercostal artery (IA). If the SubA derives from the sixth cervical ISA (ISA 6), and the costocervical trunk provides the first and second IAs (ISA 8

and 9), the seventh cervical ISA (ISA 7) then remains unaccounted for. The purpose of this study was to examine Padget's nomenclature in the light of modern angiographic material in order to identify the missing seventh ISA.

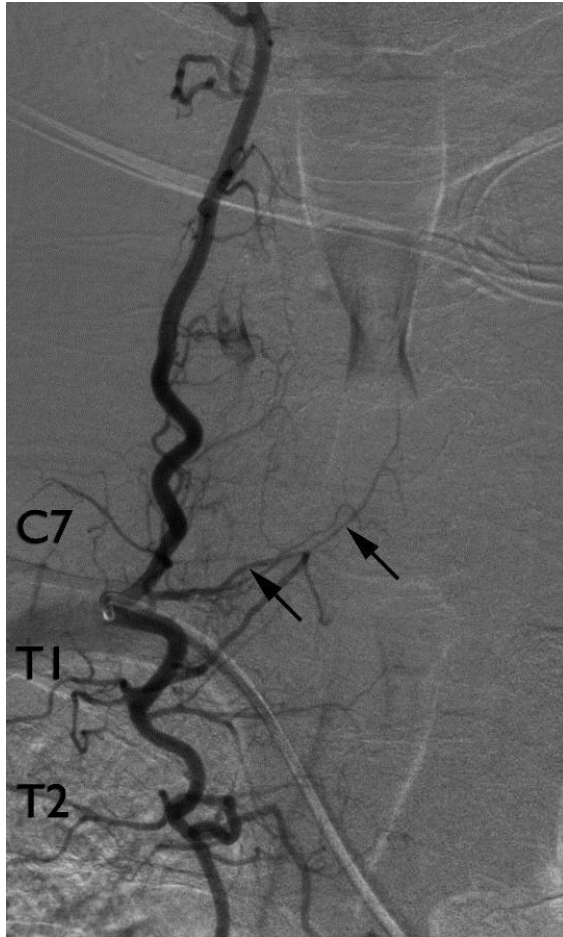
Materials and Methods

The topography of the radicular arteries is defined early during development, and their relationships with somitic elements, the intervertebral foramina in particular, remain unchanged at the adult stage. Prominent radiculomedullary arteries, readily visualized with modern angiography, therefore constitute a robust anatomical method to distinguish and correctly label ISAs. Nine angiographic cases are used to define the anatomy of the ISAs 5 to 9. Each observation is documented by a subtracted view depicting the vascular anatomy under consideration, and a native view allowing to correlate the described arterial structures with osseous landmarks for level identification.

Results

Our findings proved entirely consistent with Padget's nomenclature, confirming in particular that vascular elements attributable to the seventh ISA originate from the proximal portion of the supreme IA. The "normal" configuration of the supreme IA includes the last cervical ISA (ISA 7) and the first IA (ISA 8), while the second IA (ISA 9) appears to be a more variable component. As a consequence, in its most rudimentary form, a supreme IA should only consist of contributions from the seventh ISA, i.e., a radicular artery coursing along the 8th nerve as well as a few small branches aiming for the seventh vertebral body and the upper aspect of the first rib. Figure 1 shows a selective angiogram of a right costocervical trunk: the supreme IA provides the seventh, eighth, and ninth ISAs (C7, T1, and T2), with a prominent anterior radiculomedullary branch originating from the C7 ISA, and passing through the C7-T1 neural foramen along the eighth cervical nerve.

Note: Scanned images are included in the proceedings. Some submitted images were reduced during editing thereby decreasing clarity. Also, refer to the Program Planner. Proceedings Content as of 3/28/2014.



Conclusions

Our findings validate the terminology used by Padget, including the addition of a pro-atlantal artery and the identification of the ISA most commonly associated with the SubA as the sixth ISA. They also emphasize the need to redefine the anatomy of the supreme IA to incorporate the seventh cervical ISA.

KEYWORDS: Anatomy, Angiography, Spinal Vascular Disorders

0-567 3:14PM - 3:21PM
Advanced CT Imaging Predictors of Outcome in Acute Large Vessel Stroke Treated with Stent-Retrievers

S Patro¹, C Lum^v, M Ahmed^v, D Iancu^v, M dos Santos^v, R Thornhill^v, H Lesiuk^v

¹The Ottawa Hospital, Ottawa, Ontario, Canada, ²University of Ottawa, Ottawa, Ontario, Canada

Purpose

Recanalization rates are higher in acute anterior stroke patients treated with stent retrievers. Despite faster recanalization, some still have sizeable infarcts and poor outcome. The ASPECTS (Alberta Stroke CT Score) suggests >7 have better outcome. Smaller infarcts and better outcomes have been reported in patients with better

computed tomography angiography (CTA) collateral scores (CS). We sought to evaluate imaging predictors of outcome in acute proximal anterior circulation stroke patients undergoing comprehensive stroke imaging with NECT, CTA and CT perfusion and good recanalization with stent retrievers and newer generation intra-arterial therapies. Materials and Methods

We studied consecutive anterior circulation stroke patients presenting <12 hours onset with good (>TIMI 2) endovascular recanalization in the ICA or M1. An interventional neuroradiologist, blinded to outcome, retrospectively scored ASPECTS on NECT assessing subtle gray-white (GW) blurring (NECT-EI), hypodensity (NECT-hyp), loss of GW on CTA-source images (CTA-SI) and areas of low CBV. The 24-hour NECT ASPECT score was the reference standard. Two neuroradiologists blinded to outcome independently scored CTA collaterals using a four-point (0-3) scale. Intraclass correlation was used to assess agreement in collateral score between reviewers. Good outcomes were defined as mRS less than or equal to 2 and NIHSS>10. Sensitivity, specificity and accuracy by region were calculated. Repeated-measure ANOVA, Bonferroni multiple comparison and linear regression were used.

Results

Of 44 patients, 36(82%) had stent retrievers, 19 had CTP. Mean NIHSS and recanalization time = 17 and 67 mins, 34 (77%) had good outcomes. ASPECTS (IQR) was highest for NECT-EI=9.5 (8.5, 10.0), NECT-hyp=10,CBV=8.0, lowest for CTA-SI mean 6.8 (SD=2.7). Computed tomography angiography (CTA)-SI had highest acc=79%, sens=73%, spec=82% followed by CBV (75%, 62%, 82%). Linear regression correlated CBV and 24-hour CT (R2=0.22,p=0.04) and CTA-SI and 24-hour CT (R2=0.30, p=0.0001). There was good agreement between reviewers for CTA-CS (ICC=0.68, CI =0.4848-0.8088). There was no significant correlation with NECT-EI/Hyp and 24-hour CT or CTA-CS and 24-hour CT. Patients with good outcomes had less infarct (mean 8.2 versus 4.1, p<0.0001) and better CTA-SI (mean7.1 versus 5.1p=0.02) and CBV (mean7.8 versus 5.3, p=0.02). Median CTA-CS was 2.5 versus 2 in patients with good versus poor outcomes (p=0.11). ANOVA revealed differences between all imaging except CTA-SI versus CBV.

Conclusions

Computed tomography angiography-SI performed better than CBV in predicting final infarct in acute anterior stroke patients undergoing good recanalization. NECT underestimates the amount of infarct. There was a trend towards better CTA-CS in patients experiencing good outcomes after successful recanalization.

KEYWORDS: CT, Stents, Stroke

Note: Scanned images are included in the proceedings. Some submitted images were reduced during editing thereby decreasing clarity. Also, refer to the Program Planner. Proceedings Content as of 3/28/2014.

0-568 3:21PM - 3:28PM
Dose Reduction in Contrast-Enhanced MR Angiography of the Head and Neck: Reader Confidence, Quantitative Impact, and Field Strength Dependency

S Dehkharghani¹, A Saindane², D Qiu², L Albin³
¹Emory University Hospital, Atlanta, GA, ²Emory University, Atlanta, GA, ³Emory University School of Medicine, Atlanta, GA

Purpose

To test the feasibility of dose reduction in contrast-enhanced MRA (CE-MRA). Past studies suggest superiority of CE-MRA compared to noncontrast alternatives; however, concerns over untoward effects of gadolinium preclude use in some settings. We report the systematic comparison of full and reduced-dose CE-MRA at 1.5 and 3.0 T, with attention to reader confidence, signal-to-noise (SNR) and contrast-to-noise (CNR), hypothesizing feasibility and heightened tolerance to dose reduction at 3.0 T.

Materials and Methods

One hundred eight patients (60 female, ages 21-94) were included. Contrast-enhanced MRA protocols included: A-half dose (0.05mmol/kg) 1.5 T (n=23); B-full dose (0.1mmol/kg) 1.5 T (n=29); C-half dose 3.0 T (n=27); or D-full dose 3.0 T (n=29), with the iv power injection (2cc/s) of gadobenate dimeglumine (Multihance, Bracco Diagnostics) on Siemens systems (Siemens Healthcare, Erlangen, Germany). Imaging included 3D FLASH-based CE-MRA employing: 1) 1.5 T, TR/TE(ms)=3.09/1.11, $\theta=30^\circ$, voxel size=1.1mm isotropic, NEX=1, bandwidth=300Hz/Pixel; or 2) 3.0 T, TR/TE(ms)=2.78/1.03, $\theta=25^\circ$, voxel size=1.1x0.9x1.1 mm, NEX=1, bandwidth=650Hz/Pixel. Quantitative analysis included SNR, as well as CNR relative to reference fat (CNR_{fat}) or muscle (CNR_{muscle}) for the following: aortic arch (AA), common carotids, carotid bifurcations, and cervical ICA. Qualitative assessment of raw and maximum intensity images was performed by two neuroradiologists with attention to overall quality and reader confidence as follows: 3=exceptional; 2=good, diagnostic quality; 1=limited, but diagnosis possible; 0=severely limited. Segments interrogated for qualitative analysis included AA, CCA, ICA, and proximal (V1), intraforaminal (V2) and cervical-extraforaminal (V3) vertebral arteries.

Results

No significant qualitative differences were identified for most segments, with the exception of bilateral V2 and V3 segments ($p<0.03$). Among these four segments, pair-wise comparison demonstrated significant inferiority of half dose 1.5 T compared with the remaining three protocols, however still meeting diagnostic quality (mean rating V2_{right}=2.44; V2_{left}=2.52; V3_{right}=2.48; V3_{left}=2.52). No differences were present among the remaining protocols. Quantitative analysis comparing SNR and CNR between doses at 1.5 T demonstrated no significant difference at most segments, with the exception of cervical ICA bilaterally for all three measure (SNR, CNR_{fat}, CNR_{muscle}

$p<0.002$). By comparison, no significant differences in SNR or CNR were noted among any segments at 3.0 T, irrespective of dose.



Conclusions

Dose-reduced CE-MRA is achievable at 3.0 T without detriment to reader confidence or vascular enhancement. Even at 1.5 T, dose reduction generally may be tolerated from a qualitative standpoint in most vascular segments, however a negligible general degradation of image quality may be anticipated. These findings suggest that dose reduction is feasible at both field strengths, and may be considered where contraindications to full dose CE-MRA exist.

KEYWORDS: Angiography, Carotid Angiography, MRA

0-569 3:28PM - 3:35PM
Carotid Artery Dissection in CT. Does the colour improve the diagnostic confidence of the readers ?

L Saba¹, E Genovese², R Montisci², F Zaccagna³, E Raz⁴
¹University of Cagliari, Monserrato, Italy, ²University of Cagliari, Cagliari, Italy, ³University of Rome - Sapienza, Rome, Italy, ⁴New York University Medical Center, New York, NY

Purpose

The purpose of this work was to evaluate if the use of chromatic analysis, instead of the use of gray-scale, in the MDCTA study of carotid artery dissection (CAD) modify the observer's diagnostic accuracy.

Materials and Methods

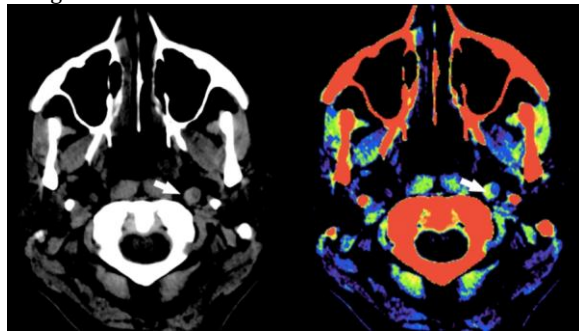
One hundred patients (61 men, 39 women; mean age, 51 years; range, 25 - 78 years) 40 with and 60 without CAD, that underwent MDCTA for suspected CAD formed the study cohort. In this study patients from three different groups were included (patients with MR confirmation of CAD, n = 40; patients with MR confirmation of CAD absence, n = 20; patients that underwent MDCTA of carotid arteries for atherosclerosis analysis, n = 40). Four blinded observers with different level of expertise (expert, intermediate A, intermediate B and trainee) analyzed the randomized basal scan of the MDCTA dataset using a cross-model (one case gray-scale and the following case using

Note: Scanned images are included in the proceedings. Some submitted images were reduced during editing thereby decreasing clarity. Also, refer to the Program Planner. Proceedings Content as of 3/28/2014.

the Chromatic-scale) and the presence of CAD was scored on a 5-point scale in order to assess the diagnostic confidence. After three months the four observers evaluated the same datasets by using the same cross-model with the inversion of the reading (one case Chromatic-scale and the following case using the gray-scale). Statistical analysis included receiver operating characteristics (ROC) curve analysis, the Cohen-weighted test and sensitivity, specificity, PPV, NPV, accuracy, LR+ and LR-.

Results

The ROC curve analysis showed that for all observers the use of Chromatic-scale produced an improvement of the diagnostic confidence with AUC values from 0.896 to 0.936; from 0.823 to 0.849; from 0.84 to 0.909 and 0.749 to 0.861 for expert, intermediate A, intermediate B and trainee observers. In particular the variation of diagnostic confidence (between the AUC areas) for the trainee was statistically significant (p = 0,036). Also accuracy, as well as sensitivity, specificity, PPV, NPV, LR+ and LR- were better using the chromatic scale.



Conclusions

Results of our study suggest that the use of chromatic scale instead the classic gray-scale improves the diagnostic confidence of the readers, in particular of the junior ones, by improving also the accuracy, sensitivity and specificity.

0-570 3:35PM - 3:42PM
Assessment of Anemia on Non-contrast Computed Tomography of the Head

A Chaudhry¹, M Gul², A Aivazi³, A Chaudhry⁴, J Dunkin³
¹Stony Brook University Medical Center, Westbury, NY, ²Winthrop University Hospital, Mineola, NY, ³Stony Brook University Medical Center, Stony Brook, NY, ⁴St Johns University, Westbury, NY

Purpose

We aim to evaluate whether diagnosis of anemia can be made on noncontrast CT of head by measuring attenuation of the intracranial dural venous sinuses.

Materials and Methods

A retrospective IRB-approved analysis of 280 randomly selected patients who underwent noncontrast CT head for various symptoms (headache, syncope, vertigo, etc.) at a tertiary care center in an emergency room or inpatient setting. Regions of interest (ROIs) (approx 3 mm in diameter) were placed on the superior sagittal sinus,

confluence of sinuses and bilateral transverse sinuses. Computed tomography (CT) attenuation values were obtained within a plus-minus of less than five units by two readers. These values were correlated with patients' hemoglobin and hematocrit values. Blood work for all patients was obtained within 24 hours of the CT scan. Patients were excluded from the study due to limitations including motion or streak artifact or unavailability of blood work within 24 hour of the CT scan. The two readers reviewed the studies in different locations and at different times and both blinded to patients' hemoglobin and hematocrit values.

Results

Two hundred forty-three patients (110 males, 133 females) mean age 59 (range 5 – 99 years) had CT attenuation values for all the dural venous sinuses averaged and categorized according to hemoglobin values of less than 8, 8-10, 10-14 and greater than 14, respectively. Mean CT attenuation values for reader A were for Hb < 8, 8-10, 10-14 and > 14 were 3.85, 42.66, 48.18 and 53.43 and with standard deviations of 5.91, 3.43, 3.43 and 4.25 respectively. Mean CT attenuation values for reader B were: 36.75, 42.05, 47.81 and 53.06 with standard deviation of 10.41, 4.87, 5.76 and 5.78, respectively. Linear regression analysis reveal highest positive correlation of hemoglobin and hematocrit values with CT attenuation at the confluence of sinuses with R2 value of 0.63. Interobserver agreement was found to be good using the kappa statistic.

Mean Age Range	Female	Male	Male:Female				
58.989 [5,99]	133	110	01:01.2				
	H/H <8	H/H 8-10		H/H <8	H/H 8-10	H/H >10	
Number pts	5	32	125	81	5	32	125
	Superior Sagittal (HU)				Superior Sagittal (HU)		
	Mean HU, Hb <8	Mean HU, Hb 8-10	Mean HU, Hb 10-14	Mean HU, Hb >14	Median HU, Hb <8	Median HU, Hb 8-10	Median HU, Hb 10-14
	34.2	42.438	46.63	51.34	36	42	47
ST.DEV	6.4807	3.1921	2.9918	3.4146			
	Transverse [R] (HU)				Transverse [R] (HU)		
	Mean HU, Hb <8	Mean HU, Hb 8-10	Mean HU, Hb 10-14	Mean HU, Hb >14	Median HU, Hb <8	Median HU, Hb 8-10	Median HU, Hb 10-14
	39.8	44.06	50.2	56.07	38	44	50
ST.DEV	7.4409	3.2422	3.4617	5.1395			
	Transverse [L] (HU)				Transverse [L] (HU)		
	Mean HU, Hb <8	Mean HU, Hb 8-10	Mean HU, Hb 10-14	Mean HU, Hb >14	Median HU, Hb <8	Median HU, Hb 8-10	Median HU, Hb 10-14
	37.2	43.47	50.37	55.98	37	43	50.5
ST.DEV	4.3243	3.4918	3.9887	5.016			
	Confluence (Torcula) (HU)				Confluence (Torcula) (HU)		
	Mean HU, Hb <8	Mean HU, Hb 8-10	Mean HU, Hb 10-14	Mean HU, Hb >14	Median HU, Hb <8	Median HU, Hb 8-10	Median HU, Hb 10-14
	32.2	40.656	45.52	50.34	32	41	46
ST.DEV	5.3821	3.7812	3.2969	3.41			
	Mean HU, Hb <8	Mean HU, Hb 8-10	Mean HU, Hb 10-14	Mean HU, Hb >14	Median HU, Hb <8	Median HU, Hb 8-10	Median HU, Hb 10-14
MEAN HU	35.85	42.66	48.18	53.43	35.75	42.5	48.38
Mean St. Dev	5.91	3.43					

Conclusions

Our study shows a direct positive correlation between attenuation value of the dural venous sinuses with patient's hemoglobin and hematocrit values with good interobserver agreement. Subset analysis reveals the highest positive correlation between patient's hemoglobin

Note: Scanned images are included in the proceedings. Some submitted images were reduced during editing thereby decreasing clarity. Also, refer to the Program Planner. Proceedings Content as of 3/28/2014.

and hematocrit with the attenuation values at the confluence of sinuses.

KEYWORDS: Dizziness, Dural Sinus, Vertigo

0-571 3:42PM - 3:49PM
Increased Number of White Matter Lesions in Patients with Familial Cerebral Cavernous Malformations

M Golden, L Morrison, B Hart
University of New Mexico, Albuquerque, NM

Purpose

Familial cerebral cavernous malformations (fCCMs) represent an autosomal dominant disorder which results in significant morbidity and mortality in affected patients. The disorder is most prevalent in the Southwest, where the affected families usually are carriers of the Common Hispanic Mutation (KRIT 1 or CCM1). The brain parenchyma is affected by increased numbers of cavernous malformations. Multiple studies have shown abnormalities of endothelial cell junctions and the blood-brain barrier in CCMs. Endothelial cell abnormalities also have been described in pathologic studies of WMHI. We examined WMHI in a population with fCCM.

Materials and Methods

We examined 191 subjects with familial CCMs, enrolled into an IRB-approved study. All carry the same CCM1 mutation. Each subject had 3 T MRI, including GRE, SWI and FLAIR sequences. The number of cavernous malformations was counted, as well as the number of nonhemorrhagic WMHI. Subjects over age 60 years were excluded. The fCCM subjects then were compared to a normal population. Logistic regression was performed for possible correlations of WMHI in the fCCM group with age, gender, headaches, hypertension, hyperlipidemia or seizure history.

Results

Familial CCM1 carriers have an abnormally increased rate of nonhemorrhagic white matter lesions compared to a normal population. Logistic regression showed mild age effect and no statistical association with gender, headaches, hypertension, hyperlipidemia or seizure history.

Conclusions

Familial CCM1 carriers have not only an increased rate of cerebral cavernous malformations, but also have white matter T2 hyperintensities, spatially distinct from CCMs, that exceed that of a normal population. To our knowledge this relationship has not been reported previously. This finding suggests an additional manifestation of endothelial abnormalities in this population.

KEYWORDS: Cavernous Malformation, White Matter Disease

0-572 3:49PM - 3:56PM
Ultralow radiation for neck CT angiograms. CTA as a screening test for carotid disease?

D Lira¹, R Gonzalez¹, M Lev², M Kalra¹, S Singh¹, J Romero²
¹Massachusetts General Hospital, Boston, MA,
²Massachusetts General Hospital, Harvard Medical School, Boston, MA

Purpose

The purpose of the study is to develop a neck computed tomography angiography (CTA) protocol that drastically reduces radiation dose while maintaining diagnostic image quality. Computed tomography angiography has become a method of choice for evaluation of carotid artery disease, allowing precise delineation of arterial walls and surrounding tissues, assessment of obstructed lumen and plaque configuration for disease diagnosis, follow up and surgical planning. Widespread use has led to concerns regarding radiation dose, particularly on young patients and repeat examinations, with special consideration of anatomical proximity to the thyroid and lenses, both radiosensitive organ.

Materials and Methods

A new reduced radiation dose scanning protocol for neck CTA (100 Kv, 140 Ma, Pitch 0.5, rot time 0.5 seg) was developed at our institution and applied on 10 patients who underwent the exam with indication of vascular disease. The exams were reviewed by two staff radiologists who assessed image quality and diagnostic capability, both on standard thin slice (0.625 mm) images, orthogonal views and dedicated high resolution individual vessel reconstructions. Total radiation doses were obtained, and compared against the standard of care protocol (120 Kv, 235 Ma, Pitch 0.5, rot time 0.5 seg). Measurements of vessel contrast (Hounsfield Units), noise (expressed by SD of the vessel ROI measurement), CNR and SNR were calculated on 10 different areas from the aortic arch to the base of the skull, then compared between the two protocols.

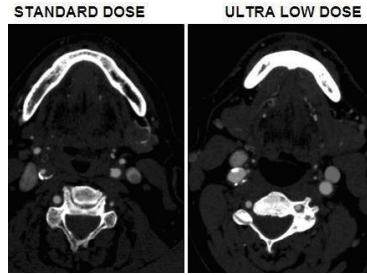
Results

All 10 exams were considered satisfactory regarding image quality and possessed full diagnostic capabilities. Adequate image resolution was obtained for the neck soft tissues. Compared to standard of care protocol, a 62% reduction was obtained for radiation dose (CTDI 42 mGy vs 16 mGy) and estimated dose for thyroid (14.2 mSv versus 5.1 mSv). Objective measurements showed higher contrast (430 HU versus 500 HU), similar noise (19.7 versus 19.4), slightly elevated CNR and SNR (24.1 versus 26.4 and 28.5 versus 29.9, respectively).

Table 1: Comparison of vessel contrast parameters between two different protocols

	Standard Dose	Ultra Low Dose	% Difference
Vessel HU	430.4	500.2	16
Noise	19.7	19.4	1
CNR	24.1	26.4	9
SNR	28.5	29.9	5

Note: Scanned images are included in the proceedings. Some submitted images were reduced during editing thereby decreasing clarity. Also, refer to the Program Planner. Proceedings Content as of 3/28/2014.



	Standard Dose	Ultra Low Dose	% Difference
Vessel HU	430.4	500.2	16
Noise	19.7	19.4	1
CNR	24.1	26.4	9
SNR	28.5	29.9	5

Conclusions

With the number of neck CTA exams rising, efforts must be made in order to keep radiation doses in the minimum possible without compromising image quality. This new low dose protocol enables full diagnostic capabilities of vascular disease with significant dose reduction, maintaining the quality of advanced high resolution individual vessel reconstructions. There is potential for further dose reduction, which can be researched and applied in future studies.

KEYWORDS: Carotid Artery, Radiation Dose Reduction, Stroke

O-573 3:56PM - 4:03PM
Cervical Injury Patterns in Blunt Cerebrovascular Injury

M Booker¹, J Lammering², M Shiroishi³, M Law³, J Go⁴
¹Keck School of Medicine, Los Angeles, CA, ²University of Southern California, Glendale, CA, ³University of Southern California, Los Angeles, CA, ⁴LAC/University of Southern California Medical Center, Los Angeles, CA

Purpose

Blunt cerebrovascular injury (BCVI) is thought to occur in 1% of blunt trauma patients and 15% of high-risk patients. While most patients are asymptomatic at presentation, the early identification and treatment of blunt carotid artery (BCAI) or blunt vertebral artery injury (BVAI) can greatly reduce mortality and stroke rates. This study examines the cervical injury patterns associated with BCVI along with the screening efficacy, incidence, and outcome of patients. Materials and Methods

A retrospective search between January 1, 2009 and June 30, 2013 was conducted at the LAC+USC Medical Center, a level 1 trauma center, to identify all patients either screened for or diagnosed with BCVI. Images were acquired on a Toshiba 64 MDCT scanner reconstructed to 1 mm in all three orthogonal planes. Cervical and skull base injuries were recorded for all patients (Table 1); a documented seatbelt sign was noted for those patients experiencing a motor vehicle collision (MVC). Statistical analysis was conducted with JMP 10 using log and Chi-square Likelihood tests.

Results

There were 14,055 total patients (4,418 post-MVC) evaluated for blunt trauma to the head or neck with 517 (249 post-MVC) screening CTAs performed (screening rate 3.7%). Thirty-seven screened patients were diagnosed with BCVI for a screening yield of 7.2%; additionally, seven unscreened patients later developed BCVI for a total BCVI population of 44 (incidence rate 0.32%). These 44 patients had 25 BVAIs and 32 BCAIs, with multivessel injury occurring in 10 patients. Ten patients suffered stroke (7 of whom were unscreened) with two subsequent deaths (both were unscreened). Of note, BCAI was present in every stroke or death. To our knowledge there were no imaging false negatives. A cervical or skull base injury was recorded in the BCVI, BVAI, and BCAI subgroup in 16 (36%), 14 (58%), and five (18%) cases, respectively. Please see Table 1 for specific injury pattern, age, and gender correlation statistics. A seatbelt sign was documented in 118 of 249 MVC cases (47%) - 4 of 22 (18%) in the BCVI group and 114 of 227 (50%) in the non-BCVI group. Consequently, the seatbelt sign was not predictive of BCVI (p-value 0.99) but, in fact, negatively correlated (OR 0.22)

Table 1: Injury Patterns in BCVI, BVAI, and BCAI

Blunt Cerebrovascular Injury (BCVI)	BCVI	No-BCVI	All	OR	OR CI (95%)	Uni p-val	Multi p-val
Displacement into Transverse foramen	4 (9.0%)	2 (0.4%)	6 (1.1%)	23.9	4.25-134.5	0.00*	0.04*
Transverse foramina involvement	6 (13%)	13 (2.7%)	19 (3.6%)	5.67	2.04-16.77	0.00*	0.77
Transverse process fracture	4 (9.0%)	12 (2.5%)	16 (3.0%)	3.9	1.20-12.65	0.04*	0.61
Facet subluxation/di/slocation	4 (9.0%)	13 (2.7%)	17 (3.2%)	3.59	1.12-11.53	0.05*	0.29
Any cervical-basilar fracture	16 (36%)	75 (16%)	91 (17%)	3.09	1.99-4.98	0.00*	0.16
C1-C2 fracture	5 (11%)	20 (4.1%)	25 (4.7%)	2.95	1.05-8.28	0.05*	0.71
Skull base fracture	4 (9.0%)	34 (7.0%)	38 (7.2%)	1.31	0.44-3.88	0.4	0.67
MVA	22 (5%)	227 (47%)	249 (47%)	1.11	0.50-2.07	0.75	0.41
(Gender (Female)	14 (31%)	163 (33%)	177 (33%)	0.91	0.47-1.76	0.87	0.7
Age	47.9 ± 21.6	40.4 ± 20.6	41.0 ± 20.8	1.02		0.02*	0.00*
Blunt Vertebral Artery Injury (BVAI)	BVAI	No-BVAI	All	OR	OR CI (95%)	Uni p-val	Multi p-val
Displacement into Transverse foramen	4 (16%)	2 (0.4%)	6 (1.1%)	49.8	8.61-288	0.00*	0.04*
Transverse foramina involvement	6 (25%)	13 (2.6%)	19 (3.6%)	12.49	4.26-36.6	0.00*	0.8
Transverse process fracture	4 (16%)	12 (2.4%)	16 (3.0%)	8.13	2.41-27.5	0.00*	0.47
Any cervical-basilar fracture	14 (56%)	77 (16%)	91 (17%)	7.69	3.30-17.94	0.00*	0.02*
Facet subluxation/di/slocation	4 (16%)	13 (2.6%)	17 (3.2%)	7.49	2.24-25.0	0.01*	0.24
C1-C2 fracture	5 (20%)	20 (4.1%)	25 (4.7%)	6.32	2.14-18.5	0.00*	0.95
MVA	14 (56%)	235 (47%)	249 (47%)	1.58	0.69-3.62	0.3	0.3
Skull base fracture	2 (8.3%)	36 (7.2%)	38 (7.2%)	1.17	0.26-5.18	0.53	0.31
(Gender (Female)	6 (25%)	171 (34%)	177 (33%)	0.64	0.25-1.85	0.51	0.37
Age	43.9 ± 23.6	40.9 ± 20.7	41.0 ± 20.8	1.01		0.5	0.29
Blunt Carotid Artery Injury (BCAI)	BCAI	No-BCAI	All	OR	OR CI (95%)	Uni p-val	Multi p-val
Skull base fracture	3 (10%)	35 (7.0%)	38 (7.2%)	1.85	0.47-5.75	0.31	0.68
Transverse process fracture	1 (3.7%)	15 (3.0%)	16 (3.0%)	1.24	0.16-9.72	0.58	0.74
Any cervical-basilar fracture	5 (18%)	86 (17%)	91 (17%)	1.09	0.40-2.95	0.52	0.74
Facet subluxation/di/slocation	1 (3.7%)	19 (3.6%)	19 (3.6%)	1.02	0.13-7.97	0.64	0.43
Transverse foramina involvement	9 (33%)	168 (33%)	177 (33%)	0.98	0.43-2.23	1	0.82
(Gender (Female)	12 (44%)	237 (47%)	249 (47%)	0.88	0.40-1.91	0.84	0.37
MVA	0 (0%)	25 (5.0%)	25 (4.7%)	0		1	1
C1-C2 fracture	0 (0%)	6 (1.2%)	6 (1.1%)	0		1	1
Displacement into Transverse foramen	0 (0%)	17 (3.4%)	17 (3.2%)	0		1	1
Facet subluxation/di/slocation	0 (0%)	17 (3.4%)	17 (3.2%)	0		1	1
Age	52.5 ± 20.8	40.4 ± 20.6	41.0 ± 20.8	1.03		0.00*	0.00*

Conclusions

BCVI is a rare event overall (incidence 0.32%) but relatively common in high-risk patients (screening yield

Note: Scanned images are included in the proceedings. Some submitted images were reduced during editing thereby decreasing clarity. Also, refer to the Program Planner. Proceedings Content as of 3/28/2014.

7.2%). Despite its widespread use, the cervical seatbelt sign had no predictive value in our data. However, the negative correlation is likely a result of statistical bias introduced from its active use as a screening factor at our institution. In addition, many classic BCVI injury patterns were associated only with vertebral artery injury - notably those involving the transverse foramen. Blunt carotid injury remains very difficult to predict as "skull base fracture" was only weakly associated.

KEYWORDS: Carotid Artery, Motor Vehicle Crash, Vertebral Artery

0-574 4:03PM - 4:10PM
Developmental venous anomalies are commonly associated with metabolic abnormality in otherwise normal-appearing brain parenchyma

M Larvie¹, J Thum², D Timerman²
¹Massachusetts General Hospital, Boston, MA, ²Harvard Medical School, Boston, MA

Purpose

Developmental venous anomalies (DVAs) are the most common intracranial vascular abnormality. Although the deleterious effects of large DVAs on brain parenchyma have been well documented, small DVAs typically are regarded as inconsequential and of no clinical significance. We recently have noticed that cortical hypometabolism, as identified on 18F-fluorodeoxyglucose (FDG) PET, commonly is associated even with small DVAs with no other apparent abnormality in the adjacent brain tissues. To better understand the features typical of brain parenchyma associated with DVAs, we analyzed all DVAs that we could identify that have been characterized at our institution with both FDG positron emission tomography (PET) and magnetic resonance imaging (MRI).

Materials and Methods

This study consists of a retrospective analysis of DVAs that have been characterized by both FDG PET and MRI at our institution. A total of 25 DVAs were identified in 22 subjects. These DVAs were characterized qualitatively for degree of metabolic abnormality in the adjacent brain parenchyma (none, mild, moderate and severe) and classified by size (small, medium and large). Abnormalities in the adjacent brain parenchyma were assessed, including MRI signal abnormality, atrophy, calcification, cavernous malformation, hemorrhage and calcification.

Results

Cortical hypometabolism was identified in a majority, 68%, of DVAs. Features correlated with higher degrees of hypometabolism include older age and larger size of the DVA. In contrast, a much smaller fraction of lesions demonstrated brain parenchymal abnormalities that were apparent on structural imaging, including atrophy (12%), T2 hyperintensity (8%), calcification (8%) and cavernous malformation (8%). Of note, one of the DVAs in our sample demonstrated marked hypermetabolism on an FDG PET scan performed at the time of a seizure.

Conclusions

Although most DVAs have no associated brain parenchymal abnormality, we find that a majority of DVAs are associated with hypometabolism as assessed by brain FDG PET. The degree of metabolic abnormality is positively correlated with greater age and size. The common understanding of small DVAs as clinically insignificant deserves reconsideration, and in certain clinical contexts, particularly in patients with epilepsy, further evaluation may be warranted, in particular through FDG PET.

KEYWORDS: Brain Development, Developmental Venous Anomalies, PET

0-575 4:10PM - 4:17PM
Admission CTA without additional MRI allows reliable diagnosis of cervical artery dissection.

U Hanning, M Schmiedel, W Heindel, T Niederstadt, R Dittrich
University Hospital of Muenster, Münster, Germany

Purpose

Spontaneous dissections of the cervical arteries are an important etiology of juvenile stroke. The currently accepted diagnostic gold standard is the contrast-enhanced MR angiography of the cervical arteries in combination with fat suppressed T1-weighted axial sequences of the neck. In this retrospective study we sought to find out the diagnostic value of the CT angiography in comparison to the MR-investigation in the acute phase of the disease.

Materials and Methods

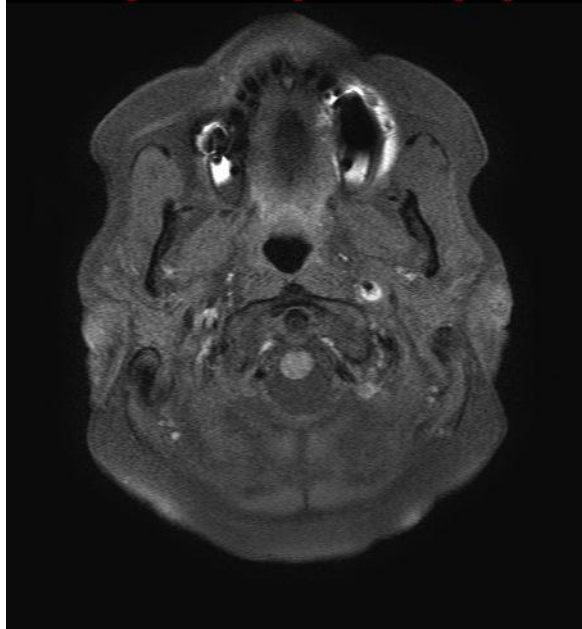
One hundred eighty-eight consecutive patients with the diagnosis of cervical artery dissection have been screened for the study within the time period from January 2005 to May 2013. Forty patients with 43 dissected arteries have been included for further analysis since these patients received both imaging modalities CT angiography and MR angiography with fat suppressed axial sequences. All images have been reviewed by two experienced neuroradiologists concerning the occurrence of the following characteristic radiological features: (1) smooth or slightly irregular tapered stenosis (CT/MR), (2) arterial occlusion (rattail-shaped tapered, flame-like) (CT/MR), (3) lumen irregularity, irregular dilatation (CT/MR), (4) pseudoaneurysm (saccular or fusiform aneurysmal dilatation) (CT/MR), (5) intimal flap (CT/MR), (6) wall thickening (e.g., suboccipital ring sign) (CT), (7) crescent sign (methemoglobin of the intramural hematoma in axial T1-weighted fat-suppressed images) (MR).

Results

In 29 cases a dissection of the internal carotid artery and in 14 cases a dissection of the vertebral artery have been found. The mean time from symptom onset to hospitalization was four days. In 39 patients, the CT angiography was the first diagnostic procedure followed by the MR investigation with a mean delay of 3.6 days. Characteristic radiological features of a cervical artery dissection could be detected in all arteries with both imaging modalities namely the smooth or slightly irregular

Note: Scanned images are included in the proceedings. Some submitted images were reduced during editing thereby decreasing clarity. Also, refer to the Program Planner. Proceedings Content as of 3/28/2014.

tapered stenosis/occlusion and the lumen irregularity or irregular arterial dilatation.



ACI (40 patients – 27 ACI)		
features	CT	MRI
1. smooth or slightly irregular stenosis	100%	100%
1. arterial Occlusion	26%	26%
1. lumen irregularity, irregular dilatation	100%	100%
1. Pseudoaneurysm	22%	22%
1. intimal flap	7%	7%
1. wall thickening (only CT)	81%	X
7. crescent sign (only MRI)	X	93%
VA (40 patients – 13 VA)		
features	CT	MRI
1. smooth or slightly irregular stenosis	100%	100%
1. arterial Occlusion	69%	77%
1. lumen irregularity, irregular dilatation	100%	100%
1. Pseudoaneurysm	0%	8%
1. intimal flap	0%	0%
1. wall thickening (only CT)	46%	X
7. crescent sign (only MRI)	X	92%

Conclusions

Both imaging modalities have a high diagnostic sensitivity in the detection of cervical artery dissection with an equivalent diagnostic value. Even if the pathognomonic intramural hematoma is visible by MRI only, other characteristic features of cervical artery dissection can be detected by very reliably CT angiography. With the typical clinical presentation in the absence of severe atherosclerosis it is possible to make the diagnosis of cervical artery dissection with CT angiography.

KEYWORDS: Carotid Dissection, Dissection, Vertebral Artery Dissection

Spots and Swirls: Relationship between Hematoma Heterogeneity, CTA Spot Sign, and Hematoma Expansion

T Huynh¹, D Connor¹, A Demchuk², D Dowlatshahi³, D Gladstone¹, S Subramaniapillai¹, S Symons¹, R Aviv¹
¹University of Toronto and Sunnybrook Health Sciences Centre, Toronto, ON, Canada, ²University of Calgary, Calgary, AB, Canada, ³University of Ottawa, Ottawa, ON, Canada

Purpose

Hematoma heterogeneity on noncontrast CT (NCCT) in acute intracranial hemorrhage (ICH), characterized both by qualitative and quantitative means, has been shown to be predictive of hematoma expansion and mortality. This may be partially related to the presence of active extravasation in which uncoagulated blood appears iso- or hypodense relative to the surrounding clot, previously coined the 'Swirl Sign'. Recently the quantitative CT densitometry (qCT) parameter coefficient of variation was found to be the best predictor of absolute hematoma volume expansion. Analysis of qCT parameters may be automated to further improve rapid and reliable prediction of expansion in the acute setting. Noncontrast CT predictors of expansion may be helpful in identifying patients who may benefit from hemostatic therapy without the need of intravenous contrast administration. We sought to evaluate the ability of hematoma heterogeneity, characterized by the Swirl Sign and qCT parameters, to predict hematoma expansion and the presence of a CT angiography (CTA) Spot Sign.

Materials and Methods

This retrospective study reviewed all primary ICH patients entered into a departmental stroke database between September 2006 and December 2012. Study inclusion criteria were all patients presenting to a tertiary hospital emergency department with stroke symptoms attributable to ICH. Patients with secondary ICH were excluded. Patients underwent standard institutional acute ICH CT protocol including noncontrast CT, CTA, and postcontrast CT. A semi-automated region of interest algorithm was applied to determine hematoma boundaries originating from a user-defined seed. Low density regions were included in the region of interest (ROI) only if they were surrounded by hematoma. Hematoma volumes and qCT parameters including mean, standard deviation, coefficient of variation, skewness, and kurtosis were calculated from hematoma regions on NCCT. Each hematoma was assessed by a blinded staff neuroradiologist for the presence of Spot Signs and to dichotomize cases into homogeneous or heterogeneous. Heterogeneous hematomas were defined as those with enclosed regions which were iso- or hypodense relative to brain parenchyma on NCCT. Those cases with heterogeneities were examined to determine whether the heterogeneity was a Swirl Sign. Logistic regression analyses were performed to assess predictors of hematoma expansion (>6ml or >33% hematoma expansion) and CTA spot sign presence.

Results

Note: Scanned images are included in the proceedings. Some submitted images were reduced during editing thereby decreasing clarity. Also, refer to the Program Planner. Proceedings Content as of 3/28/2014.

In total, 71 patients were included in the study. Mean (SD) age and gender of included patients were 68.2 ± 15.6 years and 46/71 (65%) male respectively. Median (interquartile range, IQR) NIHSS, TTS, time from baseline to follow-up CT, baseline and follow-up hematoma volumes were 10 (6 – 16), 1.9 (1.3 – 4.6) hours, 23.0 (17.8 – 27.2) hours, 18.1 (5.3 – 37.6) mL, and 18.7 (7.6 – 39.6) mL respectively.

Intraventricular hemorrhage was present in 36 (51%) patients. A Swirl Sign was present in 33 (47%) hematomas and 36 (51%) were characterized as heterogeneous.

Hematoma expansion of >6 ml or >33% occurred in 21 (30%) patients. A CTA spot sign was present in 26 (37%) patients and in patients with a spot sign present, median (IQR) number of spots was 2 (1 – 3). Univariate predictors of hematoma expansion included the Swirl Sign ($p=0.031$), qCT standard deviation ($p=0.029$), Spot Sign presence ($p=0.020$), and Spot Sign number ($p=0.009$). Trend associations were noted for time from onset < 3 hours ($p=0.059$), $\text{INR}>1.5$ ($p=0.057$), hematoma heterogeneity ($p=0.062$), mean density ($p=0.052$), and coefficient of variation ($p=0.059$). Backwards stepwise logistic regression excluding variables obtained on CTA identified that Swirl Sign and standard deviation of hematoma density were independent predictors of expansion.

Including CTA variables, Spot Sign number was the best predictor of expansion. Univariate predictors of Spot Sign included time to scan < 3 hours ($p=0.045$), Swirl Sign ($p=0.002$), heterogeneous hematomas ($p=0.002$).

Multivariable regression identified that time to scan and Swirl Sign were independent predictors of expansion.

Conclusions

Noncontrast CT predictors of expansion include Swirl Sign, hematoma heterogeneity, and qCT standard deviation.

Swirl Sign and hematoma heterogeneity also were predictive of Spot Sign presence. Time from symptom onset < 3 hours was predictive of both hematoma expansion and Spot Sign presence. Noncontrast CT may be helpful in identifying patients at risk for hematoma expansion and demonstrating a Spot Sign.

KEYWORDS: Intracerebral Hemorrhage

0-577 4:24PM - 4:31PM
Hereditary Hemorrhagic Telangiectasia: Spectrum of CNS Manifestation

D Lin¹, G Robinson², A Zessler³

¹The Johns Hopkins University School of Medicine, Baltimore, MD, ²Johns Hopkins Hospital, Baltimore, MD,

³Johns Hopkins University, Baltimore, MD

Purpose

Patients with hereditary hemorrhagic telangiectasia (HHT), an autosomal dominant disease, present with epistaxis, mucocutaneous telangiectasia and visceral vascular malformations. While brain arteriovenous malformations (AVMs) occur in HHT at a lower frequency than pulmonary and GI vascular malformations, the potentially life-threatening risk of cerebral hemorrhage makes an early and accurate diagnosis of cerebral AVMs particularly

important. Current recommendation is for all patients with the diagnosis of HHT to undergo a screening brain MRI. The purpose of this presentation is to review the spectrum of central nervous system (CNS) manifestations revealed by current standard MR imaging (MRI)/MR angiography (MRA) protocol.

Materials and Methods

Between 2009 and 2012, 191 patients were evaluated in our HHT Clinical Center and fulfilled Curaçao diagnostic criteria. One hundred fifty-one of these patients had screening brain MRI with contrast and MRA, and five had MRI of the spine in addition to the brain.

Results

Forty (26%) of the 151 patients had imaging abnormalities. Eleven (7%) had cerebral AVMs, majority of which were micro AVMs (< 1cm). Nine had developmental venous anomalies, in some cases with multiplicity. Eight had old infarcts, six had old hemorrhage or punctate hemosiderin deposit, two had cerebral aneurysms, one had infundibulum, and one had brain abscess related to pulmonary AVM. There were two cases of spinal perimedullary arteriovenous fistulas (AVF) that were large at presentation, both occurring in children (at age 2 and 6).

Conclusions

A spectrum of CNS vascular abnormalities occur in patients with HHT at a rate of 26%, similar to what is recorded in the literature. Of note, spinal AVF is currently not part of the diagnostic criteria, but should raise the suspicion in a child presenting with back symptoms as the current screening MRI does not routinely include evaluation of the spine.

KEYWORDS: AVF, AVM

0-578 4:31PM - 4:38PM
Susceptibility MRI Clot Width - Normalized to Thin Slice CT Hyperdense Clot Width – is a Highly Accurate Marker for the Development of Any Intra-parenchymal Hemorrhage Following Intra-arterial Clot Retrieval Therapy in Acute MCA Stroke

S Kamalian¹, A Yoo¹, S Kamalian¹, J Romero², J Hirsch¹, M Lev¹

¹Massachusetts General Hospital, Boston, MA,

²Massachusetts General Hospital, Harvard Medical School, Boston, MA

Purpose

We previously have shown that MCA clot susceptibility artifact width <5 mm on admission GRE T2* (and/or PWI) may identify acute stroke patients at very low-risk (NPV 98%) for developing parenchymal hematoma (PH), following intra-arterial clot-retrieval therapy. Our current purpose is to determine if a more refined measure of the precise degree of susceptibility "blooming" artifact – specifically, the ratio of clot susceptibility width (CSW) to that of corresponding hyperdense MCA clot width on thin-slice CT scans – could more accurately correlate with the risk of developing ANY intraparenchymal hemorrhage (IPH) following endovascular clot retrieval.

Note: Scanned images are included in the proceedings. Some submitted images were reduced during editing thereby decreasing clarity. Also, refer to the Program Planner. Proceedings Content as of 3/28/2014.

Materials and Methods

From a dataset of 125 consecutive AIS patients who received intra-arterial therapy (IAT) between 1/1/2010 to 12/1/2013, and had available admission THIN-SECTION noncontrast CT (ts-NCCT) for review, we identified 62 who met the following additional inclusion criteria: (1) MCA M1 or M2 occlusion; (2) Available admission gradient recalled echo (GRE); and (3) Follow-up noncontrast CT. We measured both the maximum width of clot-related susceptibility artifact (CSW) and the corresponding width of hyperdense MCA clot width at the same location on thin-slice CT scans. Clot susceptibility width was normalized to CT clot-width ("nCSW"). SCW, CT clot-width, and nCSW were compared in three groups according to the degree of IPH as defined by the ECASS classification.

Results

There were 40 patients without IPH (Group 1), 14 patients with hemorrhagic infarction (HI1 and HI2 petechial hemorrhage), and eight patients with parenchymal hematoma (PH1 and PH2). Both SCW and nCSW were significantly higher in Groups 2 (medians 6.5 mm, 2.5 mm) and 3 (medians 7.6 mm, 2.8 mm) compared to group 1 (medians 3.9 mm, 1.3 mm; Mann-Whitney all $P < 0.01$). SCW and nCSW were not significantly different when comparing Group 2 to Group 3 (Mann-Whitney, $P < 0.01$). CT clot-width was not significantly different between any combination of Groups (Kruskal-Wallis, $P > 0.05$). ROC curve analysis for distinguishing between patients with and without hemorrhage (Group 1 versus Groups 2 & 3) using SCW showed: AUC = 0.83, optimal threshold = 5.5, sensitivity = 80% and specificity = 77%. Receiver operator characteristic (ROC) curve analysis for nCSW showed: AUC = 0.92, optimal threshold = 1.8, sensitivity = 86% and specificity = 89%.

Conclusions

In acute MCA stroke patients, the width of maximal MRI clot susceptibility blooming artifact - normalized to the corresponding clot width on thin-slice unenhanced CT, with a threshold of approximately 2 - is highly accurate for determining the risk of developing any IPH following intra-arterial clot-retrieval therapy. We speculate that blooming artifact may not only be a marker for overall clot burden, but also may reflect the degree of regional vessel wall injury and blood-brain barrier breakdown - both risk factors for PH development.

KEYWORDS: Hemorrhagic Transformation, Intraarterial Thrombolysis, Stroke

Wednesday, May 21
3:00PM - 4:30PM
Room 520

69 - PARALLEL PAPERS: Pediatrics: New Techniques

0-579 3:00PM - 3:07PM
HARDI Tractography for Quantitative Assessment of the Auditory System in Autism

J Berman¹, D Chudnovskaya¹, L Blaskey¹, T Roberts¹

¹Children's Hospital of Philadelphia, Philadelphia, PA

Purpose

Given the social and language impairments common in autism spectrum disorder (ASD), research has focused on cortices and white matter related to the temporal lobe structures. Prior studies have examined the structure of the superior temporal gyrus and arcuate fasciculus in autism and discovered developmental abnormalities including abnormal lateralization (1). The auditory radiation provides sensory input to the superior temporal gyrus, but can not be studied reliably with diffusion tensor imaging because of the presence of crossing fibers. High angular resolution diffusion imaging is necessary to reliably perform tractography of the auditory radiation tracts and generate tract-specific metrics of microstructure (2). This study applies HARDI tractography to quantitatively assess the auditory radiation and to probe microstructural differences in ASD.

Materials and Methods

Imaging was performed on 34 right-handed children (11 controls, 23 with ASD, mean age 11.3 years) at 3 T. Whole-brain HARDI acquisition included 64 gradient directions at $b = 3000 \text{ s/mm}^2$; TR 16.9s; TE 110ms; voxel size $2 \times 2 \times 2 \text{ mm}$. Eight children received two HARDI acquisitions to access reproducibility. Probabilistic HARDI tractography (2) of the auditory radiation was performed to generate tract-specific measures of generalized fractional anisotropy (GFA) and traditional DTI parameters including FA, mean, axial, and radial diffusivities. Left to right hemispheric asymmetry of diffusion metrics was measured as a percent difference. Group differences in the marginal means of the diffusion measures were assessed with age and perceptual reasoning index covaried in a general linear model.

Results

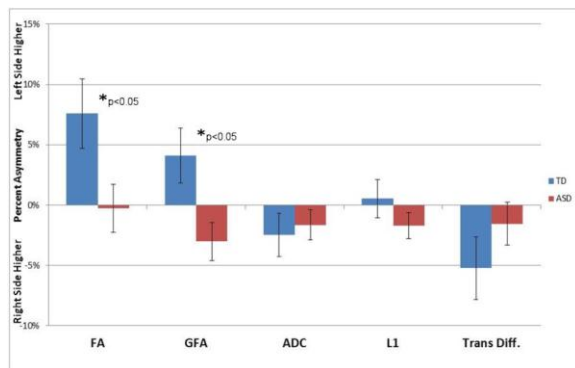
Measurements of the auditory radiation had a reproducibility intraclass correlation coefficient of 0.92 for mean diffusivity and 0.74 for FA. Significant changes of hemispheric asymmetry in ASD was observed with FA and GFA, but not mean, axial, or radial diffusivities (see Figure). Fractional anisotropy (FA) asymmetry was biased towards the left hemisphere in controls 7.58% and slightly towards the right 0.25% in ASD, with a significant difference between the two groups ($p = 0.033$). Generalized FA asymmetry was biased towards the left 4.11% in controls and 3.02% towards the right in ASD, with a significant difference between the two groups ($p = 0.016$). Linear regression of the diffusion metrics with social responsiveness scores (SRS) showed a significant positive correlation with volume of fiber tracks ($p = 0.021$).

Note: Scanned images are included in the proceedings. Some submitted images were reduced during editing thereby decreasing clarity. Also, refer to the Program Planner. Proceedings Content as of 3/28/2014.

Conclusions

HARDI tractography is capable of quantifying the entire auditory radiation which is inaccessible with diffusion tensor imaging (DTI) tractography because of crossing fibers. The pattern of diffusion anisotropy asymmetry in ASD indicates an alteration of the auditory radiation's structure. This study contributes evidence of the biological basis of autism's symptoms. The structural abnormalities previously observed in Heschl's gyrus and cortico-cortico connections also are present in the core thalamocortico tracts. The structural abnormalities to the auditory sensory tract are expected to be closely linked to the auditory and language dysfunctions common in ASD.

KEYWORDS: Autism Spectrum Disorder, Diffusion MR Imaging, Fiber Tracking



0-580

3:07PM - 3:14PM

Patterns of Structural Co-Variance Associated with Autism Spectrum Disorder in Extremely Preterm Neonates: A Novel Voxel-Wise Graph Theoretic Approach

C Whitlow¹, N Padilla², E Eklöf², G Mårtensson², M O'Shea¹, J Maldjian¹, B Skiöld², M Blennow², B Vollmer², U Ådén²

¹Wake Forest University, School of Medicine, Winston-Salem, NC, ²Karolinska Institutet, Stockholm, Sweden

Purpose

Evidence is growing that there is structural co-variance between spatially distributed areas of the brain, such that cortical thickness in one region affects thickness in other regions that are functionally connected (1). We hypothesize that brain structural co-variance will be present at voxel-wise magnetic resonance imaging (MRI) resolution, and can be evaluated using graph theoretical analysis to identify patterns of spatially distributed

volumetric brain abnormality associated with autism spectrum disorder in extremely preterm neonates.

Materials and Methods

Conventional high-resolution T1-weighted structural MRI was acquired at term-equivalent age from 25 extremely preterm neonates (<27 weeks of gestation), and 15 healthy term controls born in Stockholm, Sweden between January 2004 and March 2007. Six of the 25 preterm neonates were diagnosed with autism spectrum disorder based upon Social Responsiveness Scale and/or clinical diagnosis at a 6.5-year follow-up examination. Automatic segmentation of 3D T1-weighted images using neonatal probabilistic atlases and VBM-DARTEL in SPM8 was performed. Processed gray matter volume images from all subjects in each group were concatenated into a 4D image data file that was used to construct a group-specific voxel-wise 60,542 x 60,542 correlation matrix. Binarized adjacency matrices then were generated at a cost of 0.1 from which modularity maps were computed, with each color representing a different module containing voxels of similar gray matter volume.

Results

Modularity maps from graph theoretical analysis demonstrated qualitative whole-brain differences in patterns of structural co-variance in preterm neonates with autism spectrum disorder compared to nonautistic preterm and term controls (Figure 1). Specifically, between-group differences were identified in regions comprising the frontal, occipito-parietal, and temporal cortices, where gray matter volumetric differences have been described in other MRI studies of extremely preterm neonates. The maps also reveal between-group differences in the spatial organization of modules, with a less complex pattern of modularity in extremely preterm neonates compared to term-born controls. Such findings may reflect abnormal cortical differentiation associated with extremely preterm birth.

Conclusions

Graph theoretic techniques applied to voxel-wise structural brain MRI data can reveal whole-brain patterns of structural co-variance that differ between extremely preterm neonates with autism spectrum disorder and nonautistic preterm and term controls. Additional investigation, however, is necessary to determine if this approach can be used to identify novel biomarkers of abnormal cortical differentiation associated with autism spectrum disorder in extremely preterm neonates.

KEYWORDS: Autism Spectrum Disorder, MR Imaging Brain, Preterm

Note: Scanned images are included in the proceedings. Some submitted images were reduced during editing thereby decreasing clarity. Also, refer to the Program Planner. Proceedings Content as of 3/28/2014.

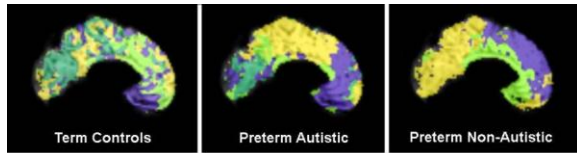


Figure 1. Modularity maps (sagittal views) from graph theoretical analysis overlaid on neonatal template brain. Each color represents a different module containing voxels of similar gray matter volume covariance.

O-581

3:14PM - 3:21PM

Volumetric Interpolated Breath-hold Examination (VIBE) of Pediatric Orbit - Initial Experience and Qualitative Analysis

S Krishna1, S El Haddi2, J Rykken1, M Rischall1, A McKinney3, D Nascene1

1University of Minnesota, Minneapolis, MN, 2University of Minnesota Medical School, Chaska, MN, 3University of Minnesota and Hennepin County Medical Centers, Roseville, MN

Purpose

Volumetric interpolated breath-hold examination (VIBE) has been utilized in thoracic and abdominal imaging for over a decade, but there is scant literature describing its usefulness in orbital imaging. Its potential utility lies in its volumetric acquisition with multiplanar reconstruction as well as the relatively short acquisition time. We studied its usefulness in contrast-enhanced imaging of the pediatric orbit and compared it to a routine T1-weighted imaging (T1WI) technique [fast low angle shot (FLASH)].

Materials and Methods

After Institutional Review Board approval, 73 consecutive pediatric orbit examinations (each with VIBE and FLASH imaging in the same encounter) performed on a 3 T magnet over a nine-month period were independently scored by three reviewers, with the sequences reviewed independent from each other. The VIBE sequences consisted of a volumetric acquisition at 1 mm slice thickness (acquisition time of about 4 minutes), which then were reconstructed into axial and coronal planes at 3mm thickness. The FLASH sequences were obtained in axial and coronal planes at 3mm thickness (4 minute acquisition time per plane). Qualitative parameters then were analyzed, including fat

suppression (intraconal, extraconal, and preseptal), degree of artifacts, and definition of structures (orbital musculature, vasculature, and orbital apex). A Wilcoxon Ranked Sum Test was performed to compare the two sequences' performance for each parameter.

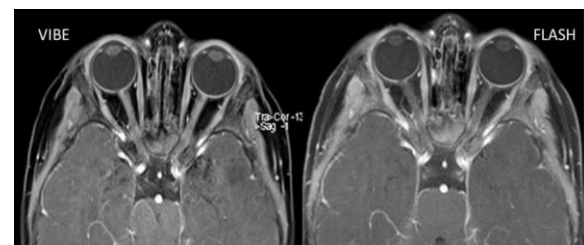
Results

All three reviewers rated the VIBE T1WI sequence superior with regard to fat suppression of extraconal, intraconal, and preseptal fat ($p \leq 0.05$). All three consistently scored VIBE as having a lower degree of intraorbital artifact as compared to FLASH, although only two readers achieved statistical significance ($p < 0.05$), while one did not ($p = 0.078$). Visualization of the ophthalmic artery was rated better on FLASH by all three readers; however, only two readers reached statistical significance ($p < 0.05$), while one did not ($p = 0.248$). Regarding the conspicuity of structures at the orbital apices, the findings were mixed, where one reviewer consistently rated VIBE with higher scores ($p < 0.05$), the second rating FLASH with higher scores ($p < 0.05$), and the third as having no statistical difference between the two sequences. There were no statistically significant differences in scores of contrast enhancement, definition of the superior ophthalmic vein, or conspicuity of the superior oblique muscle between the two sequences (all $p > 0.05$).

Conclusions

This preliminary qualitative evaluation of contrast-enhanced VIBE for pediatric orbital imaging indicates that VIBE has consistently better fat suppression than FLASH and likely a lesser degree of artifact. This was despite the fact that the native 1mm slice thickness VIBE volumetric data sets were reformatted to 3mm planar images to ensure direct comparability with 3mm FLASH images. Further analysis (currently under progress by our group) comparing the source VIBE images and the FLASH images may demonstrate further superiority of VIBE in orbital imaging vis-à-vis FLASH sequences, and prospective studies are pending.

KEYWORDS: Orbits, Pediatric Head And Neck, Volumetric Interpolated Breath-Hold



O-582

3:21PM - 3:28PM

Note: Scanned images are included in the proceedings. Some submitted images were reduced during editing thereby decreasing clarity. Also, refer to the Program Planner. Proceedings Content as of 3/28/2014.

Initial Evaluation of Three Dimensional Fluid Attenuated Inversion Recovery (3D FLAIR) and Three Dimensional Double Inversion Recovery (3D DIR) MR Sequences in Pediatric Neuroimaging at 3T

S Palasis¹, L Hayes¹, S Little¹, D Grattan-Smith¹, T Leong², R Jones¹

¹Children's Healthcare of Atlanta, Atlanta, GA, ²Emory University School of Public Health, Atlanta, GA

Purpose

Lesion detection can be challenging in pediatric neuroimaging due to the evolving state of myelination. The FLAIR sequence which is utilized widely for lesion detection often is plagued by cerebrospinal fluid (CSF) flow artifacts in young children and the poor gray white differentiation inherent to the technique, especially in the setting of incomplete myelination, can make lesion detection and localization difficult. Double inversion recovery (DIR) is a technique that recently has been implemented in adult patients suffering from multiple sclerosis due to its improved lesion detectability. The utility of the DIR sequence in lesion detection has not been evaluated yet in children. We performed the FLAIR and DIR sequences as 3D and conducted a quantitative and qualitative evaluation of these techniques at 3 T across a range of pediatric age groups.

Materials and Methods

We conducted a retrospective evaluation of 25 children aged 6 months to 17 years. IRB approval was obtained for this HIPAA-compliant study with waived informed consent. The pathology included nonspecific gliosis, neoplasia, migration anomalies, and infectious/inflammatory etiologies. The 3D DIR and 3D FLAIR sequences were performed on a 3 T scanner during the same MRI evaluation using the same slice thickness and similar spatial resolution and matrix. Lesions were categorized into gray matter (GM) only, white matter (WM) only, and mixed (MX) GM/WM. Three-dimensional FLAIR and 3D DIR sequences of all subjects were evaluated independently on a workstation by two pediatric neuroradiologists to determine image quality, extent of artifacts, lesion detectability and conspicuity. Before conducting the evaluation, the two readers underwent a training data set and agreed on the interpretations and scores for each of the evaluated parameters. This training data set was not included in the study. The reviewers were blinded to the clinical information and the images were de-identified. Qualitative assessment was performed for lesion detectability and conspicuity, GM/WM conspicuity, CSF/parenchymal conspicuity, and image artifact using a 4-point scale. Signal intensity measurements were obtained using region-of-interest analysis of the lesions, normal GM, and normal WM. Quantitative evaluation of contrast ratios between the lesion and GM/WM was performed. All quantitative measurements were performed by a pediatric

neuroradiologist in conjunction with a medical physicist after the qualitative analysis was completed. Inter-rater agreement was assessed using Kappa statistics. The 3D FLAIR and 3D DIR sequences were compared using a Mann Whitney test.

Results

Our results showed statistically significant inter-rater agreement for lesion detection and lesion conspicuity ($p < .001$) on both 3D FLAIR and 3D DIR sequences. Artifact on the 3D FLAIR images was significantly lower than on the DIR ($p < .001$). Parenchymal/CSF conspicuity was significantly less on DIR than FLAIR ($p < .001$). FLAIR GM/WH conspicuity was significantly lower on the DIR ($p < .001$). Lesion conspicuity was not significantly different between the two sequences ($p = .359$). Lesion to WM contrast ratios were greatest on the 3D DIR. The lesion to GM contrast ratios were similar on the FLAIR and DIR sequences.

Conclusions

Our study demonstrates that both 3D FLAIR and 3D DIR sequences have their strengths and limitations in pediatric neuroimaging. The 3D technique has virtually eliminated the CSF flow artifacts that often are seen on 2D FLAIR images. Overall, artifacts were greater on the DIR than the FLAIR sequence. Gray matter/WM conspicuity was greatest on the DIR sequence; however, performing DIR in children that aren't completely myelinated (less than 24 months old), is difficult. The second inversion recovery pulse is variable and needs to be adjusted accordingly to the degree of myelination. Double inversion recovery offers the greatest lesion to WM contrast and this can aid in lesion detection. Lesion conspicuity was improved on DIR and lesions could be localized more accurately to GM or WM.

KEYWORDS: Fluid-Attenuated Inversion Recovery, Inversion Recovery, Pediatric Brain

0-583

3:28PM - 3:35PM

Abnormal Iron Levels in the Brain of Pediatric Sickle Cell Disease Patients: a Study using Quantitative Susceptibility Mapping (QSM)

S Palasis¹, D Qiu², R Brown¹, B Sun¹, T Burns¹, L Hayes¹, R Jones¹

¹Children's Healthcare of Atlanta, Atlanta, GA, ²Emory University, Atlanta, GA

Purpose

Note: Scanned images are included in the proceedings. Some submitted images were reduced during editing thereby decreasing clarity. Also, refer to the Program Planner. Proceedings Content as of 3/28/2014.

Pediatric sickle cell disease (SCD) patients with high cerebral blood flow receive chronic blood transfusion to reduce the risk of stroke. As a result they suffer from systematic iron overload that affects multiple organs. While iron overload of the liver and heart has attracted much interest, the effects of blood iron overload on brain iron level of these patients have received less attention. Quantitative susceptibility mapping (QSM) is a recently developed MR method that measures tissue magnetic susceptibility from phase images and is sensitive to iron content in the brain. In the current study, we used QSM to quantify iron store in the brain of patients with SCD and compare the findings with age-matched normal subjects.

Materials and Methods

Twenty-five sickle cell patients and 23 age-matched healthy normal volunteers were recruited for the study. The mean/SD of age was 13.3/2.8 and 14.0/3.3 years for the patient and the control groups respectively. MR imaging (MRI) scan was performed using a Siemens 3 T scanner, and included a 3D multi-echo gradient-echo sequence for QSM (FOV=256x192mm, matrix=256x192, slice thickness = 2mm, 72 slices, TR = 50 ms, first TE = 3.7ms, 12 echoes, echo spacing = 3.8ms) and a T1-weighted (T1W) structural imaging sequence using MPRAGE for anatomical identification and image normalization. Only the even echoes were used for QSM processing since the even echoes are flow-compensated in the readout direction. The processing was performed using a software package developed in-house. The phase image from each echo was first unwrapped using a Laplacian method followed by spherical mean filtering to remove the background field to generate the filtered field map. The filtered field maps from each echo then were averaged to increase the signal-to-noise ratio. An L1-norm optimization-based method was used to reconstruct the susceptibility map from the mean field map. All QSM images were normalized to a standard brain template in SPM using the T1W image as a medium, and the mean susceptibility image was created. Regions of interest (ROIs) were drawn on the mean susceptibility map and included bilateral caudate nucleus (CN), putamen (PT), globus pallidus (GP), red nucleus (RN), substantia nigra (SN), dentate nucleus (DN) and choroid plexus (CP). The mean susceptibility value (SV) was calculated as the mean value of all voxels with positive susceptibility values within a ROI as defined above; the restriction to positive voxels was imposed to improve the sensitivity and avoid the inclusion of neighboring white matter. General linear model analysis was performed to compare differences in the susceptibility value of the ROIs between the patient and control groups using age as a covariate.

Results

Qualitatively, QSM nicely depicts regions known with high iron concentration, including the globus pallidus, substantia nigra and dentate nucleus. Table 1 shows the mean and standard deviation of the susceptibility values of different ROIs between the patient and control groups. After controlling for the effect of age, significantly higher

susceptibility values were found in the patient group in choroid plexus, red nucleus and dentate nucleus, suggesting high iron loading in these regions. The analysis also showed significantly increasing susceptibility values with age in many of the regions including caudate nucleus, putamen, globus pallidus, substantia nigra, red nucleus and dentate nucleus.

Conclusions

Quantitative susceptibility mapping is sensitive to iron deposition in the brain, and can nicely visualize areas with high concentrations of iron. We found significantly increasing susceptibility values in multiple ROIs examined, which is consistent with the literature. After controlling for the effect of age, significantly higher iron concentration was found in SCD patients in the choroid plexus, red nucleus and dentate nucleus. The former recently has been proposed as having an important role in brain iron transport, while the latter two are known sites of iron deposition. A possible contributing factor to the increased iron content in these regions is the high systemic iron level of these patients due to their blood transfusion therapy. The ability to image brain iron level with QSM provides valuable information that may permit customized treatment strategy for individual patients. In conclusion, QSM is sensitive for measuring iron concentration in the brain of sickle cell patients and provides a valuable tool for iron assessment for both clinical trials and individual evaluations.

KEYWORDS: Iron Deposition, Sickle Cell Disease

O-584

3:35PM - 3:42PM

Comparison of Diagnostic Value of CT-Venography and MR-Venography in Diagnosis of Neonatal Sinus Vein Thrombosis.

A Ben Ely¹, M Shroff¹, H Branson¹, M Joshi², M Moharir¹

¹The Hospital for Sick Children, Toronto, ON, Canada,
²University of Toronto, Toronto, Ontario, Canada

Purpose

Pediatric cerebral sinovenous thrombosis (CSVT) occurs most commonly in neonates. The subsequent morbidity, mortality and adverse neurodevelopmental sequelae highlight the importance of establishing an early diagnosis, which primarily is based on imaging findings. The aim of our study is to compare the diagnostic value of CTV and time of flight (TOF) MRV in the diagnosis of neonatal CSVT. In contrast to most studies on pediatric CSVT, which

Note: Scanned images are included in the proceedings. Some submitted images were reduced during editing thereby decreasing clarity. Also, refer to the Program Planner. Proceedings Content as of 3/28/2014.

include children of all ages, our study is dedicated to imaging of CSVT exclusively in neonates.

Materials and Methods

We undertook a retrospective review of the medical records and brain MRI/MRV, CT/CTV studies of the neonates (0- 28 days old, term and preterm) with presumed CSVT, presented between January 1994 and December 2011, who underwent both MRV and CTV - in total 63 neonates. We excluded patients who had more than a 24-hour time interval between the two exams. The final study population included 16 neonates (12M: 4F). Computed tomography venography technique: unenhanced and contrast-enhanced scans were performed in 15 patients and direct contrast-enhanced scan in one patient. Magnetic resonance venography technique: DWI, Ax. and Sag. T1, Ax. and Cor. FSE T2 and cor. Two-dimensional time-of-flight MRV + 3D MIPs were performed in all patients, additional GE images and susceptibility-weighted imaging (SWI) were performed in nine patients. Independent review was performed by two certified pediatric neuroradiologists, blinded to clinical data. We used Kappa Statistics to measure agreement between rater and modality.

Results

Clinical findings: The majority of our patients (62.5%) had early presentation of the disease during the first postnatal week. Seizures, either isolated or in combination with other symptoms, were the most common clinical presentation, found in 75% of our patients. Two patients (12.5%) died from the disease. Imaging findings: The majority of patients (75%) had involvement of multiple venous structures. Superficial venous structures were involved more often than deep venous structures. Intracranial bleeding was found in 12 (75%) patients. Statistical results: Overall, there was a substantial agreement between CTV and MRV (kappa=0.5639 for rater 1 and kappa=0.6988 for rater 2) as well as between raters (kappa=0.6092 and 0.6435 for CTV and MRV, respectively).

Conclusions

CT venography is as accurate as MR venography in the diagnosis of neonatal CSVT. Clinicians should be informed that both studies have a similar ability to depict CSVT in neonates and that other parameters, such as the clinical status of the neonate, the risk of radiation and iodinated contrast material and the availability of MRI, should be considered in making a choice between these two modalities.

KEYWORDS: Neonatal, Neonatal MR Imaging, Venous Sinus Thrombosis

0-585

3:42PM - 3:49PM

Radiologic-Based Algorithmic Approach to Surveillance Cranial MRI and MRA in Sickle Cell Anemia

D Russell¹, J Loewen¹, C Brown², M Quarmyne², J Kang¹, Y Zhao¹, N Desai¹

¹Emory University, Atlanta, GA, ²Children's Healthcare of Atlanta, Atlanta, GA

Purpose

Purpose: Currently, evidence-based appropriateness criteria for magnetic resonance imaging (MRI)/magnetic resonance angiography (MRA) surveillance are needed to guide clinicians when monitoring sickle cell anemia (SCA) patients with high risk of stroke. The purpose of this study is to evaluate the interrelationship of subtypes of infarction and vessel stenosis, using a numerical scoring system that recapitulates the presence of stenosis within the circle of Willis vessels, infarction within their known vascular territories, and radiologic progression on follow-up imaging. This scoring system allows statistical evaluation of progression in vessel stenosis and/ or infarction and thereby attempts to aid in identifying patients benefitting most from surveillance MRI/MRA.

Materials and Methods

IRB approval was obtained. A retrospective review of MRI/MRA reports in patients with SCA(SS/S beta0) linked to a database containing patients undergoing chronic transfusion therapy was performed noting the presence of chronic white matter disease (CWMD), basal ganglia and large territory infarcts, vessel stenosis and progression between exams. Exclusion criteria included blood disorders other than SCA and patients older than 21 years. For each study performed, a value of 1 was given to each of the three aforementioned infarct subtypes if present (0 if absent). Each major vascular territory to include the ACA, MCA, ICA, PCA/PCOM and vertebrobasilar system was scored similarly with an additional point added for each vessel territory found to be bilaterally affected. Additional points (1 for each) were added for advancement of area of infarction and for worsening of stenosis, thereby yielding a total potential score of 13 for each MRI/MRA. A total score per exam and average score per patient was calculated. Data were analyzed for both descriptive and inference-based statistics.

Results

Five hundred ninety-five MRI/MRA reports in 140 patients were reviewed. Forty patients had progression of stenosis, and 19 patients had progression of infarcts. The presence of CWMD and basal ganglia infarction was positively related to the presence of ACA stenosis (p-value=0.007 and 0.002, respectively) and MCA stenosis (p-value=0.003 and 0.002, respectively) but not with posterior circulation stenosis. Large territory infarcts were positively related to the presence of ACA (p-value<0.001), MCA (p-value<0.001), and PCA/PCOM (p-value=0.008) stenosis.

Note: Scanned images are included in the proceedings. Some submitted images were reduced during editing thereby decreasing clarity. Also, refer to the Program Planner. Proceedings Content as of 3/28/2014.

The mean point total in the group was 2.56 (SD 2.6, range 0-10.1). In patients with a total score in the first quartile (e.g., highest), 14 patients had progression of stenosis (44% of total cases of progression) and 11 had progression of infarcts (58% of total cases of progression). Conversely, in patients with total score in the 4th quartile, eight patients had progression of stenosis (16% of total cases of progression) and 0 had progression of infarcts (0% of total cases of progression).

Conclusions

The radiologic point system proposed herein is able to broadly identify a significant population at high and low risk for temporal progression of infarction and/or arterial stenosis and therefore may be a complement to a honed algorithm to identify SCA patients ideal for long-term MRI/MRA surveillance. Further analysis via a prospective trial is needed especially to arrive at the specific clinical and radiologic factors that ought to prompt MRI/MRA screening.

KEYWORDS: Infarct, Sickle Cell Disease, Stenosis

0-586

3:49PM - 3:56PM

High-Angular Resolution Diffusion Tractography of Emerging Cerebellar Pathways from Newborns to Young Adults

T Re1, K Im2, M Paldino2, A Righini3, P Grant2, E Takahashi2

1University of Milan, Milan, Italy, 2Boston Children's Hospital, Harvard University, Boston, MA, 3Milan Children's Hospital V. Buzzi, Milan, Italy

Purpose

To describe the evolution of the cerebellar pathways of the superior (SCP), middle (MCP), inferior peduncles (ICP) and the deep nuclei (DN) in developing human subjects ranging from newborn to adult, using high angular resolution diffusion imaging (HARDI) tractography (1-3).

Materials and Methods

For 90 apparently healthy individuals, aged 30GW to 28Y, we performed T1-weighted MPRAGE imaging, T2-weighted turbo spin-echo imaging, and an isotropic diffusion-weighted measurements ($b = 1,000 \text{ sec/mm}^2$) and five nondiffusion-weighted measurements ($b = 0 \text{ sec/mm}^2$) were acquired on a 3 T Siemens MR system with TR= 10 sec; TE= 88 msec; small delta= 12.0 ms; large delta= 24.2 ms; field of view= 22 x 22 cm; slice thickness= 2.0 mm; matrix size= 128 x 128, iPAT= 2. DiffusionToolkit and

TrackVis (trackvis.org) were used to reconstruct and visualize tractography pathways. A streamline algorithm with a 45° angle threshold was applied for the fiber reconstruction using all HARDI-detected local maxima. A coordinate-based tractography atlas was used to guide region of interest (ROI) placement in order to delineate the pathways of interest (4). Fractional anisotropy (FA), apparent diffusion coefficient (ADC), number, length, and volume of tracts per pathway were quantified in each subject.

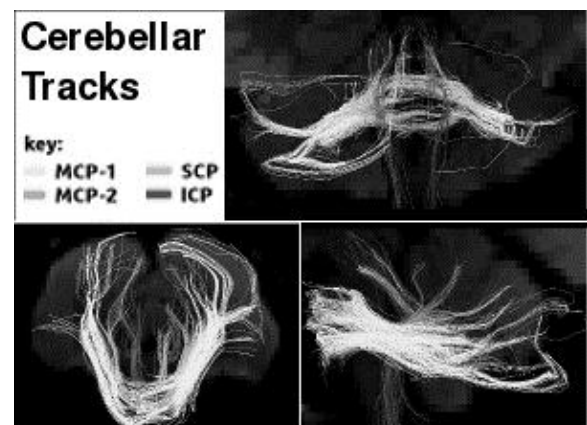
Results

An example of cerebellar tracks for a 6Y subject is provided in Figure 1. 1. Starting from the earliest ages, the MCP could be divided into two distinct subgroups: a rostral pons to caudal cerebellum group (MCP-1) and a caudal pons to rostral cerebellum group (MCP-2). These two pathways were distinctly identifiable starting from the earliest ages, and the volume of MCP-1 was consistently greater than the volume of MCP-2 (2-way ANOVA, $p < 0.05$). 2. Number and volume of all studied pathways increased progressively with age with an initial plateau varying across pathways (DN at 2Y, MCP-2 at 3Y, MCP-1 at 5Y, ICP at 6Y, SCP at 8Y,) (chi-square test, $p < 0.05$). 3. Mean apparent diffusion coefficient (ADC) for all studied pathways decreased in the first five years post-term then plateaued, while mean FA increased until adult ages (chi-square test, $p < 0.05$).

Conclusions

This work may add to our understanding of cerebellar track development and represent an initial step towards the creation of an atlas for the developing cerebellar tracts as viewed by diffusion tractography. Such an atlas would serve as a reference when looking for abnormalities of cerebellar connectivity in many cognitive disorders.

KEYWORDS: Cerebellar, DTI Tractography, Pediatric Brain



Note: Scanned images are included in the proceedings. Some submitted images were reduced during editing thereby decreasing clarity. Also, refer to the Program Planner. Proceedings Content as of 3/28/2014.

O-587

3:56PM - 4:03PM

Does Apparent Diffusion Coefficient Scalars Correlate with Near Infrared Spectroscopy as Marker of Brain Autoregulation in Neonates Who Were Treated with Brain Cooling for Perinatal Hypoxic Ischemic Injury?

A Tekes¹, A Poretti¹, J Lee², S Chung², F Northington¹, T Huisman¹

¹The Johns Hopkins University School of Medicine, Baltimore, MD, ²Johns Hopkins Medical Institutions, Baltimore, MD

Purpose

Despite therapeutic hypothermia (TH), incidence of neurologic morbidity remains high in neonates with perinatal hypoxic-ischemic injury (HII). Diffusion tensor imaging (DTI) gives qualitative and quantitative information about the brain micro-architecture while near infrared spectroscopy (NIRS) measures the brain autoregulation at bedside. We hypothesized that lower apparent diffusion coefficient (ADC) values correlate with worse autoregulation.

Materials and Methods

Thirty neonates with perinatal HII were included in this institutional review board approved study. MR imaging (MRI) was done at day of life (DOL) 4-14 after completion of TH. Apparent diffusion coefficient scalars were measured in the anterior and posterior centrum semiovale (ACS and PCS), basal ganglia, thalamus, posterior limb of the internal capsula (PLIC), pons and cerebellar white matter. NIRS autoregulation data were collected during TH, rewarming, and normothermia. The optimal mean arterial blood pressure (MAP) with most robust autoregulation was identified. To account for pseudonormalization of ADC values, data were dichotomized into neonates who received MRI before and after day of life 10. Autoregulation and ADC scalars were analyzed with Spearman correlations.

Results

Low ADC scalars of the PCS and PLIC correlated with worse autoregulation during hypothermia ($r = -0.83$; $p = 0.006$ and $r = -0.68$; $p = 0.04$), and in basal ganglia during rewarming ($r = -0.71$; $p = 0.05$) in neonates that had MRI at DOL ≥ 10 . No statistically significant correlation between ADC scalars and autoregulation were identified in neonates who had MRI done DOL < 10 .

Conclusions

Low ADC scalars correlated with worse autoregulation in PCS and PLIC during TH, and in basal ganglia during rewarming in neonates who had MRI at DOL ≥ 10 . Optimizing blood pressure during TH and rewarming may

decrease the risk of brain injury. Performing MRI until DOL 10 could be considered.

KEYWORDS: Autoregulation, Diffusion Tensor Image, Hypothermia

O-588

4:03PM - 4:10PM

Readout-Segmented EPI for Diffusion-Tensor Imaging in the Evaluation of Tumors Involving the Pediatric Spine.

L Hayes¹, S Palasis¹, R Jones¹, D Aguilera¹, C Mazewski¹, D Grattan-Smith¹, D Porter²

¹Children's Healthcare of Atlanta, Atlanta, GA, ²Siemens AG, Erlangen, Bavaria

Purpose

Diffusion-weighted imaging (DWI) is a helpful MR tool in central nervous system (CNS) tumor imaging. A new technique, readout-segmented (RS) echo planar imaging (EPI), also known as RESOLVE (Readout-segmentation of long echo trains), can produce high quality diffusion tensor images of the spine that have not been attainable with other types of DWI. In this study, we used (RS) EPI as a DWI technique in magnetic resonance imaging (MRI) of the spine in children with tumors in an effort to identify specific applications in which it would be useful.

Materials and Methods

IRB approval was obtained. Readout-segmented EPI was performed on a 1.5 T Avanto and a 3 T Trio scanner with five segments, a parallel imaging factor of two, a b factor of 500 s/mm² and an in-plane resolution of 1.25 mm². A sagittal slice orientation was chosen in nearly every case, as it allowed an entire section of the spine to be assessed with a single acquisition. This sequence was added to standard protocols for imaging children being evaluated for tumors of the spine. A total of 223 spine DWI studies of 104 children were performed. Diffusion imaging was added to standard imaging protocols for either drop metastases or primary tumors involving the spine. Of the 104 subjects, 41 had medulloblastoma. Other tumors included ependymoma (n=12), germ cell tumor (GCT) (n=9), glioblastoma multiforme (n=6), primitive neuroectodermal tumor (n=5), disseminated neuroepithelial tumor (n=5), juvenile pilocytic tumor (JPA) (n=5), neuroblastoma (n=4), atypical teratoid rhabdoid tumor (ATRT) (n=4), glioma (n=2), choroid plexus carcinoma (n=2), ganglioglioma (n=2), rhabdomyosarcoma (n=2), epidermoid (n=2), anaplastic astrocytoma (n=1), acute lymphoblastic leukemia (n=1), and Ewing's sarcoma (n=1).

Note: Scanned images are included in the proceedings. Some submitted images were reduced during editing thereby decreasing clarity. Also, refer to the Program Planner. Proceedings Content as of 3/28/2014.

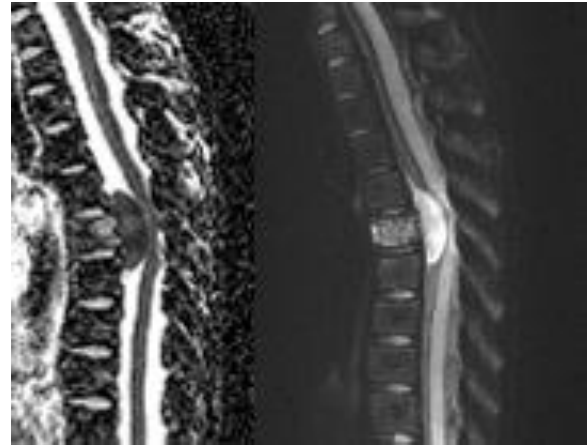
Results

Of the 94 subjects evaluated for drop metastases, 32 were positive for cerebrospinal fluid (CSF) metastases to the spine. Diffusion-weighted imaging correctly identified drop metastases from primary brain tumors that restricted diffusion in every case where metastases were seen on conventional sequences. In at least five cases where metastases were not visible on conventional images, drop metastases were clearly identified with DWI (ATRTR, GCT, and medulloblastoma). Drop metastases measuring only a few millimeters were discernable. In 23 scans for medulloblastoma, diffusion imaging was very helpful in excluding questionable metastatic disease, especially in the distal thecal sac. In paravertebral and bony lesions such as neuroblastoma, rhabdomyosarcoma, and Ewing's sarcoma (small round blue cell tumors), DWI allowed good definition of the tumor margins and aided in detection of marrow abnormalities. In all evaluations of primary spinal tumors, DWI was helpful to narrow the differential diagnosis. Diffusion-weighted imaging was not found to be helpful in detecting drop metastases from primary CNS tumors that do not restrict diffusion (neuroepithelial tumors, JPA, gliomas) In one case, hemorrhage was misinterpreted as a drop metastasis on DWI.

Conclusions

Diffusion-weighted imaging of the spine using (RS) EPI was not found to be very helpful in evaluating tumors that did not restrict diffusion. However, it was found to have exquisite sensitivity for identifying drop metastases from CNS tumors that restrict diffusion, especially those that demonstrate no or minimal enhancement with contrast (as in some medulloblastomas, ATRTs, and germ cell tumors). Metastases from these types of tumors were much more conspicuous with DWI than T1- or T2-weighted sequences. Furthermore, DWI was helpful when there were questionable findings on conventional images, allowing a more confident diagnosis of metastases when restricted diffusion was present. Diffusion-weighted imaging was useful to exclude metastases, especially when there was vague enhancement in the distal thecal sac, contrast leakage into the CSF, and arachnoiditis. As in the brain, DWI was helpful in grading spinal cord tumors. Paraspinal and vertebral small round blue cell tumors were well delineated. The results of our study support (RS) EPI to be a promising DWI technique for imaging the pediatric spine in the evaluation for tumor.

KEYWORDS: Diffusion Tensor Image, Pediatric Spine, Spinal Neoplasm



O-589

4:10PM - 4:17PM

Hippocampal biometry in the normal and abnormal fetal brain

B Kunzendorf¹, G Kasprian¹, E Schwartz¹, G Langs¹, M Weber¹, D Prayer¹

¹Medical University of Vienna, Vienna, Austria

Purpose

By 15 gestational weeks (GW) the hippocampus appears as vertically oriented "S" shaped structure. During the second trimester it gradually loses this orientation and is finally positioned horizontally in the depth of the temporal horn. As this process is arrested in cases of various developmental brain pathologies, we aimed to systematically quantify differences in hippocampal positioning between normal fetuses and cases with lissencephaly using fetal magnetic resonance imaging (MRI).

Materials and Methods

Standardized coronal T2-weighted fetal MR (1.5 T) sequences of 19 cases with the neuropathological/imaging diagnosis of lissencephaly were compared to 36 normal fetuses (age range 20-39 GW). The boundaries of the hippocampi were segmented using ITK Snap in order to define four lines, using four characteristic hippocampal landmarks and 3D Slicer. The angles (I-IV) between these lines were correlated between both sides (paired t-test), normal and abnormal fetuses. A midline served as a reference line to assess the positioning of the hippocampus as a whole.

Results

Normal age-related reduction of hippocampal angles (r^2 : 0,387; Sig.: 0,000) and positioning (r^2 : 0,278; Sig.: 0,001;

Note: Scanned images are included in the proceedings. Some submitted images were reduced during editing thereby decreasing clarity. Also, refer to the Program Planner. Proceedings Content as of 3/28/2014.

regression analysis linear) could not be observed in fetuses with lissencephaly (r^2 : 0,010; Sig.: 0,674 and r^2 : 0.045; Sig.: 0,369). Significant left right differences occurred in healthy patients in angle 2 (p-value 0,009; T-test for dependent samples), whereas side differences were found in angle 1, 2, and tilting angle (p-value 0,031; 0,021; 0,045; T-Test for dependent samples) in lissencephaly patients. In lissencephaly the angles were significantly wider than in normal age-matched controlled (p-value 0,000; Welch's Test). Already two angles discriminated healthy from lissencephaly fetuses with a sensitivity of 80% and a specificity of 94.4%.

Conclusions

Normal and abnormal developmental positioning of the hippocampal formation can be quantified by biometry of various angles, geometrically describing its vertical axis. These can be used to support the neuroradiologic detection of major developmental brain pathologies.

KEYWORDS: Fetal Brain Development, Fetal MR Imaging

O-590

4:17PM - 4:24PM

Quantitative Evaluation of Thickened Lumbar Spinal Nerves in Krabbe Disease: Preliminary Findings and Clinical Implications

M Hwang¹, G Zuccoli², A Panigrahy², D Rodriguez¹, M Poe², M Escolar²

¹University of Pittsburgh Medical Center, Pittsburgh, PA,
²Childrens Hospital of Pittsburgh of University of Pittsburgh Medical Center, Pittsburgh, PA

Purpose

Krabbe disease is an autosomal recessive lysosomal storage disease known for its rapidly progressive and fatal clinical course. Early diagnosis is crucial as advanced therapeutic interventions such as umbilical cord blood transplantation have shown promising results. Of note, the screening criteria for Krabbe disease utilizes the modified Loes scoring system which encompasses the central but not the peripheral nervous system changes, despite the accepted knowledge that myelin loss occurs in both the central and peripheral nervous systems. We show for the first time quantitative evaluation of thickened lumbar spinal nerve roots in Krabbe patients which has potential implications in improving the current screening system and therapeutic guidance.

Materials and Methods

Lumbar spine MR images (MRIs) obtained between March 2013 and September 2013 of 16 symptomatic infants (ages

ranging from 3 to 24 months) with Krabbe disease were evaluated retrospectively. Retrospective review was performed after approval by the Institutional Review Board at the University of Pittsburgh Medical Center. Of these, 15 cases were analyzed with the exclusion of one case due to severe scoliosis noted on imaging. As controls, 10 normal spine MRIs of infants of similar ages and with initial MRI indications for evaluation of tethered cord were evaluated retrospectively. Quantitative evaluation of the terminal nerve roots was performed on the axial plane obtained approximately 5 mm below the conus medullaris. The spinal canal was divided into anterior and posterior quadrants, after which the anterior quadrant was further divided into right and left quadrants. Given the technical challenge of measuring the area of smaller posterior quadrant nerve roots on an axial plane, only the anterior quadrant nerve roots were evaluated. Areas of the largest nerve root in anterior right and left quadrants were acquired, in addition to the area of the anterior thecal sac.

Results

The average values for the area (cm²) of anterior right and left nerves in Krabbe patients were 0.014 and 0.017 (average 0.016) while that of controls were 0.006 and 0.007 (average 0.007). The average area of the anterior thecal sac in Krabbe cases was 1.09 while that of controls was 0.94. Our results demonstrate that terminal nerve roots of Krabbe infants are more than twice as thick as that of controls on average. The area of the anterior thecal sac also was slightly larger in Krabbe infants than in controls.

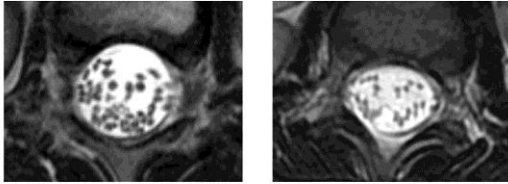
Conclusions

We present for the first time thickened terminal spinal nerves in 15 infants with Krabbe disease as confirmed by quantitative evaluation on spine MRI. Interestingly, the average anterior thecal sac area was slightly larger in Krabbe patients than in controls. Of note, preliminary evidence using the Twitcher mice model of Krabbe disease showed widening of the spaces between axons in the dorsal and ventrolateral spinal cord white matter due to perineural edema (Hofling, Kim et al., 2009). Whether this explains the peripheral nerve thickening in Krabbe patients is yet unknown, but we can begin to study the mechanism in vivo with advanced imaging techniques such as diffusion tensor imaging (Morisaki, Kawai et al., 2011; Cauley and Filippi, 2013). Further studies with a larger cohort while evaluating for the effects of disease course and therapeutic intervention on the peripheral nerve manifestations undoubtedly will improve the current screening system for Krabbe disease which fails to account for the imaging findings of peripheral nerve abnormalities.

KEYWORDS: Congenital Anomalies, Pediatric Spine, Spinal Imaging

Note: Scanned images are included in the proceedings. Some submitted images were reduced during editing thereby decreasing clarity. Also, refer to the Program Planner. Proceedings Content as of 3/28/2014.

Representative Krabbe Patient's Axial Slice 5 mm Below the Conus Representative Control Patient's Axial Slice 5 mm Below the Conus



O-591

4:24PM - 4:31PM

Birth Injuries of the Brachial Plexus: MR Neurography and Tractography with Clinical Correlation

M Ho1, M Kliot1, N Gupta1, J Strober1, C Chin1

1University of California San Francisco, San Francisco, CA

Purpose

To assess the utility of MR neurography and tractography in birth injuries of the brachial plexus. We will present our 13-year institutional experience with pediatric cervical MR neurography/tractography and correlate with patient age at presentation, clinical history, neurologic examination, electromyography (EMG)/nerve conduction studies (NCS), intraoperative findings, and clinical outcomes.

Materials and Methods

We queried the radiology information system for cervical MR neurograms performed between January 2000 and December 2013. Inclusion criteria were pediatric patients (< 18 years) referred for birth-related injury and/or upper extremity paralysis. Exclusion criteria were history of nonbirth-related trauma, suspected infection, brachial neuritis, malignancy, and prior surgery. A neuroradiology attending and neuroradiology fellow concurrently reviewed images for presence and location of brachial plexus enlargement, signal changes, enhancement, pseudomeningocele, and neuroma formation. In cases with diffusion-weighted imaging (DWI)/diffusion tensor imaging (DTI), apparent diffusion coefficient (ADC) values were measured at sites of nerve injury, and tractography was performed to assess nerve fiber integrity. Imaging findings were correlated with data from the medical record including presenting history, neurologic examination, EMG/NCS, intraoperative findings, and degree of functional recovery.

Results

Our study included 26 pediatric patients (ages: 6 weeks - 10 years, median: 6 months). Gender was 54% (14/26)

male and 46% (12/26) female. Affected side was right in 54% (14/26) and left in 46% (12/26). Neurologic examination suggested Erb palsy in 73% (19/26) of cases and total brachial plexus injury in 27% (7/26). Electromyography/NCS was performed in 15 patients, showing high correlation with MR findings in 53% (7/15) and moderate correlation in 47% (8/15). MR neurography demonstrated nerve enlargement in 81% (21/26), T2-hyperintense signal in 85% (22/26), and pseudomeningocele formation in 50% (13/26). Gadolinium contrast was administered in 18 patients, of which 89% (16/18) showed abnormal nerve enhancement in the region of injury. Diffusion-weighted imaging/DTI was performed in 18 patients, demonstrating complete nerve fiber transection in 56% (10/18). In the region of injury, apparent diffusion coefficient (ADC) was less than 1.0 in 50% (9/18), between 1.0-1.2 in 22% (4/18), and greater than 1.2 in 28% (5/18). Treatment involved physical therapy in 62% (16/26), neuromuscular stimulation in 4% (1/26), and peripheral nerve surgery in 23% (6/26) of patients. Follow-up data were available in 23 patients, with mean time interval of 1.1 years (range 2 months - 5 years). Clinical recovery was near-complete in 57% (13/23), partial in 35% (8/23), and minimal in 9% (2/23).

Conclusions

Pediatric brachial plexus injury is an important cause of upper extremity paralysis following difficult delivery. Although the majority of patients recover spontaneously, complex cases may necessitate surgical intervention. MR neurography and tractography are useful in assessing the extent and severity of injury, and correlate well with neurologic examination and EMG/NCS. At imaging, nerve enlargement, edema, and enhancement serve as general markers of injury. When there is concern for nerve transection, DTI fiber tracking, ADC measurements, and morphologic evaluation for pseudomeningocele/neuroma are promising metrics for prediction of patient prognosis and therapy.

KEYWORDS: Brachial Plexopathy, MR Neurography, Pediatric Spine

O-592

4:31PM - 4:38PM

High Resolution CT of Ossicular Abnormalities in Children with Limited Stenosis of the External Canal Associated with a Normal or Minimally Malformed External Ear.

R Jacob1, S Gupta2, B Isaacson2, J Kutz2, P Roland2, T Booth1

1Children's Medical Center, University of Texas, Southwestern Medical School, Dallas, TX, 2University of Texas, Southwestern Medical Center, Dallas, TX

Note: Scanned images are included in the proceedings. Some submitted images were reduced during editing thereby decreasing clarity. Also, refer to the Program Planner. Proceedings Content as of 3/28/2014.

Purpose

To describe clinical presentation, audiometric and high resolution CT findings in patients with limited congenital external auditory canal (EAC) stenosis associated with normal or minimally abnormal pinna.

Materials and Methods

This was a retrospective case series at a tertiary referral center. A PACS search was performed with Boolean function combining "external canal", "external auditory canal" and "stenosis" or "stenotic". Inclusion criteria were patients with congenital EAC stenosis of less than 50% diameter on CT and a normal pinna or grade I microtia. Exclusion criteria included syndromic ear malformations, EAC greater than 50% stenosis, and grades II or III microtia. Clinical presentation, audiometry and CT studies were reviewed. Intra-operative findings and success of reconstruction were reviewed when available. Clinical data and surgical results were reviewed by an experienced (8 years) fellowship trained neuro-otologist. Imaging studies were reviewed by an experienced (16 years) pediatric neuroradiologist and a neuroradiology fellow. The images were evaluated for normal or abnormal shape and size of the ossicles, presence of fixation as well as widening or narrowing of their associated joints. The distance of the inferior handle of the malleus to the cochlear promontory was measured on both abnormal and the contralateral normal ear. The oval/round windows were classified as normal, stenotic, or atretic. The facial nerve was evaluated for normal position with the posterior genu at or posterior to the round window. The inner ear also was evaluated for anomalies of the osseous labyrinth and a normal or stenotic cochlear nerve canal.

Results

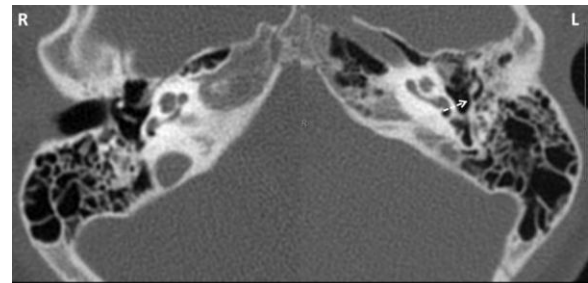
Nine patients were found with 20 excluded (12 moderate to severe stenosis, 7 grade II/III microtia, 1 syndromic). M:F ratio = 5:4 and mean age was seven years (range 3 – 12 years). All patients presented with unilateral conductive hearing loss (CHL) with seven patients having isolated CHL as the given history. On physical examination, five of the patients had normal pinna and clinically normal EACs. Four patients had grade I microtia. The mean pure tone average was 49.4 dB (SD 14.2, range 28-68), and the mean air-bone gap was 49.4 dB (SD 12.9, range 25-65). Computed tomography (CT) showed the mean EAC axial diameter to be 5.1 mm on the affected side and 7.7 mm on the normal hearing ear. Computed tomography demonstrated ossicular abnormalities in all patients. Abnormal orientation of the handle of the malleus with abnormal increased distance to the cochlear promontory was present in all ears. Average distance of the cochlear promontory to inferior aspect of the malleus handle was significantly increased 3.9mm versus 1.6 mm ($p < .0001$). Fixation of the handle of the malleus to the anterior tympanic annulus was seen in 8/9 ears. Posterior fixation of the long process of the incus was present in 2/9 ears. Other ossicular abnormalities include decreased size of malleus head (7/9), narrowed incudomalleal joint (7/9), widening of the

incudostapedial joint (5/9), and abnormal appearance of the stapes (1/9). The facial nerve was essentially normal in position in all ears with only mild anterior displacement of the vertical segment of the facial nerve seen in two ears. The oval and round windows were normal in all ears. No inner ear anomalies were found. Surgical correlation was present in 3 patients with agreement in most findings on CT. Tympanoplasty was performed in all with ossiculoplasty performed in two ears. Ossicular chain reconstruction in 1 ear. Significant improvement in hearing was noted in 2 patients on postoperative audiogram and 1 patient was lost to follow up.

Conclusions

Anomalies of the pinna commonly are absent or subtle in children with limited congenital EAC stenosis. These children typically present with unilateral conductive hearing loss and characteristic ossicular malformations. The EAC should be evaluated carefully in all children presenting with unilateral CHL, even in the absence of anomalies of the pinna. Surgical outcome is good in this cohort of patients.

KEYWORDS: Conductive Hearing Loss, Congenital Anomalies, Temporal Bone



Axial CT image at the level of the long process of Incus shows abnormal posterior fixation of the long process of Incus on the left side. Normal ossicles are present on the right side.

Wednesday, May 21

3:00PM - 4:30PM

Room 524

70 - PARALLEL PAPERS: Radiology Practice:
Quality, Safety and Economics

0-593

3:00PM - 3:07PM

Radiation protection of different lens protection systems in cranial CT-scans

Note: Scanned images are included in the proceedings. Some submitted images were reduced during editing thereby decreasing clarity. Also, refer to the Program Planner. Proceedings Content as of 3/28/2014.

A Ringelstein¹, N Guberina¹, B Mukherjee¹, M Schlamann¹

¹University Hospital Essen, Essen, Germany

Purpose

The purpose of this phantom study was to evaluate the potential dose-attenuation of different eye lens protectors for patients undergoing various cranial computed tomography (CT) scans at different scanners.

Materials and Methods

Radiation exposure of the eye lens of seven common CT algorithms at two different CT scanners [(SOMATOM® Definition AS (CT 1) and SOMATOM® Definition Flash (CT 2))] was measured (α -Al₂O₃:C thermoluminescence dosimeters TLD-500) using two different lens protectors (Somatex (SOM) and Medical Imaging Systems (MIS).

Results

Dose attenuation accomplished by the different lens protectors is summarized as follows: for CT 1 (a) unenhanced CT (nCT) with gantry angulation: SOM (0%), MIS (0%); (b) CT angiography (CTA): SOM (37%), MIS (9%); (c) CT perfusion (CTP): SOM (61%), MIS (64%); for CT 2 (d) nCT without gantry angulation: SOM (19%), MIS (9%); (e) CTA Safire®: SOM (61%), MIS (26%); (f) dual energy CTA without Safire®: SOM (31%), MIS (7%); (g) CTP: SOM (56%), MIS (31%). Depending on the CT protocol but independent from the scanner used, lens protector SOM attenuated the dose up to 1.9 times more effectively compared to MIS. Physical analysis revealed that the two lens protectors differ with respect to their density and thickness.

Conclusions

The efficacy of the two evaluated lens protectors differs widely due to various material properties but also is highly dependent from the applied CT protocol. Lens protectors are most effective in CTA protocols when reducing direct dose exposure. Considering both CT protocol and material of the lens protectors is mandatory to reduce radiation exposure of the eye lens of patients undergoing CT scans.

KEYWORDS: Dose Reduction

0-594

3:07PM - 3:14PM

High Negative Predictive Value of a Negative Spot Sign Can Potentially Reduce Subsequent Imaging in Acute Intracranial Hemorrhage.

R Hito¹, V Ciura¹, J Ortiz Leviano¹, R Gonzalez¹, J Romero²

¹Massachusetts General Hospital, Boston, MA,
²Massachusetts General Hospital, Harvard Medical School, Boston, MA

Purpose

A positive spot sign, the presence of active extravasation at computed tomography angiography (CTA), has been shown to be associated with an increased risk of significant hematoma expansion in nontraumatic intracerebral hemorrhage. The purpose of the current study is to determine the negative predictive value of a negative spot sign for significant hematoma expansion in acute nontraumatic intracranial hemorrhage, evaluate the clinical course of patients with a negative spot sign who subsequently developed significant expansion of the intracranial hematoma and to determine whether routine follow-up head CTs after intracranial hemorrhage can be reduced in patients with a negative spot sign in the absence of clinical deterioration.

Materials and Methods

An IRB approved retrospective review of patients who presented to the Massachusetts General Hospital Emergency Department with acute nontraumatic intracranial hemorrhage and a negative spot sign on a CT angiogram within 24 hours of presentation was performed, with a focus on patients with a negative spot sign who subsequently developed significant hematoma expansion (defined as an increase in the volume of greater than 33%), excluding those with intraventricular hemorrhage. The results were tabulated and the negative predictive value of a negative spot sign for significant hematoma expansion was calculated from the database. A chart review focusing on the clinical course of those patients with a negative spot sign who subsequently developed significant hematoma expansion was performed. Medical records were reviewed for International Normalized Ratio (INR), history of hypertension and antiplatelet therapy at the time of presentation. The administration of fresh-frozen plasma, vitamin K, and platelet transfusions on admission was recorded, as well as any changes in the clinical status of the patient leading up to the hematoma expansion. Additionally the average number of follow-up head CTs in patients with a negative spot sign was calculated.

Results

Of the 159 patients with a negative spot sign on CTA, four patients subsequently developed significant hematoma expansion. The negative predictive value of a negative spot sign on CTA for subsequent hematoma expansion was calculated at 97%. Three of the four patients were on anticoagulation therapy on presentation or shortly before presentation. The fourth patient had hepatocellular carcinoma with an elevated PT. On average patients with negative spot sign on initial CTA had three head CTs during the course of their hospitalization.

Conclusions

The high negative predictive value of a negative spot sign for expansion of an intracerebral hematoma in the absence of anticoagulation on admission could allow for a reduction in routine follow-up head CTs in the absence of clinical deterioration. Reducing the number of head CTs would not

Note: Scanned images are included in the proceedings. Some submitted images were reduced during editing thereby decreasing clarity. Also, refer to the Program Planner. Proceedings Content as of 3/28/2014.

only reduce the unnecessary patient exposure to radiation but also would be cost effective as the average Medicare reimbursement for a noncontrast head CT is approximately \$191.89, and on average this group of patients had three follow-up head CTs over the course of their hospitalization.

KEYWORDS: Hemorrhage
O-595

3:14PM - 3:21PM

Assessment of Adverse Reaction Rates to Gadobenate Dimeglumine: Review of over 140,000 Administrations over The Last 7.5 Years

S Fakhran¹, H Kale¹, L Alhilali¹, A Reynolds¹, C Qu¹, E Kanal¹

¹University of Pittsburgh Medical Center, Pittsburgh, PA

Purpose

To determine the incidence of adverse events with gadobenate dimeglumine at a major hospital system, consisting of both academic and community-based centers, over the last 7.5 years.

Materials and Methods

As part of regular and continuous prospective approved quality assurance project, MR technologists contemporaneously recorded all gadolinium-based contrast administrations and any associated adverse reactions to those administrations, including the type of reaction and treatment rendered, since July, 2007. Weekly data review was performed by the institutional director of MR services, and were evaluated both by site as well as in comparison to results obtained from other participating hospitals and sites with our institution's health system. Comparison between reaction rates at different sites was performed using a Chi Squared test.

Results

Over 7.5 years, 142,929 doses of gadobenate dimeglumine were administered. Two hundred forty-seven reactions were recorded (0.17% of contrast-enhanced examinations), of these, 135 cases (54.7% of all adverse reactions) required treatment and 14 (5.6% of reactions) qualified as serious. Reaction rates were significantly different between the academic and community hospital (0.2% versus 0.1% respectively, $p < 0.001$). Further, reaction rates were higher in the initial years of the study and tapered to a lower baseline rate which has been maintained over the last three plus years of the study. These findings are consistent with the reported Weber and Lalli effects noted in the literature on other agents as well.

Conclusions

Adverse reaction rates to gadobenate dimeglumine recorded over 7.5 years were comparable to those reported and published for other gadolinium-based contrast agents examined over smaller time ranges and

populations. The findings again reinforce the relatively robust safety profile of this agent. The Weber and Lalli effects seemed to have been observed within our population as a whole as well as within individual participating hospitals/sites, reinforcing the observations of Davenport (1) and others. Considering the low incidence of all adverse events observed, a statistically but likely not clinically significant difference was observed between academic and community hospitals.

KEYWORDS: Contrast Agents, MR Contrast Agents

O-596

3:21PM - 3:28PM

Analysis of Medicare Referral Network Size for Neuroradiologists.

A Pyrros¹, M King², R Weald³, P Nikolaidis⁴, A Flanders⁵

¹Community Hospital, Munster, IN, ²Indiana University-Purdue University Indianapolis, Indianapolis, IN, ³Sharethrough, San Francisco, CA, ⁴Northwestern University Feinberg School of Medicine, Chicago, IL, ⁵Thomas Jefferson University Hospital, Philadelphia, PA

Purpose

Recent trends in healthcare, such as reductions in reimbursements, consolidation and increased self-referral behavior, are impacting the business of radiology. Given radiologists' unique dependence on referrals, it is critical they understand referral networks so they can begin to actively manage them. An important part of understanding referral networks is to recognize there may be differences among medical specialties. We define network size as the number of unique referrers. We hypothesize that neuroradiologists may have smaller referral networks than other radiologists.

Materials and Methods

In this IRB exempt retrospective study, we analyzed the publicly available Docgraph data set. The Docgraph data set is one of the largest known directed social graph networks, based on 2011 Medicare claims data, containing over one million entities or nodes which provide Medicare services. The graph is a 1.3 gigabyte text file with each line of the file representing a relationship (vertex) between two providers (nodes) and a weighting number representing the number of patients that were billed for in a rolling thirty-day window by both providers. National provider identifier (NPI) numbers identify the provider nodes. The National Plan & Provider Enumeration System (NPES) file contains additional details of all providers including geographic location and specialty taxonomy codes. Utilizing all available taxonomy codes for radiology, 37,993 relevant NPI numbers were identified. Radiology facilities and institutions were excluded and filtered from this search. The radiologist's name, city, and state from the

Note: Scanned images are included in the proceedings. Some submitted images were reduced during editing thereby decreasing clarity. Also, refer to the Program Planner. Proceedings Content as of 3/28/2014.

NPESS file then was cross-referenced against the American Board of Radiology (theabr.org) public web search tool utilizing an automated script. Data then were imported into Excel (2010) NodeXL software (version 1.0.1.245) for analysis. Results then were plotted utilizing R (version 3.0.2).

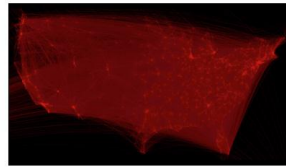
Results

There were 26,649 radiologists that were not matched and 11,275 that were matched. Of the 11,275 matches, 1,393 were identified as CAQ certified neuroradiologists. One thousand two hundred and seventy-four of those neuroradiologists also were identified in the Docgraph file. In all, 8,990 ABR verified radiologists were identified in the Docgraph file. One thousand two hundred and seventy-four NPI neuroradiology nodes were identified within 674,964 vectors/referrals within the dataset representing 13.9% out of the 4,823,135 vectors in which a radiologist was identified. Neuroradiologist in-degrees or inbound referrals average 275 with a standard deviation (SD) of 197. Out-degrees or outbound referrals average 258 with a SD of 194. Among all radiologists, the average in-degrees are 281 SD 216 and out-degrees are 269 SD 211, and when excluding neuroradiologists in-degrees 282 SD 219 and out-degrees 270 SD 214. The most common in-degree referrer physician taxonomy code for all radiologists was internal medicine (62,447). A geographic plot of this data shows the geographic distribution of neuroradiologists correlates strongly with major U.S. population centers.

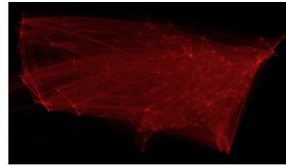
Conclusions

Neuroradiologists have a slightly smaller referral network based on the in-degree averages and standard deviations as compared to all radiologists. Interestingly, the 1,274 neuroradiologists identified represented approximately 12.3% of the total radiologists verified and a proportional 13.9% of all the radiologist connections or vectors identified, suggesting a linear relationship. This also may indicate that many subspecialty neuroradiologists practice general radiology. Not surprisingly, the docgraph data show that radiologists and neuroradiologists have very large referral networks. In a separate analysis, the only groups of providers in the graph with a larger number of referrers are medical institutions. High quality referrers are preferable to a high quantity since care must be taken to manage the relationships with other physicians. Failure to do so may contribute additionally to the commoditization of radiology services caused by the national trend of increased study volumes.

KEYWORDS: Medicare



Geographic plot of all radiologists and referrers



Geographic plot of only neuroradiologists and referrers

O-597

3:28PM - 3:35PM

Utility of Head and Neck MRA in Addition to Brain MRI in the Emergency Department Evaluation of Suspected Stroke

A Cunqueiro1, J Bello2

1Albert Einstein College of Medicine, Montefiore Medical Center, Bronx, NY, 2Montefiore Medical Center, Bronx, NY

Purpose

Concerns over healthcare spending and in particular, imaging costs, have become more acute. As radiologists, we are well positioned to identify areas of overutilization in imaging. We hypothesize that routine addition of magnetic resonance angiography (MRA) of the head and neck to magnetic resonance imaging (MRI) of the brain in the Emergency Department (ED) evaluation of "acute stroke" is an area in which overutilization may occur. Our goal is to examine the frequency with which the two additional MRA examinations add important information in the ED setting when no infarct is present on MRI of the brain, and to determine whether significant cost savings could be achieved by omitting the MRA examinations when diffusion-weighted imaging (DWI) of the brain is negative for acute infarct.

Materials and Methods

A series of over 500 consecutive patients in whom MRI of the brain and MRA of the head and neck were performed from the ED were included in the study. Patient demographic information, presenting symptoms, known stroke risk factors, and findings on initial computed tomography (CT) of the head were recorded. The presence or absence of acute infarct on MRI, as well as significant findings on the MRA examinations, reported by the interpreting neuroradiologists, also was recorded. We then compared the frequency with which significant MRA

Note: Scanned images are included in the proceedings. Some submitted images were reduced during editing thereby decreasing clarity. Also, refer to the Program Planner. Proceedings Content as of 3/28/2014.

findings were identified in patients with and without acute infarct on DWI. Within the subcategory of patients without acute infarct on MRI, we sought to discover whether any demographic factors, stroke risk factors, presenting symptoms, or initial head CT factors predicted a higher likelihood of significant findings on MRA.

Results

Preliminary review of the data showed that approximately 35% of the MRIs of the brain were positive for acute infarct. In the 65% of patients without acute infarct, 2% of the MRAs demonstrated a moderate or severe cervical internal carotid stenosis. An additional 7% of these patients had occluded cervical or intracranial internal carotid or vertebral arteries. A larger number of patients in this group without acute infarct on MRI had cervical or intracranial stenoses not specified in severity, in many cases related to technical limitations of the exam.

Conclusions

Up to 9% of patients without acute infarct on MRI were found to have a moderate or severe internal carotid stenosis on MRA, or an occluded cervical or intracranial artery. While this information is clinically relevant to subsequent management of patients with suspected cerebral ischemia, the benefit, relative to cost of obtaining head and neck MRAs can be questioned in the absence of acute ischemia. Additional review of the data might identify a constellation of presenting symptoms, risk factors, or demographic information which serve as positive predictors of a higher likelihood of significant findings on MRA. These criteria, once identified, would allow for more careful patient selection for MRAs in the absence of acute infarct on MRI.

KEYWORDS: Cost-Effective, Stroke, Utilization Management

O-598

3:35PM - 3:42PM

Differences in Neuroradiology Training Programs Around the World.

T Schneider¹, R Lima Santos², D Yousem¹

¹The Johns Hopkins University, Baltimore, MD, ²Hospital Beneficência Portuguesa de São Paulo, São Paulo, Brazil

Purpose

The USA considers itself a leader in medical education and training amongst nations. Along with most subspecialties, radiology residency and fellowship programs are known for being well structured, highly competitive and outstanding in teaching. At a national level, radiology

residents and fellows in the United States are obliged to take yearly in-training examinations as well as board certification examinations, but it is virtually impossible to realistically compare the quality and the outcome of various international radiology training schemes. In order to better understand foreign program concepts in neuroradiology, we analyzed differences in training program variables between one USA department and a variety of the departments abroad.

Materials and Methods

The parameters of radiology residency and fellowship training at foreign institutions were analyzed. Information about the respective departmental organization (number of trainees and attendings), structural concepts (length of program, case logs), teaching schedules (number of weekly lectures, case reviews, etc.), and national examinations were collected for eight countries and the USA spanning four continents.

Results

While many countries do not provide fellowship training in Neuroradiology (Italy, Greece, Lithuania, Guatemala, Pakistan), others have formal post residency curriculums, including Belgium, Sweden, Germany, Brazil, Saudi Arabia, Thailand, Japan, and South Korea. Additionally there are some countries, such as Portugal, that offer a program following medical school that is focused solely on neuroradiology. Compared to the USA program, all countries have fewer fellows and lectures, but the duration of training is almost equal (1-2 years). Big differences were observed regarding the type and the complexity of national examinations at the end of a residency or fellowship program.

Conclusions

Regarding international neuroradiology training, there is a wide variety in terms of fellowship offering, teaching quantity and assessment of learning progresses. The results of our study suggest that the general diagnostic radiology residency and neuroradiology fellowship program in the USA is more specialized and tends to focus on highly defined goals and learning objectives.

KEYWORDS: Fellowship, Neuroradiology Training

Note: Scanned images are included in the proceedings. Some submitted images were reduced during editing thereby decreasing clarity. Also, refer to the Program Planner. Proceedings Content as of 3/28/2014.

GENERAL									
Country	USA	Belgium	Sweden	Germany	Brazil	Saudi Arabia	Thailand	Japan	South Korea
Hospital name	Johns Hopkins University Baltimore	University Hospital KU Leuven	Uppsala Akademiska Sjukhuset	Charité Berlin	Beneficência Portuguesa de São Paulo	King Faisal Specialist Hospital Riyadh	Siriraj Hospital Bangkok	-	Chungnam National University Hospital
Years of medical school	4+4	3+3	5.5	6	6	6	6	6	6 or 2-4+4
Internship	1 year	no	1.75 years	no	1-2 years	1 year	1-3 years	2 years	1 year
RESIDENCY									
Years	4	5	5	5	3-4	4	3	3	4
No. of residents	40	55	10	56	70	16	75	-	8
No. of attendings	140	36	10	22	22	23	40	-	13
Neuro radi lecture s / w	1 (+ month-long course)	sporadic	sporadic	sporadic	2	1	1-2	-	sporadic
Case log	yes	yes	no	yes	no	yes	yes	-	no
Exams	w	w, o	no	o	w	w, o	w, o	(yes)	w
FELLOWSHIP									
Type offered	DNR / INR	DNR	DNR	"NR"	DNR / INR	DNR / INR	DNR / INR	DNR / INR	"NR"
Years	2 / 2	2	2	2-3	2 / 1	2 / 1	2 / 2	2 / 2	1-3
No. of fellows	8 / 3	1	3	3	6	3 / 1	2 / 2-3	-	1
No. of attendings	16 / 3	3	3	3	6	3 / 1	9	-	2
Lectures / w	daily	no	sporadic	sporadic	3	daily	3	-	sporadic
Case log	yes	no	no	yes	no	yes	no	-	no
Exams	w	w, o (ESNR)	no	o	no	o	non-uniform	-	no

0-599

3:42PM - 3:49PM

Sequence Reduction for Emergency Lumbar Spine MR Imaging

S Patel1, J Johnson2, S Stalcup1, S Kamalian3, P Schaefer3

1Massachusetts General Hospital, Cambridge, MA,
2University of California San Francisco, San Francisco, CA,
3Massachusetts General Hospital, Boston, MA

Purpose

In emergency room settings with MR imaging (MRI) availability, lumbar spine MRI is a commonly performed diagnostic procedure. The purpose of this study is to determine the efficacy of a screening lumbar spine MRI protocol (comprised of sagittal T1 and sagittal fat-suppressed T2-weighted sequences) for emergency lumbar spine MRI indications.

Materials and Methods

IRB approval was obtained for this HIPPA compliant retrospective study. Two hundred consecutive emergency room patients who underwent lumbar spine MRI examinations from January 2011 – January 2013 were chosen. Exclusion criteria included: prematurely aborted examinations, total spine survey examinations not dedicated to the lumbar spine, and patients scanned on an alternate MRI machine outside of the emergency department. All relevant clinical data for each patient (age, gender, history, physical exam findings, laboratory findings, and prior imaging) were recorded. Two neuroradiologists evaluated only the sagittal T1 and sagittal fat-suppressed T2-weighted sequences of each study, and documented the imaging findings. Readers could recommend axial imaging and/or postcontrast imaging if warranted. All imaging findings and recommendations of each reader were recorded. The readers' findings were compared with the final reports of each study and any relevant clinical follow up to determine discrepant findings. Major discrepancies were assigned if a missed finding might have changed clinical management. Minor discrepancies were assigned if a missed finding would not have changed clinical management. Clinical metrics were correlated with axial and/or postcontrast imaging recommendations and reader discrepancies utilizing a step-wise multivariate logistic regression.

Results

Of the 200 patients, 107 were female and 93 male, with average age of 60 ± 20 years. Of the 200 lumbar spine MRIs, 117 were performed without contrast and 87 were performed with contrast. The underlying lumbar spine pathologies included: 169 cases with degenerative disease; 22 cases with acute fracture; 19 cases with primary

Note: Scanned images are included in the proceedings. Some submitted images were reduced during editing thereby decreasing clarity. Also, refer to the Program Planner. Proceedings Content as of 3/28/2014.

neoplasm or metastases; 10 cases with infection; one case with epidural hemorrhage. Reader 1 recommended no further imaging in 136 cases, axial imaging in 53 cases, and postcontrast imaging in 43 cases. Reader 2 recommended no further imaging in 134 cases, axial imaging in 41 cases, and postcontrast imaging in 46 cases. In 57% of contrast-enhanced MRIs, reader 1 did not recommend contrast. In 54% of contrast-enhanced MRIs, reader 2 did not recommend contrast. Known lumbar spine metastases [(p=0.0007), adjusted OR 11 (95%CI: 2.7 to 42.5)] and prior lumbar spine surgery [(p=0.003), adjusted OR 3 (95%CI: 1.5 to 6.3)] were significant predictors of axial imaging recommendation. History of malignancy [(p=0.0004), adjusted OR 3.9 (95%CI: 1.8 to 8.4)], radicular pain [(p=0.007), adjusted OR 0.35 (95%CI: 0.16 to 0.75)], and prior lumbar spine surgery [(p=0.048), adjusted OR 2.2 (95%CI: 1.005 to 4.9)] were significant predictors of postcontrast imaging recommendation. Reader 1 had two major discrepancies (missed leptomeningeal metastasis, missed infected facet joint) and seven minor discrepancies. Reader 2 had one major discrepancy (missed lymphoma marrow infiltration) and eight minor discrepancies. In the missed cases of leptomeningeal metastasis and lymphoma marrow infiltration, the patients had a known history of malignancy (metastatic squamous cell carcinoma and lymphoma respectively) prior to imaging. In the missed case of infected facet joint, the patient presented with fever, elevated ESR/CRP, and low back pain prior to imaging. The clinical metrics demonstrated no statistically significant correlation with discrepancies.

Conclusions

Lumbar spine MRI protocol comprised of sagittal T1 and sagittal fat-suppressed T2-weighted sequences serves as an effective screening imaging examination for emergency indications, demonstrating very low rates of major discrepancies and the potential for marked reduction in imaging time and cost. To avoid missed findings utilizing this protocol, we have developed an algorithm to identify the need for additional sequences. Education in interpreting studies with limited sequences and active radiologist monitoring of the studies also are required.

KEYWORDS: Low Back Pain, Lumbar Spine MR

0-600

3:49PM - 3:56PM

Co-branding of Radiology Practices and Large Academic Medical Centers: Can't We All Just Get Along?

M Keiper¹, L Grignon¹

¹University of Nebraska Medical Center, Omaha, NE

Purpose

Branding of a radiology practice is essential to establish an identity in the marketplace and to compete with alternative options for imaging services. The purpose of this abstract is to demonstrate the seemingly insurmountable barriers but tremendous opportunities in co-branding radiology practices with large academic institutions in order to provide a formidable force in the outpatient imaging market.

Materials and Methods

This study is a primer for introducing the concept of co-branding, establishing a framework for building a brand recognition and marketing plan, and successfully implementing the concepts in the market place in the setting of an academic institution with strict prohibition of individual departmental brand initiatives. The development of a tag line, unique recognizable logo, collateral marketing material, individual business web site separate from the academic website and a radiology-specific marketing campaign within the confines of marketing guidelines of the parent institution will be delineated. The radiology department branding initiative occurred over a two-year period from 2011-2013 culminating in the initial introduction of the new brand proposition to the market in late 2013 and 2014. Optimization of service and access benchmarks in the parent academic medical center and the assessment of change in radiology imaging volumes over this time period were documented during the project and upon initial roll out into the market.

Results

Optimization of scheduling and access benchmarks to levels surpassing aggressive private practice standards was attained in a large academic institution and served as a framework of a radiology-specific marketing campaign emphasizing service to referring clinicians and patients as a primary distinguishing feature of the radiology practice in the local marketplace. Pre-existing institutional brand identity of best practices in terms of regional clinical expertise and quality care also were successfully emphasized in the marketing campaign. Co-branding of the two entities, promotion of two brand concepts and improvement of service barriers to the institution yielded an increase in the radiology practice's identity, ultimately increasing imaging volumes 15% over a two-year period by allowing the radiology department to effectively compete in an aggressive private marketplace and shed previous preconceived notions of difficult access and less than optimal service. The co-branding technique also provided a separate recognizable radiology identity, thereby reducing commoditization of radiology services.

Conclusions

Although seemingly an insurmountable task, individual unique branding of a radiology department within an academic institution is not only possible but gives both the radiology practice and the parent institution a competitive advantage in the marketplace. Co-branding academic

Note: Scanned images are included in the proceedings. Some submitted images were reduced during editing thereby decreasing clarity. Also, refer to the Program Planner. Proceedings Content as of 3/28/2014.

radiology practices with the larger parent academic medical centers is essential in creating a unique identity for the radiology department in the marketplace. The established identity allows the practice to develop marketing and service campaigns with the parent institution that surpass outpatient imaging market standards and ultimately increase radiology imaging volumes and revenue to the benefit of both entities.

KEYWORDS: Economics, Utilization Management

O-601

3:56PM - 4:03PM

Modified Neuroradiology Reports: What are the Critical Neuroradiological Findings that Trainees Miss or Misinterpret?

J Huntley¹, L Babiarz¹, D Yousem¹

¹Johns Hopkins Hospital, Baltimore, MD

Purpose

Trainees' initial interpretations of neuroradiological studies typically are reviewed and finalized by neuroradiologists on staff. Our critical findings (CF) policy requires urgent communication and electronic documentation of certain critical neuroradiology imaging findings that can have an effect on patient care. When a trainee has missed or misinterpreted a CF, that report is corrected by a faculty and electronically flagged as modified, and the change is communicated to the referring clinician. In this study we set out to identify which critical neuroradiological pathologies our trainees tend to miss or misinterpret most frequently.

Materials and Methods

Study protocol was approved by our internal review board (IRB). Using our radiology information system (RIS) database, we searched for all neuroradiology reports electronically marked to indicate a missed or misinterpreted CF by a trainee during Jan-Oct 2011. These reports were reviewed to determine what CF was amended to the report. Our CF policy includes the following 17 items: airway compromise, brain edema, child abuse, congenital variant, cord compression, cord infarction, fracture, globe/retina injury, hardware malfunction, hemorrhage, herniation, hydrocephalus, infection, mass, stroke, spinal instability, and vascular abnormality. The training level of the trainee was noted as a resident or fellow. The imaging modality was recorded as CT or MRI. Two months-worth of neuroradiology reports (Jan-Feb 2011) were reviewed to establish the baseline rate of CF entities seen at our institution. Summary statistics were calculated. The relative frequency of all individual CFs was

compared between the baseline measurement and modified reports for all trainees combined and residents and fellows separately using Fisher's exact test. Statistical significance was rated at $p < 0.05$.

Results

332 modified reports with CFs were identified. These included 143 (43.1%) CT and 189 (56.9%) MRI exams and contained 352 missed or misinterpreted CFs. 130 (39.2%) reports were read by residents and 202 (60.8%) were read by fellows. During Jan-Feb 2011, 12,607 neuroradiology reports contained 755 CFs. The baseline practice CF rates were: hemorrhage 154/755 (20.4%), stroke 145/755 (19.2%), fracture 88/755 (11.7%), vascular abnormality 68/755 (9%), mass 65/755 (8.6%), herniation 53/755 (7%), hydrocephalus 50/755 (6.6%), infection 48/755 (6.4%), brain edema 29/755 (3.8%), cord compression 19/755 (2.5%), spinal instability 15/755 (2%), globe/retina injury 13/755 (1.7%), hardware malfunction 3/755 (0.3%), child abuse 3/755 (0.3%), congenital variant 1/755 (0.1%), cord compression (0.1%), and airway compromise (0.1%). Modified reports, CF rates were: mass 52/332 (15.7%), hemorrhage 46/332 (13.9%), vascular abnormality 40/332 (12%), fracture 38/332 (11.4%), infection 35/332 (10.5%), stroke 26/332 (7.8%), brain edema 16/332 (4.8%), hydrocephalus 11/332 (3.3%), cord compression 6/332 (1.8%), hardware malfunction 4/332 (1.2%), herniation 3/332 (0.9%), and globe/retina injury 2/332 (0.6%). Not a single case of spinal instability, child abuse, congenital variant, cord compression, and airway compromise were found. Stroke, herniation, and spinal instability were found at a lower rate in modified reports than what was seen in our practice at baseline ($p < 0.0001$, $p < 0.0001$, and $p = 0.016$, respectively), whereas vascular abnormality and mass were found at a higher rate ($p = 0.024$ and $p < 0.0001$, respectively). In modified cases read by the fellows only, stroke ($p < 0.0001$) and herniation ($p = 0.0002$) occurred at a lower rate than expected and vascular abnormality ($p = 0.027$), mass ($p = 0.0001$), and infection ($p = 0.001$) were missed at a higher rate. For residents, herniation occurred at a lower rate ($p = 0.036$) and mass was overlooked at a higher rate ($p = 0.025$), compared to the baseline.

Conclusions

Our analysis of the modified neuroradiology reports identified mass, hemorrhage, vascular abnormality, fracture, infection, and stroke as the most common missed or misinterpreted CFs. Compared to the baseline CF frequency in our practice, residents disproportionately erred in cases with intracranial mass, and fellows in cases with vascular abnormality, mass, and infection. These data can be helpful in exposing trainee deficiencies and can be used to facilitate educational interventions.

KEYWORDS: Quality Control, Quality Improvement

O-602

4:03PM - 4:10PM

Note: Scanned images are included in the proceedings. Some submitted images were reduced during editing thereby decreasing clarity. Also, refer to the Program Planner. Proceedings Content as of 3/28/2014.

Is duplicated content an indicator of article quality and acceptance or rejection?

R Sharma¹, K Halm², M Castillo¹

¹University of North Carolina Chapel Hill, Chapel Hill, NC,
²American Journal of Neuroradiology, Oak Brook, IL

Purpose

Duplicated and/or plagiarized contents are well accepted indicators of poor quality in scientific articles. Here we tried to determine the relationship between duplicated contents and acceptance or rejection of articles submitted to a major journal. Additionally, we sought to determine if duplications are more common in articles from different parts of the world. Thus, we tested our hypothesis that duplicated content percentage is an indicator of acceptance/rejection and indirectly of the quality of an article.

Materials and Methods

Retrospectively we used a commercially available duplication/plagiarism web-based program (iThenticate) to examine duplicated content rate in 120 randomly selected articles published in AJNR to serve as a control (accepted) group. We then examined 120 rejected articles in the same fashion. We divided each group equally according to geographic region of article origin as: Asia, North America, and Europe (Turkey was counted in Europe data, India in Asia data, Mexico in North American data; Australia, Brazil, Egypt, Iran, and Israel were not included). Calculated duplications for each group were compared with those of other groups and we arbitrarily set a 15% rate of duplicated content from a single source as significant. Results: Two of 120 accepted articles (1.7%) had a >15% duplication rate based on iThenticate analysis. One published article from Asia showed a 23% duplication rate and one from Europe scored 17%. No published articles from North America exceeded the 15% limit. Four of 120 rejected articles (3.3%) had a >15% duplication rate. Three rejected articles from Asia were over the limit of 15% from any one source (36%, 42%, and 43%) and one from Europe scored 15%. No rejected articles from North America exceeded the 15% limit.

Results

Two of 120 accepted articles (1.7%) had a >15% duplication rate based on iThenticate analysis. One published article from Asia showed a 23% duplication rate and one from Europe scored 17%. No published articles from North America exceeded the 15% limit. Four of 120 rejected articles (3.3%) had a >15% duplication rate. Three rejected articles from Asia were over the limit of 15% from any one source (36%, 42%, and 43%) and one from Europe scored 15%. No rejected articles from North America exceeded the 15% limit.

Conclusions

Articles arising from Asia, accepted and rejected, contain higher duplication rates than those from Europe and North America. Duplication rates in rejected articles were nearly twice as high as those found in accepted articles. Thus, a priori detection of high duplication rates may be an indication of article quality and may predict acceptance or rejection.

KEYWORDS: Outcomes, Quality Control, Quality Improvement

O-603

4:10PM - 4:17PM

Frequency and Severity of Allergic-Like Reactions to the Gadolinium-Based Contrast Agent Gadobutrol: A Three Year Study at a Single High Volume Center

S Power¹, N Talbot², W Kucharczyk³, D Mandell¹

¹University Health Network: Toronto Western Hospital, Toronto, Ontario, Canada,
²University Health Network: Princess Margaret Hospital, Toronto, Ontario, Canada,
³University of Toronto, Toronto, Ontario, Canada

Purpose

Gadobutrol (Gadovist/Gadavist) is a nonionic macrocyclic gadolinium-based magnetic resonance imaging (MRI) contrast agent. The drug has been approved for use in the United States since 2011, Canada since 2004, and in some European countries since 1998. Practice guidelines suggest that gadobutrol may pose a lower risk of nephrogenic systemic fibrosis (NSF) than some other agents (1). Allergic-like reactions to gadolinium-based agents are rare, but they do occur, and reported reaction rates vary among the agents (2, 3). Most of the allergic-like reaction literature pertains to drugs other than gadobutrol. The literature for gadobutrol is mainly from postmarket surveillance and a post-hoc meta-analysis of clinical trial data, which reported widely discrepant adverse reaction rates of 0.02% and 4%, respectively (1). Surveillance results are biased by reliance on physician reporting, and the meta-analysis includes fewer than 5,000 patients gathered from 34 different trials. The purpose of our study was to determine the frequency and severity of allergic-like reactions to gadobutrol in a single high volume center.

Materials and Methods

We prospectively recorded details of every allergic-like reaction to gadolinium-based MRI contrast agents at a single center from January 1, 2010 to December 31, 2012. Each event was graded as mild, moderate, or severe, according to previously published criteria (3, 4). Physiologic reactions such as nausea and vomiting were

Note: Scanned images are included in the proceedings. Some submitted images were reduced during editing thereby decreasing clarity. Also, refer to the Program Planner. Proceedings Content as of 3/28/2014.

not included as they are not allergic-like reactions (3). The frequency of mild, moderate and severe reactions was calculated, as well as the frequency of allergic-like reactions occurring despite prophylaxis. Treatments administered for the allergic-like reactions were recorded. We also calculated the frequency of delayed reactions, with symptom onset after the patient had left the medical imaging department. The delayed reaction data was limited to reactions for which the patient contacted the department.

Results

There were 25,603 gadolinium-enhanced MRI examinations during the study period, and 80 (0.31%) allergic-like reactions. Gadobutrol was the most commonly used contrast agent (91.1% of injections) and it accounted for 76 (0.33%) of allergic-like reactions. Three of the gadobutrol reactions were moderate (dyspnea n=2, soft-palate swelling n=1) and the remainder were mild. The frequency of specific symptoms in the 76 adverse reactions is listed in the accompanying table. No treatment was administered for 37 (48.7%) reactions. Diphenhydramine was given for 35 (46.1%) reactions. Prednisolone (oral) was given for two (2.6%) reactions. There were two reactions (2.6%) for which medication was administered outside our center for a delayed reaction and the medication details were not recorded. In no case was epinephrine given, and no patients were transferred to the Emergency Department or admitted for observation. Allergic-like reactions despite corticosteroid prophylaxis, so-called "breakthrough reactions," accounted for 12 (15.8%) of the 76 adverse reactions. Delayed reactions accounted for 11 (14.5%) of the 76 reactions.

Conclusions

The frequency of allergic-like reactions to gadobutrol is low, and most are mild and self-limiting. Our rate of 0.33% is more than ten-fold lower than the 4% previously reported from post-hoc meta-analysis of clinical trials, and greater than the 0.02% from postmarket surveillance data. Breakthrough reactions and delayed reactions are relatively common, occurring in approximately 15% of cases.

KEYWORDS: Allergic, Contrast-Enhanced MR Imaging, MR Contrast Agents

Table: Frequency of symptoms characterizing the 76 contrast reactions which occurred in the 23,313 gadobutrol enhanced MRI examinations performed over a 3 year period.

Symptoms	Frequency of Symptom
Hives/Urticaria	53
Rash	16
Pruritis	14
Limited erythema	9
Localized facial edema	3
Itchy eyes	3
Dyspnea	2

Coughing	2
Soft palate swelling	1
Nasal congestion	1
Sneezing	1
Scratchy throat	1

O-604

4:17PM - 4:24PM

Integrated Sinus CT Protocol for Diagnostic Imaging and Intraoperative Navigation: Potential for Cost Savings and Radiation Dose Reduction

J Hoxworth¹, D Lal¹

¹Mayo Clinic, Phoenix, AZ

Purpose

The use of computed tomography (CT)-based surgical navigation during endoscopic sinus surgery (ESS) has become standard of care. Traditionally, this was acquired as an incremental CT scan after the patient previously had undergone a routine diagnostic sinus CT. The objective of this retrospective review was to determine the potential for cost-savings and radiation dose reduction that results from using a common sinus CT protocol for diagnostic imaging and intra-operative navigation.

Materials and Methods

This HIPAA-compliant study was approved by the Institutional Review Board, and the need for informed consent was waived. Effective October 1, 2010, sinus CT at the authors' institution began using a common imaging protocol that was deemed mutually acceptable by neuroradiologists and sinus surgeons for both diagnostic imaging and intraoperative navigation (Fusion ENT Navigation System, Medtronic, Inc.). Images were acquired on a 64-detector CT scanner (Lightspeed VCT or Discovery CT750HD, General Electric) using 120 kVp, 180 mA, 0.5-second rotation time, 0.531 pitch, and 0.625-mm section collimation. An axial fusion-compatible data set (standard reconstruction algorithm, 22 cm field of view) was created and archived for all patients. The electronic patient medical records for all sinus CT scans performed between October 1, 2010 and October 1, 2013 were reviewed to determine the number of sinus CT scans performed, the specialty of the referring physician, the percentage of CT scans used for intra-operative navigation, and the amount of time that elapsed between CT and ESS.

Results

A total of 4,658 sinus CT scans were performed during the study period (F:M 2,050: 2,608; age 53.9 +/- 16.2 years). During this time, 427 ESS cases utilized intraoperative CT guidance with 401 of these CT scans having been acquired

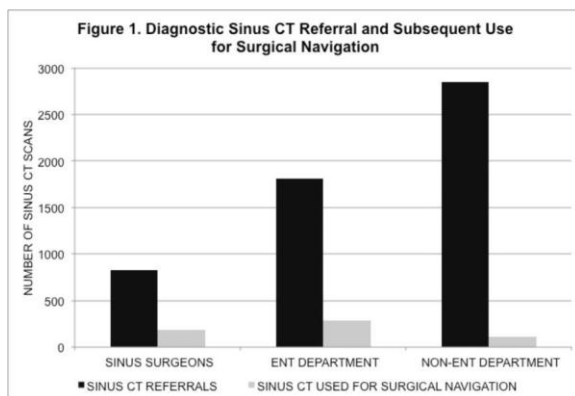
Note: Scanned images are included in the proceedings. Some submitted images were reduced during editing thereby decreasing clarity. Also, refer to the Program Planner. Proceedings Content as of 3/28/2014.

at the authors' institution. Of the 2,848 sinus CT scans ordered by non-ENT providers, 115 ESS (4.0%) ultimately were performed and did not require a new CT for surgical navigation because of the combined CT protocol. As illustrated in Figure 1, a higher percentage of sinus CT scan referrals from ENT (15.8%) and sinus surgeons (22.2%) were used for ESS ($p < 0.001$). The time interval between sinus CT and ESS was greater for non-ENT providers compared with ENT (45.1 versus 63.1 days, $p < 0.01$).

Conclusions

Using a combined sinus CT protocol for diagnostic imaging and surgical navigation prevents a significant number of patients from incurring the added cost and radiation exposure of a repeat CT. However, this approach requires neuroradiologists and sinus surgeons to agree on the CT imaging parameters, which may not be practical at centers that perform very low dose screening sinus CT.

KEYWORDS: Cost-Effective, Radiation Dose Reduction, Sinonasal Disease



O-605

4:24PM - 4:31PM

Multiple Procedure Payment Reduction (MPPR): How are Neurodiologists Affected

B Rehani¹, J Hirsch²

¹Massachusetts General Hospital, Harvard Medical School, Boston, MA, ²Massachusetts General Hospital, Boston, MA

Purpose

To understand the basic tenets of multiple procedure payment reduction (MPPR) and mechanisms by how it may affect the future of healthcare. To outline in comprehensible terms MPPR's effect on neuroradiologists and on the specialty of radiology at large.

Materials and Methods

The MPPR legislation was studied extensively and key elements are summarized. The history, implementation and potential future impact also was studied.

Results

Imaging-specific MPPRs have been applied to advanced diagnostic imaging services, which the federal government defines as computed tomography (CT), MR imaging (MRI), and Ultrasound (US). Furthermore, imaging MPPRs apply when multiple diagnostic imaging services are administered to the same patient, by the same physician, during a single health care encounter. With an MPPR, Medicare fully reimburses the most expensive procedure; however, the second and all subsequent procedures are reduced by a specific percentage. MPPR has evolved over time with multiple legislations including Deficit Reduction Act (DRA), 2006 Medicare Physician Fee Schedule Final Rule, The Patient Protection and Affordable Care Act (PPACA) and 2011 Medicare Physician Fee Schedule Final Rule. In the beginning it only involved technical component but now has expanded to Professional Component. CMS recently applied the 25% decrease to the professional component (PC) and 50% cut to the technical component (TC) to multiple physicians within the same practice for a second imaging done within the same day.

Conclusions

There is a general lack of awareness regarding the implementation of MPPR and unanswered questions about how MPPR will impact radiology. After detailed study of the legislation, there are specific key points which can help simplify the understanding of MPPR for neuroradiologists and allow them to be better prepared for the future.

KEYWORDS: Economics

O-606

4:31PM - 4:38PM

Patient Protection And Affordable Care Act (PPACA): Overview, Study Of The General Effects On Radiology, How Far Have We Come And The Future

B Rehani¹, J Hirsch², P Schaefer², R Gonzalez², D Rosman²

¹Massachusetts General Hospital, Harvard Medical School, Boston, MA, ²Massachusetts General Hospital, Boston, MA

Purpose

To understand the basics of health care reform, mechanisms by which patient protection and affordable care act (PPACA) expands health care coverage, how PPACA pays for its coverage and the future. To outline in

Note: Scanned images are included in the proceedings. Some submitted images were reduced during editing thereby decreasing clarity. Also, refer to the Program Planner. Proceedings Content as of 3/28/2014.

comprehensible terms PPACA's effect on consumers, on neuroradiologists specifically and radiology at large and understand what is yet to come.

Materials and Methods

The PPACA legislation was studied extensively and key elements of health reform are summarized. The pertinent legislation that has a potential to directly impact radiologists was studied. The roll out and the legislations, which will impact in the future, were studied.

Results

PPACA expands coverage to nearly all U.S. citizens and legal residents through two principle mechanisms: a mandate to require most U.S. citizens and legal residents to purchase health insurance; and an expansion of Medicaid. Each of these mechanisms achieves approximately half of the 30+MM people who will be newly insured due to the Act. The insurance products are made available on a state by state basis through insurance exchanges and the mandate is enforced through the tax code. Individuals who do not meet the expanded criteria for Medicaid and who meet other income eligibility criteria (from 133%-400% of federal poverty level) will be given subsidies for purchase of insurance on the exchange. Other important components of PPACA include cost controls, incentives to form Accountable Care Organizations and health plan regulation. Specific to radiology is legislation that includes utilization rate, self-referral, appropriateness criteria and a 2.3% excise tax on medical devices.

Conclusions

There is a general lack of awareness regarding the implementation of PPACA and unanswered questions about how health reform will impact radiology. After detailed study of the legislation, there are specific key points which can help simplify the understanding of PPACA for neuroradiologists and be better prepared for the future in healthcare.

KEYWORDS: Economics

Wednesday, May 21

4:45PM - 6:15PM

Room 517bc

**71 - SNIS SESSION - INTERVENTIONAL
NEURORADIOLOGY - A LOOK TO THE
FUTURE**

O-607

4:45PM - 5:15PM

The ARUBA Trial and the Interventionalist

Pride, G.
UT Southwestern Med Ctr
Dallas, TX

Abstract/Presentation Summary

Brain arteriovenous malformations (BAVM) are heterogeneous lesions known to produce intracerebral hemorrhage. There is little controversy in offering treatment to prevent recurrent hemorrhage for individuals whose hemorrhagic presentation carries a high re-rupture risk 1. On the other hand, uncertainties regarding risks associated with unruptured BAVM, coupled with increasing imaging diagnosis prompted the organization of "A Randomized Trial of Unruptured Brain Arteriovenous Malformations" (ARUBA), comparing expectant medical management of unruptured BAVM to a strategy of interventional management aimed at obliteration of the BAVM2. This multicenter, prospective, randomized, non-blinded trial compared the risks of death and symptomatic stroke between the two groups where interventional management paradigms consisted of any combination of microsurgical resection, embolization or radiation therapy. The trial was halted early after 7 years of enrollment when interim analysis of the 223 participating subjects suggested higher rates of the primary outcome, death or symptomatic stroke, in the interventional group (31% vs. 10%, hazard ratio 0.27). While not surprising that higher rates of the primary outcome occurred over the relatively short mean follow-up of 33 months in the interventional group exposed to procedural morbidity and mortality, the difference was striking. The study, its design, conduct and results have introduced controversy among physicians caring for patients harboring unruptured BAVM, with some calling for widespread applicability of the results3 and others questioning the trial's external validity4-6. Embolization as an intervention was heavily represented in the trial, applied in 58/96 (60.4%) of the treated patients in the interventional arm, 30 of whom had embolization as the only form of interventional therapy2. While endovascular treatment of BAVM with embolization has long provided an adjunct to microsurgical resection or radiation therapy, modern agents such as ethylene vinyl alcohol copolymer (EVOH) and n-butyl cyanoacrylate (n-BCA), as well as innovative embolization techniques have enabled application as primary treatment for BAVM. Large series and registries recently report AVM angiographic obliteration rates ranging from 23.5-51%7,8, with reported peri-procedural rates of morbidity/mortality ranging from 8.1% to 9.4%. The relatively high rates of death and symptomatic stroke in the interventional cohort in ARUBA (31% over 33 months of follow-up), where embolization was applied in such a large percentage of subjects, presumably aiming to obliterate the BAVM, raise questions about individual treatment modality contribution that are not elucidated in the trial report. Planned potential extension of follow-up to 5 or 10 years may add more information, although the study was not

Note: Scanned images are included in the proceedings. Some submitted images were reduced during editing thereby decreasing clarity. Also, refer to the Program Planner. Proceedings Content as of 3/28/2014.

powered to evaluate individual treatment modalities. Heterogeneity of BAVM patients clinically, AVM angioarchitecture and treatment modality nuance may dictate better analysis through organized prospective multicenter registries and studies examining structural and flow determinants of individual AVM risk. Information gathered through these types of studies may offer opportunity to answer questions left wanting in the wake of ARUBA. This talk will summarize the results of the ARUBA trial, discuss its application to current treatment paradigms, highlight limitations in applicability and discuss future directions in AVM treatment with emphasis on the contribution of endovascular therapy.
O-608

5:15PM - 5:45PM

Endovascular Simulation: Benefits and Should it be Used for Credentialing

Brook, A.

Montefiore Medical Center

Bronx, NY

Abstract/Presentation Summary

Simulation in Endovascular training is becoming not only a training tool similar to the aviation industry, but with high fidelity units and technology it is allowing for feedback and the ability to consider credentialing. Decision algorithms, preparation time and practice, as well as rehearsing calamity reversal are some of the advantages of utilizing this technology. The ease and growing computer simulated anatomically correct cases will ultimately allow for testing new equipment and the skills of the operator at various tasks. The growing haptic accuracy is not perfect but allows for sufficient feedback and guides expertise and training. The validation of these high fidelity systems is improving rapidly and numerous peer reviewed papers are documenting the necessity for trainees to practice on these simulators prior to patients. The goal is clearly to decrease human error and to decrease complications. The Government has mandated this when carotid stenting was introduced and as part of FDA approval. It is only time that will add this criteria as new devices are utilized by different disciplines using endovascular techniques. No other field like cerebrovascular highlights this as neurologists, radiologists, and surgeons treat the same diseases, in the same patient populations, with different skill sets and training backgrounds.

O-609

5:45PM - 6:15PM

SNIS President's View of the Future of Interventional Neuroradiology

Meyers, P.

Columbia University

New York, NY

Wednesday, May 21

4:45PM - 6:15PM

Room 517d

72 - GENERAL PROGRAMMING -
EMERGENCY NEURORADIOLOGY

O-700

4:45PM - 5:05PM

Neurography in the Emergency Setting

Chin, C.

University of California, San Francisco

San Francisco, CA

O-701

5:05PM - 5:25PM

Cranio-Cervical Injuries in the Elderly

Nunez, D.

Yale-New Haven Hospital

Orange, CT

Abstract/Presentation Summary

Older age is a variable that contributes to negative outcome in patients who sustain traumatic injury to the brain, as well as the spinal column and cord. This presentation will illustrate the trauma mechanics and anatomic changes that predispose this patient population to specific injury patterns that are well depicted by CT and MR imaging. Contra coup type lesions and varied presentation of subdural hematomas are more prevalent in the elderly, in whom a higher frequency of co-morbidities and anticoagulation contribute to a more rapid progression and severe manifestations of primary and secondary traumatic brain events, including cerebral herniation syndromes and ischemic complications. Likewise, the altered biomechanics associated with spinal lesions that are more prevalent in the elderly such as degenerative spondyloarthropathy, ankylosing spondylitis and central canal stenosis, contribute to a group of injury patterns that differ from the general population, typically associated with hyperextension of the neck. Elderly patients have a higher incidence of: 1. Injuries of the proximal cervical spine as well as lesions of the craniocervical and cervicothoracic junctions, 2. Fractures that are transversely oriented with frequent extension to the posterior elements, 3. Lesions of the spinal cord resulting from alleged trivial trauma and often without obvious osseous injury, 4. Associated cranial and facial fractures, 5. Injuries at multiple levels of the spine.

Note: Scanned images are included in the proceedings. Some submitted images were reduced during editing thereby decreasing clarity. Also, refer to the Program Planner. Proceedings Content as of 3/28/2014.

O-702

5:25PM - 5:50PM

MR in Spine Trauma

Kubal, W.
University of Arizona Medical Center
Tucson, AZ

Abstract/Presentation Summary

We will consider how to most effectively image acute spinal trauma. Specifically, we will consider appropriate use of both CT and MR utilizing guidelines developed by the American College of Radiology. We will review basic anatomy and introduce the concept of stability as described by the three column model. We will discuss the potential advantages of obtaining a spinal MR. We will illustrate the CT and MR appearance of various spine injuries utilizing a case-based approach. The case material will illustrate several types of ligamentous injury. The case material will also illustrate the difficulty in predicting the extent and severity of cord injury from the bony injury as detailed by CT. The MR appearance of various cord injuries will be illustrated and the prognostic significance of these injuries will be reviewed. We will consider newer imaging techniques for the evaluation of spinal trauma which may not yet be part of the clinical mainstream. Specifically, we will consider diffusion tensor imaging in the evaluation of cord injury.

O-703

5:50PM - 6:15PM

Imaging of Spinal Trauma: Pearls and Pitfalls

Rothman, S.
TBD
Los Angeles, CA

Abstract/Presentation Summary

Over the last 25 years I have had the opportunity to review more than 15,000 patients imaging studies on people involved in litigation. These include plain films, MR and CT scans. Those imaging studies were performed for the evaluation of the traumatized patient. The ultimate issues in these cases from a radiologic standpoint were to determine the presence or absence of traumatic injury. In many of those cases radiologic reports of those films incorrectly diagnosed or suggested traumatic injury when none were present. In some cases injuries were missed which should not have been missed. This talk presents a variety of commonly misdiagnosed lesions and defines some "pearls and Pitfalls" in the assessment of the

allegedly traumatized patient. The anatomic bases for the missed diagnoses will be discussed wherever possible

Wednesday, May 21

4:45PM - 6:15PM

Room 517a

73 - GENERAL PROGRAMMING: IMAGING GENOMICS

O-704

4:45PM - 5:15PM

Genomic Imaging of Human Glioma-State of the Art: Associating Genotypes with Imaging Phenotypes

Colen, R.
MD Anderson Cancer Center
Houston, TX
O-705

5:15PM - 5:45PM

Imaging Genomics in Psychosis and Other Neuropsychiatric Diseases: The Psychiatric Genetics Consortium

Szeszko, P.
The Zucker Hillside Hospital
Glen Oaks, NY

Abstract/Presentation Summary

The field of psychiatric genetics has evolved quickly over the last several years. A growing list of replicable risk alleles for severe psychiatric disorders has emerged following many unsuccessful attempts. This progress has been facilitated by the Psychiatric Genomics Consortium (PGC), which was established to conduct meta-analyses of genome-wide genetic data for psychiatric disorders, including schizophrenia and bipolar disorder. There is considerable evidence, however, that the underlying genetics and brain pathophysiology of these disorders do not respect traditional DSM-5 diagnostic boundaries, and have substantial overlap. For example, recent data from large scale genome-wide association studies have identified more than two dozen independent loci that have attained genome-wide significant criteria for one or both disorders and the number is rapidly climbing as sample sizes increase. Based on forthcoming work of the PGC, it is anticipated that the number of loci meeting genome-wide significance for schizophrenia and bipolar disorder will exceed 100, with perhaps hundreds more soon to be discovered. Recent progress in psychiatric imaging-genetics has laid the groundwork for characterizing the structural and functional significance of these risk genes using magnetic resonance imaging. For example, imaging

Note: Scanned images are included in the proceedings. Some submitted images were reduced during editing thereby decreasing clarity. Also, refer to the Program Planner. Proceedings Content as of 3/28/2014.

associations with these disorders have been reported with putative risk single nucleotide polymorphisms in ZNF804A, DISC1, MIR137, DTNBP1 and CACNA1C among others. With the recent explosion in potential risk alleles to be discovered, there will, however, be a considerable gap in the imaging-genetics literature. Moreover, a current challenge in the field of imaging-genetics is the interrogation of circuit-based measures using multimodal imaging approaches including structural, functional and diffusion tensor imaging. Such studies will inform the molecular basis of psychotic phenomenology and have significant implications for translational psychiatry. Specifically, a critical next step in the field will be to characterize the biological implications of these risk alleles to identify biomarkers for treatment response to ultimately identify new treatment targets. Understanding how a particular polymorphism affects brain structure and/or function could further enhance treatment strategies such as dosing, the use of medications with different pharmacologic properties and neurobiological mechanisms underlying individual differences in treatment response.

0-706

5:45PM - 6:15PM

How to Conduct an Imaging Genomic Analysis: Overview of Publicly-Available Tools and Datasets

Gutman, D.
Emory University
Atlanta, GA

Abstract/Presentation Summary

With the rapidly diminishing costs of obtaining detailed genomic data, increasing interest has focused on identifying imaging based features that are associated with genetic analysis. The Cancer Genome Atlas (TCGA) in conjunction with the Cancer Imaging Archive (TCIA) provided a rich (and public) data set to begin exploring these associations. In this presentation, we will describe how to obtain and manipulate these data sets. Using Glioblastoma as an example, we will also illustrate the basic steps needed to conduct an analysis identifying gene sets that correlate with specific imaging features (e.g. extent of necrosis) as an example workflow.

Wednesday, May 21

4:45PM - 6:15PM

Room 520

74 - SOCIOECONOMIC PROGRAMMING:
QUALITY (SAM)

0-707

4:45PM - 5:15PM

Update on ACA

McClellan, M.
Engelberg Center for Health Care Reform, Brookings
Washington DC, Washington DC

0-708

5:15PM - 5:50PM

Quality Scorecard in a Multi-Specialty Group Practice:
Emphasizing the Needs of the Customer

Krecke, K.
Mayo Clinic
Rochester, MN

Abstract/Presentation Summary

Quality and safety are cornerstones of medical professionalism. We strive to improve the lives of our fellow women and men and we commit to the bedrock principle "...first, do no harm". In 1999, the Institute of Medicine (IOM) published *To Err is Human: Building a Safer Health System* (1). The report's authors estimated as many as 100,000 preventable deaths at medical centers each year caused by errors of omission, commission, communication and other sources. The IOM's 2001 publication *Crossing the Quality Chasm* identified the six aims of safety, effectiveness, patient-centeredness, timeliness, efficiency, and equity (2). We need to accelerate the industry's steady evolution from skilled independent craftspeople to deeply connected interdependent team members with a common vision and systems smarts. Twenty-first century quality and safety will be built on standardization, process improvement, and evidence-based, patient-centered care (3). Rugged individualism among health care providers is not necessarily a virtue. This fall, RSNA 2014, will mark the tenth anniversary of the Sun Valley Group. The primary purpose of this think-tank was to develop a forum to "share quality improvement experiences, consider a strategy for promoting quality improvement initiatives within the radiology community, and begin efforts for benchmarking quality data.....Without timely action, our specialty runs the risk of the government and payers dictating quality metrics and defining what represents a quality radiology practice" (4). Mayo Clinic Radiology's activities spring from this group's vision. Our first pass at quality was creating a concise process map that focused on our primary customers and Radiology Department roles and responsibilities (5). Desire to understand physical flow of patients, and information flow to providers, led to process metrics reflecting our perception of value to those customers. We have successfully measured and improved access times, wait times, standard imaging protocols, performance outcomes, patient satisfaction, templated reports, and report

Note: Scanned images are included in the proceedings. Some submitted images were reduced during editing thereby decreasing clarity. Also, refer to the Program Planner. Proceedings Content as of 3/28/2014.

finalization times. We have struggled to assess and improve appropriateness and global outcomes, in part because these items have significant components that begin or end well outside the walls of the department. Collection and display of data points and trends has value in assessing the stability of our workflow and our baseline efficiencies. Over time we will continue to improve our median values, narrow the outliers, and create flags of eroding processes. Obsession with errors and mistakes is a critical trait of high reliability organizations. Equally critical is the principle of process flaws leading to human errors. Admonishing our colleagues to try harder is a limited-value strategy. Fixing process flaws that lead humans into ambiguous situations requiring rework, work-arounds or guessing is the target. Our error data comes from two sources. The first is the institution's Sentinel Event reporting process. Secondly, the department has its own Safety Event Reporting Form (SERF) which relies on frontline staffs to document errors, near-misses and "good catches" revealing process vulnerabilities below the threshold of Sentinel Events. I will share information on several years of Sentinel Event and SERF experience. We cherish the engagement of our front line staffs and the growth in SERF reporting is emblematic of high engagement and our no-blame culture of event/opportunity analysis (6). A Culture of Safety is necessary to improve immediate and future patient care. Each individual, irrespective of role, MUST feel empowered and obliged to flag a situation placing the patient or team at risk (7). Metrics are not answers. Measures can become lazy and tired if not viewed and reviewed with healthy skepticism and wide perspective. While it is true that one manages what one measures, it is equally true that one gets what one measures - frequently leading to unintended imbalance or "gaming". Quality and safety metrics are highly useful to counterbalance productivity and pure process efficiency metrics. The voice of the customer needs to be heard above the hum of the shop floor. We are in the infancy of process-oriented quality improvement in medicine. Patients and families are not sheets of steel to be molded or widgets to be shipped. Manufacturing deals little with the ill-defined pedigree and psychosocial aspects of its raw materials or the once- and twice-removed payment for goods delivered. Patient, family, provider, gatekeeper and government make each health care situation unique but it is equally evident that medical knowledge allied with process science makes our patients safer and our contributions more efficacious.

5:50PM - 6:15PM

Questions and Answers

Wednesday, May 21
4:45PM - 6:15PM
Room 524

**75 - CSI: MONTREAL PROGRAMMING:
BASIC INFORMATICS**

O-709

4:45PM - 5:15PM

Basic Informatics for the Neuroradiologist

Quigley, E.
University of Utah
Salt Lake City, UT

Abstract/Presentation Summary

"An introduction to informatics: How Neuroradiologists interact with Patients, Information, and Information Systems to deliver health care."

O-710

5:15PM - 5:45PM

Value Added Medicine: Implementing Appropriateness Criteria and Imaging Decision Making in an Electronic Environment

Phillips, C.
Weill Med. College Of Cornell/NY Presby'n
New York, NY

Abstract/Presentation Summary

The current reimbursement environment is reasonably entitled "hostile". More than ever, it is falling to the radiologist to insure billable indications for studies that are ordered by our clinical colleagues. The weight of responsibility for obtaining pre-authorization or pre-certification for the studies we perform has fallen to us. Clearly, it is too late to find that a study is not appropriate or reimbursable after the exam has been performed. Currently, there are a number of techniques to assist the ordering physician regarding indications for "high tech" imaging exams. Order-entry decision support has become a buzz word for clinical organizations to improve diagnostic algorithms and also to insure a reimbursable indication for an exam. It can also be very important for the radiologist to have information present regarding authorization and billing when protocoling examinations. For example, if a study without contrast is the authorized examination and a study with contrast has been ordered, early communication with either an ordering physician or with the insuring organization can work through a potential reimbursement issue.

Note: Scanned images are included in the proceedings. Some submitted images were reduced during editing thereby decreasing clarity. Also, refer to the Program Planner. Proceedings Content as of 3/28/2014.

0-711

5:45PM - 6:15PM

3D Printing: Basics and Application for the
Neuroradiologist

Javan, R.
Duke University
Durham, NC

Abstract/Presentation Summary

3D Printing: Basics and Application for the
Neuroradiologist Ramin Javan, MD 1. Introduction • What is 3D printing? • Why all the hype? • Connecting the dots as radiologists... 2. Rapid Prototyping Techniques • Stereolithography • Fused deposition modeling • Polyjet technology • Laser sintering • 3D printing technology • 3D bio-printing 3. 3D reconstruction and CAD software • 3D mesh (STL file format) • Open source software • Commercial software 4. Postprocessing and digital optimization • 'Manifoldness' of meshes • Creating hollow objects • Minimum wall thickness • Polygon count reduction • Skull stripping • Optimal CT algorithm (bone vs soft tissue) and window/level • Creating mechanical or fitting parts • Creating multi-color models 5. Materials and Cost • Polyamide • Multicolor • Rubber-like • Resin • Metals 6. Buying 3D printers vs commercial on-demand services • Cost • Troubleshooting • Materials 7. Practical Applications in Neuroradiology a) Educational i. Anatomic (Base of skull anatomy with cranial nerves, Pterygopalatine fossa and contents, Fiber tractography, Circle of Willis, Brain surface for gyral and sulcal anatomy in fMRI, Neck anatomic divisions) ii. Interventional phantom (Lumbar spine for CT-guided pain management interventions, Neck phantom for CT- and US-guided procedures consisting of cervical spine vertebrae, spinal cord with nerve roots, neck vessels, airway, thyroid and skin mold) iii. Surgical and interventional phantoms (Base of skull disposable surgical models, Cerebral aneurysm with hollow vessels) b) Clinical i. Surgical planning and interdisciplinary consulting (Craniosynostosis repair, Scoliosis, Facial plastic reconstruction, Conjoined twins, Practicing complicated surgeries beforehand e.g. facial vascular malformations) ii. Patient and parental counseling and consenting (Dermatome distribution for symptomatology of radiculopathy, Craniosynostosis) iii. Intraoperative drill guides (Craniotomy, Spinal fusion) iv. Implants (Cranioplasty, zygomoplasty, post-traumatic mandibular reconstruction) c) Research and Quality Control i. Fluid dynamics in vessels ii. Imaging phantoms iii. Efficacy of custom 3D printed educational models

Thursday, May 22
7:00AM - 8:30AM
Room 517d

77 - MINI SYMPOSIUM ACUTE STROKE
IMAGING: PART I: WHAT IMAGING SHOULD
WE BE DOING?

0-714

7:00AM - 7:15AM

The MGH Algorithm and Experience for Acute Stroke
Imaging?

Gonzalez, R.
Massachusetts General Hospital
Boston, MA

Abstract/Presentation Summary

The MGH Stroke Imaging Algorithm is a high-precision medical tool for patients with major anterior circulation acute ischemic strokes. It is an experience and evidence-based clinical triage tool that uses advanced imaging to identify INDIVIDUAL patients most likely to benefit from endovascular stroke therapy. It was based on over a decade of using advanced imaging (CT, CTA, CT perfusion, DWI, MR perfusion) in acute stroke patients and a critical review of the literature. The key questions and optimal imaging to answer them include: 1. Is there a hemorrhage? Noncontrast CT 2. Is there an occlusion of the distal ICA and/or proximal MCA? CTA 3. Is irreversible brain injury below a specific threshold (e.g. <70ml)? DWI Perfusion imaging is not employed unless patients cannot undergo MRI, or they do not meet the criteria for intervention. Investigations to understand the reasons for the unsuitability of perfusion CT to substitute for DWI revealed that the most likely reason is the low signal-to-noise (SNR) ratio of CT perfusion that results in a poor contrast-to-noise (CNR) ratio in severely ischemic brain. In a comparison between DWI and CTP in over 50 consecutive patients with acute anterior circulation occlusions, the mean CNR of DWI was >4 while it was <1 for CTP derived CBF. The poor CNR results in large measurement error: using Bland-Altman analyses it was found that the 95% confidence interval was $\sim \pm 50$ ml for ischemic lesion volume measurements in individual patients. The Cleveland Clinic adopted a nearly identical algorithm and their results were recently published. They reported that after the new algorithm was adopted, there was a $\sim 50\%$ reduction in mortality and a ~ 3 -fold increase in good outcomes, despite a $\sim 50\%$ decrease in the number of procedures.

Note: Scanned images are included in the proceedings. Some submitted images were reduced during editing thereby decreasing clarity. Also, refer to the Program Planner. Proceedings Content as of 3/28/2014.

O-717

7:30AM - 7:45AM

Imaging Evidence for Acute Stroke Patients Who Are Candidates for IV Thrombolysis

Sanelli, P.
Weill Cornell Medical College
New York, NY

Abstract/Presentation Summary

Stroke is a leading cause of death and disability worldwide. Imaging plays a critical role in evaluating patients suspected of acute stroke and transient ischemic attack (TIA), especially prior to initiating treatment. Over the past few decades, major advances have occurred in stroke imaging and treatment, including Food and Drug Administration (FDA) approval of recanalization therapies for treatment of acute ischemic stroke. The primary goal of imaging patients with acute stroke symptoms is to distinguish between hemorrhagic and ischemic stroke. In ischemic stroke patients, secondary goals of imaging prior to initiating revascularization interventions with intravenous (IV) thrombolysis or endovascular therapies include identification of the location and extent of intravascular clot as well as the presence and extent of "ischemic core" (irreversibly damaged tissue) and "penumbra" (hypoperfused tissue at risk for infarction). In addition, early identification of the stroke etiology or mechanism (e.g., carotid atherosclerotic disease, vascular dissection or other treatable structural causes) is critical to treatment decisions and long-term management. A wide variety of imaging techniques have become available to assess vascular lesions and brain tissue status in acute stroke patients. In addition to scientific evidence of effectiveness, important variables that influence imaging choices include constraints of time, cost, access to imaging modalities, preferences of treating physicians, availability of expertise, and availability of endovascular therapy. Thereby, it has become challenging to standardize and optimize the imaging evaluation of patients with suspected acute stroke across sites. A simple, pragmatic approach will be presented to assist in developing an optimal imaging algorithm for stroke patients at individual institution. The strength of the available evidence supporting various imaging options is presented, as well as considerations of available resources. This review and its recommendations will provide a foundation for optimizing the value of imaging in the acute stroke patient.

O-721

8:00AM - 8:15AM

Imaging Evidence for Acute Stroke Patients who are Candidates for Endovascular Revascularization

Wintermark, M.
University of Virginia
Charlottesville, VA

Abstract/Presentation Summary

In acute stroke patients who are candidates for endovascular therapy, vascular imaging (CTA, MRA, DSA) is strongly recommended during the initial imaging evaluation. Perfusion imaging may be considered to assess the target tissue "at risk" for reperfusion therapy. However, the accuracy and usefulness of perfusion imaging to identify and differentiate viable tissue have not been well established. 1. Acute large-vessel intracranial thrombus is accurately detected by CTA, MRA, and DSA. 2. Patients with large infarctions tend to have poor outcomes. The ischemic core is determined most accurately with DWI. Appropriately thresholded PCT-CBV and PCT-CBF can also be used to identify the ischemic core despite immediate reperfusion. 3. A poor collateral pattern has a high specificity for poor tissue and clinical outcome.

O-715

7:15AM - 7:21AM

SPAN-100 Predicts Vascular Imaging Profiles in Acute Ischemic Stroke

P Krishnan¹, G Saposnik², B Ovbiagele³, S Symons¹, R Aviv¹

¹University of Toronto and Sunnybrook Health Sciences Centre, Toronto, Ontario, Canada, ²St. Michael's Hospital, University of Toronto, Toronto, Ontario, Canada, ³University of South Carolina, Charleston, SC

Purpose

Stroke Prognostication using SPAN-100 facilitates stroke outcomes. We aimed to assess imaging markers associated with SPAN-100 and their additional impact on outcome determination.

Materials and Methods

Note: Scanned images are included in the proceedings. Some submitted images were reduced during editing thereby decreasing clarity. Also, refer to the Program Planner. Proceedings Content as of 3/28/2014.

Of 273 consecutive patients with acute ischemic stroke <4.5 hours, 55 were characterized as SPAN-100 positive (age + NIHSS score \geq 100). A comprehensive imaging review evaluated the differences: presence of hyperdense vessel sign, ASPECTS, clot burden score (CBS), collateral score, planimetric blood flow, volume, and transit time (CBV, CBF, MTT) volumes. The primary outcome assessed was favorable outcome (modified Rankin score; mRS \leq 2). Secondary outcomes included recanalization, lack of neurological improvement and hemorrhagic transformation (HT). Uni- and multivariate analysis assessed factors associated with favorable outcome. AUC evaluated predictors of favorable clinical outcome.

Results

Compared to SPAN-100 negative group, SPAN-100 positive patients (55/273; 20%) demonstrated larger cerebral blood volumes (CBVs) (<0.001), poorer collaterals ($p=0.0002$) and increased HT rates (56.0% versus 36%, $p=0.02$) despite earlier time to rtPA ($p=0.03$). Favorable outcome was less common among SPAN-100 positive compared to SPAN-100 negative (10.9% versus 42.2%; $p<0.0001$). Multivariate regression revealed poorer outcome for SPAN-100 [(OR) 0.17; 95% CI 0.06-0.38; $p=0.0001$], CBS [(OR) 1.14; 95% CI 1.05-1.25; $p=0.0025$] and CBV [(OR) 0.58; 95% CI 0.46-0.72; $p=0.0001$]. The addition of CBS and CBV improve the predictive value of SPAN-100 alone for a favorable outcome from 60% to 68% and 74% respectively.

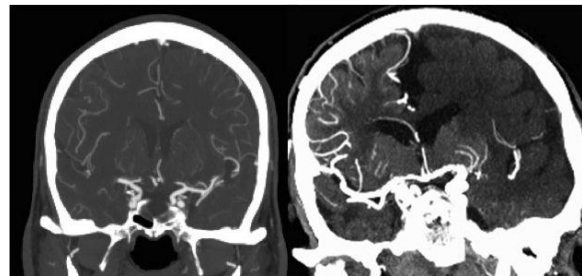
Conclusions

SPAN-100 predicts lower likelihood of favorable outcome and increased HT. Cerebral blood volume and CBS contribute to poorer outcomes among high risk patients and improve stroke outcome prediction.

KEYWORDS: Imaging Biomarker, Ischemia, Stroke

Imaging Parameters and Outcome in SPAN 100 positive and SPAN 100 negative patients			
	SPAN 100 Negative	SPAN 100 Positive	p value
Hyperdense Sign	114 (52.53)	35 (63.64)	0.1395
ASPECTS Median (IQR)	7 (6-9)	7 (5-8)	0.3969
Clot Burden score	6 (4-9)	6 (5-9)	0.2902
Collateral score	2 (2-3)	2 (1-2)	0.0002
CBVvol (median IQR)	14.7 (4.7-34.7)	34.7 (13.8-60.5)	<0.0011
CBF volume	101.6 (55.3-133.1)	98.2(74.6-129.5)	0.7503
MTT volume	104.5 (58.5-133.4)	98.4 (74.7-130.5)	0.6903
Outcome			
Recanalization	119 (55.35)	33 (61.1)	0.4451
mRS (at follow-up)	3 (1-4)	5 (4-6)	0.0001

Imaging Parameters and Outcome in SPAN 100 positive and SPAN 100 negative patients			
	SPAN 100 Negative	SPAN 100 Positive	p value
MRS \leq 2	92 (42.2)	6 (10.9)	<.0001
NIHSS improve > 3 24hrs	101 (46.3)	27 (49)	0.7139
Hemorrhagic transform'n	78 (38.6)	28 (56.0)	0.0258
Hemorrhage Infarct	64 (29.4)	23 (41.8)	0.0764
Parenchymal Hemorrhage	26 (11.9)	9 (16.4)	0.3791



0-716

7:21AM - 7:27AM

A Six Minute MRI Protocol for Evaluation of Acute Ischemic Stroke: Pushing the Boundaries

K Nael¹, R Khan¹, G Choudhary¹, A Meshksar¹, K Drake¹, J Tay¹, C Kidwell¹, B Coull¹

¹University of Arizona, Tucson, AZ

Purpose

Multimodal cerebrovascular computed tomography (CT) and MR imaging (MRI) now can provide information about tissue viability, site of occlusion, and collateral status in patients with acute ischemic stroke (AIS). If MRI is to compete with CT for evaluation of AIS, there is need for further improvements in acquisition speed. The purpose of this study was to establish the feasibility of a fast MR protocol with a six-minute acquisition time for evaluation of AIS.

Materials and Methods

The inclusion criteria for this prospective study were patients with suspicion of AIS and absence of MRI contraindications. A combination of echo-planar imaging (EPI) and parallel acquisition technique was used on a 3 T MR scanner (Skyra, Siemens) to accelerate the acquisition time. The imaging protocol included: diffusion-weighted imaging (DWI) (TR/TE 4600/65 ms, 1 min acquisition),

Note: Scanned images are included in the proceedings. Some submitted images were reduced during editing thereby decreasing clarity. Also, refer to the Program Planner. Proceedings Content as of 3/28/2014.

EPI-FLAIR1 (TR/TE/TI: 10000/88/2500 ms, 52 sec acquisition), EPI-GRE (TR/TE: 1860/48 ms, 50 sec acquisition), contrast-enhanced MR angiography (CE-MRA) of the entire supra-aortic arteries (TR/TE: 3.4/1.2 ms, 20 sec acquisition), and dynamic susceptibility contrast (DSC) perfusion (TR/TE: 1450/22 ms, 120 sec acquisition). Using a modified 2-phase contrast injection scheme, high spatial resolution CE-MRA of the supra-aortic arteries and DSC perfusion were accomplished without the need for additional contrast (2). Image analysis was performed independently by two neuroradiologists and interobserver agreement was calculated using Kappa test.

Results

A total of 50 patients (29 M, age 42-91 years old) met our inclusion criteria. The NIH stroke scale ranged from 4-19. Diagnostic image quality was achieved in 100% of DWI, 97% EPI-FLAIR, 98% EPI-GRE, 90% neck MRA and 96% of brain MRA, and 94% of DSC perfusions. Thirty-six patients (72%) had acute infarction. Using Tmax perfusion maps and applying DEFUSE criteria, 36% of patients had perfusion-diffusion mismatch with interobserver agreement of $k=0.90$. The mean of the signal-intensity-ratio values of the DWI lesion on EPI-FLAIR was 1.12 for patients with time of onset to MR imaging of < 4.5 hours and 1.40 for patients with time of onset to MR imaging of > 4.5 hours concordant with prior reports (1). Three patients had intracranial hemorrhage detected on noncontrast CT confirmed by EPI-GRE. In addition, five microhemorrhages were detected by EPI-GRE that were undetected by CT. Contrast-enhanced MRA showed 12 segmental stenoses of the extracranial arteries and 19 segmental stenoses of the intracranial arteries with interobserver agreement of $k=0.84$ and 0.78 respectively.

Conclusions

Described multimodal MR protocol is feasible for evaluation of patients with AIS and can result in significant reduction in scan time rivaling of the multimodal CT protocol.

KEYWORDS: Echo Planar Imaging, MR Imaging Brain, Stroke

0-718

7:45AM - 7:51AM

The Role of Imaging in Clinical Stroke Scales that Predict Functional Outcome.

F Soliman1, A Gupta1, H Kamel1, A Pandya1

1New York Presbyterian Hospital, Weill Cornell Medical College, New York, NY

Purpose

Numerous stroke scales have been developed to predict functional outcome following acute ischemic stroke. Such prediction models have the potential to contribute prognostic information in both the clinical and research settings. The complexity of these models varies, with the simplest including solely a scale of stroke severity [National Institutes of Health Stroke Scale (NIHSS)] and others including a combination of factors related to stroke severity, demographics, clinical presentation and medical history, and/or neuroimaging. The goal of this study was to compare the numerous prognostic stroke models, both with and without imaging, to determine whether imaging should play a role in predicting functional outcome status.

Materials and Methods

A comprehensive systematic literature search was performed to identify stroke prognosis scoring systems using multiple reference databases including PubMed. We included studies which describe stroke prognosis models or scoring systems that incorporate baseline patient stroke clinical data on presentation to predict functional outcome. Risk scores for transient ischemic attacks and specific risk scores for stroke risk in atrial fibrillation were excluded. Those models which included neuroimaging data as a predictor of prognosis were identified separately. Scores were evaluated based on area under the receiver operator characteristic (ROC) curve and statistical significance of neuroimaging predictors.

Results

Our initial search in PubMed yielded over 5000 articles. After manually searching the titles and abstracts of these references, we identified 26 risk scores that were derived from stroke cohorts to predict functional outcome and mortality; 14 of these included CT or MRI imaging results along with clinical variables as predictors and three were dedicated imaging scales. Specific neuroimaging variables used in stroke prognosis scales included lesion volume on diffusion-weighted imaging (DWI) or computed tomography (CT), CT hypodensity, and presence of arterial occlusion on MR angiography (MRA) or CT angiography (CTA). Neuroimaging variables were statistically significant predictors in 10 out of the 17 scores that evaluated these parameters. AUC results ranged from (0.72-0.90), mean 0.84 and (0.68-0.90), mean 0.81 for scores that did and did not include neuroimaging predictors, respectively, with no difference between the groups ($p<0.16$).

Conclusions

The stroke models that incorporate neuroimaging predictors demonstrate mixed results in terms of their utility in outcome prediction, while many scales without imaging are equally or more effective. Despite previous evidence that neuroimaging improves stroke prediction after transient ischemic attack, it is unclear whether imaging-based scores should be favored over simpler approaches for predicting post-stroke function.

Note: Scanned images are included in the proceedings. Some submitted images were reduced during editing thereby decreasing clarity. Also, refer to the Program Planner. Proceedings Content as of 3/28/2014.

KEYWORDS: Outcome, Stroke

O-719

7:51AM - 8:57AM

Admission Insular Infarction >50% Identifies Acute Stroke Patients Most Likely to Clinically Benefit from Robust Reperfusion

R Hu1, S Kamalian1, S Kamalian1, G Harris1, S Aneesh1, P Schaefer1, F Karen1, R Gonzalez1, O Wu1, M Lev1

1Massachusetts General Hospital, Boston, MA

Purpose

The goal of our prospective, multi-center, Specialized Programs of Translational Research in Acute Stroke (SPOTRIAS) project has been to determine reliable, practical, imaging markers to help select patients for advanced stroke therapies. Although large admission diffusion-weighted imaging (DWI) (>70 ml) is an established marker for treatment exclusion (i.e., "risk"), no validated markers exist to identify patients likely to deteriorate absent early, robust reperfusion (i.e., "benefit"). We previously have shown that admission percent insular infarction in proximal anterior-circulation occlusive stroke patients correlates with both (i) infarct growth into "at-risk" penumbra, and (ii) poor clinical outcome. Our goal was to establish - in a more generalized cohort - the value of percent admission insular infarction as a marker of the potential benefit from reperfusion.

Materials and Methods

We studied 65 consecutive acute MCA territory stroke patients who received both CTP/DWI within 9 hours of onset and follow-up perfusion imaging (CTP/MRP) within 30 hours. Reperfusion was defined as >90% improvement in admission DWI-MTT mismatch volume; 14 patients without mismatch were excluded. Percent insula infarction was rated as > or < 50% on admission DWI. Images were rated by consensus of two independent readers. Clinical outcome was determined by 90-day modified Rankin score (mRS) and clinical worsening as the change between pre-admission (all mRS<2) and 90-day mRS (delta-mRS).

Results

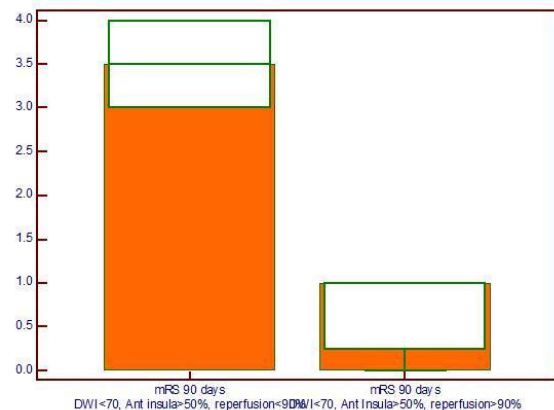
With respect to absolute clinical outcome (final mRS), the 23 patients with admission insula infarction >50% had significantly better outcomes with reperfusion (n=3/23, median mRS=1) versus without reperfusion (n=20/23, median mRS=3.5, p=0.005). Of the 28 patients with admission insula-infarction <50%, there was not a significant difference in outcome between patients with (n=13/28, median mRS=1) versus those without (n=15/28, median mRS=2, p=0.097) reperfusion. With respect to

delta-mRS from a pre-admission baseline as the outcome measure, the results were similar (p=0.01 for the reperfusion group and p=0.16 for the nonreperfusion group). In the subgroup with admission DWI volume <70 ml, there was similarly a significantly better outcome with versus without reperfusion for insular infarction >50% patients (median 3 versus 1, respectively, p = 0.02), but not in insular infarction <50% patients (median 2 versus 1, p = 0.10). Using a threshold of anterior insula infarction < or > 50%, the difference between 90-day clinical outcome in patients with compared to without reperfusion also was highly significant (median 3.5 versus 1, p=0.03).

Conclusions

For patients with acute MCA territory acute stroke, the percentage of insula infarcted at admission strongly correlates with the likelihood of clinical worsening and poor outcome in the absence of reperfusion. When assessing the risks-versus-benefits of IV and/or IA thrombolytic treatments (i.e., those with DWI<70 ml), patients with large insular infarctions at presentation (>50% insula) are likely to derive the greatest benefit from robust reperfusion.

KEYWORDS: Insula, Penumbra, Stroke



O-720

8:57AM - 8:03AM

FLAIR Vascular Hyperintensities in Acute Ischemic Stroke: a Surrogate Marker of PWI-DWI mismatch?

L Legrand1, M Tisserand2, G Turc1, W Ben Hassen1, O Naggara1, M Edjlali1, C Mellerio1, J Baron3, J Mas1, J Meder1, C Oppenheim4

1Centre Hospitalier Sainte-Anne, Paris, France, 2Sainte-Anne Hospital, Paris, France, 3Neurology, Paris, France,

Note: Scanned images are included in the proceedings. Some submitted images were reduced during editing thereby decreasing clarity. Also, refer to the Program Planner. Proceedings Content as of 3/28/2014.

4CH Sainte-Anne, Université Paris Descartes, INSERM U894, Paris, France

Purpose

FLAIR vascular hyperintensities (FVH) are defined as linear or serpentine hyperintensities corresponding to typical arterial courses (1). They frequently are encountered in acute ischemic stroke (AIS) (2) and are related to slow retrograde flow in leptomeningeal collaterals (3). Our goal was to evaluate the usefulness of FVH beyond the boundaries of the diffusion-weighted imaging (DWI) lesion (FVH-DWI mismatch) and its ability to predict perfusion-weighted imaging (PWI)-DWI mismatch in AIS before thrombolysis.

Materials and Methods

Two independent observers retrospectively analyzed 141 consecutive AIS patients with a proximal middle cerebral artery (MCA) occlusion who had MR imaging (MRI) before and after iv thrombolysis. They evaluated the presence of FVH-DWI mismatch, i.e., FVH on FLAIR seen beyond the DWI lesion on MRI before treatment. Pre- and post-treatment characteristics were compared between patients with or without FVH-DWI mismatch in univariate analyses. The association between FVH-DWI mismatch and PWI-DWI mismatch, examined as a continuous or a categorical variable ($PWI_{vol} > 1.8 \times DWI_{vol}$, $T_{max} > 6s$), was studied.

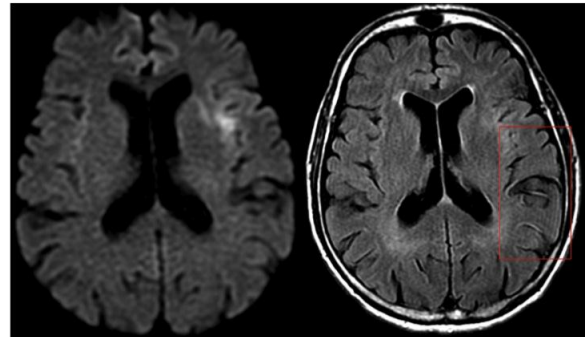
Results

All patients had FVH next to the insular region. The interobserver reliability for FVH-DWI mismatch was excellent ($\kappa=0.91$). Patients with FVH-DWI mismatch (72% of patients) had smaller initial infarcts and larger infarct growth ($p < 0.001$) than those without FVH-DWI mismatch, even though their final infarcts remained smaller ($p < 0.001$). FVH-DWI mismatch detected PWI-DWI mismatch with a sensitivity of 92% (CI95%: 85-99%) and a specificity of 64% (CI95%: 47-80%). The positive and negative predictive values were 82% and 81%, respectively.

Conclusions

Flair vascular hyperintensities are consistently present within the first 4.5 hours after proximal MCA occlusion. The FVH-DWI mismatch, i.e., presence of FVH beyond the infarct's boundaries, could be used as a surrogate marker of PWI-DWI mismatch and help identify tissue at risk before treatment decision, when PWI is missing.

KEYWORDS: Fluid-Attenuated Inversion Recovery, Mismatch, Stroke



O-722

8:21AM - 8:27AM

Role of Arterial Tissue Delay derived from Bayesian Probabilistic Method to Predict Recanalization in Patients with Acute Stroke: A comparison with Normalized Collateral Flow Index

A Meshksar¹, G Choudhary², R Khan², J Becker¹, W Kubal², K Nael²

¹University of Arizona Medical Center, Tucson, AZ,
²University of Arizona, Tucson, AZ

Purpose

The normalized collateral circulation index (nCCI) derived from DSC-time to maximum (T_{max}) recently has been proposed to determine the status of collateral flow in patients with acute stroke and a predictive measure of recanalization after thrombolysis (1). Arterial tissue delay (ATD) calculated by Bayesian probabilistic method (2) can be a more accurate estimate of collateral flow and actual tissue perfusion delay in ischemic regions. In this study, we evaluate the potential role of ATD derived from Bayesian method to predict recanalization in patients with acute stroke who underwent thrombolysis and compare the result with nCCI index derived from block-circulant singular value deconvolution (cSVD).

Materials and Methods

Twenty-four patients (15 M, 9 F, mean age 66.2 years old) with acute ischemic stroke who underwent MR imaging (MRI) stroke protocol and had proximal arterial (M1) occlusion were enrolled. All patients underwent thrombolysis. Dynamic susceptibility contrast (DSC) perfusion was performed using a gradient-EPI sequence (TR/TE: 1450/22 msec) after iv injection of 0.1 mmol/kg of gadolinium contrast. Using a FDA approved software (Olea Medical, La Ciotat, France), all prethrombolysis DSC

Note: Scanned images are included in the proceedings. Some submitted images were reduced during editing thereby decreasing clarity. Also, refer to the Program Planner. Proceedings Content as of 3/28/2014.

scans were processed with cSVD and Bayesian probabilistic method. The nCCI was calculated from cSVD derived Tmax using previously reported method (1). Volume of tissue with severe ATD (>6 sec) also was calculated from Bayesian derived ATD maps. Data were compared and analyzed by unpaired t-test.

Results

Seventeen patients (70%) had successful recanalization after thrombolysis. There was only modest correlation between nCCD and volume of ATD>6s (r=0.512). There was statistically significant difference (P=0.04) between ATD volume (mean ± SD) of recanalized (50.1 ± 29.7 cc) versus nonrecanalized (28.7 ±19.4 cc) patients. There was no statistically significant difference (P= 0.86) between the nCCI of recanalized (172.8± 205) and nonrecanalized patients (188.3 ± 139).

Conclusions

In comparison to the nCCI index, the ATD >6s volume is more accurate and a better predictor of recanalization after thrombolysis in patients with acute ischemic stroke.

KEYWORDS: Actue Stroke, Deconvolution, Dynamic Susceptibility Contrast-Enhanced

O-723

8:15AM - 8:21AM

Flow weighted and volume weighted collateral vessel signal in MR-angiography independently predicts efficacy of reperfusion in acute proximal occlusive anterior circulation stroke

M Ernst1, L Brehmer1, N Forkert1, G Thomalla2, J Fiehler1, A Kemmling3

1Department of Diagnostic and Interventional Neuroradiology, Hamburg, Germany, 2Neurology, Hamburg, Germany, 3University Medical Center Hamburg-Eppendorf, Hamburg, Germany

Purpose

In proximal anterior circulation occlusive strokes collateral flow is essential for good outcome. Vessel intensity in time of flight (TOF) and contrast-enhanced (CE) MR angiography (MRA) is variable due to acquisition method. The purpose was to quantify collateral supply including both, flow-weighted signal from TOF-MRA and volume-weighted signal from CE-MRA, and determine each predictive contribution to tissue outcome.

Materials and Methods

Consecutively (2009 to 2013), 44 stroke patients with acute proximal anterior circulation occlusion met inclusion

criteria with available TOF- and CE-MRA and penumbral imaging. Collateralized vessels were separately measured in TOF- and CE-MRA employing two methods: 1) a visual 3-point collateral score (CS) to rate the relative abundance of MCA vascularity in the ischemic hemisphere. 2) a rater-independent automated atlas based collateral index (CI) to quantify the relative collateral signal intensity in the ischemic hemisphere. Collateral measures were tested by receiver operating characteristic (ROC) curve and multivariate analysis against good outcome based on final infarct volume (FIV) and percentage of penumbra saved (PPS).

Results

Visual CE-MRA CS were significantly negatively correlated with FIV (Spearman's rho= -0.44, P<0.003) but not PPS. Visual TOF CS did not correlate significantly with each tissue outcome parameters. For good FIV (< 90 mL), the overall independently best discriminator was CICHEMRA (AUC 0.94). For effective reperfusion (PPS >50%) both, CITOF and CICHEMRA, were independent contributors and CI combined was the best overall discriminator (AUC 0.89, P<0.001).

Conclusions

Visual collateral assessment by CE- but not TOF-MRA is useful for discriminating good infarct outcome in patients with proximal occlusive strokes. Our study suggests an independent predictive utility for penumbral reperfusion using combined flow-weighted vessel signal from TOF-MRA and volume-weighted signal from CE-MRA for collateral assessment.

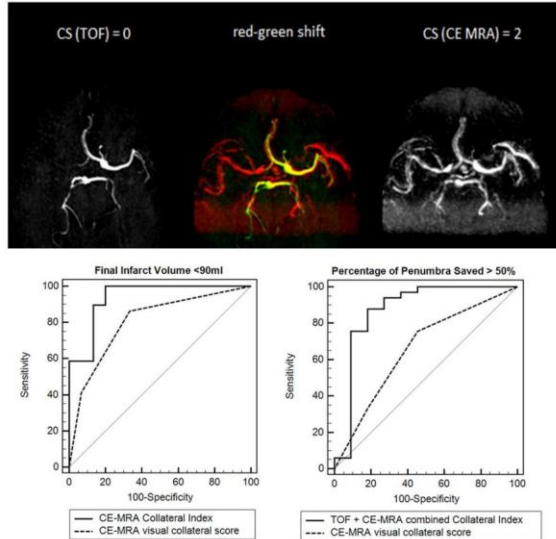
KEYWORDS: Collateral Circulation, MR Imaging/MR Angiography, Stroke

Table 3 ROC curve analysis of visual and automated collateral measured for discriminating good tissue outcome (FIV <90ml and PPS >50%)

Collateral measure	Final Infarct <90ml		P	Penumbra saved >50		P
	AUC (±SD)	Optima I criterion Youden index		AUC (±SD)	Optima I criterion Youden index	
Visual scoring (CS)						
CE-MRA	0,81(0,07)	>= 1 0,53	< 0,01	0,67(0,10)	> 1 0,27	0,04
TOF	0,53(0,02)	>= 1 0,07	0,15	0,53(0,05)	>= 1 0,09	0,52
TOF + CE-MRA	0,81(0,07)	>= 1 0,53	< 0,01	0,65(0,10)	>= 1 0,30	0,16
Atlas based collateral index (CI)						
CE-MRA	0,94(0,04)	> 0,62 0,80	< 0,01	0,83(0,10)	> 0,64 0,70	< 0,01
TOF	0,74(0,08)	> 0,37 0,43	0,01	0,86(0,06)	> 0,41 0,64	< 0,01
TOF + CE-MRA	0,95(0,03)	> 1,13 0,80	< 0,01	0,89(0,08)	> 1,51 0,76	< 0,01

Note: Scanned images are included in the proceedings. Some submitted images were reduced during editing thereby decreasing clarity. Also, refer to the Program Planner. Proceedings Content as of 3/28/2014.

AUC, Area under the ROC curve shown with associated significance level P. Optimal criterion defines collateral parameter cut off for maximized sensitivity and specificity by Youden index.



Thursday, May 22
7:30AM - 8:30AM
Room 517bc

76 - SPINE SESSION (SAM)

0-712

7:30AM - 7:50AM

Pediatric Spine

Schwartz, E.
Children's Hosp. Of Philadelphia
Philadelphia, PA

Abstract/Presentation Summary

The phrase "children are not just small adults" is commonly used in pediatric neuroimaging, and is equally applicable in the spine as in the brain. There are numerous spinal pathologies that are seen nearly exclusively in the pediatric population or have different imaging appearances and presentations when affecting children. These include congenital spinal anomalies (spinal dysraphism), certain neoplastic processes, and conditions such as Langerhan cell histiocytosis. Prenatal magnetic resonance imaging (MRI) is increasingly being used to evaluate spinal anomalies in utero. Conditions such as the myelomeningocele and lipomyelomeningocele have imaging features that usually allow for their differentiation,

as well as differentiating between these and other forms of spinal dysraphism. Patterns of traumatic injury in the spines of children are frequently different than those seen in adults, particularly cervical spine injuries. Understanding these patterns and their typical imaging features should result in an increase in physician comfort when interpreting these neuroimaging studies, and an increase in accuracy of diagnoses.

0-713

7:50AM - 8:10AM

Adult Spine

Malhotra, A.
Yale University School of Medicine
New Haven, CT

Abstract/Presentation Summary

Cauda equina syndrome (CES) refers to a typical set of neuromuscular and urogenital symptoms that result from the simultaneous involvement of multiple lumbosacral nerve roots below the level of the conus medullaris. These symptoms include low back pain, sciatica (unilateral or, usually, bilateral), saddle sensory disturbances, bladder and bowel dysfunction, and variable lower extremity motor and sensory loss. Imaging often plays a critical role in evaluation and management of these patients. CES mainly affects middle aged individuals, particularly men in their forties and fifties. Although disc herniation and canal stenosis are the most frequent causes, the conus and the cauda equina nerve roots can be involved by a range of pathologies, including vascular, neoplastic, infective and inflammatory. Presentation can be acute or chronic. Although the cauda equina lesions involve nerve roots and represent a "peripheral" nerve injury, damage may be irreversible and cauda equina syndrome may be a surgical emergency. Optimization of imaging is important for diagnosis of lesions affecting the conus and cauda equina nerve roots. Delayed or incorrect diagnosis can have significant medicolegal implications.

8:10AM - 8:30AM

Questions and Answers

Note: Scanned images are included in the proceedings. Some submitted images were reduced during editing thereby decreasing clarity. Also, refer to the Program Planner. Proceedings Content as of 3/28/2014.

Thursday, May 22
8:30AM - 10:00AM
Room 517b

78 - ASSR PROGRAMMING

O-724

8:30AM - 8:50AM

Understanding Spine Care: Clinical Visit to Imaging to Surgery to Controversy, and Health Care Policy

Cho, C.
Brigham & Womans Hospital
Boston, MA

Abstract/Presentation Summary

As medicine moves from treatment of patient illness to management of health, it becomes imperative for physicians to understand the driving forces that ultimately dictate the way we practice. Radiologists must recognize the changes happening in many parts of the country, such as CMS lead Accountable care organizations through share savings, and innovative global payment strategies pushed by private payers. This transformation points to a direction of understanding the entire care spectrum through collaboration, and in this case, spine care. Using one common disease, degenerative disc disease, this presentation reviews the limitations of medical treatment, restrictions on imaging, surgical approaches, and controversy in the surgical arena. The hope of this presentation is to stimulate the radiology audience to recognize the wave of care redesign, and the need to understand the entire treatment spectrum. Learning Points
1. ACO concept 2. Global payment of 2014 3. Initiatives from hospital networks on healthcare change 4. Non-surgical treatment process for degenerative disc disease 5. Imaging limitations by regulations 6. Surgical treatment options and approach 7. Controversy in surgical arena

O-725

8:50AM - 9:10AM

Leading Edge for Bone Augmentation

Muto, M.
AORN Cardarelli Hosp.
Naples

Abstract/Presentation Summary

Vertebral augmentation is a percutaneous treatment in which a synthetic material (poly-methyl-metacrylate-PMMA) is injected in a vertebral body that has wide the applications in the last 10 years having been used not only for the typical vertebral porotic fracture but also for the

treatment of primary and secondary spine tumors and vertebral trauma. Vertebral porotic compression fracture still represent the major indications to vertebral augmentation and usually it is performed in case of porotic fracture refractory to medical therapy 6-8 weeks after the onset of acute spine pain. MR is the method of choice to diagnose bone marrow edema that is the most important imaging finding to decide to treat or not to treat the patient. Usually 2/3 of patients show a clinical improvement and recover within 6-8 weeks after the onset of clinical symptomatology, so statistically 1/3 of the patients with porotic vertebral fractures can be potentially treated with vertebral augmentation. The standard medical therapy includes analgesic, orthosis devices, CA and Vit D plus bisphosphonates and for this reason it is always very important to cooperate with a bone metabolic center to prescribe the best medical therapy is possible to patients. Many papers are published in the literature showing not many differences in terms of clinical results between vertebral cementoplasty performed with only cement injection (vertebroplasty -VP) or if the treatment is preceded by the creation of a cavity with a balloon or any type of metallic implant (assisted techniques- AT). The biomechanic target to reduce kyphotic deformity is certainly obtained more frequently with AT compared to simple VP but this does not mean a gain in terms of clinical results that is usually good in 85-90% of the treated patients with both systems. The common question performing VP or AT is if there is an increased risk of new fractures to adjacent or distant metamer related to the stiffness of the injected material compared to normal bone. Theoretically this stiffness could represent a problem but in practice statistically there are no major changes in terms of new fractures to new metamer in patients with porotic fracture treated or not treated with a previous vertebral cementoplasty. We know in fact by the natural history of patients with vertebral porotic fracture, the risk of new fractures in the year following a previous one is 20% higher than patients without porotic fracture and this risk does not increase after VP or AT. In the last years it has been shown it is useful to perform a preventive VP to the superior and inferior vertebral body to reduce the incidence of new fracture in case of osteoporotic fractures. In case of multiple fractures in patients with long history of steroid assumption for collagenopathies, or Chron's disease or patients in chronic treatment for epilepsy it is possible to perform one session vertebroplasty up to 10 levels in neuroleptoanalgesia. It is always important to perform those treatments with the best technologies available such as angio suite or CT-Fluoro guidance. Vertebral hemangioma is a common finding performing MR examination but only the aggressive type with vascular epidural component and the symptomatic hemangioma needs to be treated with VP that also reaches a stabilization of the metamer with antalgic effects. In those cases VP is the treatment of choice obtaining a venous embolization with arterial vascular deafferentation and reducing the vascular epidural compression. There is no indication for AT in spine hemangioma. Aneurysmal bone cyst (ABC) is a rare benign spine tumor causing pain and less stability

Note: Scanned images are included in the proceedings. Some submitted images were reduced during editing thereby decreasing clarity. Also, refer to the Program Planner. Proceedings Content as of 3/28/2014.

that has been treated in the past in many ways causing potential spinal cord damage with acute clinical onset. Surgical, endovascular and percutaneous treatment with glue can be performed. Now it is also available a new treatment with osteoconductive material that has the properties to rebuilt normal bone with normal stiffness and embolizing properties. Another common application of vertebral augmentation are spine metastasis. We cannot apply the same concept of traumatic spine instability to oncological spine instability. Oncological Spinal Instability is poorly defined in the literature and presently there is a lack of guidelines available to aid in defining the degree of spinal instability in the setting of neoplastic spinal disease. The concept of oncological spinal instability remains important in the clinical decision-making process for patients with spine tumors. The Spine Oncologic Study Group (SOSG) has defined it as the loss of spinal integrity associated with pain related to movement, symptomatic deformity, and progressive neurological deficit under physiological load. Malignant primary tumors or metastases can disrupt the normal biomechanics of the spine via bone destruction or deformity resulting in a decrease in its load-bearing capacity. The loadbearing capacity is determined by a number of factors, including tumor size as well as cross-sectional area of the intact body and its bone mineral density. Krishaney has divided the vertebral body in 27 Similar cubes. When the destruction of all the cubes within 1/3 of the axial soma occurs, it creates an instability due to a deficit of the anterior and middle column. In case of sagittal destruction only, the spinal stability is maintained and not altered. The location of the tumor (and hence bone destruction) within the vertebral body may also play a role in the patient's risk of fracture and instability. There is a distinct discrepancy between the thoracic and thoracolumbar or lumbar spine and spinal oncological instability. In fact, according to Taneichi, the most important risk factor of fracture of thoracic spine instability is the disruption of costo-vertebral joint and , only after, the vertebral body. The costo-vertebral joint and all thoracic muscular structure increase the stiffness and the resistance of the thoracic spine maintaining the spinal biomechanical. In fact, in thoracic level, it is demonstrated that it is necessary to have about 50-60% vertebral disruption to have pathologic vertebral fracture and instability versus 35-40% of Thoraco-Lumbar and Lumbar level. A comprehensive classification system based on patient symptoms and radiographic criteria of the spine was developed to aid in predicting spine stability of neoplastic lesions. The classification system includes: -global spinal location of the tumor, -type and presence of pain, -bone lesion quality, spinal alignment, -extent of vertebral body collapse, - posterolateral spinal element involvement. By the combinations of all these elements a score - The Spine Instability Neoplastic Score - comes out that can guide clinicians in identifying when patients with neoplastic disease of the spine may benefit from surgical treatment. A score between 0 and 6 results in spinal stability, between 7 and 12 possible instability, and between 13 and 18 results in oncological instability. The management of patients

affected by neoplastic lesions involving the spine have to respond to two major concepts: • Pain treatment • Stability treatment especially for the spinal metastasis. Certain type of vertebral spine fracture such as Magerl A1.1 type represent another good indication for vertebral augmentation avoiding orthosis devices and kyphotic deformities.

O-726

9:10AM - 9:30AM

Intra-Operative Imaging Correlates: Surgical Anatomy of Spine

Groff, M.
Brigham and Women's Hospital
Boston, MA

O-777

9:30AM - 9:50AM

Interventional Pain Management in Failed Back Surgery Syndrome

Georgy, B.
North County Radiology

-, --

Abstract/Presentation Summary

In this presentation, common interventional procedures performed on patients with failed back surgery syndrome (FBSS) will be discussed in details regarding the indications, techniques and potential complications. Procedures presented will include epidural steroid injections, selective trans-foraminal epidural injections, median branch blocks and sacroiliac joint injections. The evolving role of spinal cord stimulation will be discussed in more details.

9:50AM - 10:00AM

Discussion

Thursday, May 22
8:30AM - 10:00AM
Room 517d

79 - MINI SYMPOSIUM STROKE - PART II:
IMAGING FOR STROKE PREVENTION

Note: Scanned images are included in the proceedings. Some submitted images were reduced during editing thereby decreasing clarity. Also, refer to the Program Planner. Proceedings Content as of 3/28/2014.

O-779

8:30AM - 8:45AM

Carotid Stenosis and Plaque Imaging

Wasserman, B.
Johns Hopkins University
Baltimore, MD

O-783

9:00AM - 9:15AM

Transient Ischemic Attack

Zaharchuk, G.
Lucille Packard Children's Hosp. at Stanford
Stanford, CA

O-786

9:30AM - 9:45AM

Intracranial Artery Wall Imaging

Mandell, D.
University Health Network and the University of Toronto
Toronto, Ontario
O-780

8:45AM - 8:51AM

Plaque Component Thickness Measurements in Carotid Artery Stenosis: A Potential CTA Marker of Symptomatic Plaque

A Gupta¹, H Baradaran¹, H Kamel¹, A Pandya¹, A Mangla¹,
A Dunning¹, R Marshall², P Sanelli¹

¹Weill Cornell Medical College, New York, NY, ²Columbia University Medical Center, New York, NY

Purpose

In light of improvements in the effectiveness of nonsurgical therapy for carotid atherosclerotic disease in the past two decades, there has been renewed interest in evaluating imaging techniques for risk stratification beyond luminal stenosis severity, including direct carotid plaque imaging to evaluate for vulnerable plaque. Most of the recent carotid plaque imaging literature has been MR imaging (MRI)-based. There are several challenges, however, in the wide implementation of multisequence carotid MRI as a risk stratification tool in the clinical setting, including the need for specialized MRI coils, lengthy acquisition times, and the complexity of image interpretation. We correlated recently proposed CT markers, soft and hard plaque thickness measurements on axial CT angiography (CTA)

source images, with symptomatic disease status (ipsilateral stroke or TIA) in high-grade carotid disease.

Materials and Methods

Soft plaque and hard plaque thickness were measured by a board certified neuroradiologist with a recently validated technique using CTA source images in subjects with $\geq 70\%$ extracranial carotid artery stenosis. Figure demonstrates technique on a magnified axial CTA image (left panel) of the proximal right ICA. Asterisk represents the residual patent ICA lumen. Measurements are shown with the calipers, with the white calipers representing maximum soft plaque thickness and black calipers representing maximum hard plaque thickness measurement. The right panel demonstrates a coronal view from a curved multiplanar reconstruction in the same subject showing the patent vessel lumen (asterisk) significantly narrowed by predominantly soft plaque, as measured on axial image. We used multiple logistic regression analysis to measure the strength of association between each 1 mm increase of soft plaque thickness and symptomatic disease status while controlling for the percent degree of NASCET stenosis and any additional covariate risk factors found to be statistically significant in univariate analyses at a threshold of $p < 0.05$. In addition, receiver operating characteristic (ROC) curve analysis was performed to determine which imaging feature (maximum total plaque thickness, maximum soft plaque thickness, or maximum hard plaque thickness) had the best discrimination for symptomatic carotid disease status. Finally, to test for reliability of measurements, a second board-certified neuroradiologist blinded to the initial measurements repeated linear axial dimension measurements on a subset of 20 subjects.

Results

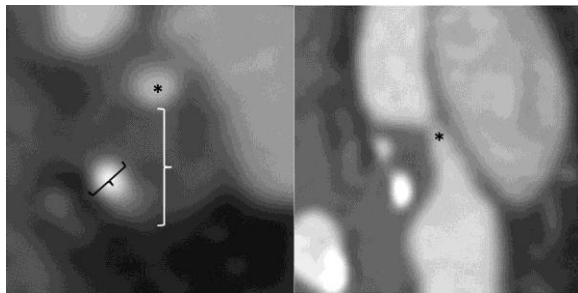
A total of 42 of 76 subjects meeting inclusion criteria had symptomatic carotid disease. Compared to asymptomatic subjects, those with symptomatic carotid disease had significantly larger soft plaque and total plaque thickness measurements and smaller hard plaque thickness measurements. For every 1 mm increase in maximum soft plaque thickness, there was approximately a 2.7 times greater likelihood (OR = 2.7) of prior ipsilateral stroke or TIA ($p < 0.0001$). Conversely, for each 1 mm increase in hard plaque thickness, there was 45% (OR = 0.55) decreased likelihood of prior ipsilateral stroke or TIA ($p = 0.007$). Soft plaque thickness measurements provided excellent discrimination between symptomatic and asymptomatic disease with ROC analysis showing an area under the curve of 0.90. A cutoff of 3.5 mm maximum soft plaque thickness provided a sensitivity of 81%, specificity of 83%, positive predictive value of 85%, and a negative predictive value of 78%. Inter-reader correlation coefficients for measurements of maximum total wall thickness, maximum soft plaque thickness, and maximum hard plaque thickness were 0.93, 0.91, and 0.88, respectively, indicating excellent inter-observer reliability.

Conclusions

Note: Scanned images are included in the proceedings. Some submitted images were reduced during editing thereby decreasing clarity. Also, refer to the Program Planner. Proceedings Content as of 3/28/2014.

Increasing maximum soft plaque thickness measurements are strongly associated with symptomatic disease status in carotid artery stenosis. Prospective validation of these results may translate into a widely accessible stroke risk stratification tool in high grade carotid artery atherosclerotic disease.

KEYWORDS: Carotid Artery, Carotid Artery Stenosis, CTA



O-781

8:51AM - 8:57AM

High-resolution 3T MR protocols for detection and quantification of the vulnerable hemorrhagic plaque

M Vargas¹, M Scheffler¹, I Barnaure-Nachbar¹, R Sztajzel¹, B Delattre¹, V Cuvinciuc¹, V Mendes-Pereira¹, K Lovblad¹

¹Geneva University Hospitals, Geneva, Switzerland

Purpose

We aimed to detect carotid hemorrhagic plaque using a black blood fat sat T1 sequence and quantify the degree of stenosis at 3 T.

Materials and Methods

The inclusion criteria was the diagnosis of symptomatic carotid plaque; 29 patients (10 women and 19 men, ages 37 - 89 years, average of 72 years) were studied on a 3 T MR Philips Ingenuity TF PET/MR Unit. The technical protocol performed comprised axial diffusion, axial EG T2 and coronal FLAIR of the brain and 3DTOF and a 3DT1 black blood sequence at the level of the carotid bifurcation. Both carotids were analyzed in each patient and the NASCET scale was used for quantification of degree of stenosis.

Results

We analyzed 58 carotid arteries at the level of the bifurcation; all of our 29 patients had plaques (right=10, left=14, both= 5). Hemorrhagic plaque appears as a localized hyperintensity on the black blood 3D T1 sequence. We detected 13 hemorrhagic plaques, and 18

patients without hemorrhagic plaque; three carotid arteries in two patients (2 right and one left) were not interpretable due to kinetic movement. The NASCET scale measurement showed: 9=40-50% stenosis, 7=between 60-65% stenosis, 3=70%, 3=80% 4=90% stenosis, 4=nonsignificant stenosis. Five patients of 13 patients with hemorrhagic plaques had brain ischemia. No statistical difference was found between the two groups (with hemorrhagic plaque and without) and the degree of stenosis (p=0.116).

Conclusions

MR imaging with black blood technique fat sat T1 is a safe, confident and noninvasive tool useful for detection and quantification of hemorrhagic vulnerable plaque. The capacity to detect hemorrhage will help in defining patients that need treatment.

KEYWORDS: Fat Suppression, MR Imaging/MR Angiography, MR Plaque Imaging



O-782

8:57AM - 9:01AM

MRI-detected Intraplaque Hemorrhage, Stenosis and Current Smoking are Essential Markers of Stroke Risk

J McNally¹, D Parker¹, M McLaughlin¹, G Treiman¹

¹University of Utah, Salt Lake City, UT

Purpose

Carotid atherosclerosis accounts for 20-30% of the >690,000 strokes occurring annually in the United States, according to the American Heart Association 2013 update. Stroke risk stratification based on carotid stenosis results in many unnecessary surgeries on asymptomatic patients each year. Lumen evaluation does not detect plaque

Note: Scanned images are included in the proceedings. Some submitted images were reduced during editing thereby decreasing clarity. Also, refer to the Program Planner. Proceedings Content as of 3/28/2014.

components, and recent studies suggest that plaque components such as intraplaque hemorrhage (IPH) may account for the majority of carotid source strokes. The purpose of this study was to determine essential markers of acute ischemic stroke in a multivariate logistic regression model including IPH and standard imaging and clinical markers.

Materials and Methods

Over four years, 450 patients with suspected acute stroke were imaged with MR imaging (MRI)/MR angiography (MRA). Carotid MRA was used to measure lumen markers of plaque vulnerability (stenosis, plaque thickness, ulceration and intraluminal thrombus). Intraplaque hemorrhage was detected with the magnetization prepared rapid acquisition gradient-recalled echo (MPRAGE) sequence. Ipsilateral embolic ischemic events were detected with brain diffusion tensor imaging (DTI). Of the 450 patients, 141 were excluded due to noncarotid stroke sources (e.g., atrial fibrillation). This provided 309 patients with 618 carotid artery and ipsilateral brain image pairs. After excluding eight vessels due to occlusion, 610 carotid arteries were used in the final analysis.

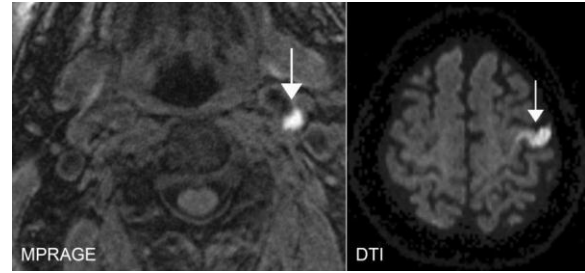
Results

Carotid IPH was associated with acute territorial ischemic events [odds ratio (OR)=55.1, 95% confidence interval (CI)=17.3-176.5]. After adjusting for covariates including the above lumen markers of plaque vulnerability and clinical markers (current smoking, prior smoking, diabetes, hypertension, dyslipidemia, age and male sex), IPH remained significantly associated with acute territorial ischemic events (OR=12.1, 95% CI=4.1-35.4). In addition, two of the covariates remained significantly associated with ischemic events, including stenosis (OR=8.2, 95% CI=1.9-36.1) and current smoking (OR=2.8, 95% CI=1.1-7.1).

Conclusions

In this cross-sectional study, carotid IPH was an independent risk factor for ischemic stroke. After adjusting for the confounders in our logistic regression model, only IPH, stenosis and current smoking remained significantly associated with carotid source embolic events. These results strongly argue against using carotid stenosis as the sole imaging determinate of stroke risk and argue for the additional use of carotid IPH imaging techniques. Interestingly, current smoking was the lone clinical covariate resulting in stroke risk unexplained by current plaque imaging techniques. Advances in positron emission tomography (PET) imaging of plaque inflammation and dynamic contrast-enhanced (DCE) MRI measures of plaque permeability may shed further light on this association.

KEYWORDS: Carotid, Intraplaque Hemorrhage, Stroke



O-784

9:15AM - 9:21AM

Tissue Negative-Transient Ischemic Attack: Is There a Role for MR Perfusion?

R Grams¹, C Kidwell¹, S Shroff¹, K Drake¹, K Nael¹

¹University of Arizona, Tucson, AZ

Purpose

Conventional imaging is inconclusive in the majority of clinically diagnosed transient ischemic attack (TIA) patients. The purpose of this study is to evaluate the added diagnostic value of dynamic susceptibility contrast (DSC) perfusion in detection of perfusion deficits as a footprint of ischemia in diffusion-weighted imaging (DWI)-negative patients with TIA.

Materials and Methods

Electronic charts of TIA patients who presented to the emergency department between October 2012-October 2013 were reviewed by stroke neurologists. The inclusion criteria were: 1) clinical presentation of TIA at the time of admission and discharge confirmed by stroke neurologist, 2) Negative conventional imaging including DWI, and 3) acquisition of DSC perfusion imaging. The MR imaging was performed within first 24 hours after the clinical presentation. Dynamic susceptibility contrast perfusion was performed using a gradient-EPI sequence (TR/TE: 1450/22 msec, FA 90°, FOV: 22x22-cm, matrix 128 mm, voxel size 1.7 x 1.7 x 4 mm³, GRAPPA x3) after intravenous injection of 0.1 mmol/kg of Multihance-gadolinium contrast. Using a FDA-approved software (Olea Medical, La Ciotat, France), all DSC scans were processed with block-circulant singular value deconvolution. The perfusion parametric maps of cerebral blood flow (CBF) and time to maximum (Tmax) were scored using a 1-3 scoring scale for the presence and location of perfusion disturbance by two independent observers (stroke neurologist and neuroradiologist) blinded to patients history. Statistical analysis was performed by Kappa and Wilcoxon tests.

Note: Scanned images are included in the proceedings. Some submitted images were reduced during editing thereby decreasing clarity. Also, refer to the Program Planner. Proceedings Content as of 3/28/2014.

Results

Thirty patients (16 M, 14 F), age (range 20-95 years old, median 74) who met our inclusion criteria were evaluated. The ABCD2 score ranged 2-7 with median of 5. In 7/30 (23%) TIA patients, a perfusion abnormality was identified by both observers. There was a high agreement ($k=0.82$) between both readers. In 6/7 (86%) TIA patients with a positive perfusion scan, the brain regions where perfusion abnormalities were identified matched with the neurologic deficits at TIA presentation. The mean of ABCD2 scores in patients with positive perfusion abnormalities was higher ($p=0.05$) than in patients without perfusion deficit.

Conclusions

MR perfusion has an added diagnostic value in approximately a quarter of DWI-negative TIA patients. There is high correlation between presence of location of perfusion deficit with patient clinical presentation and ABCD2 score, suggesting the perfusion deficit is a footprint of hemodynamic disturbance in this population.

KEYWORDS: DSC MR Imaging, MR Imaging Perfusion, TIA

O-785

9:21AM - 9:27AM

Comparison of Susceptibility-Weighted Imaging and CT Angiography for Evaluation of Clot Burden in Acute Ischemic Stroke

A Agarwal¹, K Thamburaj², S Kanekar³

¹Penn State University, Hummelstown, PA, ²Penn State University, Hershey, PA, ³Penn State Milton Hershey Medical Center, Hershey, PA

Purpose

1. To evaluate the diagnostic accuracy of the magnetic resonance imaging (MRI) susceptibility-weighted images (SWI) for the detection of clot in acute ischemic stroke. 2. To compare the diagnostic accuracy of susceptibility-weighted imaging against computed tomography (CT) angiography for estimation of clot length and burden in acute ischemic stroke.

Materials and Methods

The University Institutional Review Board approved the study. A series of 79 patients with acute MCA stroke was selected using 'MCA infarct' in our search engine software (Primordial Design, Inc., San Mateo, CA); under the time frame of January 2009 to May 2012. Inclusion criteria included: (1) Diffusion positive cases of acute onset MCA infarct, (2) CT angiogram of the brain and MRI performed within 24 hours of clinical onset, (3) SWI included in the MRI protocol. All patients with SWI, included in our study,

had minimum intensity projection (mIP) images which were used for detection of thrombus. Computed tomography angiogram was performed on a Siemens 128 slice dual tube (Definition Flash) scanner. MR imaging was done on Siemens Magnetom Aera 1.5 T, Siemens Magnetom Skyra 1.5 T, or Philips Intera 1.5 T. The interval between CT and MR imaging ranged from four hours to 21 hours (mean, 13 hours 36 minutes). We finally had 35 patients who satisfied all the criteria. All of these patients were evaluated with the new 3D-GRE SWI MR technique in addition to other conventional MRI techniques, including DWI with apparent diffusion coefficient (ADC) maps. All the cases, which finally were included in our study, were reviewed by two fellowship trained neuroradiologists. We first reviewed the SWI-mIP images only, being completely blinded to the clinical history and other imaging sequences. Observations were made for the presence of MCA thrombus, extent of thrombus, and segments of MCA involved. Following these observations, other MR sequences including DWI and the CT angiogram of the brain were reviewed.

Results

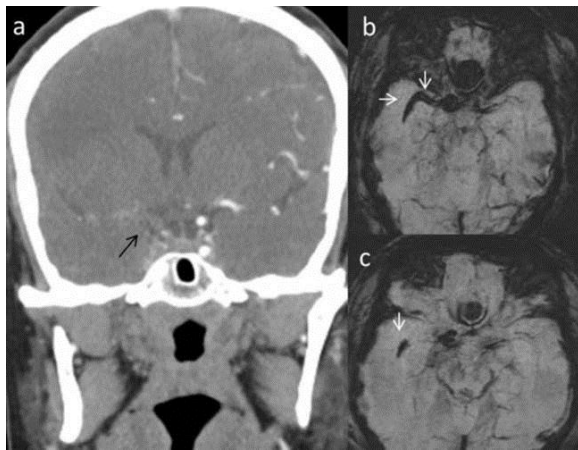
The clinical and imaging standard for our study was the presence of DWI positive MCA infarct. Intra-arterial MCA thrombus was seen on SWI in 30 cases (86%) of the 35 reviewed. Of the 30, SWI showed thrombus in more than one MCA segments in seven patients. M1 segment was most commonly involved, with thrombus seen in this segment in 19 of 30 cases. Thrombus was seen in the M2 segment in 12 cases. One patient had involvement of the opercular M3 MCA segment. Six patients had involvement of the cortical M4 branch of MCA. We excluded any case with frank hemorrhagic transformation from our study; however, few scattered foci of petechial hemorrhages were seen in 13 cases (37%). More than 50% of cases positive for branch occlusion on CTA had poor distal reconstitution. Estimation of thrombus burden or the number of MCA segments involved was therefore difficult for most cases on CTA (Figure 1). The mean length of the clot on SWI was 14.9 ± 6.4 mm (range: 5-39) and on CTA was 11.1 ± 4.1 mm (range: 5-27). Thrombus was noted in two patients on SWI only, with no corresponding abnormality seen on CTA. Both of these patients had branch occlusion of distal M4 segment of MCA. Two patients with acute MCA infarct showed no vascular occlusion or thrombus on either CTA or SWI.

Conclusions

Recanalization is a powerful predictor of stroke outcome in patients with arterial occlusion treated with either intravenous (iv) recombinant tissue plasminogen activator (rt-PA) or an endovascular approach. Many factors impact the success of recanalization therapy, including clot composition, clot burden and site of clot impaction. Our study demonstrates that SWI is a very sensitive tool for detection of intra-arterial thrombus in acute MCA stroke, compared with other techniques including CT angiography. Moreover, SWI can provide an accurate estimation of thrombus burden.

Note: Scanned images are included in the proceedings. Some submitted images were reduced during editing thereby decreasing clarity. Also, refer to the Program Planner. Proceedings Content as of 3/28/2014.

KEYWORDS: Clot, Stroke, Susceptibility-Weighted Imaging



O-788

9:51AM - 9:57AM

Vessel Wall MRI in Acute Ischemic Stroke: Effects of Embolus and Mechanical Thrombectomy on the Arterial Wall

S Power¹, F Silver², T Krings², D Mikulis², D Mandell¹

¹University Health Network: Toronto Western Hospital, Toronto, Ontario, Canada, ²Toronto Western Hospital, Toronto, Ontario, Canada

Purpose

Secondary prevention of ischemic stroke requires determination of stroke etiology. High resolution contrast-enhanced vessel wall MR imaging (MRI) (VW-MRI) is a potential method of differentiating among intracranial etiologies such as atherosclerosis, vasculitis, and vasoconstriction syndromes (1-3). However, it is not known whether an embolus from a proximal source may itself injure the arterial wall and mimic the VW-MRI appearance of primary intracranial arteriopathy. Similarly, it is not known whether mechanical thrombectomy alters the VW-MRI appearance of the arterial wall. The purpose of this study was to determine the VW-MRI appearance of the arterial wall in the days after acute occlusion of large intracranial arteries.

Materials and Methods

This was a cross-sectional study of consecutive patients with acute intracranial arterial occlusion who underwent contrast-enhanced VW-MRI using a 3 T MR system as part of a secondary prevention clinical imaging protocol. Studies were performed over an 18-month period. The

VW-MRI technique has been described in detail elsewhere (2, 3). We performed a detailed chart review for each case and categorized stroke etiology as cardioembolic, carotid embolic, or other/unknown. A neuroradiologist, blinded to clinical data including management, reviewed the imaging. Using the contralateral arteries as a reference standard, the neuroradiologist evaluated the site of occlusion and categorized the lumen (occluded, partially recanalized, fully recanalized), arterial wall thickening (none/minimal, mild, moderate, severe), and arterial wall enhancement (same four categories). We used the Fisher exact test to compare presence versus absence of arterial wall thickening and presence versus absence of wall enhancement in patients treated with medical therapy alone versus mechanical thrombectomy.

Results

Sixteen patients satisfied the inclusion criteria. There were eight women and eight men; median age was 58.5 years (interquartile range 18.5 years.) The accompanying table provides the results for each patient. The majority of patients (69%) had occlusion of a middle cerebral artery M1 or M2 segment (n=11), and most of the remainder (25%) had a carotid terminus occlusion. There were 10 patients managed without endovascular therapy and six patients who underwent mechanical thrombectomy using a stent-retriever device, either Solitaire FR (Covidien, EV3 Neurovascular, Irvine, California) or Trevo (Stryker Neurovascular, Mountain View, California). Unless contraindicated, intravenous tissue plasminogen activator (tPA) was administered, with 12 of 16 patients (75%) receiving iv tPA. Median time from symptom onset to vessel wall MRI was three days (interquartile range 2 days). The arterial occlusion had completely recanalized at the time of vessel wall MRI in 14 cases and there was mild residual narrowing in two cases. Vessel wall MRI demonstrated two main patterns: the underlying arterial wall appeared essentially normal with no/minimal wall thickening or enhancement in eight cases (50%) and there was mild/moderate wall thickening and enhancement in eight cases (50%). In one case (subject 1), the arterial wall abnormality was focal and had the appearance (1, 3) of an intracranial atherosclerotic plaque. This was the only patient with moderate arterial wall abnormality who had not undergone mechanical thrombectomy. Arterial wall thickening and enhancement were more frequent in patients who had undergone mechanical thrombectomy than nonendovascular therapy alone (p=0.03 for thickening; p=0.05 for enhancement).

Conclusions

Preliminary investigation suggests that acute embolic occlusion of intracranial arteries may itself result in concentric arterial wall thickening and enhancement but this is usually very mild. In contrast, mechanical thrombectomy commonly results in pronounced concentric segmental arterial wall thickening and enhancement. Knowledge of these appearances may be important for accurate interpretation of VW-MRI in patients with recent intracranial arterial occlusion.

Note: Scanned images are included in the proceedings. Some submitted images were reduced during editing thereby decreasing clarity. Also, refer to the Program Planner. Proceedings Content as of 3/28/2014.

KEYWORDS: Mechanical Thrombectomy, Stroke, Vessel Wall

0-877

9:45AM - 9:51AM

Towards a better assessment of vascular clots in acute ischemic stroke

V Macaigne¹, P Roux¹, M Obadia¹, A Gueguen², K Malkani³, E Tollard⁴, A Halimi-Cohen², J Savatovsky¹

1Fondation Ophthalmologique Adolphe de Rothschild, Paris, France, 2Fondation Rothschild, Paris, France, 3University of Angers, Saint Sylvain d'Anjou, Pays de la Loire, France, 4CHU Charles Nicolle, Rouen, France

Purpose

Acute ischemic stroke is a major cause of morbidity and mortality worldwide. Brain imaging, which plays an important role in the initial evaluation of the disorder including the assessment of vascular clot location and length, is being used increasingly as a decision-making tool in selecting patients for recanalization treatments, such as intravenous thrombolysis and intra-arterial therapy. Here we compare the efficacy of 3D contrast-enhanced magnetic resonance angiography (CEMRA) with those of time of flight (TOF) angiography, T2* sequences, and TOF angiography combined with T2* sequences, in the evaluation of middle cerebral arterial clots in patients with acute ischemic stroke.

Materials and Methods

The records of 70 consecutive eligible patients were selected from those of 253 patients having undergone brain MRI within 12 hours of an acute neurological deficit during the period from November 2011 to August 2013. All patients had been scanned on the same 3 T MRI system with a 16-channel neurovascular coil. Two independent observers retrospectively analyzed the results of the various MRI sequences performed to determine the location and length of cerebral arterial clots using CEMRA, TOF angiography, T2* sequences, and TOF angiography combined with T2*sequences. Interobserver reproducibility in the determination of vascular clot location and length with each of these techniques then was assessed.

Results

Interobserver reproducibility for appreciating vascular clot location and length was better with CEMRA than with the other techniques. Contrast-enhanced MRA gave results similar to those of TOF angiography combined with T2* sequences for the detection and location of the clots. In contrast, clot length was poorly assessed when using TOF angiography alone, and compared to the results of CEMRA, the combination of TOF angiography and T2* sequences

Table: Study Results. Left (Lt), Right (Rt). Carotid terminus (carotid T). Mechanical thrombectomy (MT). Intravenous tissue plasminogen activator (IV tPA). Imaging interval is time in days from symptom onset to VW-MRI. M1 and M2 segments of the middle cerebral artery (M1, M2). P2 and P3 segments of the posterior cerebral artery (P2/3).

1	2	M	Lt M1	Mod erate	Mode rate	N	N	2	Unknown
2	2	M	Lt M1	Non e/mi nimal	None/ minimal	N	Y	11	Unknown
3	2	F	Lt M2	Non e/mi nimal	None/ minimal	N	Y	2	Cardioembolic
4	2	M	Rt P2/3	Non e/mi nimal	Mild	N	Y	1	Unknown
5	2	M	Lt M1	Non e/mi nimal	None/ minimal	N	N	3	Cardioembolic
6	2	M	Lt M1	Non e/mi nimal	None/ minimal	Y	Y	5	Cardioembolic
7	2	F	Rt M2	Mod erate	Mode rate	Y	Y	1	Cardioembolic
8	2	M	Lt M2	Non e/mi nimal	None/ minimal	N	Y	3	Carotidembolic
9	2	F	Lt Carotid T	Mod erate	Mode rate	Y	Y	4	Unknown
10	2	F	Lt Carotid T	Mod erate	Mode rate	Y	N	4	Cardioembolic
11	2	M	Lt M1	Mild	Mild	N	Y	1	Carotidembolic
12	2	F	Rt M1	Non e/mi nimal	None/ minimal	N	Y	4	Cardioembolic
13	2	F	Rt M2	Non e/mi nimal	None/ minimal	N	Y	3	Cardioembolic
14	2	F	Rt M1	Non e/mi nimal	None/ minimal	N	N	7	Unknown
15	2	F	Lt Carotid T	Mild	Mode rate	Y	Y	2	Cardioembolic
16	2	M	Lt carotid T	Mild	Mild	Y	Y	2	Unknown

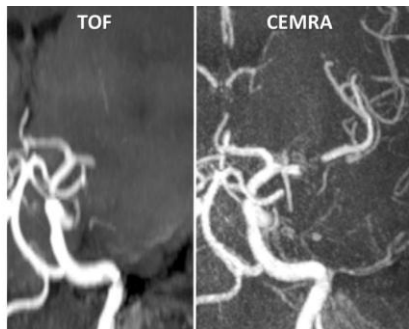
Note: Scanned images are included in the proceedings. Some submitted images were reduced during editing thereby decreasing clarity. Also, refer to the Program Planner. Proceedings Content as of 3/28/2014.

appeared to overestimate the length of the arterial occlusion.

Conclusions

Our retrospective study suggests that satisfactory intracranial assessment of the presence, and of vascular clots in patients with acute ischemic stroke can be obtained either with TOF angiography combined with T2* sequences or with CEMRA. However, CEMRA appears to offer better interobserver reproducibility and more reliable results for thrombus length without compromising examination time. These preliminary results would need to be tested by a prospective controlled study based on digital subtraction angiography as the reference technique. If confirmed, they would allow the use of CEMRA as a unique tool in cases of acute ischemic stroke for the selection of patients likely to benefit from revascularization strategies.

KEYWORDS: Clot, MR Imaging/MR Angiography, Stroke



Thursday, May 22
8:30AM - 10:00AM
Room 517a

80 - SNIS PROGRAMMING: UPDATE ON CEREBRAL ANEURYSMS (SAM)

O-790

8:30AM - 8:50AM

Endovascular Aneurysm Therapy: Current State of the Art and What the Future Holds

Turk, A.
Med. Univ. Of So. Carolina
Charleston, SC

Abstract/Presentation Summary

Cerebral aneurysms are the most frequent cause of non traumatic hemorrhagic stroke. Approximately 1 in 50 people harbor an unruptured brain aneurysm. The annual rate of rupture is approximately 8-10 of 100,000. When aneurysms rupture, as many as 65% of patients do not survive and approximately half of those that survive are

disabled. The endovascular treatment of cerebral aneurysms continues to expand, with many now viewing this approach as the preferred method over open surgical clipping. Endovascular therapy has traditionally focused on coiling of aneurysms. Utilizing adjunctive devices such as balloons and stents have allowed operators to treat more difficult wide-necked aneurysms and often to achieve better angiographic outcomes. However, recurrence of treated aneurysms requiring retreatment occurs as frequently as 15% of the time. There have been significant advances in aneurysm endovascular device technology to address this potential limitation. In efforts to overcome this potential limitation, coils have been coated with bioactive substances to accelerate healing. Coils have been developed with substances that swell to increase the volume filling or complex into compact mass to increase packing density. Stents have been developed to provide better covering of the aneurysm neck and easier to interact with coil catheters. This has naturally progressed to high density stents that function as flow diverters that can treat aneurysms without having to enter into the aneurysm. However, this type of device is limited to sidewall aneurysms. More recently, intrasaccular flow diverters have been developed and are in initial human use in Europe. Other next generation experimental devices are seeing limited initial human use or are being evaluated in the pre-clinical arena. This talk will focus on the evolution of cerebral aneurysm treatment and focus on next generation technology coming to the US.

O-791

8:50AM - 9:10AM

Endovascular Management of Dissecting Intracranial Aneurysms

Tampieri, D.
Montreal Neurological Hospital and Institute
Montreal, Quebec

Abstract/Presentation Summary

Arterial dissections originate from the disruption of the lamina intima of an artery which allows blood to accumulate in the arterial wall. A cerebral arterial dissection may give rise to the formation of a dissecting aneurysm. This pathological process results in an increased risk of rupture of the arterial wall and can therefore lead to SAH. When unruptured, dissecting aneurysms likely present with mass effect related symptoms such as headache, seizure, focal neurological deficit and they are often associated with pain. In the past various treatments, surgical and endovascular, have been applied in the management of these lesions, often leading to the sacrifice of the parent artery. Surgical and endovascular approaches include wrapping, clipping and trapping, and neurointerventional treatments consist of proximal occlusion, coiling. More recently the use of stent-

Note: Scanned images are included in the proceedings. Some submitted images were reduced during editing thereby decreasing clarity. Also, refer to the Program Planner. Proceedings Content as of 3/28/2014.

assisted techniques have permitted to perform reconstructive interventions with successful preservation of the parent artery. The use of endovascular techniques and in particular the stent assisted coiling or flow diverters techniques enables preservation of the parent artery, with relative low risks procedure and stable long terms follow up. The management of anticoagulation represents certainly one of the major challenges in these treatments mainly if the patients presents acutely with a SAH.

O-792

9:10AM - 9:30AM

Flow Diversion: Is it the Solution to the Aneurysm Problem or Another Tool in the Kit?

Fiorella, D.
Stonybrook Univ. Medical Center
Stonybrook, NY

Abstract/Presentation Summary

Flow diversion represents a conceptually new approach to the endovascular treatment of brain aneurysms. These new devices have provided us with the ability to achieve a durable and complete reconstruction of even the most complex cerebral aneurysms, many of which were not previously amenable to surgical or endovascular repair¹. The devices work to redirect flow away from the aneurysm, causing the aneurysm to proceed to thrombosis. Eventually tissue grows over the device and definitively excludes the aneurysm from circulation. Finally, the thrombus mass within the aneurysm is resorbed and the mass effect dissipates². As this technology is increasingly applied, we are continuously learning more about its capabilities and limitations. We will review the theoretical basis for the mechanism of action of flow diverters, the existing clinical data and the existing indications and contraindications for treatment³.

9:30AM - 10:00AM Questions and Answers

Thursday, May 22
8:30AM - 10:00AM
Room 520

81 - ASFNR PROGRAMMING: DEMENTIA

O-793

8:30AM - 8:50AM

Pathophysiology of Alzheimer's Disease Revealed by Neuroimaging

Black, S.
Sunnybrook Health Sciences Center
Toronto, ON

Abstract/Presentation Summary

The pathophysiology of Alzheimer's Disease (AD) is becoming clearer, but is much more complex than first imagined. Oligomers of amyloid beta 40-42 are thought to be a key instigator in the pathological cascade. Overproduction appears to drive neurodegeneration in autosomal dominant cases, but impaired clearance is likely an important mechanism in sporadic AD, exacerbated by aging, genetic (e.g. apolipoprotein E e4), and other factors such as oxidative stress and innate immune activation. Alzheimer pathology combined with vascular lesions is the common substrate of dementia postmortem, and comorbid synucleinopathy is also frequent. Advances in MRI and computational analysis can reveal a typical pattern of cortical thinning in AD along with hallmark hippocampal atrophy. Functional and structural connectivity using diffusion tensor, resting state and activation fMRI, have added new optics to neurodegenerative patterns, exemplified by decreased functional connectivity in the Default Mode Network in AD. Small vessel disease (SVD) is evident in 95% of elders on FLAIR or T2-weighted MRI, and is increasingly important to understand relationships between SVD and AD, including amyloid angiopathy, which is a potent cause of hemorrhagic stroke, as well as microbleeds. 18Fglucose PET has been available for 30 years with hypometabolic signatures discernable using statistical parametric mapping and surface projections. However, the most exciting development over the last decade is C-11 and now 18F amyloid PET ligands. Now we can visualize the culprit pathologies in the living brain. We can credential patients for participation in clinical trials of anti-amyloid therapies. In the A4 study, for example, normal individuals aged 65 to 85 considered at risk of AD are now being recruited to undergo a florbetapir scan. If appropriate uptake is seen, they are offered randomization to solanezumab vs placebo, infused monthly over 3 years, with the goal of preventing cognitive decline. Similar interventions are being considered in patients with autosomal dominant AD. Tau ligands are also in development to make tau pathology visualizable in AD and Fronto-Temporal tauopathies. Synuclein ligands are also actively being pursued. It is now possible to identify pathologies in vivo to guide therapeutics, monitor target engagement and clinical outcomes. Whether or not this will translate into clinically meaningful slowing and prevention remains to be seen and How to affordably integrate this into the clinic will be challenging. Cost-benefit analyses will be needed to determine clinical utility even before proven effective disease-modifying therapies become available. Irrefutably, however, our ability to document amyloid beta and tau pathology in vivo as it is unfolding (or perhaps folding!) is a game changer for neuroimaging in vascular and neurodegenerative cognitive impairment.

Note: Scanned images are included in the proceedings. Some submitted images were reduced during editing thereby decreasing clarity. Also, refer to the Program Planner. Proceedings Content as of 3/28/2014.

O-794

8:50AM - 9:10AM

The Value of PET Tracers in the Assessment of Dementia

Rabinovici, G.
University of California, San Francisco
San Francisco, CA

O-795

9:10AM - 9:30AM

The Utility of Diffusion Imaging in the Assessment of Dementia

Helpert, J.
The Medical University of South Carolina
Charleston, SC

Abstract/Presentation Summary

Water molecules diffusing in the brain can be used to probe tissue microstructure non-invasively with diffusion MRI (dMRI). The microstructural distances to which dMRI is most sensitive is set by the typical distance a water molecule diffuses during the approximately 100 ms needed to acquire an individual dMRI signal. This distance of about 10 μm makes dMRI ideal for investigating cell-sized microstructural features (i.e. dendritic, axonal, myelin). In this sense, dMRI overcomes the resolution limits of other MRI techniques and bestows upon dMRI a unique ability to non-invasively assess the microstructure of human brain tissue *in vivo*. This makes dMRI particularly useful for investigating brain tissue microstructural changes that occur during the evolution of AD pathology.

O-796

9:30AM - 9:50AM

Resting State BOLD MRI Methods in the Assessment of Dementia

Ances, B.
Washington University
Saint Louis, MO

Abstract/Presentation Summary

Recent advances in neuroimaging may allow for earlier diagnosis of preclinical late onset Alzheimer's disease (sAD). One marker that has gained increasingly application is resting state functional connectivity (rs-fc). Correlations in oscillations in the blood oxygen level dependent (BOLD) signal are used to map out resting state networks (RSNs) in an individual while they lie quietly in the scanner. These networks nicely recapitulate those seen when performing a functional task. Using rs-fc MRI significant differences

between cognitively normal and sAD individuals for multiple RSNs, including the default mode network (a group of brain areas that is most active at rest when not performing a task). A decrease in rs-fc in the DMN sAD nicely overlaps changes seen in amyloid imaging. In addition, to the DMN additional networks including the dorsal attention network (DAN) and control (CON) are affected with increasing disease progression. When comparing known risk factors for AD, the presence of at least one APOE e4 allele causes decreases in rs-fc in the DMN, even in cognitively normal individuals. Using rs-fc we have begun to distinguish healthy aging from early preclinical changes in sAD. Changes in rs-fc may not be the earliest biomarker for preclinical sAD but instead may be a therapeutic measure that could evaluate the efficacy of potential therapeutics. Finally, genetic mutations in presenilin and amyloid precursor protein can lead to autosomal dominant AD (ADAD). Recent comparisons between sAD and ADAD have shown similar changes using rs-fc.

9:50AM - 10:00AM Discussion

Thursday, May 22
8:30AM - 10:00AM
Room 524

82 - INTERNATIONAL SESSION: SILAN

O-797

8:30AM - 8:40AM

Introduction to SILAN.ORG and SILAN Foundation

Figueroa, R.
Medical College of Georgia
Augusta, GA

O-798

8:40AM - 9:00AM

Current Impact of Imaging in Selecting ICH patient's Treatment

Romero, J.
Massachusetts General Hospital, Harvard Medical School
Boston, MA

O-799

9:00AM - 9:20AM

MR Imaging of the Brachial Plexus

Note: Scanned images are included in the proceedings. Some submitted images were reduced during editing thereby decreasing clarity. Also, refer to the Program Planner. Proceedings Content as of 3/28/2014.

Torres, C.
The Ottawa Hospital
Ottawa, Ontario

Abstract/Presentation Summary

Magnetic Resonance Imaging (MRI) is the imaging modality of choice for the evaluation of the brachial plexus due to its superior soft tissue resolution and multiplanar capabilities. The evaluation of the brachial plexus however represents a diagnostic challenge for the clinician and the radiologist. The imaging assessment of the brachial plexus, in particular, has been traditionally challenging due to the complexity of its anatomy, its distribution in space and due to technical factors. During the presentation, we will describe a modified technique used in our institution for the evaluation of the brachial plexus which led to a substantial decrease in scanning time and to better visualization of all the segments of the brachial plexus from the roots to the branches, in only one or two images, facilitating therefore the understanding of the anatomy and the interpretation of the study. We illustrate the benefit of this modified technique with an example of a patient with a lesion in the proximal branches of the left brachial plexus that was clinically suspected but missed on conventional brachial plexus imaging for 6 consecutive years. In addition, we will review the common and infrequent benign and malignant pathology that can affect the brachial plexus.

O-800

9:20AM - 9:40AM

Eight Years of Experience - Update and Current Status in Flow Diverters

Lylyk, P.
ENERI - SAGRADA FAMILIA
Buenos Aires

Abstract/Presentation Summary

INTRODUCTION The introduction of the flow diversion concept in the treatment of intracranial aneurysms emerged as a paradigm shift in the endovascular field. It also represents the evolution of the endovascular treatment: starting with balloon aneurysm filling, coiling, balloon assisted coiling, stent assisted coiling and finally flow diversion for vessel repair. Since the first flow diverter device, four different generations were introduced in the practice, including monolayers, multilayers, retrievable devices, and we experienced all these generations. **MATERIALS AND METHODS** Since March 2006, intracranial aneurysms were treated with different flow diverter devices. The first device used was Pipeline Endovascular Device (PED), with more than 599 aneurysms, 497 patients and 739 devices. SNEG was used in 66 aneurysms, 57 patients and 73 devices. CMFM in 67

aneurysms, 61 patients, 83 devices. P64FMD in 41 aneurysms, 29 patients, 33 devices. WEB single or dual layer in 26 aneurysms, 24 patients, 26 devices. All patients were followed up with MRI and DSA images every 3 months during the first year, and annually after. Clinical and angiographic data were reported. **RESULTS** A total of 804 aneurysms were treated with flow diverter devices, 673 patients and 959 devices. 85% of the aneurysms were located in anterior circulation, 51% were large or giant aneurysms. The range of clinical and angiographic follow up was at 3 months and up to 8 years. Occlusion rate at 6 months and 12 months was 80% and 90%, and 100% after the third year. Technical success up to 90%. The combined morbidity and mortality rate was 4.6% for all flow diverter devices. **CONCLUSION** Flow diversion technique proved to be a feasible, safe and effective technique, with acceptable number of complications and morbidity/mortality rate. We learned about the clinical management over the years and its limitations. Better devices with specific characteristics as greater sizes, retrievability, surface coating are needed to continue improving this technique.

O-801

9:40AM - 10:00AM

Dyna CT for Planning the Endovascular Treatment of Spinal Epidural Arteriovenous Fistula

Diaz, O.
The Methodist Hospital
Bellaire, TX

Abstract/Presentation Summary

Spinal extradural (epidural) arteriovenous fistulas (AVFs) are uncommon vascular lesions of the spine with arteriovenous shunting located primarily in the spinal epidural venous plexus. Understanding the complex anatomical variations of these uncommon lesions is important for management. We will present the most common neuroaxial location of the spinal extradural AVFs as well a practical and treatment oriented classification according to the hemodynamic status and the venous drainage. According to that the spinal extradural AVFs we have divided into 3 types. In Type A spinal extradural AVFs, arteriovenous shunting occurs in the epidural space and these types have an intradural draining vein causing venous hypertension and spinal cord edema with associated myelopathy or cauda equina syndrome. Type B1 malformations are confined to the epidural space with no intradural draining vein, causing compression of the spinal cord and/or nerve roots with myelopathy and/or radiculopathy. Type B2 malformations are also confined to the epidural space with no intradural draining vein and no mass effect, and are asymptomatic. The current description of the different types of spinal extradural AVFs can help in understanding their pathophysiology and guide management. DynaCT was found to be useful in understanding the complex anatomy of these lesions.

Note: Scanned images are included in the proceedings. Some submitted images were reduced during editing thereby decreasing clarity. Also, refer to the Program Planner. Proceedings Content as of 3/28/2014.

Endovascular treatment with Onyx is a good alternative for spinal extradural AVF management.

Thursday, May 22
10:30AM - 12:00PM
Room 517bc

83 - PARALLEL PAPERS: Spine: New Techniques and Neurography

O-802

10:30AM - 10:37AM

Spinal Cord DTI in Motor Neuron Disease

A Meoded¹, C Blackstone², M Floeter¹, C Pierpaoli³, R Roda², J Sarlls⁴, O Schanz¹

¹National Institute of Neurological Disorders and Stroke, National Institutes of Health, SSPU, Baltimore, MD, ²National Institute of Neurological Disorders and Stroke, National Institutes of Health, Neurogenetic, Bethesda, MD, ³Program on Pediatric Imaging and Tissue Sciences, NICHD, NIH, Bethesda, Maryland, Bethesda, MD, ⁴National Institute of Neurological Disorders and Stroke, National Institutes of Health, NMRF, Bethesda, MD

Purpose

The hereditary spastic paraplegias (HSPs) comprise a large group of inherited neurologic disorders. Hereditary spastic paraplegia type 4 (SPG4), is the most common form in a heterogeneous group of autosomal dominant HSP's. Pathologically, there is a bilateral fiber loss: corticospinal tract (CST) and posterior columns (PCs) of opposite gradients of progression. In uncomplicated HSP there is insidiously progressive spastic paraplegia often accompanied by decreased vibratory sensation in the toes. Primary lateral sclerosis (PLS) is a sporadic disorder characterized by slowly progressive CST dysfunction. Primary lateral sclerosis is recognized clinically by its nearly exclusive involvement of upper motor neurons, initially affecting the legs and later involving upper extremities and bulbar muscles. The description of MR imaging (MRI) findings in the literature of the spinal cord in these patients is scarce and mainly qualitative. Diffusion tensor imaging (DTI) permits the investigation of white matter organization and microstructure. The aims of our study were: (a) calculate the DTI metrics, and fiber volume and perform 3D-tractography of the lateral CSTs and the PC in the cervical spine in healthy subjects, and (b) compare these metrics between healthy controls (HCs) and HSP and PLS patients.

Materials and Methods

Primary lateral sclerosis and HSP patients, and age-matched healthy-controls (HC) were enrolled. Clinical ratings for motor/sensory functions were assessed with finger/foot tapping and vibration sense of the index finger/great toe, respectively. Reduced field-of-view DTI at 2mm isotropic resolution with 60 diffusion directions was acquired of the cervical spinal cord. We performed region of interest (ROI)/deterministic-tractography analysis for the lateral CSTs and PC. Statistical analysis was performed using ANCOVA with age as covariate in order to evaluate the mean differences of DTI metrics: fractional anisotropy (FA), Trace, axial and radial diffusivity (AD, RD) and cord volume, measured as number of fibers per voxel normalized for slice number, between groups. This study was approved by the local IRB.

Results

Six healthy control, seven PLS and four HSP patients (mean age: 51.8, 58.2, 51.75 years), were studied. Sensory and motor ratings in PLS patients were lower compared to HSP (foot>finger). The following DTI-metrics in the regions studied were statistically different between groups: Left CST-FA: (F(2,13)=6.48, p=0.01) HV>PLS p=0.021, HV>HSP p=0.056; Trace: (F(2,13) =8.94, p=0.003), PLS>HV p= 0.01, PLS>HSP p=0.006; RD: (F(2,13)=9.32,p=0.003), PLS>HV p=0.004, PLS>HSP p=0.012. Fiber volume (spinal-cord C0-C4): F(2,13)= 2.752, p=0.104; HSP<HC (p=0.046, LSD corrected for multiple comparison).

Conclusions

Precise localization of focal pathologies in the spinal cord requires accurate depiction of its intrinsic anatomical structures, in particular differentiation of gray and white matter structures. In our study both patient groups demonstrated more motor/vibration sense deficit (foot>hands) compared to controls. Primary lateral sclerosis>HSP patients more abnormalities of DTI metrics, and HSP demonstrated more volume loss compared to controls. The combination of reduced FA, increased Trace and RD, and volume loss in the spinal cord may reflect tissue loss, due to axonal degeneration, gliosis, or expanded extracellular space. The relative preservation of upper extremity sensory/motor function may explain the lesser degree of change in diffusion metrics at this upper cervical level. Additional patients will be studied in order to assess the relationship with clinical measures.

KEYWORDS: Diffusion Tensor Image, Neurodegenerative, Spinal Cord

O-803

10:37AM - 10:44AM

Cervical Spine 3D Double Inversion Recovery (DIR) Sequence in Multiple Sclerosis

Note: Scanned images are included in the proceedings. Some submitted images were reduced during editing thereby decreasing clarity. Also, refer to the Program Planner. Proceedings Content as of 3/28/2014.

I Riederer¹, D Karampinos¹, M Settles¹, C Preibisch¹, J Bauer¹, J Kleine¹, M Mühlau¹, C Zimmer¹

¹Klinikum Rechts der Isar, Technical University of Munich, Munich, Germany

Purpose

The double inversion recovery (DIR) sequence suppresses simultaneously the signal from both the cerebrospinal fluid (CSF) and the white matter. It became apparent that this sequence is widely accepted and crucial in MR imaging (MRI) diagnostic of multiple sclerosis (MS) in the brain, especially for the detection of intracortical lesions. Spinal cord imaging in MS is still challenging, though very important for diagnosis and prognosis. The application of the DIR sequence on the spine, however, has not been established yet. Therefore, we developed and evaluated a cervical spine 3D DIR sequence in this study.

Materials and Methods

We examined 30 patients with suspected multiple sclerosis (16 female, mean age 39 years) and 10 healthy controls (4 female, mean age 33 years) in a 3 T Philips Ingenia MR scanner. The 3D DIR sequence (TR: 5500 ms, scan time: 7:36 min, acq. voxel size: 1,2 x 1,2 x 1,3 mm) was compared with the conventional T2 TSE sequence (sag/ax, TR: 3000 ms, scan time: 3:47/1:48 min, acq. voxel size: 0,94 x 1,18 x 2/0,65 x 0,82 x 4 mm). Axial and coronal multiplanar reconstructions (MPR) were done postprocessing. Lesions were counted independently by two neuroradiologists. Furthermore, the standardized contrast to noise ratio (sCNR) was calculated. No abnormalities were found in the control group.

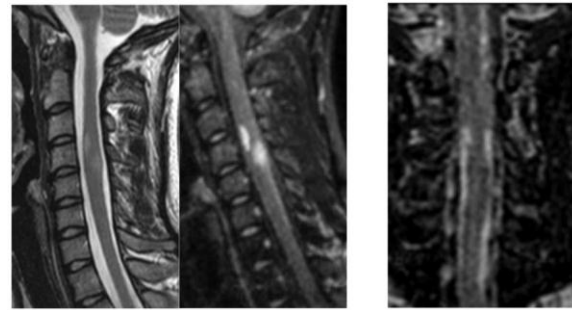
Results

Many more lesions could be detected with the 3D DIR sequence than with the conventional T2 TSE sequence (121 versus 92; = 32%). The sCNR was significantly higher ($p < 0.001$) in the 3D DIR sequence compared to the T2 TSE sequence (left image). Therefore, it was easier for the raters to interpret the images using the DIR sequence. The lesion load ranged from multiple focal lesions to confluent lesions. The coronal reconstructions have proven helpful especially in the localization of lesions and delineation of elongated lesions (right image). Particularly, lesions in the border of the spinal cord were very conspicuous.

Conclusions

The 3D DIR sequence has proven essential in the detection of cervical spine lesions in MS. The number of detected lesions was higher and the sCNR was significantly stronger than with the conventional T2 TSE sequence. The 3D DIR sequence might be a helpful supplement for the conventional MRI protocol for the examination of spinal cord lesions, especially in MS.

KEYWORDS: MRI Spine, Multiple Sclerosis



T2 TSE

3D DIR

3D DIR

O-804

10:44AM - 10:51AM

Evaluation of Monochromatic Imaging to Reduce Metallic Artifacts in Computed Tomography of the Spine with Fusion Hardware

P Komlosi¹, D Grady¹, A Goode¹, P Judy¹, M Wintermark¹

¹University of Virginia, Charlottesville, VA

Purpose

Monochromatic imaging with dual energy computed tomography (CT) has been proposed to reduce metallic artifacts as compared to conventional polychromatic CT. The purpose of this study is to systematically evaluate and define the optimal dual-energy CT imaging parameters for specific spinal implant alloy compositions.

Materials and Methods

Spinal fixation rods of chromium-cobalt (Cr-Co) or titanium (Ti) alloys inserted in the cervical spine section of Alderson Rando anthropomorphic phantom were imaged ex vivo with fast-kV switching CT at 80 and 140 kVp. The collimation width and field of view were varied between 20-40 mm and medium-large, respectively. Extrapolated monochromatic images were generated at 70, 90, 110 and 130 keV. The standard deviation of voxel intensities along a circular line profile around the spine was used as an index of the magnitude of metallic artifact.

Results

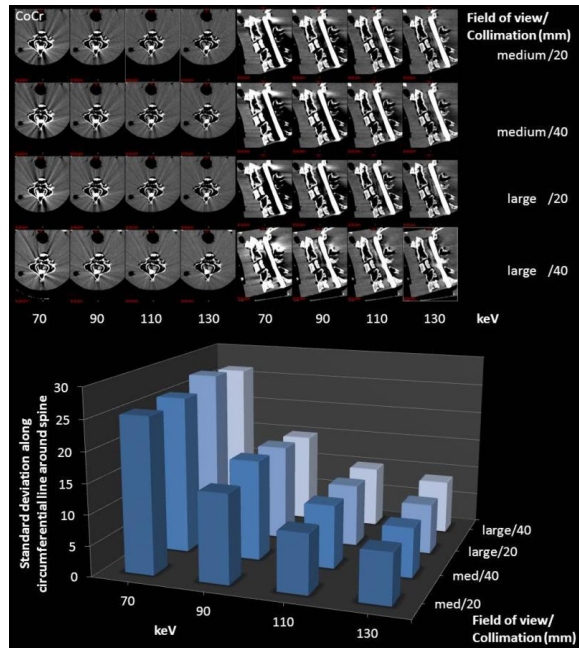
The metallic artifact was more conspicuous around the fixation rods made of Cr-Co than those of Ti alloys. The magnitude of metallic artifact seen with Cr-Co fixation rods was minimized at 130 keV using a collimation width of 40 mm and medium field of view settings.

Conclusions

Note: Scanned images are included in the proceedings. Some submitted images were reduced during editing thereby decreasing clarity. Also, refer to the Program Planner. Proceedings Content as of 3/28/2014.

Optimization of acquisition settings used with monoenergetic CT studies yields reduced metallic artifacts. As compared to Cr-Co, spinal fixation rods manufactured from Ti cause less metallic artifacts on cervical spinal CT images.

KEYWORDS: CT, Dual-Energy CT, Metal Artifact



O-805

10:51AM - 10:58AM

Diffusion tensor imaging detects the spatial variation in fiber angle and lamellar number in intact human discs

R Alkalay¹, D Meier², C Westin², D Hackney¹

¹Beth Israel Deaconess Medical Center, Boston, MA,
²Brigham and Women's Hospital, Boston, MA

Purpose

The biological and physiological modifications of the disk tissue's structure underlie the loss of its functional integrity and ultimately, loss of its performance as a mechanical joint. This study investigated the use of tensor diffusion imaging to directly interrogate the spatial orientation of collagen fibers in intact human disks.

Materials and Methods

Four human lumbar cadaver spinal disk units (L2-L3), from donors age 48 and 52 years, were scanned using a 9.4

T scanner (Bruker Biospin MRI GmbH, Ettlingen, Germany) equipped with an actively shielded 400 mT/m gradient coil (Bruker, BGA12S). The disks were imaged in 72 mm inner-diameter quadrature birdcage coil with the disk's caudal-cranial axis aligned with the main static magnetic field direction (laboratory z-axis). Diffusion tensor imaging (DTI): 3D spin-echo echo-planar imaging (SE-EPI) diffusion tensor image data were acquired using 30 noncollinear directions and two averaged b₀ images with: b = 670 s/mm², TE/TR = 29/700ms, NEX = 8, FOV = (56 x 50 x 16)mm, acquisition matrix = 290 x 176 x 16, reconstructed resolution = (193 x 195 x 500) μm. Imaging time = 10 hours. Diffusion tensor imaging data were reconstructed in Slicer 3D (v.4.1, www.slicer.org) and a weighted least-squares algorithm used to estimate the 3D diffusion tensor from the diffusion-weighted images. Diffusion tensor imaging data set was analyzed directly from the 3x3 diffusion tensor (V.14, Matlab, Mathworks) and the orientation angle relative to the axial plane of the disk computed at each voxel.

Results

The DTI analysis showed clear demarcation of the AF and NP regions [Figure 1(A)] with fine details of the annulus structure demonstrated by the number of laminae. In agreement with histological studies (1), analysis of fiber angles at the anterior, lateral and posterior regions (B) shows the increase in fiber angle as a function of region within the AF. Of note is the increase in the fibers angle dispersion at the posterior region.

Conclusions

In close agreement with histological studies (1), fiber angle within the AF increased from the anterior to the posterior aspect of the disk with respect to its transverse plane. We are able to count the number of lamellae as a function of location around the circumference of the disk. Since disk degeneration produces, among other things, a loss in the number of laminae, this permits a more detailed assessment of the structural effects of disk degradation. This approach also permits evaluating the range of fiber orientations as a function of degeneration. This protocol will enable us to provide novel data on the effects of degenerative changes in the disk, on the relationships between structure and composition and, in turn, their effect on the mechanical behavior of the disk. This study, for the first time, showed the ability to directly visualize fiber angle and the number of lamina in the AF within the intact disk.

KEYWORDS: Diffusion Tensor Image, Disk, Spinal Imaging

Note: Scanned images are included in the proceedings. Some submitted images were reduced during editing thereby decreasing clarity. Also, refer to the Program Planner. Proceedings Content as of 3/28/2014.

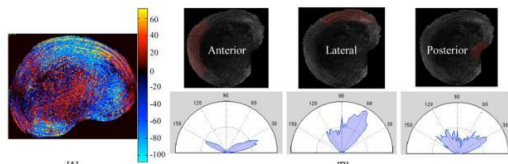


Fig. 1. Fiber angle based segmentation of the DTI data set shows discrete, alternating, lamella structure in the AF and a near uniform structure in the NP [A].

O-806

10:58AM - 11:05AM

MR Diffusion is Sensitive to Mechanical Loading in Human Intervertebral Discs

R Alkalay¹, D Burstein¹, C Westin², D Meier², D Hackney¹

1Beth Israel Deaconess Medical Center, Boston, MA,
2Brigham and Women's Hospital, Boston, MA

Purpose

Though quantitative measurements MR have targeted the assessment of disk composition, water and proteoglycan content, as markers of the severity of degeneration, it is the loss of the disk's mechanical function and its tissues structural integrity that underlie the degradation of its primary role as a mechanical joint. This study investigated the use of MR diffusion imaging to directly interrogate the loss of dynamic and viscoelastic properties of intact human disks.

Materials and Methods

Five complete human L2-L3 disk units were isolated from donors age 39, 65, 69, 72 and 81 years. The disks were rehydrated (37°C saline, 4 hours, 200N compression), conditioned (10 compressive load cycles (100 - 300N, 0.5Hz)) and mechanically characterized by a) Dynamic test:

Fifty cycles of compressive strain (0-9.1%, 1Hz), simulating endplate deformation under daily loads, b) Stress-relaxation: A constant displacement, computed to impose 9.1% strain, applied for a period of 4500 seconds. For each disk, dynamic stiffness (S_y), elastic ($E1$) and viscous ($E2$) stiffness and viscosity ($h1$), were computed from the curves. The disks were scanned in a 72 mm inner-diameter quadrature birdcage coil using a 4.7 T scanner (Bruker Biospin MRI GmbH, Ettlingen, Germany) with the disk's caudal-cranial axis aligned with the main static magnetic field direction (laboratory z-axis). Two MR experiments were performed: a) T2 relaxation: MSME sequence (TR/TE=5000/7..186 ms, 11.6ms spacing), matrix=256², Slice=1mm. b) Diffusion: Diffusion sensitization gradients [(1,0,0), (0, 1, 0), (0,0,1)] with four equally spaced b-values (100-1000)mm²/s, large delta=14ms, small delta=8ms, Matrix=128², Slice=1mm. These experiments were performed with the disk loaded at 200N and at 800N, simulating a sitting and standing load conditions (2). Repeated measure MANOVA (JMP 8.0, SAS, NC) tested for the effects of loading, tissue (nucleus versus annulus) on the change in either the mean or COV as main effects. Tukey's HSD was used for post-hoc analysis. Linear models were used to test for correlation between MR and mechanical parameters.

Results

Loading caused a significantly lower mean diffusivity ((11.3 versus 10.1)10⁻⁴.mm/sec, $p<0.001$) and higher variance (COV: 22.0% versus 30.1%, $p<0.001$) of diffusivity. No such effect was seen for the T2 values. The nucleus (NP) showed higher T2 (45%) and MD (25%) compared to the annulus(AF) ($p<0.001$ for both). Under load tissue-based differences were observed only for diffusion values with the AF showing lower MD (21%) but higher COV (31.9)% compared to the NP ($p<0.001$). Loading had no significant effect on diffusion anisotropy ($p>0.05$). Degenerative grade was significantly associated with the reduction in MD and T2 ($p<0.001$ for both). Diffusivity and T2 were correlated with the disk's dynamic ($p<0.01$ and $p<0.05$) and long term viscoelastic ($p<0.05$ and $p<0.05$) stiffness. Diffusivity but not T2, was correlated with its viscoelastic dampening ($p<0.01$) and instantaneous stiffness ($p<0.05$). MR estimated hydration was significantly correlated with the reduction in the disk's dynamic ($r^2=0.66$, $p<0.05$) and instantaneous ($E1$: $r^2=0.89$, $p<0.01$) stiffness.

Conclusions

In contrast to the T2, diffusion measures detected the effect of loading on the disk. Strong tissue-based differences for both MR metrics appear to reflect the difference between the highly structured AF versus the less structured but highly hydrated NP, Figure 1. Increased degenerative state of the disk was associated with loss of tissue definition, decreased variability in the NP and conversely, increased variability in the AF, suggesting a loss of tissue demarcation. In effect, the disks appeared more "cartilaginous" - one of the hall marks of disk degeneration. The strong correlations between diffusivity

Note: Scanned images are included in the proceedings. Some submitted images were reduced during editing thereby decreasing clarity. Also, refer to the Program Planner. Proceedings Content as of 3/28/2014.

and the rheological assessments of disk mechanics, suggests that MR might permit quantitative assessment of disk functional status and structural integrity.

KEYWORDS: Diffusion MR Imaging, Disk Degeneration, Mean Diffusivity

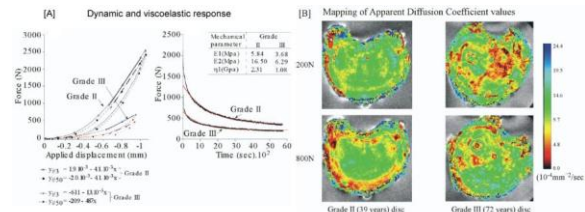


Fig. 1. Comparison of the cyclic and time dependent response [A] and corresponding change in MR diffusivity for a grade II and III discs [B]

O-807

11:05AM - 11:12AM

MR-Neurography: Sensitivity of Nerve T2-Signal and Nerve Caliber in Hereditary Transthyretin Familial Amyloid Polyneuropathy

J Kollmer¹, E Hund¹, B Hornung¹, S Schönland¹, U Hegenbart¹, A Kristen¹, M Bendszus¹, M Pham¹

¹University of Heidelberg, Heidelberg, Germany

Purpose

Transthyretin familial amyloid polyneuropathy (TTR-FAP) is a fatal autosomal dominantly transmitted hereditary disease leading to misfolding and extracellular deposition of transthyretin amyloid. TTR-FAP usually manifests with a rapidly progressive and incapacitating axonal, distal-symmetric, sensory-motor polyneuropathy (1, 2). Recently, we were able to show that lower limb nerve injury in TTR-FAP is detectable in vivo by an increase of nerve T2-lesions using high resolution MR neurographic (MRN) sequences. The aim of the current study is to evaluate whether nerve caliber can be used as an additional MRN criterion to detect amyloid-related nerve injury in TTR-FAP. Furthermore, we compared the sensitivity of nerve T2-signal and nerve caliber to differentiate between symptomatic TTR-FAP, asymptomatic gene carriers and healthy volunteers.

Materials and Methods

We prospectively examined 20 patients with rare genetically confirmed TTR-FAP [13 with manifest polyneuropathy (PNP), seven asymptomatic gene carriers] and 60 healthy volunteers, age/gender matched. All participants received detailed neurological/electrophysiological examinations. High resolution imaging was done on a 3 T MR scanner Magnetom/Trio/Siemens: (1) axial T2-TSE-fs-sequences

from proximal thigh to distal ankle (140 slices/leg; TE/TR 55/5970ms, voxel-size 0.4x0.3x3.5mm); 2) 3D-T2-IR-SPC-sequence with axial reformation (50 images) for the lumbar plexus/spinal nerves (TE/TR 202/3000, voxel-size 1.0x1.0x1.0). Manual segmentation of the lumbar plexus/sciatic/tibial nerve as nerve tissue voxels and voxel-based measurement of nerve caliber was performed on each axial imaging slice (320/subject).

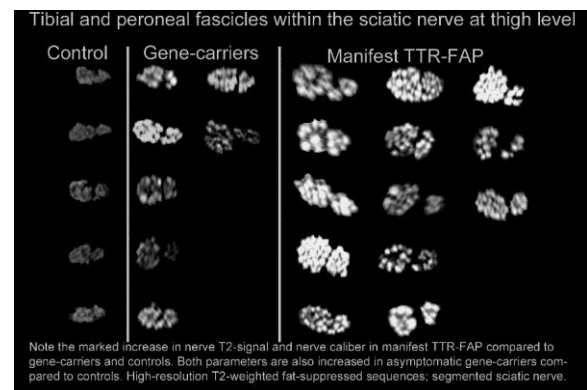
Results

Proximal thigh to ankle level: Cumulative nerve lesion-voxel number was significantly higher in manifest TTR-FAP than in controls: 8282 ± 1585 versus 0 ± 328 ; $p < 0.00001$. Lesion-voxel number in asymptomatic gene carriers (4079 ± 1503) also was increased significantly compared to controls ($p = 0.008$) but decreased compared to manifest TTR-FAP ($p = 0.033$). In both TTR-FAP groups a clear proximal focus of nerve lesions ($p < 0.00001$) was observed. Here, nerve caliber also was increased significantly and with proximal predominance in manifest TTR-FAP ($p < 0.00001$) and gene carriers ($p = 0.0084$) compared to controls. Lumbar plexus/spinal nerves: Evaluation at plexus level revealed also statistical differences of nerve T2-lesions between controls and both TTR-FAP groups (both: $p = 0.0002$), but not between the two TTR-FAP groups ($p = 0.843$), while differences in nerve caliber were highly significant between all three groups: manifest TTR-FAP versus controls, $p < 0.00001$; asymptomatic gene carriers versus controls, $p < 0.00001$; manifest TTR-FAP versus gene carriers, $p = 0.0157$.

Conclusions

We could show for the first time, that TTR-FAP related nerve lesions are detectable in vivo not only by an increase of nerve T2-lesions, but also by an increase of nerve caliber with a proximal focus in both, manifest and asymptomatic TTR-FAP. Furthermore, our results especially at plexus level may indicate that nerve T2-signal has a particularly strong sensitivity to detect early nerve injury, while nerve caliber may help to differentiate between severe and even more severe cases of nerve impairment.

KEYWORDS: Amyloid, High-Resolution Imaging, MR Neurography



Note the marked increase in nerve T2-signal and nerve caliber in manifest TTR-FAP compared to gene-carriers and controls. Both parameters are also increased in asymptomatic gene-carriers compared to controls. High-resolution T2-weighted fat-suppressed sequences; segmented sciatic nerve.

Note: Scanned images are included in the proceedings. Some submitted images were reduced during editing thereby decreasing clarity. Also, refer to the Program Planner. Proceedings Content as of 3/28/2014.

O-808

11:12AM - 11:19AM

In-Vivo Detection of Nerve Injury in Systemic Light Chain (AL) Amyloidosis by High-Resolution MR-Neurography

J Kollmer¹, J Purrucker¹, B Hornung¹, E Hund¹, S Schönland¹, U Hegenbart¹, M Bendszus¹, M Pham¹

¹University of Heidelberg, Heidelberg, Germany

Purpose

Systemic light chain (AL) amyloidosis, a chronic hematological disorder caused by plasma cell dyscrasia or B-cell lymphoproliferative disorders, is the most common form of amyloidosis in the western world. It leads to an extracellular deposition of amyloid fibrils, which are components of immunoglobulins, known as light chains (1). Clinically, it presents as a multisystem disorder with progressive dysfunction of several organs, including heart, liver and kidneys due to an accumulation of amyloid (2). Untreated, prognosis is very bad. A peripheral neuropathy is relatively rare and manifests as a symmetrical distal sensory-motor polyneuropathy (PNP) (3, 4). For the first time, we investigated, whether lower limb nerve injury in AL amyloidosis can be detected and localized in vivo by using high resolution T2-weighted imaging with large anatomical coverage.

Materials and Methods

Prospective investigation in a relatively large sample of 10 patients with rare PNP due to AL amyloidosis (no former therapy with neurotoxic agents such as Velcade or Vincristin) and 38 healthy volunteers, matched for gender and age. All participants received a neurological examination, including scoring for NIS-LL (Neuropathy-Impairment-Score-Lower-Limbs), NDS (Neuropathy-Deficit-Score), NSS (Neuropathy-Symptom-Score), and detailed electrophysiological studies of the tibial, peroneal and sural nerve as well as small-fiber testing (sympathetic skin response). Imaging was done feet-first and supine in a 3 T MR scanner (Magnetom/Trio/Siemens) with high resolution axial T2-weighted turbo-spin-echo, fat-suppressed sequences separately for each leg from proximal thigh to distal ankle (140 slices/leg): TE/TR 55/5970ms, voxel-size 0.4x0.3x3.5mm. Nerve T2-signal was evaluated as contrast-to-noise ratio (CNR) by manually delineating the nerve circumference as intraneural region-of-interest (ROI) on each axial imaging slice. Additional ROIs were read out in adjacent muscles for normalization of nerve T2-signal.

Results

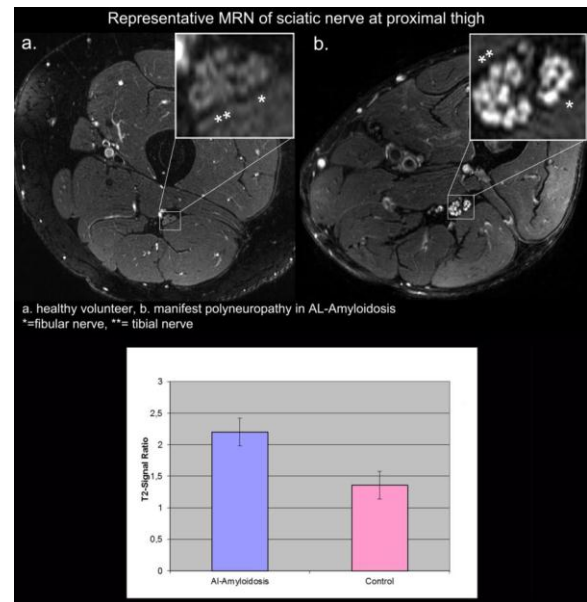
Quantitative evaluation revealed a marked increase of nerve T2-signal in all AL patients (Signal Ratio 2.20±0.24)

with strong statistical significance compared to the group of healthy volunteers (Signal Ratio 1.36±0.04, p=0.02; Figure). These nerve lesions appear completely symmetrically. Furthermore, we found a clear proximal focus of nerve lesions in all our patients with distally symmetric polyneuropathy due to AL amyloidosis (Figure).

Conclusions

Our study results present for the first time, that nerve lesions in AL amyloidosis are detectable in vivo by using high resolution MR neurography. While we could show that nerve lesions appear symmetrically inconsistent with the clinical appearance, we surprisingly found a clear proximal focus of nerve lesions at thigh level, although symptoms prevail distally. This suggests that MRN can serve as a novel and sensitive diagnostic marker of amyloid-related nerve injury and may help to better understand the underlying and yet not completely understood pathomechanism in polyneuropathy due to AL amyloidosis. Furthermore, MRI may hold potential to identify patients with early or subclinical polyneuropathic nerve lesions, and therefore an increased risk to develop neurotoxic side effects due to Velcade or Vincristin therapy.

KEYWORDS: Amyloid, MR Neurography



O-809

11:19AM - 11:26AM

Proximal Nerve Lesions in Distally Symmetric Hereditary and Non-Hereditary Amyloid Polyneuropathies

Note: Scanned images are included in the proceedings. Some submitted images were reduced during editing thereby decreasing clarity. Also, refer to the Program Planner. Proceedings Content as of 3/28/2014.

J Kollmer1, J Purrucker1, E Hund1, B Hornung1, S Schönland1, U Hegenbart1, M Bendszus1, M Pham1

1University of Heidelberg, Heidelberg, Germany

Purpose

Among cardiac and autonomic manifestations patients with either hereditary transthyretin associated, or nonhereditary primary systemic light-chain amyloidosis can manifest with a severe polyneuropathy (PNP) due to an extracellular deposition of amyloid (1, 2). Peripheral nerve affection occurs in form of a nerve length-dependent impairment, first involving unmyelinated or small myelinated fibers causing spontaneous, often burning pain sensations, loss of temperature and numbness in the lower extremities. Later patients develop increasing sensory and motor deficits due to an alteration of larger motor and sensory fibers undergoing wallerian degeneration (3-5). Like in other metabolic PNP, clinically it presents distally symmetric. However, the exact pathomechanism of peripheral nerve injury is still a matter of research. Therefore, we investigated the spatial appearance and focus of nerve lesions in the lower extremities from proximal-to-distal in both hereditary and nonhereditary amyloid PNP by using MR neurography (MRN) with high spatial resolution.

Materials and Methods

We prospectively examined a large sample of 23 patients with manifest amyloid-related polyneuropathy [13 with genetically confirmed, manifest transthyretin familial amyloid polyneuropathy (TTR-FAP) and 10 with systemic light-chain amyloidosis (AL)], seven asymptomatic gene-carriers for TTR-FAP and 38 healthy volunteers. First, all participants received detailed neurological and electrophysiological examinations, including scoring for three established scores used in PNP. Then high resolution MRN of proximal thigh, distal thigh, proximal lower leg, ankle region was done in a 3 T MR scanner separately for both legs with axial T2-TSE-fs sequences (140 slices/leg; TE/TR 55/5970ms, voxel size 0.4x0.3x3.5mm). In the TTR-FAP group manual segmentation of the sciatic/tibial/peroneal nerve was performed as nerve-tissue-voxels on each axial imaging slice (320/subject) with subsequently fully automated and operator-independent classification of lesion voxels. In AL nerve T2-signal was evaluated quantitatively as contrast-to-noise ratio (CNR) by manually delineating the nerve circumference as intraneural region-of-interest (ROI) on each axial imaging slice, followed by normalization of nerve T2 signal with respect to adjacent intramuscular T2 signal.

Results

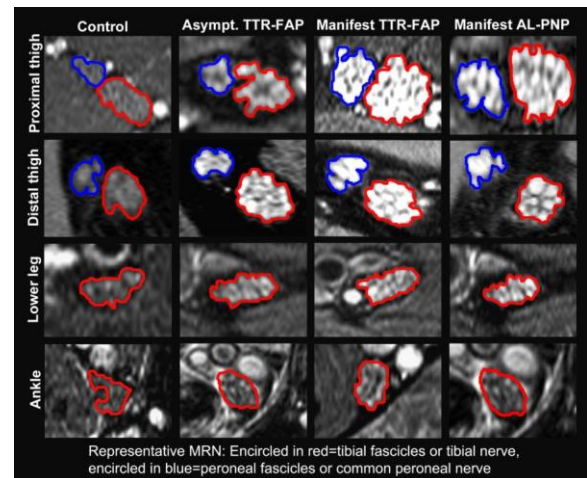
In the TTR-FAP group, two-way ANOVA revealed significantly more proximal than distal nerve lesions (f-value 76.06, p-value <0.00001) with a gradient between increased proximal and distal nerve lesions being most pronounced in symptomatic patients (f-value 67.65, p-

value <0.00001). Post-hoc pairwise comparisons between proximal (0-60) and distal slice positions (80-139) and between manifest TTR-FAP and asymptomatic gene carriers revealed for nerve T2 lesion voxels per position a predominant proximal focus at thigh level in both groups (p<0.00001). In the AL group we also found a strong and statistical significant gradient between proximal and distal nerve lesions by an increase of normalized nerve T2-signal intensity compared to our healthy volunteers (p=0.0023).

Conclusions

For the first time, MRN could accomplish to determine the precise localization of nerve lesions in hereditary and nonhereditary amyloid PNP in vivo. Our findings of a surprisingly clear proximal focus of nerve lesions in distal symmetric PNP may lead to a better understanding of the underlying and possibly same pathomechanism in all metabolic PNP, at least in all amyloid-related PNP. One possible explanation may be a metabolic-toxic mechanism leading to microvascular dysfunction and therefore ischemia in the watershed areas of peripheral nerves prior to distal axonal degeneration. That is supported by the proximal predominance of nerve lesions in complete asymptomatic gene carriers for TTR-FAP.

KEYWORDS: MR Neurography, Nerve Imaging, Peripheral Nerve



0-810

11:26AM - 11:33AM

Denervation Changes are Detectable on MRI after Botulinum Toxin A Injection into the Rat Hind Limb.

K Fink1, C Marder2, I Odderson1, S Oh1, W Hwang1, D Casey3, K Maravilla1

Note: Scanned images are included in the proceedings. Some submitted images were reduced during editing thereby decreasing clarity. Also, refer to the Program Planner. Proceedings Content as of 3/28/2014.

1University of Washington, Seattle, WA, 2Simon Med Imaging, Tucson, AZ, 3North Oaks Hospital, Hammond, LA

Purpose

Patient response to chemodenervation with Botulinum Toxin A (BTX) injection for painful muscle syndromes is variable. One possible reason is a difference in degree of muscular denervation, but to date there has been no objective measure of chemodenervation effect. This study describes an MRI method to document muscular denervation, and seeks to characterize the time course, nature, and intensity of such changes following BTX-mediated chemodenervation of the rat hind limb.

Materials and Methods

MR imaging of the hind limbs were performed on 14 adult male Sprague Dawley rats. Animals were anesthetized with 5% isoflurane by facemask and MRI was performed at 3 T using a phased array rat coil. Imaging sequences included short-tau inversion recovery (STIR) and multi-echo T2-weighted images with quantitative T2 mapping. Twelve rats were injected with 2.5 U botulinum toxin A in 0.05 to 0.1 mL 0.9% preservative-free saline into the left hamstring muscles. Two additional rats underwent sham injection with 0.1 ml 0.9% preservative-free saline without BTX. The right hind limb served as an internal control for all animals. MR imaging was performed at baseline and at weekly intervals postinjection for six weeks, then at two months and three months. Gait track analysis was performed at baseline and at each MRI session to assess functional effects of chemodenervation. MR images were analyzed using OsiriX v5.8 64-bit software. STIR signal changes were evaluated visually. The area of maximal STIR abnormality was selected on the four-week scan, and regions-of-interest (ROIs) were placed on the injected left hind limb. Similar ROIs were placed over the homotopic area of the uninjected right hind limb. Mean values and standard deviations were recorded for each ROI at each time point. For each animal at each time point, STIR and quantitative T2 values were recorded from each limb. STIR and T2 values were normalized to the contralateral side (Left/Right *100). Values were compared at each time point using a two-tailed paired Student's t-test. Animals were donated to the animal-use training program at the conclusion of the study.

Results

All BTX-injected animals demonstrated increased STIR signal in the affected hind limb (Figure 1). Mean normalized STIR values increased significantly in the BTX-injected limb by one week postinjection ($p < 0.001$), remained significantly elevated compared to the baseline scan through the two-month study ($p \leq 0.01$), but were not significantly different compared to baseline scan at the three-month time point ($p = 0.2$, Figure 2). Normalized quantitative T2 values were significantly elevated beginning at week one scan ($p < 0.001$), and remained significantly elevated through the two month scan ($p \leq 0.02$). The control animals showed no increase in STIR

signal or T2 values in the sham-injected limb. Quantitative T2 values in the uninjected right leg also did not significantly differ from baseline at any time-point in BTX rats or controls.

Conclusions

MR imaging signal changes are evident on STIR and quantitative T2 images after chemodenervation with botulinum toxin A but not after sham injection. Signal changes are evident at one week and gradually normalize over a three-month period. Therefore, MRI may provide an objective measure to evaluate extent of chemodenervation after BTX injection.

KEYWORDS: MR Imaging, Muscle Denervation, Pain

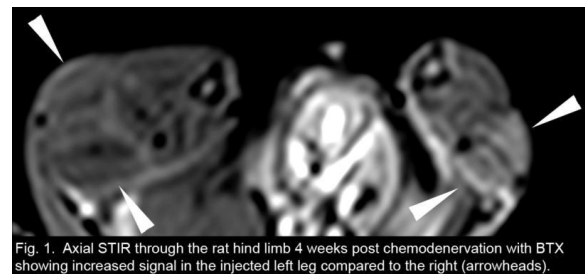


Fig. 1. Axial STIR through the rat hind limb 4 weeks post chemodenervation with BTX showing increased signal in the injected left leg compared to the right (arrowheads).

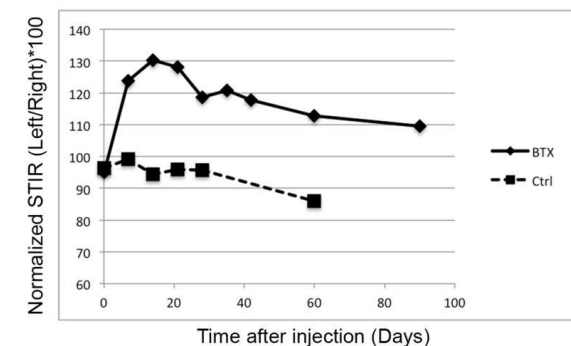


Fig. 2. Normalized STIR signal in experimental versus control animals.

O-811

11:33AM - 11:40AM

Imaging Genital Nerves with a Molecular Imaging Agent: Preliminary Animal Studies

D Schellingerhout¹, L Flores¹, D Gomez¹, L Le Roux¹

¹University of Texas MD Anderson Cancer Center, Houston, TX

Purpose

Erectile dysfunction (ED) is a common complication of all forms of prostate cancer treatment, with incidence varying from 13-97% depending on the series quoted. Damage to

Note: Scanned images are included in the proceedings. Some submitted images were reduced during editing thereby decreasing clarity. Also, refer to the Program Planner. Proceedings Content as of 3/28/2014.

the neurovascular bundles is a root cause, with strong indications from many studies that preservation of the neurovascular bundles avoids post-treatment ED. The goal of this study is to use a novel neural imaging agent based on the nontoxic Tetanus Toxin C-fragment (TTc) to allow the visualization of the anatomy of genital nerves in prostate cancer. This will reduce the clinical impact of prostate cancer by reducing the nerve complications associated with the treatment of prostate disease, predominantly erectile dysfunction (ED).

Materials and Methods

Male rats were anesthetized (1-2% isoflurane/oxygen) and stereotactically injected with 50 µg of fluorescently labeled TTc546 in a total volume of 20 µl in the tunica albuginea of the left corpus cavernosum. Animals were imaged live one hour postinjection with a Xenogen IVIS 200 small animal imager. Animals then were killed, and the cavernosal nerves, prostates, nerve plexi were dissected, followed by ex vivo imaging as well as confocal imaging of cleared prostate tissues.

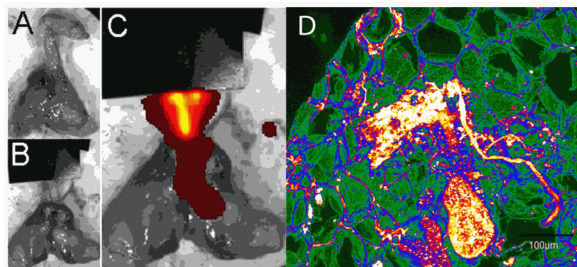
Results

En bloc excision of the prostate with the penis allowed imaging of the genital nerves. We note fluorescent TTc-related signal uptake along the expected course of the nerve tract ipsilateral to the injection site (Figure 1 A-C). Postdissection we visualized TTc signal along the corpus cavernosum, urethra and within the prostate lobes and seminal vesicles. Detailed histological assessment of the prostate after clearing with BABB clearing agent allowed visualization of the pelvic nerve ganglion (Figure 1 D), a key structure in nerve preserving surgery of the prostate.

Conclusions

We demonstrate preliminary data suggesting that TTc could be used as a nerve imaging agent to demonstrate the cavernosal nerves by imaging. This suggests that with further work, image guidance could be provided to physicians and surgeons to spare these nerves during treatment for prostate carcinoma, allowing the preservation of genital nerve function and quality of life in prostate cancer survivors.

KEYWORDS: Nerve Imaging, Neuronavigation



O-812

11:40AM - 11:47AM

Diabetic Neuropathy Can be Demonstrated by Molecular Neurographic Imaging and Parallels Neurologic/Behavioral Findings

D Schellingerhout¹, L Flores¹, D Gomez¹, L Le Roux¹

¹University of Texas MD Anderson Cancer Center, Houston, TX

Purpose

The purpose of our study was to utilize neurography, a molecular imaging technology evaluating retrograde transport, to demonstrate the development of diabetic neuropathy and correlate it with neurological function in an animal model of diabetes.

Materials and Methods

Male CD1 28-30 gm nonfasting mice received multiple doses of Streptozotocin (STZ) at 55 mg/kg body weight for five consecutive days injected intraperitoneally. Control animals received citrate buffer (n=6). Blood glucose was determined with tail vein puncture and a blood glucometer (ReliOn, Arkray, Shiga, Japan) and body weights were taken every three days. Mice were considered to be diabetic when their nonfasted blood glucose levels were ≥ 200 mg/dl and those experimental animals that did not develop diabetes were excluded from further assessment (final n=9). We assessed the development of diabetic neuropathy by means of both imaging and Von Frey testing for mechanical sensitivity. For each imaging session, animals received fluorescently labeled TTc-Alexa790 (15 µg/20 µL) via intramuscular injection into the calf muscle. Fluorescent imaging using a small animal optical imager (Xenogen IVIS 200) was used to image the distribution of TTc over 60 minutes, with region of interest (ROI) measurements taken over the thoracic spine to quantitate fluorescent uptake. Region of interest measurements had background activity subtracted, and were normalized to the signal intensity at time=0. Mechanical sensitivity was assessed through the use of von Frey nylon filaments by applying calibrated force to the palmar surface of the hind paw, and the 50% withdrawal threshold was calculated. At the end of the study tissue was harvested for immunohistochemical analysis.

Results

Blood glucose values (mg/dl) were at baseline 148.00 ± 17.09 and 167.89 ± 51.05 , 145.00 ± 24.62 and 312.00 ± 80.97 1st week, 135.00 ± 14.31 and 350.44 ± 42.23 2nd week, 107.33 ± 34.77 and 377.78 ± 61.78 3rd week, 156.33 ± 54.54 and 414.13 ± 59.82 5th week, 133.67 ± 12.24 and 394.38 ± 42.58 7th week, 126.83 ± 25.47 and 384.00 ± 59.00 9th week, 102.67 ± 11.96 and 467.13 ± 61 11th week, 126.60 ± 18.51 and 492.38 ± 60.44 14 week,

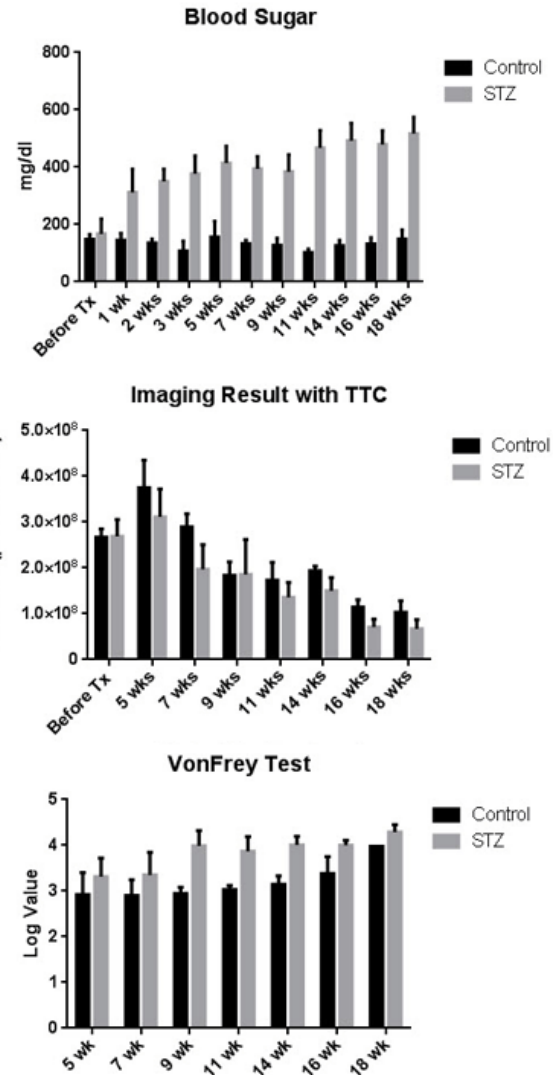
Note: Scanned images are included in the proceedings. Some submitted images were reduced during editing thereby decreasing clarity. Also, refer to the Program Planner. Proceedings Content as of 3/28/2014.

132.40±21.73 and 478.71±48.98 16th week and 149.2032.54 and 517.38±57.07 18th week for the control and diabetic animals. These values were statistically different from the 1st week onward (two-tailed T-test $p < 0.0001$). The mean Radiance of TTC imaging (photons/s/cm²/steradian) were 2.67E+08±1.77E+07 and 2.69E+08±3.68E+07 before treatment, 3.75E+08±6.04E+07 and 3.11E+08±6.08E+07 5th week, 2.89E+08±2.94E+07 and 1.97E+08±5.31E+07 at 7th week, 1.84E+08±2.97E+07 and 1.86E+08±7.62E+07 at 9th week, 1.73E+08±3.88E+07 and 1.36E+08±3.31E+07 at 11th week, 1.94E+08±1.00E+07 and 1.50E+08±2.86E+07 at 14th week, 1.15E+08±1.59E+07 and 7.12E+07±1.68E+07 at 16th week and 1.04E+08±2.44E+07 and 6.72E+07±2.01E+07 at 18th week for control and diabetic animals. Statistical significant difference were noted at 7th week ($p=0.0179$) and from 14 weeks onward ($p=0.0240$, 0.0029 and 0.0248). Log transformed Von Frey values were 2.92±0.48 and 3.31±0.41 5th week, 2.90±0.34 and 3.35±0.49 at 7th week, 2.95±0.13 and 3.99±0.33 at 9th week, 3.03±0.09 and 3.87±0.31 at 11th week, 3.14±0.19 and 4.01±0.18 at 14th week, 3.38±0.37 and 4.05±0.07 at 16th week and 3.98±0.00 and 4.29±0.16 at 18th week for control and diabetic animals. These showed statistically significant differences from 9th week onward ($p=0.0003$, 0.0002, <0.001, 0.0025, 0.0134).

Conclusions

The development of diabetic neuropathy could be detected via molecular imaging targeting the retrograde axonal transport mechanism (neurography). This suggests that defective retrograde axonal transport is important in the development of diabetic neuropathy, and that imaging can play a role in diagnosing and monitoring the disease. Behavioral and imaging data were well correlated.

KEYWORDS: Diabetes, Nerve Imaging, Neurography



0-813

11:47AM - 11:54AM

Semi-Automated 3D Segmentation of Peripheral Nerves Using a Novel MR Neurography Postprocessing Software Tool

C Potter¹, J Fuller¹, L Lenkinski², A Rutman¹, K Maravilla¹

¹University of Washington, Seattle, WA, ²NerveVision, Toronto, Ontario, Canada

Purpose

MR neurography is limited in its ability to optimally display peripheral nerves due to their small size, low contrast and

Note: Scanned images are included in the proceedings. Some submitted images were reduced during editing thereby decreasing clarity. Also, refer to the Program Planner. Proceedings Content as of 3/28/2014.

complex course that does not conform well to traditional orthogonal imaging planes. This study seeks to evaluate and test a novel MR neurography program that provides 3D nerve segmentation for improved nerve display.

Materials and Methods

We retrospectively segmented and evaluated images from a series of patients who previously underwent MR neurography (MRN) of the ulnar, sciatic and femoral nerves to determine clinical utility. Images were obtained using a 3 T scanner and standard MRN imaging techniques, including high resolution STIR and fat suppressed T2 sequences to highlight nerve structures and suppress background tissues. Using the newly developed 3D MR neurography program (3D NerveVision, Milwaukee, WI), we were able to segment the peripheral nerves and display them in 3D. They then could be manipulated for optimal evaluation, including rotating the nerve in any plane, applying variable degrees of background tissue suppression, and highlighting various nerve features.

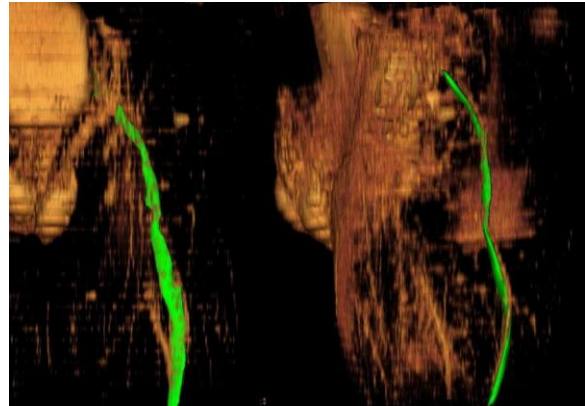
Results

The process requires initial nerve location/selection by the user at several points along its course with subsequent automatic tracking and contour formation. The user then confirms the programmatic selection and modifies the nerve boundary at any level for optimal segmentation. The resulting postprocessing provided excellent nerve visualization in the upper and lower extremities. Since the program utilizes semi-automated techniques for segmentation of the nerve tissue from adjacent structures, processing time was reasonable for an initial learner, taking approximately 5-10 minutes per nerve on average. Importantly, the nerve was well segmented while accurately maintaining the contour of the nerve and preserving signal intensity variation across the length of the nerve. Nerve intensity and size at each slice is measured easily for comparison using standard measurement tools. Next steps will be to improve the speed and accuracy of segmentation and test its clinical utility in a series of patients with blinded reader evaluations with and without nerve segmentation display.

Conclusions

This new 3D neurography postprocessing tool appears to provide excellent quality 3D peripheral nerve image display that can be used to display nerve structures in various projections for clinical interpretation and for treatment planning.

KEYWORDS: Nerve Imaging, Peripheral Nerve, Postprocessing



O-814

11:54AM - 12:01PM

Utility of MR neurography in identifying extraspinal disease in patients with lumbosacral neuropathy

N Benedetti¹, V Douglas¹, N Robbins¹, C Chin¹

¹University of California San Francisco, San Francisco, CA

Purpose

Low back pain/radiculopathy is the most common cause of disability in the United States and is experienced by 80% of the population at some point in their lives. MR imaging (MRI) has emerged as the imaging modality of choice for diagnosing the cause of low back pain. A newer technique, MR neurography of the lumbosacral plexus, is being used increasingly as an adjunct technique when standard lumbar spine MRI sequences fail to provide a diagnosis. MR neurography can be used to follow peripheral nerves as they course outside spine and is more sensitive than standard MRI sequences for detecting peripheral nerve disease that can present as low back pain and radiculopathy. We aim to demonstrate the added utility of neurography over standard lumbar spine MRI.

Materials and Methods

We conducted a retrospective chart review of 145 consecutive patients undergoing MR neurography of the lumbosacral plexus at our institution from 12/9/2012 to 11/6/2013. A GE MR imaging (MRI) scanner was used to produce axial and coronal STIR images through the lumbosacral plexus. All of the patients had prior lumbar spine MRI scans that failed to diagnose an etiology for their symptoms. The patient demographic information was obtained, and we categorized the indication for the studies as sensory symptoms, motor symptoms (i.e., weakness) or peripheral nerve tumors. Results of the MR lumbosacral neurograms were characterized as normal, nerve compression, nonspecific inflammation in a single nerve,

Note: Scanned images are included in the proceedings. Some submitted images were reduced during editing thereby decreasing clarity. Also, refer to the Program Planner. Proceedings Content as of 3/28/2014.

peripheral nerve tumor, iatrogenic radiation or surgical nerve damage, musculoskeletal abnormality, diffuse lumbosacral plexopathy and miscellaneous. The results also were correlated with the referring clinician's follow-up notes and clinical diagnosis.

Results

Of the 145 patients undergoing lumbosacral MR neurograms, 54% (n=79) of the patients were female and 45% (n=66) of the patients were male. Patient ages ranged from 16 to 89 years old. The indications for the studies were: sensory symptoms such as pain, numbness and tingling mostly in a sciatic nerve distribution (74%, n=107); weakness (13%, n=19), mixed motor and sensory symptoms (6%, n=8) and peripheral nerve tumors (8%, n=11). The results of the lumbosacral plexus MR neurograms for our 145 patients were abnormal in 56% (n=81), and only four of these studies had abnormal findings that the referring clinicians felt did not correlate with the symptoms, yielding a very low false positive rate of 6%. The most common abnormality identified was nerve compression (31%, n=25) caused by piriformis syndrome, ischiofemoral impingement, spinal hardware, neuroforaminal narrowing, or discosteophytes. Additional abnormalities that were identified include nonspecific inflammation in a single nerve (17%, n=14), peripheral nerve tumor (14%, n=11), iatrogenic radiation or surgical nerve damage (12%, n=10), musculoskeletal abnormality (11%, n=9), diffuse lumbosacral plexopathy (4%, n=3) and miscellaneous (6%, n=5).

Conclusions

In patients with unexplained low back pain or lower extremity neuropathic symptoms, lumbosacral MR neurography can be a useful imaging modality for demonstrating etiologies not identifiable on routine lumbar spine MRIs.

KEYWORDS: Neurography



O-815

12:01PM - 12:08PM

Ulnar Nerve Entrapment: MR Neurography Evaluation with Clinical and Surgical Correlation

K Sharma¹, Z Rumboldt¹, A Varma,¹ M Vittoria-Spampinato¹

¹Medical University of South Carolina, Charleston, SC

Purpose

Ulnar nerve entrapment at the elbow is the second most common entrapment neuropathy. High resolution magnetic resonance neurography (MRN) is used increasingly in the evaluation of entrapment neuropathy due to its ability to assess fine morphological features of the nerves as well as their relation to surrounding structures. We correlated MRN features of ulnar nerve entrapment at the elbow with clinical, electrophysiological and surgical findings, with the hypothesis that MRN would provide information complementary to electrophysiology.

Materials and Methods

We retrospectively reviewed MRN studies of 10 patients with suspected ulnar nerve entrapment at the elbow. All studies were performed using a 3 T MR scanner equipped with a dedicated extremity coil. Inclusion criteria were the following: suspected ulnar neuropathy; clinical evaluation at our institution; preoperative MRN; surgical treatment. All cases were reviewed by two radiologists in consensus and a score of 0 to 7 was calculated based on the imaging features including nerve T2 signal intensity (0:Normal;1:Increased), nerve caliber (0:Normal; 1:Mild

Note: Scanned images are included in the proceedings. Some submitted images were reduced during editing thereby decreasing clarity. Also, refer to the Program Planner. Proceedings Content as of 3/28/2014.

increase; 2: Moderate increase; 3: Severe increase), nerve fascicular pattern (0: Normal; 1: Abnormal), perineural fat stranding (0: Absent; 1: Present), and signs of muscle denervation (0: Absent; 1: Present). Patients were classified into three groups based on presurgical electrophysiological and clinical findings as follows: sensory neuropathy only (grade I); sensory and motor neuropathy (grade II); sensory neuropathy, motor neuropathy and muscle atrophy (grade III). Magnetic resonance neuropathy assessment of longitudinal extent of T2 signal hyperintensity of the nerve and likely site of entrapment (proximal to, within, or distal to the cubital tunnel) also were noted and correlated with surgical findings. Mann-Whitney test was used for statistical comparisons. P-value less than 0.05 was considered significant.

Results

Seven of 10 patients had grade III and three had grade II ulnar neuropathy. Magnetic resonance neuropathy scores varied between the grade II (1 to 4 MRN score) and grade III (5 to 7 MRN score) neuropathy groups and the difference was statistically significant ($p < 0.017$). Electrophysiological testing conclusively demonstrated focal ulnar neuropathy in seven of 10 patients with grade II and grade III neuropathy; it showed nonfocal nerve abnormality in two cases (clinically grade III) and was normal in one patient (clinically grade II). Imaging findings included T2 hyperintensity of the nerve (10/10), abnormal fascicular pattern (9/10), nerve thickening (9/10), perineural fat stranding (8/10) and muscle denervation changes (2/10). T2 hyperintensity, abnormal fascicular pattern, and perineural fat stranding were observed in both groups of patients. In patients with grade II neuropathy there was none to mild nerve thickening, while mild to severe nerve thickening was present with grade III. Magnetic resonance neuropathy identified the site of entrapment with 90% accuracy. In one patient MRN and surgical findings were discordant: MRN showed T2 hyperintensity and increased caliber of the ulnar nerve within the cubital tunnel; however, at surgery a fibrous band compressing the nerve was found proximal to the tunnel.

Conclusions

Magnetic resonance neuropathy is a promising modality for detection and localization of nerve abnormality in patients with ulnar nerve entrapment at the elbow. Integration of high resolution MRN into diagnostic algorithm of patients with ulnar entrapment can improve presurgical planning and influence patient management.

KEYWORDS: MR Neurography, Neurography

Thursday, May 22
10:30AM - 12:00PM
Room 517d

84 - MINI SYMPOSIUM STROKE - PART III:
BEYOND ROUTINE IMAGING

O-816

10:30AM - 10:45AM

Cerebrovascular Reserve and Oxygen Extraction Fraction

Lin, W.
Univ. of North Carolina at Chapel Hill
Chapel Hill, NC

Abstract/Presentation Summary

The search for means to identify patients who may benefit from tPA treatment beyond the approved therapeutic window has been actively pursued, particularly in light of recent success on the ECASS III (European Cooperative Acute Stroke Study III) trial, which demonstrated efficacy of tPA treatment could be extended from the original 3hrs to 4.5hrs from onset. In addition, with an accumulating arsenal of mechanical clot retrieval devices promising to achieve more effective reperfusion than IV-tPA, it is likely that the therapeutic windows for these retrieval devices will differ from that of IV-tPA. Toward this end, imaging approaches have been actively sought to potentially provide a signature for tissue viability. The diffusion/perfusion mismatch (DPM) concept represents the most widely adopted imaging approach to depict the "ischemic penumbra" to potentially select patients who may benefit from treatment beyond approved therapeutic windows. However, recent negative results from MR-RESCUE have called for additional refinements to the DPM approach and/or new imaging methods that exploit underlying metabolic alterations during hyper-acute stroke. Positron emission tomography (PET)-measured cerebral metabolic rate of oxygen utilization (CMRO₂) is capable of discerning brain tissue viability in both transient and permanent middle cerebral artery occlusion in primate models. However, the need for an onsite cyclotron as well as invasive arterial lines for quantitative measures have largely limited the clinical utility of PET, particularly for imaging acute stroke patients. Alternative MR approaches have recently been developed that are capable of providing information similar to PET derived CMRO₂. Here, we will discuss the current status of MR imaging approaches aimed at measuring oxygen metabolism/oxygen extraction fraction with special emphasis on their potential clinical applications. In

Note: Scanned images are included in the proceedings. Some submitted images were reduced during editing thereby decreasing clarity. Also, refer to the Program Planner. Proceedings Content as of 3/28/2014.

addition, new approaches on the horizon will also be discussed.

O-819

11:00AM - 11:15AM

Assessing Collateral Circulation

Liebeskind, D.
David Geffen School of Medicine at UCLA
Los Angeles, CA

O-823

11:30AM - 11:45AM

Chronic Neurovascular Uncoupling Syndrome

Mikulis, D.
Toronto Western Hospital
Toronto, ON

O-818

10:51AM - 10:57AM

Long-term survival probability following conservative therapy according to simple time-intensity curve's types of perfusion-weighted images in severe stroke patients due to the ipsilateral carotid-middle cerebral artery occlusion

T Mori¹, T Iwata¹, Y Miyazaki¹, Y Tanno¹, S Kasakura¹, Y Aoyagi¹

1Shonan Kamakura General Hospital Stroke Center,
Kamakura, Japan

Purpose

It is difficult to anticipate long-term survival probability (SP) in acute stroke setting. The aim of our study was to investigate whether or not simple time-intensity curve (TIC) types of perfusion-weighted images (PWI) was useful for anticipating long-term SP in severe acute stroke patients due to the ipsilateral carotid-middle cerebral artery occlusion.

Materials and Methods

Included were patients 1) who were transferred to our institution within 24 hours of onset between January 2005 and August 2013, 2) who underwent MR angiography (MRA) displaying the affected internal carotid and middle cerebral artery (IC-MCA) occlusion and 3) who were treated without any reperfusion therapy. We evaluated TIC types, any death within 90 days and clinical outcome at 90

days. Time-intensity curves were generated on regions of interest set at symmetrical positions of the bilateral MCA territories. According to the time to peak (TP) and the peak signal (PS) comparing the affected side (a) with the contralateral side (c), we classified TIC pattern into four types and defined type 1 as [TPa-TPc of 1 second (s) or more and PSa less than 0.25xPSc] or TPa-TPc of 18 s or more, type 2 as TPa-TPc of 1 s or more and less than 18 s and PSa of 0.25xPSc or more and less than 0.75xPSc, type 3 as TPa-TPc of 1 s or more and less than 18 s and PSa of 0.75xPSc or more, and type 4 as TPa-TPc less than 1 s.

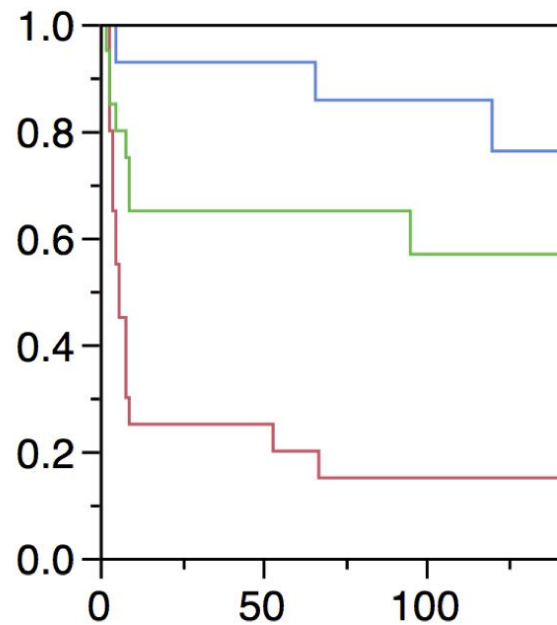
Results

Fifty-four patients were analyzed. There were 20, 20, 14 and 0 patients in type 1, 2, 3 and 4 of TICs. Twenty-seven patients (50%) died within 90 days, mostly within 10 days. In type 1, 2 and 3 of TIC, 17, eight and two patients died within 90 days, and SP of the Kaplan-Meier method at 90 days was 15%, 56.9% and 85.7% ($p < 0.0001$), respectively. Among 12 survivors of type 2 at 90 days, there were two of mRS of 3, two of mRS of 4 and eight of mRS of 5. Among 12 survivors of type 3 at 90 days, there were two of mRS of 2, two of mRS of 3, five of mRS of 4 and three of mRS of 5.

Conclusions

Time-intensity curve types of PWI were useful for anticipating long-term survival probability in acute stroke setting. We must rescue patients with type 1 and improve clinical outcome of patients with type 2 or 3.

KEYWORDS: MR Perfusion-Weighted Imaging, Outcome, Stroke



Note: Scanned images are included in the proceedings. Some submitted images were reduced during editing thereby decreasing clarity. Also, refer to the Program Planner. Proceedings Content as of 3/28/2014.

O-821

11:15AM - 11:21AM

Analysis of Reperfusion, Clinical, and Safety Results of Intra-arterial Ultrasound vs. Standard Microcatheter in The IMS Trials

T Evans1, T Tomsick2

1University of Cincinnati Medical Center, Springboro, OH, 2University Hospital/University of Cincinnati College of Medicine, Cincinnati, OH

Purpose

The purpose of this study was to further investigate the efficacy and safety of intra-arterial (IA) microcatheter versus IA-ultrasound (US) microcatheter-assisted thrombolysis in acute ischemic stroke in the Interventional Management of Stroke (IMS) Trials.

Materials and Methods

Interventional Management of Stroke I, II, and III subjects with ICA (ICAO) and M1 occlusions following reduced-dose rtPA were compared based upon whether IA thrombolytic therapy was administered via microcatheter or in conjunction with high frequency (1.7 MHz)/low energy US via EKOS Micro-Infusion US microcatheter. Comparisons of the primary clinical (mRS 0-2), reperfusion (mTICI 2-3), and safety endpoints, including symptomatic intracranial hemorrhage (SICH), and death, were recorded and compared for each study individually and cumulatively according to treatment method.

Results

Table 1 outlines individual study and cumulative total results for reperfusion, clinical, and safety end points for IMS I, II, III according to treatment method. Symptomatic intracranial hemorrhage was more common with US-catheter-assisted thrombolysis than with standard microcatheter in the IMS Trials (p=0.013).

Conclusions

The IMS III Trials yielded experienced higher percent SICH with use of US-assisted thrombolysis, with no differences in reperfusion or good outcome, compared to standard microcatheter treatment. While the data are not adjusted as yet for relevant clinical variables, data suggest risks of ICH should be monitored closely in future studies of ultrasound-assisted thrombolysis following administration of IV rtPA.

KEYWORDS: Stroke, Thrombolysis, Ultrasonography

Table	Standard Thrombolysis	Ultrasound-Assisted
1	(n=109)	(n=37)

	I	II	III	Total	I	II	III	Total
	(n=46)	(n=12)	(n=51)			(N=23)	(n=14)	(n=37)
mTICI	56.5 %	66.6 %	70.6% ³	64.5 %	*	56.5 %	71.4%	62.2%
I		8/12	6/51	71/109		13/23	10/14	23/37
2-3	26/46							
mRS	26.1%	50 %	29.4%	30.3%	*	30.4 %	28.6%	29.7%
0-2	12/46	6/12	15/51	33/109		7/23	4/14	11/37
	6.5%	7.7%	3.9%	5.5 %		21.7 %	14.3 %**	18.9 %
SICH			2/51		*			
	3/46	1/13		6/109		5/23	2/14	7/37

O-821

11:21AM - 11:27AM

Time and Infarct Size Dynamics in Major Anterior Circulation Ischemic Strokes

B Vachha1, R Hakimelahi2, J He1, M Higazi1, W Copen1, A Yoo1, M Lev1, P Schaefer1, R Gonzalez1

1Massachusetts General Hospital, Boston, MA, 2University of Texas Medical Branch, Galveston, TX

Purpose

Major anterior circulation ischemic strokes caused by occlusion of the distal internal carotid artery (ICA) or proximal middle cerebral artery (MCA) or both are an important subset of strokes, which account for about a third of all ischemic strokes and produce the most poor outcomes in this disease. These strokes are treatable by iv tPA and by endovascular methods with management governed primarily by time since stroke onset. However, the dynamics of infarct growth in these strokes are not well documented. The purpose of this study was to gain insight into infarct growth dynamics by measuring acute infarct size by diffusion-weighted (DWI) MR imaging (MRI) at known times after stroke onset in patients with documented ICA/MCA occlusions.

Materials and Methods

A total of 188 patients were included in the study. Forty-seven consecutive patients with terminal ICA or proximal MCA occlusions or both who underwent diffusion MRI within 30 hours of stroke onset were included in the retrospective part of this investigation. Prospectively, 141 patients were identified with the same inclusion criteria. Diffusion-weighted imaging lesion volumes were measured and compared to time since stroke onset.

Results

Note: Scanned images are included in the proceedings. Some submitted images were reduced during editing thereby decreasing clarity. Also, refer to the Program Planner. Proceedings Content as of 3/28/2014.

Acute infarct volumes ranged from 0.4 ml to 319 ml. There was no correlation between infarct size and time ($r^2 < 0.0006$, $p > 0.5$). The mean infarct volume was 61 ml and was similar when grouped into temporal cohorts. Using 70 ml as a threshold, the majority of patients fell under this threshold regardless of whether they were imaged less than or more than eight hours after stroke onset. In a subset of patients imaged over multiple time points, the majority had diffusion lesion growth that was less than 2 ml per hour.

Conclusions

The lack of correlation between infarct volume and time after stroke onset suggests that there are factors more powerful than time that determine infarct size within the first 24 hours. The observations may be explained if infarct dynamics are determined primarily by the collateral circulation; that there is wide variation in the vigor of this circulation; and that the pattern of infarct growth may be logarithmic, similar to animal models where a rapid early growth of infarcts is followed by a slower infarct growth phase. If verified, the clinical implications include the possibility of treating many patients outside traditional time windows.

KEYWORDS: Infarct Prediction, Stroke, Treatment Assessment

O-822

11:27AM - 11:31AM

Early Neurological Deterioration After Thrombolysis: Extra-penumbra Infarct Growth?

M Tisserand¹, P Seners¹, G Turc¹, L Legrand¹, M Labeyrie¹, J Méder¹, J MAS¹, J Baron¹, C Oppenheim¹

¹Sainte-Anne Hospital, INSERM U894, Paris, France

Purpose

Early neurological deterioration (END) without obvious cause (intracerebral hemorrhage, malignant edema...) is observed in about 7% of thrombolized patients. This could be explained by infarction of extra-penumbra tissue. To test this hypothesis, we compared infarct growth after treatment in patients with and without unexplained END (END+ and END-, respectively).

Materials and Methods

A case-control design was used for this study. From a population of 308 consecutive patients (2003-13) treated by iv rtPA ≤ 4.5 hours for anterior circulation stroke, we selected patients with unexplained END (END+ defined as Δ NIHSS 0-24 hours ≥ 4 points without obvious cause) with MR imaging (MRI) before [diffusion-weighted imaging

(DWI)+perfusion-weighted imaging (PWI)] and ~24 hours after treatment. Control patients (END-) were selected (3 controls per case) by individual matching for initial DWI volume, initial NIHSS, occlusion and 24 hour-recanalization. Automated coregistration of MRI images before and after treatment and semi-automated segmentation of DWI and PWI lesions were performed blind to clinical status and visually checked. We studied the volume of Progressing Acute DWI lesions (PAD, defined as hyperintense voxels on 24 hour DWI without any abnormality on initial DWI) within or beyond the penumbra ($T_{max} > 6s$).

Results

There were 10 eligible cases (END+). They did not differ from controls (END-) for age (mean \pm SD 73 ± 14 versus 63 ± 17 ; $p = 0.08$), initial NIHSS [median (IQR) 10 (8-12) versus 11 (7-15); $p = 0.52$], onset-to-treatment time [168 (122-210) versus 142 (110-185) min; $p = 0.27$], proximal occlusion i.e., internal carotid artery or proximal MCA [$n = 10$ (100%) versus $n = 25$ (83%); $p = 0.31$], initial DWI volume [13 (4-21) versus 14 (6-24) cc; $p = 0.98$] or mismatch volume [86 (49-142) versus 56 (32-104) cc; $p = 0.27$]. The volume of symptomatic tissue before treatment (core+penumbra) was also similar [END+ 97 (56-188) versus END- 87 (47-130) cc; $p = 0.44$]. PAD volume was larger in END+ than END- patients [median (IQR) 38 (24-81) versus 10 (3-31) cc, $p = 0.014$]. Furthermore, END+ had larger extra-penumbra PAD than END- patients [16 (10-350) versus 5 (1-16) cc, $p = 0.047$].

Conclusions

Unexplained early neurological deterioration after intravenous thrombolysis is associated significantly with, and probably caused by, infarct growth beyond penumbra.

KEYWORDS: MR Imaging/Diffusion, Stroke, Thrombolysis

O-824

11:45AM - 11:51AM

White matter Ischemic Changes in Patients with Hyperacute Ischemic Stroke: A Voxel-based Analysis Using Fractional Anisotropy and DSC Perfusion

K Nael¹, S Lafleur¹, B Coull¹, C Kidwell¹, E Krupinski¹, T Trouard¹

¹University of Arizona, Tucson, AZ

Purpose

Using diffusion tensor imaging (DTI)-fractional anisotropy (FA), the ischemic microstructural changes can be heterogeneous and variable between the infarction core and ischemic regions (1). The purpose of this study was to

Note: Scanned images are included in the proceedings. Some submitted images were reduced during editing thereby decreasing clarity. Also, refer to the Program Planner. Proceedings Content as of 3/28/2014.

evaluate the DTI-FA changes of white matter infarction and hypoperfusion in patients with acute ischemic stroke (AIS) using a quantitative voxel-based analysis.

Materials and Methods

The inclusion criteria for this prospective study were: patients with AIS who presented within six hours from symptom onset with acquisition of both DTI and DSC perfusion on a 3 T MR scanner (Skyra, Siemens). Dynamic susceptibility contrast perfusion was performed using a gradient-EPI sequence (TR/TE: 1450/22 msec, FA 90°, FOV: 22×22-cm, matrix 128 mm, voxel size 1.7 x 1.7 x 4 mm³, GRAPPA x3) after intravenous injection of 0.1 mmol/kg of Multihance-gadolinium contrast. Diffusion tensor imaging were acquired by using single-shot echo-planar imaging (TR/TE, 5500/82 ms; FOV: 22×22-cm; matrix 128 mm; voxel size 1.5 x 1.5 x 2 mm). Diffusion-sensitized gradients were applied along 20 noncolinear directions with a b-value of 1000 s/mm² resulting in four minutes acquisition time. The measured FA, apparent diffusion coefficient (ADC), and Tmax images were coregistered for voxel-based quantification using a region-of-interest (ROI) approach in the ipsilateral affected side and in the homologous contralateral white matter (WM). The infarction core and hypoperfusion were determined by threshold method defined as an ADC value less than 600 x 10⁻⁶ mm²/s and DSC-Tmax > 2 sec. A mask of the gray matter (FA threshold > 0.15) was generated for each patient to ensure extraction of voxel values is limited only to WM. The image analysis was performed by combination of FDA approved software (Olea Medical, La Ciotat, France) and Matlab. Data were analyzed by unpaired t-test.

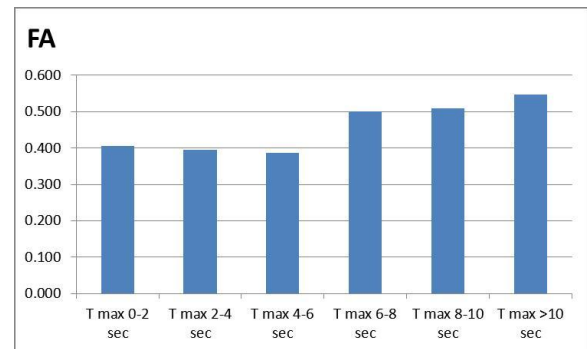
Results

Fifteen patients (9M, age 48-83 years old) met our inclusion criteria. The average time from onset to MR imaging was 4.3 hours and the NIH stroke scale range was 4-12. Total number of voxels included were 1100 for WM infarction, 5100 for WM hypoperfusion and 3300 for normal contralateral WM. The mean of FA values were significantly higher in the regions of WM hypoperfusion ($p < 0.0001$, $t: 7.90$) and significantly lower in the regions of WM infarction ($p < 0.0001$, $t: 6.52$), compared to FA values in the contralateral normal WM. In subanalysis of hypoperfused regions with different Tmax, the FA values were significantly higher ($p < 0.0001$, $t: 32.0$) in the hypoperfused WM with Tmax ≥ 6 sec in comparison to regions with Tmax < 6 sec with a mean difference of 0.14 (see Figure 1). The mean of Tmax values was significantly higher in both WM hypoperfusion ($p < 0.0001$, $t: 58.31$) and WM infarction ($p < 0.0001$, $t: 42.70$), compared to Tmax values in the contralateral normal WM. The mean ADC values were significantly lower in the WM infarction ($p < 0.0001$, $t: 58.3$) in comparison to hypoperfused WM and normal WM. There was no statistically significant difference between the mean ADC values in the WM hypoperfusion and normal WM ($p = 0.07$, $t: 2.1$).

Conclusions

Diffusion tensor imaging-FA is decreased in regions of WM infarction and increased in hypoperfused WM in patients with AIS. The FA values are significantly higher in the hypoperfused WM with Tmax ≥ 6 sec suggestive of early microstructural changes related to ischemia.

KEYWORDS: Actue Stroke, Diffusion Tensor Image, Dynamic Susceptibility Contrast-Enhanced



O-825

11:51AM - 11:57AM

Wake-up Stroke: Multimodal CT based Measurement of % Water-Increase in Ischemic Lesions as possible Surrogate Marker for Time of Onset

A Kemmling¹, G Broocks¹, M Ernst¹, J Minnerup², J Fiehler¹

¹University Medical Center Hamburg-Eppendorf, Hamburg, Germany, ²University Medical Center Münster, Münster, Germany

Purpose

In wake-up strokes, obtaining the time of symptom onset (T₀) has been a major focus of acute stroke imaging. In the early infarct core there is unidirectional increase of percent water content (edema) with time. The CT value calibrated at 100% water content (HU=0) correlates linearly with tissue density. The purpose of this study was to apply CT-based quantification percent water increase within early infarct core and test this physiological marker for determining T₀.

Materials and Methods

In CT, the product of volume and its density remains constant regardless of any amount of water added. When water of volume V_E is added to a volume V₀ with density D₀ resulting in a new volume V₁ and density D₁, then V₀×D₀=V₁×D₁=(V₀+V_E)×D₁ (Eq. 1). The proportion of

Note: Scanned images are included in the proceedings. Some submitted images were reduced during editing thereby decreasing clarity. Also, refer to the Program Planner. Proceedings Content as of 3/28/2014.

added water within V1 is $VE/V1$ which can be expressed as $1/(D1/(D0-D1)+1)$ (Eq. 2). The edematous infarct at time T1 with volume V1 and lowered density D1 has a percent water increase of $VE/V1$ which can be calculated from Eq. 2, where D1 is the density within the ischemic lesion at T1 (identified by CTP) and D0 is the density at T0 (measured in the healthy contralateral hemisphere). Precision of Eq. 1 and Eq. 2 was tested in a set of increasingly diluted iodine solutions. In 50 acute proximal MCA occlusive strokes, measurements of percent water content were correlated with time between symptom onset (T0) to imaging (T1). Receiver operating characteristic (ROC) curve analysis was performed to predict $(T1-T0) < 4.5$ hours.

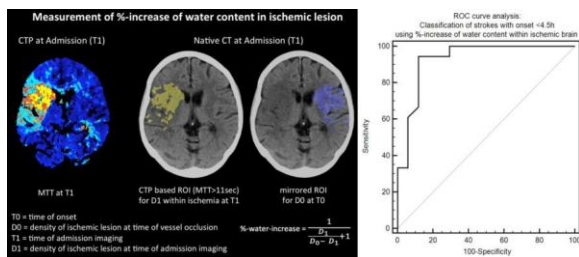
Results

The optimal cut-off value of percent water increase within the ischemic lesion to predict symptom onset < 4.5 hours was 7.0% (94.4% sensitivity, 88.2% specificity, AUC 0.93, $p < 0.0001$).

Conclusions

This novel approach of CT-based measurement of percent water increase within early ischemic brain is a reliable method to identify patients with time of symptom onset < 4.5 hours.

KEYWORDS: CT And Stroke, CT Perfusion, Stroke



Thursday, May 22
10:30AM - 12:00PM
Room 517a

85 - PARALLEL PAPERS: Brain: Functional
Imaging III

0-826

10:30AM - 10:37AM

Increased Between-Network Causal Connectivity in
Substance Dependence

N Saenz¹, K Maharajh², J Tregellas², Y Dorothy², R Perry²,
J Tanabe²

¹University of Colorado, Denver, CO, ²University of
Colorado, Aurora, CO

Purpose

Drug addiction may be associated with changes in the functional organization of the brain. The default mode network (DMN) and networks that underlie habit and executive control have been implicated in drug-seeking behavior (1, 2). While seed-based resting state analyses have demonstrated altered connectivity in brains of drug users (3, 4), the strength and direction of connectivity between larger functional networks has not been explored. The goal of this study was to investigate between-network connectivity and the direction of such connections using Granger causality analysis. We hypothesized that compared to controls, substance dependent individuals (SDI) would have stronger connectivity between the DMN (internal mental processing) and basal ganglia (habit formation) networks and weaker connectivity between executive control and DMN.

Materials and Methods

Fifty SDI (28M/22F, 34 ± 8 years) were compared to 50 controls (25M/25F, 32 ± 9 years). Substance dependent individuals met DSM-IV criteria for dependence on amphetamine and/or cocaine. Gradient recalled echo (GRE) functional MR imaging (fMRI) scans were acquired over five minutes during quiet rest with eyes closed. Data analysis using group independent component analysis was conducted on SDI and controls separately (GIFT toolbox). Fourteen independent components were selected automatically using template matching to a standardized set of resting state networks (http://findlab.stanford.edu/functional_ROIs.html) (5). Each network time series was concatenated across subjects. Signals were adjusted for motion, cerebrospinal fluid (CSF), and white matter signal fluctuations. Between-network connectivity was calculated using Granger causality. Group comparisons were conducted using nonparametric permutation statistical testing (200 iterations). Significance levels were set at $p < 0.05$, FDR-corrected for multiple comparisons.

Results

Substance dependent individuals showed more bidirectional connectivity whereas controls showed more unidirectional connectivity among the 14 network components (Figure 1). Furthermore, among 182 possible between-network pairs, only three pairs differed significantly in patients compared to controls. Compared to controls, SDI showed stronger connectivity from the DMN to the basal ganglia network and from the right executive control network to the DMN.

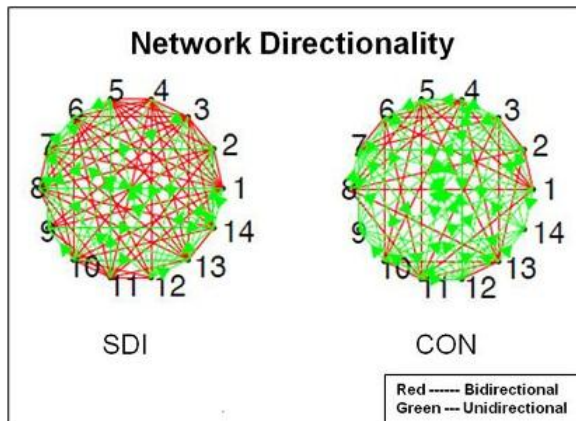
Conclusions

Greater connectivity from DMN to basal ganglia resting state networks in SDI compared to controls is consistent with the hypothesis that internal mental processes (DMN)

Note: Scanned images are included in the proceedings. Some submitted images were reduced during editing thereby decreasing clarity. Also, refer to the Program Planner. Proceedings Content as of 3/28/2014.

influence habit formation (basal ganglia) to a greater extent in SDI than controls. Pathological habit has been implicated in the persistence of drug-seeking behavior in SDI. Contrary to prediction, there was greater connectivity from the executive control network to DMN in SDI. Increased bidirectional connectivity may suggest overall less efficient functional organization in brains of drug users.

KEYWORDS: Functional Connectivity MR, Functional Networks, Resting-State FMRI



O-827

10:37AM - 10:44AM

Iron Particles as an MRI Contrast Agent May Differentiate Dural-Based Masses Better than Gadolinium Contrast

J Wagner¹, R Woltjer¹, S Gahramanov¹, G Nesbit¹, E Neuwelt¹, B Hamilton¹

¹Oregon Health & Science University, Portland, OR

Purpose

Enhancing dural-based intracranial masses often are diagnosed as meningiomas, however this may lead to inappropriate management when other pathology is encountered. Unlike gadolinium-based contrast agents (GBCA), ferumoxytol enhancement characteristics may better differentiate among causes of dural-based disease and may contribute to a better understanding of pathophysiology.

Materials and Methods

We searched the clinical records in our research database comprising two separate ferumoxytol neuroimaging protocols to retrieve all studies in patients imaged with dural-based intracranial masses. Cases from these

protocols with the same histopathology elsewhere in the central nervous system (CNS) and extracranial head and neck also were included. We retrospectively evaluated immediate and 24-hour delayed postferumoxytol scans using T1- and T2-weighted sequences and compared enhancement patterns to GBCA-enhanced scans obtained concurrently.

Results

Fifteen cases were identified in eight females and seven males (aged 34-76 years). Five meningiomas, one case each of hemangiopericytoma and schwannoma showed no intratumoral enhancement with ferumoxytol at any time. One extracranial hemangiopericytoma and transcranial paraganglioma showed only delayed enhancement. One meningioma showed delayed postferumoxytol enhancement. Three dural metastases showed delayed enhancement that was more prominent compared to GBCA-enhanced MR imaging (MRI). One dural and one intramedullary cavernous malformation showed immediate enhancement that increased at delayed imaging.

Conclusions

Ferumoxytol-enhanced MRI may better differentiate among causes of dural-based masses than GBCA-enhanced MRI. Nonenhancement likely reflects intact capillary tight junctions in benign disease. Blood-brain barrier compromise in malignant dural disease presumably leads to vascular exit and intracellular uptake. Immediate postferumoxytol enhancement is typical of vascular lesions and allows differentiation from benign and malignant dural neoplasms.

KEYWORDS: Brain Perfusion, Cancer, MR Imaging Perfusion

O-828

10:44AM - 10:51AM

Subject-Level Characterization of Functional Connectivity in Schizophrenia Utilizing Region-Specific Graph Theoretic Analysis

R Airan¹, J Pillai¹, S Gujar¹, H Sair¹

¹Johns Hopkins Medical Institutions, Baltimore, MD

Purpose

Given the heterogeneity across individual patients, to apply resting state functional MR imaging (rs-fMRI) assessed functional connectivity for clinical use, methods are needed that can assess individual subject whole-brain functional connectivity while retaining region-specific resolution. Here we develop methodology for quantification of inter-

Note: Scanned images are included in the proceedings. Some submitted images were reduced during editing thereby decreasing clarity. Also, refer to the Program Planner. Proceedings Content as of 3/28/2014.

network connectivity patterns in individual subjects, for assessing the contribution of individual brain regions to these results, and for comparison of individual subject connectivity to a control distribution. We apply this methodology to characterizing functional connectivity perturbations in a cohort of schizophrenic patients.

Materials and Methods

A publicly available dataset from the COBRE (1) research group was utilized. Briefly, the data included 72 schizophrenic patients spanning a variety of DSM 295 codes, with 75 group age-matched controls (ages 18-65 in each group). Available phenotypic information included DSM category, handedness, age, and gender. Each subject underwent T1 MPRAGE and five min BOLD fMRI (TR=2 sec) sequences. Data were preprocessed using FSL (FMRIB, Oxford, UK), SPM8 (Wellcome Trust, UK) and custom MATLAB (Mathworks, MA) scripts to complete slice-timing correction, rigid-body motion correction, segmentation and normalization to a standard template (MNI, 2mm), COMPCOR nuisance regression, bandpass temporal filtering (0.01-1Hz), and spatial smoothing (6mm Gaussian kernel). The whole brain gray matter (cortical, deep, and cerebellar) was parcellated automatically into 875 anatomically and functionally compact (2) regions of interest (ROIs). Each timecourse was extracted as the first eigenvariate of the set of voxel timecourses across the ROI. Pearson correlation coefficients between each pair of ROI timecourses were calculated. The set of average control correlation coefficients were fed as a weighted adjacency matrix (thresholded at the false discovery rate, FDR, for $\alpha=0.05$) into the infomap modularity algorithm (3) to generate a map of functional networks spanning gray matter. For each network and for each subject, the intra-network efficiency of the FDR thresholded adjacency submatrix was calculated using the Brain Connectivity Toolbox (4), with a similar measure applied to the internetwork efficiency. Individual subject network efficiency maps were calculated as z-scores relative to the distribution of control subjects.

Results

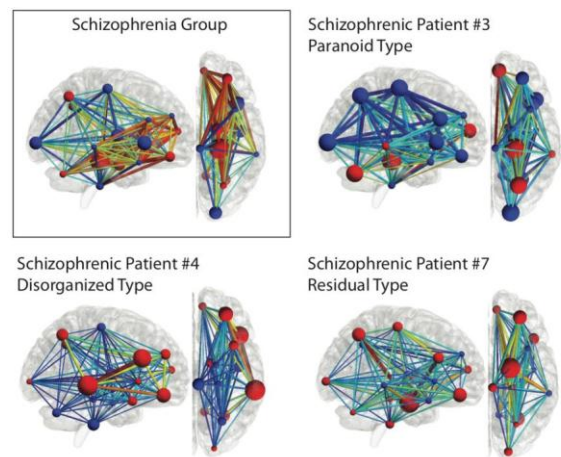
As shown, 17 networks spanning all of brain gray matter were detected (Figure, each node is plotted at the left hemisphere network centroid; networks were symmetric across midline) (5). Without any a priori information of expected network structure, the methods produced spatially compact, left-right symmetric, functionally related modules corresponding to known resting state networks (6). The differences in network efficiency between schizophrenics and control for each pair of networks (Figure, top left; red indicates increased efficiency in schizophrenics) show that this population has reduced internetwork efficiency in regions considered part of the salience network (anterior insula, dorsal anterior cingulate) but increased internetwork efficiency in limbic regions such as the amygdala, hippocampus and orbitofrontal cortex, overall consistent with prior studies (7, 8). In individual subjects, differing patterns of connectivity are seen seemingly dependent on the

particular DSM category of the schizophrenia (Figure, top right and bottom left and right).

Conclusions

We have developed a methodology for rs-fMRI analysis that allows for interrogation of whole-brain functional connectivity that can be traced back to individual brain regions of particular networks in individual subjects. We find patterns of group differences between schizophrenics and controls that are commensurate with those described in the literature (7, 8). We further identify particular patterns of connectivity in individual patients that show interesting variations depending on the individual subtype of schizophrenia.

KEYWORDS: Graph Theory, Psychiatry, Resting-State FMRI



0-829

10:51AM - 10:58AM

Brain Tumor Identification Using Gaussian Mixture Model Features and Decision Trees Classifier

A Chaddad¹, P Zinn¹, R Colen²
1MD Anderson Cancer Center, Houston, TX

Purpose

Image processing enhances the accuracy of imaging information for medical diagnosis; this is particularly the case with magnetic resonance imaging (MRI). The feature extraction process is the main step to obtain the information from raw medical images, and each feature can be described within image; most features are based on statistical computation. We propose a novel image processing method for glioblastoma (GBM) detection based on the Gaussian mixture model (GMM) features which represent the weighted sum of Gaussian component densities. Gaussian mixture model provides some features,

Note: Scanned images are included in the proceedings. Some submitted images were reduced during editing thereby decreasing clarity. Also, refer to the Program Planner. Proceedings Content as of 3/28/2014.

namely, mean, standard deviation and weight. These features are extracted from MR (T1, T2 and FLAIR) images in order to enhance GBM identification.

Materials and Methods

Multithresholding segmentation technique was applied on the morphological MR images (T1WI, T2WI, and FLAIR) to detect the abnormal area (GBM tumor); redundant features were discarded, thereby improving the performance of the feature-based scheme to detected GBM. The Decision Trees classifier was applied on the GMM features and reduced using three principal components to evaluate the classifier accuracy of cancer and normal area discrimination. The discrimination between GBM and normal tissue in the images, was compared using three performance indicators, namely, accuracy, false alarm and missed detection, and three modes of MRI images T1, T2 and FLAIR were employed.

Results

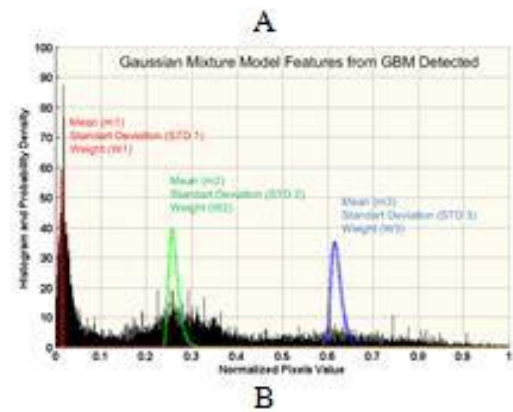
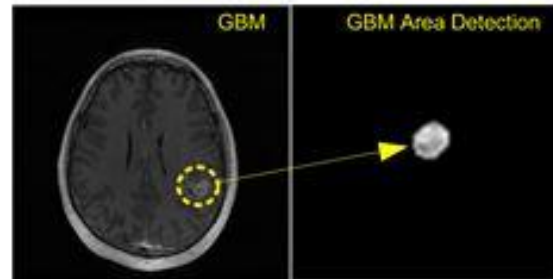
Seventeen images from each sequence T1-, T2-weighted and FLAIR were analyzed. We successfully applied new imaging features using the raw data images from 17 patients. Using the Decision Trees classifier, the GMM features demonstrated the best performance overall. For the T10- and T20-weighted images, the accuracy performance was 100% with 0% missed detection and 0% false alarm respectively. In the FLAIR mode, the accuracy decreased to 94.11% with 2.95% missed detection and 2.95% false alarm. The following figures show the simulation results of the present proposal.

Conclusions

Gaussian mixture model features successfully discriminate between GBM and normal tissue. The high accuracy of this technique demonstrates the efficiency of this work, and promises to enhance the GBM diagnosis. This is important as robust feature extraction is needed in order to develop imaging biomarkers that accurately reflect the genomic and pathologic composition of the tumor.

KEYWORDS: Classification, Glioblastoma

Simulation result of performance indicators based on the reduced GMM features			
MR mode	Accuracy	Flase alarm	Missed detection
T1	100	0	0
T2	100	0	0
FLAIR	94.11	2.95	2.95



O-830

10:58AM - 11:05AM

High Resolution DTI of the Optic Pathway in NF1 Patients with Readout-segmented, Multi-shot Echo Planar Imaging at 3T

C Ho1, J West1, C Lin1, S Kralik1, Y Wang1, D Porter2, A Saykin1, C Shih3

1Indiana University School of Medicine, Indianapolis, IN, 2Siemens AG Munich, Munich, Germany, 3Riley Hospital for Children, Indianapolis, IN

Purpose

Children with neurofibromatosis type 1 (NF1) have up to a 40% incidence in developing optic nerve glioma associated with visual loss. Diffusion tensor imaging (DTI) may be helpful in assessing optic pathway integrity as a marker for treatment in these patients. However, susceptibility artifacts that are common in conventional DTI using single-shot echo planar imaging (EPI) can severely distort areas of interest such as the optic tracts and optic chiasm. As such, a readout-segmented multi-shot EPI technique (rsEPI) (Siemens RESOLVE, Erlangen Germany) was utilized to minimize susceptibility distortions of the skull base which may preclude accurate diffusion tensor evaluation of the optic apparatus.

Note: Scanned images are included in the proceedings. Some submitted images were reduced during editing thereby decreasing clarity. Also, refer to the Program Planner. Proceedings Content as of 3/28/2014.

Materials and Methods

IRB approval was obtained for this prospective pilot study. Healthy adult volunteers, children with NF1 with and without optic gliomas as previously diagnosed with MR imaging were recruited. A final axial protocol, consisting of seven shots, 12 diffusion directions, b-values of 0, 250, 500, and 800, 1.2 x 1.2 x 2.2 mm³ voxel resolution, and 16 slices was chosen on 3 T scanners (Siemens Verio and Trio, Erlangen, Germany). Positioning of the slices was done to cover the optic tracts, optic chiasm, and as much of the optic radiations as possible. Healthy adult volunteers were scanned with both the conventional product DTI and rsEPI technique, matching FOV, resolution, b-values, and diffusion direction scheme. Fractional anisotropy (FA) maps of the optic nerves and tracts for both product and rsEPI were evaluated for significant differences. Fractional anisotropy data sets consisting of subjects with NF1 with and without optic gliomas were evaluated by two fellowship-trained neuroradiologists separately for region of interest (ROI) placement along the bilateral intraorbital, intracanalicular, and prechiasmatic optic nerves, chiasm, bilateral optic tracts and Meyer's loops. The resulting FA and mean diffusivity (MD) values were analyzed for appreciable changes in patients with NF1 with and without optic gliomas.

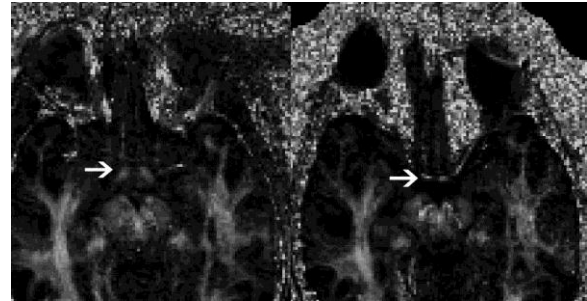
Results

Five healthy adult volunteers, three children (ages 7-15 years) with NF1 without optic glioma, and four children (ages 4-18 years) with NF1 with optic glioma were imaged. T-test of the means of the FA on the optic nerves and tracts on healthy volunteers were significantly higher in the rsEPI (0.49 ± 0.14) compared to product DTI (0.29 ± 0.12) ($t=2.94$, $p=0.011$). The mean of the FA values from both neuroradiologists were significantly higher ($t=3.07$, $p=0.0025$) in NF1 patients without tumor (0.59 ± 0.12) versus NF1 patients with optic gliomas (0.52 ± 0.14). Conversely, mean MD values from both neuroradiologists were significantly higher ($t=3.26$, $p=0.0014$) in NF1 patients with tumor (0.00098 ± 0.0003 mm²/s) versus NF1 patients without optic gliomas (0.00082 ± 0.0003 mm²/s). Comparison of FA values between healthy volunteers (0.49 ± 0.14) and NF1 patients without optic gliomas (0.59 ± 0.12) were not significant ($t=1.93$, $p=0.09$). Figure A shows axial FA map from rsEPI technique with visualization of the chiasm (arrow) in a healthy adult volunteer. In contrast, Figure B of the same volunteer shows product DTI FA map at the same level with significant distortion of the chiasm (arrow).

Conclusions

High resolution DTI with readout-segmented multi-shot EPI technique can better visualize the optic pathway and allow more confident measurements of anisotropy. This is shown by a significant increase in FA with rsEPI versus product DTI. Also, in patients with NF1, FA decreases and MD increases with the development of optic gliomas. Further study with a larger patient population would be necessary to establish treatment thresholds.

KEYWORDS: DTI, Neurofibromatosis, Optic Nerve



O-831

11:05AM - 11:12AM

Intracranial Atherosclerotic Disease: Impact of Regional Stenotic Lesions on Systemic Intracranial Hemodynamics

C Wu¹, S Prabhakaran¹, T Carroll¹, P Vakil¹, N Chatterjee¹, A Honarmand¹, S Ansari², J Carr¹, M Markl¹

¹Northwestern University, Chicago, IL, ²Northwestern University Feinberg School, Chicago, IL

Purpose

Digital subtraction angiography (DSA) is the gold standard for the diagnosis and evaluation of intracranial atherosclerotic disease (ICAD). Cerebral hemodynamic factors were considered to be critical in the development and risk stratification of ICAD. The purpose of this study was to evaluate the feasibility of 4D flow MR imaging for the comprehensive evaluation of the impact of regional stenotic lesions on intracranial hemodynamics in all major vascular territories of the brain including quantitative analysis of peak velocity and mean blood flow in the large intracranial vessels.

Materials and Methods

Twenty-one symptomatic ICAD patients (11 male + 10 female, age=65±16 years) with mild to severe intracranial vascular stenosis and three normal volunteers were included in this study. The stenosed vessels in these patients were internal carotid artery (ICA, n=8), middle cerebral artery (MCA, n=7), vertebral artery (VA, n=2), basilar artery (BA, n=5), and posterior cerebral artery (PCA, n=3). Four-dimensional flow data acquisition with ECG synchronization (TR/TE=5.2/2.8ms, flip angle=15°, VENC=80-100cm/s, spatial resolution=1.1mm×1.1mm×1.5mm, temporal resolution=42ms, acquisition time=15-20min) was performed for all subjects on a 1.5 T MRI scanner (Siemens, Germany). Intracranial hemodynamics was visualized by time-integrated 3D pathlines demonstrating the

Note: Scanned images are included in the proceedings. Some submitted images were reduced during editing thereby decreasing clarity. Also, refer to the Program Planner. Proceedings Content as of 3/28/2014.

cumulative flow path over one cardiac cycle in all major intracranial arteries and veins (example for left ICA and right MCA stenosis in the figure). Peak velocity (m/s) and mean blood flow (ml/s) in manually positioned planes were quantified at different vascular regions (EnSight, CEL, USA). Due to limited spatial resolution of 4D flow MRI, locations proximal to the stenosis were used for flow quantification. Blood flow and peak velocity ratios of the nonaffected versus affected side (N/A) or the right versus left side (R/L) for BA stenosis and volunteers were calculated in four vascular territories (ICA, MCA, PCA, and ACA) for all subjects.

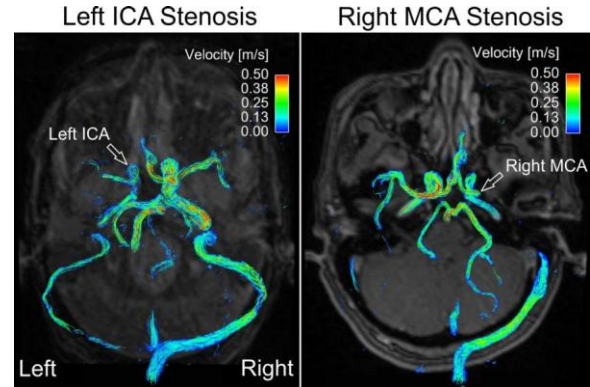
Results

For the healthy subjects, blood flow velocities were distributed coherently across the brain vessels [R/L blood flow and peak velocity ratios: ICA (1.03±0.03, 0.92±0.10), MCA (1.01±0.07, 1.04±0.16), PCA (0.98±0.05, 1.06±0.09), ACA (1.12±0.15, 1.00±0.20)]. For the patients with ICA stenosis, highly asymmetric blood flow and peak velocity were observed in the other three vascular territories in MCA (2.27±2.31, 1.34±0.52), PCA (0.70±0.19, 0.86±0.25), and ACA (5.16±6.25, 1.13±0.60). Similarly for those patients with MCA stenosis, highly asymmetric flow and peak velocity were observed in the vascular territories in ICA (2.46±2.14, 1.60±1.16), PCA (0.76±0.24, 0.95±0.53) and ACA (0.77±0.39, 0.80±0.23). We also noted that the blood flow ratios in PCA were opposite to the ratios in ICA and MCA, which indicated intracranial blood flow redistribution due to regional stenotic lesions. However, the impact of regional PCA and BA stenosis on the hemodynamics in other vascular territories (e.g., ICA, MCA) were not significant. In addition, we found that the blood flow proximal to the stenosis (ICA: 3.16±1.45ml/s; MCA: 1.20±0.52ml/s) were significantly lower compared with the normal contralateral vessels (ICA: 7.17±2.38ml/s; MCA: 3.65±0.82ml/s) in two subgroups with ICA (p=0.002) and MCA (p<0.001) stenosis.

Conclusions

Our findings demonstrated significant impact of regional stenotic lesions on the hemodynamics in other vascular territories. Quantitative hemodynamic markers in the major intracranial vessels may provide additional insight into the pathophysiology and risk stratification for ICAD patients. In addition, 4D flow imaging may be useful for the monitoring of intracranial hemodynamic alterations for ICAD patients during interventions.

KEYWORDS: Hemodynamics, Intracranial Atherosclerosis, Phase Contrast Imaging



0-832

11:12AM - 11:19AM

Diffusion Tensor Imaging Measures in Posterior Limb of the Internal Capsule Correlate with Motor Function Outcome in Stroke Patients

J Song¹, L Walton¹, B Young¹, V Nair¹, S Vergun¹, M Tyler¹, J Sattin¹, D Farrar-Edwards¹, J Williams¹, V Prabhakaran¹

¹University of Wisconsin Madison, Madison, WI

Purpose

Motor outcome prediction is important in determining the effective rehabilitation strategy provided for stroke patients. Recent advances in neuroimaging techniques have contributed to motor outcome prediction after stroke. Studies using magnetic resonance imaging (MRI) suggest that stroke location rather than the volume of an infarct is more important for predicting functional outcomes (1, 2) and that lesions of the internal capsule were associated with a significantly lower probability of return of isolated hand motor function than lesions of the cortical, subcortical regions and corona radiata (3). In this study, we examined the relationship between structural integrity of the posterior limb of internal capsule (PLIC) measured using diffusion tensor imaging (DTI) and upper limb motor outcome in stroke patients.

Materials and Methods

Diffusion tensor imaging (DTI) data were obtained from nine stroke patients (6 male, chronicity of stroke range 2-23 months) with persistent upper-extremity motor deficits who completed maximum 15 sessions' interventional rehabilitation facilitated by Brain-Computer Interface (BCI) and Functional Electrical muscle Stimulation (FES). Neuroimaging scans and clinical motor outcome assessment including the hand function domain of Stroke Impact Scale (SIS) and the Action Research Arm Test (ARAT), were conducted at four time points for all patients:

Note: Scanned images are included in the proceedings. Some submitted images were reduced during editing thereby decreasing clarity. Also, refer to the Program Planner. Proceedings Content as of 3/28/2014.

pre-, mid-, post- and one-month-after intervention. Values of fractional anisotropy (FA), axial diffusivity (AD), radial diffusivity (RD) and mean diffusivity (MD) were computed for the white matter tracts of PLIC. Asymmetry index of each DTI-derived metric comparing ipsilesional and contralesional PLIC--(Value_contralesional - Value_ipsilesional)/(Value_contralesional + Value_ipsilesional), was further calculated. The asymmetry scores range from -1 to 1, with positive and negative values indicating reduced or increased DTI measures respectively in ipsilesional PLIC relative to the contralesional PLIC, a value of 0 indicating an equivalent measurement between the two hemispheres. Values of DTI-derived metrics and asymmetry index of each metric were assessed in relation to the motor outcome measurements, respectively.

Results

Ipsilesional PLIC showed significantly reduced FA and increased diffusivity (AD, RD and MD) compared with contralesional side. Regression analyses on the PLIC DTI and motor function measurements revealed that better performance in motor outcome measures was related to higher FA values and lower diffusivity in ipsilesional PLIC. Asymmetry indices of DTI-derived metrics also showed significant correlation with motor function outcomes (all p-values < 0.00001 for regression coefficients), with lower FA asymmetry scores and higher diffusivity asymmetry scores associated with better motor function performance (Figure 1; Table 1).

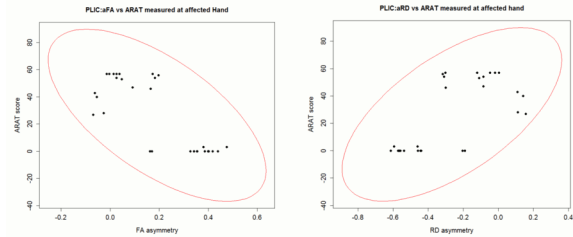
Conclusions

The results of this study suggest that motor functional recovery of upper-limb extremity in stroke patients receiving BCI-facilitated intervention relates to microstructural status of the PLIC. Thus DTI-derived measures may be applicable for upper-limb motor outcome prediction and in monitoring the effect of therapy. Asymmetry indices of DTI-derived measures were shown to be stronger predictors compared to pure DTI measures, which may reflect a potential remodeling of both the ipsilesional and contralesional PLIC in stroke recovery.

KEYWORDS: Biomarkers, Diffusion Tensor Image, Stroke

		FA	AD	RD	MD	aFA	aAD	aRD	aMD
SIS-Hand function	Regression coefficient	234.98	-12.79	-50.51	-53.53	-138.95	163.29	87.35	110.62
	p-value	1e-05	0.73	2.81e-03	0.026	1.01e-08	5.66e-05	4.39e-05	2.47e-05
ARAT	Regression coefficient	80.26	-36.48	-34.46	-34.67	-114.94	135.78	71.18	91.17
	p-value	0.13	0.067	1.25e-04	1.55e-03	6.05e-08	1.49e-05	3.05e-05	1.38e-05

Figure 1: Shown are asymmetry indices of FA and RD correlating with upper limb function measured by ARAT.



O-833

11:19AM - 11:26AM

White Matter Diffusion Abnormalities in Carotid Artery Disease: A Systematic Review and Meta-analysis

H Baradaran¹, E Mtui², A Dunning¹, J Richardson¹, D Delgado¹, P Sanelli², A Gupta²

¹Weill Cornell Medical College, New York, NY, ²New York Presbyterian Hospital, Weill Cornell Medical College, New York, NY

Purpose

Abnormalities in apparent diffusion coefficient (ADC), fractional anisotropy (FA), and mean diffusivity (MD) values can be used to assess microstructural damage to white matter tracts and could represent a quantitative marker of chronic ischemia and thereby potentially serve as a stroke risk factor. We performed a systematic review and meta-analysis to evaluate the association between unilateral carotid stenosis/occlusion and ipsilateral ADC, FA, or MD abnormality.

Materials and Methods

With the aid of an experienced medical librarian, we performed a comprehensive literature search evaluating the association of carotid stenosis/occlusion and quantitative white matter diffusion imaging, including ADC, FA, and MD values. The included studies were retrospective or prospective studies examining patients for ADC, FA, and MD values ipsilateral and contralateral to the site of carotid artery disease. A meta-analysis using standardized mean differences with assessment of study heterogeneity and publication bias was performed.

Results

Of the 2920 manuscripts screened, seven met eligibility for systematic review including a total of 257 patients. Of the manuscripts included for meta-analysis, three studied ADC values, six studied FA values, and three studied MD values. The standardized mean difference for ADC, FA, and MD values between cerebral hemispheres ipsilateral and

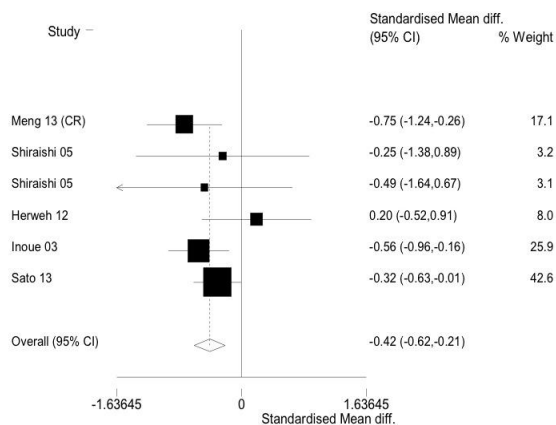
Note: Scanned images are included in the proceedings. Some submitted images were reduced during editing thereby decreasing clarity. Also, refer to the Program Planner. Proceedings Content as of 3/28/2014.

contralateral to carotid artery disease site were 1.13 (95% CI: 0.79-1.47, $p < 0.001$), -0.42 (95% CI: -0.62 to -0.21, $p < 0.001$), and 0.23 (95% CI: -0.32-0.77, $p = 0.41$), respectively. Measures of heterogeneity showed mild heterogeneity and no statistically significant publication bias in any of the three meta-analyses.

Conclusions

Carotid artery steno-occlusive disease is associated with significant ADC and FA value changes, suggesting that carotid disease is associated with quantifiable white matter microstructural damage. Further work is warranted to assess the ability of white matter diffusion imaging abnormalities to predict clinically evident ischemic events.

KEYWORDS: Carotid Stenosis, Stroke, White Matter Tracts



O-834

11:26AM - 11:33AM

Diffusion and Perfusion Weighted Imaging in Acute Stroke: How Well Do Diffusion Restricted, Perfusion-Diffusion Mismatch Ratios and Hypoperfused Volumes Correlate with Clinical Outcomes?

L Vaughn1, M Bajaj1, A Capizzano1, T Moritani1

1University of Iowa Hospitals and Clinics, Iowa City, IA

Purpose

Treatment decisions in patients with acute stroke often are made based upon imaging findings at MR imaging (MRI) including diffusion (DWI) and perfusion (PWI) sequences. The role of "penumbra" imaging, however, is still not established in clinical practice. Our aim is to correlate stroke outcome with DWI restricted lesion volume and volume of hypoperfused brain tissue.

Materials and Methods

We obtained IRB approval for this retrospective study. We did a search for MRI performed with PWI for evaluation of acute stroke. Our search returned 197 patients. Thirteen patients were excluded from the final analysis (12 had no PWI performed and 1 PWI study was performed for evaluation of brain tumor, not stroke). On a Vitrea workstation, we utilized OLEA software for postprocessing of PWI and DWI studies. The arterial input function was selected automatically by the software. The following perfusion parameters were obtained: mean transit time (MTT), cerebral blood flow (CBF), cerebral blood volume (CBV) and Tmax. The DWI lesion volume was calculated by setting an ADC value threshold level to match the DWI abnormality. The volume of hypoperfused brain tissue was calculated using the Tmax, with threshold level typically set at six seconds. Finally, we performed a chart review to correlate the clinical outcomes with the DWI restricted volumes and volumes of hypoperfused brain tissue. In our initial evaluation, we assessed the first 35 patients. Treatment outcomes were defined as the change in NIH Stroke scale value (NIHSS) between admission and discharge. A poor clinical outcome was defined as a decrease in NIHSS less than four. We performed a statistical analysis utilizing the SPSS Statistics Data Editing software. We performed a Pearson correlation in order to identify how well hypoperfused volume, DWI restricted lesion volumes and PWI-DWI Mismatch Ratios correlated with NIHSS values at admission and discharge.

Results

There were 35 patients in our initial evaluation with average age 69 years (range 40-92 years). There were 15 males and 20 females. Eight patients were excluded from our final analysis due to the absence of either an admission or discharge NIHSS value. The range of diffusion restricted lesion volumes included in the initial evaluation was 2.3-153 mL. The range of hypoperfused volumes included in the initial evaluation was 0.46-243 mL. Fourteen patients had a poor clinical outcome as defined by our study. The mean of DWI restricted lesion volumes in this subset of patients was 48.6 mL [standard deviation (std. dev.) 43.6]. The mean of hypoperfused volumes in this subset of patients was 92.5 mL (std. dev. 53.5). Thirteen patients had a good clinical outcome as defined by our study. The mean of DWI restricted lesion volumes in this subset of patients 35.2 mL (std. dev. 36.7). The mean of hypoperfused volumes in this subset was 61.9 mL (std. dev. 55.5). No significant difference in DWI restricted lesion volumes or hypoperfused volumes between our two subsets of patients was seen. A statistically significant correlation was detected between hypoperfused volumes and DWI restricted volumes ($r=0.753$, $p < 0.001$), NIHSS at admission ($r=0.700$, $p < 0.001$), and NIHSS at discharge ($r=0.748$, $p < 0.001$). The DWI restricted lesion volumes also correlated significantly with the NIHSS values at admission ($r=0.535$, $p=0.004$) and discharge ($r=0.507$, $p=0.01$), although to a lesser degree. The PWI-DWI mismatch ratios showed no significant correlation to either NIHSS value at admission or discharge. A partial correlation of

Note: Scanned images are included in the proceedings. Some submitted images were reduced during editing thereby decreasing clarity. Also, refer to the Program Planner. Proceedings Content as of 3/28/2014.

hypoperfused volumes and NIHSS values was performed, controlling for age, sex and DWI restricted volume. This showed that hypoperfused volume has a statistically significant correlation with NIHSS values at admission ($r=0.592$, $p=0.004$) and discharge ($r=0.662$, $p=0.001$), independently of the other variables.

Conclusions

In our initial assessment of 35 patients, those with poor outcomes tended to have higher DWI restricted volumes and hypoperfused volumes relative to those who had good clinical outcomes, although this did not reach statistical significance. We were able to show that there is a statistically significant correlation between hypoperfused volumes and NIHSS values at admission and discharge. A significant correlation also is seen between DWI restricted volumes and NIHSS values, although to a lesser degree. The correlation of hypoperfused volumes with NIHSS values was independent of DWI restricted lesion volume, age and sex. No significant correlation is seen with PWI-DWI mismatch ratios and NIHSS values at admission or discharge, emphasizing that mismatch ratios must be interpreted in the context of DWI restricted lesion and hypoperfused volumes. We believe that a further analysis of the remaining patients in our study will allow us to better delineate the relative importance of DWI restricted lesion and hypoperfused volumes in stratifying patients for potential treatment.

KEYWORDS: Diffusion-Perfusion Mismatch, Diffusion-Weighted Imaging, Stroke

0-835

11:33AM - 11:40AM

Variables of 123I-IMP SPECT by graph plot method relating to elevation of blood sampling global oxygen extraction fraction in patients with a high-grade carotid stenosis

T Mori1, T Iwata1, Y Miyazaki1, Y Tanno1, S Kasakura1, Y Aoyagi1, K Yoshioka1

1Shonan Kamakura General Hospital Stroke Center, Kamakura, Japan

Purpose

Hyperperfusion syndrome is likely to occur in patients who undergo CEA or CAS for a high-grade carotid stenosis causing hemodynamic failure of stage 2 or 3 compared to stage 1. However, it is difficult to identify patients with stage 2 or 3 in general hospitals. In patients with stage 2 failure, oxygen extraction fraction (OEF) is elevated to maintain cerebral metabolic rate of oxygen (CMRO₂). Not regional but global OEF can be calculated from blood

sampling and SPECT also can be performed in general hospitals. The aim of our study was to investigate whether or not some variables of 123I-IMP SPECT by graph plot method is related to elevation of blood sampling oxygen extraction fraction (OEF).

Materials and Methods

Included in our study were patients 1) who underwent elective CAS for symptomatic or asymptomatic lesions between September 2010 and July 2013, 2) who underwent 123I-IMP SPECT before CAS and 3) in whom blood sampling OEF was calculated just before CAS. Oxygen extraction fraction was calculated from cerebral arteriovenous oxygen difference. Arterial blood was sampled from the common carotid artery and venous blood from the dominant-sided superior jugular bulb. Variables of 123I-IMP SPECT calculated with graph plot method were as follows; supra- and infra-tentorial cerebral blood flow (CBF) on regions of interest (ROIs) set in the affected (a) and contralateral (c) sided MCA territory before and after 1 gram acetazolamide challenge (D). Cerebral blood flow against ipsilateral cerebellar blood flow (MCA/CE) was calculated as CBF(a) divided by cerebellar BF(a) x 100, cerebral vasoreactivity (CVR) as (D_CBF(a) - CBF(a)) divided by CBF(a) x100 and asymmetry index (AI) as CBF(a) divided by CBF(c) x 100. Evaluated were relationship between elevated OEF and SPECT variables.

Results

During the study period, 142 patients matched to our criteria. Average age, OEF, CBF(a), CBF(c), MCA/CE(a) and CVR(a) were 74.4±6.7 years, 0.42±0.075, 39.3±7.5 ml/min/100g, 39.9±7.9 ml/min/100g, 87.3±16% and 26.9±21, respectively. Median OEF and MCA/CE were 0.41 (0.37-0.47; IQR) and 88.9% (76-98). When cut-off value of significant elevation of OEF was defined as 0.47 (the third quartile), there were significant differences in MCA/CE(a) ($p<0.05$), CBF(a) ($p<0.05$) and CBF(c) ($p<0.05$) between elevated and nonelevated OEF groups. Stepwise regression analysis showed that MCA/CE was only an independent significant variable ($p<0.05$) for OEF elevation of 0.47 or more. Receiver operating characteristic curve displayed that cut-off point of MCA/CE was 88.9%. Two by two table showed that there was a significant difference between MCA/CE of 88.9% or less and OEF of 0.47 or more ($p<0.01$, odds ratio of 3.1). AI, CVR and D_MCA/CE were not related to elevated OEF.

Conclusions

Middle carotid artery/CE in the affected side calculated from 123I-IMP SPECT values by graph plot method significantly related to elevation of blood sampling global OEF.

KEYWORDS: Carotid Artery Stenting, Hemodynamics, Oxygen

Note: Scanned images are included in the proceedings. Some submitted images were reduced during editing thereby decreasing clarity. Also, refer to the Program Planner. Proceedings Content as of 3/28/2014.

O-836

11:40AM - 11:47AM

Highly Selective MRI-Guided Targeting of Chemotherapy to the Brainstem Across a Focally Disrupted Blood Brain Barrier in a Rabbit Model.

M Pearl¹, M Janowski¹, E Wyse², E Ngen¹, A Gilad¹, A Bar-Shir¹, P Walczak¹

¹Johns Hopkins University School of Medicine, Baltimore, MD, ²Johns Hopkins Hospital, Baltimore, MD

Purpose

Inadequate penetration of chemotherapeutic agents across an intact blood-brain barrier (BBB) and lack of methodology for precise drug delivery represents a major therapeutic challenge in the treatment of pontine gliomas. The purpose of this study is to demonstrate that intra-arterial (IA) chemotherapy administration can be performed with high precision after focal blood-brain barrier disruption (BBBD) and that parenchymal penetration of drug-sized molecules can be validated with fluorescent microscopy.

Materials and Methods

Our IACUC approved this protocol. Using a hybrid MR imaging (MRI) angiography suite (Miyabi, Siemens), the left vertebral artery of 4-kg New Zealand white rabbits was catheterized with a 4-French catheter. A 1.7-French microcatheter then was advanced into the basilar artery. The rabbits were transported to a 3 T MRI (Magnetom Trio, Siemens) for anatomical reference images [horizontal and sagittal T2-weighted (TR/TE=1500/105)]. Real-time assessment of trans-catheter contrast-enhanced perfusion territory using GE-EPI sequence (TR/TE=3000/30; 60 measurements) was performed during infusion of iron oxide nanoparticle solution (Feraheme) (rates of 0.001-0.1ul/s). Intra-arterial mannitol (25% over 5 minutes at the predetermined optimized infusion rate) was administered for focal BBBD. Intravenous gadolinium (Magnevist, 0.5 mM, 0.125 mmol/kg) was administered followed by T1-weighted (TR/TE=300/9.1) images. Intra-arterial fluorescein isothiocyanate (FITC) (19 μmol), a surrogate marker for the chemotherapy drug melphalan, then was infused. The brains were immediately harvested and snap frozen on crushed dry ice. Cryo-sectioned tissue slices were counterstained with DAPI and imaged by fluorescence microscopy (Zeiss) for detection of extravasated fluorescein. The drug (melphalan) was conjugated to a fluorescent moiety (fluorescein) to obtain a melphalan-fluorescein conjugate, for subsequent studies of direct monitoring of this drug across the BBB. The conjugate then was purified using silica-gel columns and characterized by HPLC, NMR, and MS.

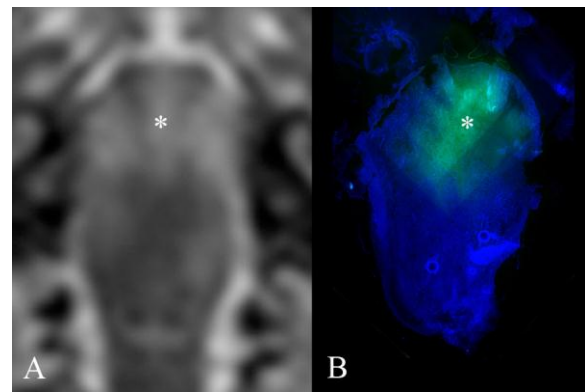
Results

Feraheme-enhanced real-time MRI demonstrated an optimal injection rate of 0.01 ml/sec to selectively perfuse the pons. Using this rate, IA mannitol resulted in specific pontine BBBD as visualized by gadolinium enhanced T1-weighted images. Post-mortem evaluation of fluorescein distribution correlated well with T1 enhancement (Figure 1). Horizontal postgadolinium T1-weighted image (A) and histological preparation of a brain slice through the pons and medulla demonstrate pontine enhancement (asterisk) and pontine uptake of FITC (green) with nuclear DAPI counterstain (blue).

Conclusions

MRI-guided targeted IA mannitol-induced BBBD in rabbit brainstems can be performed allowing for highly selective delivery of chemotherapeutic agents to the pons. Assessment of therapeutic drug delivery after BBBD can be depicted with fluorescent microscopy.

KEYWORDS: Blood-Brain Barrier, Brainstem, Intraarterial Chemotherapy



O-837

11:47AM - 11:54AM

Comparison of connectivity from simultaneous direct intracranial stimulation and fMRI, with subsequent diffusion and resting state connectivity

S Jones¹, J Gonzalez-Martinez¹, M Zhang²

¹Cleveland Clinic, Cleveland, OH, ²Ohio State Medical School, Columbus, OH

Purpose

We recently developed the capability to perform simultaneous direct intracranial stimulation and fMRI, on patients undergoing invasive evaluation for intractable epilepsy. This technique can successfully produce maps of BOLD activation, both local and distal to the stimulating

Note: Scanned images are included in the proceedings. Some submitted images were reduced during editing thereby decreasing clarity. Also, refer to the Program Planner. Proceedings Content as of 3/28/2014.

electrodes, whose patterns may reflect underlying maps of connectivity. We now compare these maps with those obtained subsequently in the same patient using diffusion MRI and resting-state MRI measures.

Materials and Methods

To date, five patients with medically refractory epilepsy have been studied using the technique of DES-fMRI. All used a block paradigm for the temporal pattern of stimulation (typically 32 seconds at 8 mA/20Hz), with the recent addition of a successful event paradigm (2 second stimulation at 8 mA/20Hz). Connectivity measures from this method are simply the t-statistic of induced BOLD activation. After DES-fMRI, and prior to resective surgery, the patients underwent HARDI (61 direction) and resting state fMRI, with each providing its measure of connectivity. Thereafter, these two measures of connectivity were compared with DES-fMRI measures, using the location of the stimulating electrodes as the seed point. Measures were compared on a voxelwise basis, using all voxels in the brain, and two-dimensional scatter plots produced. Correlation values and significance were computed.

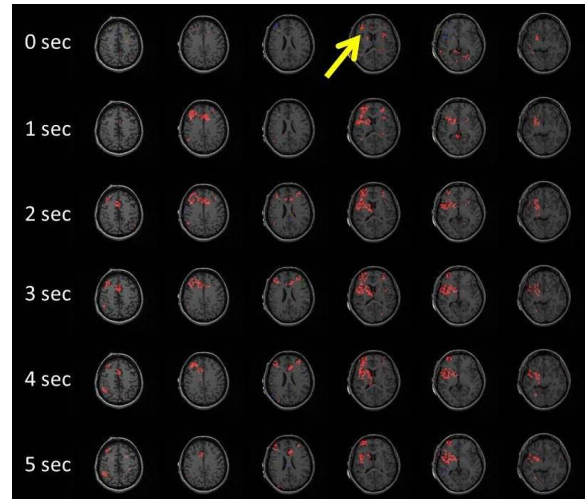
Results

DES-fMRI has been now extended to five patients, recently including an event paradigm that can show the temporal evolution of BOLD signal changes across the brain due to stimulation of a single electrode pair (see attached figure, where each row shows a BOLD map at one second intervals. The yellow arrow shows the location of the stimulating electrode pair, at 8 mA 20Hz for a duration of 2 seconds). Correlation of the fMRI t-statistic to a diffusion-weighted imaging (DWI) connectivity score shows a significant but weak correlation ($R^2=0.04$, $p<1e-6$). Similarly, voxelwise correlation with resting state connectivity shows a significant but weak correlation ($R^2=0.0004$, $p=3e-5$).

Conclusions

We compare voxelwise connectivity maps made from three methods: direct intracranial stimulation and fMRI, diffusion MRI, and resting state MRI. While the correlations are significant, they are modest such that there are many brain regions strongly connected by one measure, but weakly connected using another measure. These results raise questions about the meaning of connectivity, and any possibility of a "gold standard".

KEYWORDS: Deep Brain Stimulator, Epilepsy, Functional Brain Mapping



O-838

11:54AM - 12:01PM

Perfusion in evaluating Pediatric tumor

Z Khademian1

1Children's National Medical Center, Washington, DC

Purpose

Arterial spin labeling (ASL) has a special appeal for study of the brain function in the pediatric population for two important reasons; it eliminates the need for intravenous contrast injection and secondly removes the ionizing radiation. Tumor pediatric population does receive contrast on a routine basis for tumor evaluation. But, it is the differences in ASL measured blood flow that can assist in further evaluation of underlying tumor histology. The aim of this research was to measure blood flow of tumor population presented in our pediatric hospital.

Materials and Methods

Arterial spin labeling was institutionalized in our hospital about 24 months ago. We reviewed all tumor population magnetic resonance images (MRIs) for the last 24 months. There were 38 patients with new and known tumor population that had ASL. There were 20 additional patients that did not have ASL, either there was post-tumor removal or ASL was not technically viable. The latter 20 patients therefore were not in our study. Of the 38 patients in our study with ASL there were 19 male and 19 female patients. The youngest male patient reviewed was 14 months old; the oldest 12 years old. The youngest female patient was nine months old; the oldest 19 and a half years old. We measured and documented the tumor blood flow for all of the 38 cases. In case of heterogeneous tumor population we measured multiple sites. In addition, we used cerebral

Note: Scanned images are included in the proceedings. Some submitted images were reduced during editing thereby decreasing clarity. Also, refer to the Program Planner. Proceedings Content as of 3/28/2014.

blood flow (CBF) of the right mesial temporal lobe as a baseline. We then used this baseline flow against the tumor flow. Arterial spin labeling measurements then were compared and grouped against the known histology the tumor.

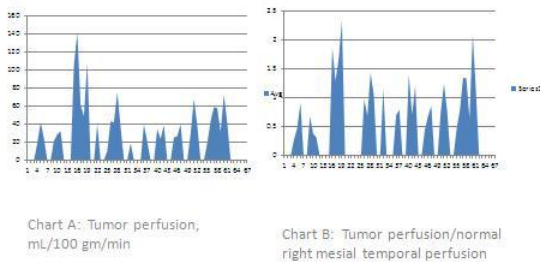
Results

We measured perfusion of 10 to 11 subcategories of tumor. Chart A shows perfusion peak for each subcategory. Chart B shows peak ratios of tumor to normal brain perfusion. By reviewing the charts, it is clear that there is variation in perfusion of each tumor subcategory. We also noted that ependymoma tumors (the third peak) had the highest perfusion in both charts. Anaplastic astrocytomas (fifth peak in Chart A and fourth peak in Chart B) had the second highest values. While the medulloblastomas and PNET tumors, the first and second peaks, had actually lower perfusion than pilocystic astrocytomas or glioma.

Conclusions

Our data showed that high grade tumors may not have a higher perfusion than a low grade glioma. Also perfusion values are influenced by the heterogeneity of the tumor. There were even some variation in perfusion measurements of the same tumor, even the tumor appeared homogenous on T2 and postenhancement imaging.

KEYWORDS: Arterial Spin-Labeling



Thursday, May 22
10:30AM - 12:00PM
Room 520

86 - PARALLEL PAPERS: Interventional:
Malformations/Stroke/Misc

0-839

10:30AM - 10:37AM

Endovascular Embolization of Vein of Galen Aneurysmal Malformations: Noninvasive Assessment of Intracranial Hemodynamic Alterations with 4D Flow MR Imaging

C Wu¹, S Schoeneman², A Honarmand¹, J Deng², S Ansari³, M Markl¹, A Shaibani¹

¹Northwestern University, Chicago, IL, ²Ann & Robert H. Lurie Children's Hospital of Chicago, Chicago, IL, ³Northwestern University Feinberg School, Chicago, IL

Purpose

Intracranial hemodynamics in patients with rare vein of Galen aneurysmal malformations (VGAM) and the impact of treatment on cerebral blood flow are still poorly understood. The purpose of this study was to evaluate the feasibility of serial 4D flow MR imaging for the noninvasive characterization of changes in intracranial hemodynamic in three pediatric VGAM patients treated by endovascular embolization.

Materials and Methods

Three VGAM patients (2 male +1 female; age=10±8 months) treated by endovascular embolization were included in this study. Electrocardiogram (ECG)-gated 4D flow MRI (TR/TE=5.5/2.9ms, flip angle=15°, velocity sensitivity VENC=100-150cm/s, spatial resolution=1.2mm×1.2mm×1.4mm, temporal resolution=44ms, acquisition time=8.9±1.8min) was performed for all patients (patient 1: pre- and post-1st embolization; patient 2: post-1st and 2nd embolization; patient 3: post-2nd and 3rd embolization) on a 1.5 T MRI scanner. Intracranial 3D hemodynamics were visualized by time-integrated 3D pathlines depicting the cumulative flow path over the cardiac cycle in all MR visible vessels. Color coding was used to visualize the distribution of regional blood flow velocities. Peak velocity (m/s) and mean blood flow (ml/s) were quantified in manually positioned planes perpendicular to the major vessels.

Results

The figure illustrates 3D blood flow characteristics in patient 1 at pre- and post-1st embolization, demonstrating marked reduction of VGAM size and significant hemodynamic alterations after endovascular occlusion of the feeding right posterior choroidal artery (RPChA, open white arrow in the figure). Considerable VGAM shrinkage and hemodynamic changes also were observed in patient 2. The VGAM was not visible in patient 3 at post-2nd and 3rd embolization, but hemodynamic alterations in the surrounding cerebral vasculature clearly were evident. Blood flow through the VGAMs decreased for all patients after intervention (patient 1: from 27.92ml/s to 11.86ml/s; patient 2: from 11.69ml/s to 8.57ml/s; patient 3: from 3.84ml/s to 2.12ml/s). We also observed that the peak velocity in the straight sinus was decreased in patient 1

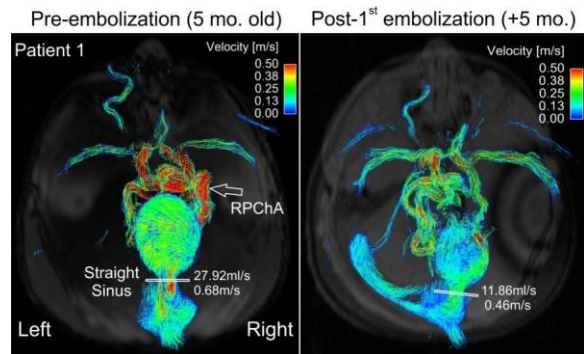
Note: Scanned images are included in the proceedings. Some submitted images were reduced during editing thereby decreasing clarity. Also, refer to the Program Planner. Proceedings Content as of 3/28/2014.

(from 0.68m/s to 0.46m/s) and patient 2 (from 0.44m/s to 0.37m/s) but increased in patient 3 (from 0.40m/s to 0.75m/s). In addition to regional hemodynamic alterations in the VGAMs, we also observed a systemic impact of focal embolization of the feeding artery on the hemodynamics in other intracranial vessels territories.

Conclusions

The results demonstrated the feasibility and potential of 4D flow MR imaging for the comprehensive noninvasive assessment of hemodynamic alterations in VGAMs before and during staged embolization. We were able to identify shunt reduction and blood flow redistribution after endovascular embolization. The full volumetric coverage by 4D flow MRI allows for the analysis of VGAM blood flow in combination with hemodynamics in other intracranial vessels. Future studies are needed to evaluate the potential of 4D flow MRI to complement existing diagnostic tool to better determine optimal timing for treatment, to evaluate the efficacy of therapeutic interventions, to monitor treatment effects, and to predict outcome.

KEYWORDS: Endovascular Embolization, Hemodynamics, Vein Of Galen



Vein of Galen malformations (VOGMs) are rare and complex congenital arteriovenous fistulas. Clinical and radiological features of VOGMs and their relation to long-term clinical outcomes are not fully characterized. Thus, we examined these features and the predictors of outcome in patients with VOGM.

Materials and Methods

We retrospectively reviewed records of all patients with VOGM treated at our hospital (1986-2013), and measured outcomes via a survey performed in 2012. Thirty-nine cases were confirmed as VOGM. We applied the modified Rankin Scale to determine functional outcome by chart review.

Results

Most patients (89%) were diagnosed with VOGM in the first year of life. Age at treatment was distributed bimodally, with predominantly urgent embolization at <10 days of age and elective embolization after one year of age. Patients commonly presented with hydrocephalus (78%) and congestive heart failure (68%). The mixed-type (31%) VOGM was more common in our cohort than purely mural (25.5%) or choroidal (25.5%) types. The most common feeding arteries were choroidal and thalamoperforating. Transarterial embolization with coils was the most common technique used to treat VOGMs at our institution. Functional outcome (N=28) was normal or only mildly disabled in 50% of the cases at last follow up (median=1.1 years, range=0 to 23 years). Younger age at first diagnosis (p=0.006) and seizures (p=0.014) were predictive of adverse clinical outcome. Validated questionnaires (N=6) showed that children treated for VOGMs are affected variably in multiple functional domains.

Conclusions

VOGMs continue to be challenging to treat and manage. However, the long-term neurodevelopmental outcomes of affected children may be good in many cases.

KEYWORDS: Outcomes, Vein Of Galen

O-840

10:37AM - 10:44AM

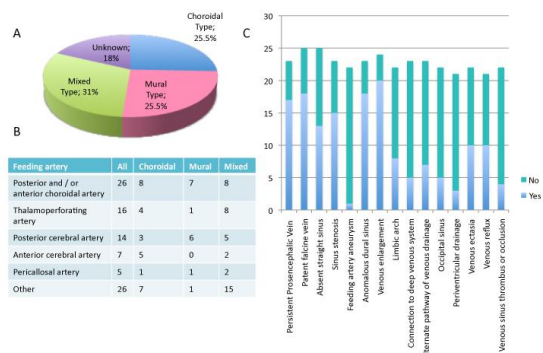
Vein of Galen Malformations: radiological and clinical features, and long-term outcome following endovascular treatment

M Chow¹, D Cooke¹, H Fullerton¹, H McSwain¹, M Amans¹, J Narvid¹, C Dowd¹, R Higashida², V Halbach¹, H Kim¹, S Hetts¹

¹University of California San Francisco, San Francisco, CA, ²University of California Medical Center, San Francisco, CA

Purpose

Figure 1. Angioarchitecture of VOGMs



Note: Scanned images are included in the proceedings. Some submitted images were reduced during editing thereby decreasing clarity. Also, refer to the Program Planner. Proceedings Content as of 3/28/2014.

O-841

10:44AM - 10:51AM

Effect of Venous Angioarchitecture on Hemorrhagic Presentation of Arteriovenous Malformations of the Brain

M Alexander¹, H Kim², D Cooke², S Hetts²

¹Santa Clara Valley Medical Center, San Jose, CA,
²University of California San Francisco, San Francisco, CA

Purpose

Intracranial hemorrhage accounts for the majority of morbidity and mortality caused by arteriovenous malformations (AVMs). Several angiographic features of the venous components of these malformations have been identified as affecting hemorrhage risk. The current study examines the association between the angiographic appearance of the venous components of AVMs with initial presentation of hemorrhage in a large prospectively maintained cohort using standardized digital subtraction angiographic (DSA) characterization.

Materials and Methods

Under an IRB-approved protocol, patients with an AVM were identified from a prospectively maintained cerebrovascular database between 2000 and 2011. Patients with VOGM, DAVF, or NGAVF were excluded. Demographics, clinical presentation, and angioarchitectural features of the lesions were noted. Univariate and multivariate regression models were constructed.

Results

Seven hundred fifty-three patients were evaluated during the study period. Three hundred thirty-nine (45.0%) patients had initial presentation of hemorrhage. Univariate analysis identified exclusively deep venous drainage ($p < 0.001$) and single draining vein ($p < 0.001$) as associated with initial presentation of hemorrhage. Lesions with venous ectasia ($p < 0.001$) were less likely to present initially with hemorrhage. No statistical significance was noted for gender ($p = 0.711$), venous stenosis ($p = 0.205$), venous reflux ($p = 0.093$), or sinus thrombosis ($p = 0.614$). A multivariate Cox regression model was created to evaluate venous angiographic characteristics that were statistically significant in the univariate analysis. Exclusively deep venous drainage remained the most strongly predictive characteristic for initial presentation of hemorrhage (OR: 4.0, 95% CI: 2.1 to 7.5, $p < 0.001$). Lesions with two or more draining veins (OR: 0.76, 95% CI: 0.63 to 0.92, $p = 0.004$) and venous ectasia (OR: 0.48, 95% CI: 0.31 to 0.74, $p = 0.001$) also retained statistical significance, with these findings found less commonly in patients presenting with hemorrhage.

Conclusions

Risk stratification for predicting future rupture of brain AVMs is of tremendous clinical interest, particularly following publication of the ARUBA study. In agreement with previously published literature, brain AVMs with deep venous drainage in our cohort were more likely to present with hemorrhage, as were patients with a single draining vein. Interestingly, patients with venous ectasia were less likely to present with hemorrhage. No statistically significant association was noted for previously implicated venous features including venous stenosis, venous reflux, or sinus thrombosis.

KEYWORDS: Arteriovenous Malformation, Hemorrhage, Venous Drainage

O-842

10:51AM - 10:58AM

Cerebral venous thrombosis after embolization of pediatric AVM with jugular bulb stenosis or occlusion: management and prevention.

G Saliou¹, F Puccinelli², K Deiva², C Bellesme², P Durand², L Chevret², B Husson², M Sachet², D Ducreux²

¹Toronto Western Hospital, Toronto, Ontario, Canada,
²Hopital Bicetre, Le Kremlin Bicetre, val de Marne, France

Purpose

Thrombosis of cerebral arteriovenous malformation (AVM) after embolization is rare, but can involve the normal venous network with extensive venous thrombosis. We report angioarchitecture findings, our management and prevention strategy for this complication in pediatric AVMs.

Materials and Methods

Between January 2008 and Jun 2013, 181 patients under the age of 15 years (vein of Galen aneurysmal malformation: $n = 101$; pial AVM and pial fistulas: $n = 68$; dural sinus malformation: $n = 12$) were treated by NBCA or ONYX embolization in a total of 359 sessions. We retrospectively reviewed the chart of all 13 patients under 15 years who were anticoagulated after embolization. In our initial experience four children who didn't receive any prophylactic anticoagulation presented with extensive venous thrombosis after embolization (group 1). Following this, nine children with similar angioarchitecture and embolization modalities were treated with prophylactic anticoagulation immediately after embolization (group 2). We analyzed the type of AVM, angioarchitecture, dose of prophylactic anticoagulant, efficacy/complications of treatment and late outcome.

Results

Note: Scanned images are included in the proceedings. Some submitted images were reduced during editing thereby decreasing clarity. Also, refer to the Program Planner. Proceedings Content as of 3/28/2014.

All patients in group 1 had severe jugular bulb stenosis/occlusion associated with cerebral venous dilatation. In group 2 with similar angioarchitecture, only three patients (33%) developed extensive thrombosis. In both groups, thrombosis occurred within two days of treatment in six children and two weeks in one child. The diagnosis was suspected on ICH in five patients and oculomotor disorder in one. One was asymptomatic. All children were treated with therapeutic doses of LMWH (anti-Xa: 0.5-1). No hemorrhagic complications occurred. Good venous remodeling was observed in all but one patient.

Conclusions

Anticoagulation in extensive venous thrombosis after AVM embolization in children appears to be safe and effective. In cases with angioarchitectural features of dilatation of the cerebral venous network and occlusion/severe stenosis of the jugular bulbs, full dose anticoagulation may be required to prevent thrombosis.

KEYWORDS: AVM, Pediatric Cerebrovascular Disease, Venous Sinus Thrombosis

O-843

10:58AM - 11:05AM

Management of Tongue Venous and Lymphatic Malformations

W Yakes¹

¹Vascular Malformation Center, Englewood, CO

Purpose

To determine the efficacy of ethanol embolization in management of tongue venous and lymphatic malformations.

Materials and Methods

Thirty-nine patients (22 females, 17 males; mean age: 38 years) presented with tongue low-flow malformations. Forty-seven patients had undergone 61 failed previous procedures (embo, laser, surgery, steroid injection, alpha-interferon, radiation). All patients had baseline arteriograms and MRs. All patients underwent direct puncture ethanol endovascular therapy.

Results

Of 39 patients with venous and lymphatic malformations, 32 patients had dramatic reduction and seven patients' therapy is on-going with concurrent reductions (mean f/up: 60 months). One patient with AVM required additional surgery and one patient with mixed veno-lymphatic malformation required surgical debulking of excess tissues. Minor complications such as tongue blisters (9 instances) healed spontaneously; three tongue focal necrosis injuries healed spontaneously; three infections

responded to antibiotic treatment; one focal tongue hemi numbness resolved.

Conclusions

Ethanol embolotherapy is a primary and consistent form of therapy to eradicate low-flow vascular malformations of the tongue permanently at long term follow up. Rarely is concurrent surgery required. Ethanol sclerotherapy is a curative treatment in which recurrences do not occur and permanent ablations are the rule. Complications that occur are minor and rare.

KEYWORDS: Embolization, Tongue, Venous Malformations

O-844

11:05AM - 11:12AM

High resolution endovascular imaging during intracranial interventions - a paradigm shift in neurointerventional therapeutics ?

R Sacho¹, P McVeigh², V Mendes Periera³, B Wilson⁴, T Krings¹

¹Toronto Western Hospital, Toronto, Ontario, Canada,
²University of Toronto, Toronto, Ontario, Canada,
³University Hospital of Geneva, Geneva, Switzerland,
⁴Princess Margaret Hospital/University Health Network, Toronto, Ontario, Canada

Purpose

Direct endoluminal visualization during endovascular therapy is an attractive concept which previously has received little attention due to the poor imaging quality and delicate nature of existing angioscopes. The potential benefits include enhancing existing techniques as well as extensive research opportunity. We report on the first application of a novel ultrathin high resolution scanning fiber endoscope (SFE) to directly visualize endovascular interventions in real time.

Materials and Methods

The physics and design of the SFE have been previously described (1). Under general anesthesia three Yorkshire pigs (35-40kg) underwent transfemoral cannulation and catheterization of common carotid and cervical arteries (3-5mm) using fluoroscopic angiography. Standard 6F guide catheters and distal access catheters were used to navigate the SFE. Our initial experiments concentrated on achieving reliable endovascular visibility which was achieved via a combination of saline irrigation through the guide catheter, the occlusive nature of the catheter in distal vessels and proximal balloon inflation via a 9F balloon guide catheter as needed. Subsequent experiments focused on recording standard endovascular techniques in real time: through microcatheters introduced via a second 'working' guide catheter we recorded high quality endoluminal views of

Note: Scanned images are included in the proceedings. Some submitted images were reduced during editing thereby decreasing clarity. Also, refer to the Program Planner. Proceedings Content as of 3/28/2014.

microwire vessel cannulation, aneurysm coil deployment, stent retrieval of experimentally introduced thrombus using the Trevo and Solitaire stent retrievers and deployment of the Pipeline embolization device across a blind pouch created by sidebranch coiling.

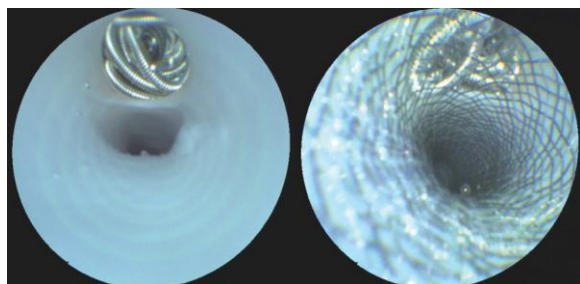
Results

Endoscopy allowed visualization of neck coverage during coil embolization, the completeness and extent of clot retrieval during stent-retriever deployment and we were able to visualize the true and false lumens of an iatrogenic dissection flap. Accurate positioning and deployment of the flow diverter were achieved under direct vision. We were able to visualize flow stagnation within a blind vessel pouch area covered by flow diversion. Stent tine position and wall apposition could be assessed accurately.

Conclusions

Endovascular angioscopy is feasible and has tremendous potential as a tool to diagnostic and therapeutic enhancement during standard endovascular procedures. The SFE is a potential powerful research tool to understand endovascular therapeutics.

KEYWORDS: Endovascular Management, Endovascular Therapy



O-845

11:12AM - 11:19AM

Reduction of Radiation Exposure during Pediatric Cerebral Angiography

P Morris¹

¹Wake Forest University, Winston Salem, NC

Purpose

To identify imaging parameters under operator control during pediatric angiography most easily adjusted to

reduce patient exposure and dose without compromise of patient care and safety.

Materials and Methods

In-vitro DSA and fluoroscopy exposures using a Rando phantom and an ArtisZee biplane unit (Siemens) were performed under standardized conditions for exposure settings, magnification, and source-image distance (SID). Recordings of dose-area product (DAP) and estimated skin dose (ESD) were recorded and standardized for controlled conditions in which kV, dose per frame, copper filtration, field of view, frames per second, and insertion or removal of the grid were independently varied. Image quality was evaluated using a line-pair resolution card and adjustment of post-processing edge-enhancement features.

Results

For DSA the most substantial reductions in exposure and dose were obtained through curtailing the length and fps setting of the DSA protocol with savings directly proportional to the degree of adjustment. For example, adjusting a single phase DSA run of 8 seconds at 3 fps to a multiphase run of 2 fps for 4 s and 1 fps for 4 s results in a 50% reduction of dose. Reductions in proportion to the adjustment in dose-per-frame were also evident, e.g. reduction of dose/fr from 0.54 mcGy/f to 0.17 mcGy/f resulted in a 56% reduction of DAP and ESD. Grid removal resulted in a reduction of DAP of between 33-51% and of ESD of between 31-50% in the AP plane. Introduction of copper filtration of above 0.3mm resulted in lower recordings of DAP and ESD but with undesirable upward adjustments of kV. Adjustments of the edge-enhancement settings above the default setting of 30% compensated favorably for the impact on image quality of removal of the grid.

Conclusions

1. Substantial radiation savings during pediatric cerebral angiography are possible through self-evident procedures such as reduction of the number of DSA runs, reduction of the frame rate during DSA, and reduction of the pulse-rate during fluoroscopy and roadmap. Depending on the operator's starting baseline, these reductions can reduce exposure by greater than 50%. 2. Less evident points of adjustment, but equally substantial in their impact on exposure, include settings such as dose-per-frame for DSA and dose-per-pulse for fluoroscopy, resulting in similar magnitudes of dose reduction. Furthermore, a single pediatric setting of dose-per-frame for DSA is probably not optimized for all children and smaller children likely will benefit from even lower dose/fr settings depending on body size, without compromise of image quality. 3. Grid removal results in substantial radiation savings of up to 50% just by itself independently of all other factors, with minimal impact on image quality some of which can be attenuated by edge-enhancement postprocessing. 4. Copper filtration in excess of 0.3mm is likely an adjustment of diminishing and unfavorable returns due to its impact on kV. In conclusion, thorough familiarity with the available adjustments relating to radiation exposure under

Note: Scanned images are included in the proceedings. Some submitted images were reduced during editing thereby decreasing clarity. Also, refer to the Program Planner. Proceedings Content as of 3/28/2014.

operator control and inclusion of these factors in the preprocedure "Time-Out" can redound to the patient's advantage considerably with reductions of dose and exposure to a small fraction of those generated by default pediatric settings.

KEYWORDS: Radiation Dosage, Radiation Dose Reduction, Radiation Exposure

O-846

11:19AM - 11:26AM

Transbrachial approach as a first access route for neurointervention

T Mori¹, Y Aoyagi¹, T Iwata¹, S Kasakura¹, Y Miyazaki¹, Y Tanno¹

¹Shonan Kamakura General Hospital Stroke Center, Kamakura, Japan

Purpose

Transfemoral approach for neuroendovascular treatment is widely used but sometimes limited by aortic or peripheral arterial conditions. Purpose: The purpose of our study was to investigate the feasibility and safety of transbrachial procedures using the sheath-guide specifically designed for transbrachial cannulation into the carotid artery.

Materials and Methods

Included in our retrospective analysis were patients who underwent transbrachial neurointervention from January 2012 to December 2012. We used the particular sheath-guides, MSK-guide sheath (Medikit Co.Ltd., Tokyo, Japan), with two types of distal length; 1: (1) MSK-guide 7.5x90; 6Fr (2.24 mm, 0.088 inch) (ID: internal diameter) guiding sheath with 7.5cm-distal part and 90 cm in length; This sheath guide was developed for direct cannulation into the common carotid artery (CCA) without an inner catheter and used mainly for CAS. (2) MSK-guide 7.5x70; 6Fr (ID) guiding sheath with 7.5cm-distal part and 70 cm in length; This sheath guide was used for inserting the 2nd guiding catheter with up to 6Fr (outer diameter: OD) co-axially and positioning it in the internal carotid artery. 2: MSK-guide 15x90(3D); It is designated for transbrachial direct cannulation into the internal carotid artery (ICA) and for fitting to the anatomical feature of the ICA. This catheter was used for intracranial neurointervention, mainly intracranial angioplasty or stenting, or embolization of aneurysms with two or three microcatheters required.

Results

During the study period, 188 procedures were done. Among them, 135 were elective and 53 emergent. MSK-

guide were used in 101 (75%) of 135 elective cases and in 29 (55%) of 53 emergent cases. Among 135 elective transbrachial procedures, 56 CAS, 17 intracranial angioplasty or stenting, 16 coiling and others were included. Among 29 emergent transbrachial procedures, 28 cases were reperfusion therapy for ischemic stroke. All transbrachial cannulation into the target CCA or ICA were successful in all cases. All transbrachial neurointervention were completed, too. The MSK-guide provided good support-force. Transbrachial procedures didn't depend on anatomical features of the abdominal aorta and/or peripheral arteries. Transbrachial procedures didn't depend on vascular diseases of the abdominal aorta and/or peripheral arteries.

Conclusions

Transbrachial neurointervention was feasible and safe by using the MSK-guide sheath specifically designated for transbrachial cannulation into the carotid arteries. Routine transbrachial approach can open the door for patients and neuroendovascular physicians.

KEYWORDS: Brachial Artery, Carotid Artery Stenting, Endovascular Therapy

O-847

11:26AM - 11:33AM

Significant Acquisition Dose Reduction Maintains Diagnostic Quality of Biplane Cerebral Digital Subtraction Angiography

A Honarmand¹, A Shaibani¹, M Hurley², B Patel², V Daruwalla², C Sammet³, T Morgan⁴, S Ansari²

¹Northwestern University, Chicago, IL, ²Northwestern Feinberg School of Medicine, Chicago, IL, ³Ann & Robert H. Lurie Children's Hospital of Chicago, Chicago, IL, ⁴Northwestern Memorial Hospital, Chicago, IL

Purpose

Digital subtraction angiography (DSA) remains the gold standard modality for evaluation, diagnosis, and treatment planning of several intracranial vascular abnormalities. However, patient radiation dose can be considerable with both diagnostic and especially complex neurointerventional procedures. Modern biplane flat-detector angiography units provide several possibilities for automatic dose reduction by modifying X-ray tube potential, current, pulse width, and filtration thickness. We aimed to investigate the feasibility of reducing the radiation exposure dose in diagnostic DSA examinations while preserving the overall image quality for diagnostic purposes.

Note: Scanned images are included in the proceedings. Some submitted images were reduced during editing thereby decreasing clarity. Also, refer to the Program Planner. Proceedings Content as of 3/28/2014.

Materials and Methods

Following IRB approval and informed consent, a prospective study was performed on patients undergoing diagnostic cerebral DSA using biplane flat detector rotational fluoroscopy and angiography unit (Artis zee/zeego, Siemens). DSA images were acquired using a predefined manufacturer standard DSA program by selecting detector dose of 3.6 $\mu\text{Gy}/\text{frame}$ (mean typical tube voltage (TTV): 80.6 kVP, mean tube current (TC): 230.6 mA, using focal spot size (FS) of 0.6 and inherent filtration) and reduced DSA detector dose of 1.2 $\mu\text{Gy}/\text{frame}$ (mean TTV: 73.6 kVP, mean TC: 153.5 mA, using FS of 0.3 with additional 0.1/0.2 copper filter) dose protocols for each patient. Using identical contrast agent, contrast injection rate, and fluoroscopy time, randomly selected internal carotid arteries or vertebral arteries and their contralateral equivalent arteries were injected to obtain standard radiation dose and low radiation dose AP and lateral DSA images, respectively. Images were not included for image quality assessment if any significant technical issue and/or flow limiting vascular stenosis/occlusion, or steal phenomenon from AV shunts were present. Image quality assessment was performed independently by two neurointerventionalists on a de-identified PACS workstation. A 5 point scale (5: Very good: excellent large and small vessel visualization; 4: Good: excellent large vessel and minimal compromise of small vessel visualization; 3: Average: diagnostic value for large vessel, but compromised small vessel visualization 2: Poor: compromised large and small vessel visualization; 1: Nondiagnostic) was used for qualitative evaluation of arterial, capillary, and venous phases of DSA images respectively. The total score was defined as the overall diagnostic value. Paired sample t-test and Wilcoxon's signed rank test compared the kerma-area product (KAP) and scores assigned to image quality parameters, respectively. P value <0.05 was considered statistically significant.

Results

Twenty-three DSA image series were obtained from nine patients (8M/1F, mean age: 65.9 \pm 9.16) undergoing diagnostic DSA. Mean KAP was significantly reduced by 60% or 2.5 fold (1408.90 \pm 419.18 $\mu\text{Gy}/\text{m}^2$ versus 557.08 \pm 214.56 $\mu\text{Gy}/\text{m}^2$, P <0.0001). No significant difference was observed between image quality scores assigned by the observers while assessing arterial (observer 1: P=1.0; observer 2: P=0.24), capillary (observer 1: P=0.54; observer 2: P=0.3), venous (observer 1: P=0.14; observer 2: P=0.7) phases, and overall diagnostic value (observer 1: P=0.34; observer 2: P=0.8).

Conclusions

Radiation exposure dose can be reduced significantly without compromising image quality for diagnostic purposes in cerebral DSA studies.

KEYWORDS: Image Quality, Radiation Dose Reduction

O-848

11:33AM - 11:40AM

A Prospective Trial of Venous Sinus Stenting for Idiopathic Intracranial Hypertension Refractory to Medical Therapy

A Patsalides¹, F Laage-Gaup¹, P Singh¹, M Dinkin¹

¹Weill Cornell Medical College, New York, NY

Purpose

Stenosis of the transverse-sigmoid sinus junction has been observed in a majority of patients with idiopathic intracranial hypertension (IIH), but whether it is a result of intracranial hypertension (IH), a contributor to IH or both remains controversial. Since Higgins demonstrated clinical improvement in a patient with IIH, multiple studies have demonstrated clinical improvement in select patients treated with venous sinus stenting. However, most of these studies have been retrospective, only some have included careful analysis of visual field data, and most have not demonstrated repeat opening pressure measurements following the procedure. We set out to perform a clinical trial (ClinicalTrials.gov Identifier: NCT01407809) of the effect of venous stenting on clinical symptoms, visual acuity and field data, papilledema and opening pressure on lumbar puncture (LP) in patients with medically refractive IIH. We hypothesized that there would be improvement in these parameters in a majority of patients.

Materials and Methods

We selected eight patients who were either medically refractory to or intolerant of acetazolamide and/or topiramate or presented with fulminant vision loss requiring a procedure for inclusion in the trial. Alternative options were discussed including optic nerve sheath fenestration and ventriculoperitoneal shunt placement, and for those who opted for stenting, informed consent was obtained. All patients satisfied the Dandy criteria for IIH including MR imaging (MRI) showing no mass lesion and LP showing elevated opening pressure with normal contents. Preprocedure fields, OCT and fundus photography were performed in all patients. Only patients whose MR venography (MRV) either demonstrated venous sinus stenosis bilaterally, or in a dominant transverse sinus, were included. Catheter venography was performed and trans-stenotic gradients were measured. Venous stents were placed only in patients with a gradient of 10 mm Hg or more. Venous stenting was performed under general anesthesia. Stent placement required aspirin and Plavix for one month and aspirin for six months.

Results

Out of the eight patients, clinical presentation included headache in 100%, pulsatile tinnitus in 87.5%, and diplopia in 63%. Out of 16 eyes, 16 (100%) demonstrated a visual

Note: Scanned images are included in the proceedings. Some submitted images were reduced during editing thereby decreasing clarity. Also, refer to the Program Planner. Proceedings Content as of 3/28/2014.

field defect, 15 (94%) showed papilledema, and nine (56%) showed loss of visual acuity. MR venography showed bilateral stenosis in 50% and unilateral stenosis where the fellow sinus was hypoplastic in 50%. Stenting was feasible in all patients. Prestenting trans-stenotic gradients ranged from 14 to 28 mmHg (mean 19) and improved in all patients postprocedure (range 0-5mmHg, mean 3). At follow-up visits ranging from 2-9 months after stent placement, 63% reported an improvement in headache, 86% in pulsatile tinnitus and 100% in diplopia. Out of 16 eyes with visual field defects, eight (50%) showed an improvement, three (19%) worsened at the first follow up but subsequently improved past their baseline (2 to normal), and the remaining five (31%) were stable. Out of nine eyes with loss of visual acuity at presentation, five (44%) showed an improvement and the remaining four were stable. Visual acuity never worsened. Out of 15 eyes with papilledema, seven (47%) showed an improvement in Frisén grade and the remaining eight were stable. Of eight eyes that presented with Frisén grade 2 or more, six (75%) showed improvement. In those eyes that showed no improvement in papilledema grade on funduscopy, a decrease in the retinal nerve fiber layer (RNFL) thickness towards the normal range was demonstrated in 100% (8/8). Opening pressure improved in 100%. Complications included one small retroperitoneal hematoma without need for transfusion or surgery.

Conclusions

We present interim data in one of the first prospective FDA-approved studies of venous sinus stenting for IIH. Following stenting procedure, all patients demonstrated an improvement in trans-stenotic gradient on venography and intracranial pressure as demonstrated by LP. The majority of patients showed an improvement in headache, diplopia and pulsatile tinnitus, but the response was less vigorous in headache, possibly owing to the multifactorial nature of this symptom in IIH patients. While clinical funduscopy showed an improvement in only 47% of eyes, this appears to be the result of the inclusion of some eyes that were Frisén grade I at presentation, where clinical improvement would not be obvious. Looking only at Frisén grade II eyes, all demonstrated either a clinical improvement, or a reduction in RNFL thickness towards the normal range. Most importantly, the vast majority of patients showed improvement in visual field defects with stability demonstrated in the remainder. These preliminary results suggest that venous stenting for IIH is efficacious, as demonstrated in prior retrospective studies, but larger numbers of patients will be required to confirm the long term efficacy and safety of this procedure.

KEYWORDS: Cerebral Venous System, Increased Intracranial Pressure, Venous Sinus Stenting

O-849

11:40AM - 11:47AM

Analysis of 24 False Negative Spinal Angiograms Performed in 16 Patients with Vascular Malformations Subsequently Documented by Angiography: What Went Wrong and How to Avoid It.

P Gailloud¹, E Wyse¹, B Greenberg², D Heck¹, C Pardo¹

¹The Johns Hopkins Hospital, Baltimore, MD²University of Texas Southwestern Medical Center, Dallas, TX

Purpose

The diagnosis of spinal vascular malformations often is delayed by the lack of specific clinical signs and symptoms, and the nonspecific appearance on MR imaging (MRI). Spinal angiography is the gold standard imaging technique for the investigation of spinal vascular anomalies. But it is a technically demanding method, which must be conducted using a methodical approach to offer a high diagnostic yield. The possibility of falsely negative angiographic studies is particularly distressing when one addresses progressive conditions with a limited therapeutic window. This review analyzes 26 false positive spinal angiograms obtained in 16 patients later diagnosed with and treated for a spinal vascular malformation.

Materials and Methods

Twenty-six false-negative spinal angiograms obtained in 16 patients with spinal vascular malformations subsequently documented by angiography were reviewed. Thirteen patients were referred to our services for further evaluation and/or second medical opinions after prior negative investigations, while three patients had their initial negative spinal study performed by two of the study's authors. In all cases, further investigations were warranted by the lack of clinical improvement or by symptoms progression.

Results

Sixteen patients with 17 spinal arteriovenous fistulas (AVFs) underwent a total of 26 negative spinal angiograms (average 1.6, range 1 to 6). At the time of report, 16 out of the 17 lesions had been treated successfully, either endovascularly (14) or surgically (2). The distribution of the lesions was as follows: 10 spinal epidural AVFs (SEAVFs) (59%), 5 spinal dural AVFs (SDAVFs) (29%), and 2 perimedullary AVFs (PmAVF) (12%). The SEAVFs/SDAVFs were found at the thoracic (n=3, 20%), lumbar (n=10, 67%), or sacral (n=2, 13%) levels. Both PmAVFs were located at the conus medullaris, and supplied by thoracic feeding arteries (T8 and T10). The list of initial diagnoses included transverse myelitis (TM) (n=8, 50%), spinal venous thrombosis (n=2, 13%), spine degenerative disease (DGD) (n=2, 13%), spinal stroke (n=1, 6%), or other (n=3, 18%). Twenty-one out the 26 the false negative angiograms were available for review. The reasons behind the negative studies could be categorized as follows: 1 - the level with the lesion was not investigated

Note: Scanned images are included in the proceedings. Some submitted images were reduced during editing thereby decreasing clarity. Also, refer to the Program Planner. Proceedings Content as of 3/28/2014.

(11 cases). In this instance, the angiogram was either incomplete (e.g., no evaluation of the pelvis, 9 cases) or the level was skipped during the procedure (e.g., mislabeling, 2 cases), 2 - the level with the lesion was investigated, but the lesion was outside of the field of view (1 case) or the injection was inadequate (1 case) (see Figure 1), 3 - the lesion was documented by the angiogram, but not recognized (7 cases), 4 - in one instance, the level with the lesion was investigated adequately, but the lesion was not visible. This case represents the only instance of truly false negative spinal angiogram in this series. Figure 1 legends: the left panel shows a right L3 SEAVF (arrow) draining into a radiculomedullary vein (arrowheads). The right panel shows a nonselective injection of the same vessel during the false negative study; while the ISA is opacified, the lesion is not detectable.

Conclusions

The most important lesson learned from our retrospective analysis of false negative spinal angiograms obtained in a series of 16 patients is that in all but one instance, the false negative result was related directly to a correctable, operator-dependent technical factor. Incomplete or missing investigation of the lumbosacral vasculature was singled out as the most common cause of false negative studies (52%), followed by the nonrecognition of angiographically documented lesions (33%). The potential for false negative studies therefore can be minimized by adoption of rigorous technical and training standards.

KEYWORDS: Spinal Angiography, Spinal Arteriovenous Malformation, Spinal Imaging



O-850

11:47AM - 11:54AM

Susceptibility Clot Width >5 mm is a Highly Sensitive Marker for Development of Parenchymal Hematoma Following Intra-arterial Clot Retrieval in Acute Stroke

S Kamalian1, L Morais1, A Yoo1, A Franceschi2, S Kamalian1, J Hirsch1, L Schwamm1, M Lev1

1Massachusetts General Hospital, Boston, MA, 2SUNY at Stony Brook, Stony Brook, NY

Purpose

The degree of proximal middle cerebral artery (MCA) "blooming artifact" on susceptibility MR imaging (MRI) of acute ischemic stroke (AIS) patients is highly specific for occlusive clot burden, and hence – potentially – of the degree of endothelial vascular injury locally, in the adjacent MCA perforator vessels, and in the more distal capillary bed. Our purpose was to determine if there is a relationship between the width of clot-related susceptibility artifact and the likelihood of parenchymal hematoma (PH) following endovascular clot retrieval in these patients.

Materials and Methods

We retrospectively reviewed 213 consecutive AIS patients who received intra-arterial therapy (IAT) between 6/1/2004 and 12/1/2013. Of these, 138 met the following inclusion criteria: (1) MCA M1 or M2 occlusion; (2) Available admission gradient recalled echo (GRE) T2* and/or perfusion-weighted imaging (PWI); and (3) Follow-up noncontrast CT. We measured the maximum width of clot-related susceptibility artifact (CSW) and stratified patients into two groups: CSW≤5 mm (Group 1) and CSW>5 mm (Group 2). The findings were correlated with development of postprocedural parenchymal hematoma (ECASS PH1 and PH2).

Results

There were 74 patients in Group 1 and 64 patients in Group 2. Parenchymal hematoma occurred in 15 patients, of which 1/64 (2%) was from Group 1 and 14/74 (19%) were from Group 2. Thus, of the 15 PH bleeds, 14/15 (93%) had SCW>5 mm. Sensitivity, specificity, positive predictive value, and negative predictive value for determining the risk of PH following IAT using a SCW cutoff of 5 mm were 93%, 51%, 19%, and 98%, respectively.

Conclusions

Width of clot-related susceptibility artifact <5 mm on admission GRE T2* and/or PWI may identify patients at very low-risk (NPV 98%) of developing parenchymal hematoma following intra-arterial clot-retrieval therapy. We speculate that blooming artifact may not only be a marker for overall clot burden, but also may reflect the degree of regional vessel wall injury and blood-brain barrier breakdown – both risk factors for PH development.

KEYWORDS: Hemorrhagic Transformation, Intraarterial Thrombolysis, Stroke

Note: Scanned images are included in the proceedings. Some submitted images were reduced during editing thereby decreasing clarity. Also, refer to the Program Planner. Proceedings Content as of 3/28/2014.

O-851

11:54AM - 12:01PM

Mechanical Thrombectomy With The « ERIC »™ Device: Initial Experience

H Raoult¹, H Redjem², A Lintia-Gaultier³, J Ferré¹, R Blanc², S Pistocchi², R Bourcier⁴, B Bartolini², D Benjamin⁴, H Desal², J Gauvrit¹, M Piotin²

¹University Hospital of Rennes, Rennes, France, ²Rothschild Foundation, Paris, France, ³Laennec Hospital, University of Nantes, Nantes, France, ⁴University Hospital of Nantes, Nantes, France

Purpose

Ischemic stroke is one of the major causes of mortality and long-term disability (1). Mechanical endovascular thrombectomy recently merged as an efficient and safe technique to recanalize large occluded arteries, especially using stent retriever devices (2). We aimed at evaluating a device with an innovative design, the "ERIC" (Embolus Retriever with Interlinked Cage), in revascularization of patients with acute ischemic stroke.

Materials and Methods

Twenty-five patients (16 men; median age: 59.2 years) treated with the "ERIC" device (Microvention, Tustin, CA) for large intracranial artery occlusion at the acute phase of a stroke were included consecutively in three French centers, from April to November 2013. The "ERIC" is a 3rd generation device, differing from the "stent retriever": it is composed of five interconnected and mobile nitinol spheres, allowing to capture and withdraw the thrombus without delay. Main data about imaging, interventional technique and clinical status were recorded.

Results

The occlusion site was terminal carotid artery in eight cases and middle cerebral artery (M1) in 15 cases, associated with cervical carotid occlusion in seven cases; and basilar artery in two cases. Intravenous thrombolysis was associated for 18 patients. For 22 patients, « ERIC » was the first intention device, allowing complete recanalization (TICI ≥2B) in 19 cases (86%), after one to four passes (median: 2); in three cases of failure, a rescue stent was used (successfully in two cases). For three patients, "ERIC" was used after stent failure, then allowing complete recanalization in two cases. The median time from symptoms onset to recanalization was 325 min. The median time from groin puncture to recanalization was 78 min. Median baseline and at discharge NIHSS were 17 and 8.5, respectively. Five cases of asymptomatic secondary hemorrhagic transformation were recorded on the 24-hours CT scan.

Conclusions

The « ERIC » device can rapidly, safely and effectively retrieve clots from large intracranial arteries.

KEYWORDS: Stroke, Thrombectomy

O-852

12:01PM - 12:08PM

Endovascular Management of Basilar Artery Occlusion: Clinical and Radiological Prognostic Factors for 3 Months' Neurological Outcome

R Fahed¹, N Sourour¹, D Federico¹, J Gabrieli¹, C Rosso¹, S Crozier¹, V Degos¹, Y Samson¹, J Chiras¹, F Clarençon¹

¹Hopital de la Pitie-Salpetriere, Paris, France

Purpose

Basilar artery occlusion (BAO) is a rare (1%) but very severe subtype of stroke, with a very high mortality and disability rate. Intravenous thrombolysis is a poorly effective treatment, explaining the rise of endovascular treatment, which has gained acceptance in this indication. But even though recanalization rate is higher in endovascular treatment of BAO, a favorable neurological outcome, defined by a modified Rankin scale (mRS) = 0-2 at 3 months follow up, remains low (30%). Our study aimed to evaluate the effectiveness and safety of endovascular treatment of basilar artery occlusion, and to identify clinical and radiological prognostic factors that may help predict the clinical outcome.

Materials and Methods

We retrospectively analyzed the charts of 29 consecutive patients (21 males, 8 females; mean age/SD = 61.1 ± 14.1 years, range: 29-88) who presented BAO (diagnosed with a positive MRI with 3D time-of-flight angiography or brain CT with CT angiography) and underwent endovascular treatment between April 2006 and June 2013 in our institution. Clinical data (including National Institute of Health Stroke Scale [NIHSS] at admission/day 1/day 7, delay between symptoms and beginning of endovascular procedure), radiological data [including prognostic scores on initial MRI and follow-up MRI within 48 hours after the procedure: Bern score (1), Cho et al. score (2), Renard et al. score (3), DWI-pc-ASPECTS (4)], angiographic data [including duration of the procedure, vascular anatomy, drugs and devices used during the procedure, recanalization rate using the following scales: Thrombolysis In Cerebral Ischemia (TICI) score, Thrombolysis In Myocardial Ischemia (TIMI) score and Arterial Occlusive Lesion (AOL) score] were assessed retrospectively. Patients were divided in two groups: good

Note: Scanned images are included in the proceedings. Some submitted images were reduced during editing thereby decreasing clarity. Also, refer to the Program Planner. Proceedings Content as of 3/28/2014.

outcome was defined by a mRS=0-2 at three months follow up, whereas poor outcome was defined by a mRS=3-6 at three months follow up.

Results

Nine of 29 patients (31%) had a good outcome, and 20/29 patients (69%) had a poor outcome, including 8/29 deceased patients (27.6%). There was a statistically significant difference between the groups regarding NIHSS at day one and day seven ($p<0.0001$), all four prognostic scores on initial and/or follow-up MR imaging (MRI) ($p<0.05$ for each score), thalamic infarction on follow-up MRI ($p=0.04$), AOL score ($p=0.02$). There was no significant difference between the groups regarding delay from symptoms to endovascular procedure ($p=0.272$), TIMI score ($p=0.1$), TICI score ($p=0.22$).

Conclusions

Endovascular treatment of BAO is a safe and effective treatment. Recanalization seems to be a necessary but not sufficient prognostic factor for a good outcome. Further studies need to identify other clinical and/or radiological prognostic factors.

KEYWORDS: Endovascular Mechanical Recanalization, MR Imaging, Stroke

	Good outcome (mRS=0-2)	Poor outcome (mRS=3-6)	p
Clinical Data			
Number of patients	9/29 (31 %)	20/29 (61 %)	
Number of deceased patients	0	9/20 (45 %)	
Number of male patients	8/9 (88.9 %)	13/20 (65 %)	$p=0.37$
Mean age (years)	59.1	62.05	$p=0.61$
mean NIHSS at admission	22	26.75	$p=0.34$
mean NIHSS at day 1	2.7	31.26	$p<0.0001$
mean NIHSS at day 7	1	25.8	$p<0.0001$
Radiological Data before endovascular procedure			
Number of MRI before procedure	8/9 (88.9 %)	18/20 (90 %)	$p=1$
Mean Cho score	1.625	3.5	$p=0.01$
Mean Renard score	1.625	3.78	$p=0.007$
Mean Bern score	2.375	5.28	$p=0.0007$
Mean pc-ASPECTS	8.125	6.1	$p=0.007$
Number of uni-/bilateral thalamic infarction	0/8	6/18 (33.3 %)	$p=0.13$
Endovascular Procedure			
Mean delay between symptoms and procedure (min)	308.6	410.3	$p=0.27$
Mean procedure length (minutes)	106	119.5	$p=0.53$
Mean TIMI score	2.22	1.65	$p=0.11$
Mean AOL score	2.56	1.85	$p=0.024$

Number of patients with TICI = 2b-3	6/9 (66.7 %)	7/20 (35 %)	$p=0.23$
Number of patients with use of Solitaire device	5/9 (55.6 %)	4/20 (20 %)	$p=0.09$
Mean number of retriever tentatives (Solitaire only)	1	2.75	$p=0.02$
Radiological Data after endovascular procedure			
Number of MRI 24-48 hours after procedure	9/9 (100 %)	16/20 (80 %)	$p=0.28$
Mean Cho score	2	4.94	$p=0.006$
Mean Renard score	2.5	5	$p=0.0005$
Number of uni-/bilateral thalamic infarction	1/9 (11.1 %)	11/20 (55 %)	$p=0.04$
Number of hemorrhagic transformation	1/9 (11.1 %)	10/20 (50 %)	$p=0.096$

Thursday, May 22
10:30AM - 12:00PM
Room 524

87 - PARALLEL PAPERS: Excerptas

O-853

10:30AM - 10:35AM

Location, Location, Location! – A Valuable Discriminator for Diagnosing Pigmented Villonodular Synovitis (PVNS) of the Cervical Spine.

N Koontz¹, E Quigley², B Witt², R Sanders², E Stevens², L Shah²

¹University of Utah School of Medicine, Salt Lake City, UT,
²University of Utah, Salt Lake City, UT

Purpose

Pigmented villonodular synovitis (PVNS) is an uncommon benign, but locally aggressive lesion characterized by synovial proliferation of synovial joints, usually the appendicular large joints. Pigmented villonodular synovitis of the spine is rare, typically involving the posterior elements. We present a case of PVNS of the cervical spine, highlighting useful imaging features and describing pathologic correlation.

Materials and Methods

A 49-year-old woman presented with a two-year history of progressive neck stiffness and occasional left jaw pain. MR imaging (MRI) revealed a heterogeneously enhancing low T1, markedly low T2 signal intensity (SI) mass involving the dens, extending across the atlanto-axial joint into the C1 anterior arch and into prevertebral space. NECT demonstrated a soft tissue density lesion with sharp zone

Note: Scanned images are included in the proceedings. Some submitted images were reduced during editing thereby decreasing clarity. Also, refer to the Program Planner. Proceedings Content as of 3/28/2014.

of transition and thin, sclerotic margins with focal cortical disruption of the dens and C1 anterior arch. The lesion was hypermetabolic (max SUV 24.53) on FDG-PET/CT imaging. Histopathology from a CT-guided biopsy revealed numerous histiocytes, several multinucleated giant cells, foamy macrophages, and pigmented macrophages. The majority of the cells were CD68 positive on immunohistochemical stains, indicating a histiocytic differentiation.

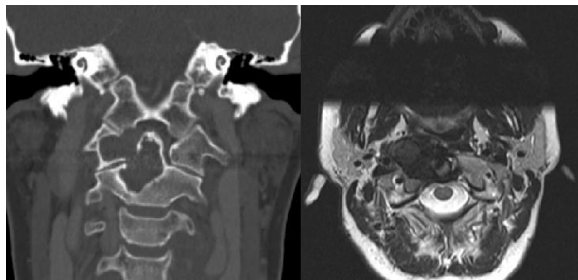
Results

Three subtypes of PVNS (diffuse intra-articular, localized intra-articular, localized extra-articular) can affect virtually any joint. The lesion in this case is centered about the joint space, which is helpful in differentiating that this is a tumor of synovial origin (such as PVNS), rather than a juxta-articular lesion [such as giant cell tumor of bone or gout, which may demonstrate very similar imaging characteristics, particularly on MR imaging (MRI)]. On MRI, PVNS classically demonstrates intermediate to low signal intensity on T1- and T2-weighted sequences due to the presence of hemosiderin, accounting for the "blooming" artifact seen on GRE sequences. The absence of hemosiderosis does not exclude PVNS. Variability in SI may be due to varying amounts of blood products, fibrous tissue, and edema. Moderate, inhomogeneous postcontrast enhancement is typical. On CT, there are well defined erosions with sclerotic margins and a soft tissue component without matrix calcification. Lesions may be hypermetabolic on FDG-PET.

Conclusions

Pigmented villonodular synovitis is a benign but locally aggressive lesion of synovial proliferation that rarely occurs in the cervical spine and may pose a diagnostic dilemma for radiologists. The lytic nature and FDG-avidity may mimic a metastatic lesion and the low signal intensity on T1-weighted, T2-weighted imaging and gradient recalled echo (GRE) may mimic giant cell tumor of bone, gout, or amyloid. Recognizing that the lesion is centered about the joint space is a valuable discriminator to identify a synovial lesion, including the diagnosis of PVNS.

KEYWORDS: Differential Diagnosis, Spinal Neoplasm, Tumor-Like Conditions



O-854

10:35AM - 10:40AM

Acute Cerebral Fat Embolism Secondary to Left Ventricular Assist Device Placement

A Chaudhry1, M Gul2, L Gerges3, R Peyster4

1Stony Brook University Medical Center, westbury, NY, 2Winthrop University Hospital, Mineola, NY, 3Stony Brook University Medical Center, Bellport, NY, 4Stony Brook University Medical Center, Stony Brook, NY

Purpose

Left ventricular assist device (LVAD) is a fairly common intervention that is used as a supportive measure for patients in circulatory failure usually from severe cardiomyopathy and are awaiting heart transplant. Common complications of this procedure include: hemorrhage (secondary to anticoagulation), infection, arrhythmias, pulmonary insufficiency, thromboembolic events (acute MI and cerebrovascular accidents). We present a rare case of acute central nervous system (CNS) fat embolism resulting from LVAD placement. Previously reported cases of CNS fat embolism have resulted from trauma, cardiac surgery or from angiography.

Materials and Methods

A 67-year-old male with past medical history of CAD w/ MI s/p CABG x 4, paroxysmal atrial flutter s/p ablation, stage 3b/4 heart failure (LVEF 15-20%) on heart transplant list was admitted to the hospital for left ventricular assist device placement. Postprocedure, when the patient woke up, he noticed right upper and lower extremity weakness. Physical exam revealed 0/5 strength in the right upper and lower extremity, otherwise, the remainder of the neurologic exam was unremarkable. Routine laboratory values were within expected postop range. The patient was last seen normal prior to the surgery and at the time of physical exam was intubated, but was alert and oriented * 3 and not on any sedations. No hemorrhage was seen on the noncontrast CT; however, it revealed diffuse hypoattenuation of the left ganglia and caudate nucleus with evidence of edema, concerning for acute ischemic infarct. Additionally, a long segment abnormal tubular low density was seen within the left MCA which correspond to the left MCA filling and perfusion defects seen on the angiogram and perfusion study, respectively. The tubular hypoattenuation measured fat density on CT, raising concern for fat embolus. The patient was unable to undergo brain MR imaging (MRI) because of his AICD. Computed tomography perfusion of the brain revealed decreased flow and perfusion in the left MCA territory.

Results

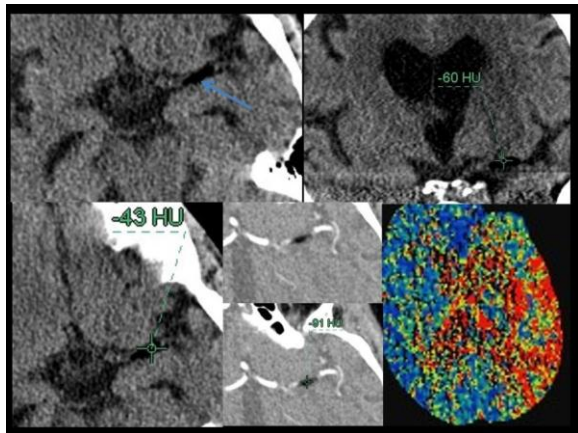
Note: Scanned images are included in the proceedings. Some submitted images were reduced during editing thereby decreasing clarity. Also, refer to the Program Planner. Proceedings Content as of 3/28/2014.

Noncontrast CT brain revealed a long segment left MCA tubular hypodensity measuring fat attenuation, suggestive of a fat embolus. Computed tomography brain with contrast revealed a long segment filling defect in the M1 branch of the left MCA measuring fat attenuation, compatible with a fat embolus. Computed tomography perfusion images revealed diminished blood flow and mean transit time, likely related to the fat embolus. However, there was less than expected perfusion defect, likely due to residual blood flow in the left MCA through the pliable fat embolus, resulting in more of an acute ischemic state rather than a total gross large territory infarction, which one would expect from a blood clot.

Conclusions

Although thrombotic stroke are reported to occur in up to 12 to 16% of patients, central nervous system (CNS) fat embolism is rarely encountered. To our knowledge, there has not been a case reported of acute fat embolism in patients with LVAD placement. Most common reported cases of CNS fat embolism were seen in the setting of traumatic long bone fractures with subsequent embolization of bone marrow fat to the brain via patent foramen ovale. Given the degree of advanced atherosclerosis in our patient, placement of LVAD probably dislodged a cholesterol plaque from the heart or the aorta to the brain leading to CNS fat embolism. Unique imaging findings of CNS fat embolism include presence of tubular clot that measures fat attenuation on unenhanced CT head and follows MRI signal characteristics of fat on all sequences. Additional interesting finding is that there appears to be a less than expected size of brain infarct in these patients, possibly secondary to the pliable nature of the fat embolus which allows for passage for some blood thereby resulting in severe ischemia more so than gross infarction. Our patient was treated with anticoagulation and had gradually near full recovery to baseline. This perhaps suggests better prognosis in patients with CNS fat embolism as compared to those with same sized thrombotic embolus.

KEYWORDS: Fat Emboli



O-855

10:40AM - 10:45AM

A SMART Case: Stroke Like Migraine Attacks after Radiation Therapy

S Karnezis¹, B Yoo², N Salamon²

¹University of California Los Angeles, Los Angeles, CA,
²David Geffen School of Medicine at University of California Los Angeles, Los Angeles, CA

Purpose

We report a case of a patient with reversible clinical and radiologic features suggestive of SMART syndrome (Stroke-Like Migraine Attacks after Radiation Therapy), a late, uncommon and reversible complication after radiation therapy for brain tumors.

Materials and Methods

A 54-year-old man presented to an outside hospital with new onset of altered mental status and generalized seizures. His past medical history was significant for a left frontal lobe oligodendroglioma status postresection and chemoradiation therapy in 1991. Prior to his current presentation, the patient was doing well, without evidence of tumor recurrence; he was discharged from care with regards for his brain tumor for the past six years. Recurrent seizures characterized by staring and unresponsiveness were observed with progression to generalized seizure activity. Following transfer to our institution, the patient continued to have witnessed seizures. He was intubated and put on burst suppression on day eight. His work up included repeated cerebrospinal fluid (CSF) analyses, which revealed slightly elevated protein, but no evidence of bacterial, viral, fungal or tuberculosis. His CSF cytology revealed no malignant cells. The patient was treated empirically with antibiotics and antivirals, despite having no evidence of infection. During his hospital course, the patient seizures gradually improved, and his anti-seizure medications were tapered off. Upon discharge, the patient was seizure free, and EEG revealed no subclinical seizures or epileptic discharges.

Results

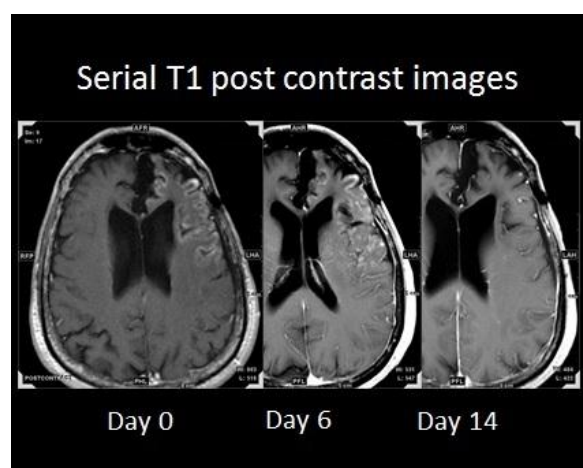
Admission MR imaging (MRI) demonstrated left frontal lobe cortical edema, mild patchy gyral enhancement, mild restricted diffusion, and normal vessel imaging. Subsequent imaging demonstrated increasingly prominent gyral enhancement, prominent cortical edema, and restricted diffusion with enhancement reaching peak intensity on day six. A small area of cortical laminar necrosis developed along the left middle frontal sulcus. By day 14, enhancement completely resolved, and cortical edema gradually decreased.

Note: Scanned images are included in the proceedings. Some submitted images were reduced during editing thereby decreasing clarity. Also, refer to the Program Planner. Proceedings Content as of 3/28/2014.

Conclusions

SMART is a rare syndrome with transient, reversible neurological symptoms often manifesting with headaches and seizures, occurring years after radiation therapy for brain tumors. While often mistaken on presentation for cerebral infarction, encephalitis, and recurrent malignancy, radiologic features are suggestive with salient findings including transient unilateral gyral enhancement and focal cortical edema. Early consideration of this entity can prevent unnecessary treatment including neurosurgical procedures with potentially significant neurologic sequelae.

KEYWORDS: Migraine, Seizure, Stroke



O-856

10:45AM - 10:50AM

Transthyretin-related Familial Amyloidosis: a cause of leptomeningeal enhancement and superficial siderosis

J Hunsaker¹, G Miller¹, N Campeau¹

¹Mayo Clinic, Rochester, MN

Purpose

Present the imaging findings of transthyretin-related familial amyloidosis, a rare and progressively disabling inherited disease.

Materials and Methods

A 43-year-old male presented with reported history of severe meningoencephalitis 10 years previously, manifesting as extremity paresthesias, severe aphasia, profound weakness, and incontinence. This was followed by spontaneous improvement without identification of a

causative infectious, inflammatory, or autoimmune etiology. He experienced subsequent transient episodes of aphasia and extremity paresthesias superimposed on persistent mild gait and cognitive deficits from his initial event. The patient had experienced bowel and bladder dysfunction with progressive lower extremity fatigue in the nine months preceding his presentation at our tertiary referral center. Brain MR imaging (MRI) performed 18 months previously showed diffuse intracranial leptomeningeal enhancement and superficial siderosis which persisted on a repeat brain MRI. Lumbar puncture was notable only for elevated protein. PET/CT was negative for malignancy. Additional MRI of the spinal cord was performed demonstrating diffuse leptomeningeal enhancement and possible superficial siderosis. Enlarged vessels were noted at the time of lumbar spine MRI, raising suspicion of a dural arteriovenous fistula. However, two subsequent spinal angiograms were negative. Open biopsy of the dura and leptomeninges was performed at L3. Although no gross dural or leptomeningeal abnormality was seen, engorged, but not arterialized, veins were present along the nerves of the cauda equina. Final pathology demonstrated prominent amyloid deposition with further analysis characterizing the amyloid as the transthyretin-type associated with familial amyloidosis, confirmed with gene sequencing. Liver transplant was considered, but ultimately not recommended due to severe leptomeningeal involvement. Four months following initiation of treatment with doxycycline and ursodeoxycholic acid, the patient had made marked subjective improvement with repeat MRI demonstrating objective improvement in leptomeningeal enhancement.

Results

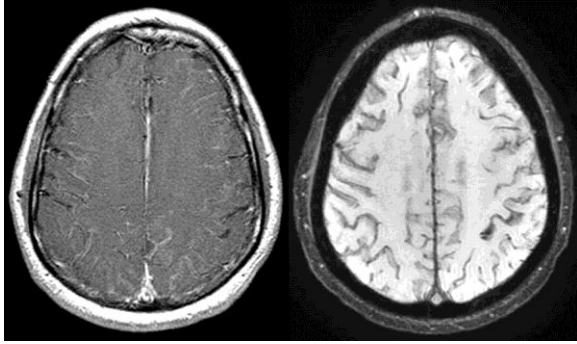
Enhanced T1 and susceptibility-weighted imaging demonstrated diffuse cerebral leptomeningeal enhancement and superficial siderosis. Additional images (not shown) demonstrated leptomeningeal enhancement of the spinal cord, enlarged vessels along the inferior spinal cord and cauda equina nerve roots.

Conclusions

Differential considerations of leptomeningeal enhancement and superficial siderosis are broad. However, the presence of both in the setting of elevated cerebrospinal fluid (CSF) protein suggests the unifying diagnosis of leptomeningeal transthyretin related familial amyloidosis.

KEYWORDS: Amyloid, Leptomeningeal, Superficial Hemosiderosis

Note: Scanned images are included in the proceedings. Some submitted images were reduced during editing thereby decreasing clarity. Also, refer to the Program Planner. Proceedings Content as of 3/28/2014.



O-857

10:50AM - 10:55AM

Cauda Equina Syndrome Secondary to Tophaceous Gout of the Spine

A Agarwal¹, S Kanekar², K Thamburaj³

¹Penn State University, Hummelstown, PA, ²Penn State Milton S Hershey Medical Center, Hershey, PA, ³Penn State University, Hershey, PA

Purpose

This report describes a case of cauda equina syndrome due to gouty tophus of the lumbar facet joints involving the epidural space, which caused marked epidural inflammation and compression. The clinical details of the symptoms, investigations, which included computed tomography (CT) and the results of operative treatment are presented. A Medline search of the literature for the past 50 years yielded only 11 other reported cases of tophaceous gout involving the facet joints of the spine. This particular case illustrates the difficulties in making the diagnosis, especially from common lesions like spinal metastases.

Materials and Methods

A 85-year-old man was admitted to the Emergency Department (ED) because of the inability to pass urine and a 1-day history of right thigh pain. He had a history of hypertension and gouty arthritis with gouty tophi in both hands and both feet. Urinary retention and overflow incontinence developed on the day of admission. Physical examination showed that the power of the lower limbs was normal; however perianal sensation was impaired. Patient had a cardiac pacemaker, hence CT of the lumbar spine was ordered instead of MR imaging (MRI).

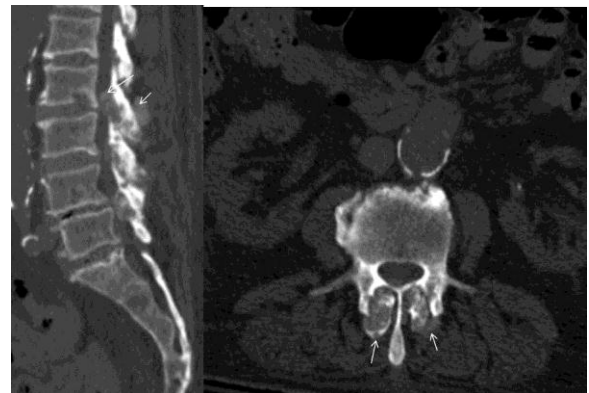
Results

Computed tomography revealed multiple juxta-articular erosions involving the lumbar facet joints with large posterior epidural soft tissue components causing severe canal stenosis and compression of the cauda equina roots at L2-L3 level (Figure 1). The epidural soft tissue was hyperdense. The joint space was relatively preserved. Emergency posterior decompression with L2-L5 laminectomies was performed. The facet joints were distended because of chalky material; the facet joint on the left side was affected more severely than the right. The chalky material was extending into the epidural space, which caused marked inflammation of the epidural tissue, as well as cauda equina compression. The chalky material was removed from the epidural space and the facet joints, and was sent for histological examination. Pathological examination revealed that the chalky material was a tophaceous deposit with an associated granulomatous response. The neurological deficit gradually improved postoperatively.

Conclusions

Although rare, pseudogout should be considered in the differential diagnosis of low back pain, radiculopathy or cauda equina syndrome in patient with known gouty arthritis. Making a correct diagnosis is difficult because symptoms and signs resemble those of degenerative lumbar spinal disease and radiological features of chondrocalcinosis may not be present. Classic imaging finding include a dense asymmetrical, well defined soft tissue mass, juxta-articular erosion, and relative preservation of the joint space.

KEYWORDS: Cauda Equina, Gout



O-858

10:55AM - 11:00AM

MR Imaging Findings in Acute Hyperammonemic Encephalopathy

Note: Scanned images are included in the proceedings. Some submitted images were reduced during editing thereby decreasing clarity. Also, refer to the Program Planner. Proceedings Content as of 3/28/2014.

E Flaherty¹, C Bazan¹, B Winegar¹, W Altmeyer¹

¹University of Texas Health Science Center San Antonio, San Antonio, TX

Purpose

Acute hepatic encephalopathy is a potentially reversible clinical disorder, with significant morbidity and mortality if prompt treatment is not initiated. Elevated plasma ammonia levels have been implicated as the major contributor in the development of hepatic encephalopathy, and the degree of hyperammonemia has been shown to correlate with the severity of symptoms. We present the MR imaging (MRI) findings of acute hyperammonemic hepatic encephalopathy.

Materials and Methods

Three patients who presented with acute hyperammonemic encephalopathy resulting from acute or chronic hepatic failure and hepatic failure following hydrochlorothiazide-induced necrotizing pancreatitis were included. Peak plasma ammonia levels ranged from 123 - 472 umol/L. Each patient underwent MR imaging of the brain, with symmetric involvement of the cingulate gyri and subinsular cortices identified in all cases. Two of the three patients whose peak ammonia levels reached 423 umol/L and 472 umol/L died, as it was determined that their prognosis for a meaningful recovery was poor.

Results

Extensive cortical signal changes were seen in each case, with notable symmetric restricted diffusion and increased T2/FLAIR signal intensity involving the bilateral cingulate gyri and insular cortices visualized in all cases. Similar signal characteristics involving other regions of the brain were more variable.

Conclusions

Elevated ammonia levels can have serious central nervous system (CNS) consequences. Patients with acute hyperammonemic encephalopathy demonstrate characteristic regions of signal change on MR imaging. Thus, knowledge of the MRI findings in such patients can aid the clinician in early, aggressive treatment, and possibly minimize long term morbidity.

KEYWORDS: Encephalopathy, Hyperammonemic, MR Imaging

O-859

11:00AM - 11:05AM

Isolated Intracerebral Light Chain Deposition Disease: Novel Imaging and Pathologic Findings

J Yu¹, C Glastonbury¹

¹University of California San Francisco, San Francisco, CA

Purpose

The purpose of the abstract is to (1) describe the novel imaging and pathologic findings of a unique case of intracerebral light chain deposition disease mimicking an intracranial tumor and (2) to broaden our emerging understanding of the imaging features of light chain deposition disease within the central nervous system.

Materials and Methods

Light chain deposition disease (LCDD) is a rare clinicopathologic entity first described in 1976 and is characterized by a monoclonal gammopathy that results in nonamyloid immunoglobulin light chain tissue deposition. Light chain deposition disease most commonly presents in the setting of a plasma cell dyscrasia and is associated with multiple myeloma in two thirds of reported cases and also is associated with other B-cell neoplasms such as lymphoma and chronic lymphocytic leukemia. Renal involvement is the most common manifestation of LCDD but also can involve the heart, liver, lungs and in rare instances the central nervous system. Within the central nervous system, only four cases of intracerebral LCDD have been reported previously. The case presented herein is the first instance of an intracerebral LCDD in the absence of known lymphoproliferative disease or the presence of local plasma cells and serves to widen our appreciation for the various clinical and imaging manifestations of LCDD within the central nervous system.

Results

MR imaging of the brain revealed a T1 hypointense, T2/FLAIR hyperintense, nonenhancing mass lesion centered in the right superior and middle frontal lobes measuring 4.7 x 3.9 x 3.8-cm (anteroposterior x transverse x craniocaudal) with local mass effect and effacement of overlying sulci and subjacent anterior horn of the right lateral ventricle. The large intracranial mass demonstrated no intrinsic magnetic susceptibility artifact, complete absence of postcontrast enhancement and homogeneous facilitated diffusion. Targeted dynamic gadolinium-enhanced axial perfusion imaging of the mass demonstrated no cerebral blood volume as compared to contralateral white matter.

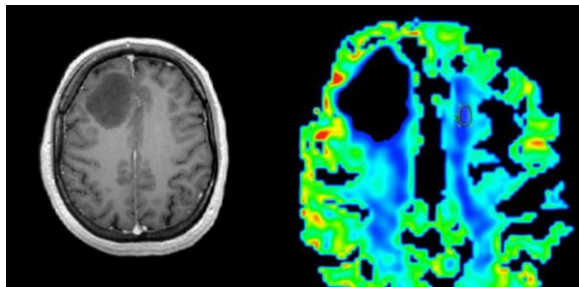
Conclusions

The previous reports of intracerebral LCDD were discovered in the setting of a known plasma cell dyscrasia or in the presence of local mature plasma cells whose local synthesis of light chains generated the intracranial mass, both of which are conspicuously absent in the case presented here. Additionally, the imaging features of this unique case of LCDD also mirror the surprising pathologic findings. Unlike the previously reported cases of intracerebral LCDD, magnetic resonance imaging of our mass reveals no evidence of postgadolinium contrast

Note: Scanned images are included in the proceedings. Some submitted images were reduced during editing thereby decreasing clarity. Also, refer to the Program Planner. Proceedings Content as of 3/28/2014.

enhancement on T1-weighted images and little to no evidence of perfusion on dynamic gadolinium-enhanced perfusion imaging. Both imaging features stand in stark contrast to the reported imaging findings of prior reports of LCDD, which demonstrated varying degrees of enhancement on postcontrast imaging. The lack of enhancement observed in our case, then, likely reflects the novel underlying pathologic findings. This unique case reflects a growing understanding of the varying radiologic and pathologic features of LCDD within the central nervous system and a growing appreciation of a more heterogeneous disease process than previously thought.

KEYWORDS: Masses, MR Imaging Brain



O-860

11:05AM - 11:10AM

AIDS Related EBV Associated Smooth Muscle Tumor Mimicking a Meningioma.

A Saad¹, L Nickell¹, S Bogale¹, M Massand², C Coimbra¹, M Opatowsky¹

¹Baylor University Medical Center, Dallas, TX, ²Cleveland Clinic, Cleveland, OH

Purpose

The purpose of this excerpt is to describe the imaging and clinico-pathologic features of Epstein-Barr virus (EBV) associated smooth muscle tumors (SMT) in the central nervous system using an illustrative case of a dural-based SMT presenting as a suspected meningioma.

Materials and Methods

A 46-year-old man with a history of HIV/AIDS and disseminated histoplasmosis treated one year prior presented with recent onset of right-sided hearing loss and dizziness. The patient underwent magnetic resonance imaging (MRI) of the brain, which revealed the interval development of a dural-based mass arising from the right petrous apex (Figures 1, 2), not present on brain MRI one year prior. A right fronto-orbitozygomatic craniotomy was

performed with resection of the lesion, which upon pathologic examination revealed features compatible with an EBV-associated smooth muscle tumor.

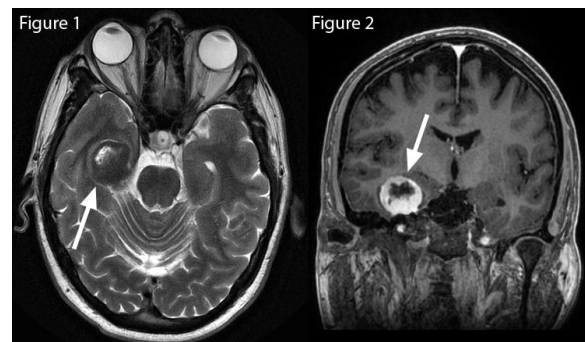
Results

Figure 1: Axial T2-weighted image reveals a hypointense extra-axial mass (white arrow) arising from the right petrous apex with a central region of cystic/necrotic change. Figure 2: Coronal T1 postcontrast image shows an avidly enhancing extra-axial mass (white arrow) arising from the right petrous apex with a broad dural attachment and a central region of nonenhancing cystic/necrotic change.

Conclusions

Epstein-Barr virus-associated smooth muscle tumors are an increasingly reported non-AIDS defining neoplasm, with the majority of reported cases arising in young severely immunosuppressed individuals. As in this case, tumors generally demonstrate spindle cells with smooth muscle actin and muscle specific actin reactivity in addition to positive in situ hybridization with EBV RNA. These neoplasms are designated as leiomyoma versus leiomyosarcoma based on necrosis and mitotic activity; however the existing data do not demonstrate a strong histologic correlation with patient prognosis. The central nervous system (CNS) is the most common reported site of AIDS-associated SMT, with reported lesions presenting as extra-axial dural-based enhancing masses. Patient treatment options include lesion resection as well as chemoradiotherapy and highly active antiretroviral therapy (HART). Tumor-related death is seen in a minority of cases.

KEYWORDS: AIDS, Epstein Barr Virus, Meningioma



O-861

11:10AM - 11:15AM

A Case of Chronic Lymphocytic Inflammation with Pontine Perivascular Enhancement Responsive to Steroids (CLIPPERS) in a Child

Note: Scanned images are included in the proceedings. Some submitted images were reduced during editing thereby decreasing clarity. Also, refer to the Program Planner. Proceedings Content as of 3/28/2014.

R Adas¹, A Samkari¹, S Abdullah¹

¹National Guard Hospital, Jeddah, Saudi Arabia

Purpose

Our purpose is to present a case of chronic lymphocytic inflammation with pontine perivascular enhancement responsive to steroids (CLIPPERS) in a nine-year-old boy. To the best of our knowledge this is the youngest patient reported with this entity in the English literature.

Materials and Methods

A nine-year-old boy presented to our neurology clinic with abnormal gait and abnormal left eye movement for one month. He had headache and repeated vomiting but reported no loss of consciousness. He gave a history of minor head trauma about a month before presentation. There was no significant past medical or family history. On examination, the patient was vitally stable and looked generally well. His central nervous system (CNS) exam showed no neurological deficits. He had mild ataxia with tendency to falling to the left side. The patient's electroencephalogram (EEG) showed inactive bi-occipital epileptic activity and he was sent home on Keppra pending his MR imaging (MRI) appointment. An MRI was performed in a private institute a week afterwards and showed bilateral brachium pontis lesions, which according to the outside report were concerning for a glioma. The patient underwent biopsy and received postoperative dexamethasone for brain edema. The patient was discharged and was later booked for a postoperative MRI in our institution where the pre-operative studies also were reviewed. The diagnosis of CLIPPERS was suggested on imaging and later confirmed by pathology. The patient currently is doing very well and is back to school. There is minimal ataxia and left eye nystagmus. He is currently on maintenance steroids.

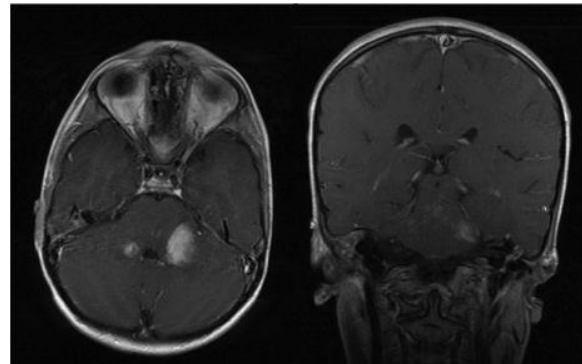
Results

The initial MRI images showed solid enhancing low T1 and high T2 lesions in both middle cerebellar peduncles with mass effect on the fourth ventricle but no hydrocephalus. There was no diffusion restriction or blooming. Abnormal subtle punctuate perivascular enhancement also were noted in the pons. No supratentorial abnormalities were identified. The postoperative MRI showed interval development of a small surgical cavity in the left brachium pontis. The lesions however had become smaller in response to the steroids with very minimal residual enhancement.

Conclusions

CLIPPERS is a new inflammatory entity described in 2010. Since then only adult and adolescent cases have been reported. Knowing that this entity can affect young children will raise the index of suspicion and guide clinicians and pathologist to making the correct diagnosis to avoid unnecessary measures.

KEYWORDS: Inflammatory, MR Imaging



O-862

11:15AM - 11:20AM

Another Boring Case of NF2 – NOT! Schwannomatosis

N Koontz¹, A Agarwal², K Mosier², L Shah³

¹University of Utah School of Medicine, Salt Lake City, UT,
²Indiana University School of Medicine, Indianapolis, IN,
³University of Utah, Salt Lake City, UT

Purpose

Schwannomatosis is an under-recognized entity characterized by multiple schwannomas without involvement of the vestibular nerves. Given its similarity to NF2, the two diagnoses are easily confused. We present a case of schwannomatosis predominantly involving the spine, describe the similarities and differences between schwannomatosis and NF2, highlight useful imaging and clinical discriminators, and discuss the importance of distinguishing between these diagnoses.

Materials and Methods

A 36-year-old woman with history of prior resection of a cervical schwannoma presented with severe back pain. Past medical history, family history, and physical examination were unremarkable. MR imaging (MRI) of the lumbar spine revealed numerous T1 hypointense, T2 hyperintense, enhancing extramedullary, intradural masses along the course of the cauda equina nerve roots, as well as within the paraspinous muscles and presacral pelvis. MR imaging of the cervical and thoracic spine revealed numerous other spinal and dural-based lesions, and MRI of the brain was negative for vestibular schwannomas. No pathologic mutation of the NF2 gene was found after comprehensive genetic analysis.

Note: Scanned images are included in the proceedings. Some submitted images were reduced during editing thereby decreasing clarity. Also, refer to the Program Planner. Proceedings Content as of 3/28/2014.

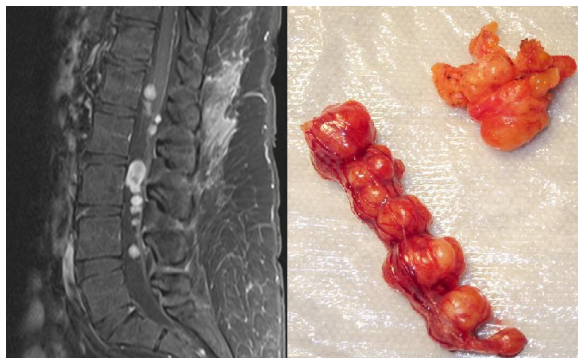
Results

Schwannomatosis is genetically different from NF2. Although the SMARCB1/INI1 gene plays a role in tumorigenesis, no genetic test exists to definitively make the diagnosis. For this reason, imaging plays a critical role in making the diagnosis. Patients who are older than 30 with two or more nonintradermal schwannomas or one pathologically confirmed schwannoma and a first degree relative with the diagnosis can be diagnosed with schwannomatosis, provided they do not have a vestibular schwannoma on MRI, fulfill diagnostic criteria for NF2, have a first-degree relative with NF2, or carry a known constitutional NF2 gene mutation. MR imaging of the brain is the primary means of evaluating these patients and excluding vestibular schwannomas. Findings include multiple round-to-oval lesions along the course of peripheral nerves. Lesions are typically low-to-intermediate signal intensity on T1-weighted imaging, high signal intensity on T2-weighted imaging, PD, and STIR, and demonstrate variable contrast enhancement. On CT, lesions are usually hypo-to-isodense to skeletal muscle with variable contrast enhancement.

Conclusions

Schwannomatosis and NF2 are unique disorders that easily are confused by imagers. It is critical for radiologists to differentiate the two on imaging grounds, as there are important differences in clinical outcomes (schwannomatosis patients do not have a decreased life expectancy, unlike NF2 patients, and do not need to worry about future sensorineural hearing loss) and clinical management of the two disorders. Location of lesions is a critical imaging discriminator and the absence of vestibular nerve lesions strongly favors the diagnosis of schwannomatosis over NF2.

KEYWORDS: Differential Diagnosis, Neurofibromatosis, Schwannoma



O-863

11:20AM - 11:25AM

Delayed Post Hypoxic Leukoencephalopathy (DPHL), A case report.

A Meshksar¹, R Khan¹, W Kubal¹, K Nael¹

¹University of Arizona, Tucson, AZ

Purpose

Delayed posthypoxic leukoencephalopathy (DPHL) is a rare consequence of hypoxic-ischemic brain injury. We describe the imaging and clinical findings of DPHL in a young patient after an episode of cardiac arrest.

Materials and Methods

The patient is a 19-year-old male who was admitted to hospital for viral cardiomyopathy and poor cardiac function. He developed cardiac arrest during his admission and was comatose for two days before gaining his normal level of consciousness. Brain MR imaging (MRI) after cardiac arrest showed restricted diffusion involving bilateral basal ganglia, corona radiata and parieto-occipital cortex with associated T2/FLAIR hyperintensity compatible with hypoxic ischemic injury. Three weeks after his arrest he developed behavioral changes and myoclonus. His level of consciousness gradually declined, developed involuntary movements of all extremities and did not follow commands. Second MRI examination six weeks after cardiac arrest revealed severe interval progressive cerebral volume loss with a central pattern predominance evidenced by enlargement of the cerebral lateral ventricles and reactive gliosis along areas of infarctions. Eventually he became comatose again, had another incident of cardiac arrest and passed away. The results of serum chemistry analyses, serum lactate and pyruvate level, thyrotropin, vitamin B12 complete blood cell count, coagulation studies, as well as CMV, HSV, West Nile virus of cerebrospinal fluid (CSF) were all normal. The result of autopsy revealed thinning of the gray matter with extensive neuronal loss in all layers of the cortex, gemistocytic astrocytes, and focal areas of laminar necrosis indicating ischemic/hypoxic encephalopathy with irreversible diffuse cortical injury.

Results

Diffusion-weighted MRI (left) after cardiac arrest shows restricted diffusion along occipitoparietal cortex and basal ganglia. FLAIR image (right) performed six weeks later reveals severe interval central predominant cerebral volume loss and reactive gliosis along the infarcted regions.

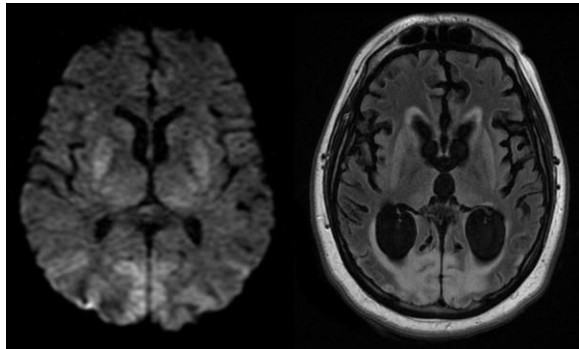
Conclusions

Delayed posthypoxic leukoencephalopathy is characterized by full or partial recovery from confusion or comatose state postcerebral hypoxia which then is followed days or weeks later by neurologic and neuropsychiatric findings including disorientation, amnesia, hyperreflexia, parkinsonism, or psychosis. Demyelination has been proposed as a pathophysiological mechanism. Widely

Note: Scanned images are included in the proceedings. Some submitted images were reduced during editing thereby decreasing clarity. Also, refer to the Program Planner. Proceedings Content as of 3/28/2014.

spaced arterioles within the white matter render it vulnerable to hypoxic injury and subsequent demyelination. Delayed posthypoxic leucoencephalopathy also has been associated with carbon monoxide poisoning, heroin inhalation, and occult abnormalities in arylsulfatase A. Prognosis is variable, usually ominous but recovery has been described in few cases.

KEYWORDS: Demyelination, Encephalopathy, Hypoxia



O-864

11:25AM - 11:30AM

A case of calcified stylopharyngeus causing globus sensation.

J Lee1, J Bello2, K Shifteh2

1Montefiore Medical Center, New York, NY, 2Montefiore Medical Center, Bronx, NY

Purpose

To present a case of a calcified stylopharyngeus muscle causing globus sensation and mimicking a foreign body.

Materials and Methods

A 64-year-old man presented to the emergency department with globus sensation after eating boneless chicken the day before. Patient reported a dull pain radiating to the right jaw and ear. A computed tomography (CT) scan of the neck was performed from the emergency department, which revealed a linear radiodense structure in the right oropharyngeal wall, interpreted as a foreign body. Patient underwent a transoral exploration, which failed to reveal a foreign body. Repeat CT scan after the exploration showed right lateral oropharyngeal edema and persistent linear radiodensity lateral to the constrictor muscles. The patient then underwent a pharyngotomy, and a calcified stylopharyngeus was excised. A month after surgery, the patient reported that the globus sensation and pain had resolved.

Results

Unenhanced CT of the neck revealed a linear radiodensity measuring approximately 5 cm in length arising just inferomedial to the distal tip of the right styloid process, extending inferomedially and terminating deep to the right lateral oropharyngeal wall (Figure 1). There was edema of the right lateral oropharyngeal wall. The styloid processes were top normal in length.

Conclusions

This case highlights a rare situation of a calcified stylopharyngeus causing pain and globus sensation. The insertion of the stylopharyngeus is comprised of a descending muscle bundle surrounding the piriform recess and a second shorter component inserting into the tonsillar bed (1). The latter was calcified in this case. Awareness of the course of the stylopharyngeus will help differentiate it from an elongated stylohyoid process or a calcified stylohyoid ligament (Eagle's syndrome).

KEYWORDS: Neck Lesions

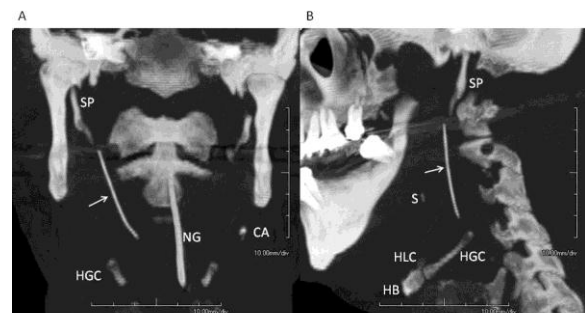


Fig. 1. Coronal and sagittal MIP images demonstrate a calcified right stylopharyngeus (arrow). SP, styloid process. NG, nasogastric tube. HB, hyoid body. HLC, hyoid lesser cornu. HGC, hyoid greater cornu. S, sialolith. CA, carotid artery calcification.

O-865

11:30AM - 11:35AM

Delayed embolization of coil fragments with associated foreign body reaction

P Alcaide Leon1, T Marotta2, L Noel de tilly3, W Montanera3, A Bharatha4

1St Michael's Hospital, Toronto, Ontario, 2St. Michael's Hospital, Toronto, Ontario, 3St Michael's Hospital, Toronto, Ontario, 4St. Michael's Hospital, Toronto, ON

Purpose

Note: Scanned images are included in the proceedings. Some submitted images were reduced during editing thereby decreasing clarity. Also, refer to the Program Planner. Proceedings Content as of 3/28/2014.

We describe a delayed complication of coil embolization of basilar tip aneurysm consistent of brain-enhancing lesions in the posterior circulation territory associated to susceptibility foci.

Materials and Methods

We report the case of a 38-year-old female who presented with a nonruptured basilar tip aneurysm and a strong family history of subarachnoid hemorrhage (grandmother who died of a subarachnoid hemorrhage at age 42 and a mother who suffered a subarachnoid hemorrhage with persistent neurological deficits at age 52). Treatment was decided and Microplex 10 Cosmos Complex and Microplex 10 Hypersoft Helical detachable coils were utilized to occlude the aneurysm.

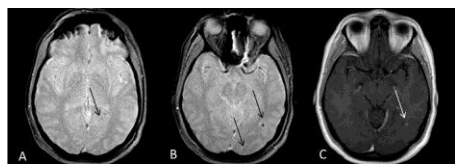
Results

Postprocedure MR performed the next day after coiling showed a few infarcts in the posterior circulation. No susceptibility foci were present at this point on T2-gradient echo images. Follow-up MR imaging (MRI) studies at three months showed new susceptibility foci at the site of the infarcts with associated nodular and ring enhancement as well as surrounding edema. Eight months follow-up MR study showed complete resolution of prior enhancement and a new rim-enhancing lesion with surrounding edema associated to a previously identified susceptibility focus. Patient remained completely asymptomatic. These findings are most in keeping with foreign body reaction secondary to embolic material of unknown source.

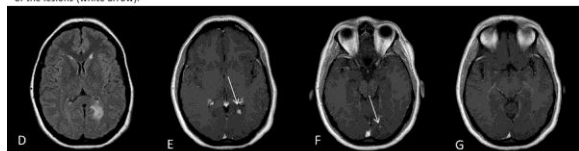
Conclusions

Very few cases of brain foreign body reaction related to aneurysm coiling have been described in the literature. Recognition of this entity is essential to avoid unnecessary brain biopsies. Characteristic features of foreign body reaction related to aneurysm coiling are enhancing lesions associated to susceptibility foci, spontaneous improvement of lesions and absence or very mild symptoms (clinikoradiological dissociation).

KEYWORDS: Aneurysm Treatment, Foreign-Body Granuloma



A, B and C: Follow up MRI performed three months after coiling. A and B. T2 weighted gradient echo sequence showing three new susceptibility foci (black arrows) - C. Contrast enhanced T1 weighted sequence showing enhancement in one of the lesions (white arrow).



D, E, F and G: Follow up MRI eight months after coiling new foci of enhancement associated to the susceptibility foci have appeared (E and F, white arrows). Previous enhancement has completely resolved (G). Edema is noted (D) in association to rim enhancing lesion in the left occipital lobe (E).

0-866

11:35AM - 11:40AM

A case of cerebral amyloid angiopathy inflammation mimicking cerebral metastasis

J Cain¹, S Wuppapapati², H Sonwalker², C Coutinho², S Mathur²

¹University of Manchester, Manchester, UK, ²Lancashire Teaching Hospitals, Preston, UK

Purpose

To describe a case of cerebral amyloid angiopathy inflammation and to highlight the salient imaging features of this condition.

Materials and Methods

A 75-year-old woman with a previous history of treated breast cancer presented with increasing confusion. She was normally cognitively intact. The patient underwent initial imaging with computed tomography (CT) both with and without contrast which were suspicious for cerebral metastasis and subsequent MRI imaging (MRI) was performed.

Results

The initial contrast-enhanced CT demonstrated three areas of vasogenic edema within the left frontal, left parietal and right temporal lobes but no discernible mass lesions were identified. The edema was presumed secondary to occult metastasis. A subsequent MRI was performed and this confirmed the presence of widespread vasogenic edema especially within the left parietal lobe but no enhancing lesions were identified. On diffusion imaging there was a subtle focal areas of susceptibility in the left parietal lobe. The patient was treated prophylactically with steroids and a subsequent MRI examination was performed two weeks later with additional gradient echo and spectroscopy sequences. The areas vasogenic edema had improved significantly since the previous imaging and the gradient echo showed multiple small focal susceptibility defects corresponding to the areas of vasogenic edema. The spectroscopy showed a subtle decrease in NAA but otherwise normal spectra within the edema. The appearances are in keeping with micro hemorrhages related to cerebral amyloid angiopathy, a diagnosis of inflammatory cerebral amyloid angiopathy. The diagnosis of cerebral metastasis was refuted.

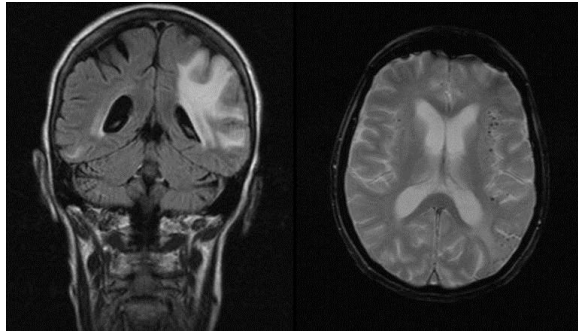
Conclusions

Cerebral angiopathy with inflammation (CAA-I) is an uncommon manifestation of amyloid angiopathy. Cerebral angiopathy with inflammation presents with acute or

Note: Scanned images are included in the proceedings. Some submitted images were reduced during editing thereby decreasing clarity. Also, refer to the Program Planner. Proceedings Content as of 3/28/2014.

subacute onset of headaches, cognitive and behavioral changes, seizures and focal neurological deficits. It is an important differential to consider in an elderly patient with behavioral change and the addition of gradient echo/susceptibility-weighted imaging is of significant diagnostic value. The condition is steroid responsive in approximately 50% of cases. This case highlights CAA-I as a possible differential diagnosis in acutely cognitively impaired patients.

KEYWORDS: Amyloid, Microbleeds, MR Spectroscopy



T8 and T10. Biopsies of the left thalamic lesion were performed and ultimately were diagnostic for Langerhans cell histiocytosis. The patient was managed with corticosteroids, chemotherapy, ventricular shunting and third ventriculostomy. On subsequent imaging the lesion showed regression, and the hydrocephalus resolved.

Results

MR imaging performed approximately six months after presentation reveals an enlarging, enhancing lesion involving both thalami. Significant surrounding edema is present extending into the medulla, and there is mass effect on the third ventricle and aqueduct resulting in mild obstructive hydrocephalus. An additional punctate enhancing lesion is noted in the right temporal lobe (arrow).

Conclusions

To the best of our knowledge we present the first case of biopsy-proven Langerhans cell histiocytosis presenting as a thalamic mass and resulting in obstructive hydrocephalus.

KEYWORDS: Hydrocephalus, Langerhans Cell Histiocytosis, Thalamic

O-867

11:40AM - 11:45AM

Langerhans Cell Histiocytosis Presenting as a Thalamic Lesion and Resulting in Obstructive Hydrocephalus

W Marashdeh¹, E Bourekas², W Slone³, R Cavaliere³, M Luttrull³

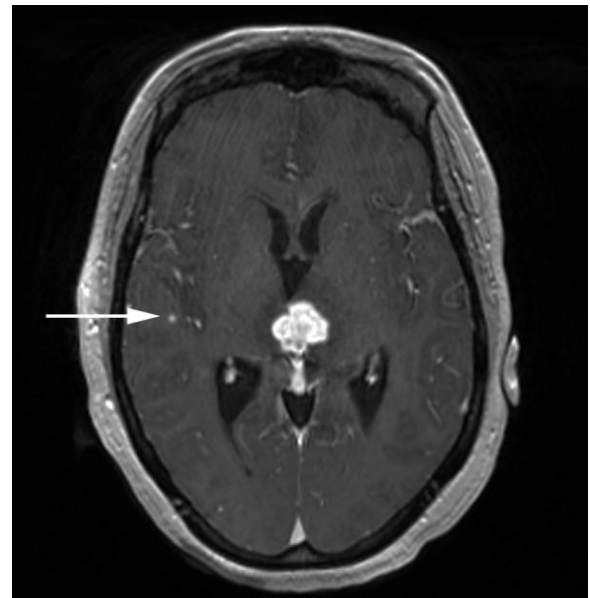
1Ohio State University Wexner Medical Center, Dublin, OH, 2Ohio State University, Columbus, OH, 3Ohio State Wexner Medical Center, Columbus, OH

Purpose

To report to the best of our knowledge the first case of Langerhans cell histiocytosis presenting as enhancing thalamic lesion and resulting in obstructive hydrocephalus.

Materials and Methods

A 27-year-old female presenting with headache and neck pain was referred for a brain MR imaging (MRI) and was found to have a nodular, ring enhancing lesion of the left thalamus abutting the third ventricle with surround T2 hyperintensity. Lesion fluctuated in size over short interval follow-up examinations, but ultimately increased in size to involve the contralateral right thalamus and resulted in mild obstructive hydrocephalus within six months of presentation. Subsequent imaging studies revealed an additional punctate enhancing lesion in the right temporal lobe and nonspecific vertebral endplate abnormalities at



O-869

11:50AM - 11:55AM

Growing Spectrum of Rhabdoid Brain Malignancies: Case of Cribriform Neuroepithelial Tumor of Intraventricular Origin.

Note: Scanned images are included in the proceedings. Some submitted images were reduced during editing thereby decreasing clarity. Also, refer to the Program Planner. Proceedings Content as of 3/28/2014.

S Zhadanov1, J Rusin2

1University of Toledo, Rossford, OH, 2Nationwide Children's Hospital, Columbus, OH

Purpose

Expanding use of genetic and neuropathologic markers in brain malignancies allows for advances in classification of central nervous system (CNS) neoplasms. However, their clinical and radiologic differentiation remains a challenging diagnostic dilemma. Atypical teratoid rhabdoid tumor (ATRT) is a devastating group of highly aggressive pediatric brain neoplasms with poor prognosis and overall survival. Meta-analysis of available cases implies that ATRT might be under-diagnosed radiologically but yet represents the most common brain malignancy in infant population. It recently has been suggested that ATRT may not constitute a single entity. Cribriform neuroepithelial tumor (CRINET) is recognized as a distinct desmoplastic neoplasm based on specific histopathologic markers and favorable clinical behavior. We present a case of CRINET with unique supratentorial manifestation arising in the lateral ventricle. Using the index case and data published elsewhere, we exemplify imaging characteristics of CRINET in attempt to increase awareness of this new type of pathology and explicate its role in differential diagnostics of pediatric CNS malignancies.

Materials and Methods

A 14-month-old male infant with unremarkable developmental milestones presented with mental status change and lethargy following a minor head trauma. Subsequent CT head performed in ER incidentally found a multiloculated lesion in the right hemisphere. Further MR imaging suggested a broad range of differential diagnoses including PNET, ATRT, ependymoma or choroid plexus carcinoma. Craniotomy and surgical exploration achieved a subtotal tumor resection. Postoperative recovery was uneventful with induction chemotherapy consisted of cisplatin, cyclophosphamide, etoposide and vincristine, reinforced by high-dose methotrexate. Subsequent chemotherapy and radiation will be contemplated depending on follow-up imaging. Histopathology found a highly cellular biphasic neoplasm with cells forming distinct cribriform strands specific for CRINET. Characteristically, tumor cell nuclei showed no immunohistochemical staining for INI1 tumor suppressor protein. Molecular analysis confirmed bi-allelic INI1 inactivation due to microdeletion of 22q accompanied by a somatic nonsense mutation. It is unclear however, as to what extent genetic alterations may affect clinical aggressiveness of CRINET and its imaging manifestations.

Results

Multimodal MR imaging of the brain demonstrated a large complex right parietal mass emanating from the atrium of the lateral ventricle. It was composed of mixed cystic and solid components with the latter exhibiting impeded water

diffusion suggestive of high cellularity. Solid areas revealed subtle signal prolongation on both T1- and T2-weighted sequences and heterogeneously enhanced. It contained foci of hemosiderin staining on gradient MRI due to varying age intrinsic hemorrhage accompanied by some perilesional vasogenic edema. Marked mass effect resulted in solid component extrusion into basal cisterns with ventricular and midbrain displacement. Despite the size of a primary lesion, there was no evidence of cerebrospinal fluid (CSF) dissemination or extracranial spread.

Conclusions

Cribriform neuroepithelial tumor is a newly described neuroepithelial CNS tumor with distinct histopathologic cribriform pattern and relatively benign prognosis. It further contributes to a genetic continuum of INI1-deficient pediatric malignancies but remains an under-recognized clinical entity and not yet included in 2007 WHO nomenclature. We discuss CRINET presentation and its pictorial profile to familiarize radiologists with growing spectrum of ATRT neoplasms. Specific genetic alterations may provide future avenues for molecular imaging of CRINET and other INI1 brain malignancies. However, a limited number of known observations warrants additional analysis to further corroborate association of specific imaging pattern in CRINET.

KEYWORDS: ATRT, Neurogenetics, Pediatric Brain Tumors



O-870

11:55AM - 12:00PM

A rare case of duplication of the pituitary gland in an adult with multiple associated congenital midline cranial and cervical lesions.

C Hilditch1, A Herwadkar1, K Gnanalingham1, D Hughes1, G Potter1

Note: Scanned images are included in the proceedings. Some submitted images were reduced during editing thereby decreasing clarity. Also, refer to the Program Planner. Proceedings Content as of 3/28/2014.

1Salford Royal Foundation NHS Trust, Salford, UK

Purpose

To demonstrate a rare case of adult pituitary gland duplication with multiple associated midline cranial and cervical abnormalities, and to discuss potential clinical implications.

Materials and Methods

A 33-year-old lady with a history of cleft palate underwent out-patient neurosurgical assessment for posterior neck pain over the preceding 12 months. Neurological examination was normal except for slightly brisk upper limb reflexes. MR imaging (MRI) and computed tomography (CT) of the spine demonstrated congenital cervical and cervico-occipital segmentation and fusion anomalies. MR imaging of the brain and pituitary region showed callosal dysgenesis and callosal lipoma, a likely left frontal epidermoid cyst, probable midline sphenoid dermoid lesion, hypothalamic hamartoma, duplication of the pituitary gland and pituitary stalk, and duplication of the distal basilar artery. The left frontal extraaxial epidermoid lesion was not associated with mass effect or adjacent parenchymal signal abnormality. The configuration of the basilar artery duplication suggested a low risk of aneurysm formation. Pituitary function tests were normal. Clinical symptoms were felt to be unrelated to the radiological findings. The patient was reviewed by skull base, neuro-oncology and endocrine multidisciplinary teams, with a plan for conservative management including clinical and radiological follow up.

Results

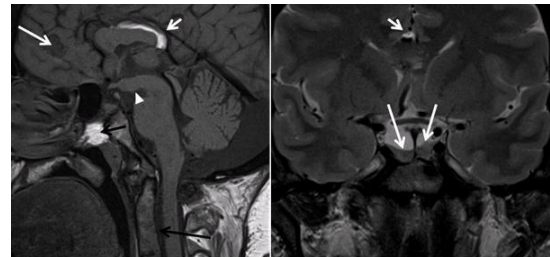
Computed tomography and MRI of the cervical spine demonstrated nonsegmentation of the C2-C3 and C3-C4 vertebrae, atlanto-occipital fusion anomalies, nonfusion of the anterior and posterior C1 arches and asymmetric jugular foramina. Junctional degenerative changes were seen at C4-5 and C5-6. MR imaging of the head and pituitary region, including diffusion-weighted imaging, demonstrated multiple midline abnormalities as follows: 1) Callosal dysgenesis with callosal lipoma, 2) Likely left frontal epidermoid cyst, 3) Fat-containing sphenoid lesion most suggestive of a dermoid lesion, 4) Likely hypothalamic hamartoma, 5) Duplication of the pituitary gland and stalk, separated by a bony septum on CT, 6) Distal basilar artery duplication, giving rise to superior cerebellar and posterior cerebral arteries.

Conclusions

Pituitary gland duplication, a rare embryonic anomaly with a poorly understood pathogenesis, is found most often in childhood, with many patients not surviving beyond puberty. Pituitary gland duplication may be associated with basilar artery duplication (with the potential for aneurysm formation) as well as several other craniofacial abnormalities such as cleft palate, agenesis of the corpus callosum, hypothalamic hamartoma and nasopharyngeal

teratoma. The wide range of lesions may be assessed by a combination of CT and MRI/MRA; we believe this is the first documented case of a midline inter-sellar bony spur in pituitary gland duplication with an intracranial epidermoid. In adult patients presenting with such lesions, the need for clinical and radiological follow up should be based on the size, nature and site of the lesions, with assessment of the likelihood of future neurological and endocrine complications, following appropriate multidisciplinary review.

KEYWORDS: Callosal Dysgenesis, Epidermoid, Pituitary Gland



Thursday, May 22

1:00PM - 2:30PM

Room 517bc

**88 - PARALLEL PAPERS: Adult Brain:
Inflammatory Diseases**

0-871

1:00PM - 1:07PM

1000 Clinically Isolated Syndromes: the "Barcelona cohort"
Defines a New Natural History Study

A Rovira¹, M Tintoré¹, C Auger¹, G Arrambide¹, R Mitjana¹, S Otero¹, J Rio¹, J Sastre-Garriga¹, X Montalban¹

¹Hospital Vall d'Hebron, Barcelona, Spain

Purpose

To determine the effect of baseline demographic, clinical, MR imaging (MRI) and biological factors on conversion to clinically definite multiple sclerosis (CDMS) and

Note: Scanned images are included in the proceedings. Some submitted images were reduced during editing thereby decreasing clarity. Also, refer to the Program Planner. Proceedings Content as of 3/28/2014.

development of disability in a prospective cohort of patients with clinically isolated syndromes (CIS).

1Biogenidec, Cambridge, MA

Materials and Methods

From 1995 to 2012, 1058 CIS patients underwent clinical and MRI follow-up (within 5 months of the CIS, at 12 months and every five years). We studied the influence of age, gender, topography, number and location of lesions at baseline (Barkhof criteria-BC) and IgG oligoclonal bands (OB) on the risk of CDMS and development of disability (EDSS 3.0) using Cox univariate and multivariate regression analysis.

Results

We included 1015 patients followed for a mean of 81 (SD 57) months with positive OB in 453/798 (57.2%) and normal MRI in 299/951 (31%). Thirty-eight percent of the patients and 57% of those with abnormal MRI were on disease modifying treatment (DMT). Gender was not associated with the development of CDMS [HR 1 (0.8 - 1.3)] or disability progression [HR 0.7 (0.5 - 1.1)]. Younger age at onset showed a higher risk of CDMS [HR 1.9 (1.1 - 3.1)] but no effect on disability progression. Patients with ON had a lower risk of conversion [HR 0.6 (0.5 - 0.8)] and disability progression [HR 0.5 (0.3 - 0.8)], however this protective effect disappeared when adjusting for MRI and DMT. Presence of OB increased the risk of CDMS [HR 1.5 (1.1 - 2)] and EDSS 3.0 [HR 2.3 (1.3 - 4.0)] independently of other factors. In the adjusted model, the presence of 3-4 BC criteria increased the risk of CDMS [HR 6.6 (4.6 - 9.5)], and disability progression [HR 2.4 (1.3 - 4.2)]. Treating patients before the second attack resulted in a reduced risk of CDMS [HR 0.6 (0.4 - 0.8)] and disability progression [HR 0.5 (0.2 - 0.9)] irrespective of MRI and other factors.

Conclusions

MR imaging baseline characteristics have a high impact in the long term. OB and topography/demographic characteristics are of medium and low impact, respectively. Early DMT decreases the risk of CDMS and accumulation of disability.

KEYWORDS: MR Imaging Brain, Multiple Sclerosis

O-872

1:07PM - 1:14PM

Asymptomatic progressive multifocal leukoencephalopathy in multiple sclerosis patients treated with natalizumab

T Dong-si1, S Richman1, G Bloomgren1, M Wenten1, J Philip1, S Datta1, J McIninch1, C Bozic1, N Richert1

Purpose

To evaluate MR imaging (MRI) findings and clinical outcomes in natalizumab-treated multiple sclerosis (MS) patients who were asymptomatic at the time they were diagnosed with progressive multifocal leukoencephalopathy (PML).

Materials and Methods

Asymptomatic patients, diagnosed by MRI findings consistent with PML and JC virus DNA detected in cerebrospinal fluid (CSF), were compared with patients who were symptomatic for PML at diagnosis. Demographics, MRI, functional status, and survival data were analyzed. Expanded Disability Status Scale (EDSS) and Karnofsky Performance Scale (KPS) scores were recorded pre-PML, at diagnosis, and at six and 12 months post-PML diagnosis.

Results

As of June 5, 2013, 372 natalizumab-associated PML cases were confirmed in multiple sclerosis patients. At diagnosis, 30 PML patients (8.1%) were asymptomatic (mean age 42.7 years; 70% female; median natalizumab exposure 40.5 months) and 342 were symptomatic (mean age 45.1 years; 70.8% female; median natalizumab exposure 40.0 months). Progressive multifocal leukoencephalopathy lesions on MRI in asymptomatic versus symptomatic patients were 68% versus 37% unilobar, 21% versus 24% multilobar, and 11% versus 40% widespread, respectively. In both groups, frontal lesions predominated. Symptoms developed in eight of 19 asymptomatic patients a median of 20 days (range 3-130) after PML diagnosis, including five patients with cognitive deficits and/or behavioral changes. Prior to PML, mean EDSS and KPS scores in asymptomatic and symptomatic patients were similar. At PML diagnosis, mean EDSS score in asymptomatic patients was significantly lower than symptomatic patients [4.1 (n=11) versus 5.4 (n=193); P=0.038]. These differences persisted six months after PML diagnosis [4.9 (n=11) versus 6.6 (n=87); P=0.007] but not 12 months after diagnosis [5.1 (n=6) versus 6.5 (n=59); P=0.169]. Similarly, mean KPS scores in asymptomatic patients showed significant improvement compared with symptomatic patients at six months [71.5 (n=10) versus 47.1 (n=108); P<0.001] but not at 12 months [56.0 (n=5) versus 46.6 (n=67); P=0.178] after PML diagnosis. As of June 5, 2013, 96.7% (29 of 30) of asymptomatic patients and 75.4% (258 of 342) of symptomatic PML patients were alive.

Conclusions

Preliminary data suggest that PML in asymptomatic patients was associated with better survival and functional outcomes compared with PML patients who were symptomatic at diagnosis. Additional research is needed to evaluate whether routine MRI monitoring may improve outcomes in natalizumab-treated patients developing PML, as a result of earlier PML detection.

Note: Scanned images are included in the proceedings. Some submitted images were reduced during editing thereby decreasing clarity. Also, refer to the Program Planner. Proceedings Content as of 3/28/2014.

KEYWORDS: Leukoencephalopathy, MR Imaging Brain, Multiple Sclerosis

O-873

1:14PM - 1:21PM

Changes in white matter fiber tracts in patients with systemic lupus erythematosus.

G Shah¹, R Shastri², I Meesa², P Cagnoli², W McCune², P Wang², S Gebarski², P Maly Sundgren²

¹University of Michigan Health System, Ann Arbor, MI,
²University of Michigan, Ann Arbor, MI

Purpose

Systemic lupus erythematosus (SLE) is a chronic inflammatory, immune-mediated, autoimmune, connective tissue disease that affects 0.1% of the general population. Neuropsychiatric SLE (NPSLE) is a severe and life-threatening condition, reported to occur in 30% to 72% of patients with SLE and associated with increased morbidity and mortality. The purpose of this study was to investigate with tractographic analysis of diffusion tensor imaging, if there are differences in white matter integrity in specific white matter tracts in NPSLE and SLE patients.

Materials and Methods

Using a 3 T MR scanner (Philips, Netherlands) DTI MR images (15 gradient directions at $b=800\text{s/mm}^2$, plus one $b=0$ image) were obtained of 18 healthy controls (HC), 19 NPSLE patients and 19 non-NPSLE patients. Groups were matched for age and sex. Tractographic analysis was performed for genu of corpus callosum (GCC), inferior fronto occipital fasciculus (IFO), anterior corona radiata (ACR), anterior limb internal capsule (AIC), superior longitudinal fasciculus (SLF), external capsule (EC), posterior limb internal capsule (PIC), inferior longitudinal fasciculus (ILF), cingulate gyrus part (CGC) and frontal part of uncinate fasciculus (UNC). Lesion burden also was analyzed on conventional MR imaging (MRI).

Results

Statistical analyses revealed decreased fractional anisotropy in GCC, IFO, ACR, AIC, SLF, EC. On the conventional MRI, severe lesion burden was seen in 10.5% (2/19), moderate in 21% (4/19), and mild in 38.8% of the NPSLE patients (7/19). Moderate lesion burden was seen in 15.8% (3/19), and mild in 42% of the non-NPSLE patients (8/19). In the HC group, six patients had mild, one patient had moderate and one patient had severe lesion burden.

Conclusions

Our data suggest that decreased fractional anisotropy is seen in some of the frontal white matter tracts in patients with NPSLE and SLE as compared to healthy volunteers.

KEYWORDS: Diffusion Tensor Image, Systemic Lupus Erythematosus

O-874

1:21PM - 1:28PM

Feasibility Study of Flow Compensation to Improve Diagnostic Quality of T1 Post Contrast Spin Echo Magnetic Resonance Images

R Khan¹, M Covington¹, A Jedd¹, P Sharma¹, E Krupinski², K Nael²

¹University of Arizona Medical Center, Tucson, AZ,
²University of Arizona, Tucson, AZ

Purpose

Phase-related pulsation artifact has long been a problem with T1 postcontrast MR imaging (MRI). Flow compensation can be applied to decrease this phase-related artifact which results in increased image clarity and improved diagnostic accuracy. In this study, we compared flow compensated (FC) with conventional nonflow compensated (non-FC) T1 postcontrast MR images.

Materials and Methods

Forty-two patients (29 F, 8 M, mean age 53 years old, age range 6-82 years old) who underwent routine contrast-enhanced MRI of the brain had both FC T1 postcontrast MR images (TR/TE 535/18) and non-FC (TR/TE 550/7.7) after intravenous injection of 0.1 mmol/kg of gadolinium contrast. Image series were randomized, reviewed blinded, and scored on a four point scale as follows: 4: Excellent image quality, none to minimal pulsation artifact. 3: Mild flow artifact; no hyperintensity that can be confused for a lesion and less than six slices with pulsation artifact. 2: Prominent pulsation artifact, with hyperintensity that may be confused for a lesion; or pulsation artifact on six or more slices. 1: Poor image quality, not interpretable. Data were analyzed with an ANOVA using the ratings as the dependent variable and condition (FC versus non-FC) and reader as independent variables. Interobserver agreement was tested with Spearman rank correlation.

Results

Twenty-eight of 42 (66%) of studies were rated nondiagnostic (score ≤ 2) in non-FC technique versus 6/42 (14%) in FC group. The image quality score was statistically significantly higher ($F = 106.502$, $p < 0.0001$) for FC technique versus non-FC. The mean \pm SD of image quality score were 2.124 (sd = 0.413) for non-FC and 3.036

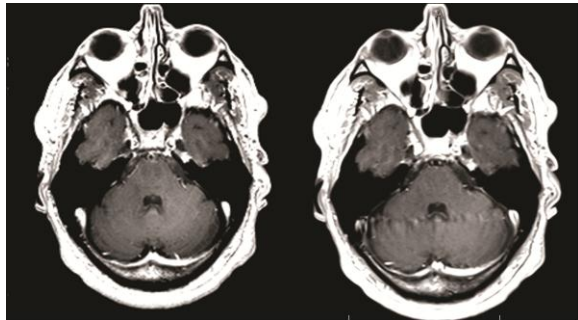
Note: Scanned images are included in the proceedings. Some submitted images were reduced during editing thereby decreasing clarity. Also, refer to the Program Planner. Proceedings Content as of 3/28/2014.

(sd = 0.633) for FC technique. The Spearman rank correlation and 95% CI for image quality scores between readers were 0.64, 95% CI 0.25-0.73 for FC and 0.56, 95% CI 0.20-0.67 for non-FC technique.

Conclusions

Postcontrast T1 with flow compensation significantly improves pulsation artifact which can help with diagnostic accuracy.

KEYWORDS: MR Imaging, MR Imaging Brain, Quality Improvement



O-875

1:28PM - 1:35PM

Cervical Cord Atrophy and Clinical Disability in Primary Progressive Multiple Sclerosis Patients

A Rovira¹, X Aymerich¹, C Auger¹, C Tur¹, J Sastre-Garriga¹, X Montalban¹

¹Hospital Vall d'Hebron, Barcelona, Spain

Purpose

To measure spinal cord atrophy in a group of patients with primary progressive multiple sclerosis (PPMS); and assess correlations between spinal cord atrophy and different brain measures (T2 lesion load, brain atrophy, magnetization transfer ratio), and clinical disability.

Materials and Methods

3D T1-weighted isotropic MR images of the cervical cord were acquired from 67 PPMS patients (34 men, 33 women; mean age: 48.7 years, range: 31–65 years; median expanded disability status scale –EDSS– score: 6.0, range: 3.0–7.0; median disease duration: 10 years, range: 0–33 years). An additional group of 9 healthy control subjects (5 men, 4 women; mean age: 45.0 years, range: 37–56 years) was also included for comparison. Spinal cord from C1 to C5 was segmented in each subject using a segmentation method [Horsfield, 2010] based on the application of an

active surface model of the cord surface. Using this method we evaluated cross-sectional spinal cord area (CSA) from spinal cord volume divided by cord length. CSA was then normalized (CSAn) to the intra-cranial cross-sectional area (ICCSA). T2 lesion load (T2LL), brain parenchymal fraction (BPF), and magnetization transfer ratio (MTR) in normal appearing brain tissue (MTRNAB) and the whole parenchyma (MTRWP) were calculated. Apart from EDSS, 25-foot timed walk test (TWT) and the inverse of the nine-hole peg test (1/NHPT) were also evaluated. Partial correlations controlled for age, gender and disease duration were performed to evaluate relationship between clinical (EDSS, TWT, 1/NHPT) and radiological variables (T2LL, BPF, MTRNAB, MTRWP, SCAn). Stepwise multiple linear regression analyses controlled for age, gender and disease duration were also carried out to investigate the ability of radiological variables to predict clinical outcomes.

Results

CSAn had a moderate correlation with EDSS ($r=-0.381$, $p=0.02$) and TWT ($r=-0.269$, $p=0.038$). CSAn was also the only predictor of greater disability as measured by EDSS and TWT, resulting in a significant improvement of a 12.5% and a 6.3% of the variance being explained by covariate variables, respectively. Models including CSAn and covariate variables also presented significance predicting EDSS ($p=0.001$) and TWT ($p=0.013$). Finally, none of the brain MR measures correlated with clinical data.

Conclusions

The findings of this study indicate that normalized cross-sectional spinal cord area measure is clinically relevant in PPMS patients. These results also suggest that CSAn seems to be more relevant than brain MRI variables to predict clinical disability.

KEYWORDS: Atrophy, Multiple Sclerosis, Spinal Cord

O-876

1:35PM - 1:42PM

Molecular Magnetic Resonance Immunoradiology Reveals Differential Effects of Interferon- β and Glatiramer Acetate on Murine Multiple Sclerosis

B Pulli¹, G Wojtkiewicz¹, M Ali¹, J Chen¹

¹Massachusetts General Hospital, Boston, MA

Purpose

Conventional contrast-enhanced MR imaging (MRI) measures blood-brain barrier breakdown, but not necessarily inflammation in multiple sclerosis (MS). We

Note: Scanned images are included in the proceedings. Some submitted images were reduced during editing thereby decreasing clarity. Also, refer to the Program Planner. Proceedings Content as of 3/28/2014.

hypothesized that MPO-Gd (bis-5HT-DTPA-Gd), a molecular MRI probe sensitive and specific for the inflammatory enzyme myeloperoxidase (MPO) (1), can detect the immunotherapeutic effects of Interferon- β (Ifn- β) and Glatiramer Acetate (GA), two current first-line drugs on the molecular level noninvasively.

Materials and Methods

Thirty female SJL mice were injected with proteolipid protein (PLP139-151) to induce experimental autoimmune encephalomyelitis, a mouse model of MS, and treated with Ifn- β (1 μ g/day), GA (150 μ g/day), or saline. To determine effects of these drugs on MPO, mice underwent MRI at 4.7 T with MPO-Gd at the disease peak (day 11-13). Lesion volumes and contrast-to-noise ratio (CNR) at 10 and 60 minutes post MPO-Gd injection were quantified. Myeloperoxidase activity and secretion experiments were conducted.

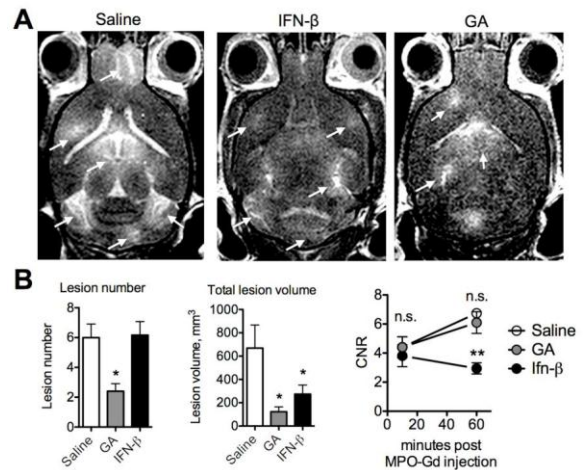
Results

Disease severity was ameliorated with both Ifn- β and GA ($p < 0.05$ compared to saline). Myeloperoxidase-Gd-enhanced MRI detected decreased number of lesions with GA (2.4 ± 1.1 , $p < 0.01$) but not with Ifn- β (6.2 ± 2.2 , $p = 0.90$) compared to saline (6.0 ± 1.8). Total lesion volume was decreased significantly with both Ifn- β and GA compared to saline (123.0 ± 92 mm² for GA, 273.3 ± 193.8 mm² for Ifn- β , and 669.0 ± 395.8 mm², $p < 0.01$). Lesion CNR at 10 minutes post MPO-Gd injection, which mostly represents blood-brain barrier breakdown, was not changed with either treatment (4.41 ± 1.44 for GA, 3.82 ± 1.84 for Ifn- β , and 4.37 ± 1.51 for saline, $p = 0.81$). Interestingly, lesion CNR at 60 minutes post MPO-Gd injection, which represents specific MPO activity *in vivo*, was reduced with Ifn- β treatment (2.95 ± 0.94 , $p < 0.01$) but not with GA treatment (6.10 ± 1.49 , $p = 0.43$) compared to saline (6.74 ± 0.29). Neither Ifn- β nor GA directly inhibited MPO activity *in vitro* ($p > 0.05$). Myeloperoxidase secretion experiments on isolated myeloid cells revealed that Ifn- β significantly reduces extracellular MPO activity upon stimulation with a secretagogue (1.45 ± 0.30 Units/second for 10ng/ml Ifn- β and 0.11 ± 0.15 for 100ng/ml versus 3.68 ± 0.11 for vehicle, $p < 0.01$), while no such effect was detected for GA (3.88 ± 1.36 for 1 μ g/ml GA and 3.56 ± 1.92 for 15 μ g/ml GA, $p > 0.05$).

Conclusions

Myeloperoxidase-Gd-enhanced MRI detected unique treatment effects of two first-line therapeutics for MS. While Ifn- β markedly decreases MPO activity, it does not reduce the number of inflammatory lesions. This corresponds to a novel, hitherto undescribed mechanism of action: Ifn- β directly acts on myeloid cells to decrease MPO secretion. In contradistinction, GA does not decrease lesion MPO activity, but instead decreases the number of inflammatory lesions seen on MRI. Upon translation, MPO-Gd molecular imaging could be used to monitor treatment efficacy in MS patients.

KEYWORDS: Imaging Biomarker, Molecular Imaging, Multiple Sclerosis



0-877

1:42PM - 1:49PM

MPO-Gd Enhanced Molecular MRI Detects Murine Multiple Sclerosis Disease Activity at Remission and Relapse better than DTPA-Gd

B Pulli1, G Wojtkiewicz1, M Ali1, J Chen1

1Massachusetts General Hospital, Boston, MA

Purpose

Clinical diagnosis of multiple sclerosis (MS) is challenging. DTPA-Gd enhanced imaging often under-reports active MS lesions and correlates poorly with clinical disability. We aim to evaluate if MPO-Gd, a molecular MR imaging (MRI) probe that specifically detects the inflammatory enzyme myeloperoxidase (MPO) activity (1), can detect disease activity at remission and relapse better than DTPA-Gd in a mouse model of MS.

Materials and Methods

A total of 18 female SJL mice were injected with proteolipid protein (PLP139-151) to induce experimental autoimmune encephalomyelitis, a mouse model of MS. To investigate detection of chronic disease, mice underwent MRI with MPO-GG or DTPA-Gd at the interval between acute disease and relapse (=remission, day 21 postinduction) and at the relapse (days 24-30 postinduction). Lesion number and volumes were quantified on postcontrast T1 images. Flow cytometry for brain leukocytes and MPO was conducted.

Results

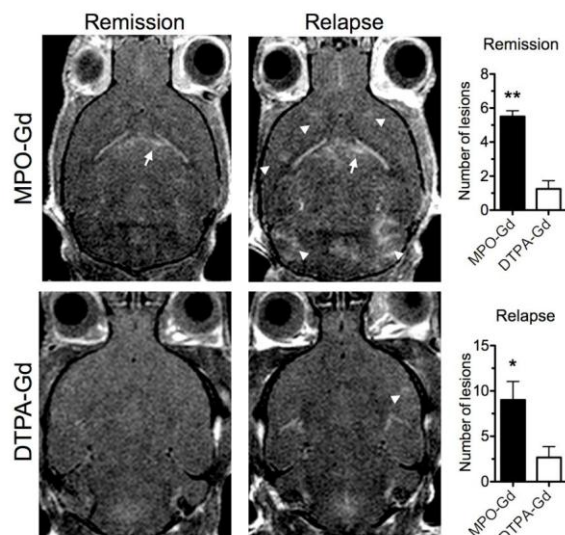
Note: Scanned images are included in the proceedings. Some submitted images were reduced during editing thereby decreasing clarity. Also, refer to the Program Planner. Proceedings Content as of 3/28/2014.

There was no difference in clinical disease severity or disease onset between mice imaged with MPO-Gd versus DTPA-Gd ($p > 0.05$). At remission, when disease activity is thought to be silent, more MPO-active lesions (5.5 ± 0.84 versus 1.25 ± 0.96 , $p < 0.01$) and a greater total lesion volume (0.047 ± 0.02 versus 0.010 ± 0.006 cm³, $p < 0.05$) were detected with MPO-Gd compared to DTPA-Gd. Significantly more lesions (9.0 ± 4.1 versus 2.7 ± 2.1 , $p < 0.05$) and a greater total lesion volume (0.219 ± 0.186 versus 0.013 ± 0.011 cm³, $p < 0.05$) also were detected at the relapse with MPO-Gd. The majority of MPO-active lesions appeared in areas previously unremarkable compared to imaging at remission (arrowheads in figure represent new lesions, while arrows represent lesions already present at remission), suggesting that MPO-Gd not only detects higher disease activity at remission, but also is capable of revealing the highly dynamic nature of this inflammatory disease model noninvasively in vivo. Flow cytometry demonstrated a marked increase of MPO-positive inflammatory cells even during remission compared to sham (2392 ± 894 versus 132 ± 43 cells/brain, $p < 0.01$). At relapse, MPO-positive inflammatory cells were further increased (4245 ± 1430 cells/brain, $p < 0.01$). The majority ($62 \pm 14\%$) of these MPO-positive cells were found to be Ly-6C-high inflammatory monocytes.

Conclusions

MPO-Gd-enhanced MRI can detect disease activity at remission and relapse better than nonspecific enhancement from DTPA-Gd. This corresponds to the presence of MPO-secreting inflammatory immune cells, and most of them were identified as monocytes. Upon translation, earlier and more sensitive detection of subclinical disease activity could greatly improve timely diagnosis in MS patients, and could be used as a better surrogate to evaluate treatment efficacy.

KEYWORDS: Imaging Biomarker, Molecular Imaging, Multiple Sclerosis



O-878

1:49PM - 1:56PM

In Search of Criteria Supporting Chronic Cerebrospinal Venous Insufficiency (CCSVI) in Patients with Multiple Sclerosis

C Torres¹, M Hogan¹, S Chakraborty¹, C Lum¹, T Nguyen¹, B Schwarz¹, L Legault-Kingstone¹, S Belanger¹, M Bussiere², M Freedman¹, H Dabirzadeh¹, M Schweitzer³, R Thornhill¹

¹The Ottawa Hospital, University of Ottawa, Ottawa, Ontario, Canada, ²Grey Nuns Community Hospital, Edmonton, Alberta, Canada, ³SUNY Stony Brook University Medical Center, Stony Brook, NY

Purpose

Chronic cerebrospinal venous insufficiency (CCSVI) is a proposed condition to cause or be closely associated with multiple sclerosis (MS) and is caused by stenoses within the venous drainage of the brain and spinal cord. The original observation was based on Doppler ultrasound and criteria for its diagnosis were defined by Paolo Zamboni. We undertook the current study to confirm if these observations are present in a cross-section of MS patients.

Materials and Methods

This was a single-center, prospective, observational study of 50 subjects with confirmed multiple sclerosis and 50 age-matched controls undergoing Doppler ultrasound evaluation. Ethics approval and informed consent were obtained. Subjects were randomly selected from a list of volunteers divided into six MS categories [relapsing remitting (RR), secondary progressive (SP), and primary progressive (PP) of less than or greater than 10 years duration]. Ten subjects were selected from each RR and SP MS category and five subjects from the two PP MS categories. Controls were age-matched acquaintances. An ultrasonographer blind to subject group evaluated the intra and extracranial venous circulation. Deep cerebral veins (DCV) were insonated through temporal bone windows. The evaluation order of subject-control pairs was assigned randomly. Two neuroradiologists blind to subject group independently evaluated CCSVI criteria. A positive study had two or more criteria present. Evaluators were asked to reach consensus on positive studies.

Results

Recruitment was completed over five months. Median ages were 52 (range 27-72) for patients and 52.5 (range 25-73) for controls. The female to male ratio was 1.9 for patients

Note: Scanned images are included in the proceedings. Some submitted images were reduced during editing thereby decreasing clarity. Also, refer to the Program Planner. Proceedings Content as of 3/28/2014.

and 0.6 for controls. Interobserver variability for CCSVI criteria was good [ICC 0.89 (0.85-0.93)]. Consensus between observers was required for four positive CCSVI results and no adjudication was required. Our primary outcome of a positive CCSVI score ≥ 2 was found in 13 subjects in the patient group with no positive results in the control group ($p < 0.001$, Fisher's exact test). No interaction with MS categories was observed. Deep cerebral veins signal was identified in 77% of subjects but there was no reflux and DCV measures did not contribute to the CCSVI scores.

Conclusions

We identified CCSVI criteria in a small subset of subjects with MS. While this can suggest some degree of association, our results do not support CCSVI as a cause or key pathogenetic factor in MS.

KEYWORDS: CCSVI, Doppler Ultrasound, Multiple Sclerosis

O-879

1:56PM - 2:03PM

Predictive Value of Susceptibility Weighted Imaging appearance of Multiple Sclerosis Lesions

S Siemonsen¹, W Schmidt¹, J Sedlacik¹, C Heesen¹, J Fiehler¹

¹University Medical Center Hamburg-Eppendorf, Hamburg, Germany

Purpose

Purpose: Multiple sclerosis (MS) lesions display different imaging characteristics in susceptibility-weighted imaging (SWI) phase in comparison to T2- and T1-weighted images. The purpose of this study was to evaluate SWI phase signal intensity characteristics of MS lesions and their association with overall lesion number and their predictive value for lesion development.

Materials and Methods

Twenty-eight patients with relapsing remitting MS underwent MR imaging (MRI) examination on a 3 T Siemens scanner including T2-weighted, T1-weighted imaging and SWI. Seventeen of these underwent a second MRI follow up (FU) after 6-12 months. Total number of T2 lesions and number of lesions appearing clearly bright in SWI phase was determined for each patient. For patients with FU, the number of new T2 lesions was determined. Patients were dichotomized due to a new T2 lesion in FU scans. The number of black holes was generated from T1-weighted images.

Results

The number of lesions displaying clearly bright signal in SWI phase images showed significant correlation with T2 lesion number ($p < 0.001$, $R = 0.71$) and number of black holes ($p < 0.01$, $R = 0.79$). Additionally the accuracy of bright phase lesion number to predict the occurrence of a new T2 lesion in FU was 0.94 with an optimal cut off value of six hyperintense phase lesions. The positive predictive value of bright phase lesion number greater or equal to six for prediction of a new T2 lesion in the next 6-12 months was 0.91 (CI 0.62 - 0.99, $p < 0.01$).

Conclusions

Bright SWI phase lesions can be found regularly in MS patients. High SWI phase signal might indicate increased iron deposition or other changes associated with inflammation. A higher number of bright phase lesions seems to be associated with new lesion formation and therefore higher activity in MS patients.

KEYWORDS: MR Imaging, MR Imaging Brain, Multiple Sclerosis

O-880

2:03PM - 2:10PM

Temporal Evolution of Multiple Sclerosis Lesions in Susceptibility Weighted Imaging

S Siemonsen¹, W Schmidt¹, J Sedlacik¹, C Heesen¹, J Fiehler¹

¹University Medical Center Hamburg-Eppendorf, Hamburg, Germany

Purpose

Multiple sclerosis (MS) lesions visualized in susceptibility-weighted imaging (SWI) display different imaging characteristics if assessed in phase in comparison to regular T2- and T1- weighted imaging. The purpose of this study was to evaluate SWI phase signal intensity characteristics of acute, contrast enhancing MS lesions and their temporal development.

Materials and Methods

Ten MS patients underwent baseline MR imaging (MRI) examination on a 3 T Siemens MRI scanner including T1- and T2-weighted imaging and SWI and follow-up scans after one and two months. Thirty-one contrast enhancing lesions were identified on baseline T1-weighted and signal characteristics of lesions were evaluated on SWI phase images on baseline and follow-up images.

Results

In baseline scans 16 of the contrast enhancing lesions were identified as hyperintense lesions on phase images, 13

Note: Scanned images are included in the proceedings. Some submitted images were reduced during editing thereby decreasing clarity. Also, refer to the Program Planner. Proceedings Content as of 3/28/2014.

were not visible, one showed a hyperintense ring configuration and one lesion presented as prominent vein. Among the invisible lesions in the baseline phase scan two remained invisible in both monthly follow-up scans, while seven emerged as hyperintense lesions and two as hyperintense ring lesions on follow-up SWI phase scans. Of those lesions that appeared with hyperintense signal in baseline scans, three lesions showed decreasing signal intensity in follow-up scans.

Conclusions

Contrast-enhancing MS lesions display different characteristics in SWI phase images and show variable temporal evolution. Most MS lesions seem to display characteristics of iron deposition either initially with contrast enhancement or during their temporal evolution. Nevertheless, these changes can be reversible and lesions are still evolving months after their initial appearance.

KEYWORDS: MR Imaging, MR Imaging Brain, Multiple Sclerosis

O-881

2:10PM - 2:17PM

Clinical significance of dural enhancement on magnetic resonance imaging.

K Lam¹, P Lee¹, P Shen¹, M Bobinski¹, A Nidecker¹

¹University of California Davis, Sacramento, CA

Purpose

Dural (pachymeningeal) enhancement is a common yet potentially confounding finding on brain MR imaging (MRI) with broad differential diagnosis including postoperative or procedural enhancement, spontaneous intracranial hypotension, infection or inflammation as well as malignant processes such as dural metastasis or primary brain tumors. Typically, the diagnosis is made with relevant clinical history and imaging follow up. This management strategy creates a diagnostic dilemma for radiologists, due to frequent lack of clinical history and prior imaging at the time of interpretation. In this single institutional study, our objective was to systematically determine clinical and imaging outcomes of patients with dural enhancement.

Materials and Methods

We retrospectively studied 50 consecutive patients with imaging findings of dural enhancement on MRI using the PACS imaging system and Electronic Medical Record at UC Davis between 01/2002 – 05/2013. Patients greater than 10 years of age with dural enhancement on one or more MRI studies were included in the study. We excluded cases

that involved focal dural enhancement (either directly under a surgical cavity or associated with an extra-axial mass), immediate postoperative, immediate post-traumatic with intracranial injuries, or lost to clinical follow up. All patients were imaged on a 1.5 T General Electric Healthcare (Waukesha, WI) MRI with contrast-enhanced T1-weighted sequences. Any thin and discontinuous meningeal enhancement was considered normal. Dural enhancement patterns were further classified as focal (smooth only, smooth with nodular, or mass-like) versus diffuse (smooth only, smooth with focal nodular pattern, or mass-like). Dural enhancement was defined as focal when present fewer than 75% and diffuse over 75% of the dural surface of one cerebral hemisphere on all imaging planes. Mass-like dural enhancement was defined as greater than 10mm in thickness.

Results

The 50 included cases were grouped into four major etiologic categories, including 28 intracranial hypotension [recent lumbar puncture (5), chronic cerebral shunts (17), or spontaneous (6)], 13 metastasis, five inflammatory or infectious causes, three chronic postoperative effects, and one idiopathic hypertrophic pachymeningitis (IHP). In the intracranial hypotension category, we observed only focal-smooth, diffuse-smooth and diffuse-smooth/nodular patterns (14%, 68%, 18%, respectively). Inflammatory/infectious and chronic postoperative categories also demonstrated only focal-smooth/nodular and diffuse-smooth/nodular patterns. None of benign etiologies demonstrated mass-like dural enhancement. The metastasis category showed enhancement patterns of focal-smooth/nodular (23%), focal mass-like (23%), diffuse-smooth only (7%), diffuse-smooth/nodular (16%), diffuse mass-like (31%). Among the metastatic foci, 8% of the cases had concurrent intraparenchymal metastases, 16% had concurrent leptomeningeal metastases, 69% had concurrent calvarial metastases and 54% had secondary dural metastases on contralateral hemisphere or posterior fossa; however these are not mutually exclusive. The case of IHP showed diffuse-smooth enhancement pattern.

Conclusions

Uniform dural enhancement on MR imaging has a relatively broad differential of diagnoses, thus clinical correlation proves to be crucially important in identifying the underlying cause(s). Within our small cohort of 50 patients, smooth dural enhancement pattern is seen predominantly in the intracranial hypotension, inflammatory/infectious and chronic postoperative categories. Conversely, cases with metastasis have more nodular and/or mass-like dural enhancement pattern. Interestingly, 100% metastases were observed to have concurrent intraparenchymal, calvarial and/or remote dural metastases, thus significantly improving diagnostic confidence of metastasis in the setting of dural enhancement.

KEYWORDS: Dural

Note: Scanned images are included in the proceedings. Some submitted images were reduced during editing thereby decreasing clarity. Also, refer to the Program Planner. Proceedings Content as of 3/28/2014.

O-882

2:17PM - 2:24PM

Infratentorial Lesions in Multiple Sclerosis: Double Inversion Recovery superior to FLAIR and T2

R De Leacy¹, I Corcuera-Solano¹, A McLellan¹, A Doshi¹, P Pawha¹, L Tanenbaum¹

1Icahn School of Medicine at Mount Sinai, New York, NY

Purpose

Magnetic resonance (MR) techniques have had a major impact in understanding and managing multiple sclerosis (MS). At present, multiplanar or 3D T2 FLAIR is the dominant method to evaluate the presence and extent of disease, however it has well documented shortcomings for cortical and infratentorial pathology, some of which are compensated for with T2WI. Double inversion recovery (DIR) is a recently available 3D imaging technique in which both white matter (WM) and cerebrospinal fluid (CSF) signals are suppressed, greatly increasing the conspicuity of cortical lesions. Early experience suggests that WM suppression increases the relative conspicuity of white matter lesions as well as cortical/subcortical lesions with particular benefits below the tentorium where FLAIR is particularly challenged. The purpose of this retrospective study is to investigate the incremental benefit of DIR over the traditional diagnostic MR sequences, T2WI and FLAIR, with focus on the detection of posterior fossa lesions in the study of MS. We expect this validation study to serve as a foundation for widespread use of DIR for the follow up of MS patients.

Materials and Methods

Thirty patients with MS lesions involving the posterior fossa were enrolled in this retrospective study from among 44 consecutive patients who underwent 3 T MRI for the study of MS between 6/2013 and 12/2013. MR protocol included 3D DIR, T2 and 3D FLAIR. All studies were performed on Siemens Aera 1.5 T and Skyra 3 T scanners using commercially available software. Two reviewers recorded the number of lesions identified in the posterior fossa and visualized upper cervical spinal cord on independent serial, randomized consensus reviews of the DIR, T2 and FLAIR sequences. Two experienced neuroradiologists used a five-point scale to assess individual lesion conspicuity and image quality. Only lesions larger than 1 mm in diameter were included in the analysis. The data were analyzed as medians and the groups were compared with the use of the Wilcoxon signed-rank test.

Results

Double inversion recovery is significantly better than FLAIR and T2 in identifying MS lesions of the posterior fossa (p<0.005) (Table 1). The number of lesions detected with DIR was 212 versus 166 identified with FLAIR, and

131 with T2, representing a 28% and 66% improvement over traditional sequences. Qualitative analysis demonstrated superior lesion conspicuity on DIR than the traditional T2 and FLAIR sequences (Figure 1).

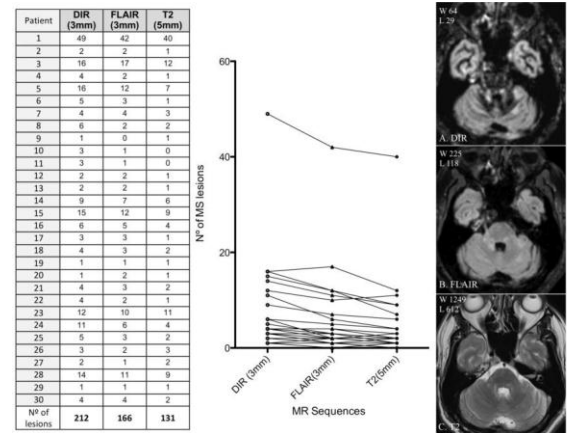
Conclusions

Double inversion recovery is superior in identifying MS lesions in the posterior fossa adding to its documented benefits for cortical and subcortical lesions. Double inversion recovery will augment and may supplant FLAIR in combination with T2 and for the routine evaluation of patients with symptoms suggesting MS.

KEYWORDS: MR Imaging Brain, Multiple Sclerosis, Posterior Fossa

Table 1. Comparison of the average of the numbers of lesions identified in DIR, FLAIR and T2

Table 1. Comparison of the average of the numbers of lesions identified in DIR, FLAIR and T2								
DIR	FLAIR	p	DIR	T2	p	FLAIR	T2	p
7.07±9.20	5.53±8.03	0.0001	7.07±9.20	4.37±7.49	<0.0001	5.53±8.03	4.37±7.49	0.0002



O-883

2:24PM - 2:31PM

Comparison of Visual Conspicuity between Contrast-Enhanced T1-Weighted Gradient Echo and Spin Echo Sequences in the Detection of Multiple Sclerosis Lesions with 3.0T MRI

Note: Scanned images are included in the proceedings. Some submitted images were reduced during editing thereby decreasing clarity. Also, refer to the Program Planner. Proceedings Content as of 3/28/2014.

X Aymerich¹, C Auger², P Alcaide Leon³, E Huerga², J Corral², R Mitjana², J Sastre-Garriga², X Montalban², A Rovira²

¹Hospital Vall d'Hebron/Universitat Politècnica de Catalunya, Barcelona, Spain, ²Hospital Vall d'Hebron, Barcelona, Spain, ³St Michael's Hospital, Toronto, Ontario, Canada

Purpose

High field MR imaging (MRI) (3.0 T) offers higher contrast-enhancing multiple sclerosis (MS) lesion detection rates than lower field MRI equipment. However, it is not well established whether gradient-echo (GE) or spin-echo (SE) is the sequence of choice for this purpose. The aim of this study was to compare the ability of these two sequences to detect active MS lesions.

Materials and Methods

One hundred relapsing MS patients [73 women; mean age, 35.8 years; age range (23, 50) years, median EDSS, 3; EDSS range, (0, 8)], underwent 3.0 T brain MRI including enhanced GE and SE T1-weighted sequences. Gradient echo images were acquired 15 minutes after injection of a double dose (0.2 mmol/kg) of gadobutrol. In half of patients, SE images were acquired just before, and in the other half just after, acquisition of the GE images. To define the gold standard, an experienced neuroradiologist identified and marked contrast-enhanced MS lesions in these sequences using Jim 5.0 software. Differentiation of MS lesions in GE and SE images was evaluated using a 5-point qualitative scale. The anatomical location (periventricular, subcortical, infratentorial, and juxtacortical) and the pattern of contrast uptake (nodular, ring, open-ring, and heterogeneous) also were assessed. Each of the two sets of contrast-enhanced T1weighted scans then was evaluated in a random fashion and using objective image interpretation criteria by three experienced neuroradiologists. The results were compared with the gold standard reference to obtain the number of true-positive (TP), false-negative (FN), and false positive (FP) evaluations. Quantitative assessment of lesion conspicuity and the effect of spatial location were based on image contrast and the contrast-to-noise ratio between lesions and their 3-pixel-width surroundings, and division of the intracranial region into four quadrants in each slice.

Results

We found 607 MS lesions (105 periventricular, 274 subcortical, 165 juxtacortical, and 63 infratentorial). Most lesions showed a nodular pattern of contrast uptake (nodular, 527; ring, 13; open-ring, 34; heterogeneous, 33). The qualitative approach showed slightly better lesion differentiation with SE images. However, analysis of agreement between readers and gold standard segmentations showed better sensitivity to detect lesions with GE images (0.828) than with SE (0.767), and a similar mean number of FPs (GE, 16.33; SE, 16.67). Spin echo images showed a higher image contrast ratio (TP, 0.37; FN,

0.20; FP, 0.25) than GE images (TP, 0.23; FN, 0.11; FP, 0.16), whereas the contrast-to-noise ratio was higher for GE (TP, 37.76; FN, 17.02; FP, 20.71) than for SE (TP, 27.26; FN, 13.69; FP, 14.85). Both comparisons presented significant statistical differences ($p < 0.05$) using ANOVA and the post-hoc T3 Dunnett test. Finally, in both SE and GE sequences, most misclassifications occurred in the right posterior quadrant.

Conclusions

Selection of the best sequence requires the use of visual indices that study greater surrounding complexity of lesions than the image contrast ratio. The results obtained suggest that visual conspicuity of MS lesions in images acquired at 3.0 T is better in GE sequences than in SE.

KEYWORDS: Contrast Enhancement, MR Imaging, Multiple Sclerosis

Thursday, May 22

1:00PM - 2:30PM

Room 517d

**89 - MINI SYMPOSIUM STROKE - PART IV:
ENDOVASCULAR THERAPY: WHERE ARE
WE NOW?**

0-885

1:00PM - 1:15PM

Endovascular Thrombolysis and Devices

Yoo, A.
Massachusetts General Hospital
Boston, MA

0-889

1:30PM - 1:45PM

Carotid Stenting

Sunshine, J.
University Hospitals Case Medical Center
Cleveland, OH

Abstract/Presentation Summary

We will discuss the major antecedent randomized prospective clinical trials that directly affect treatment decisions for carotid stenosis. The conclusions from the North American Symptomatic Carotid Endarterectomy Trial (NASCET) and the Asymptomatic Carotid Atherosclerosis Study (ACAS) will be quickly reviewed. The presentation will then focus on the (CREST) data and its

Note: Scanned images are included in the proceedings. Some submitted images were reduced during editing thereby decreasing clarity. Also, refer to the Program Planner. Proceedings Content as of 3/28/2014.

implications for selection of today's patient for endovascular placement of a carotid stent or surgical endarterectomy. These data will be parsed to review implications for specific subsets of patients for whom one technique may offer a more complementary alignment. We will then turn our attention from use of carotid stent for stroke prevention to use in treatment of acute onset of cerebral ischemia in any attempts to restore flow and rescue cerebral tissue. In particular we will discuss use of carotid stents when faced with revascularization through tandem lesions most often of the cervical internal carotid and the ipsilateral middle cerebral artery. As time permits we will show some of the advanced imaging techniques for image characterization of the carotid plaque and how these may be useful in patient selection or treatment guidance. These can include high-resolution black blood MRI, intravascular ultrasound or most recently intravascular optical coherence tomography. We will look at restenosis occurrence, stent placement soon after thrombolysis, and in relation to patient age or life expectancy. The discussion will close by offering one or more models to guide treatment choice in either the setting of acute vascular occlusion or the more common application to prevent new or recurrent cerebral infarction.

O-892

2:00PM - 2:15PM

Intracranial Stenting

Derdeyn, C.
Mallinckrodt Inst. Radiology
St. Louis, MO

Abstract/Presentation Summary

The current landscape of angioplasty and stenting for intracranial occlusive disease is still dominated by emerging data from the recently completed Stenting and Aggressive Medical Management for the Prevention of Recurrent Ischemic Stroke (SAMMPRIS) trial [1]. Final results with long term follow up were published in the Fall of 2013 [2]. The early superiority of the medical arm persisted, with similar late recurrent stroke rates in the medical and interventional arms. SAMMPRIS has provided critical information on the benefit of aggressive medical management (dual antiplatelet medication for 90 days as well as good blood pressure and lipid control) in patients presenting with recent ischemic stroke or TIA secondary to severe atherosclerotic stenosis of a major intracranial artery. These data have narrowed the definition of the patient population that may have benefit from angioplasty and stenting and provided new information on the nature of early and late complications of angioplasty and stenting

[3]. This short talk will review this recent information, discuss current indications for intracranial angioplasty and stenting, and explore future directions for research in this area.

O-886

1:15PM - 1:21PM

Endovascular Therapy of Anterior Circulation Stroke: Clinical, Radiological and Angiographic Prognostic Factors for 3 Months' Neurological Outcome

R Fahed¹, H Redjem¹, R Blanc¹, B Bartolini¹, S Pistocchi¹, A Rouchaud¹, E Shotar¹, G Ciccio¹, B Gilboa¹, T Robert¹, M Piotin¹

¹Fondation Rothschild, Paris, France

Purpose

Despite recent studies that did not show any superiority of endovascular treatment of ischemic stroke versus iv thrombolysis, mechanical thrombectomy (MT) is getting more and more importance in the management of acute ischemic stroke. Recent devices have drastically increased efficiency in terms of revascularization with a relatively low rate of complications. However, patient selection for MT remains challenging.

Materials and Methods

We prospectively gathered the charts of 88 consecutive patients (50 males, 38 females; mean age/SD = 63.4±14 years old) who presented anterior circulation acute ischemic stroke and underwent MT from December 2011 to September 2013 in our institution. Initial NIHSS score, DWI-ASPECT score, therapeutic data (iv thrombolysis prior to MT, time from initiation of MT to revascularization, procedure duration), angiographic prognostic scores as Capillary Index Score (CIS), Collateral Flow Grading System (CFGs) and TICI score. NIHSS scores (at admission, at day one and at discharge) and the three-month mRS were analyzed. Patients were dichotomized into two groups: favorable (mRS≤2) and poor (mRS≥3) outcomes at three-month follow up.

Results

Forty-seven out of 88 patients (53.4 %) had a good outcome. The three-month mortality was 17.0% (15/88). Intravenous thrombolysis was performed in 30/47 (63.8%) patients with a good outcome, and 22/41 (53.7%) patients with a poor outcome (p=0.45). Recanalization (TICI ≥ 2b) was obtained in 66.7% (58/87) of the patients. Mean procedure duration was 71.2 minutes. Patients with a three-month good outcome had statistically lower NIHSS at admission, at day one and at discharge (p<0.0001), a

Note: Scanned images are included in the proceedings. Some submitted images were reduced during editing thereby decreasing clarity. Also, refer to the Program Planner. Proceedings Content as of 3/28/2014.

higher CIS and CFGS score (p<0.05), a higher recanalization rate (p=0.0004). An initial CT instead of a MR imaging (MRI) was statistically associated with a poor outcome (p=0.02). There was no statistical difference between the two groups regarding DWI-ASPECTS (p=0.07), delay between symptoms and iv thrombolysis (p=0.19), delay between stroke onset and recanalization (p=0.32), procedure duration (p=0.1). Seven out of 88 patients (7.9%) had a delayed intracerebral hemorrhage, including five patients with an ECASS-1 or ECASS-2 hemorrhage.

Conclusions

Intravenous thrombolysis prior to MT does not confer better outcome. Time from stroke onset to revascularization does not influence the outcome. A low initial NIHSS is associated with a better outcome. The most striking prognostic factor regarding outcome is the presence of arterial collateral supply. Further studies should focus on better collateral scoring in order to select patients that are more likely to benefit from MT.

KEYWORDS: Collateral Circulation, Endovascular Revascularization, Stroke

	Good Outcome (mRS=[0-2] at 3 months follow-up)	Poor Outcome (mRS=[3-6] at 3 months follow-up)	p
Clinical Data:			
Number of patients	47/88 (53.4 %)	41/88 (46.6 %)	
Number of male patients	25/47 (53.2 %)	25/41 (61 %)	0.6
Mean age (years)	64	62.6	0.64
High blood pressure	26/47 (55.3 %)	23/41 (56.1 %)	0.89
Diabetes	5/47 (10.6 %)	3/41 (7.3 %)	0.72
Dislipidemia	16/47 (34 %)	14/41 (34.1 %)	0.83
Smoking	14/47 (29.8 %)	12/41 (29.3 %)	0.86
Antiplatelet drugs	6/47 (12.8 %)	11/41 (26.8 %)	0.16
Anticoagulant drugs	7/47 (14.9 %)	7/41 (17.1 %)	0.99
Mean NIHSS at admission	14.3	19.3	0.0001
Radiological data:			
Initial brain CT	7/47 (14.9 %)	16/41 (39 %)	0.02
Initial brain MRI	40/47 (85.1 %)	25/41 (61 %)	0.02
Mean DWI-ASPECTS score	7.5	6.6	0.07
Right brain stroke	25/47 (53.2 %)	19/41 (46.3 %)	0.67
Left brain stroke	22/47 (46.8 %)	22/41 (53.7 %)	0.67
Angiographic and endovascular data			
Patients with previous IV thrombolysis	30/47 (63.8 %)	22/41 (53.7 %)	0.45
Mean delay between symptoms and IV thrombolysis (minutes)	137.9	157	0.19
TICI ≥2B	39/46 (84.8 %)	19/41 (46.3 %)	0.0004
Mean delay between symptoms and recanalization	335.1	360.8	0.32

	(minutes)		
Mean procedure duration (minutes)	62.3	77.4	0.1
Capillary Index Score (CIS) = 0	1/32 (3.1 %)	8/36 (22.2 %)	0.03
CIS = 1	3/32 (9.4 %)	8/36 (22.2 %)	0.2
CIS = 2	12/32 (37.5%)	11/36 (30.6 %)	0.61
CIS = 3	16/32 (50 %)	9/36 (25 %)	0.04
Collateral Flow Grading System (CFGS) = 0	1/33 (3 %)	8/36 (22.2 %)	0.03
CFGS = 1	6/33 (18.2 %)	8/36 (22.2 %)	0.77
CFGS = 2	16/33 (48.5 %)	12/36 (33.3 %)	0.23
CFGS = 3	5/33 (15.1 %)	4/36 (11.1 %)	0.73
CFGS = 4	5/33 (15.1 %)	4/36 (11.1 %)	0.73
Follow-up:			
Mean NIHSS at day 1	5	21.4	<0.0001
Craniectomy	1/47 (2.1 %)	6/41 (14.6 %)	0.06
Mean NIHSS at discharge	4	17.1	<0.0001
Mean mRS at discharge	1.8	4.7	<0.0001
mRS at 3 months follow-up	0.9	4.5	<0.0001
Number of deceased patients at 3 months	0/47	15/41 (36.6 %)	

O-887

1:21PM - 1:27PM

Successful Intra-Arterial Reperfusion Therapy Improves Clinical Outcomes in Acute Stroke Secondary to Large Vessel Occlusions – TICI Based Analysis.

S Mangla¹, R Loganathan², P Moh², T Victor², B Kanna², M Schori²

1SUNY Downstate Health Science Center, Brooklyn, NY, 2Lincoln Medical Center, Bronx, NY

Purpose

Acute ischemic stroke secondary to large vessel occlusion within the proximal vessels of the circle of Willis remains a devastating clinical event. Intravenous tPA remains as first-line therapy in patients presenting within early (<4.5 hours) windows however, has had limited success in achieving reperfusion and favorable clinical outcomes in large vessel occlusions. Our study analyzed our experience utilizing currently available intra-arterial reperfusion strategies, technical success at achieving reperfusion, and its effects on clinical outcomes at discharge.

Materials and Methods

We performed an IRB-approved retrospective review of a prospectively maintained clinical database of patients receiving intra-arterial reperfusion therapy at Lincoln Medical Center from 9/1/2009 – 1/31/2013. Forty-seven

Note: Scanned images are included in the proceedings. Some submitted images were reduced during editing thereby decreasing clarity. Also, refer to the Program Planner. Proceedings Content as of 3/28/2014.

consecutive patients triaged with CTA/CTP imaging for large vessel occlusions within eight hours of symptom onset underwent intra-arterial therapy [IA alone (25/47 – 54.2%)], or iv followed by IA (22/47 – 46.8%) based on the presence of a large vessel occlusion, independent of perfusion imaging parameters. Combinations of therapies were employed, primarily mechanical thrombectomy with the Penumbra aspiration system (42/47 – 89.4%), secondarily MERCI device (8/47 – 17.0%), with low dose (1-10 mg) IA tPA (16/47 – 34.0%). Clinical imaging (CT, DSA, and MRI), and clinical outcomes (NIHSS, mRS) were reviewed through discharge. Angiographic outcomes were graded based on thrombolysis in cerebral ischemia system (TICI).

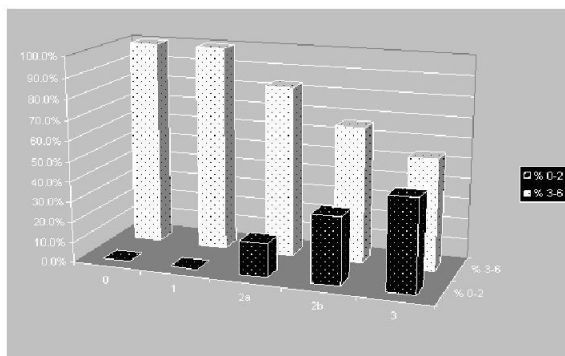
Results

TICI 0, 1, 2a, 2b, 3 was achieved in five (10.6%), one (2.1%), 12 (25.5%), 18 (38.3%), 11 (23.4%) patients respectively. Favorable mRS outcome at discharge (0-2) was associated positively with higher grades of TICI reperfusion (mRS), TICI 0 (0/5 – 0%); 1 (0/1 – 0%); 2a (2/12 – 16.7%); 2b (6/18 – 33.3%); 3 (5/11 – 45.5%) (Figure). Twenty-one of 47 (44.7%) patients experienced an eight-point or greater improvement in NIHSS at discharge, overall 13/47 (27.7%) achieved mRS (0-2) at discharge, with 5/47 (10.6%) mortality and symptomatic intracranial hemorrhage in 4/47 (8.5%).

Conclusions

Our experience with IAT suggests that significant clinical improvement can be experienced in prolonged therapeutic windows (< 8 hours); however, the threshold for reperfusion to achieve favorable clinical outcome may be higher than previously thought (TICI 2b or greater). A significant percentage of patients may still suffer significant functional brain injury despite reperfusion.

KEYWORDS: Acute Ischemic Stroke, Clinical Outcome, Mechanical Thrombectomy



0-888

1:27PM - 1:33PM

Opportunities for Reducing Delays in Endovascular Reperfusion Therapy of Acute Ischemic Stroke Patients

A Honarmand¹, S Prabhakaran¹, R Beck², C Beck², J Conners³, V Lee³, A Shaibani¹, M Hurley⁴, S Ansari⁴

¹Northwestern University, Chicago, IL, ²Northwest Community Hospital, Arlington Heights, IL, ³Rush University, Chicago, IL, ⁴Northwestern University Feinberg School of Medicine, Chicago, IL

Purpose

It has been demonstrated that every 30-minute delay in time to revascularization is associated with 10% absolute decrease in the probability of a good outcome from intra-arterial therapy (IAT) in acute ischemic stroke (AIS) patients. We investigated the potential critical time intervals among patients with direct presentation compared to inter-hospital transfers to comprehensive stroke centers (CSCs) for IAT.

Materials and Methods

We performed a retrospective review of consecutive AIS patients who underwent IAT at four institutions since 2012 and abstracted symptom onset time (SOT), first emergency department arrival time (EDAT), and time of groin puncture (GP). Patients were categorized into those who were transferred from outside institutions and those who presented directly to the CSCs (nontransferred). We compared times using Mann-Whitney tests and proportions using Fisher's exact tests.

Results

Sixty-three patients (59% male, mean age 65.4 years) were studied, of which 34 (54%) patients were interhospital transfers. Of the studied time intervals, SOT to CSC arrival time in nontransferred group was significantly less than that of transferred group (mean: 53.4 versus 271.1 min, respectively; $p < 0.0001$). Additionally, SOT to GP time was reduced significantly in nontransferred group (233.6 versus 308.5 min; $p = 0.004$). Likewise, first EDAT to GP was reduced significantly in nontransferred compared with transferred group (186.3 versus 215.7 min; $p = 0.01$). In nontransferred group, eight (27.6%), 18 (62%), and three (10.4%) patients and in transferred group two (6%), 26 (76%), and six (17%) patients achieved SOT to GP time of <3, 3-6, >6 hours, respectively ($p = 0.06$). Additionally, first EDAT to GP time of <120 minutes was achieved in only four cases in both groups (4.3%).

Conclusions

Although SOT to GP time is significantly lower in direct referrals, among direct referrals and interhospital transfer patients, onset and initial arrival to treatment times are far from optimal. Majority of the delay (90%) from symptom onset to treatment is accounted for prior to CSC arrival among transfers while nearly 80% of the time elapses at

Note: Scanned images are included in the proceedings. Some submitted images were reduced during editing thereby decreasing clarity. Also, refer to the Program Planner. Proceedings Content as of 3/28/2014.

CSCs among nontransfers. There are considerable opportunities for reducing delays in several key steps in the process including early team activation, interhospital transport, and rapid multimodal imaging protocols.

KEYWORDS: Endovascular Therapy, Stroke

0-890

1:45PM - 1:51PM

Safety and Outcomes of Carotid Endarterectomy versus Stenting: Evidence from a Large National Hospital Discharge Database

R McDonald1, J McDonald1, T Therneau1, D Kallmes1, H Cloft1

1Mayo Clinic, Rochester, MN

Purpose

Clinical equipoise of carotid revascularization therapies remains controversial. We sought to determine if adverse outcomes following carotid endarterectomy (CEA) or carotid angioplasty and stenting (CAS) were equivalent on a population scale by using propensity score matched analysis of a large hospital discharge database.

Materials and Methods

All surgical cases of CEA (ICD9: 38.12) or CAS (ICD9: 00.63) were identified from the 2008-2012 Premier Perspective database and grouped by clinical presentation (asymptomatic (ICD9: 433.10 or 433.30); symptomatic (ICD9: 435.9, 362.34, or 433.11)). Additional data associated with each revascularization procedure including demographics, clinical characteristics, and outcomes were also retrieved. The primary outcomes for this study were in-hospital mortality, intra- or post-operative stroke (subarachnoid hemorrhage (SAH, ICD9: 430) or intracranial hemorrhage (ICH, ICD9: 431)), or acute myocardial infarction (AMI, ICD9: 410). Outcomes were evaluated individually, as a composite endpoint (mortality, stroke, or AMI), and as a modified composite endpoint (mortality or stroke only). All CEA and CAS records were subjected to 1:1 matching on the propensity score, derived from 33 covariates associated with clinical status or established treatment assignment criteria, to simulate the randomization of an RCT. Multivariate-adjusted odds ratios (OR) and/or hazard ratios (HR) from cox-proportional hazard models were computed to determine if individual or composite outcomes were similar between CEA and CAS.

Results

Among 109,632 carotid revascularizations recorded within the 2008-2012 Perspective database, 95,742 CEA and

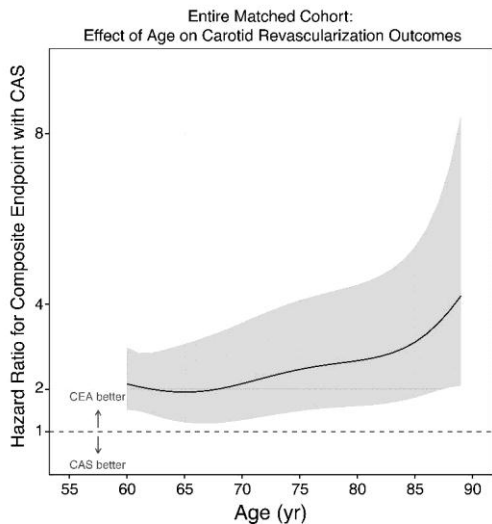
13,980 CAS procedures were performed. Asymptomatic stenosis comprised 90% (N=98,729) of all carotid revascularizations. Following 1:1 propensity score-based matching, 24,004 asymptomatic (12,002 CEA : 12,002 CAS) and 3,506 symptomatic (1,753 CEA : 1,753 CAS) procedures were included for further study. Asymptomatic patients who underwent CAS had significantly higher rates of in-hospital mortality (0.7% vs. 0.5%, HR = 1.47 (1.04-2.08), p = .02), SAH (0.2% vs. 0%, OR = 24.51 (4.54-402), p = .0012), and ICH (0.3% vs. 0.1%, OR = 3.23 (1.54-7.14), p = .0013) compared to a matched cohort of patients who received CEA. Similarly, symptomatic patients who received CAS also had significantly higher rates of mortality (mortality: 4.1% vs. 0.9%, OR = 4.55 (2.64-8.33), p < .0001), SAH (1.1% vs. 0.2%, OR = 6.67 (1.98-33.4) p = .0022), ICH (1.4% vs. 0.3%, OR = 5.00 (1.89-16.7), p = .0010) compared to CEA recipients. Using the composite endpoint (mortality, stroke, or AMI), CAS recipients had worse overall outcomes than CEA recipients for both asymptomatic (3.0% vs. 2.2%, HR = 1.40 (1.19-1.65), p < .0001) and symptomatic presentations (11.1% vs. 5.1%, HR = 2.31 (1.78-3.00), p < .0001); the treatment effect on the entire matched cohort was not modified by age (p = .28) or sex (p = .35). Similar results were observed using the modified composite endpoint (mortality or stroke alone) for both asymptomatic (CAS = 2.5% vs. CEA = 1.7%, HR = 1.49 (1.25-1.78), p < .0001) and symptomatic presentations (CAS = 10.0% vs. CEA = 3.5%, HR = 3.02 (2.25-4.07), p < .0001).

Conclusions

Among individuals treated for atherosclerotic disease of the carotid artery in a large sample of hospitals in the United States, CAS was associated with higher risk of peri-operative mortality, stroke, and unfavorable discharges when compared to CEA for all ages and clinical presentations.

KEYWORDS: Carotid Artery Stenting, Comparative Effectiveness, Outcomes

Note: Scanned images are included in the proceedings. Some submitted images were reduced during editing thereby decreasing clarity. Also, refer to the Program Planner. Proceedings Content as of 3/28/2014.



O-891

1:51PM - 1:57PM

Safety evaluation of primary carotid stenting: Embolic detection on intraprocedural transcranial Doppler and correlation with diffusion-weighted imaging lesions on post-procedural MRI.

P Lopez-Ojeda¹, C Muñoz¹, K Solo¹, S Lownie¹, D Pelz¹

¹London Health Sciences Centre, London, Ontario, Canada

Purpose

A major limitation of carotid artery stenting (CAS) is the potential for embolic stroke. Standard CAS technique involves placement of an embolic protection device (EPD) distal to the stenosis, stent insertion, pre- and post-insertion balloon angioplasty. It has been shown that every step, particularly stent deployment and balloon angioplasty, generate emboli. Our experience has shown that balloon angioplasty is not required to successfully treat the majority of patients. Decreasing the number of manipulations and avoiding the use of balloons may reduce the risk of distal embolization and stroke. We evaluated the safety of primary carotid stenting (PCS), using self-expanding stents alone without deliberate use of balloons and EPDs, by correlating the findings of intraprocedural transcranial Doppler (TCD) with diffusion weighted imaging (DWI) on postprocedural MR imaging (MRI).

Materials and Methods

A sample size of 30 consecutive patients was chosen for feasibility. Between March and December 2013, 14 patients were prospectively enrolled. Transcranial Doppler

monitoring was performed in all patients during CAS procedures, which were divided into six steps. Embolic signals on TCD were counted and classified based on their relative energy index of microembolic signals (REIM) as either benign (<1) or malignant (≥1). Pre-stenting (within 30 days) and poststenting (within 24 hours) MRI with diffusion-weighted imaging (DWI) was performed in all cases.

Results

Preliminary results in 14 patients (15 stents deployed) are described. All patients were symptomatic with atherosclerotic stenosis >60% by NASCET criteria (median 80%). All patients underwent primary carotid stenting, bilateral in one patient. Balloon angioplasty was required in two cases. The median embolic signal count was 90 (70 benign, 22 malignant). The stent deployment stage generated the highest median embolic signal count (66). Three patients (21.4%) had new DWI lesions post CAS. The median DWI count was one. There was no correlation between incidence of malignant microemboli and DWI lesions, although the sample size is small. One patient (7.1%) had a postoperative transient ischemic attack (TIA) within 12 hours postprocedure. None of the patients had new or worsening postprocedural clinical deficits.

Conclusions

Although numerous microembolic signals were observed during PCS, the numbers of both benign and malignant emboli are remarkably lower than those observed with standard CAS techniques. Only 21.4% of patients developed new DWI lesions, also lower than reported with standard techniques, and none developed new clinical deficits. There was no correlation between malignant microemboli and DWI lesions in this small, preliminary sample. Initial results suggest that PCS may be safer than standard CAS techniques. Results from the full sample of 30 patients will be presented.

KEYWORDS: Carotid Artery Stenting, MR Imaging/Diffusion, Transcranial Ultrasound

O-893

2:15PM - 2:21PM

Iatrogenic Reactions Due To Polymer Coatings Originating From Vascular and Interventional Devices: Neuroradiological Findings with Pathological Correlation

R Mehta¹, R Mehta²

¹SUNY Upstate Medical University, Syracuse, NY,
²University of Maryland, Baltimore, MD

Purpose

Note: Scanned images are included in the proceedings. Some submitted images were reduced during editing thereby decreasing clarity. Also, refer to the Program Planner. Proceedings Content as of 3/28/2014.

Hydrophilic polymers are commonly applied as coating on endovascular device surfaces. These materials have the potential to dissociate during clinical use, occasionally causing embolic and other iatrogenic phenomena. Rare reports document morbidity in affected patients. The focus of this study was to evaluate neuroradiological features associated with this phenomenon.

Materials and Methods

On retrospective review of the literature and the archives at a tertiary care hospital (1997-2013), 16 cases of intracerebral iatrogenic polymer reactions were identified. Twelve cases with available neuroradiological data were reviewed retrospectively.

Results

Mean patient age was 54 years (age range: 2.5 months to 87 years; four patients were male). Patients had undergone aneurysm coil embolization (n=6), angiography (n=4), cardiac catheterization (n=1) and Norwood procedure (n=1). Radiologic changes on magnetic resonance (MR), magnetic resonance angiography (MRA) and/or computed tomography (CT) studies included acute multifocal embolic infarcts (n=4); hydrocephalus (n=3); parenchymal hematoma (n=2); white matter lesions (n=2); perianeurysmal enhancement (n=2); perianeurysmal wall thickening (n=1); perianeurysmal parenchymal edema (n=1); small intra-arterial clot at site of coiled aneurysm (n=1); vessel occlusion (n=1); focal abscess formation (n=1); and intraventricular hemorrhage (n=1). Histopathologic data, available on eight patients (66%), confirmed neuroradiological changes due to embolic and/or inflammatory (neutrophilic, mononuclear, and/or granulomatous) sequelae associated with iatrogenic polymer deposits. Iatrogenic changes were symptomatic in all cases. Four patients without available pathological correlation exhibited aseptic chemical meningitis that was clinically attributable to polymeric reactions. On postmortem analysis, associated scattered microinfarcts directly resulted in death of two patients (17%).

Conclusions

Intracerebral polymer deposits may elicit variable neuroradiological patterns of injury within the brain. The primary findings include embolic and/or inflammatory changes. Since neuroradiologic features may be nonspecific, increased awareness of this potential iatrogenic phenomenon and clinical correlation may facilitate earlier diagnosis. Additional studies are needed to further characterize this iatrogenic complication resulting from modern interventional techniques.

KEYWORDS: Foreign-Body Granuloma, Hydrocoil, Hydrophilic Catheters

Emergent Intracranial Angioplasty with or without Stenting for Underlying Atherosclerosis in Patients with Acute Ischemic Stroke

W Yoon¹, H Kang¹, S Kim¹

1Chonnam National University Hospital, Gwangju, South Korea

Purpose

The goal of our study was to evaluate the outcome of emergent angioplasty with or without stenting for treatment of underlying atherosclerotic steno-occlusive lesions in patients with acute ischemic stroke.

Materials and Methods

Between January 2011 and March 2013, a total of 175 acute stroke patients presented within eight hours of stroke onset and were treated with endovascular revascularization therapy at a tertiary academic center. Thirty-eight of these 175 patients who underwent emergent angioplasty with (n=24) or without stenting (n=14) for treatment of underlying atherosclerotic lesions were included in this study. Successful recanalization was defined as thrombolysis in cerebral ischemia grades 2b to 3. Outcome measure was the modified Rankin Scale (mRS) score of 0-2 at 3 months. All patients underwent follow-up CT angiography within one week after the treatment.

Results

Data from 38 patients were analyzed. Nineteen patients had atherosclerotic lesions in M1 segment of middle cerebral artery (MCA), 12 patients had lesions in basilar artery, and seven patients had lesions in intracranial internal carotid artery. Twenty-four patients were treated with intracranial angioplasty after mechanical thrombectomy with Solitaire stent, and 14 patients were treated with angioplasty alone. Successful recanalization was achieved in 95% (36/38) of patients. Twenty-three patients (61%) had a good clinical outcome at three months. Arterial rupture occurred in one patient. Mortality rate was 18% (7/38). Acute reocclusion of treated vessel occurred in 16% (6/38) of patients on follow-up CT angiography.

Conclusions

This study suggests that emergent intracranial angioplasty is feasible and safe for treatment of underlying atherosclerotic steno-occlusive lesions in patients with acute ischemic stroke.

KEYWORDS: Acute Ischemic Stroke, Angioplasty And Stenting

O-894

2:21PM - 2:27PM

Thursday, May 22
1:00PM - 2:38PM

Note: Scanned images are included in the proceedings. Some submitted images were reduced during editing thereby decreasing clarity. Also, refer to the Program Planner. Proceedings Content as of 3/28/2014.

Room 520

90 - PARALLEL PAPERS: Spinal Cord and Trauma

O-900

1:35PM - 1:42PM

The Diaphragmatic Crus Syndrome - A Treatable Cause of Spinal Cord Ischemia

L Higginbotham¹, J Wolinsky¹, C Pardo¹, P Gailloud¹

¹The Johns Hopkins Hospital, Baltimore, MD

Purpose

The diaphragmatic crus syndrome (DCS) was described in 2000 by Rogopoulos and co-authors. The DCS is linked to the compression of lumbar intersegmental arteries (ISA) as they pass through the tendinous portion of the crus, generally at the L1 and L2 levels. Medullary ischemia can result from crus compression when the involved vessel provides a significant contribution to the spinal cord vascularization. This report describes six cases of DCS.

Materials and Methods

The clinical and imaging findings of six observations of DCS (1 woman and 5 men, average age 35 years, range 11-56) were reviewed.

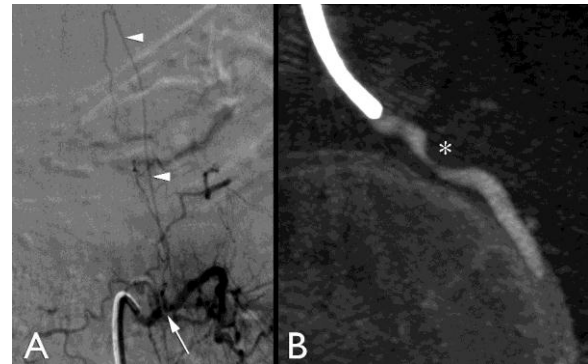
Results

In each patient, a spinal cord stroke was documented by MR imaging (MRI), while compression of an ISA providing significant supply to the spinal cord was confirmed by angiography (Figure 1). The symptomatology was progressive in four cases, unclear in the other two. The onset followed heavy physical activity in three instances. The initial diagnosis was transverse myelitis in three cases, spine degenerative disease, nonspecific myelopathy or spinal stroke in one case each. At the time of accurate diagnosis, four patients were paraplegic, and one had stable leg monoplegia. Only one patient with progressing symptoms was considered a good candidate for surgical therapy. In this case, section of the diaphragmatic crus was performed, with excellent outcome. Figure 1 legends: A shows a selective injection of the left L1 ISA, which provides the artery of Adamkiewicz (arrowheads). The compression by the diaphragmatic crus, indicated by an arrow in A, is confirmed by an axial reconstruction of the selective left L1 flat-panel catheter angiogram (FPCA). (Asterisk=diaphragmatic crus).

Conclusions

Although rarely reported, the DCS may represent a more common cause of spinal cord ischemia than usually appreciated. While accurate anatomical diagnosis requires spinal angiography, the prospect of a potentially treatable etiology of spinal cord ischemia is exciting, particularly if one considers the young age of presentation in our series (average of 35 years). Two-thirds of our patients had a progressive course consistent with worsening ischemia. In half of the cases, the ischemic event followed unusual physical activity.

KEYWORDS: Spinal Angiography, Spinal Imaging, Spinal Stroke



O-901

1:42PM - 1:49PM

Intramedullary Spinal Cord Metastases: Prognostic Value of MRI and Clinical Features from a 13-year Institutional Case Series

F Diehn¹, J Wald¹, L Eckel¹, C Hunt¹, K Schwartz¹, C Wood¹, T Kaufmann¹

¹Mayo Clinic, Rochester, MN

Purpose

Intramedullary spinal cord metastases (ISCM) are rare. Recent studies have elucidated MR imaging (MRI) features of ISCM (1, 2). Our goal was to identify both MRI and clinical features with prognostic value among patients with ISCM from a large single-institution retrospective series.

Materials and Methods

Search of our radiology and clinical databases previously identified patients with ISCM from 1999 to 2011. The relevant MRI examination for each patient from a consecutive group of ISCM patients had been reviewed previously by two neuroradiologists for various imaging characteristics, and baseline clinical data had been obtained. Additional relevant clinical data were extracted. Influence of the clinical and imaging characteristics on survival was assessed by Kaplan Meier survival curves and

Note: Scanned images are included in the proceedings. Some submitted images were reduced during editing thereby decreasing clarity. Also, refer to the Program Planner. Proceedings Content as of 3/28/2014.

log rank test for categorical characteristics, and by Cox models for continuous characteristics.

Results

Forty-nine patients harbored 70 ISCM, with 10 (20%) having multiple ISCM. Lung cancer was the most common primary malignancy (49%). From the date of ISCM diagnosis, the median survival for all patients was 3.5 months. One clinical feature was associated with decreased median survival: lung or breast primary malignancy compared to all other malignancy types ($p=0.0004$); 1.9 months for lung/breast primary malignancies, versus 10.3 months for patients with all other types of primary malignancies. Three MRI features were associated with decreased median survival: 1) multiple ISCM ($p=0.0217$); 1.8 versus 4.0 months for multiple versus solitary ISCM; 2) greater longitudinal extent of cord T2 hyperintensity ($p=0.0184$); 3.7 months for patients with ≥ 3 segments, versus 6.1 months for patients with ≤ 2 segments; and 3) visualization of the primary tumor or non-CNS metastases on the reference MRI ($p=0.0124$); 1.9 versus 10.3 months for patients in whom these findings were present versus absent.

Conclusions

This study describes the prognostic value of pertinent clinical and MRI features in a large single institution series of patients with ISCM. Spinal cord edema spanning multiple segments, the presence of multifocal ISCM, and evidence for non-CNS metastases or the primary tumor should be specifically sought, as these MRI features are associated with decreased survival. Patient with either a lung or breast primary malignancy are expected to have decreased survival. The visualized lungs should be evaluated carefully on MRI since lung cancer is the most common primary malignancy and imparts a worse prognosis compared to other nonlung/nonbreast malignancies.

KEYWORDS: Metastases, Spinal Cord, Spinal Neoplasm

O-902

1:49PM - 1:56PM

2D MEDIC vs 2D T2TSE FS in the Evaluation MS Plaques and Foraminal Narrowing in the Cervical Spine

M Shapiro¹, A Kravtsova²

¹Neuro Imaging Institute of Winter Park, Winter Park, FL,
²University of Central Florida Medical School, Winter Park, FL

Purpose

The purpose of this study was two fold: 1. To determine whether 2D MEDIC or 2D TSE FS is best for detecting

multiple sclerosis (MS) plaques in the cervical cord. 2. To determine which of the above two sequences is better for detecting foraminal narrowing in the cervical spine.

Materials and Methods

One hundred patients with known multiple sclerosis (MS) were prospectively imaged brain and cervical spine on a 3 T (Siemens Verio) MR imaging (MRI) system. All were scanned with MS protocols. The cervical spine protocol included both MEDIC and T2TSE FS in the axial plane in addition to T1 FLAIR, STIR, T1 FLAIR with phase sensitivity reconstruction, T1 VIBE FS pre and postgadolinium and T1 FLAIR FS postcontrast. MEDIC and T2TSE FS sequences (both with 2.5mm slice thickness) were independently evaluated by the neuroradiologist and a fourth year medical student with a two month experience reviewing MRIs for the number and conspicuity of MS plaques. MEDIC, T2TSE fs and T1 VIBE fs were compared by the two reviewers for foraminal narrowing at three levels C 4-5, C 5-6 and C 6-7. Interobserver variation was significant and will be discussed.

Results

Two hundred eight MS plaques were detected by the MEDIC pulse sequence. Two hundred three were detected by the T2 TSE fs sequence. The conspicuity (1-3 scale) was significantly better on MEDIC for most plaques. The postcontrast VIBE sequence was superior for foraminal narrowing. MEDIC most exaggerated foraminal narrowing. T2TSE fs exaggerated foraminal narrowing less than MEDIC but more than postgadolinium VIBE fs. Susceptibility with metal in postfusion patients most effected MEDIC negatively. At the cervico- thoracic junction the signal to noise (SNR) MEDIC was diminished.

Conclusions

MEDIC in the axial plane is slightly superior to T2TSE in the detection of MS plaques in the cervical cord. T2TSE fs is superior in the detection of MS plaques in patients who are postop with anterior or posterior fusions with metal. Postcontrast VIBE fs best delineates foraminal narrowing. MEDIC exaggerates foraminal narrowing the most. T2TSE fs exaggerates foraminal narrowing less than MEDIC. At the cervico thoracic junction, the SNR of MEDIC is somewhat suboptimal particularly, in large patients. Because of the above results, the authors recommend both MEDIC and T2TSE fs be obtained on the patients initial cervical spine scan in patients with known or suspected MS. On follow-up scans MEDIC alone is probably sufficient as the axial T2 pulse sequence unless the patient has had a cervical fusion or is extremely large.

KEYWORDS: Cervical Spine

O-903

1:56PM - 2:03PM

Does Lumbar Epidural Fat Amount Affect Spinal Canal CSF Volume?

Note: Scanned images are included in the proceedings. Some submitted images were reduced during editing thereby decreasing clarity. Also, refer to the Program Planner. Proceedings Content as of 3/28/2014.

KEYWORDS: Epidural Space, Idiopathic Intracranial Hypotension, Image Processing

N Alperin¹, A Bagci¹, B Lam¹, E Sklar²

¹University of Miami, Miami, FL, ²Jackson Memorial Hospital/University of Miami, Miami, FL

Purpose

Female obesity is a risk factor for idiopathic intracranial hypertension (IIH). The exact mechanism however is not yet understood. Thickness measurements of epidural fat suggest that there is no direct link between the amount of body fat and epidural fat. We aimed to study whether the amount of epidural fat affects the spinal canal cerebrospinal fluid (CSF) volume, and thus spinal canal compliance, as a potential link between obesity and IIH.

Materials and Methods

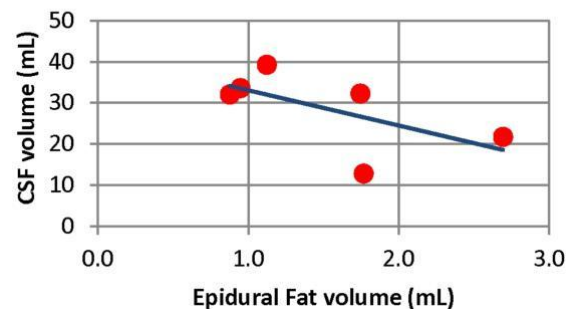
High resolution whole spine 3D T2W FSE and 3D T1W GRE volumes covering the lower portion of the spine was used to scan young (age range 22-30 years) female subjects with a wide range of BMI values (range 20-40) and 2 female IIH patients with ages 17 and 25 years with BMI values of 31 and 25 for the purpose of quantifying spinal canal CSF volume and posterior epidural fat. The study was performed on a 1.5 T Siemens Symphony scanner. The imaging parameters for the 3D T2-weighted sequence with isotropic voxel size of 1.0 mm, TR/TE of 1500/250ms and the 3D T1-weighted sequence with isotropic voxel size of 1.0 mm, FA :12 degrees TR/TE: 10.5/4.8 ms. The epidural fat was delineated manually from T12-L1 through L5-S1 levels on T1-weighted images, and the CSF within the spinal column was segmented using FSL FAST on T2-weighted images. Associations between the CSF and epidural fat volumes, and BMI and epidural fat volumes were determined using linear regression.

Results

An example demonstrating the segmentation of the epidural fat and the segmentation of CSF in the lumbar spine is shown in Figure 1 (top). A scatter plot of the epidural fat volumes versus CSF volumes in lumbar spine is shown in Figure 1 (bottom). While there seems to be no association between epidural fat volume and BMI ($R=-0.16$, $P=0.75$) there was a moderate inverse correlation between the epidural fat volumes and the CSF volumes ($R=-0.62$, $P=0.19$).

Conclusions

In agreement with previous reports, no association was demonstrated between epidural fat volume and BMI. However, epidural fat seems to restrict the CSF space in the lumbar spinal canal, which provides the majority of the spinal canal compliance. These preliminary results suggest that further investigations of the role of epidural fat and how it is being affected by weight gain and/or loss are warranted for understanding of the underlying link between obesity and IIH.



O-904

2:03PM - 2:10PM

Predictors of Vertebral Artery Injury in Isolated C2 Fractures Based on Fracture Morphology Using CT Angiography

D Durand¹, V Kalra¹, A Malhotra¹

¹Yale University School of Medicine, New Haven, CT

Purpose

The incidence of C2 fractures have increased 21% within the last decade. C2 fractures have a known association with vertebral artery injury as the vertebral arteries frequently course through the C2 transverse foramen. We determine predictors of vertebral artery injury defined on CTA in

Note: Scanned images are included in the proceedings. Some submitted images were reduced during editing thereby decreasing clarity. Also, refer to the Program Planner. Proceedings Content as of 3/28/2014.

isolated C2 fractures based on fracture pattern using previously published orthopedic and neurosurgical imaging-based fracture classification schemes.

Materials and Methods

Three hundred CTs containing the words "C2 fracture" based on keyword search performed at a single, large academic institution in the past 10 years were evaluated retrospectively after obtaining IRB approval. Studies were excluded if there was a history of penetrating injury, if there were additional cervical or occipital condyle fractures, or if no CTA was subsequently performed. Three blinded reviewers classified fractures based on multiplanar CT images and independently evaluated CTA images. Disagreements were resolved by consensus. Fractures were classified based on fracture pattern, angulation, and displacement criteria set by Bono et al., Levine et al., and Benzel et al. Morphology was classified into Type I-III spondylolisthesis of the axis, Type I-III odontoid fractures, foramen transversarium involvement with or without comminution, and miscellaneous coronal/sagittal vertebral body fractures. Vertebral artery injury on CTA was defined as the presence of luminal irregularity, luminal narrowing, dissection, pseudoaneurysm, occlusion, or transection. Chi-square, Fisher exact, and logistic regression were performed using Minitab statistical software (Minitab, State College, PA) to determine the association between C2 fracture morphologies and vertebral artery injury.

Results

Seventy-one patients met inclusion criteria. Patient ranged from 17-99 years (mean 57.1, SD 22.2) and included 39 males and 32 females. Fifteen patients (21.1%) had vertebral artery injury on CTA. Thirty-three patients (46.5%) had traumatic spondylolisthesis type fractures. Twenty-three patients (32.4%) had dens fractures. Fifty-five patients (77.5%) had fractures involving the foramen transversarium. Fracture patterns significantly associated with vertebral artery injury were significant traumatic spondylolisthesis fractures (type II - defined as 3-12 mm of displacement and angulation between 0-25 degrees) ($p=0.028$), dens fractures ($p=0.015$), and comminuted foramen transversarium fractures ($p=0.016$).

Conclusions

Isolated C2 fractures demonstrating statistically significant association with vertebral artery injury as defined on CTA were significant traumatic spondylolisthesis fractures, dens fractures, and comminuted foramen transversarium fractures. Simple fractures extending through the foramen transversarium did not demonstrate a statistically significant association with vertebral artery injury. Fracture angulation, translation, and maximum displacement were not significant predictors of vertebral artery injury. These data can be used to determine which patients with isolated C2 fractures should obtain further evaluation with CTA.

KEYWORDS: Cervical Fractures, Thrombosis, Vertebral Artery Dissection

O-907

2:24PM - 2:31PM

MRI and Pediatric Cervical Trauma: Is Bright Always Bad?

J Wagner¹, D Bardo¹

¹Oregon Health & Science University, Portland, OR

Purpose

Imaging evaluation of the pediatric cervical spine in the setting of trauma remains controversial, as no universally accepted standards exist. Typically, institutional patterns dictate imaging protocol ranging from routine use of radiographs to computed tomography (CT) and/or MR imaging (MRI) when cervical spine injury is apparent or suspected. Age and mechanism of injury are important considerations in evaluating cervical spine injury in children because anatomical and physiologic maturity of spinal structures varies tremendously, especially in early childhood. These factors and a child's ability or inability to provide history or participate in, and cooperate with, physical exam emphasize that reliable radiographic imaging findings are essential in children. Traumatic injuries of the cervical spine in children most often involve ligaments, cartilage, spinal cord and the peri- and paraspinal soft tissues rather than bone fracture. While CT or radiographs may readily reveal findings of fracture, STIR and other heavily weighted T2 MRI sequences are most sensitive to detection of joint and soft tissue injury or radiographically occult fracture. Alternatively, the presence of fluid signal in or surrounding a growing joint or ligament may represent a normal physiologic finding. It is therefore paramount to recognize normal MRI findings of cervical spine structures in children in order to differentiate pathologic from normal physiologic findings. The purpose of our study is to recognize and compare the appearance of paraspinal soft tissues and hyperintense STIR signal in cervical spine joints and other structures in children receiving cervical spine MRI both in the absence of trauma as well as in the evaluation of trauma.

Materials and Methods

IRB approval was granted. An electronic query was used to identify patients with cervical spine MR, age 0 – 17 years from 10/1/2010 to 11/13/2013 ($n = 1871$). Patients were first stratified by exam indication into two groups: "trauma" and "nontrauma," and into seven age groups based on spinal maturity, ability to reliably provide clinical history, and likely types of trauma, such as participation in sports. Exams were eliminated due to artifact, absent STIR sequence, or congenital, neoplastic, infectious pathology

Note: Scanned images are included in the proceedings. Some submitted images were reduced during editing thereby decreasing clarity. Also, refer to the Program Planner. Proceedings Content as of 3/28/2014.

and postsurgical changes in a nontrauma patient. Sagittal STIR images were reviewed by two board certified radiologists (one with Neuroradiology MOC and one with Neuroradiology CAQ eligibility) and hyperintense signal in the atlanto-occipital and atlanto-axial joints, spinal ligaments, and peri- and para-spinous tissues was recorded as the binary observation of "present" or "absent".

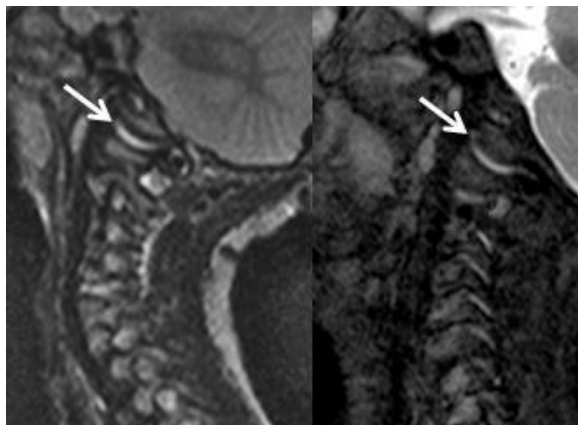
Results

In the nontrauma group, hyperintense STIR signal was identified in atlanto-occipital and atlanto-axial joints in 96% and 98% of all patients, respectively. Hyperintense STIR signal also was identified within the paraspinal tissues in 90% of nontrauma patients. In the pediatric group receiving cervical MRI for suspected traumatic injury, hyperintense STIR signal was identified in the atlanto-occipital and atlanto-axial joints in 95% and 99% of all patients, respectively. In these patients, hyperintense STIR signal also was identified in the paraspinal soft tissues in 99% of patients.

Conclusions

STIR hyperintense signal frequently is seen in atlanto-occipital and atlanto-axial joints of children of all ages without and with traumatic injury. Peri- and para-spinal and spinal ligament signal hyperintensity may be seen due to vascular flow artifact. Findings should not be diagnosed as indication of traumatic injury.

KEYWORDS: Cervical Spine, Pediatric Spine



O-895

1:00PM - 1:07PM

Radiologic and Clinical Features of Radiation Induced Myelitis

P Ambady¹, D Kimbrough², S Terezakis¹, J Blakeley¹, S Newsome², I Izbudak²

¹The Sidney Kimmel Comprehensive Cancer Center at Johns Hopkins, Baltimore, MD, ²Johns Hopkins University, Baltimore, MD

Purpose

Radiation-myelitis (RM) is a rare but dreaded complication of radiation exposure to the spinal cord. Symptom-onset may be delayed and can range from a few weeks up to several years following exposure. The extent of RM in a given patient is influenced by several factors, including the radiation technique, individual radiosensitivity, exposure to radio-sensitizing chemotherapies, and co-morbidities. We present a systematic review of clinical and magnetic resonance imaging (MRI) findings in RM patients treated at a tertiary care institution during the last 20 years.

Materials and Methods

The Institutional Review Board approved this retrospective study. A radiology departmental database of MRI spine studies between 1993 and 2013 was searched using keywords 'myelitis' and 'radiation'. A neuro-oncologist and a neuro-immunologist reviewed clinical records of the queried scans and identified patients with a history of radiation treatment and subsequent myelitis. A single neuroradiologist (II) confirmed the diagnosis and identified relevant imaging characteristics in these patients.

Results

The database inquiry yielded 15935 MRI scans (6759 individual patients), of which 550 scans had diagnostic features of transverse myelitis. Eleven patients fulfilled criteria for final analysis [6 males, 5 females; mean age: 30 years (range 5 -38 years)]. Six received whole body radiation with mediastinal boost with autologous stem cell transplantation for recurrent nonhodgkins lymphoma. Five others received radiation for recurrent multiple myeloma, gastric carcinoma, acute lymphocytic lymphoma, brainstem glioma and medulloblastoma. All patients received at least one radio-sensitizing chemotherapy before or concurrently with radiation. Cervical and/or thoracic cord was involved in all patients in a longitudinally extensive pattern. Maximum myelopathic changes corresponded to the central field of radiation identified by apparent fatty vertebral bone marrow on T1-weighted images. The central 2/3 of the cord on axial T2-weighted images was involved in 10 patients, and one patient presented with focal small area of central and dorsal cord involvement. Lower extremity sensorimotor dysfunction and bladder dysfunction were the predominant presenting complaints (8 of 11 patients). Median time to symptom-onset was 14 months (range 1 month to 180 months). All received steroids while two received hyperbaric oxygen at initial presentation. Seven improved on follow up while one did not. Follow up was not available for three patients.

Conclusions

Note: Scanned images are included in the proceedings. Some submitted images were reduced during editing thereby decreasing clarity. Also, refer to the Program Planner. Proceedings Content as of 3/28/2014.

Radiation-induced myelitis (RM) is a rare but potentially devastating complication of radiation treatment to the central nervous system (CNS). Because clinical presentations of RM may be delayed, diagnosis requires a high index of suspicion and long term follow-up. This study provides relevant clinical background and associated MRI findings that may be helpful in making a diagnosis of RM. Further studies are necessary to ascertain the optimum radiation dose to the CNS in the context of radio-sensitizing chemotherapy in patients with recurrent malignancies, who have received prior treatments with potentially neuro-toxic agents.

KEYWORDS: Radiation, Spinal Cord, Transverse Myelitis

0-896

1:07PM - 1:14PM

Super-resolution tract density images of the spinal cord derived from probabilistic tractography predicts functional impairment in patients with cervical spondylosis

B Ellingson¹, N Salamon², D Woodworth¹, L Holly¹

¹University of California Los Angeles, Los Angeles, CA,
²David Geffen School of Medicine at University of California Los Angeles, Los Angeles, CA

Purpose

The purpose of this study was to explore the use of super-resolution tract density images (TDI) derived from probabilistic tractography performed using diffusion tensor images (DTI) of the spinal cord as a biomarker for microstructural integrity and functional impairment in patients with cervical spondylosis.

Materials and Methods

All experiments were performed on a 3 T Siemens Trio (Siemens Healthcare, Erlangen, Germany). Structural MR imaging (MRI) and DTI were collected on 27 patients with cervical spondylosis with (N=21) or without (N=6) functional impairment as defined by the modified Japanese Orthopedic Scale (mJOA). Diffusion tensor imaging was performed axially through the site of compression using a custom 2D RF excitation pulse combined with a reduced field-of-view EPI readout (Zoomed-EPI) in a total of 20 directions with 10 averages. Probabilistic tractography was performed at 0.5 mm isotropic spatial resolution using the streamline technique combined with constrained spherical deconvolution (model order=4, 0.1-mm step size, 1 million seed points randomly placed throughout the volume). Measurements of maximum tract density at the site of compression, average tract density in rostral normal-appearing spinal cord, the ratio of max tract density to normal tract density, and the volume of tissue

with tract density > 3000 tracts/voxel were calculated for each patient.

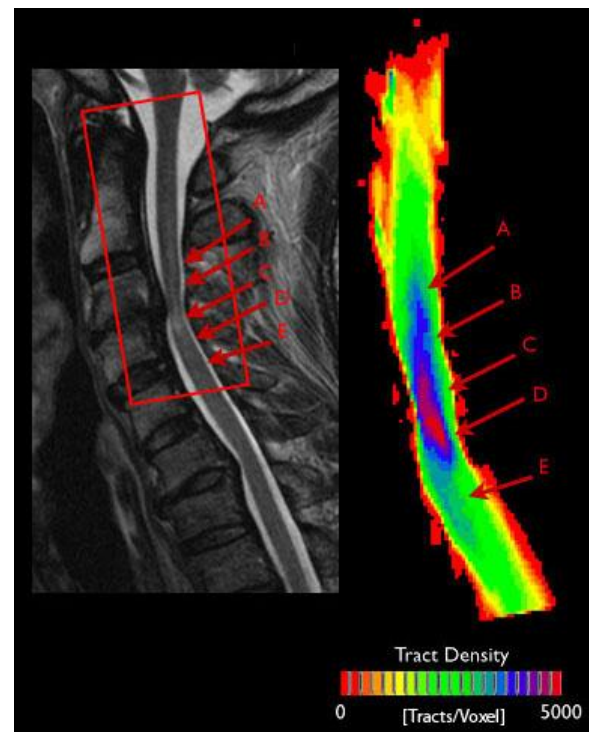
Results

Qualitatively, results demonstrated elevated fiber tract density at the site of compression in all people compared to normal tissue, and a higher fiber tract density in focal areas at the site of compression in patients with functional impairment. Quantitative results suggest that there was a negative correlation between maximum tract density and mJOA ($R^2=0.6324$, $P<0.0001$) and the ratio of maximum tract density to normal tract density ($R^2=0.6648$, $P<0.0001$). A weak negative correlation also was observed between the volume of tissue with tract density > 3000 tracts/voxel and mJOA ($R^2=0.1619$, $P=0.0375$). When grouped according to severity of impairment (mild, $18>mJOA>16$; moderate, $15>mJOA>11$; severe, $mJOA<11$), results showed a significant difference in the ratio between groups (Kruskal-Wallis, $P=0.0015$) and a significant difference between severe and both no impairment ($P<0.01$) and mild impairment ($P<0.05$). No correlation between standard MRI measures of compression or T2 hyperintensity correlated with impairment.

Conclusions

Super-resolution TDI provides unique information about the compression and functional integrity of specific fiber tracts within the spinal cord.

KEYWORDS: MR Diffusion, MR Imaging Spine, Spinal Stenosis



Note: Scanned images are included in the proceedings. Some submitted images were reduced during editing thereby decreasing clarity. Also, refer to the Program Planner. Proceedings Content as of 3/28/2014.

O-897

1:14PM - 1:21PM

Radiation Injury Can be Detected with Neurographic Molecular Imaging

D Schellingerhout¹, S Bredow¹, D Grosshans¹, L Le Roux¹

¹University of Texas MD Anderson Cancer Center, Houston, TX

Purpose

The goal of this study was to detect changes in the spinal cord in response to radiation injury by means of molecular imaging.

Materials and Methods

The lower thoracic spinal cord of adult female BALB/c mice was irradiated with single doses of 2, 10, and 80 Gy. Fluorescently labeled Tetanus Toxin C-fragment (TTc) was used to evaluate changes in the retrograde axonal transport mechanism by means of optical imaging. Hematoxylin-Eosin staining served to assess pathologic changes in radiated cords.

Results

Transport of TTc in the spinal cord was impaired in a dose-dependent manner as early as two days after radiation. Transport was decreased significantly by 16 days in animals exposed to either 10 or 80, while animals exposed to 2 Gy remained unaffected. Further, animals exposed to the highest dose also experienced significant weight loss by 9 days and developed posterior paralysis by 45 days. Pathologic changes of radiation damage could be seen in radiated cords after 30 days in mice exposed to 80 Gy.

Conclusions

Radiation of the spinal cord induces dose-dependent changes in the axonal transport mechanism which can be monitored by molecular imaging. This approach suggests a novel diagnostic modality to assess nerve injury and monitor therapeutic interventions.

KEYWORDS: Nerve Imaging, Radiation Injury, Radiation Protection

O-898

1:21PM - 1:28PM

Intrathecal Chemotherapy and Reversible Cord Myelopathy: Critical identification of treatable myelopathy

E Quigley¹, K Juster-Switlyk¹, N Pierson², L Ledbetter¹, N Satovick³, S Pulst¹, L Shah¹

¹University of Utah, Salt Lake City, UT, ²University of Utah Health Science Center, Salt Lake City, UT, ³University of Utah Hospitals and Clinics, Salt Lake City, UT

Purpose

Intrathecal chemotherapy, such as methotrexate, can induce an acute/chronic myelopathy by interruption of the B12 pathway. This treatable pathology in a subacute combined degeneration pattern may be underreported in patients receiving intrathecal chemotherapy. The goal of this paper is to examine the clinical manifestation and imaging occurrence of subacute combined degeneration (SCD) of spinal cord in patients receiving intrathecal chemotherapy. Additional complicating risk factors, such as radiation therapy, also were characterized. It is hypothesized that the high local concentration of chemotherapeutics that interrupt B12 metabolism can cause SCD in the cord while systemic levels of B12 are normal. Homocysteine may be a more sensitive marker of B12 metabolism. Recognizing this treatable form of myelopathy in patients receiving intrathecal chemotherapy is critical, as "rescue" B12 can be administered early in the onset of symptoms to prevent permanent loss of dorsal column function.

Materials and Methods

Retrospective clinical chart review and imaging database review was performed over eight years. All patients receiving intrathecal chemotherapy in radiology were identified. Those with concurrent MR of the brain, cervical and thoracic spine were identified. Clinical chart review was performed by neurologist. Subsequently, imaging on those patients was reviewed retrospectively by a CAQ neuroradiologist. The presence of abnormal T2 signal in the dorsal or lateral columns of the medulla, cervical, and thoracic cord was characterized. Clinical laboratory data were collected where available including MCV, Hb, or homocysteine levels. Clinical presentations were blinded to the neuroradiologist on imaging review.

Results

Three hundred forty-seven intrathecal chemotherapeutic injections (methotrexate, cytarabine) were identified in 118 separate patients over eight-year duration. Of the 118 patients receiving intrathecal methotrexate (iMTX), 36 patients had imaging of the brain and spine after iMTX. Clinical symptoms included: lower extremity weakness, paresthesia, loss of reflexes and proprioception, decreased pain and temperature, ataxia, imbalance. These neurologic symptoms were present clinically and diagnosed in 17/36 patients. Of these patients, clear dorsal column abnormality was present in 1/36. Subtle dorsal column

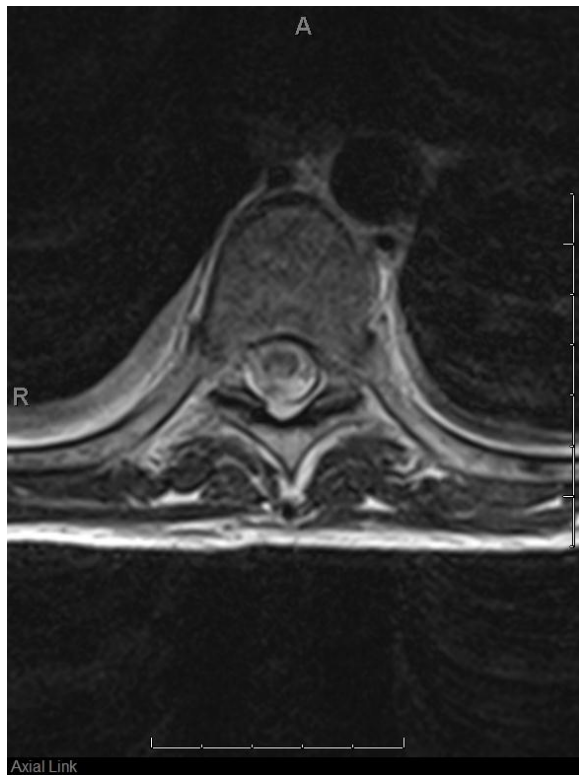
Note: Scanned images are included in the proceedings. Some submitted images were reduced during editing thereby decreasing clarity. Also, refer to the Program Planner. Proceedings Content as of 3/28/2014.

cord or medullary T2 hyperintensity was present in four additional patients on axial T2 imaging. A patient with unilateral dorsal column T2 signal with associated enhancement was excluded due to presence of widespread leptomeningeal disease. Of the five patients with florid or subtle dorsal column signal abnormality, an average of six doses of iMTX were administered. The patient with classic holocord SCD presentation received eight doses of iMTX, doxorubicin, and spinal radiotherapy. Cord abnormality presented two months after iMTX. High dose B12 was administered to this patient with resolution of clinical symptoms.

Conclusions

Intrathecal chemotherapy, such as methotrexate, can cause an acute or subacute presentation SCD pattern of cord myelopathy. High local concentrations, possibly potentiated by radiation therapy, may contribute to this treatable pathology. If suspected or documented on imaging, "rescue" intravenous B12 can treat symptoms. Consider early spine imaging in any patient undergoing intrathecal chemotherapy presenting with loss of dorsal column function. B12 and homocysteine levels can be assessed. However, systemic B12 levels often are normal in patients with clear clinical symptoms of dorsal column involvement.

KEYWORDS: Drugs, Metabolic, Spinal Cord



0-899

1:28PM - 1:35PM

The Periconal Arterial Anastomotic Circle and the Posterior Thoracolumbar Watershed Zone of the Spinal Cord

P Gailloud1, L Gregg1, C Pardo1

1The Johns Hopkins Hospital, Baltimore, MD

Purpose

The concept of spinal cord watershed territories was suggested in the 1950s, but their location remains ill-defined. Isolated spinal gray ischemia constitutes one type of watershed injury related to the higher metabolic need of the gray substance. This report describes the existence of another type of watershed territory related to the particular configuration of the spinal vasculature in the region of the conus medullaris.

Materials and Methods

The MR imaging (MRI) and angiographic data of three patients (56-year-old man, 53-year-old woman, 11-year-old-boy) with documented ischemic injuries in the posterior thoracolumbar watershed zone of the spinal cord are presented.

Results

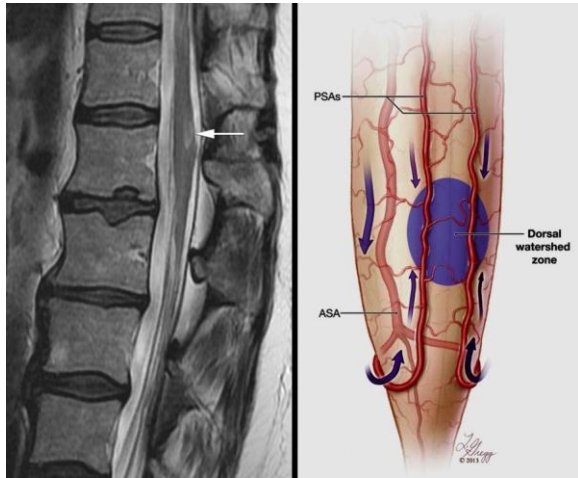
In all three cases, intersegmental arteries providing one or more significant radiculomedullary contribution for the lower cord were compromised by a compressive mechanism responsible for decreased spinal cord perfusion (diaphragmatic crus syndrome in two cases, disk herniation in one). The ischemic injury, located at the junction of the anterior and posterior spinal artery territories along the dorsal aspect of the conus medullaris, was consistent with a watershed mechanism. An example is shown in Figure 1A (arrow). Figure 1B illustrates the periconal arterial anatomy; note in particular the direction of flow, indicated by arrows, with ascending flow in the most caudal segment of the posterior spinal arteries. This portion of the posterior spinal distribution is therefore, from a functional standpoint, under the dependence of the anterior spinal artery.

Conclusions

The posterior thoracolumbar watershed zone of the spinal cord represents an area at increased risk for ischemic injuries, in particular in the context of partial flow impairment related to arterial compression mechanisms.

Note: Scanned images are included in the proceedings. Some submitted images were reduced during editing thereby decreasing clarity. Also, refer to the Program Planner. Proceedings Content as of 3/28/2014.

KEYWORDS: Anatomy, Spinal Angiography, Spinal Vascular Disorders



Thursday, May 22
1:00PM - 2:31PM
Room 520

91 - PARALLEL PAPERS: Spine: Interventional

0-909

1:00PM - 1:07PM

Development of quantitative and objective method to predict fracture risk in patients with vertebral metastases

R Alkalay¹, D Meier², D Hackney¹

¹Beth Israel Deaconess Medical Center, Boston, MA,
²Brigham and Women's Hospital, Boston, MA

Purpose

Breast and prostate cancer are the second leading cause of cancer death in the western world in women and men respectively (1). Vertebral bone is the most frequent site of skeletal metastasis. Although pathologic vertebral fractures (PVF) represents the most dreaded complication associated with metastatic disease in the spine, no objective or quantitative method exists for estimating PVF risk in patients with spinal metastasis. This study is the application of quantitative computed tomography-based structural analysis system (CTA-FRx) to accurately predict the failure of human lumbar spinal units with simulated lytic defect (1).

Materials and Methods

Twenty-eight three-level human cadaveric spine segments (T6-T8, T9-T11, T12-L2, L3-L4), obtained from four male and six female donors aged 48-57 years, were CT scanned (Aquilion 64, Toshiba Medical, USA) using a clinical scanning protocol (field of view: 16 cm, 125kV, Matrix:512²). A six-chamber calcium hydroxyapatite phantom (0-1.5 g/cc³, CIRS, Norfolk, VR) was imaged with the spines to allow bone density calibration. Clinically relevant lytic defects, identified to impose a high risk of failure (Figure 1A) were created in the middle vertebra of each segment. The segments were rescanned in the same spatial orientation, prepared for mechanical testing and tested to failure under axial compression. Using a novel segmentation algorithm, the vertebrae were segmented and the stack of segmented gray level (Hounsfield units) CT images mapped, on a pixel by pixel basis, to density values using the calibration phantom data and the resulting apparent density values converted to elastic modulus. For each vertebral cross-section the following structural parameters were computed; Axial rigidity: estimating the axial load carrying capacity of the vertebra; sagittal (Elmax) and transverse (Elmin) bending rigidities: (estimating the vertebra's resistance to bending load in a chosen axis). The latter were computed about the section modulus-weighted centroid (GCw) with the section's principal axes (Eigenvectors) and second moment of area's computed from the tensor. This computation established the CT-FRx parameters.

Results

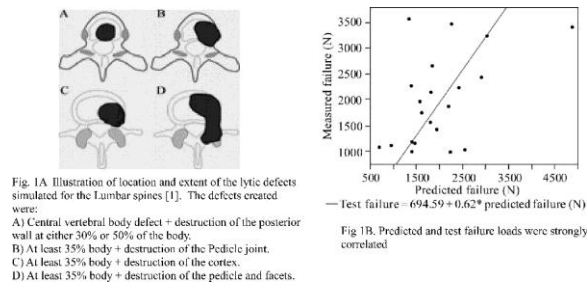
For each of the segmented spines with simulated osteolytic defects, CT-FRx was used to compute the expected failure load. Regression models (JMP 9.0, SAS, NC), fitted to the predicted CT-FRx versus test failure loads, showed a highly significant correlation (ANOVA, F=16.6, p<0.001) with a coefficient of determination (R² =0.71), Figure 1B. As observed from the scatter plot, the failure loads of several spine segments presented a large departure from that predicted. These outliers were attributed to the existence of large osteophytes, often bridging across the disk space, significantly altering the loading acting on the spine.

Conclusions

In agreement with previous studies the location of the defect had no significant effect on the prediction. This study demonstrating high correlation between CT-FRx theoretically predicted spinal failure loads and the measured test values, demonstrates the ability of our protocol to predict failure loads for human vertebrae with lytic defects with a high degree of accuracy. This work will provide a qualitative, and importantly, objective assessment of the changes in the risk of vertebral fracture for breast and prostate cancer patients. We expect this novel approach to facilitate patient management and resource utilization by providing guidelines for selecting among the various treatment options based on fracture risk.

KEYWORDS: Algorithmn, CT, Metastases

Note: Scanned images are included in the proceedings. Some submitted images were reduced during editing thereby decreasing clarity. Also, refer to the Program Planner. Proceedings Content as of 3/28/2014.



O-910

1:07PM - 1:14PM

Safety and Effectiveness of Sacroplasty in a Large Single Center Experience

A Gupta¹, A Yoo¹, R Chandra¹, D Bell¹, B Mehta¹, M Larvie¹, T Leslie-Mazwi¹, J Rabinov¹, J Hirsch¹

¹Massachusetts General Hospital, Boston, MA

Purpose

Sacral insufficiency fractures (SIF) are a common cause of severe low back pain and immobilization in the osteoporotic and cancer populations. Frequently missed on plain film radiography, SIF lesions often require computed tomography (CT) or magnetic resonance imaging (MRI) for diagnosis. Current practice guideline recommendations range from physical therapy with analgesia to surgical fixation/resection in those patients who qualify. For many patients, these options may be ineffective and associated with significant morbidity. Sacroplasty has emerged as a minimally invasive therapeutic strategy for such fractures. Here we study the safety and effectiveness of sacroplasty in a single-center cohort of 53 patients.

Materials and Methods

Under institutional review board approval, we retrospectively reviewed 53 sacroplasty cases completed at our institution from January 2004 to September 2013. Informed consent was obtained prior to procedure and HIPAA compliance was maintained. Chart review was performed to obtain patient demographics and to assess pre- and post-treatment assessments on the Visual Analog Scale (VAS), Functional Mobility Scale (FMS), and Analgesic Scale (AS). Also, a four-point pain improvement scale was used to assess overall response rate to sacroplasty intervention (1 – complete resolution of pain; 2 – improvement of pain; 3 – no change; 4 – worsened pain). Statistical correlation was assessed using the Wilcoxon signed-rank test.

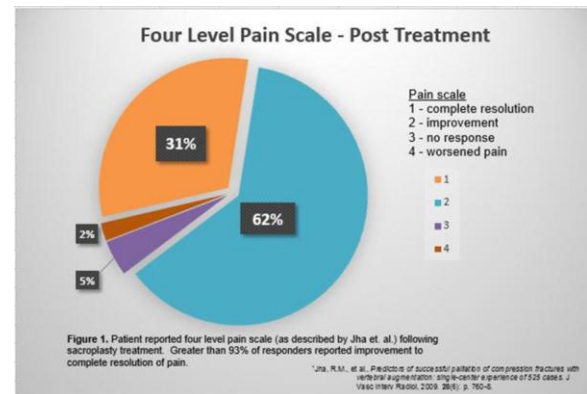
Results

A total of 53 procedures was completed. In this cohort (83.0% female), sacral fracture etiology included metastatic (54.7%), osteoporotic (30.2%), and traumatic (15.1%). Among 27 patients with available pre- and post-treatment scores, there was a statistically significant decrease in patient VAS score ($p < 0.001$), FMS score ($p < 0.001$), and AS score ($p < .01$). Pretreatment median [IQR] VAS (9.0 [8.0-10]), FMS (3.0 [2.0-3.0]) and AS (3.0 [3.0-4.0]) were reduced to median post-treatment [IQR] VAS (3.0 [0.0-5.8]), FMS (1.0 [0.25-2.8]), and AS (3.0 [2.0-3.8]). There were no major complications or procedure-related morbidity reported. Using the four level pain scale, greater than 93% of the total 53 patients reported either complete resolution of pain or improvement in overall pain. Average time to follow up was 27.0 (23.2 – 30.7) days.

Conclusions

In this single-center experience, sacroplasty is a safe and effective procedure for the palliation and treatment of sacral insufficiency fractures. Our results show significant short-term gains in pain relief, increased mobility, and decreased dependence on pain medication.

KEYWORDS: Bone Metastases, Sacroplasty, Spine Interventions



O-911

1:14PM - 1:21PM

Chronic Back Pain after Percutaneous Vertebroplasty: Risk Factors

J Blasco Andaluz¹, L San Roman¹, J Macho¹, A Lopez Rueda¹, C Ruiz¹, N Macias¹, P Peris¹

¹Hospital Clinic of Barcelona, Barcelona, Spain

Purpose

Note: Scanned images are included in the proceedings. Some submitted images were reduced during editing thereby decreasing clarity. Also, refer to the Program Planner. Proceedings Content as of 3/28/2014.

Nearly 25% of patients enrolled in a recent randomized controlled trial comparing vertebroplasty (VP) versus conservative treatment (CT) in patients with symptomatic vertebral fractures (VF) developed severe chronic back pain (CBP). We analyzed the risk factors related to the development of CBP.

Materials and Methods

Severe CBP was defined as residual pain of VAS \geq 7 at the end of follow up (12 months). Several risk factors were evaluated: visual analog scale (VAS) at baseline and during follow up, age, gender, symptom onset time, number, type and severity of VF at baseline, number of vertebral bodies treated, incidental VF, and antiosteoporotic treatment.

Results

Severe CBP was observed in 23% of patients treated with VP and same percentage was found in the CT arm. Patients developing CBP after VP showed a longer symptom onset time (82% \geq 4 months). In the univariate analysis, female gender, number of acute VF (>1), VAS \geq 7 two months after treatment and the type of antiosteoporotic therapy (teriparatide) were risk factors related to CBP development in both groups. In the multivariate analysis the main risk factors were having a baseline and a post-treatment VAS value \geq 7, longer symptom onset time and type of antiosteoporotic treatment.

Conclusions

Nearly 25% of patients with symptomatic osteoporotic VF developed severe CBP independently of type of treatment. Symptom onset time previous to VP and persistence of severe CBP after treatment were the main factors related to CBP. Treatment with teriparatide was related to decreased risk of this complication.

KEYWORDS: Osteoporosis, Vertebral Augmentation, Vertebral Compression Fractures

O-912

1:21PM - 1:28PM

A SECOND LOOK AT SPINE MRIs: Adding Clinical Focus for Optimal Care.

J Rivera¹, P Baghai¹, U Waheed¹, S Curran-Melendez², M Fukui¹

¹Allegheny Health Network, Pittsburgh, PA, ²Allegheny General Hospital, Pittsburgh, PA

Purpose

Many patients may suffer without a diagnosis of a treatable source for their spine pain, if imaging reports are too general or fail to report relevant findings. Our purpose

was to determine if second interpretations of spine MRIs by a neuroradiologist, in collaboration with the neurosurgeon, were concordant with the initial interpretation provided by a nonspecialized radiologist. The interpretations then were correlated with clinical findings and a surgical intervention or nerve root block was offered.

Materials and Methods

We retrospectively reviewed second reports of MRI exams of the cervical, thoracic or lumbar spine by one neuroradiologist in collaboration with one referring neurosurgeon. Second interpretations were compared with the outside interpretation. Discordant interpretations were defined as failure to describe an epidural or spinal canal lesion, cord contusion, degree of spinal canal and lateral recess stenosis, disk extrusion with migration or sequestration, nerve root impingement, and acute fracture. Radiologic interpretations were compared to clinical records, surgical notes, and postoperative symptoms.

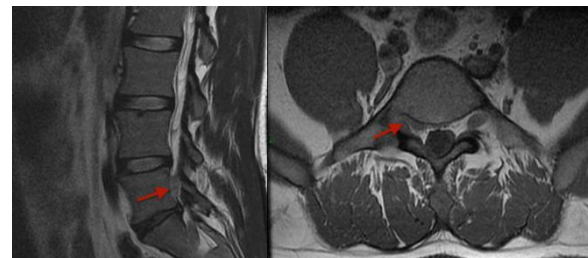
Results

Sixty MRIs (26 cervical, 5 thoracic and 29 lumbar spines) were reviewed in 57 patients. There were 33 out of 60 concordant interpretations. Out of the 33 concordant interpretations, 20 were offered surgery or nerve root block. There were 27 out of 60 discordant interpretations. Out of the 27 discordant interpretations, 21 were offered surgery or a nerve root block. A total of 19 surgeries were performed on 18 patients. Of the 19 surgeries, 10 were from discordant interpretations. In all 19 surgeries, the described pathological disks or foramina were confirmed.

Conclusions

A collaborative approach to spine pain contributes to effective treatment. Detailed history and exam findings are vital to spine MRI interpretation. Reports by a neuroradiologist, with detailed description of pathology, more than doubled the population of patients offered surgery. Interpretations by neuroradiologists permits the neurosurgeon to devise a targeted treatment approach beyond analgesics and offers patients an avenue for a reduction or cure for their pain. We hope that future studies may demonstrate improved outcomes with this approach.

KEYWORDS: Second Opinion Consultation, Specific Findings, Spine Interventions



Note: Scanned images are included in the proceedings. Some submitted images were reduced during editing thereby decreasing clarity. Also, refer to the Program Planner. Proceedings Content as of 3/28/2014.

O-913

1:28PM - 1:35PM

Spontaneous Intracranial Hypotension: Long Term Clinical Outcomes after Treatment with Image-guided Epidural Blood Patch

V Agarwal¹, K Ching¹, J McPhilomy¹, D Laughlin¹, W Rothfus¹

¹University of Pittsburgh Medical Center, Pittsburgh, PA

Purpose

Spontaneous intracranial hypotension (SIH) is an under-diagnosed cause of persistent and often debilitating headaches. Patients commonly present with orthostatic headaches associated with decreased cerebrospinal fluid (CSF) volume and low opening pressure without history of prior instrumentation or trauma. Etiologies of CSF leakage include tears of spinal nerve root sleeves, cervical bone spurs, meningeal/arachnoid diverticula, underlying connective tissue disorders, and perineural cysts. Recent literature reports associate SIH with degenerative disk disease, specifically calcified thoracic intradural disk herniations. In most cases, SIH responds well to conservative management which includes bed rest, increased fluid intake and caffeine. Image-guided epidural blood patches have been shown to be effective treatment for CSF leaks in patients who do not respond to conservative measures. Only a handful of studies have evaluated the long-term outcomes of image-guided epidural blood patches for treatment of spontaneous intracranial hypotension. The aim of this study is to evaluate the long term outcomes of image-guided blood patches for treatment of refractory SIH.

Materials and Methods

An IRB-approved retrospective single institution review was performed of all patients who underwent image-guided epidural blood patch for treatment of refractory SIH and had a minimum of one year followup. The diagnosis of SIH was established by either a neurologist or neurosurgeon prior to the procedure and in some patients was confirmed with lumbar puncture and/or cross-sectional imaging. Patient demographics, technical details, complications, and clinical outcomes were reviewed. For long term follow up, patients were contacted by a trained nurse from our interventional spine service for a short telephone interview. Participation was voluntary and no compensation was provided. Survey questions followed the diagnostic criteria for headache attributed to spontaneous (or idiopathic) low CSF pressure as defined by the International Headache Society (IHS). In cases where patients reported diffuse and/or dull headaches

with or without a postural component, the Headache Disability Index was administered. Any additional treatments that patients underwent for persistent symptoms also were recorded. A total of 42 patients were identified and six patients were excluded (n=4 could not be reached for follow up and n=2 could not recall undergoing the blood patch procedure).

Results

Thirty-six patients (M:F = 8:28) with a mean age of 43 years (range 19-65) underwent a total of 74 image-guided blood patch procedures (34 blind lumbar and 40 targeted) without complications. The average volume of blood injected was 23.9 mL for blind injections and 6.5 mL for targeted injections. The mean follow-up period was 3.4 years (range 1.4-6.9 years). Fifty percent of patients (n=18) reported immediate and complete relief of symptoms. 8.3% of (n=3) patients reported an initial partial response with eventual complete relief of headache symptoms. 5.5% of patients (n=2) patients reported immediate initial relief, however symptoms recurred within < 6 months. 36.1% (n=13) did not respond to blood patch treatment and had persistent symptoms. Of these 13 patients, nine underwent surgical intervention and the remaining four patients continued medical management. After surgery, 55.5% (n=5) patients had complete relief of symptoms while 44.4% (n=4) reported continued symptoms. Of the four patients who elected for medical management, 50% had complete relief of symptoms while the remaining had persistent symptoms. Patients who reported complete relief of symptoms at follow up had undergone 29 procedures (15 blind, 14 targeted) with mean number of 1.4 blood patch procedures. Patients who reported persistent symptoms at follow up had undergone 45 procedures (19 blind, 26 targeted) with mean number of three blood patch procedures.

Conclusions

Image-guided epidural blood patches have been shown to be effective treatment for patients with refractory spontaneous intracranial hypotension. Although no consensus as to the optimal method between targeted and blind epidural blood patch can be reached, an overall 58% success rate of long term symptom relief supports image-guided epidural blood patches as first-line therapy. The minimally invasive technique and low complication rate make it an ideal treatment for SIH. In patients who do not respond to epidural blood patch therapy, surgery may be considered; however cure rates are only slightly higher than medical management.

KEYWORDS: Epidural Blood Patch, Intracranial Hypotension, Spinal CSF Leak

O-914

1:35PM - 1:42PM

Rebound Intracranial Hypertension: A Complication of Epidural Blood Patching for Intracranial Hypotension

Note: Scanned images are included in the proceedings. Some submitted images were reduced during editing thereby decreasing clarity. Also, refer to the Program Planner. Proceedings Content as of 3/28/2014.

P Kranz¹, T Amrhein², L Gray¹

¹Duke University Medical Center, Durham, NC, ²Medical University of South Carolina, Charleston, SC

Purpose

To describe the presentation of patients with confirmed rebound intracranial hypertension (RIH), a complication of epidural blood patching characterized by increased intracranial pressure, with an emphasis on common features that may suggest the diagnosis and potential treatment strategies.

Materials and Methods

Patients treated for intracranial hypotension with epidural blood patch (EBP) who subsequently developed symptoms consistent with elevated intracranial pressure, and who were confirmed to have cerebrospinal fluid (CSF) pressure >20cm H₂O measured by lumbar puncture were included in this retrospective review. Pre-EBP and post-EBP clinical symptoms, CSF pressure measurements, and treatment details were recorded.

Results

Nine cases were identified; eight patients had been treated for spontaneous intracranial hypotension, and one for post-LP headache. All patients had positional headache prior to EBP. Mean pre-EBP opening pressure was 8.6 cm H₂O (range, 1.0-15.0). Median time to onset of RIH was one day (range, 2 hours-1 year). Six of nine patients (66%) developed symptoms of RIH within 48 hours of blood patching. Mean opening pressure measured after development of RIH was 30 cm H₂O (range, 22-55). Headache location associated with RIH was different compared to pre-EBP location in 66% of cases; occipital headaches were most common prior to EBP (66%), while frontal (44%) and peri- or retro-orbital (33%) headaches were most common after RIH development. Most patients with RIH reported new blurred vision (78%) or new nausea/vomiting (89%). All patients improved after drainage of cerebrospinal fluid. In eight of nine cases, patients subsequently were treated with oral acetazolamide, ranging in duration from 5 days to 3+ years.

Conclusions

Rebound intracranial hypertension is a potential complication of epidural blood patching that should be considered in patients who report headache after treatment. Particularly suggestive features include change in headache phenotype, development of new nausea, vomiting, or blurred vision, and symptom development in close relationship to blood patching. Patients should be monitored closely for development of these symptoms, and can be treated with CSF drainage and/or acetazolamide.

KEYWORDS: Epidural Blood Patch, Intracranial Hypertension, Intracranial Hypotension

O-915

1:42PM - 1:49PM

Transforaminal versus intra-articular facet steroid injections for the treatment of cervical radiculopathy: a randomized, double-blind, controlled study.

N Bureau¹, T Moser¹, J Dagher², D Shedid¹, M Li³, P Brassard⁴, B Leduc¹

¹Centre Hospitalier de l'Université de Montréal, Montréal, Québec, Canada, ²Institut de Réadaptation de Montréal, Montréal, Québec, Canada, ³Université de Montréal, Montréal, Québec, Canada, ⁴McGill University Health Center, Montréal, Québec, Canada

Purpose

Transforaminal steroid injections (TFSI) are part of the management of cervical radiculopathy (CR). In recent years, catastrophic complications following TFSI have been reported. This study aims to evaluate and to compare the efficacy of TFSI and of intra-articular facet steroid injections (IFSI) in the treatment of chronic CR.

Materials and Methods

This study was approved by the institutional review board and all study subjects signed an informed consent. We randomly assigned 56 subjects diagnosed with chronic CR by a neurosurgeon (D.S., M.L.) or a physiatrist (B.E.L., J.D.) according to standardized criteria, to receive CT-guided TFSI (15 men, 13 women; mean age 52 years; range 29 - 72 years) or CT-guided IFSI (8 men, 20 women; mean 44 years; range 26 - 60 years). The CT-guided injections were performed by one of two musculoskeletal radiologists (N.B., T.M.) with 18 and 10 years experience respectively. The subjects were blinded to the type of injection they received. The subjects were evaluated on the day of the procedure (Pre) and one month later (Post) by a research assistant who also was blinded to the type of injection administered to the subjects. A pain score, using a Visual Analog Scale (VAS), and the Neck Disability Index (NDI) were used as outcome measures. Two outcome variables, the VAS_Diff and the NDI_Diff (difference between Post and Pre scores, relative to the Pre score, in percentage) were used. The efficacy of each technique, in terms of pain score reduction and of NDI improvement, was defined as a VAS_DIFF > 30% and a NDI_DIFF > 10%, respectively. To compare the efficacy between both techniques, in terms of the VAS pain score and NDI outcomes, ANCOVA analysis was used with the Pre score as covariable. Noninferiority of the IFSI to the TFSI was claimed when the mean and 95% confidence interval (CI) of the outcome variables of IFSI were superior to, or not less than 15% the outcome variables of TFSI.

Note: Scanned images are included in the proceedings. Some submitted images were reduced during editing thereby decreasing clarity. Also, refer to the Program Planner. Proceedings Content as of 3/28/2014.

Results

In the intention-to-treat and per-protocol analyses, for a mean Pre VAS pain score, IFSI demonstrated a significant pain score reduction of 35% (CI: 17.7% - 52.4%) and of 30.9% (CI: 12.7% - 49.3%) respectively, while TFSI showed nonsignificant pain score reduction of 12.6% (CI: +4.7% - 29.9%) and 15.7% (CI: +3.3% - 34.7%) respectively. Regarding the NDI outcome, both techniques demonstrated a significant improvement, in the intention-to-treat analysis with IFSI 24.5% (CI: 5.5% - 43.5%) and TFSI 25.5% (CI: 6.5% - 44.5%) and in the per-protocol analysis with IFSI 24.5% (CI: 5.9% - 43.2%) and TFSI 25.5% (CI: 6.2% - 44.8%). When comparing both techniques, an interaction between both groups and the Pre VAS pain score was found. Hence, in the intention-to-treat and per-protocol analyses, noninferiority of IFSI to TFSI was demonstrated for Pre VAS pain score ≤ 60 , while the efficacy of IFSI was inferior to TFSI for Pre VAS pain score ≥ 80 . Regarding the NDI outcome, noninferiority of IFSI to TFSI was demonstrated in both analyses.

Conclusions

Intra-articular facet steroid injections are effective for the treatment of chronic CR. The efficacy of IFSI is noninferior to TFSI when the initial level of pain score is low to moderate. IFSI can be an effective and a safer alternative to TFSI for the treatment of CR as no serious complications have been reported to date with this approach.

KEYWORDS: Cervical Spine, Nerve Root, Spine Injections

0-916

1:49PM - 1:56PM

3D T2 MR-based Measurements of the Posterior Cervical Thecal Sac in Flexion and Extension for Cervical Puncture.

M Bazylewicz1, A Sayah1, F Berkowitz1

1Medstar Georgetown University Hospital, Washington, DC

Purpose

Current technique for cervical puncture traditionally is performed with neck extension. The purpose of this study is to compare anatomical measurements of the posterior cervical thecal sac during neck flexion and extension in normal volunteers using high resolution MR imaging to aid in positioning for cervical puncture.

Materials and Methods

High resolution 3D T2 SPACE magnetic resonance imaging (MRI) images were obtained of the cervical spine in 10 subjects. Subjects included healthy volunteers of age 18 or older. Exclusion criteria included: history of cervical spine injury or surgery, acute or chronic neck pain, and history of degenerative disk disease. Sagittal T2 SPACE images were obtained in the following neck positions: supine extension, supine flexion, prone extension, and prone flexion. Measurements of the degree of flexion and extension were

recorded for each of the four positions. The AP dimension of the posterior cervical thecal sac (distance between the spinal cord and the posterior spinal canal at the C1-2 level) was measured in each of the four positions.

Results

Mean angle of extension was 38 degrees for supine and 35 degrees for prone position. Mean angle of flexion was 20.5 degrees for supine and 21 degrees for prone position. Mean size of the AP dimension of the posterior thecal sac at the C1-C2 level were as follows: 0.37 cm for supine extension, 0.26 cm for supine flexion, 0.4 cm for prone extension, and 0.33 cm for prone flexion.

Conclusions

Based upon our measurements of healthy volunteers, the posterior cervical thecal sac is larger with neck extension than with neck flexion. This difference is independent of prone or supine positioning. This suggests that extension is the ideal neck position for performing cervical puncture and that the decision for prone versus supine positioning can be made based on operator comfort and patient preference.

KEYWORDS: Cervical Spine, Myelography, Spine Interventions

0-917

1:56PM - 2:03PM

Reducing the Dose for CT-guided Spine Biopsies: Let's Shift the Paradigm

K Shpilberg1, B Delman1, S Esses1, L Tanenbaum1, R Subramaniam1, A Doshi1

1Mount Sinai Hospital, New York, NY

Purpose

Imaging-guided biopsies are a commonly used method to obtain tissue sample for diagnosis in suspected cases of malignancy. In particular, CT guidance provides a reliable method of image guidance for spinal lesions. The purpose of this study is to demonstrate that using a low-dose (LD) protocol for CT-guided spine biopsies can be as effective in tissue sampling, procedural time and complication rate as a regular-dose (RD) protocol.

Materials and Methods

After obtaining Institutional Review Board approval, we retrospectively reviewed all patients who underwent CT-guided spine procedures at our institution between May 2010 and October 2013. Patients who underwent disk space aspirations for suspected diskitis/osteomyelitis and spinal pain injections were excluded. Patients for whom dose reports were not available in our institution's PACS were excluded. Sixty-four patients were included. The

Note: Scanned images are included in the proceedings. Some submitted images were reduced during editing thereby decreasing clarity. Also, refer to the Program Planner. Proceedings Content as of 3/28/2014.

following data were recorded: age, gender, lesion biopsied, kVp, mAs, pitch, CT dose index (CTDIvol) per series (mGy), total CTDIvol, dose length product (DLP) per series (mGy-cm), scan range (mm), total DLP, number of biopsy-guiding scans, number of pre- and post-biopsy diagnostic scans, number of needle passes, total number of scans, duration of each biopsy, pathology results and complications. Low-dose biopsies were defined as those with a kVp of 80, mAs of 40-60 and pitch of 0.875-1.35. Regular-dose biopsies were defined as those with a kVp of 120 and mAs >200. Scans performed at kVp and mAs parameters outside the above-mentioned criteria for LD and RD biopsies were classified based on average CTDIvol (CTDIvol <10mGy LD; CTDIvol >10mGy RD). Age, biopsy duration, total number of scans, total CTDIvol and total DLP of LD and RD groups were compared using unpaired t-test. Diagnostic tissue yield was compared using Fisher exact test. $P < 0.05$ was considered to be statistically significant.

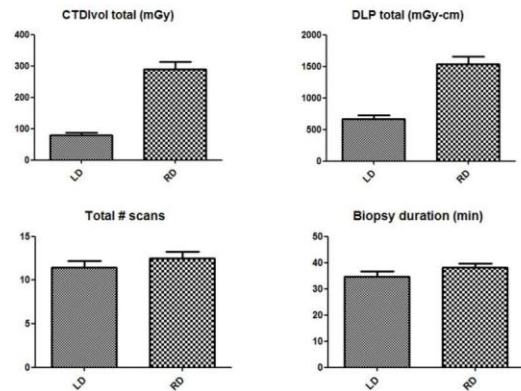
Results

Thirty-one patients underwent LD CT-guided spine biopsies and 33 patients underwent RD biopsies. There was no significant difference in patient age between the two groups (64.13 ± 2.44 years for LD versus 58.97 ± 2.54 years for RD; $p=0.149$). There was a statistically significant difference in total CTDIvol between the LD and RD groups (79.06 ± 8.336 mGy versus 289.3 ± 23.48 mGy respectively; $p < 0.0001$) as well as in total DLP (667.2 ± 62.2 mGy-cm for LD versus 1536 ± 115.9 mGy-cm for RD; $p < 0.0001$). There was no significant difference in total number of scans obtained (11.42 ± 0.78 for LD versus 12.48 ± 0.79 for RD; $p=0.3422$), duration of procedure (34.55 ± 2.15 min for LD versus 38.18 ± 1.57 min for RD; $p=0.1732$) or diagnostic tissue yield (21/31 or 67.74% for LD versus 20/33 or 60.61% for RD positive for malignancy; $p=0.61$). There were sufficient specimens for diagnosis in all patients in both biopsy groups. No significant complications were noted in either group.

Conclusions

Low CT-dose spine biopsies have a significantly lower cumulative radiation exposure (CTDIvol and DLP) when compared to regular CT-dose biopsies without significantly affecting procedural time or diagnostic tissue yield. Use of a LD protocol should be considered as an alternative to RD protocol when performing CT-guided spinal biopsies, thus allowing the operator to reduce ionizing radiation dose while maintaining overall quality and efficiency of the procedure.

KEYWORDS: Biopsies, Dosimetry, Spinal Neoplasm



0-918

2:03PM - 2:10PM

Achieving Integrated, Collaborative Management of Spinal Tumors using CT Myelography based Stereotactic Radiosurgery Planning: A Preliminary Experience.

V Zohrabian¹, Z Husain¹, M Laurans¹, V Chiang¹, A Mahajan¹, M Johnson¹

¹Yale-New Haven Hospital, New Haven, CT

Purpose

Computed tomography (CT) myelography has been employed to distinctly delineate neural structures, allowing for precise treatment of tumor with high-dose irradiation. Here, we discuss collaborative efforts between the Departments of Diagnostic Radiology, Radiation Oncology, and Neurosurgery in the creation of a robust spine stereotactic radiosurgery pre-treatment planning program at a large cancer center designed to increase patient throughput and enhance therapeutic accuracy.

Materials and Methods

In November 2012, a spine tumor board was created to review patients with metastatic disease to the spine and to explore a variety of treatment options, including conventional radiation therapy, chemotherapy, stereotactic radiosurgery, minimally invasive and conventional surgery, vertebral augmentation with vertebroplasty/kyphoplasty, and palliative care. The enhancement of the spine radiosurgery program was largely sought because of increasing numbers of patients with spinal metastatic disease and the difficulty of acquiring efficient co-registration from MR imaging (MRI) and CT simulation scan data sets with conventional radiation planning. In cases where tumor closely approximated radiosensitive neural structures, a decision was made to obtain CT myelography for pretreatment

Note: Scanned images are included in the proceedings. Some submitted images were reduced during editing thereby decreasing clarity. Also, refer to the Program Planner. Proceedings Content as of 3/28/2014.

planning. Calibration between the diagnostic radiology CT and radiation oncology simulation CT were evaluated and documented by both diagnostic and therapeutic radiology physicists. Electronic transfer of data from the diagnostic radiology CT scanner to the radiation oncology simulation CT also was tested and found to be successful.

Results

Patients were scheduled for CT myelography-based simulation approximately one week prior to treatment. The patient arrived in the Diagnostic Radiology department as the first case in the morning. Patient registration, chart review, consent, and iv access were performed, and the patient was on the table within one hour of arrival. A lumbar puncture was performed with instillation of a standard dose of 20 mL of Omnipaque 180 into the thecal sac to opacify the subarachnoid space. Approximately 1-3 mL of CSF fluid was obtained for analysis in each patient. Contrast was advanced into the area of interest and fluoroscopic spot films obtained. For tumors in the thoracic area, a gold fiducial localization marker was placed to provide an internal fiducial for correlation with the external fiducials and the immobilization bag. The spinal needle was removed and the patient was immediately transported across the hall to a CT scanner with flat table top. There, the radiology and radiation oncology technologists met the patient, and the patient was immobilized in a pre-molded standard mask system or stereotactic body frame system utilizing double-vacuum technology to provide motion stability. The patient then was positioned on the CT table and scanned using a 60-65 cm FOV to include the immobilization device, and the images checked by the radiologist for diagnostic quality. The CT myelographic dataset subsequently was reformatted with a smaller field of view and thin sections, including sagittal and coronal reconstructions, for diagnostic interpretation. Following this, the patient was taken to the diagnostic radiology recovery area for monitoring for 1-2 hours following the procedure prior to home discharge. The pretreatment CT imaging was immediately available to the radiation oncologist and neurosurgeon for treatment planning utilizing inverse planning IMRT software.

Conclusions

We performed CT myelography pretreatment planning in 20 patients between December 2012 and December 2013. None of the patients in our series experienced radiation myelitis or compression fractures as a complication of radiosurgery. We have documented tumor type and primary versus recurrent, time from initial consult to pretreatment planning CT myelogram, time from CT planning stage to radiation treatment, and mean radiosurgical doses. Our overall experience has been positive, and has fostered a close working relationship between the radiologists, oncologists, and neurosurgeons, which we expect to translate into improved clinical outcomes.

KEYWORDS: Radiation Therapy, Spinal Imaging, Spine Interventions

O-919

2:10PM - 2:17PM

Radiation Induced Osteoradionecrosis and Osteomyelitis of the Sub-axial Cervical Spine Following Radiation Therapy and Posterior Pharyngeal Wall Surgery

H Su¹, A Khorsandi², W Mourad², C Lazarus², M Urken², A Jacobson²

¹Thyroid, Head and Neck Cancer Foundation, New York, NY, ²Beth Israel Medical Center, New York, NY

Purpose

To report our experience with radiation-induced osteoradionecrosis (RIORN) of the subaxial cervical spine. RIORN is a serious long term complication of radiation therapy (RT) for head and neck cancers (HNC). RIORN involving the mandible is well documented. RIORN of the skull base, C1 and C2 also has been documented in patients being treated for nasopharyngeal carcinomas. However, RIORN of the subaxial cervical spine is described much less frequently, and can lead to vertebral instability, kyphosis and pain requiring aggressive surgical intervention and hyperbaric oxygen therapy.

Materials and Methods

This is a single-institution retrospective review of patients diagnosed and treated for RIORN of the subaxial cervical spine following treatment for HNC. From January 2000 through January 2013, all radiologic imaging, operative reports and pathologic findings were retrieved from the Department of Radiology, Radiation Oncology and Otolaryngology databases and reviewed.

Results

Four patients were identified, each with an extensive history of recurrent HNC treated with surgery and multiple courses of RT with a cumulative dose of ≥ 100 Gy. All patients had previous surgical treatment involving the posterior pharyngeal wall (PPW). RIORN involved multiple cervical vertebrae between C3 and T1. Positron emission tomography (PET)/ computed tomography (CT) imaging was performed for two patients and initially was interpreted as recurrent disease. MR imaging was performed for all patients and initially was interpreted as diskitis and osteomyelitis. Two patients were treated with intravenous antibiotics and/or antifungal medication, and two were treated with surgical debridement and fixation.

Note: Scanned images are included in the proceedings. Some submitted images were reduced during editing thereby decreasing clarity. Also, refer to the Program Planner. Proceedings Content as of 3/28/2014.

Conclusions

RIORN of the subaxial spine has variable imaging appearance and needs to be differentiated from recurrent or metastatic disease. We propose that surgical violation of the PPW on top of compromised vasculature in HNC patients treated heavily with RT may predispose the subaxial cervical vertebrae to RIORN. Previous irradiation combined with exposure to upper aerodigestive tract secretions from PPW defects may lead to vertebral body osteomyelitis, systemic infection, vertebral compression fracture and fistula formation.

KEYWORDS: Cervical Spine, Radiation Necrosis

O-920

2:17PM - 2:24PM

18F-NaF PET Evaluation of Facet Joints of the Lower Lumbar Spine Compared with CT and MRI Graded Arthropathy

M Brus-Ramer¹, S Behr¹, J Talbott¹, W Dillon²

1University of California San Francisco, San Francisco, CA,
2University of California San Francisco Medical Center, San Francisco, CA

Purpose

Lumbar facet syndrome is a major cause of morbidity in the United States. Commonly employed radiographic studies, including CT, show poor correlation with outcomes following diagnostic facet blocks. Noninvasive imaging techniques that more accurately identify patients who will benefit from interventional therapies for facet syndrome are needed. As a measure of bone turnover and blood flow, 18F-NaF (NaF) PET may identify functional changes in the facet joint not reflected by simple structural abnormalities seen on CT. Correlation between NaF uptake and CT grade of facet arthropathy was tested. Additionally, separately obtained MRI in a subset of patients was compared to findings in the PET and CT studies.

Materials and Methods

Thirty patients who underwent NaF PET-CT imaging over a year period (2009-2013) for cancer restaging were identified retrospectively. No patient had imaging or clinical evidence for metastatic disease. Whole body PET-CT images were acquired approximately 45 minutes following iv administration of 160 MBq 18F-NaF. Maximum (SUVmax) and mean (SUVavg) NaF uptake within the bilateral L3-L4, L4-L5, and L5-S1 facet joints was measured using a volumetric region of interest (ROI) encompassing the entire facet joint. Values subsequently were standardized to uptake within the normal mid-femoral diaphysis. Facet arthropathy was graded on CT images using Pathria classification. Facet joints were divided into three groups: high uptake (SUVavg \geq 4),

moderate uptake ($4 >$ SUVavg \geq 2) and low uptake joints (SUVavg $<$ 2) on the basis of their SUVavg. Computed tomography scores of facet arthropathy were averaged within each of these groups and compared via Student's t-test and ANOVA. Correlation analyses also were performed. In a subset of patients. MR imaging of the lumbar spine performed within 12 months of the PET-CT also was reviewed. Pathria CT grading and modified Pathria scoring for MRI facet arthropathy was compared with NaF SUV using ANOVA and Student's t test.

Results

Computed tomography evidence for facet arthropathy was present in 91% (grade 1 through 3) of interrogated joints (n= 180), with 53% of joints graded as moderate (grade 2) or severe (grade 3) by Pathria CT criteria. The mean SUVavg within a facet joint was 3.4 (range 1.4 - 9.8, SDEV = 1.5) while the mean SUVmax was 7.0 (range 2.3 - 30.4, SDEV = 4.3). A statistically significant variation between groups by ANOVA was present (F = 4.19, p = 0.017), with significant individual group CT Pathria score differences between high NaF uptake group and moderate and low uptake groups (p < 0.015). Overall, only weak correlation between SUVavg and CT grade of arthropathy ($\rho = 0.30$) was observed. In the subset of patients with recent MRI, the presence of pathologic facet joint fluid was associated with elevated SUVavg (p < 0.05).

Conclusions

High NaF uptake within a facet joint is associated with significantly worse facet arthropathy as assessed by Pathria grading. However, overall weak correlation between NaF PET and CT arthropathy grade suggests that NaF PET and CT findings might reflect different ongoing abnormalities in the setting of chronic ongoing facet arthropathy. Interestingly, the presence of pathologic facet joint fluid on MRI is highly associated with increased NaF uptake. Further prospective studies utilizing NaF-PET in low back pain patients are warranted to correlate with clinically confirmed sites of facetogenic pain.

KEYWORDS: Bone Scan, Facet, PET/CT

O-921

2:24PM - 2:31PM

Intracardiac Cement Embolism During Percutaneous Vertebroplasty: Incidence, Risk Factors and Clinical Management

S Fadili¹, F Clarençon², R FAHED³, E Cormier⁴, J Gabrieli², L Le Jean¹, C Zeghal¹, J CHIRAS²

1Pitié-Salpêtrière Hospital, Paris, Ile de France, 2Hopital de la Pitie-Salpetriere - Service de Neuroradiologie Interventionnelle - Pr. CHIRAS, PARIS, France, 3Hôpital de

Note: Scanned images are included in the proceedings. Some submitted images were reduced during editing thereby decreasing clarity. Also, refer to the Program Planner. Proceedings Content as of 3/28/2014.

la Pitie-Salpetriere, PARIS, France, 4Pitié-Salpêtrière
Hospital, Paris, France

O-922

1:00PM - 1:07PM

Purpose

To evaluate the incidence of intracardiac cement embolism during percutaneous vertebroplasty (PV).

Materials and Methods

Single-center retrospective analysis of 1512 consecutive patients (996 females, 516 males; mean age = 68 y) who underwent 1855 PV with PMMA cement for thoracic and/or lumbar vertebral compression fracture (VCF) (tumor lesion: 45.5%, osteoporosis: 33.7%, trauma: 10%, other: 10.8%). A chest imaging (plain X-ray and/or CT-scan) was performed when a venous leakage was suspected by the operator during the procedure. The rate of cement cardiac migration (CCM) was evaluated. Age, sex, operator's experience, lesion type (tumor, osteoporosis, trauma), sub-type of tumor lesions (blastic, osteolytic or mixed) were evaluated as risk factors for CCM. Clinical consequences of CCM were evaluated in post-procedure and at 1-month follow-up.

Results

In 65.4 % post-PV chest imaging was available. Seventy-one patients (4.7%) had CCM during the 1855 procedures. These CCMs were isolated in 14% of the cases and associated with lung cement embolism in 86% of the cases. The rate of CCM was independent from age, sex, operator's experience, lesion type, tumor lesions' sub-type. Five patients (7%) with CCM had symptoms potentially related to this complication: one cardio-respiratory arrest, that immediately recovered and without any clinical consequence, one pericardial effusion, and 3 cases of transitory dyspnea without further consequence. All these patients had an associated lung cement migration.

Conclusions

CCM during PV with PMMA cement are not exceptional (4.7% the cases) but are asymptomatic in most cases (93%).

KEYWORDS: Cement, Cement Augmentation, Complications

Clinical Confounds in Volumetric Analysis: A Comparison of Intracranial and Posterior Fossa Volumetry in the Adult Chiari 1 Malformation, Idiopathic Intracranial Hypertension, and Controls

A Saindane1, B Bruce2, A Saindane2, L Albin2

1Emory University, Atlanta, GA, 2Emory University School of Medicine, Atlanta, GA

Purpose

Measurement of posterior fossa volume (PFV) has been proposed to have diagnostic utility and physiologic significance in the Chiari malformation type 1 (CM1), however, this remains debatable in adults. This study evaluated the effects of demographics on PFV and total intracranial volume (TICV) in adult CM1 patients, patients with idiopathic intracranial hypertension (IIH) who may share some imaging features of CM1, and in healthy controls using reproducible methods of MRI-based volumetric assessment.

Materials and Methods

Twenty-eight confirmed CM1 patients, 21 IIH patients, and 113 asymptomatic control subjects underwent brain MR imaging (MRI) including contrast-enhanced 3D GRE T1-weighted imaging. Linear measurements of the posterior fossa (PF) and intracranial (IC) space were obtained, and manual segmentation of the PF and IC was performed to yield PFV and TICV (Figure 1). Intra and inter-observer measurement variability and the utility of using linear measurements to predict PFV and TICV were assessed. The effects of age, gender, race, and BMI on PFV and TICV were evaluated in controls, and differences in these demographic variables were controlled for in comparisons of linear and volumetric measurements between CM1, IIH, and control patients.

Results

Three of the 12 linear measurements were significant predictors of TICV (accounting for 74% of variance), and four predicted PFV (accounting for 54% of variance). Both linear and volumetric measurements demonstrated good to excellent intra and interobserver reliability, with greater variability for linear dimensions than volumes. Age, race, gender, and BMI each significantly influenced PFV and TICV in controls. White race, male sex, and high BMI correlated significantly with both larger PFV and larger TICV, while older age corresponded with smaller volumes. No significant differences in PFV, TICV, or PFV:TICV ratio were seen between the CM1 group and the control group after controlling for demographics; however, IIH patients were more likely to have smaller PFVs (OR 1.81, p= 0.1) and trended towards having larger TICVs (OR 1.24, p =

Thursday, May 22

1:00PM - 2:38PM

Room 524

92 - PARALLEL PAPERS: Structural and Volumetric Analysis in the CNS

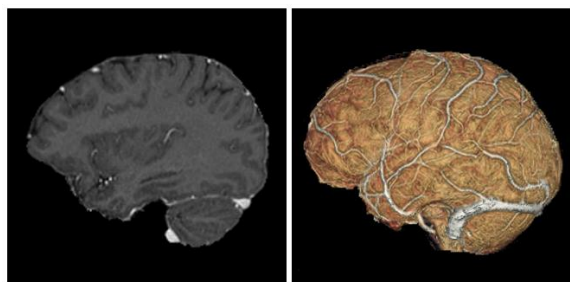
Note: Scanned images are included in the proceedings. Some submitted images were reduced during editing thereby decreasing clarity. Also, refer to the Program Planner. Proceedings Content as of 3/28/2014.

0.06). The figure demonstrates two-dimensional tracing and three-dimensional volume renderings of TICV. Similar images were generated for PFV.

Conclusions

Linear measurements of the PF and IC space are not strong predictors of PFV and TICV. Age, race, gender, and BMI have significant effects on intracranial measurements that must be considered, particularly with respect to PFV in CM1. Even when these demographic variables are appropriately accounted for, other similarly presenting diseases may demonstrate small PFVs. Overall, this emphasizes the need for caution in interpreting the significance of differences in intracranial dimensions between various groups.

KEYWORDS: Chiari Malformation type 1, Idiopathic Intracranial Hypotension, Volumetric Analysis



O-923

1:07PM - 1:14PM

Changes in Total Intracranial Vascular Volume and Dural Sinus Volume following Lumbar Puncture in Patients with Suspected Idiopathic Intracranial Hypertension

A Saindane¹, V Biousse², N Newman², B Bruce², A Saindane¹, L Albin²

¹Emory University, Atlanta, GA, ²Emory University School of Medicine, Atlanta, GA

Purpose

Intracranial pressure (ICP) is determined by contributions of brain volume, cerebrospinal fluid (CSF) volume, and vascular volume. In conditions of abnormally elevated ICP such as idiopathic intracranial hypertension (IIH), the dural venous sinuses have been demonstrated to be abnormal with stenosis of the distal transverse sinuses. In the setting of low intracranial pressure from a CSF leak, the dural venous sinuses have been shown to increase in size. This pilot study assessed the changes in total intracranial

vascular volume and dural venous sinus volume following lumbar puncture (LP) with CSF removal.

Materials and Methods

Six patients with suspected IIH underwent imaging evaluation including contrast-enhanced MR venography at 1.5 T (Siemens Avanto, Erlangen, Germany or GE Signa, Milwaukee, Wisconsin) using a standard head coil. MRV precontrast and postcontrast sequences were obtained in the axial plane with TR of 4-6 ms, TE of 1-2 ms, and flip angle of 22-30 degrees with slice thickness of 0.8-1.4 mm. A subtracted dataset was generated from the precontrast and postcontrast sources images. All patients underwent MRV evaluation both prior to and following LP for opening pressure assessment and CSF removal. Subtracted MRV datasets were segmented manually to determine the total intracranial volume (TICV) inside the cranial vault. This volumetric dataset then was thresholded to yield only enhancing vascular intracranial structures as a measure of total vascular volume (TVV). The superior sagittal, straight, transverse, and sigmoid sinuses then were manually segmented from the TVV dataset to yield dural sinus volume (DSV). Measures of TICV, TVV, and DSV, as well as %TVV/TICV and %DSV/TICV were compared within patients pre- and post- LP.

Results

There were five female and one male patients with median BMI was 44.5. Median OP was 30.0 cm water (range 10 to 54). Four of six patients ultimately met diagnostic criteria for IIH. The median time from the initial MRV to LP was five days (range 0 to 29 days), and the median time from the LP to the MRV was 0 days (four patients with LP on same day as MRV, two others with MRV 51 and 171 days following LP). Pre- and Post-LP volumes are summarized in the table. Only minimal difference in TICV between MRV examinations was noted (0.3%, $p=0.218$) indicating good reproducibility of the segmentation process. Following LP and CSF removal, TVV increased by 14.0% ($p=0.010$), as did TVV normalized to TICV (13.3% increase; $p=0.007$). While on average the DSV increased 10.8% following LP, this did not achieve statistical significance ($p=0.166$). The mean increase in TVV following LP was 14 cc, while the mean increase in DSV was only 3 cc. The figure demonstrates pre-LP (A) and post-LP (B) appearance of the dural venous sinuses.

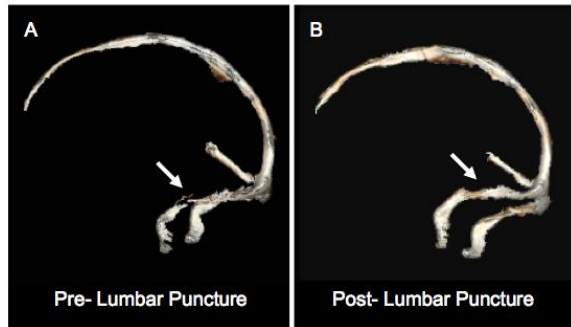
Conclusions

Following LP and CSF removal there is a significant increase in intracranial TVV as well as TVV normalized to TICV. The dural venous sinus volume increases in size in some patients following LP but across all patients this was not a significant increase. The overall increase in TVV also is not be accounted for by the dural venous sinuses, indicating that small venous and perhaps arterial and capillary bed increases in vascular volume account for this change post LP and CSF removal.

KEYWORDS: Dural Sinus, Idiopathic Intracranial Hypertension, Lumbar Puncture

Note: Scanned images are included in the proceedings. Some submitted images were reduced during editing thereby decreasing clarity. Also, refer to the Program Planner. Proceedings Content as of 3/28/2014.

(N = 6)	TICV	TVV	% TVV/TICV	DSV	%DSV/TVV
Pre-LP	1434.6	102.2	0.07	22.6	0.22
Post-LP	1439.1	116.5	0.08	25.0	0.21
% Change	0.3%	14.0%	13.3%	10.8%	-2.9%
P	0.218	0.010	0.007	0.166	0.570



O-924

1:14PM - 1:21PM

Is the foramen magnum line reliable for measuring cerebellar tonsil position? An interobserver study of cerebellar tonsillar tip location using three different imaging landmarks

A Moore¹, D Gomez-Hassan², D Quint¹, H Garton¹, C Maher¹, A Srinivasan¹

¹University of Michigan Health System, Ann Arbor, MI,
²University of Michigan, Ann Arbor, MI

Purpose

The aim of our study was to evaluate the interobserver agreement in assessment of cerebellar tonsil position using three different bony landmarks on magnetic resonance imaging (MRI) (foramen magnum, C1 arch and C2 arch).

Materials and Methods

Our IRB approved, HIPAA-compliant retrospective study consisted of consecutive brain MRIs performed at our institution between January 2010 and December 2012. Exclusion criteria included skull base osseous abnormalities (e.g., basilar invagination/impression, platybasia, Paget's disease, etc.), poor quality sagittal T1-weighted images, significant motion artifacts, and congenital or acquired osseous abnormalities of C1 and C2 vertebrae. Sagittal T1-weighted images in these patients were interpreted by two board certified neuroradiologists (blinded to underlying clinical diagnoses) with measurement of bilateral tonsil position based on lines drawn perpendicular from the tonsillar tip to the: (i) Foramen magnum (FM) line (joining the anterior and posterior margins), (ii) C1 arch line (joining superior

cortical margins of the anterior and posterior arches), (iii) C2 line (joining the anterior and posterior margins of the inferior endplate). The readers evaluated the entire stack of sagittal images on each scan and measured the tonsil position on the image that showed the most caudal position of a tonsil. Pertinent medical records including surgical reports also were reviewed. Nonparametric Spearman correlation coefficients between the readers were calculated for each of the three techniques. Interobserver agreement between the readers was assessed using Bland-Altman analysis.

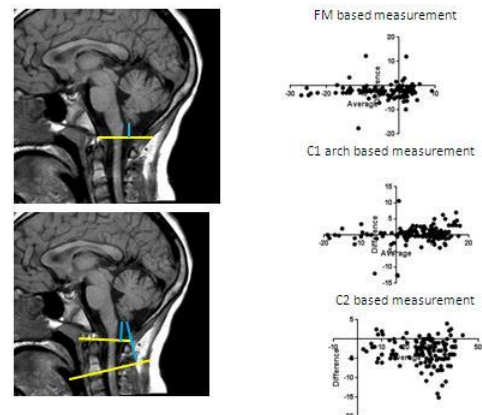
Results

A total of 130 cerebellar tonsils on 65 patients (mean age - 22 + 13 yrs; 41 females, 24 males) were studied that included 13 patients with Chiari I malformation suspected based on clinical and radiologic features (>5mm tonsillar descent below FM) and 52 without Chiari I malformation. The Spearman correlation coefficients for the three techniques were 0.864, 0.939 and 0.899 respectively for FM, C1 and C2 landmarks. Bland-Altman analysis showed the best interobserver agreement for C1 line (0.25mm bias) and the least for C2 line (3.2 mm bias), implying that the differences in measurements between the two readers were the least when the C1 line was employed.

Conclusions

Our results demonstrate better interobserver agreement in localization of the cerebellar tonsillar tip when osseous landmarks based on C1 vertebra are used compared to the FM line (which is currently widely used). This may be due to better delineation of the bony cortices at C1 compared to the margins of the FM on sagittal T1-weighted images. We plan to expand this study in the future to include a larger sample group and to evaluate the differences in "misclassification" rates of patients with respect to the presence or absence of Chiari I malformations using these three different techniques.

KEYWORDS: Cerebellar Tonsils



Note: Scanned images are included in the proceedings. Some submitted images were reduced during editing thereby decreasing clarity. Also, refer to the Program Planner. Proceedings Content as of 3/28/2014.

O-925

1:21PM - 1:28PM

Surface Expansion of the Hippocampal Dentate Gyrus in Multiple Sclerosis: an In-Vivo Evidence of Neurogenesis?

R Messina¹, M Rocca¹, G Longoni¹, E Pagani¹, B Colombo¹, M Rodegher¹, G Comi¹, A Falini¹, M Filippi¹

¹San Raffaele Scientific Institute, Vita-Salute San Raffaele University, Milan, Italy

Purpose

The subgranular zone of the dentate gyrus (DG) of the hippocampus has long been thought to support neurogenesis in the adult mammalian brain (1, 2). Inflammatory responses within the central nervous system (CNS) have the potential to alter the homeostasis of the stem cell niche and enhance neurogenesis within the DG, but the functional significance of adult neurogenesis in CNS pathology is still debated. (3, 4). The purpose of our work was to assess, using magnetic resonance (MR) radial mapping analysis of hippocampal surface, whether there are detectable morphological alterations of the DG in patients with multiple sclerosis (MS).

Materials and Methods

Brain 3D T1-weighted scans were acquired from 115 MS patients [28 relapsing remitting (RR), 34 secondary progressive (SP), 27 primary progressive (PP), and 26 benign (B) MS] and 28 healthy controls (HC)]. Hippocampal segmentation was performed manually according to standardized procedures (5). From contours, radial distances were calculated and between-group vertex analysis performed (independent sample t-test, age adjusted). Percentage difference of average medial distance (AMD) in clusters of significant difference ($p < 0.05$) was calculated. Results are reported for the DG region only.

Results

Compared to HC, all MS phenotypes revealed an increase AMD in correspondence of the DG. The percentage change of AMD and the cluster dimensions (number of vertices) were, for RRMS vs HC: right DG +24.5%, 55; left DG +31.5%, 235; for SPMS vs HC: right DG +24.2%, 18; left DG +20.8%, 234; for PPMS vs HC: right DG +11.5%, 102; left DG +22.2%, 122, and for BMS vs HC: right DG n.s.; left DG +21.2%, 33. Comparisons among MS clinical phenotypes revealed a significant increase in AMD, for the left hippocampus only, in RRMS compared to SPMS (+14.2%, 17).

Conclusions

Surface expansion of the DG of the hippocampi might represent an inflammation-induced alteration of the

neurogenic niche in the adult subgranular zone. This seems to be strengthened by the pronounced effect found in the early and most inflammatory phase of the disease. In vivo imaging of neurogenesis could provide a tool for monitoring the effects of new therapeutic strategies, which are emerging in the field of regenerative medicine. This work has been partially supported by a grant from Fondazione Italiana Sclerosi Multipla (FISM2012/R/8).

KEYWORDS: Hippocampus, MR Imaging, Multiple Sclerosis

O-926

1:28PM - 1:35PM

Towards In vivo Detection of Single Cells in Brain by MRI

E Shapiro¹, S Mukherji¹

¹Michigan State University, East Lansing, MI

Purpose

The use of magnetic resonance imaging (MRI) to detect specific cell populations in intact organisms has been supporting major developments in stem cell therapies, immunotherapies and cellular diagnostics. The basic tenet behind MRI-based cell tracking is to incorporate an MRI contrast agent inside cells and then to use imaging to detect their presence against a biological background. Our group has been pioneering the development of novel imaging agents, MRI detection schemes and postprocessing data analysis algorithms for ultrasensitive detection of cells, down to single cell sensitivity. In this work, we describe advances in iron oxide nanoparticles that will facilitate clinical translation of MRI-based cell tracking to humans. Further, we demonstrate the capabilities to use MRI to detect single cells in vivo in rodent brain. Next, we introduce an image processing framework for quantifying cell tracking. Lastly, we describe a way forward for accomplishing in vivo detection of single cells in humans.

Materials and Methods

Clinically viable iron oxide nanoparticles (NPs) for MRI-based cell tracking were fabricated by oil-in-water emulsion using an FDA approved polymer, PLGA, and 10 nm iron oxide nanocrystals. Multiple stem cell differentiation and immune cell functional assays were performed on magnetically labeled cells. Nanoparticle biodegradation was assayed as well. A model of single, dispersed cells in the rat brain was created by intracardiac injection of either magnetically labeled, CFSE labeled mesenchymal stem cells (MSCs) or nonmagnetic cells. Adult rats were anesthetized and 200,000 magnetically labeled MSCs or unlabeled MSCs were injected into the left cardiac ventricle. Animals were imaged at 11.7 T with high resolution gradient echo MRI, followed by pathology to

Note: Scanned images are included in the proceedings. Some submitted images were reduced during editing thereby decreasing clarity. Also, refer to the Program Planner. Proceedings Content as of 3/28/2014.

identify green CFSE stained MSCs with red particles. Automated spot detection and quantification was accomplished using similar techniques used for automated vessel detection. However, instead of selecting for snake-like vessel structures, spheres were selected. Spots were quantified from the resulting binary images through cluster thresholds.

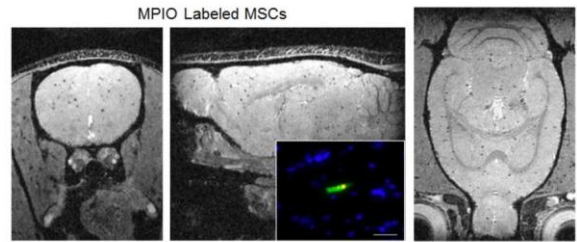
Results

Highly magnetic PLGA encapsulated iron oxide NPs can be fabricated, incorporating as much as 84 weight% magnetite. Total particle size is ~ 100 nm. An in vivo biodegradation study revealed that nanoparticles degraded ~80% over the course of 12 weeks. Cells can be labeled in culture by simple incubation, with both dose and time dependent labeling kinetics. The capability of magnetically labeled MSCs or neural stem cells to differentiate down multiple lineages, or for magnetically labeled immune cells to release cytokines following stimulation, is uncompromised. Magnetically labeled MSCs appear as punctate, dark spots in high resolution gradient echo MRI in rodent brain following intracardiac delivery. Histology confirms that 70% of dark contrast spots are due to single cells, the remaining 30% are due to either two or three cells. Calculated numbers of cells in the brain were between 1,504 and 7,765, or between 0.8% to 3.9% of the total number of injected cells, depending on threshold.

Conclusions

In regenerative medicine, single cell detection enables a strategy on quantifying the cell transplants based on enumeration of contrast spots in the image. In immunotherapy, single cell detection opens up enormous possibilities for sensitivity, enabling the detection of the first infiltrative cell to enter a tumor and a way to monitor therapy. In cancer diagnostics, single cell detection capabilities may allow one to image early inflammatory or neoplastic events as a way for early detection of disease. To achieve single cell MRI in humans will require an FDA-approved particle and high field MRI. The particle we describe here has a positive trajectory for potential FDA approval, while the proliferation of high field human MRI systems will enable the high resolution MRI we can achieve on animals, as shown here, to be performed on humans.

KEYWORDS: Molecular Imaging, MR Imaging, Stem Cell



Detection of magnetically labeled single cells in the rat brain in vivo. Purple circles show a single spot in all three orthogonal planes, confirming the susceptibility effects induced by the labeled cells are spherical at this acquired resolution. Inset is a single MSC in green, MPIOs in orange, nuclei in blue.

O-927

12:01PM - 12:08PM

High-Resolution CT/MR Fusion Demonstrates Sites and Patterns of Flow in Patients with Skull Base CSF Leaks

B Delman¹, A Agbetoba¹, S Govindaraj¹, J Bederson¹, L Tanenbaum², R Shrivastava¹

¹Icahn School of Medicine at Mount Sinai, New York, NY, ²Mount Sinai Medical Center, New York, NY

Purpose

Cerebrospinal fluid (CSF) leaks present with variable symptoms, including diplopia, tinnitus, nausea, and headaches relieved or diminished by supine positioning. Traditional diagnosis depended on history of such symptoms with detection of beta-2-transferrin from collected fluid and imaging confirmation. Computed tomography cisternography is frequently used modality, requiring intrathecal injection of contrast and provocative positioning to opacify a leak site. However this is invasive and relies on adequate opacification of CSF. Other techniques, such as nuclear cisternography, require intrathecal In-111 injection and placement of six pledgets in the nasal cavity, which can be uncomfortable and is a time-consuming process. A noninvasive modality to assess CSF leaks may make diagnosis more pleasant for patients, and might increase the diagnostic yield. Computed tomography/MR fusion has been described previously but at lower resolution (Mostafa). The purpose of this investigation was to determine what patterns of leak or defect can be seen in fusion of HRCT/MR in patients with abnormalities proven surgically.

Materials and Methods

Candidates included patients suspected of CSF leak in whom high resolution CT and MR were obtained on the same day, between 10/2011 and 11/2013. Patients derived from the practices of otolaryngology and neurosurgery in our institution. Patients were included if they ultimately underwent surgery at our site, and had a surgically proven leak or a defect such as meningo(encephalo)coele. Computed tomography and MR data were fused on a dedicated postprocessing workstation to match position, scale, and rotation, which ensured portrayed planes matched perfectly. For all cases, images were generated as a fused set (CUBE T2 in colorscale superimposed over CT in grayscale), and as

Note: Scanned images are included in the proceedings. Some submitted images were reduced during editing thereby decreasing clarity. Also, refer to the Program Planner. Proceedings Content as of 3/28/2014.

separate CT and T2 datasets in grayscale alone. For some cases a similar set of sagittal images was generated, if the interpreting radiologist felt a different plane would add to diagnosis. The same radiologist interpreted all of the studies. Recorded data included the following: 1) site of defect(s) or other osseous abnormalities such as bony remodeling on the CT; 2) presence and location of T2 hyperintense fluid near any of these osseous abnormalities; 3) whether a change in such fluid was resolvable during the course of the exam; 4) site of any herniated tissue [i.e., meningo(encephalo)coele]; 5) ancillary findings such as prominent arachnoid granulations or pitting, or changes in the sella such as sellar expansion or pituitary flattening.

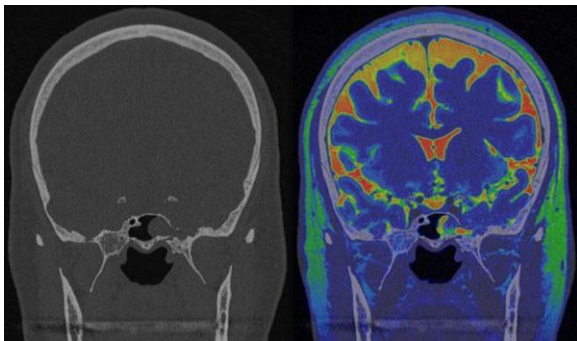
Results

During the time period surveyed, we found 16 patients who underwent same-day CT and MR and had surgical exploration at our site. In 15/16 (94%) the site of the defect matched the site or the surgically confirmed lesion; in one patient (6%), a definite site could not be resolved. The presence of fluid on T2 (13 cases) or local air (1 case) was a strong indicator of sidedness of leak: this conformed in 14/16 cases (88%), while lateralization could not be determined in one case and there was no clear extracranial fluid in another. Changes in CSF configuration (including pooling) during the scan session were seen in six of the 13 studies that had high resolution series at the start and end of the MRI (46%). Empty sella was identified in 11/16 (69%), and ancillary findings of CSF pulsatility other than empty sella were seen in 13/16 (82%), including enlarged Meckel's caves (+/- Meckel's meningoceles) in 5/16 (31%) and prominent arachnoid granulations in 8/16 (50%). Although superimposition of colorscale T2 over CT may obscure some findings, the superimposed image can nicely demonstrate abnormalities efficiently and effectively once they are diagnosed (for example, see the left sphenoid encephalocele in Figure 1).

Conclusions

Fusion of high resolution CT and MR allows advantages of each to be exploited in characterizing CSF leak defects, without requiring intrathecal contrast. Site of fluid, or changes during the imaging session, can aid in ultimate localization of skull base defect.

KEYWORDS: CSF Leak, Fusion, Postprocessing



0-928

1:42PM - 1:49PM

What Determines Workup of Incidental Thyroid Nodules Reported on CT and MRI? Review of Outcomes in 375 Patients

T Tanpitukpongse¹, A Grady², K Choudhury², J Sosa², J Hoang²

¹Duke University Medical Center, Chapel Hill, NC, ²Duke University Medical Center, Durham, NC

Purpose

Incidental thyroid nodules (ITN) commonly are reported on CT and MRI scans, but not all receive workup. The purpose of this study is to determine the proportion of reported ITNs on CT or MRI that receive workup and the factors that influence clinicians' deciding to evaluate them further. A secondary aim is to estimate how adoption of CT/MRI guidelines would affect the number of ITN reported.

Materials and Methods

This is a retrospective study of 401 patients with ITNs reported on CT or MRI studies between January and December 2011. Patients were identified by searching CT and MRI reports for the phrase "thyroid nodule". Patients were excluded if they had prior evaluation of their thyroid or history of thyroid cancer. Medical records and radiology reports were reviewed for 1) workup, 2) characteristics of the patient, ITN, and referring clinician, and 3) radiologists' reporting styles. Analyses were performed to identify factors associated with workup. For the secondary aim, a 3-tiered system was applied retrospectively to ITNs to estimate how application of these guidelines would change the number of nodules reported. The proposed 3-tiered system criteria are based on suspicious imaging features, patient age, and nodule size (1, 2); that is, indeterminate nodules <15 mm in patients <35 years do not meet criteria for reporting (3TS-).

Results

Three hundred seventy-five patients met inclusion criteria, and 30 received workup (Table 1). Twenty-four patients underwent an ultrasound, 21 FNA, and two surgery. There were two cases of thyroid malignancy: one anaplastic and one papillary cancer. One hundred thirty-eight (37%) ITNs were reported in the impression of the report, of which 19% received workup. The odds ratio (OR) for workup of a nodule in the impression section of the report was 14 (95%CI 5-40), which was higher than that of nodules recommended for ultrasound (OR 9, 95%CI 4-19). On multivariate analysis, the only two factors associated with workup were patient age and nodule size ($p \leq 0.01$, Table 1); younger patients and larger nodules were more likely

Note: Scanned images are included in the proceedings. Some submitted images were reduced during editing thereby decreasing clarity. Also, refer to the Program Planner. Proceedings Content as of 3/28/2014.

to undergo additional workup. When the 3-tiered system was applied retrospectively, the result was that there would have been a reduction in ITNs reported in the impression section of the report: 57 reported were 3TS- and 25 mentioned only in the body were 3-tiered system positive.

Conclusions

Less than one in five ITNs reported in the impression section of CT/MRI radiology reports receive additional workup, which raises the question of whether the nodules reported by radiologists are of significance to clinicians. The factors associated with a greater likelihood of workup are younger patient age and larger nodule size. These are already criteria incorporated into a 3-tiered system. Such guidelines have the potential to improve consistency of radiology reports and reduce the number of nodules reported.

KEYWORDS: Thyroid

	Ultrasound	FNA	Surgery	Any Workup	All Nodules	Univariate p-value ^a	Multivariate p-value ^a
(N)(%)							
US recommended (N)(%)	16 (67)	11 (52)	1 (50)	18 (60)	69 (19)	<0.0001	0.09
Workup Results by Bethesda Cytopathology Categories (%)							
I - Nondiagnostic / Unsatisfactory		0		0	0		
II - Benign		16 (77)		16 (77)	16 (77)		
III - Atypia		2 (10)		2 (10)	2 (10)		
IV - Follicular neoplasm		1 (5)		1 (5)	1 (5)		
V - Suspicious for malignancy		0		0	0		
VI - Malignant		2 (10)		2 (10)	2 (10)		

^a p-values for factors associated with any workup of ITN.
^b Not all patients had sizes reported in the radiology report. The nodules were measured on the CT/MRI images for cases that had workup with missing nodule sizes in order to categorize nodules by the 3-tiered system.

	Ultrasound	FNA	Surgery	Any Workup	All Nodules	Univariate p-value ^a	Multivariate p-value ^a
N	24	21	2	30	375		
Age (years, SD)	58 (13)	60 (10)	53 (9)	59 (13)	64 (14)	0.04	0.009
Female (%)	18 (75)	19 (91)	2 (100)	23 (77)	250 (67)	0.23	
Nodule Characteristics							
Mean size in mm (SD)	17 (12)	18 (12)	19 (14)	18 (12)	5 (9)	0.02	0.002
Size (N)(%) ^b							
<10mm, subcentimeter	6 (25)	4 (19)	1 (50)	7 (23)	75 (20)		
10-14 mm	6 (25)	6 (29)	0	7 (23)	52 (14)		
15-19 mm	3 (13)	3 (14)	0	4 (13)	26 (7)		
> 20 mm	9 (38)	8 (38)	1 (50)	12 (40)	47 (13)		
Morphology (N)(%)							
Calcifications	4 (17)	5 (24)	1 (50)	6 (20)	63 (17)	0.87	
Cystic	0	0	0	0	4 (1)		
Hypervascular	0	0	0	0	2 (1)		
Study Indication (%)							
Malignancy	5 (21)	4 (19)	0	6 (20)	196 (52)	<0.0001	0.18
Vascular	5 (21)	5 (24)	0	8 (27)	63 (17)		
Trauma	1 (5)	1 (5)	0	1 (3)	43 (11)		
Infection / Inflammation	6 (29)	3 (14)	0	6 (20)	24 (6)		
Other	7 (29)	8 (38)	2 (100)	9 (30)	49 (13)		
Radiology Division (%)							
Chest imaging	10 (42)	11 (52)	1 (50)	14 (47)	92 (25)	0.002	0.12
Neuroradiology	11 (46)	7 (33)	1 (50)	11 (37)	103 (27)		
Body imaging	3 (13)	3 (14)	0	5 (17)	172 (46)		
Other	0	0	0	0	8 (2)		
Reporting style (%)							
Reported in impression	21 (88)	18 (86)	2 (100)	26 (87)	138 (37)		

0-929

1:49PM - 1:56PM

Structural Brain Changes Following Long-term Bedrest

D Roberts¹, T Brown¹, K Garrett¹, J Helpert¹, A Tabesh¹

¹Medical University of South Carolina, Charleston, SC

Purpose

Following long term missions aboard the International Space Station, ophthalmic changes, including papilledema, and increased intracranial pressure (ICP) have been documented in NASA astronauts (Mader et al., 2011). It has been hypothesized that these changes may result from the loss of gravitational hydrostatic pressure gradients and large cephalad fluid shifts. Altered gravitational pressure gradients also occur in chronically ill patients who are confined to long term bedrest. The consequences of fluid redistribution on the brain are poorly understood but may include alterations in brain structure, cerebral blood vessels, and brain function. In this study, we used long term bedrest as an analog for spaceflight to study any potential structural changes of the human brain.

Materials and Methods

Eight normal subjects underwent 60 days of bedrest at the NASA Flight Analogs Facility at the University of Texas Medical Branch. The subjects were positioned in 6° head down tilt and maintained on a strict diet. T1-weighted 3D SPGR MR images of the brain were acquired before undergoing bedrest (baseline) and on day 60 (d60) of

Note: Scanned images are included in the proceedings. Some submitted images were reduced during editing thereby decreasing clarity. Also, refer to the Program Planner. Proceedings Content as of 3/28/2014.

bedrest. We applied voxel-based morphometry (VBM, VBM8 toolbox, available at <http://dbm.neuro.uni-jena.de/vbm/>) to the baseline and d60 MR image pairs to map longitudinal changes in local tissue volume. We assessed these changes in both gray and white matter. We also evaluated the global brain shift upwards and posteriorly following bedrest. This was accomplished by quantifying the brain shift along the direction perpendicular to the plane passing through the anterior commissure (AC) and interpeduncular fossa (IPF) [Figure 1(a)].

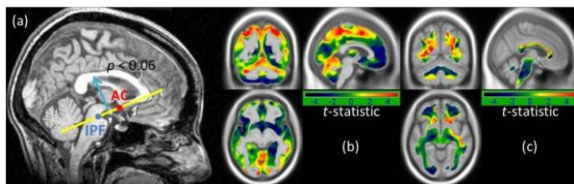
Results

Group analysis showed a trend toward global brain tissue shift upwards and posteriorly following bedrest ($p < 0.06$) [Figure 1(a)]. Voxel-based morphometry indicated that compared to baseline, frontal lobe tissue expanded at d60 while the sulci along the vertex became more crowded. Figure 1(b, c) show the t-statistic map of the difference between the d60 and baseline tissue volume for all eight subjects, after mapping to a common MRI template and smoothing. There is a consistent contraction (red) of the cerebrospinal fluid (CSF) spaces along the vertex with expansion (blue) of brain tissue and surrounding sulcal CSF in the anterior frontal lobes.

Conclusions

Changes in body position, and resultant changes in gravitational gradients, have been found to impact brain physiology and function. Moving from an upright to supine position alters venous outflow, with collapse of the internal jugular veins and redirection of venous return through the vertebral venous plexuses. Clinically, altered venous outflow has been implicated in disease processes such as pseudotumor cerebri and multiple sclerosis. The consequences of long term maintenance of a supine or head-down body position is unknown, and therefore in this study, we investigated associated changes in brain structure. We use this model as an analog for spaceflight and hypothesize that our observed structural alterations may lead to changes in CSF flow dynamics and compression of the dural venous sinuses along the vertex. This in turn may contribute to venous outflow obstruction and the spectrum of intra-orbital and intracranial findings described in astronauts. We have planned future studies to include vascular imaging in the astronaut population. These findings may be applicable to long term bedridden patients as well.

KEYWORDS: Brain Volume, Volumetric Analysis, Voxel-Based Morphometry



0-930

1:56PM - 2:03PM

Sex modulates the effects of substance-dependence on neuroanatomical volumes

M Regner¹, M Dalwani¹, J Sakai¹, J Honce¹, Y Dorothy¹, R Perry¹, J Tanabe¹

¹University of Colorado, Aurora, CO

Purpose

The natural history of substance-dependence is known to differ between men and women (4). While structural neuroimaging studies have demonstrated volumetric differences between healthy control subjects and substance-dependent individuals (SDI) in numerous brain regions, the effect of sex on these differences is poorly understood. Few studies that have investigated these interactions provide conclusions mitigated by small sample sizes, confounding population characteristics, or experimental design (1, 2, 5-7). We investigated the sex and group effects of substance-dependence on cortical gray matter volumes (GMV).

Materials and Methods

One hundred twenty-seven age- and sex-matched participants (28F/40M controls, 28F/31M SDI) were scanned on a 3 T MR system. Substance-dependent individuals met DSM-IV criteria for lifetime dependence on psychostimulants but were abstinent an average of 13.5 months. T1-weighted SPGR-IR images were acquired, segmented using SPM8 with the VBM8 toolbox, and registered using Diffeomorphic Anatomical Registration Through Exponentiated Lie Algebra (DARTEL). Main effects of group, sex, and group by sex interactions were analyzed over the whole brain using ANCOVA, adjusting for age and intracranial volume by modulation (SPM8). Family-wise cluster-based corrections voxel-wise ($p < 0.001$) for multiple comparisons ($p < 0.05$) were used. ANCOVA on parahippocampal gyrus (PHG), medial frontal gyrus (MedFG), anterior cingulate gyrus (ACG), insula, and orbitofrontal cortex (OFC) region of interest (ROI) volumes was performed based on a priori hypotheses.

Results

There were main effects of sex on GMV, with women showing significantly more GMV than men in the bilateral frontal-temporal lobes, consistent with previous literature (3). Main effects of group on GMV were driven primarily by GMV differences observed between female controls and female SDI. Compared to female controls, female SDI had significantly less GMV in bilateral OFC, MedFG, insula, ACG, medial temporal lobe (including PHG), ventral striatum, cerebellar vermis, and superior temporal gyrus (Figure).

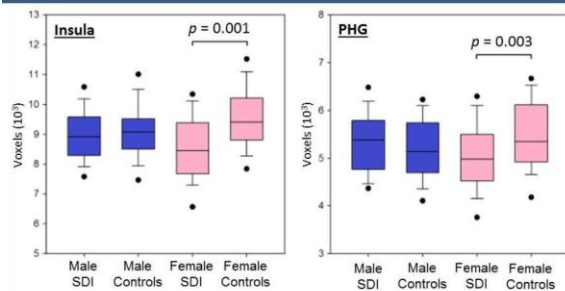
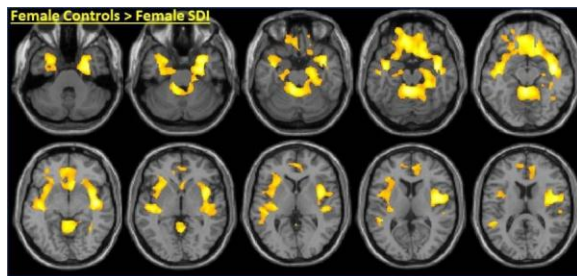
Note: Scanned images are included in the proceedings. Some submitted images were reduced during editing thereby decreasing clarity. Also, refer to the Program Planner. Proceedings Content as of 3/28/2014.

There were no significant differences in GMV in male controls versus male SDI. A significant group by sex interaction was contained entirely within the effect of group within females. Whole brain results were corroborated by ROI analyses (box plots).

Conclusions

In this largest sample size to date investigating the effects of abstinent substance-dependence on neuroanatomical volumes, significant differences in frontal, limbic, and cerebellar regional volumes were found between controls versus SDI, female controls versus female SDI, and sex by group interactions. These findings may elucidate mechanisms underlying the differences in the natural history of substance dependence in men compared to women. Our results illustrate the need for sufficiently powered studies to control for sex effects in brain morphometry studies.

KEYWORDS: Psychiatry, Sex Differences, Voxel-Based Morphometry



0-931

2:03PM - 2:10PM

Canal diameter and compression ratio in patients with cervical spondylotic myelopathy: is there a difference in patients' subgroups

M Ibrahim1, Z Sayedahmad2, A Srinivasan1, H Parmar3

1University of Michigan Health System, Ann Arbor, MI, 2Harper University Hospital, Detroit, MI, 3University of Michigan, Ann Arbor, MI

Purpose

Myelopathy of the cervical cord is a common complication related to degenerative disk disease. Cervical spondylotic myelopathy (CSM) is more likely to occur in patients with developmentally narrow spinal canal. Cord signal changes in patients with CSM are variable and can be associated with abnormal cord enhancement. The imaging changes on T2-weighted images can be focal or segmental (more than one vertebral level), with or without intramedullary contrast enhancement. Patients with segmental disease or cord enhancement typically have a worse prognosis. The purpose of this study is to evaluate the canal diameter and compression ratio in patients with enhancing versus nonenhancing cord signal changes as well as in patients with segmental versus focal disease.

Materials and Methods

We retrospectively reviewed 653 patients with CSM who had undergone magnetic resonance (MR) imaging between January 2008 and December 2012. Common indication for MR imaging included: pain, sensory changes and motor dysfunction. We identified 48 patients with cord signal changes. The imaging features on T1, T2, cord enhancement, canal diameter and compression ratio were evaluated. Independent samples t-test was performed for statistical analysis.

Results

Intramedullary enhancement was seen in 14 patients, whereas cord signal changes without enhancement was seen in 34 patients. Focal intramedullary signal changes were more common in patients with nonenhancing CSM (32 versus 7). Patients with intramedullary enhancement typically had segmental disease with involvement of more than one vertebral level (7 versus 2). The average anteroposterior (AP) cord diameter in patients with enhancing CSM was 5.3 mm with a compression ratio of 37% in comparison to patients with nonenhancing CSM whose AP cord diameter was 4.8 mm with similar compression ratio of 37% (p value 0.77). The compression ratio was minimally larger in patients with segmental disease in comparison to patients with focal disease (39% versus 37%; p value 0.77). The average canal diameter was similar between the two groups measuring 10 mm (segmental versus focal and enhancing versus nonenhancing; p value 0.93).

Conclusions

Canal diameter and compression ratio are not significantly different in CSM patients with cord enhancement and segmental disease in comparison to CSM patients with no intramedullary enhancement and focal disease. This indicates that other factors might be responsible for the development of cord enhancement and segmental cord changes in CSM patients.

Note: Scanned images are included in the proceedings. Some submitted images were reduced during editing thereby decreasing clarity. Also, refer to the Program Planner. Proceedings Content as of 3/28/2014.

KEYWORDS: Myelopathy

O-932

2:10PM - 2:17PM

The occipital emissary vein: part 1, a radio-anatomical study

A Piveteau¹, P Gailloud², D San Millan¹

1Hôpital de Sion, Réseau Santé Valais, Sion, Switzerland,
2The Johns Hopkins Hospital, Baltimore, MD

Purpose

Emissary veins of the base of the skull and posterior fossa play an important role in directing cerebral venous blood towards the cervical venous outflow pathways. The occipital emissary vein (OEV) has received little attention in the past anatomical and clinical literature. It connects the torcular herophili to the suboccipital veins of the external vertebral venous system. The purpose of the present study was to determine its prevalence and evaluate its potential functional and clinical implications.

Materials and Methods

1.5 T magnetic resonance imaging (MRI) studies including gadolinium-3DT1-SPGR from 100 patients (64% females, average 56 years old) were analyzed retrospectively. Patients with venous thrombosis, intracranial arteriovenous shunts or posterior fossa surgery were excluded. The presence of an OEV was recorded. Maximum diameters of the OEV were measured within its osseous segment in the occipital squama and in front of its extracranial orifice. The presence of the osseous canal of the OEV was sought for on CT (64MDCT) when available.

Results

An OEV was found in 32% of the patients. Two OEVs were found in two occasions and a triple OEV was encountered once. The average diameter of the OEV was 1.6 mm (range 0.5-3 mm) both in its osseous segment and extracranially. The exit point of the OEV always was located between the external occipital protuberance and the foramen magnum. Seventy-seven percent of patients also underwent CT. Five patients had an OEV canal on CT but not visible OEV on MRI.

Conclusions

An OEV was observed in 32% of the cases, a much higher incidence than previously reported in the anatomical literature (up to 14%). Because it is located proximally to the transverse and sigmoid sinuses it may provide an outflow pathway in case of stenosis or occlusion of the transverse/sigmoid sinuses (see The occipital emissary vein, part 2).

KEYWORDS: Venous Anatomy, Venous Drainage

O-933

2:17PM - 2:24PM

The 5-minute Brain MRI: Rapid Parallel Imaging with 32- and 64-Channel Coils at 3T

D Boulter¹, M Borja¹, T Witzel², E Ratai¹, C Jaimes³, P Schaefer¹, O Rapolino¹

1Massachusetts General Hospital, Harvard Medical School, Boston, MA, 2Massachusetts General Hospital, Harvard Medical School, Charlestown, MA, 3Massachusetts General Hospital, Boston, MA

Purpose

Parallel imaging techniques, such as generalized autocalibrating partially parallel acquisitions (GRAPPA), utilize spatial information inherent in phased array coils to shorten MRI acquisition times by under-sampling of k-space. These techniques are compatible with most pulse sequences, and commonly are used to accelerate imaging by a factor of 2 or more using 8 - 32 channel head coils. Acceleration factors (AF) above 2-3 are limited by decreasing signal-to-noise ratios (SNR). However, SNR losses can be partially offset with higher order coil arrays, high field strength systems, and advantageous pulse sequences, thereby maintaining image quality at higher AF. Our purpose was to develop an accelerated five-minute brain magnetic resonance imaging (MRI) protocol by optimizing routine clinical sequences for use with a 32-channel or 64-channel coil at 3 T, and to assess image quality in normal volunteers.

Materials and Methods

Our institutional review board approved this study. Brain MRIs of healthy volunteers were performed on a 3 T scanner using both a 32-channel head coil and a 64-channel head and neck coil. Existing routine clinical sequences for the 32-channel coil at 3 T were optimized and further accelerated using GRAPPA parallel imaging AF ranging from 3 to 4. Sequences performed included: Scout, T1 sagittal, FLAIR, T2, DWI and Susceptibility.

Results

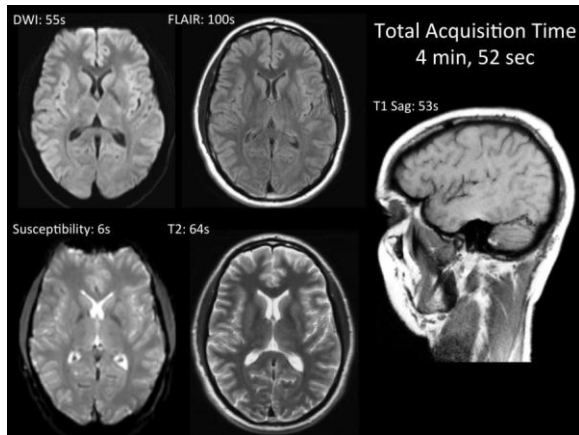
Total image acquisition time for the rapid protocol was four minutes, 52 seconds, compared with nine minutes, 50 seconds for the standard clinical protocol. Individual sequence acquisition times for the rapid versus standard protocols were: Scout (14 versus 46 s), T1 Sag (53 versus 172 s), DWI (55 versus 58 s), FLAIR (100 versus 128 s), T2 (64 versus 70 s), and Susceptibility (6 versus 124 s). Image quality for the rapid protocol was comparable to the standard clinical protocol for both 32-channel and 64-channel coils.

Note: Scanned images are included in the proceedings. Some submitted images were reduced during editing thereby decreasing clarity. Also, refer to the Program Planner. Proceedings Content as of 3/28/2014.

Conclusions

An accelerated brain MRI protocol requiring less than 5 minutes is feasible using parallel imaging, advantageous pulse sequences, and either a 32- or 64-channel coil at 3 T.

KEYWORDS: MR Imaging Brain, Parallel Imaging, Phased-Array Head Coils



O-934

2:24PM - 2:31PM

The occipital emissary vein: part 2, a marker for pseudotumor cerebri?

A Piveteau¹, P Gailloud², D San Millan¹

¹Hôpital de Sion, Réseau Santé Valais, Sion, Switzerland,
²The Johns Hopkins Hospital, Baltimore, MD

Purpose

Transverse sinus stenosis is increasingly recognized as a cause of pseudotumor cerebri. Transverse sinus stenosis may be primary (post-thrombosis or large arachnoid granulations) or secondary to increased intracranial CSF-pressure, but in both situations may induce increased venous pressure resulting in venous pseudotumor cerebri (VPTC). The occipital emissary vein (OEV) connects the torcular herophili with the suboccipital veins of the external vertebral plexus and, therefore, represents a potential collateral pathway in VPTC.

Materials and Methods

The presence of an OEV was evaluated in 42 patients with documented VPTC underwent 320-multidetector subtracted venography (320MDCTV). Maximum diameters of the OEV were measured within its osseous segment in the occipital squama and in front of its extracranial orifice.

25 patients underwent transverse sinus stenting after documented significant trans-stenotic pressure gradient. Of these, 15 had follow-up 320MDCTV. Post-stenting OEV diameters were recorded in this subgroup of stented patients.

Results

An OEV was found in 60% of the patients. Average maximum diameters of the OEV were 2.4mm (range 1-7mm) at the osseous segment and 3.4mm (range 1.8-10mm) extracranially. In the 15 patients undergoing stenting, average OEV intraosseous and extracranial diameters were 2.2 and 3.2 respectively prior to stenting and 1.8 and 2.6 after stenting.

Conclusions

An OEV is frequently encountered in patients with VPTC, with an incidence of 60% compared to 32% in the normal population*. Additionally, the diameter of the OEV in patients with VPTC is larger than in patients without VPTC*, further suggesting that the OEV is recruited as a collateral venous pathway in cases of significant transverse sinus stenosis. Venous stenting results in a diameter reduction the OEV in keeping with the normalization of the intracranial venous pressure by the stenting procedure. * OEV is present in 32% of normal patients and average maximum diameter is 1.6mm (range 0.5-3mm), see The occipital emissary vein, Part 1).

KEYWORDS: Venous Anatomy, Venous Sinus Stenting, Venous Stenosis

Thursday, May 22

3:00PM - 4:30PM

Room 517bc

93 - SNIS PROGRAMMING: ENDOVASCULAR MANAGEMENT OF ACUTE STROKE AND STROKE PROPHYLAXIS

O-935

3:00PM - 3:30PM

Carotid Angioplasty and Stenting: Where We Are and Where We Are Going?

Heck, D.
The Johns Hopkins Hospital
Baltimore, MD

Abstract/Presentation Summary

This presentation will cover the imaging evaluation of carotid artery disease and the data supporting the use of carotid stenting for primary prevention and secondary prevention of stroke. Trials comparing carotid stenting and carotid endarterectomy will be summarized. Future areas

Note: Scanned images are included in the proceedings. Some submitted images were reduced during editing thereby decreasing clarity. Also, refer to the Program Planner. Proceedings Content as of 3/28/2014.

of research will be discussed, and the rationale and design of the upcoming CREST 2 trial will be presented.

O-936

3:30PM - 4:00PM

New Insights from the IMS Trials: Hints at Future Directions in Acute Stroke Revascularization Trials

Tomsick, T.
University Hospital/University of Cincinnati College of Medicine
Cincinnati, OH

O-937

4:00PM - 4:30PM

The Angio Suite as the Stroke Resuscitation/Management Unit: Possible Future of Acute Stroke Management

Strother, C.
University of Wisconsin
Madison, WI

Abstract/Presentation Summary
Paralleling the rapid development of the tools and techniques used in endovascular therapy has been a simultaneous dramatic enhancement in the imaging capabilities of x-ray angiographic equipment. The 2D and 3D images of the intracranial and spinal vasculature now obtainable have spatial and temporal resolution that is superior to ones obtained with any other technique. The high resolution CT like images obtained with new flat detectors allow imaging of implantable devices, vasculature and brain parenchyma with image quality that is, in many instances, superior to that of multi-detector CT; this is achievable with radiation exposures significantly lower than that used with conventional CT. Measurement of physiologic parameters i.e. perfusion in the angiographic suite is now a reality. New developments in 4D DSA and Omni-plane fluoroscopy will further enhance the capabilities of the angiographic suite. The modern angiographic suite now offers an environment where it is feasible for some patients with acute ischemic and hemorrhagic strokes to go from arrival at the hospital to the angiographic suite for diagnosis, triage and, if appropriate, treatment. In this presentation I will discuss and illustrate these capabilities. A proposed workflow showing the feasibility of a "one stop shop" approach to the management of patients with acute strokes will be described and illustrated. In theory, such an approach, by saving time and improving patient selection, should result in improved outcomes.

Thursday, May 22
3:00PM - 4:30PM
Room 517d

94 - Mini Symposium Stroke – Part V:
Clinical Scenarios: What Would the Experts Do? An Interactive Plan

Thursday, May 22
3:00PM - 4:30PM
Room 517a

95 - ASSR PROGRAMMING:
CONTROVERSIES IN SPINE PROCEDURES

3:00PM - 3:20PM

Vertebral Augmentation: Myths and Reality
Ortiz, A.
Winthrop University Hospital
Mineola, NY

O-941

3:20PM - 3:40PM

Controversies in Spine Intervention
Barr, J.
California Center for Neurointerventional Surgery
La Jolla, CA

O-942

3:40PM - 4:00PM

Epidural Injections: To Be or Not To Be

Brook, A.
Montefiore Medical Center
Bronx, NY
O-943

4:00PM - 4:20PM

Augmentation for Malignant Spinal Lesions: Is there A Role for RF Ablation?

Georgy, B.
North County Radiology

Abstract/Presentation Summary
The role of vertebral augmentation for malignant compression fractures has been described extensively in the literature. Cement augmentation helps pain control and stabilization of the vertebral bodies. Recently, radio-

Note: Scanned images are included in the proceedings. Some submitted images were reduced during editing thereby decreasing clarity. Also, refer to the Program Planner. Proceedings Content as of 3/28/2014.

frequency ablation of the tumor tissue has been described for tumor debulking before cement augmentation. This presentation outlines the evolving role of this technique and the potential benefits. Early clinical results and potential benefits in the treatment algorithm of malignant compression fractures will be also discussed.

4:20PM - 4:30PM Discussion

Thursday, May 22

3:00PM - 4:30PM

Room 520

96 - GENERAL PROGRAMMING: FILM
PANEL, STUMP THE STARS

Thursday, May 22

3:00PM - 4:30PM

Room 524

97 - PARALLEL PAPERS: Tumor - New
Techniques and fMRI

O-946

3:00PM - 3:07PM

Simultaneous Measurement of ADC Probability Density Functions and Functional Connectivity in Brain Tumor Patients Using DREAM-MRI

B Ellingson¹, T Cloughesy¹, W Pope¹

¹University of California Los Angeles, Los Angeles, CA

Purpose

Diffusion magnetic resonance imaging (MRI) is an important, yet controversial quantitative cancer imaging biomarker. The apparent diffusion coefficient (ADC), or magnitude of random water movement, within tumors can be used to estimate tumor cell density, allowing clinicians to monitor and predict treatment response. Apparent diffusion coefficient maps acquired clinically are only an estimate of ADC within the tissue, and therefore are prone to measurement and physiologic noise. Additionally, resting-state functional MRI (fMRI) information on patients with brain tumors typically is not acquired, mostly due to the additional scan time requirements of this sequence.

The purpose of the current study was to develop and test a new MR sequence to simultaneously acquire estimates of the ADC probability density function (ADC PDF) as well as estimate functional connectivity in patients with primary brain tumors.

Materials and Methods

We have developed a new technique to quickly estimate ADC PDFs for each image voxel using a "diffusion reproducibility evaluation and measurement" (DREAM) MR sequence. Additionally, the nondiffusion-weighted (reference) images collected simultaneously can be used as resting-state fMRI data to measure functional connectivity, an unbiased parameter thought to reflect neurological integrity. We tested this sequence in a variety of phantoms, 20 healthy control participants, and 40 patients with primary gliomas.

Results

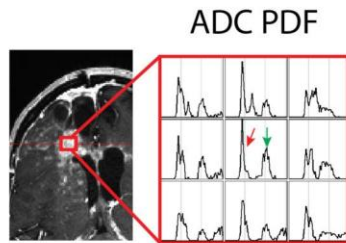
Phantom studies suggest an optimal b-value of 500 s/mm² for minimal variance in ADC. Apparent diffusion coefficient variability changed linearly with choice of repetition time, but not number of acquisitions, direction, or tissue T1. Test-retest reliability demonstrated good concordance between serial measurements in both phantoms and healthy tissues. We observed complex ADC PDF characteristics in biologically heterogeneous tumors, suggesting ADC PDFs may be a novel method of quantifying tumor heterogeneity. These complex ADC PDFs were independent of tissue perfusion and diffusion direction, but occurred most frequently in metabolically active tumor as measured using 18F-FDG PET. Apparent diffusion coefficient coefficient of variation (ADC CV) measurements of less than 5% appeared to isolate and label regions of nonenhancing tumor and predict future enhancement independent of FLAIR, T2, or average ADC maps. Functional diffusion mapping (fDMs) using voxel-wise changes in ADC PDFs could be used to spatially visualize and statistically quantify treatment response. Resting-state fMRI networks extracted from DREAM-MRI data in volunteers and patients were anatomically consistent with known functional networks, including in the default mode network.

Conclusions

DREAM-MRI is a potentially valuable technique for simultaneously characterizing brain tumor microstructure and neurological integrity by estimating the voxel-wise ADC PDF, exploring new image contrasts including ADC CV, statistically comparing diffusion measurements over time, and simultaneously estimating functional connectivity from resting-state fMRI signals.

KEYWORDS: Biomarkers, Brain Neoplasms, MR Diffusion

Note: Scanned images are included in the proceedings. Some submitted images were reduced during editing thereby decreasing clarity. Also, refer to the Program Planner. Proceedings Content as of 3/28/2014.



O-947

3:07PM - 3:14PM

Diffusion Imaging Genomic Mapping Identifies Genomic Targets Involved in Invasion and Poor Prognosis

G Thomas¹, J Wang², Z Mahmood¹, M ElBanan¹, P Zinn¹, R Colen¹

¹MD Anderson Cancer Center, Houston, TX, ²The University of Texas MD Anderson Cancer Center, Houston, TX

Purpose

To create an imaging genomic map, linking MR imaging traits with gene and miRNA expression profiles, in GBM patients to determine genomic correlates of a MR diffusion radiophenotype to possibly find new genomic targets for GBM treatment. Decreases in diffusion in tumors, specifically GBM, is associated with increase in cellular density and higher nuclear to cytoplasm (N:C) ratio. Here, we present the first study examining in a quantitative way diffusion imaging genomics in GBM to determine novel and targetable genomic biomarkers in GBM.

Materials and Methods

We identified 60 treatment-naive GBM patients from The Cancer Genome Atlas (TCGA) who had both gene- and miRNA expression profiles and pretreatment MR-neuroimaging specifically ADC maps. Image segmentation analysis was done in Slicer 3.6 (slicer.org) using segmentation module, where regions of FLAIR hyperintensity, contrast enhancement, and necrosis were segmented to obtain accurate tumor volumetric data. Diffusion was analyzed and patients were grouped into

those with restricted diffusion and facilitated diffusion (those with mixed diffusion were excluded). Biostatistical image-genomic analysis was performed for gene and miRNA sets in restricted versus facilitated diffusion group. Comparative Marker Selection (Broad Institute) identified preferentially up-regulated genomic events in the restricted versus facilitated groups. All the genomic data also were analyzed to determine the most upregulated mRNAs/miRNAs using ingenuity pathway analysis (IPA).

Results

IPA identified molecular networks, as well as canonical and functional pathways highly associated with cancer and invasion in those patients with low ADC values (areas of restricted diffusion).

Conclusions

The diffusion radiophenotype identified genes and miRNAs and corresponding molecular networks that were highly associated with tumor invasion. By these means we were able to identify possible key genes and miRNAs involved in the latter regulation. The uncovered genes and miRNAs represent new insight into tumors with restricted diffusion seen on MRI. The discovery of imaging biomarkers reflecting specific genomic compositions associated with presence of restricted diffusion are clinically relevant as they can determine tumor aggressiveness/growth. Differences in the genomic composition of GBMs with restricted versus facilitated diffusion provide insight into possible genomic-based therapeutics that target more aggressive tumors with restricted diffusion.

KEYWORDS: Diffusion MR Imaging, GBM, Genomic Mapping

O-949

3:21PM - 3:28PM

Dynamic Susceptibility Weighted Perfusion MR Imaging Metrics are Predictive of Overall Survival in Patients with Recurrent Primary Central Nervous System Lymphoma

R Barajas¹, S Cha¹, M Mabray¹, J Rubenstein¹, F Valles¹

¹University of California San Francisco, San Francisco, CA

Purpose

Primary central nervous system lymphoma (PCNSL), an aggressive primary brain neoplasm of immunocompetent patients is occurring with a rising incidence. Morphologic magnetic resonance imaging (MRI) characteristics have not proven to be clinically prognostic. We previously have demonstrated that baseline pretherapeutic dynamic susceptibility weighted (DSC) perfusion MR imaging metrics quantified at the time of initial diagnosis are

Note: Scanned images are included in the proceedings. Some submitted images were reduced during editing thereby decreasing clarity. Also, refer to the Program Planner. Proceedings Content as of 3/28/2014.

prognostic of progression free and overall survival (OS). Given the variable response to therapy and clinical outcomes in patients with recurrent PCNSL, we investigated if DSC MR imaging-derived relative cerebral blood volume (rCBV), peak height (rPH), and percentage of signal intensity recovery (rPSR) were prognostic of clinical outcome.

Materials and Methods

Thirty-two patients treated at our institution between June 2001 and 2013 were included in this study on the basis of the following criteria; histopathologic diagnosis of B-cell PCNSL, negative HIV status, and absence of disease outside the central nervous system (CNS). All patients had a pathologic diagnosis of large B-cell CNS lymphoma and demonstrated full resolution of enhancing disease following high dose methotrexate-based chemotherapy treatment as described previously. All 32 patients developed clinical and imaging evidence of recurrent PCNSL. Of this cohort, 11 patients underwent DSC MRI prior to re-initiation of high dose methotrexate therapy for recurrence of disease. Standard of care morphologic MR images (T2, FLAIR, and T1 Postcontrast) were obtained in addition to DSC perfusion imaging (TR/TE 1250/54; Flip Angle 35°) on a 1.5 T clinical scanner. Imaging data were transferred to a GE advantage workstation for processing (GE Functool 4.4). Regions of interest (ROIs) were drawn about the enhancing lesion allowing for the calculation of mean, minimum, and maximum rCBV, rPH, rPSR values and enhancing disease volume as described previously. Dichotomous high and low DSC imaging metric groups were stratified based on receiver operating curve (ROC) analysis. Overall survival was defined from the imaging diagnosis of recurrent disease until death or loss to follow up. Survival analysis was performed by using log-rank test. A P-value <0.05 was considered to indicate statistical significance.

Results

The mean OS time for the entire cohort following development of recurrent disease was 17.7 ± 26.9 months. Patients were stratified into low and high DSC imaging groups for each perfusion metric (low group = CBVmean <1.0; CBVmin <0.6; CBVmax < 1.6; rPH <1.5, and rPSR <1.0). Karnofsky Performance Score and time to disease recurrence from initial diagnosis of PCNSL was not observed to be statistically different when stratified between groups ($P > 0.05$). Volume of recurrent disease burden also was not significantly different between the low and high groups (1312 m3 vs 857 m3; $P = 0.29$). Six patients stratified into the low CBVmean and CBVmax groups were found to have a significantly increased risk of death (Figure 1). Multivariate analysis demonstrated enhancing disease volume did not influence overall survival ($P > 0.05$). rCBVmin, rPH, and rPSR values were not observed to significantly risk stratify patients for death at time of recurrent PCNSL diagnosis (Relative Risk < 2.97; $P > 0.19$).

Conclusions

This preliminary study suggests that DSC perfusion MR imaging obtained prior to chemotherapy for recurrent PCNSL may be used as a prognostic biomarker of survival. Specifically, mean and maximum CBV metrics may identify patients at risk for adverse prognosis. If the findings of this study are supported in a larger patient cohort then the use of DSC perfusion MR imaging as a possible means of risk stratification prior to initiation of high dose methotrexate-based chemotherapy for recurrent PCNSL would be prudent. The implementation of this prognostic noninvasive imaging biomarker could prove to alter the clinical treatment strategy. The validation of this preliminary finding is currently underway in a larger cohort of patients with recurrent PCNSL.

KEYWORDS: Dynamic Susceptibility Contrast-Enhanced, Lymphoma, Primary CNS Neoplasms

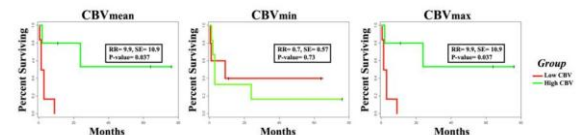


Figure 1: Patient survival outcome as a function of CBV metric stratification into low and high groups. Kaplan Meier analysis of overall survival for patients stratified into the low rCBVmean group (red line; left, cutoff value= 1.0) and rCBVmax (right, cutoff value= 1.6) with mean survival of 17.6 months versus those stratified into the high rCBV groups (green line) with a mean survival of 26.8 months was found to be significantly different ($P = 0.037$). rCBVmin (center, cutoff value= 0.6) did not demonstrate a statistically significant overall survival benefit.

0-950

3:28PM - 3:35PM

A Comparative Study of DCE-derived Permeability Metrics Obtained Using Different Software Platforms in Intracranial Neoplasms

S Kingston1, D Treister1, S Cen2, D Hwang2, C Liu2, A Lerner2, J Go2, N Muradyan3, H Huhdanpaa2, M Law2, M Shiroishi2

1University of Southern California Keck School of Medicine, Los Angeles, CA, 2University of Southern California, Los Angeles, CA, 3iCAD, Nashua, NH

Purpose

The implementation of image-processing software to dynamic contrast-enhanced magnetic resonance imaging (DCE-MRI) data allows for acquisition of quantitative metrics that reflect tissue microvascular physiology. Variability in data acquisition, post-processing, and analysis methods can limit the accuracy and reproducibility of these studies. It is known that differences in postprocessing software can influence measured values, however the actual magnitude of variability in brain tumors is unclear. We sought to investigate the effect of software platforms that utilize different postprocessing algorithms on the calculation of quantitative values in patients with intracranial neoplasms.

Note: Scanned images are included in the proceedings. Some submitted images were reduced during editing thereby decreasing clarity. Also, refer to the Program Planner. Proceedings Content as of 3/28/2014.

Materials and Methods

Twenty patients with intracranial neoplasms (12 glioblastoma multiforme and 8 intracranial metastases) who had received DCE-MRI imaging protocol were retrospectively selected. The same raw DCE-MRI brain tumor data were analyzed using two different software: CADvue, which utilizes the extended-Tofts pharmacokinetic model and TOPPCAT, which utilizes the Patlak model. In addition, CADvue uses an institutionally derived arterial-input function (AIF) to generate one set of DCE parametric maps, while TOPPCAT uses both the superior sagittal sinus (SSS) and an arterial source to generate two sets of parametric maps, one for each vascular input function (VIF). Regions of interest (ROI's) were placed manually over enhancing regions of tumor on traditional T1 postcontrast images and coregistered to DCE-MRI data. Lesion ROI's were used to extract permeability metrics on a voxel-wise basis. Statistical correlation analysis was performed voxel-by-voxel on the transfer coefficient (Ktrans) and fractional blood plasma volume (vp) values obtained from CADvue and TOPPCAT.

Results

There was no statistically significant correlation between CADvue and SSS VIF-derived TOPPCAT Ktrans values ($r=0.084$, $p=0.155$). Weak correlation was found between CADvue and arterial VIF-derived TOPPCAT Ktrans ($r=0.155$, $p=0.0258$). There was moderate correlation between the two software for vp, particularly between CADvue and arterial VIF-derived TOPPCAT vp ($r=0.425$, $p<0.01$) but also between CADvue and SSS VIF-derived TOPPCAT vp ($r=0.326$, $p<0.01$). The strongest correlation was found between the TOPPCAT SSS and arterial-derived VIF data sets for both Ktrans ($r=0.57$, $p<0.01$) and vp ($r=0.689$, $p<0.01$).

Conclusions

Using identical brain tumor source data, we found inconsistencies in quantitative DCE-MRI pharmacokinetic parameters between different software platforms and analysis methods. We found variable correlation of vp between TOPPCAT and CADvue platforms. Ktrans showed either weak or no statistically significant correlation, depending on the VIF selected for analysis. However within TOPPCAT, the use of SSS or arterial-derived VIF appeared to demonstrate good correlation. Our results indicate that the choice of software and post-processing methods can have significant implications for the quantification of brain tumor DCE metrics, particularly with regard to Ktrans. This should be kept in mind when performing a multi-vendor study or interpreting results across the literature.

KEYWORDS: Dynamic Contrast-Enhanced MR

O-951

3:35PM - 3:42PM

Comparison of Restriction Spectrum Imaging and FDG-PET for Prediction of Recurrent GBM

N Farid¹, A Dale², J Hattangadi-Gluth², S Kesari², C McDonald², N White¹

¹University of California San Diego, San Diego, CA,
²University of California San Diego, La Jolla, CA

Purpose

Assessing treatment response in patients with glioblastoma multiforme (GBM) is a challenging issue. On these patients' posttreatment magnetic resonance (MR) scans, areas of new or increasing enhancement and/or edema frequently are detected. Determining whether these areas represent recurrent tumor versus radiation injury is often difficult with standard MR imaging. Therefore, many investigations have studied the ability of advanced imaging techniques such as diffusion-weighted imaging (DWI), MR spectroscopy, MR perfusion, and fluorodeoxyglucose-positron emission tomography (FDG-PET) to differentiate between recurrent tumor and radiation injury. Given its ability to depict tumor cellularity, DWI has shown particular promise in predicting recurrent tumor and differentiating it from radiation injury. High b-value DWI has been shown to be superior to standard DWI in this regard due to its greater sensitivity to restricted diffusion. Our group has developed a new advanced DWI technique, called Restriction Spectrum Imaging (RSI), that shows even greater sensitivity to restricted diffusion compared to both standard and high-b value DWI by utilizing multiple b-values and diffusion times to separate out the spherically restricted water compartment from the hindered water compartment. We previously have shown that RSI offers improved tumor conspicuity relative to high b-value DWI/ADC in patients with primary and metastatic brain tumor. In the current investigation, we aim to determine whether RSI can provide improved detection of recurrent GBM compared to FDG-PET.

Materials and Methods

Retrospective review of our brain tumor database between April 2011 and July 2013 revealed 16 patients with pathologically proven recurrent GBM who had both RSI and FDG-PET data available within the six months prior to surgical resection. RSI and FDG-PET images were reviewed for each patient. The sensitivity of each of these techniques for predicting recurrent tumor then was calculated.

Results

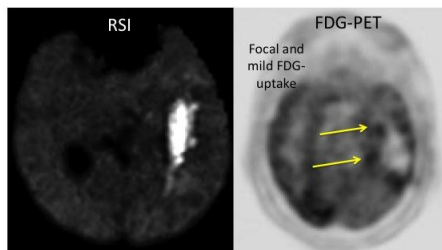
RSI was positive (i.e., showed some area of restricted diffusion) in all 16 patients with recurrent GBM (100% sensitivity), whereas FDG-PET demonstrated FDG uptake in 13 of the 16 patients with recurrent GBM (81% sensitivity). In addition, three of the 13 cases which were positive on FDG-PET only showed mild FDG uptake with SUV values less than 4 (see Figure).

Note: Scanned images are included in the proceedings. Some submitted images were reduced during editing thereby decreasing clarity. Also, refer to the Program Planner. Proceedings Content as of 3/28/2014.

Conclusions

Due to RSI's greater sensitivity to restricted diffusion compared to both standard and high-b value DWI, it previously has been shown to offer improved tumor conspicuity in patients with primary and metastatic brain tumor. In the current study, we show that it also offers improved detection of pathologically proven recurrent GBM compared to FDG-PET.

KEYWORDS: Advanced MR Imaging, Glioma Recurrence, Restricted Diffusion



0-952

3:42PM - 3:49PM

Semi-automated, Computer-assisted Quantification of Neuroimaging Characteristics of Glioblastoma: Correlation with Histopathologic Subtypes.

L Furusawa-Stratton¹, D Chow², E Kwak², D Lin², B Lanzman², J Neira², X Guo², P Canoll², A Lignelli³, K Cauley⁴, B Zhao², L Schwartz², C Filippi²

¹Columbia University Medical Center, Fort Lee, NJ, ²Columbia University Medical Center, New York, NY, ³Columbia University, New York, NY, ⁴Columbia Presbyterian, New York, NY

Purpose

Glioblastoma (GBM) is a malignant and highly infiltrative tumor. Recent analysis of the Cancer Genome Atlas (TCGA) has revealed four subtypes (mesenchymal, classical, neural, and proneural) of GBM based on gene patterns. Disease course and treatment response varies according to genomic subtype. The development of reproducible, quantitative imaging biomarkers that can be used to

classify the subtypes of GBM preoperatively may provide a useful tool for treatment guidance and prognosis. Using semi-automated computer-assisted technique, the purpose of this study is to correlate the quantitative imaging features of glioblastoma from the TCGA data set with the four histopathologic subtypes of GBM.

Materials and Methods

This was a retrospective review using pathology results and images from the TCGA database and Cancer Imaging Archive, respectively. The Cancer Imaging Archive maintains images corresponding to TCGA patients. Only patients with presurgical MRI with T1 precontrast, T1 postcontrast, and FLAIR imaging were included. Patients without presurgical imaging or pathology were excluded. Magnetic resonance (MR) images were analyzed using a semi-automated algorithm that combines the region-based active contours and level set approach. The volume of peritumoral edema (Ed), contrast enhancing tumor (CE), noncontrast enhancing tumor (nCE), and necrosis (NE) was obtained for each patient. Additionally, the edema to contrast enhancing ratio (Ed:CE) and edema to noncontrast enhancing ratio (Ed:nCE) were calculated. Peritumoral heterogeneity was quantified objectively by measuring the skew in signal intensity within the peritumoral edema on FLAIR imaging. Statistical analysis with multiple regression was performed with SPSS for each variable. A $p < 0.05$ was considered statistically significant for this study.

Results

A total of 82 patients were available, of which 59 met inclusion criteria. Subtypes distribution was 32.2% (19/59) proneural, 18.6% (11/59) neural, 18.6% (11/59) classical, and 30.5% (18/59) mesenchymal class GBM tumors. We observed a significant relationship between nCE, Ed:nCE ratio, and peritumoral edema heterogeneity with the Verhaak classification ($p < 0.001$ for each category). For example, the mesenchymal subtype displayed the lowest mean nCE (2.9%), whereas other tumor types had higher amounts. Additionally, mesenchymal subtypes displayed a higher Ed:nCE ratio and peritumoral heterogeneity compared to other GBM subtypes. With regard to other studied variables, CE, peritumoral edema, and NE did not display a significant difference among the subtypes. Ed:CE ratio also did not demonstrate a significant difference amongst tumor subtypes.

Conclusions

In summation, the use of semi-automated computer-assisted analysis of neuroimaging characteristics provides quantifiable and objective metrics in the evaluation of the four subtypes of GBM. The mesenchymal subtype of GBM demonstrates statistically significantly lower noncontrast enhancing tumor, higher edema to noncontrast enhancing tumor ratio, and higher peritumoral heterogeneity compared to the other subtypes.

KEYWORDS: Computer Modeling, Glioblastoma

Note: Scanned images are included in the proceedings. Some submitted images were reduced during editing thereby decreasing clarity. Also, refer to the Program Planner. Proceedings Content as of 3/28/2014.

	Verhaak GBM Subtype				p [†]
	Mesenchymal	Classical	Neural	Proneural	
Proportional Involvement					
%CE	24.30%	21.80%	25.60%	19.10%	0.298
%Nec	28.90%	33.20%	29.80%	40.80%	0.09
%nCE	2.90%	10.20%	9.90%	39.30%	<0.001
%Ed	64.20%	62.90%	58.90%	65.40%	0.938
Tumor Infiltration					
Ed:CE	3.42	3.57	2.77	2.27	0.097
Ed:nCE	4.83	4.00	3.44	1.53	<0.001
Peritumoral Edema Heterogeneity					
Edema Skewness	0.83	0.25	0.57	0.36	<0.001

[†] Statistical analysis assessed with multiple regressions

Abbreviations:

%CE, proportion contrast enhancing; %Nec, proportion necrosis; %nCE, proportion non-contrast enhancing disease; %Ed, proportion peritumoral edema.

O-953

3:49PM - 3:56PM

Diffusion Restriction Precedes Contrast Enhancement in Glioblastoma Multiforme

J Shankar1, A Bata2

1QEII Health Science Center, Dalhousie University, Halifax, Nova Scotia, 2Dalhousie University, Halifax, Nova Scotia

Purpose

Glioblastoma multiforme (GBM) are known to have highly variable responses to currently used therapies. The current imaging standard for detecting and assessing tumor progression in these patients depends on the presence of or changes in contrast-enhancing abnormality on brain MR imaging. Diffusion-weighted images (DWI) have become important in characterization of tumors. In tumors, restricted diffusion is seen in areas showing very high cellularity. We have observed that isolated foci of diffusion restriction precedes the enhancement in cases of GBM. The aim of our study was to assess the incidence of isolated diffusion restriction preceding corresponding enhancement and to determine whether diffusion restriction can predict the development of new enhancing mass lesions.

Materials and Methods

Magnetic resonance imaging (MRI) of brain, including diffusion-weighted imaging (DWI) and apparent diffusion coefficient (ADC) maps, of 102 consecutive patients with confirmed cases of glioblastoma were examined retrospectively. Images were assessed to determine

whether there were nonconcordant areas of restricted diffusions (areas where low ADC lesions were present without corresponding postgadolinium enhancement). If found, these regions of interest (ROIs) for each patient were further followed for development of corresponding areas of tumor enhancement on follow-up MRI. Data were collected to assess where low ADC regions exist without enhancement, the normalized ADC (comparing tumor regions to normal regions), the length of time that enhancement takes to appear, and the overall survival of patients from the time of the appearance of corresponding enhancement.

Results

In 97 of 102 patients, restricted diffusion was detected at some point during treatment. The study cohort was formed by 41 patients (42.3%) who had low ADC lesions without an enhancement in a corresponding location on Post-Gad MR imaging. Ten (24.3%) patients developed enhancing tumor at the site of the low ADC lesion. In these ten patients, there were 12 instances where isolated diffusion restriction preceded the development of enhancing tumor. Enhancements appeared in follow-up imaging an average of 145 days after detection of corresponding low ADC lesions. In one case, detection of a nonconcordant low ADC lesion occurred 359 days before gadolinium enhancement appeared in MR imaging. Isolated low ADC lesions had an average apparent diffusion coefficient value of 721.4 GY (compared to 888.7 GY for the comparison group). Progress could not be tracked in 10 patients of the 41 (24.3%) who lacked follow-up imaging after detection of low ADC lesion. In nine (21.9%) more patients, potential development of enhancing tumor could not be accurately examined because of surgical changes, incomplete image sets, or a lack of timely follow up. The remaining 12 patients (29.2%) had low ADC lesions that did not precede the development of corresponding enhancement.

Conclusions

Isolated low ADC lesions indicating restricted diffusion preceded the development of enhancing tumor in approximately 1/5th of GBM patients. Further examination of this phenomena will be necessary, but we believe that these areas of restricted diffusion should be included in the treatment planning of GBM both of surgery or radiotherapy. Inclusion of these potentially may result in more predictive outcome in these patients.

KEYWORDS: Diffusion-Weighted Imaging, Glioblastoma, Restricted Diffusion

O-954

3:56PM - 4:03PM

Note: Scanned images are included in the proceedings. Some submitted images were reduced during editing thereby decreasing clarity. Also, refer to the Program Planner. Proceedings Content as of 3/28/2014.

Image Optimizing in Retinoblastoma: RESOLVE Diffusion Technique for Evaluation of Tumor Expansion and Activity in the Orbit.

KEYWORDS: Diffusion MR Imaging, MR Imaging, Retinoblastoma

S Goericke¹, S Sirin¹, S Maderwald², M Forsting¹, M Schlamann¹

¹University Hospital Essen, Essen, Germany, ²Erwin L. Hahn Institute for Magnetic Resonance Imaging, Essen, Germany

Purpose

Retinoblastoma is the most common orbital malignancy in childhood. Planning therapeutic strategies information on tumor extension and activity is needed. The aim of this prospective study (04/2013-12/2013) was to assess the value of RESOLVE (readout segmented diffusion technique) in MR diagnostic in currently 40 children with retinoblastoma.

Materials and Methods

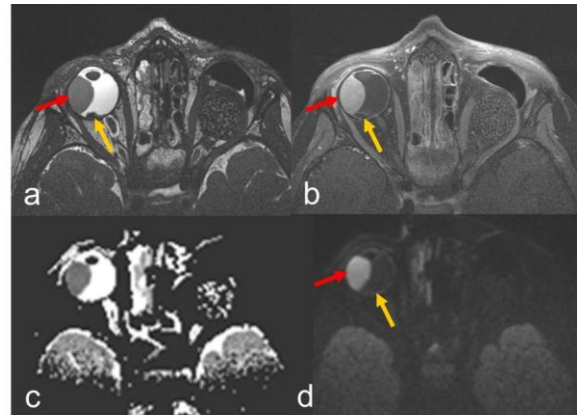
This study was approved by the local hospital ethics committee. Magnetic resonance imaging (MRI) was performed on a 1.5 T scanner (Magnetom Aera, Siemens, Erlangen, Germany) with the use of two orbit surface coils. A standardized high resolution examination protocol with additional RESOLVE sequence of the orbit was applied. Image analysis concerning image quality, evaluation of orbital structures, tumor detection and artifacts was performed by two neuroradiologists in consensus using a three point scale (1-poor to 3-very good). Additionally the mean signal intensity of tumor and vitreous body was evaluated and detection of tumor in RESOLVE, CISS (constructive interference in steady-state) sequence and T1 weighted images with fat saturation and contrast agent were compared.

Results

RESOLVE imaging shows very good image quality (2.4 ± 0.5) and a very good delineation of tumor ($b1000$ 2.8, $b0$ 2.0, ADC 2.3). Some artifacts ($b1000$ 2.1) are detectable however without compromising tumor detection. In evaluation of tumor detection the RESOLVE was inferior to the CISS sequence (1.6 ± 0.3) but superior to the T1+CE (2.6 ± 0.8). Inactive tumor lesions in funduscopy are not diffusion restricted in RESOLVE [hypointense [26.0 ± 20.6 , vitreous body 22.6 ± 7.8]]; active tumors show diffusion restriction [hyperintense [117.5 ± 38.2]], with drop in the ADC maps. Even very small lesions can be assessed successfully concerning tumor activity.

Conclusions

The RESOLVE technique allows detection of retinoblastoma. First experiences demonstrate its value in evaluation of tumor expansion and activity even in small lesions.



O-955

4:03PM - 4:10PM

Optimization of conditional probabilities of a Bayesian Expert System for Neuroradiology differential diagnosis

I Nasrallah¹, M Salehi Sadaghiani¹, M Tanwar¹, E Herskovits², H Kundel¹, S Mohan¹, C Li¹, M Lynch¹, R Bryan¹

¹University of Pennsylvania, Philadelphia, PA, ²University of Maryland, Baltimore, MD

Purpose

Decision-support applications are being designed to help physicians analyze the growing amount of medical data, but have not been applied broadly within radiology. We have developed a Bayesian network expert system (BES) model for neuroradiology differential diagnosis (DDx). This network integrates reader-extracted data from brain magnetic resonance imagings (MRIs) using predefined conditional probabilities (CPs) to output posterior probability for eleven diseases and normal. An initial model (M1P1) based upon the opinion of one expert neuroradiologist was used to generate DDx from key features (KFs) extracted from cases by blinded readers. This model showed reasonable performance compared to the radiologists' DDx (Rad-DDx) (1). In this study, we test the hypothesis that models based upon consensus agreement of neuroradiologists or derived from data extracted from cases would show improved performance.

Materials and Methods

Note: Scanned images are included in the proceedings. Some submitted images were reduced during editing thereby decreasing clarity. Also, refer to the Program Planner. Proceedings Content as of 3/28/2014.

Three readers of varying experience (resident, fellow, attending) extracted KFs and generated Rad-DDx from 101 cases: six of each disease and 35 normals. Modified Delphi method was used for expert consensus CP modification (2). Conditional probabilities independently generated by three neuroradiologists were blinded, shared, and discussed. Independent CP changes then were permitted. After two rounds, the final CPs were averaged yielding model M1P2. For the data driven approach (M1P3), CPs were calculated from the KFs extracted by the case readers. Conditional probabilities were initially set to equivalence and then proportionally modified based upon reader extracted KFs. BES network structure was identical for all models. Reader extracted KFs were run through each BES model to generate DDx and evaluated by complete and partial receiver operating curve (ROC) analysis using Proproc curve fitting. Area under the curve (AUC) was compared between Model DDxs and Rad-DDx using ANOVA.

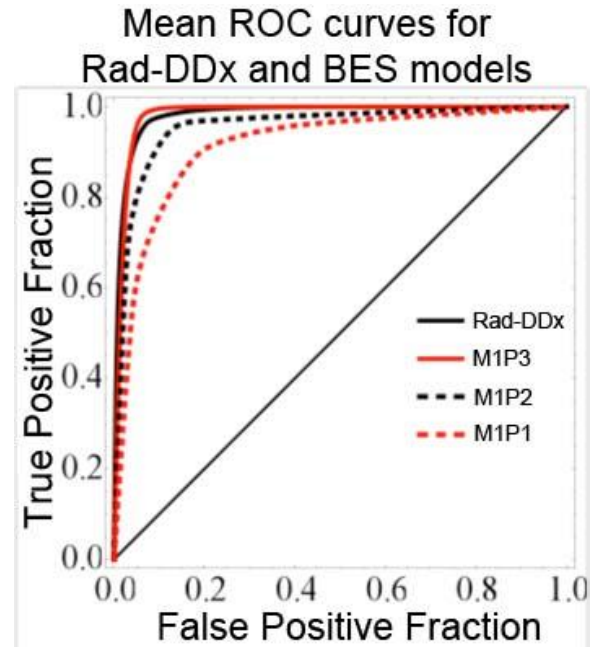
Results

The figure shows mean ROC curves. Rad-DDx and M1P3 had the highest AUC while M1P1 had the lowest. Compared to Rad-DDx, M1P1 showed significant difference ($p < 0.01$) while M1P2 and M1P3 did not. Partial curve analysis showed significant difference between M1P3 and M1P1 ($p = 0.026$) and a trend towards significance between M1P2 and M1P1 ($p = 0.09$) while M1P2 and M1P3 did not differ. Complete ROC analysis did not show significant differences reflecting insufficient power.

Conclusions

Expert consensus, which can reduce personal and recall bias, and a data driven method, limited by the size and representativeness of the sample it was derived from, resulted in improved performance of a prototype differential diagnosis system for neuroradiology.

KEYWORDS: Differential Diagnosis, Informatics, Report Content



0-956

4:10PM - 4:17PM

"Overshoot"-induced Variability in DSC-MR PWI rCBV Measurement of Intracranial Tumors among FDA-approved and Public Research Software programs

X Liu¹, W Tian¹, A Hussain¹, H Wang¹, S Ekholm¹

¹University of Rochester Medical Center, Rochester, NY

Purpose

The first-pass effect in dynamic susceptibility contrast (DSC)-MR perfusion weighted imaging (PWI) leads to decrease of T2* signal intensity followed by recovery after the peak. In most of brain tumors, the T2* signal intensity could recover back close to the base line. The phenomenon that T2* signal intensity recovers higher than the base line is defined as "overshoot". The "overshoot" is less common in DSC MR PWI of intracranial tumors; in this study, we compared the relative blood volume (rCBV) value in the intracranial tumors with "overshoot", which was calculated by three FDA-approved and public research DSC MR PWI software programs.

Materials and Methods

We retrospectively reviewed 32 cases with pathology confirmed intracranial tumors, including 12 cerebral lymphomas, three brain metastases, three meningiomas, and 14 high grade gliomas. Three DSC MR PWI software programs were applied to generate rCBV maps, including

Note: Scanned images are included in the proceedings. Some submitted images were reduced during editing thereby decreasing clarity. Also, refer to the Program Planner. Proceedings Content as of 3/28/2014.

GE BrainStat and nordicICE are FDA-approved products, LUPE (Lund University Perfusion Evaluation) is a public research software program. The rCBV image derived from GE BrainStat is without blood-brain barrier (BBB)-leakage correction. The nordicICE and LUPE calculate BBB-leakage corrected rCBV images. Two neuroradiologists measured the rCBV in the same localized ROIs of rCBV maps generated from these three software programs, and the difference among the three software programs was evaluated.

Results

The interoperator analysis between two neuroradiologists showed that the intraclass correlation coefficient (ICC) was 0.917. The mean rCBV value of "overshoot" intracranial tumors in GE BrainStat rCBV without BBB-leakage correction was 0.38 ± 0.33 , ranged from 0.21 to 1.36. The mean value of LUPE BBB-leakage corrected rCBV was 0.72 ± 0.38 , ranged from 0.47 to 1.79. The mean value of nordicICE BBB-leakage corrected rCBV was 2.97 ± 2.15 , ranged from 1.86 to 4.31.

Conclusions

There is significant difference of rCBV value in "overshoot" intracranial tumors among three FDA-approved and public research DSC MR PWI software programs. The "overshoot" can cause underestimation of rCBV in such intracranial tumors, even in BBB-leakage corrected rCBV maps. Therefore, interpretation of rCBV findings in "overshoot" intracranial tumors must be careful.

KEYWORDS: Cerebral Blood Volume, MR Perfusion-Weighted Imaging, Neoplasm

O-957

4:17PM - 4:24PM

Value of Quantitative Apparent Diffusion Coefficients in Differentiating Low-grade Gliomas from Mixed Neuronal-glioma Tumors

A Agarwal¹, K Thamburaj², S Kanekar³

¹Penn State University, Hummelstown, PA, ²Penn State University, Hershey, PA, ³Penn State Milton S Hershey Medical Center, Hershey, PA

Purpose

To retrospectively assess if diffusion-weighted MR imaging (DWI) and quantitative apparent-diffusion coefficient maps (ADC) could be used to differentiate between low grade gliomas and mixed neuronal-glioma tumors (Dysembryoplastic Neuroepithelial Tumor or Ganglioglioma).

Materials and Methods

This institutional review board-approved, Health Insurance Portability and Accountability Act-compliant retrospective study involved 46 patients with histologically verified tumors: 24 with low grade gliomas (LGGs), 13 with dysembryoplastic neuroepithelial tumor (DNETs) and nine with ganglioglioma. All these patient had conventional MRI and diffusion-weighted imaging done within one month prior to surgery. Apparent diffusion coefficient (ADC) values of tumor (enhancing regions or the solid portion of tumor) and ADC ratios (ADC of tumor to ADC of contralateral white matter) were compared with the histologic diagnosis. Apparent diffusion coefficient values and ratios of low-grade gliomas and mixed neuronal tumors were compared by using the t-test. Optimal thresholds of ADC values and ADC ratios for distinguishing low grade gliomas from mixed neuronal-glioma tumors were determined by receiver operating characteristic (ROC) curve analysis.

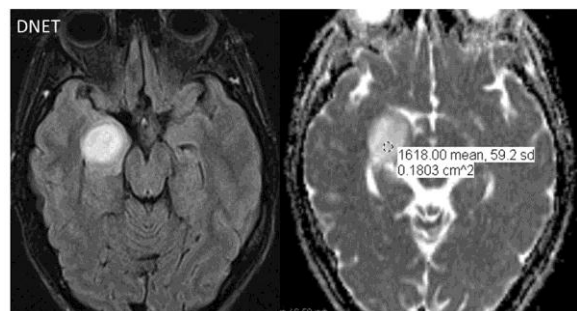
Results

Statistically significant differences were found for minimum and mean of ADC tumor and ADC tumor ratio values between low grade gliomas and mixed neuronal tumors when including only one factor at a time (Figure 1). Including a combination of in total four parameters (mean ADC tumor, and minimum, maximum and mean ADC tumor ratio) resulted in sensitivity, specificity, positive (PPV), and negative predictive values (NPV) of 88.9, 78.6, 91.5, and 77.1% respectively. In the receiver operating characteristic (ROC) curve analysis, the area under the curve of the combined four parameters was the largest (0.86), indicating a good test.

Conclusions

The ADC value, minimal ADC value, and ADC ratios of solid tumoral or enhancing region appeared to be useful for differentiating low grade tumors from mixed neuronal tumors.

KEYWORDS: DNET, Ganglioglioma, Glioma



O-958

4:24PM - 4:31PM

Note: Scanned images are included in the proceedings. Some submitted images were reduced during editing thereby decreasing clarity. Also, refer to the Program Planner. Proceedings Content as of 3/28/2014.

Characterisation of Choroid Plexus Perfusion and Permeability Characteristics Using DCE-MRI in Health and Disease: Glioma.

G Thompson¹, R McCreary², S Mills³, A Jackson¹

¹University of Manchester, Manchester, UK, ²Salford Royal NHS Foundation Trust, Salford, UK, ³Salford Royal NHS Foundation Trust, Manchester, UK

Purpose

There is a continuous process of cerebrospinal fluid (CSF) production and resorption in the central nervous system (CNS) which is crucial to normal function (1). Abnormalities in CSF equilibrium have been implicated in a number of CNS conditions from the straightforward mechanical situations including communicating and noncommunicating hydrocephalus, to less well understood phenomena relating to neurodegenerative disorders such as multiple sclerosis and Alzheimer disease. It also has been hypothesized that disequilibrium in CSF dynamics may contribute to morbidity and mortality in the setting of high grade glioma (HGG) (2). The choroid plexus (CP) is a key vascular structure in the production and regulation of CSF, but to date, only very limited assessment has been made in vivo using noninvasive techniques such as imaging (3). Since CP is known to have leaky endothelium, and large intravascular and extravascular, extracellular spaces, we proposed the use of dynamic contrast-enhanced MRI (DCE-MRI) to assess the perfusion and permeability characteristics of CP in both healthy volunteers in a test-retest setting, and in HGG to assess any variability in normal function detectable by MR, and investigate any possible link with HGG tumor size and degree of perifocal FLAIR abnormality.

Materials and Methods

Fifteen healthy volunteers underwent DCE-MRI at 3 T using an optimized whole brain protocol with baseline variable flip angle T1 relaxometry, and pharmacokinetic analysis based on the Tofts model (4). Time of day and potential modifiers of CSF production such as alcohol, caffeine and prescription medications were controlled for, and the volunteers were scanned on two separate occasions. Brain volumes were segmented using FSL FAST, with manual segmentation of the CP in the lateral ventricles. Twenty-eight patients with histology proven HGG underwent preoperative imaging with the same DCE-MRI protocol. Tumor regions and lateral CP were segmented manually, with FAST segmentation of the remaining brain. Median values of K_{trans}, v_e, v_p, and bolus arrival delay were calculated for each segmented region and in each individual and compared. The image shows the tumor, brain, and choroid plexus segmentation results for an example patient.

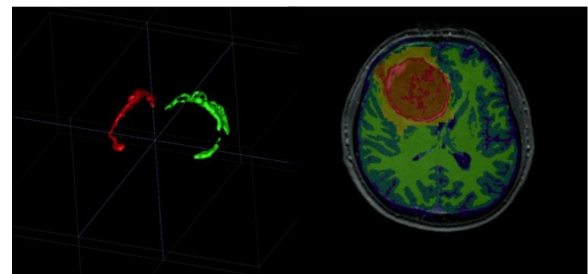
Results

There was no difference between left and right lateral CP v_e, v_p, and bolus arrival delay in healthy volunteers, or between visits. K_{trans} was the only parameter to vary between visits in the healthy volunteers. In tumor patients, values for all parameters were comparable to healthy volunteers, and there was no difference between the choroid plexus parameters between ipsilateral and contralateral hemispheres to tumor. There also was no significant relationship between tumor size, enhancing volume, necrotic volume, nor FLAIR abnormal volume and any of the CP DCE-MRI parameters.

Conclusions

Assessment of choroid plexus perfusion and permeability characteristics is feasible at 3 T in healthy individuals and in disease. There is no intervisit variability in vascular or extravascular, extracellular volume in CP in healthy volunteers, although K_{trans} does change. This may indicate that variance in permeability is the main baseline contributor to variability in CSF production in healthy individuals. In tumors, there is no significant variance in CP characteristics when compared to healthy volunteers, and there also is no difference between ipsilateral and contralateral vascular characteristics, even when taking into account the size of the lesions and significant differences in local and global mass effect, indicating that CP may maintain its functional characteristics even in the setting of significant lesion burden. Further work is required to assess the pathological significance, although the technique can now be utilized to assess a number of neurological disorders of differing etiologies.

KEYWORDS: Cerebral Neoplasm, Cerebrospinal Fluid, Choroid Plexus



0-959

4:31PM - 4:38PM

Rapid Development of Diffusion Restricting Lesions Following Bevacizumab Initiation in High-grade Gliomas is Associated with Male Sex, Older Age, and high MIB-1 proliferation.

J Mettenburg¹, R Hamilton¹

Note: Scanned images are included in the proceedings. Some submitted images were reduced during editing thereby decreasing clarity. Also, refer to the Program Planner. Proceedings Content as of 3/28/2014.

1University of Pittsburgh Medical Center, Pittsburgh, PA

Purpose

To identify characteristics of high grade gliomas associated with rapid development of diffusion restricting lesions (DRLs) following initiation of bevacizumab.

Materials and Methods

Diffusion-weighted imaging (DWI) before and after initiation of bevacizumab was reviewed for 34 patients with high grade gliomas either resected or biopsied during 2012. Patient age ranged from 22 – 77 years (17 M/ 17 F). All patients underwent initial resection or biopsy and chemoradiation, and were started on bevacizumab as salvage therapy following evidence of progression of disease. Histologic and molecular data evaluated included: MIB-1% (a marker of proliferation), IDH-1 mutation analysis, p53 expression, EGFR expression, 1p19q FISH, p16 (CDKN2A) FISH and loss of heterozygosity in 9p. Magnetic resonance images (MRIs) obtained before (0-24 days) and after (1-2 months) bevacizumab initiation were reviewed for new DRLs in the absence of other evidence of interval disease progression. Demographics, histologic and molecular pathology were compared to the DWI findings by chi squared and Student T-tests, with a p-value of <0.05 deemed significant. The study was IRB approved.

Results

Sixteen of 34 patients rapidly developed new DRLs after bevacizumab initiation. There was no significant difference in the average age between men or women or between those that developed DRLs and those that did not. Men were more likely to develop DRLs (11/17) than women (5/17) of any age ($p=0.0393$). For those over 70 years, 5/5 men developed DRLs, while 0/3 women did ($p<0.00001$). There was no significant difference in average percent tumor MIB-1 expression between those that developed DRLs and those that did not; however, patients with tumors demonstrating MIB-1 > 20% were more likely to develop DRLs ($p=0.0019$). Diffusion restricting lesions were associated with 15/28 glioblastomas, but only 1/6 anaplastic astrocytomas (NS, $p=0.10$). Tumors with loss of heterozygosity in 9p were more likely to develop DRLs ($p=0.011$). Homozygous loss of p16 and a greater percentage of polysomy 19q trended toward a greater number of DRLs, but did not reach significance in either case. No association was seen with IDH-1 mutations, p53 or EGFR expression or 1p19q FISH.

Conclusions

In this study, a subset of patients started on bevacizumab as salvage therapy rapidly developed DRLs in the absence of other signs of disease progression. Development of DRLs following bevacizumab is not well understood, though these lesions have been reported as atypical necrosis. Delayed onset of diffusion restriction often precedes progression of disease. The rapidly developing DRLs were associated significantly with patient age, sex and aggressive tumor pathology such as an elevated

proliferation marker (MIB-1 > 20%) and loss of heterozygosity in 9p, a chromosomal region rich in tumor suppression genes such as p16. These preliminary studies suggest that tumors with these aggressive pathologic and demographic features are characterized by rapid development of DRLs following bevacizumab initiation. Future studies will include multivariate analysis and evaluate the relationship of DRLs with overall and progression free survival, as well as characterizing location of recurrence relative to location of the DRLs.

KEYWORDS: Anaplastic Astrocytoma, DWI, Glioblastoma